Natural Resources Canada | Ressources naturelles Canada

GEOLOGICAL SURVEY OF CANADA
OPEN FILE 7894

Quartz provenance in the Mesozoic of the eastern Scotian Basin

C.E. Sales de Oliveira, Y. Zhang, G. Pe-Piper,
D.J.W. Piper, and R. Corney

2015

Canada



GEOLOGICAL SURVEY OF CANADA
OPEN FILE 7894

Quartz provenance in the Mesozoic of the eastern Scotian Basin

C.E. Sales de Oliveira[1], Y. Zhang[1], G. Pe-Piper[1], D.J.W. Piper[2], and R. Corney[1]

[1] Saint Mary's University, Halifax, Nova Scotia
[2] Geological Survey of Canada (Atlantic), Bedford Institute of Oceanography, Dartmouth, Nova Scotia

2015

© Her Majesty the Queen in Right of Canada, as represented by the Minister of Natural Resources Canada, 2015

doi:10.4095/296834

This publication is available for free download through GEOSCAN (http://geoscan.nrcan.gc.ca/).

Recommended citation
Sales de Oliveira, C.E., Zhang, Y., Pe-Piper, G., Piper, D.J.W., and Corney, R., 2015. Quartz provenance in the Mesozoic of the eastern Scotian Basin; Geological Survey of Canada, Open File 7894, 507 p. doi:10.4095/296834

Publications in this series have not been edited; they are released as submitted by the author.

Preface

This study forms part of a joint project between the Geological Survey of Canada and Saint Mary's University to evaluate an integrated approach of scanning electron microscope - backscattered electron (SEM-BSE) imaging, SEM - cathodoluminescense (SEM-CL) imaging, hot-cathode cathodoluminescense (HCL) imaging, and optical microscopic petrography on detrital quartz grains for provenance study in the eastern Scotian Basin. This report documents microscopic, SEM-BSE, SEM-CL and HCL images of selected quartz grains from sandstones in the Bandol-1 well. Different types of detrital quartz grains have been identified in this study: plutonic quartz, very-low-grade- to low-grade- metamorphic quartz (with brittle deformation), low-medium-grade- metamorphic quartz (with/without ductile deformation) and medium-high-grade- metamorphic quartz. Possible sources of sediments to Bandol-1 well were suggested in the Gander terrane of southern Newfoundland, Humber terrane of western Newfoundland, and part of southern Dunnage terrane by the integration of this study and previous detrital mineral and geochronological studies.

Acknowledgements

This work was funded by a grant from the Nova Scotia Offshore Energy Research Association, EnCana, and the Natural Sciences and Engineering Research Council of Canada. We thank Xiang Yang for assistance with scanning electron microscopy at Saint Mary's University. This report was reviewed by Peter S. Giles.

Author's addresses:

CADU SALES DE OLIVEIRA, YUANYUAN ZHANG, GEORGIA PE-PIPER, RANDOLPH CORNEY
Department of Geology, Saint Mary's University, Halifax, Nova Scotia, B3H 3C3, Canada;
gpiper@smu.ca

DAVID J.W. PIPER, Natural Resources Canada, Geological Survey of Canada (Atlantic), Bedford Institute of Oceanography, P.O. Box 1006, Dartmouth, Nova Scotia, B2Y 4A2, Canada;
david.piper@nrcan-rncan.gc.ca

Table of Contents

ABSTRACT 6
INTRODUCTION 7
GEOLOGICAL SETTING 8
LITERATURE REVIEW 10
METHODOLOGY 12
RESULTS AND DISCUSSION 17
Integration and Evaluation of Different Techniques 17
Diagnostic Characteristic Features of Different Quartz Types 20
Plutonic Quartz (Type 1) 20
Metamorphic Quartz (Types 2, 3, 4) 22
Very Low-Grade to Low-Grade Metamorphic Quartz with Brittle Deformation (Type 2) 22
Low-grade to Medium-grade Metamorphic Quartz with no Significant Ductile Deformation (Type 3A) 24
Low-grade to Medium-grade Metamorphic Quartz with Ductile Deformation (Type 3B) 25
Medium-grade to High-grade Metamorphic Quartz (Type 4A and 4B) 26
Volcanic Quartz (not observed in this study) 27
Distribution of Quartz Types in this Study 28
Comparison with Previous Detrital Mineral and Geochronological Studies 29
Provenance Implications 31
CONCLUSIONS 32
REFERENCES 34

List of Figures

Fig. 1. Location of investigated samples. 39
Fig. 2. Inferred Tithonian paleogeography of the Scotian Basin and its hinterland. 40
Fig. 3. Nomenclature for describing the SEM-CL images of detrital quartz. 41
Fig. 4. Data presentation from HCL method. 43
Fig. 5. Examples of SEM-CL images for different quartz types. 44
Fig. 6. Histograms of the distribution of quartz grains. 45
Fig. 7. Pie diagrams of summarized distribution of quartz types. 46
Fig. 8. Annotated bedrock geologic map of Newfoundland 47

List of Tables

Table 1. Summary of research activities applied to studied samples. 48
Table 2: Description of characteristic features of quartz types from various rock lithologies using SEM-CL. 49
Table 3: Summarized diagnostic features in SEM-CL, HCL, and optical images for identified quartz types.. 50

Table 4A: Summary data of detrital quartz grains of sample 2565 (petrography and SEM-CL image). 51
Table 4B. Summary data of sample 2565 (petrography and HCL image). 52
Table 5A. Summary data of sample 2860 (petrography and SEM-CL image). 53
Table 5B. Summary data of sample 2860 (petrography and HCL image). 54
Table 6A. Summary data of sample 2995 (petrography and SEM-CL image). 55
Table 6B. Summary data of sample 2995 (petrography and HCL image). 56
Table 7A. Summary data of sample 3000 (petrography and SEM-CL image). 57
Table 7B. Summary data of sample 3000 (petrography and HCL image). 58
Table 8A. Summary data of sample 3150 (petrography and SEM-CL image). 59
Table 8B. Summary data of sample 3150 (petrography and HCL image). 60
Table 9A. Summary data of sample 3425 (petrography and SEM-CL image). 61
Table 9B. Summary data of sample 3425 (petrography and HCL image). 62
Table 10A. Summary data of sample 3900 (petrography and SEM-CL image). 63
Table 10B. Summary data of sample 3900 (petrography and HCL image). 64

Appendices

Appendix 1A. Microphotos, SEM-BSE images, SEM-CL images, and EDS analyses of quartz grains in sample 2565. 65
Appendix 1B. HCL images and blue colour shift of quartz grains in sample 2565. 108
Appendix 2A. Microphotos, SEM-BSE images, SEM-CL images, and EDS analyses of quartz grains in sample 2860. 130
Appendix 2B. HCL images and blue colour shift of quartz grains in sample 2860. 172
Appendix 3A. Microphotos, SEM-BSE images, SEM-CL images, and EDS analyses of quartz grains in sample 2995. 193
Appendix 3B. HCL images and blue colour shift of quartz grains in sample 2995. 235
Appendix 4A. Microphotos, SEM-BSE images, SEM-CL images, and EDS analyses of quartz grains in sample 3000. 256
Appendix 4B. HCL images and blue colour shift of quartz grains in sample 3000. 298
Appendix 5A. Microphotos, SEM-BSE images, SEM-CL images, and EDS analyses of quartz grains in sample 3150. 319
Appendix 5B. HCL images and blue colour shift of quartz grains in sample 3150. 361
Appendix 6A. Microphotos, SEM-BSE images, SEM-CL images, and EDS analyses of quartz grains in sample 3425. 382
Appendix 6B. HCL images and blue colour shift of quartz grains in sample 3425. 424
Appendix 7A. Microphotos, SEM-BSE images, SEM-CL images, and EDS analyses of quartz grains in sample 3900. 445
Appendix 7B. HCL images and blue colour shift of quartz grains in sample 3900. 487

ABSTRACT

The provenance of quartz, the predominant framework mineral in sandstone reservoirs, is an important exploration tool in petroleum basins. An integrated approach of scanning electron microscope-cathodoluminescense (SEM-CL), hot-cathode cathodoluminescense (HCL), and petrographic microscopy using grain-by-grain comparison was used to interpret provenance of sandstones in the Bandol-1 well in the eastern Scotian Basin. Information provided by SEM-CL features, HCL colours and colour shift, and optical properties such as extinction, fluid inclusion trails and polycrystallinity were combined to distinguish different quartz types. The integration of the three techniques reduces uncertainties inherent to each individual technique. The three techniques were compared and all the characteristic features for each quartz type under the three different microscopes were summarized in detail. This study suggests that the integration of SEM-CL and petrographic microscopy appears to be enough to differentiate between major quartz types such as plutonic and metamorphic quartz, while HCL analyses are important to constrain and confirm the classification of quartz types. In addition, HCL analyses were demonstrated to be very useful in assigning detrital quartz to a specific metamorphic grade. Previous detrital mineral and geochronological studies of the same samples were also used for comparison and better understanding of potential provenance sources. Possible sources of sediments to Bandol-1 well were suggested in the Gander terrane of southern Newfoundland, Humber terrane of western Newfoundland, and part of southern Dunnage terrane.

INTRODUCTION

Quartz is the predominant framework mineral in reservoir sandstones in petroleum basins. The study of detrital quartz provenance thus is a significant predictor for the availability of reservoir sandstones in frontier basins. Several techniques based on petrology and geochemistry have been developed over the years to interpret the provenance of detrital quartz. Scanning electron microscope-cathodoluminescense (SEM-CL) has been intensively used for quartz provenance analysis (e.g. Milliken 1994; Seyedolali et al., 1997; Kwon and Boggs, 2002; Bernet and Basset, 2005; Boggs and Krinsley, 2006). In addition, hot-cathode cathodoluminescense (HCL), which often provides characteristic CL color for quartz with different sources, has likewise been used as a tool in provenance studies (e.g. Zinkernagel, 1978; Matter and Ramseyer, 1985; Watt et al., 1997; Götte and Richter, 2006; Hooker and Laubach, 2007; Sawatzky and Pe-Piper, 2013). The petrographic microscope also provides important clues to interpret quartz provenance, such as undulatory extinction, polycrystallinity, nature of sub-grain boundaries, fluid inclusion trails, deformation lamellae, and deformation banding, (e.g. Basu et al., 1975; Bernet and Basset, 2005; Sawatzky and Pe-Piper, 2013). These petrographic microscope features have been combined with SEM-CL analyses in order to improve identification of quartz provenance groups (Kwon and Boggs, 2002; Bernet and Basset, 2005). This new provenance analysis technique, using integrated SEM-CL and optical analysis on the same individual quartz grain, was used by Bernet and Basset (2005) to distinguish among plutonic, volcanic, and metamorphic quartz. However, no studies have yet combined the three provenance techniques (SEM-CL, HCL and petrographic microscopy) on detrital quartz grains. Also a problematic overlap of features is present in low-, medium- and high-grade metamorphic quartz, which impedes the attempt of assigning detrital quartz to a specific metamorphic grade.

The Scotian Basin hosts producing gas fields in Upper Jurassic-Lower Cretaceous deltaic sandstones. They are all situated in the Sable subbasin in the central part of the basin. No gas fields have yet been discovered in the Laurentian subbasin. However, since the latter subbasin also contains abundant deltaic sandstones, similar to the Sable subbasin, potential reservoir sandstones might be present. In this study, the three detrital quartz provenance techniques were applied to seven sandstone samples from the Bandol-1 well located in the Laurentian subbasin in northeastern part of the Mesozoic-Cenozoic Scotian Basin on the eastern Canadian margin (Fig. 1A). We used the integration of the three techniques on the same quartz grains to assign individual detrital quartz grains to provenance quartz types and also to specific metamorphic grades based on SEM-CL features, HCL colours, and optical properties such as extinction and polycrystallinity.

The objectives thus of this study are (1) to develop a comprehensive provenance analysis technique using integrated SEM-CL, HCL, and petrographic microscope analysis of detrital quartz grains based on the identification and detailed description of diagnostic features of quartz from different sources, e.g. volcanic, plutonic or metamorphic quartz type; (2) to compare and evaluate these three techniques; (3) to summarize and further improve diagnostic features for each quartz-type group and especially for the identification of the grade of metamorphic quartz; (4) to assess our results from detrital quartz by comparing with previous geochemical and detrital mineralogical data from the Bandol-1 well; and (5) to synthesize the potential sources of sediments to the Bandol-1 well in the Laurentian subbasin.

GEOLOGICAL SETTING

The Scotian Basin is located offshore Nova Scotia. It formed after Triassic rifting and early Jurassic separation of the North American and African continents. The Scotian Basin is a passive-

margin sedimentary basin that underlies the present continental shelf and slope (McIver, 1972; Wade and MacLean, 1990). Distinctive depocentres, which are Shelburne, Sable, Abenaki and Laurentian subbasins, are identified in the Scotian Basin (Fig. 1B). The deposition of sediments was initiated during Triassic rifting and persisted through the Mesozoic (Wade and MacLean, 1990) (Fig. 1B). During the Late Jurassic, deltaic sandstones and shales of the Mic Mac Formation and the lower Missisauga Formation were deposited from an influx of clastic sediment in the Scotian Basin. Deltaic sedimentation persisted through the Neocomian supplying the upper Missisauga Formation and the Aptian-Early Cenomanian Logan Canyon Formation (Wade and MacLean, 1990). Several detrital mineral and geochemical provenance studies suggested that the sediments in the eastern and central Scotian Basin were supplied by two distinct rivers, the Banquereau and Sable rivers respectively (Pe-Piper et al., 2008; Triantafyllidis et al., 2010; Tsikouras et al., 2011; Pe-Piper and Piper, 2012). The Banquereau river flowed along the Humber Fault and drained mainly western Newfoundland, while the Sable river flowed through the Cabot Strait and drained southern Labrador, the west coast of Newfoundland, the present Gulf of St. Lawrence, and parts of New Brunswick (Pe-Piper and Piper, 2012) (Fig. 2). In addition, small local rivers added sediments from the Meguma terrane south of the Cobequid-Chedabucto fault zone. In the Laurentian subbasin, where the studied well is located, there is some evidence from the Hermine E-94 well for supply from the Avalon terrane of southern Newfoundland during the Late Jurassic and Early Cretaceous (Pe-Piper et al., 2014).

Bandol-1 well was drilled on the shelf in the central Laurential subbasin in 2001. The samples analysed in this study are from the Missisauga Formation and the underlying Mic Mac Formation, with the base-Cretaceous unconformity at 2632 m. Previous mineralogical study of the Bandol-1 well suggested Gander terrane of southern Newfoundland, Humber terrane of western Newfoundland, and part of southern Dunnage terrane (Fig. 1A) as potential sources of sediments (Pe-Piper, 2007).

LITERATURE REVIEW

Cathodoluminescence (CL) properties of quartz have been used as a provenance-identification technique (Zinkernagel, 1978; Matter and Ramseyer, 1985; Hooker and Laubach, 2007). The cause of luminescence of quartz has been credited to a diversity of factors, and it is not yet completely understood (Bernet and Basset, 2005; Boggs and Krinsley, 2006). The cause includes Al substitution for Si, intracrystalline variation in trace element concentrations, and point or linear defects in the crystal lattice of the quartz (Perny et al., 1992; Watt et al., 1997; Ramseyer and Mullis, 2000; Bernet and Basset, 2005). Each of these may affect the intensity and spectral characteristics of luminescence during irradiation by the electron beam. Due to difference in luminescence intensity within different parts of grains, various distinctive textural cathodoluminescence features appear in quartz crystals, such as CL colour, zoning, healed fractures, patches, streaks (spiders), deformation lamellae, and mottling. These distinctive features of detrital quartz grains have been used collectively to differentiate grains of differing provenance.

Both SEM-CL and HCL have been used to get CL images. SEM-CL images of detrital quartz display different shades of grey extending from black to white, where black or dark grey corresponds to low luminescence, and white or light grey corresponds to high luminescence. Some quartz grains can show up nearly uniform CL, appearing homogeneous in black, dark grey or light grey. These grains are low in defects or chemical variation such as trace elements in the crystal structure (Seyedolali et al., 1997; Bernet and Basset, 2005; Boggs and Krinsley, 2006). Seyedolali et al. (1997) proposed a set of traits for discriminating quartz for different sources by analysing quartz from known volcanic, plutonic and metamorphic rocks. Kwon and Boggs (2002) suggested that to properly determine sediment provenance, SEM-CL must be combined

with optical microscopy analysis, since SEM-CL by itself may provide discrepant provenance inferences for the same sample. Optical microscopy analyses provide important auxiliary information to interpret provenance, such as extinction behavior, mono-, poly-, and microcrystallinity, and the presence of sub-grain boundaries. In addition, mineral and fluid inclusions are also useful to distinguish different types of quartz. Bernet and Basset (2005) combined SEM-CL with optical microscopy analysis on single quartz grains to interpret sediment provenance. In this study, reference data based on Seyedolali et al. (1997), Kwon and Boggs (2002), and Bernet and Basset (2005) was summarized to discriminate quartz grains from different groups of parent rocks in the sandstones (Tables 2, 3).

Three main quartz types, volcanic, plutonic and metamorphic quartz, have been described in the literature (Seyedolali et al., 1997; Bernet and Basset, 2005; Boggs and Krinsley, 2006). Volcanic quartz is usually monocrystalline and displays non-undulose to weak undulose extinction and large open fractures under the optical microscope. The main distinctive SEM-CL features are homogeneous CL and frequent zoning. Typical plutonic quartz under optical microscopy is mainly identified by non-undulose or weakly undulose extinction and fluid inclusion trails. The main distinctive SEM-CL features are light grey CL with randomly oriented healed fractures, and irregular dark patches and streaks termed spiders (Boggs and Krinsley, 2006). Metamorphic quartz displays weakly to strongly undulose extinction and presence of deformation lamellae and healed fractures with preferred orientation. The SEM-CL images for metamorphic quartz may show homogeneous, patchy or mottled CL, but commonly are dark grey to black colour. No good discrimination between low, medium, and high-grade metamorphic quartz has yet been established.

HCL microscopy, which provides CL colour images, has also been frequently used as a tool to interpret provenance of quartz (Zinkernagel, 1978; Matter and Ramseyer, 1985; Marshall and Mariano, 1988; Götze and Zimmerle, 2000). The following classification scheme is commonly applied to identify different quartz types: (1) blue to violet: plutonic quartz, as well as quartz phenocrysts in volcanic rock, and high-grade metamorphic quartz; (2) red: groundmass quartz in volcanic rocks; (3) brown: quartz from regionally metamorphosed rocks; (4) non-luminescent or weakly luminescent: authigenic quartz; (5) short-lived green or blue CL: hydrothermal and pegmatitic quartz (Götze and Zimmerle, 2000; Boggs and Krinsley, 2006; Sawatzky and Pe-Piper, 2013).

METHODOLOGY

Seven sandstone samples from the Missisauga and underlying Mic Mac Formations from the Bandol-1 well in northeastern part of the Scotian Basin were selected to be studied for detrital quartz (Table 1). The name of each sample corresponds to its depth in meters. One sample (2565) is from the Missisauga Formation and the other six samples (2860, 2995, 3000, 3150, 3425, and 3900) are from the Mic Mac Formation. They are all fine-grained cuttings, which were carefully brushed and washed, and then dried. The following steps were used during this process: First, the cutting samples were broken down using only fingertips and homogenized, and then washed with detergent and centrifuged down in order to remove any remnant drilling mud and other contaminants such as minerals evaporated from residual seawater. No inorganic flocculants or other contaminants were used. Then, the samples were dry sieved at 1 mm to remove large cuttings. The remainder of the sample was then wet sieved, using detergent for removal of the drilling oil, at 250 µm and 54 µm. The heavy liquid used was an aqueous solution of sodium polytungstate powder prepared to a specific gravity of 2.8. The upper

layer, containing lighter fraction (<2.8 specific gravity) was poured off into a reinforced paper filter and vacuumed to retain heavy liquid for possible reuse. The filter and the washed contents were moved to a drying oven. The filtered grains were then transferred to a second vacuum flask for washing with pure water (reverse osmosis filtered lab water). The light fraction from each of these samples was used to make polished thin sections used in this study. A polished thin section for each sample was studied consecutively under petrographic microscope, scanning electron microscopy (SEM), and hot-cathode cathodoluminescense (HCL) microscope at the Regional Analytical Centre, Saint Mary's University.

Forty detrital quartz grains, covering as many different characteristics of detrital quartz as possible, were selected for each sample with the petrographic microscope. Two microphotographs of each quartz grain were taken under plane-polarized light (PPL) and crossed-polarized light (XPL). The investigation of the detrital quartz grains by the petrographic microscope include the description of extinction character, roundness, the presence and the nature of mineral inclusions, the number of sub-grains, and the presence of mosaic texture, deformation lamellae, fluid inclusions and melt inclusion trails.

These forty quartz grains in each sample were then studied with the SEM. Backscattered electron (BSE) images, cathodoluminescence (CL) images, and mineral chemical analyses, especially from inclusions in the detrital quartz grains, were taken using a LEO 1450 VP SEM. This SEM is equipped with a one channel Gatan Mini CL detector and an Oxford X-max 80 mm^2 SDD energy dispersive spectrometer (EDS) at 30 kV with an acquisition time of 60 seconds. BSE images were utilized to observe fracture, secondary porosity and melt inclusion; EDS analyses were taken for further identification of melt inclusions and mineral inclusions. SEM-CL images were utilized to observe distinctive CL fabrics in quartz and to describe CL appearance in

panchromatic images (Fig. 3). The description of SEM-CL appearance was expressed in grey-level scale with the intensity extending from 0-255, which is extracted from ImageJ, an open source java based software developed at National Institute of Health, Bethesda, Maryland, USA, by Wayne Rosband. Since the working conditions of the SEM such as voltage and beam current vary for each sample, the mounting epoxy has been designated as comparative reference in order to minimize the effects of varied SEM conditions for determining the brightness of quartz grain for different samples. Therefore, a comparison between the brightness of individual quartz grain and its surrounding epoxy is used to classify dark grey (or black), grey, and light grey for the appearance of SEM-CL image. Even though, slight changes in working conditions, like beam size, occurred for a few grains in one sample in order to get a clearer SEM-CL images, the above criteria for SEM-CL appearance was still applied to most of the quartz grains within one sample. The other distinctive features of SEM-CL images are described later (Tables 2, 3). All the features of the SEM-CL image of individual quartz grains for each sample have been summarized in Tables 4-10.

The quartz grains were studied using a HC4-LM cathodoluminescense microscope from Lumic. This is a hot cathode luminescence system comprised of a modified Olympus polarizing optical microscope, an aluminum vacuum sample chamber, an electron gun, a high vacuum pump, and a high voltage power supply. Images were captured with a Kappa DX40C Peltier-cooled digital CCD camera and Kappa Camera Control software. The magnification of HCL images is controlled by the optical microscope equipped with 40, 100, and 1000 times lenses. Sets of four consecutive pictures were taken after 3s, 6s, 9s, and 12s exposure at the CL beam respectively. Each image was taken with 2 seconds exposure time and 1 second latency. Detailed description of this method is in Sawatzky and Pe-Piper (2012). All HCL images were taken in

RGB (R: red, G: green, B: blue) colour mode, in which each parameter defines the intensity of the colour and can be an integer between 0 and 255. For example, RGB (0, 0, 255) value is rendered as blue in the image. With the aid of program ImageJ, HCL images with 3s and 12s exposure named as the first and last HCL images for each grain, were investigated. First, an area of interest (AOI) was defined on the first image, and then transferred to the last image to ensure identical AOI was being analysed. The RGB values within each AOI were graphed in ImageJ and then exported to software Graph (Fig. 4). HCL images of all analysed quartz grains were found to be predominantly in the blue channel, with little or no changes to the red and green parameters. Therefore, only blue values were extracted from HCL images and used to quantify the colour shift between the first image and the last image.

Microphotos under PPL and XPL, BSE images, SEM-CL images, and HCL images of detrital quartz for all samples are provided in Appendices 1-7. The following nomenclature were used to define diagnostic characteristics of detrital quartz in our samples observed in this study.

1. **Homogenous CL:** Nearly uniform CL intensity across the grain (Fig. 3A).

2. **Fractures** in quartz have been divided into two types: healed fractures and open fractures.
   - **Healed fractures** (after Boggs and Krinsley, 2006) are fractures filled with secondary silica that appear as thin (commonly < 10 μm) black lines in SEM-CL images (Fig. 3B). They are usually not shown in BSE images. **Open fractures** appear in CL images as dark lines or bright lines; they are also visible in BSE images and microphotographs. Sometimes open fractures appear only in BSE images, not in SEM-CL images (Boggs and Krinsley, 2006).

3. **Tectonic deformation lamellae**: Tectonic deformation lamellae (Fig. 3C) appear in SEM-CL image as numerous sets of thin, parallel, closely spaced and dark grey lines (Bernet and Basset, 2005). According to Hamers and Drury (2011), tectonic deformation lamellae can either appear as dark grey lines or bright lines in SEM-CL images, and can show slightly

wavy features with varying thickness. They usually also appear in XPL images under petrographic microscope.

4. **Spiders**: They are made up of dark CL patches and streaks. **Dark CL patches** mainly range from 10-100 µm. **Streaks** are random and irregular in the appearance of black broad (>10 µm) elongated form. The spiders are commonly associated with healed fractures, giving them the appearance in SEM-CL images of spiders sitting on a web (Fig. 3D). They cannot be seen in BSE images, since they are made up of secondary silica (Boggs and Krinsley, 2006).
5. **Bright patches or mottling**: Some grains show irregular CL intensities across grains, creating a mottled pattern due to the presence of patches (Boggs and Krinsley, 2006). Three types of bright patches or mottling were seen.
   - **Random bright patches** (Fig. 3E1)
   - **Bright streaky patches fabric** (Fig. 3E2)
   - **Subtle mottling** (Fig. 3E3)
6. **Overgrowth**: Overgrowth appears in SEM-CL images as dark areas in the border of the quartz grains (Fig. 3F).
7. **Fluid inclusion trail**: They are usually associated with secondary porosity and commonly located along healed fractures, boundaries between detrital quartz grains and quartz overgrowth. They are easily observed in microphotos under PPL. The fluid inclusion trails are separated in two kinds:
   - **Detrital fluid inclusion trails:** fluid inclusions are original and do not cut any quartz overgrowth.
   - **Diagenetic fluid inclusion trails**: fluid inclusions originate from diagenesis and thus cut quartz overgrowths.
8. **Melt inclusion**: Large fluid inclusions (>10 µm) in which crystallised minerals are visible.
9. **Secondary porosity**: Porosities usually caused by dissolution and/or fractures. They are easily observed in microphotos under PPL and BSE images.
10. **HCL colour:** The classification of the intensity of the blue colour in HCL image was based on the blue colour scale with values from 0-255 (0=no blue or "black", 255=blue). The following criteria were used to classify the colour: very dark blue (0-10), dark blue (11-

50), medium dark blue (51-100), medium blue (101-150), bright-medium blue (151-200), and bright blue (201-255) (Fig. 4).

11. **HCL colour shift**: Colour shift is used to describe colour change between the first and the last HCL images of each quartz grain. Four ranks of colour shift have been identified by using the change of statistical mean blue values (ΔB) of AOI determined by ImageJ: no colour shift ($\Delta B < 5$), slight colour shift ($5 \leq \Delta B < 15$), moderate colour shift ($15 \leq \Delta B < 30$), strong colour shift ($\Delta B \geq 30$) (Fig. 4).

RESULTS AND DISCUSSION

Integration and Evaluation of Different Techniques (Petrographic Microscopy, SEM-CL and HCL)

Petrographic microscope analysis alone does not provide significant provenance information for a reliable provenance interpretation (Kwon and Boggs, 2002; Bernet and Basset, 2005; Boggs and Krinsley, 2006). There are also no clear-cut CL features for different quartz types. Therefore, SEM-CL images were considered jointly with petrographic microscope data in order to reduce ambiguities in distinguishing quartz provenance types (Bernet and Basset, 2005). In addition, HCL images were also used to improve the identification of quartz provenance.

The main petrographic features used in this study to identify quartz types were extinction, presence of quartz mosaics, mono-, poly-, and microcrystallinity, formation of sub-grain boundaries, roundness, and presence of fluid inclusion trails and deformation lamellae. Extinction characteristics are considered to be extremely important to distinguish quartz types since they vary with deformation. Plutonic quartz usually displays non-undulose or weak undulose extinction (5°-10°), while low-grade to high- grade metamorphic quartz frequently displays weak undulose to strong undulose extinction (>10°). The presence of quartz mosaics, common in medium-grade to high-grade metamorphic quartz, usually indicates high

deformation. This type of quartz can be monocrystalline or polycrystalline. Those that are polycrystalline usually display sutured sub-grain boundaries, which are related to high pressure at medium to high grade metamorphic conditions. Deformation lamellae and deformation banding are also very useful to identify quartz types, since they are the main features which characterize ductily deformed quartz under low-grade to medium-grade metamorphic conditions. Deformation lamellae appear in petrographic microscope or in SEM-CL images, or in both, whereas deformation banding can only be observed with the petrographic microscope.

Both primary and secondary characteristic features of quartz grains can be shown in SEM-CL images (Table 2), which are very helpful in identifying quartz types. The primary features include those originating from crystallisation and/or cooling after crystallisation, such as zoning, randomly oriented healed fractures, spiders, homogeneous CL (only in volcanic quartz and vein quartz), and bright patches or mottling (in volcanic quartz and vein quartz, less common in plutonic quartz). The secondary features include those that modify or overprint previously existing features, and they originate from deformation and/or recrystallisation. These features comprise microfractures with preferred orientation, deformation lamellae, homogeneous CL, and bright patches or mottling. Some features such as homogenous CL and bright patches or mottling can also be either primary feature or secondary feature. For instance, bright patches or mottling indicates uneven distribution of activator ions or defect structures within the grain, which can be preserved as a primary feature in volcanic, vein and plutonic quartz (less commonly) or caused by secondary recrystallisation or annealing due to metamorphism (Boggs and Krinsley, 2006). Therefore, collaborative investigation from observations on other features should be made for the correct identification of quartz type.

The quartz grains in this study were also analysed under the HCL microscope, which provides different CL colour images according to the physicochemical and thermodynamic conditions under which the quartz formed. However, magnification of HCL technique in this study could not be as high as SEM-CL, so detailed fabrics in luminescing quartz should be better shown in SEM-CL images than HCL images. Various investigations of an extensive array of quartz-bearing rocks have shown that a provenance correlation of quartz grains constructed only using HCL colour is not always possible since different samples of quartz that formed under varying genetic conditions may display similar HCL colour (Götze and Zimmerle, 2000; Sawatzky and Pe-Piper, 2013). Nevertheless, HCL features can fully constrain and confirm the identification of distinct quartz types when considered jointly with petrographic and SEM-CL microscopic data.

In order to evaluate different techniques in provenance study, identifications of quartz types from two integrated methods were made respectively: combined microscopic and SEM-CL techniques (Tables 4A-10A), and combined microscopic and HCL techniques (Tables 4B-10B). A final classification was made by integrating the results from these two methods (Tables 4B-10B). Quartz types identified by these two different methods turned out to be similar even though HCL features for different quartz types are not as distinct as SEM-CL features. Therefore, the microscopic observation is significant and should be considered more rigorously in the study of quartz provenance. We also discovered that the integration of HCL images and petrographic microscope data was not sufficient to identify brittle deformed quartz, since the HCL resolution provided was not enough to reveal sets of healed fractures with preferred orientation, nor did these healed fractures appear under petrographic microscope examination. Neither bright patches or mottling could be seen with these techniques. Therefore, attention

should be focused on SEM-CL images in order to assign quartz types for some brittle deformed quartz grains or some grains with bright patches or mottling.

The integration of HCL images, SEM-CL images and petrographic microscopic observations was very useful to differentiate quartz types that were deformed, metamorphosed, and/or recrystallised under low, medium, or high-grade metamorphic conditions. For example, low-grade metamorphic quartz displays medium to dark blue or medium to dark brownish blue HCL colour, while medium and high-grade metamorphic quartz (type 5A in table 3) displays bright to bright-medium blue HCL colour. Since there is no distinct division between these two quartz groups from SEM-CL, nor from optical features for some grains, the features in HCL images are crucial to distinguish them.

Diagnostic Characteristic Features of Different Quartz Types

Two main quartz types, plutonic and metamorphic quartz are identified in studied samples from the Bandol-1 well. Further subtypes of the metamorphic quartz have also been recognized. All the quartz types and their diagnostic characteristic features from SEM-CL images, HCL images, and petrographic microscopic observations are summarized in Table 3 and exemplified in Fig. 5. Even though volcanic quartz was not found in our samples, it is described in this report due to its provenance importance in other regions.

Plutonic Quartz (Type 1 Quartz)

Plutonic quartz grains in our samples show non-undulose or weak undulose extinction (5°-10°) under petrographic microscope. Most of them are monocrystalline (94%), and a few polycrystalline grains contain less than four sub-grains without sutured sub-grain boundaries. Fluid inclusions trails, which can be seen under petrographic microscope, are present in more

than 95% of the plutonic quartz grains. Melt inclusions and mineral inclusions such as apatite and zircon are also present.

In SEM-CL images, all plutonic quartz grains show oriented healed fractures (Fig. 3B1 and 3B2). Lots of fractures in plutonic quartz could possibly be created during cooling at the transition of beta quartz to alpha quartz (570 to 600°C) since large distortional strains accompanied with this transition can cause widespread cracking of the quartz grains (Sprunt and Nur, 1979; Müller et al., 2000; Boggs and Krinsley, 2006). The percolation and precipitation of silica-rich fluids at lower temperatures allowed these fractures to be filled and thus healed, resulting in healed fractures (Boggs and Krinsley, 2006). The fluid inclusion trails were commonly observed under petrographic microscope where healed fractures occurred in the SEM-CL images. This also suggests that the fluids first filled previously established open fractures, and then filled the fractures to form healed fractures. Therefore, the occurrence of fluid inclusion trails in plutonic quartz under the petrographic microscope usually indicates the presence of healed fractures.

Another SEM-CL feature that was commonly seen in plutonic quartz in our samples is dark-CL patches and streaks, termed spiders (Fig. 3D). The spiders are frequently associated with healed fractures and are present in 80% of the analysed plutonic quartz grains in this study. The spiders cannot be seen in the petrographic microscope or in SEM-BSE images, which indicates that they are composed of SiO_2 and are in optical continuity with the host quartz grain. Spiders are formed during cooling of quartz crystals (Boggs and Krinsley, 2006). Most of the plutonic quartz grains display light grey-CL, and some display grey-CL. Zoning does not occur in any of our plutonic quartz grains, even though several authors found zoning in plutonic quartz (Seyedolali et al., 1997; D'Lemos et al., 1997; Bernet and Basset, 2005; Boggs and Krinsley,

2006). We observed random bright patches in a few plutonic quartz (<10%) without any preferred orientation, which was not dominant enough to erase primary features such as healed fractures and spiders. Therefore, it is believed that these random bright patches are not related to deformation.

HCL colour of the plutonic quartz ranges from bright blue to medium-dark blue. Most grains (91%) display medium blue or medium-dark blue. A slight or moderate colour shift in most grains (87%) is observed. These findings are in accord with the results in Sawatzky and Pe-Piper (2013). Problems remained to identify detailed CL features such as healed fractures and spiders in HCL images due to the restricted magnifications using this technique.

Metamorphic Quartz (Types 2, 3, 4 Quartz)

Since metamorphic rocks form from diverse protoliths and under variable ranges of temperature, pressure and fluid conditions, it is of great value to assign metamorphic grade in identifying metamorphic quartz type. However, previous studies showed that it was difficult to associate specific SEM-CL features with clear-cut metamorphic grade, because overlaps of characteristic features are present in low-, medium- and high-grade metamorphic quartz. This study attempts to differentiate metamorphic grades of quartz as indicated by its deformation, by using petrographic microscope, SEM-CL and HCL features in concert.

Very Low-Grade to Low-Grade Metamorphic Quartz with Brittle Deformation (Type 2 Quartz)

Burial, or local or regional tectonic deformation under non-metamorphic to very low-grade or low grade metamorphic conditions at temperatures lower than 300°C is dominated by quartz grains with brittle deformation (Passchier and Trouw, 1996). This brittle deformation usually creates microfractures with preferred orientation (Figs. 3B3, 5B) that match the local or

regional strain field (Kanaori, 1986; Bernet and Basset, 2005). Silica-rich fluids can precipitate SiO_2 at lower temperatures within these microfractures, resulting in healed fractures. The associated fluid inclusion trails also appear and can be seen under petrographic microscope. If these healed fractures had occurred due to burial or compaction during sedimentation, they should appear in almost all grains in the same sample. Therefore, it is considered that the sets of oriented healed fractures observed in this study are due to tectonic deformation, not burial or compaction, and related to the tectonic setting of the quartz provenance.

In terms of provenance, such grains with brittle deformation are assigned as very low-grade to low-grade metamorphic quartz (type 2) if sets of parallel microfractures (commonly healed) with preferred orientation are seen. More than one generation of oriented healed fractures are present in some grains, indicating differing strain over time. The healed fractures are associated with spiders in most grains (79%) of type 2. The brittle deformation in type 2 quartz did not cause significant changes in the SEM-CL features of the pristine quartz type. Bright streaky patches in 45% of all our brittle deformed quartz grains (Figs. 3E2, 5B) were also observed. Such patches always display the same orientation as the set of healed fractures. Therefore, the appearance of bright streaky patches can also be an indicator of brittle deformation.

Our HCL analyses show that type 2 quartz displays a variety of blue CL colours in HCL images in accord with the pristine quartz, since the metamorphism was not intense enough to cause changes in CL colour response. Therefore, the HCL technique by itself is not an effective tool to identify brittle deformation.

Low-grade to Medium-grade Metamorphic Quartz with no Significant Ductile Deformation (Type 3A Quartz)

Two subtypes of low-grade to medium-grade metamorphic quartz have been recognized depending on the appearance of ductile deformation. Low-grade to medium-grade metamorphic quartz with no significant ductile deformation is assigned as type 3A, whereas low-grade to medium-grade metamorphic quartz with ductile deformation is type 3B. Quartz grains of type 3A (Table 3) are monocrystalline or polycrystalline with sutured sub-grain boundaries. The grains display weak to strong undulose extinction under the petrographic microscope. Fluid inclusion trails are not common. Metamorphic mineral inclusions (mainly chlorite) may be present.

Low-grade to medium-grade metamorphic quartz usually displays grey to dark grey SEM-CL. Some quartz grains of type 3A (29% of the analysed grains of type 3A) display grey-black homogeneous CL (Fig. 3A1), in accord with Seyedolali et al. (1997) and Bernet and Basset (2005). Bright patches or mottling with preferred orientation were present in some grains (37%) of type 3A, which is distinct from randomly oriented bright patches in plutonic quartz. Three different types of bright patches or mottling in type 3A quartz were seen: random bright patches (Fig. 3E1), bright streaky patches (Fig. 3E2), and subtle mottling (Fig. 3E3).

Healed fractures in SEM-CL images are common in most grains (60%). They occur as primary features because the recrystallisation or annealing under this low-grade to medium-grade metamorphic condition was not intense enough to completely erase previously developed primary healed fractures. However, these features tend to continually disappear with increasing metamorphic grade, and can be totally erased if the quartz is completely recrystallised. Therefore, healed fractures are considered to be one of the diagnostic features for type 3A quartz.

Colour of HCL images of type 3A ranges from medium-dark blue to dark blue. Only a slight colour shift (or none at all) was predominantly observed in type 3A quartz (> 90%). A moderate colour shift was also occasionally observed (< 10%), which is in agreement with previous studies of this type (Götze and Zimmerle, 2000; Götte and Richter, 2006; Sawatzky and Pe-Piper, 2013).

Low-grade to Medium-grade Metamorphic Quartz with Ductile Deformation (Type 3B Quartz)

At low-grade metamorphic conditions (300-400°C), dislocation glide and creep become so important in quartz that tectonic deformation lamellae can be developed (Fig. 3C). The occurrence of deformation lamellae, deformation bands, and medium to strong undulose extinction in quartz has been considered to be correlated with the initiation of ductile deformation with increasing metamorphic grade (Passchier and Trouw, 1996). Deformation bands and undulose extinction have been observed only under the petrographic microscope examination, while deformation lamellae sometimes can be seen under the petrographic microscope and other times in SEM-CL images. Deformation lamellae in SEM-CL images appear as numerous sets of thin, parallel, closely spaced and dark gray lines, which are different from healed fractures. The reason why they appear as dark lines in SEM-CL images has not been totally understood. It is possible that defect structures are so densely distributed along line defects that phonons (heat) are emitted instead of photons, thereby reducing CL luminosity (Boggs et al., 2002; Boggs and Krinsley, 2006). Deformation lamellae usually do not appear associated with bright patches or mottling in our samples. However, when both features are present in the same grain, they show the same orientation.

HCL images of type 3B quartz display CL colour similar to type 3A, ranging from medium-dark blue to dark blue. Slight colour shift was shown for most grains of type 3B (65%). Only moderate colour shift was also observed, and some grains showed no shift at all. Sometimes the HCL images do not display deformation lamellae due to inadequate resolution.

Medium-grade to High-grade Metamorphic Quartz (Type 4A and 4B Quartz)

Homogenous SEM-CL images are a typical feature for medium-grade to high-grade metamorphic quartz. Two subtypes were identified depending on the colour of the SEM-CL images: (1) type 4A quartz with bright SEM-CL colour (Figs. 3A3, 5E) (23% in all analysed type 4 quartz grains) and (2) type 4B quartz with very dark SEM-CL colour (Figs. 3A2, 5F) (77%). Quartz grains that show bright homogeneous CL (type 4A) are usually monocrystalline or polycrystalline (<5 sub-grains), and display weak to strong undulose. Quartz mosaics and metamorphic mineral inclusions may be present in type 4A quartz. The very dark homogeneous CL quartz grains (type 4B) are easily recognised under the petrographic microscope. They are usually polycrystalline, and contain various sub-grains with sutured sub-grain boundaries due to intense deformation under medium-high metamorphic condition. Quartz mosaics with weak to strong undulose extinction are frequently observed in type 4B quartz grains. Metamorphic mineral inclusions may be present as well.

The cause for homogeneous bright CL and very dark CL in SEM-CL images under high metamorphic conditions has not yet been totally understood. Quartz grains formed at very high temperatures have tendency to be more luminous than those formed under lower temperatures, which is consistent with the general assumption that high-temperature quartz crystallises with more structural defects and more impurity ions than low-temperature quartz (Marshall and Mariano, 1988; Boggs and Krinsley, 2006). This principle should explain the bright SEM-CL

color in type 4A quartz. Matter and Ramseyer (1985) suggested that low CL luminosity might occur due to the cleaning of the quartz crystal structure in terms of trace elements and structural defects during recrystallisation, which accounts for type 4B quartz with very dark SEM-CL colour. Neither type 4A nor type 4B quartz shows widespread previously described textural features in other quartz types such as zoning, healed fractures, spiders, and deformation lamellae, because most of these CL features disappeared due to recrystallisation or annealing in such higher metamorphic conditions. However, remnants of pristine grains with pre-existing CL features like bright CL patches or mottling can be observed in small areas or sub-grains where quartz recrystallisation is not complete for some grains from both type 4A and 4B (20%).

Quartz grains from type 4A and 4B present distinct HCL colours. Type 4A quartz with bright SEM-CL colour displays bright HCL colour, ranging from bright-medium blue to medium-dark blue with moderate to strong color shift, whereas type 4B with very dark SEM-CL colour show HCL colour in dark blue, very dark blue or not luminescence with no colour shift, in accord with Sawatzky and Pe-Piper (2013). Type 4A quartz is the least stable among all provenance quartz types because they show the most intense colour shift. This feature in type 4A quartz is useful to distinguish it from plutonic quartz with similar initial CL colour but slight to moderate colour shift.

Volcanic Quartz (not observed in this study)

Volcanic quartz is monocrystalline with euhedral or hypidiomorphic crystal habit, and shows non-undulose extinction. In addition, volcanic quartz may also display melt inclusions, embayments and large open fractures, which may be formed as a result of rapid cooling (Bernet and Basset, 2005).

In SEM-CL images, most volcanic quartz is typically characterized by its zoning. The zoning often appears as oscillatory zoning with concentric light and dark bands oriented approximately parallel to grain edges. The appearance of these bands results from differences in CL intensity within the quartz grain. However, zoning is not visible in petrographic image or SEM-BSE image, indicating that variations in dominant element chemistry are not the cause of zoning (Boggs and Krinsley, 2006). Nevertheless, the exact causes of CL zoning in volcanic quartz are not yet completely understood. Peppard et al. (2001) suggested that the difference in colour bands was attributed to the changes in composition of the magma from which the quartz phenocrysts grew, and the following magma differentiation. Watt et al. (1997) suggested that oscillatory zoning in quartz may reproduce chemical variation of the melt during crystallisation or changes in the rate of crystal growth. Although most volcanic quartz is zoned, Bernet and Basset (2005) reported significant quantity of unzoned volcanic quartz that displays homogenous CL, or inhomogeneous CL with a few bright CL patches in some New Zealand volcanic rocks.

HCL colour of volcanic quartz was described from blue to violet (Götze and Zimmerle, 2000). However, Sawatzky and Pe-Piper (2013) reported it to range from bright blue to medium blue in volcanic quartz present in sandstones from the Scotian Basin. They also found a moderate to strong colour shift in such grains, whereas Götte and Richter (2006) suggested a slight colour shift because the CL colour of volcanic quartz was thought to be the most stable among different quartz types.

Distribution of Quartz Types in this Study

All the features from SEM-CL, HCL, and petrographic microscopic images of individual quartz grain for each sample were summarized in Tables 4-10. The overall distribution of two major quartz types, plutonic and metamorphic quartz, with depth is illustrated in Fig. 6.

Metamorphic quartz abundance is higher than plutonic in all samples. Samples 3000 and 3425 show the highest abundances of metamorphic quartz (85%) and the lowest plutonic quartz (15%). Samples 2565 and 3150 show the lowest metamorphic quartz (61% and 62.5% respectively) and the highest plutonic (39% and 37.5% respectively). In general, the abundance of metamorphic quartz increases downwards from 2565 to 3425 m, except sample 3150, with a similar distribution to sample 2565.

The dominant metamorphic subtype is the low- to medium-grade metamorphic quartz, ranging from 40% to 55% (Fig. 7). Very low- to low-grade metamorphic quartz, with brittle deformation, is present in all samples with relatively similar abundance varying from 7.5% in samples 2995 and 3150 to 17.5% in sample 3900. The abundance of medium-grade to high-grade metamorphic quartz is similar (ca. 5%) in samples 2565, 3159 and 3425, whereas samples 2995, 3000 and 3425 show the highest abundance (20%). This suggests that there was a significant sediment input from high-grade metamorphic sources at the interval 2995-3000 m. For all studied samples, detrital quartz is mainly sourced from very low- to medium-grade metamorphic rocks (Fig. 7).

Comparison with Previous Detrital Mineral and Geochronological Studies

Study of detrital quartz grains shows major low- to medium-grade metamorphic quartz (40%–50%), subordinate plutonic quartz (15%–39%), and minor medium- to high-grade metamorphic quartz (5%–20%) and very low to low-grade metamorphic quartz (7.5%–17.5%) in the sandstones from the lower member of the Missisauga Formation and the Mic Mac Formation in Bandol-1 well.

Previous study on compositions of detrital minerals such as tourmaline, garnet, and chromite, and lithic clasts and detrital monazite geochronology has identified two distinct

sources for the Missisauga and Mic Mac Formations in the Bandol-1 well: a pelitic metasediment source and a granitoid plutonic source (Pe-Piper, 2007). This result is consistent with our study. An additional ophiolitic source was also suggested for the deeper beds of the Mic Mac Formation (Pe-Piper, 2007), which can not be confirmed by our study since ophiolites are mainly composed of mafic and ultramafic rocks which are poor in quartz.

High K_2O content of whole rock analyses of both sandstones and mudstones in Bandol-1 well was used as a further indication for a granitic or syenitic source (Pe-Piper, 2007). The abundance of K-feldspar detrital grains in the light fraction is also supportive. There is no evidence for an important source of sand-sized plagioclase. All these findings strongly support a granite source for the identified plutonic quartz grains.

Upward increase in the concentrations TiO_2, Zr and the light rare earth elements (LREE) and tourmaline abundance of granitic origin may indicate a progressively more important granitoid source upwards in the Missisauga Formation and the upper Mic Mac Formation (Pe-Piper, 2007). This agrees with the high abundance of plutonic quartz observed at 2565 m and 2860 m in this study. The lowest concentrations of TiO_2, Zr and LREE were reported by Pe-Piper (2007) at 3425 m, which is also consistent with the lowest plutonic abundance and the highest abundance of metamorphic quartz at 3425 m (Fig. 6).

An important high-grade metamorphic source at 3000 m was inferred from necking quartz inclusions in spessartine garnet (Mn-rich). The presence of tourmaline, almandine garnet (Fe-rich), and staurolite also indicate an important pelitic metasedimentary source, particularly to the deeper part of the Mic Mac Formation (Pe-Piper, 2007). This high metamorphic source at 3000 m is in accord with the high frequency of medium- to high-grade metamorphic quartz type found at 2995 m and 3000 m (20%, Fig. 7) in our study. In addition, the more important pelitic

metasediments source in the deeper part of the Mic Mac formation is also supported by the higher metamorphic quartz frequency observed at 3425 m and 3900m (Figs. 6, 7).

Provenance Implications

The Bandol-1 well lies 100 km east of the principal distal deposits supplied by the Banquereau River marked by a Lower Cretaceous sand-rich tongue (Tyrrell, 2007). Seismic profiles (OETR, 2011) suggest that upper Jurassic deltas in the Eastern Scotian Basin prograded from Newfoundland. Western and southern Newfoundland are considered to be the main possible source areas for Bandol-1 well (Fig. 2) during Late Jurassic–Early Cretaceous. Low-grade metamorphic rocks and plutonic rocks are widespread in Newfoundland, with a wider distribution of low metamorphic rocks in central Newfoundland, whereas high-grade Paleoproterozoic metamorphic rocks are common in northwestern Newfoundland (Fig. 2). Plutonic rocks are widely distributed in southern Newfoundland.

Detrital monazite dating reported by Pe-Piper (2007) suggests one source in Devonian granites (mean age 371, 388, 390 ±9 Ma). Devonian peraluminous granites (Gd7 of Whalen et al., 1996) are widespread in the Gander terrane of southern Newfoundland and Mid Devonian granites of similar age to the samples at 3900 m from Bandol-1 well have been dated in southwest Newfoundland by Dubé et al. (1996) (Fig. 8). In addition, the Mid-Devonian Port aux Basques granites located in the southwest Newfoundland are rich in tourmaline. Therefore, that area can also be a candidate source for the tourmaline of granitic origin found at Bandol-1 well. Pe-Piper (2007) also suggested the K-feldspar rich granites located at Dunnage terrane and at the southeast end of Gander terrane as possible rock sources to Bandol-1 well. One detrital monazite of latest Paleoproterozoic (~1.65 Ga) age was also reported in the Bandol-1 well (Pe-Piper, 2007); grains of this age are common in both detrital monazite and zircon dating of the Scotian

Basin (Piper et al., 2012; Pe-Piper et al., 2014). It corresponds to the Trans-Labrador-Manicougan intrusions of Quebec and Labrador (Gower et al., 2008).

During the Late Jurassic–Early Cretaceous, the Mid-Devonian granite in the Gander terrane of southern Newfoundland, the tourmaline granite in southwest Newfoundland, and the mostly K-feldspar granite in the Dunnage terrane and southeast Gander terrane are the potential source of plutonic quartz. The low-grade metamorphic rocks located mainly in central Newfoundland are the potential sources of low- to medium-grade metamorphic quartz. The Paleoproterozoic gneissic rocks that are overthrust by the Humber terrane are the potential sources of medium- to high-grade metamorphic quartz (Fig. 8). The sediments from these source areas were transported by means of the Banquereau River and/or another local river during the Late Jurassic–Early Cretaceous to the eventual site of the Bandol-1 well (Figs. 2 and 8). No volcanic quartz was found in our samples, so the Avalon terrane, composed mainly of volcanic rocks, contributes little to the sediments for Late Jurassic –Early Cretaceous sandstones in Bandol-1 well. The increase in plutonic quartz at higher stratigraphic levels might indicate a change in provenance or might result from uplift and unroofing of granitic basement from beneath metamorphic cover.

CONCLUSIONS

1. The integration of SEM-CL, HCL and petrographic microscope analysis on detrital quartz grains was demonstrated to be effective in distinguishing quartz types. SEM-CL combined with petrographic microscope examination appears to be effective to differentiate between major quartz types such as plutonic and metamorphic quartz. HCL technique is important to further constrain and confirm the identification of distinct quartz types. In addition, HCL

analyses are very useful in assigning detrital quartz to a specific metamorphic grade. For example, low-grade metamorphic quartz (type 3) displays medium to dark blue or medium to dark brownish blue HCL colour, whereas medium- to high-grade metamorphic quartz (type 4A) displays bright to bright-medium blue HCL colour. Furthermore, the colour shift in HCL images is also demonstrated to be crucial to distinguish between plutonic quartz and medium- to high-grade metamorphic quartz (type 4A), since the latter displays the largest colour shift.

2. Comparing the integration of HCL and petrographic microscope with the integration of SEM-CL and petrographic microscope, results for the identification of quartz types were similar.
3. Metamorphic quartz abundance is higher than plutonic in all studied samples. In general, the metamorphic abundance increases downward from 2565 to 3425 m. The dominant quartz type is low- to medium-grade metamorphic quartz, followed by plutonic quartz, medium- to high grade metamorphic quartz, and very low- to low-grade metamorphic quartz.
4. Our findings from detrital quartz are consistent with previous studies based on the composition of detrital minerals and lithic clasts, and detrital monazite geochronology (Pe-Piper, 2007), suggesting a pelitic metasediment source and a granitoid plutonic source for the Bandol-1 well sediments. A progressively more important granitoid plutonic source upwards, and a more important pelitic metasediments source in the deeper part of the Mic Mac Formation are also suggested in our study.
5. The Mid-Devonian granite in the Gander terrane of southern Newfoundland, the tourmaline granite in southwest Newfoundland, and the K-feldspar-rich granite in Dunnage terrane and southeast Gander terrane are the potential source of plutonic quartz in the Bandol-1 well. The low-grade metamorphic rocks located mainly in the central Newfoundland are the potential sources of low- to medium-grade metamorphic quartz type and the Paleoproterozoic gneissic

rocks overthrust by the Humber terrane are the potential sources of medium- to high-grade metamorphic quartz in the Bandol-1 well.

REFERENCES

Basu, A., Young, S. W., Suttner, L. J., James, W. C., & Mack, G. H. (1975). Re-evaluation of the use of undulatory extinction and polycrystallinity in detrital quartz for provenance interpretation. Journal of Sedimentary Research, 45(4), 873–882.

Bernet, M., & Bassett, K. (2005). Provenance analysis by single-quartz-grain SEM-CL/optical microscopy. Journal of Sedimentary Research, 75(3), 492–500.

Boggs, S., Kwon, Y. I., Goles, G. G., Rusk, B. G., Krinsley, D., & Seyedolali, A. (2002). Is quartz cathodoluminescence color a reliable provenance tool? A quantitative examination. Journal of Sedimentary Research, 72(3), 408–415.

Boggs, S., & Krinsley, D. H. (2006). Application of cathodoluminescence imaging to the study of sedimentary rocks. Cambridge University Press, Cambridge, 165p.

D'Lemos, R. S., Kearsley, A. T., Pembroke, J. W., Watt, G. R., & Wright, P. (1997). Complex quartz growth histories in granite revealed by scanning cathodoluminescence techniques. Geological Magazine, 134(4), 549–552.

Dubé, B., Dunning, G. R., Lauzière, K., & Roddick, J. C. (1996). New insights into the Appalachian Orogen from geology and geochronology along the Cape Ray fault zone, southwest Newfoundland. Geological Society of America Bulletin, 108(1), 101–116.

Götte, T., & Richter, D. K. (2006). Cathodoluminescence characterization of quartz particles in mature arenites. Sedimentology, 53(6), 1347–1359.

Götze, J., & Zimmerle, W. (2000). Quartz and silica as guide to provenance in sediments and sedimentary rocks. KG Saur Verlag Gmbh & Co, Contribution to Sedimentary Geology, v. 21, 91p.

Gower, C. F., Kamo, S. L., Kwok, K., & Krogh, T. E. (2008). Proterozoic southward accretion and Grenvillian orogenesis in the interior Grenville Province in eastern Labrador: Evidence from U–Pb geochronological investigations. Precambrian Research, 165(1), 61–95.

Hamers, M. F., & Drury, M. R. (2011). Scanning electron microscope cathodoluminescence (SEM-CL) imaging of planar deformation features and tectonic deformation lamellae in quartz. Meteoritics & Planetary Science, 46(12), 1814–1831.

Hooker, J. N., & Laubach, S. E. (2007). The geologic history of quartz grains, as revealed by color SEM-CL. Gulf Coast Association of Geological Societies Transactions, 57, 375–386.

Kanaori, Y. (1986). A SEM cathodoluminescence study of quartz in mildly deformed granite from the region of the Atotsugawa fault, central Japan. Tectonophysics, 131(1), 133–146.

Kwon, Y. I., & Boggs Jr, S. (2002). Provenance interpretation of Tertiary sandstones from the Cheju Basin (NE East China Sea): a comparison of conventional petrographic and scanning cathodoluminescence techniques. Sedimentary Geology, 152(1), 29–43.

Marshall, D. J., & Mariano, A. N. (1988). Cathodoluminescence of geological materials. Unwin Hyman, Boston, 146p.

Matter, A., & Ramseyer, K. (1985). Cathodoluminescence microscopy as a tool for provenance studies of sandstones. In Zuffa, G.C. (ed), Provenance of arenites. Springer Netherlands, pp. 191–211.

McIver, N. L. (1972). Cenozoic and Mesozoic stratigraphy of the Nova Scotia shelf. Canadian Journal of Earth Sciences, 9(1), 54–70.

Milliken, K. L. (1994). Cathodoluminescent textures and the origin of quartz silt in Oligocene mudrocks, South Texas. Journal of Sedimentary Research, 64(3), 567–571.

Müller, A., Seltmann, R., & Behr, H. J. (2000). Application of cathodoluminescence to magmatic quartz in a tin granite – case study from the Schellerhau Granite Complex, Eastern Erzgebirge, Germany. Mineralium Deposita, 35(2-3), 169–189.

OETR (Offshore Energy Technical Research) (2011). Play fairway analysis atlas: offshore Nova Scotia. Nova Scotia Department of Energy Report 88-11-0004-01, 349p.

Passchier, C. W., & Trouw, R. A. (1996). Microtectonics. Springer, Berlin, 366p.

Pe-Piper, G. (2007). Detrital petrology and provenance of Mesozoic sediments in the Bandol well. Halifax, NS. Saint Mary`s University Internal Report.

Pe-Piper, G., Triantafyllidis, S., & Piper, D. J. W. (2008). Geochemical identification of clastic sediment provenance from known sources of similar geology: the Cretaceous Scotian Basin, Canada. Journal of Sedimentary Research, 78(9), 595–607.

Pe-Piper, G., & Piper, D. J. W. (2012). The impact of early Cretaceous deformation on deposition in the passive margin Scotian Basin, offshore eastern Canada. In Busby, C. and Azor, A. (eds), Tectonics of Sedimentary Basins: Recent Advances. John Wiley & Sons, Ltd, Chichester, U.K., pp. 270–287.

Pe-Piper, G., Piper, D. J. W., & Triantafyllidis, S. (2014). Detrital monazite geochronology, Upper Jurassic-Lower Cretaceous of the Scotian Basin: significance for tracking first-cycle sources. Geological Society, London, Special Publications, 386(1), 293–311.

Peppard, B. T., Steele, I. M., Davis, A. M., Wallace, P. J., & Anderson, A. T. (2001). Zoned quartz phenocrysts from the rhyolitic Bishop Tuff. American Mineralogist, 86(9), 1034–1052.

Perny, B., Eberhardt, P., Ramseyer, K., Mullis, J., & Pankrath, R. (1992). Microdistribution of Al, Li, and Na in alpha quartz; possible causes and correlation with short-lived cathodoluminescence. American Mineralogist, 77(5-6), 534–544.

Piper, D. J. W., Pe-Piper, G., Tubrett, M., Triantafyllidis, S., & Strathdee, G. (2012). Detrital zircon geochronology and polycyclic sediment sources, Upper Jurassic–Lower Cretaceous of the Scotian Basin, southeastern Canada. Canadian Journal of Earth Sciences, 49(12), 1540–1557.

Ramseyer, K., & Mullis, J. (2000). Geologic application of cathodoluminescence of silicates. In Pagel, M. et al. (eds), Cathodoluminescence in geosciences. Springer, Berlin, pp. 177–191.

Sawatzky, C., & Pe-Piper, G. (2012). Provenance identification of detrital quartz using hot-cathode cathodoluminescence: An atlas of source rocks. Geological Survey of Canada, Open File 7060, 149 p.

Sawatzky, C. C., & Pe-Piper, G. (2013). Detrital quartz sources in the Scotian Basin, eastern Canada, using hot-cathode cathodoluminescence: Availability of coarse-grained sand for reservoirs. AAPG Bulletin, 97(9), 1503–1520.

Seyedolali, A., Krinsley, D. H., Boggs, S., O'Hara, P. F., Dypvik, H., & Goles, G. G. (1997). Provenance interpretation of quartz by scanning electron microscope cathodoluminescence fabric analysis. Geology, 25(9), 787–790.

Sprunt, E. S., & Nur, A. (1979). Microcracking and healing in granites: new evidence from cathodoluminescence. Science, 205(4405), 495–497.

Triantafyllidis, S., Pe-Piper, G., MacKay, R., Piper, D. J. W., & Strathdee, G. (2010). Monazite as a provenance indicator for the Lower Cretaceous reservoir sandstones, Scotian Basin. Geological Survey of Canada, Open File 6732, 452p.

Tsikouras, B., Pe-Piper, G., Piper, D. J. W., & Schaffer, M. (2011). Varietal heavy mineral analysis of sediment provenance, Lower Cretaceous Scotian Basin, eastern Canada. Sedimentary Geology, 237(3), 150–165.

Tyrrell, M. 2007. Major depositional environment of the Lower Cretaceous in the Stonehouse area [abstract]: Nova Scotia Offshore Basin Forum, 2007.

Wade, J. A., & MacLean, B. C. (1990). Chapter 5 The geology of the southeastern margin of Canada. In Keen, M. J. and Williams, G. L. (eds), Geology of the continental margin off eastern Canada. Geological Survey of Canada, Ottawa, Canada, pp. 167–238.

Watt, G. R., Wright, P., Galloway, S., & McLean, C. (1997). Cathodoluminescence and trace element zoning in quartz phenocrysts and xenocrysts. Geochimica et Cosmochimica Acta, 61(20), 4337–4348.

Weston, J. F., MacRae, R. A., Ascoli, P., Cooper, M. K. E., Fensome, R., Shaw, D., & Williams G. L. (2012). A revised biostratigraphic and well log sequence-stratigraphic framework for the Scotian Margin, offshore eastern Canada. Canadian Journal of Earth Science, 49(12), 1417–1462.

Whalen, J. B., Fyffe, L. R., Longstaffe, F. J., & Jenner, G. A. (1996). The position and nature of the Gander-Avalon boundary, southern New Brunswick, based on geochemical and isotopic data from granitoid rocks. Canadian Journal of Earth Sciences, 33(2), 129–139.

Zinkernagel, U. (1978). Cathodoluminescence of quartz and its application to sandstone petrology. Schweizerbart, Stuttgart, 69p.

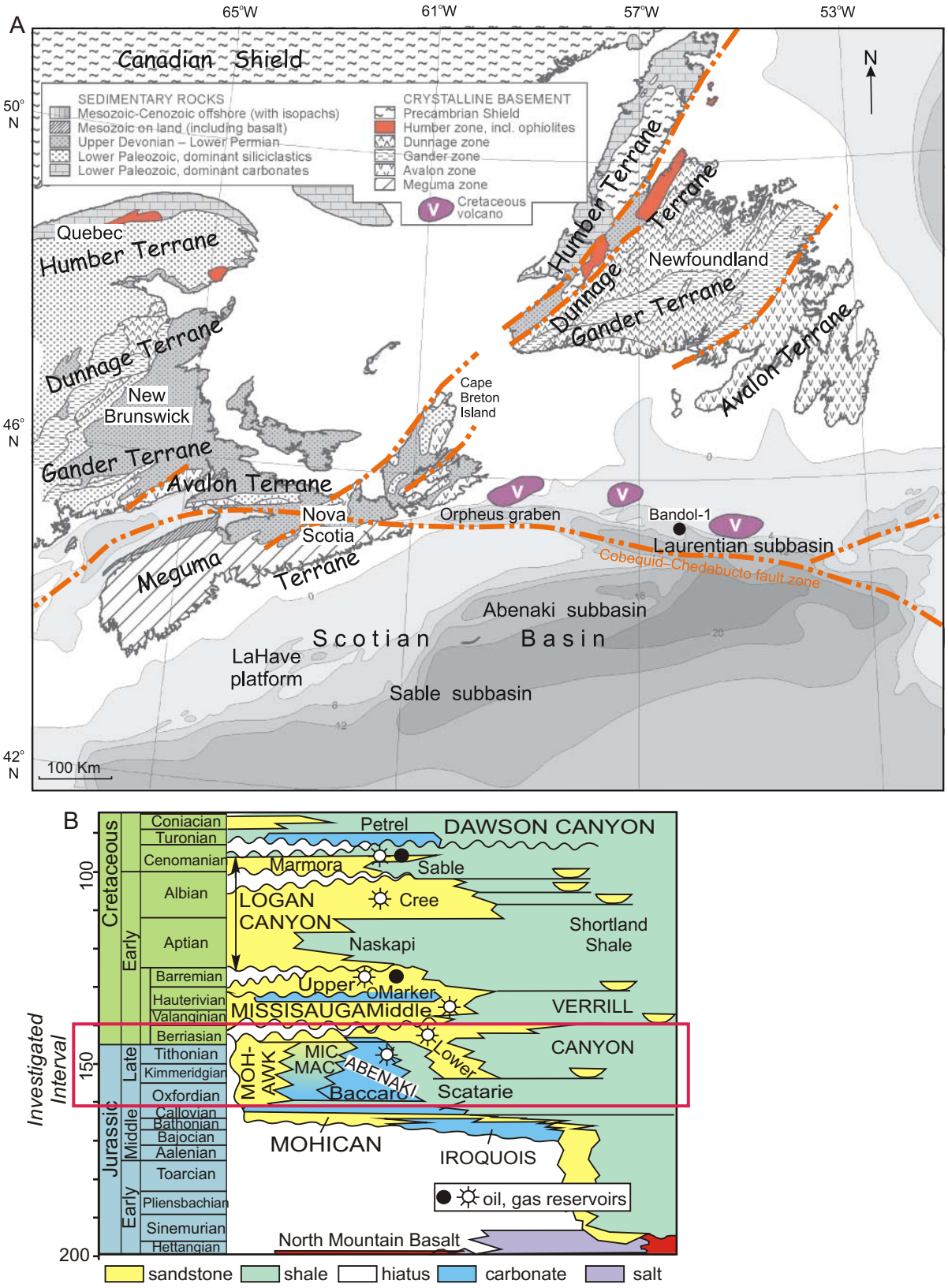

Figure 1. Location of investigated samples. (A) Summary geologic map of the Scotian Basin and its hinterland, showing the location of sampled Bandol-1 well. Basin isopachs in kilometers from Wade and MacLean (1990). (B) Stratigraphic column for the Upper Jurassic and Lower Cretaceous of the Scotian Basin (modified from OETR, 2011, using data from Weston et al., 2012), showing the investigated interval.

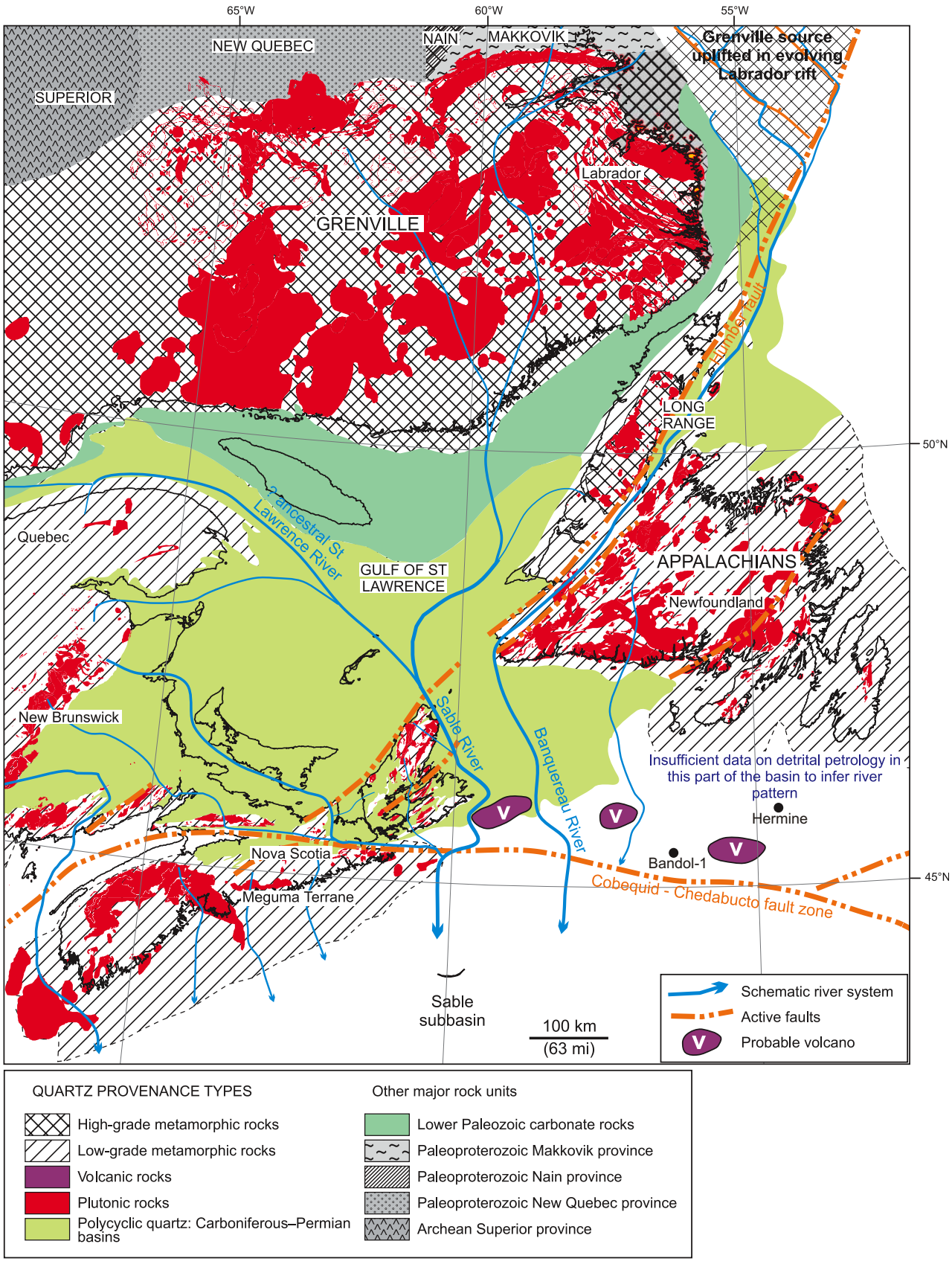

Figure 2. Inferred Tithonian paleogeography of the Scotian Basin and its hinterland, showing the location of Bandol-1 well river pattern in the Scotian Basin (modified from Sawatzky and Pe-Piper , 2013).

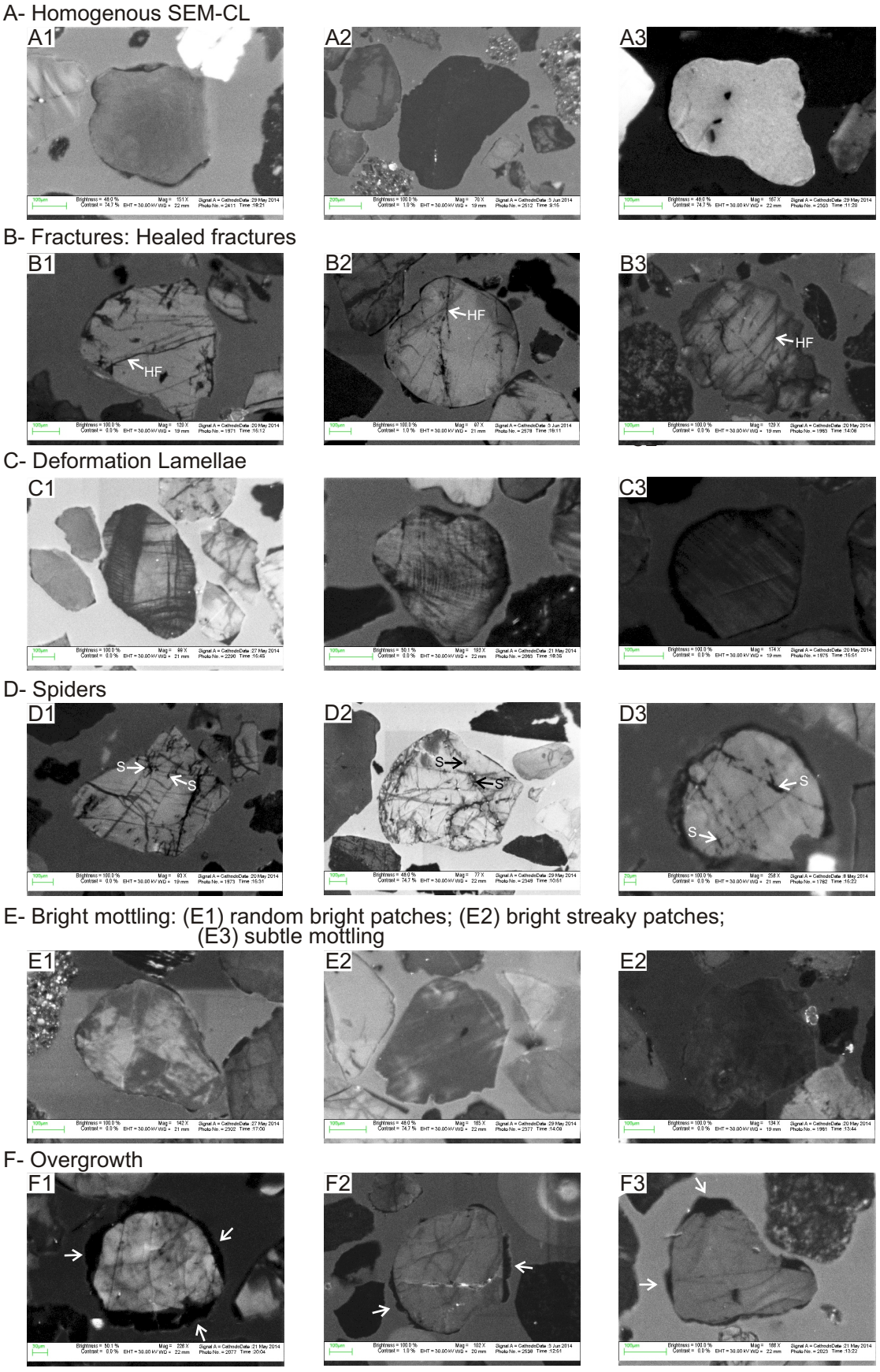

Figure 3. Nomenclature used for describing the SEM-CL images of detrital quartz. (A) Grains showing homogeneous CL (little difference in CL brightness), (A1) low- to medium-grade

metamorphic quartz with homogeneous grey CL, (A2) medium- to high-grade metamorphic quartz showing homogeneous black CL, (A3) medium- to high-grade metamorphic quartz showing homogeneous bright CL. (B) Grains showing healed fractures (HF), (B1, B2) plutonic quartz showing randomly oriented healed fractures, (B3) Brittle deformed quartz showing a set of parallel healed fractures with preferred orientation. (C) Ductile deformed quartz showing deformation lamellae. (D) Plutonic quartz showing spiders (S). (E) Low- to medium metamorphic quartz showing bright mottling pattern, which can appear as (E1) Random bright patches, (E2) bright streaky patches, and (E3) subtle mottling. (F) Overgrowth showing as dark areas surrounding the detrital quartz.

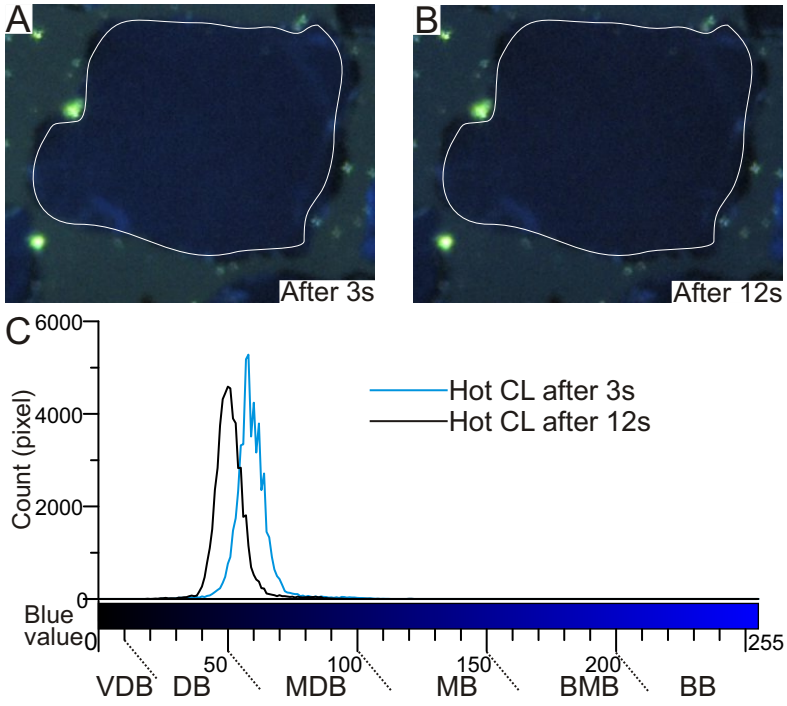

Figure 4. Data presentation from HCL method. (A) HCL image of one detrital quartz grain after 3s exposure at the CL beam and its AOI indicated by white line. (B) HCL image after 12s exposure at the CL beam and its respective AOI. (C) The histogram of blue colour within AOI for both images, where X axis is the intensity of blue colour indicated by the colour bar with values from 0-255 (0=no blue or "black", 255=blue), and Y axis indicates the pixel amount at different blue values. Abbreviations: VDB = very dark blue, DB = dark blue, MDB = medium dark blue, MB = medium blue, BMB = bright-medium blue, BB = bright blue.

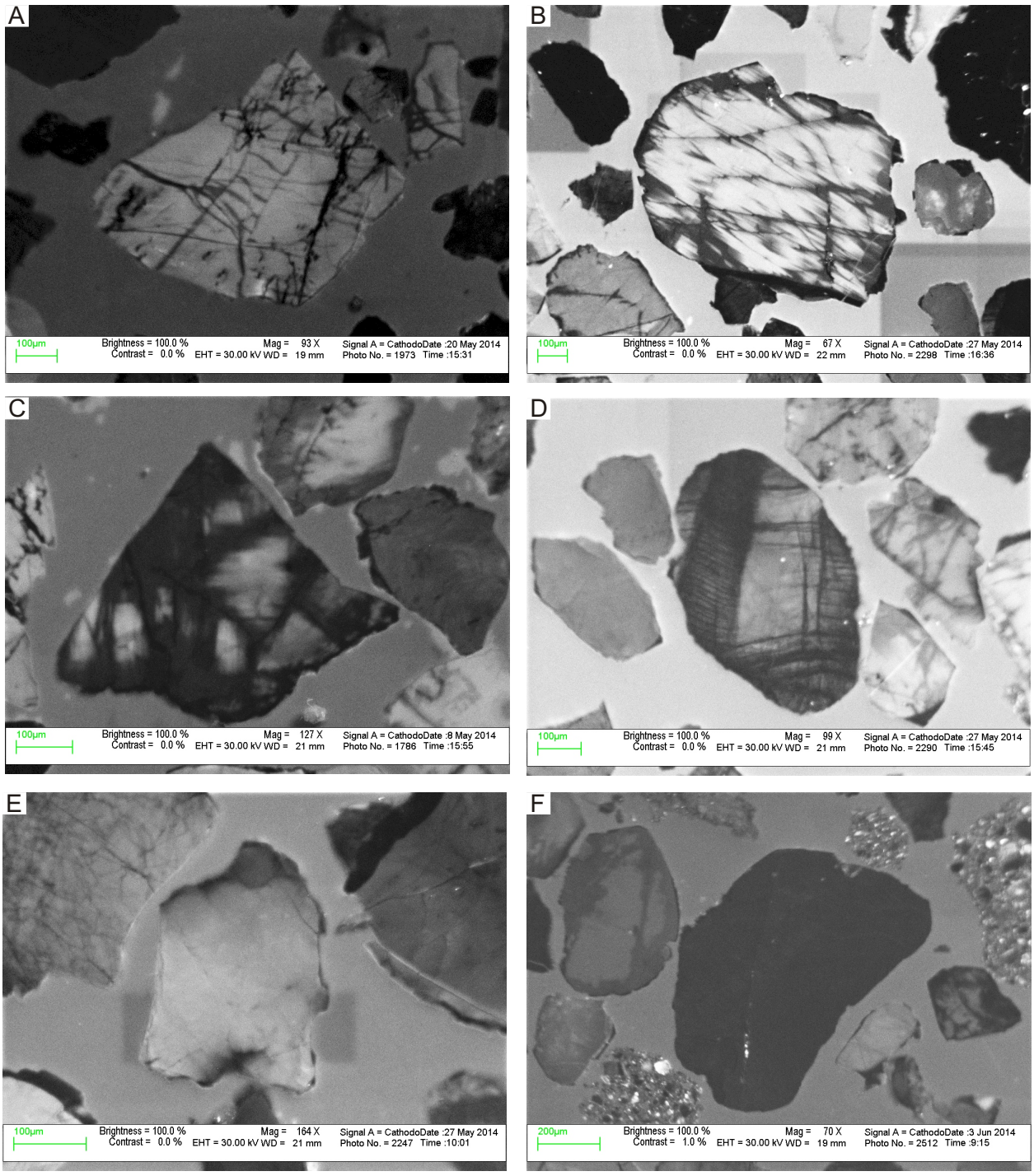

Figure 5. Examples of SEM-CL images showing CL features for different quartz types identified in this study. (A) Plutonic quartz (type 1) showing typical light grey CL and randomly oriented healed fractures and spiders. (B) Brittle deformed quartz (type 2) showing two sets of sub-parallel healed fractures with preferred orientation. Note that the bright streaky patches show the same orientation as one set of healed fractures. (C) Low- to medium-grade metamorphic quartz (type 3A) showing dark grey appearance and random bright patches. (D) Ductile deformed quartz (type 3B) showing typical deformation lamellae. (E) Medium- to high-grade metamorphic quartz showing typical bright homogeneous CL (type 4A). (F) Medium- to high-grade metamorphic quartz showing black homogeneous CL (type 4B). Note that the absence of CL features due to total recrystallisation.

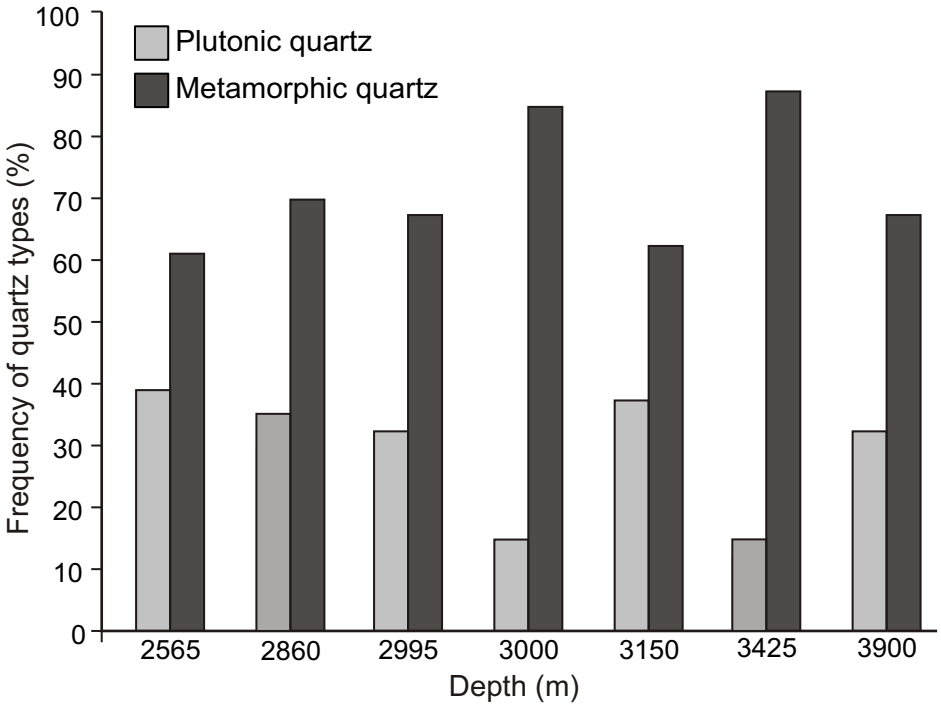

Figure 6: Histograms of the distribution of plutonic and metamorphic quartz grains in all analysed samples.

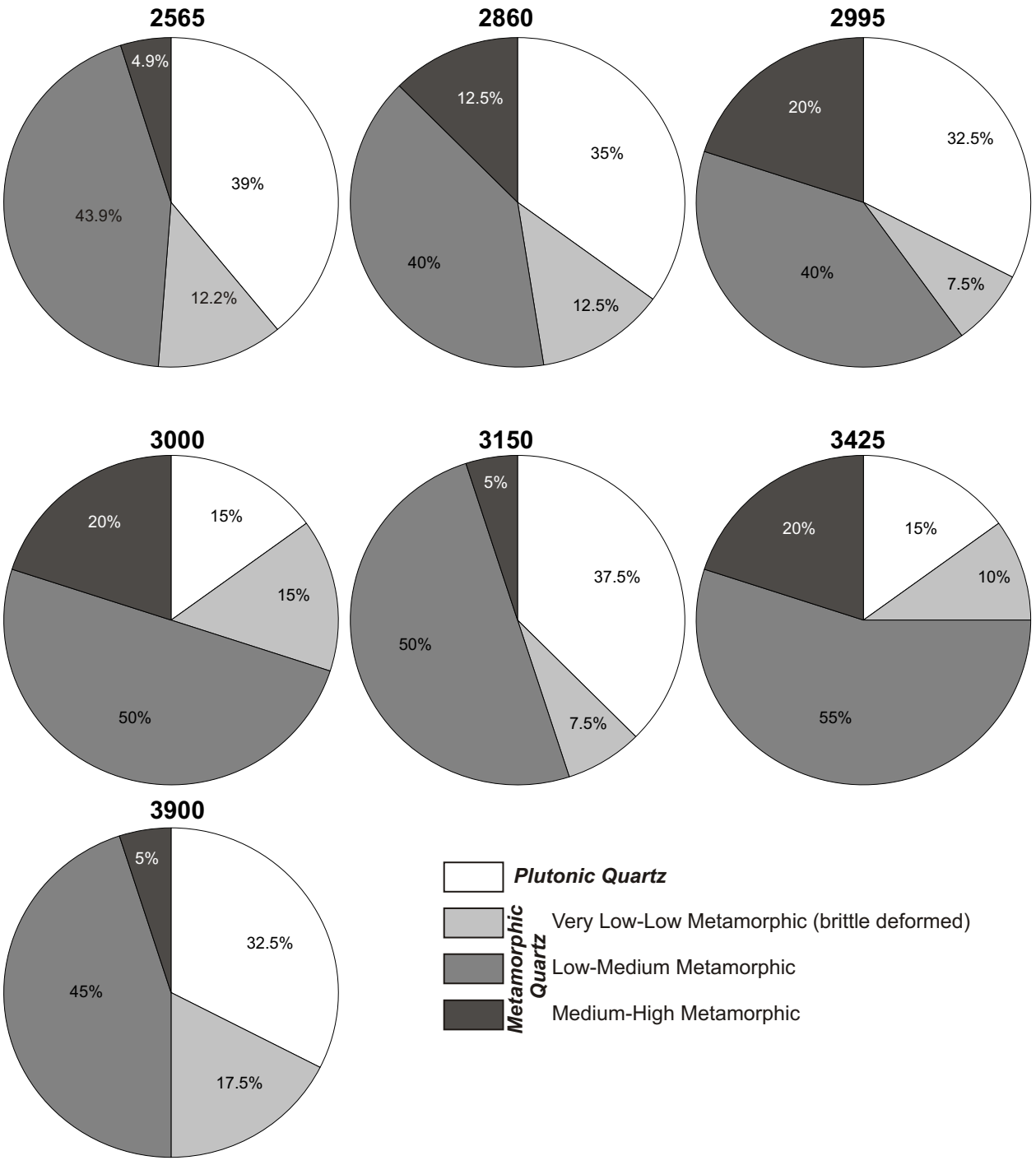

Figure 7: Pie diagrams of summarized distribution of detrital quartz types for all analysed samples.

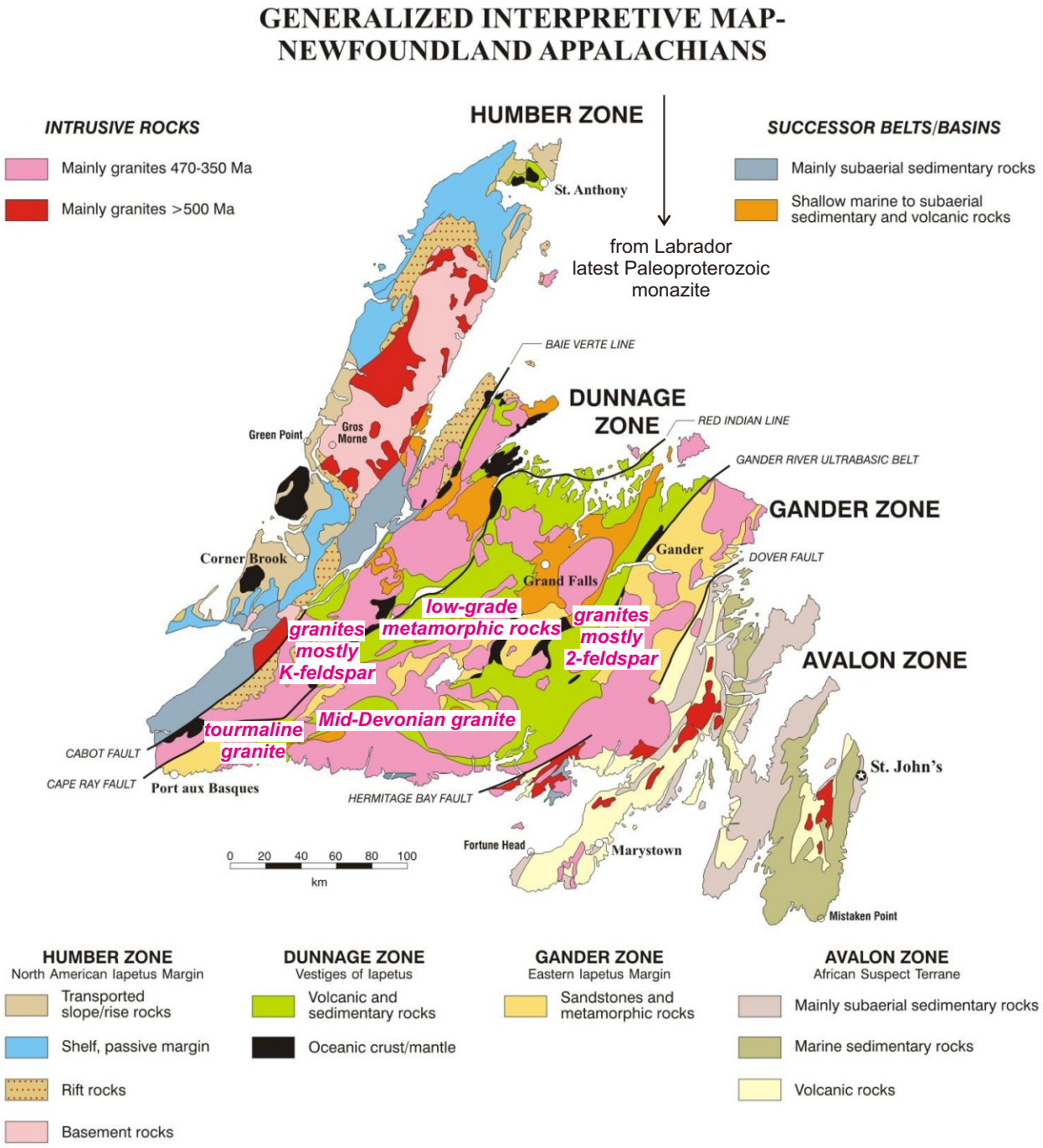

Figure 8: Annotated bedrock geologic map of Newfoundland (after Natural Resources of Newfoundland - Labrador, Canada <http://www.nr.gov.nl.ca/nr/mines/maps/>), showing potential sources for Bandol-1 well.

Table 1: Summary of research activities applied to studied samples.

Sample	Depth (m)	Stratigraphical level	Lithology	Type	Petrographic Microscope	SEM-BSE image	SEM-CL image	Hot-CL image	Quartz type summary	Appendix	Notes from Pe-Piper (2007)
2565	2565	Lower Missisauga Fm	grey sandstone	fine cuttings	40 grains	40 grains	40 grains	36 grains	Table 4A&4B	1A&1B	fine; with few coarse grains; heavy mineral and whole-rock geochemical analyses
2860	2860	Mic Mac Fm	beige sandstone		40 grains	40 grains	40 grains	37 grains	Table 5A&5B	2A&2B	fine; with coarse grains, heavy mineral and whole-rock geochemical analyses
2995	2995	Mic Mac Fm	beige sandstone		40 grains	40 grains	40 grains	40 grains	Table 6A&6B	3A&3B	fine; with coarse grains; 1 large cutting; whole-rock geochemical analyses
3000	3000	Mic Mac Fm	beige sandstone		40 grains	40 grains	40 grains	38 grains	Table 7A&7B	4A&4B	fine; with coarse grains; heavy mineral and whole-rock geochemical analyses
3150	3150	Mic Mac Fm	light grey shaly sandstone		40 grains	40 grains	40 grains	39 grains	Table 8A&8B	5A&5B	fine; with few coarse grains; heavy mineral analyses
3425	3425	Mic Mac Fm	beige sandstone		40 grains	40 grains	40 grains	37 grains	Table 9A&9B	6A&6B	fine; with coarse grains; heavy mineral and whole-rock geochemical analyses
3900	3900	Mic Mac Fm	beige sandstone		40 grains	40 grains	39 grains	38 grains	Table 10A&10B	7A&7B	fine; with some coarse grains; heavy mineral and whole-rock geochemical analyses

Table 2: Description of characteristic features of quartz types from various rock lithologies using SEM-CL.

Characteristic Feature	Description in SEM-CL image	Quartz type identified in this study (Table 3)	Ocurrence in this study (% out of specific quartz type)	Primary/ Secondary feature	Comments
Bright patches or mottling	Irregular CL intensities across grains, creating a mottled pattern due to the presence of patches. Three types of bright patches or mottling were observed in this study (Fig. 3E)	Low- to medium-grade metamorphic quartz	37%	Secondary	They can show preferred orientation or be random in this study. Bright patches or mottling in volcanic and vein quartz occur as primary features.
		Medium- to high-grade metamorphic quartz	20%		
		Plutonic quartz	<10%	Secondary, less primary	
Healed fractures with preferred orientation	Healed fractures that are parallel aligned, more than one set are common.	Very low-grade to low-grade metamorphic quartz with brittle deformation	100%	Secondary	The orientation matches to the local or regional strain field during deformation.
Homogeneous CL	Nearly uniform CL intensity across the grain, light gray to dark grey or black	Low- to medium-grade metamorphic quartz	29%	Secondary	Homogeneous CL in volcanic quartz and vein quartz is primary features.
		Medium- to high-grade metamorphic quartz (type 4A)	87%		
		Medium- to high-grade metamorphic quartz (type 4B)	86%		
Randomly oriented healed fractures	Fractures filled with secondary silica that appear as thin (commonly < 10µm) black lines in SEM-CL images. They are usually not shown in back-scattered images (BSE).	Plutonic quartz	100%	Primary	Healed fractures tend to disappear in high grade metamorphic conditions due to recrystallisation or annealing.
		Low- to medium-grade metamorphic quartz	60%		
Spiders	Dark-CL patches and streaks. Dark-CL patches mainly range from 10-100µm. Streaks are random and irregular in the appearance of black broad (>10 µm) elongated form.	Plutonic quartz	80%	Primary	Commonly associated with healed fractures.
		Low-grade metamorphic quartz with brittle deformation	79%		
		Low- to medium-grade detamorphic quartz	18%		
Tectonic deformation lamellae	Numerous sets of thin, parallel, closely spaced and dark gray lines; occasionally appear as bright lines and show slightly wavy features with varying thickness	Low- to medium-grade metamorphic quartz with ductile deformation	100%	Secondary	Particularly characteristic of ductile deformed quartz
Zoning (not observed in this study)	either as oscillatory zoning with concentric light and dark bands oriented approximately parallel to grain edges; or as non-oscilatory zoning	not observed in this study	—	Primary	Very common in volcanic quartz; present in some plutonic and vein quartz (Bernet and Basset, 2005; Boggs and Krinsley, 2006)

Table 3: Summarized diagnostic features in SEM-CL, HCL, and optical images for identified quartz types in the studied samples.

Quartz Type		SEM-CL Features	HCL Features	Optical Features	Comments
Plutonic quartz (type 1)		– grey to light grey CL – randomly oriented healed fractures – spiders are common – random bright patches can be present – no zoning	– initial CL colour ranges from bright blue to medium dark blue (medium blue and medium dark blue are common) – final CL colour ranges from bright medium blue to dark blue – slight to moderate colour shift	– mono- or polycrystalline (<3 subgrains) – non-undulose to weak undulose extinction – fluid inclusion trails are common –some mineral inclusions (e.g., apatite or zircon).	Fluid inclusion trails usually appear along healed fractures.
Very low-grade to low-grade metamorphic quartz with brittle deformation (type 2)		– healed fractures with preferred orientation – Bright streaky patches fabric with preferred orientation	– variety of CL colors in accord with the pristine quartz type	– mono- or polycrystalline – weak to strong undulose extinction	More than one generation of healed fractures can be seen. Bright streaky patches have the same orientation as healed fractures, matching to the local or regional strain field during deformation.
Low-medium grade metamorphic quartz	quartz with no significant ductile deformation (type 3A)	– light grey to black CL (dark colour are more common) – patchy or bright mottling	– initial CL colour ranges from medium-dark blue to dark blue – final CL colours ranges from medium-dark blue to dark blue – no to slight colour shift	– mono- or polycrystalline with sutured sub-grain boundaries – weak to strong undulose extinction – may contain metamorphic mineral inclusions (mainly chlorite)	Presence of healed fractures is interpreted to be as an indicator of low-grade metamorphism. Patches can be in preferred orientation.
	ductile deformed quartz (type 3B)	– tectonic deformation lamellae – complex shear	– initial CL colour ranges from medium-dark blue to dark blue – final CL colours ranges from medium-dark blue to dark blue – no to slight colour shift	– mono- or polycristalline – weak to strong undulose extinction – deformation lamellae – deformation banding	Complex shear patterns reported in literatures were not observed in this study.
Medium-high grade metamorphic quartz	type 4A	– light grey CL – homogeneous CL	– initial CL colour ranges from brigh-medium blue to medium-dark blue – final CL colours ranges from medium blue to medium-dark blue – moderate colour shift	– mono- or polycristalline – weak to strong undulose extinction – quartz mosaics – sutured sub-grain boundaries can be present – may contain metamorphic mineral inclusions	Typical textural features in other quartz types such as zoning, healed fractures, spiders, and deformation lamellae disappear due to intensive recrystallisation or annealing under medium to high-grade metamorphic conditions .
	type 4B	– very dark grey or black CL – homogeneous CL	– initial CL colour ranges from dark blue to very dark blue or not luminescense – final CL colours also ranges from dark blue to very dark blue or not luminescense – no colour shift	– polycrystalline with sutured subgrain boundaries (monocrystalline are less common) – quartz mosaics with non undulose to strong undulose extinction – may contain metamorphic mineral inclusions	
Volcanic quartz (not observed in this study)		– light grey to black CL – common zoning – large open fractures – either homogeneous or patchy CL	– initial CL colour ranges from bright blue to medium blue – final CL colours ranges from medium to medium-dark blue – moderate to strong colour shift (Sawatzky and Pe-Piper, 2013) – no to slight colour shift (Götze and Richter, 2006)	– monocrystalline – non-undulose extinction – embayments	Information from Bernet and Basset (2005), Boggs and Krinsley (2006), Götze and Richter (2006), and Sawatzky and Pe-Piper (2013).

Table 4A: Summary data of detrital quartz grains of sample 2565 (petrography and SEM-CL image).

Grain No	Roundness (angular (A), sub-angular (SA), sub-rounded (SR), rounded (R))	Mono-/Poly-crystalline (M/no. of grains)	Extinction (None- weak+, strong++)	Mosaic Texture	Deformation Lamellae	Deformarion Banding	Zoning	Overgrowth	Homo-geneous SEM-CL image	Grayscale in SEM-CL Image				Fractures (rare-,some+,common++)			Fluid Inclusion Trail		Mineral Inclusion[3]	Spiders (rare-, some+. Common++)	Bright Mottling Random, Streaky, Subtle (R/St/Sb)	Quartz Type (Met.: metamorphic; L, M, H: low, medium, high grade)
										Quartz	Epoxy	Difference (=Quartz - Epoxy)	Colour[1]	Total amount	Open fracture	Healed fracture[2]	Occurrence (rare-, some+, Common++)	Detrital/ Diagenetic (Det/Dgn)				
1	A	M	(-)	–	–	–	–	√	–	62.0	62.2	-0.2	G	(-)	(-)	(+)	(+)	Det	–	(-)	–	Plutonic
2	SR	M	(++)	–	–	–	–	√	–	87.2	67.5	19.8	G	(+)	(+)	(+)	(+)	Det	–	(-)	–	Met. (L-M)
3	R	M	(-)	–	–	–	–	√	–	147.8	72.3	75.5	L	(+)	(-)	(++)	(++)	Det/Dgn	–	(++)	–	Plutonic
4	SR	M	(-)	–	–	–	–	√	–	148.3	98.5	49.8	L	(+)	(+)	(+)	(+)	Det	–	(+)	–	Plutonic
5	A	> 7	(++)	–	–	–	–	√	–	40.5	105.8	-65.3	D	(-)	(-)	(+)	(++)	Det/Dgn	–	(-)	St	Met. (L-M)
6	SR	M	(+)	–	–	–	–	√	–	43.9	83.2	-39.3	D	(+)	(+)	(++) (O)	(++)	Det	–	(+)	St	Met. (L); brittle deformed
7	SA	3	(++)	–	–	√	–	√	–	62.8	81.6	-18.9	G	(+)	(+)	(+)	(++)	Det	–	(-)	–	Met. (L-M); ductily deformed
8	SA	> 7	(++)	–	–	–	–	√	√	62.0	84.8	-22.8	G	(+)	(+)	(-)	(++)	Det	–	(-)	–	Met. (L-M)
9	R	M	(-)	–	–	–	–	√	–	186.4	86.9	99.5	L	(+)	(-)	(++)	(++)	Det	–	(++)	–	Plutonic
10	R	M	(++)	–	–	–	–	–	–	30.1	55.0	-24.9	D	(++)	(+)	(++) (O)	(+)	Det	–	(-)	Sb	Met. (L-M)
11	SA	M	(++)	–	–	–	–	√	–	75.1	63.4	11.7	L	(+)	(-)	(+)	(+)	Det	–	(-)	–	Met. (L-M)
12	SA	M	(++)	–	–	–	–	√	–	145.7	93.8	51.9	L	(+)	(-)	(+)	(+)	Det	–	(-)	–	Plutonic
13	SA	M	(+)	–	–	–	–	–	–	147.4	89.6	57.9	L	(+)	(+)	(+)	(++)	Det	–	(+)	–	Plutonic
14	SR	M	(+)	–	–	–	–	√	–	153.2	83.4	69.8	L	(+)	(+)	(+)	(+)	Det	–	(+)	–	Plutonic
15	A	M	(+)	–	–	–	–	–	–	100.3	61.7	38.7	L	(++)	(-)	(++)	(++)	Det	Ms/Sp	(++)	R	Plutonic
16	SR	M	(-)	–	–	–	–	√	–	55.4	72.4	-17.0	G	(+)	(+)	(++)	(++)	Det	Mag	(++)	–	Plutonic
17	A	M	(-)	–	–	–	–	–	–	181.2	111.5	69.7	L	(+)	(+)	(+)	(++)	Det	Bt/Py+Ilt/Kfs	(+)	–	Plutonic
18	SR	M	(-)	–	–	–	–	√	–	82.3	68.2	14.1	G	(+)	(+)	(+)	(+)	Det	–	(+)	–	Plutonic
19	SR	3	(++)	–	–	–	–	–	–	60.7	70.9	-10.2	G	(+)	(+)	(-)	(++)	Det	Kfs/Rt	(-)	–	Met. (L-M)
20	SA	M	(+)	–	–	–	–	√	–	55.1	38.9	16.2	G	(+)	(+)	(++) (O)	(++)	Det	–	(-)	St	Met. (L-M)
21	SR	M	(+)	√	–	–	–	√	–	79.7	126.0	-46.3	G*	(+)	(+)	(-)	(++)	Det	–	(-)	R	Met. (L-M)
22	SA	M	(++)	–	–	–	–	√	–	126.5	123.4	3.1	D & L	(+)	(+)	(+)	(++)	Det	–	(-)	R	Met. (L-M)
23	SR	M	(++)	–	–	–	–	–	√	41.2	49.8	-8.6	G	(+)	(+)	(-)	(-)	–	Zrn	(-)	Sb	Met. (L-M)
24	SR	2	(+)	√	–	–	–	√	–	87.8	78.2	9.6	G	(++)	(+)	(++) (O)	(++)	Det	–	(+)	–	Met. (L); brittle deformed
25	SR	2	(++)	–	–	–	–	–	–	84.2	109.0	-24.8	G	(+)	(-)	(+)	(++)	Det	Ap	(+)	R	Met. (L-M)
26	SA	4	(++)	–	–	–	–	√	–	35.1	62.3	-27.3	D	(-)	(+)	(-)	(+)	Det	–	(-)	Sb	Met. (L-M)
27	SR	M	(-)	–	–	–	–	√	–	120.1	117.5	2.6	G	(+)	(-)	(+) (O)	(++)	Det/Dgn	–	(+)	St	Met. (L); brittle deformed
28	SR	M	(+)	–	–	–	–	√	–	113.0	69.6	43.4	L	(++)	(+)	(++)	(++)	Det	–	(++)	–	Plutonic
29	SA	M	(+)	–	–	–	–	–	–	126.6	63.2	63.4	L	(++)	(++)	(++)	(++)	Det	–	(++)	–	Plutonic
30	R	M	(++)	–	√	–	–	√	–	32.6	38.5	-5.9	G	(-)	(+)	(-)	(+)	Dgn	–	(-)	–	Met. (L-M); ductily deformed
31	SR	M	(-)	–	–	–	–	√	–	51.3	36.0	15.3	G	(-)	(+)	(-)	(++)	Dgn	–	(-)	–	Plutonic
32	SR	3	(+)	√	–	–	–	–	√	25.9	53.7	-27.7	D	(+)	(+)	(-)	(++)	Det	Py+Ms/Kfs	(-)	–	Met. (H); type 4B
33	SR	M	(++)	–	–	–	–	–	√	30.6	111.6	-81.0	D	(+)	(+)	(+)	(++)	Det	–	(-)	–	Met. (L-M)
34	SA	M	(+)	–	–	–	–	√	–	149.4	113.4	36.0	G	(++)	(+)	(++) (O)	(++)	Det	Bt	(++)	–	Met. (L); brittle deformed
35	SR	M	(+)	–	–	–	–	√	–	110.0	120.0	-10.0	G	(+)	(-)	(+)	(++)	Det/Dgn	Kfs/Rt	(+)	St	Met. (L-M)
36	A	M	(++)	–	–	–	–	√	–	60.2	60.9	-0.7	G	(+)	(+)	(+) (O)	(++)	Det	–	(-)	St	Met. (L); brittle deformed
37	SA	> 7	(++)	–	–	–	–	–	–	55.2	128.3	-73.1	G*	(+)	(+)	(+)	(++)	Det	–	(+)	Sb	Met. (L-M)
38	SA	6	(+)	√	–	–	–	√	–	46.8	36.2	10.6	G	(-)	(+)	(-)	(+)	Det	–	(-)	–	Met. (H); type 4B
39	SR	M	(-)	–	–	–	–	√	–	73.5	38.5	35.0	L	(-)	(-)	(+)	(-)	–	–	(+)	–	Plutonic
40	A	M	(-)	–	–	–	–	√	–	61.2	32.3	28.9	L	(+)	(+)	(+)	(++)	Det	–	(+)	–	Plutonic
41	R	M	(++)	–	–	–	–	√	–	26.2	52.5	-26.3	D	(+)	(+)	(+)	(++)	Det	–	(-)	–	Met. (L-M)

Notes: [1] D=dark gray to black SEM-CL: value of difference < -25; G=gray SEM-CL: -25 < value of difference < 25; L=light gray SEM-CL: values of difference > 25; some grains were indicated with two distinct colours because both colours were shown in SEM-CL images and it is impossible to identify one main appearance. * indicates that the observed grain colour does not match the colour in this table due to a substantial change in the contrast for the purpose of high-quality SEM-CL image.

[2] (O) was marked in cases that the grain shows microfractures with preferred orientation.

[3] Ap=apatite; Bt=biotite; Ilt=illite; Kfs=K-feldspar; Mag=magnetite; Ms=muscovite; Py=pyrite; Rt=rutile; Sp=sphalerite; Zrn=zircon.

Table 4B: Summary data of detrital quartz grains of sample 2565 (petrography and HCL image).

Grain No	Roundness (angular (A), sub-angular (SA), sub-rounded (SR), rounded (R))	Mono-/Poly-crystalline (M/no. of grains)	Extinction (None- weak+, strong++)	Mosaic Texture	Deformation Lamellae	Deformarion Banding	Zoning	Overgrowth	Fractures (rare-,some+,common++)	Fluid Inclusion Trail		Mineral Inclusion[1]	Hot CL			Quartz Type[3] *(from HCL & Petrography)*	Quartz Type *(from SEM-CL & Petrography)*	Final Classification
										Occurrence (rare-, some+, Common++)	Detrital/ Diagenetic (Det/Dgn)		3s colo-ur[2]	12s colo-ur[2]	Colour Shift			
1	A	M	(-)	–	–	–	–	√	(-)	(+)	Det		DB	DB	no	Plutonic	Plutonic	Plutonic
2	SR	M	(++)	–	–	–	–	√	(+)	(+)	Det	–	DB	DB	slight	Met. (L-M)	Met. (L-M)	Met. (L-M)
3	R	M	(-)	–	–	–	–	√	(-)	(++)	Det/Dgn	–	MB	MB	slight	Plutonic	Plutonic	Plutonic
4	SR	M	(-)	–	–	–	–	√	(+)	(+)	Det	–	MDB	MDB	slight	Plutonic	Plutonic	Plutonic
5	A	> 7	(++)	–	–	–	–	√	(-)	(++)	Det/Dgn	–	DB	DB	no	Met. (L-M)	Met. (L-M)	Met. (L-M)
6	SR	M	(+)	–	–	–	–	√	(+)	(++)	Det	–	DB	DB	slight	Plutonic*	Met. (L); brittle deformed	Met. (L); brittle deformed
7	SA	3	(++)	–	–	√	–	√	(+)	(++)	Det	–	MDB	DB	slight	Met. (L-M)	Met. (L-M); ductily deformed	Met. (L-M); ductily deformed
8	SA	> 7	(++)	–	–	–	–	√	(+)	(++)	Det	–	DB	DB	no	Met. (L-M)	Met. (L-M)	Met. (L-M)
9	R	M	(-)	–	–	–	–	√	(-)	(++)	Det	–	BB	BB	slight	Plutonic	Plutonic	Plutonic
10	R	M	(++)	–	–	–	–	–	(+)	(+)	Det	–	DB	DB	slight	Met. (L-M)	Met. (L-M)	Met. (L-M)
11	SA	M	(++)	–	–	–	–	√	(-)	(+)	Det	–	–	–	–		Met. (L-M)	Met. (L-M)
12	SA	M	(++)	–	–	–	–	√	(-)	(+)	Det	–	MDB	MDB	slight	Met. (L-M)*	Plutonic	Plutonic
13	SA	M	(+)	–	–	–	–	–	(+)	(++)	Det	–	MDB	MDB	slight	Plutonic	Plutonic	Plutonic
14	SR	M	(+)	–	–	–	–	√	(+)	(+)	Det	–	MDB	MDB	no	Plutonic	Plutonic	Plutonic
15	A	M	(+)	–	–	–	–	–	(-)	(++)	Det	Ms/Sp	MDB	MDB	slight	Plutonic	Plutonic	Plutonic
16	SR	M	(-)	–	–	–	–	√	(+)	(++)	Det	Mag	DB	DB	slight	Plutonic	Plutonic	Plutonic
17	A	M	(-)	–	–	–	–	–	(+)	(++)	Det	Bt/Py+Ilt/Kfs	MB	MB	slight	Plutonic	Plutonic	Plutonic
18	SR	M	(-)	–	–	–	–	√	(+)	(+)	Det	–	MDB	MDB	slight	Plutonic	Plutonic	Plutonic
19	SR	3	(++)	–	–	–	–	–	(+)	(++)	Det	Kfs/Rt	DB	DB	no	Met. (L-M)	Met. (L-M)	Met. (L-M)
20	SA	M	(+)	–	–	–	–	√	(+)	(++)	Det	–	MDB	MDB	slight	Plutonic*	Met. (L-M)	Met. (L-M)
21	SR	M	(+)	√	–	–	–	√	(+)	(++)	Det	–	DB	DB	slight	Met. (L-M)	Met. (L-M)	Met. (L-M)
22	SA	M	(++)	–	–	–	–	√	(+)	(++)	Det	–	MDB	MDB	slight	Met. (L-M)	Met. (L-M)	Met. (L-M)
23	SR	M	(++)	–	–	–	–	–	(+)	(-)	–	Zrn	DB	DB	slight	Met. (L-M)	Met. (L-M)	Met. (L-M)
24	SR	2	(+)	–	–	–	–	√	(+)	(++)	Det	–	MDB	MDB	slight	Met. (L-M)	Met. (L); brittle deformed	Met. (L); brittle deformed
25	SR	2	(++)	–	–	–	–	–	(-)	(++)	Det	Ap	MDB	MDB	slight	Plutonic*	Met. (L-M)	Met. (L-M)
26	SA	4	(++)	–	–	–	–	√	(+)	(+)	Det	–	DB	DB	no	Met. (L-M)	Met. (L-M)	Met. (L-M)
27	SR	M	(-)	–	–	–	–	√	(-)	(++) (O)	Det/Dgn	–	MDB	MDB	slight	Plutonic*	Met. (L); brittle deformed	Met. (L); brittle deformed
28	SR	M	(+)	–	–	–	–	√	(+)	(++)	Det	–	–	–	–		Plutonic	Plutonic
29	SA	M	(+)	–	–	–	–	–	(++)	(++)	Det	–	MB	MB	moderate	Plutonic	Plutonic	Plutonic
30	R	M	(++)	–	√	–	–	√	(+)	(+)	Dgn	–	DB	DB	slight	Met. (L-M)	Met. (L-M); ductily deformed	Met. (L-M); ductily deformed
31	SR	M	(-)	–	–	–	–	√	(+)	(++)	Dgn	–	MDB	DB	slight	Plutonic	Plutonic	Plutonic
32	SR	3	(+)	–	–	–	–	–	(+)	(++)	Det	Py+Ms/Kfs	DB	DB	no	Met. (L-M)*	Met. (M-H); type 4B	Met. (M-H); type 4B
33	SR	M	(++)	–	–	–	–	–	(+)	(++)	Det	–	DB	DB	no	Met. (L-M)	Met. (L-M)	Met. (L-M)
34	SA	M	(+)	–	–	–	–	√	(+)	(++)	Det	Bt	DB	DB	slight	Met. (L-M)	Met. (L); brittle deformed	Met. (L); brittle deformed
35	SR	M	(+)	√	–	–	–	√	(-)	(++)	Det/Dgn	Kfs/Rt	MDB	MDB	slight	Met. (L-M)	Met. (L-M)	Met. (L-M)
36	A	M	(++)	–	–	–	–	√	(+)	(++)	Det	–	MDB	MDB	slight	Met. (L-M)	Met. (L); brittle deformed	Met. (L); brittle deformed
37	SA	> 7	(++)	–	–	–	–	–	(+)	(++)	Det	–	MDB	MDB	slight	Met. (L-M)	Met. (L-M)	Met. (L-M)
38	SA	6	(+)	√	–	–	–	√	(+)	(+)	Det	–	–	–	–		Met. (M-H); type 4B	Met. (M-H); type 4B
39	SR	M	(-)	–	–	–	–	√	(-)	(-)	–	–	–	–	–		Plutonic	Plutonic
40	A	M	(-)	–	–	–	–	√	(+)	(++)	Det	–	MB	MDB	slight	Plutonic	Plutonic	Plutonic
41	R	M	(++)	–	–	–	–	√	(+)	(++)	Det	–	DB	DB	no	Met. (L-M)	Met. (L-M)	Met. (L-M)

Notes: [1] Ap=apatite; Bt=biotite; Ilt=illite; Kfs=K-feldspar; Mag=magnetite; Ms=muscovite; Py=pyrite; Rt=rutile; Sp=sphalerite; Zrn=zircon.

[2] VDB=very dark blue; DB=dark blue; MDB=medium dark blue; MB=medium blue; BMB=bright-medium blue; BB=bright blue.

[3] * indicates that the classification from combined HCL and petrography does not match the classification from combined SEM-CL and petrography.

Table 5A: Summary data of detrital quartz grains of sample 2860 (petrography and SEM-CL image).

Grain No	Roundness (angular (A), sub-angular (SA), sub-rounded (SR), rounded (R))	Mono-/Poly-crystalline (M/no. of grains)	Extinction (None- weak+, strong++)	Mosaic texture	Deformation Lamellae	Deformarion Banding	Zoning	Overgrowth	Homo-geneous SEM-CL image	Grayscale in SEM-CL Image				Fractures (rare-,some+,common++)			Fluid Inclusion Trail		Mineral Inclusion[3]	Spiders (rare-, some+. Common ++)	Bright Mottling Random, Streaky, Subtle (R/St/Sb)	Quartz Type (Met.: metamorphic; L, M, H: low, medium, high grade)
										Quartz	Epoxy	Difference (=Quartz - Epoxy)	Colour[1]	Total amount	Open fracture	Healed fracture[2]	Occurrence (rare-, some+, Common++)	Detrital/ Diagenetic (Det/Dgn)				
1	SR	M	(++)	–	–	–	–	–	–	151.6	221.7	-70.1	D*	(+)	(+)	(+)	(+)	Det	–	(-)	–	Met. (L-M)
2	SR	4	(++)	–	–	–	–	–	–	125.1	218.1	-93.0	D	(++)	(++)	(++)	(++)	Det	–	(-)	–	Met. (L-M)
3	SA	2	(+)	√	–	–	–	√	√	167.2	150.1	17.1	L	(+)	(+)	(+)	(+)	Det	–	(-)	–	Met. (L-M)
4	SA	M	(+)	–	–	–	–	√	–	160.0	200.9	-40.9	G & L	(+)	(+)	(-)	(+)	Det	–	(+)	R	Plutonic
5	SA	M	(++)	–	–	–	–	√	–	103.1	227.2	-124.1	D	(+)	(-)	(+)	(+)	Det	–	(-)	–	Met. (L-M)
6	SR	M	(-)	–	–	–	–	√	–	177.9	219.4	-41.5	L*	(+)	(++)	(-)	(+)	Det	–	(+)	–	Plutonic
7	SR	M	(++)	–	–	–	–	–	√	104.0	212.1	-108.1	D	(+)	(-)	(+)	(-)	–	–	(-)	–	Met. (L-M)
8	SR	M	(-)	–	–	–	–	√	–	166.5	223.8	-57.3	G	(+)	(-)	(+)	(+)	Det	–	(-)	St	Met. (L-M)
9	SR	3	(++)	–	–	–	–	√	√	111.8	137.1	-25.3	G	(+)	(+)	(+)	(+)	Det	–	(-)	Sb	Met. (L-M)
10	SR	M	(-)	–	–	–	–	√	–	238.7	235.6	3.2	L	(++)	(++)	(-)	(++)	Det/Dgn	Mnz	(++)	R	Plutonic
11	SR	3	(+)	–	–	–	–	√	–	133.1	227.5	-94.4	G*	(++)	(++)	(++) (O)	(++)	Det	–	(++)	–	Met. (L); brittle deformed
12	SR	M	(+)	–	–	–	–	–	√	97.5	220.4	-122.8	D	(+)	(-)	(+)	(-)	–	–	(-)	–	Met. (L-M)
13	SR	M	(++)	–	–	–	–	√	–	92.9	120.2	-27.3	G	(++)	(+)	(++)	(-)	–	–	(-)	Sb	Met. (L-M)
14	SR	2	(-)	–	–	–	–	√	–	123.8	59.8	64.0	L	(++)	(+)	(++)	(+)	Dgn	–	(+)	–	Plutonic
15	SA	M	(-)	–	–	–	–	√	–	73.8	97.9	24.1	L	(++)	(+)	(++)	(+)	Det	–	(++)	R	Plutonic
16	A	M	(+)	√	–	–	–	–	√	107.7	194.1	-86.4	D	(++)	(-)	(++)	(+)	Det	Chl	(-)	–	Met. (M-H); type 4B
17	SA	M	(+)	–	–	–	–	√	–	225.5	189.7	35.8	L	(++)	(++)	(+)	(++)	Det	Bt	(++)	–	Plutonic
18	SR	M	(+)	–	–	–	–	√	–	126.7	91.8	34.9	L	(++)	(+)	(++)	(++)	Det/Dgn	–	(-)	Sb	Plutonic
19	A	> 10	(++)	–	–	–	–	–	√	80.1	174.3	-94.3	D	(+)	(-)	(+)	(-)	–	–	(-)	–	Met. (M-H); type 4B
20	R	M	(+)	–	–	–	–	√	√	110.7	190.4	-79.7	G	(-)	(-)	(-)	(++)	Det	–	(-)	–	Met. (L-M)
21	SR	M	(-)	–	–	–	–	√	–	160.4	202.7	-42.3	G	(+)	(+)	(+)	(++)	Det/Dgn	Ap	(-)	St	Plutonic
22	R	M	(++)	–	–	–	–	√	–	99.9	111.6	-11.8	G	(++)	(++)	(++)	(+)	Det	–	(-)	–	Met. (L-M)
23	SA	M	(+)	–	–	–	–	√	–	136.6	175.0	-38.3	G	(++)	(++)	(++)	(++)	Det	Ms	(++)	–	Plutonic
24	R	M	(++)	–	√	–	–	√	–	157.7	222.3	-64.5	G	(+)	(++)	(+)	(+)	Det	–	(-)	–	Met. (L-M) ductily deformed
25	SA	M	(++)	–	–	–	–	√	–	197.6	196.7	0.9	L	(++)	(++)	(+)	(++) (O)	Det/Dgn	–	(++)	R	Met. (L); brittle deformed
26	SA	M	(++)	–	–	–	–	√	–	97.0	118.0	-21.0	G	(+)	(-)	(+)	(+)	Det	–	(-)	Sb	Met. (L-M)
27	A	> 8	(++)	√	–	–	–	√	–	101.9	180.0	-78.1	G	(+)	(-)	(+)	(-)	–	Ilt	(-)	–	Met. (L-M)
28	SA	2	(+)	–	–	–	–	√	–	225.5	220.8	4.7	G & L	(++)	(++)	(+)	(++)	Det/Dgn	–	(+)	St	Met. (L); brittle deformed
29	SR	4	(++)	√	–	–	–	√	–	122.3	126.5	-4.3	G	(++)	(++)	(+)	(++)	Det/Dgn	–	(++)	–	Met. (L-M)
30	R	M	(-)	–	–	–	–	√	–	82.9	121.5	-38.6	G	(+)	(+)	(+)	(++)	Det	–	(-)	R	Met. (L-M)
31	R	M	(++)	–	–	–	–	√	–	54.8	60.6	-5.8	G	(+)	(+)	(+)	(+)	Det	–	(-)	St	Met. (L-M)
32	R	> 5	(+)	√	–	–	–	√	√	104.5	70.6	33.8	L	(-)	(+)	(-)	(+)	Det	Bt, Kfs	(-)	–	Met. (L-M)
33	SR	M	(-)	–	–	–	–	√	–	114.9	119.6	-4.6	G	(+)	(+)	(+)	(++)	Det	–	(+)	–	Plutonic
34	SA	M	(+)	–	–	–	–	√	–	128.9	180.1	-51.2	G	(++)	(++)	(++) (O)	(++)	Det/Dgn	Kfs	(+)	R	Met. (L); brittle deformed
35	SA	M	(+)	√	–	–	–	√	–	98.2	175.5	-77.3	G	(+)	(+)	(+)	(++)	Det	–	(-)	–	Met. (L-M)
36	A	M	(-)	–	–	–	–	–	–	83.9	188.6	-104.7	G & L	(++)	(+)	(++)	(++)	Det	Ms	(++)	R	Plutonic
37	A	M	(+)	–	–	–	–	√	–	145.0	110.1	35.0	L	(++)	(++)	(++)	(+)	Det	–	(++)	–	Plutonic
38	R	M	(-)	–	–	–	–	√	–	92.4	214.7	-122.3	G*	(+)	(++)	(++) (O)	(+)	Det	Ms, Ap	(+)	St	Met. (L); brittle deformed
39	SA	M	(+)	–	–	–	–	√	–	127.0	190.6	-63.6	G	(++)	(+)	(++)	(+)	Det/Dgn	Chr, Anh	(-)	–	Plutonic
40	SR	M	(-)	–	–	–	–	√	–	114.4	177.2	-62.8	G	(++)	(++)	(++)	(++)	Det/Dgn	Ms	(++)	–	Plutonic

Notes: [1] D=dark gray to black SEM-CL: value of difference < -80; G=gray SEM-CL: -80 < value of difference < 0; L=light gray SEM-CL: values of difference > 0; some grains were indicated with two distinct colours because both colours were shown in SEM-CL images and it is impossible to identify one main appearance. * indicates that the observed grain colour does not match the colour in this table due to a substantial change in the contrast for the purpose of high-quality SEM-CL image.

[2] (O) was marked in cases that the grain shows microfractures with preferred orientation.

[3] Anh=anhydrite; Ap=apatite; Bt=biotite; Chl=chlorite; Chr=chromite; Ilt=illite; Kfs=K-feldspar; Ms=muscovite; Mnz=monazite.

Table 5B: Summary data of detrital quartz grains of sample 2860 (petrography and HCL image).

Grain No	Roundness (angular (A), sub-angular (SA), sub-rounded (SR), rounded (R))	Mono-/Poly-crystalline (M/no. of grains)	Extinction (None- weak+, strong++)	Mosaic texture	Deformation Lamellae	Deformarion Banding	Zoning	Overgrowth	Fractures (rare-, some+, Common++)	Fluid Inclusion Trail		Mineral Inclusion[1]	Hot CL			Quartz Type[3] *(from HCL & Petrography)*	Quartz Type *(from SEM-CL & Petrography)*	Final Classification
										Occurrence (rare-, some+, Common++)	Detrital/ Diagenetic (Det/Dgn)		3s colo-ur[2]	12s colo-ur[2]	Colour Shift			
1	SR	M	(++)	–	–	–	–	–	(+)	(+)	Det	–	DB	DB	no	Met. (L-M)	Met. (L-M)	Met. (L-M)
2	SR	4	(++)	–	–	–	–	–	(++)	(++)	Det	–	DB	DB	slight	Met. (L-M)	Met. (L-M)	Met. (L-M)
3	SA	2	(+)	√	–	–	–	√	(+)	(+)	Det	–	MB	MDB	moderate	Met. (M-H); type 4A*	Met. (L-M)	Met. (M-H); type 4A
4	SA	M	(+)	–	–	–	–	√	(+)	(+)	Det	–	MDB	MDB	moderate	Plutonic	Plutonic	Plutonic
5	SA	M	(++)	–	–	–	–	√	(-)	(+)	Det	–	DB	DB	slight	Met. (L-M)	Met. (L-M)	Met. (L-M)
6	SR	M	(-)	–	–	–	–	√	(++)	(+)	Det	–	MDB	MDB	slight	Plutonic	Plutonic	Plutonic
7	SR	M	(++)	–	–	–	–	–	(-)	(-)	–	–	DB	DB	no	Met. (L-M)	Met. (L-M)	Met. (L-M)
8	SR	M	(-)	–	–	–	–	√	(-)	(+)	Det	–	MDB	DB	slight	Plutonic*	Met. (L-M)	Met. (L-M)
9	SR	3	(++)	–	–	–	–	√	(+)	(+)	Det	–	MDB	MDB	moderate	Met. (M-H); type 4A*	Met. (L-M)	Met. (M-H); type 4A
10	SR	M	(-)	–	–	–	–	√	(++)	(++)	Det/Dgn	Mnz	MDB	MDB	moderate	Plutonic	Plutonic	Plutonic
11	SR	3	(+)	–	–	–	–	√	(++)	(++)	Det	–	MDB	MDB	slight	Plutonic*	Met. (L); brittle deformed	Met. (L); brittle deformed
12	SR	M	(+)	–	–	–	–	–	(-)	(-)	–	–	DB	DB	no	Plutonic*	Met. (L-M)	Met. (L-M)
13	SR	M	(++)	–	–	–	–	√	(+)	(-)	–	–	DB	DB	no	Met. (L-M)	Met. (L-M)	Met. (L-M)
14	SR	2	(-)	–	–	–	–	√	(+)	(+)	Dgn	–	BB	MB	moderate	Plutonic	Plutonic	Plutonic
15	SA	M	(-)	–	–	–	–	√	(+)	(+)	Det	–	DB	DB	slight	Plutonic	Plutonic	Plutonic
16	A	M	(+)	√	–	–	–	–	(-)	(+)	Det	Chl	DB	DB	no	Met. (L-M)*	Met. (M-H); type 4B	Met. (M-H); type 4B
17	SA	M	(+)	–	–	–	–	√	(++)	(++)	Det	Bt	–	–	–		Plutonic	Plutonic
18	SR	M	(+)	–	–	–	–	√	(+)	(++)	Det/Dgn	–	MDB	MDB	slight	Plutonic	Plutonic	Plutonic
19	A	> 10	(++)	–	–	–	–	–	(-)	(-)	–	–	DB	DB	no	Met. (M-H); type 4B	Met. (M-H); type 4B	Met. (M-H); type 4B
20	R	M	(+)	–	–	–	–	√	(-)	(++)	Det	–	–	–	–		Met. (L-M)	Met. (L-M)
21	SR	M	(-)	–	–	–	–	√	(+)	(++)	Det/Dgn	Ap	MDB	MDB	moderate	Plutonic	Plutonic	Plutonic
22	R	M	(++)	–	–	–	–	√	(++)	(+)	Det	–	DB	DB	slight	Met. (L-M)	Met. (L-M)	Met. (L-M)
23	SA	M	(+)	–	–	–	–	√	(++)	(++)	Det	Ms	MB	MDB	moderate	Plutonic	Plutonic	Plutonic
24	R	M	(++)	–	√	–	–	√	(++)	(+)	Det	–	DB	DB	slight	Met. (L-M)	Met. (L-M) ductily deformed	Met. (L-M) ductily deformed
25	SA	M	(++)	–	–	–	–	√	(++)	(++)	Det/Dgn	–	MB	MB	moderate	Met. (M-H)*	Met. (L); brittle deformed	Met. (L); brittle deformed
26	SA	M	(++)	–	–	–	–	√	(-)	(+)	Det	–	MDB	MDB	slight	Plutonic*	Met. (L-M)	Met. (L-M)
27	A	> 8	(++)	√	–	–	–	√	(-)	(-)	–	Ilt	DB	DB	slight	Met. (L-M)	Met. (L-M)	Met. (L-M)
28	SA	2	(+)	–	–	–	–	√	(++)	(++)	Det/Dgn	–	MDB	DB	strong	Plutonic*	Met. (L); brittle deformed	Met. (L); brittle deformed
29	SR	4	(++)	√	–	–	–	√	(++)	(++)	Det/Dgn	–	MDB	MDB	slight	Plutonic*	Met. (L-M)	Met. (L-M)
30	R	M	(-)	–	–	–	–	√	(+)	(++)	Det	–	MDB	MDB	slight	Plutonic	Met. (L-M)	Met. (L-M)
31	R	M	(++)	–	–	–	–	√	(+)	(+)	Det	–	MDB	DB	slighjt	Met. (L-M)	Met. (L-M)	Met. (L-M)
32	R	> 5	(+)	√	–	–	–	√	(+)	(+)	Det	Bt, Kfs	MB	MB	moderate	Met. (M-H); type 4A*	Met. (L-M)	Met. (M-H); type 4A
33	SR	M	(-)	–	–	–	–	√	(+)	(++)	Det	–	DB	DB	no	Met. (L-M)*	Plutonic	Plutonic
34	SA	M	(+)	–	–	–	–	√	(++)	(++)	Det/Dgn	Kfs	MB	MB	moderate	Plutonic*	Met. (L); brittle deformed	Met. (L); brittle deformed
35	SA	M	(+)	√	–	–	–	√	(+)	(++)	Det	–	–	–	–		Met. (L-M)	Met. (L-M)
36	A	M	(-)	–	–	–	–	–	(+)	(++)	Det	Ms	MDB	DB	slight	Plutonic	Plutonic	Plutonic
37	A	M	(+)	–	–	–	–	√	(++)	(+)	Det	–	DB	DB	slight	Plutonic	Plutonic	Plutonic
38	R	M	(-)	–	–	–	–	√	(++)	(+)	Det	Ms, Ap	MDB	DB	slight	Met. (L-M)	Met. (L); brittle deformed	Met. (L); brittle deformed
39	SA	M	(+)	–	–	–	–	√	(+)	(+)	Det/Dgn	Chr, Anh	DB	DB	no	Plutonic	Plutonic	Plutonic
40	SR	M	(-)	–	–	–	–	√	(++)	(++)	Det/Dgn	Ms	MDB	MDB	slight	Plutonic	Plutonic	Plutonic

Notes: [1] Anh=anhydrite; Ap=apatite; Bt=biotite; Chl=chlorite; Chr=chromite; Ilt=illite; Kfs=K-feldspar; Ms=muscovite; Mnz=monazite.

[2] VDB=very dark blue; DB=dark blue; MDB=medium dark blue; MB=medium blue; BMB=bright-medium blue; BB=bright blue.

[3] * indicates that the classification from combined HCL and petrography does not match the classification from combined SEM-CL and petrography.

Table 6A: Summary data of detrital quartz grains of sample 2995 (petrography and SEM-CL image).

Grain No	Roundness (angular (A), sub-angular (SA), sub-rounded (SR); rounded (R))	Mono-/Poly-crystalline (M/no of grains)	Extinction (None- weak+, strong++)	Mosaic texture	Deformation Lamellae	Deformarion Banding	Zoning	Overgrowth	Homo-geneous SEM-CL image	Grayscale in SEM-CL Image				Fractures (rare-,some+,common++)			Fluid Inclusion Trail		Mineral Inclusion[3]	Spiders (rare-, some+. Common ++)	Bright Mottling Random, Streaky, Subtle (R/St/Sb)	Quartz Type (Met.: metamorphic; L, M, H: low, medium, high grade)
										Quartz	Epoxy	Difference (=Quartz - Epoxy)	Colour[1]	Total amount	Open fracture[2]	Healed fracture[2]	Occurrence (rare-, some+, Common++)	Detrital/ Diagenetic (Det/Dgn)				
1	A	3	(++)	–	–	–	–	–	–	26.9	49.0	-22.1	D*	(++)	(++)	(++) (O)	(++)	Det	–	(-)	–	Met. (L); brittle deformed
2	SR	M	(-)	–	–	–	–	√	–	148.2	51.3	96.9	L	(++)	(++) (O)	(+)	(+)	Det	–	(+)	–	Plutonic
3	A	2	(+)	√	–	–	–	√	–	70.6	40.8	29.8	G	(++)	(++)	(+)	(++)	Det	–	(-)	–	Met. (L-M)
4	R	M	(+)	–	–	–	–	√	–	84.9	93.5	-8.6	G	(++)	(+)	(+)	(++)	Det	–	(+)	–	Plutonic
5	A	M	(-)	–	–	–	–	√	–	160.0	111.2	48.8	L	(++)	(++)	(+)	(+)	Det	–	(+)	–	Plutonic
6	SA	M	(++)	√	√	–	–	√	–	97.5	108.4	-10.9	G	(+)	(+)	(+)	(++)	Det	–	(+)	–	Met. (L-M); ductily deformed
7	SR	2	(+)	√	–	–	–	√	–	101.8	159.6	-57.8	D	(+)	(+)	(+)	(++)	Det	–	(-)	–	Met. (L-M)
8	SR	M	(+)	√	–	–	–	√	√	97.1	70.2	26.9	G	(-)	(+)	(-)	(++)	Det/Dgn	–	(-)	–	Met. (L-M)
9	R	M	(+)	–	–	–	–	√	–	117.5	88.1	29.4	G	(++)	(++)	(++)	(++)	Det	–	(++)	–	Plutonic
10	SR	>10	(+)	√	–	–	–	–	√	127.1	136.6	-9.5	D*	(-)	(-)	(-)	(-)	–	–	(-)	–	Met. (M-H); Type 4B
11	R	>10	(+)	√	–	–	–	–	√	96.3	128.3	-32.0	D	(+)	(+)	(-)	(+)	Det	–	(-)	–	Met. (M-H); Type 4B
12	SR	M	(-)	–	–	–	–	√	–	146.2	125.5	20.7	G	(++)	(++)	(-)	(+)	Det	Kfs	(-)	–	Plutonic
13	SR	6	(++)	–	–	–	–	–	–	141.2	117.4	23.8	G	(++)	(++) (O)	(-)	(-)	–	–	(-)	–	Met. (L-M)
14	SR	2	(++)	–	–	–	–	√	–	–	–	–	G	(++)	(-)	(++) (O)	(++)	Det	–	(-)	St	Met. (L); brittle deformed
15	SR	M	(+)	√	–	–	–	–	√	98.6	152.8	-54.2	D	(-)	(-)	(-)	(++)	Det	–	(-)	–	Met. (L-M)
16	SA	M	(++)	–	–	–	–	√	–	152.0	152.3	-0.3	G	(+)	(+)	(+)	(++)	Det/Dgn	–	(-)	–	Met. (L-M)
17	SA	M	(+)	–	–	–	–	√	–	125.0	144.5	-19.5	G	(++)	(++)	(++)	(++)	Det	–	(++)	R	Plutonic
18	SA	M	(++)	–	–	–	–	–	–	88.3	86.4	1.9	G	(++)	(+)	(++)	(+)	Det	–	(-)	Sb	Met. (L-M)
19	R	M	(-)	–	–	–	–	√	√	132.3	90.9	41.4	L	(-)	(-)	(-)	(-)	–	–	(-)	–	Plutonic
20	R	7	(+)	√	–	–	–	–	√	103.4	156.7	-53.3	D	(-)	(-)	(-)	(-)	–	–	(-)		Met. (M-H); Type 4B
21	SR	M	(++)	–	–	–	–	√	–	66.2	80.3	-14.1	G	(+)	(+)	(-)	(++)	Det/Dgn	–	(-)	–	Met. (L-M)
22	SR	M	(-)	–	–	–	–	√	–	101.6	116.4	-14.8	G	(+)	(+)	(+)	(++)	Det	–	(-)	–	Plutonic
23	R	M	(+)	–	–	–	–	√	–	–	–	–	G	(++)	(++)	(+)	(++)	Det	–	(++)	–	Plutonic
24	SR	3	(+)	–	√	–	–	√	–	110.9	161.9	-51.0	D	(+)	(+)	(+)	(++)	Det	–	(-)	R	Met. (L-M); ductily deformed
25	SR	5	(+)	√	–	–	–	√	√	103.3	136.5	-33.2	D	(+)	(-)	(+)	(-)	–	–	(-)	–	Met. (M-H); Type 4B
26	SA	M	(++)	–	–	–	–	√	√	120.4	65.0	55.4	L	(+)	(-)	(+)	(+)	Dgn	–	(-)	–	Met. (L-M)
27	R	3	(+)	√	–	–	–	–	√	132.2	204.9	-72.7	D	(-)	(-)	(-)	(+)	Det	–	(-)	–	Met. (M-H); Type 4B
28	SR	2	(+)	–	√	–	–	–	–	133.7	184.0	-50.3	D	(++)	(++)	(+) (O)	(+)	Det	–	(-)	–	Met. (L-M); ductily deformed
29	SR	M	(++)	–	–	√	–	√	–	136.6	139.9	-3.3	G	(-)	(-)	(-)	(++)	Det/Dgn	–	(-)	–	Met. (L-M); ductily deformed
30	SA	M	(++)	–	–	–	–	√	√	91.8	110.1	-18.3	G	(-)	(-)	(-)	(+)	Det	Rt	(+)	–	Met. (L-M)
31	SR	>8	(+)	√	–	–	–	–	√	97.3	135.7	-38.4	D	(+)	(+)	(-)	(+)	Det	Py	(-)	–	Met. (M-H); Type 4B
32	SR	M	(+)	√	–	–	–	√	–	166.9	148.6	18.3	L	(++)	(++)	(+) (O)	(++)	Det	–	(+)	–	Met. (L); brittle deformed
33	R	>10	(++)	√	–	–	–	√	√	108.4	136.5	-28.1	G	(+)	(+)	(-)	(-)	–	–	(-)	–	Met. (M-H); Type 4B
34	R	>12	(+)	√	–	–	–	√	–	104.1	130.2	-26.1	G	(+)	(+)	(-)	(-)	–		(-)	Sb	Met. (M-H); Type 4B
35	SR	M	(+)	–	–	–	–	√	–	119.3	135.5	-16.2	G	(+)	(++)	(-)	(++)	Det	–	(+)	–	Plutonic
36	SR	M	(+)	–	√	–	–	√	–	94.1	104.0	-9.9	G	(+)	(+)	(+)	(++)	Det	–	(-)	Sb	Met. (L-M); ductily deformed
37	A	M	(-)	–	–	–	–	√	–	74.4	59.5	14.9	G	(+)	(+)	(-)	(++)	Det	–	(-)	–	Plutonic
38	SR	M	(-)	–	–	–	–	√	–	94.4	58.7	35.7	L	(+)	(+)	(+)	(+)	Det	Ap	(-)	–	Plutonic
39	SR	M	(-)	–	–	–	–	√	–	105.2	84.2	21.0	G	(+)	(+)	(+)	(-)	–	Ilt, Brt	(+)	–	Plutonic
40	SA	M	(++)	–	–	–	–	√	–	85.3	125.7	-40.4	D	(-)	(-)	(-)	(+)	Det	Tur, Bt	(-)	Sb	Met. (L-M)

Notes: [1] D=dark gray to black SEM-CL: value of difference < -30; G=gray SEM-CL: -30 < value of difference < 30; L=light gray SEM-CL: values of difference > 30. * indicates that the observed grain colour does not match the colour in this table due to a substantial change in the contrast for the purpose of high-quality SEM-CL image.

[2] (O) was marked in cases that the grain shows microfractures with preferred orientation.

[3] Ap=apatite; Brt=barite; Bt=biotite; Ilt=illite; Kfs=K-feldspar; Py=pyrite; Rt=rutile; Tur=tourmaline.

Table 6B: Summary data of detrital quartz grains of sample 2995 (petrography and HCL image).

Grain No	Roundness (angular (A), sub-angular (SA), sub-rounded (SR), rounded (R))	Mono-/Poly-crystalline (M/no. of grains)	Extinction (None- weak+, strong++)	Mosaic Texture	Deformation Lamellae	Deformarion Banding	Zoning	Fractures (rare-, some+, Common++)	Fluid Inclusion Trail		Mineral Inclusion[1]	HCL Color			Quartz Type[3] *(from HCL & Petrography)*	Quartz Type *(from SEM-CL & Petrography)*	Final Classification
									Occurrence (rare-, some+, Common++)	Detrital/ Diagenetic (Det/Dgn)		3s colo-ur[2]	12s colo-ur[2]	Colour Shift			
1	A	3	(++)	–	–	–	–	(++)	(++)	Det	–	DB	DB	slight	Met. (L-M)	Met. (L); brittle deformed	Met. (L); brittle deformed
2	SR	M	(-)	–	–	–	–	(++) (O)	(+)	Det	–	MB	MB	moderate	Plutonic	Plutonic	Plutonic
3	A	2	(+)	√	–	–	–	(++)	(++)	Det	–	MDB	MDB	slight	Met. (L-M)	Met. (L-M)	Met. (L-M)
4	R	M	(+)	–	–	–	–	(+)	(++)	Det	–	MDB	DB	slight	Plutonic	Plutonic	Plutonic
5	A	M	(-)	–	–	–	–	(++)	(+)	Det	–	MB	MB	moderate	Plutonic	Plutonic	Plutonic
6	SA	M	(++)	√	√	–	–	(+)	(++)	Det	–	DB	DB	no	Met. (L-M)	Met. (L-M); ductily deformed	Met. (L-M); ductily deformed
7	SR	2	(+)	√	–	–	–	(+)	(++)	Det	–	DB	DB	no	Met. (L-M)	Met. (L-M)	Met. (L-M)
8	SR	M	(+)	√	–	–	–	(+)	(++)	Det/Dgn	–	MDB	MDB	slight	Met. (L-M)	Met. (L-M)	Met. (L-M)
9	R	M	(+)	–	–	–	–	(++)	(++)	Det	–	MDB	MDB	slight	Plutonic	Plutonic	Plutonic
10	SR	>10	(+)	√	–	–	–	(-)	(-)	–	–	DB	DB	no	Met. (M_H); type 4B	Met. (M_H); type 4B	Met. (M_H); type 4B
11	R	>10	(+)	√	–	–	–	(+)	(+)	Det	–	DB	DB	no	Met. (M_H); type 4B	Met. (M-H); type 4B	Met. (M-H); type 4B
12	SR	M	(-)	–	–	–	–	(++)	(+)	Det	Kfs	MDB	MDB	slight	Plutonic	Plutonic	Plutonic
13	SR	6	(++)	–	–	–	–	(++) (O)	(-)	–	–	MDB	MDB	slight	Met. (L-M)	Met. (L-M)	Met. (L-M)
14	SR	2	(++)	–	–	–	–	(-)	(++)	Det	–	MDB	MDB	slight	Met. (L-M)	Met. (L); brittle deformed	Met. (L); brittle deformed
15	SR	M	(+)	√	–	–	–	(-)	(++)	Det	–	DB	DB	no	Met. (L-M)	Met. (L-M)	Met. (L-M)
16	SA	M	(++)	–	–	–	–	(+)	(++)	Det/Dgn	–	DB	DB	no	Met. (L-M)	Met. (L-M)	Met. (L-M)
17	SA	M	(+)	–	–	–	–	(++)	(++)	Det	–	MDB	DB	slight	Plutonic	Plutonic	Plutonic
18	SA	M	(++)	–	–	–	–	(+)	(+)	Det	–	MDB	DB	slight	Met. (L-M)	Met. (L-M)	Met. (L-M)
19	R	M	(-)	–	–	–	–	(-)	(-)	–	–	MDB	MDB	slight	Plutonic	Plutonic	Plutonic
20	R	7	(+)	√	–	–	–	(-)	(-)	–	–	DB	DB	no	Met. (M_H); type 4B	Met. (M-H); type 4B	Met. (M-H); type 4B
21	SR	M	(++)	–	–	–	–	(+)	(++)	Det/Dgn	–	DB	DB	moderate	Met. (L-M)	Met. (L-M)	Met. (L-M)
22	SR	M	(-)	–	–	–	–	(+)	(++)	Det	–	DB	DB	slight	Plutonic	Plutonic	Plutonic
23	R	M	(+)	–	–	–	–	(++)	(++)	Det	–	MDB	DB	slight	Plutonic	Plutonic	Plutonic
24	SR	3	(+)	–	√	–	–	(+)	(++)	Det	–	DB	DB	no	Met. (L-M)	Met. (L-M); ductily deformed	Met. (L-M); ductily deformed
25	SR	5	(+)	√	–	–	–	(-)	(-)	–	–	DB	DB	slight	Met. (L-M)*	Met. (M-H); type 4B	Met. (M-H); type 4B
26	SA	M	(++)	–	–	–	–	(-)	(+)	Dgn	–	MDB	MDB	slight	Met. (L-M)	Met. (L-M)	Met. (L-M)
27	R	3	(+)	√	–	–	–	(-)	(+)	Det	–	DB	DB	no	Met. (HP)	Met. (M-H); type 4B	Met. (M-H); type 4B
28	SR	2	(+)	–	√	–	–	(++)	(+)	Det	–	DB	DB	no	Met. (L-M)	Met. (L-M); ductily deformed	Met. (L-M); ductily deformed
29	SR	M	(++)	–	–	√	–	(-)	(++)	Det/Dgn	–	DB	DB	no	Met. (L-M)	Met. (L-M); ductily deformed	Met. (L-M); ductily deformed
30	SA	M	(++)	–	–	–	–	(-)	(+)	Det	Ttn	DB	DB	no	Met. (L-M)	Met. (L-M)	Met. (L-M)
31	SR	>8	(+)	√	–	–	–	(+)	(+)	Det	Py	DB	DB	no	Met. (M_H); type 4B	Met. (M-H); type 4B	Met. (M-H); type 4B
32	SR	M	(+)	√	–	–	–	(++)	(++)	Det	–	MDB	DB	slight	Met. (L-M)	Met. (L); brittle deformed	Met. (L); brittle deformed
33	R	>10	(++)	√	–	–	–	(+)	(-)	–	–	DB	DB	no	Met. (L-M)*	Met. (M-H); type 4B	Met. (M-H); type 4B
34	R	>12	(+)	√	–	–	–	(+)	(-)	–		DB	DB	slight	Met. (L-M)*	Met. (M-H); type 4B	Met. (M-H); type 4B
35	SR	M	(+)	–	–	–	–	(++)	(++)	Det	–	MDB	MDB	slight	Plutonic	Plutonic	Plutonic
36	SR	M	(+)	–	√	–	–	(+)	(++)	Det	–	MDB	MDB	slight	Met. (L-M)	Met. (L-M); ductily deformed	Met. (L-M); ductily deformed
37	A	M	(-)	–	–	–	–	(+)	(++)	Det	–	MDB	MDB	slight	Plutonic	Plutonic	Plutonic
38	SR	M	(-)	–	–	–	–	(+)	(+)	Det	Ap	DB	DB	no	Plutonic	Plutonic	Plutonic
39	SR	M	(-)	–	–	–	–	(+)	(-)	–	Ilt, Brt	MDB	MDB	slight	Plutonic	Plutonic	Plutonic
40	SA	M	(++)	–	–	–	–	(-)	(+)	Det	Tur, Bt	DB	DB	slight	Met. (L-M)	Met. (L-M)	Met. (L-M)

Notes: [1] Ap=apatite; Brt=barite; Bt=biotite; Ilt=illite; Kfs=K-feldspar; Py=pyrite; Rt=rutile; Tur=tourmaline.

[2] VDB=very dark blue; DB=dark blue; MDB=medium dark blue; MB=medium blue; BMB=bright-medium blue; BB=bright blue.

[3] * indicates that the classification from combined HCL and petrography does not match the classification from combined SEM-CL and petrography.

Table 7A: Summary data of detrital quartz grains of sample 3000 (petrography, SEM-CL image).

Grain No	Roundness (angular (A), sub-angular (SA), sub-rounded (SR), rounded (R))	Mono-/Poly-crystalline (M/no of grains)	Extinction (None- weak+, strong++)	Mosaic texture	Deformation Lamellae	Deformarion Banding	Zoning	Overgrowth	Homo-geneous SEM-CL image	Grayscale in SEM-CL Image				Fractures (rare-,some+,common++)			Fluid Inclusion Trail		Mineral Inclusion[3]	Spiders (rare-, some+. Common++)	Bright Mottling Random, Streaky, Subtle (R/St/Sb)	Quartz Type (Met.: metamorphic; L, M, H: low, medium, high grade)
										Quartz	Epoxy	Difference (=Quartz - Epoxy)	Colour[1]	Total amount	Open fracture	Healed fracture[2]	Occurrence (rare-, some+, Common++)	Detrital/ Diagenetic (Det/Dgn)				
1	SA	M	(++)	–	–	–	–	–	√	81.5	86.9	-5.3	G	(+)	(+)	(-)	(+)	Det	Ms, Ap	(-)	–	Met. (L-M)
2	SA	4	(++)	–	–	–	–	√	√	74.4	65.7	8.7	G	(+)	(+)	(-)	(-)	–	–	(-)	–	Met. (L-M)
3	SA	M	(++)	–	–	–	–	√	√	90.9	69.4	21.5	L	(+)	(++)	(+)	(+)	Det	–	(+)	–	Met. (L-M)
4	SA	7	(+)	√	–	–	–	√	√	97.5	110.0	-12.6	G	(-)	(-)	(-)	(-)	(+)	–	(-)	–	Met. (L-M)
5	SA	M	(+)	√	–	–	–	–	√	104.3	168.6	-64.2	D	(-)	(+)	(-)	(+)	Det	–	(-)	–	Met. (M-H); type 4A
6	SA	M	(+)	–	–	–	–	√	√	108.5	111.6	-3.2	G	(-)	(-)	(+)	(+)	Det	–	(+)	–	Plutonic
7	SR	3	(++)	–	–	–	–	√	–	97.1	127.8	-30.7	G & L	(+)	(+)	(-)	(-)	–	–	(-)	R	Met. (L-M)
8	SR	M	(+)	–	–	–	–	√	–	98.4	126.1	-27.7	G	(+)	(+)	(+) (O)	(++)	Det	Ms	(+)	St	Met. (L); brittle deformed
9	SR	M	(-)	–	–	–	–	√	–	86.7	84.8	2.0	G	(-)	(-)	(+)	(++)	Det/Dgn	Zrn. Py	(+)	Sb	Plutonic
10	SA	M	(+)	√	–	–	–	√	–	136.6	101.8	34.8	L	(++)	(-)	(++) (O)	(++)	Det	–	(++)	–	Met. (L); brittle deformed
11	SR	M	(++)	–	–	–	–	√	–	100.6	108.4	-7.8	G	(+)	(+)	(+)	(++)	Det	–	(++)	St	Met. (L); brittle deformed
12	R	2	(+)	√	–	–	–	–	√	72.4	122.5	-50.1	D	(-)	(+)	(-)	(++)	Det	–	(-)	–	Met. (M-H); type 4A
13	SR	M	(+)	–	–	–	–	√	–	90.6	99.5	-9.0	G	(+)	(+)	(+) (O)	(++)	Det	Zrn	(-)	–	Met. (L); brittle deformed
14	SA	M	(++)	–	–	–	–	√	–	109.1	89.3	19.8	G	(++)	(+)	(++) (O)	(++)	Det	–	(+)	–	Met. (L); brittle deformed
15	SR	M	(++)	–	–	–	–	√	√	82.7	111.8	-29.1	G	(+)	(+)	(+)	(++)	Det	–	(-)	R	Met. (L-M)
16	A	M	(+)	–	–	–	–	√	–	63.6	77.3	-13.6	G	(+)	(+)	(+)	(++)	Det	–	(+)	–	Met. (L-M)
17	SR	M	(++)	–	√	–	–	–	–	106.1	149.5	-43.4	D	(++)	(-)	(++)	(++)	Det	–	(-)	–	Met. (L-M); ductily deformed
18	SA	M	(+)	–	–	–	–	√	–	73.3	38.7	34.6	D & L	(-)	(-)	(-)	(+)	Dgn	–	(-)	–	Met. (L-M)
19	SR	4	(+)	√	–	–	–	–	–	76.6	117.4	-40.9	G*	(-)	(-)	(+)	(++)	Det	–	(+)	St	Met. (L-M)
20	A	M	(+)	–	–	–	–	√	–	63.2	96.5	-33.3	D	(+)	(-)	(++)	(++)	Det	–	(-)	St	Met. (L-M)
21	SA	M	(+)	–	–	–	–	√	√	91.3	122.8	-31.5	D	(+)	(+)	(-)	(++)	Det	Bt	(-)	–	Met. (L-M)
22	A	M	(-)	–	–	–	–	√	–	77.6	59.3	18.3	G	(+)	(-)	(+)	(++)	Det	–	(+)	–	Plutonic
23	SR	M	(+)	–	–	–	–	√	–	80.3	110.6	-30.2	G	(+)	(+)	(+)	(++)	Det	–	(-)	St	Met. (L-M)
24	SA	3	(+)	√	–	–	–	√	–	88.9	61.6	27.3	L	(+)	(+)	(-)	(++)	Det	Bt, Kfs	(+)	–	Met. (L-M)
25	R	M	(-)	–	–	–	–	√	–	91.1	75.5	15.6	G	(++)	(+)	(+)	(+)	Dgn	–	(-)	–	Plutonic
26	SA	2	(+)	√	–	–	–	√	–	104.4	78.8	25.6	L	(++)	(+)	(++) (O)	(++)	Det	–	(++)	–	Met. (L); brittle deformed
27	SR	M	(-)	–	–	–	–	√	–	82.9	71.0	11.8	G	(+)	(+)	(++)	(+)	Det/Dgn	Ilt	(+)	–	Plutonic
28	SR	M	(++)	√	–	–	–	√	–	102.9	58.1	44.8	L	(++)	(+)	(++) (O)	(++)	Det	–	(+)	–	Met. (L); brittle deformed
29	SR	M	(++)	–	–	–	–	√	√	90.1	103.5	-13.3	G	(-)	(+)	(-)	(-)	Dgn	Ms	(-)	–	Met. (L-M)
30	SA	>6	(+)	√	–	–	–	–	√	57.9	82.2	-24.3	D*	(-)	(-)	(-)	(-)	–	Ms	(-)	–	Met. (M-H); type 4A
31	R	M	(+)	√	–	–	–	√	–	107.3	141.8	-34.5	G	(+)	(+)	(-)	(+)	Dgn	Zrn	(-)	St	Met. (L-M)
32	SR	M	(+)	√	–	–	–	√	–	93.4	86.5	7.0	G	(+)	(+)	(+)	(++)	Det	Py, Ilt	(+)	–	Met. (L-M)
33	SR	M	(+)	√	–	–	–	–	√	86.9	127.2	-40.3	D	(+)	(+)	(-)	(-)	–	Ttn	(-)	–	Met. (M-H); type 4A
34	SR	M	(++)	–	–	–	–	–	–	89.0	78.5	10.6	G	(-)	(-)	(-)	(+)	Det	–	(-)	–	Met. (L-M)
35	SR	M	(+)	–	–	–	–	–	–	80.9	109.2	-28.3	G	(+)	(+)	(-)	(-)	–	–	(-)	R	Met. (L-M)
36	A	M	(+)	√	–	–	–	√	√	88.1	116.2	-28.0	D*	(-)	(+)	(-)	(-)	–	Cal	(-)	–	Met. (M-H); type 4A
37	SR	M	(-)	–	–	–	–	√	–	116.9	107.1	9.8	G	(++)	(++)	(+)	(++)	Det	–	(++)	–	Plutonic
38	SR	3	(++)	√	–	–	–	√	–	83.6	111.8	-28.2	D*	(+)	(+)	(-)	(+)	Dgn	–	(-)	–	Met. (M-H); type 4A
39	SR	>8	(++)	–	–	–	–	√	–	85.4	116.7	-31.3	G*	(++)	(+)	(++)	(++)	Det	–	(++)	–	Met. (L-M)
40	SR	M	(++)	–	–	–	–	–	–	73.2	123.5	-50.3	D	(-)	(+)	(-)	(-)	–	–	(-)	R	Met. (L-M)

Notes: [1] D=dark gray to black SEM-CL: value of difference < -30; G=gray SEM-CL: -30 < value of difference < 20; L=light gray SEM-CL: values of difference > 20; some grains were indicated with two distinct colours because both colours were shown in SEM-CL images and it is impossible to identify one main appearance. * indicates that the observed grain colour does not match the colour in this table due to a substantial change in the contrast for the purpose of high-quality SEM-CL image.

[2] (O) was marked in cases that the grain shows microfractures with preferred orientation.

[3] Ap=apatite; Bt=biotite; Cal=calcite; Ilt=illite; Kfs=K-feldspar; Ms=muscovite; Py=pyrite;Ttn=titanite; Zrn=zircon.

Table 7B: Summary data of detrital quartz grains of sample 3000 (petrography and HCL image).

Grain No	Roundness (angular (A), sub-angular (SA), sub-rounded (SR), rounded (R))	Mono-/Poly-crystalline (M/no of grains)	Extinction (None- weak+, strong++)	Mosaic texture	Deformation Lamellae	Deformarion Banding	Zoning	Overgrowth	Fractures (rare-, some+, Common++)	Fluid Inclusion Trail		Mineral Inclusion[1]	Hot CL			Quartz Type[3] *(from HCL & Petrography)*	Quartz Type *(from SEM-CL & Petrography)*	Final Classification
										Occurrence (rare-, some+, Common++)	Detrital/ Diagenetic (Det/Dgn)		3s colo-ur[2]	12s colo-ur[2]	Colour Shift			
1	SA	M	(++)	–	–	–	–	–	(+)	(+)	Det	Ms, Ap	DB	DB	slight	Met. (L-M)	Met. (L-M)	Met. (L-M)
2	SA	4	(++)	–	–	–	–	√	(+)	(-)	–	–	MDB	DB	slight	Met. (L-M)	Met. (L-M)	Met. (L-M)
3	SA	M	(++)	–	–	–	–	√	(++)	(+)	Det	–	MDB	MDB	moderate	Met. (M-H); type 4A	Met. (L-M)	Met. (M-H); type 4A
4	SA	7	(+)	√	–	–	–	√	(-)	(-)	(+)	–	DB	MDB	no	Met. (L-M)	Met. (L-M)	Met. (L-M)
5	SA	M	(+)	√	–	–	–	–	(+)	(+)	Det	–	DB	DB	no	Met. (L-M)*	Met. (M-H); type 4B	Met. (M-H); type 4B
6	SA	M	(+)	–	–	–	–	√	(-)	(+)	Det	–	BMB	MB	moderate	Plutonic	Plutonic	Plutonic
7	SR	3	(++)	–	–	–	–	√	(+)	(-)	–	–	DB	DB	slight	Met. (L-M)	Met. (L-M)	Met. (L)
8	SR	M	(+)	–	–	–	–	√	(+)	(++)	Det	Ms	MDB	DB	slight	Met. (L-M)	Met. (L); brittle deformed	Met. (L); brittle deformed
9	SR	M	(-)	–	–	–	–	√	(-)	(++)	Det/Dgn	Zrn. Py	MDB	DB	moderate	Plutonic	Plutonic	Plutonic
10	SA	M	(+)	√	–	–	–	√	(-)	(++)	Det	–	MDB	MDB	moderate	Met. (L-M)	Met. (L); brittle deformed	Met. (L); brittle deformed
11	SR	M	(++)	–	–	–	–	√	(+)	(++)	Det	–	MB	MB	moderate	Met. (M-H)*	Met. (L); brittle deformed	Met. (L); brittle deformed
12	R	2	(+)	√	–	–	–	–	(+)	(++)	Det	–	–	–	–	Met. (L-M)*	Met. (M-H); type 4B	Met. (M-H); type 4B
13	SR	M	(+)	–	–	–	–	√	(+)	(++)	Det	Zrn	MDB	MDB	slight	Plutonic*	Met. (L); brittle deformed	Met. (L); brittle deformed
14	SA	M	(++)	–	–	–	–	√	(+)	(++)	Det	–	DB	DB	slight	Met. (L-M)	Met. (L); brittle deformed	Met. (L)
15	SR	M	(++)	–	–	–	–	√	(+)	(++)	Det	–	MB	MB	moderate	Met. (M-H); type 4A	Met. (L-M)	Met. (M-H); type 4A
16	A	M	(+)	–	–	–	–	√	(+)	(++)	Det	–	DB	DB	slight	Plutonic*	Met. (L-M)	Met. (L-M)
17	SR	M	(++)	–	√	–	–	–	(-)	(++)	Det	–	DB	DB	no	Met. (L-M)	Met. (L-M); ductily deformed	Met. (L-M); ductily deformed
18	SA	M	(+)	–	–	–	–	√	(-)	(+)	Dgn	–	MDB	MDB	slight	Plutonic*	Met. (L-M)	Met. (L-M)
19	SR	4	(+)	√	–	–	–	–	(-)	(++)	Det	–	MDB	MDB	moderate	Met. (L-M)	Met. (L-M)	Met. (L)
20	A	M	(+)	–	–	–	–	√	(-)	(++)	Det	–	DB	DB	no	Plutonic*	Met. (L-M)	Met. (L)
21	SA	M	(+)	–	–	–	–	√	(+)	(++)	Det	Bt	DB	DB	no	Plutonic*	Met. (L-M)	Met. (L-M)
22	A	M	(-)	–	–	–	–	√	(-)	(++)	Det	–	MDB	DB	moderate	Plutonic	Plutonic	Plutonic
23	SR	M	(+)	–	–	–	–	√	(+)	(++)	Det	–	MDB	DB	moderate	Plutonic*	Met. (L-M)	Met. (L)
24	SA	3	(+)	√	–	–	–	√	(+)	(++)	Det	Bt, Kfs	MDB	MDB	slight	Met. (L-M)	Met. (L-M)	Met. (L)
25	R	M	(-)	–	–	–	–	√	(+)	(+)	Dgn	–	MB	MDB	moderate	Plutonic	Plutonic	Plutonic
26	SA	2	(+)	√	–	–	–	√	(+)	(++)	Det	–	MDB	MDB	moderate	Met. (L-M)	Met. (L); brittle deformed	Met. (L); brittle deformed
27	SR	M	(-)	–	–	–	–	√	(+)	(+)	Det/Dgn	Ilt	DB	DB	slight	Plutonic	Plutonic	Plutonic
28	SR	M	(++)	√	–	–	–	√	(+)	(++)	Det	–	MB	MB	moderate	Met. (M-H)*	Met. (L); brittle deformed	Met. (L); brittle deformed
29	SR	M	(++)	–	–	–	–	√	(+)	(-)	Dgn	Ms	MDB	DB	slight	Met. (L-M)	Met. (L-M)	Met. (L-M)
30	SA	>6	(+)	√	–	–	–	–	(-)	(-)	–	Ms	DB	DB	no	Met. (L-M)*	Met. (M-H); type 4B	Met. (M-H); type 4B
31	R	M	(+)	√	–	–	–	√	(+)	(+)	Dgn	Zrn	DB	DB	slight	Met. (L-M)	Met. (L-M)	Met. (L)
32	SR	M	(+)	√	–	–	–	√	(+)	(++)	Det	Py, Ilt	–	–	–	Met. (L-M)	Met. (L-M)	Met. (L)
33	SR	M	(+)	√	–	–	–	–	(+)	(-)	–	Ttn	DB	DB	no	Met. (M-H); type 4B	Met. (M-H); type 4B	Met. (M-H); type 4B
34	SR	M	(++)	–	–	–	–	–	(-)	(+)	Det	–	MDB	MDB	slight	Met. (L-M)	Met. (L-M)	Met. (L)
35	SR	M	(+)	–	–	–	–	–	(+)	(-)	–	–	DB	DB	slight	Plutonic*	Met. (L-M)	Met. (L-M)
36	A	M	(+)	√	–	–	–	√	(+)	(-)	–	Cal	–	–	–	Met. (L-M)	Met. (M-H); type 4B	Met. (M-H); type 4B
37	SR	M	(-)	–	–	–	–	√	(++)	(++)	Det	–	MDB	MDB	moderate	Plutonic	Plutonic	Plutonic
38	SR	3	(++)	√	–	–	–	√	(+)	(+)	Dgn	–	DB	DB	no	Met. (M-H); type 4B	Met. (M-H); type 4B	Met. (M-H); type 4B
39	SR	>8	(++)	–	–	–	–	√	(+)	(++)	Det	–	MDB	DB	moderate	Met. (L-M)	Met. (L-M)	Met. (L)
40	SR	M	(++)	–	–	–	–	–	(+)	(-)	–	–	DB	DB	no	Met. (L-M)	Met. (L-M)	Met. (L-M)

Notes: [1] Ap=apatite; Bt=biotite; Cal=calcite; Ilt=illite; Kfs=K-feldspar; Ms=muscovite; Py=pyrite;Ttn=titanite; Zrn=zircon.

[2] VDB=very dark blue; DB=dark blue; MDB=medium dark blue; MB=medium blue; BMB=bright-medium blue; BB=bright blue.

[3] * indicates that the classification from combined HCL and petrography does not match the classification from combined SEM-CL and petrography.

Table 8A: Summary data of detrital quartz grains of sample 3150 (petrography, SEM-CL image).

Grain No	Roundness (angular (A), sub-angular (SA), sub-rounded (SR), rounded (R))	Mono-/Poly-crystalline (M/no. of grains)	Extinction (None- weak+, strong++)	Mosaic texture	Deformation Lamellae	Deformarion Banding	Zoning	Overgrowth	Homo-geneous SEM-CL image	Grayscale in SEM-CL Image				Fractures (rare-,some+,common++)			Fluid Inclusion Trail		Mineral Inclusion[3]	Spiders (rare-, some+. Common++)	Bright Mottling Random, Streaky, Subtle (R/St/Sb)	Quartz Type (Met.: metamorphic; L, M, H: low, medium, high grade)
										Quartz	Epoxy	Difference (=Quartz - Epoxy)	Colour[1]	Total amount	Open fracture	Healed fracture[2]	Occurrence (rare-, some+, Common++)	Detrital/ Diagenetic (Det/Dgn)				
1	SR	M	(++)	–	–	–	–	–	√	87.3	133.1	-45.8	G	(+)	(++)	(-)	(-)	–	–	(-)	–	Met. (L-M)
2	SA	4	(++)	–	–	–	–	√	–	118.2	227.6	-109.4	D	(+)	(+)	(+)	(+)	Det	–	(-)	–	Met. (L-M)
3	SA	M	(++)	–	√	–	–	–	–	88.7	130.1	-41.4	G	(+)	(+)	(+)	(++)	Det	–	(-)	–	Met. (L-M); ductily deformed
4	SR	M	(-)	–	–	–	–	√	–	119.7	138.3	-18.6	G	(++)	(++)	(+)	(++)	Det	Ms	(+)	–	Plutonic
5	R	M	(+)	–	–	–	–	√	–	130.3	84.7	45.6	L	(++)	(+)	(++)	(++)	Det/Dgn	–	(++)	–	Plutonic
6	SA	M	(++)	–	–	–	–	√	–	88.3	135.2	-46.9	G	(++)	(+)	(+)	(++)	Det	–	(+)	–	Met. (L-M)
7	R	M	(++)	–	√	–	–	√	–	103.1	80.1	23.0	L	(++)	(+)	(++)	(++)	Det	–	(+)	–	Met. (L-M); ductily deformed
8	SR	M	(++)	–	–	√	–	√	√	117.1	77.9	39.2	L	(-)	(+)	(-)	(-)	–	–	(-)	–	Met. (L-M); ductily deformed
9	SR	>8	(++)	–	–	–	–	–	–	–	–	–	G	(+)	(+)	(+)	(++)	Det	–	(+)	–	Met. (L-M)
10	R	2	(-)	–	–	–	–	√	–	145.7	145.0	0.7	L	(++)	(+)	(++)	(++)	Det	Ms	(++)	–	Plutonic
11	SA	M	(++)	–	–	–	–	√		98.2	180.1	-81.9	G	(+)	(+)	(+)	(++)	Dgn	–	(-)	–	Met. (L-M)
12	SR	M	(+)	–	–	–	–	–	–	121.8	117.2	4.6	L	(++)	(++)	(++)	(++)	Det	Ilt	(++)	Sb	Plutonic
13	SR	M	(+)	–	–	–	–	√	–	–	–	–	G	(-)	(-)	(-)	(-)	–	–	(-)	–	Met. (L-M)
14	SR	M	(-)	–	–	–	–	√	–	114.4	167.6	-53.2	G	(+)	(+)	(+)	(++)	Det	Ms	(+)	–	Plutonic
15	SR	M	(-)	–	–	–	–	√	–	113.6	176.7	-63.1	G	(++)	(+)	(++)	(++)	Det	Ms, Mnz	(++)	–	Plutonic
16	SA	M	(+)	√	–	–	–	√	√	102.8	159.6	-56.8	G	(-)	(+)	(-)	(+)	Det/Dgn	–	(-)	–	Met. (L-M)
17	SA	M	(-)	–	–	–	–	√	–	164.4	106.6	57.8	L	(++)	(+)	(++) (O)	(++)	Det	Py	(++)	–	Met. (L); brittle deformed
18	SR	M	(++)	–	–	–	–	√	–	80.8	117.4	-36.6	G	(++)	(+)	(++)	(++)	Det	–	(-)	–	Met. (L-M)
19	SR	2	(+)	√	–	–	–	√	√	94.2	98.9	-4.7	G	(-)	(+)	(-)	(-)	–	–	(-)	–	Met. (L-M)
20	SA	3	(++)	–	–	–	–	–	–	105.2	226.0	-120.8	D	(+)	(+)	(+)	(++)	Det	–	(-)	–	Met. (L-M)
21	R	2	(+)	√	–	–	–	–	√	93.3	206.1	-112.8	D	(+)	(+)	(+)	(++)	Det	–	(-)	–	Met. (L-M)
22	SR	M	(-)	–	–	–	–	√	–	–	–	–	G	(++)	(+)	(++)	(++)	Det	–	(++)	St	Plutonic
23	SA	M	(+)	–	–	–	–	√	–	111.7	71.7	40.0	L	(++)	(+)	(++)	(++)	Det	Py	(++)	–	Plutonic
24	SR	4	(-)	√	–	–	–	√	–	121.6	118.5	3.1	L	(++)	(-)	(++)	(+)	Det	–	(++)	–	Met. (L-M)
25	SR	2	(+)	–	–	–	–	√	–	117.3	60.5	56.8	L	(++)	(+)	(++)	(+)	Det	–	(++)	–	Plutonic
26	SR	M	(++)	–	–	–	–	√	–	–	–	–	D & L	(++)	(++)	(+)	(-)	–	–	(-)	R	Met. (L-M)
27	SR	>5	(++)	–	–	–	–	√	√	126.8	110.3	16.5	L	(+)	(+)	(+)	(-)	–	–	(-)	–	Met. (L-M)
28	SA	M	(++)	–	–	–	–	√	√	66.2	114.3	-48.1	D*	(+)	(+)	(-)	(+)	Dgn	–	(-)	–	Met. (L-M)
29	R	M	(+)	–	–	–	–	√	–	108.9	146.1	-37.2	G	(++)	(++)	(++)	(++)	Det	–	(++)	–	Plutonic
30	SR	2	(++)	√	–	–	–	√	–	106.5	212.6	-106.1	D	(++)	(+)	(++) (O)	(++)	Det	–	(++)	St	Met. (L); brittle deformed
31	SR	M	(-)	–	–	–	–	√	–	126.3	141.1	-14.8	G	(++)	(++)	(++)	(++)	Det	Zrn	(++)	R	Plutonic
32	A	4	(+)	–	–	–	–	√	–	87.9	116.4	-28.5	G	(++)	(++)	(++)	(+)	Det	–	(+)	–	Plutonic
33	SR	M	(++)	–	–	–	–	√	–	–	–	–	D & L	(-)	(+)	(-)	(-)	–	–	(-)	R	Met. (L-M)
34	R	2	(+)	√	–	–	–	√	–	82.3	120.5	-38.2	G	(+)	(+)	(+) (O)	(++)	Det	–	(+)	St	Met. (L); brittle deformed
35	A	M	(-)	–	–	–	–	√	–	94.2	71.8	22.4	L	(++)	(+)	(++)	(++)	Det	Kfs	(-)	–	Plutonic
36	A	M	(++)	–	–	–	–	√	–	–	–	–	G	(+)	(+)	(+)	(+)	Det/Dgn	–	(-)	St	Met. (L-M)
37	SR	M	(++)	–	–	–	–	√	–	–	–	–	G	(++)	(++)	(++) (O)	(++)	Det/Dgn	–	(++)	St	Met. (L); brittle deformed
38	SA	4	(++)	–	–	–	–	√	–	94.7	156.1	-61.4	G	(++)	(++)	(++)	(++)	Det	–	(-)	–	Plutonic
39	SR	M	(++)	–	–	–	–	√	–	–	–	–	G	(++)	(++)	(++) (O)	(++)	Det/Dgn	–	(++)	St	Met. (L); brittle deformed
40	A	M	(-)	–	–	–	–	√	–	–	–	–	L	(++)	(+)	(++)	(++)	Det/Dgn	–	(++)	St	Plutonic

Notes: [1] D=dark gray to black SEM-CL: value of difference < -90; G=gray SEM-CL: -90 < value of difference < 0; L=light gray SEM-CL: values of difference > 0; some grains were indicated with two distinct colours because both colours were shown in SEM-CL images and it is impossible to identify one main appearance. * indicates that the observed grain colour does not match the colour in this table due to a substantial change in the contrast for the purpose of high-quality SEM-CL image.

[2] (O) was marked in cases that the grain shows microfractures with preferred orientation.

[3] Ilt=illite; Kfs=K-feldspar; Ms=muscovite; Mnz=monazite; Py=pyrite; Zrn=zircon.

Table 8B: Summary data of detrital quartz grains of sample 3150 (petrography and HCL image).

Grain No	Roundness (angular (A), sub-angular (SA), sub-rounded (SR), rounded (R))	Mono-/Poly-crystalline (M/no. of grains)	Extinction (None- weak+, strong++)	Mosaic texture	Deformation Lamellae	Deformarion Banding	Zoning	Overgrowth	Fractures (rare-, some+, Common++)	Fluid Inclusion Trail		Mineral Inclusion[1]	Hot CL			Quartz Type[3] *(from HCL & Petrography)*	Quartz Type *(from SEM-CL & Petrography)*	Final Classification
										Occurrence (rare-, some+, Common++)	Detrital/ Diagenetic (Det/Dgn)		3s colo-ur[2]	12s colo-ur[2]	Colour Shift			
1	SR	M	(++)	–	–	–	–	–	(++)	(-)	–	–	DB	DB	no	Met. (L-M)	Met. (L-M)	Met. (L-M)
2	SA	4	(++)	–	–	–	–	√	(+)	(+)	Det	–	DB	DB	slight	Met. (L-M)	Met. (L-M)	Met. (L-M)
3	SA	M	(++)	–	√	–	–	–	(+)	(++)	Det	–	DB	DB	slight	Met. (L-M)	Met. (L-M); ductily deformed	Met. (L-M); ductily deformed
4	SR	M	(-)	–	–	–	–	√	(++)	(++)	Det	Ms	MDB	MDB	slight	Plutonic	Plutonic	Plutonic
5	R	M	(+)	–	–	–	–	√	(+)	(++)	Det/Dgn	–	BB	BB	moderate	Plutonic	Plutonic	Plutonic
6	SA	M	(++)	–	–	–	–	√	(+)	(++)	Det	–	MDB	DB	moderate	Met. (L-M)	Met. (L-M)	Met. (L-M)
7	R	M	(++)	–	√	–	–	√	(+)	(++)	Det	–	BB	BB	strong	Met. (M-H); type 4A*	Met. (L-M); ductily deformed	Met. (L-M); ductily deformed
8	SR	M	(++)	–	–	√	–	√	(+)	(-)	–	–	MDB	MDB	moderate	Met. (L-M)	Met. (L-M); ductily deformed	Met. (L-M); ductily deformed
9	SR	>8	(++)	–	–	–	–	–	(+)	(++)	Det	–	MDB	MDB	slight	Met. (L-M)	Met. (L-M)	Met. (L-M)
10	R	2	(-)	–	–	–	–	√	(+)	(++)	Det	Ms	MDB	MDB	slight	Plutonic	Plutonic	Plutonic
11	SA	M	(++)	–	–	–	–	√	(+)	(++)	Dgn	–	MDB	DB	no	Met. (L-M)	Met. (L-M)	Met. (L-M)
12	SR	M	(+)	–	–	–	–	–	(++)	(++)	Det	Ilt	BB	BB	moderate	Plutonic	Plutonic	Plutonic
13	SR	M	(+)	–	–	–	–	√	(-)	(-)	–	–	MDB	DB	slight	Plutonic*	Met. (L-M)	Met. (L-M)
14	SR	M	(-)	–	–	–	–	√	(+)	(++)	Det	Ms	DB	DB	slight	Plutonic	Plutonic	Plutonic
15	SR	M	(-)	–	–	–	–	√	(+)	(++)	Det	Ms, Mnz	DB	DB	no	Plutonic	Plutonic	Plutonic
16	SA	M	(+)	√	–	–	–	√	(+)	(+)	Det/Dgn	–	DB	DB	no	Met. (L-M)	Met. (L-M)	Met. (L-M)
17	SA	M	(-)	–	–	–	–	√	(+)	(++)	Det	Py	MDB	MDB	moderate	Plutonic*	Met. (L); brittle deformed	Met. (L); brittle deformed
18	SR	M	(++)	–	–	–	–	√	(+)	(++)	Det	–	DB	DB	slight	Met. (L-M)	Met. (L-M)	Met. (L-M)
19	SR	2	(+)	√	–	–	–	√	(+)	(-)	–	–	MDB	MDB	slight	Met. (L-M)	Met. (L-M)	Met. (L-M)
20	SA	3	(++)	–	–	–	–	–	(+)	(++)	Det	–	DB	DB	slight	Met. (L-M)	Met. (L-M)	Met. (L-M)
21	R	2	(+)	√	–	–	–	–	(+)	(++)	Det	–	DB	DB	no	Met. (L-M)	Met. (L-M)	Met. (L-M)
22	SR	M	(-)	–	–	–	–	√	(+)	(++)	Det	–	DB	DB	slight	Plutonic	Plutonic	Plutonic
23	SA	M	(+)	–	–	–	–	√	(+)	(++)	Det	Py	MDB	MDB	slight	Plutonic	Plutonic	Plutonic
24	SR	4	(-)	√	–	–	–	√	(-)	(+)	Det	–	MB	MB	moderate	Met. (M-H); type 4A	Met. (L-M)	Met. (M-H); type 4A
25	SR	2	(+)	–	–	–	–	√	(+)	(+)	Det	–	MB	MB	moderate	Plutonic	Plutonic	Plutonic
26	SR	M	(++)	–	–	–	–	√	(++)	(-)	–	–	MDB	DB	slight	Met. (L-M)	Met. (L-M)	Met. (L-M)
27	SR	>5	(++)	–	–	–	–	√	(+)	(-)	–	–	MB	MB	moderate	Met. (M-H); type 4A	Met. (L-M)	Met. (M-H); type 4A
28	SA	M	(++)	–	–	–	–	√	(+)	(+)	Dgn	–	DB	DB	no	Met. (L-M)	Met. (L-M)	Met. (L-M)
29	R	M	(+)	–	–	–	–	√	(++)	(++)	Det	–	MDB	MB	moderate	Plutonic	Plutonic	Plutonic
30	SR	2	(++)	√	–	–	–	√	(+)	(++)	Det	–	DB	DB	slight	Met. (L-M)	Met. (L); brittle deformed	Met. (L); brittle deformed
31	SR	M	(-)	–	–	–	–	√	(++)	(++)	Det	Zrn	MB	MB	moderate	Plutonic	Plutonic	Plutonic
32	A	4	(+)	–	–	–	–	√	(++)	(+)	Det	–	MDB	DB	slight	Met. (L-M)*	Plutonic	Plutonic
33	SR	M	(++)	–	–	–	–	√	(+)	(-)	–	–	DB	DB	no	Met. (L-M)	Met. (L-M)	Met. (L-M)
34	R	2	(+)	√	–	–	–	√	(+)	(++)	Det	–	MDB	DB	slight	Met. (L-M)	Met. (L); brittle deformed	Met. (L); brittle deformed
35	A	M	(-)	–	–	–	–	√	(+)	(++)	Det	Kfs	MDB	BMB	moderate	Plutonic	Plutonic	Plutonic
36	A	M	(++)	–	–	–	–	√	(+)	(+)	Det/Dgn	–	MDB	MDB	slight	Met. (L-M)	Met. (L-M)	Met. (L-M)
37	SR	M	(++)	–	–	–	–	√	(++)	(++)	Det/Dgn	–	MDB	DB	slight	Met. (L-M)	Met. (L); brittle deformed	Met. (L); brittle deformed
38	SA	4	(++)	–	–	–	–	√	(++)	(++)	Det	–	MDB	DB	slight	Met. (L-M)*	Plutonic	Plutonic
39	SR	M	(++)	–	–	–	–	√	(++)	(++)	Det/Dgn	–	–	–	–	Met. (L-M)	Met. (L); brittle deformed	Met. (L); brittle deformed
40	A	M	(-)	–	–	–	–	√	(+)	(++)	Det/Dgn	–	MB	MDB	no	Plutonic	Plutonic	Plutonic

Notes: [1] Ilt=illite; Kfs=K-feldspar; Ms=muscovite; Mnz=monazite; Py=pyrite; Zrn=zircon.

[2] VDB=very dark blue; DB=dark blue; MDB=medium dark blue; MB=medium blue; BMB=bright-medium blue; BB=bright blue.

[3] * indicates that the classification from combined HCL and petrography does not match the classification from combined SEM-CL and petrography.

Table 9A: Summary data of detrital quartz grains of sample 3425 (petrography and SEM-CL image).

Grain No	Roundness (angular (A), sub-angular (SA), sub-rounded (SR), rounded (R))	Mono-/Poly-crystalline (M/no. of grains)	Extinction (None- weak+, strong++)	Mosaic Texture	Deformation Lamellae	Deformarion Banding	Zoning	Overgrowth	Homo-geneous SEM-CL image	Grayscale in SEM-CL Image				Fractures (rare-,some+,common++)			Fluid Inclusion Trail		Mineral Inclusion[3]	Spiders (rare-, some+. Common ++)	Bright Mottling Random, Streaky, Subtle (R/St/Sb)	Quartz Type (Met.: metamorphic; L, M, H: low, medium, high grade)
										Quartz	Epoxy	Difference (=Quartz - Epoxy)	Colour[1]	Total amount	Open fracture	Healed fracture[2]	Occurrence (rare-, some+, Common++)	Detrital/ Diagenetic (Det/Dgn)				
1	SR	M	(++)	–	–	–	–	√	√	88.1	63.4	24.7	G	(++)	(++)	(+)	(++)	Det	–	(-)	–	Met. (L-M)
2	SR	M	(++)	–	–	–	–	–	–	76.5	92.5	-16.0	D	(++)	(++)	(-)	(-)	Det	–	(-)	–	Met. (L-M)
3	SR	M	(+)	–	–	–	–	√	–	195.2	110.1	85.1	L	(++)	(++)	(++) (O)	(++)	Dgn	Bt	(-)	St	Met. (L); brittle deformed
4	SR	2	(++)	–	–	–	–	–	–	113.7	167.8	-54.1	D*	(++)	(++)	(++) (O)	(++)	Det	–	(-)	St	Met. (L); brittle deformed
5	SA	M	(+)	–	√	–	–	√	–	–	–	–	L	(++)	(+)	(+)	(+)	Det	–	(-)	St	Met. (L-M); ductily deformed
6	SR	M	(++)	–	–	–	–	–	–	114.1	144.4	-30.3	G	(++)	(++)	(-)	(+)	Det	–	(-)	Sb	Met. (L-M)
7	SR	2	(+)	√	–	–	–	–	√	92.7	185.1	-92.4	D	(-)	(-)	(-)	(-)	–	–	(-)	–	Met. (M-H); type 5B
8	R	M	(+)	√	–	–	–	–	√	127.9	229.1	-101.2	D	(+)	(+)	(+)	(++)	Det	–	(-)	–	Met. (L-M)
9	SR	>4	(+)	√	–	–	–	√	√	126.0	190.4	-64.4	G	(+)	(+)	(-)	(-)	–	–	(-)	–	Met. (L-M)
10	R	M	(+)	–	–	–	–	√	√	93	202.5	-109.5	G	(++)	(++)	(-)	(+)	Det	–	(-)	–	Met. (L-M)
11	SR	>10	(+)	√	–	–	–	–	√	88.7	197.7	-109.0	D	(+)	(+)	(-)	(+)	Det	–	(-)	–	Met. (M-H); type 5B
12	SR	M	(++)	–	√	–	–	–	–	139.9	133.5	6.4	G	(+)	(+)	(+)	(+)	Det	–	(+)	–	Met. (L-M); ductily deformed
13	SR	M	(++)	–	–	–	–	√	–	105.5	134.1	-28.6	G	(+)	(+)	(+)	(++)	Det/Dgn	Chl	(+)	–	Met. (L-M)
14	SR	>6	(++)	–	–	–	–	–	√	119.2	222	-102.8	D	(+)	(+)	(-)	(++)	Det	–	(-)	–	Met. (M-H); type 5B
15	SA	M	(-)	–	–	–	–	√	–	122.3	54.4	67.9	L	(+)	(+)	(+)	(++)	Det	–	(+)	–	Plutonic
16	SR	>5	(++)	–	–	–	–	√	–	104.5	132.2	-27.7	G	(++)	(+)	(++)	(++)	Det	–	(-)	–	Met. (L-M)
17	A	M	(+)	–	–	–	–	√	–	157.6	57.9	99.7	L	(+)	(+)	(++) (O)	(++)	Det	Bt	(-)	–	Met. (L); brittle deformed
18	R	M	(++)	–	–	–	–	–	√	87.4	195.5	-108.1	D	(-)	(-)	(-)	(+)	Det	–	(-)	–	Met. (L-M)
19	SR	>7	(+)	√	–	–	–	–	–	86.8	139.1	-52.3	G	(-)	(+)	(-)	(-)	–	–	(-)	Sb	Met. (L-M)
20	SR	>10	(+)	√	–	–	–	–	√	114.4	198.5	-84.1	D	(+)	(+)	(-)	(-)	–	–	(-)	–	Met. (M-H); type 5B
21	A	M	(++)	–	–	–	–	√	–	139.3	47.8	91.5	L	(-)	(+)	(-)	(+)	Dgn	–	(+)	–	Met. (L-M)
22	SR	M	(-)	–	–	–	–	√	–	151.9	34.2	117.7	L	(+)	(-)	(+)	(++)	Det	–	(+)	–	Plutonic
23	SR	>10	(+)	√	–	–	–	–	√	72.1	187.1	-115.0	D	(-)	(-)	(-)	(+)	Det	–	(-)	–	Met. (M-H); type 5B
24	R	M	(+)	–	–	–	–	√	–	81.1	204.3	-123.2	G	(++)	(++)	(-)	(+)	Det	Ttn	(-)	St	Met. (L-M)
25	SR	M	(+)	–	–	–	–	–	–	102.7	199.5	-96.8	D	(+)	(+)	(-)	(-)	–	–	(-)	Sb	Met. (L-M)
26	SA	>6	(+)	√	–	–	–	–	–	105.5	203.7	-98.2	D	(++)	(++)	(+)	(-)	–	Chl	(-)	–	Met. (M-H); type 5B
27	SA	M	(-)	–	–	–	–	√	–	136.8	83.3	53.5	L	(++)	(++)	(+)	(+)	Det	–	(+)	R	Plutonic
28	SR	M	(+)	–	–	–	–	–	√	82.5	224.8	-142.3	D	(++)	(++)	(-)	(++)	Det	–	(-)	–	Met. (L-M)
29	SR	>10	(+)	√	–	–	–	–	√	78.5	112.3	-33.8	G	(-)	(+)	(-)	(-)	–	–	(-)	Sb	Met. (M-H); type 5B
30	SR	M	(++)	–	–	–	–	√	–	–	–	–	G	(++)	(++)	(-)	(+)	Det	–	(-)	St	Met. (L-M)
31	SA	M	(+)	–	–	–	–	√	–	138.7	24.8	113.9	L	(-)	(+)	(+)	(-)	–	Bt	(+)	–	Plutonic
32	SA	>7	(+)	√	–	–	–	–	√	103.5	206.4	-102.9	D	(-)	(-)	(-)	(-)	–	Chloritized Ms. Bt	(-)	–	Met. (M-H); type 5B
33	SA	2	(++)	–	√	–	–	√	–	92.1	88.1	4.0	G	(+)	(+)	(+)	(+)	Det	–	(+)	–	Met. (L-M); ductily deformed
34	SR	M	(+)	√	–	–	–	√	–	68.5	165.1	-96.6	D	(++)	(++)	(+)	(+)	Det/Dgn	–	(-)	Sb	Met. (L-M)
35	SR	M	(+)	√	–	–	–	–	–	84.8	51.2	33.6	G	(++)	(++)	(+)	(++)	Det/Dgn	–	(+)	–	Met. (L-M)
36	SR	3	(+)	√	–	–	–	√	–	133.3	38.2	95.1	L	(++)	(++)	(++)	(++) (O)	Det	–	(++)	–	Met. (L); brittle deformed
37	SR	M	(++)	√	–	–	–	√	√	86.5	121	-34.5	G	(-)	(+)	(-)	(-)	–	–	(-)	–	Met. (L-M)
38	SA	M	(-)	–	–	–	–	√	√	180.2	41.6	138.6	L	(-)	(+)	(-)	(-)	Dgn	–	(-)	–	Plutonic
39	SR	M	(++)	–	–	–	–	–	√	48	145.5	-97.5	D	(+)	(+)	(-)	(+)	Det	–	(-)	–	Met. (L-M)
40	SR	M	(++)	–	–	–	–	√	–	144.8	33	111.8	L	(++)	(++)	(++)	(++)	Det/Dgn	–	(++)	–	Plutonic

Notes: [1] D=dark gray to black SEM-CL: value of difference < -80; G=gray SEM-CL: -80 < value of difference < 50; L=light gray SEM-CL: values of difference > 50. * indicates that the observed grain colour does not match the colour in this table due to a substantial change in the contrast for the purpose of high-quality SEM-CL image.

[2] (O) was marked in cases that the grain shows microfractures with preferred orientation.

[3] Bt=biotite; Chl=chlorite; Ms=muscovite; Ttn=titanite.

Table 9B: Summary data of detrital quartz grains of sample 3425 (petrography and HCL image).

Grain No	Roundness (angular (A), sub-angular (SA), sub-rounded (SR), rounded (R))	Mono-/Poly-crystalline (M/no. of grains)	Extinction (None- weak+, strong++)	Mosaic Texture	Deformation Lamellae	Deformarion Banding	Zoning	Overgrowth	Fractures (rare-, some+, Common++)	Fluid Inclusion Trail		Mineral Inclusion[1]	HCL			Quartz Type[3] *(from HCL & Petrography)*	Quartz Type *(from SEM-CL & Petrography)*	Final Classification
										Occurrence (rare-, some+, Common++)	Detrital/ Diagenetic (Det/Dgn)		3s colo-ur[2]	12s colo-ur[2]	Colour Shift			
1	SR	M	(++)	–	–	–	–	√	(++)	(++)	Det	–	DB	MDB	no	Met. (L-M)	Met. (L-M)	Met. (L-M)
2	SR	M	(++)	–	–	–	–	–	(++)	(-)	Det	–	DB	DB	no	Met. (L-M)	Met. (L-M)	Met. (L-M)
3	SR	M	(+)	–	–	–	–	√	(++)	(++)	Dgn	Bt	MDB	DB	strong	Met. (L-M)	Met. (L); brittle deformed	Met. (L); brittle deformed
4	SR	2	(++)	–	–	–	–	–	(++)	(++)	Det	–	DB	DB	no	Met. (L-M)	Met. (L); brittle deformed	Met. (L); brittle deformed
5	SA	M	(+)	–	√	–	–	√	(+)	(+)	Det	–	MDB	MDB	slight	Met. (L-M)	Met. (L-M); ductily deformed	Met. (L-M); ductily deformed
6	SR	M	(++)	–	–	–	–	–	(++)	(+)	Det	–	MDB	DB	moderate	Met. (L-M)	Met. (L-M)	Met. (L-M)
7	SR	2	(+)	√	–	–	–	–	(-)	(-)	–	–	DB	DB	no	Met. (M-H); type 4B	Met. (M-H); type 4B	Met. (M-H); type 4B
8	R	M	(+)	√	–	–	–	–	(+)	(++)	Det	–	DB	DB	no	Met. (L-M)	Met. (L-M)	Met. (L-M)
9	SR	>4	(+)	√	–	–	–	√	(+)	(-)	–	–	DB	DB	slight	Met. (L-M)	Met. (L-M)	Met. (L-M)
10	R	M	(+)	–	–	–	–	√	(++)	(+)	Det	–	DB	DB	no	Met. (L-M)	Met. (L-M)	Met. (L-M)
11	SR	>10	(+)	√	–	–	–	–	(+)	(+)	Det	–	DB	DB	no	Met. (M-H); type 4B	Met. (M-H); type 4B	Met. (M-H); type 4B
12	SR	M	(++)	–	√	–	–	–	(+)	(+)	Det	–	MDB	MDB	slight	Met. (L-M)	Met. (L-M); ductily deformed	Met. (L-M); ductily deformed
13	SR	M	(++)	–	–	–	–	√	(+)	(++)	Det/Dgn	Chl	DB	DB	no	Met. (L-M)	Met. (L-M)	Met. (L-M)
14	SR	>6	(++)	–	–	–	–	–	(+)	(++)	Det	–	DB	DB	no	Met. (M-H); type 4B	Met. (M-H); type 4B	Met. (M-H); type 4B
15	SA	M	(-)	–	–	–	–	√	(+)	(++)	Det	–	MB	MDB	slight	Plutonic	Plutonic	Plutonic
16	SR	>5	(++)	–	–	–	–	√	(+)	(++)	Det	–	DB	DB	no	Met. (L-M)	Met. (L-M)	Met. (L-M)
17	A	M	(+)	–	–	–	–	√	(+)	(++)	Det	Bt	–	–	–	Met. (L) or Plutonic	Met. (L); brittle deformed	Met. (L); brittle deformed
18	R	M	(++)	–	–	–	–	–	(-)	(+)	Det	–	–	–	–	Met. (L-M)	Met. (L-M)	Met. (L-M)
19	SR	>7	(+)	√	–	–	–	–	(+)	(-)	–	–	DB	DB	no	Met. (L-M)	Met. (L-M)	Met. (L-M)
20	SR	>10	(+)	√	–	–	–	–	(+)	(-)	–	–	DB	DB	no	Met. (M-H); type 4B	Met. (M-H); type 4B	Met. (M-H); type 4B
21	A	M	(++)	–	–	–	–	√	(+)	(+)	Dgn	–	MDB	DB	slight	Met. (L-M)	Met. (L-M)	Met. (L-M)
22	SR	M	(-)	–	–	–	–	√	(-)	(++)	Det	–	MDB	MB	no	Plutonic	Plutonic	Plutonic
23	SR	>10	(+)	√	–	–	–	–	(-)	(+)	Det	–	VDB	VDB	no	Met. (M-H); type 4B	Met. (M-H); type 4B	Met. (M-H); type 4B
24	R	M	(+)	–	–	–	–	√	(++)	(+)	Det	Ttn	DB	DB	no	Met. (L-M)	Met. (L-M)	Met. (L-M)
25	SR	M	(+)	–	–	–	–	–	(+)	(-)	–	–	DB	DB	no	Met. (L-M)	Met. (L-M)	Met. (L-M)
26	SA	>6	(+)	√	–	–	–	–	(++)	(-)	–	Chl	DB	DB	no	Met. (M-H); type 4B	Met. (M-H); type 4B	Met. (M-H); type 4B
27	SA	M	(-)	–	–	–	–	√	(++)	(+)	Det	–	MDB	DB	slight	Plutonic	Plutonic	Plutonic
28	SR	M	(+)	–	–	–	–	–	(++)	(++)	Det	–	VDB	VDB	no	Met. (L-M)	Met. (L-M)	Met. (L-M)
29	SR	>10	(+)	√	–	–	–	–	(+)	(-)	–	–	–	–	–	Met. (M-H); type 4B	Met. (M-H); type 4B	Met. (M-H); type 4B
30	SR	M	(++)	–	–	–	–	√	(++)	(+)	Det	–	DB	DB	moderate	Met. (L-M)	Met. (L-M)	Met. (L-M)
31	SA	M	(+)	–	–	–	–	√	(+)	(-)	–	Bt	MDB	MDB	slight	Plutonic	Plutonic	Plutonic
32	SA	>7	(+)	√	–	–	–	–	(-)	(-)	–	Chloritized Ms. Bt	DB	DB	no	Met. (M-H); type 4B	Met. (M-H); type 4B	Met. (M-H); type 4B
33	SA	2	(++)	–	√	–	–	√	(+)	(+)	Det	–	DB	DB	slight	Met. (L-M)	Met. (L-M); ductily deformed	Met. (L-M); ductily deformed
34	SR	M	(+)	√	–	–	–	√	(++)	(+)	Det/Dgn	–	DB	DB	slight	Met. (L-M)	Met. (L-M)	Met. (L-M)
35	SR	M	(+)	√	–	–	–	–	(++)	(++)	Det/Dgn	–	MB	MDB	slight	Plutonic*	Met. (L-M)	Met. (L-M)
36	SR	3	(+)	√	–	–	–	√	(++)	(++) (O)	Det	–	BMB	MB	moderate	Met. (M-H)*	Met. (L); brittle deformed	Met. (L); brittle deformed
37	SR	M	(++)	√	–	–	–	√	(+)	(-)	–	–	DB	DB	slight	Met. (L-M)	Met. (L-M)	Met. (L-M)
38	SA	M	(-)	–	–	–	–	√	(+)	(-)	Dgn	–	MB	MB	moderate	Plutonic	Plutonic	Plutonic
39	SR	M	(++)	–	–	–	–	–	(+)	(+)	Det	–	DB	DB	slight	Met. (L-M)	Met. (L-M)	Met. (L-M)
40	SR	M	(++)	–	–	–	–	√	(++)	(++)	Det/Dgn	–	MB	MDB	slight	Met. (L-M)*	Plutonic	Plutonic

Notes: [1] Bt=biotite; Chl=chlorite; Ms=muscovite; Ttn=titanite.

[2] VDB=very dark blue; DB=dark blue; MDB=medium dark blue; MB=medium blue; BMB=bright-medium blue; BB=bright blue.

[3] * indicates that the classification from combined HCL and petrography does not match the classification from combined SEM-CL and petrography.

Table 10A: Summary data of detrital quartz grains of sample 3900 (petrography and SEM-CL image).

Grain No	Roundness (angular (A), sub-angular (SA), sub-rounded (SR), rounded (R))	Mono-/Poly-crystalline (M/no. of grains)	Extinction (None- weak+, strong++)	Mosaic texture	Deformation Lamellae	Deformarion Banding	Zoning	Overgrowth	Homo-geneous SEM-CL Image	Grayscale in SEM-CL Image				Fractures (rare-,some+,common++)			Fluid Inclusion Trail		Mineral Inclusion[3]	Spiders (rare-, some+. Common ++)	Bright Mottling Random, Streaky, Subtle (R/St/Sb)	Quartz Type (Met.: metamorphic; L, M, H: low, medium, high grade)
										Quartz	Epoxy	Difference (=Quartz - Epoxy)	Colour[1]	Total amount	Open fracture	Healed fracture[2]	Ocurrence (rare-, some+, Common++)	Detrital/ Diagenetic (Det/Dgn)				
1	SR	M	(-)	–	–	–	–	–	–	138.8	157.2	-18.4	L	(+)	(+)	(-)	(+)	Det	Ilt, Ap, Py	(+)	–	Plutonic
2	SR	M	(++)	–	–	–	–	–	–	101.5	184.7	-83.2	G	(-)	(-)	(+)	(+)	Det	Ilt, Py	(-)	R	Met. (L-M)
3	SR	M	(++)	–	–	–	–	–	√	122.3	179.5	-57.2	D*	(-)	(-)	(-)	(-)	–	Cal	(-)	–	Met. (L-M)
4	SR	M	(++)	–	–	–	–	–	–	143.2	237.2	-94.0	D	(-)	(-)	(-)	(-)	–	Ms	(-)	R	Met. (L-M)
5	SR	M	(-)	–	–	–	–	√	–	204.1	223.7	-19.6	L	(++)	(++)	(++)	(++)	Det	–	(++)	–	Plutonic
6	SR	M	(-)	–	–	–	–	–	–	–	–	–	G	(+)	(+)	(+)	(++)	Det	–	(-)	R	Plutonic
7	R	M	(-)	–	–	–	–	√	√	186.4	20.3	166.1	L	(-)	(-)	(-)	(++)	Dgn	Fe oxide, Hc	(-)	–	Met. (L-M)
8	SR	>9	(++)	–	–	–	–	–	–	–	–	–	G	(++)	(+)	(+) (O)	(+)	Det	–	(++)	R	Met. (L); brittle deformed
9	SR	M	(++)	–	–	–	–	–	–	105.5	177.6	-72.1	G	(++)	(++)	(++)	(++)	Det	–	(+)	R	Met. (L-M)
10	SR	>9	(+)	√	–	–	–	–	–	113.6	242.9	-129.3	D	(+)	(+)	(-)	(++)	Det	–	(-)	Sb	Met. (M-H); type 4B
11	SA	2	(++)	–	√	–	–	–	–	115.6	224.0	-108.4	G	(++)	(+)	(++)	(++)	Det	–	(-)	–	Met. (L-M); ductily
12	SA	M	(++)	–	–	–	–	–	–	–	–	–	–	(+)	(-)	(++)	(-)	–	Bt	(-)	R	Met. (L-M)
13	R	M	(+)	–	–	–	–	–	–	150.7	170.4	-19.7	L	(+)	(-)	(+)	(+)	Det	–	(+)	–	Plutonic
14	SA	M	(-)	–	–	–	–	–	–	120.3	198.1	-77.8	G	(+)	(+)	(+)	(-)	–	Ap	(+)	–	Plutonic
15	A	3	(-)	–	–	–	–	–	–	104.6	216.2	-111.6	G	(+)	(+)	(++)	(+)	Det	Kln, Py, kfs	(++)	–	Plutonic
16	R	M	(+)	√	–	–	–	√	–	132.1	181.9	-49.8	L	(+)	(+)	(++) (O)	(+)	Det/Dgn	–	(+)	St	Met. (L); brittle deformed
17	SR	M	(-)	–	–	–	–	√	–	170.6	189.9	-19.3	L	(++)	(+)	(++)	(++)	Det	–	(++)	–	Plutonic
18	A	6	(++)	–	–	–	–	–	√	91.7	184.6	-92.9	D	(+)	(+)	(-)	(+)	Det	–	(-)	Sb	Met. (L-M)
19	SR	M	(+)	√	–	–	–	–	–	90.9	155.1	-64.2	G	(+)	(+)	(-)	(+)	Det	Ms	(-)	St	Met. (L-M)
20	SR	5	(+)	√	–	–	–	–	–	119.7	229.7	-110.0	G	(+)	(+)	(+)	(+)	Det	Ilt, Kfs, Bt, Py	(+)	–	Met. (L-M)
21	R	M	(+)	√	–	–	–	√	–	196.7	181.7	15.0	L	(++)	(++)	(++) (O)	(++)	Det	–	(++)	–	Met. (L); brittle deformed
22	R	M	(+)	–	–	–	–	√	–	140.4	142.7	-2.3	L	(++)	(-)	(++) (O)	(++)	Det	Ms	(++)	–	Plutonic
23	SA	M	(++)	–	–	–	–	√	–	140.2	243.5	-103.3	G	(++)	(+)	(++) (O)	(-)	–	Pl	(++)	–	Met. (L); brittle deformed
24	SR	M	(++)	√	–	–	–	–	–	138.9	224.1	-85.2	G	(++)	(+)	(++) (O)	(++)	Det	–	(++)	–	Met. (L); brittle deformed
25	SR	M	(+)	√	–	–	–	–	–	118.3	177.1	-58.8	G	(+)	(-)	(++)	(-)	–	Ms, Py, Ab	(-)	R	Met. (L-M)
26	SA	M	(+)	–	–	–	–	√	–	146.8	227.4	-80.6	G	(+)	(+)	(+)	(-)	–	Zrn	(+)	–	Plutonic
27	SR	M	(+)	–	–	–	–	–	–	132.4	142.4	-10.0	L	(++)	(+)	(++) (O)	(++)	Det	Zrn, Py	(+)	St	Met. (L); brittle deformed
28	R	M	(+)	–	–	–	–	–	–	138.9	196.4	-57.5	G	(+)	(++)	(+)	(+)	Det	–	(+)	–	Plutonic
29	SR	M	(++)	–	–	–	–	√	–	111.2	99.5	11.7	L	(+)	(-)	(++)	(+)	Det	–	(++)	Sb	Met. (L-M)
30	R	M	(++)	√	–	–	–	√	–	85.5	78.9	6.6	G*	(-)	(+)	(-)	(+)	Det	–	(-)	Sb	Met. (L-M)
31	SR	M	(-)	–	–	–	–	–	–	165.2	184.4	-19.2	L*	(++)	(-)	(++)	(++)	Det	–	(++)	–	Plutonic
32	SR	M	(-)	–	–	–	–	–	–	121.9	166.7	-44.8	G	(+)	(+)	(+)	(++)	Det	–	(+)	–	Plutonic
33	SR	M	(-)	–	–	–	–	–	–	160.5	192.9	-32.4	L	(++)	(++)	(+)	(+)	Det	–	(+)	–	Plutonic
34	R	M	(+)	–	–	–	–	–	–	100.4	204.5	-104.1	D	(++)	(++)	(-)	(-)	–	–	(-)	Sb	Met. (L-M)
35	SA	4	(+)	√	–	–	–	–	–	106.6	85.6	21.0	G	(++)	(+)	(++)	(+)	Det	–	(-)	–	Met. (L-M)
36	SR	M	(+)	–	–	–	–	√	√	136.6	155.8	-19.2	L	(-)	(+)	(-)	(+)	Dgn	–	(-)	–	Met. (L-M)
37	SA	M	(+)	–	–	–	–	–	√	111.9	246.5	-134.6	D	(+)	(+)	(-)	(+)	Det	Py, Kln	(-)	Sb	Met. (L-M)
38	SR	5	(++)	–	√	–	–	–	–	197.7	172.0	25.7	L	(++)	(+)	(++) (O)	(++)	Det	–	(++)	–	Met. (L-M); ductily
39	SA	M	(+)	√	–	–	–	–	–	–	–	–	L	(++)	(-)	(++) (O)	(++)	Det	–	(++)	–	Met. (L); brittle deformed
40	SR	M	(+)	√	–	–	–	–	–	–	–	–	–	–	(-)	–	(+)	Det	–	–	–	Met. (L-M)

Notes: [1] D=dark gray to black SEM-CL: value of difference < -90; G=gray SEM-CL: -90 < value of difference < -20; L=light gray SEM-CL: values of difference >-20. * indicates that the observed grain colour does not match the colour in this table due to a substantial change in the contrast for the purpose of high-quality SEM-CL image.

[2] (O) was marked in cases that the grain shows microfractures with preferred orientation.

[3] Ab=albite; Ap=apatite; Bt=biotite; Cal=calcite; Hc=hercynite; Ilt=illite; Kfs=K-feldspar; Kln=kaolinite;Ms=muscovite; Pl=plagioclase; Py=pyrite; Zrn=zircon.

Table 10B: Summary data of detrital quartz grains of sample 3900 (petrography and HCL image).

Grain No	Roundness (angular (A), sub-angular (SA), sub-rounded (SR), rounded (R))	Mono-/Poly-crystalline (M/no. of grains)	Extinction (None- weak+, strong++)	Mosaic Texture	Deformation Lamellae	Deformarion Banding	Zoning	Overgrowth	Fractures (rare-, some+, Common++)	Fluid Inclusion Trail		Mineral Inclusion[1]	HCL			Quartz Type[3] *(from HCL & Petrography)*	Quartz Type *(from SEM-CL & Petrography)*	Final Classification
										Occurrence (rare-, some+, Common++)	Detrital/ Diagenetic (Det/Dgn)		3s colo-ur[2]	12s colo-ur[2]	Colour Shift			
1	SR	M	(-)	–	–	–	–	–	(+)	(+)	Det	Ilt, Ap, Py	MB	MDB	moderate	Plutonic	Plutonic	Plutonic
2	SR	M	(++)	–	–	–	–	–	(-)	(+)	Det	Ilt, Py	MDB	MDB	no	Met. (L-M)	Met. (L-M)	Met. (L-M)
3	SR	M	(++)	–	–	–	–	–	(-)	(-)	–	Cal	DB	DB	no	Met. (L-M)	Met. (L-M)	Met. (L-M)
4	SR	M	(++)	–	–	–	–	–	(-)	(-)	–	Ms	DB	DB	slight	Met. (L-M)	Met. (L-M)	Met. (L-M)
5	SR	M	(-)	–	–	–	–	√	(++)	(++)	Det	–	MB	MDB	moderate	Plutonic	Plutonic	Plutonic
6	SR	M	(-)	–	–	–	–	–	(+)	(++)	Det	–	MDB	DB	slight	Plutonic	Plutonic	Plutonic
7	R	M	(-)	–	–	–	–	√	(-)	(++)	Dgn	Fe oxide, Hc	BB	BB	no	Plutonic*	Met. (L-M)	Met. (L-M)
8	SR	>9	(++)	–	–	–	–	–	(+)	(+)	Det	–	MDB	MDB	slight	Met. (L-M)	Met. (L); brittle deformed	Met. (L); brittle deformed
9	SR	M	(++)	–	–	–	–	–	(++)	(++)	Det	–	MDB	MDB	slight	Met. (L-M)	Met. (L-M)	Met. (L-M)
10	SR	>9	(+)	√	–	–	–	–	(+)	(++)	Det	–	DB	DB	no	Met. (L-M)*	Met. (M-H); type 4B	Met. (M-H); type 4B
11	SA	2	(++)	–	√	–	–	–	(+)	(++)	Det	–	DB	DB	slight	Met. (L-M)	Met. (L-M); ductily	Met. (L-M); ductily
12	SA	M	(++)	–	–	–	–	–	(-)	(-)	–	Bt	MB	MDB	moderate	Met. (M-H); type 4A	Met. (L-M)	Met. (M-H); type 4A
13	R	M	(+)	–	–	–	–	–	(-)	(+)	Det	–	BB	BB	moderate	Plutonic	Plutonic	Plutonic
14	SA	M	(-)	–	–	–	–	–	(+)	(-)	–	Ap	–	–	–		Plutonic	Plutonic
15	A	3	(-)	–	–	–	–	–	(+)	(+)	Det	Kln, Py, Kfs	MB	MDB	moderate	Plutonic	Plutonic	Plutonic
16	R	M	(+)	√	–	–	–	√	(+)	(+)	Det/Dgn	–	BB	BMB	moderate	Met. (M-H); type 4A*	Met. (L); brittle deformed	Met. (L); brittle deformed
17	SR	M	(-)	–	–	–	–	√	(+)	(++)	Det	–	MDB	MDB	moderate	Plutonic	Plutonic	Plutonic
18	A	6	(++)	–	–	–	–	–	(+)	(+)	Det	–	DB	DB	slight	Met. (L-M)	Met. (L-M)	Met. (L-M)
19	SR	M	(+)	√	–	–	–	–	(+)	(+)	Det	Ms	DB	DB	slight	Met. (L-M)	Met. (L-M)	Met. (L-M)
20	SR	5	(+)	√	–	–	–	–	(+)	(+)	Det	Ilt, Kfs, Bt, Py	MDB	MDB	moderate	Met. (L-M)	Met. (L-M)	Met. (L-M)
21	R	M	(+)	√	–	–	–	√	(++)	(++)	Det	–	BB	BB	moderate	Met. (M-H)*	Met. (L); brittle deformed	Met. (L); brittle deformed
22	R	M	(+)	–	–	–	–	√	(-)	(++)	Det	Ms	MB	MB	moderate	Plutonic	Plutonic	Plutonic
23	SA	M	(++)	–	–	–	–	√	(+)	(-)	–	Pl	MDB	DB	slight	Met. (L-M)	Met. (L); brittle deformed	Met. (L); brittle deformed
24	SR	M	(++)	√	–	–	–	–	(+)	(++)	Det	–	MDB	MDB	slight	Met. (L-M)	Met. (L); brittle deformed	Met. (L); brittle deformed
25	SR	M	(+)	√	–	–	–	–	(-)	(-)	–	Ms, Py, Ab	MDB	MDB	slight	Met. (L-M)	Met. (L-M)	Met. (L-M)
26	SA	M	(+)	–	–	–	–	√	(+)	(-)	–	Zrn	MB	MB	moderate	Plutonic	Plutonic	Plutonic
27	SR	M	(+)	–	–	–	–	–	(+)	(++)	Det	Zrn, Py	–	–	–		Met. (L); brittle deformed	Met. (L); brittle deformed
28	R	M	(+)	–	–	–	–	–	(++)	(+)	Det	–	BMB	MB	strong	Plutonic	Plutonic	Plutonic
29	SR	M	(++)	–	–	–	–	√	(-)	(+)	Det	–	MDB	MDB	moderate	Met. (L-M)	Met. (L-M)	Met. (L-M)
30	R	M	(++)	√	–	–	–	√	(+)	(+)	Det	–	MDB	MDB	slight	Met. (L-M)	Met. (L-M)	Met. (L-M)
31	SR	M	(-)	–	–	–	–	–	(-)	(++)	Det	–	MDB	DB	strong	Plutonic	Plutonic	Plutonic
32	SR	M	(-)	–	–	–	–	–	(+)	(++)	Det	–	MB	MB	moderate	Plutonic	Plutonic	Plutonic
33	SR	M	(-)	–	–	–	–	–	(++)	(+)	Det	–	MDB	MDB	moderate	Plutonic	Plutonic	Plutonic
34	R	M	(+)	–	–	–	–	–	(++)	(-)	–	–	DB	DB	slight	Met. (L-M)	Met. (L-M)	Met. (L-M)
35	SA	4	(+)	√	–	–	–	–	(+)	(+)	Det	–	MDB	MDB	moderate	Met. (L-M)	Met. (L-M)	Met. (L-M)
36	SR	M	(+)	–	–	–	–	√	(+)	(+)	Dgn	–	MDB	MDB	moderate	Met. (L-M)	Met. (L-M)	Met. (L-M)
37	SA	M	(+)	–	–	–	–	–	(+)	(+)	Det	Py, Kln	DB	DB	no	Met. (L-M)	Met. (L-M)	Met. (L-M)
38	SR	5	(++)	–	√	–	–	–	(+)	(++)	Det	–	MDB	MDB	slight	Met. (L-M)	Met. (L-M); ductily	Met. (L-M); ductily
39	SA	M	(+)	√	–	–	–	–	(-)	(++)	Det	–	MDB	DB	moderate	Plutonic*	Met. (L); brittle deformed	Met. (L); brittle deformed
40	SR	M	(+)	√	–	–	–	–	(-)	(+)	Det	–	MDB	MDB	slight	Met. (L-M)	Met. (L-M)	Met. (L-M)

Notes: [1] Ab=albite; Ap=apatite; Bt=biotite; Cal=calcite; Hc=hercynite; Ilt=illite; Kfs=K-feldspar; Kln=kaolinite;Ms=muscovite; Pl=plagioclase; Py=pyrite; Zrn=zircon.

[2] VDB=very dark blue; DB=dark blue; MDB=medium dark blue; MB=medium blue; BMB=bright-medium blue; BB=bright blue.

[3] * indicates that the classification from combined HCL and petrography does not match the classification from combined SEM-CL and petrography.

Appendix 1A: Microphotos, scanning electron microscopy-backscattered electron (SEM-BSE) images, scanning electron microscopy-cathodoluminescence (SEM-CL) images, and EDS analyses of detrital quartz grains in sample 2565.

Notes:

1. **Homogenous CL:** Nearly uniform CL intensity across the grain (Fig. 2A).

2. Fractures in quartz have been divided into two types: **healed fractures** (**HF**) and **open fractures** (**OF**).

   Healed fractures are fractures filled with secondary silica that appear as thin (commonly < 10 μm) black lines in SEM-CL images (Fig. 2B). They are usually not shown in back-scattered images (Boggs and Krinsley, 2006).

   Open fractures appear in cathodoluminescense images as CL-dark or CL-bright lines, and they are also visible in back-scattered images and microphotos. A few open fractures are **conchoidal fractures** (**CF**) (Boggs and Krinsley, 2006).

3. **Tectonic deformation lamellae**: Tectonic deformation lamellae (Fig. 2C) appear in SEM-CL image as numerous sets of thin, parallel, closely spaced, dark gray lines (Bernet and Basset, 2005). According to Hamers and Drury (2011), tectonic deformation lamellae can either appear as dark gray lines or bright lines in SEM-CL images, and can show slightly wavy features with varying thickness. They usually also appear in XPL image under petrographic microscope.

4. **Spiders (S):** They are made up of dark-Cl patches and streaks. Dark-CL patches mainly range from 10-100 μm. Streaks are random and irregular in the appearance of black broad (>10 μm) elongated form. The spiders are commonly associated with healed fractures, giving them the appearance in SEM-CL images of spiders sitting on a web (Fig. 2D). They cannot be seen in BSE images, since they are composed by secondary silica (Boggs and Krinsley, 2006).

5. **Bright mottling**: Some grains show irregular CL intensity across grains, creating a mottled pattern due the presence of patches (Boggs and Krinsley, 2006). Three types of bright mottling were seen.

   - **Random bright patches** (Fig. 2E1)
   - **Bright streaky patches fabric** (Fig. 2E2)
   - **Subtle mottling** (Fig. 2E3)

6. **Overgrowth:** Overgrowth appears in SEM-CL images as dark areas in the border of the quartz grains (Fig. 2F).

7. **Fluid inclusion trail** (**FI trail**): Trails formed by **fluid inclusions** (**FI**). They are usually associated with secondary porosity and commonly located along fractures and at boundaries between detritral quartz grain and the overgrowth. They are well observed in microphotos under ppl. The fluid inclusion trails can be separated in two kinds: **detrital fluid inclusion trails (**fluid inclusions that are original from the detrital quartz, they do not cut the quartz overgrowth) and **diagenetic fluid inclusion trails** (fluid inclusions originated from the diagenesis, and they thus cut the quartz overgrowth).

8. **Melt inclusion** (**MI**): Large fluid inclusions (>10 μm) in which crystallized minerals are visible.

9. **Secondary porosity** (**SP**): Porosities usually caused by dissolution and/or fractures. They are easily observed in microphotos under PPL and BSE images.

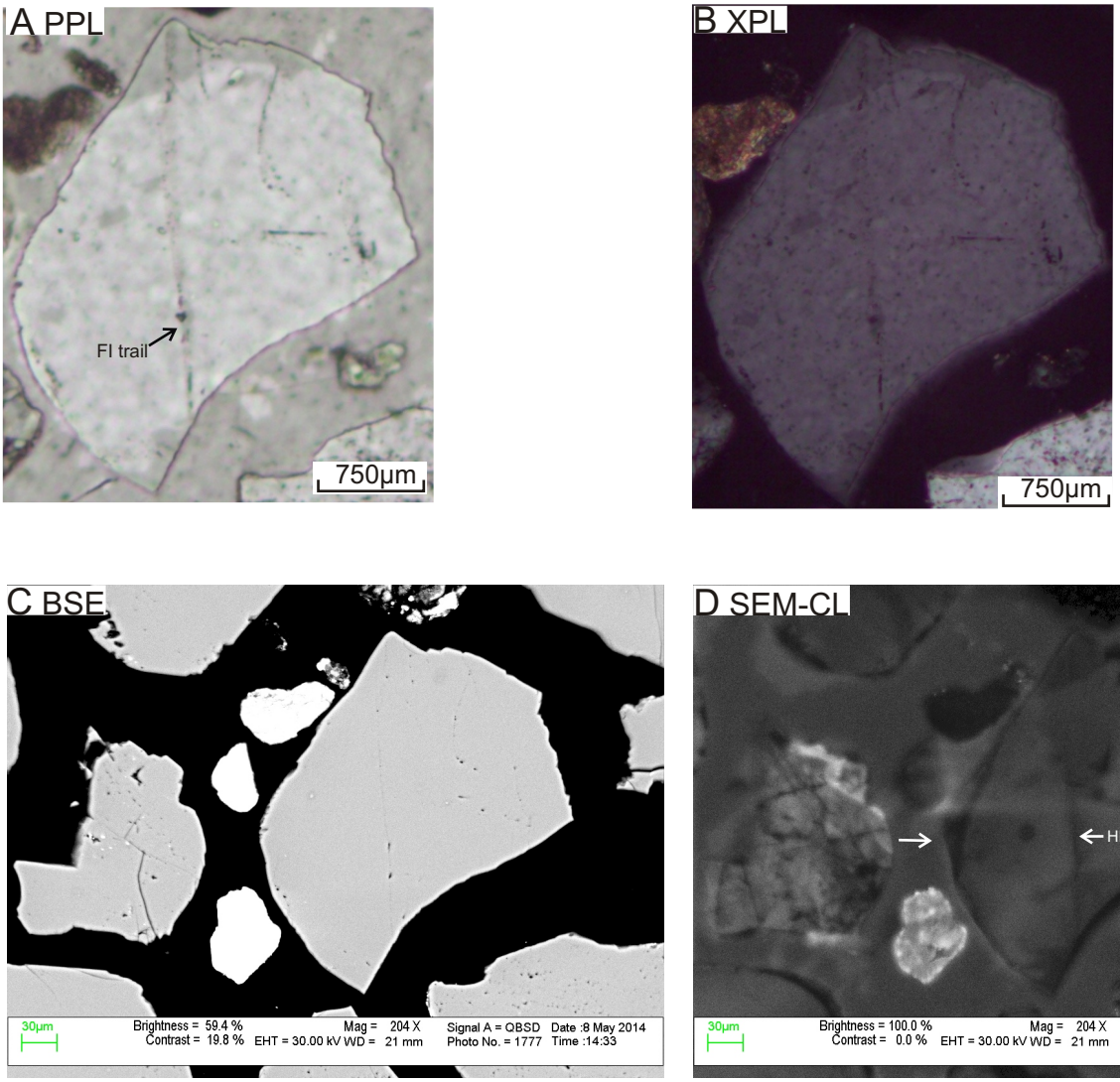

Figure 1A-1: Microphotos under ppl (A) and xpl (B), SEM-BSE image (C) and SEM-CL image (D) of quartz grain 1 in sample 2565. The grain is anhedral and angular monocrystalline with sharp margins and non-undulose extinction. The grain contains fluid inclusions trails (FI trail) associated with secondary porosity (SP) along fractures (Fig. A and C) and is weakly microfractured (Fig. C and D). Some healed fractures (HF) can be seen in Fig. D. The area with dark CL indicated by arrows in Fig. D is overgrowth.

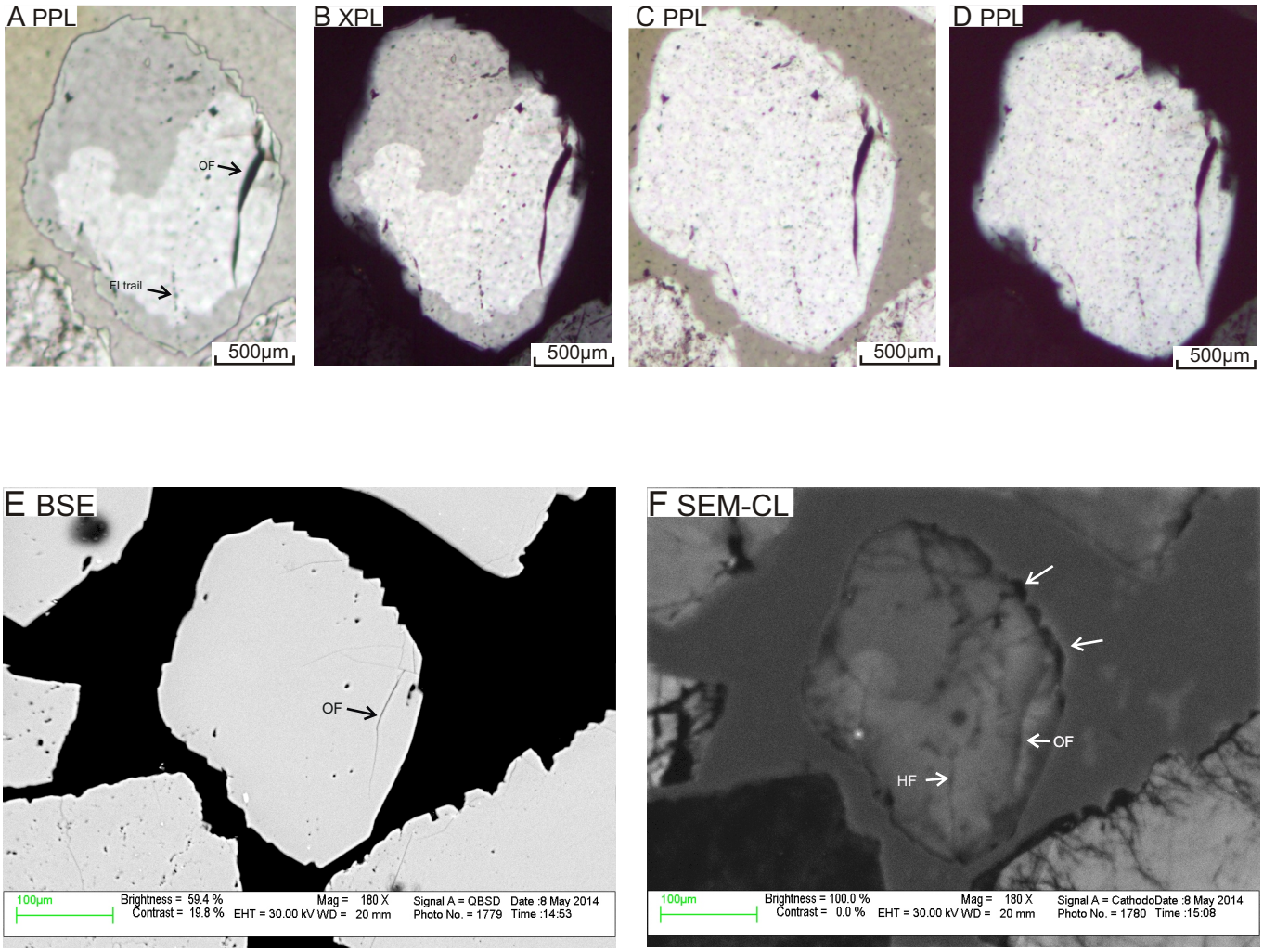

Figure 1A-2: Microphotos under ppl (A and C) and xpl (B and D), BSE image (E) and SEM-CL image (F) of quartz grain 2 in sample 2565. Fig. C and D were taken after cleaning thin section to preclude the possibility of uneven carbon coating. The occurrence of zoning in Fig. A and B, not in Fig. C and D, results from the severely uneven carbon coating on the original thin section. The grain is subhedral and sub-rounded monocrystalline with irregular margins and strong undulose extinction. The grain contains fluid inclusion trail (FIT) along fractures (Fig. A) and some irregular curved fractures (Fig. E and F). Some healed fractures (HF) can be seen in Fig. F. . The dark area indicated by arrows in Fig. F is overgrowth. The zoning that appears in Fig. F is due the uneven carbon coating on the original thin section.

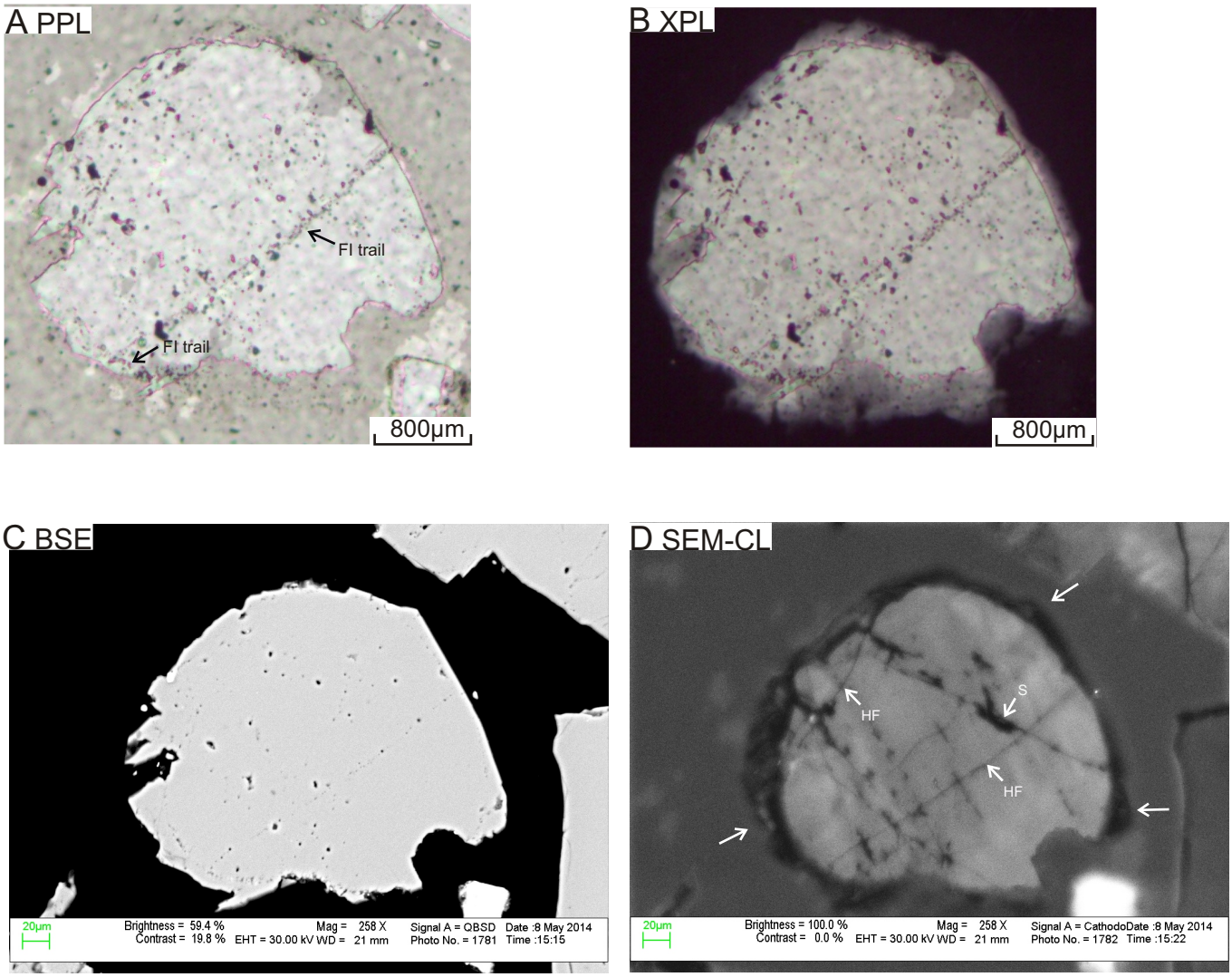

Figure 1A-3: Microphotos under ppl (A) and xpl (B), BSE image (C) and SEM-CL image (D) of quartz grain 3 in sample 2565. The grain is anhedral and rounded monocrystalline with irregular and embayed margins, and non-undulose extinction. Fluid inclusions are common; they are usually associated with secondary porosity and form trails along healed fractures and at boundaries between detritral quartz grain and the overgrowth (diagenetic fluid inclusion) (Fig. A). The grain is microfractured with two sets of parallel fractures crosscutting each other (Fig. D). Some healed fractures (HF) can be seen in Fig. D; the Spiders (S) in Fig. D indicate secondary porosity filled by diagenetic quartz along fractures. The areas indicated by arrows in Fig. D are overgrowth; these areas appear corroded in Fig. C, suggesting secondary porosity.

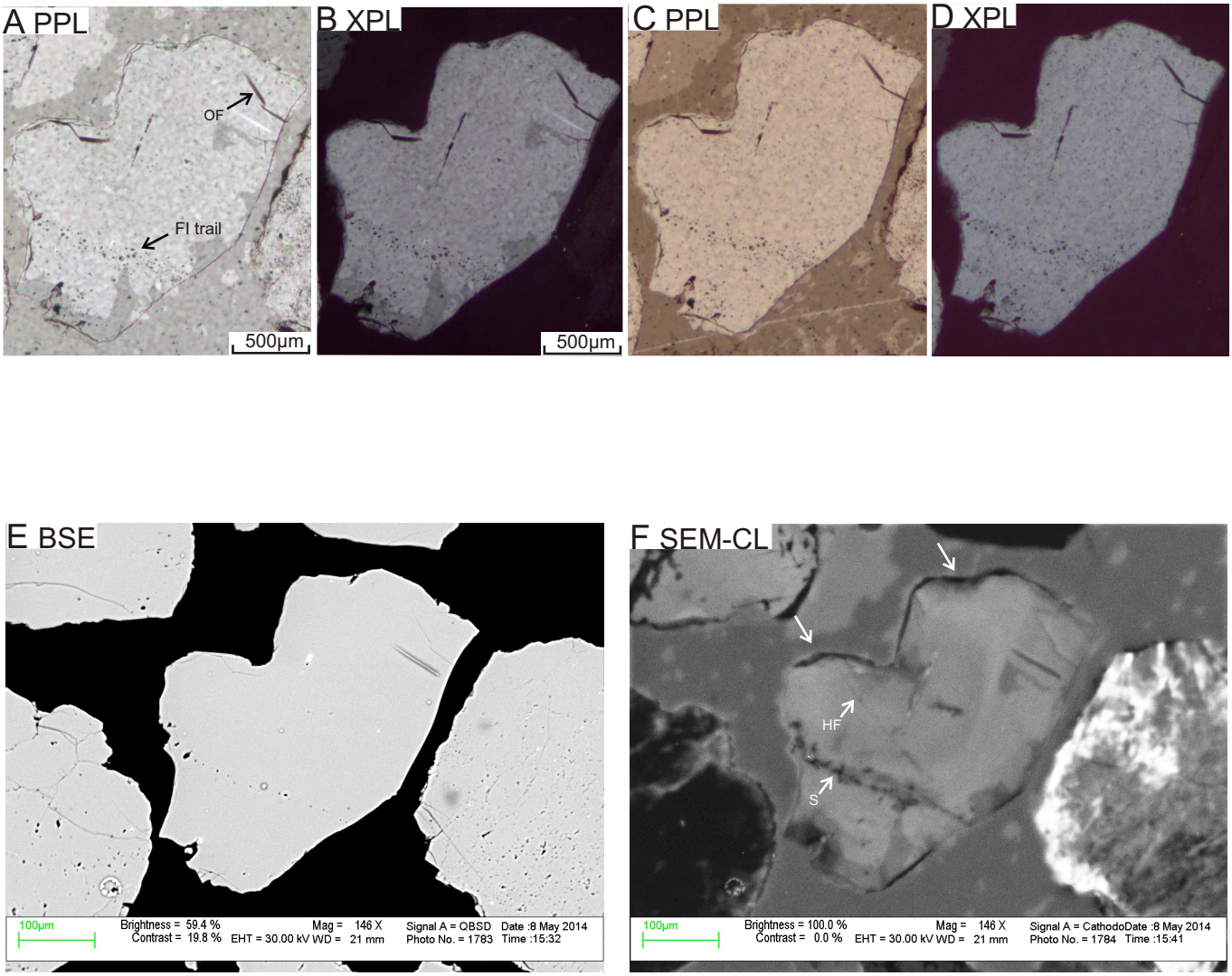

Figure 1A-4: Microphotos under ppl (A and C) and xpl (B and D), BSE image (E) and SEM-CL image (F) of quartz grain 4 in sample 2565. See details about Fig. C and D and the explanation of darker patches in Fig. A and B in the caption of Fig. 1A-2. The grain is anhedral and sub-rounded monocrystalline with embayed margins and non-undulose extinction. The grain contains fluid inclusions trails (FI trail) associated with secondary porosity along fractures (Fig. A), and is microfractured with irregular fractures. A few healed fractures (Fig. D) and open fractures (Fig. A) can be seen. Spiders (S) in Fig. F are secondary porosity filled by diagenetic quartz along fractures. The shadow indicated by arrows in Fig. F shows overgrowth. The zoning that appears in Fig. F is due the uneven carbon coating on the original thin section.

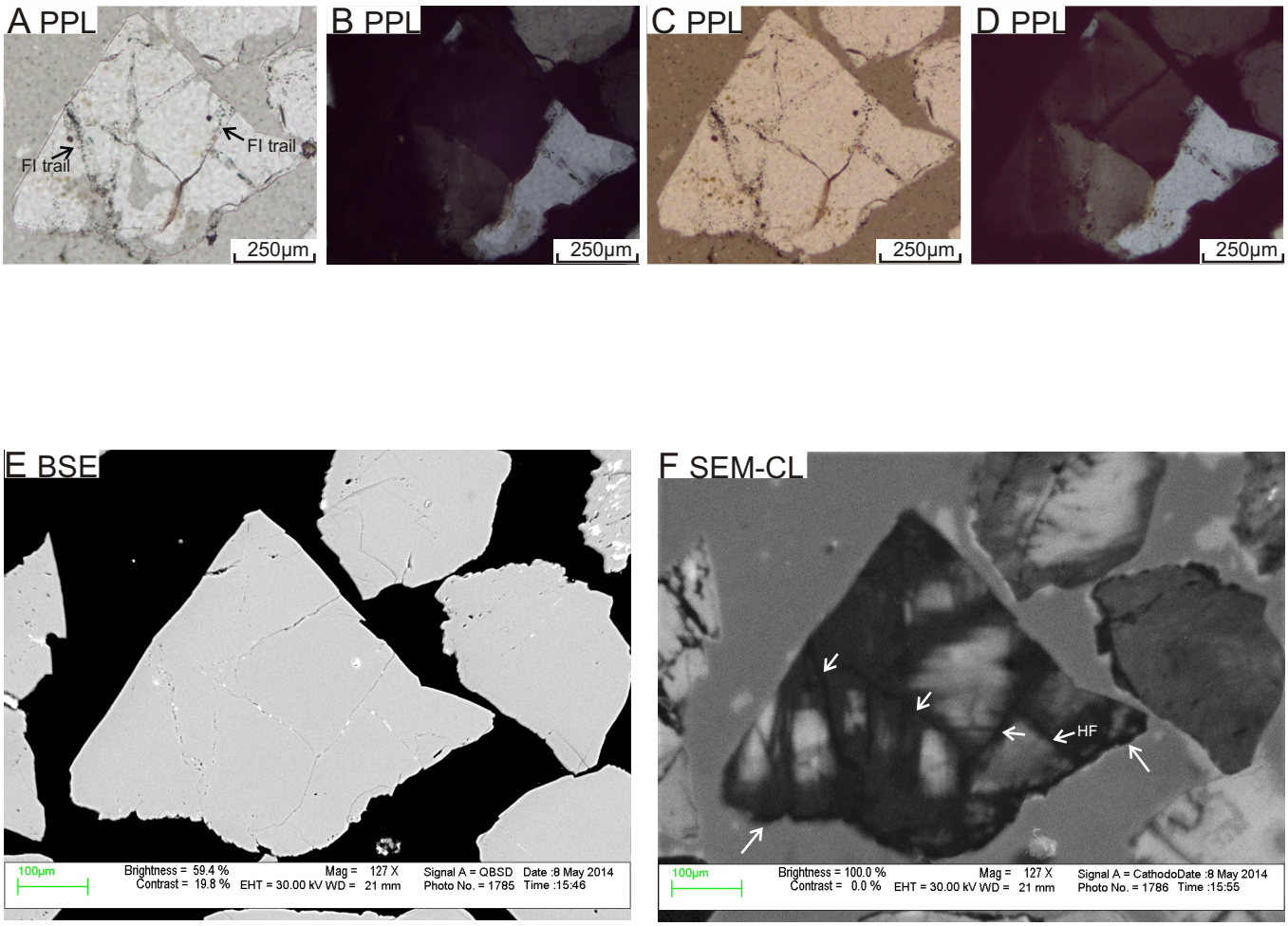

Figure 1A-5: Microphotos under ppl (A and C) and xpl (B and D), BSE image (E) and SEM-CL image (F) of quartz grain 5 in sample 2565. See details about Fig. C and D and the explanation of darker patches in Fig. A and B in the caption of Fig. 1A-2. The grain is anhedral and angular polycrystalline (more than 5 sub-grains) with strong undulose extinction. Fluid inclusions are common; they are usually associated with secondary porosity and form trails along the sub-grains boundaries (Fig. A). The grain is weakly microfractured with only a few fractures. Some healed fractures can be seen in Fig. F; however, most of the black curved lines indicated by arrows in Fig. F are the sutured sub-grains boundaries. The black areas indicated by arrows in Fig. D are overgrowth. The grain shows bright-CL streaky patches in SEM-CL image.

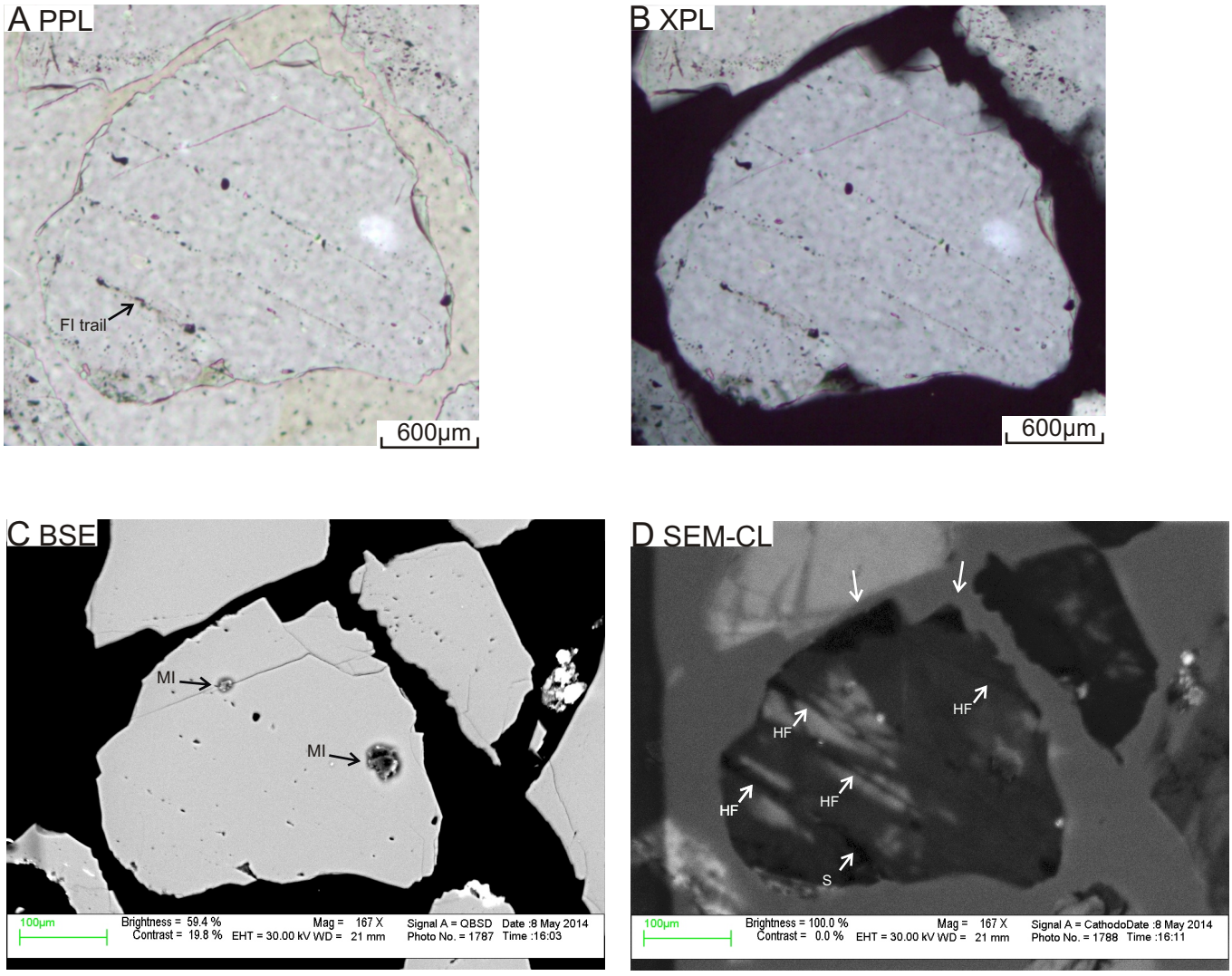

Figure 1A-6: Microphotos under ppl (A) and xpl (B), BSE image (C) and SEM-CL image (D) of quartz grain 6 in sample 2565. The grain is anhedral and sub-rounded monocrystalline with weak undulose extinction. Fluid inclusions are common; they are usually associated with secondary porosity and form trails along healed fractures (Fig. A). Melt inclusions (MI) can be seen in Fig. C. Sets of parallel healed fractures (HF) are present (Fig. C and D). The spiders (S) in Fig. D are secondary porosity filled by diagenetic quartz along fractures, and the dark areas indicated by arrows in Fig. D are overgrowth. The grain shows bright streaky patches in SEM-CL (Fig. D).

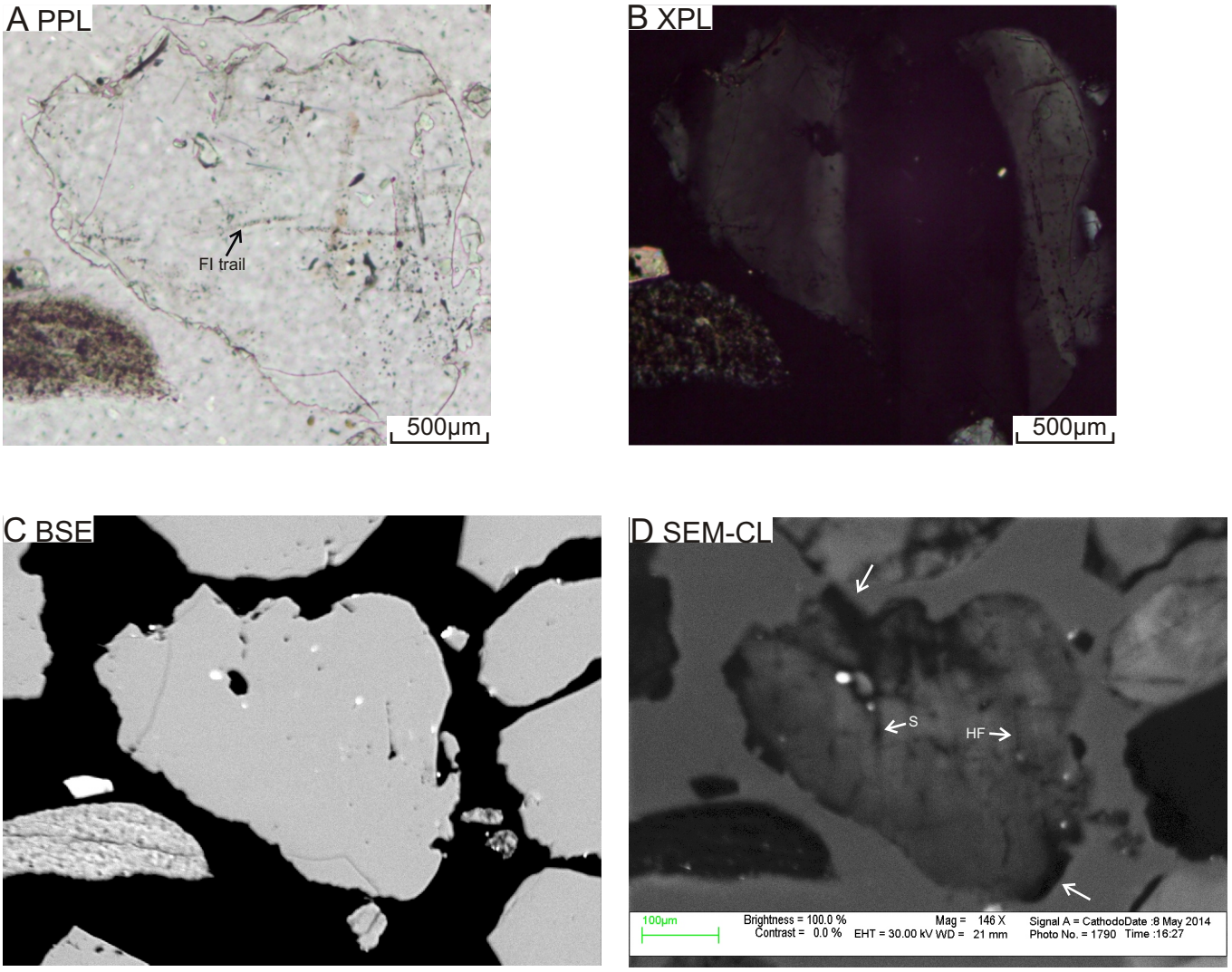

Figure 1A-7: Microphotos under ppl (A) and xpl (B), BSE image (C) and SEM-CL image (D) of quartz grain 7 in sample 2565. The grain is anhedral and sub-angular polycrystalline (only a few sub-grains) with irregular margins, deformation banding, and with strong undulose extinction. Fluid inclusions are common; they usually form trails along healed fractures (Fig. A). The grain is microfractured with sets of irregular curved fractures. A few healed fractures (HF) can be seen in Fig. D. The spiders (S) are rare. The dark areas indicated by arrows in Fig. D are overgrowth.

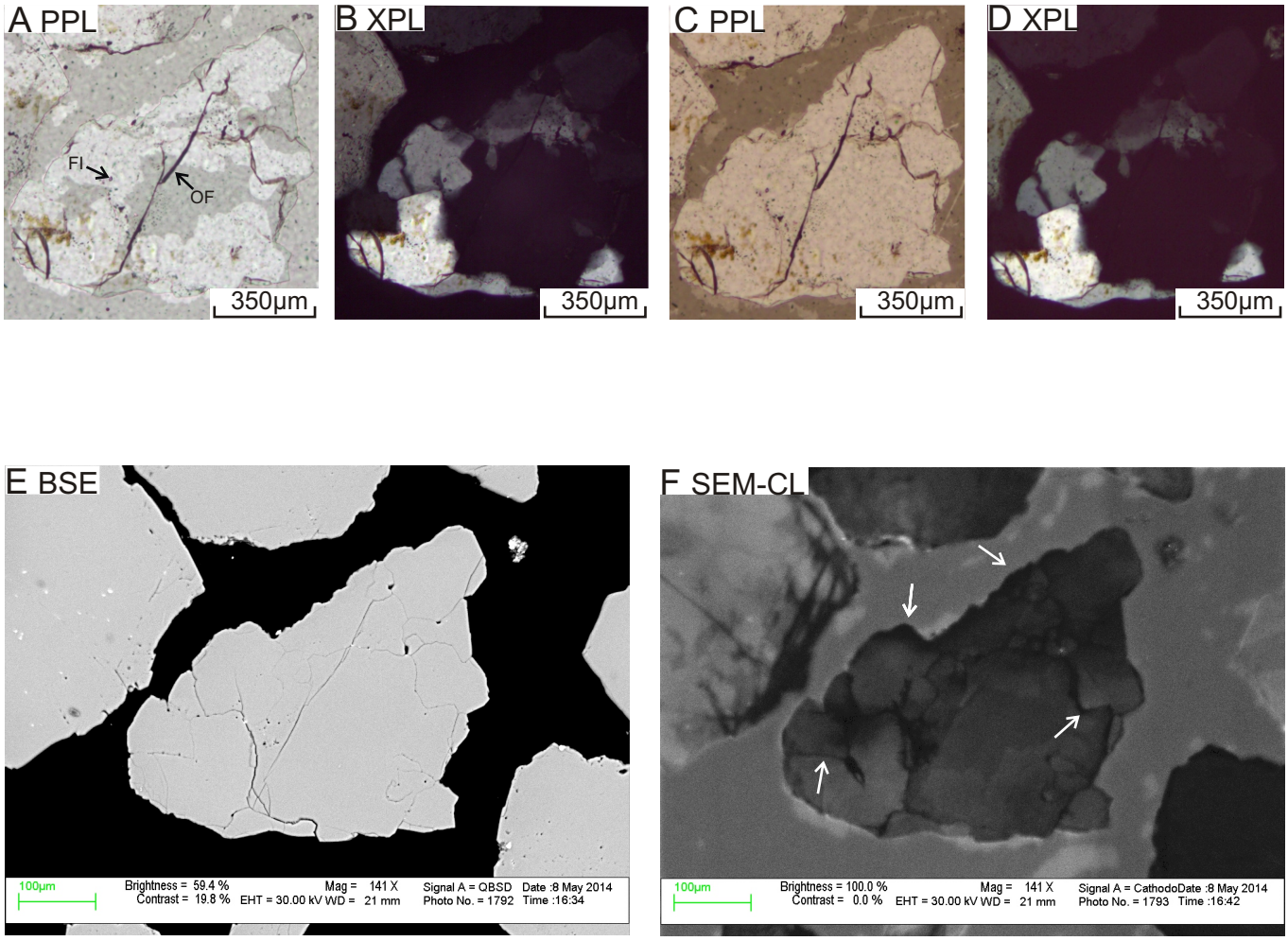

Figure 1A-8: Microphotos under ppl (A and C) and xpl (B and D), BSE image (E) and SEM-CL image (F) of quartz grain 8 in sample 2565. See details about Fig. C and D and the explanation of darker patches in Fig. A and B in the caption of Fig. 1A-2. The grain is anhedral and sub-angular polycrystalline (more than 7 sub-grains with sutured sub-grain boundaries) with irregular margins and strong undulose extinction. Fluid inclusions (FI) are common, and they are usually associated with secondary porosity (Fig A). The grain is microfractured with irregular curved fractures. A few open fractures (Fig. A) can be seen. The black curved lines indicated by arrows in Fig. F are the sutured sub-grains boundaries. The dark areas indicated by arrows in Fig. F are overgrowth.

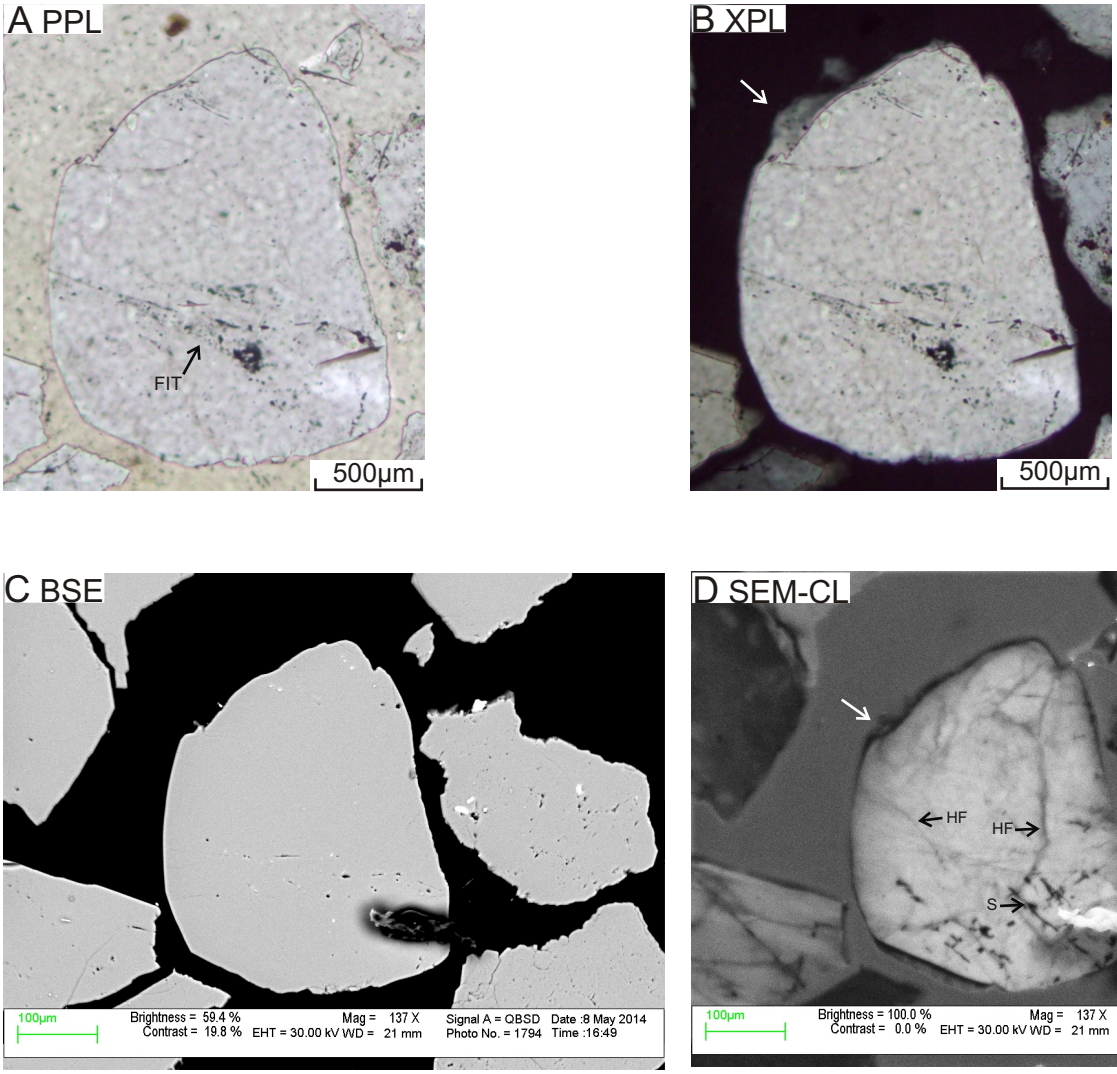

Figure 1A-9: Microphotos under ppl (A) and xpl (B), BSE image (C) and SEM-CL image (D) of quartz grain 9 in sample 2565. The grain is subhedral and rounded monocrystalline with non-undulose extinction. Fluid inclusions are common; they are usually associated with secondary porosity and form trails along healed fractures (Fig. A).The grain contains sets of parallel fractures and irregular curved fractures (Fig. D). Some healed fractures (HF) can be seen in Fig. D. The spiders (S) in Fig. D are secondary porosity filled by diagenetic quartz along fractures. The areas indicated by arrows in Fig. B and D are overgrowth.

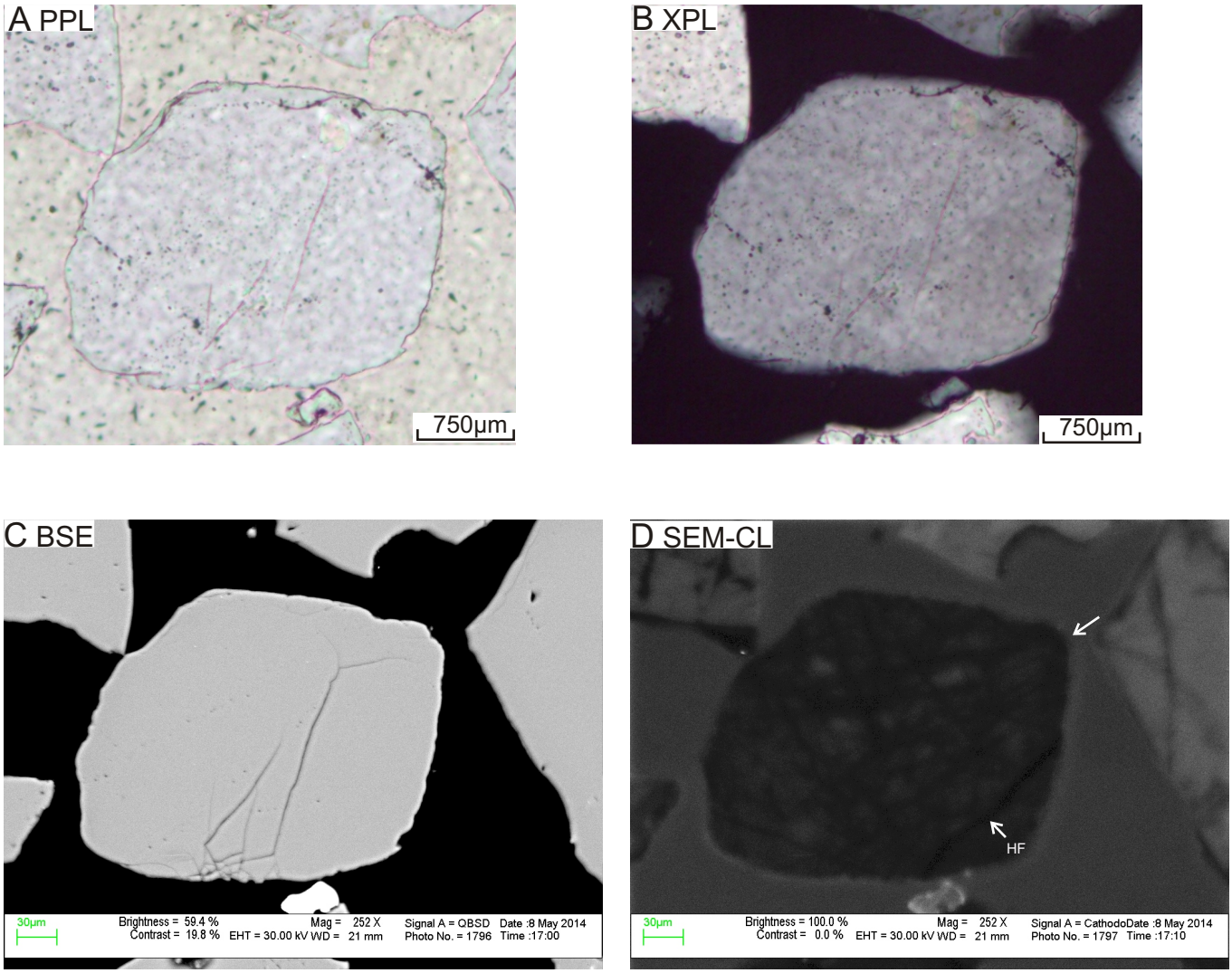

Figure 1A-10: Microphotos under ppl (A) and xpl (B), BSE image (C) and SEM-CL image (D) of quartz grain 10 in sample 2565. The grain is subhedral and rounded monocrystalline with strong undulose extinction. The grain contains fluid inclusions and is microfractured with sets of sub-parallel fractures (Fig. C and D). Healed fractures (HF) are common (Fig. D). The dark area indicated by arrow in Fig. B and D is overgrowth. The grain shows subtle mottling pattern in SEM-CL (Fig. D)

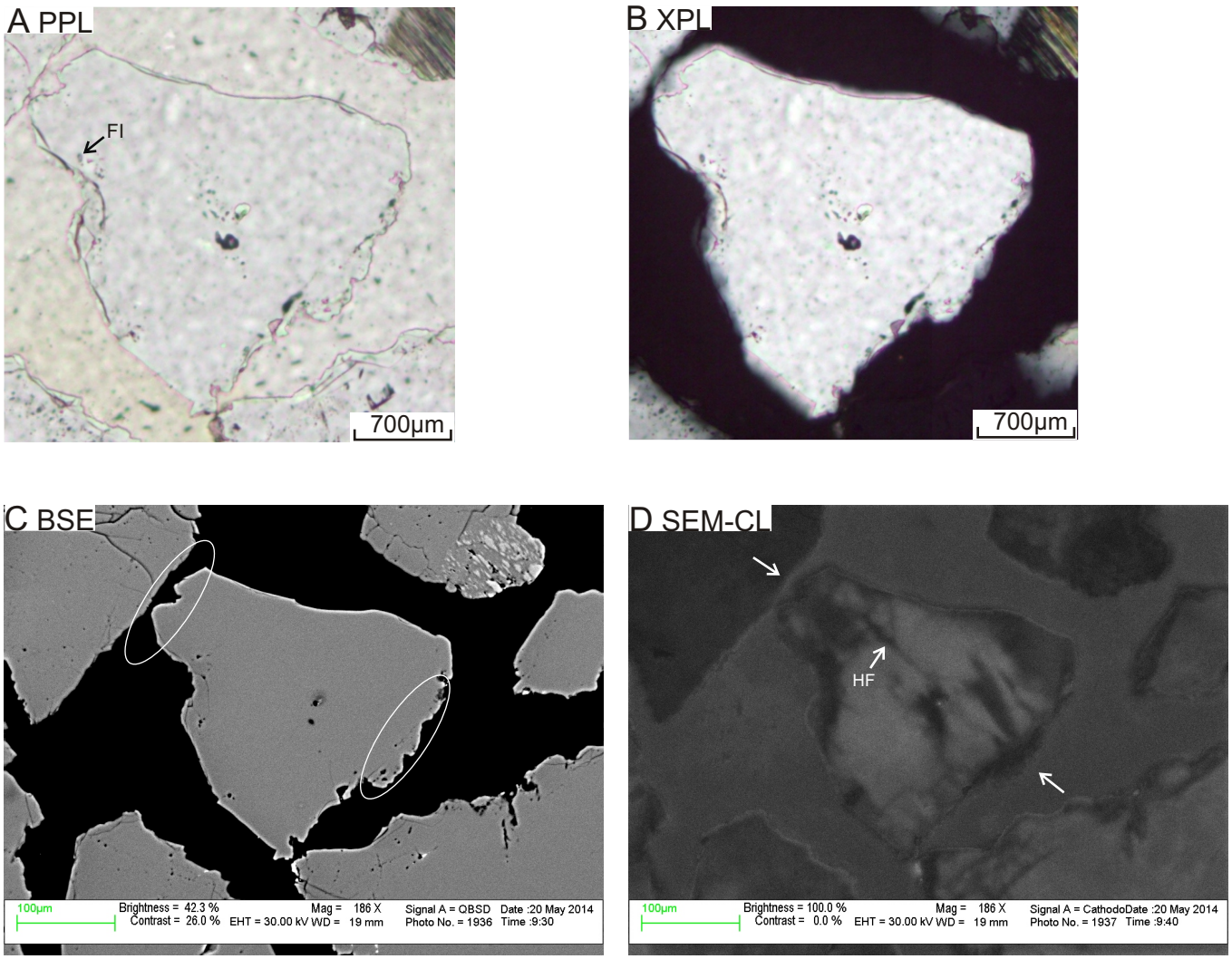

Figure 1A-11: Microphotos under ppl (A) and xpl (B), SEM-BSE image (C) and SEM-CL image (D) of quartz grain 11 in sample 2565. The grain is anhedral and sub-angular monocrystalline with strong undulose extinction. The grain contains fluid inclusions (Fig. A) and a few irregular and curved fractures (Fig. C and D). Some healed fractures (HF) can be seen in Fig. D. The areas indicated by arrows in Fig. D are euhedral faces of overgrowth. These faces appear corroded in Fig. C (circles), suggesting secondary porosity.

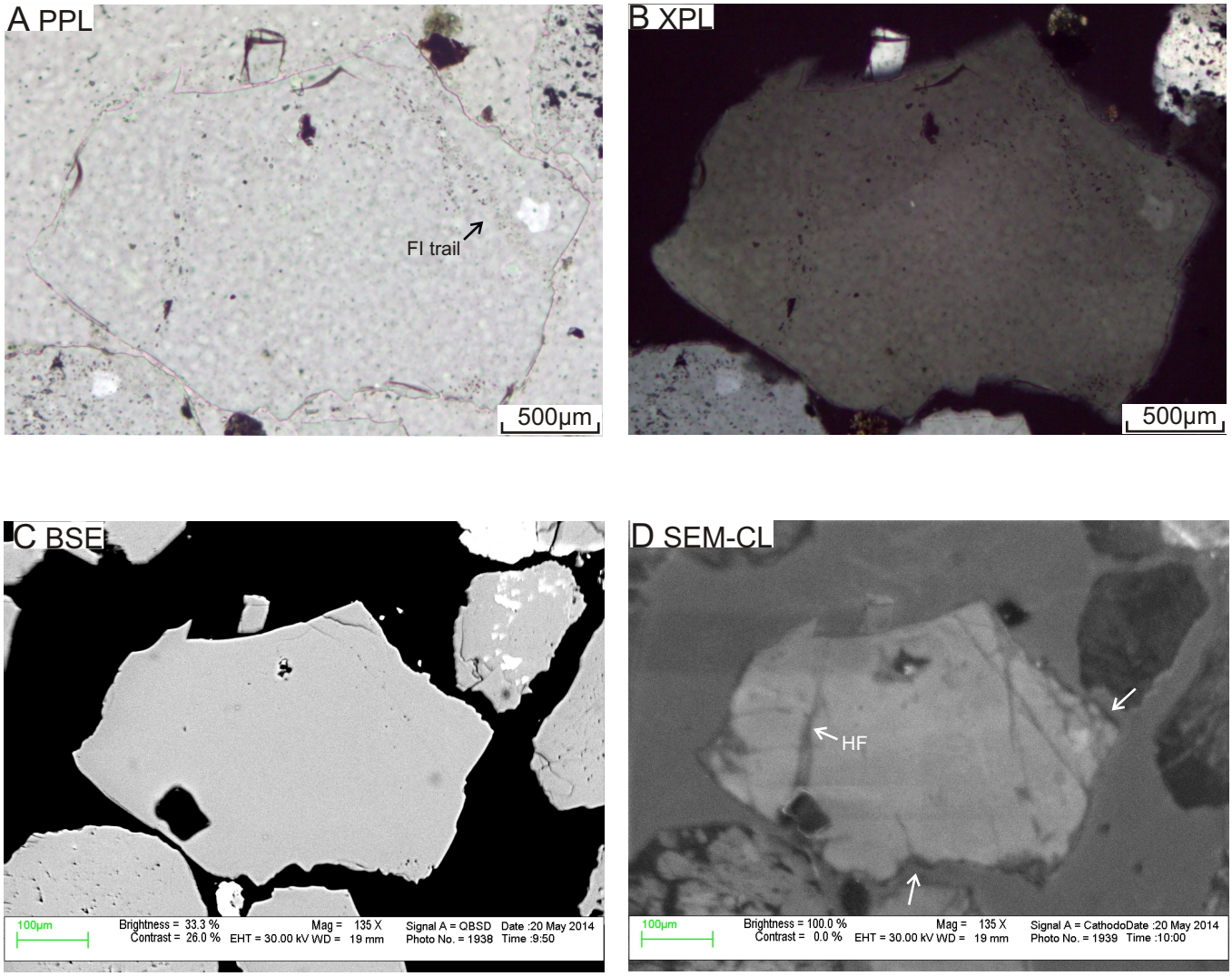

Figure 1A-12: Microphotos under ppl (A) and xpl (B), SEM-BSE image (C) and SEM-CL image (D) of quartz grain 12 in sample 2565. The grain is anhedral and sub-angular monocrystalline with mosaic texture and weak undulose extinction. Fluid inclusions are common; they are usually associated with secondary porosity and form trails along healed fractures (Fig. A). The grains is microfractured with some irregular fractures (Fig. D). Some healed fractures (HF) can be seen in Fig. D. The areas indicated by arrows in Fig. D shows overgrowth.

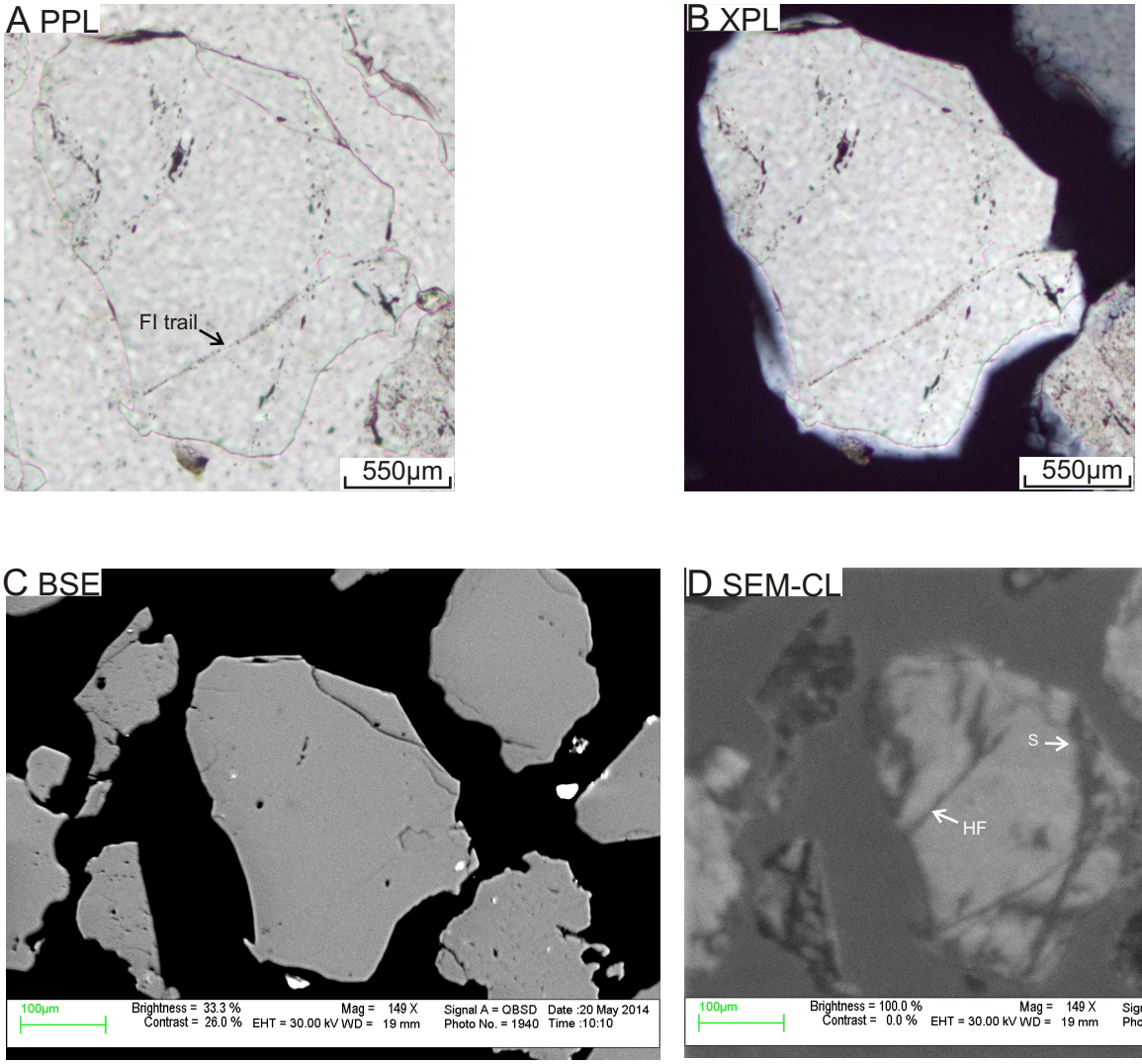

Figure 1A-13: Microphotos under ppl (A) and xpl (B), SEM-BSE image (C) and SEM-CL image (D) of quartz grain 13 in sample 2565. The grain is anhedral and sub-angular monocrystalline with weak undulose extinction, and is microfractured with a set of irregular fractures (Fig. D). Fluid inclusions are common; they are usually associated with secondary porosity and form trails along healed fractures (Fig. A). Some healed fractures (HF) and Spiders (S), that are secondary porosity filled by diagenetic quartz, can be seen in Fig. D.

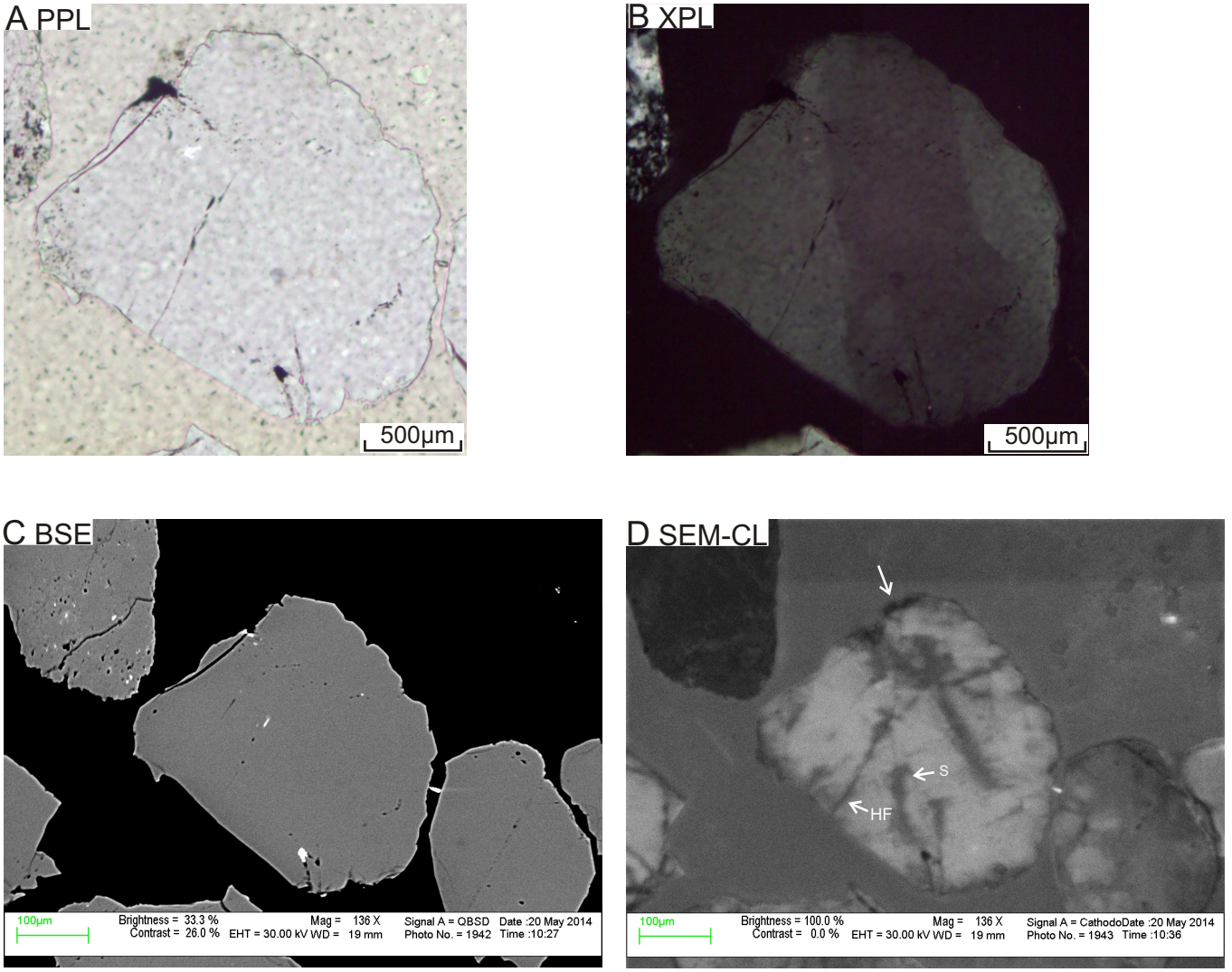

Figure 1A-14: Microphotos under ppl (A) and xpl (B), SEM-BSE image (C) and SEM-CL image (D) of quartz grain 14 in sample 2565. The grain is subhedral and sub-rounded monocrystalline with weak undulose extinction. The grain contains fluid inclusions and is microfractured with a set of irregular fractures (Fig. A and D). A few healed fractures (HF) can be seen in Fig. D. The spiders (S) in Fig. D are secondary porosity filled by diagenetic quartz along fractures. The dark area indicated by arrow in Fig. D is overgrowth.

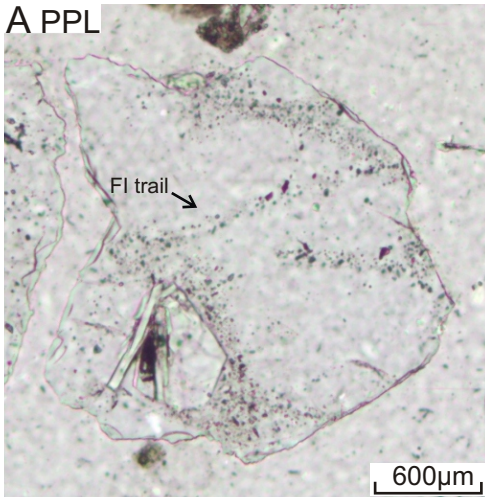

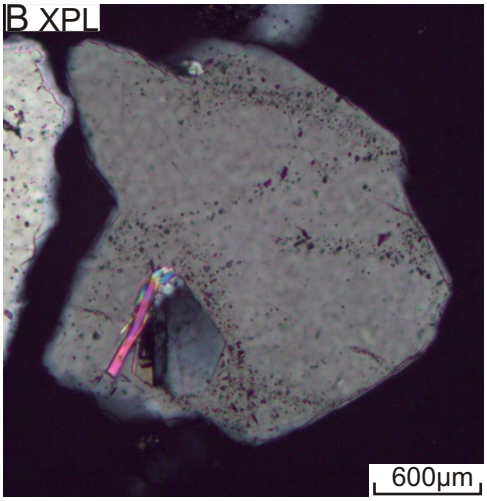

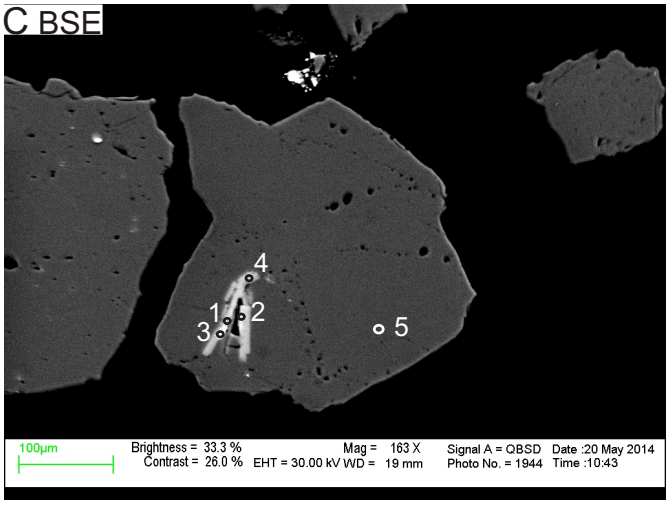

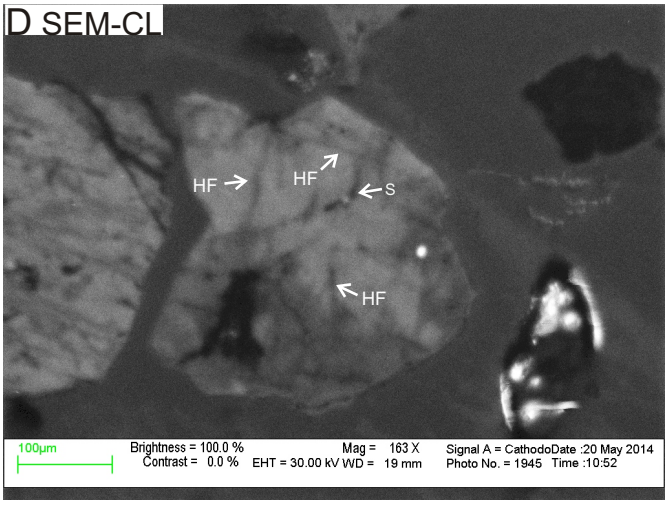

E EDS mineral analyses

Pos#	Min. ID	SiO2	TiO2	Al2O3	FeO	MgO	Na2O	K2O	SO3	ZnO	Total	Actual Total
1	Ms	47.49	0.16	34.06	1.97	0.41	0.45	10.47			95	180
2	Sp+Ms	47.43	0.23	17.38	2.28	0.28		4.66	16.56	11.19	100	209
3	Ms	48.18	0.45	32.71	2.73	0.58	0.32	10.03			95	149
4	Ms	47.55	0.27	33.53	2.14	0.41	0.37	10.73			95	166
5	Qz	99.99									100	183

Figure 1A-15: Microphotos under ppl (A) and xpl (B), SEM-BSE image (C), SEM-CL image (D), and EDS analyses table (E) of quartz grain 15 in sample 2565. The grain is subhedral and angular monocrystalline with weak undulose extinction. Fluid inclusions are common; they are usually associated with secondary porosity and form trails along healed fractures (Fig. A).The grain contains muscovite and sphalerite inclusions and is microfractured with a set of irregular fractures (Fig. A and D). Some healed fractures (HF) and spiders (S), that are secondary porosity filled by diagenetic quartz, can be seen in Fig. D. The grain shows random bright CL patches in SEM-CL image.

A PPL

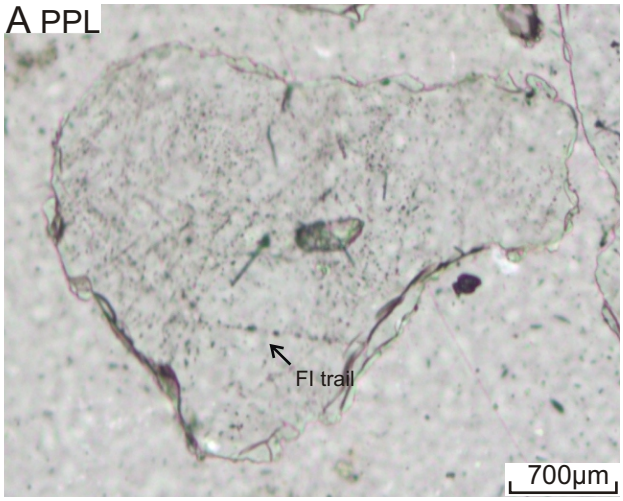

B XPL

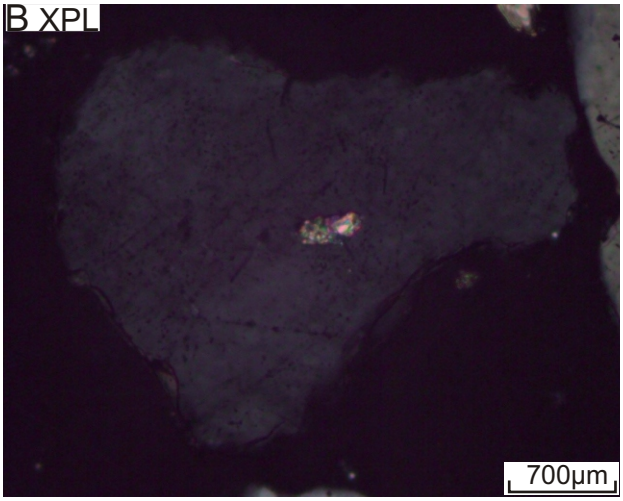

C BSE

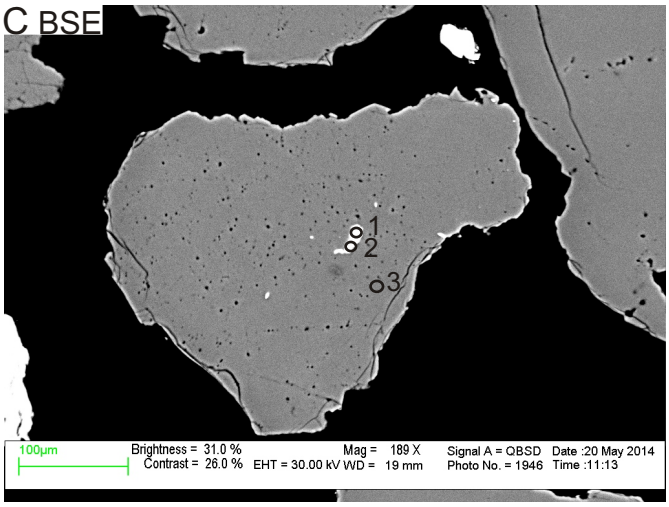

D SEM-CL

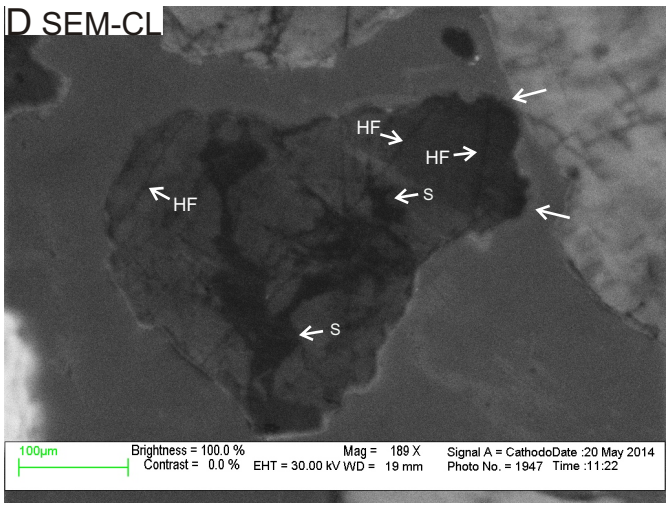

E EDS mineral analyses

Pos#	Min. ID	SiO2	Al2O3	FeO	MnO	CaO	P2O5	Total	Actual Total
1	Mag	6.48	0.62	87.43	0.75	3.13	1.58	100	95
2	Mag	10.14		84.52	0.54	3.29	1.51	100	97
3	Qz	99.99						100	184

Figure 1A-16: Microphotos under ppl (A) and xpl (B), SEM-BSE image (C), SEM-CL image (D), and EDS analyses table (E) of quartz grain 16 in sample 2565. The grain is anhedral, and sub-rounded monocrystalline with irregular margins and non-undulose extinction. Fluid inclusions are common; they are usually associated with secondary porosity and form trails along healed fractures (Fig. A). The grain contains magnetite inclusions and is microfractured with a set of sub-parallel fractures (Fig. C and D). Healed fractures (HF) and spiders (S) are common (Fig. D). The dark areas indicated by arrows in Fig. D are overgrowth; these areas appear corroded in Fig. C, suggesting secondary porosity.

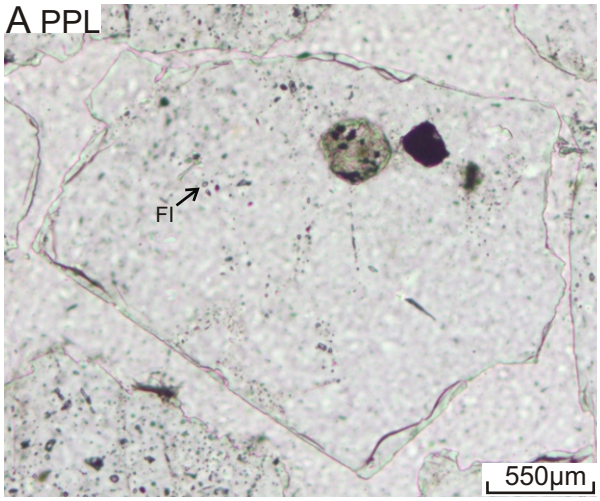

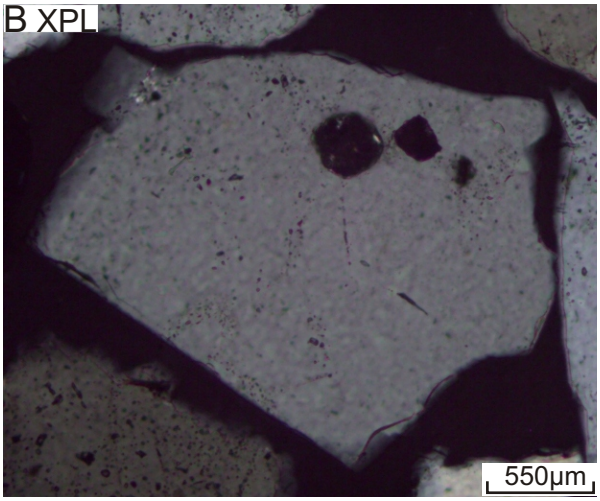

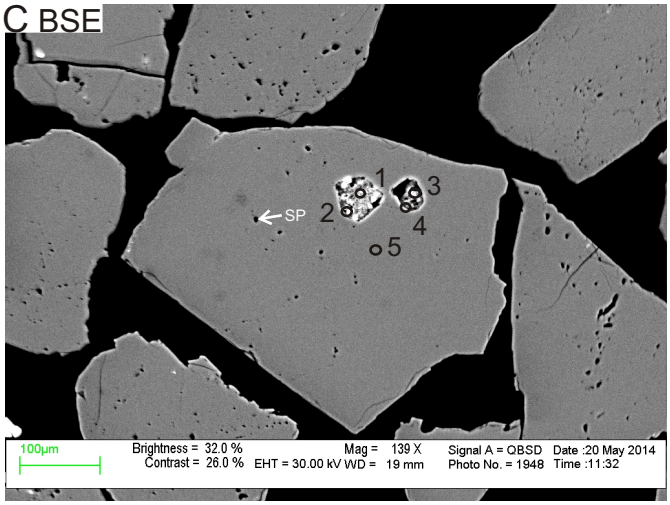

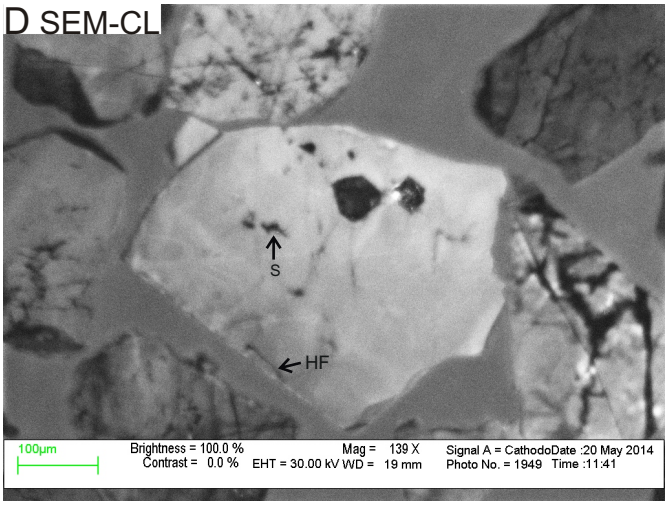

E EDS mineral analyses

Pos#	Min. ID	SiO2	TiO2	Al2O3	FeO	MnO	MgO	Na2O	K2O	SO3	Total	Actual Total
1	Bt	51.69		20.99	11.43	0.21	3.98		7.70		96	134
2	Py+Ilt	32.60		10.92	15.31		0.68		5.48	35.01	100	222
3	Kfs	53.65	0.32	32.42	2.30		1.06	0.66	9.59		100	143
4	Kfs	59.36	0.18	28.87	2.26		1.03	0.61	7.70		100	183
5	Qz	99.99									100	174

Figure 1A-17: Microphotos under ppl (A) and xpl (B), SEM-BSE image (C), SEM-CL image (D), and EDS analyses table (E) of quartz grain 17 in sample 2565. The grain is subhedral and angular monocrystalline with non-undulose extinction. The grain contains biotite, K-feldspar, and pyrite + illite inclusions, forming melting inclusions, and is weakly microfractured with irregular fractures (Fig. D). Secondary porosity (SP) and fluid inclusions are common (Fig. A and C). A few healed fractures (HF) and spiders(S), that are secondary porosity filled by diagenetic quartz, can be seen in Fig. D.

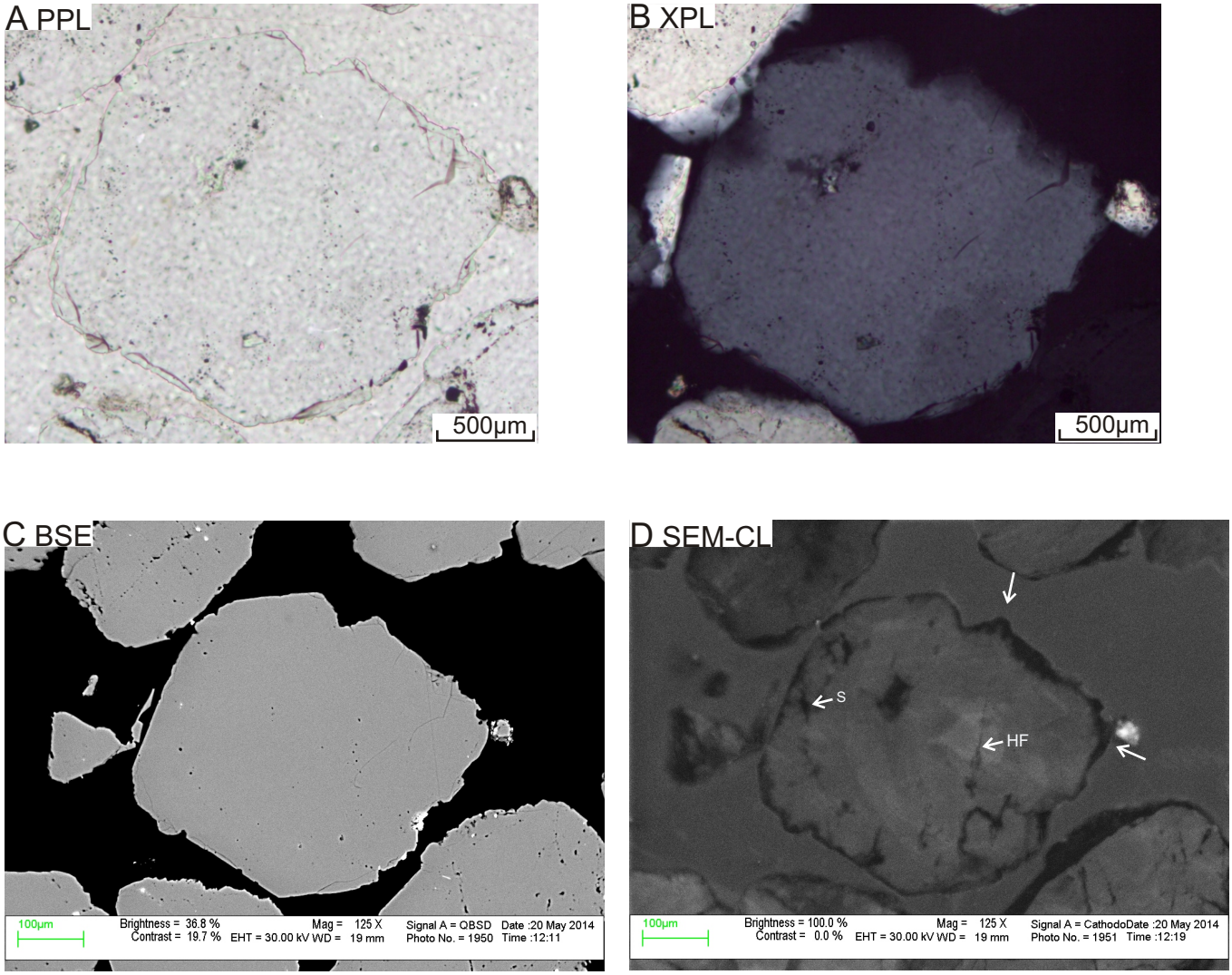

Figure 1A-18: Microphotos under ppl (A) and xpl (B), SEM-BSE image (C) and SEM-CL image (D) of quartz grain 18 in sample 2565. The grain is subhedral and sub-rounded monocrystalline with irregular margins and non-undulose extinction. The grain contains fluid inclusions and is weakly microfractured with a set of irregular fractures (Fig. D). A few healed fractures (HF) and spiders (S), that are secondary porosity filled by diagenetic quartz, can be seen in Fig. D. The areas indicated by arrows in Fig. D are euhedral faces of overgrowth. These faces appear corroded in Fig. C, suggesting secondary porosity.

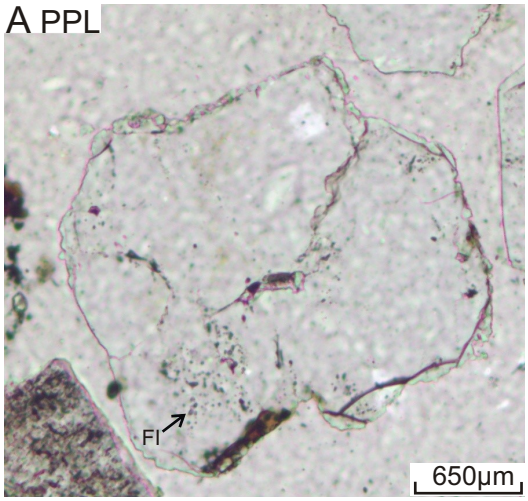

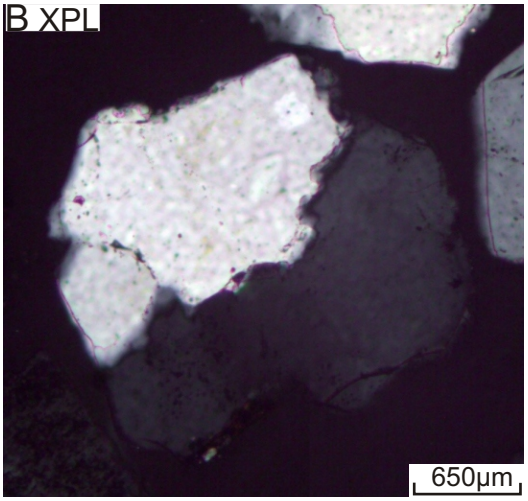

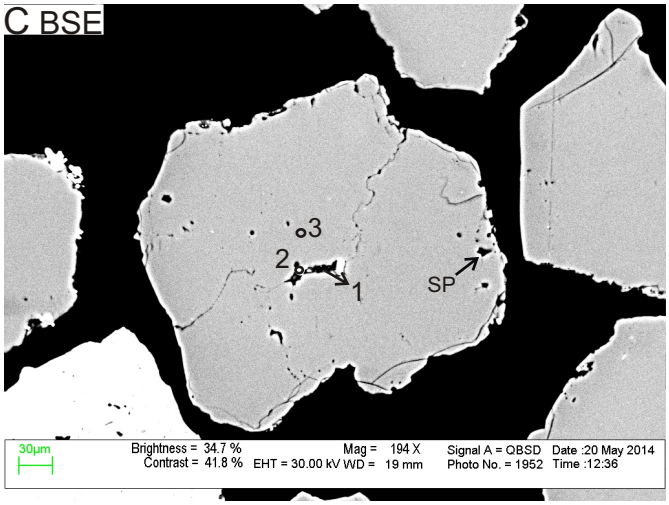

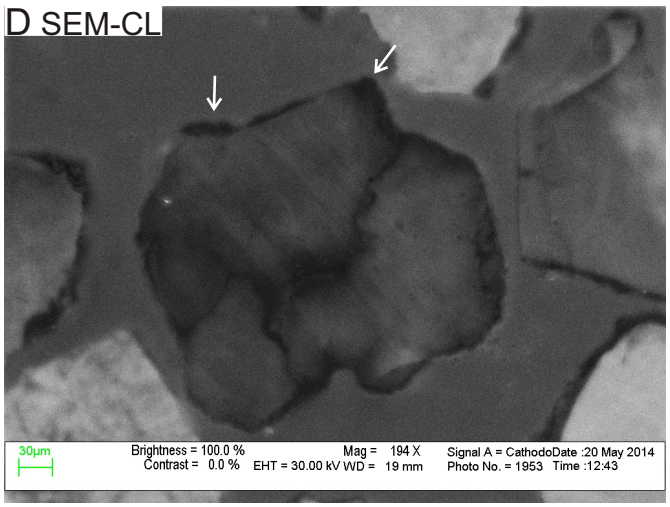

E EDS mineral analyses

Pos#	Min. ID	SiO2	TiO2	Al2O3	FeO	MgO	K2O	SO3	F	Nb2O5	Total	Actual Total
1	Kfs	77.1		16.38	0.64	0.36	0.29	0.7	4.51		100	143
2	Rt	11.85	80.1	2.48	1.34					4.22	100	153
3	Qz	99.99									100	166

Figure 1A-19: Microphotos under ppl (A) and xpl (B), SEM-BSE image (C), SEM-CL image (D), and EDS analyses table (E) of quartz grain 19 in sample 2565. The grain is subhedral, and sub-rounded polycrystalline (only 3 sub-grains with sutured sub-grain boundaries) with irregular and embayed margins, and with strong undulose extinction. Fluid inclusions and secondary porosity are common (Fig. A and C). The grain contains k-feldspar and rutile inclusions and is weakly fractured. The areas indicated by arrows in Fig. D are euhedral faces of overgrowth which appear corroded in Fig. C, suggesting secondary porosity.

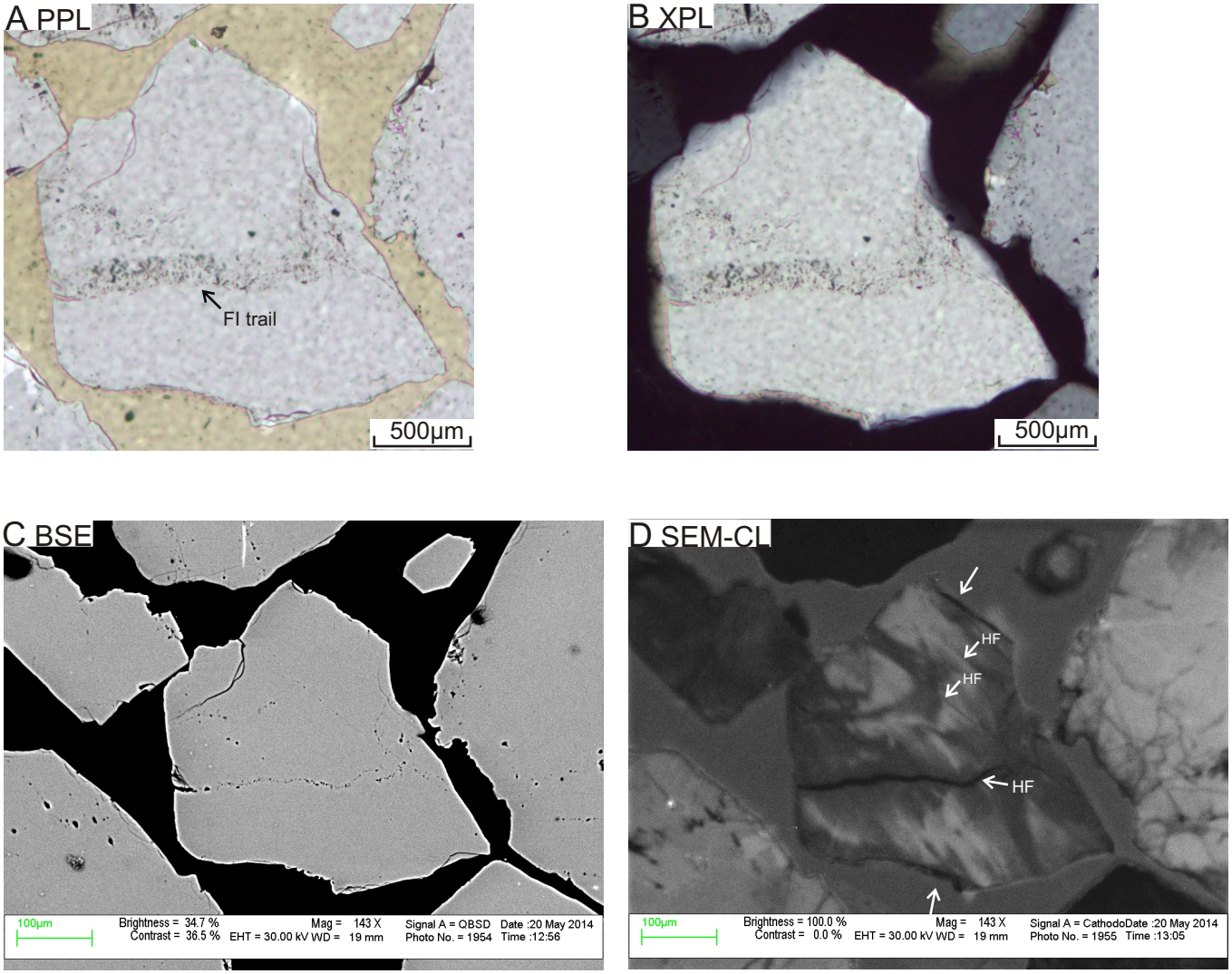

Figure 1A-20: Microphotos under ppl (A) and xpl (B), SEM-BSE image (C) and SEM-CL image (D) of quartz grain 20 in sample 2565. The grain is subhedral and sub-angular monocrystalline with weak undulose extinction. Fluid inclusions are common; they are usually associated with secondary porosity and form trails along healed fractures (Fig. A). The grain is microfractured with a set of parallel fractures and a set of irregular curved fractures (Fig. C and D). Healed fractures (HF) are common (Fig. D). The dark areas indicated by arrows in Fig. D are overgrowth; these areas appear corroded in Fig. C, forming secondary porosity. The grain shows bright CL streak patches in SEM-CL image, which have the same orientation of the set of parallel healed fractures.

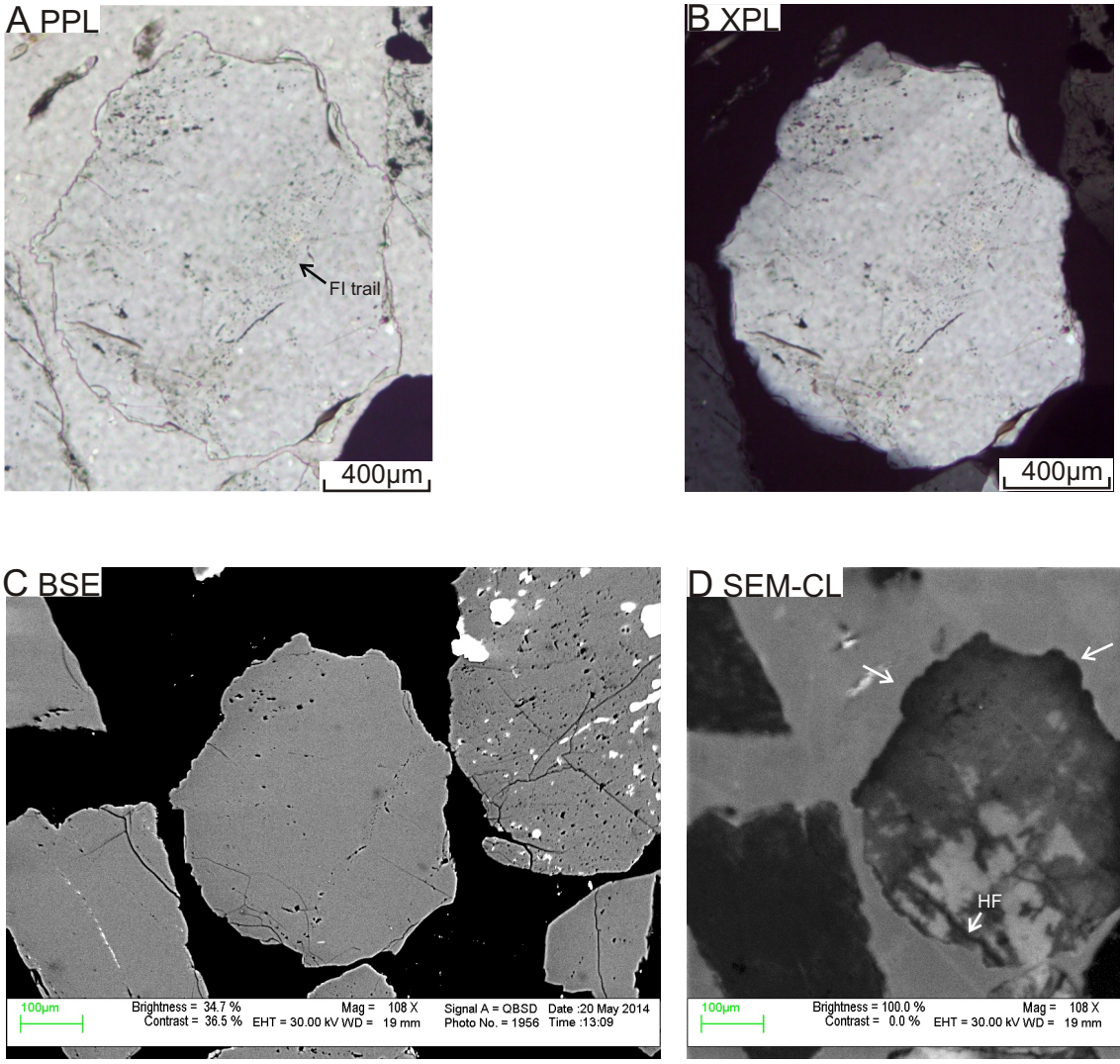

Figure 1A-21: Microphotos under ppl (A) and xpl (B), SEM-BSE image (C) and SEM-CL image (D) of quartz grain 21 in sample 2565. The grain is subhedral and sub-rounded monocrystalline with irregular margins, mosaic texture, and strong undulose extinction. Fluid inclusions are common; they are usually associated with secondary porosity and form trails along healed fractures (Fig. A). The grain is microfractured with some irregular and curved fractures (Fig. C and D). A few healed fractures (HF) can be seen in Fig. D. The areas indicated by arrows in Fig. D are overgrowth; these areas appear corroded in Fig. C, suggesting secondary porosity. The grain shows random bright CL patches in SEM-CL image.

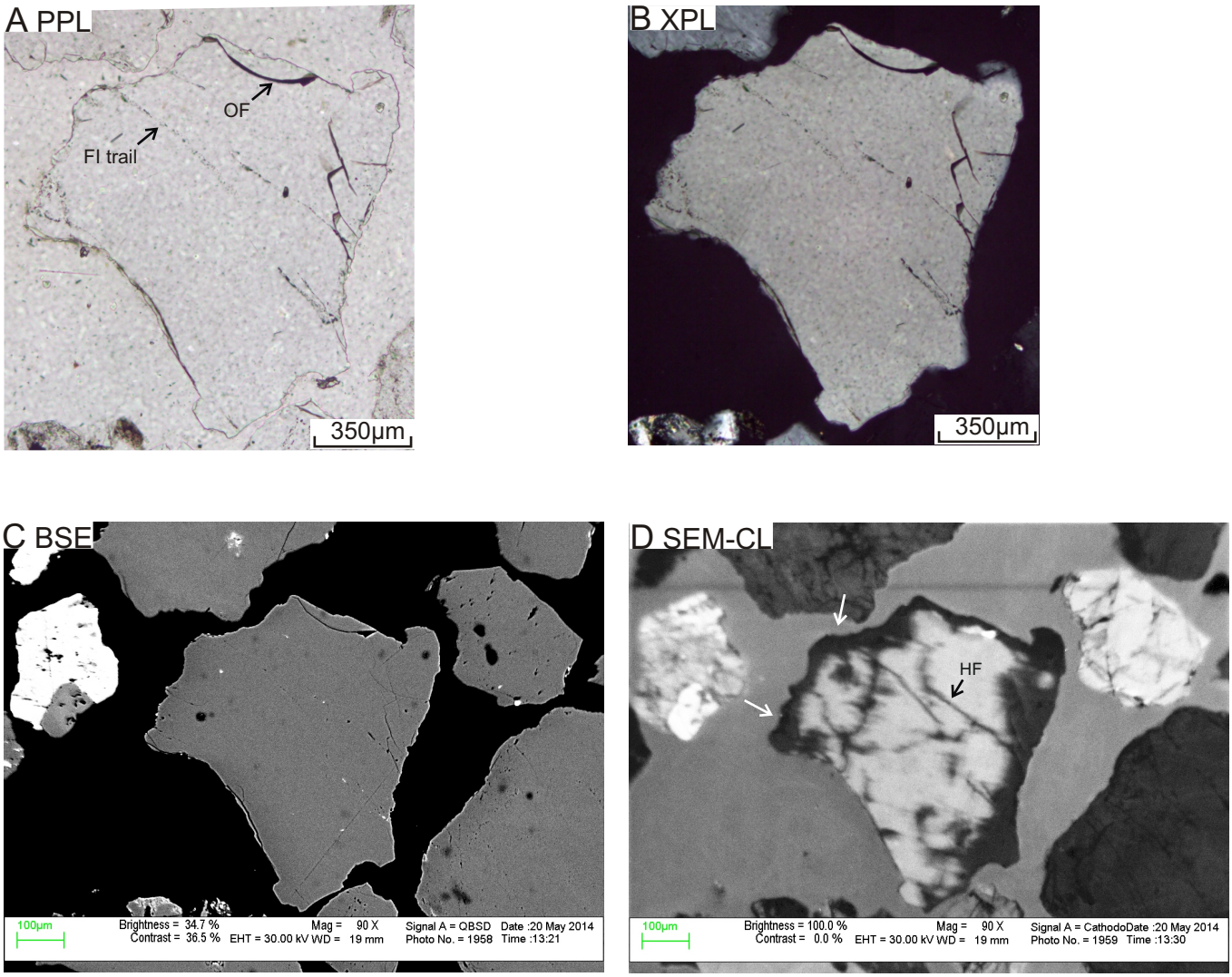

Figure 1A-22: Microphotos under ppl (A) and xpl (B), SEM-BSE image (C) and SEM-CL image (D) of quartz grain 22 in sample 2565. The grain is subhedral and sub-angular monocrystalline with irregular and embayed margins, and with strong undulose extinction. Fluid inclusions are common; they are usually associated with secondary porosity and form trails along healed fractures (Fig. A). The grain is microfractured with a set of parallel fractures and some irregular curved fractures (Fig. C and D). Some healed fractures (HF) can be seen in Fig. D. The areas indicated by arrows in Fig. D are overgrowth; these areas appear corroded in Fig. C. The grain shows bright streaky patches fabric in SEM-CL image.

A PPL

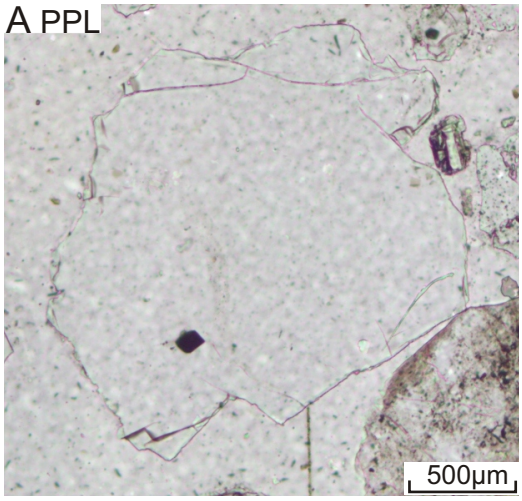

B XPL

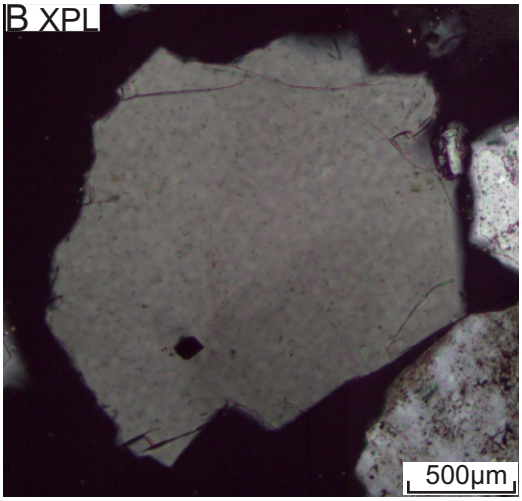

C BSE

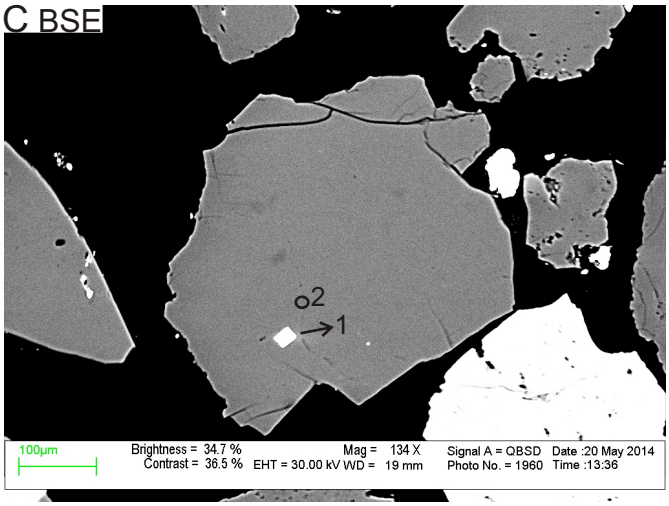

D SEM-CL

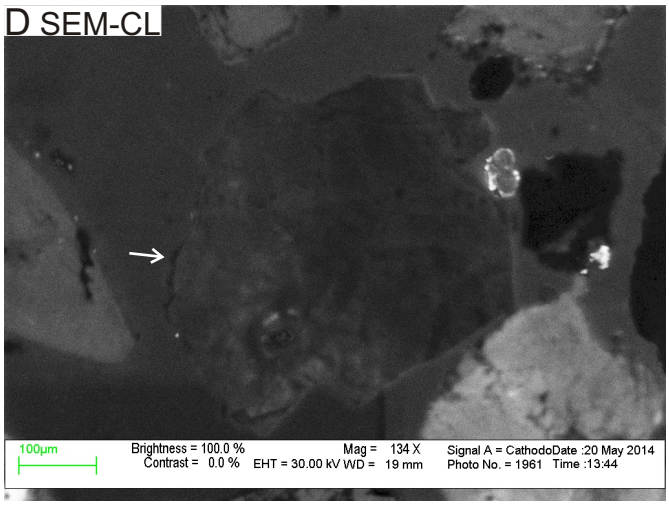

E EDS mineral analyses

Pos#	Min. ID	SiO2	Al2O3	FeO	CaO	Sc2O3	Y2O3	ZrO2	HfO2	Total	Actual Total
1	Zrn	29.86	0.47	0.39	0.97	0.55	2.31	64.07	1.39	100	127
2	Qz	99.99								100	172

Figure 1A-23: Microphotos under ppl (A) and xpl (B), SEM-BSE image (C), SEM-CL image (D), and EDS analyses table (E) of quartz grain 23 in sample 2565. The grain is subhedral and sub-rounded monocrystalline with strong undulose extinction. Fluid inclusions and secondary porosity are rare. The grain contains zircon inclusion and is microfractured with a few irregular curved fractures (Fig. C and D). Healed fractures are rare. The area indicated by arrow in Fig. D is overgrowth; this area appears corroded in Fig. C, suggesting secondary porosity. The grain shows subtle mottling in SEM-CL image.

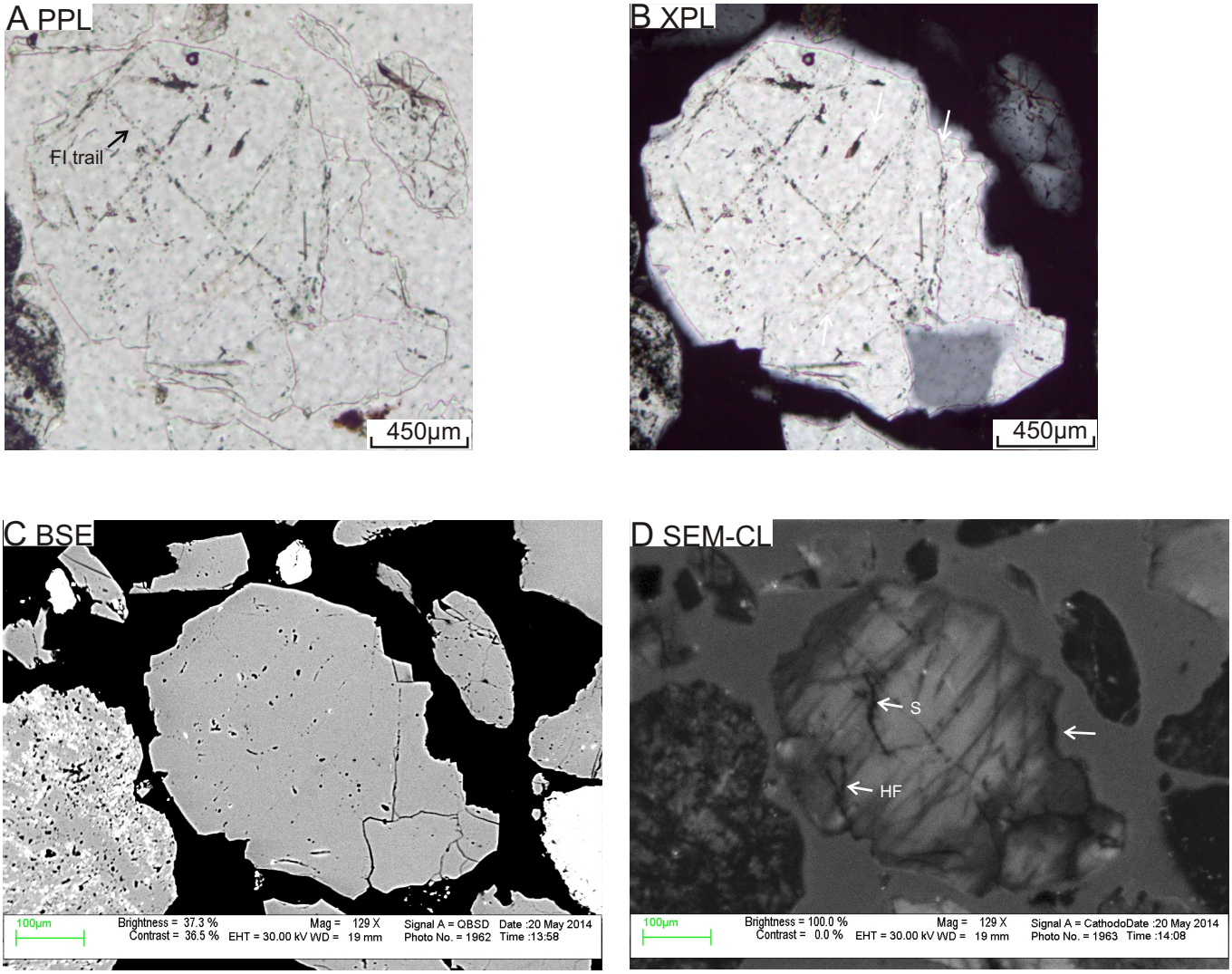

Figure 1A-24: Microphotos under ppl (A) and xpl (B), SEM-BSE image (C) and SEM-CL image (D) of quartz grain 24 in sample 2565. The grain is subhedral and sub-rounded polycrystalline (only 2 sub-grains) with irregular margins and strong undulose extinction. Fluid inclusions are common; they are usually associated with secondary porosity and form trails along healed fractures (Fig. A) The grain is strongly microfractured with a set of parallel fractures that show preferred orientation and some irregular fractures (Fig. D). Healed fractures (HF) and Spiders (S) are common (Fig. D). The area indicated by arrow in Fig. D is overgrowth; this area appears corroded in Fig. C, suggesting secondary porosity. The grain shows streaky texture in SEM-CL image.

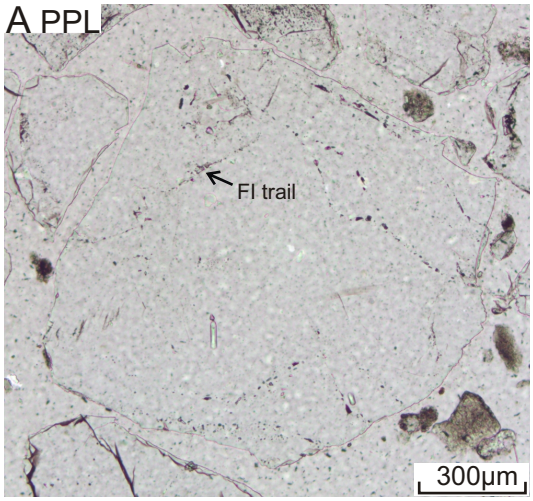

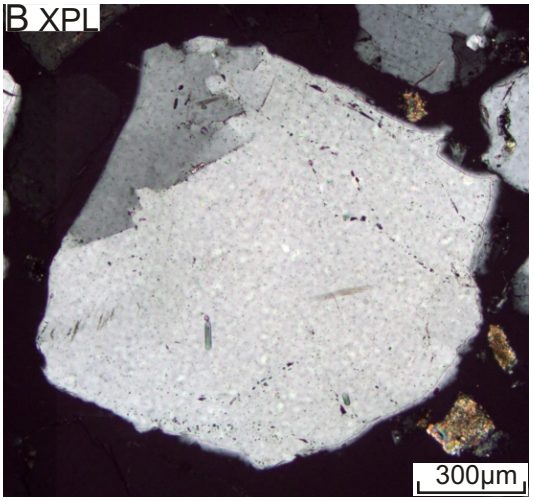

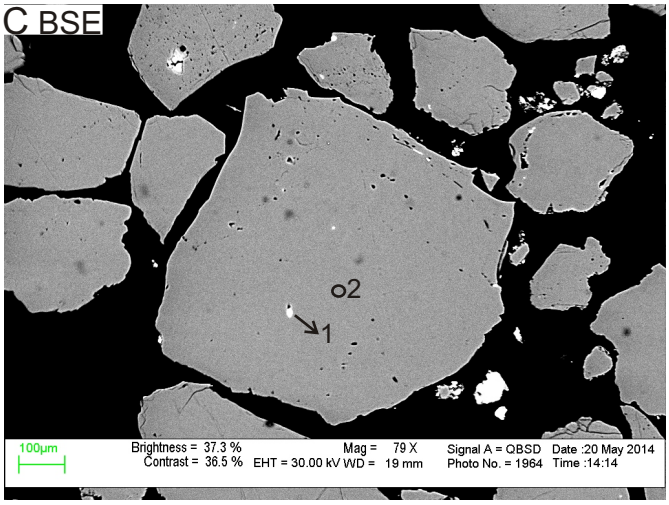

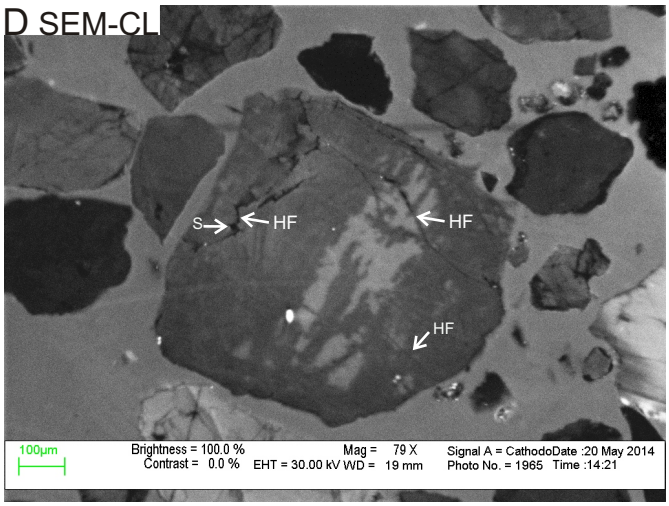

E EDS mineral analyses

Pos#	Min. ID	SiO2	CaO	P2O5	F	Total	Actual Total
1	Ap	20.77	36.85	37.51	4.87	100	186
2	Qz	99.99				100	166

Figure 1A-25: Microphotos under ppl (A) and xpl (B), SEM-BSE image (C), SEM-CL image (D), and EDS analyses table (E) of quartz grain 25 in sample 2565. The grain is subhedral and sub-rounded polycrystalline (only 2 sub-grains) with strong undulose extinction. Fluid inclusions are common; they are usually associated with secondary porosity and form trails along healed fractures (Fig. A). The grain contains apatite inclusions and some irregular curved fractures. Some healed fractures (HF) and Spiders (S) can be seen in Fig. D. The grain shows random bright CL patches in SEM-CL image.

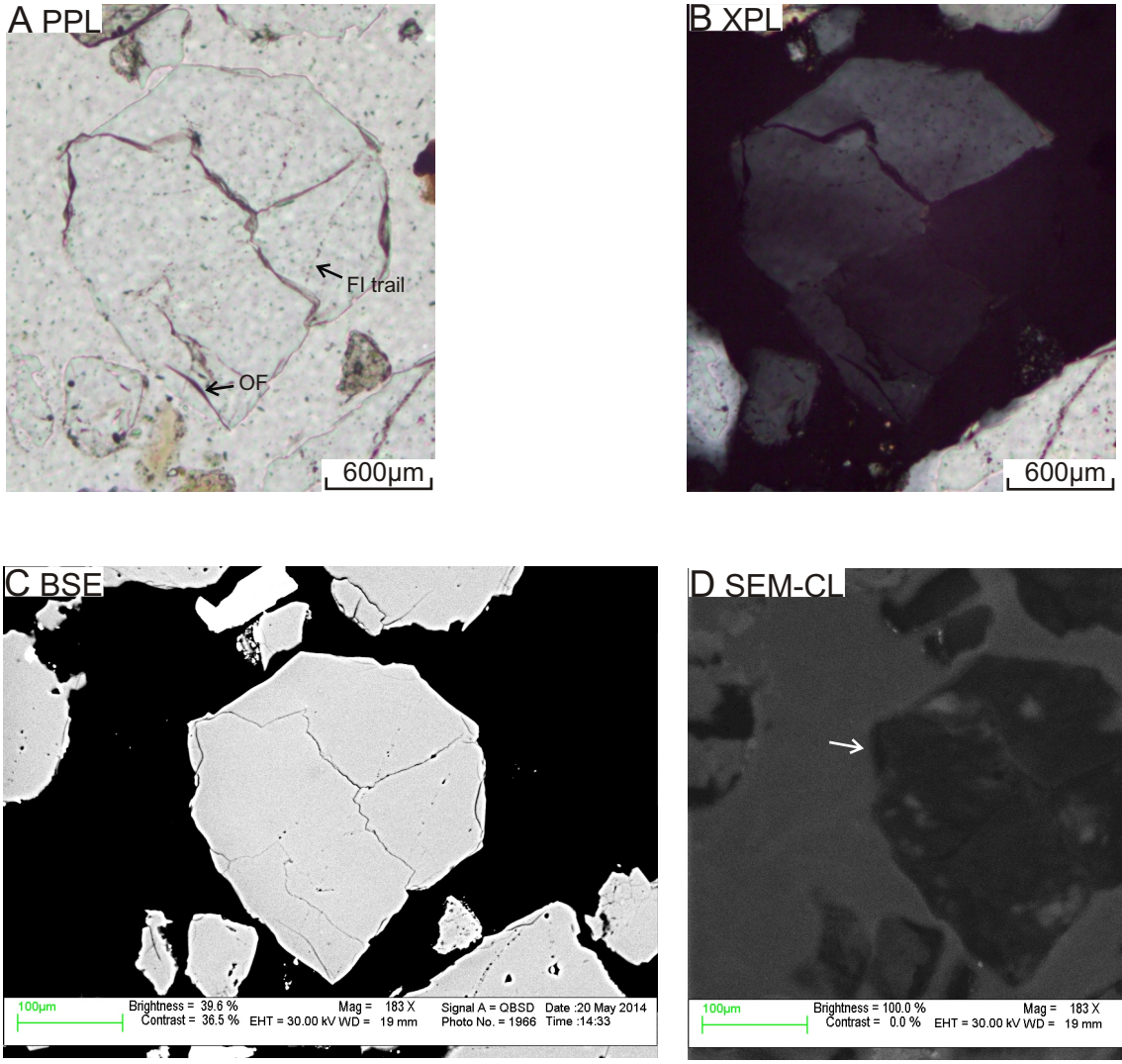

Figure 1A-26: Microphotos under ppl (A) and xpl (B), SEM-BSE image (C) and SEM-CL image (D) of quartz grain 26 in sample 2565. The grain is subhedral and sub-angular polycrystalline (only 4 sub-grains) with strong undulose extinction. Fluid inclusions are present; they are usually associated with secondary porosity and form trails along healed fractures (Fig. A). The grain contains irregular curved fractures (Fig. A and C). A few open fracture can be seen in Fig. A. The areas indicated by arrows in Fig. D are overgrowth. The grain shows subtle mottling in SEM-CL image.

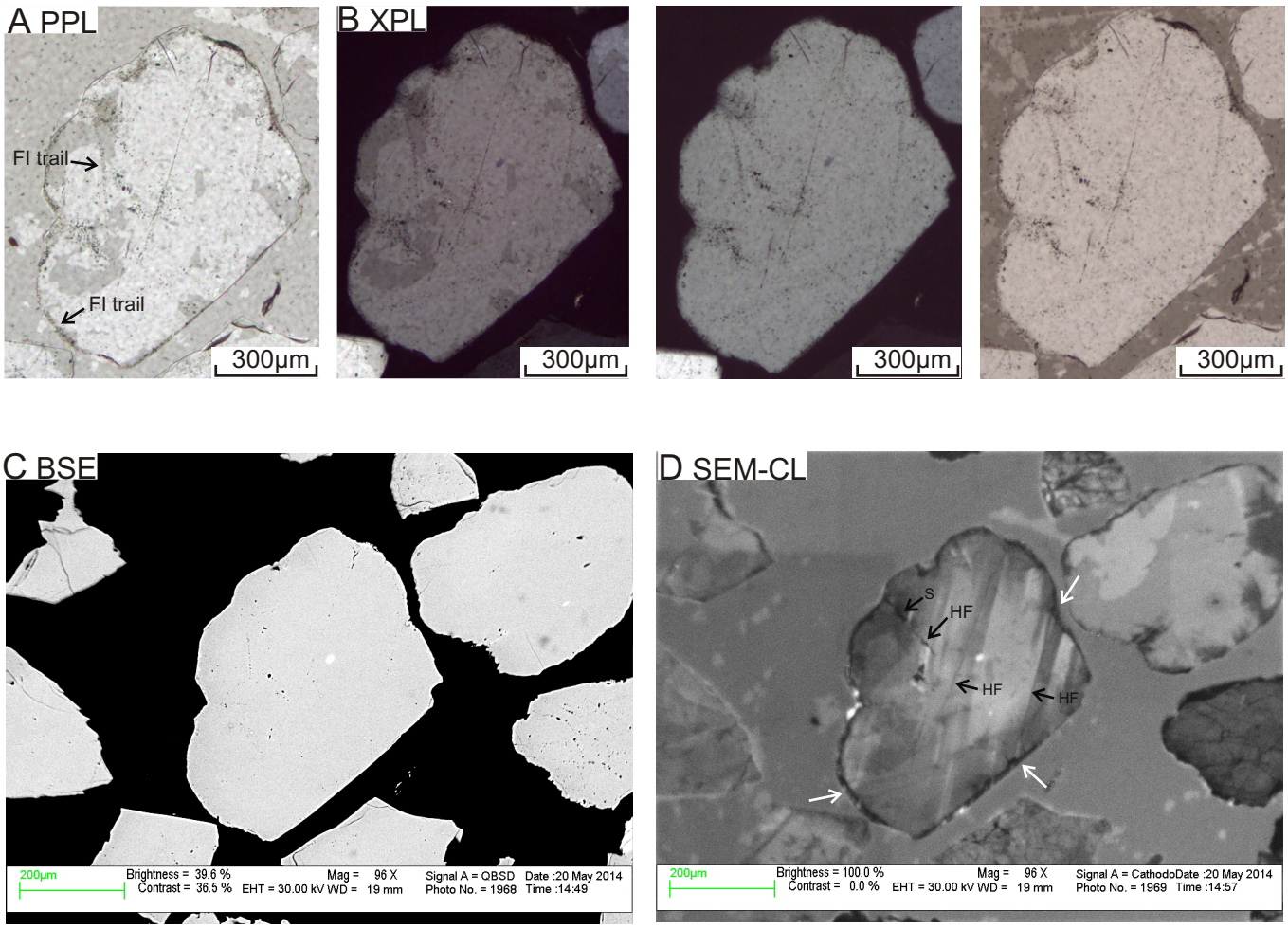

Figure 1A-27: Microphotos under ppl (A and C) and xpl (B and D), BSE image (E) and SEM-CL image (F) of quartz grain 27 in sample 2565. See details about Fig. C and D and the explanation of darker patches in Fig. A and B in the caption of Fig. 1A-2. The grain is anhehedral and sub-rounded monocrystalline with non-undulose extinction. Fluid inclusions are common (Fig. A); they are usually associated with secondary porosity and form trails along healed fractures and at the boundary between the detrital quartz grain and the overgrowth (diagenetic fluid inclusion trail). The grain is microfractured with a set of parallel fractures (Fig. F). Some healed fractures (HF) and spiders (S) can be seen in Fig. F. The areas indicated by arrows in Fig. F are overgrowth. The grain shows streaky patches pattern in SEM-CL image, which has the same orientation of the set of parallel fractures.

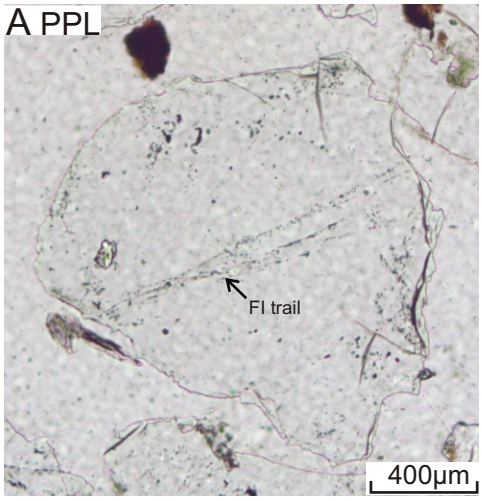

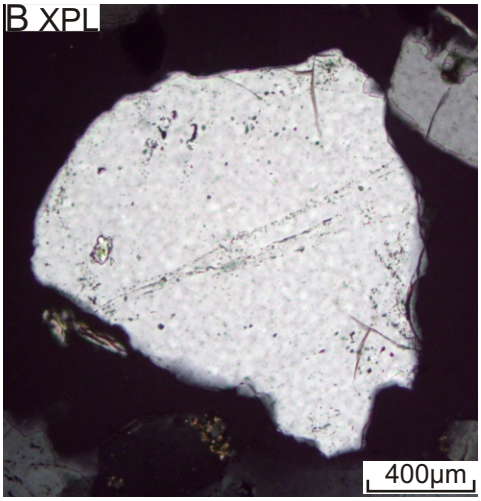

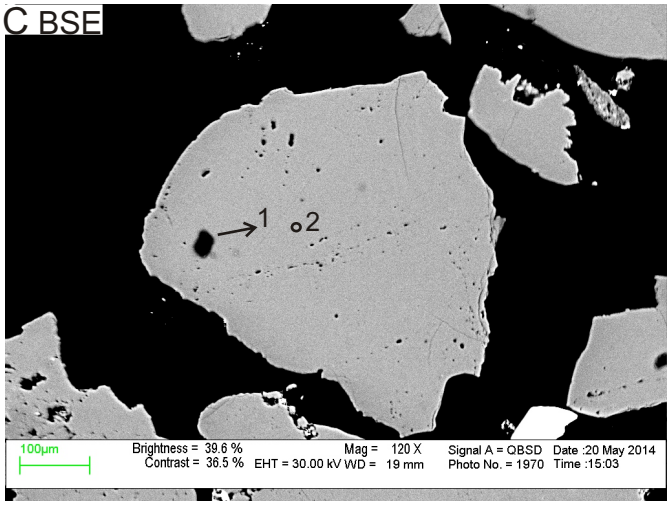

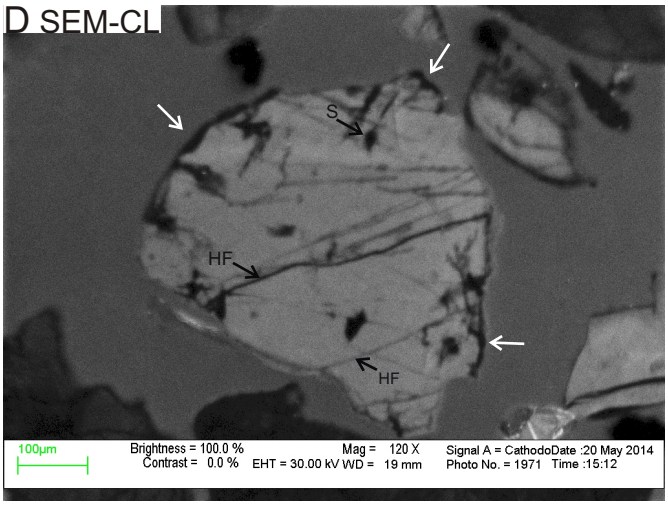

E EDS mineral analyses

Pos#	Min. ID	SiO2	CaO	Na2O	K2O	SO3	Cl	CuO	Total	Actual Total
1	Qz	92.52	0.29	1.78	1.78	1.85	1.18	0.61	100	114
2	Qz	99.99							100	160

Figure 1A-28: Microphotos under ppl (A) and xpl (B), SEM-BSE image (C), SEM-CL image (D), and EDS analyses table (E) of quartz grain 28 in sample 2565. The grain is subhehedral and sub-rounded monocrystalline with weak undulose extinction. Fluid inclusions are common; they are usually associated with secondary porosity and form trails along healed fractures (Fig. A). The grain contains sets of parallel fractures. Healed fractures (HF) and spiders (S) are common (Fig. D). The areas indicated by arrows in Fig. D are overgrowth; these areas appear corroded in Fig. C.

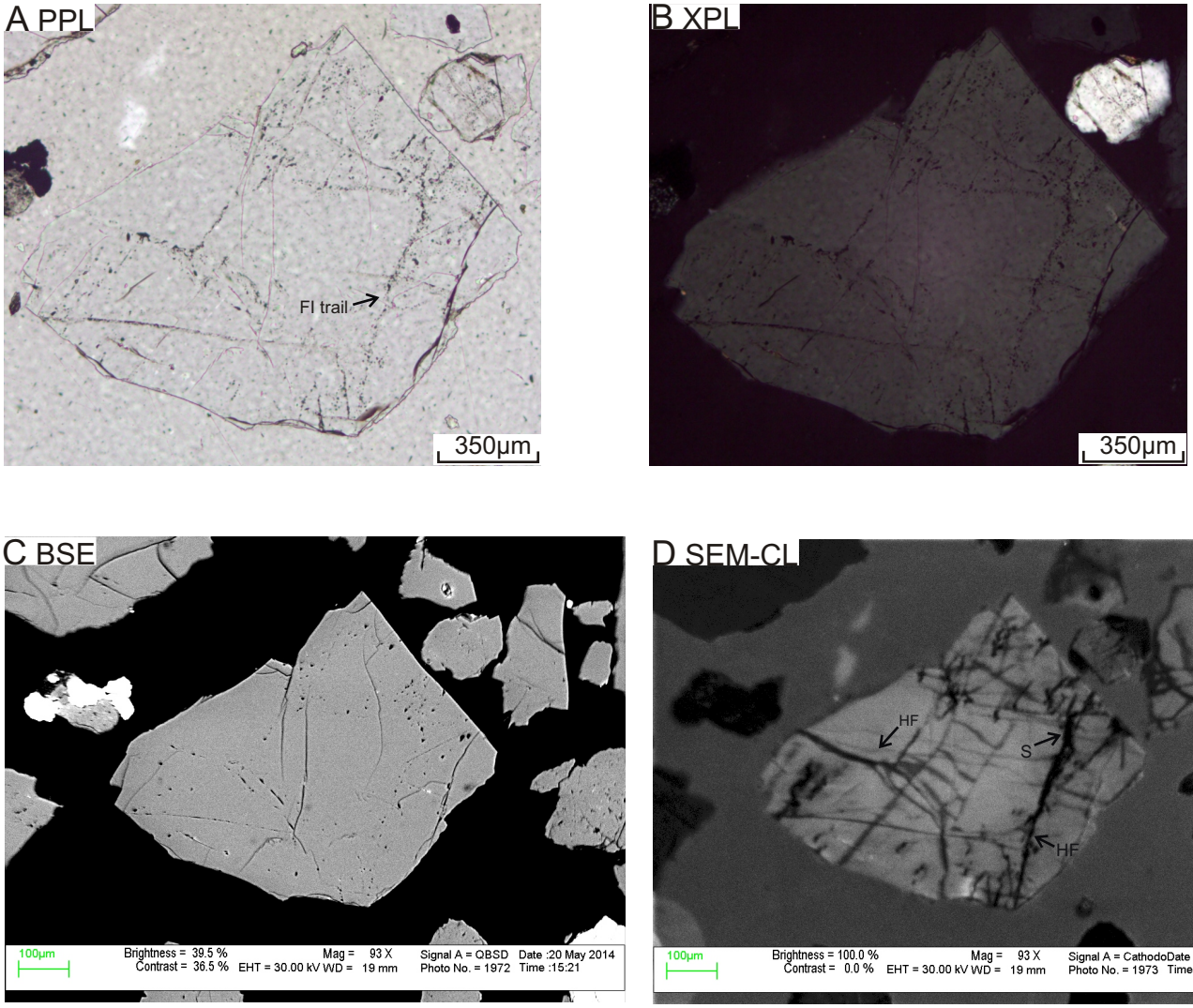

Figure 1A-29: Microphotos under ppl (A) and xpl (B), SEM-BSE image (C) and SEM-CL image (D) of quartz grain 29 in sample 2565. The grain is anhedral and sub-angular monocrystalline with weak undulose extinction. Fluid inclusions are common; they are usually associated with secondary porosity and form trails along healed fractures (Fig. A). The grain contains two sets of parallel fractures crosscutting each other. Healed fractures (HF) and spiders (S) are common (Fig. D).

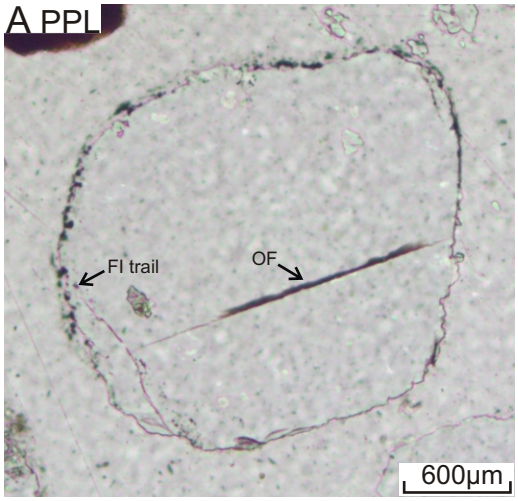

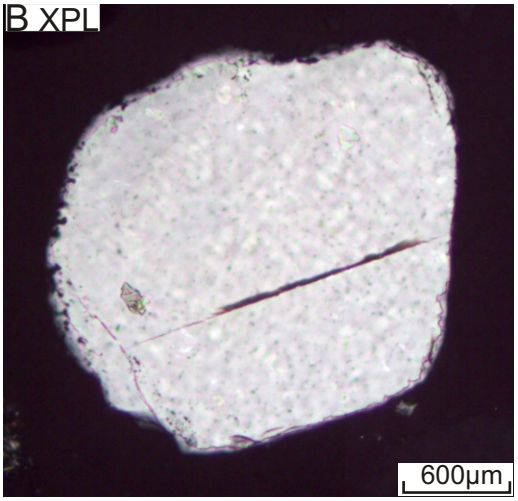

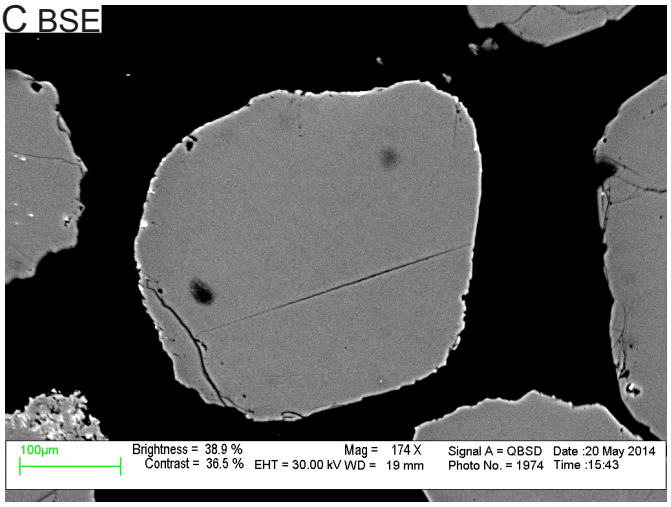

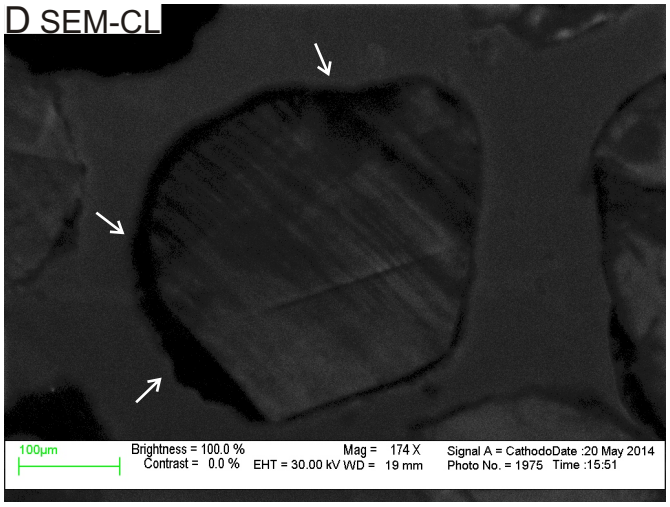

E EDS mineral analyses

Pos#	Min. ID	SiO2	Na2O	K2O	SO3	Cl	Total	Actual Total
1	Qz	98.21	0.53	0.23	0.77	0.24	100	141
2	QZ	99.99					100	154

Figure 1A-30: Microphotos under ppl (A) and xpl (B), SEM-BSE image (C), SEM-CL image (D), and EDS analyses table (E) of quartz grain 30 in sample 2565. The grain is subhedral and well rounded monocrystalline with deformation lamellae and strong undulose extinction. Fluid inclusions and secondary porosity are common (Fig. A), they are located at the boundary between the detrital quartz grain and the overgrowth (diagenetic fluid inclusion trail). The grain contains only a few irregular fractures and open fractures (Fig. A and C). The areas indicated by arrows in Fig. D are overgrowth; these areas appear corroded in Fig. C, suggesting secondary porosity. The grain shows deformation lamellae in SEM-CL image.

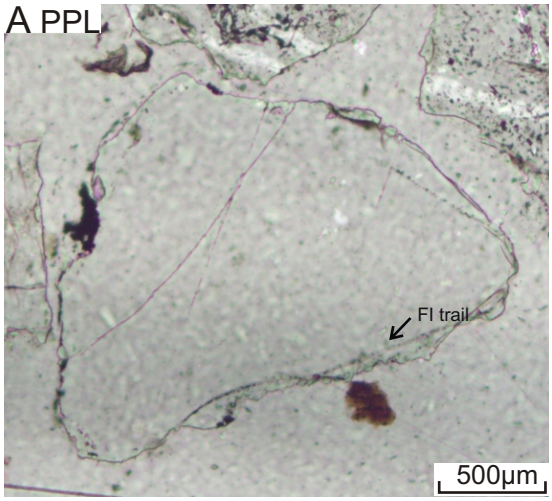

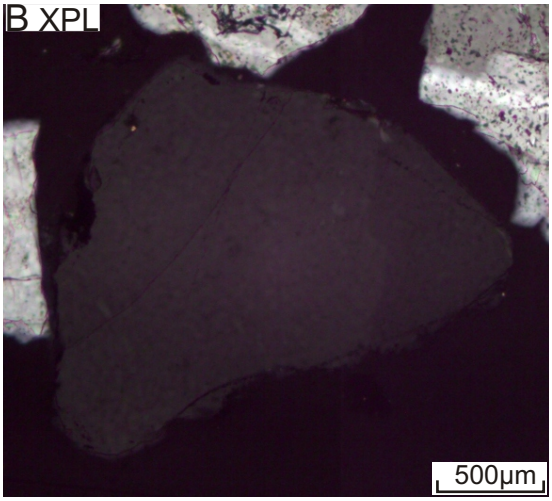

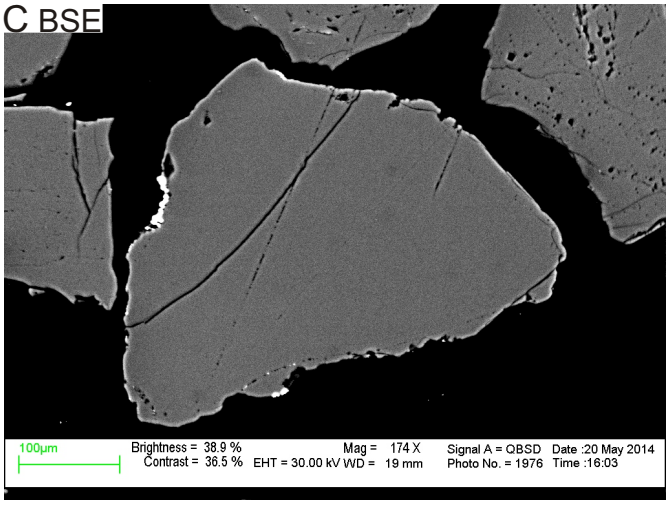

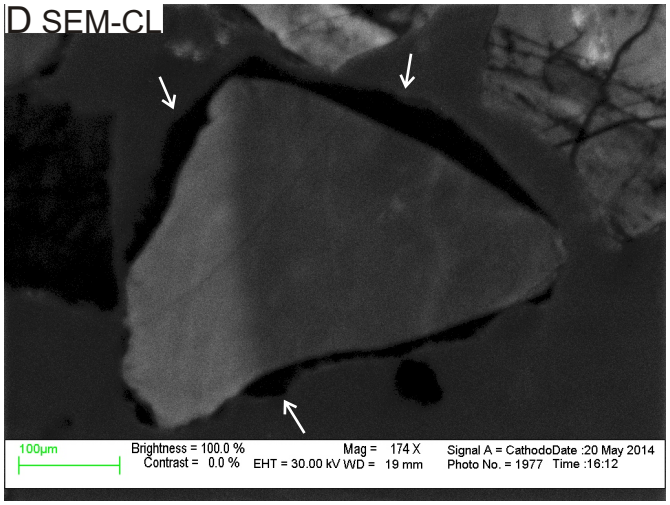

Figure 1A-31: Microphotos under ppl (A) and xpl (B), SEM-BSE image (C) and SEM-CL image (D) of quartz grain 31 in sample 2565. The grain is anhedral and sub-rounded monocrystalline with non-undulose extinction. Fluid inclusions form trails; they are associated with secondary porosity and are located at the boundary between the detrital quartz grain and the overgrowth (Fig. A). The grain is weakly fractured with irregular and curved fractures (Fig. C). The areas indicated by arrows in Fig. D are overgrowth; these areas appear corroded in Fig. C, suggesting secondary porosity. The grain shows zoning in SEM-CL image due variation in luminescense intensity within different parts.

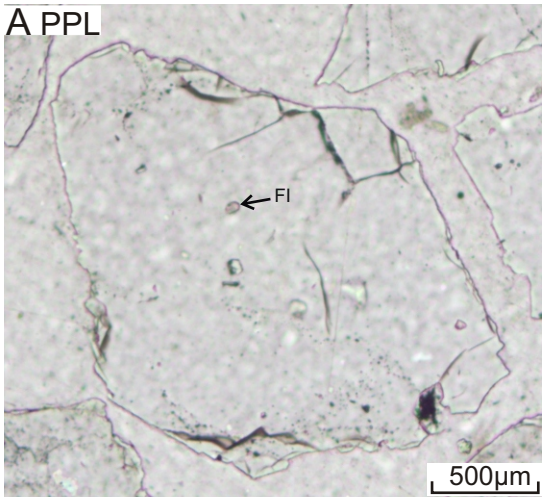

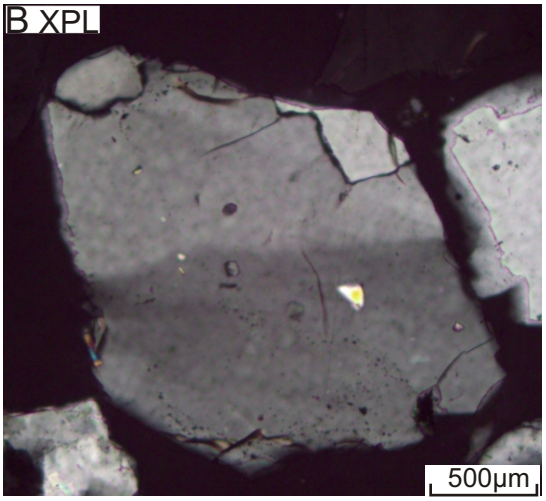

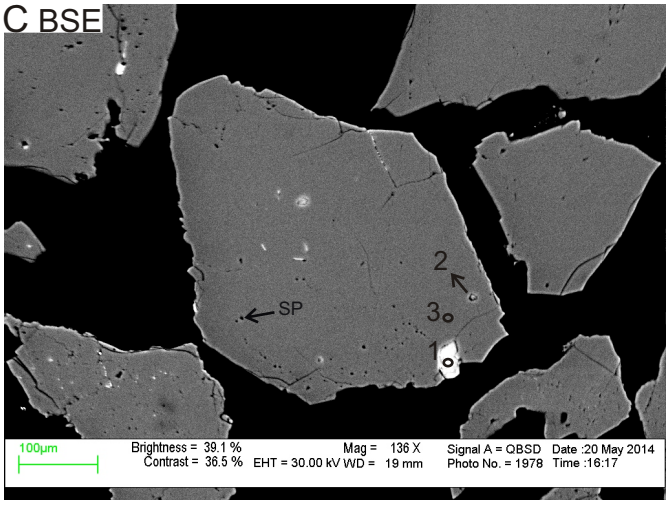

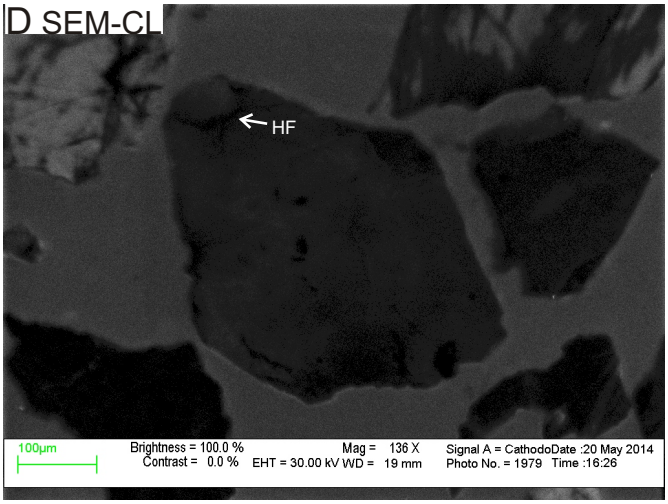

E EDS mineral analyses

Pos#	Min. ID	SiO2	TiO2	Al2O3	FeO	MgO	Na2O	K2O	P2O5	SO3	F	Total	Actual Total
1	Py+Ms	41.56	0.63	23.83	7.91	2.19	0.27	8.62	0.89	12.09	2.01	100	658
2	Kfs	78.49	0.3	12.43	1.34	0.81	0.18	4.01			2.44	100	643
3	Qz	99.99										100	640

Figure 1A-32: Microphotos under ppl (A) and xpl (B), SEM-BSE image (C), SEM-CL image (D), and EDS analyses table (E) of quartz grain 32 in sample 2565. The grain is anhedral and sub-rounded polycrystalline (only 3 sub-grains with sutured sub-grain boundaries) with mosaic texture and weak undulose extinction. Fluid inclusions (Fig. A) and secondary porosity (Fig. C) are common. The grain contains pyrite + muscovite inclusions, and K-feldspar inclusion and is microfractured with irregular curved fractures (Fig. C). Healed fractures are rare.

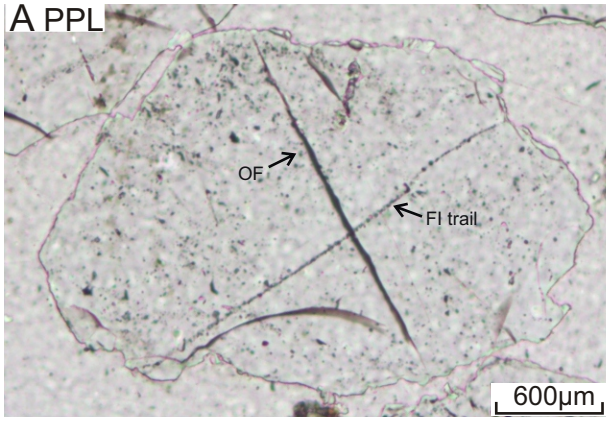

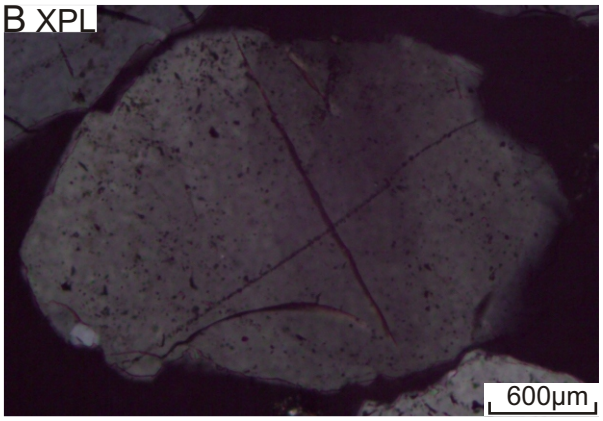

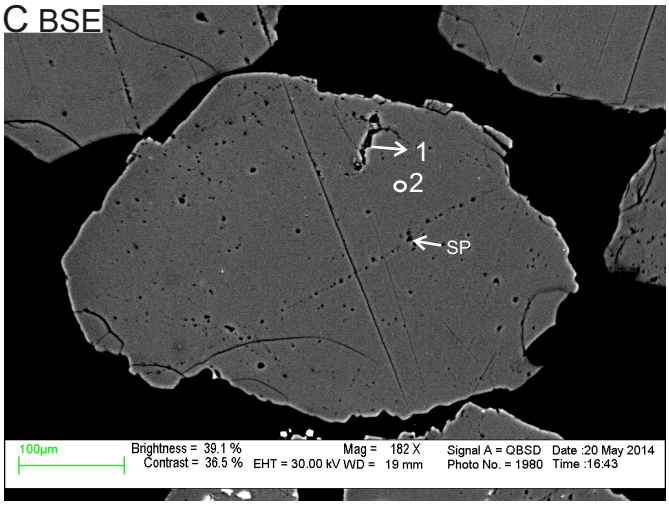

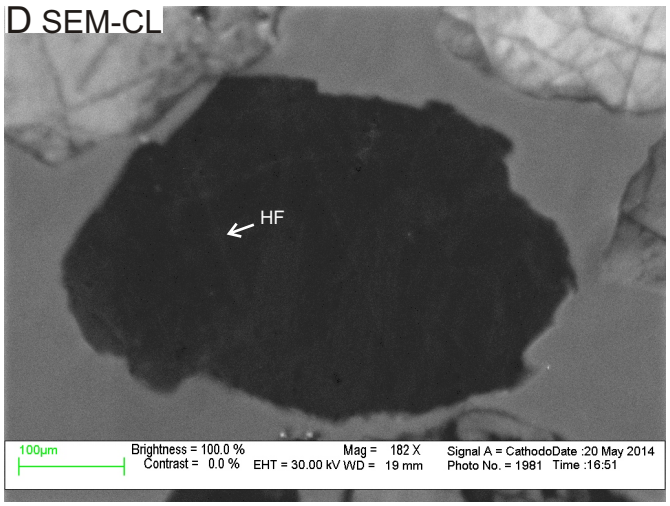

E EDS mineral analyses

Pos#	Min. ID	SiO2	Total	Actual Total
1	Qz	99.99	100	140
2	Qz	99.99	100	144

Figure 1A-33: Microphotos under ppl (A) and xpl (B), SEM-BSE image (C), SEM-CL image (D), and EDS analyses table (E) of quartz grain 33 in sample 2565. The grain is anhedral and sub-rounded monocrystalline with strong undulose extinction. Fluid inclusions are common; they are usually associated with secondary porosity and form trails along healed fractures (Fig. A and C). The grain is microfractured with sets of parallel fractures and some irregular curved fractures (Fig. C). A few open fractures can be seen in Fig. A, The healed fractures are camouflaged by the very dark gray CL colour in SEM-CL image.

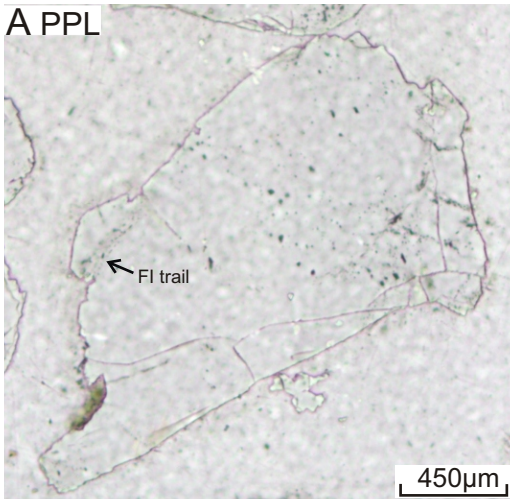

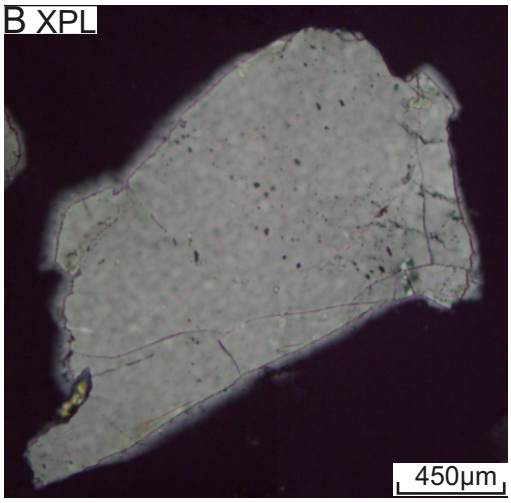

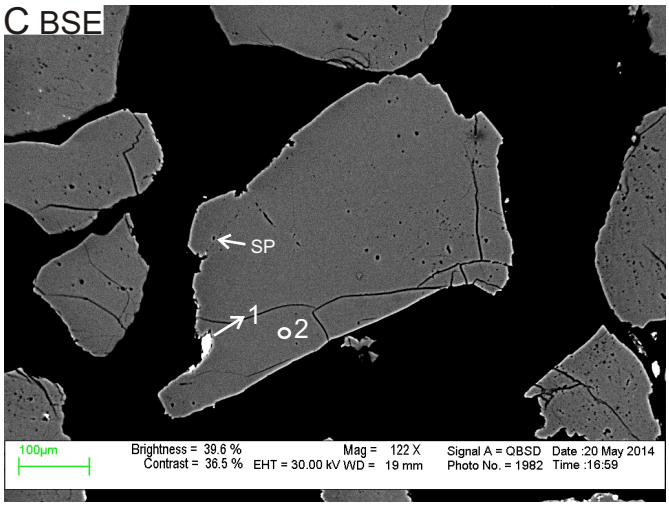

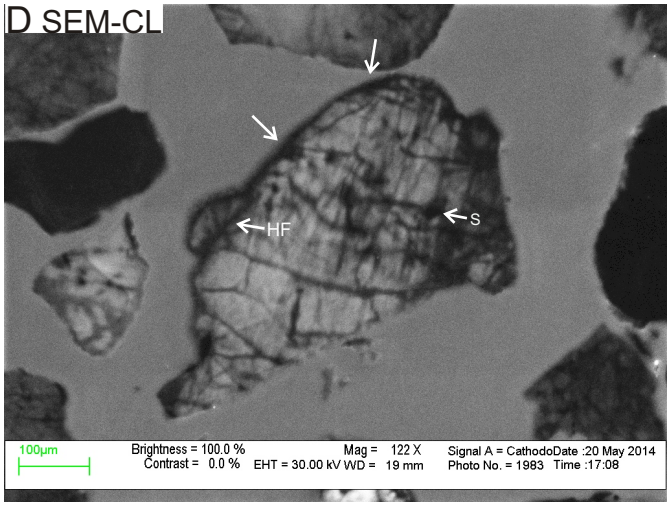

E EDS mineral analyses

Pos#	Min. ID	SiO2	TiO2	Al2O3	FeO	MnO	MgO	K2O	F	Cl	Total	Actual Total
1	Bt	38.79	2.39	16.74	23.32	0.81	1.02	8.93	3.83	0.17	96	133
2	Qz	99.99									100	146

Figure 1A-34: Microphotos under ppl (A) and xpl (B), SEM-BSE image (C), SEM-CL image (D), and EDS analyses table (E) of quartz grain 34 in sample 2565. The grain is anhedral and sub-angular monocrystalline with weak undulose extinction. Fluid inclusions are common (Fig. A); they are usually associated with secondary porosity (Fig. C) and form trails along healed fractures (Fig. A). The grain contains biotite inclusion and is microfractured with two sets of parallel fractures crosscutting each other and a set of irregular curved fractures (Fig. D). A few healed fractures (HF) and spiders (S), that are secondary porosity filled by diagenetic quartz, can be seen in Fig. D. The areas indicated by arrows in Fig. D are overgrowth; these areas appear corroded in Fig. C. The grain shows streaky texture in SEM-CL image.

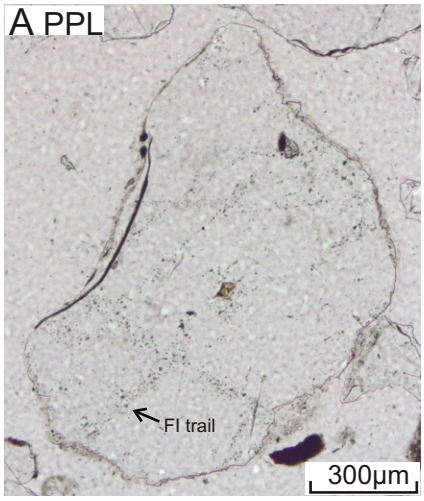

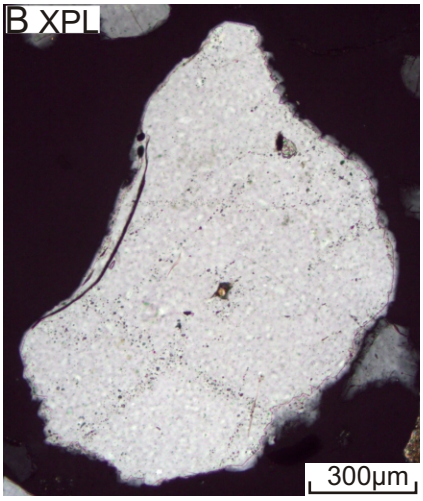

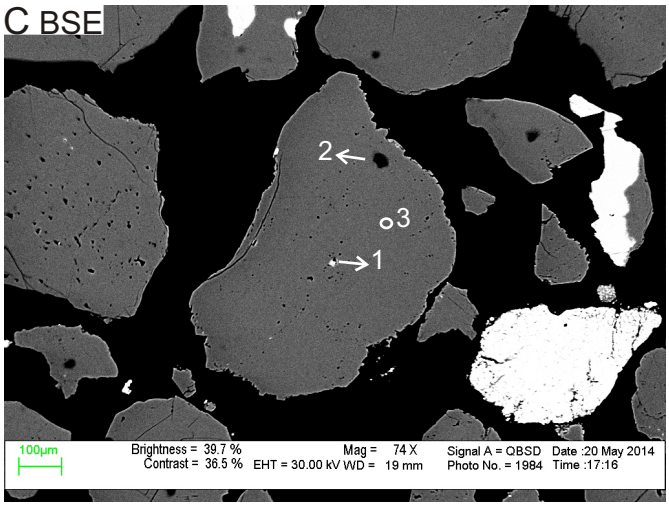

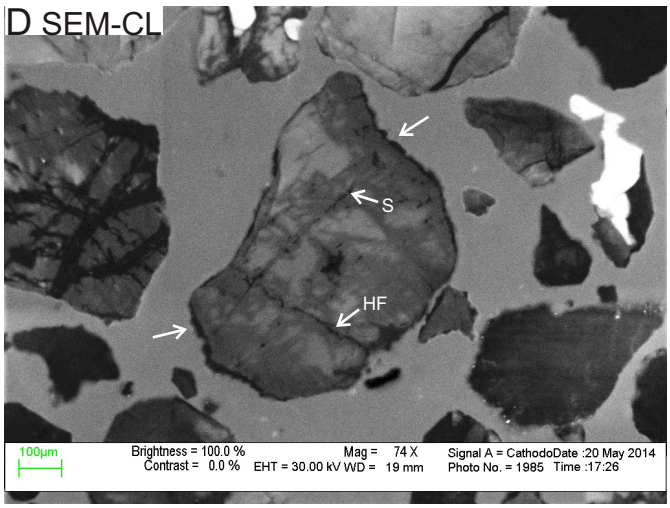

E EDS mineral analyses

Pos#	Min. ID	SiO2	TiO2	Al2O3	FeO	MnO	Na2O	K2O	SO3	Cl	Total	Actual Total
1	Kfs	49.52	0.23	36.47	1.89	0.21	0.63	11.05			100	130
2	Qz	96.63					1.12	0.86	0.87	0.5	100	126
3	Qz	99.99									100	146

Figure 1A-35: Microphotos under ppl (A) and xpl (B), SEM-BSE image (C), SEM-CL image (D), and EDS analyses table (E) of quartz grain 35 in sample 2565. The grain is anhedral and sub-rounded monocrystalline with weak undulose extinction. Fluid inclusions are common; they are usually associated with secondary porosity and form trails along healed fractures and at the boundary between detrital quartz grain and the overgrowth (Fig. A). The grain contains K-feldspar inclusion and is microfractured with a set of irregular fractures (Fig. D). Some healed fractures (HF) and spiders (S) can be seen in Fig. D. The areas indicated by arrows in Fig. D are overgrowth; these areas appear corroded in Fig. C. The grain shows bright streaky patches CL in SEM-CL image.

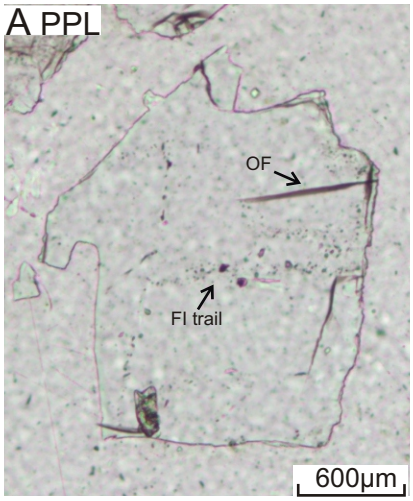

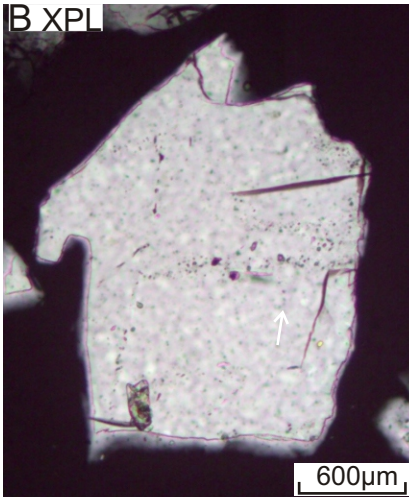

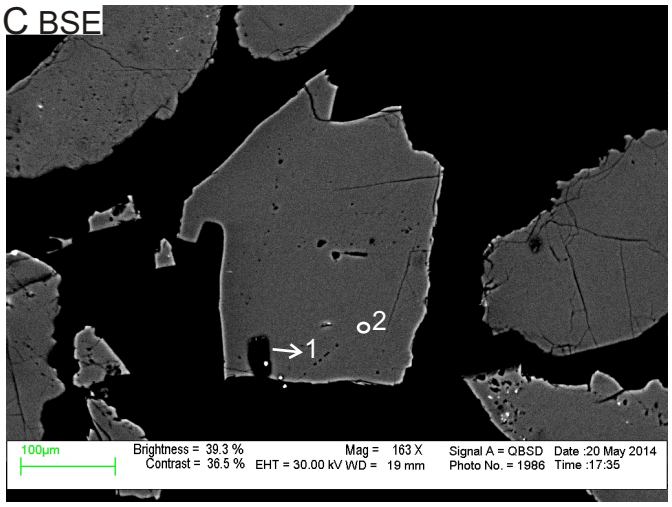

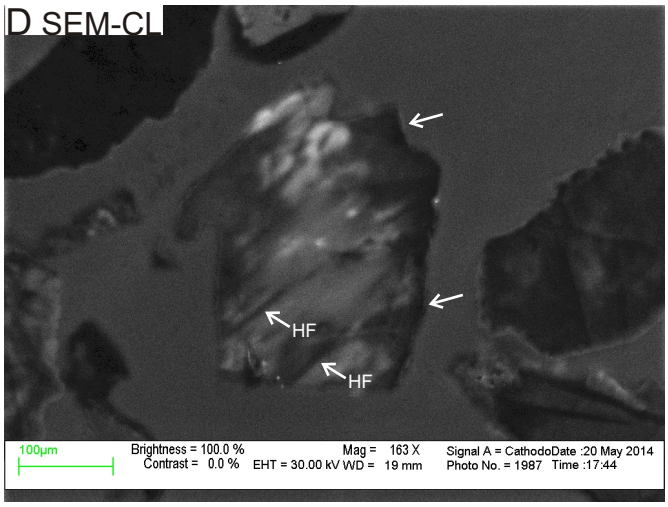

E EDS mineral analyses

Pos#	Min. ID	SiO2	Al2O3	FeO	CaO	Na2O	K2O	SO3	Cl	Total	Actual Total
1	Hole	87.28	0.68	0.19	0.36	4.11	1.88	2.45	3.03	100	90
2	Qz	99.99								100	146

Figure 1A-36: Microphotos under ppl (A) and xpl (B), SEM-BSE image (C), SEM-CL image (D), and EDS analyses table (E) of quartz grain 36 in sample 2565. The grain is anhedral and angular monocrystalline with strong undulose extinction. Fluid inclusions are common; they are usually associated with secondary porosity and form trails along healed fractures (Fig. A). The grain is microfractured with a set of parallel fractures and a set of irregular fractures (Fig. C and D). Some open fractures (OF) can be seen in Fig. A, and some healed fractures (HF) can be seen in Fig. D. The areas indicated by arrows in Fig. D are overgrowth; these areas appear corroded in Fig. C. The grain shows bright-CL streaky patches fabric in SEM-CL image.

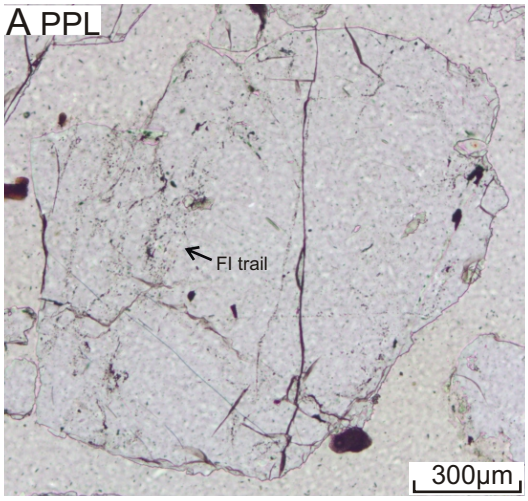

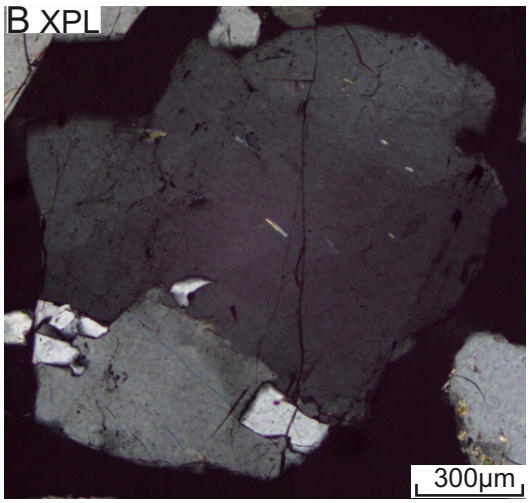

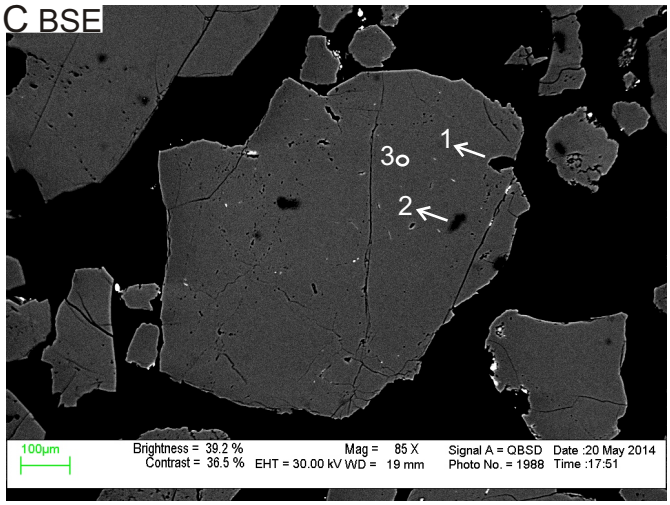

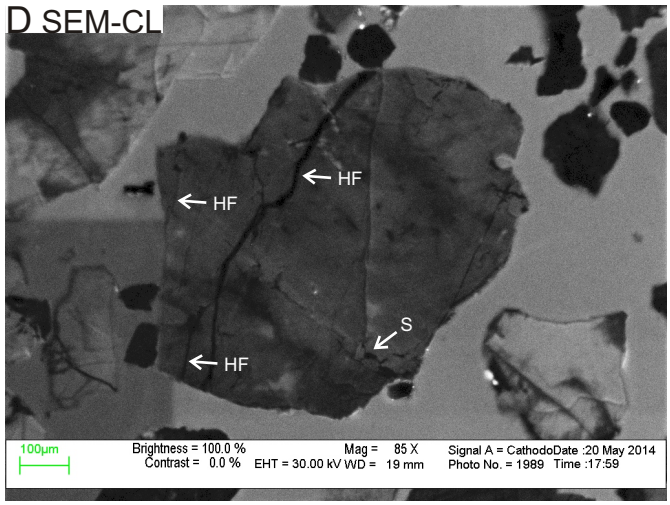

E EDS mineral analyses

Pos#	Min. ID	SiO2	F	Cl	Total	Actual Total
1	Hole		81.13	18.87	100	1
2	Qz	99.99			100	138
3	Qz	100			100	154

Figure 1A-37: Microphotos under ppl (A) and xpl (B), SEM-BSE image (C), SEM-CL image (D), and EDS analyses table (E) of quartz grain 37 in sample 2565. The grain is subhedral and sub-angular polycrystalline (more than 7 sub-grains with sutured sub-grain boundaries) with strong undulose extinction. Fluid inclusions are common; they are usually associated with secondary porosity and form trails along healed fractures (Fig. A). The grain is microfractured with irregular fractures and a set of sub-parallel fractures (Fig. D). Some healed fractures (HF) and spiders (S) can be seen in Fig. D, a thick healed fracture filled with secondary silica is indicated by arrow in Fig. D. The grain shows subtle mottling texture in SEM-CL image.

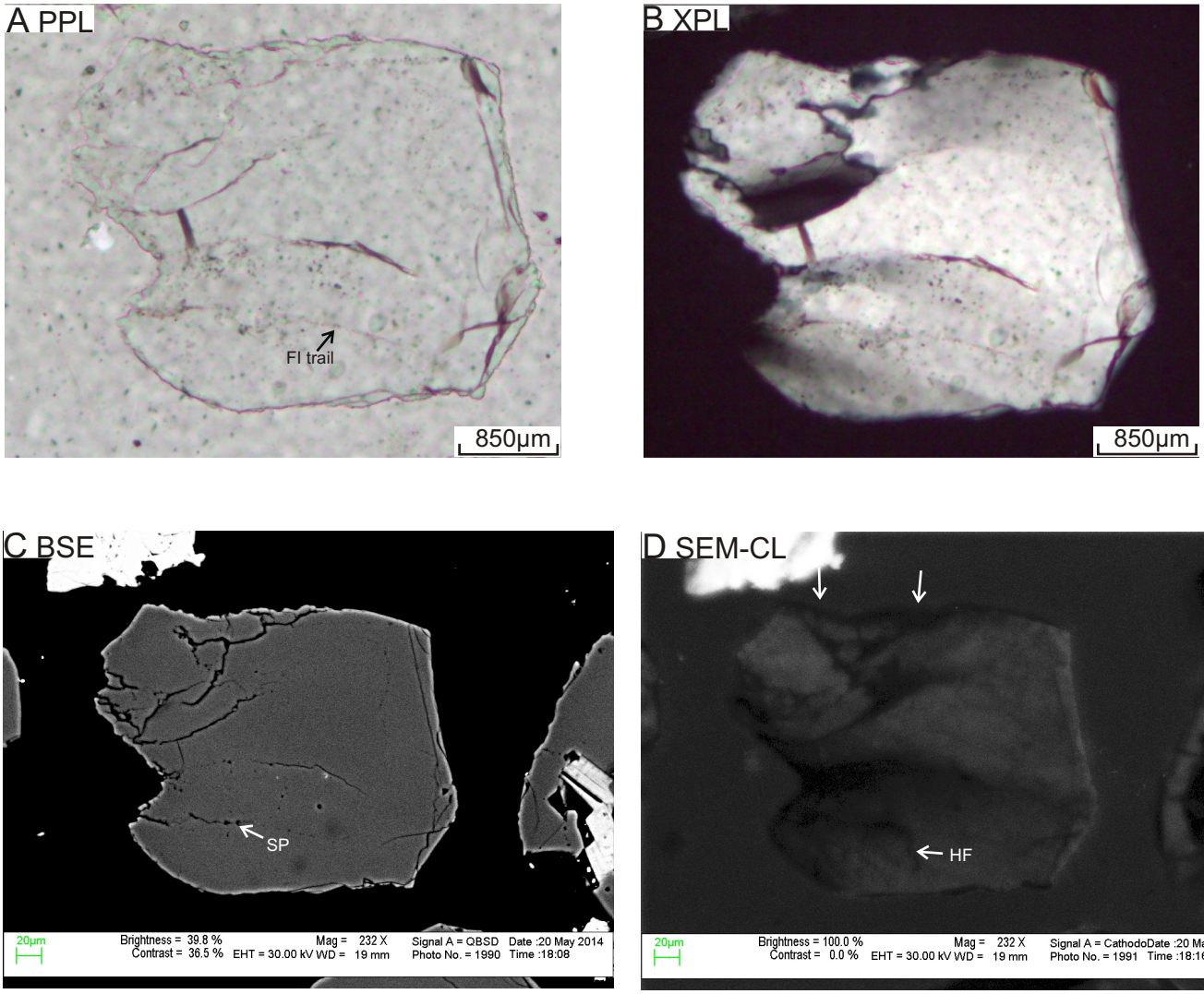

Figure 1A-38: Microphotos under ppl (A) and xpl (B), SEM-BSE image (C) and SEM-CL image (D) of quartz grain 38 in sample 2565. The grain is anhedral and sub-angular polycrystalline (6 sub-grains with sutured sub-grain boundaries) with mosaic texture and weak undulose extinction. Fluid inclusions are present; they are usually associated with secondary porosity and form trails along healed fractures (Fig. A). The grain is microfractured with a set of irregular curved fractures (Fig. C and D). Some healed fractures (HF) can be seen in Fig. D. The areas indicated by arrows in Fig. D are overgrowth; these areas appear corroded in Fig. C, suggesting secondary porosity.

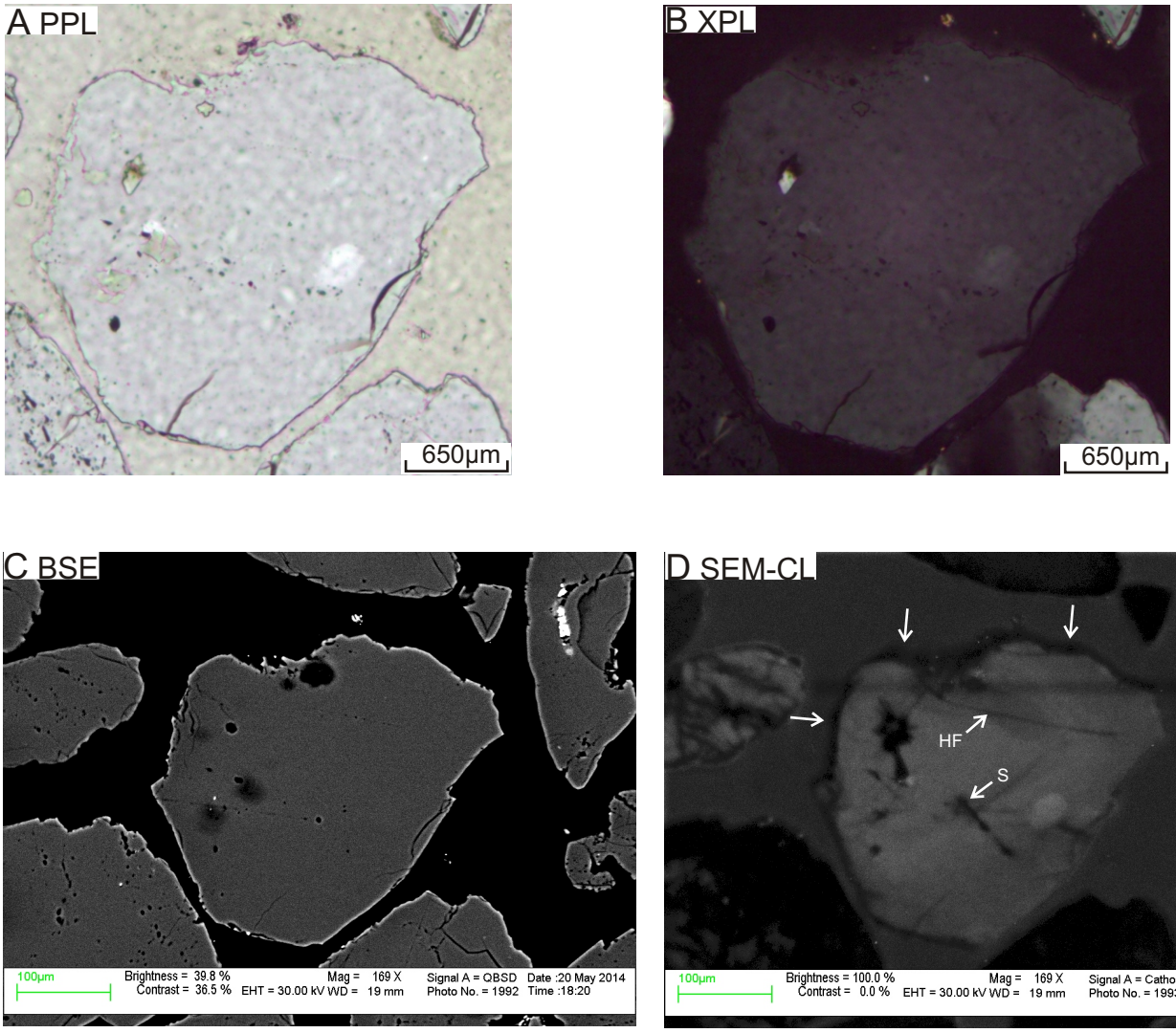

Figure 1A-39: Microphotos under ppl (A) and xpl (B), SEM-BSE image (C) and SEM-CL image (D) of quartz grain 39 in sample 2565. The grain is subhedral and sub-rounded monocrystalline with non-undulose extinction. Fluid inclusions are rare. The grains is weakly microfractured with irregular fractures (Fig. A and C). A few healed fractures (HF) and spiders (S) can be seen in Fig. D. The areas indicated by arrows in Fig. D are overgrowth; these areas appear corroded in Fig. C, suggesting secondary porosity.

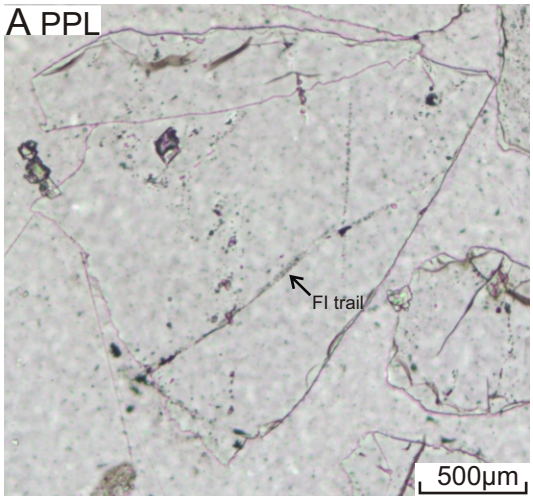

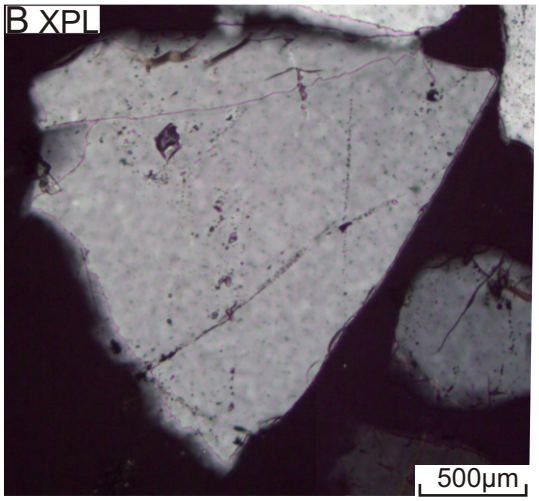

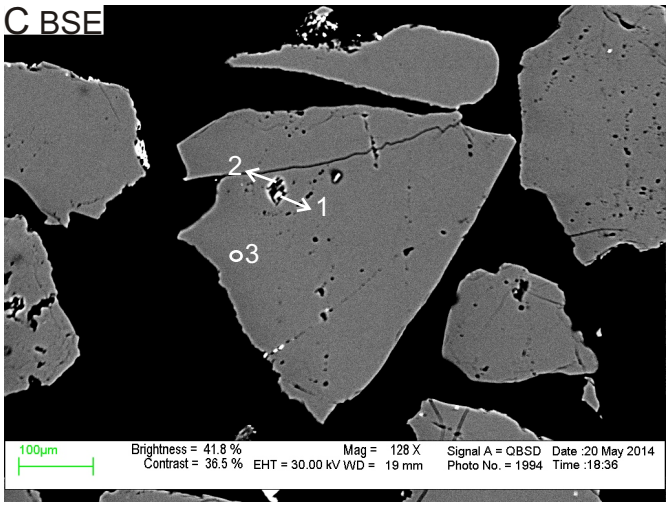

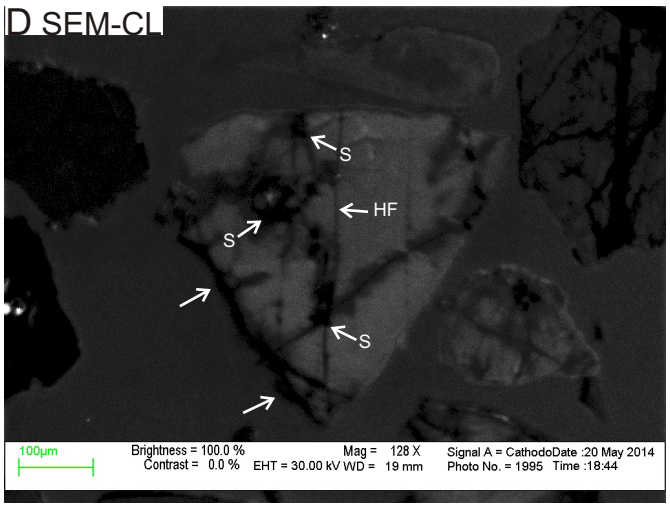

E EDS mineral analyses

Pos#	Min. ID	SiO2	Al2O3	K2O	Total	Actual Total
1	Qz	98.92	0.87	0.19	100	147
2	Qz	99.99			100	103
3	Qz	99.99			100	146

Figure 1A-40: Microphotos under ppl (A) and xpl (B), SEM-BSE image (C), SEM-CL image (D), and EDS analyses table (E) of quartz grain 40 in sample 2565. The grain is anhedral and angular monocrystalline with non-undulose extinction. Fluid inclusions are common; they are usually associated with secondary porosity and form trails along healed fractures (Fig. A). The grain is microfractured with a set of parallel fractures and some irregular fractures (Fig. C and D). Some healed fractures (HF) and spiders (S) can be seen in Fig. D. The areas indicated by arrows in Fig. D are overgrowth; these areas appear corroded in Fig. C, suggesting secondary porosity.

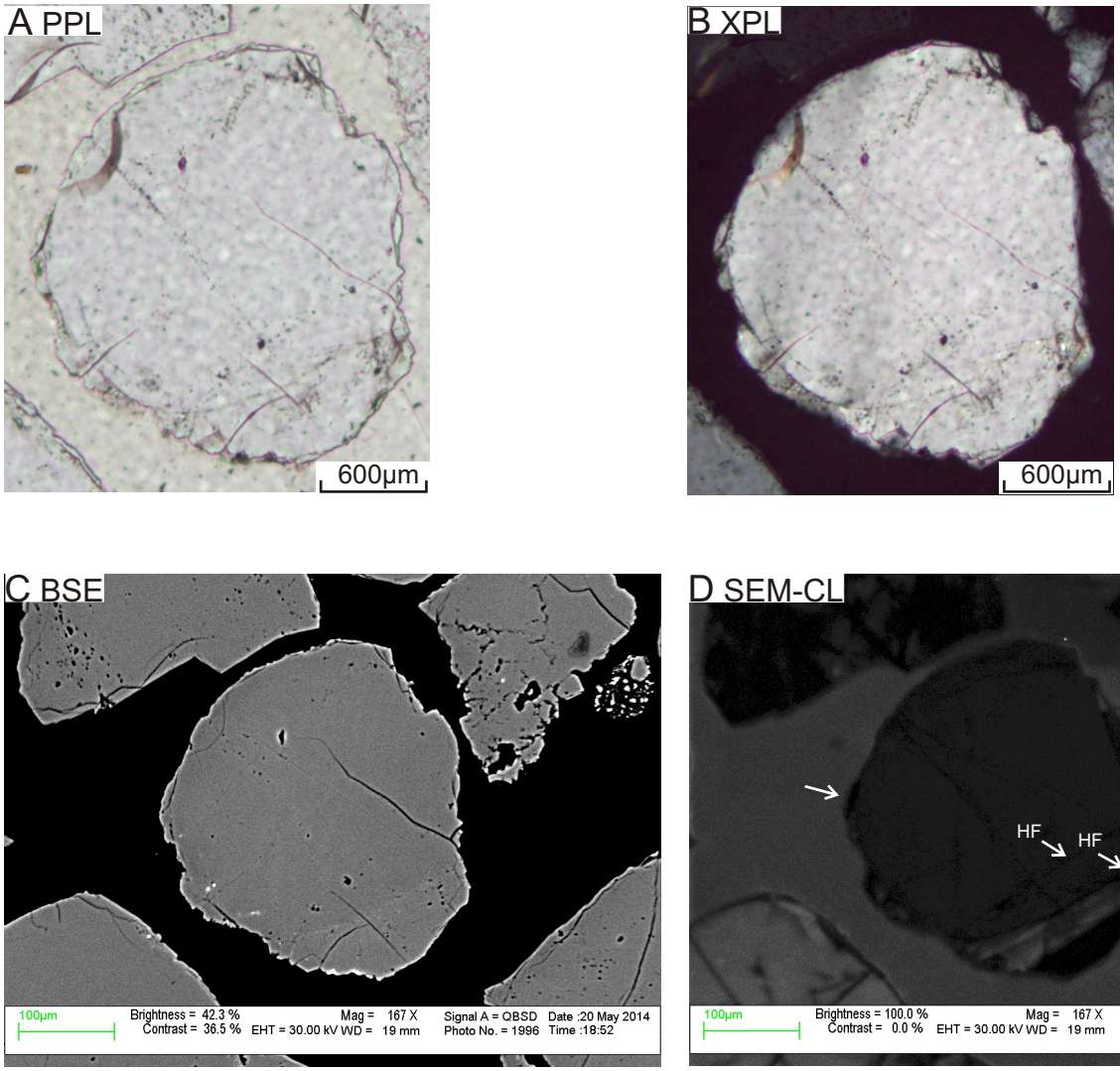

Figure 1A-41: Microphotos under ppl (A) and xpl (B), SEM-BSE image (C), SEM-CL image (D), and EDS analyses table (E) of quartz grain 41 in sample 2565. The grain is anhedral and rounded monocrystalline with strong undulose extinction. Fluid inclusions are common; they are usually associated with secondary porosity and form trails along healed fractures (Fig. A). The grain is microfractured with a set of sub-parallel fractures and irregular fracture (Fig. C and D). Some healed fractures (HF) can be seen in Fig. D. The area indicated by arrows in Fig. D is overgrowth. The grain shows streaky texture in the inferior part (SEM-CL image).

Appendix 1B: Hot cathodoluminescence (HCL) images and blue colour shift analyses of detrital quartz grains in sample 2565.

Notes:

1. All the grains with HCL images correspond to the same grain in SEM-CL images. In all the following organized HCL figures,

   Fig. A shows HCL image taken after 3 seconds;

   Fig. B shows HCL image taken after 12 seconds;

   Fig. C is the histogram of blue colour within the analysed quartz grain in Fig. A and B, where X axis is the intensity of blue colour indicated by the colour bar with values from 0-255 (0=no blue or "black", 255=blue), and Y axis indicates the pixel amount at different blue values;

   Fig. D is the statistical table of blue values within the analysed grain area, where SD corresponds to standard deviation.

2. To classify the blue colour, the following abbreviations are used:

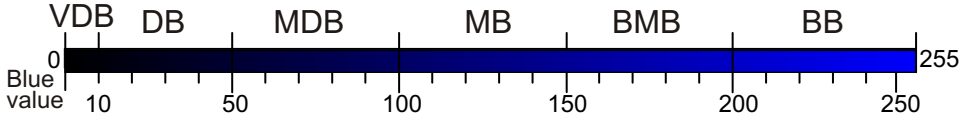

VDB: Very Dark Blue (0-10) **DB**: Dark Blue (11-50)

MDB: Medium Dark Blue (51-100) **MB**: Medium Blue (101-150)

BMB: Bright-Medium Blue (151-200) **BB**: Bright Blue (201-255)

3. To quantify the blue colour shift, the following criteria are used:

   Mean blue value change **< 5**: **No** colour shift

   5 ≤Mean blue value change **< 15**: **Slight** colour shift

   15 ≤Mean blue value change **< 30**: **Moderate** colour shift

   Mean blue value change ≥**30**: **Strong** colour shift

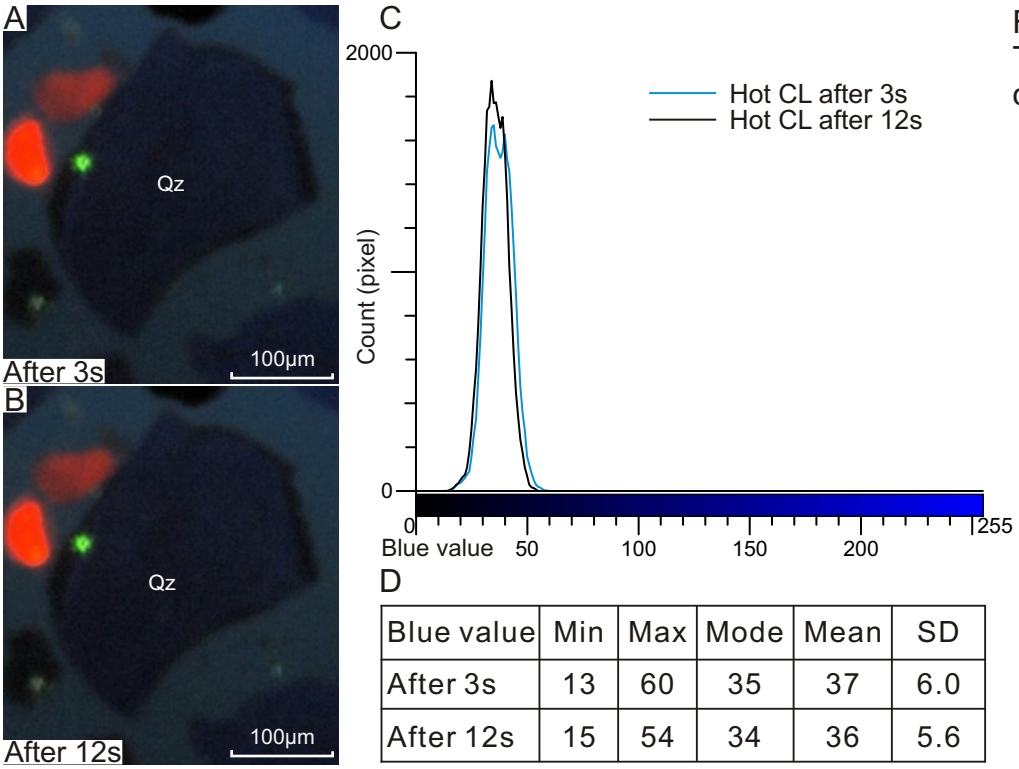

Figure 1B-1: Grain 1. The grain shows no colour shift.

D

Blue value	Min	Max	Mode	Mean	SD
After 3s	13	60	35	37	6.0
After 12s	15	54	34	36	5.6

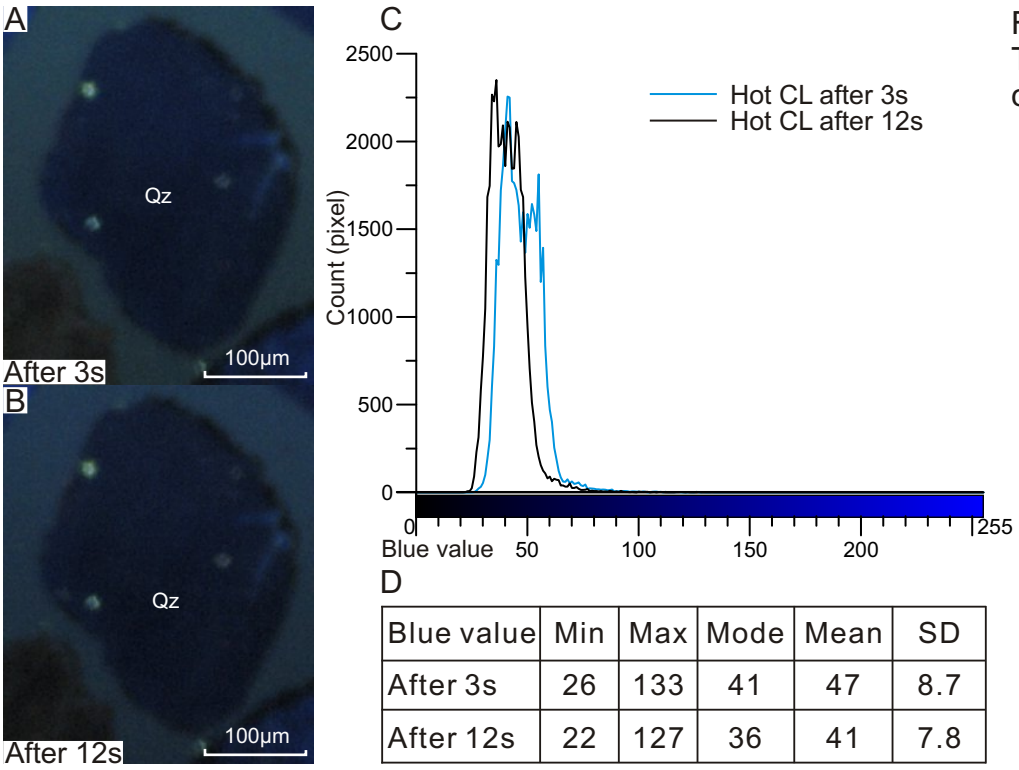

Figure 1B-2: Grain 2. The grain shows slight colour shift.

D

Blue value	Min	Max	Mode	Mean	SD
After 3s	26	133	41	47	8.7
After 12s	22	127	36	41	7.8

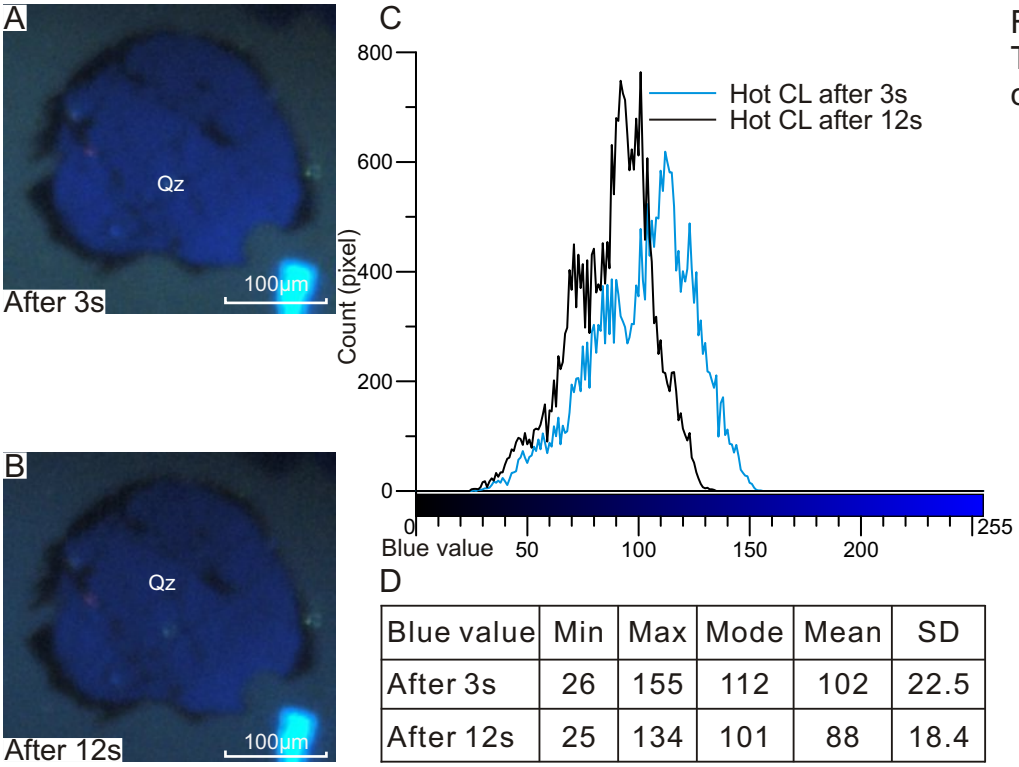

D

Blue value	Min	Max	Mode	Mean	SD
After 3s	26	155	112	102	22.5
After 12s	25	134	101	88	18.4

Figure 1B-3: Grain 3. The grain shows slight colour shift.

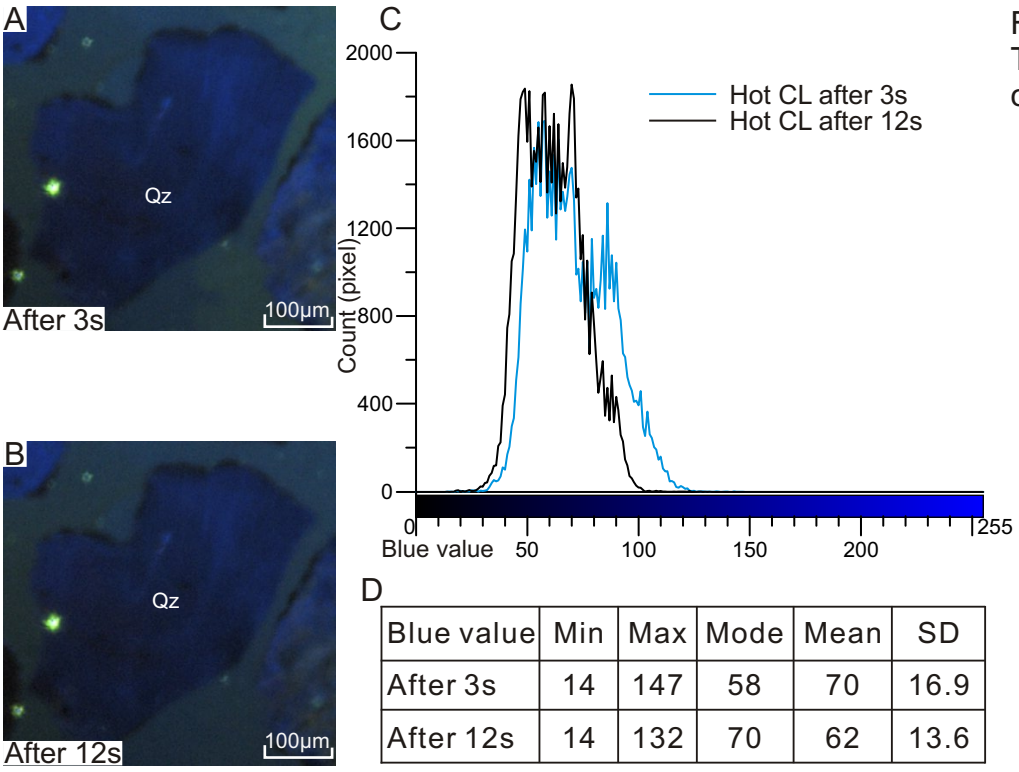

D

Blue value	Min	Max	Mode	Mean	SD
After 3s	14	147	58	70	16.9
After 12s	14	132	70	62	13.6

Figure 1B-4: Grain 4. The grain shows slight colour shift.

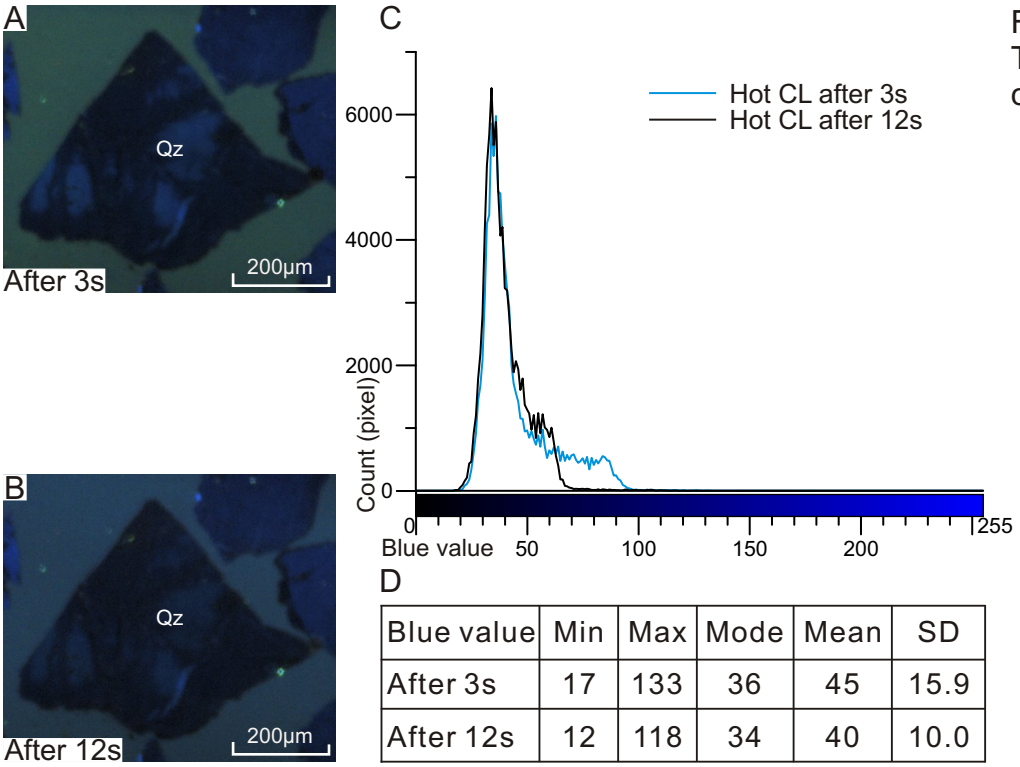

Figure 1B-5: Grain 5. The grain shows slight colour shift.

D

Blue value	Min	Max	Mode	Mean	SD
After 3s	17	133	36	45	15.9
After 12s	12	118	34	40	10.0

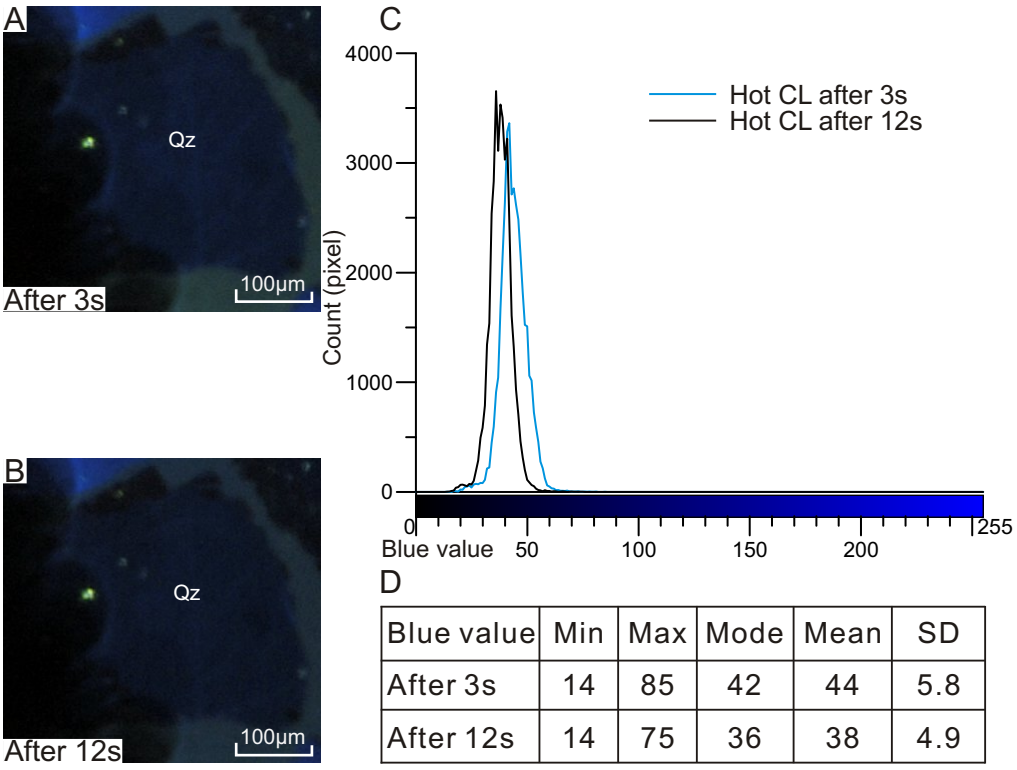

Figure 1B-6: Grain 6. The grain shows slight colour shift.

D

Blue value	Min	Max	Mode	Mean	SD
After 3s	14	85	42	44	5.8
After 12s	14	75	36	38	4.9

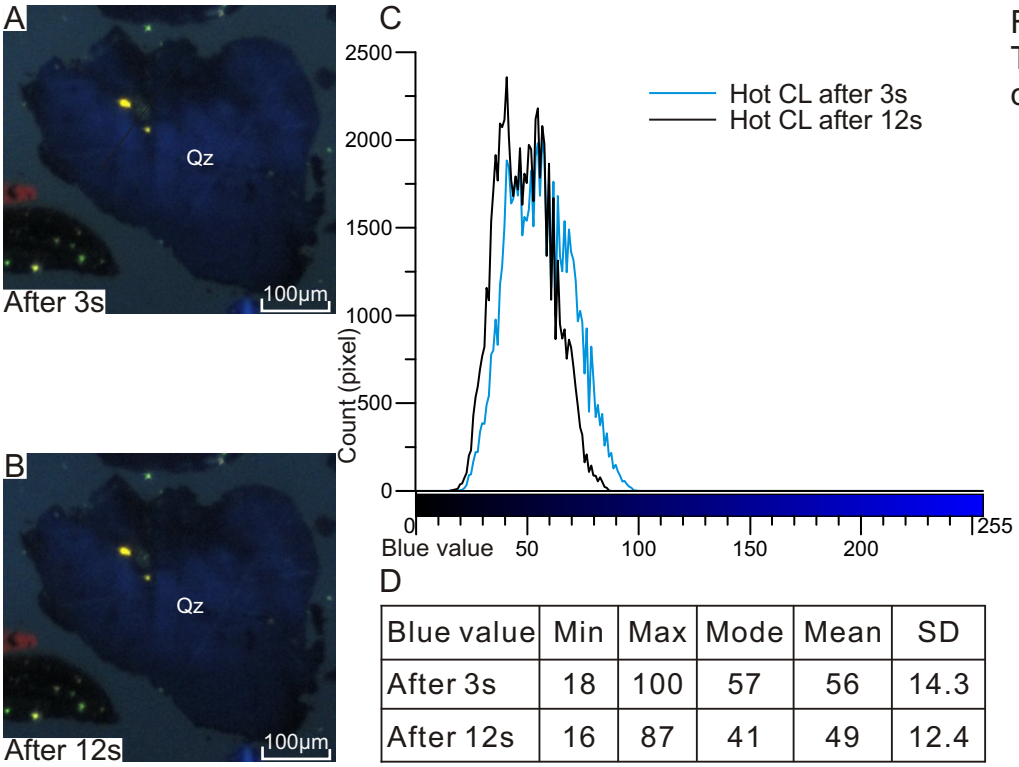

D

Blue value	Min	Max	Mode	Mean	SD
After 3s	18	100	57	56	14.3
After 12s	16	87	41	49	12.4

Figure 1B-7: Grain 7. The grain shows slight colour shift.

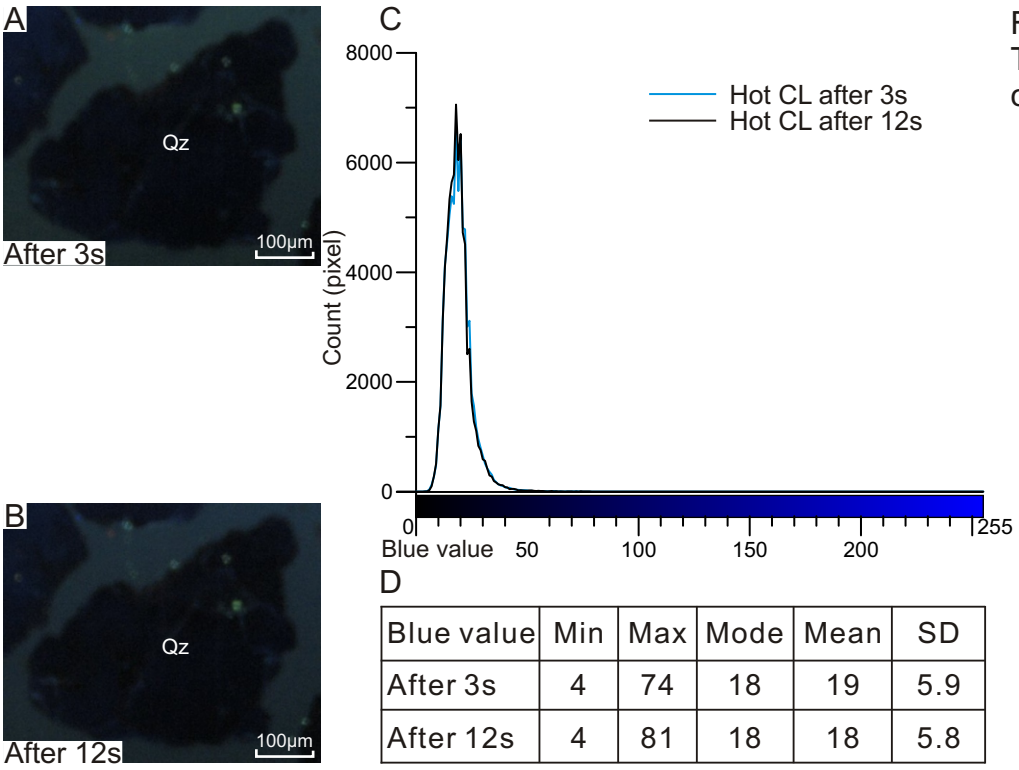

D

Blue value	Min	Max	Mode	Mean	SD
After 3s	4	74	18	19	5.9
After 12s	4	81	18	18	5.8

Figure 1B-8: Grain 8. The grain shows no colour shift.

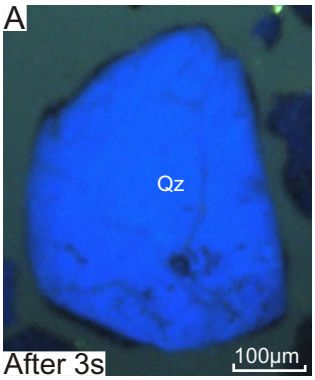

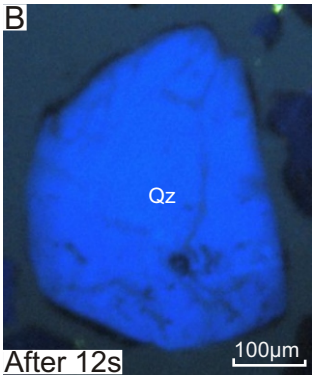

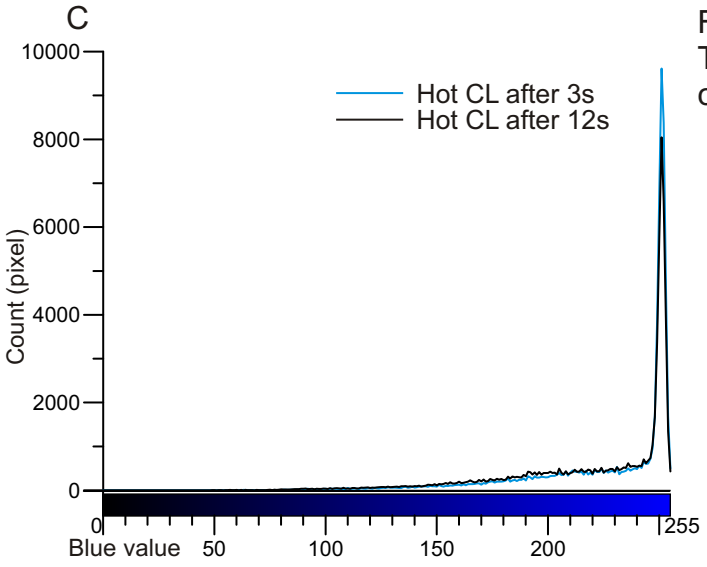

D

Blue value	Min	Max	Mode	Mean	SD
After 3s	45	255	251	228	34.7
After 12s	46	255	251	222	17.7

Figure 1B-9: Grain 9. The grain shows slight colour shift.

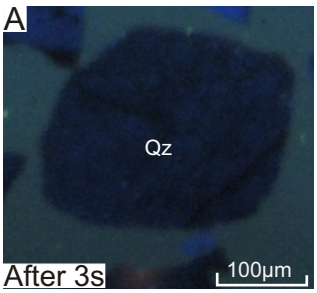

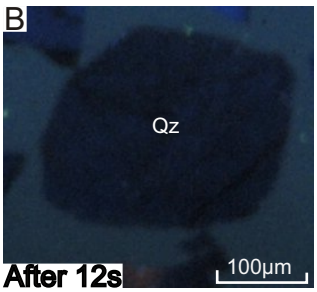

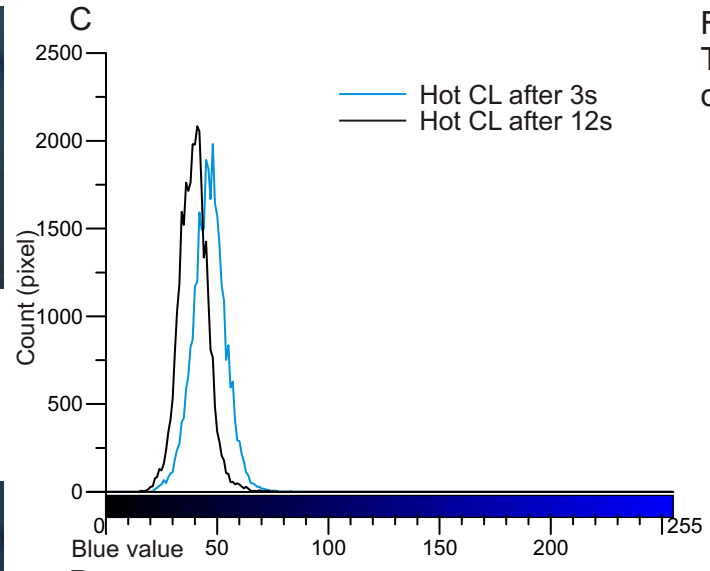

D

Blue value	Min	Max	Mode	Mean	SD
After 3s	18	83	48	46	7.3
After 12s	15	77	41	39	6.5

Figure 1B-10: Grain 10. The grain shows slight colour shift.

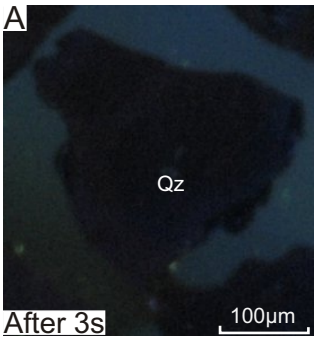

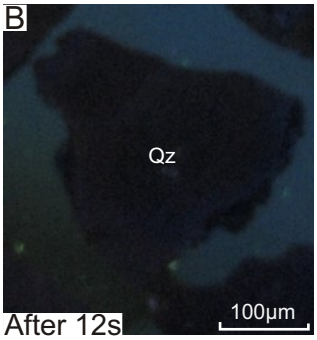

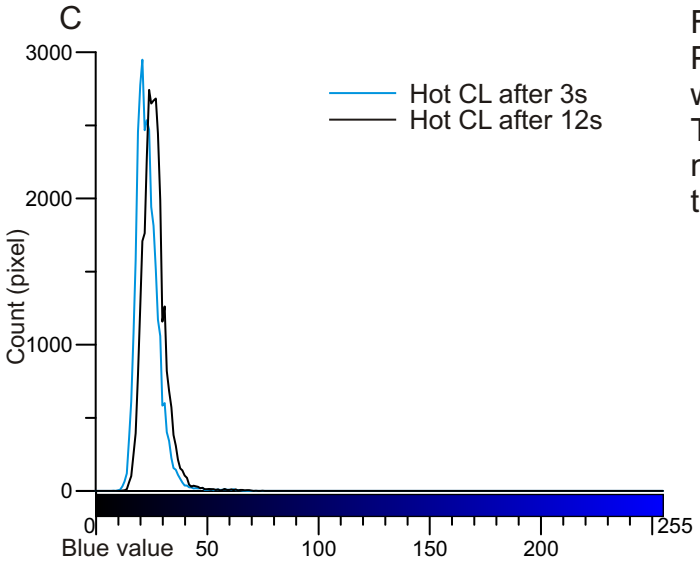

Figure 1B-11: Grain 11. Probably the first image was taken too early. Therefore, this grain is not useful to analyse the colour shift.

D

Blue value	Min	Max	Mode	Mean	SD
After 3s	8	66	21	23	5.3
After 12s	12	75	24	26	5.3

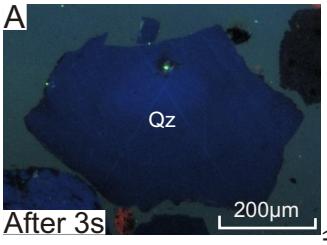

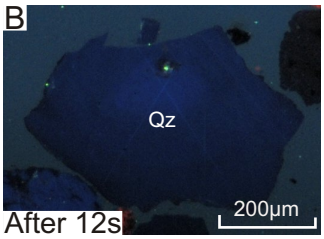

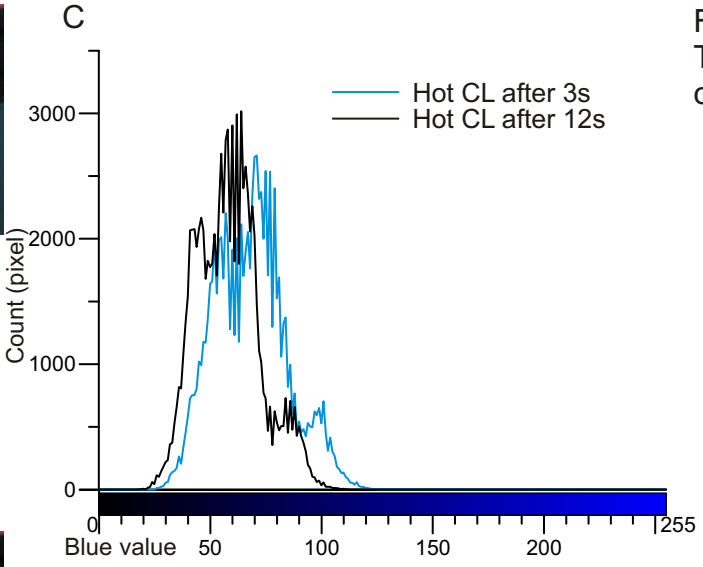

Figure 1B-12: Grain 12. The grain shows slight colour shift.

D

Blue value	Min	Max	Mode	Mean	SD
After 3s	26	126	71	68	16.3
After 12s	18	112	64	58	14.3

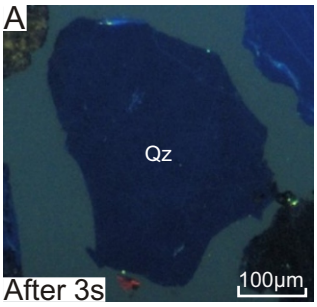

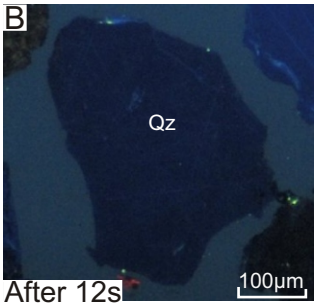

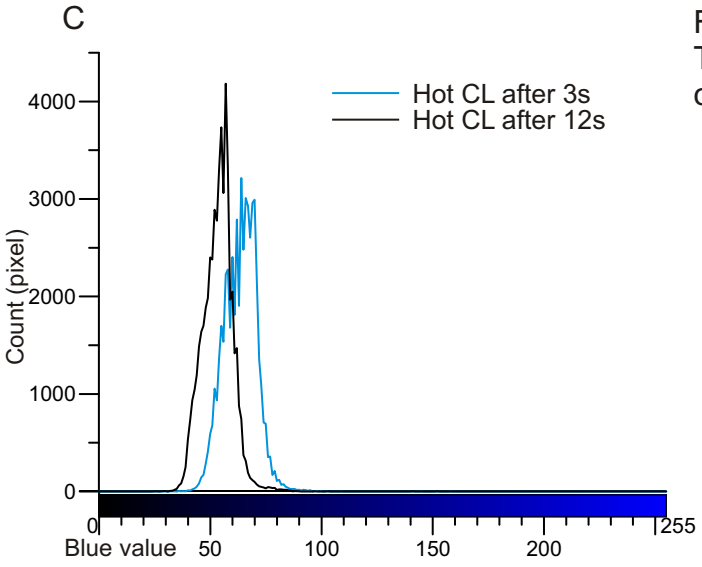

Figure 1B-13: Grain 13. The grain shows slight colour shift.

D

Blue value	Min	Max	Mode	Mean	SD
After 3s	30	158	64	63	7.2
After 12s	25	152	57	53	6.7

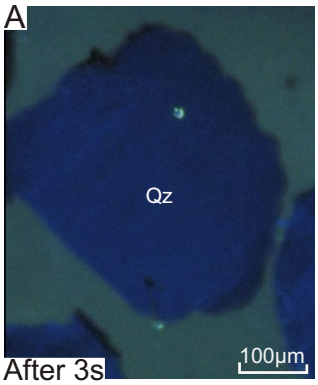

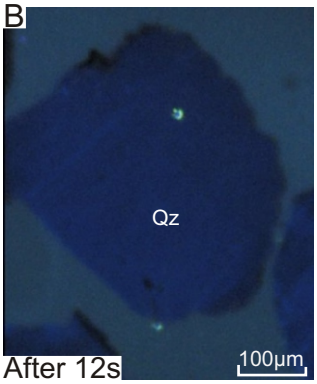

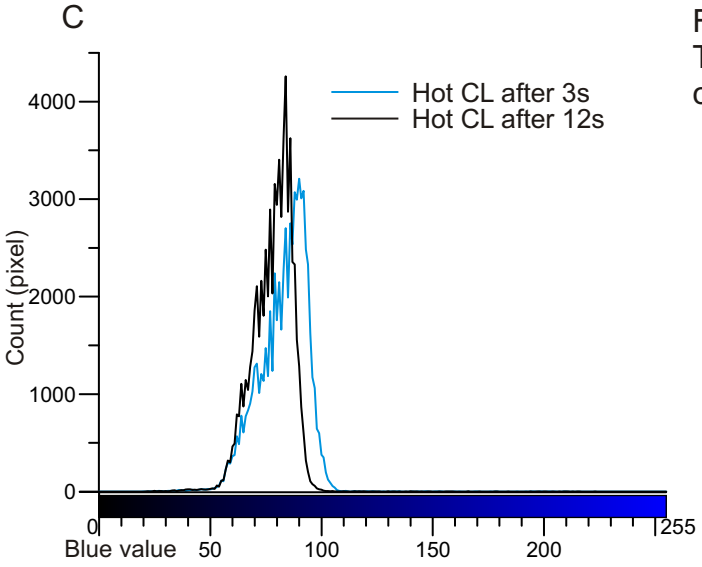

Figure 1B-14: Grain 14. The grain shows slight colour shift.

D

Blue value	Min	Max	Mode	Mean	SD
After 3s	20	210	90	83	10.8
After 12s	21	223	84	78	9.2

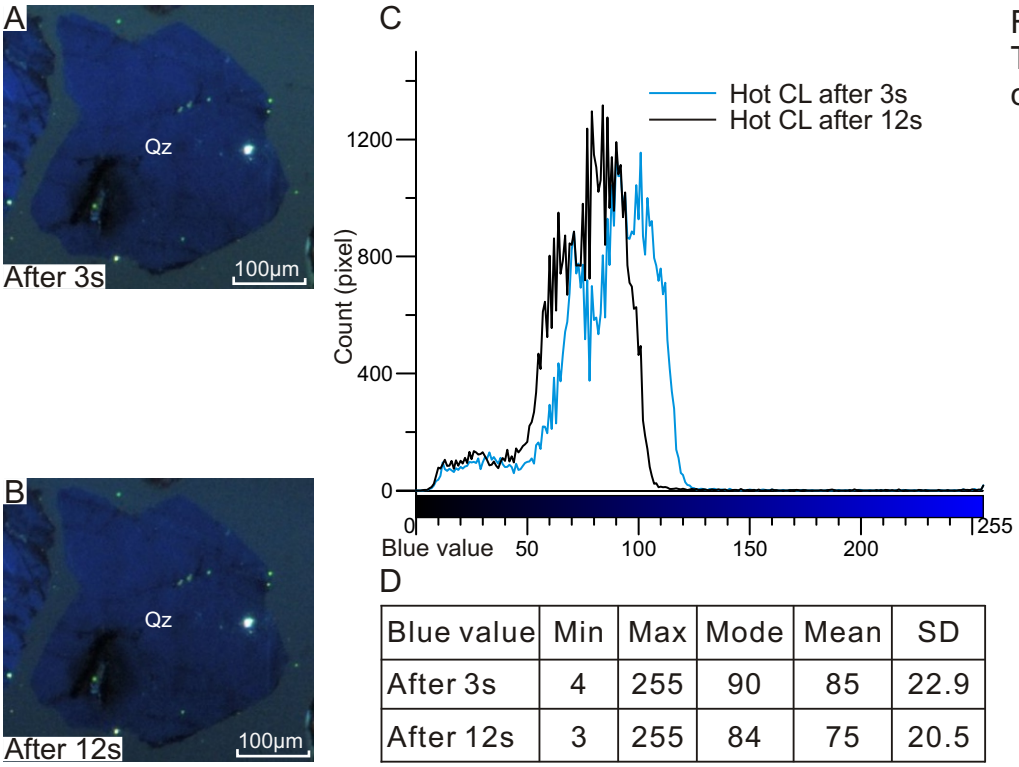

Figure 1B-15 : Grain15. The grain shows slight colour shift.

D

Blue value	Min	Max	Mode	Mean	SD
After 3s	4	255	90	85	22.9
After 12s	3	255	84	75	20.5

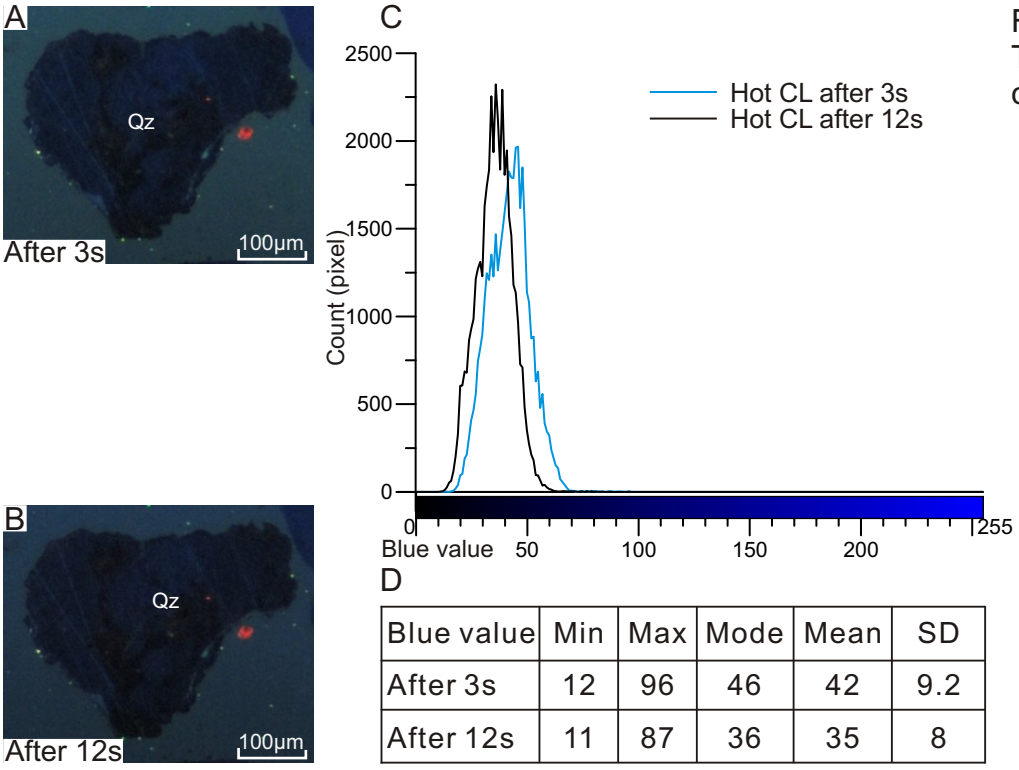

Figure 1B-16: Grain 16. The grain shows slight colour shift.

D

Blue value	Min	Max	Mode	Mean	SD
After 3s	12	96	46	42	9.2
After 12s	11	87	36	35	8

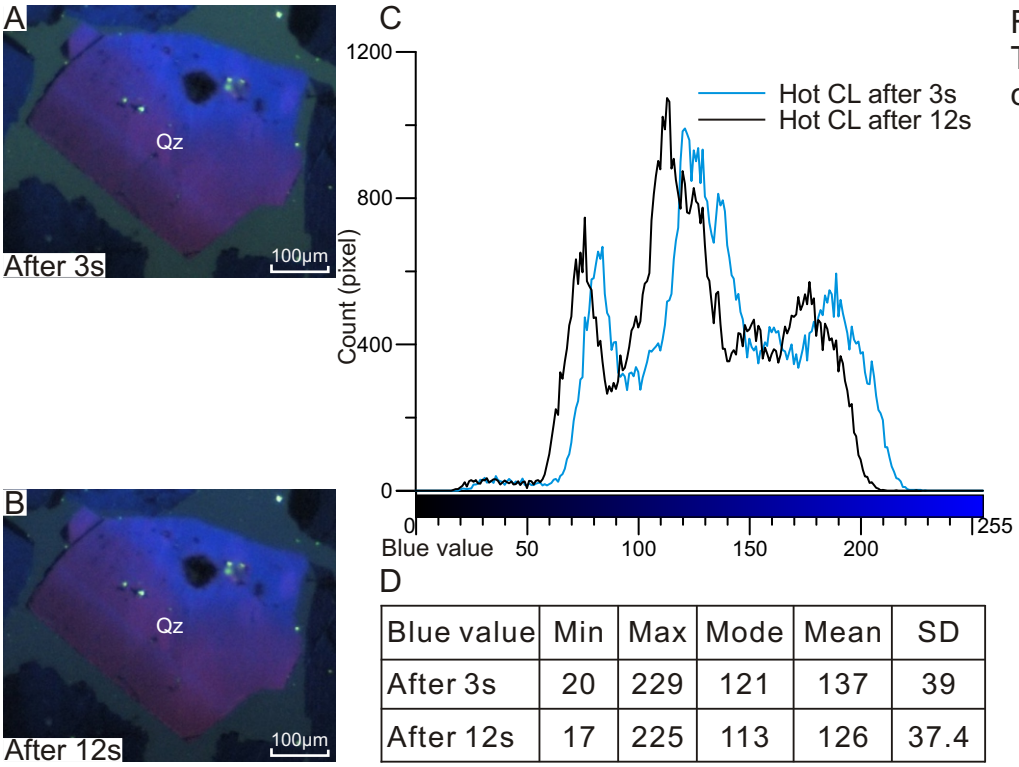

Figure 1B-17: Grain 17. The grain shows slight colour shift.

D

Blue value	Min	Max	Mode	Mean	SD
After 3s	20	229	121	137	39
After 12s	17	225	113	126	37.4

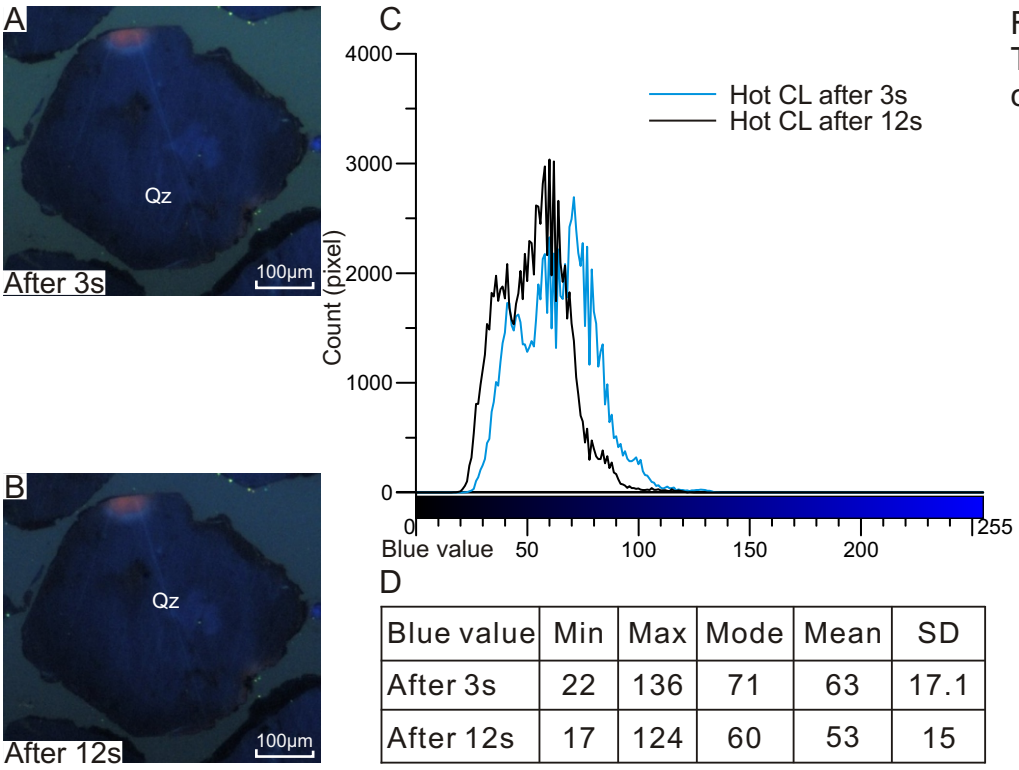

Figure 1B-18: Grain 18. The grain shows slight colour shift.

D

Blue value	Min	Max	Mode	Mean	SD
After 3s	22	136	71	63	17.1
After 12s	17	124	60	53	15

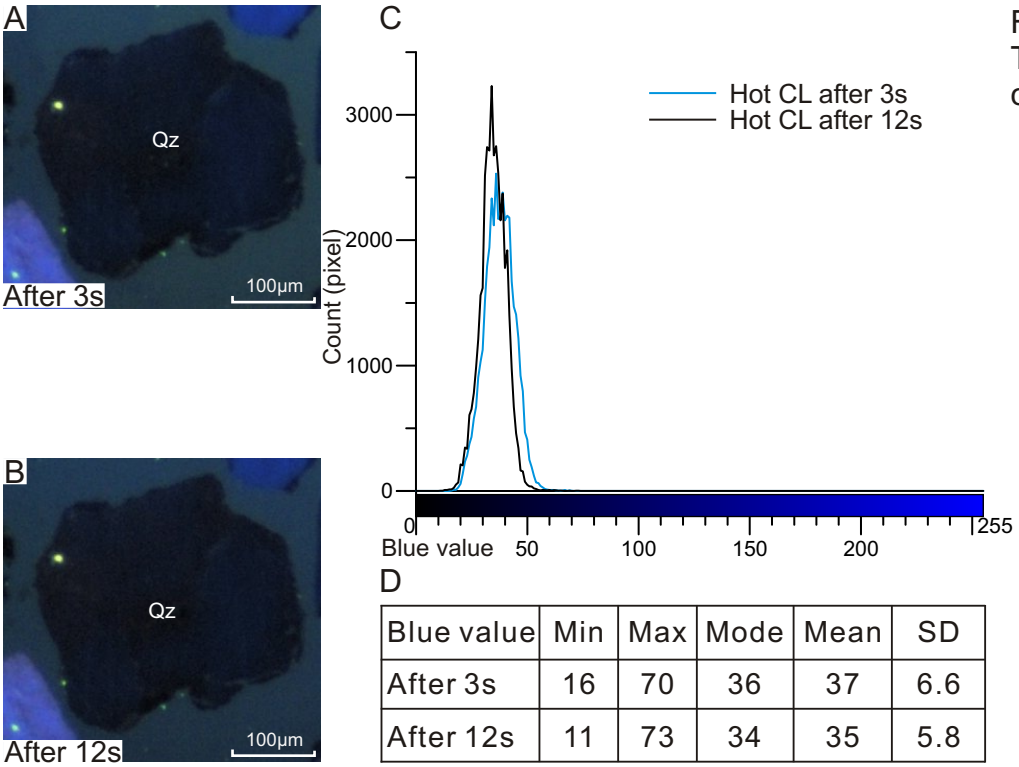

Figure 1B-19: Grain 19. The grain shows no colour shift.

D

Blue value	Min	Max	Mode	Mean	SD
After 3s	16	70	36	37	6.6
After 12s	11	73	34	35	5.8

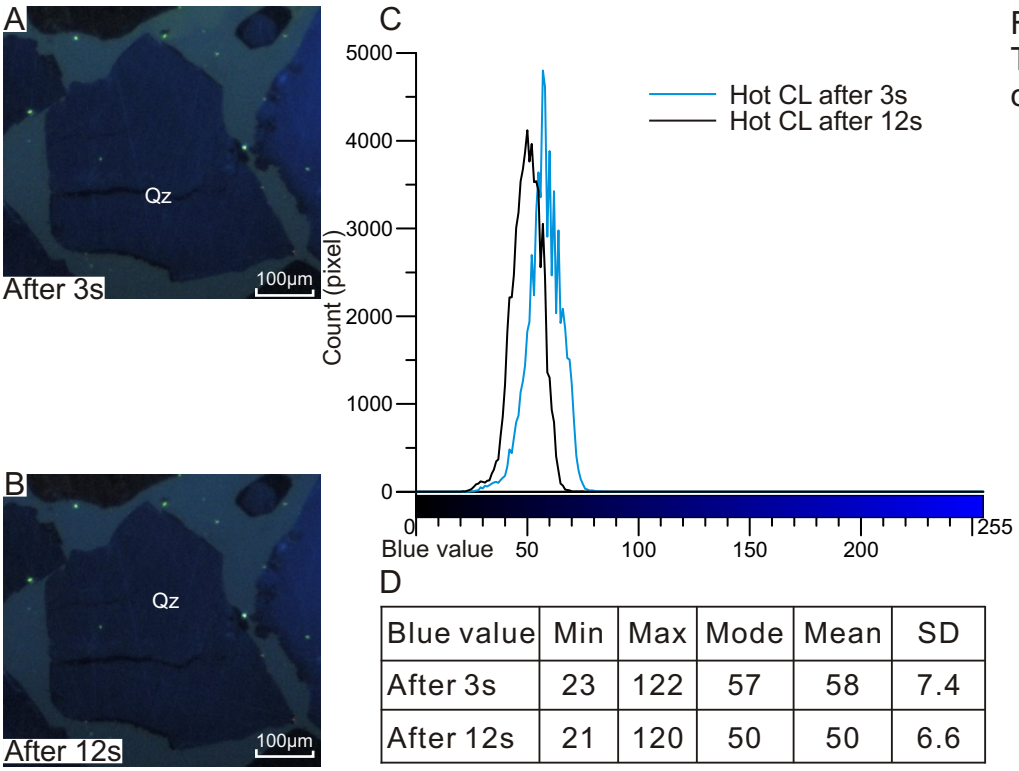

Figure 1B-20: Grain 20. The grain shows slight colour shift.

D

Blue value	Min	Max	Mode	Mean	SD
After 3s	23	122	57	58	7.4
After 12s	21	120	50	50	6.6

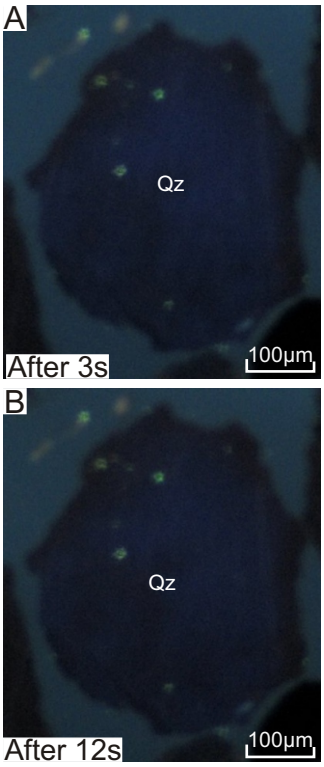

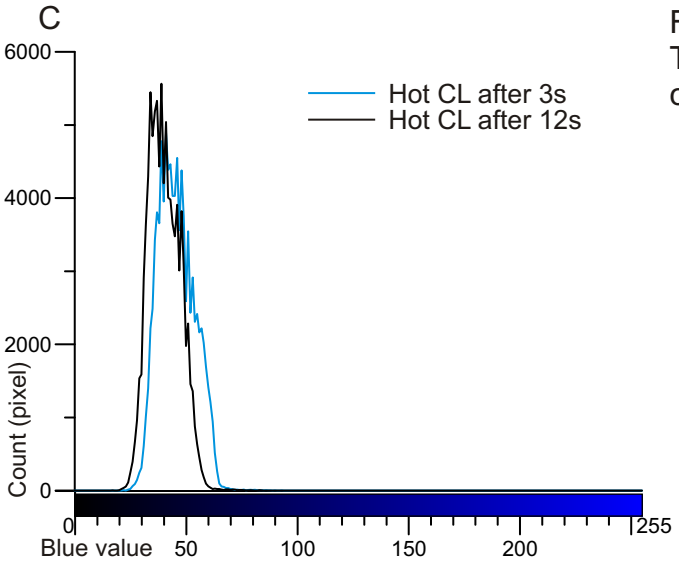

D

Blue value	Min	Max	Mode	Mean	SD
After 3s	22	94	41	46	8
After 12s	17	86	39	40	7

Figure 1B-21: Grain 21. The grain shows slight colour shift.

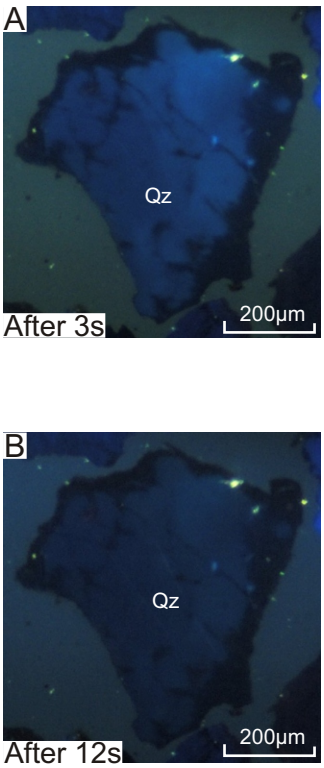

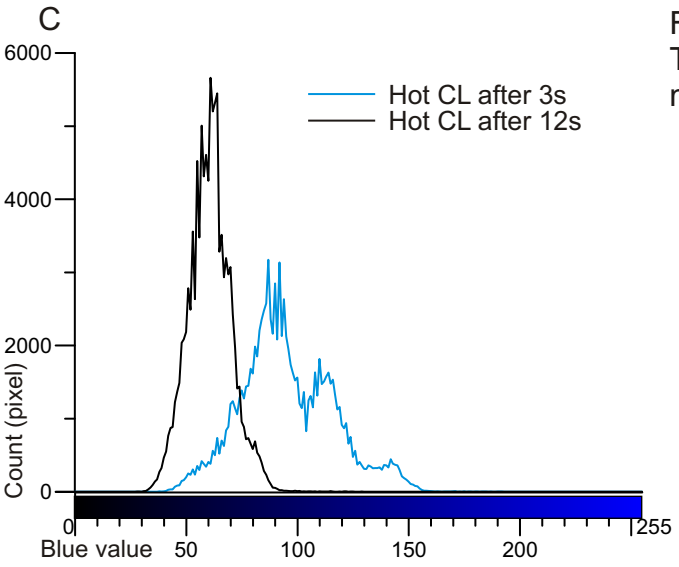

D

Blue value	Min	Max	Mode	Mean	SD
After 3s	37	196	87	95	20.9
After 12s	27	129	61	61	9.6

Figure 1B-22: Grain 22. The grain shows moderate colour shift.

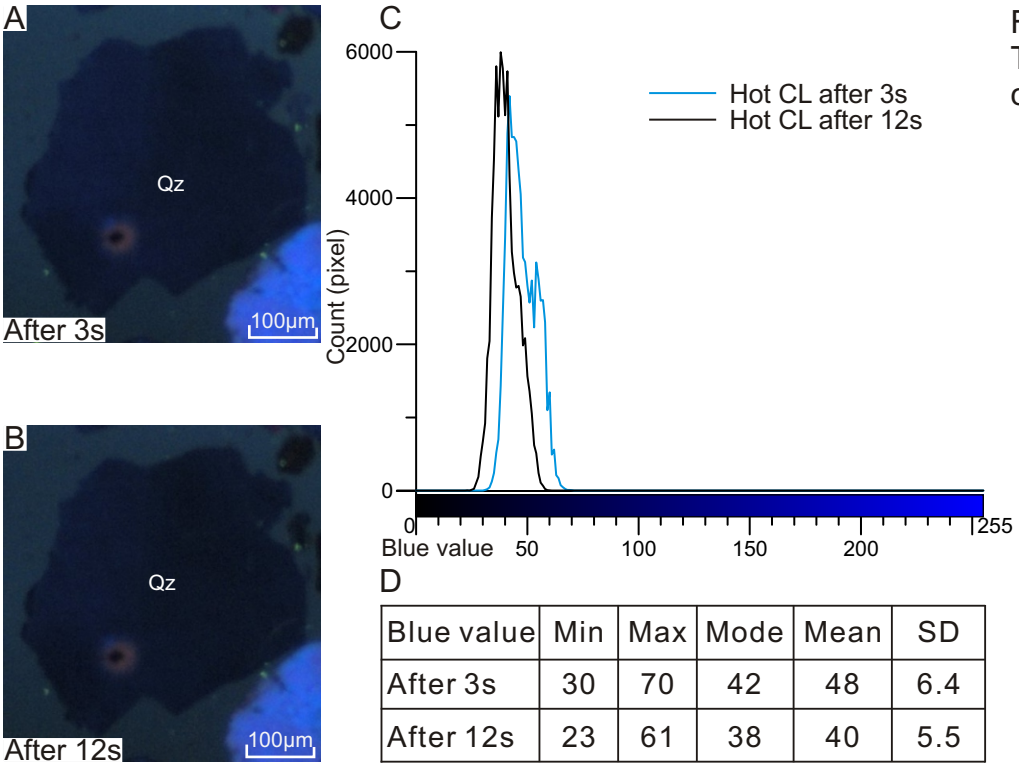

Figure 1B-23: Grain 23. The grain shows slight colour shift.

D

Blue value	Min	Max	Mode	Mean	SD
After 3s	30	70	42	48	6.4
After 12s	23	61	38	40	5.5

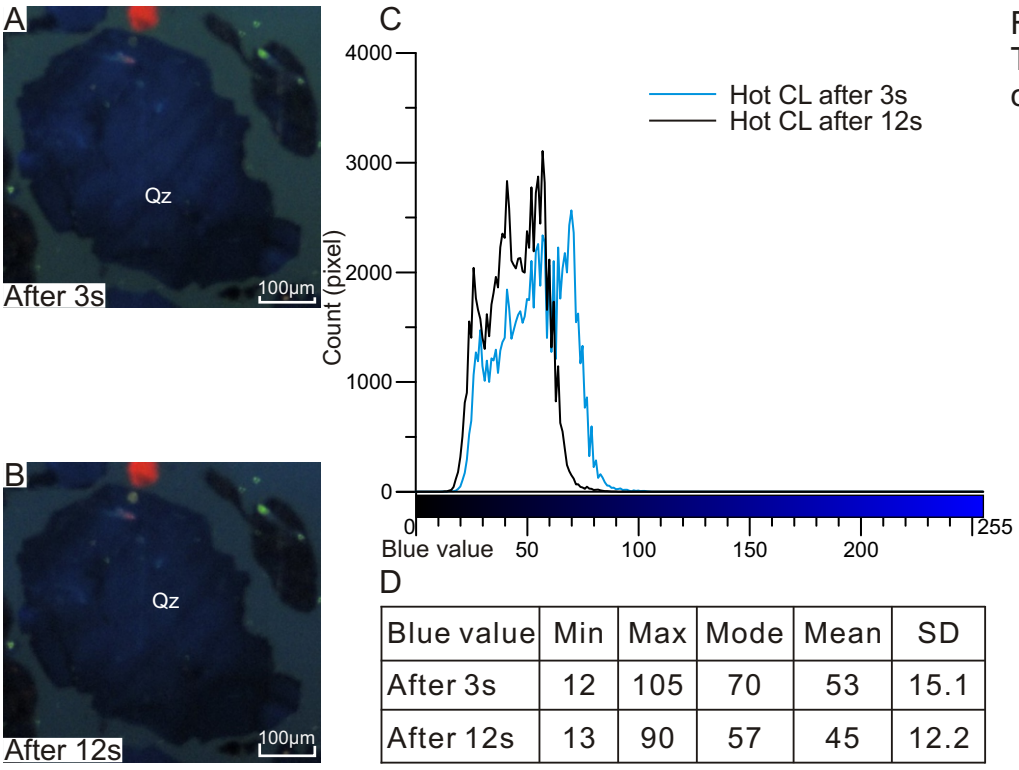

Figure 1B-24: Grain 24. The grain shows slight colour shift.

D

Blue value	Min	Max	Mode	Mean	SD
After 3s	12	105	70	53	15.1
After 12s	13	90	57	45	12.2

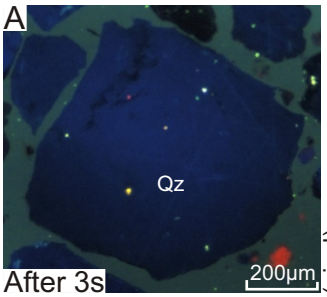

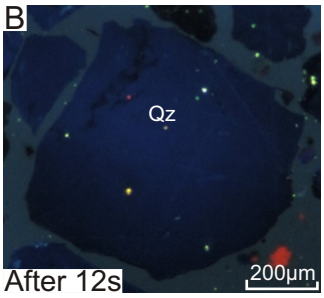

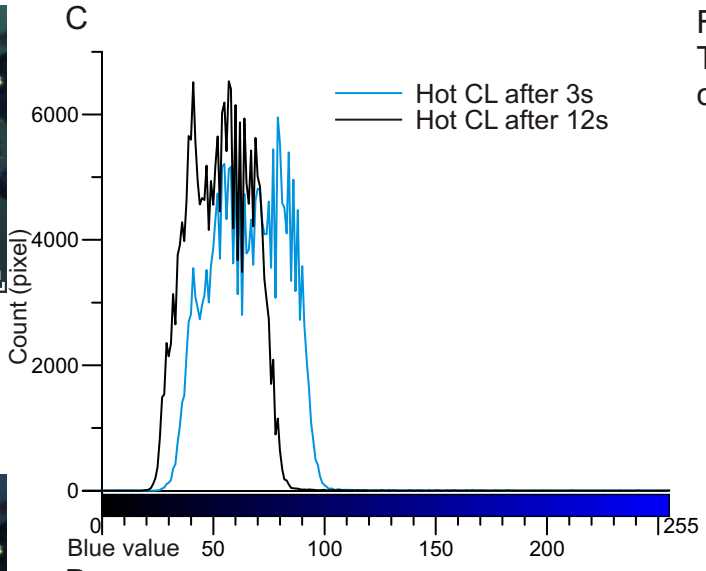

D

Blue value	Min	Max	Mode	Mean	SD
After 3s	7	255	79	66	16.2
After 12s	9	255	57	53	13.8

Figure 1B-25: Grain 25. The grain shows slight colour shift.

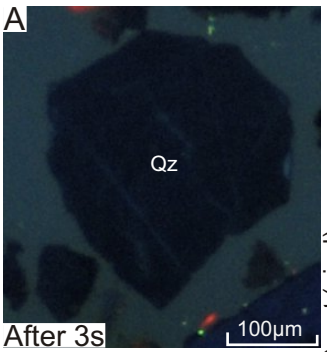

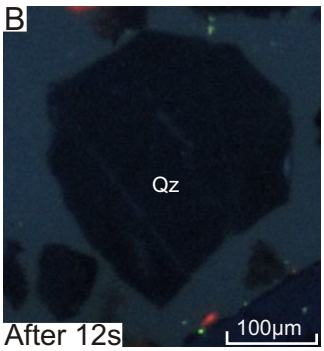

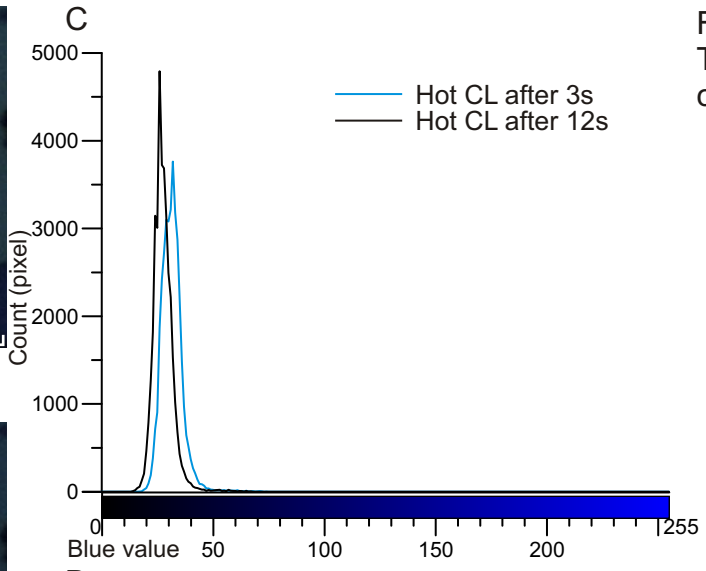

D

Blue value	Min	Max	Mode	Mean	SD
After 3s	17	75	32	31	4.8
After 12s	13	68	26	28	4.5

Figure 1B-26: Grain 26. The grain shows no colour shift.

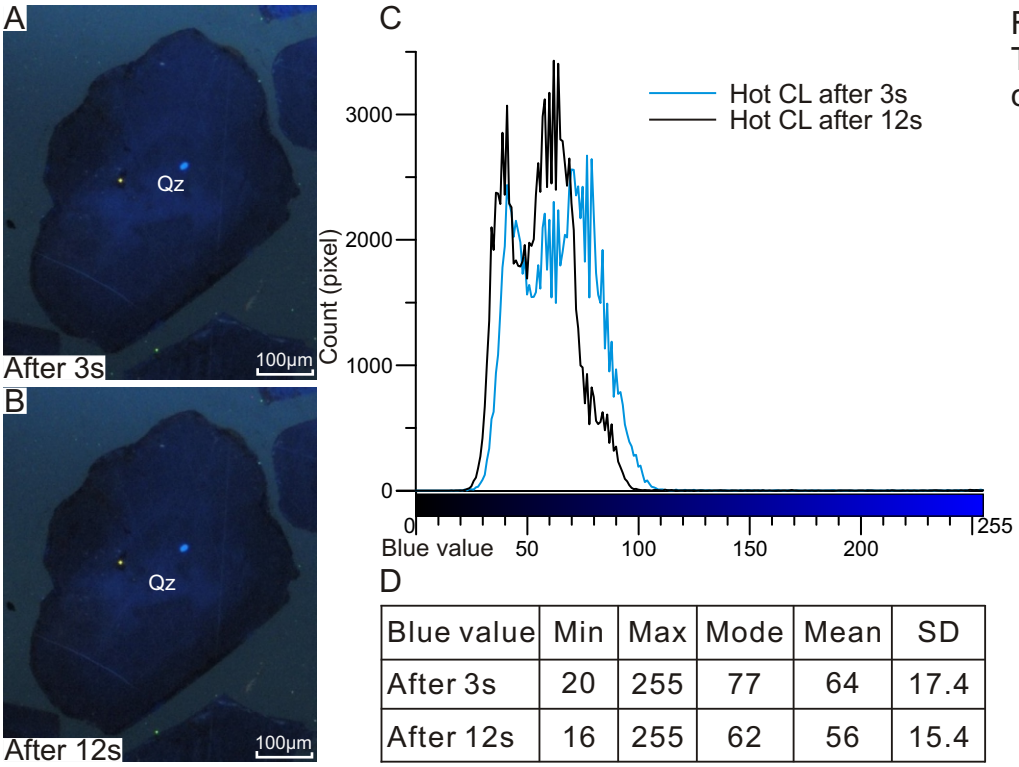

D

Blue value	Min	Max	Mode	Mean	SD
After 3s	20	255	77	64	17.4
After 12s	16	255	62	56	15.4

Figure 1B-27: Grain 27. The grain shows slight colour shift.

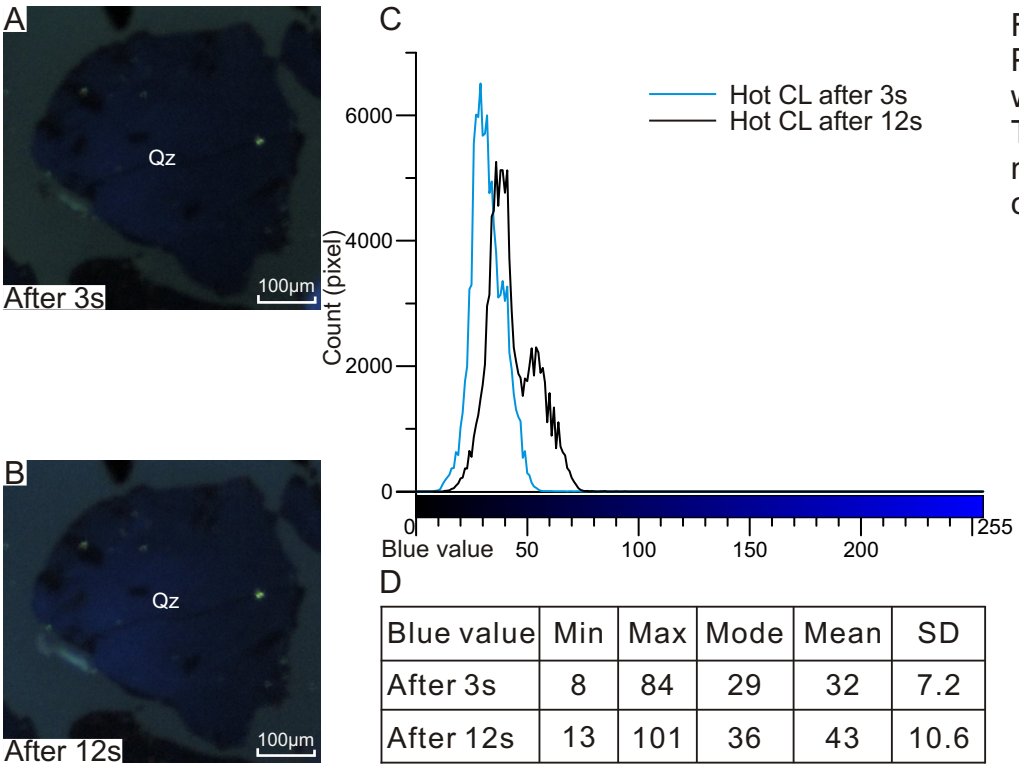

D

Blue value	Min	Max	Mode	Mean	SD
After 3s	8	84	29	32	7.2
After 12s	13	101	36	43	10.6

Figure 1B-28: Grain 28. Probably the first image was taken too early. Therefore, this grain is not useful to analyse the colour shift.

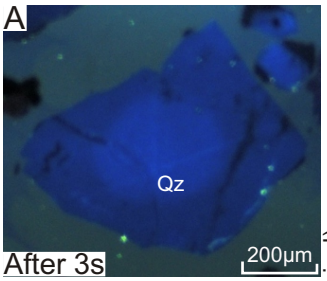

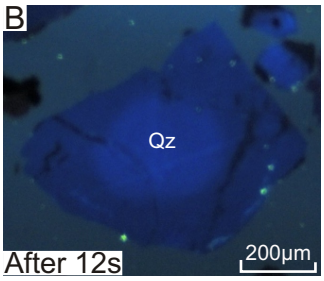

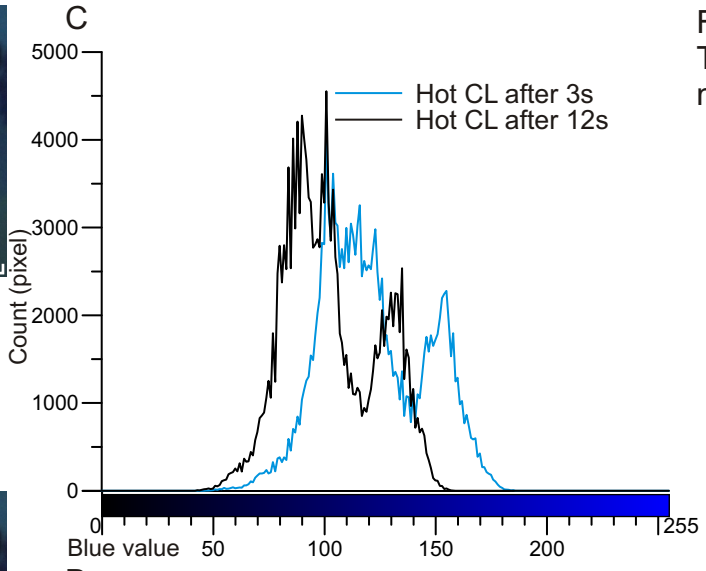

D

Blue value	Min	Max	Mode	Mean	SD
After 3s	47	186	101	122	23.3
After 12s	43	159	101	103	20.6

Figure 1B-29: Grain 29. The grain shows moderate colour shift.

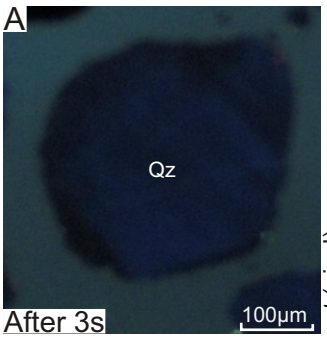

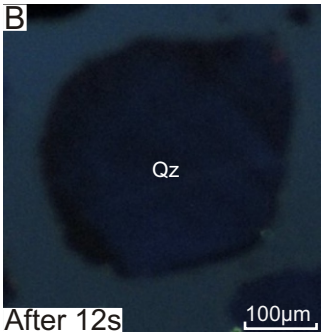

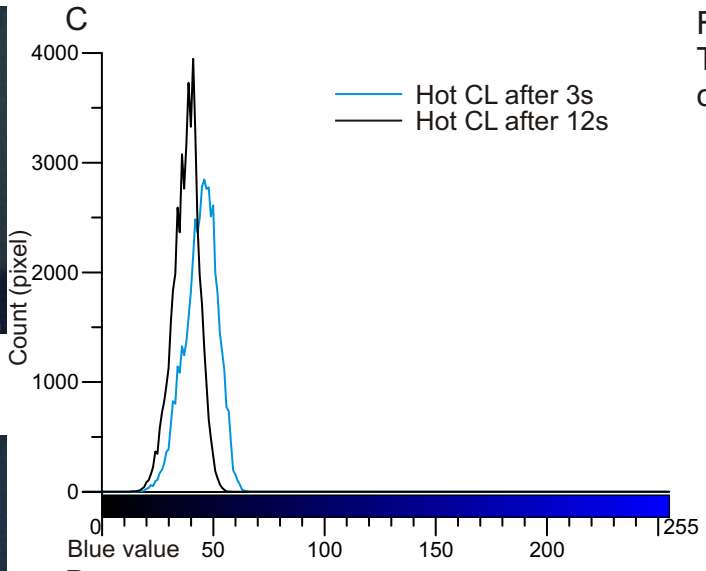

D

Blue value	Min	Max	Mode	Mean	SD
After 3s	16	66	46	44	7.6
After 12s	13	58	41	38	5.9

Figure 1B-30: Grain 30. The grain shows slight colour shift.

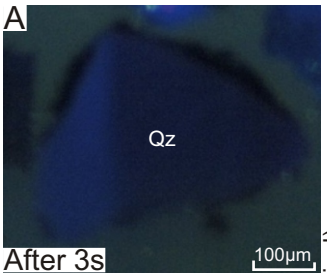

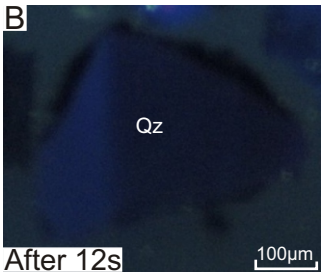

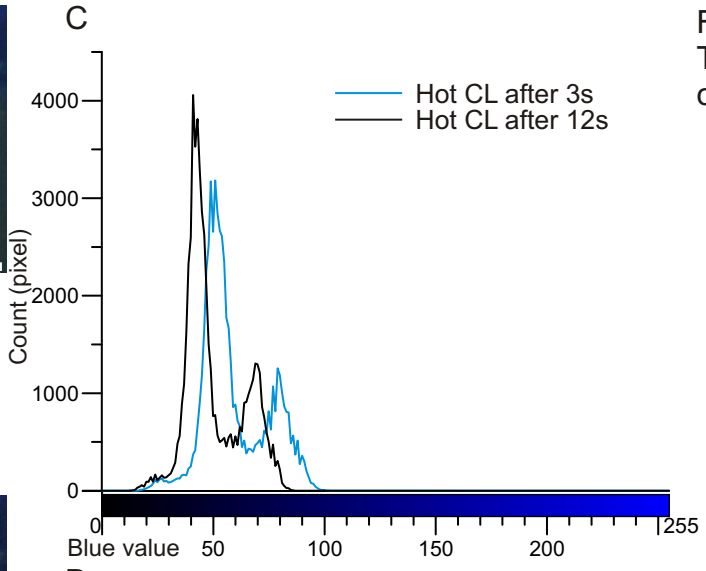

Figure 1B-31: Grain 31. The grain shows slight colour shift.

D

Blue value	Min	Max	Mode	Mean	SD
After 3s	13	102	51	59	14.6
After 12s	13	86	41	50	13

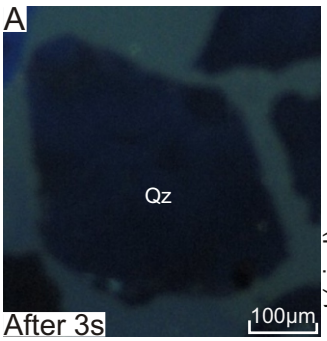

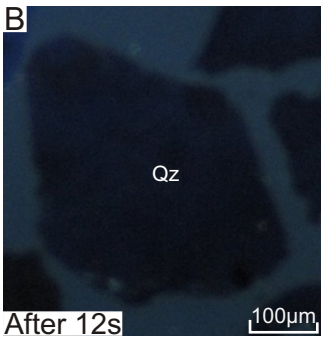

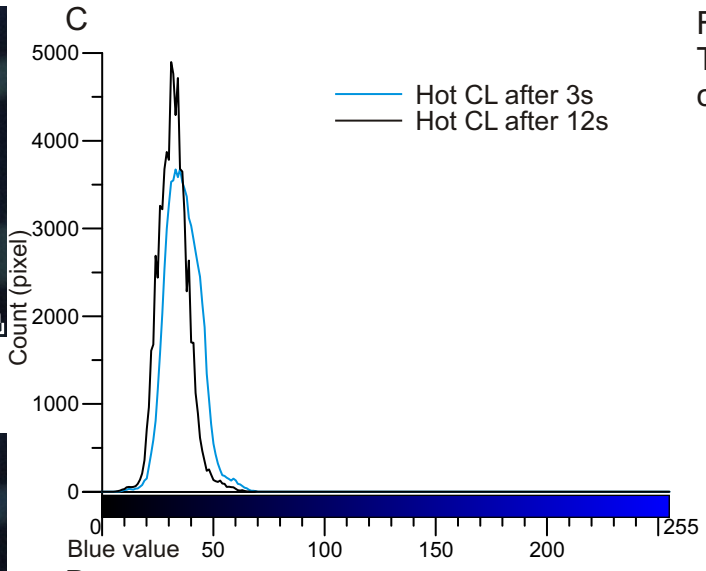

Figure 1B-32: Grain 32. The grain shows no colour shift.

D

Blue value	Min	Max	Mode	Mean	SD
After 3s	7	73	34	36	7.7
After 12s	6	72	31	32	6.7

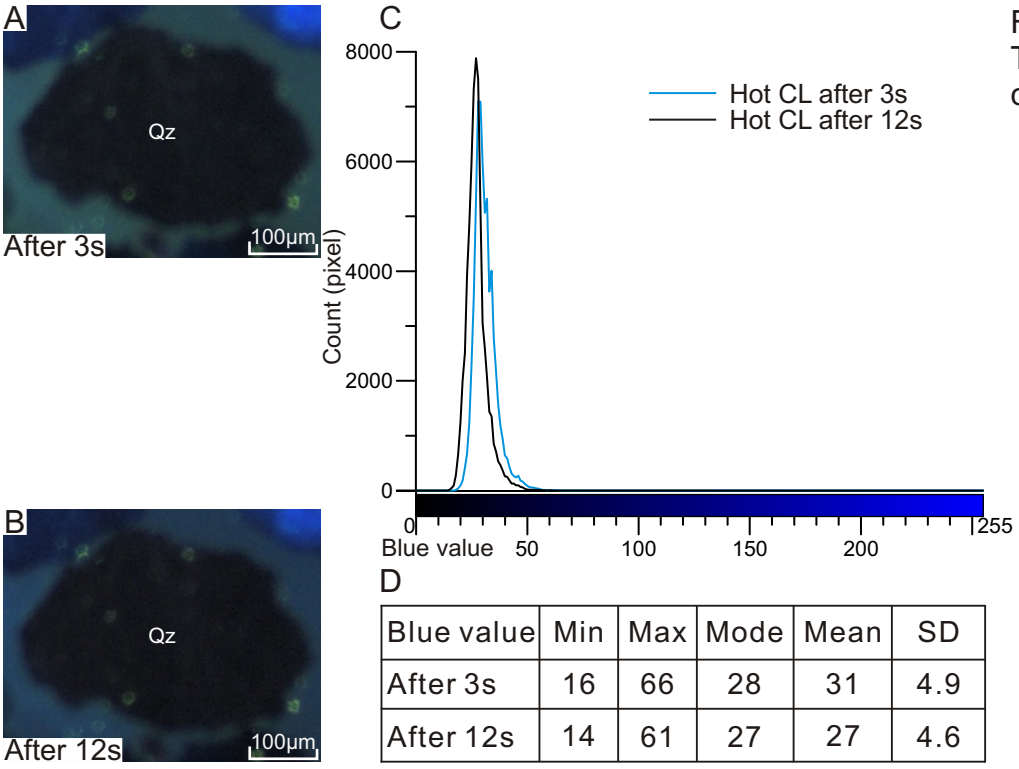

Figure 1B-33: Grain 33. The grain shows no colour shift.

D

Blue value	Min	Max	Mode	Mean	SD
After 3s	16	66	28	31	4.9
After 12s	14	61	27	27	4.6

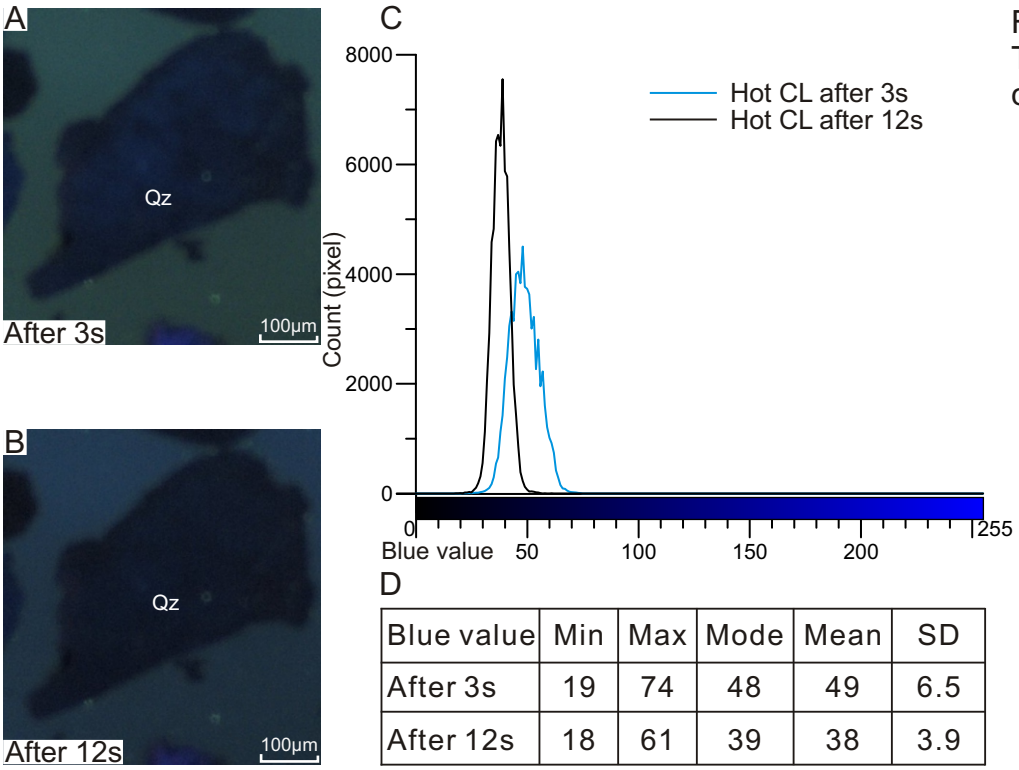

Figure 1B-34: Grain 34. The grain shows slight colour shift.

D

Blue value	Min	Max	Mode	Mean	SD
After 3s	19	74	48	49	6.5
After 12s	18	61	39	38	3.9

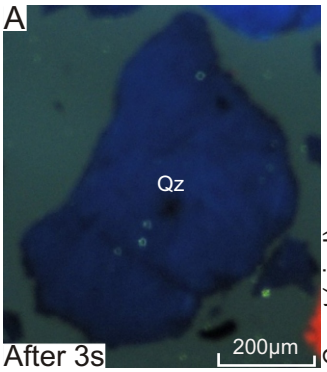

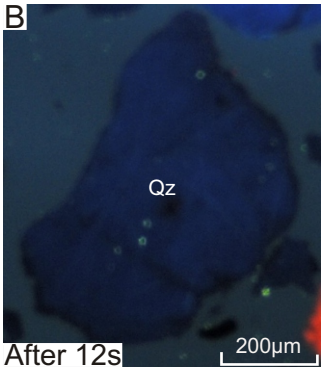

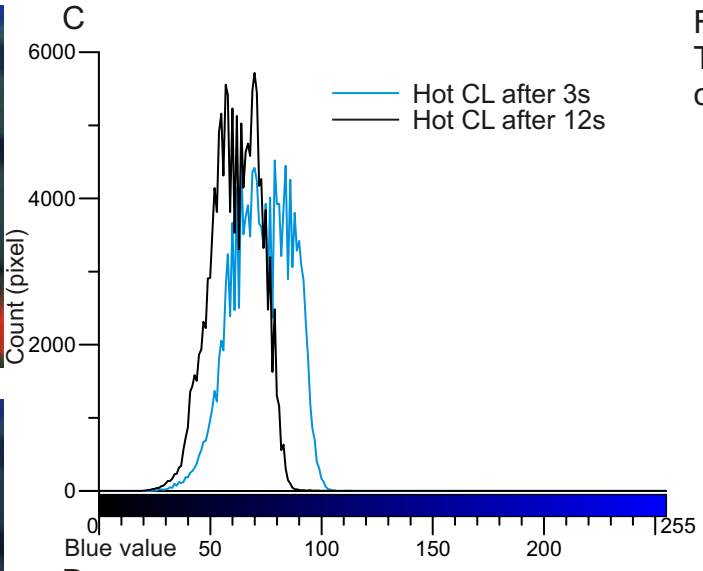

Figure 1B-35: Grain 35. The grain shows slight colour shift.

D

Blue value	Min	Max	Mode	Mean	SD
After 3s	24	119	79	73	13.1
After 12s	20	114	70	62	10.8





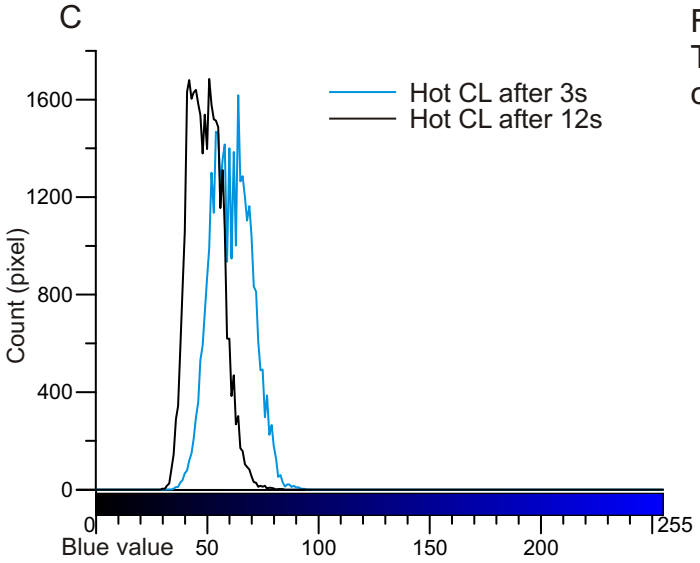

Figure 1B-36: Grain 36. The grain shows slight colour shift.

D

Blue value	Min	Max	Mode	Mean	SD
After 3s	32	96	64	61	8.9
After 12s	30	84	51	49	7.3

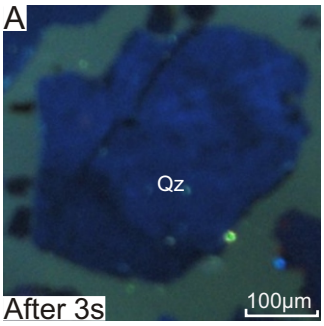

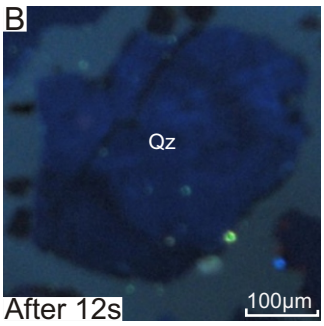

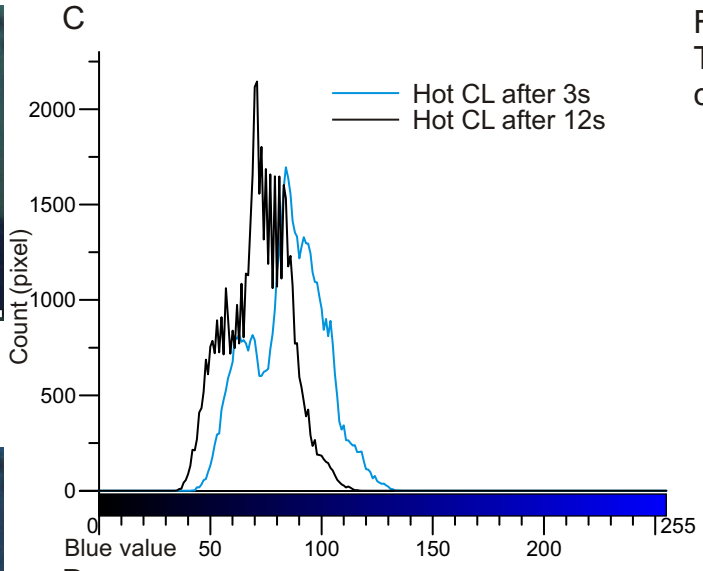

Figure 1B-37: Grain 37. The grain shows slight colour shift.

D

Blue value	Min	Max	Mode	Mean	SD
After 3s	42	135	84	85	16.2
After 12s	35	117	71	72	13.8

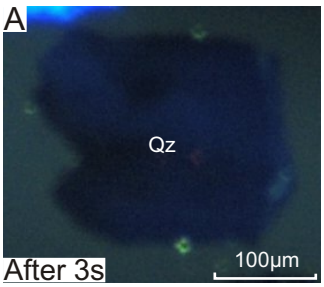

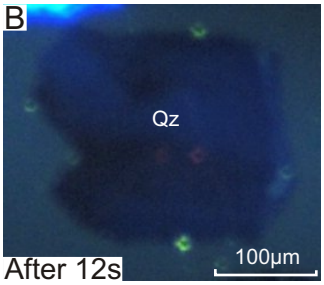

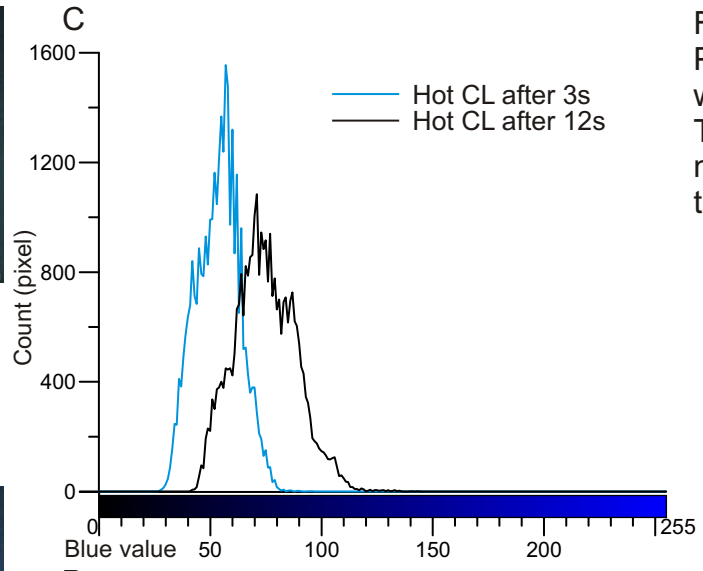

Figure 1B-38: Grain 38. Probably the first image was taken too early. Therefore, this grain is not useful to analyse the colour shift.

D

Blue value	Min	Max	Mode	Mean	SD
After 3s	27	96	57	54	9.7
After 12s	41	144	71	75	13.8

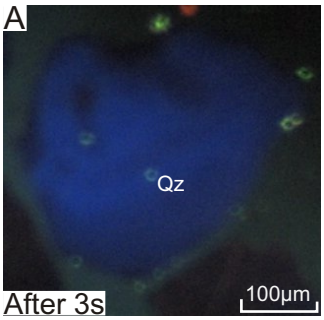

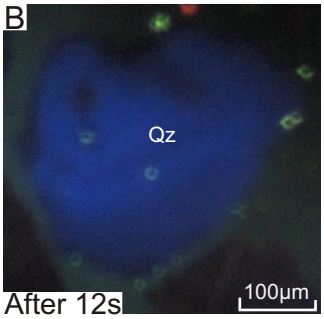

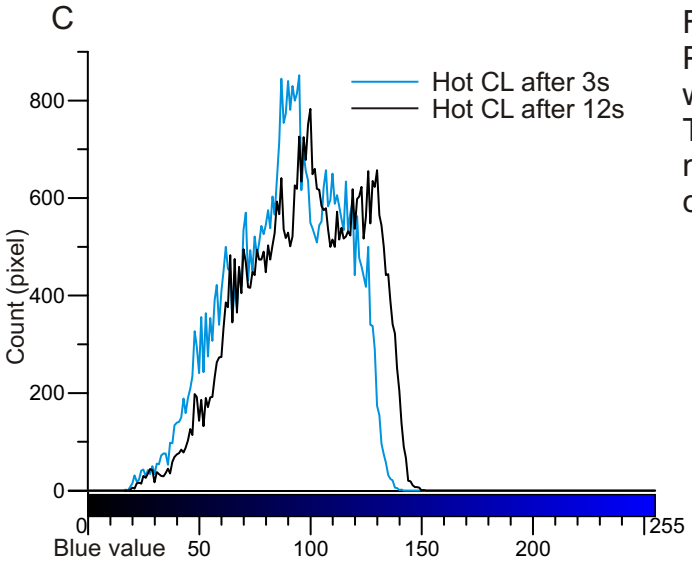

D

Blue value	Min	Max	Mode	Mean	SD
After 3s	17	141	95	89	24.3
After 12s	19	151	100	97	25.6

Figure 1B-39: Grain 39. Probably the first image was taken too early. Therefore, this grain is not useful to analyse the colour shift.

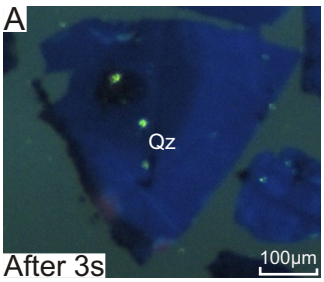

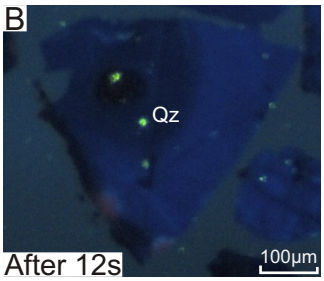

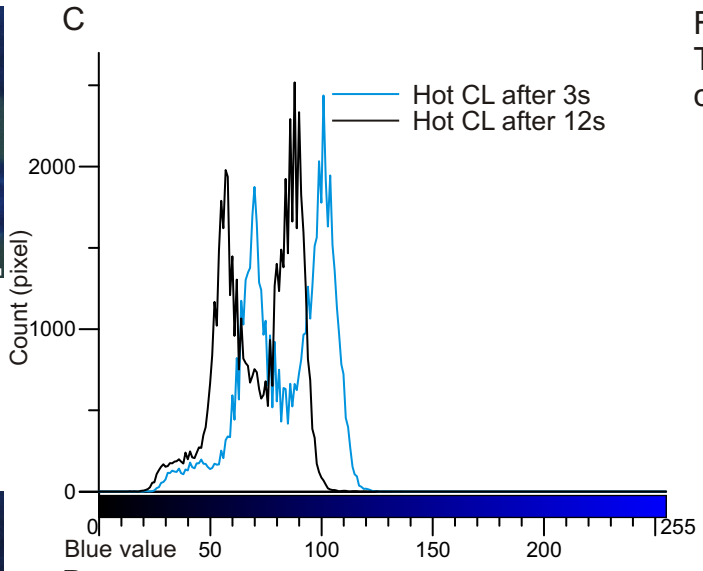

D

Blue value	Min	Max	Mode	Mean	SD
After 3s	21	136	101	84	18.9
After 12s	14	125	88	71	17

Figure 1B-40: Grain 40. The grain shows slight colour shift.

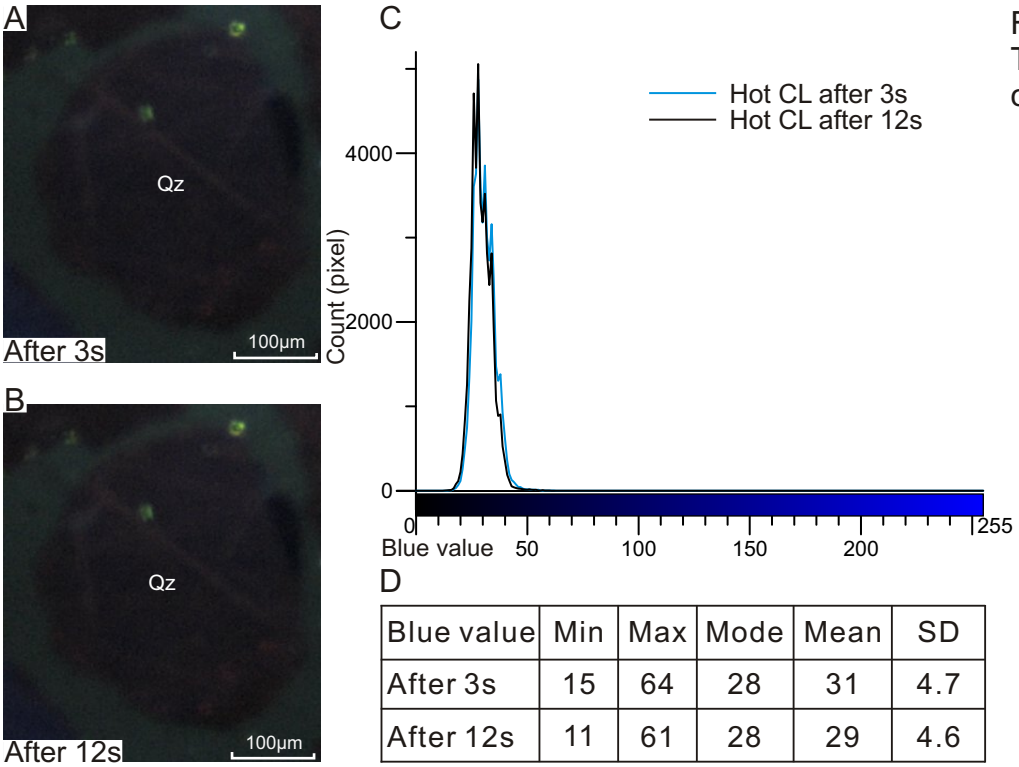

Figure 1B-41: Grain 41. The grain shows no colour shift.

D

Blue value	Min	Max	Mode	Mean	SD
After 3s	15	64	28	31	4.7
After 12s	11	61	28	29	4.6

Appendix 2A: Microphotos, SEM-BSE images, SEM-CL images, and EDS analyses of detrital quartz grains in sample 2860.

Notes:

1. **Homogenous CL:** Nearly uniform CL intensity across the grain (Fig. 2A).

2. Fractures in quartz have been divided into two types: **healed fractures** (**HF**) and **open fractures** (**OF**).

   Healed fractures are fractures filled with secondary silica that appear as thin (commonly < 10 μm) black lines in SEM-CL images (Fig. 2B). They are usually not shown in back-scattered images (Boggs and Krinsley, 2006).

   Open fractures appear in cathodoluminescense images as CL-dark or CL-bright lines, and they are also visible in back-scattered images and microphotos. A few open fractures are **conchoidal fractures** (**CF**) (Boggs and Krinsley, 2006).

3. **Tectonic deformation lamellae**: Tectonic deformation lamellae (Fig. 2C) appear in SEM-CL image as numerous sets of thin, parallel, closely spaced, dark gray lines (Bernet and Basset, 2005). According to Hamers and Drury (2011), tectonic deformation lamellae can either appear as dark gray lines or bright lines in SEM-CL images, and can show slightly wavy features with varying thickness. They usually also appear in XPL image under petrographic microscope.

4. **Spiders (S):** They are made up of dark-Cl patches and streaks. Dark-CL patches mainly range from 10-100 μm. Streaks are random and irregular in the appearance of black broad (>10 μm) elongated form. The spiders are commonly associated with healed fractures, giving them the appearance in SEM-CL images of spiders sitting on a web (Fig. 2D). They cannot be seen in BSE images, since they are composed by secondary silica (Boggs and Krinsley, 2006).

5. **Bright mottling**: Some grains show irregular CL intensity across grains, creating a mottled pattern due the presence of patches (Boggs and Krinsley, 2006). Three types of bright mottling were seen.

   - **Random bright patches** (Fig. 2E1)
   - **Bright streaky patches fabric** (Fig. 2E2)
   - **Subtle mottling** (Fig. 2E3)

6. **Overgrowth:** Overgrowth appears in SEM-CL images as dark areas in the border of the quartz grains (Fig. 2F).

7. **Fluid inclusion trail** (**FI trail**): Trails formed by **fluid inclusions** (**FI**). They are usually associated with secondary porosity and commonly located along fractures and at boundaries between detritral quartz grain and the overgrowth. They are well observed in microphotos under ppl. The fluid inclusion trails can be separated in two kinds: **detrital fluid inclusion trails (**fluid inclusions that are original from the detrital quartz, they do not cut the quartz overgrowth) and **diagenetic fluid inclusion trails** (fluid inclusions originated from the diagenesis, and they thus cut the quartz overgrowth).

8. **Melt inclusion** (**MI**): Large fluid inclusions (>10 μm) in which crystallized minerals are visible.

9. **Secondary porosity** (**SP**): Porosities usually caused by dissolution and/or fractures. They are easily observed in microphotos under PPL and BSE images.

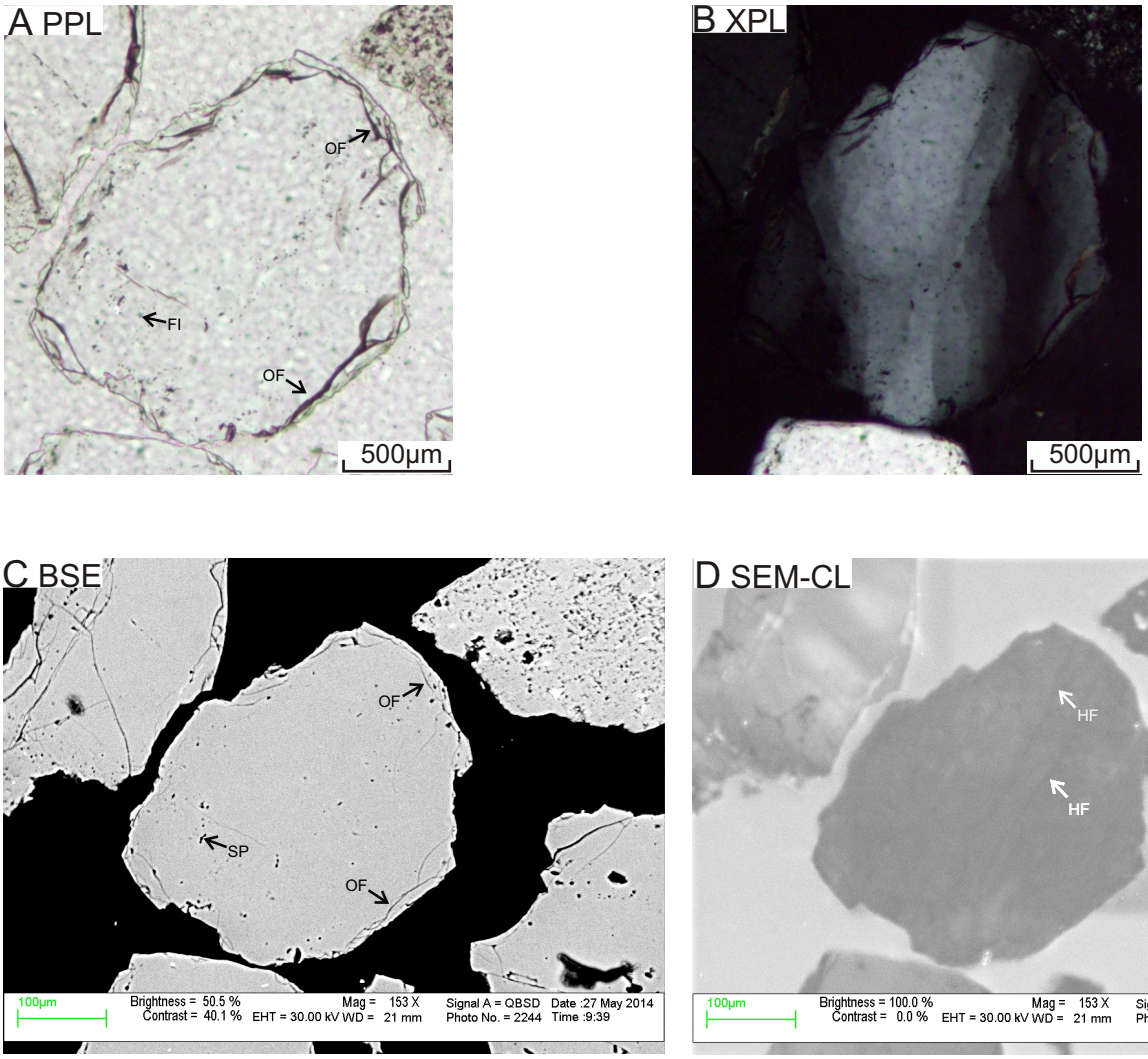

Figure 2A-1: Microphotos under ppl (A) and xpl (B), SEM-BSE image C, and SEM-CL image (D) of quartz grain 1 in sample 2860. The grain is subhedral and sub-rounded monocrystalline with strong undulose extinction. Fluid inclusions (FI) and secondary porosity (SP) are present (Fig. A and C). The grain is microfractured; a set of irregular open fractures (OF) can be seen in Fig. A and C, and a few parallel healed fractures (HF) can be seen in Fig. D.

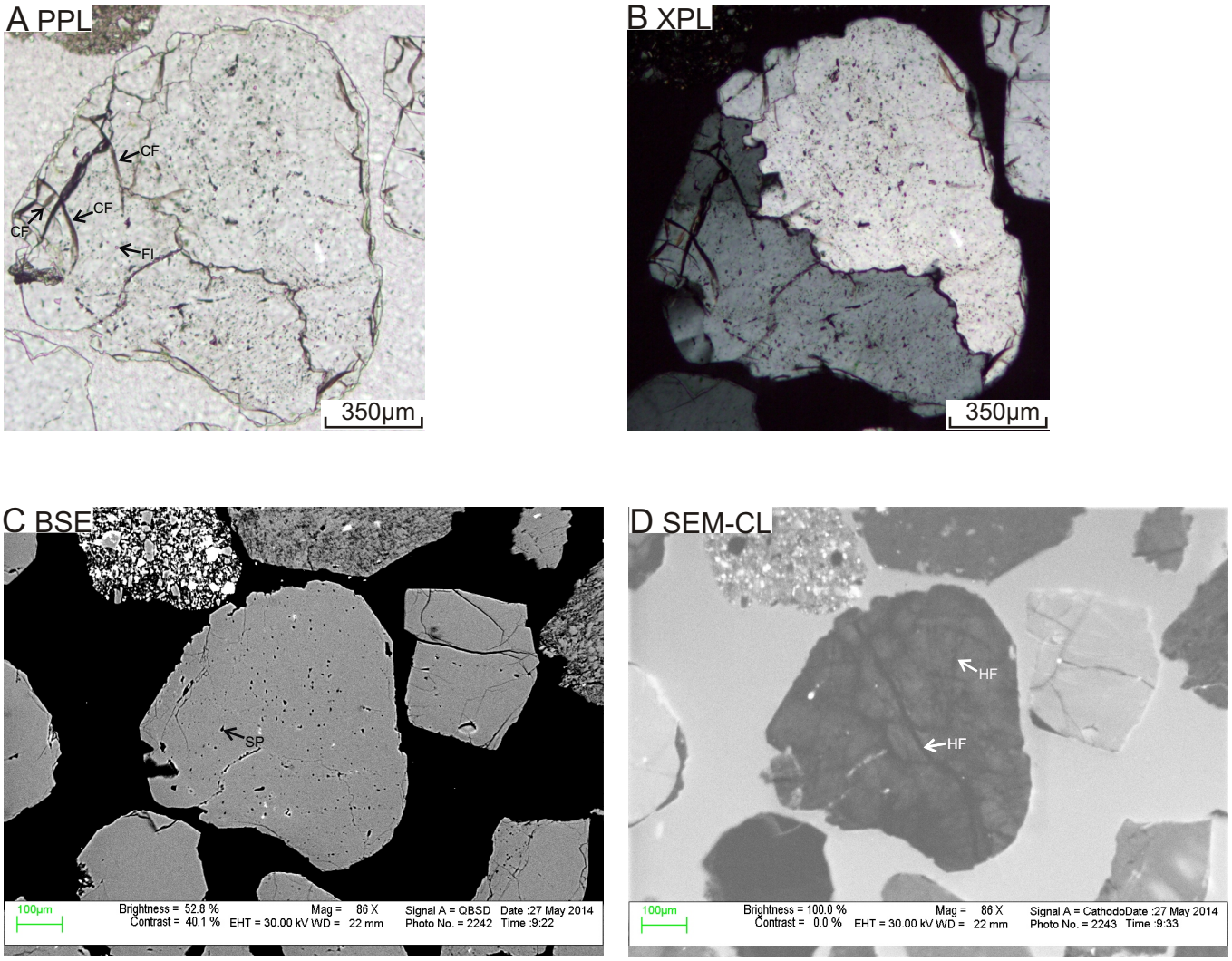

Figure 2A-2: Microphotos under ppl (A) and xpl (B), SEM-BSE image C, and SEM-CL image (D) of quartz grain 2 in sample 2860. The grain is anhedral and rounded polycrystalline (only a few sub-grains with sutured sub-grain boundaries) with strong undulose extinction. Fluid inclusions are common; they are usually associated with secondary porosity and form trails along healed fractures (Fig. A and C). The grain is microfractured with irregular fractures. A few conchoidal fractures (CF) can be seen in Fig. A, a set of randomly oriented healed fractures (HF) can be seen in Fig. D.

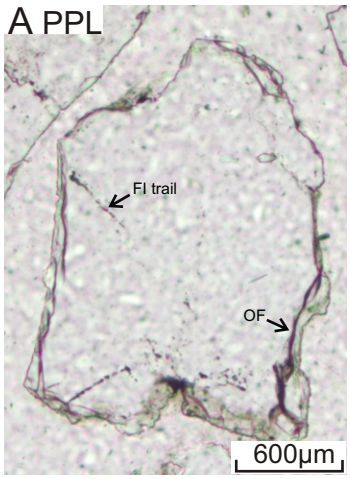

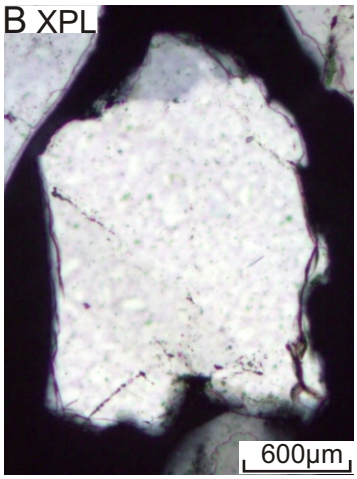

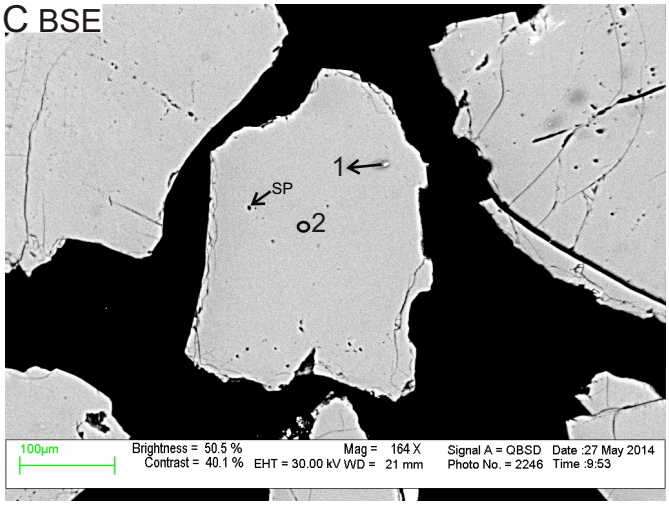

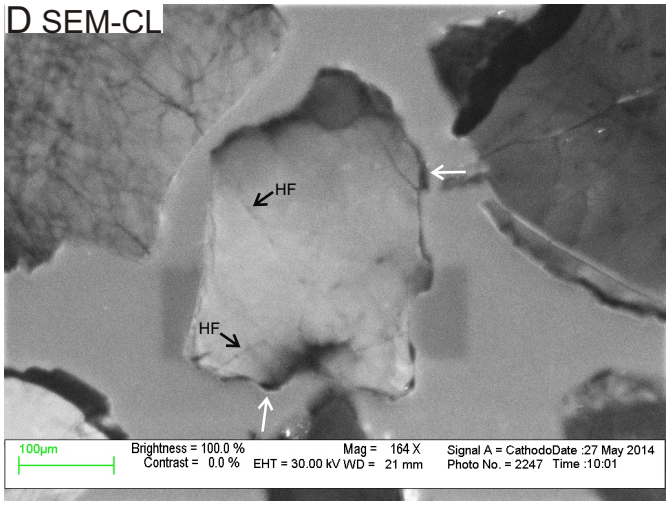

E EDS analyses

Pos#	Min. ID	SiO2	Al2O3	FeO	MgO	Na2O	Total	Actual total
1	Qz + ?	88.37	2.15	0.62	8.52	0.32	100	72
2	Qz	99.99					100	64

Figure 2A-3: Microphotos under ppl (A) and xpl (B), SEM-BSE image (C), SEM-CL image (D), and EDS analyses table (E) of quartz grain 3 in sample 2860. The grain is anhedral and sub-angular polycrystalline (only two sub-grains) with mosaic texture and weak undulose extinction. The grain contains fluid inclusions trails (FI trail) associated with secondary porosity (SP) along fractures (Fig. A and C), and is microfractured with irregular fractures. A few open fractures (Fig. A) and healed fractures (Fig. D) can be seen. The dark areas indicated by arrows in Fig. D are overgrowth.

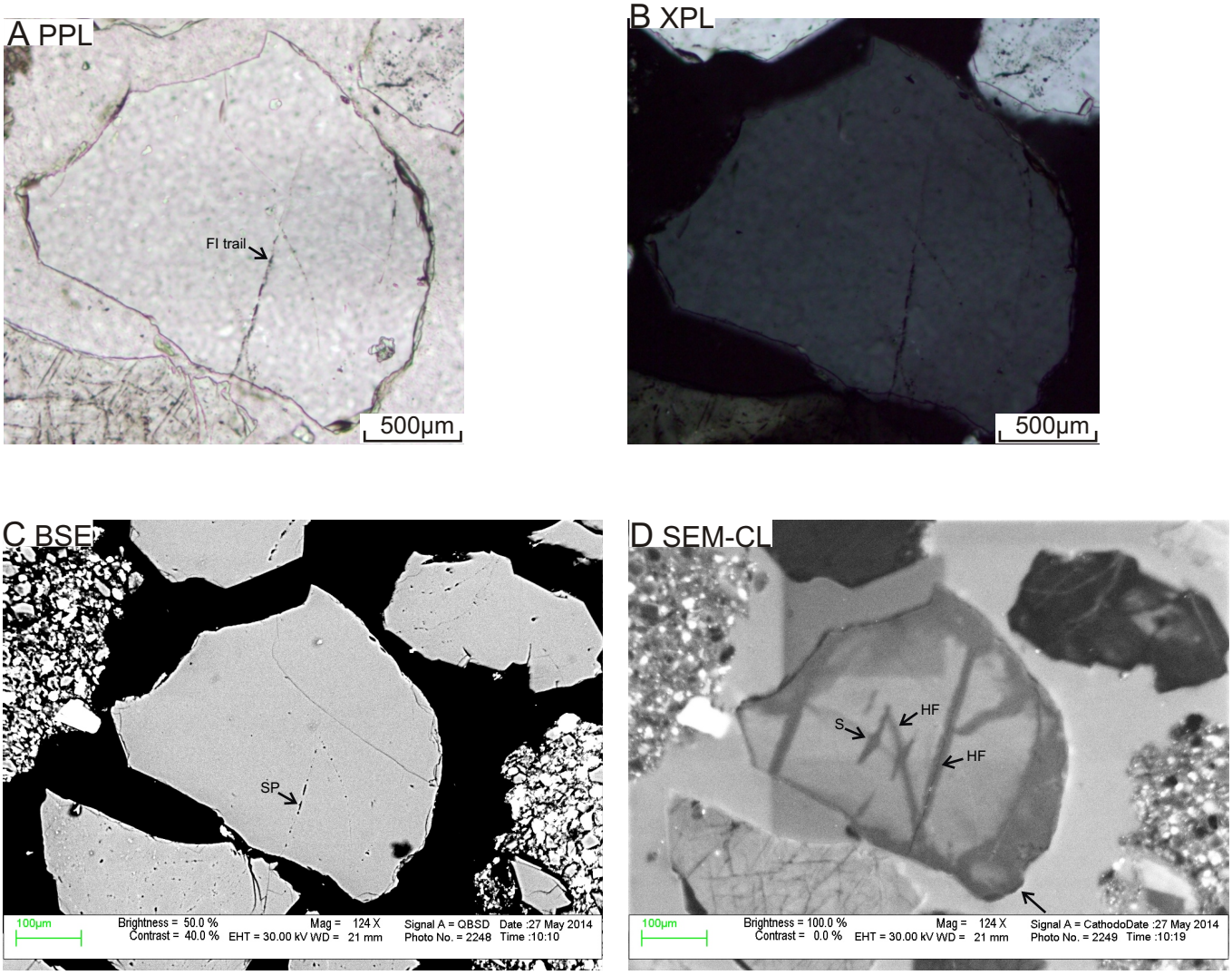

Figure 2A-4: Microphotos under ppl (A) and xpl (B), SEM-BSE image C, and SEM-CL image (D) of quartz grain 4 in sample 2860. The grain is anhedral and sub-angular monocrystalline with strong undulose extinction. Fluid inclusions are present; they are usually associated with secondary porosity and form trails along healed fractures (Fig. A and C). The grain is weakly microfractured with a set of sub-parallel healed fractures (Fig. D). The spiders (S) in Fig. D are secondary porosity filled by diagenetic quartz along fractures, and the dark area indicated by arrow in Fig. D is overgrowth. The grain shows random bright patches im SEM-CL image.

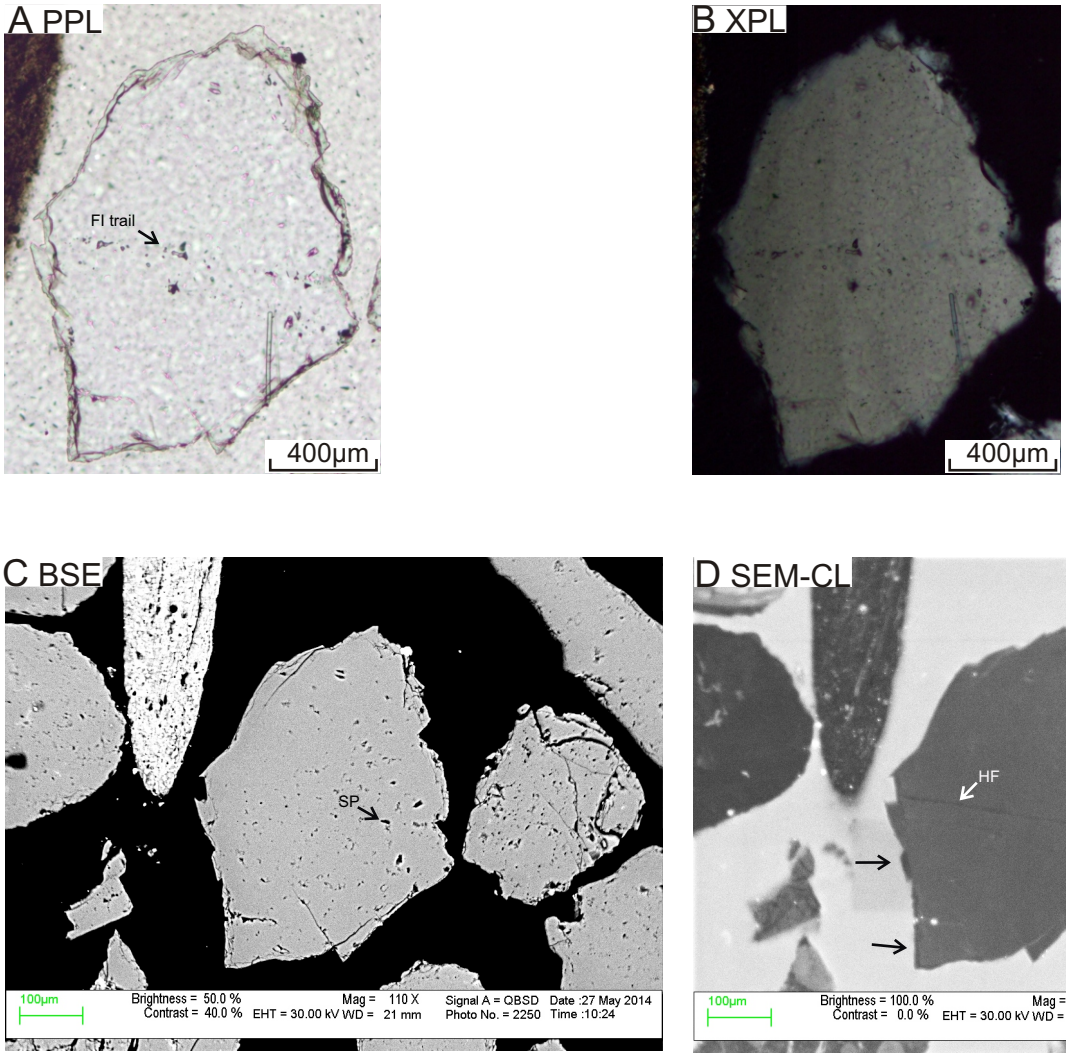

Figure 2A-5: Microphotos under ppl (A) and xpl (B), SEM-BSE image C, and SEM-CL image (D) of quartz grain 5 in sample 2860. The grain is anhedral and angular monocrystalline with strong undulose extinction. Secondary porosity filled by diagenetic quartz are common (Fig. C). The grain contains fluid inclusions that form trails along fractures (Fig. A) and is weakly microfractured with irregular fractures (Fig. A and C). A healed fracture (HF) can be seen in Fig D. The dark areas indicated by arrows in Fig. D are overgrowth.

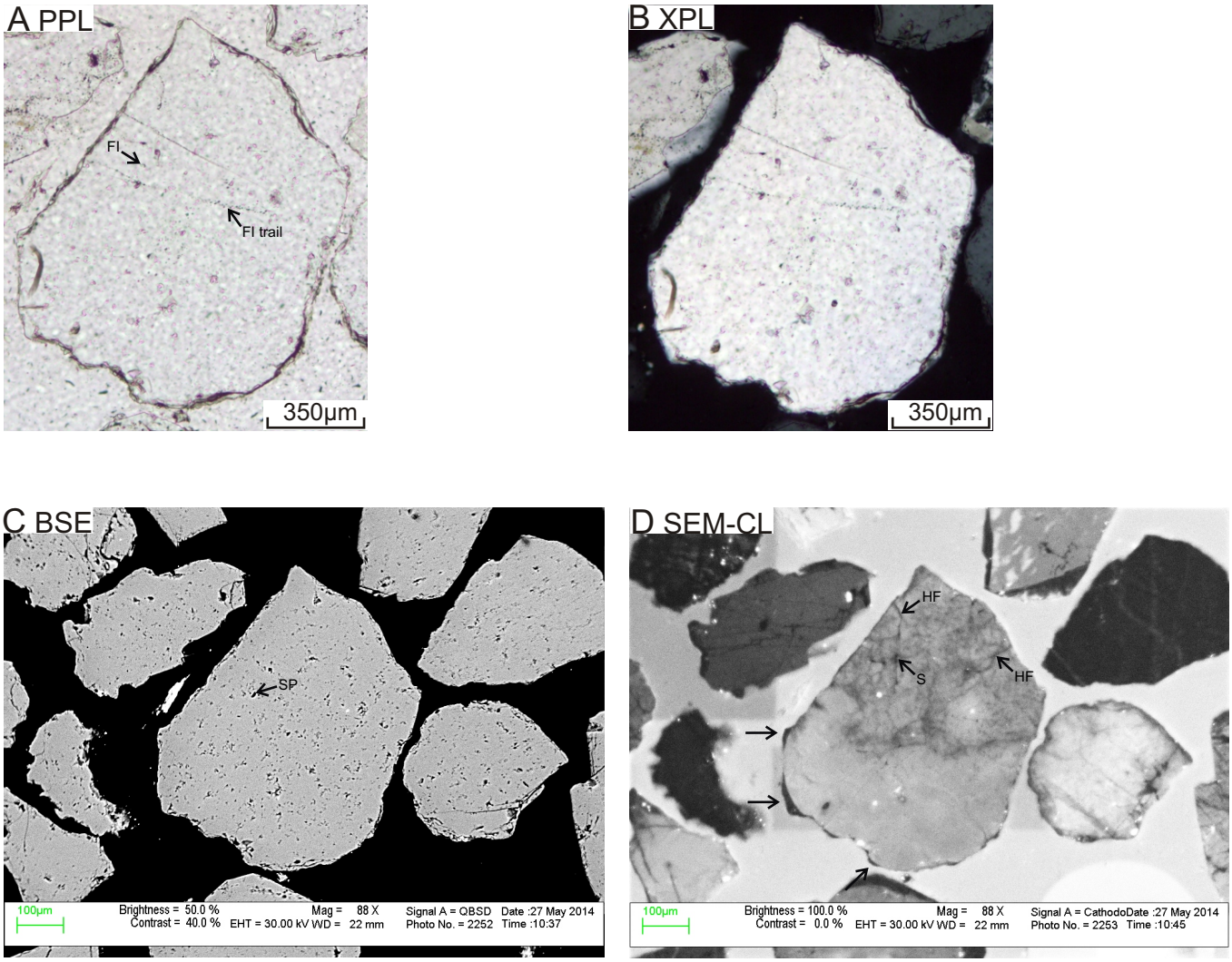

Figure 2A-6: Microphotos under ppl (A) and xpl (B), SEM-BSE image C, and SEM-CL image (D) of quartz grain 6 in sample 2860. The grain is anhedral and sub-rounded monocrystalline with non-undulose extinction. Fluid inclusion trails and secondary porosity are present (Fig. A and C). The grain is microfractured with randomly oriented irregular fractures (Fig. A and D). Some healed fractures (HF) and spiders (S) can be seen in Fig D. The dark areas indicated by arrows in Fig. D are overgrowth.

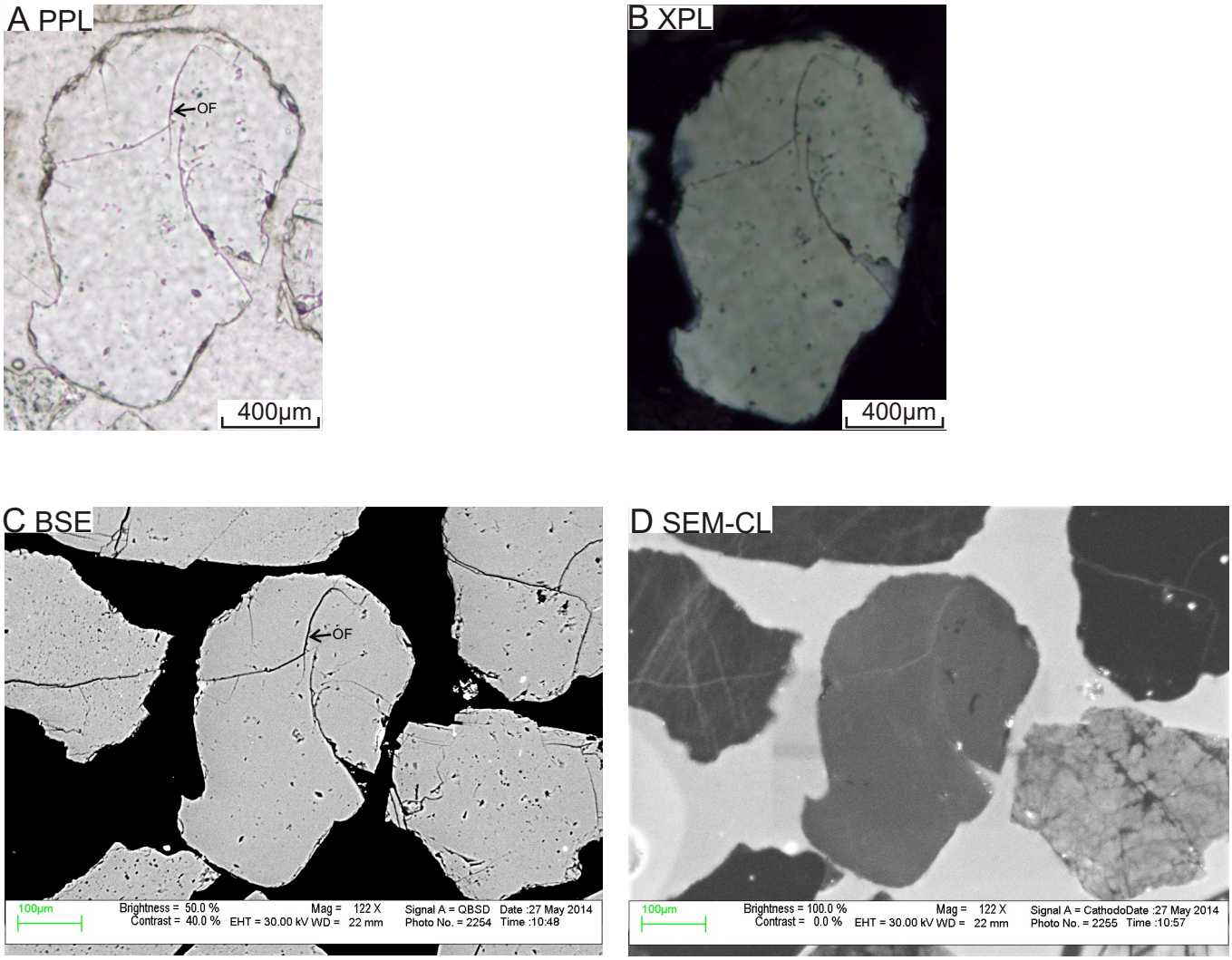

Figure 2A-7: Microphotos under ppl (A) and xpl (B), SEM-BSE image C, and SEM-CL image (D) of quartz grain 7 in sample 2860. The grain is anhedral and sub-rounded monocrystalline with strong undulose extinction. Fluid inclusion trails are rare. The grain is microfractured with irregular curved open fractures (Fig. A and C). Healed fractures and spiders are rare.

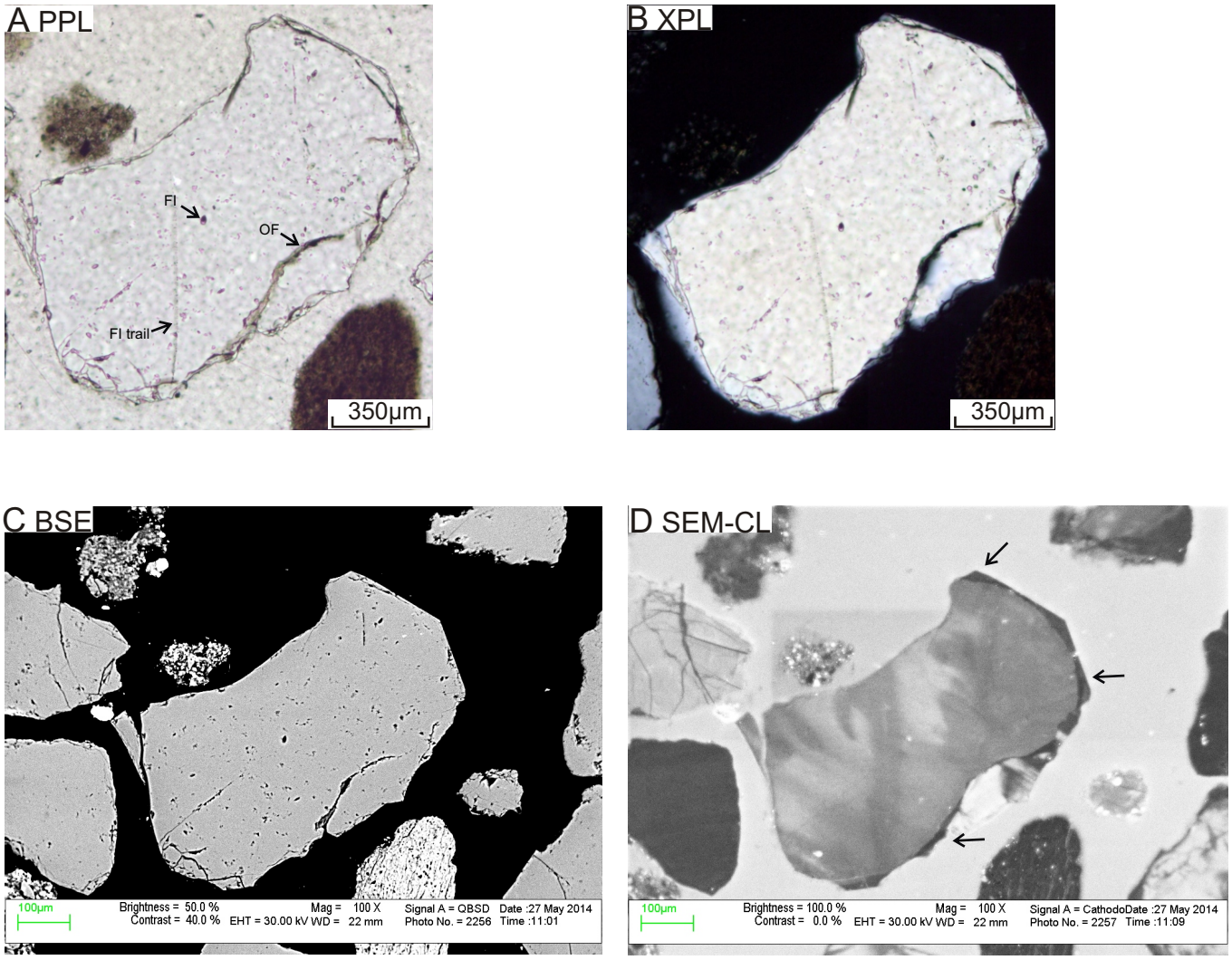

Figure 2A-8: Microphotos under ppl (A) and xpl (B), SEM-BSE image C, and SEM-CL image (D) of quartz grain 8 in sample 2860. The grain is anhedral and sub-rounded monocrystalline with non-undulose extinction. Fluid inclusion trails are present (Fig. A). The grain is weakly microfractured with irregular curved open fractures (Fig. A and C). Healed fractures are rare. The dark areas indicated by arrows in Fig. D are overgrowth. The grain shows bright streaky patches in SEM-CL image.

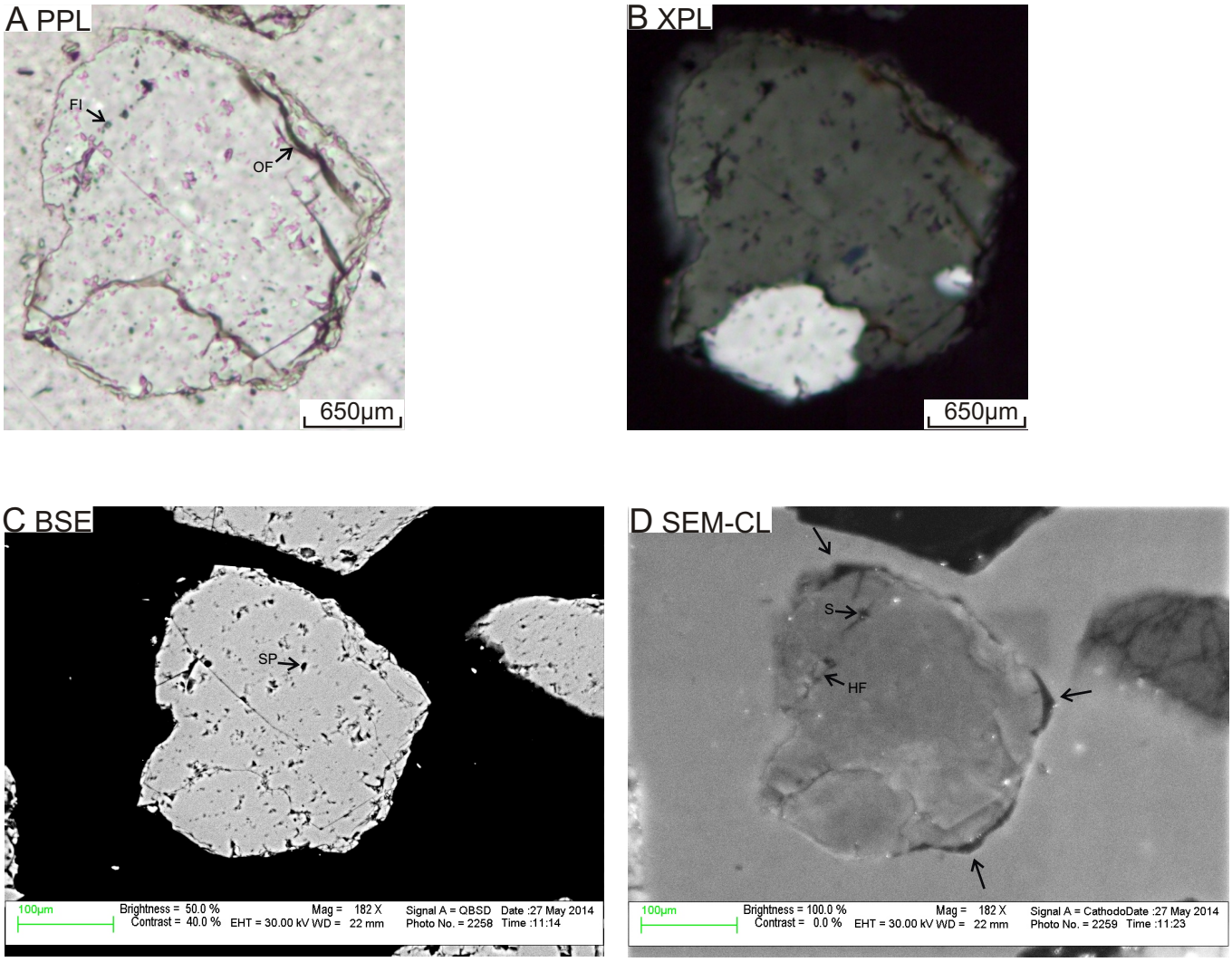

Figure 2A-9: Microphotos under ppl (A) and xpl (B), SEM-BSE image ©, and SEM-CL image (D) of quartz grain 9 in sample 2860. The grain is anhedral and sub-rounded polycrystalline (only 3 sub-grains with sutured sub-grain boundaries) with embayed margins and strong undulose extinction. Sencondary porosity (SP) are common (Fig. C), only a few fluid inclusions can be seen in Fig. A. The grain is microfractured with irregular fractures (Fig. A and C). Some open fractures (Fig. A) and only a few healed fractures (Fig. D) can be seen. The spiders (S) in Fig. D are secondary porosity filled by diagenetic quartz. The dark areas indicated by arrows in Fig. D are overgrowth. The grain shows subtle mottling texture with only a few bright-CL patches.

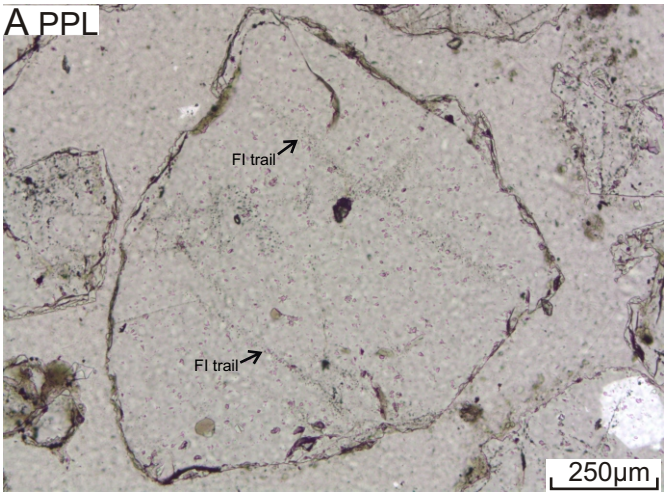

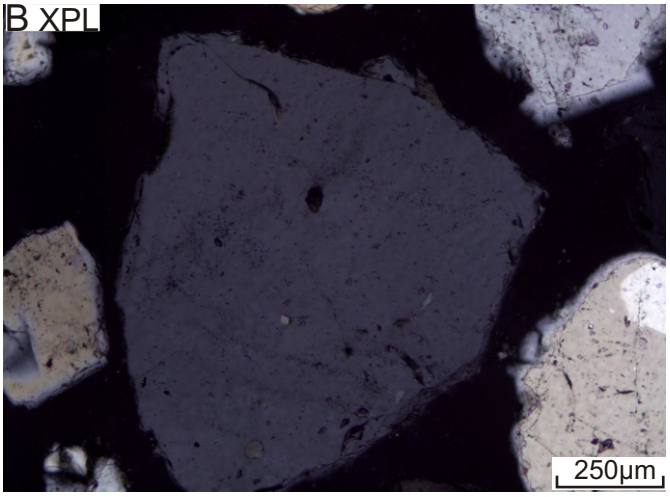

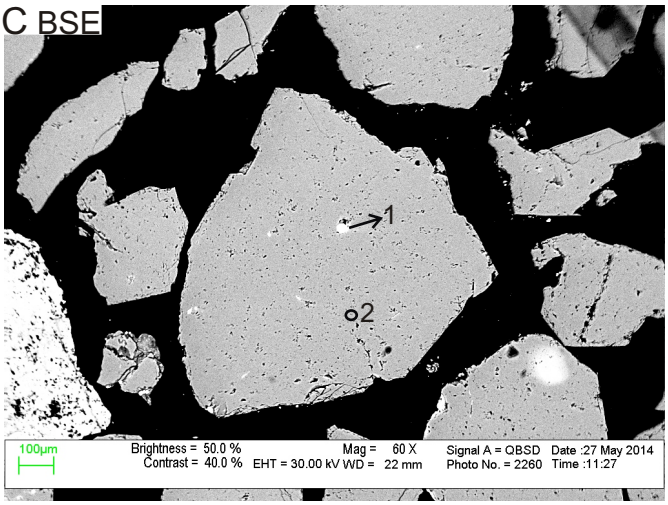

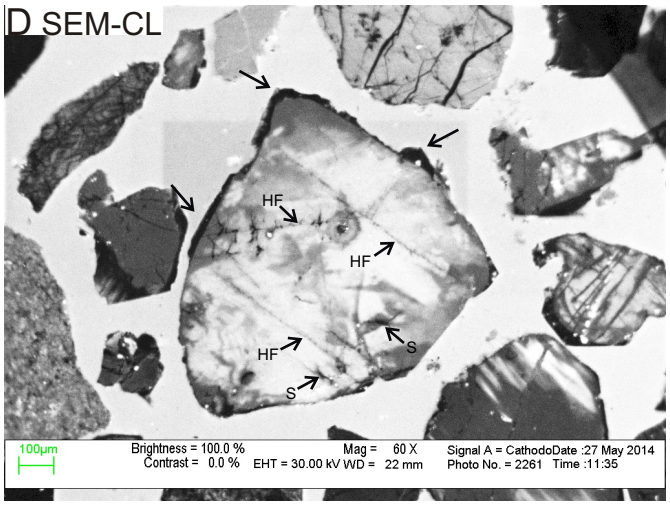

E EDS analyses

Pos#	Min. ID	SiO2	CaO	P2O5	Y2O3	La2O3	Ce2O3	Nd2O3	ThO2	Total	Actual total
1	Mnz	3.98	1.26	33.84	2.87	13.24	27.42	10.29	7.12	100	53
2	Qz	99.99								100	65

Figure 2A-10: Microphotos under ppl (A) and xpl (B), SEM-BSE image (C), SEM-CL image (D), and EDS analyses table (E) of quartz grain 10 in sample 2860. The grain is subhedral and sub-rounded monocrystalline with non-undulose extinction. Fluid inclusions are common (Fig. A); they are usually associated with secondary porosity and form trails along healed fractures and at boundaries between the detritral quartz grain and the overgrowth (diagenetic fluid inclusion). The grain contains monazite inclusion and is microfractured with a set of parallel fractures and a set of irregular fractures (Fig. D). Some healed fractures (HF) and spiders (S) can be seen in Fig. D. The dark areas indicated by arrows in Fig. D are overgrowth. The grain shows random bright CL patches in SEM-CL image.

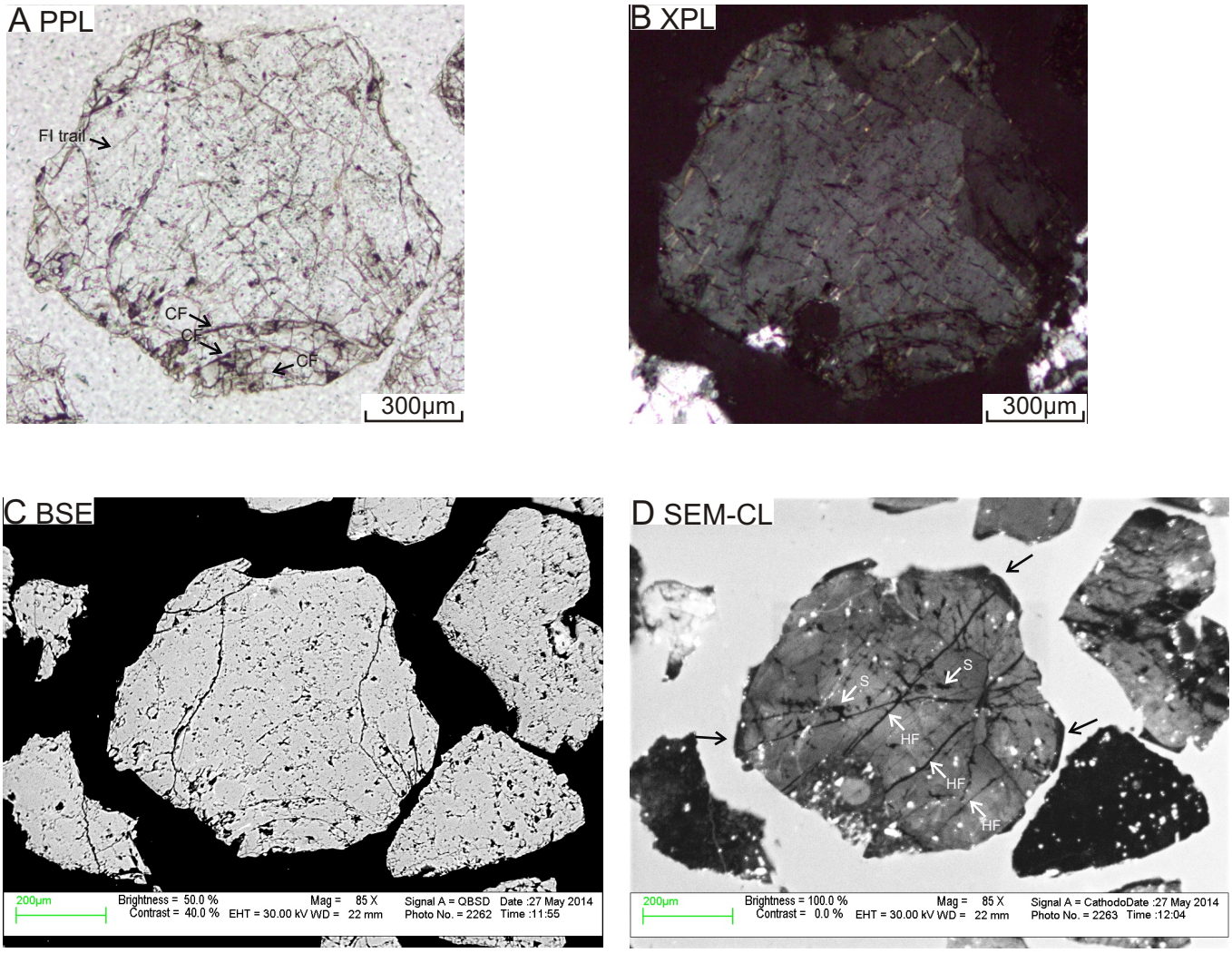

Figure 2A-11: Microphotos under ppl (A) and xpl (B), SEM-BSE image C, and SEM-CL image (D) of quartz grain 11 in sample 2860. The grain is subhedral and sub-rounded polycrystalline (only 3 sub-grains with sutured sub-grain boundaries) with weak undulose extinction. Fluid inclusions trails along fractures and secondary porosity are common (Fig. A). The grain is strongly microfractured with a set of parallel fractures and a set of irregular curved fractures (Fig. A and D). Some parallel healed fractures (HF) can be seen in Fig. D, and a set of preferably oriented conchoidal fractures (CF) can be seen in Fig. A. The spiders (S) in Fig. D are secondary porosity filled by diagenetic quartz along fractures. The dark areas indicated by arrows in Fig. D are overgrowth.

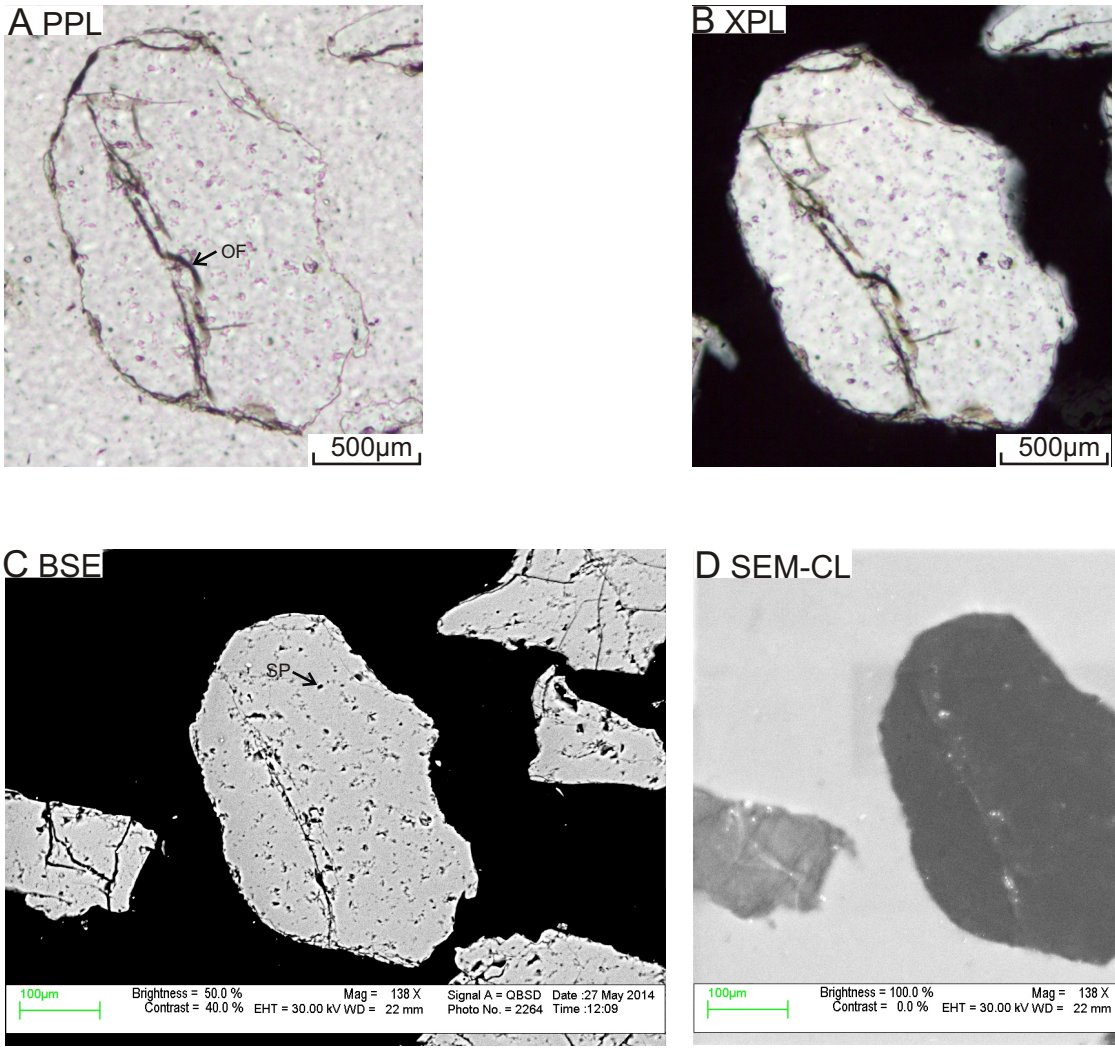

Figure 2A-12: Microphotos under ppl (A) and xpl (B), SEM-BSE image C, and SEM-CL image (D) of quartz grain 12 in sample 2860. The grain is anhedral and sub-rounded monocrystalline with weak undulose extinction. Secondary porosity (Fig. C) is common. The grain is microfractured with a set of irregular open fractures (Fig. A). Healed fracturers are rare.

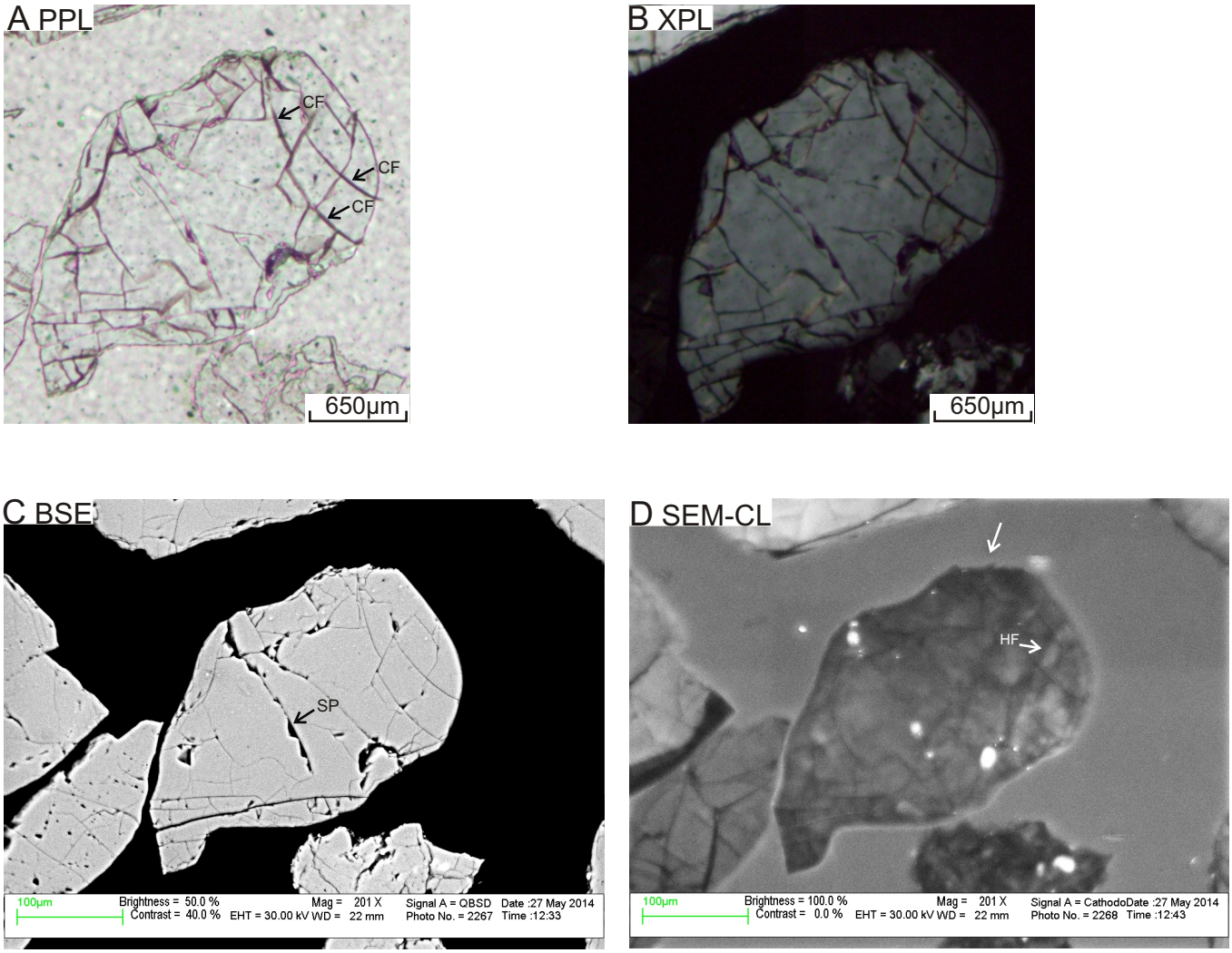

Figure 2A-13: Microphotos under ppl (A) and xpl (B), SEM-BSE image C, and SEM-CL image (D) of quartz grain 13 in sample 2860. The grain is anhedral and sub-rounded monocrystalline with strong undulose extinction. Secondary porosity is common (Fig. A). The grain is strongly microfractured with a set of irregular curved fractures (Fig. A and D). A few conchoidal open fractures (CF) with preferred orientation can be seen (Fig. A), and a only few healed fractures (HF) can be seen in Fig. D. The dark area indicated by arrow in Fig. D is overgrowth; this area appears corroded in Fig. C, suggesting secondary porosity. The grain shows subtle bright mottling texture in SEM-CL image.

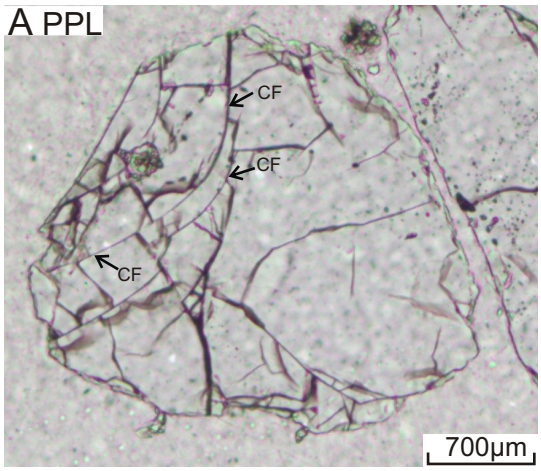

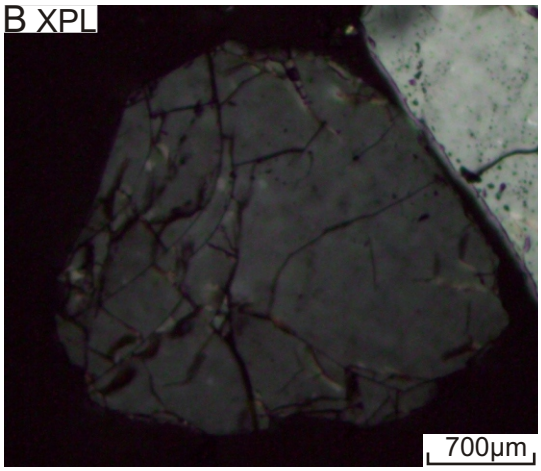

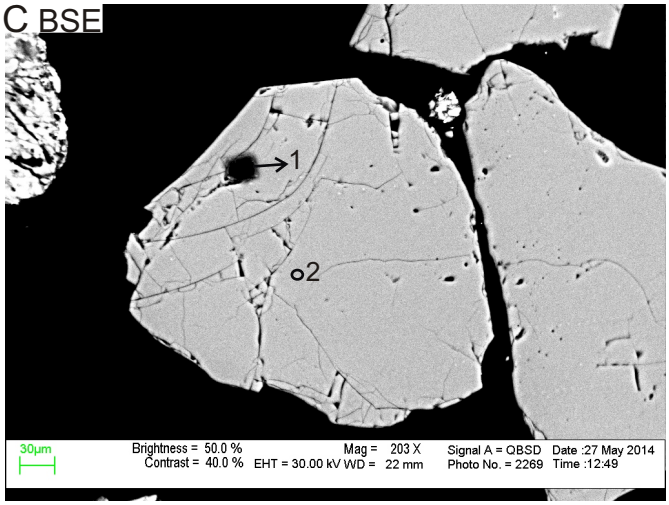

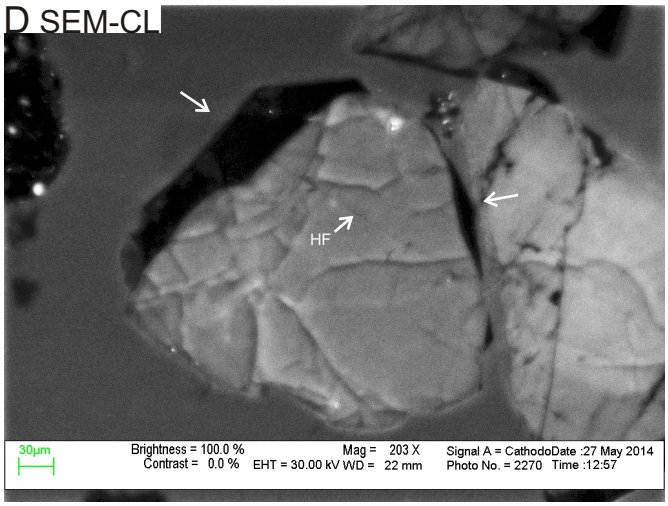

E EDS analyses

Pos#	Min. ID	SiO2	Na2O	K2O	SO3	Cl	Total	Actual total
1	Fluid inclusion	69.16	0.84	0.16	0.57	0.26	71	54
2	Qz	99.99					100	66

Figure 2A-14: Microphotos under ppl (A) and xpl (B), SEM-BSE image (C), SEM-CL image (D), and EDS analyses table (E) of quartz grain 14 in sample 2860. The grain is subhedral and sub-rounded polycrystalline (only 2 sub-grains) with non-undulose extinction. Fluid inclusions are present; they are located at boundaries between the detritral quartz grain and the overgrowth (Fig. C). The grain is strongly microfractured with a set of irregular and curved open fractures (Fig. A and D). Some conchoidal open fractures (CF) with preferred orientation can be seen (Fig. A); only a few healed fractures (HF) can be seen in Fig. D. The dark areas indicated by arrows in Fig. D are overgrowth.

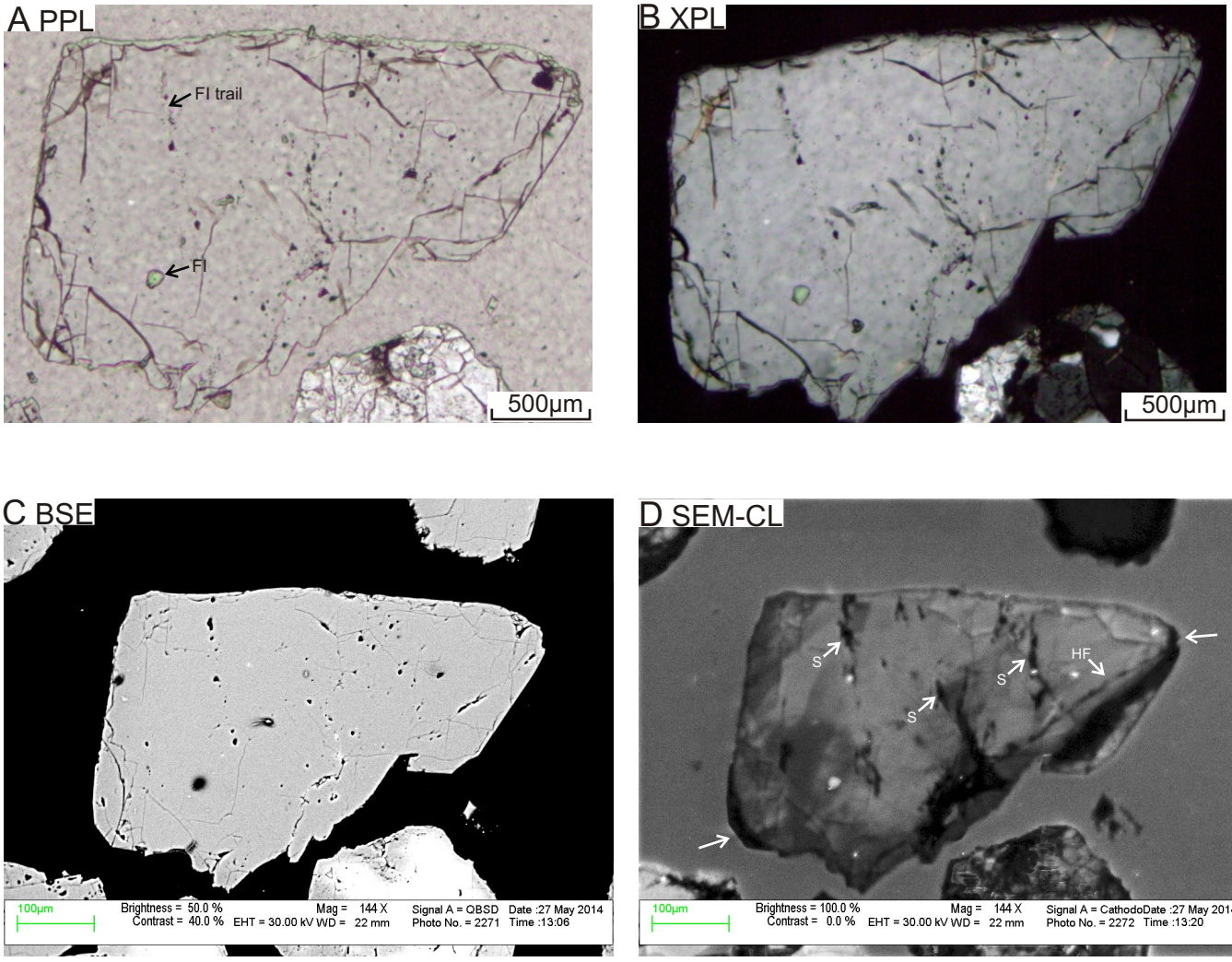

Figure 2A-15: Microphotos under ppl (A) and xpl (B), SEM-BSE image C, and SEM-CL image (D) of quartz grain 15 in sample 2860. The grain is anhedral and sub-angular monocrystalline with non-undulose extinction. Fluid inclusions are common; they are usually associated with secondary porosity and form trails along healed fractures (Fig. A). The grain is microfractured with a set of irregular fractures (Fig. A and D). Some healed fractures (HF) and spiders (S) can be seen in Fig. D. The dark areas indicated by arrows in Fig. D are overgrowth. The grain shows random bright patches in SEM-CL image.

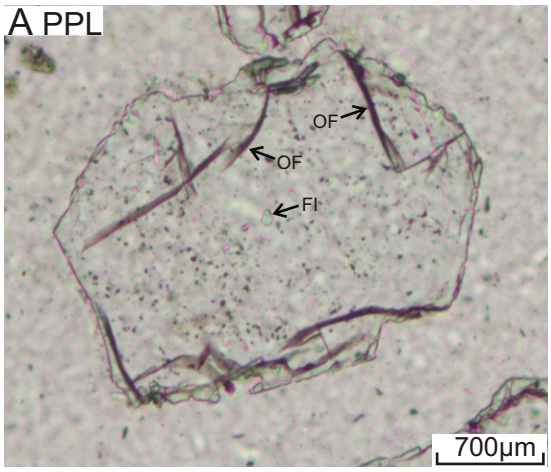

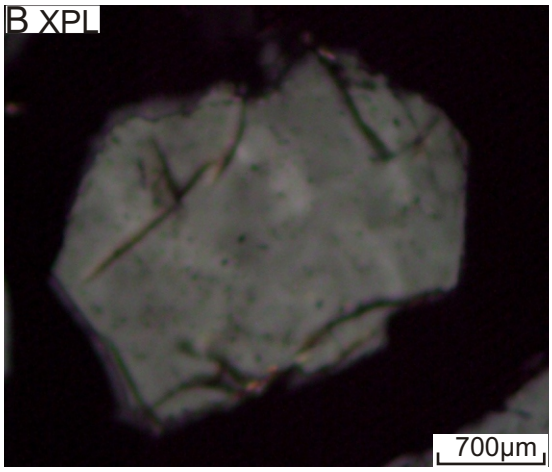

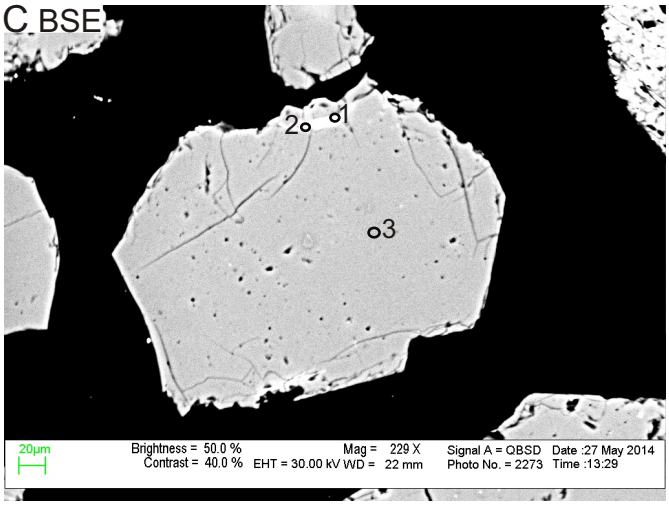

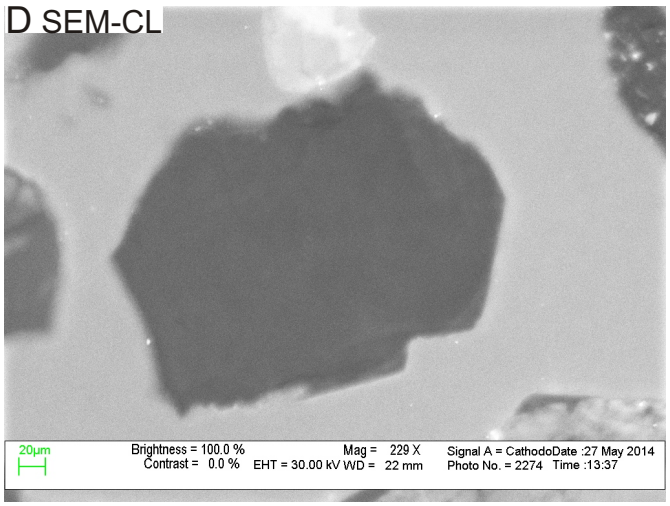

E EDS analyses

Pos#	Min. ID	SiO2	Al2O3	FeO	MnO	MgO	K2O	Total	Actual total
1	Chl	35.84	16.67	20.57	0.44	11.48		85	55
2	Chl	42.72	14.52	17.49	0.38	9.72	0.17	85	58
3	Qz	99.99						100	65

Figure 2A-16: Microphotos under ppl (A) and xpl (B), SEM-BSE image (C), SEM-CL image (D), and EDS analyses table (E) of quartz grain 16 in sample 2860. The grain is subhedral and angular monocrystalline with mosiac texture and strong undulose extinction. Fluid inclusions and secondary porosity are present (Fig. A and C). The grain contains chlorite inclusions and is microfractured with a set of irregular and curved open fractures (Fig. A).

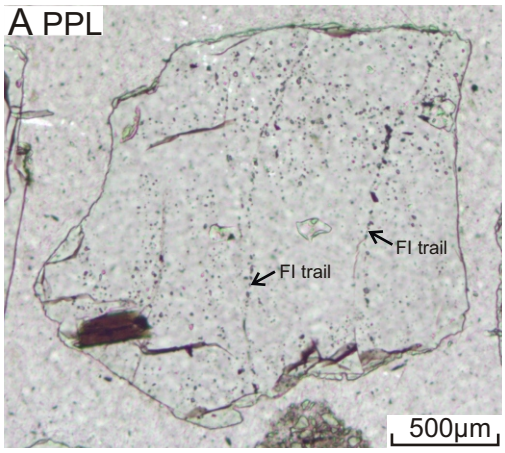

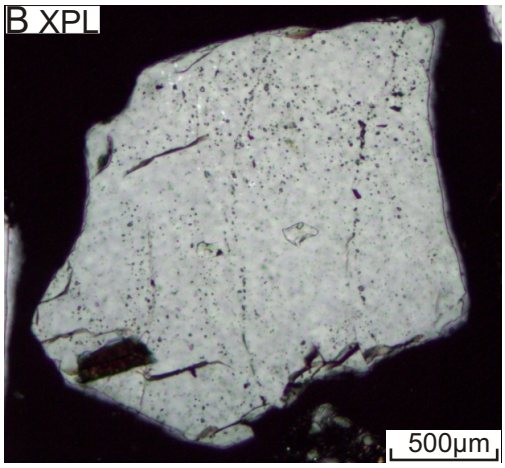

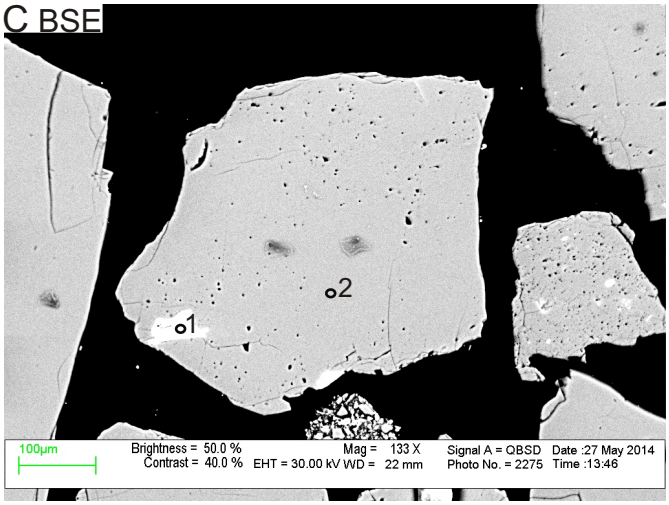

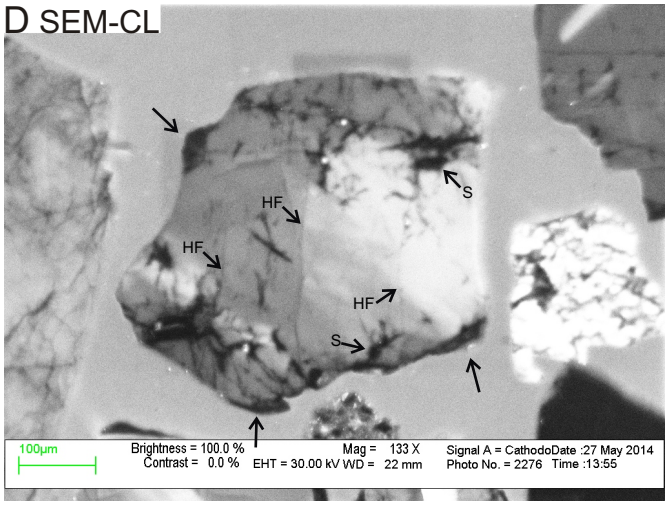

E EDS analyses

Pos#	Min. ID	SiO2	TiO2	Al2O3	FeO	MnO	MgO	K2O	Cl	Total	Actual total
1	Bt	37.54	3.09	20.17	22.52	0.25	2.80	9.39	0.23	96	54
2	Qz	99.99								100	63

Figure 2A-17: Microphotos under ppl (A) and xpl (B), SEM-BSE image (C), SEM-CL image (D), and EDS analyses table (E) of quartz grain 17 in sample 2860. The grain is anhedral and sub-angular monocrystalline with weak undulose extinction. Fluid inclusions are common; they are usually associated with secondary porosity and form trails along healed fractures (Fig. A). The grain contains biotite inclusion and is microfractured with a set of parallel fractures and a set of irregular fractures (Fig. A and D). Healed fractures (HF) and spiders (S) are common (Fig. D). The dark areas indicated by arrows in Fig. D are overgrowth.

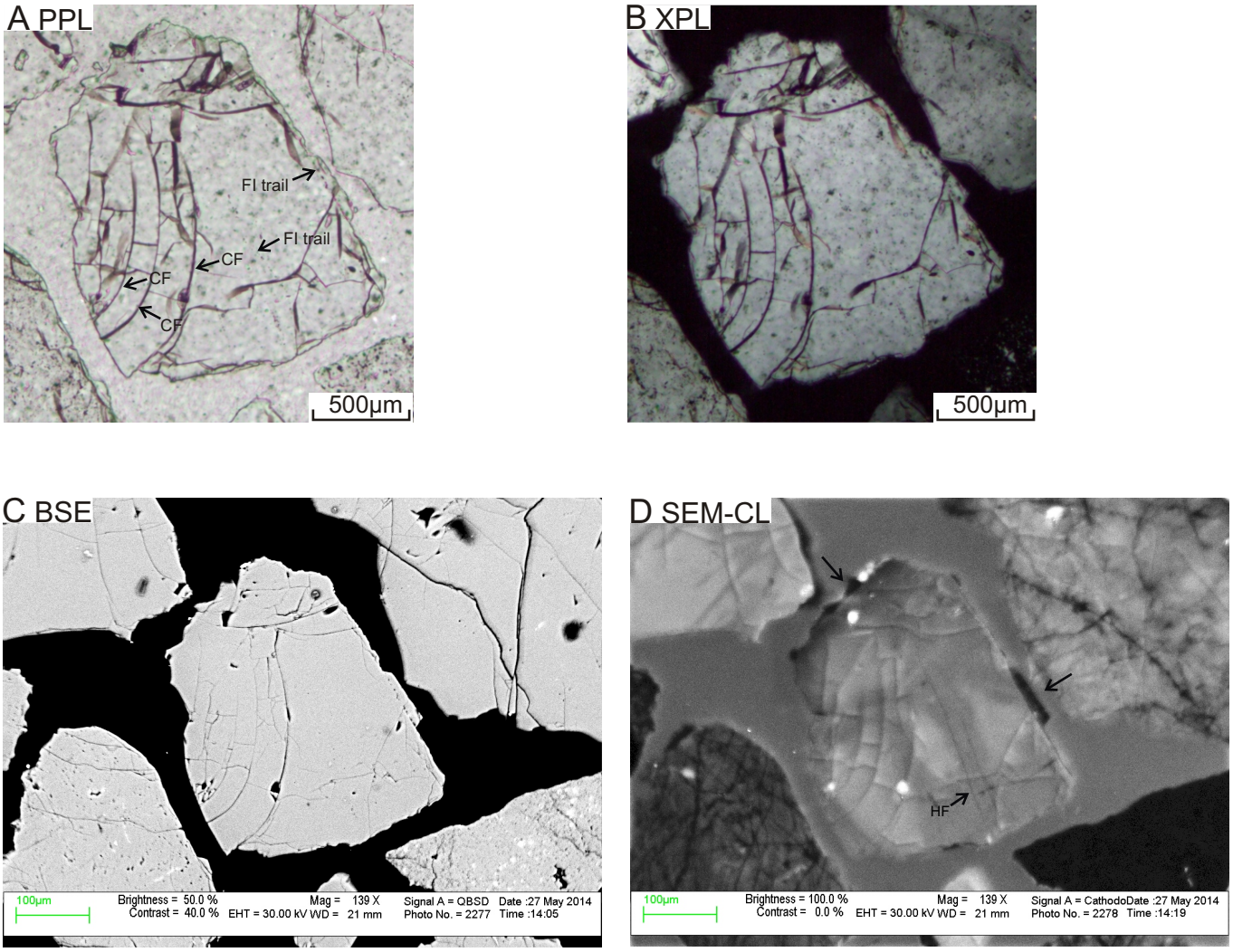

Figure 2A-18: Microphotos under ppl (A) and xpl (B), SEM-BSE image C, and SEM-CL image (D) of quartz grain 18 in sample 2860. The grain is anhedral and sub-rounded monocrystalline with weak undulose extinction. Fluid inclusions are common and form trails along healed fractures and at the boundary between the detrital quartz grain and the overgrowth (Fig. A). The grain is strongly microfractured with a set of irregular curved fractures (Fig. A and D). Some conchoidal open fractures (CF) with preferred orientation can be seen (Fig. A); only a few healed fractures (HF) can be seen in Fig. D. The dark areas indicated by arrows in Fig. D are overgrowth. The grain shows random bright-CL patches in SEM-CL image.

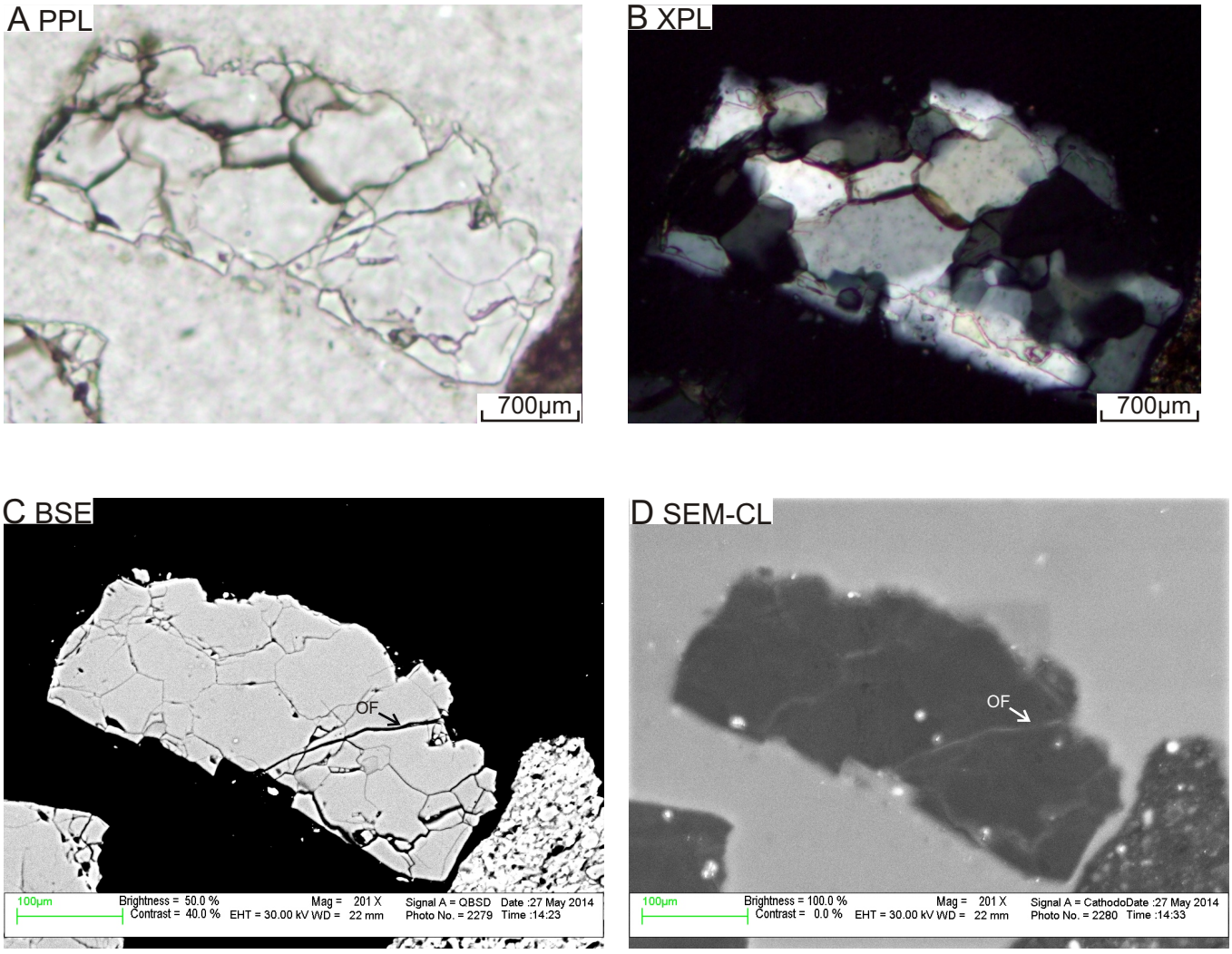

Figure 2A-19: Microphotos under ppl (A) and xpl (B), SEM-BSE image C, and SEM-CL image (D) of quartz grain 19 in sample 2860. The grain is anhedral and angular polycrystalline (more than 10 sub-grains with sutured sub-grain boundaries) with strong undulose extinction. Fluid inclusions and secondary porosity are present (Fig. A and C). The grain is microfractured with a set of irregular and curved open fractures (Fig. A and C). Healed fractures are rare, the bright lines in SEM-CL images are the sutured sub-grain boundaries.

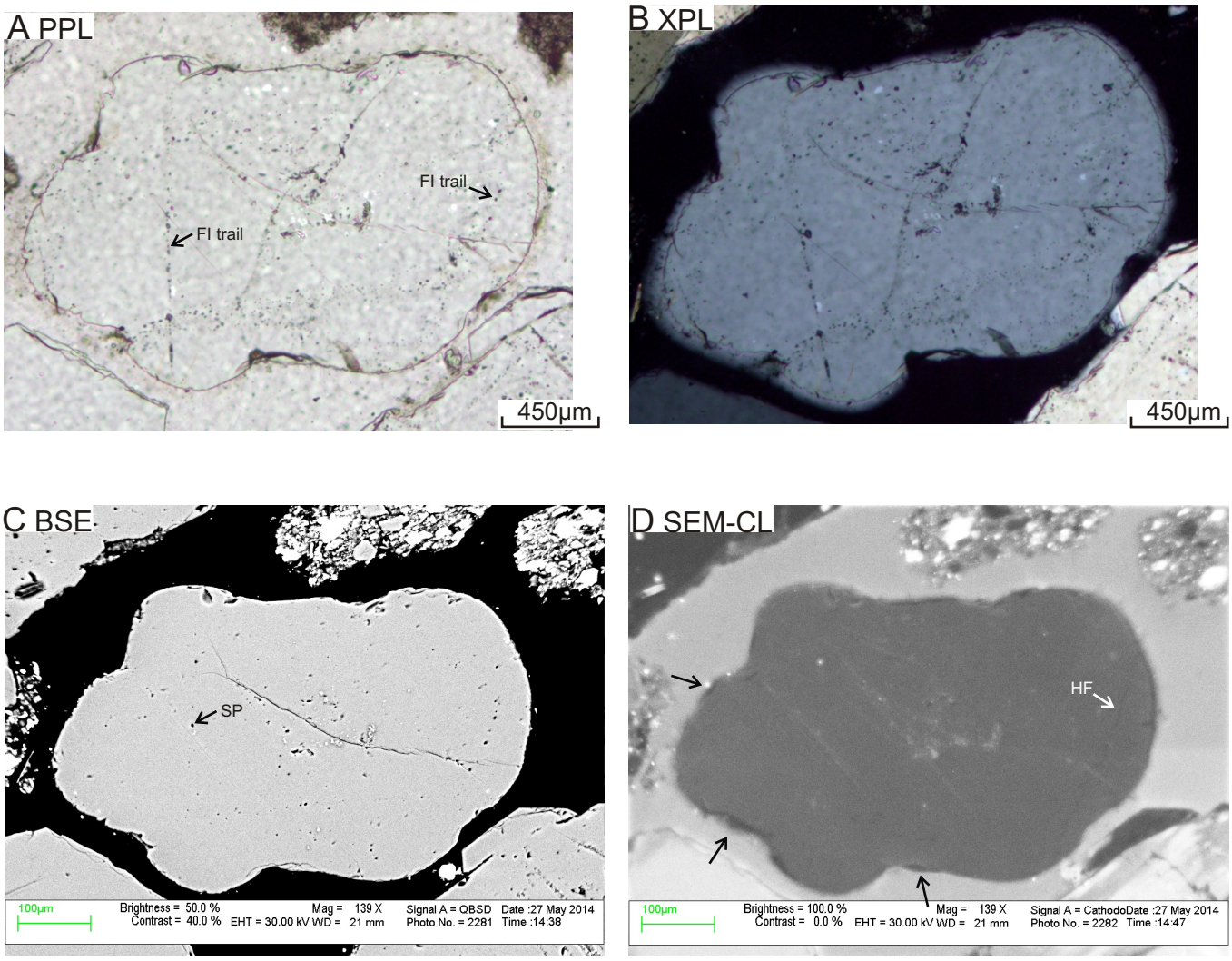

Figure 2A-20: Microphotos under ppl (A) and xpl (B), SEM-BSE image C, and SEM-CL image (D) of quartz grain 20 in sample 2860. The grain is anhedral and well-rounded monocrystalline with weak undulose extinction. Fluid inclusions are common; they are usually associated with secondary porosity and form trails along healed fractures (Fig. A). The grain is weakly microfractured with a set of irregular curved fractures (Fig. A and C). Only a few healed fractures (HF) can be seen in Fig. D. The dark areas indicated by arrows in Fig. D are overgrowth.

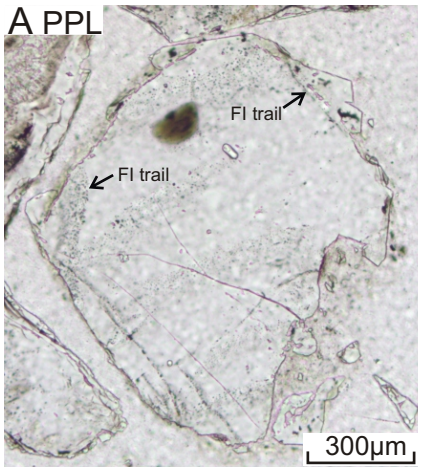

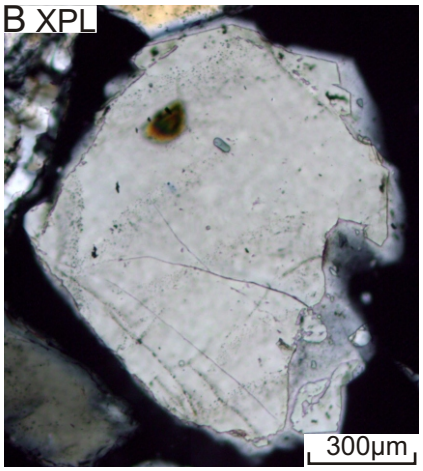

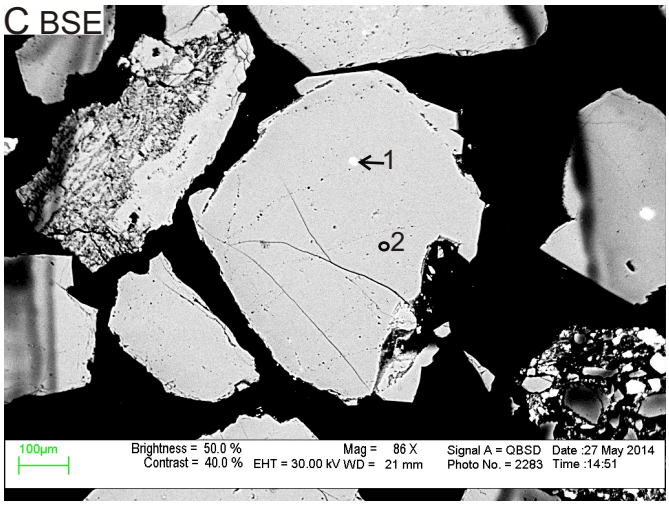

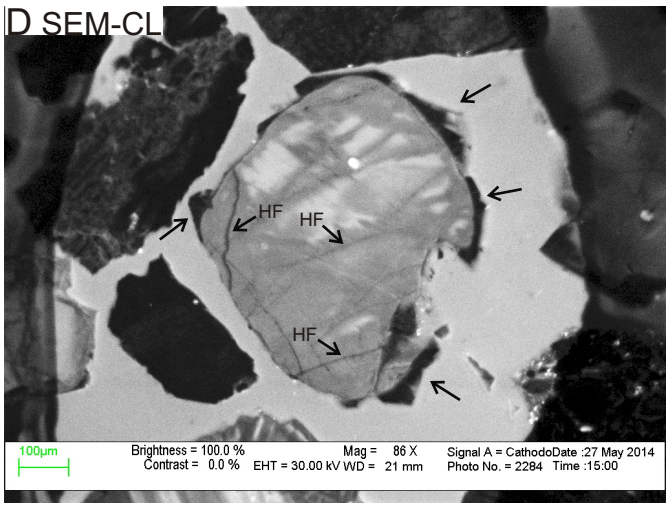

E EDS analyses

Pos#	Min. ID	SiO2	CaO	Na2O	P2O5	F	Cl	Ce2O3	Total	Actual total
1	Ap	1.39	46.75	0.5	44.06	6.17	0.34	0.8	100	64
2	Qz	99.99							100	70

Figure 2A-21: Microphotos under ppl (A) and xpl (B), SEM-BSE image (C), SEM-CL image (D), and EDS analyses table (E) of quartz grain 21 in sample 2860. The grain is anhedral and sub-rounded monocrystalline with non-undulose extinction. Fluid inclusions are common; they are usually associated with secondary porosity and form trails along healed fractures and at the boundary between the detrital quartz grain and the overgrowth (Fig. A). The grain contains apatite inclusions and is microfractured with a set of parallel fractures and a set of irregular fractures (Fig. C and D). Some healed fractures (HF) can be seen in Fig. D. The dark areas indicated by arrows in Fig. D are overgrowth. The grain shows bright-CL streaky patches fabric in SEM-CL image.

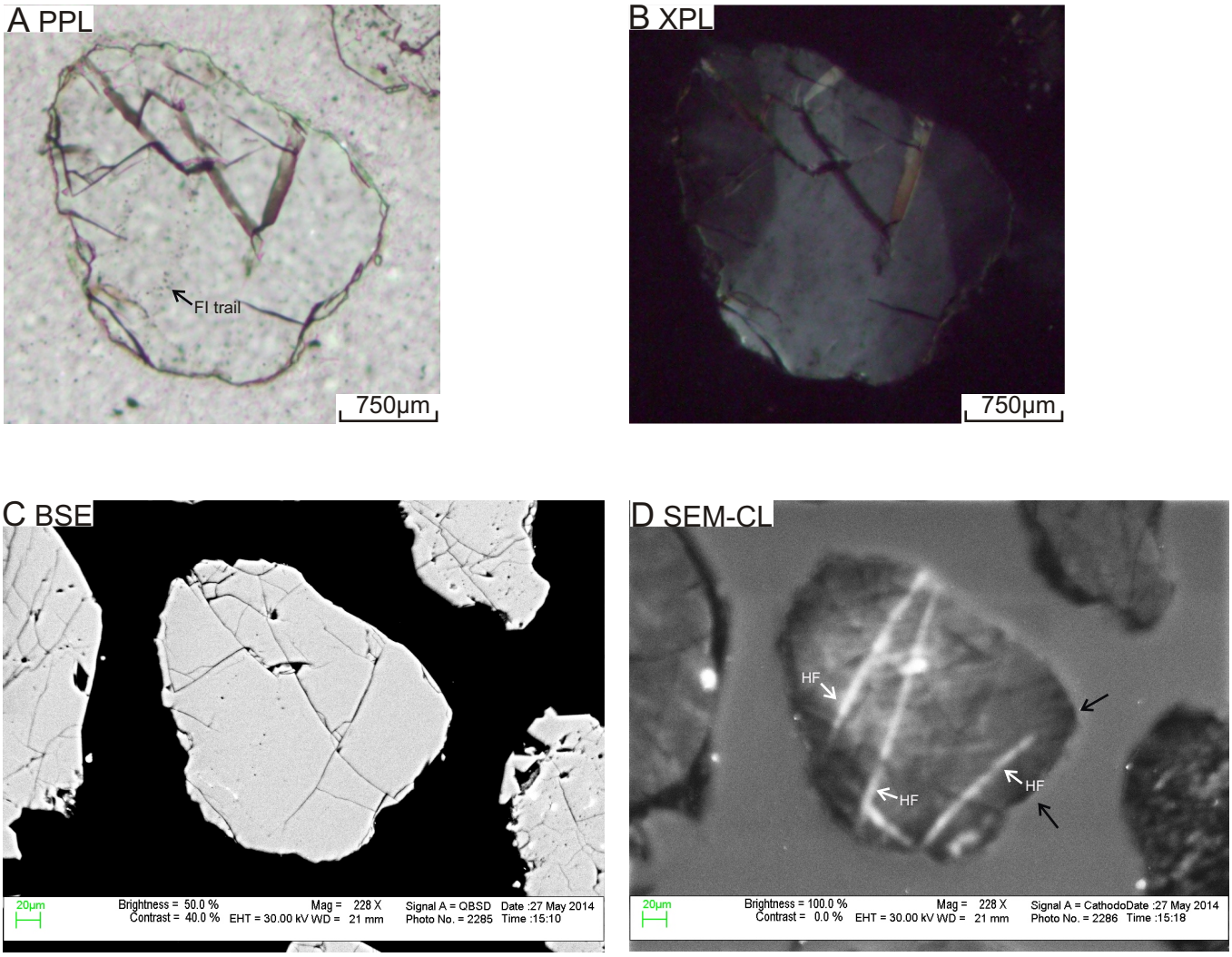

Figure 2A-22: Microphotos under ppl (A) and xpl (B), SEM-BSE image C, and SEM-CL image (D) of quartz grain 22 in sample 2860. The grain is anhedral and rounded monocrystalline with strong undulose extinction. Fluid inclusions are present; they form trails along healed fractures (Fig. A). The grain is strongly microfractured with two sets of sub-parallel fractures crosscutting each other and a set of irregular fractures (Fig. C and D). Healed fractures (HF) (Fig. D). The dark areas indicated by arrows in Fig. D are overgrowth.

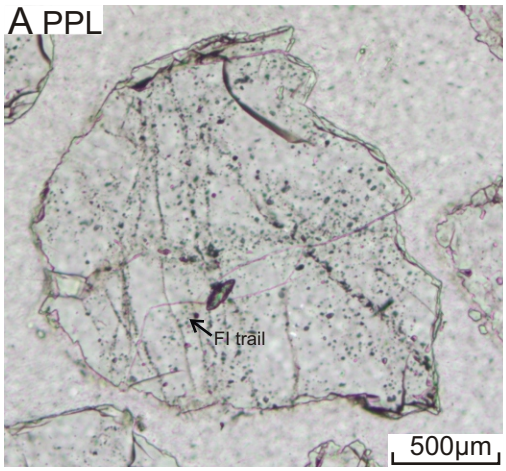

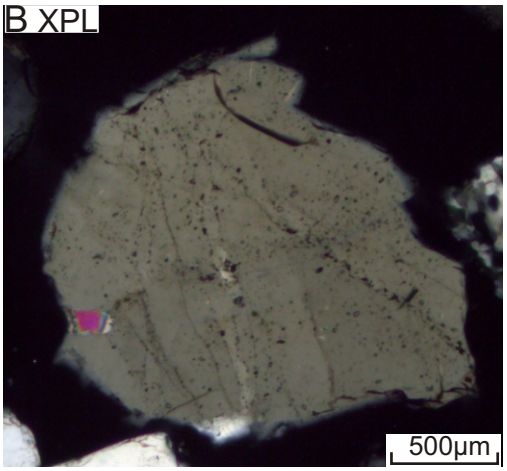

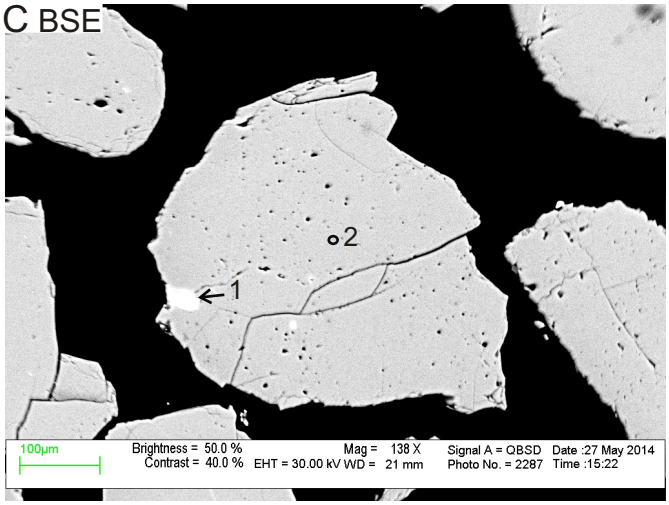

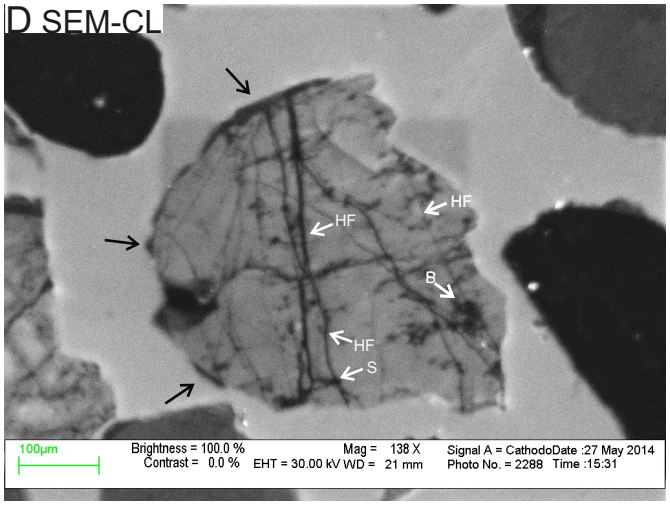

E EDS analyses

Pos#	Min. ID	SiO2	TiO2	Al2O3	FeO	Na2O	K2O	Total	Actual total
1	Ms	47.62	0.57	33.46	2.57	0.44	10.34	95	60
2	Qz	99.99						100	69

Figure 2A-23: Microphotos under ppl (A) and xpl (B), SEM-BSE image (C), SEM-CL image (D), and EDS analyses table (E) of quartz grain 23 in sample 2860. The grain is anhedral and sub-angular monocrystalline with weak undulose extinction. Fluid inclusions are common; they are usually associated with secondary porosity and form trails along healed fractures (Fig. A). The grain contains muscovite inclusions and is strongly microfractured with a set of sub-parallel fractures and a set of irregular fractures (Fig. C and D). Healed fractures (HF) and spiders (S) are common (Fig. D). The dark areas indicated by arrows in Fig. D are overgrowth.

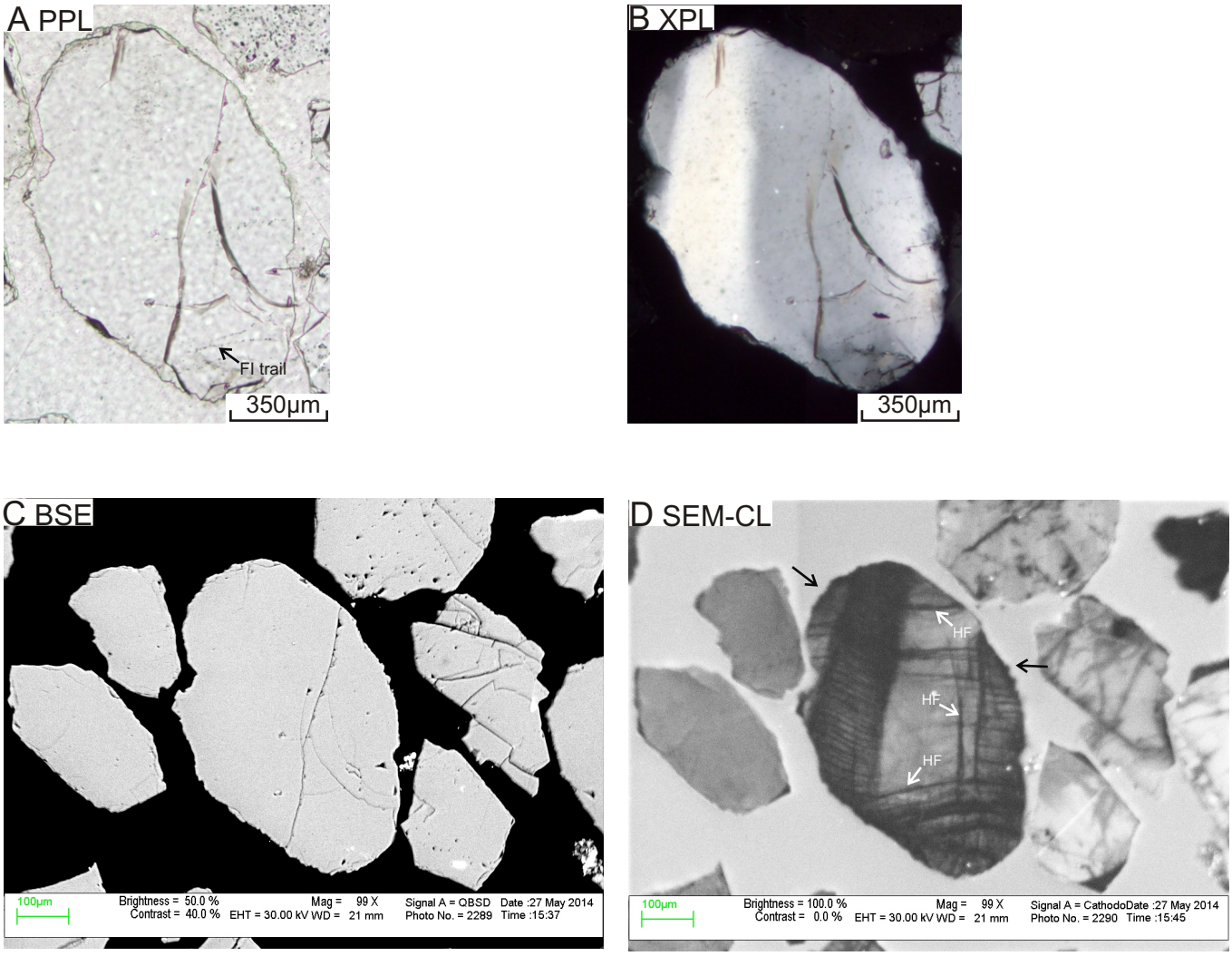

Figure 2A-24: Microphotos under ppl (A) and xpl (B), SEM-BSE image C, and SEM-CL image (D) of quartz grain 24 in sample 2860. The grain is subhedral and rounded monocrystalline with strong undulose extinction. Fluid inclusions are present; they form trails along healed fractures (Fig. A). The grain is microfractured with a set of parallel fractures and a set of irregular fractures (Fig. C and D). Healed fractures (HF) are common (Fig. D). The dark areas indicated by arrows in Fig. D are overgrowth. The grain shows a complex pattern of zoning with non-concentric bands in SEM-CL image, this pattern appears to be deformation lamellae.

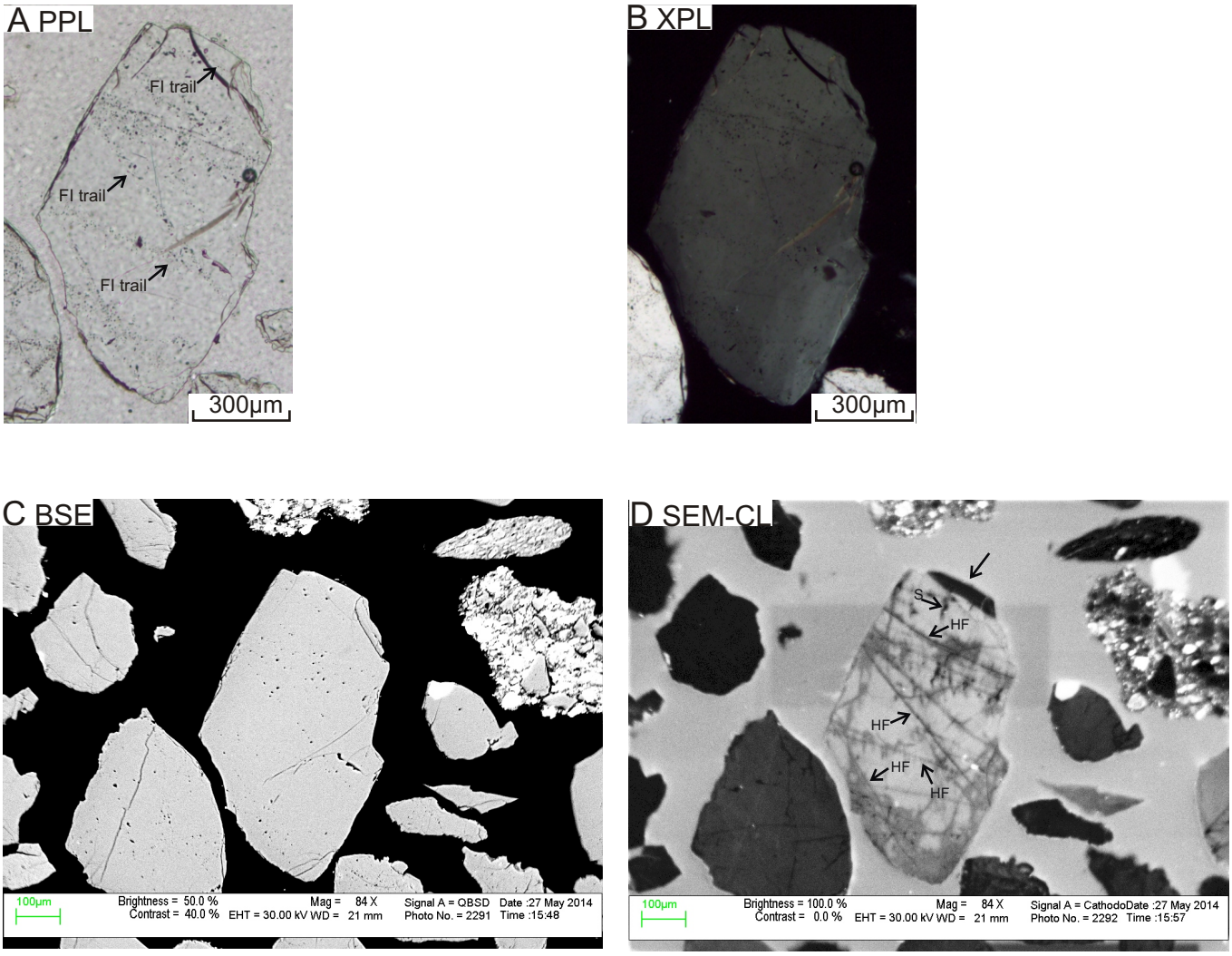

Figure 2A-25: Microphotos under ppl (A) and xpl (B), SEM-BSE image C, and SEM-CL image (D) of quartz grain 25 in sample 2860. The grain is anhedral and sub-angular monocrystalline with strong undulose extinction. Fluid inclusions are common; they are usually associated with secondary porosity and form trails along healed fractures and at the boundary between the detrital quartz and the overgrowth (Fig. A). The grain is strongly microfractured with two sets of parallel fractures crosscutting each other (Fig. C and D). Healed fractures (HF) and spiders (S) are common (Fig. D). The dark areas indicated by arrows in Fig. D are overgrowth. The grain shows random bright-CL patches in SEM-CL image.

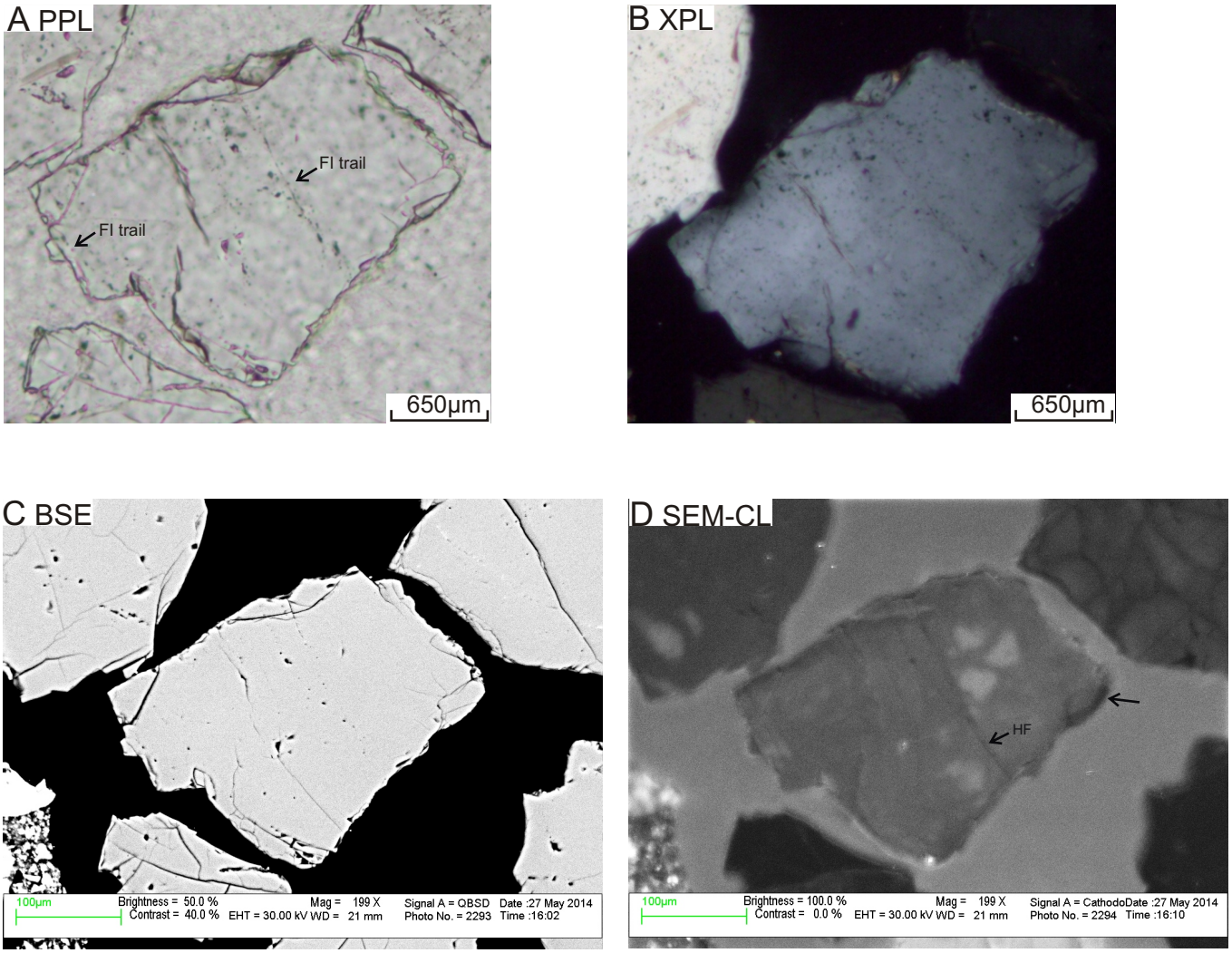

Figure 2A-26: Microphotos under ppl (A) and xpl (B), SEM-BSE image C, and SEM-CL image (D) of quartz grain 26 in sample 2860. The grain is anhedral and sub-angular monocrystalline with strong undulose extinction. Fluid inclusions are present; they form trails along healed fractures (Fig. A). The grain is microfractured with a set of irregular fractures (Fig. C and D). A few healed fractures (HF) can be seen in Fig. D. The dark area indicated by arrow in Fig. D is overgrowth. The grain shows subtle mottling in SEM-CL image.

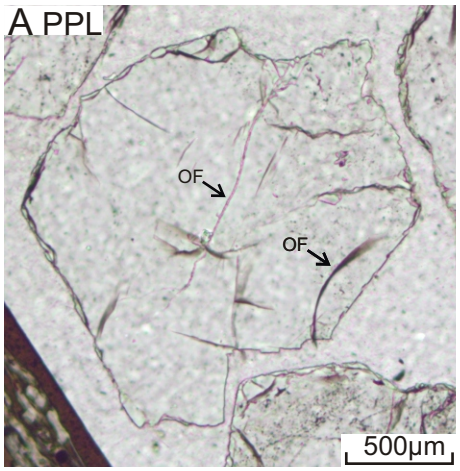

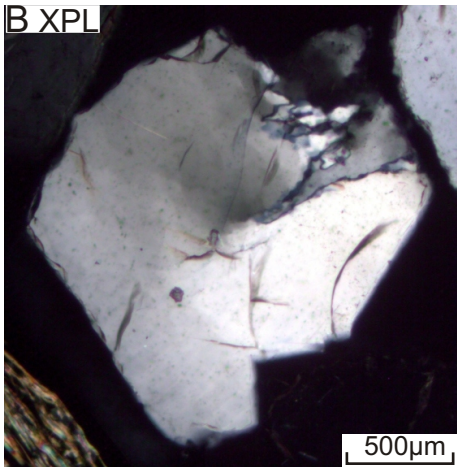

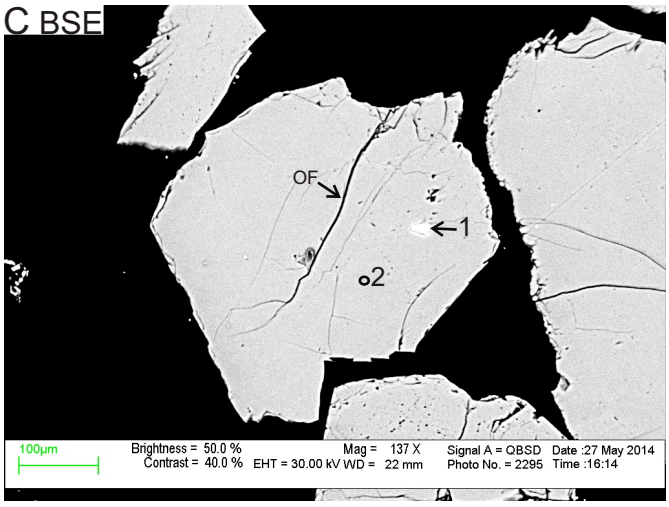

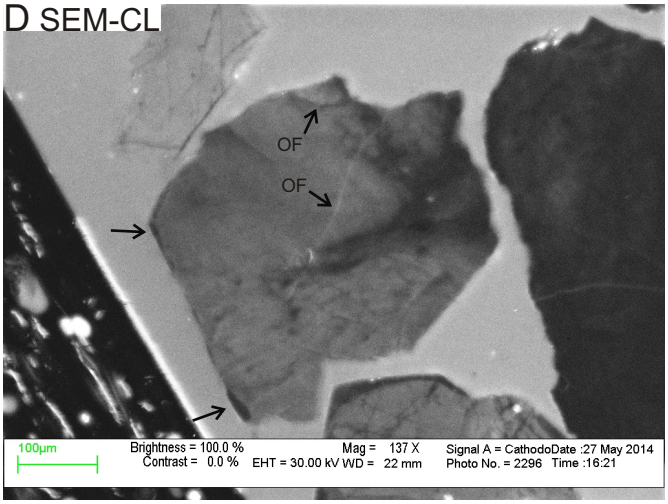

E EDS analyses

Pos#	Min. ID	SiO2	TiO2	Al2O3	FeO	MgO	Na2O	K2O	Total	Actual total
1	Ilt	46.25	0.86	26.99	4.10	1.22	0.55	10.04	90	59
2	Qz	99.99							100	66

Figure 2A-27: Microphotos under ppl (A) and xpl (B), SEM-BSE image (C), SEM-CL image (D), and EDS analyses table (E) of quartz grain 27 in sample 2860. The grain is anhedral and angular polycrystalline (more than 8 sub-grains with sutured sub-grain boundaries) with mosaic texture and strong undulose extinction. Fluid inclusions are not common. The grain contains illite inclusion and is microfractured with a set of irregular open fractures (Fig. C and D). Healed fractures are rare; the fractures that appear in Fig. D are open fractures. The dark areas indicated by arrows in Fig. D are overgrowth.

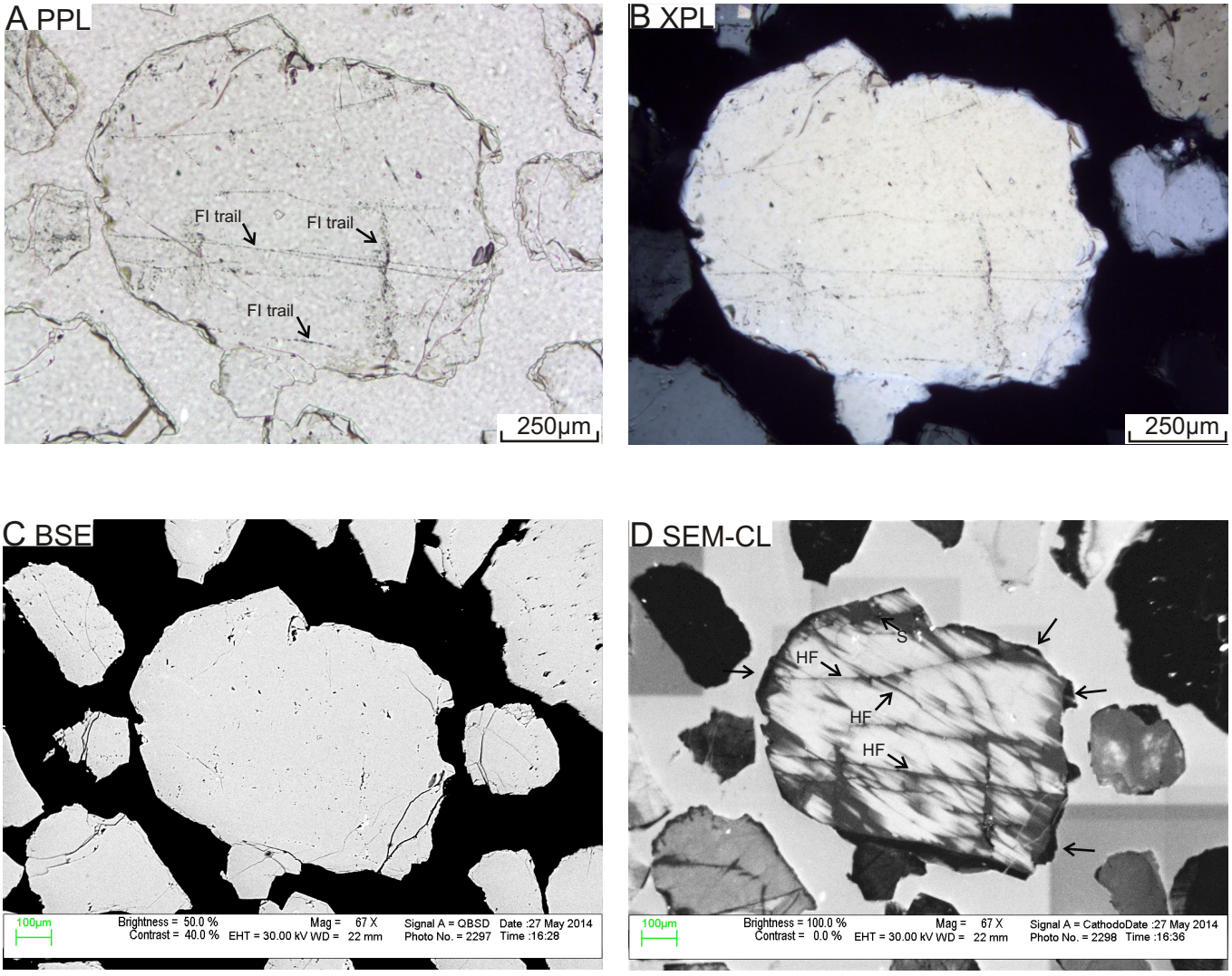

Figure 2A-28: Microphotos under ppl (A) and xpl (B), SEM-BSE image C, and SEM-CL image (D) of quartz grain 28 in sample 2860. The grain is anhedral and sub-angular polycrystalline (only 2 sub-grains) with weak undulose extinction. Fluid inclusions are common; they are usually associated with secondary porosity and form trails along healed fractures and at the boundaries between the detrital quartz and the overgrowth (Fig. A). The grain is microfractured with two sets of parallel fractures crosscutting each other (Fig. D). Healed fractures (HF) are common, and a few spiders (S) are present (Fig. D). The dark areas indicated by arrows in Fig. D are overgrowth. The grain shows bright-Cl streaky patches in SEM-CL image.

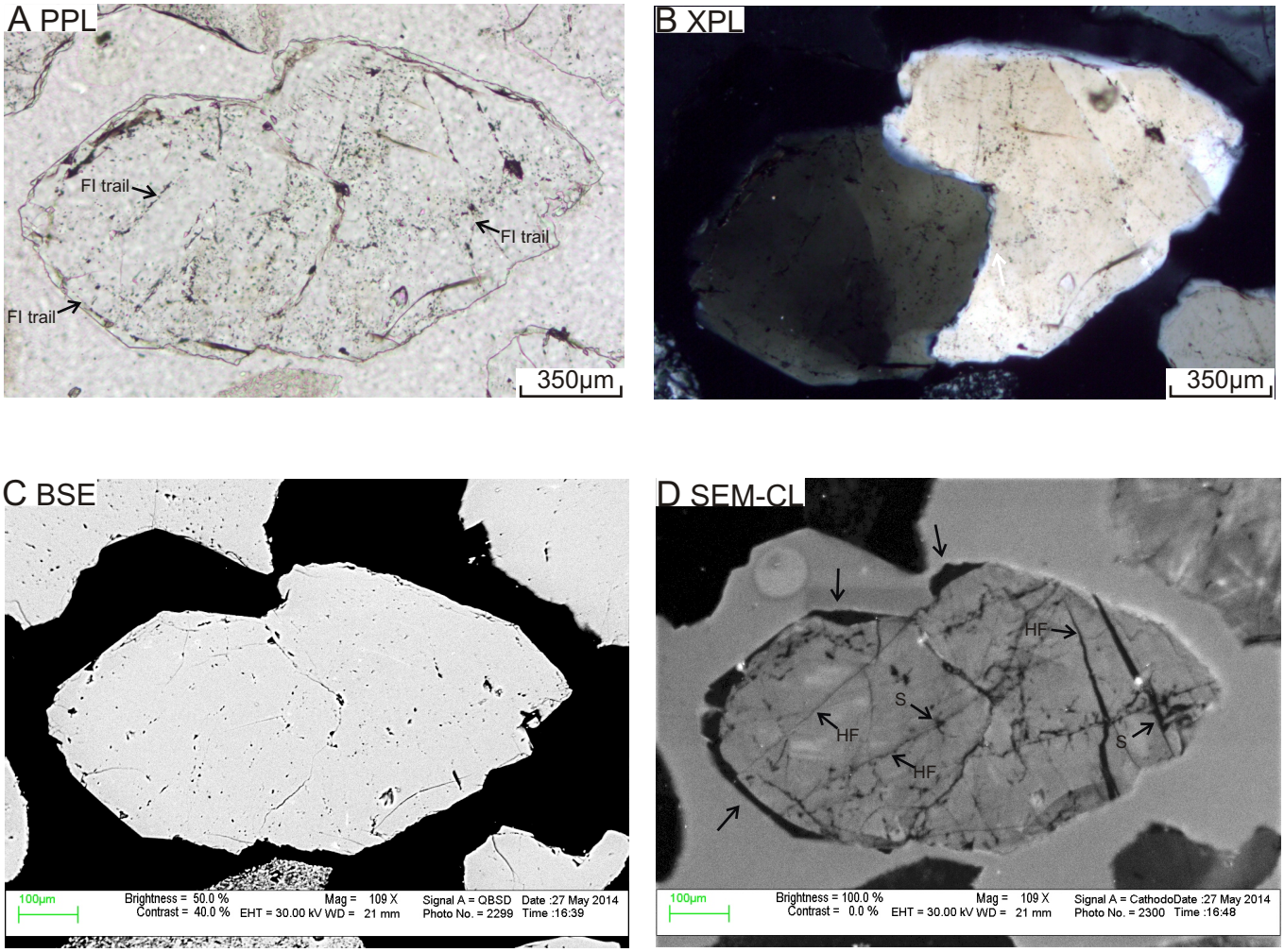

Figure 2A-29: Microphotos under ppl (A) and xpl (B), SEM-BSE image C, and SEM-CL image (D) of quartz grain 29 in sample 2860. The grain is anhedral and sub-rounded polycrystalline (only a few sub-grains with sutured sub-grain boundaries) with mosaic texture and strong undulose extinction. Fluid inclusions are common; they are usually associated with secondary porosity and form trails along healed fractures and at the boundaries between the detrital quartz grain and the overgrowth (Fig. A). The grain is microfractured with two sets of parallel fractures crosscutting each other (Fig. D). Healed fractures (HF) and spiders (S) are common (Fig. D). The dark areas indicated by arrows in Fig. D are overgrowth.

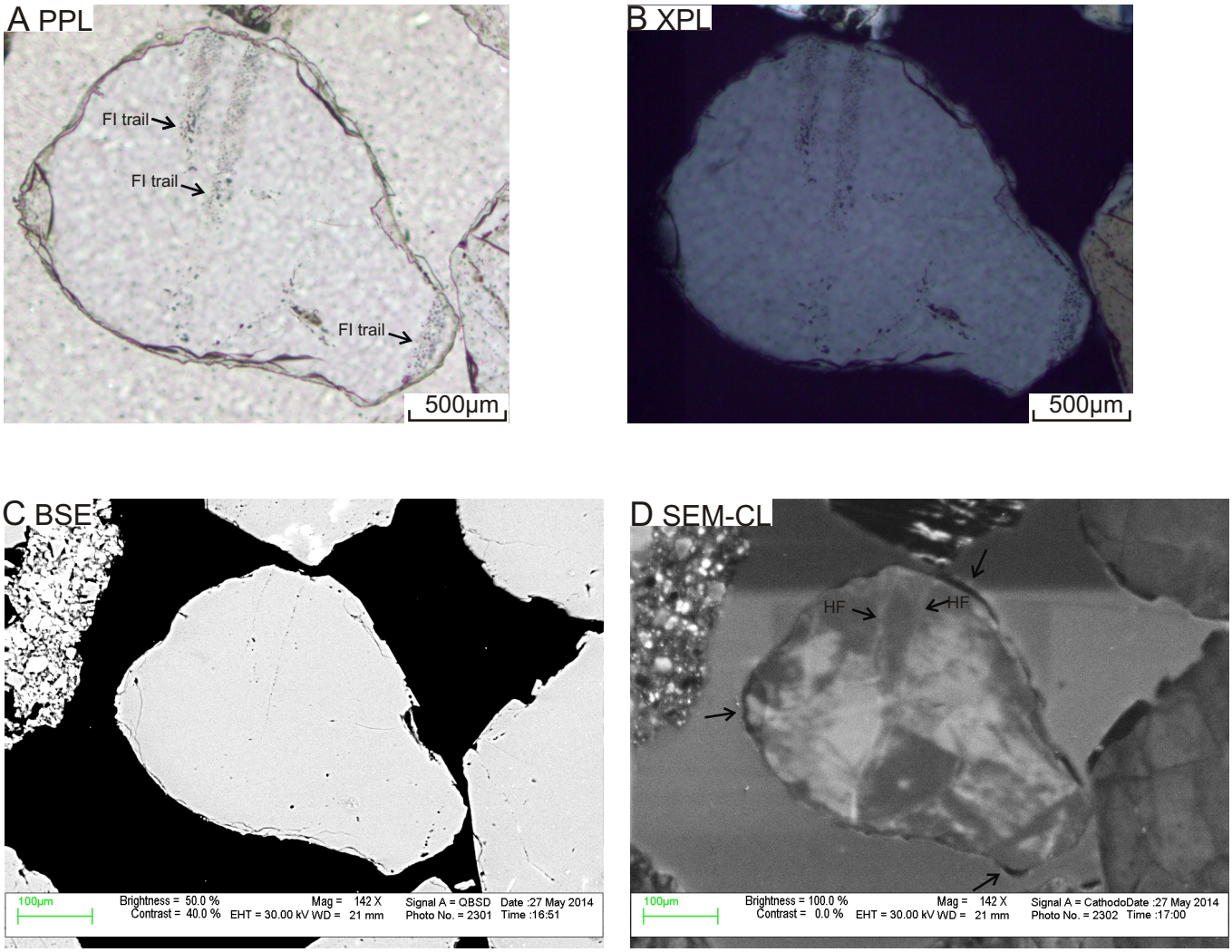

Figure 2A-30: Microphotos under ppl (A) and xpl (B), SEM-BSE image C, and SEM-CL image (D) of quartz grain 30 in sample 2860. The grain is anhedral and rounded monocrystalline with non-undulose extinction. Fluid inclusions are common; they are usually associated with secondary porosity and form trails along healed fractures (Fig. A). The grain is microfractured with a set of parallel fractures and a set of irregular fractures (Fig. C and D). A few parallel healed fractures (HF) can be seen in Fig. D. The dark areas indicated by arrows in Fig. D are overgrowth. The grain shows random bright-CL patches in SEM-CL image.

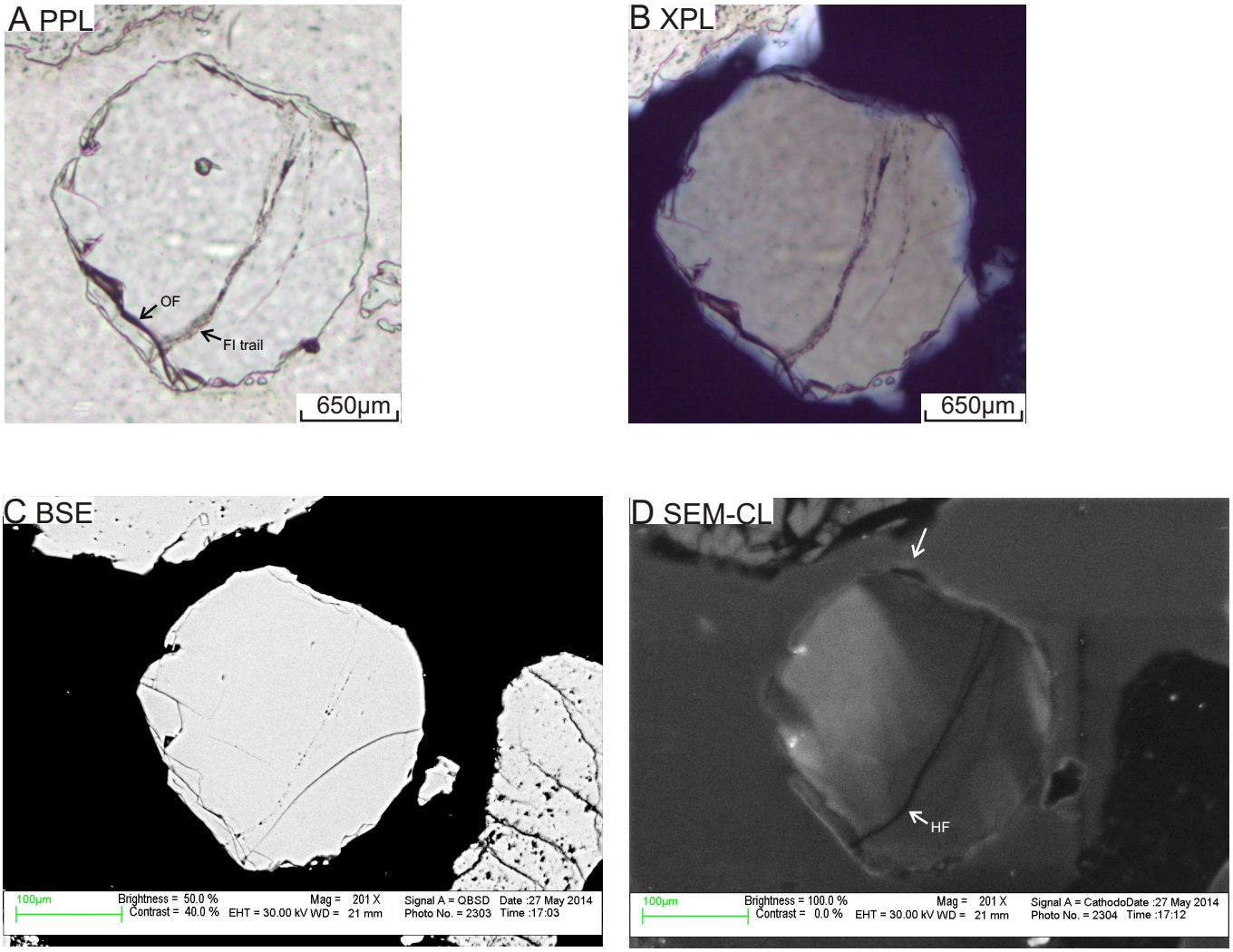

Figure 2A-31: Microphotos under ppl (A) and xpl (B), SEM-BSE image C, and SEM-CL image (D) of quartz grain 31 in sample 2860. The grain is anhedral and rounded monocrystalline with strong undulose extinction. Fluid inclusions are common; they form trails along healed fractures (Fig. A). The grain is microfractured with a set of irregular curved fractures (Fig. C and D). A few healed fractures (Fig. D) and open fractures (Fig. A) can be seen. The dark area indicated by arrow in Fig. D is overgrowth. The grain shows bright-CL streaky patches in SEM-CL image.

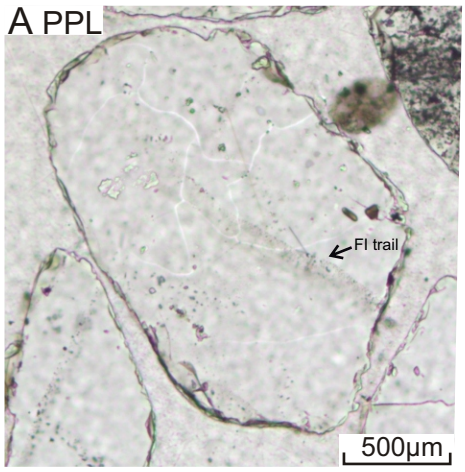

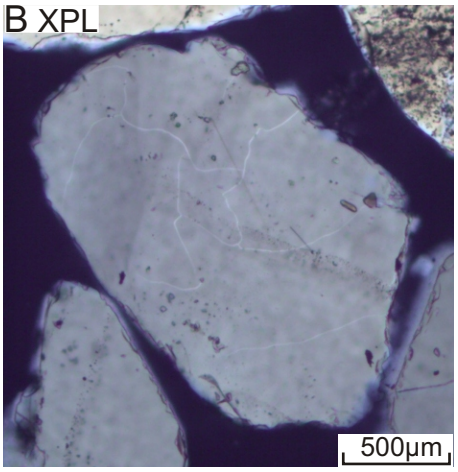

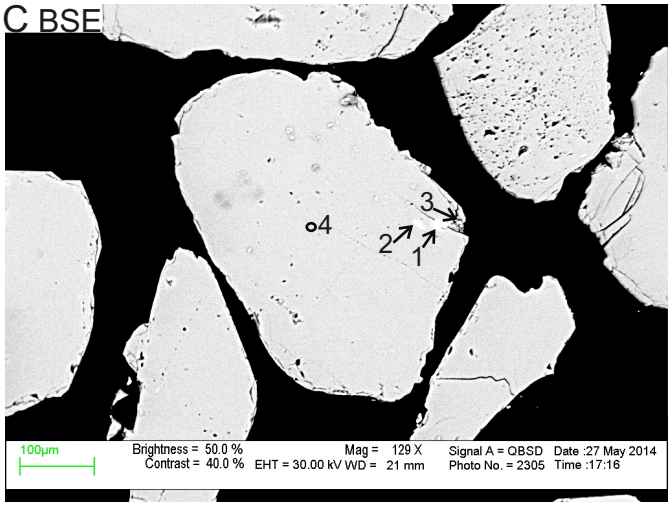

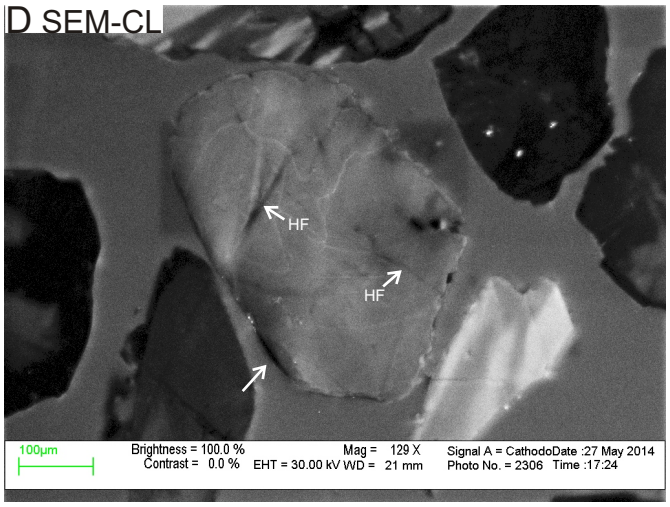

E EDS analyses

Pos#	Min. ID	SiO2	TiO2	Al2O3	FeO	MgO	Na2O	K2O	F	Cl	Total	Actual total
1	Bt	38.31	4.18	16.71	18.05	8.23	0.68	9.61		0.24	96	57
2	Bt	51.41	2.54	11.94	13.39	5.49	0.59	7.00	3.64		96	68
3	Kfs	77.01	0.7	6.84	5.34	3.88	0.44	3.13	2.65		100	65
4	Qz	99.99									100	66

Figure 2A-32: Microphotos under ppl (A) and xpl (B), SEM-BSE image (C), SEM-CL image (D), and EDS analyses table (E) of quartz grain 32 in sample 2860. The grain is anhedral and rounded polycrystalline (more than 5 sub-grains) with mosaic texture and weak undulose extinction. Fluid inclusions are common; they usually form trails along healed fractures (Fig. A). The grain contains fluid inclusion trails, biotite inclusions, k-feldspar inclusion, and is microfractured with a set of irregular fractures (Fig. C and D). A few healed fractures can be seen in Fig. D. The dark area indicated by arrow in Fig. D is overgrowth.

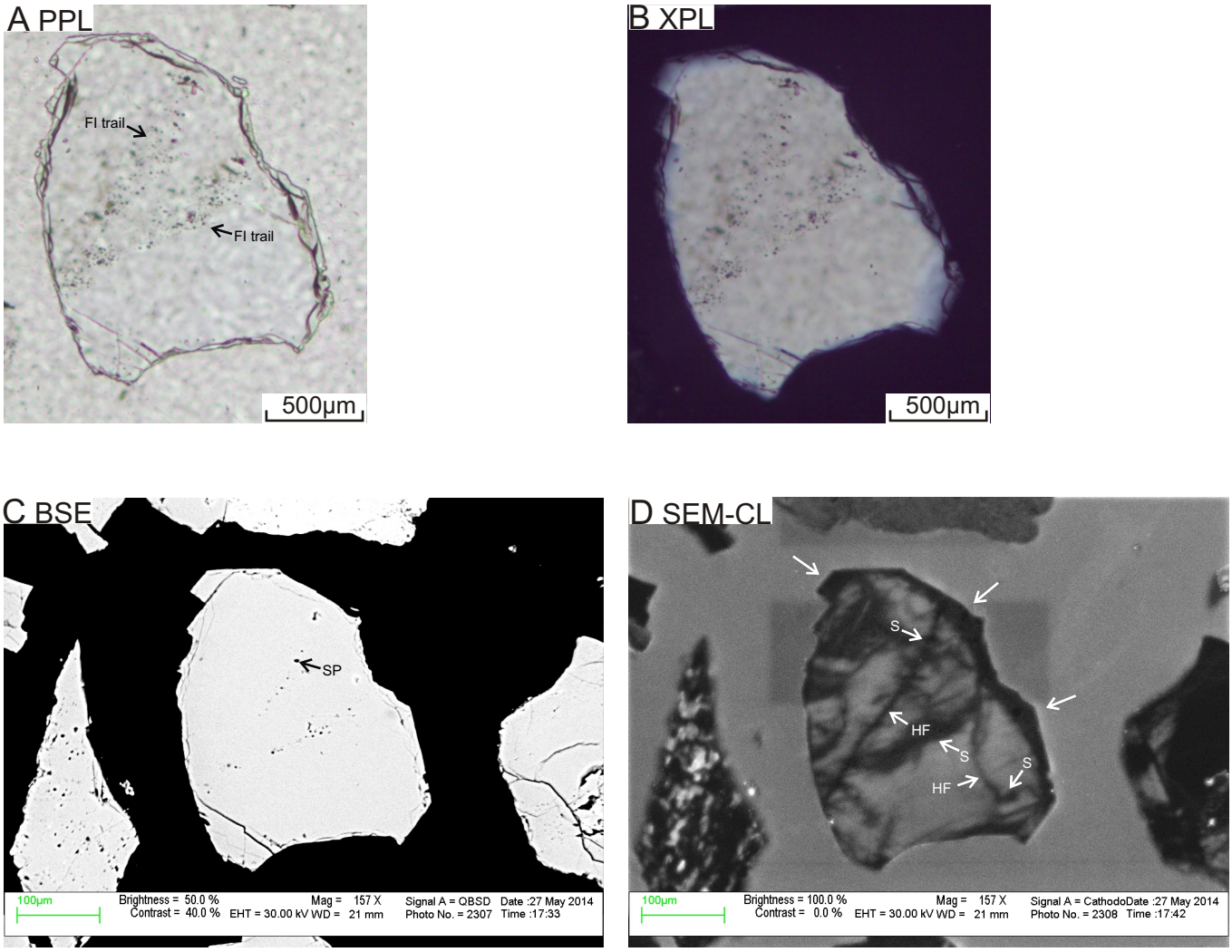

Figure 2A-33: Microphotos under ppl (A) and xpl (B), SEM-BSE image C, and SEM-CL image (D) of quartz grain 33 in sample 2860. The grain is anhedral and sub-rounded monocrystalline with non-undulose extinction. Fluid inclusions are common; they are usually associated with secondary porosity (SP) and form trails along healed fractures (Fig. A and C). The grain is microfractured with a set of irregular fractures (Fig. D). Healed fractures (HF) and spiders (S) are common (Fig. D). The dark areas indicated by arrows in Fig. D are overgrowth.

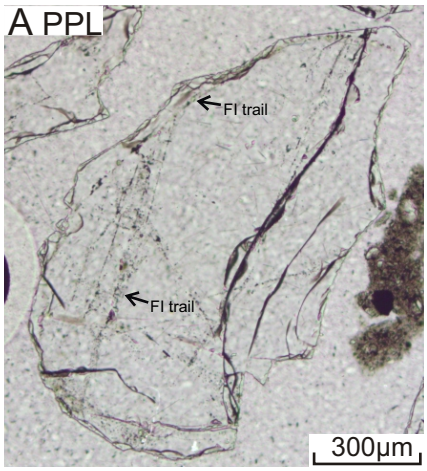

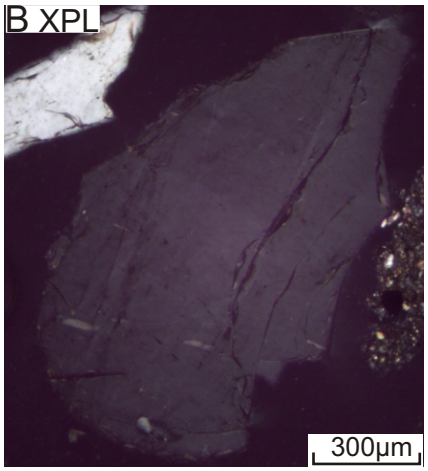

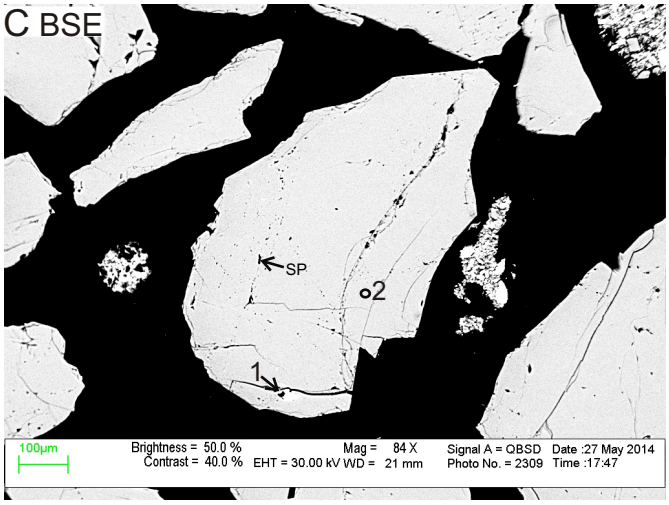

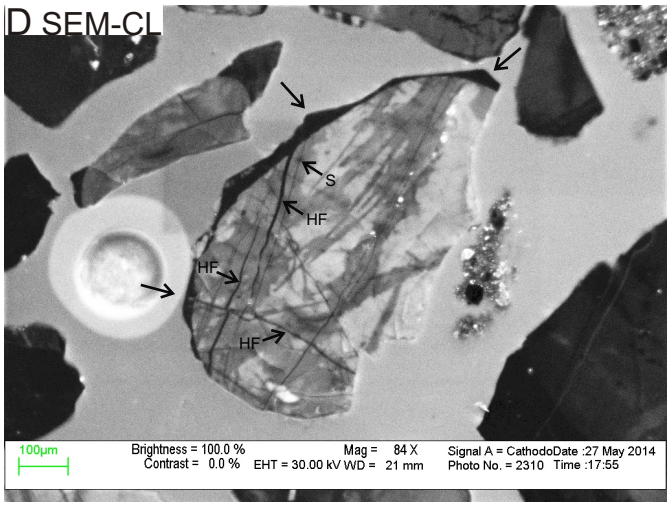

E EDS analyses

Pos#	Min. ID	SiO2	Al2O3	Na2O	K2O	F	Total	Actual total
1	Kfs	64.18	17.48	1.19	14.29	2.87	100	68
2	Qz	99.99					100	75

Figure 2A-34: Microphotos under ppl (A) and xpl (B), SEM-BSE image (C), SEM-CL image (D), and EDS analyses table (E) of quartz grain 34 in sample 2860. The grain is anhedral and sub-angular monocrystalline with weak undulose extinction. Fluid inclusions are common; they are usually associated with secondary porosity (SP) and form trails along healed fractures and at the boundaries between the detrital quartz grain and the overgrowth (Fig. A). The grain contains K-feldspar inclusions and is microfractured with two sets of parallel fractures crosscutting each other (Fig. D). Healed fractures (HF) are common and a few spiders (S) are present (Fig. D). The dark areas indicated by arrows in Fig. D are overgrowth. The grain shows random bright-CL patches in SEM-CL image.

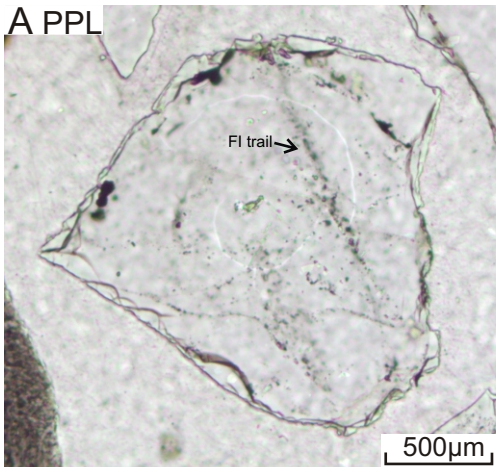

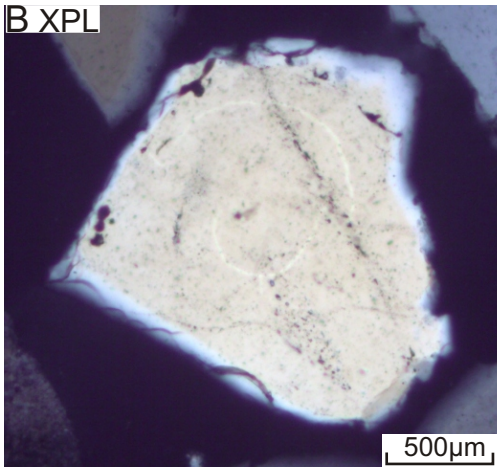

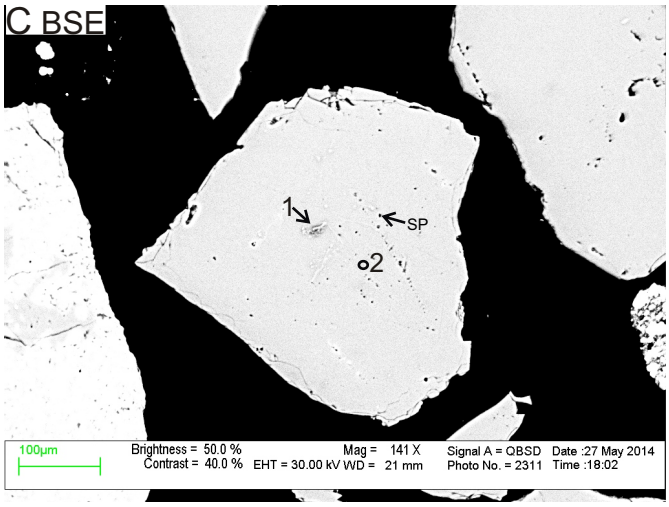

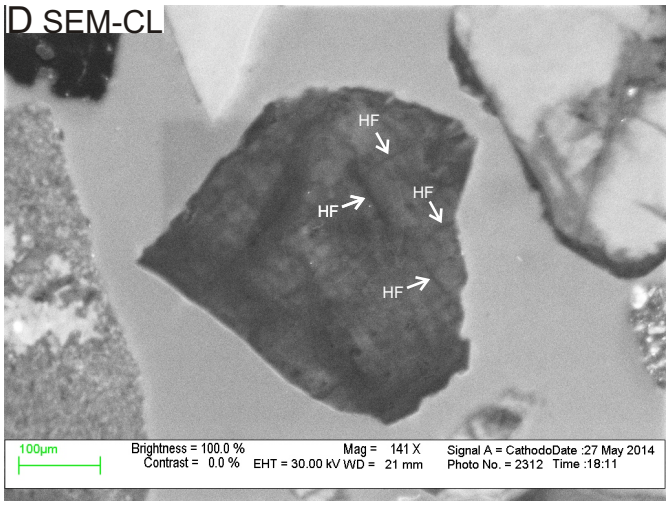

E EDS analyses

Pos#	Min. ID	SiO2	FeO	MgO	CaO	Na2O	K2O	SO3	F	Cl	Total	Actual total
1	Fluid inclusion	88.73	0.17	1.04	0.36	2.82	0.25	0.5	5.53	0.59	100	63
2	Qz	99.99									100	68

Figure 2A-35: Microphotos under ppl (A) and xpl (B), SEM-BSE image (C), SEM-CL image (D), and EDS analyses table (E) of quartz grain 35 in sample 2860. The grain is anhedral and sub-angular monocrystalline with mosaic texture and weak undulose extinction. Fluid inclusions are common; they are usually associated with secondary porosity (SP) and form trails along healed fractures (Fig. A and C). The grain is microfractured with two sets of parallel fractures crosscutting each other perpendicularly (Fig. C and D). A few healed fractures (HF) can be seen in Fig. D.

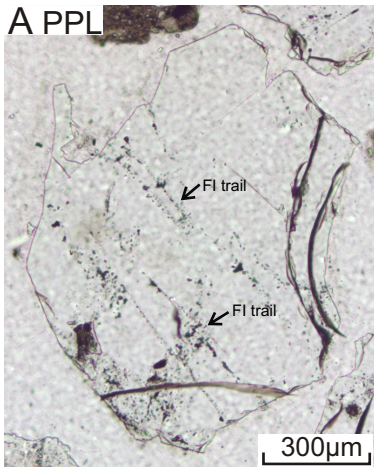

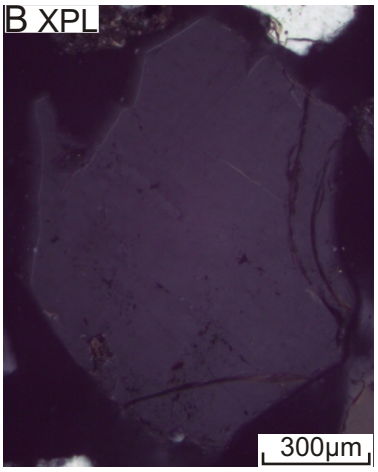

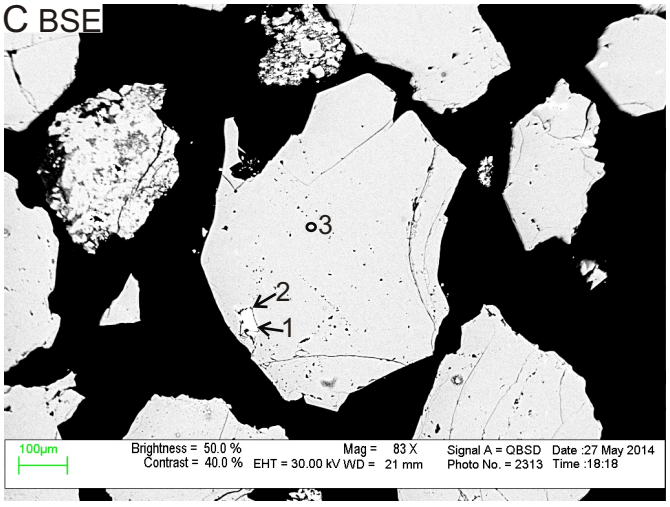

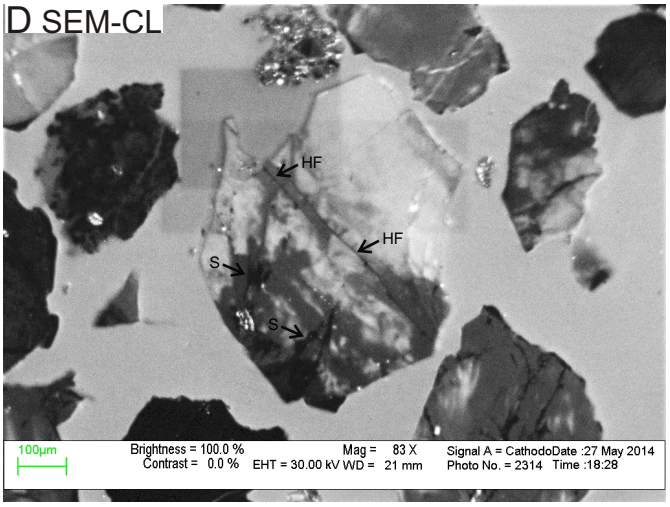

E EDS analyses

Pos#	Min. ID	SiO2	TiO2	Al2O3	FeO	MgO	CaO	Na2O	K2O	P2O5	SO3	F	Ce2O3	Nd2O3	Total	Actual total
1	Ms	44.59	0.24	30.95	1.67	0.67	1.41	0.55	8.28	2.81		1.76	1.50	0.58	95	71
2	Ms	45.60	0.43	30.88	1.67	0.76	2.40	0.48	8.13	1.94	1.16	1.55			95	76
3	Qz	99.99													100	70

Figure 2A-36: Microphotos under ppl (A) and xpl (B), SEM-BSE image (C), SEM-CL image (D), and EDS analyses table (E) of quartz grain 36 in sample 2860. The grain is anhedral and angular monocrystalline with non-undulose extinction. Fluid inclusions are common; they are usually associated with secondary porosity and form trails along healed fractures (Fig. A and C). The grain contains muscovite inclusions and is microfractured with a set of parallel fractures and a set of irregular curved fractures (Fig. C and D). Healed fractures (HF) and spiders (S) are common (Fig. D). The grain shows random bright-CL patches in SEM-CL image.

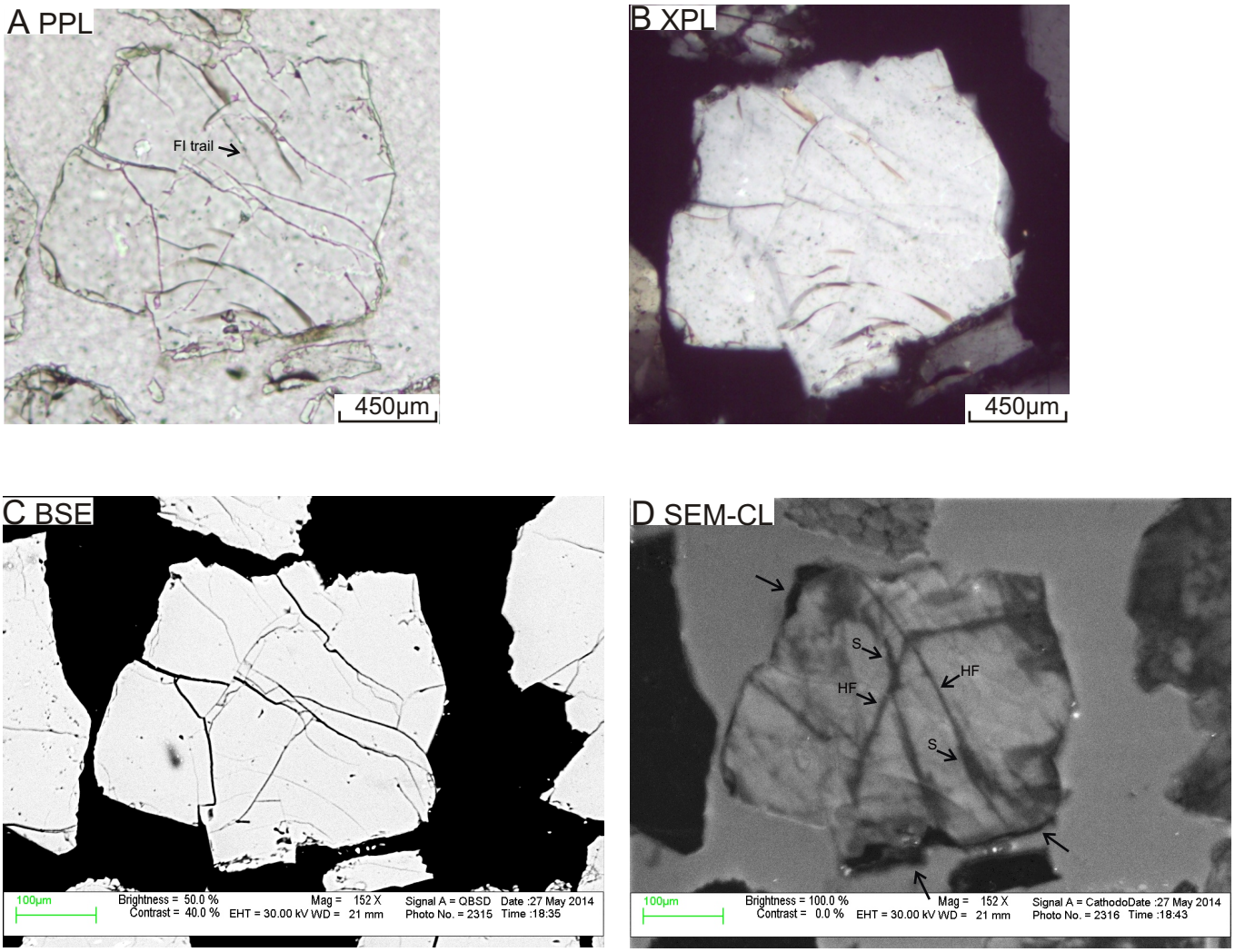

Figure 2A-37: Microphotos under ppl (A) and xpl (B), SEM-BSE image C, and SEM-CL image (D) of quartz grain 37 in sample 2860. The grain is anhedral and angular monocrystalline with weak undulose extinction. Fluid inclusions are present; they usually form trails along healed fractures (Fig. A). The grain is strongly microfractured with a set of sub-parallel fractures and a set of irregular curved open fractures (Fig. C and D). Healed fractures (HF) and spiders (S) are common (Fig. D). The dark areas indicated by arrows in Fig. D are overgrowth.

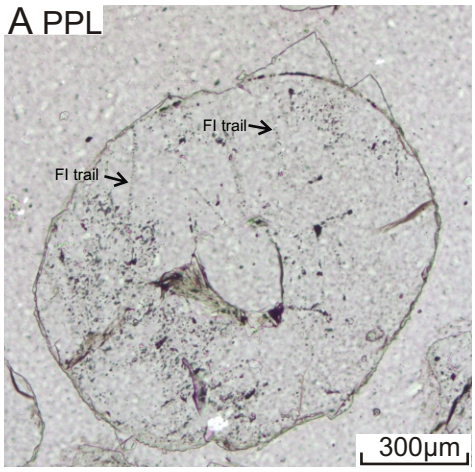

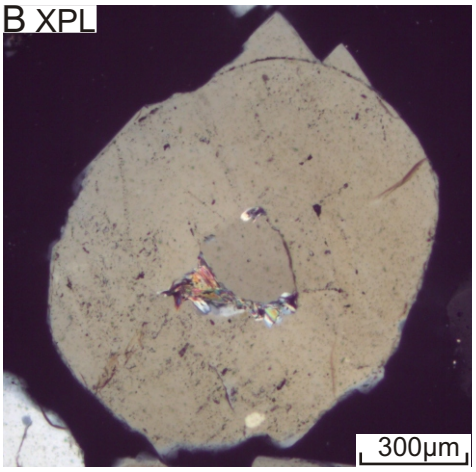

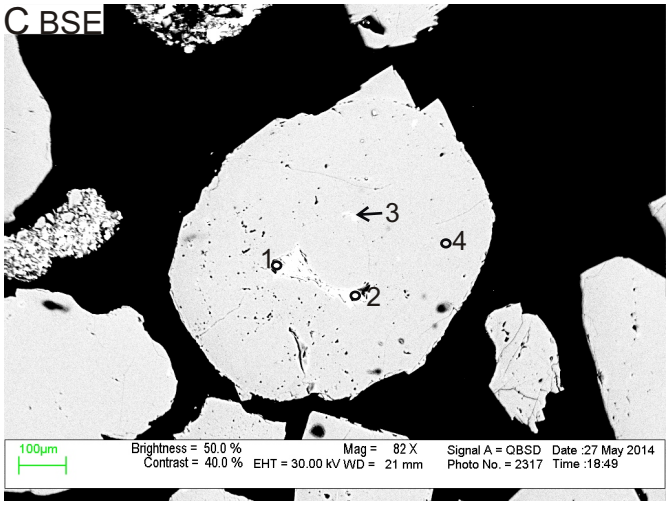

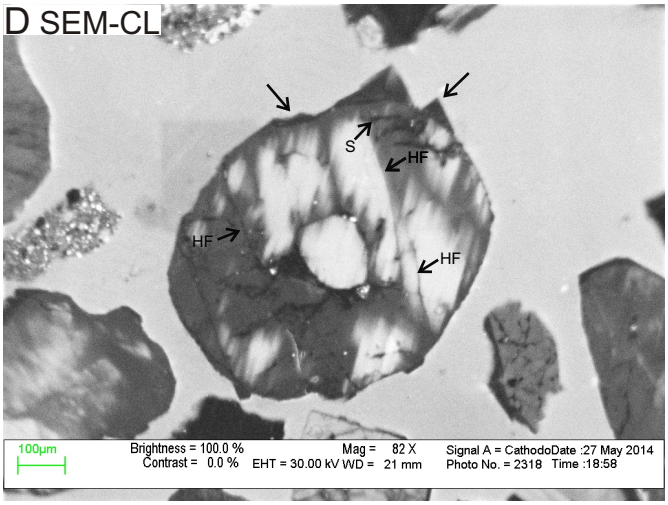

E EDS analyses

Pos#	Min. ID	SiO2	Al2O3	FeO	MgO	CaO	Na2O	K2O	P2O5	SO3	F	Cl	Total	Actual total
1	Ms	45.13	31.01	2.26	0.60		1.95	9.49			3.95	0.62	95	56
2	Ms	45.07	31.75	3.34	1.26		1.11	8.49			3.84	0.14	95	58
3	Ap+Ms	26.25	15.85	0.63		22.82	1.15	3.90	23.37	0.55	5.47		100	66
4	Qz	99.99											100	71

Figure 2A-38: Microphotos under ppl (A) and xpl (B), SEM-BSE image (C), SEM-CL image (D), and EDS analyses table (E) of quartz grain 38 in sample 2860. The grain is anhedral and rounded monocrystalline with non-undulose extinction. Fluid inclusions are present; they usually form trails along healed fractures (Fig. A). The grain contains muscovite inclusions, muscovite + apatite inclusion, and is microfractured with a set of parallel fractures and a set of irregular fractures (Fig. C and D). Healed fractures (HF) and spiders (S) are common (Fig. D). The dark areas indicated by arrows in Fig. D are overgrowth. The grain shows bright-CL streaky patches fabric in SEM-CL image.

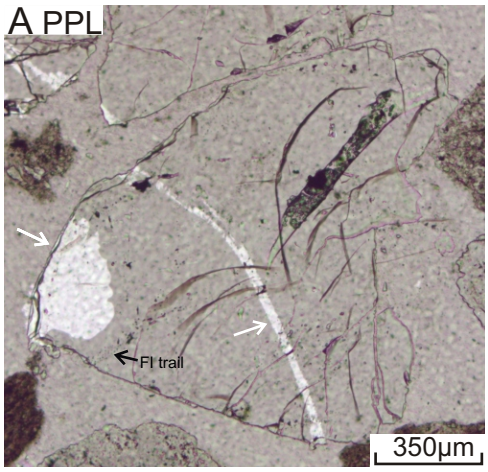

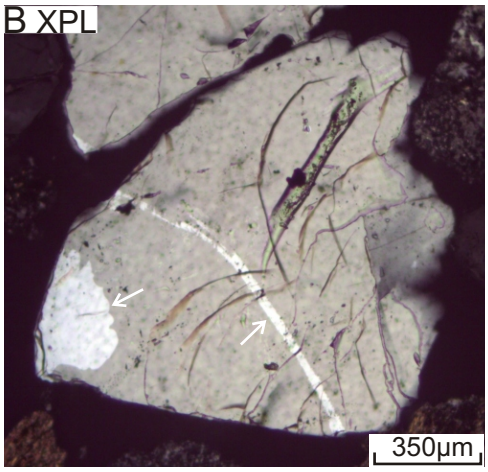

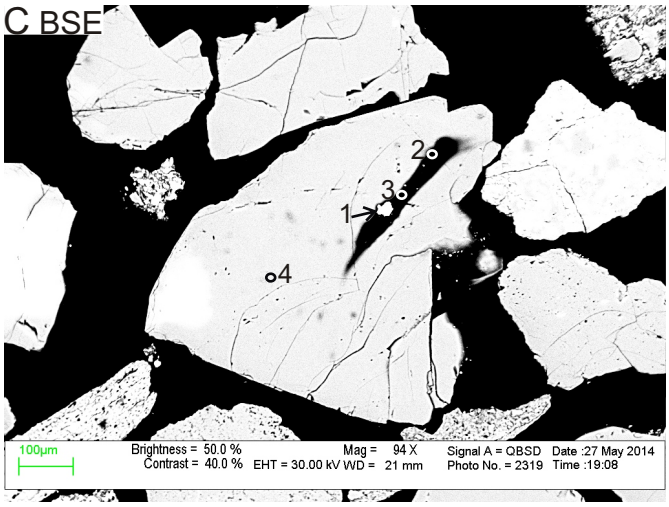

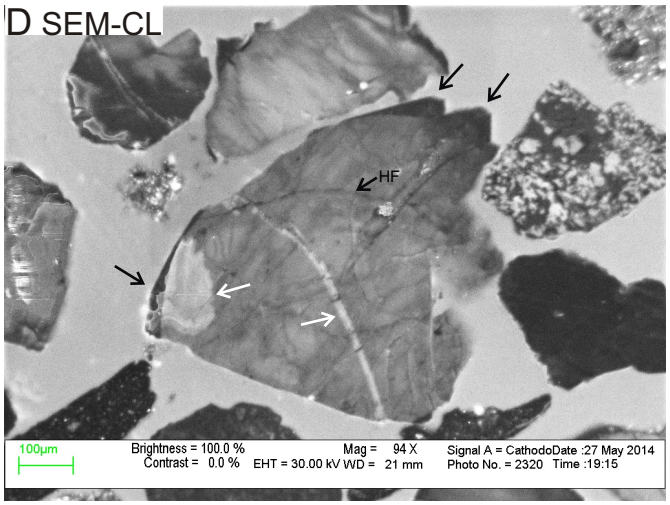

E EDS analyses

Pos#	Min. ID	SiO2	FeO	MnO	CaO	SO3	Cl	Cr2O3	NiO	CuO	ZnO	Total	Actual total
1	Chr	2.1	66.74	1.63				19.92	9.61			100	48
2	Anh+Qz	82.12			7.99	7.99	0.56			0.58	0.77	100	18
3	Anh+Qz	96.16	0.45			3.4						100	35
4	Qz	99.99										100	67

Figure 2A-39: Microphotos under ppl (A) and xpl (B), SEM-BSE image (C), SEM-CL image (D), and EDS analyses table (E) of quartz grain 39 in sample 2860. The grain is anhedral and sub-angular monocrystalline with weak undulose extinction. Fluid inclusion trails are present, they usually form trails along healed fractures and at the boundaries between the detrital quartz and the overgrowth (Fig. A). The grain contains chromite and anhydrite inclusions, and is microfractured with a set of irregular curved fractures (Fig. C and D). Most of the fractures in Fig. D are open fractures and only a few healed fractures can be seen. The dark areas indicated by black arrows in Fig. D are overgrowth. The zoning and the band that appear in Fig. A, B, and D (indicated by white arrows) is due the uneven carbon coating on the thin section.

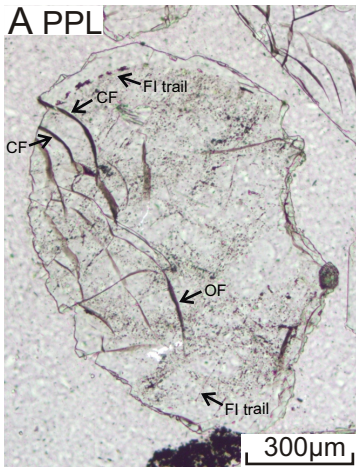

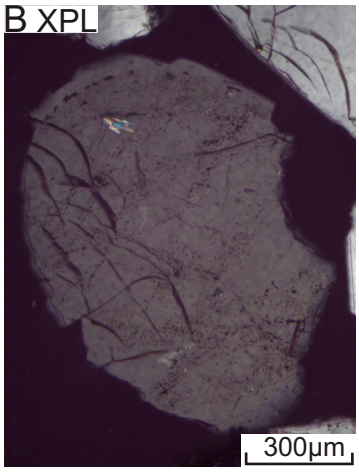

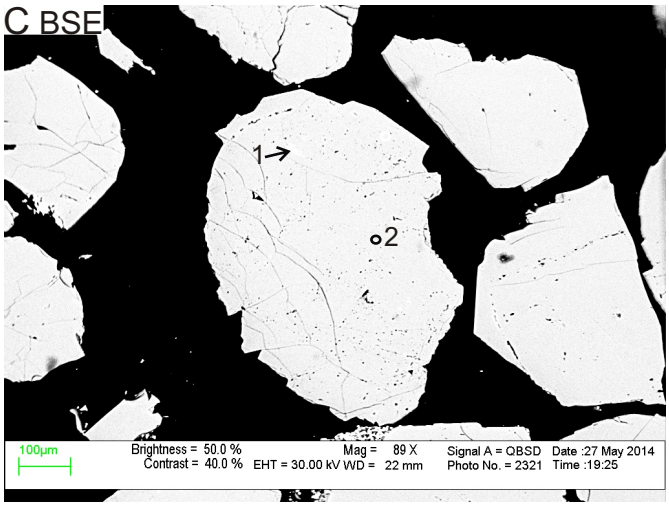

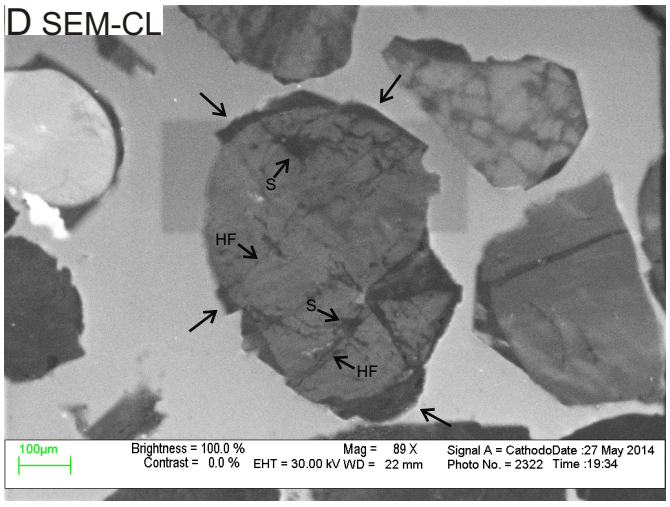

E EDS analyses

Pos#	Min. ID	SiO2	TiO2	Al2O3	FeO	Na2O	K2O	ZnO	Total	Actual total
1	Ms	49.59	0.19	33.37	1.10	0.47	9.96	0.32	95	62
2	Qz	99.99							100	70

Figure 2A-40: Microphotos under ppl (A) and xpl (B), SEM-BSE image (C), SEM-CL image (D), and EDS analyses table (E) of quartz grain 40 in sample 2860. The grain is anhedral and sub-rounded monocrystalline with non-undulose extinction. Fluid inclusions are common; they usually form trails along healed fractures and at the boundaries between the detrital quartz and the overgrowth (Fig. A). The grain contains muscovite inclusion and is microfractured with a set of parallel fractures, a set of irregular fractures, and a set of conchoidal fractures (Fig. C and D). Conchoidal fractures (CF) are indicated in Fig. A. Healed fractures (HF) and spiders (S) are common (Fig. D). The dark areas indicated by arrows in Fig. D are overgrowth.

Appendix 2B: Hot cathodoluminescence (HCL) images and blue colour shift analyses of detrital quartz grains in sample 2860.

Notes:

1. All the grains with HCL images correspond to the same grain in SEM-CL images. In all the following organized HCL figures,

   Fig. A shows HCL image taken after 3 seconds;

   Fig. B shows HCL image taken after 12 seconds;

   Fig. C is the histogram of blue colour within the analysed quartz grain in Fig. A and B, where X axis is the intensity of blue colour indicated by the colour bar with values from 0-255 (0=no blue or "black", 255=blue), and Y axis indicates the pixel amount at different blue values;

   Fig. D is the statistical table of blue values within the analysed grain area, where SD corresponds to standard deviation.

2. To classify the blue colour, the following abbreviations are used:

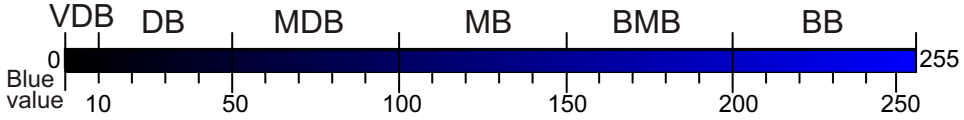

VDB: Very Dark Blue (0-10) **DB**: Dark Blue (11-50)

MDB: Medium Dark Blue (51-100) **MB**: Medium Blue (101-150)

BMB: Bright-Medium Blue (151-200) **BB**: Bright Blue (201-255)

3. To quantify the blue colour shift, the following criteria are used:

   Mean blue value change **< 5**: **No** colour shift

   5 ≤Mean blue value change **< 15**: **Slight** colour shift

   15 ≤Mean blue value change **< 30**: **Moderate** colour shift

   Mean blue value change ≥**30**: **Strong** colour shift

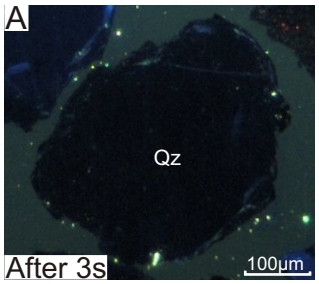

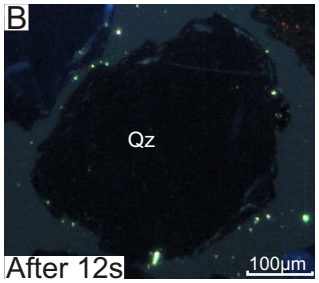

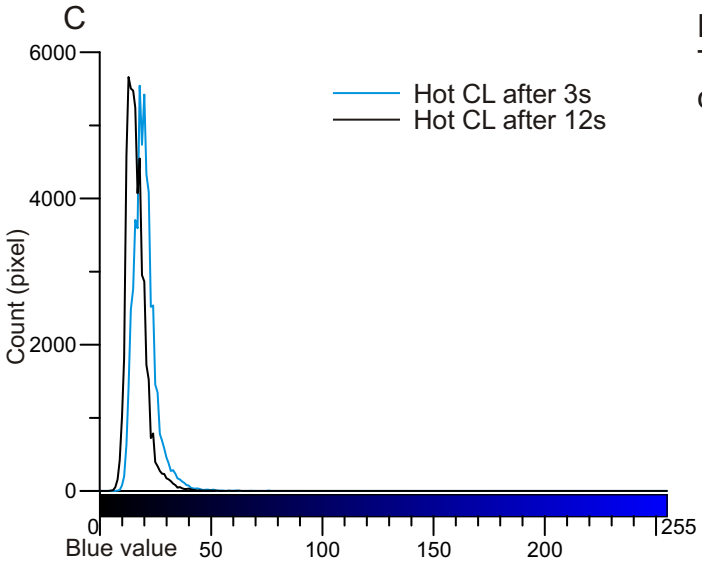

Figure 2B-1: Grain 1. The grain shows no colour shift.

D

Blue value	Min	Max	Mode	Mean	SD
After 3s	5	78	18	20	5.2
After 12s	3	74	13	16	4.6

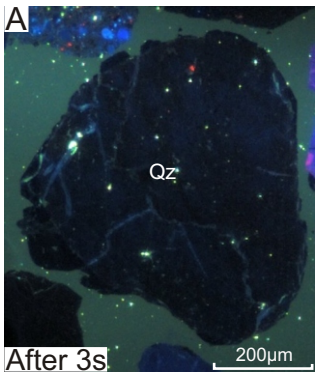

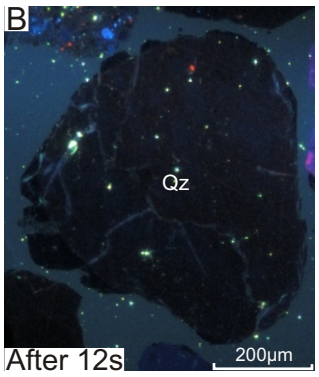

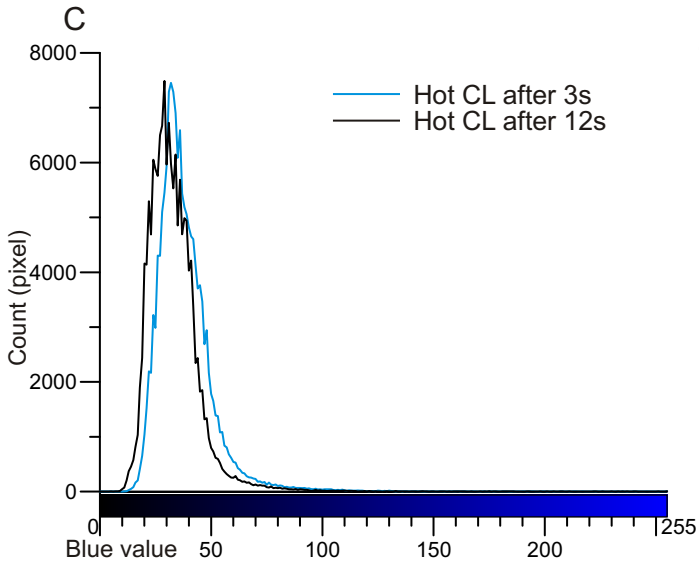

Figure 2B-2 : Grain 2. The grain shows slight colour shift.

D

Blue value	Min	Max	Mode	Mean	SD
After 3s	6	255	32	38	13.5
After 12s	5	255	29	33	12.4

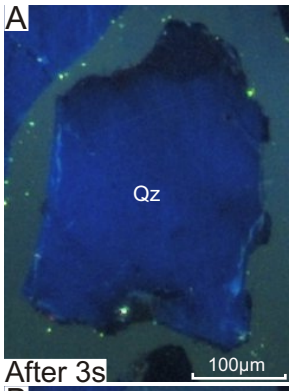

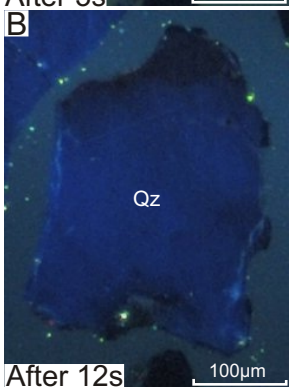

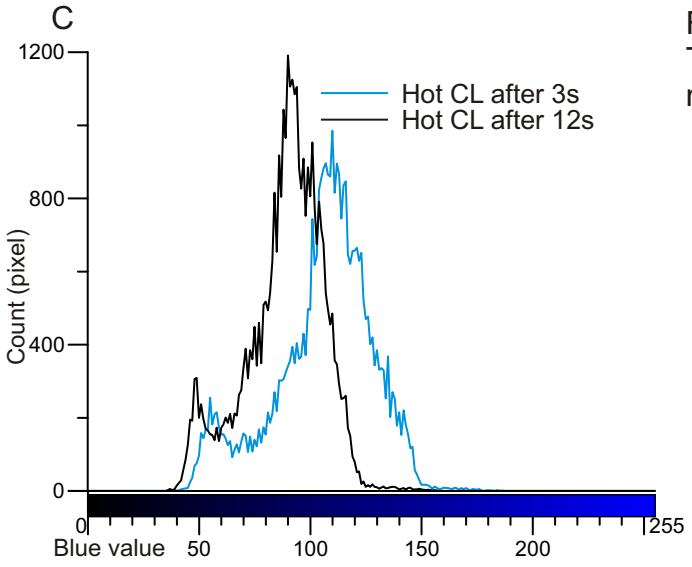

Figure 2B-3: Grain 3. The grain shows moderate colour shift.

D

Blue value	Min	Max	Mode	Mean	SD
After 3s	39	186	110	106	22.2
After 12s	36	157	90	89	17.5

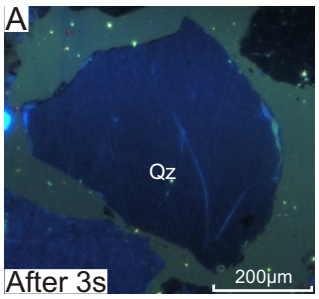

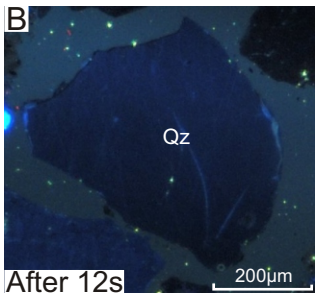

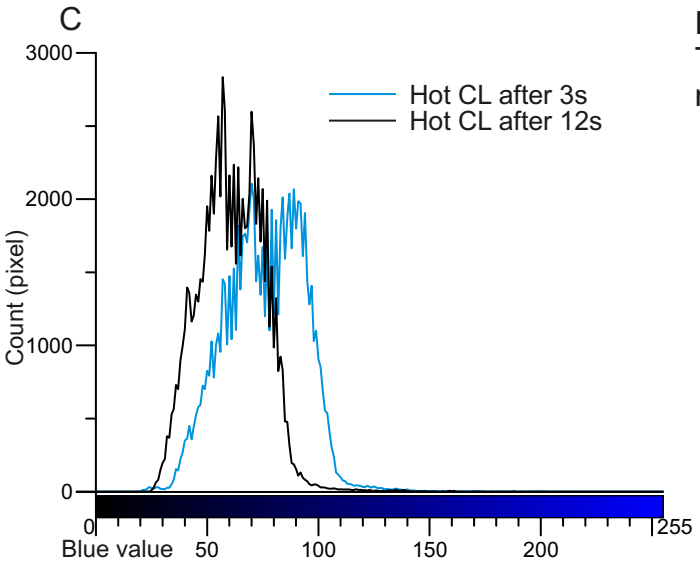

Figure 2B-4 : Grain 4. The grain shows moderate colour shift.

D

Blue value	Min	Max	Mode	Mean	SD
After 3s	19	216	70	76	17.6
After 12s	23	201	57	61	14.5

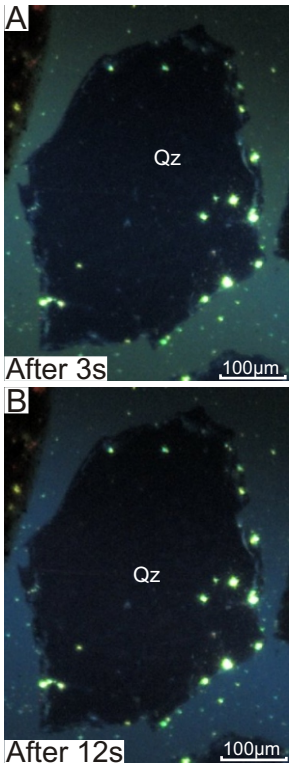

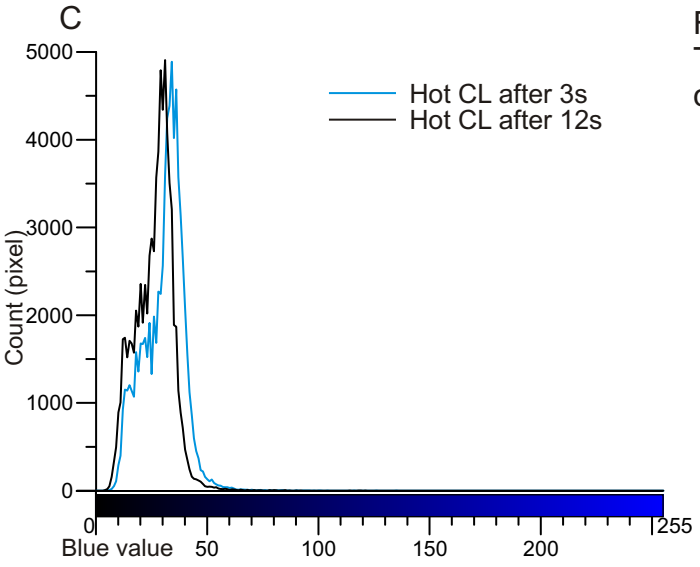

Figure 2B-5: Grain 5. The grain shows slight colour shift.

D

Blue value	Min	Max	Mode	Mean	SD
After 3s	4	165	34	31	9.2
After 12s	3	152	31	26	8.5

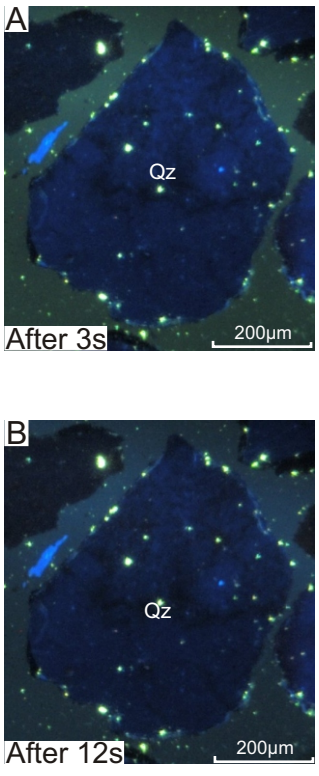

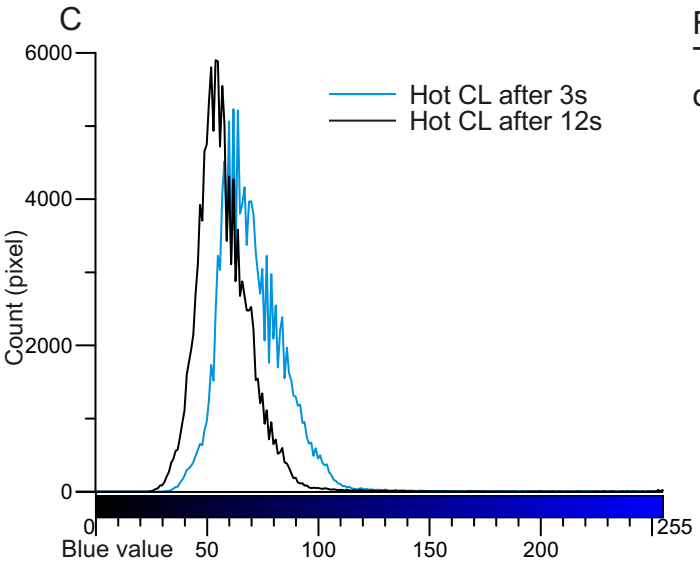

Figure 2B-6: Grain 6. The grain shows slight colour shift.

D

Blue value	Min	Max	Mode	Mean	SD
After 3s	28	255	62	70	16
After 12s	24	255	54	58	14.1

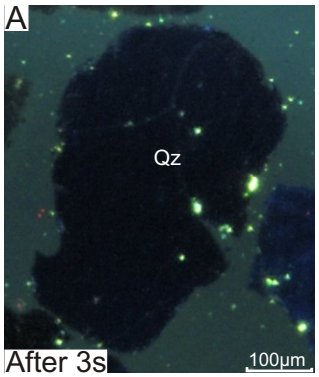

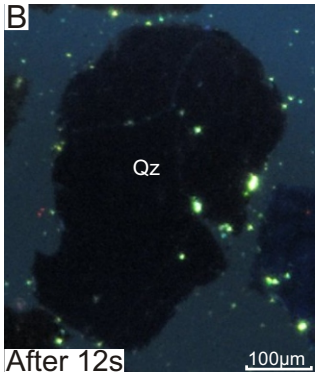

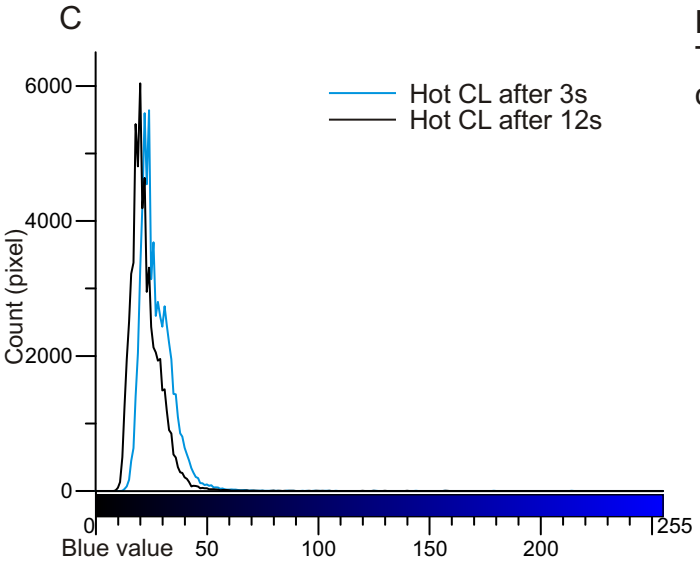

Figure 2B-7: Grain 7. The grain shows no colour shift.

D

Blue value	Min	Max	Mode	Mean	SD
After 3s	11	244	24	27	8.2
After 12s	6	245	20	23	7.8

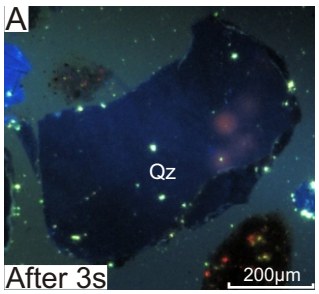

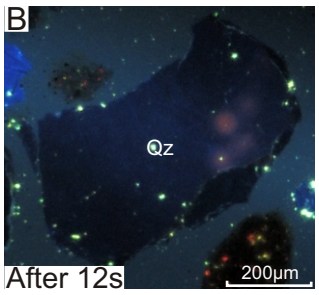

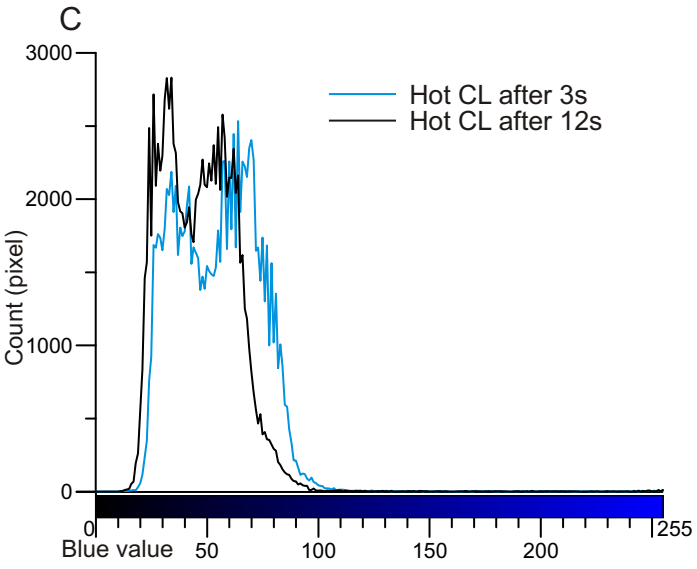

Figure 2B-8: Grain 8. The grain shows slight colour shift.

D

Blue value	Min	Max	Mode	Mean	SD
After 3s	11	255	64	55	19.1
After 12s	11	255	34	47	17.2

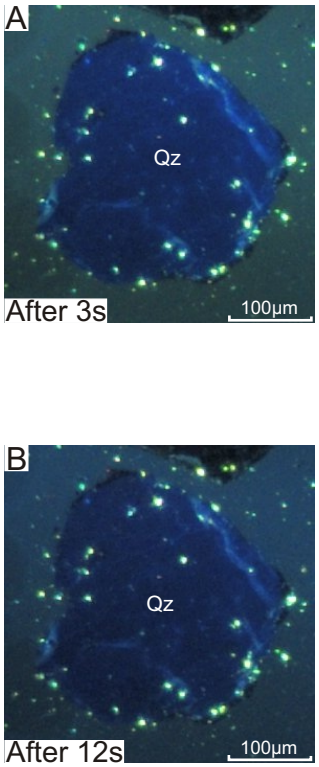

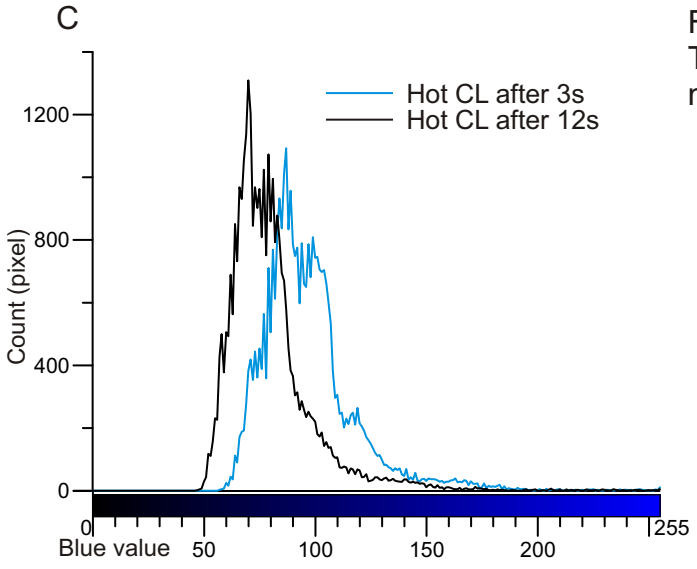

Figure 2B-9 : Grain 9. The grain shows moderate colour shift.

D

Blue value	Min	Max	Mode	Mean	SD
After 3s	57	255	87	97	21.6
After 12s	47	255	70	80	19.8

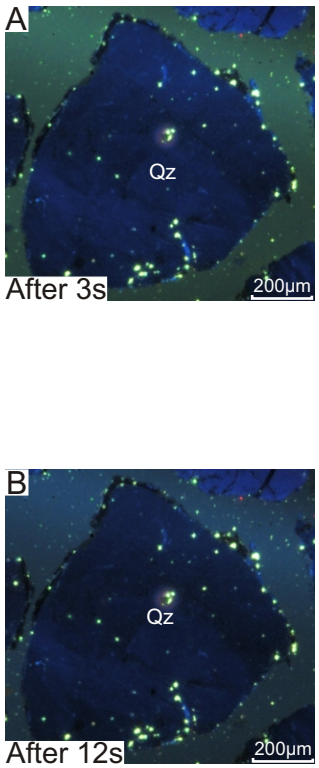

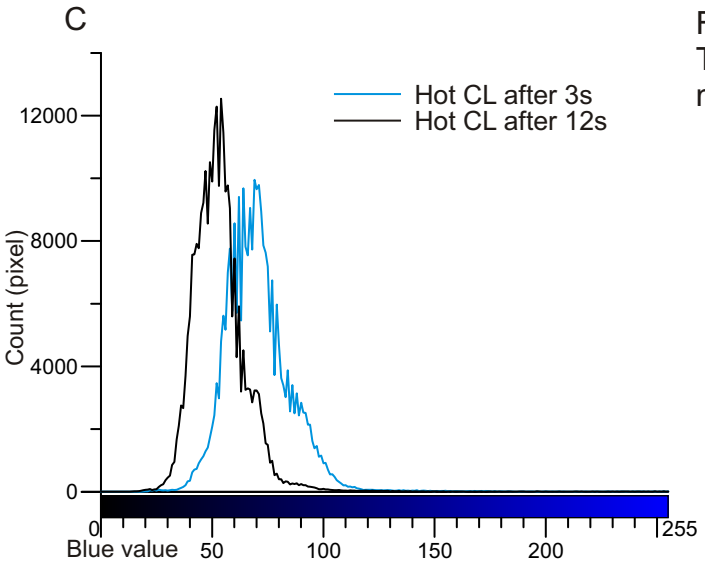

Figure 2B-10 : Grain 10. The grain shows moderate colour shift.

D

Blue value	Min	Max	Mode	Mean	SD
After 3s	16	255	69	71	15.5
After 12s	11	255	54	53	13.1

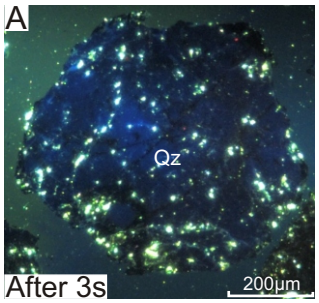

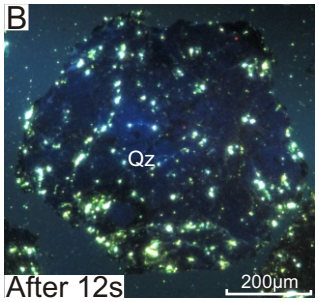

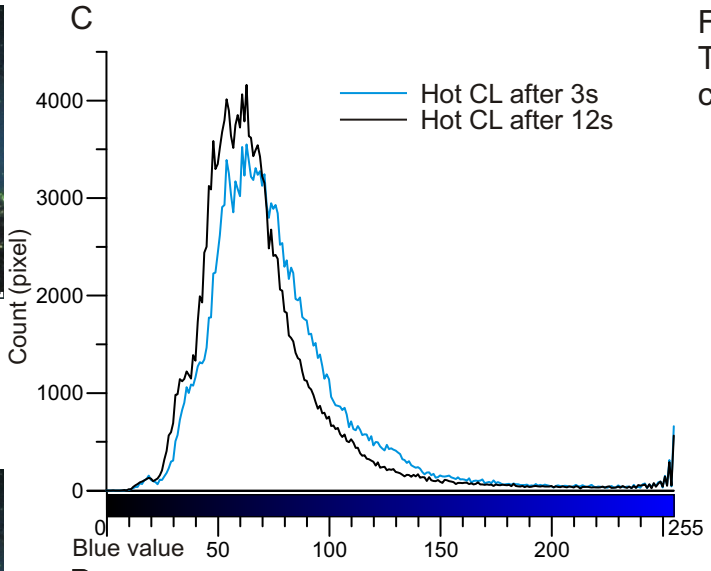

Figure 2B-11: Grain 11. The grain shows slight colour shift.

D

Blue value	Min	Max	Mode	Mean	SD
After 3s	8	255	63	78	35.6
After 12s	3	255	63	71	33.9

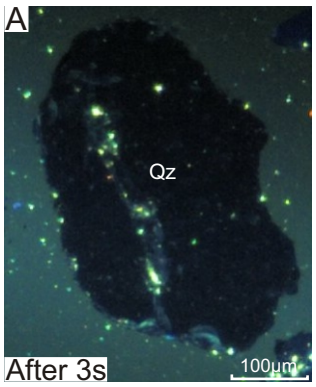

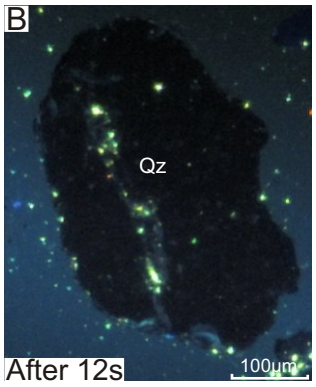

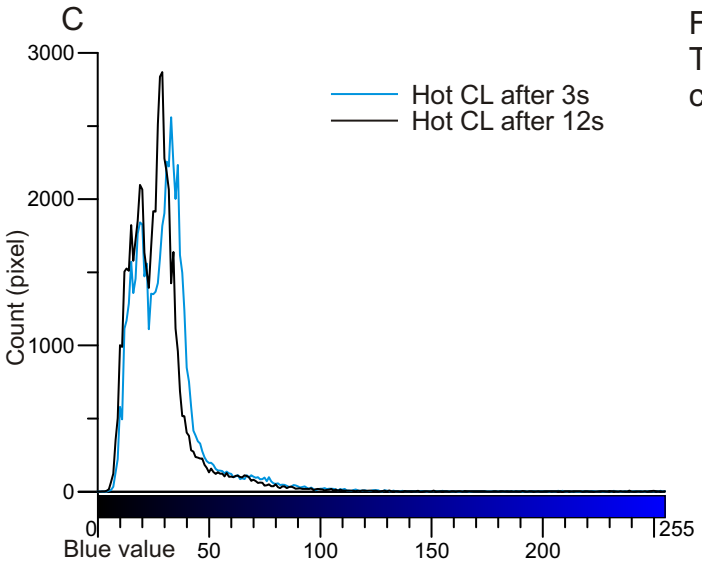

Figure 2B-12: Grain 12. The grain shows no colour shift.

D

Blue value	Min	Max	Mode	Mean	SD
After 3s	5	255	33	31	18.6
After 12s	2	255	29	28	17.7

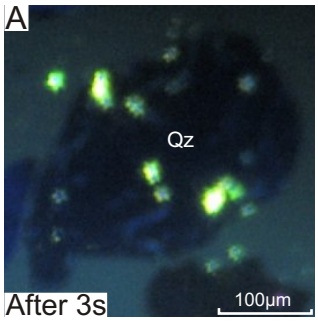

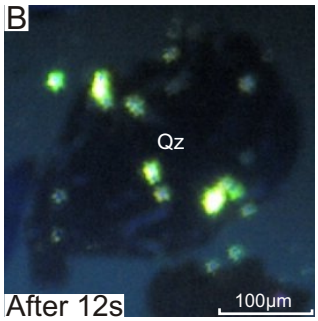

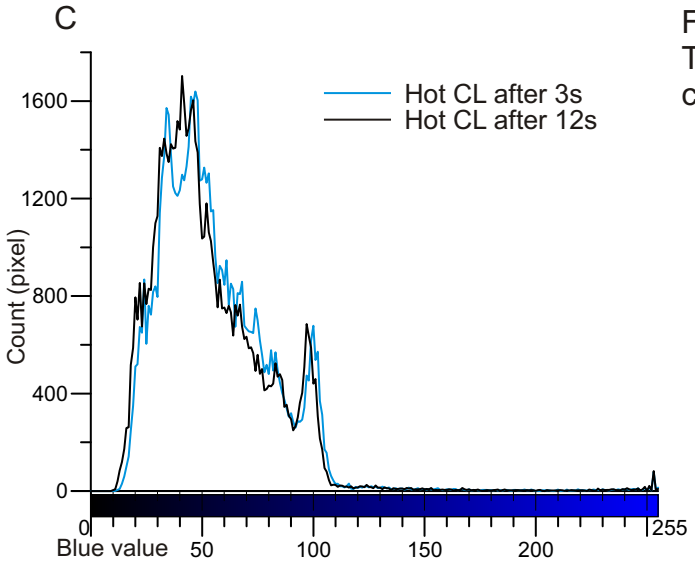

Figure 2B-13: Grain 13. The grain shows no colour shift.

D

Blue value	Min	Max	Mode	Mean	SD
After 3s	10	94	33	36	12.1
After 12s	9	85	32	33	11.3

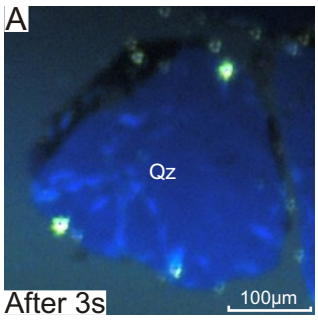

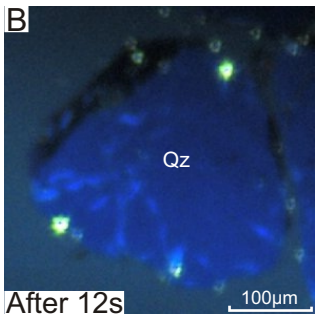

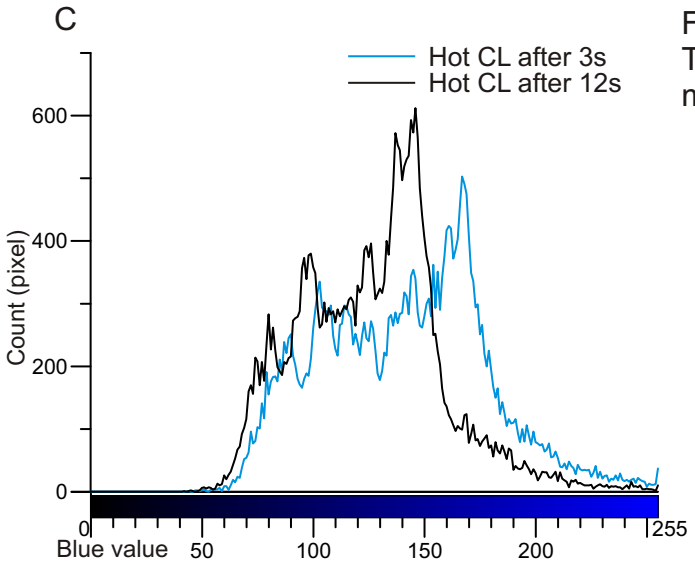

Figure 2B-14: Grain 14. The grain shows moderate colour shift.

D

Blue value	Min	Max	Mode	Mean	SD
After 3s	44	255	167	141	37.4
After 12s	42	255	146	126	32.1

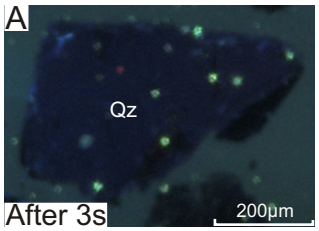

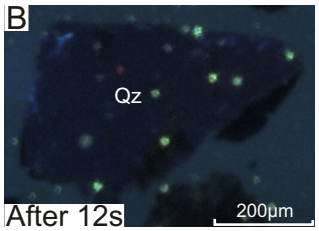

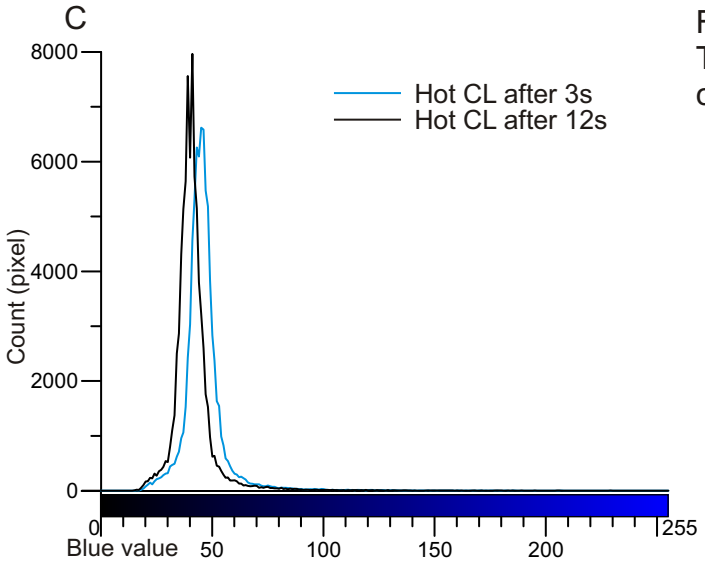

Figure 2B-15: Grain 15. The grain shows slight colour shift.

D

Blue value	Min	Max	Mode	Mean	SD
After 3s	16	228	45	46	10.6
After 12s	13	229	41	41	10.3

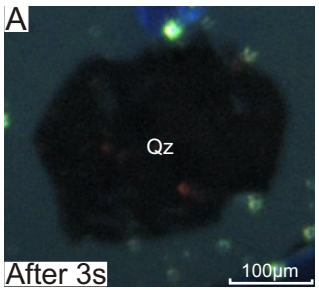

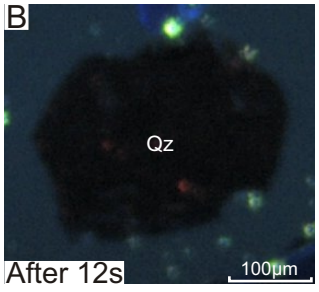

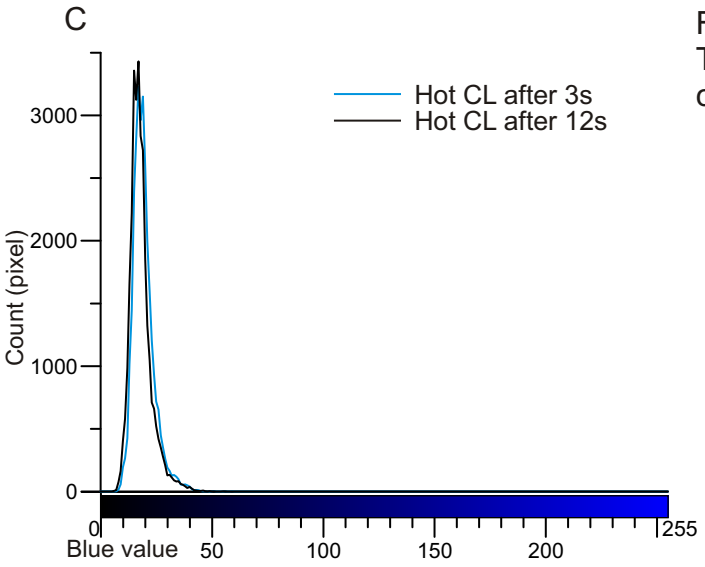

Figure 2B-16: Grain 16. The grain shows no colour shift.

D

Blue value	Min	Max	Mode	Mean	SD
After 3s	6	59	17	19	4.8
After 12s	6	56	17	18	4.9

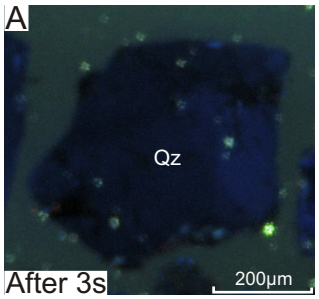

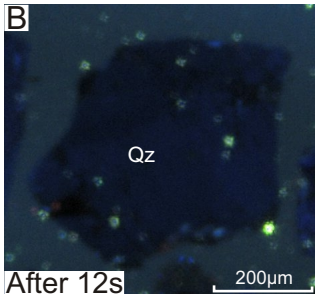

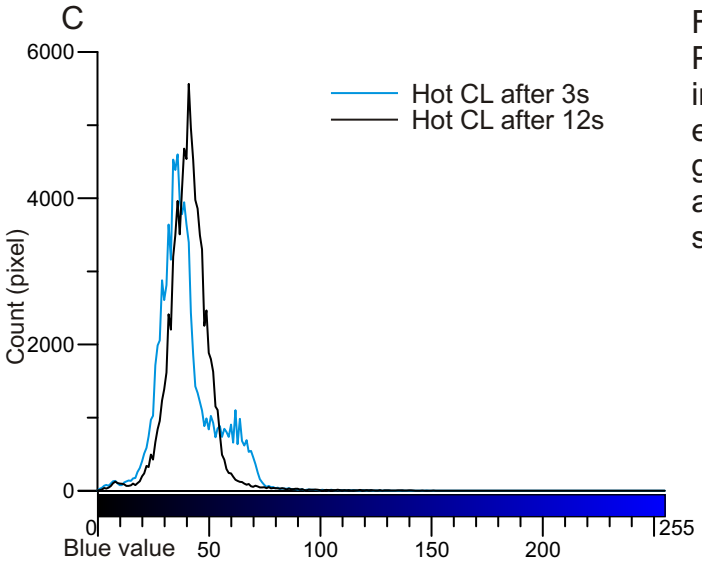

D

Blue value	Min	Max	Mode	Mean	SD
After 3s	0	182	36	40	13.4
After 12s	0	183	41	41	10.3

Figure 2B-17: Grain 17. Probably the first image was taken too early. Therefore, this grain is not useful to analyse the colour shift.

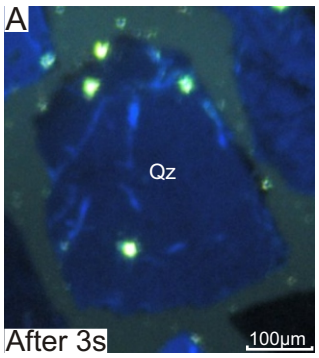

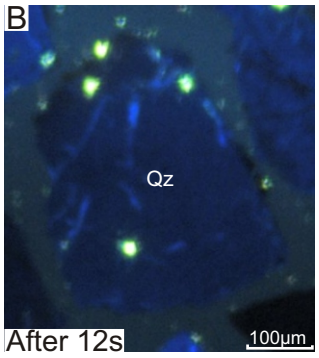

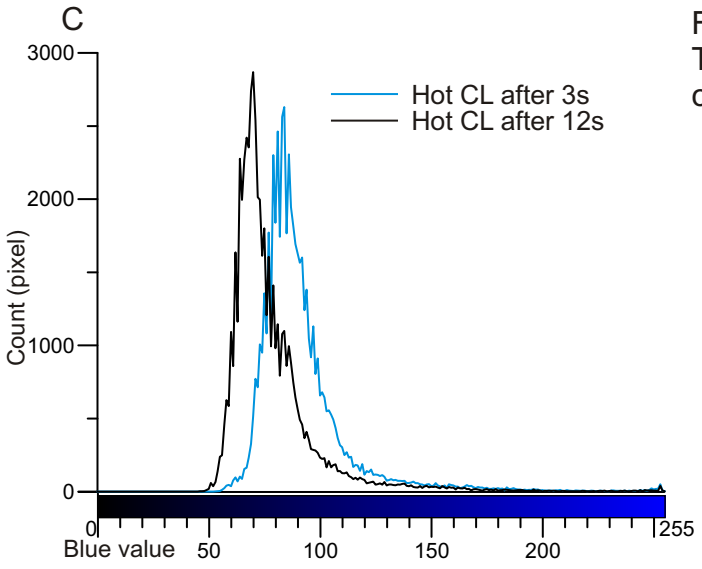

D

Blue value	Min	Max	Mode	Mean	SD
After 3s	53	255	84	92	22.1
After 12s	46	255	70	78	21.3

Figure 2B-18: Grain 18. The grain shows slight colour shift.

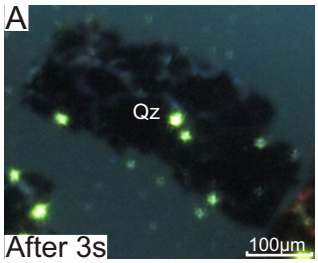

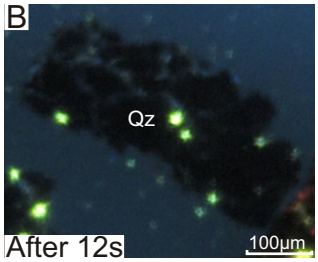

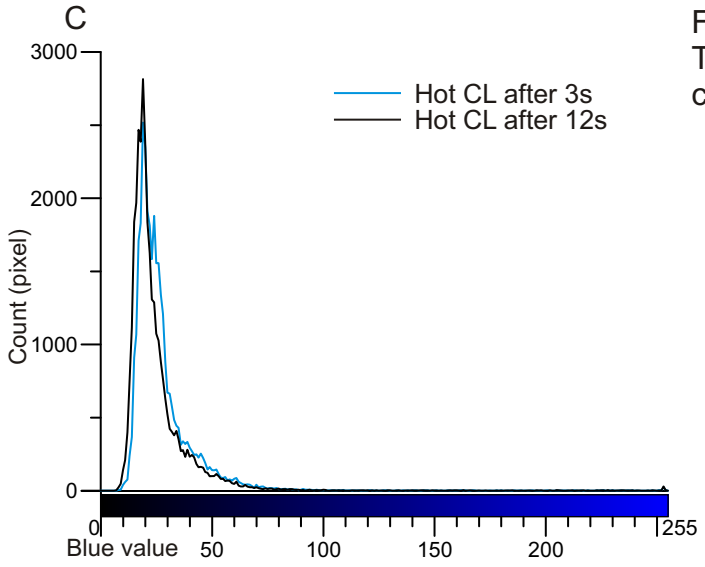

Figure 2B-19: Grain 19. The grain shows no colour shift.

D

Blue value	Min	Max	Mode	Mean	SD
After 3s	8	254	19	28	16.9
After 12s	7	254	19	25	16.6

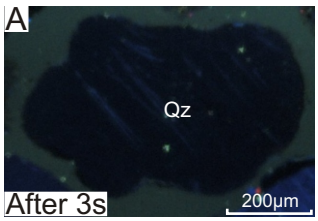

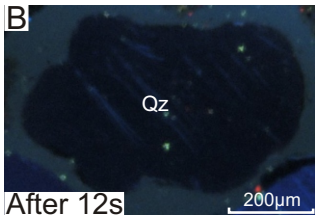

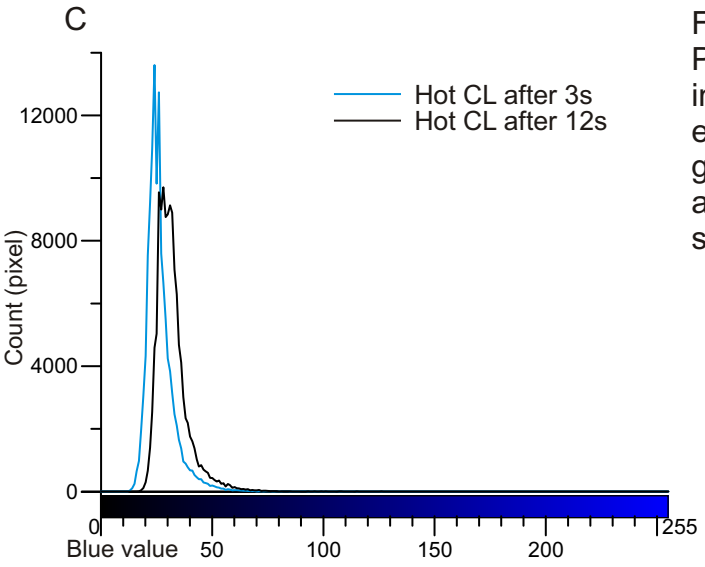

Figure 2B-20: Grain 20. Probably the first image was taken too early. Therefore, this grain is not useful to analyse the colour shift.

D

Blue value	Min	Max	Mode	Mean	SD
After 3s	10	164	24	27	6.7
After 12s	15	198	28	32	7.6

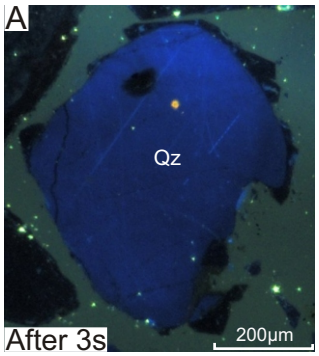

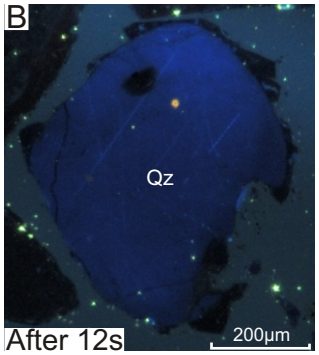

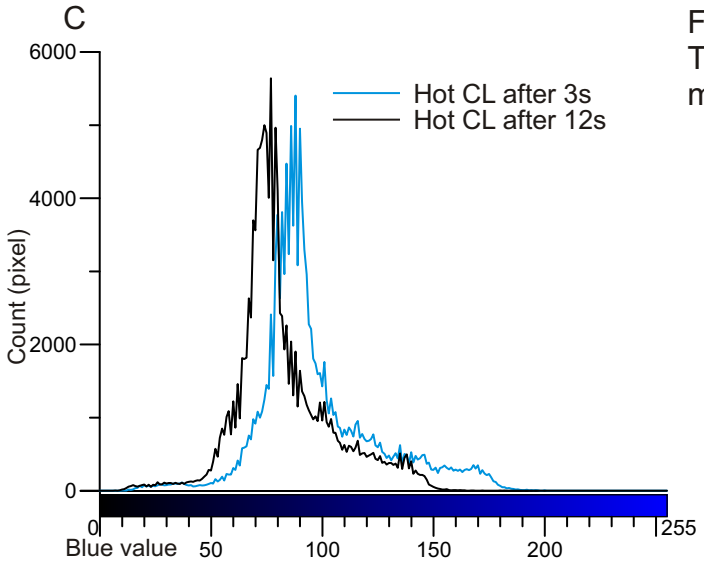

Figure 2B-21: Grain 21. The grain shows moderate colour shift.

D

Blue value	Min	Max	Mode	Mean	SD
After 3s	9	211	88	97	26.8
After 12s	6	186	77	82	21.7

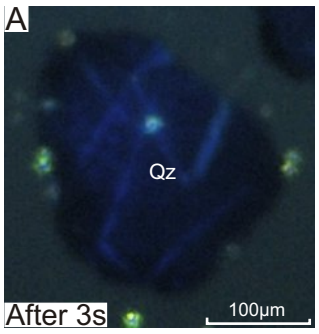

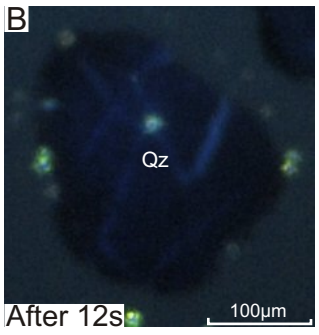

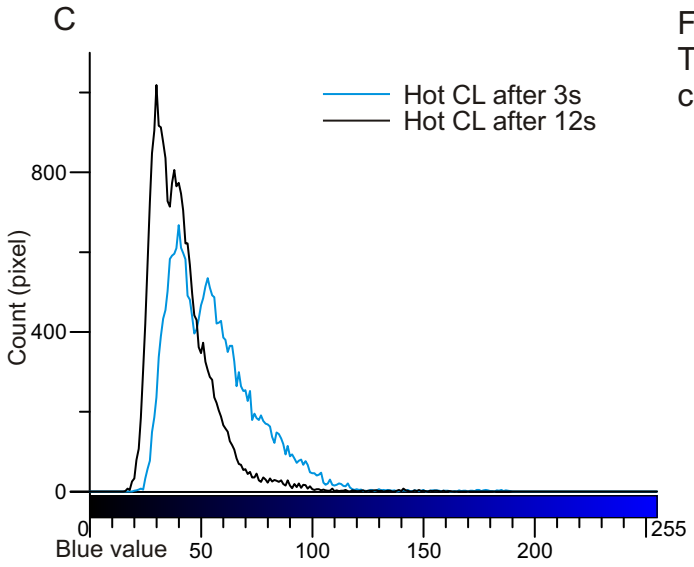

Figure 2B-22: Grain 22. The grain shows slight colour shift.

D

Blue value	Min	Max	Mode	Mean	SD
After 3s	20	189	40	55	19.8
After 12s	16	162	30	41	14.3

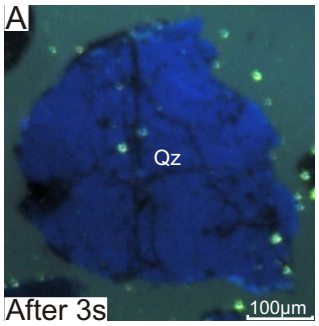

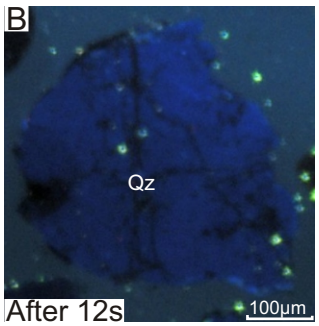

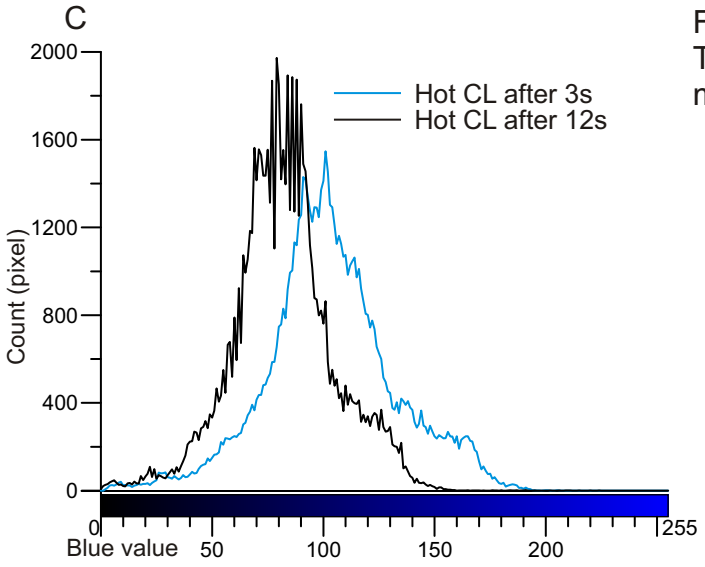

Figure 2B-23: Grain 23. The grain shows moderate colour shift.

D

Blue value	Min	Max	Mode	Mean	SD
After 3s	2	206	101	103	29
After 12s	0	224	79	82	22.9

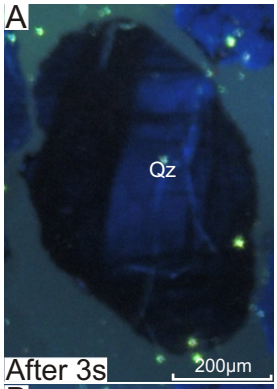

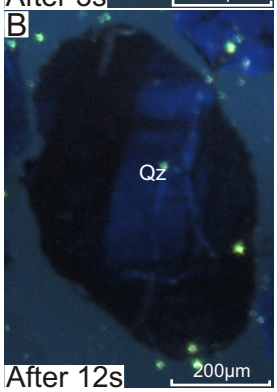

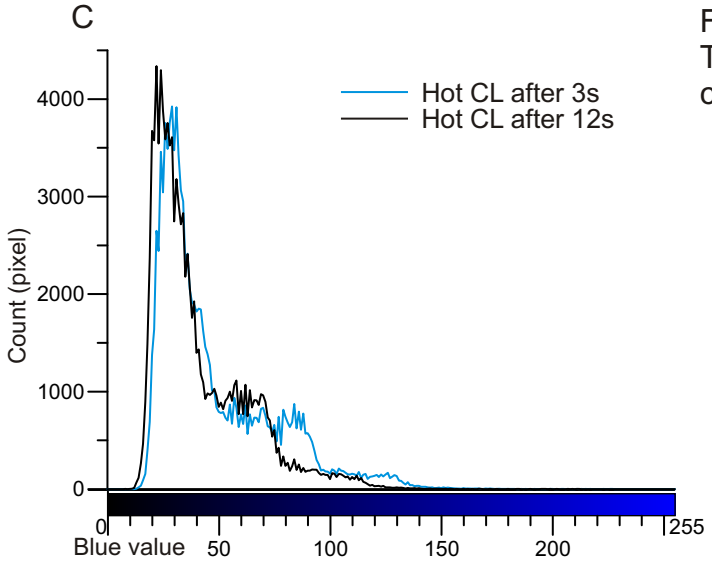

Figure 2B-24: Grain 24. The grain shows slight colour shift.

D

Blue value	Min	Max	Mode	Mean	SD
After 3s	13	227	29	48	26.1
After 12s	8	212	22	41	21.5

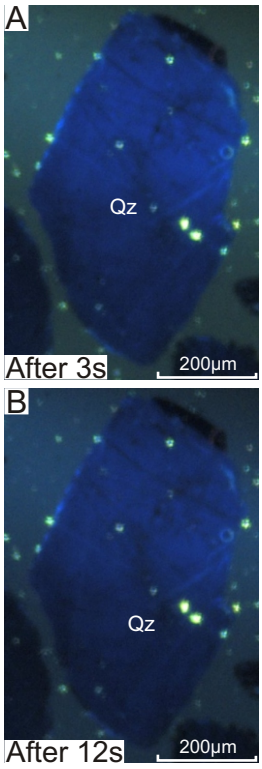

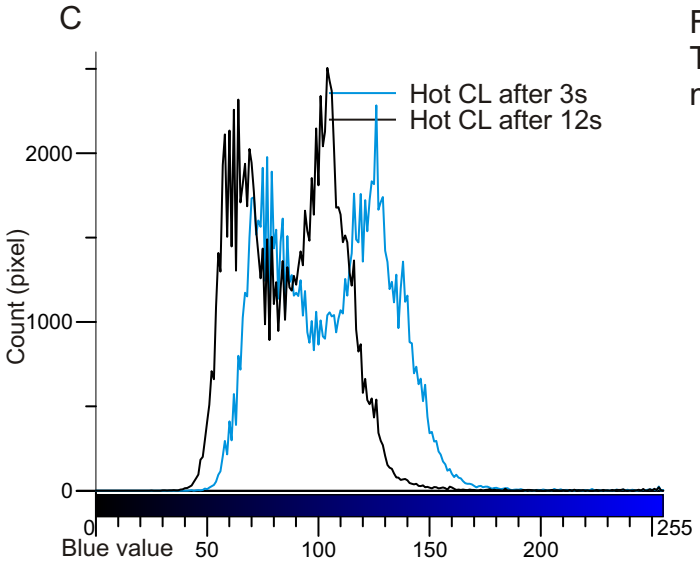

D

Blue value	Min	Max	Mode	Mean	SD
After 3s	42	255	126	106	26.7
After 12s	25	254	104	88	22.6

Figure 2B-25: Grain 25. The grain shows moderate colour shift.

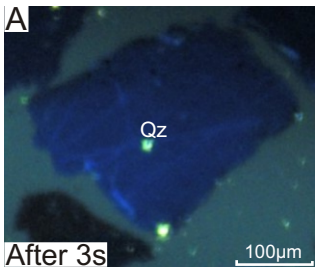

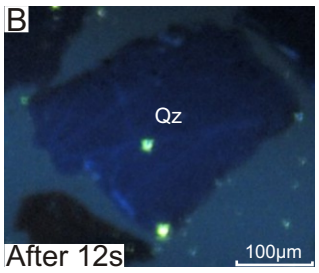

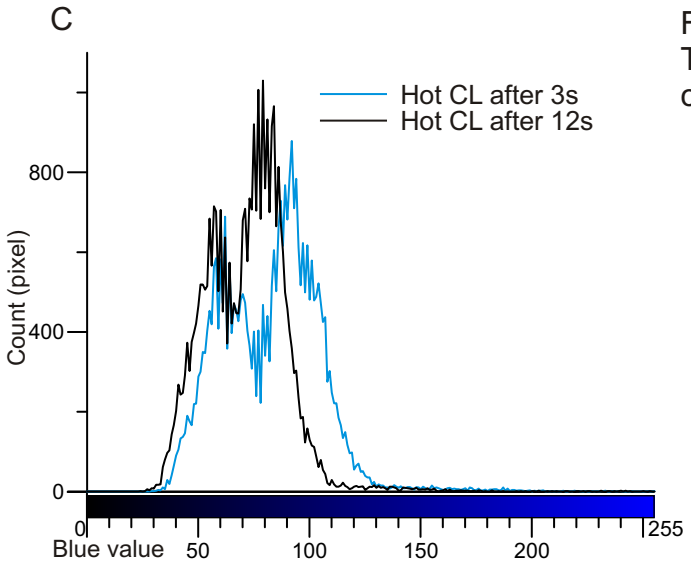

D

Blue value	Min	Max	Mode	Mean	SD
After 3s	29	255	92	82	22.2
After 12s	24	253	79	71	18.2

Figure 2B-26: Grain 26. The grain shows slight colour shift.

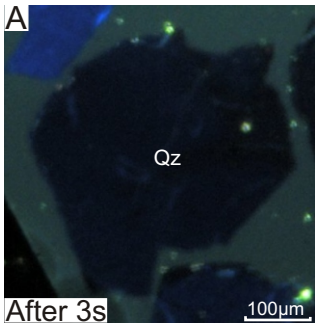

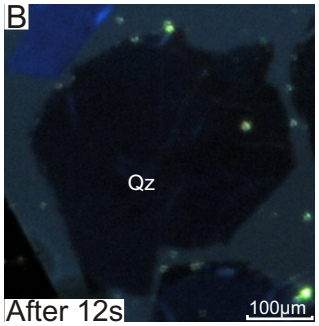

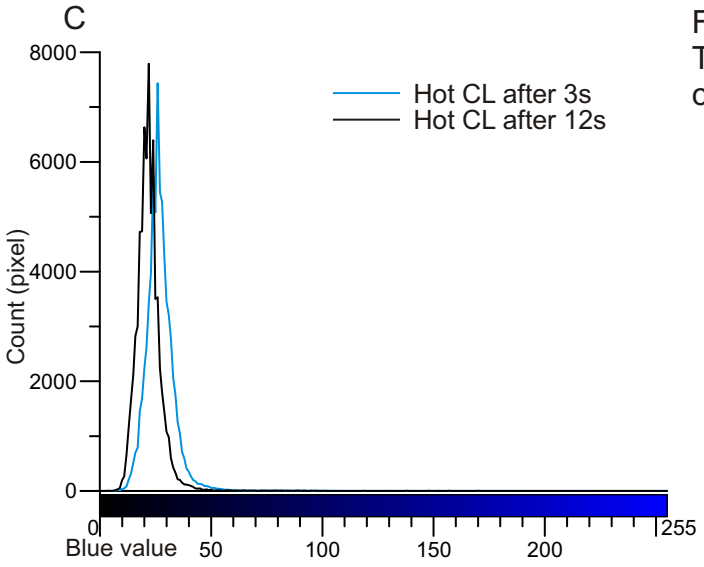

Figure 2B-27: Grain 27. The grain shows slight colour shift.

D

Blue value	Min	Max	Mode	Mean	SD
After 3s	6	222	26	27	7.2
After 12s	3	213	22	22	6.4

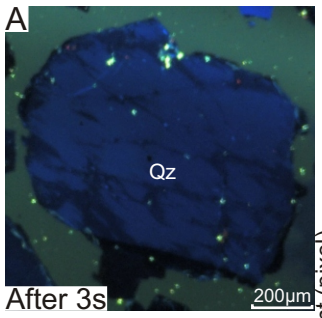

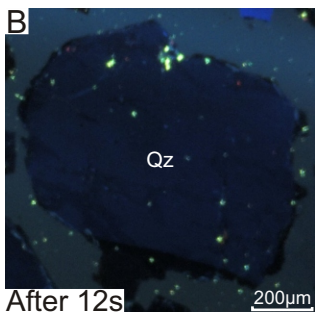

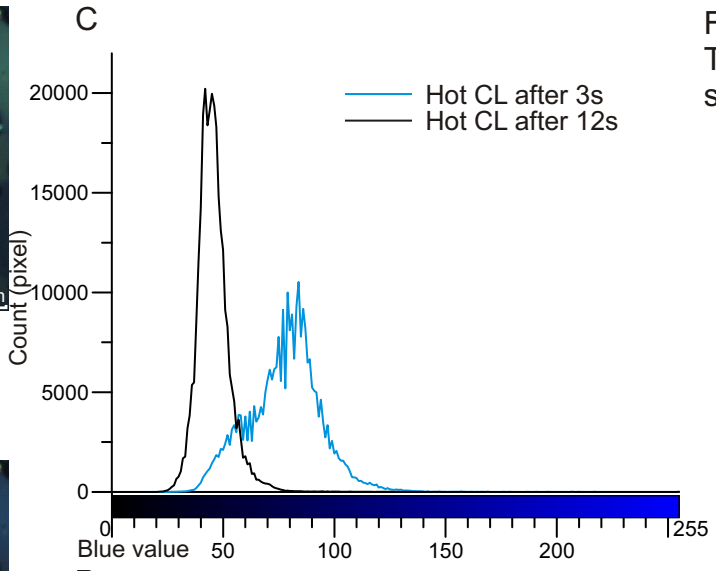

Figure 2B-28: Grain 28. The grain shows strong colour shift.

D

Blue value	Min	Max	Mode	Mean	SD
After 3s	24	255	84	78	16.4
After 12s	19	255	42	46	8.4



Figure 2B-29: Grain 29. The grain shows slight colour shift.

D

Blue value	Min	Max	Mode	Mean	SD
After 3s	27	255	90	90	16.8
After 12s	23	255	77	78	15.2

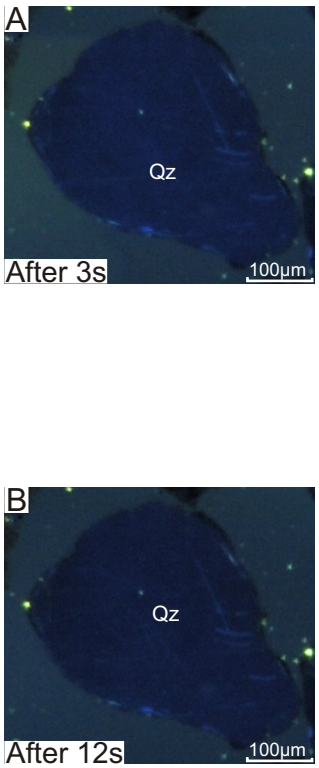

Figure 2B-30: Grain 30. The grain shows slight colour shift.

D

Blue value	Min	Max	Mode	Mean	SD
After 3s	34	179	64	66	7.5
After 12s	33	157	58	58	6.8

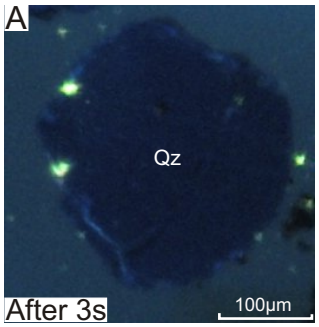

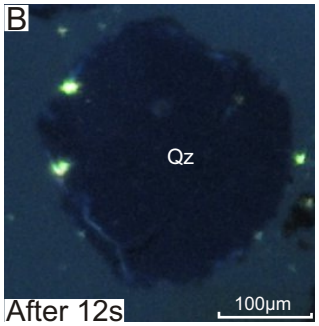

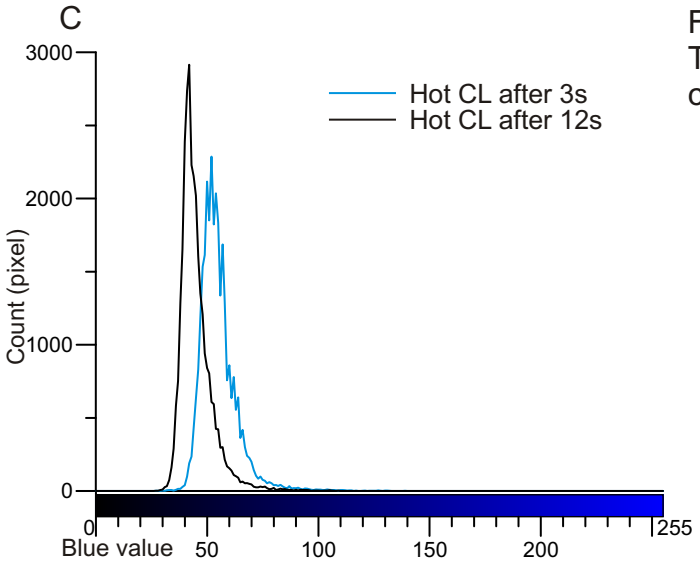

Figure 2B-31: Grain 31. The grain shows slight colour shift.

D

Blue value	Min	Max	Mode	Mean	SD
After 3s	27	139	52	55	8.5
After 12s	27	109	42	45	7.4

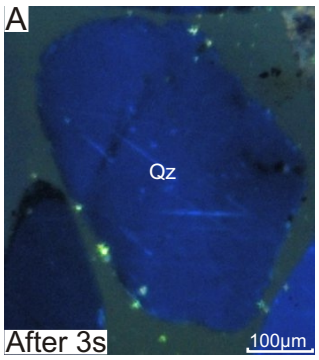

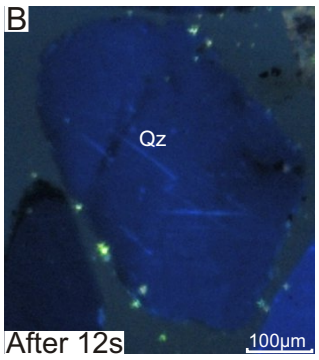

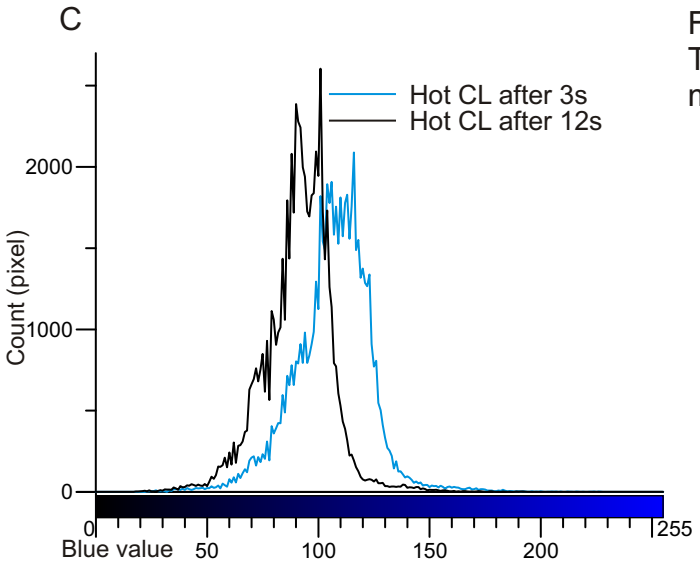

Figure 2B-32: Grain 32. The grain shows moderate colour shift.

D

Blue value	Min	Max	Mode	Mean	SD
After 3s	23	227	116	106	17.4
After 12s	18	193	101	91	15.2

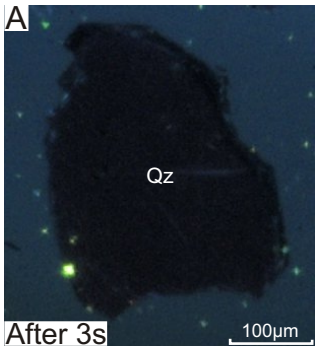

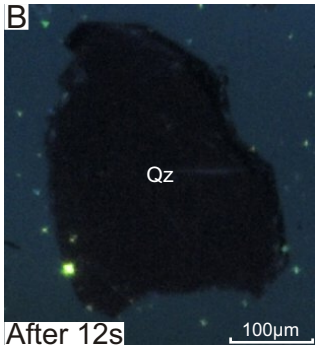

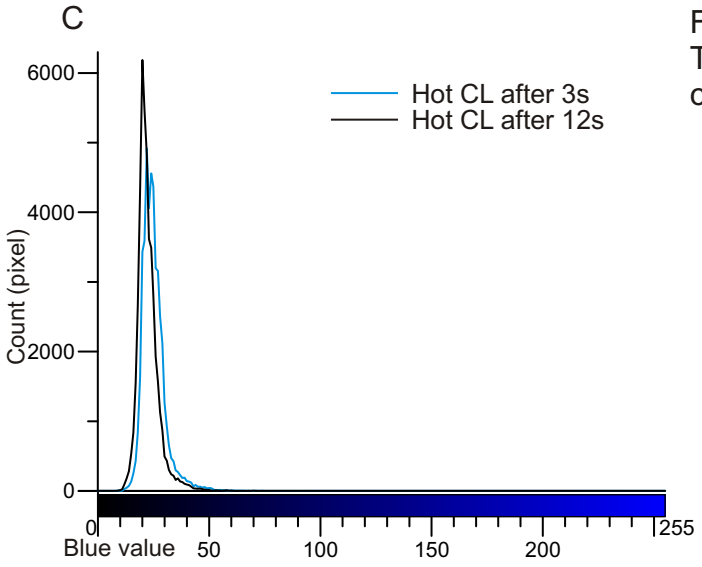

Figure 2B-33: Grain 33. The grain shows no colour shift.

D

Blue value	Min	Max	Mode	Mean	SD
After 3s	9	99	22	25	5.3
After 12s	8	105	20	22	4.8

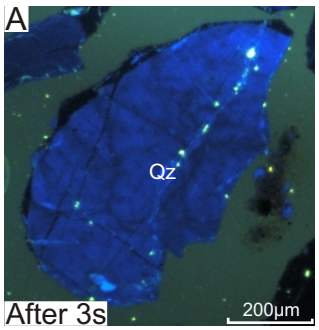

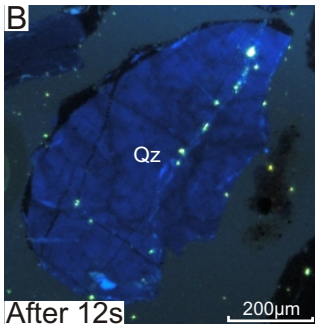

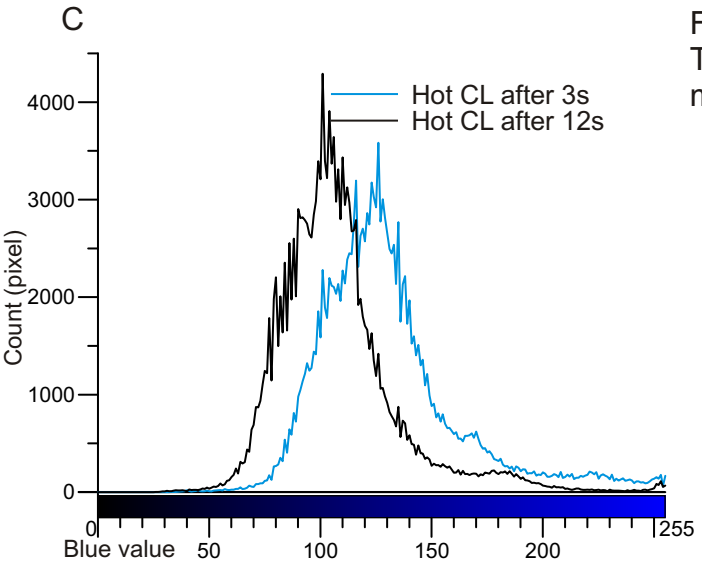

Figure 2B-34: Grain 34. The grain shows moderate colour shift.

D

Blue value	Min	Max	Mode	Mean	SD
After 3s	33	255	126	130	32.5
After 12s	26	255	101	108	27.4

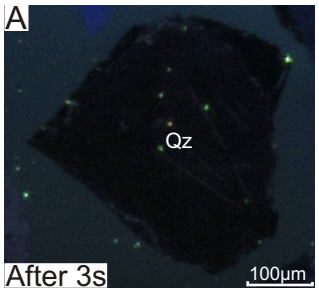

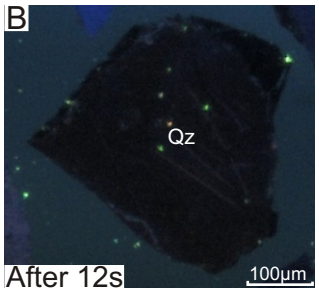

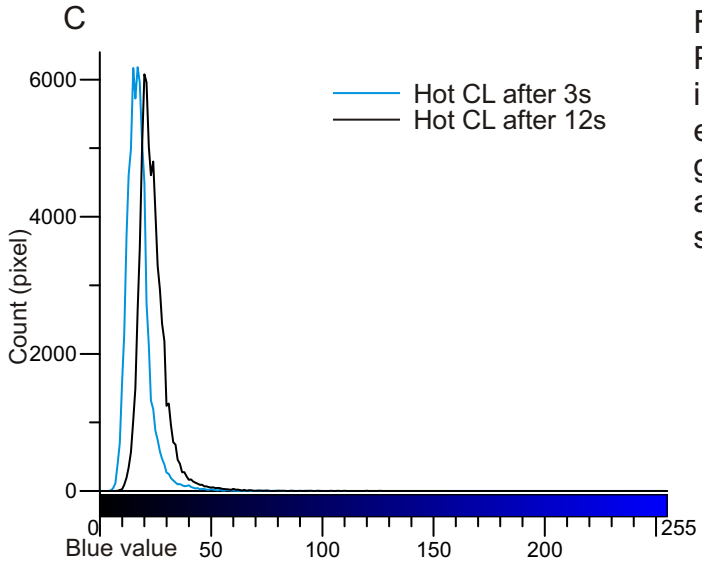

D

Blue value	Min	Max	Mode	Mean	SD
After 3s	4	135	17	17	5.8
After 12s	6	151	20	24	6.7

Figure 2B-35: Grain 35. Probably the first image was taken too early. Therefore, this grain is not useful to analyse the colour shift.

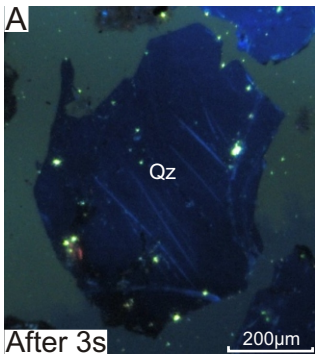

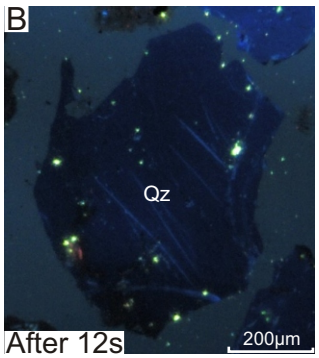

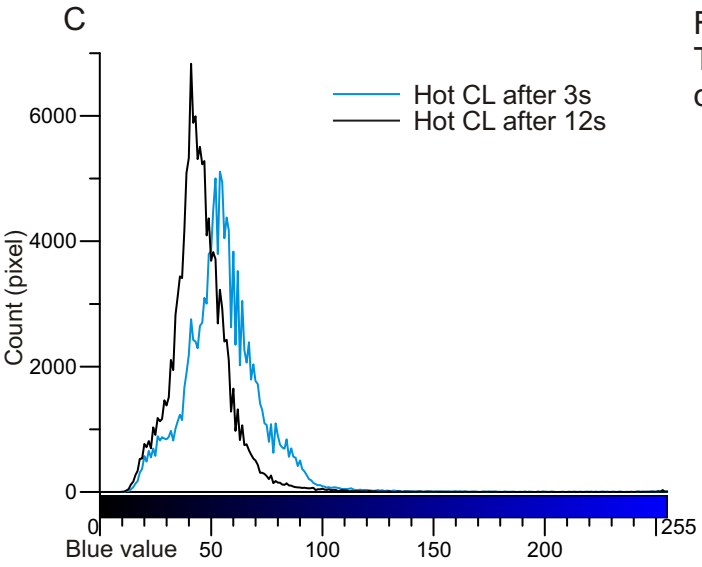

D

Blue value	Min	Max	Mode	Mean	SD
After 3s	12	255	54	56	17.8
After 12s	10	255	41	46	14.6

Figure 2B-36: Grain 36. The grain shows slight colour shift.

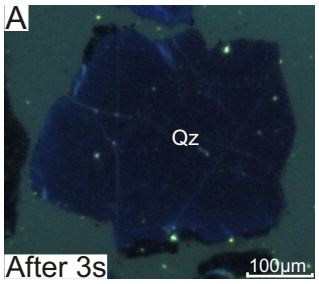

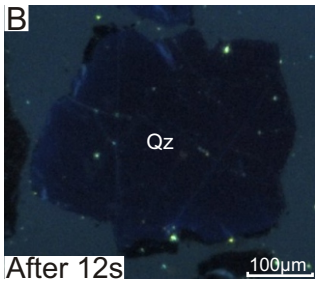

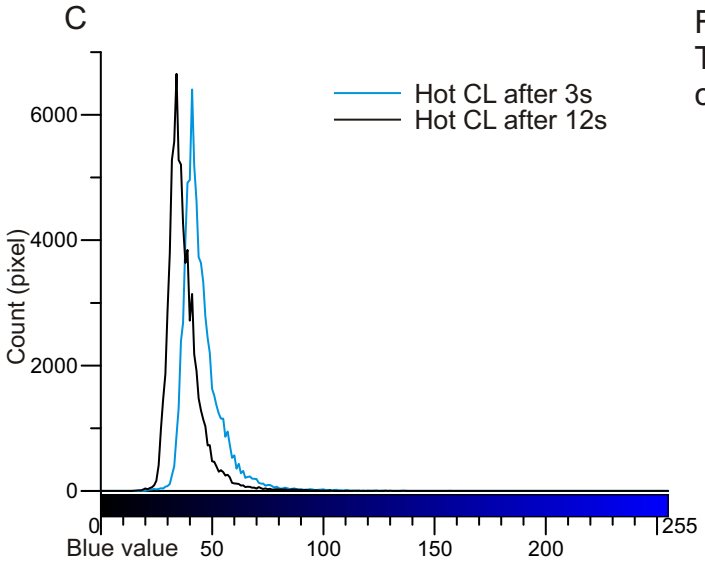

Figure 2B-37: Grain 37. The grain shows slight colour shift.

D

Blue value	Min	Max	Mode	Mean	SD
After 3s	18	175	41	45	9.5
After 12s	13	169	34	38	8.2

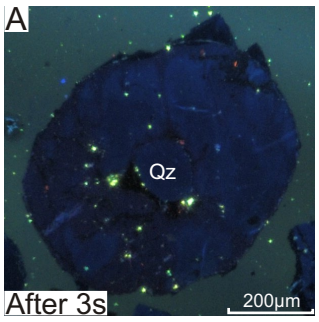

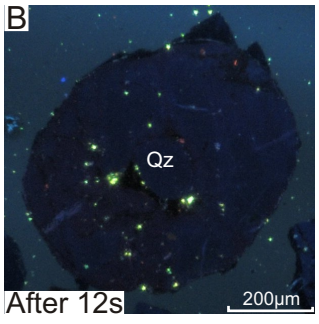

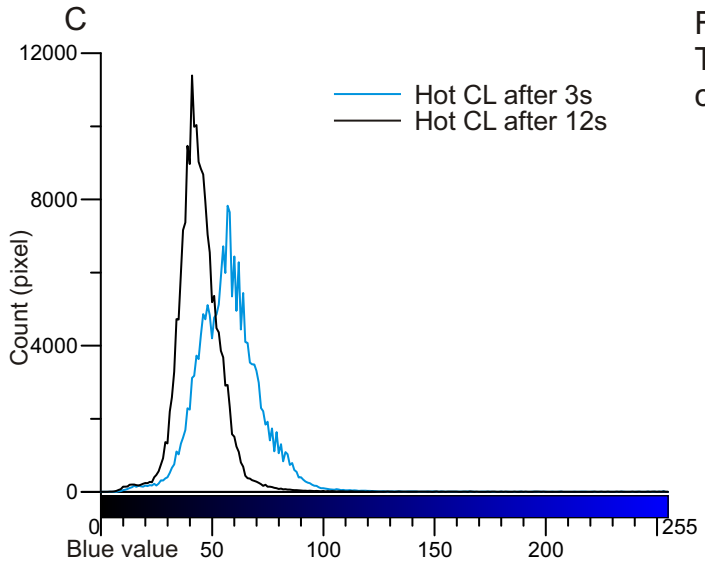

Figure 2B-38: Grain 38. The grain shows slight colour shift.

D

Blue value	Min	Max	Mode	Mean	SD
After 3s	8	254	57	58	15.1
After 12s	4	255	41	45	11.6

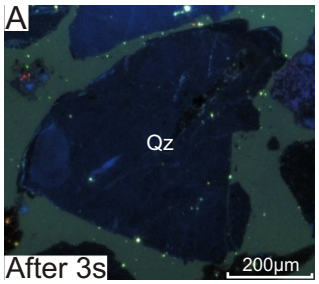

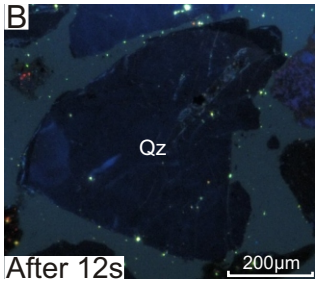

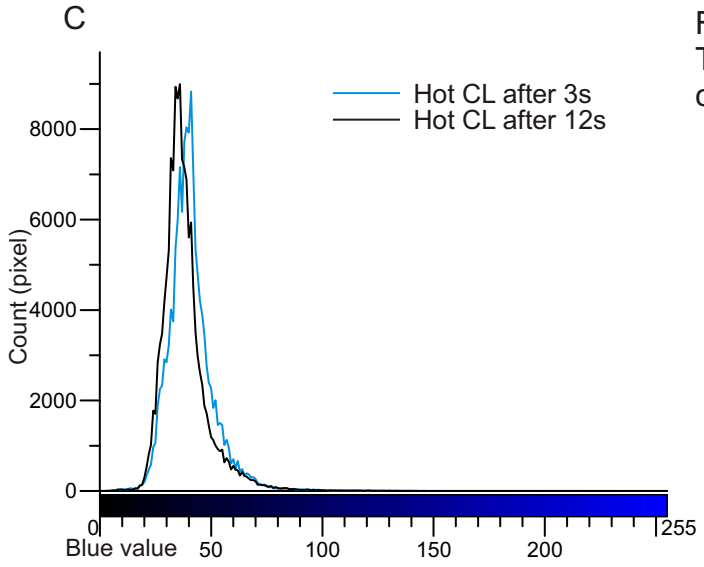

Figure 2B-39: Grain 39. The grain shows no colour shift.

D

Blue value	Min	Max	Mode	Mean	SD
After 3s	2	246	41	41	10.8
After 12s	4	235	36	38	10.5

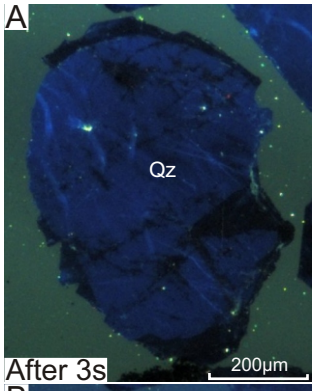

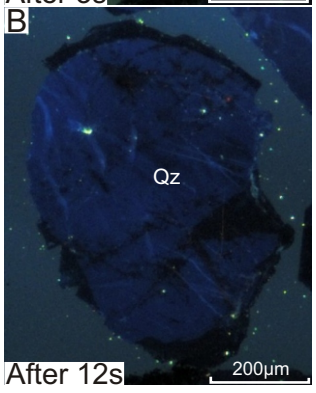

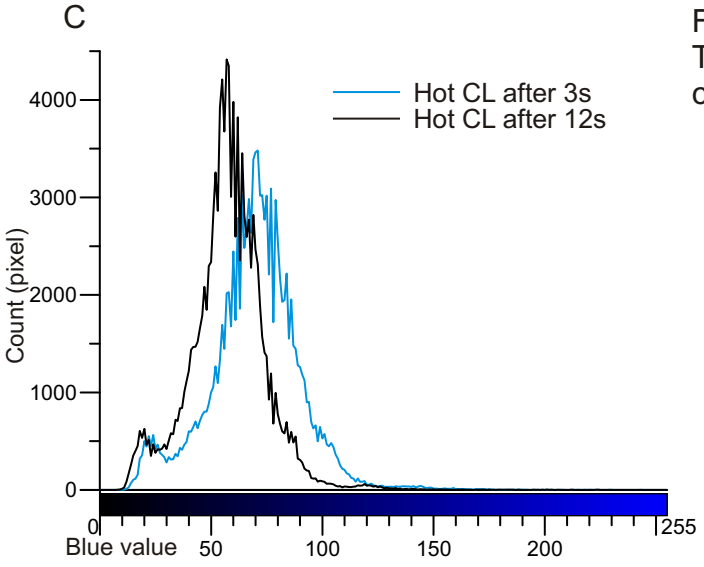

Figure 2B-40: Grain 40. The grain shows slight colour shift.

D

Blue value	Min	Max	Mode	Mean	SD
After 3s	9	243	71	69	20.3
After 12s	8	224	57	58	17

Appendix 3A: Microphotos, scanning SEM-BSE images, SEM-CL images, and EDS analyses of detrital quartz grains in sample 2995.

Notes:

1. **Homogenous CL:** Nearly uniform CL intensity across the grain (Fig. 2A).

2. Fractures in quartz have been divided into two types: **healed fractures** (**HF**) and **open fractures** (**OF**).

   Healed fractures are fractures filled with secondary silica that appear as thin (commonly < 10 μm) black lines in SEM-CL images (Fig. 2B). They are usually not shown in back-scattered images (Boggs and Krinsley, 2006).

   Open fractures appear in cathodoluminescense images as CL-dark or CL-bright lines, and they are also visible in back-scattered images and microphotos. A few open fractures are **conchoidal fractures** (**CF**) (Boggs and Krinsley, 2006).

3. **Tectonic deformation lamellae**: Tectonic deformation lamellae (Fig. 2C) appear in SEM-CL image as numerous sets of thin, parallel, closely spaced, dark gray lines (Bernet and Basset, 2005). According to Hamers and Drury (2011), tectonic deformation lamellae can either appear as dark gray lines or bright lines in SEM-CL images, and can show slightly wavy features with varying thickness. They usually also appear in XPL image under petrographic microscope.

4. **Spiders (S):** They are made up of dark-Cl patches and streaks. Dark-CL patches mainly range from 10-100 μm. Streaks are random and irregular in the appearance of black broad (>10 μm) elongated form. The spiders are commonly associated with healed fractures, giving them the appearance in SEM-CL images of spiders sitting on a web (Fig. 2D). They cannot be seen in BSE images, since they are composed by secondary silica (Boggs and Krinsley, 2006).

5. **Bright mottling**: Some grains show irregular CL intensity across grains, creating a mottled pattern due the presence of patches (Boggs and Krinsley, 2006). Three types of bright mottling were seen.

   - **Random bright patches** (Fig. 2E1)
   - **Bright streaky patches fabric** (Fig. 2E2)
   - **Subtle mottling** (Fig. 2E3)

6. **Overgrowth:** Overgrowth appears in SEM-CL images as dark areas in the border of the quartz grains (Fig. 2F).

7. **Fluid inclusion trail** (**FI trail**): Trails formed by **fluid inclusions** (**FI**). They are usually associated with secondary porosity and commonly located along fractures and at boundaries between detritral quartz grain and the overgrowth. They are well observed in microphotos under ppl. The fluid inclusion trails can be separated in two kinds: **detrital fluid inclusion trails (**fluid inclusions that are original from the detrital quartz, they do not cut the quartz overgrowth) and **diagenetic fluid inclusion trails** (fluid inclusions originated from the diagenesis, and they thus cut the quartz overgrowth).

8. **Melt inclusion** (**MI**): Large fluid inclusions (>10 μm) in which crystallized minerals are visible.

9. **Secondary porosity** (**SP**): Porosities usually caused by dissolution and/or fractures. They are easily observed in microphotos under PPL and BSE images.

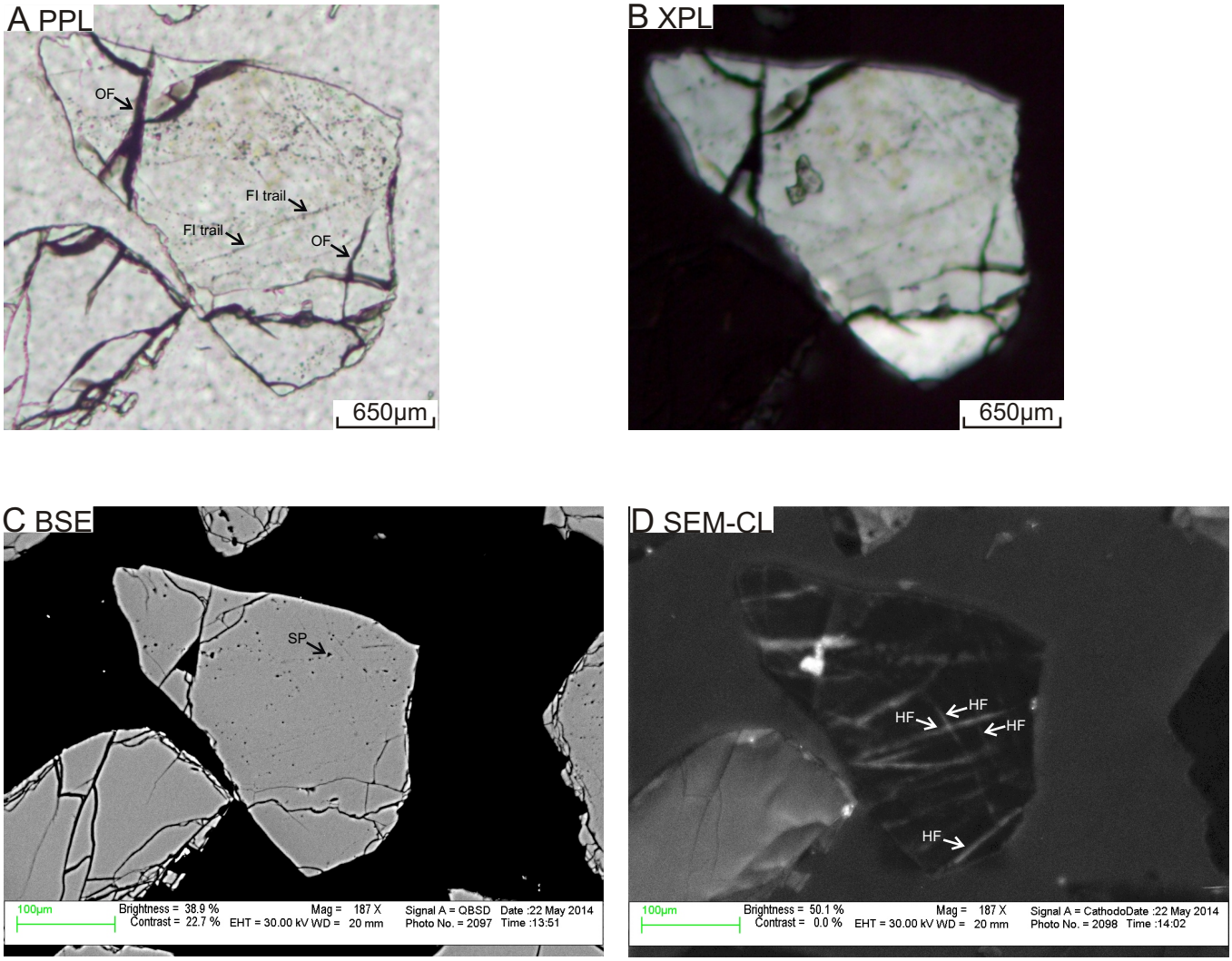

Figure 3A-1: Microphotos under ppl (A) and xpl (B), SEM-BSE image (C) and SEM-CL image (D) of quartz grain 1 in sample 2995. The grain is anhedral and angular polycrystalline (only a few sub-grains with sutured sub-grain boundaries) with strong undulose extinction. Fluid inclusions are common; they are usually associated with secondary porosity (SP) and form trails (FI trail) along healed fractures (Fig. A and C). The grain is microfractured with two sets of sub-parallel healed fractures (HF), crosscutting each other perpendicularly, and a set of irregular open fractures (OF) (Fig. A and D). Healed fractures are common.

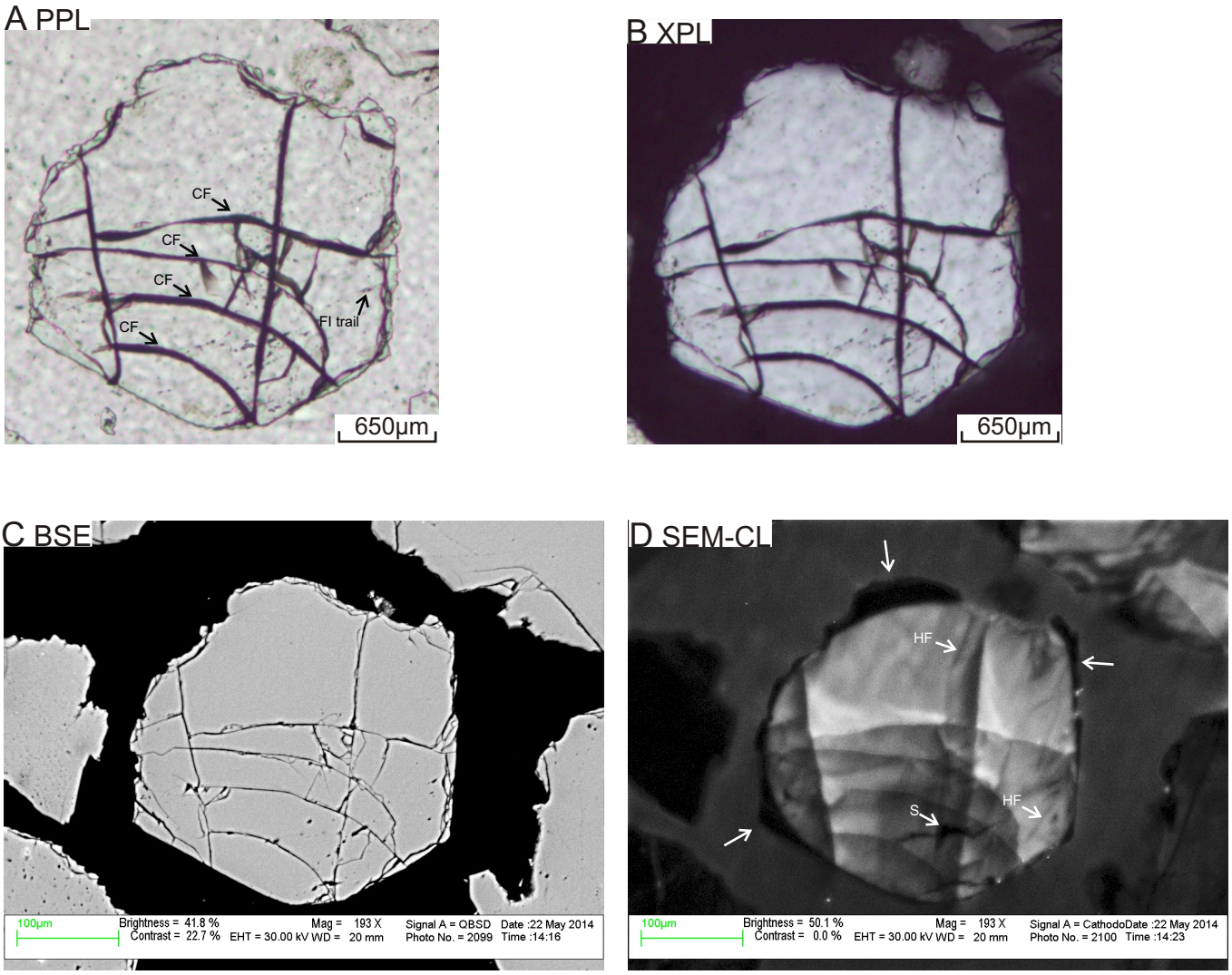

Figure 3A-2: Microphotos under ppl (A) and xpl (B), SEM-BSE image (C) and SEM-CL image (D) of quartz grain 2 in sample 2995. The grain is subhedral and sub-rounded monocrystalline with irregular margins and weak undulose extinction. Fluid inclusions are present, they usually form trails (FI trail) along healed fractures (Fig. A). The grain is microfractured with a set of sub-parallel fractures and a set of conchoidal fractures (CF) (Fig. A and D). Some healed fractures (HF) and spiders (S), which are secondary porosity filled by diagenetic quartz, can be seen in Fig. D. The dark areas indicated by arrows in Fig. D are overgrowth; these areas appear corroded in Fig. C, suggesting secondary porosity.

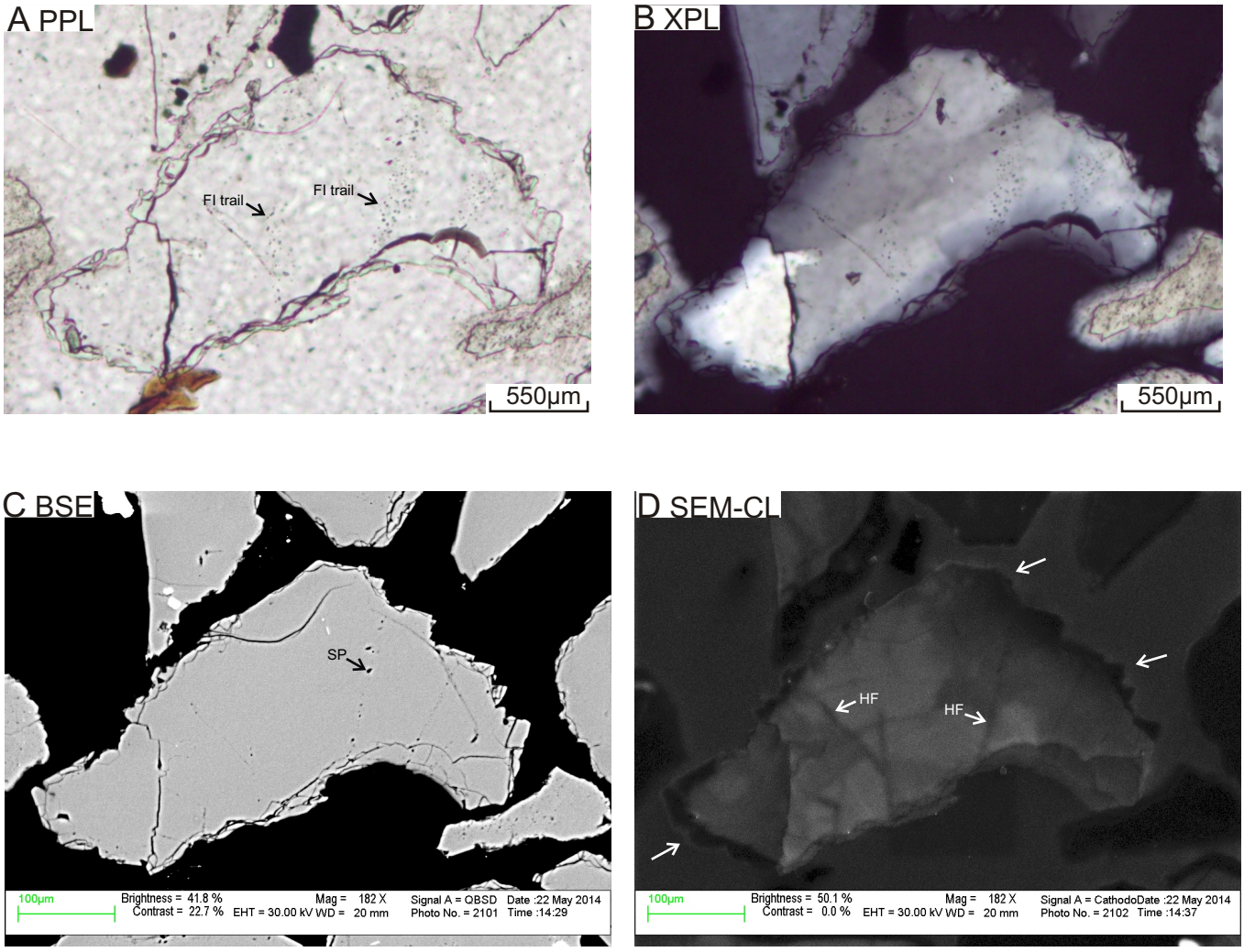

Figure 3A-3: Microphotos under ppl (A) and xpl (B), SEM-BSE image C, and SEM-CL image (D) of quartz grain 3 in sample 2995. The grain is anhedral and angular polycrystalline (only 2 sub-grains with sutured sub-grain boundaries) with irregular margins, mosaic texture, and weak undulose extinction. Fluid inclusions are common; they are usually associated with secondary porosity (SP) and form trails (FI trail) along healed fractures (Fig. A and C). The grain is microfractured with a set of irregular fractures (Fig. C and D). Some healed fractures (HF) can be seen in Fig. D. The dark areas indicated by arrows in Fig. D are overgrowth; these areas appear corroded in Fig. C, sugesting secondary porosity.

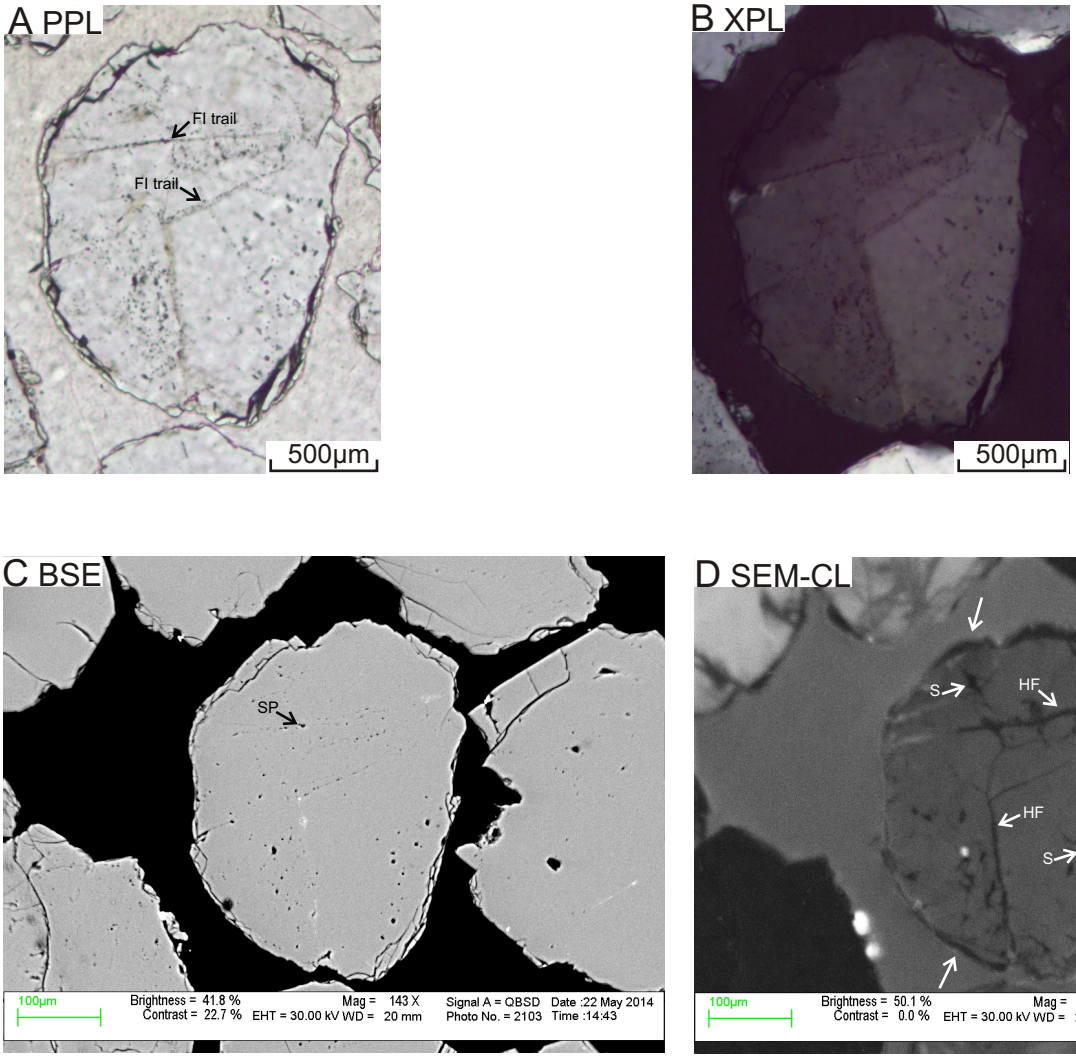

Figure 3A-4: Microphotos under ppl (A) and xpl (B), SEM-BSE image C, and SEM-CL image (D) of quartz grain 4 in sample 2995. The grain is subhedral and rounded monocrystalline with weak undulose extinction. Fluid inclusions are common; they are usually associated with secondary porosity (SP) and form trails (FI trail) along healed fractures (Fig. A and C). The grain is microfractured with a set of irregular fractures (Fig. C and D). Healed fractures (HF) and spiders (S) are common (Fig. D). The dark areas indicated by arrows in Fig. D are overgrowth; these areas appear corroded in Fig. C, suggesting secondary porosity.

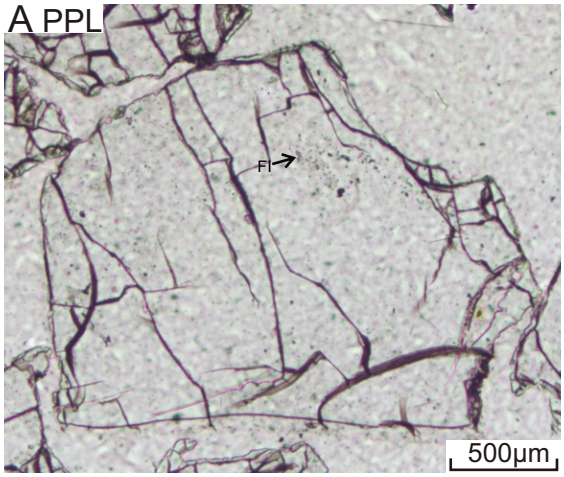

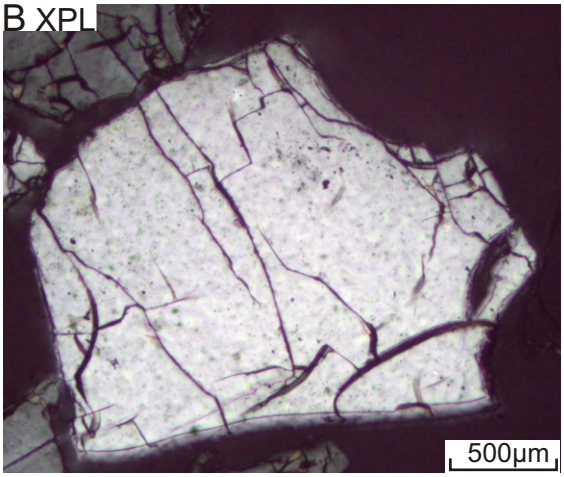

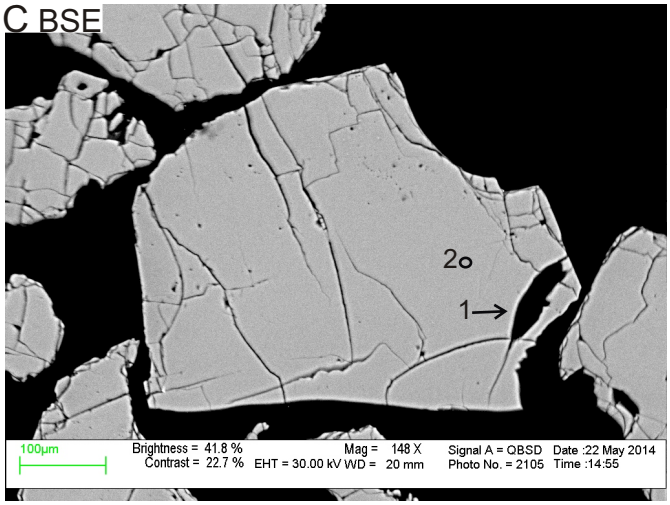

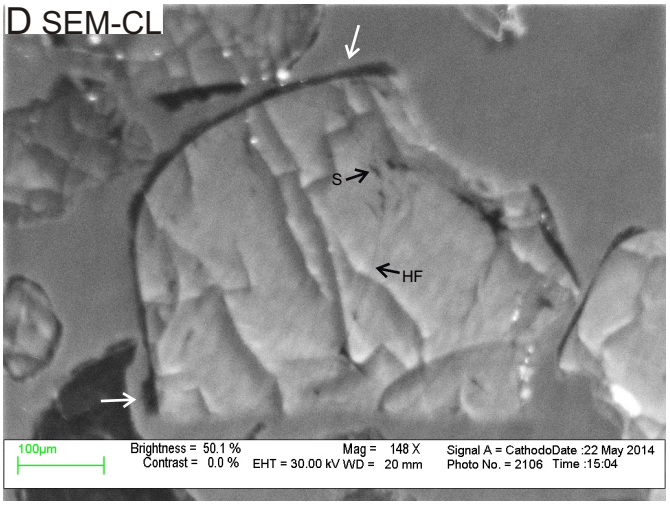

E EDS analyses

Pos#	Min. ID	SiO2	F	Cl	BaO	Total	Actual total
1	Hole	45.89	43.22	3.55	7.34	100	4
2	Qz	99.99				100	129

Figure 3A-5: Microphotos under ppl (A) and xpl (B), SEM-BSE image (C), SEM-CL image (D), and EDS analyses table (E) of quartz grain 5 in sample 2995. The grain is anhedral and angular monocrystalline with non-undulose extinction. Fluid inclusions (FI) are present (Fig. A). The grain is strongly microfractured with a set of irregular fractures (Fig. C and D). Most of the fractures are open fractures, only a few healed fractures (HF) and spiders (S) can be seen in Fig. D. The dark areas indicated by arrows in Fig. D are overgrowth.

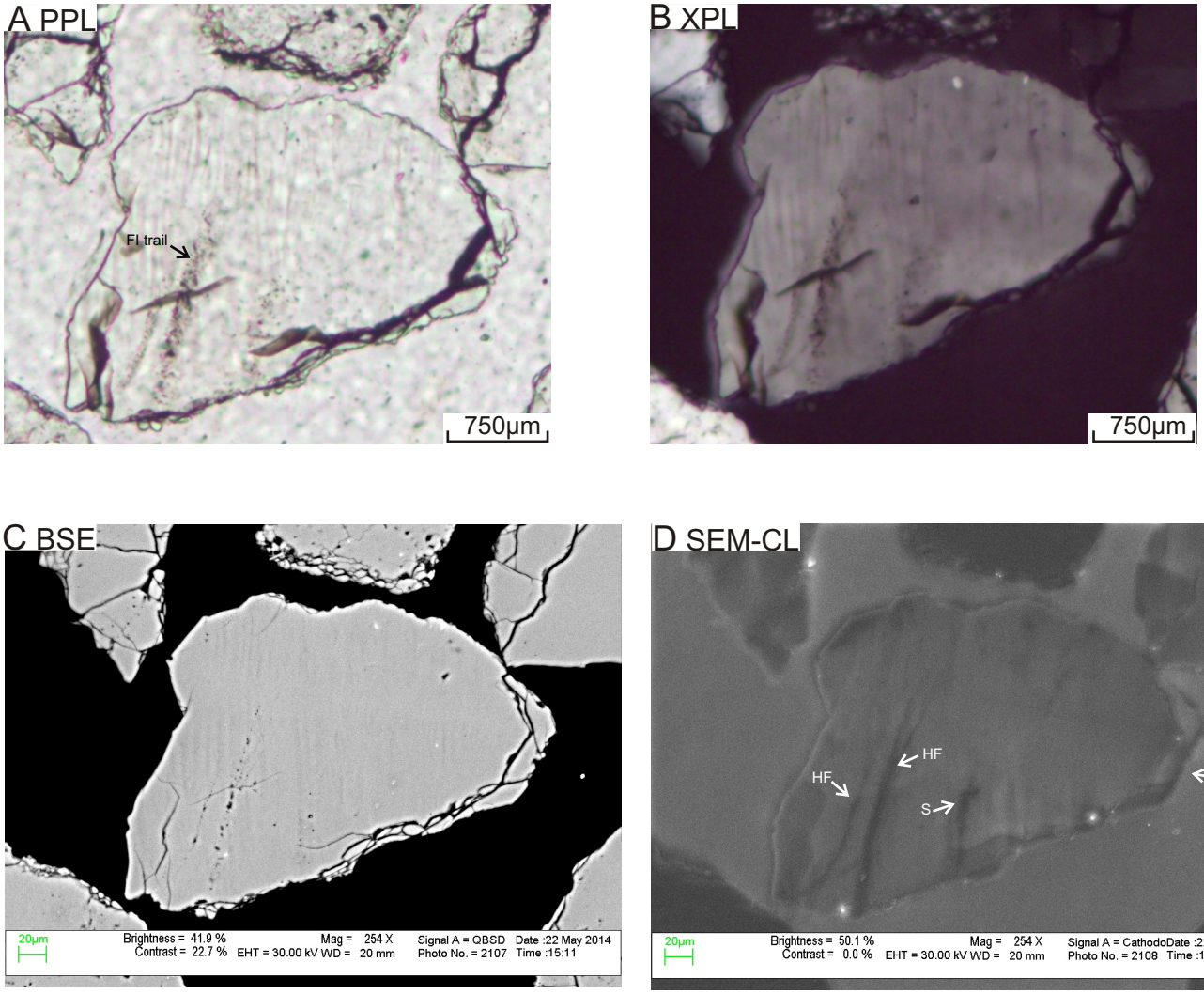

Figure 3A-6: Microphotos under ppl (A) and xpl (B), SEM-BSE image (C), SEM-CL image (D), and EDS analyses table (E) of quartz grain 6 in sample 2995. The grain is anhedral and sub-angular monocrystalline with deformation lamellae, mosaic texture, and strong undulose extinction. Fluid inclusions are common; they usually form trails (FI trail) along healed fractures (Fig. A). The grain is microfractured with a set of parallel fractures and a set of irregular fractures (Fig. C and D). Some healed fractures (HF) and spiders (S) can be seen in Fig. D. The dark area indicated by arrow in Fig. D is overgrowth.

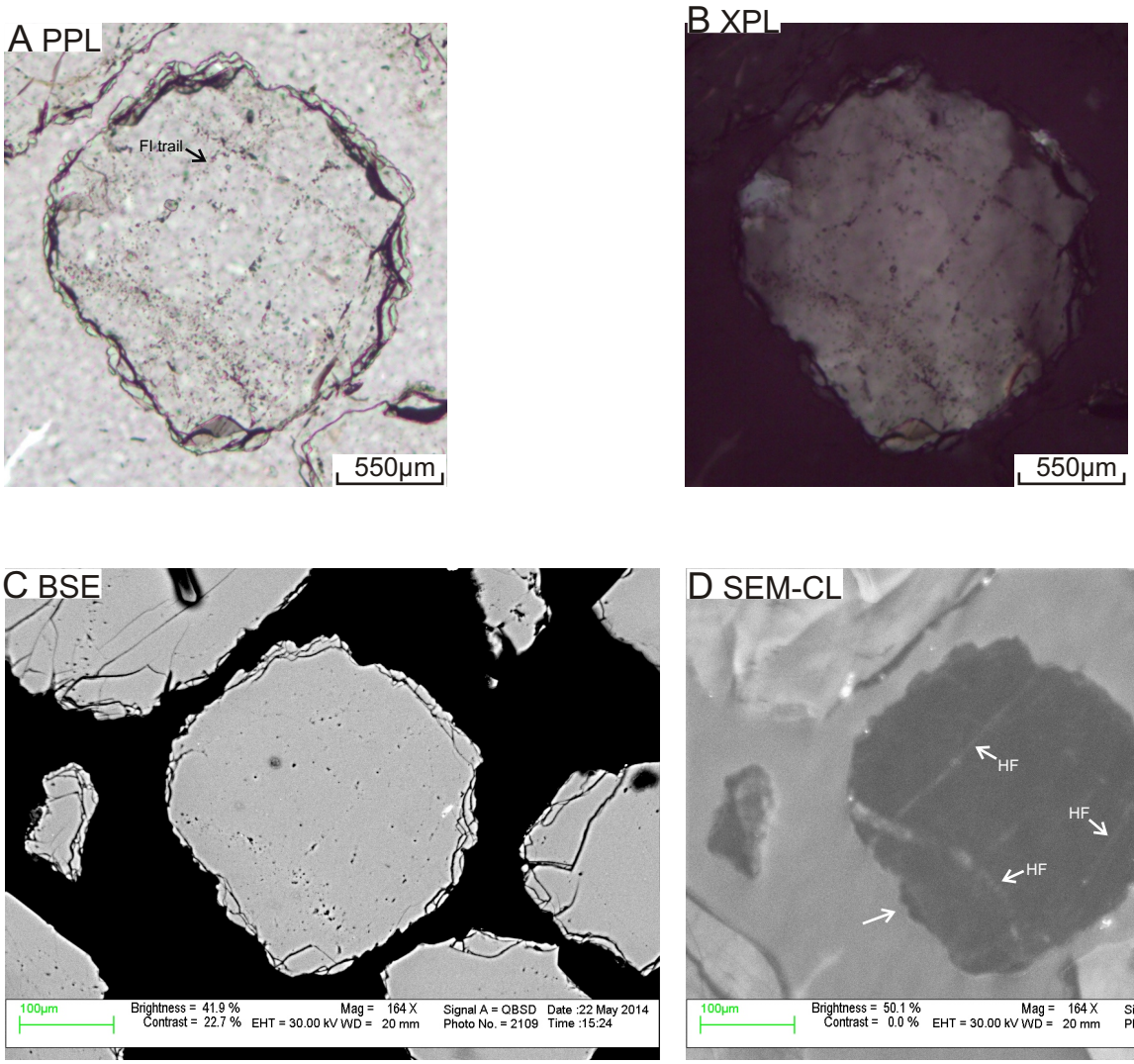

Figure 3A-7: Microphotos under ppl (A) and xpl (B), SEM-BSE image C, and SEM-CL image (D) of quartz grain 7 in sample 2995. The grain is subhedral and sub-rounded polycrystalline (only 2 sub-grains) with irregular margins, mosaic texture, and weak undulose extinction. Fluid inclusions are common; they are usually associated with secondary porosity and form trails (FI trail) along healed fractures (Fig. A). The grain is microfractured with a set of parallel fractures and a set of irregular fractures (Fig. C and D). Some healed fractures (HF) can be seen in Fig. D. The dark area indicated by arrow in Fig. D is overgrowth.



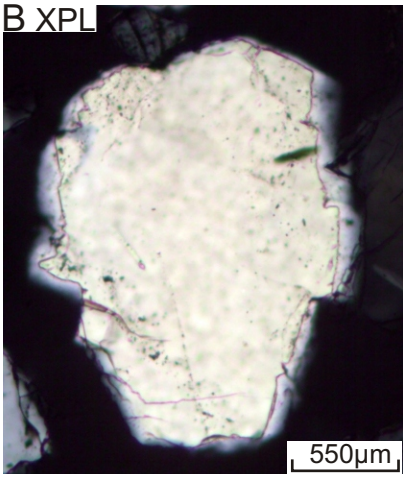

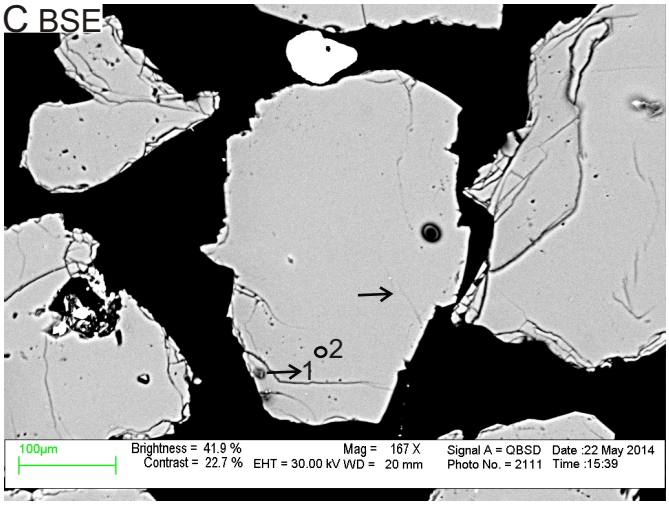

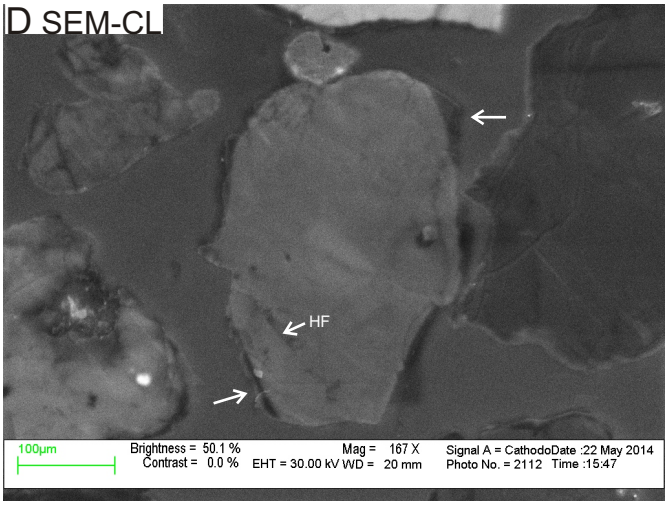

E EDS analyses

Pos#	Min. ID	SiO2	Cr2O3	Total	Actual total
1	Qz	98.32	1.68	100	116
2	Qz	99.99		100	140

Figure 3A-8: Microphotos under ppl (A) and xpl (B), SEM-BSE image (C), SEM-CL image (D), and EDS analyses table (E) of quartz grain 8 in sample 2995. The grain is subhedral and sub-angular monocrystalline with mosaic texture and weak undulose extinction. Fluid inclusions are common; they usually form trails (FI trail) along healed fractures (Fig. A). The grain is microfractured with a set of irregular fractures (Fig. C and D). Only a few healed fractures (HF) can be seen in Fig. D. The dark area indicated by arrow in Fig. D is overgrowth.

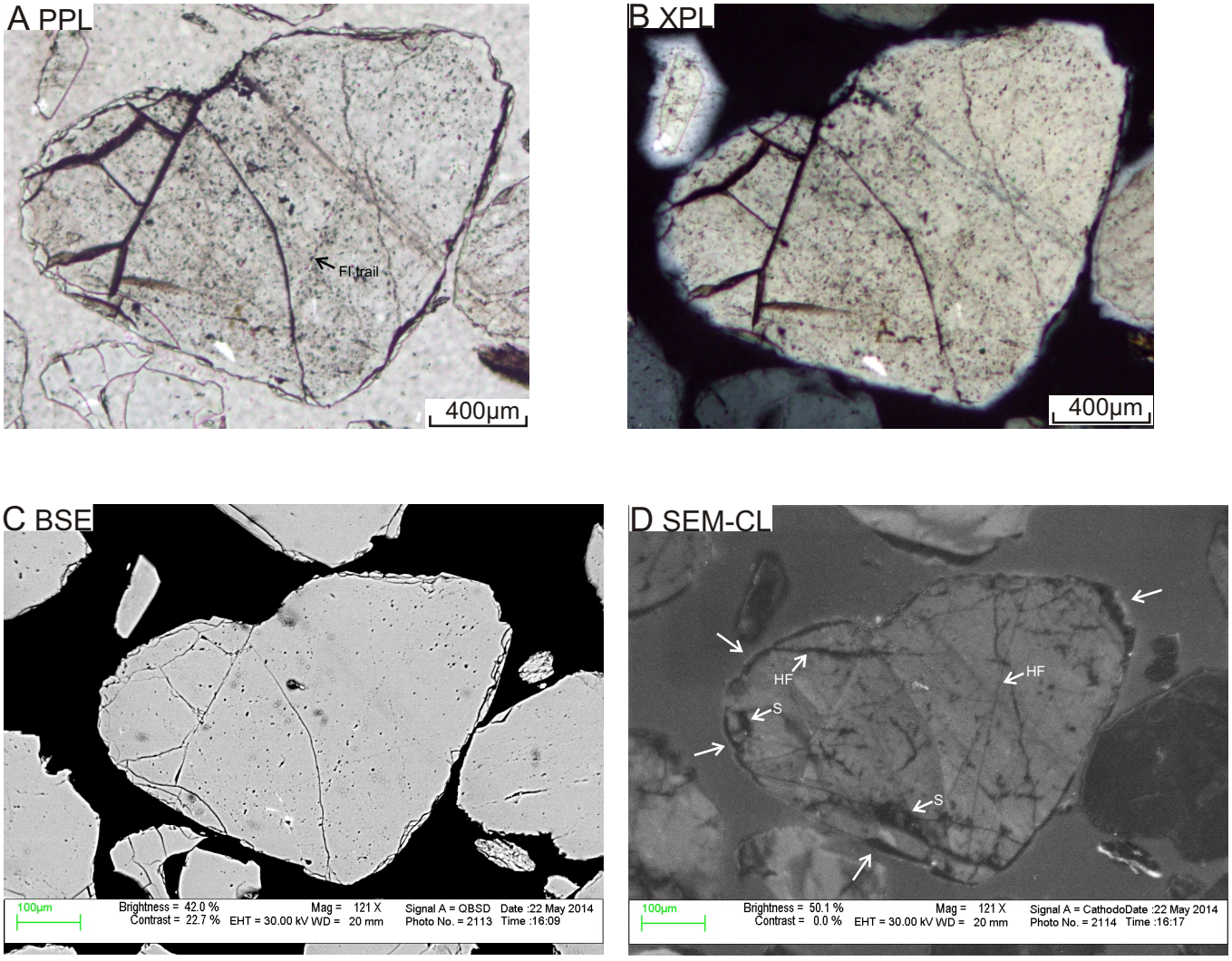

Figure 3A-9: Microphotos under ppl (A) and xpl (B), SEM-BSE image C, and SEM-CL image (D) of quartz grain 9 in sample 2995. The grain is anhedral and rounded monocrystalline with weak undulose extinction. Fluid inclusions are common; they usually are associated with secondary porosity and form trails (FI trail) along healed fractures (Fig. A). The grain is microfractured with sets of irregular fractures (Fig. C and D). Healed fractures (HF) and spiders (S) are common (Fig. D). The dark areas indicated by arrows in Fig. D are overgrowth; these areas appear corroded in Fig. C, sugesting secondary porosity.

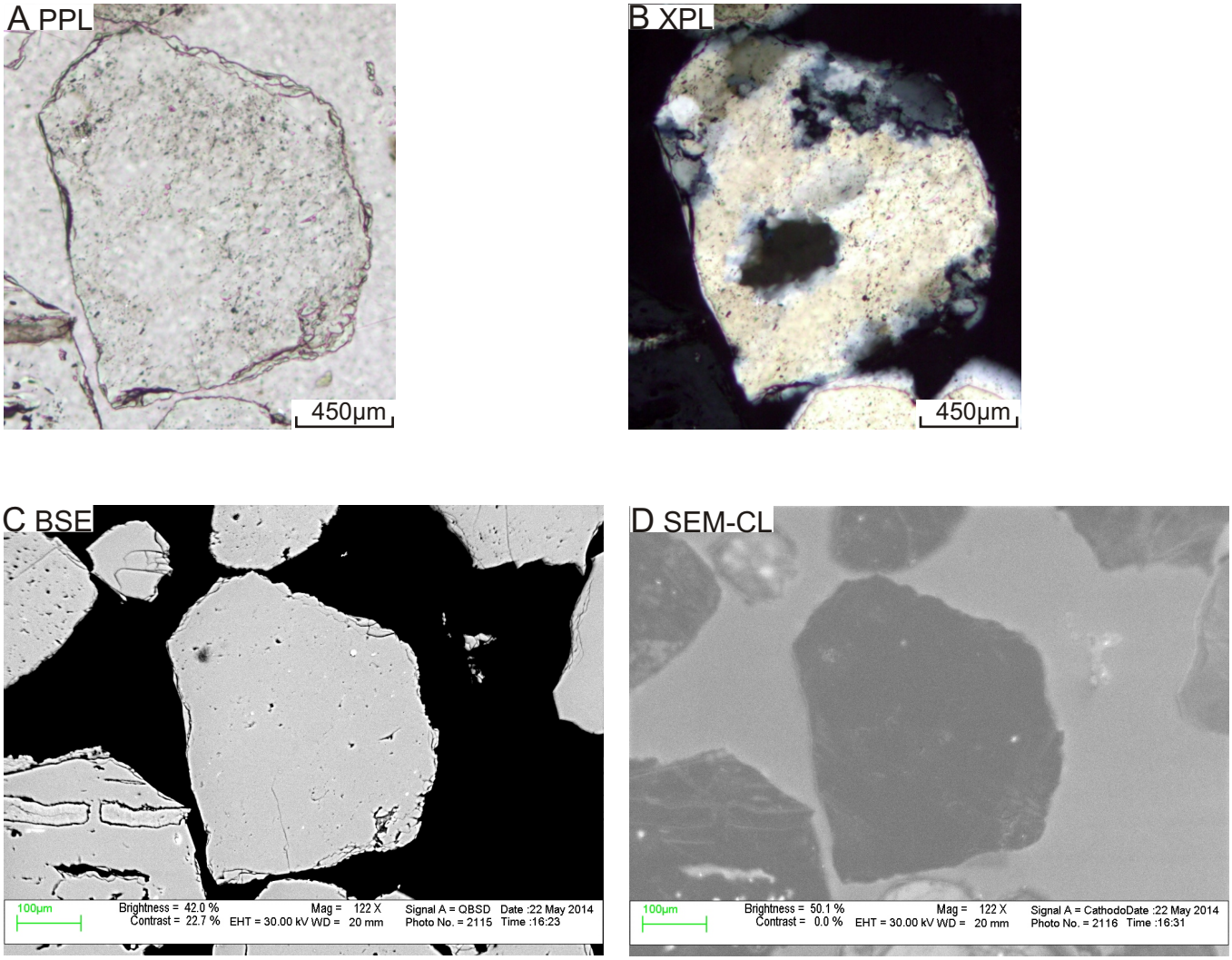

Figure 3A-10: Microphotos under ppl (A) and xpl (B), SEM-BSE image C, and SEM-CL image (D) of quartz grain 10 in sample 2995. The grain is subhedral and sub-rounded polycrystalline (more than 10 sub-grains, some with sutured sub-grain boundaries) with mosaic texture and weak undulose extinction. Fluid inclusions are rare, and the grain is weakly microfractured.

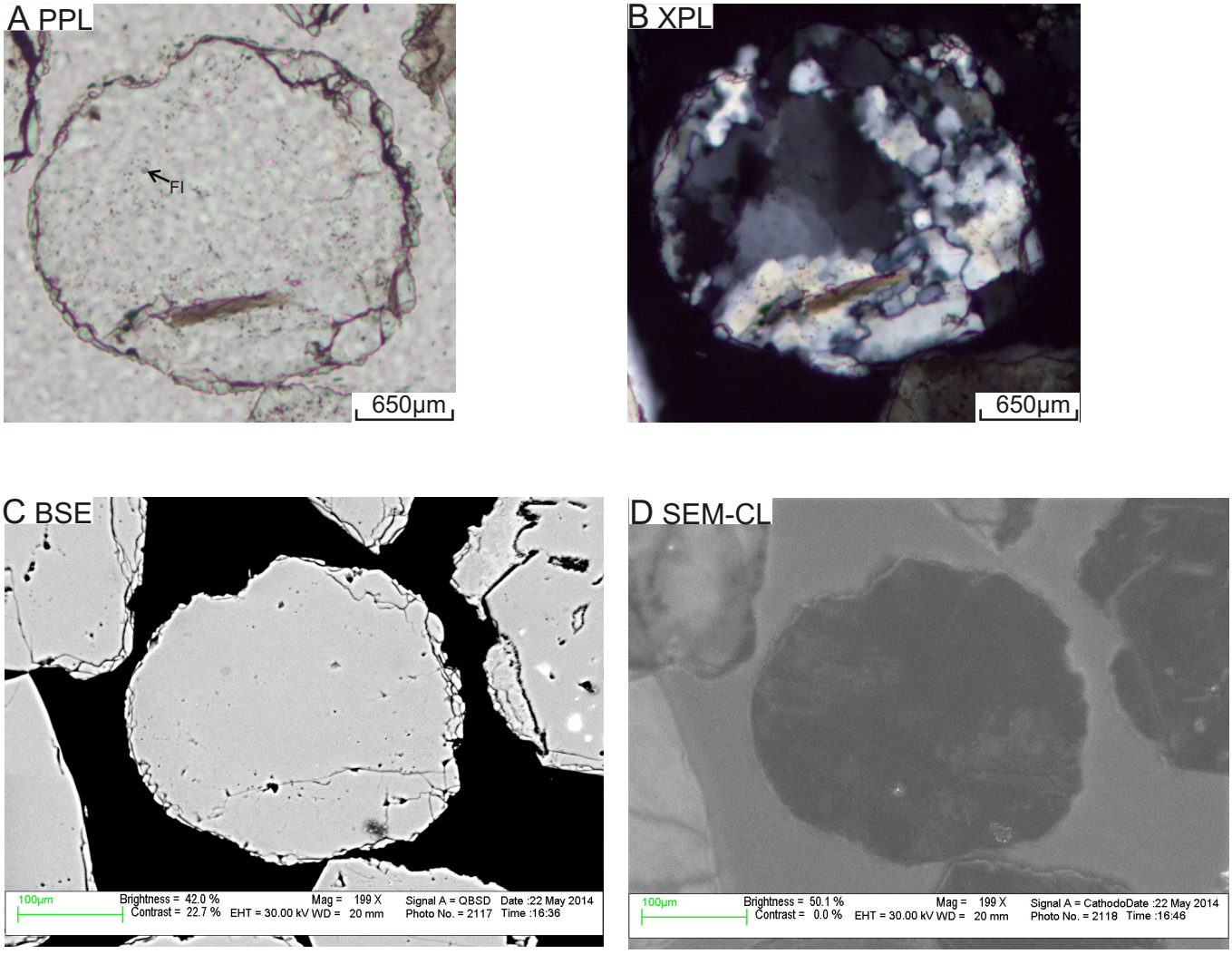

Figure 3A-11: Microphotos under ppl (A) and xpl (B), SEM-BSE image (C) and SEM-CL image (D) of quartz grain 11 in sample 2995. This grain is a rhyolite clast. The grain is subhedral and rounded polycrystalline (more than 10 sub-grains with sutured sub-grain boundaries) withmosaic texture and weak undulose extinction. Fluid inclusions (FI) are present (Fig. A). The grain is microfractured with irregular fractures (Fig. D). Healed fractures are rare.

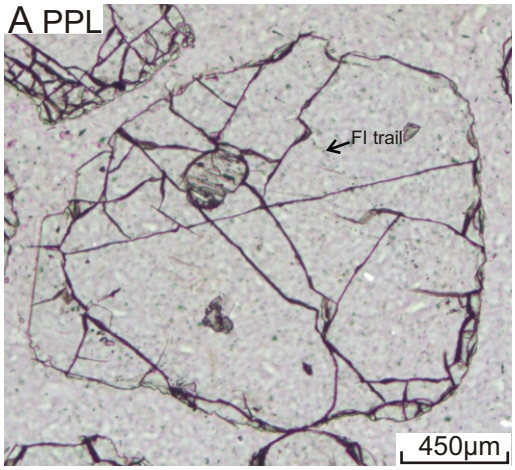

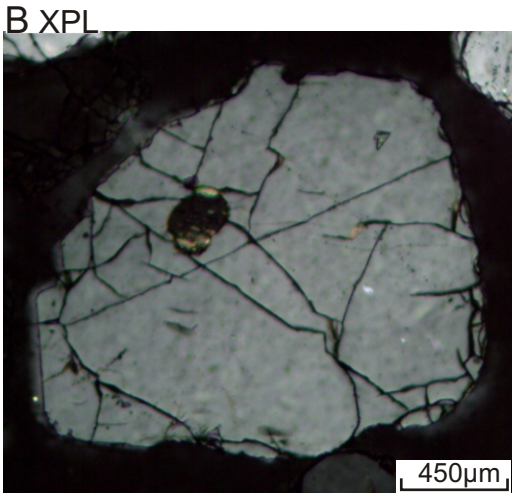

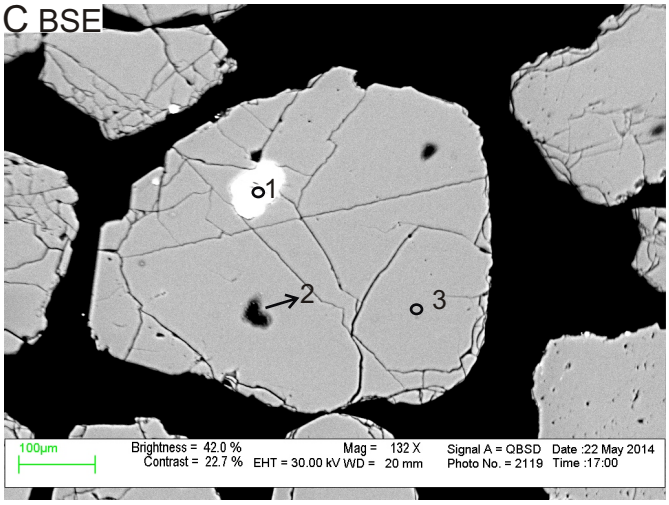

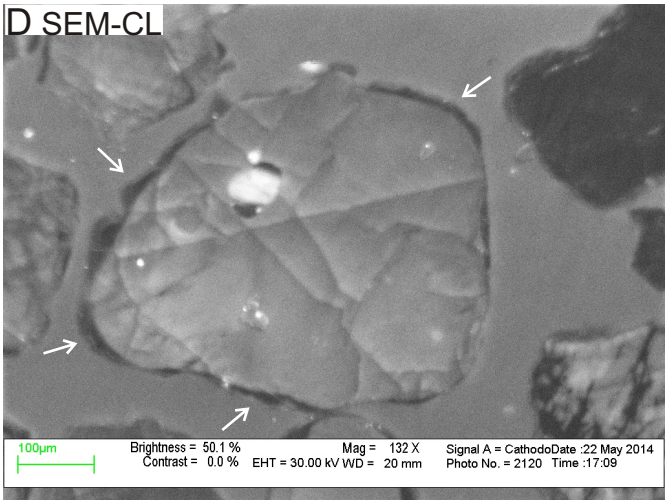

E EDS analyses

Pos#	Min. ID	SiO2	Al2O3	FeO	CaO	Na2O	K2O	SO3	Cl	Total	Actual total
1	Kfs	63.23	17.67	2.61	0.81	0.54	15.13			100	113
2	Qz	96.29				1.46	0.58	0.87	0.82	100	98
3	Qz	99.99								100	134

Figure 3A-12: Microphotos under ppl (A) and xpl (B), SEM-BSE image (C), SEM-CL image (D), and EDS analyses table (E) of quartz grain 12 in sample 2995. The grain is subhedral and sub-rounded monocrystalline with non-undulose extinction. Fluid inclusions are present, some of them form trails (Fig. A). The grain contains K-feldspar inclusion and is microfractured with a set of irregular fractures (Fig. C and D). Healed fractures are rare, most of the fractures in Fig. D are open fractures. The areas indicated by arrows in Fig. D are overgrowth; these areas appear corroded in Fig. C, suggesting secondary porosity.

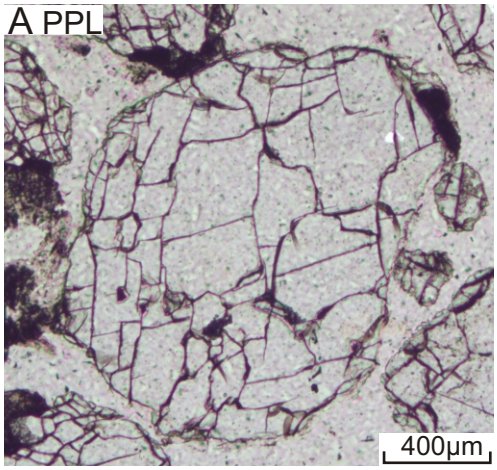

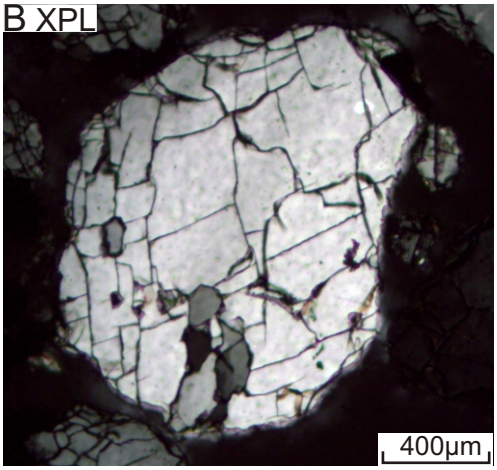

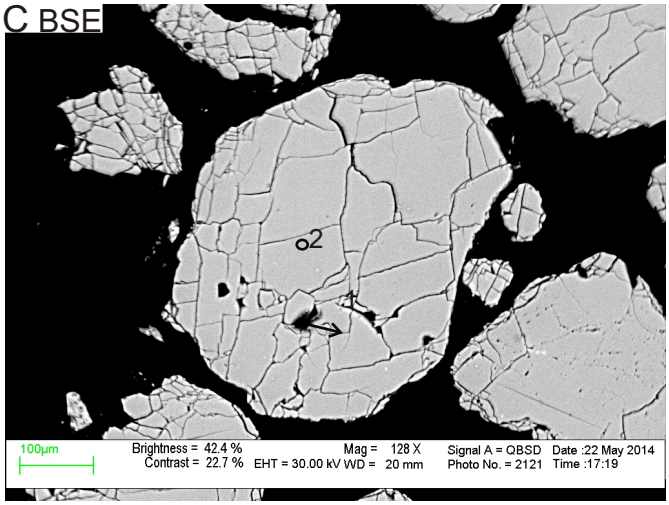

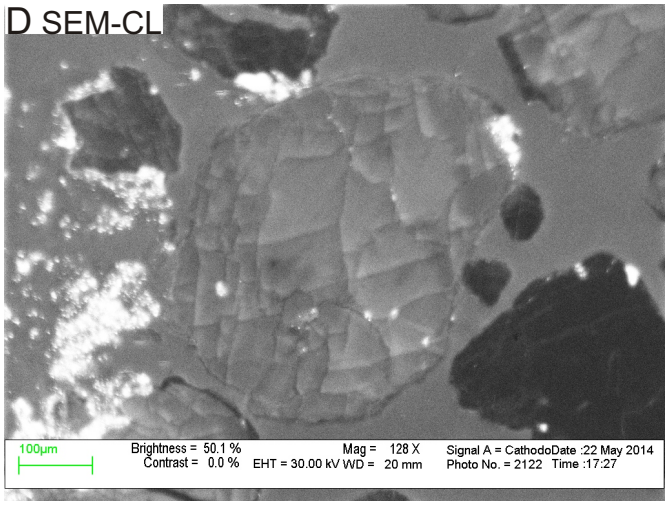

E EDS analyses

Pos#	Min. ID	SiO2	CaO	Na2O	SO3	Cl	Total	Actual total
1	Hole	96.18	0.38	0.4	2.65	0.39	100	87
2	Qz	99.99					100	129

Figure 3A-13: Microphotos under ppl (A) and xpl (B), SEM-BSE image (C), SEM-CL image (D), and EDS analyses table (E) of quartz grain 13 in sample 2995. The grain is subhedral and sub-rounded polycrystalline (more than 5 sub-grains with sutured sub-grain boundaries) with strong undulose extinction. Fluid inclusions are rare. The grain is strongly microfractured with sets of irregular fractures (Fig. C and D). Healed fractures are rare, most of the fractures in Fig. D are open fractures.

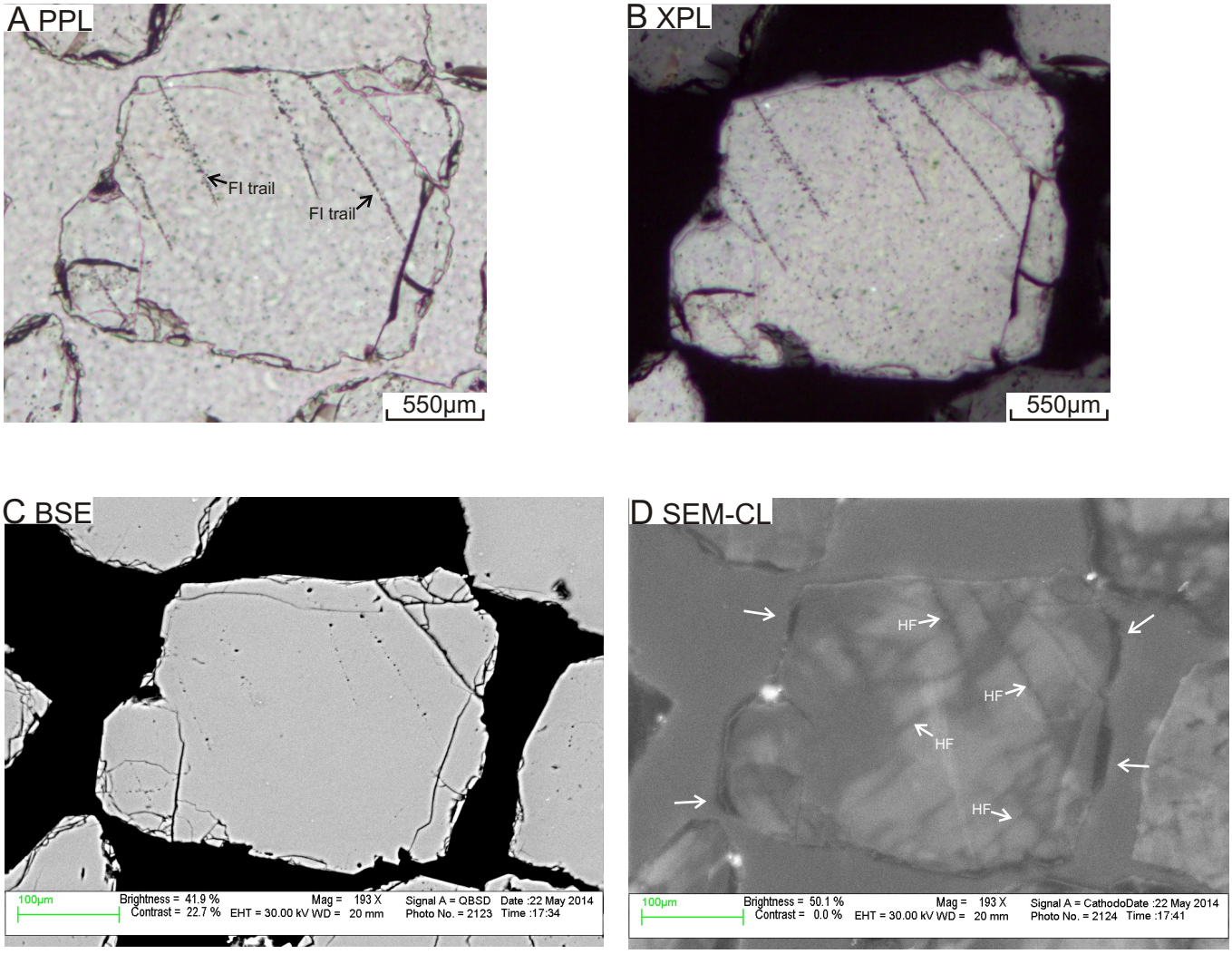

Figure 3A-14: Microphotos under ppl (A) and xpl (B), SEM-BSE image C, and SEM-CL image (D) of quartz grain 14 in sample 2995. The grain is subhedral and sub-rounded polycrystalline (only 2 sub-grains) with strong undulose extinction. Fluid inclusions are common; they usually form trails along healed fractures (Fig. A). The grain is microfractured with two distinct sets of parallel fractures crosscutting each other and a set of irregular fractures (Fig. C and D). Some healed fractures (HF) can be seen in Fig. D. The areas indicated by arrows in Fig. D are overgrowth; these areas appear corroded in Fig. C, suggesting secondary porosity. The grain shows bright streaky patches in SEM-CL image.

A PPL

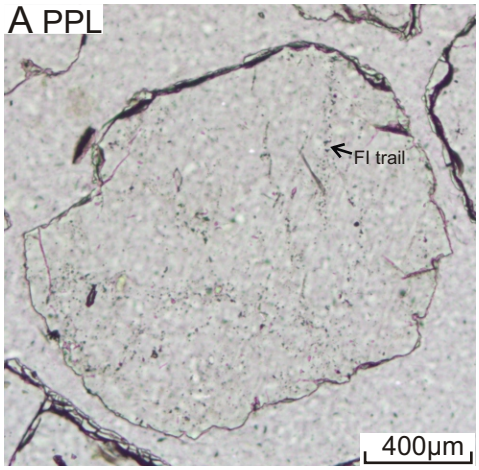

B XPL

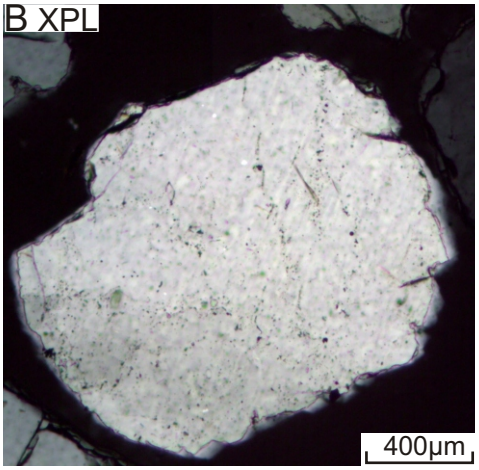

C BSE

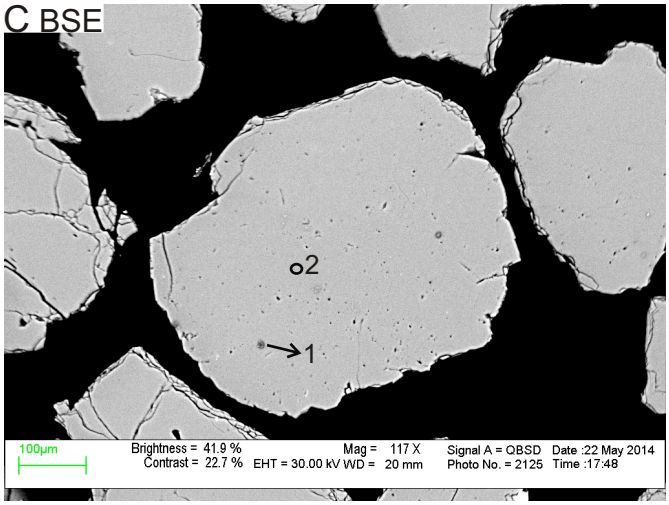

D SEM-CL

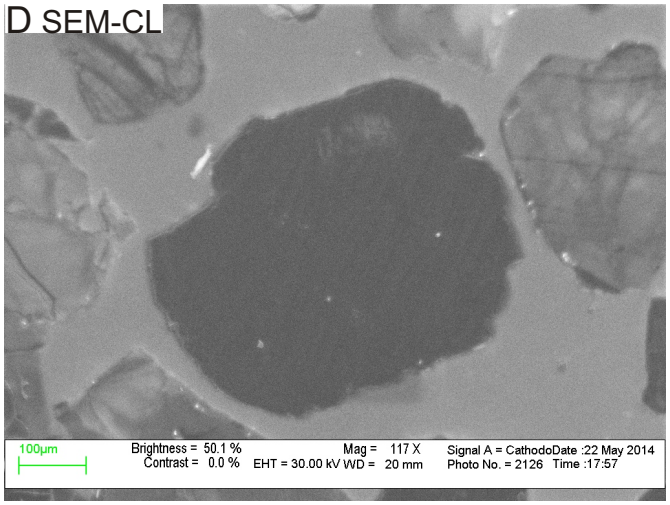

E EDS analyses

Pos#	Min. ID	SiO2	Na2O	Cl	Total	Actual total
1	Qz	98.85	0.7	0.44	100	114
2	Qz	99.99			100	136

Figure 3A-15: Microphotos under ppl (A) and xpl (B), SEM-BSE image (C), SEM-CL image (D), and EDS analyses table (E) of quartz grain 15 in sample 2995. The grain is subhedral and sub-rounded monocrystalline with mosaic texture and weak undulose extinction. Fluid inclusions are present and usually form trails (Fig. A). The grain is weakly microfractured with irregular fractures (Fig. C). The grain shows homogenous dark-Cl in SEM-CL image; therefore, healed fractures cannot be seen in Fig. D.

A PPL

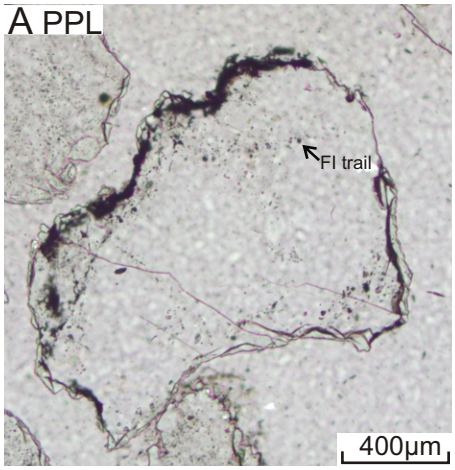

B XPL

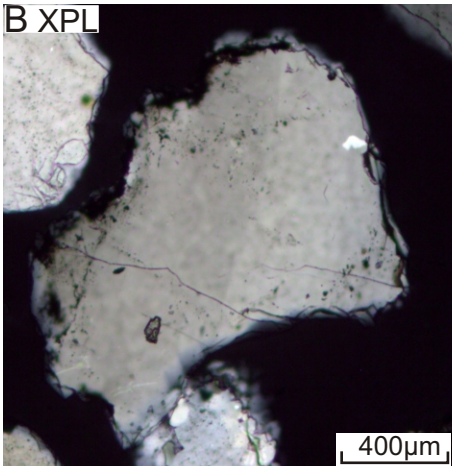

C BSE

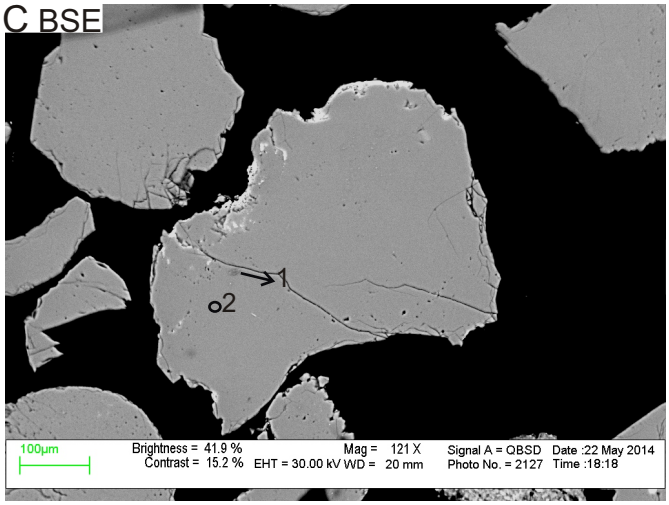

D SEM-CL

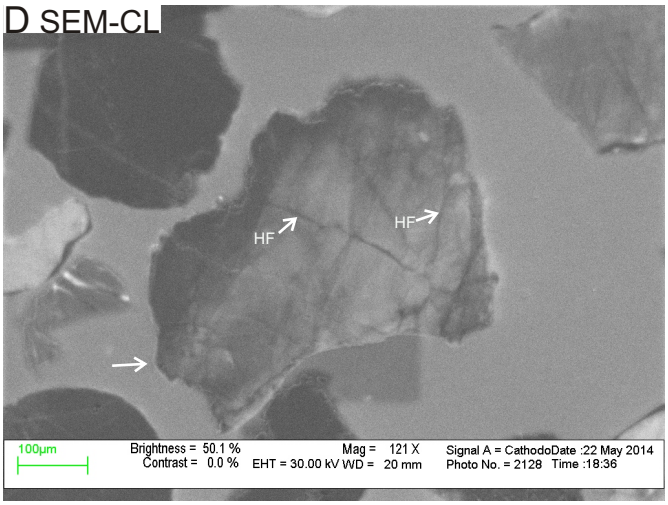

E EDS analyses

Pos#	Min. ID	SiO2	Cr2O3	Total	Actual total
1	Qz	99.54	0.47	100	133
2	Qz	99.99		100	141

Figure 3A-16: Microphotos under ppl (A) and xpl (B), SEM-BSE image (C), SEM-CL image (D), and EDS analyses table (E) of quartz grain 16 in sample 2995. The grain is anhedral and sub-angular monocrystalline with strong undulose extinction. Fluid inclusions are common; they usually form trails along fractures (Fig. A). The grain is microfractured with a set of irregular fractures (Fig. C and D). Some healed fractures (HF) can be seen in Fig. D. The dark area indicated by arrow in Fig. D is overgrowth.

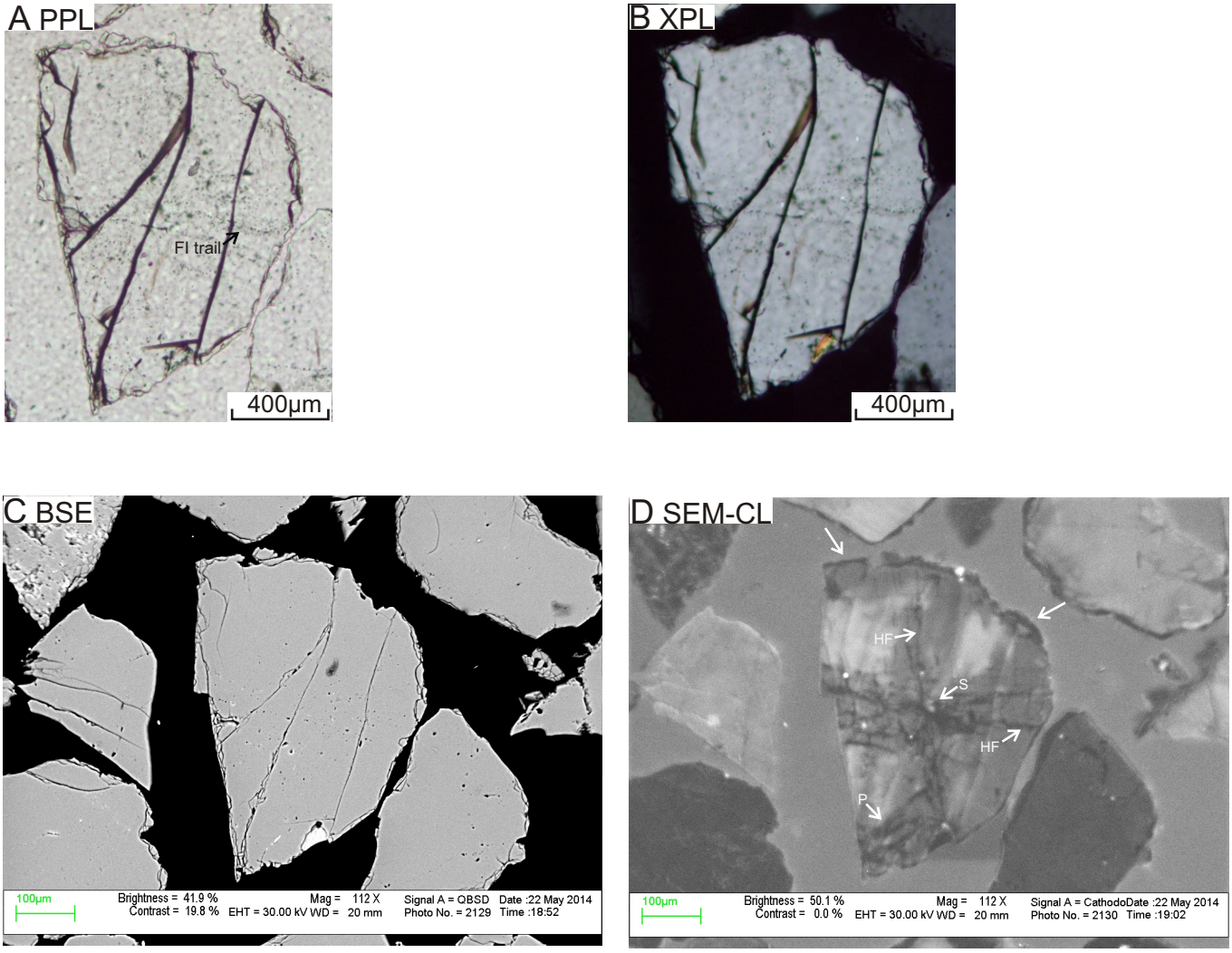

Figure 3A-17: Microphotos under ppl (A) and xpl (B), SEM-BSE image C, and SEM-CL image (D) of quartz grain 17 in sample 2995. The grain is anhedral and sub-angular monocrystalline with weak undulose extinction. Fluid inclusions are common; they usually form trails along healed fractures (Fig. A). The grain is microfractured with a set of sub-parallel fractures and a set of irregular fractures (Fig. C and D). Healed fractures (HF) and spiders (S) are common (Fig. D). The areas indicated by arrows in Fig. D are overgrowth; these areas appear corroded in Fig. C, suggesting secondary porosity. The grain shows random bright-CL patches in SEM-CL image.

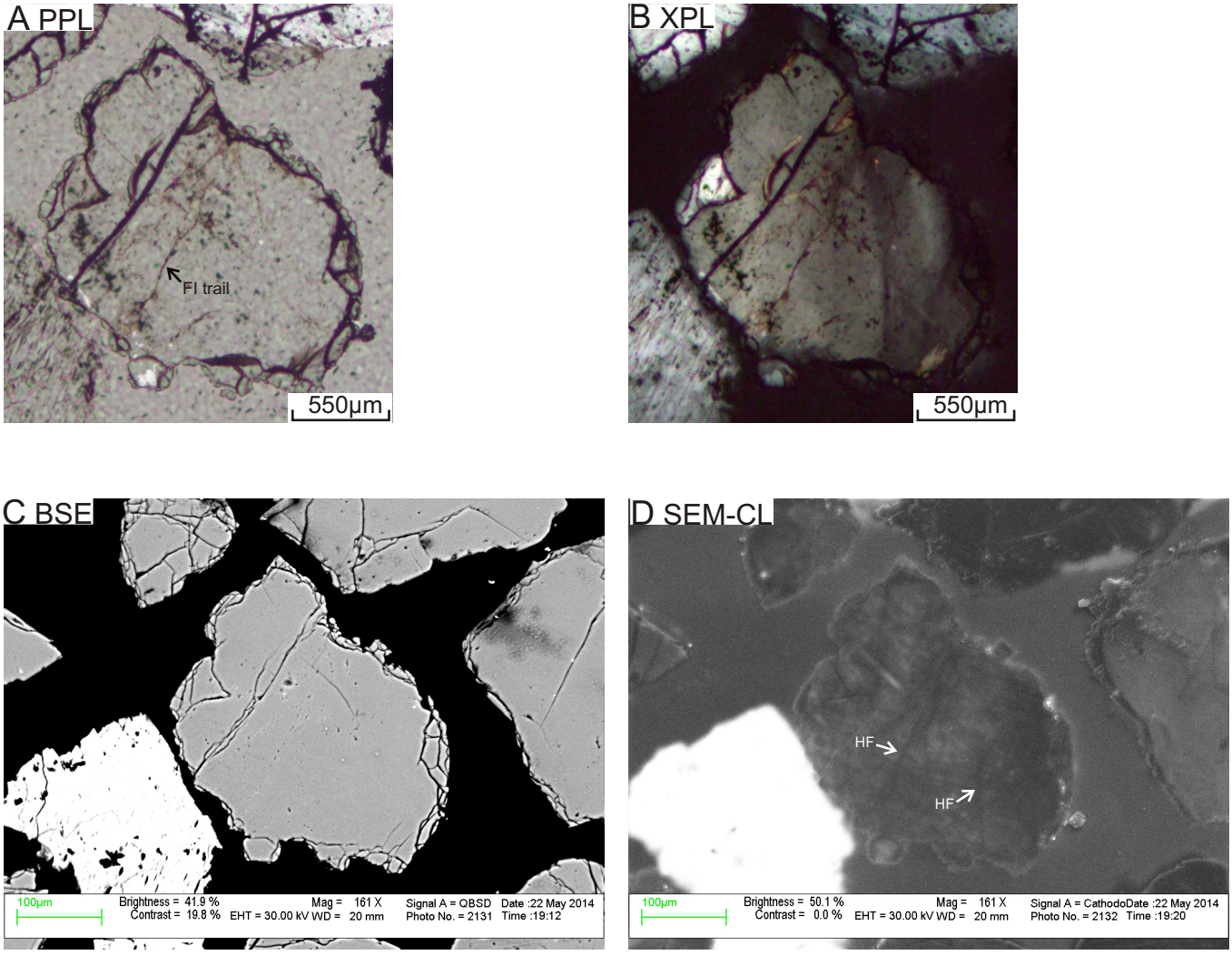

Figure 3A-18: Microphotos under ppl (A) and xpl (B), SEM-BSE image C, and SEM-CL image (D) of quartz grain 18 in sample 2995. The grain is anhedral and angular monocrystalline with strong undulose extinction. Fluid inclusions are present, some form trail along fractures (Fig. A). The grain is microfractured with a set of irregular fractures (Fig. C and D). Some healed fractures (HF) can be seen in Fig. D. The grain shows subtle bright mottling texture in SEM-CL image.

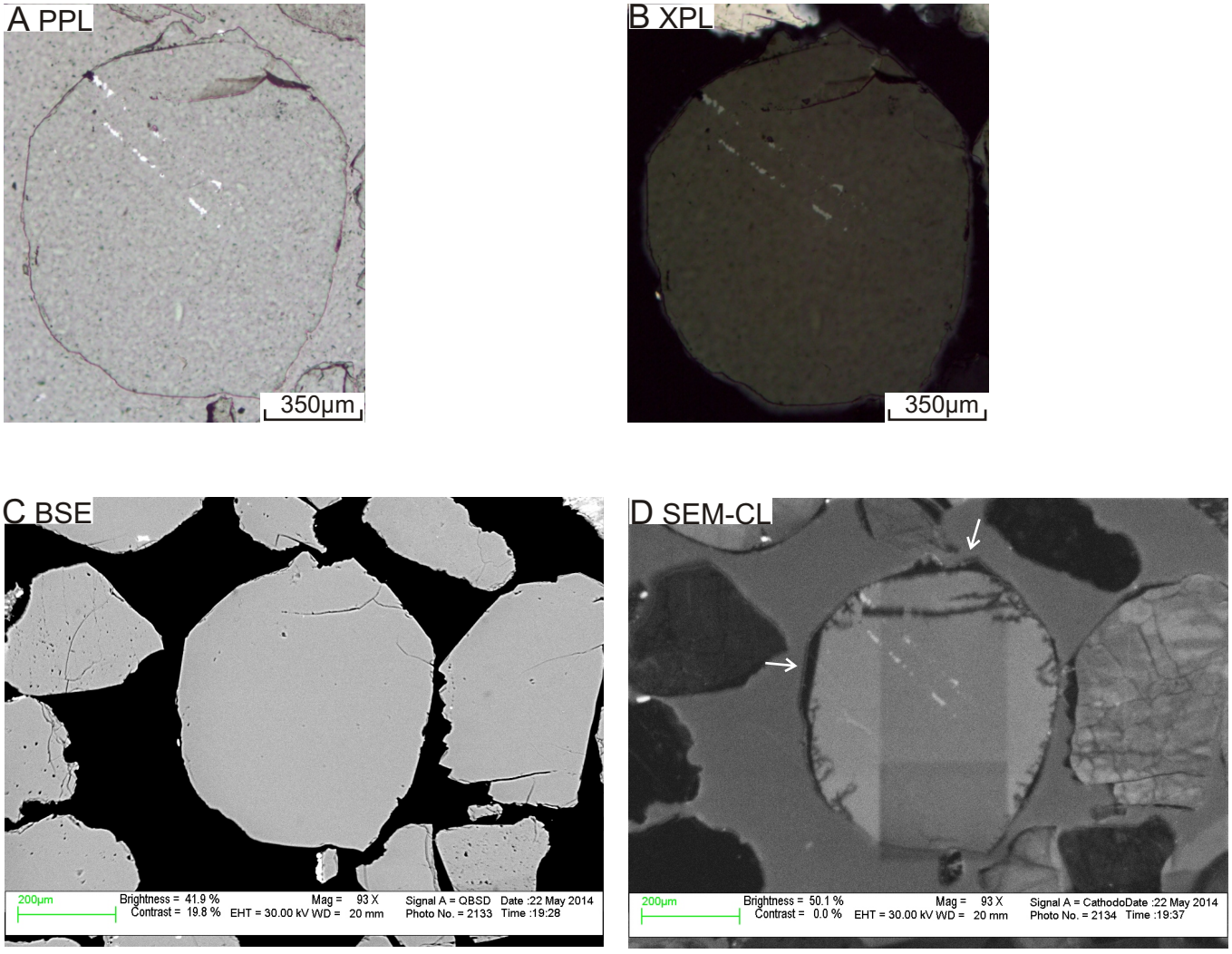

Figure 3A-19: Microphotos under ppl (A) and xpl (B), SEM-BSE image C, and SEM-CL image (D) of quartz grain 19 in sample 2995. The grain is subhedral and well-rounded monocrystalline with non-undulose extinction. Fluid inclusions are rare. The grain is weakly microfractured with only a few irregular curved open fractures (Fig. C and D). Healed fractures are rare. The areas indicated by arrows in Fig. D are overgrowth; these areas appear corroded in Fig. C, suggesting secondary porosity.

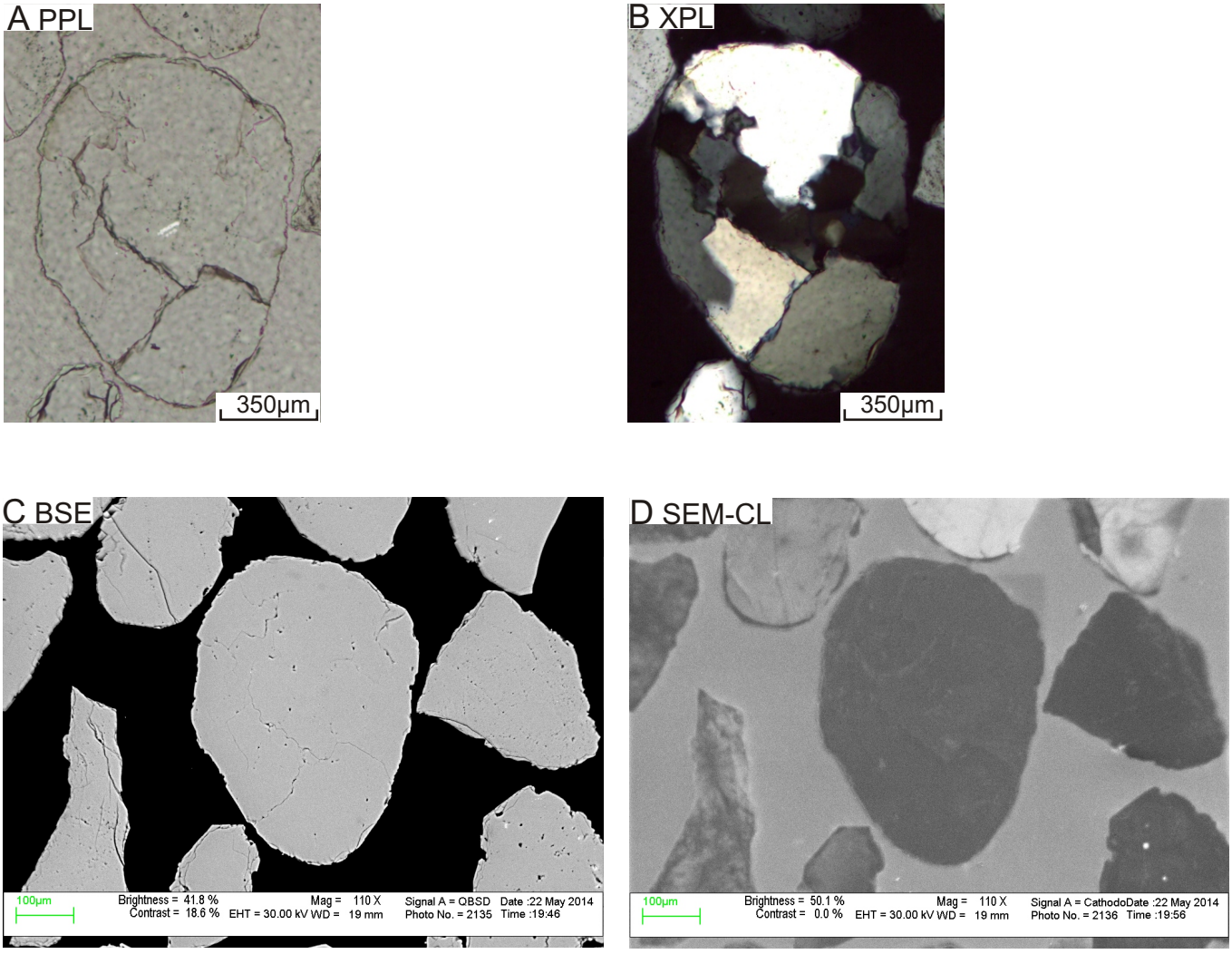

Figure 3A-20: Microphotos under ppl (A) and xpl (B), SEM-BSE image C, and SEM-CL image (D) of quartz grain 20 in sample 2995. The grain is subhedral and well-rounded polycrystalline (more than 6 sub-grains with sutured sub-grain boundaries) with mosaic texture and weak undulose extinction. Fluid inclusions are rare. The grain is weakly microfractured with only a few irregular curved open fractures (Fig. C and D). Healed fractures are rare.

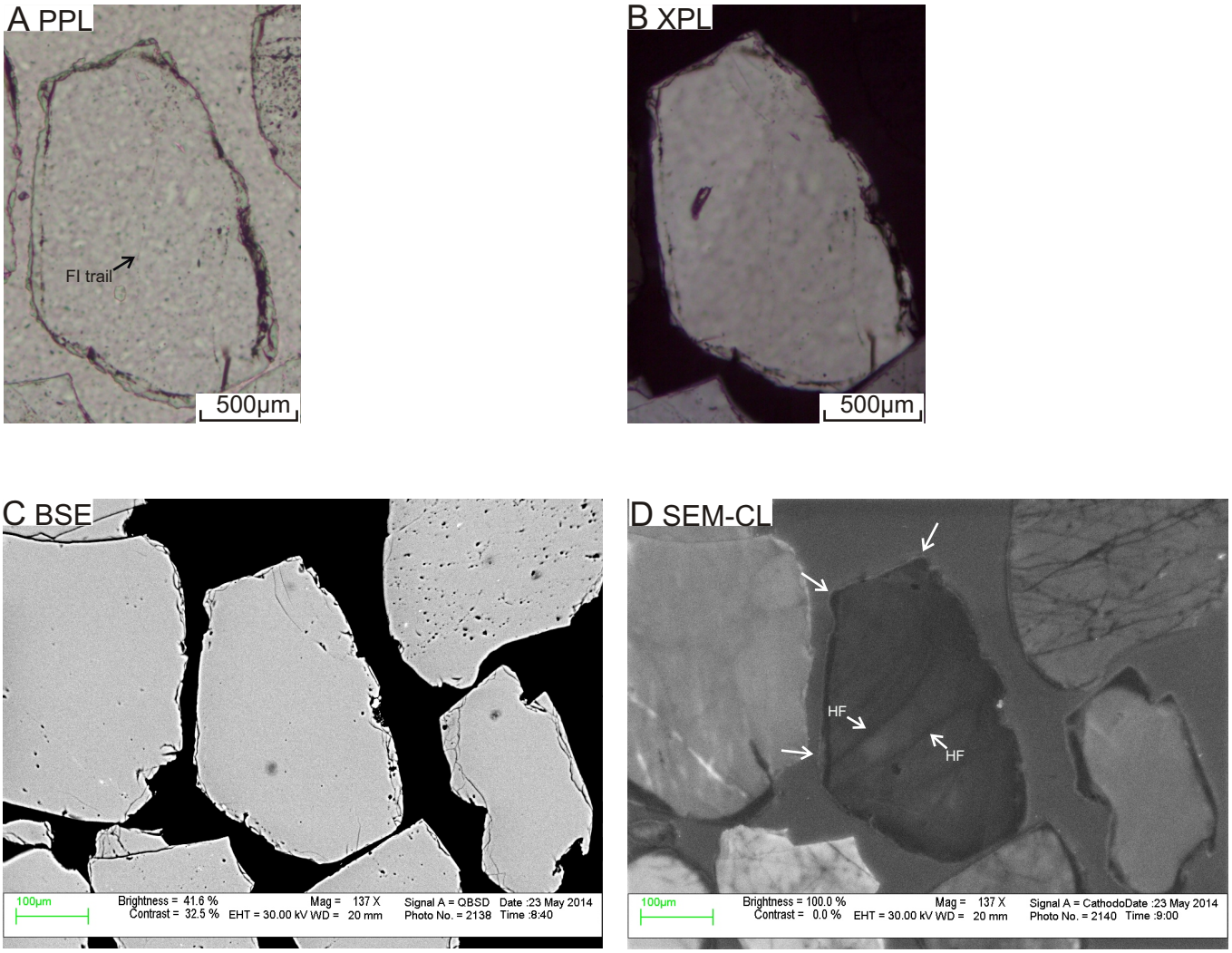

Figure 3A-21: Microphotos under ppl (A) and xpl (B), SEM-BSE image C, and SEM-CL image (D) of quartz grain 21 in sample 2995. The grain is subhedral and sub-rounded monocrystalline with strong undulose extinction. Fluid inclusion trails are present, they are located at boundaries between detrital quartz and the overgrowth. The grain is weakly microfractured with a set of sub-parallel fractures (Fig. D). Some healed fractures (HF) can be seen in Fig. D. The dark areas indicated by arrows in Fig. D are overgrowth.

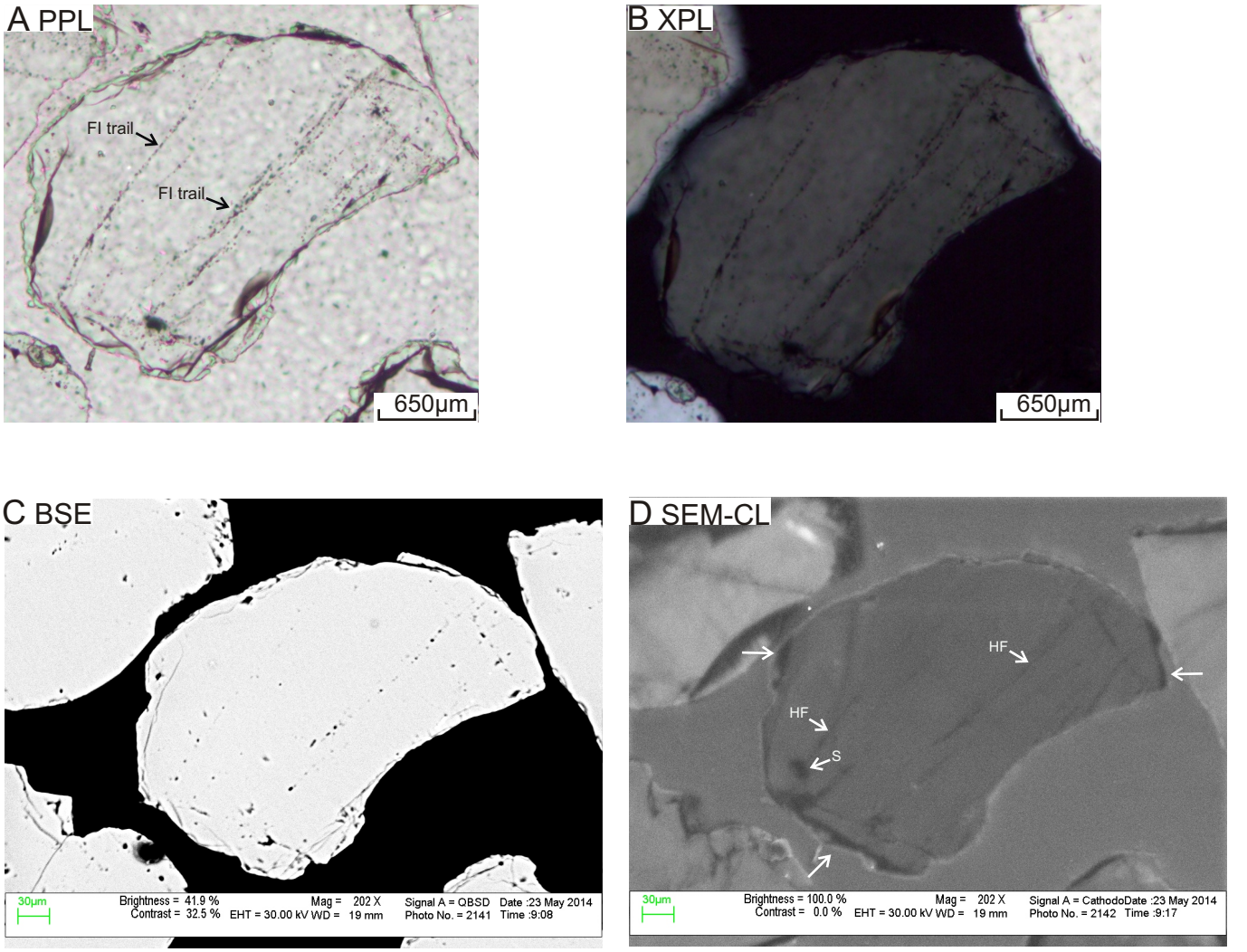

Figure 3A-22: Microphotos under ppl (A) and xpl (B), SEM-BSE image C, and SEM-CL image (D) of quartz grain 22 in sample 2995. The grain is anhedral and sub-rounded monocrystalline with non-undulose extinction. Fluid inclusions are common; they are usually associated with secondary porosity and form trails (FI trail) along healed fractures (Fig. A). The grain is microfractured with a set of parallel fractures and a set of irregular fractures (Fig. C and D). Some healed fractures (HF) and a few spiders (S) can be seen in Fig. D. The dark areas indicated by arrows in Fig. D are overgrowth.

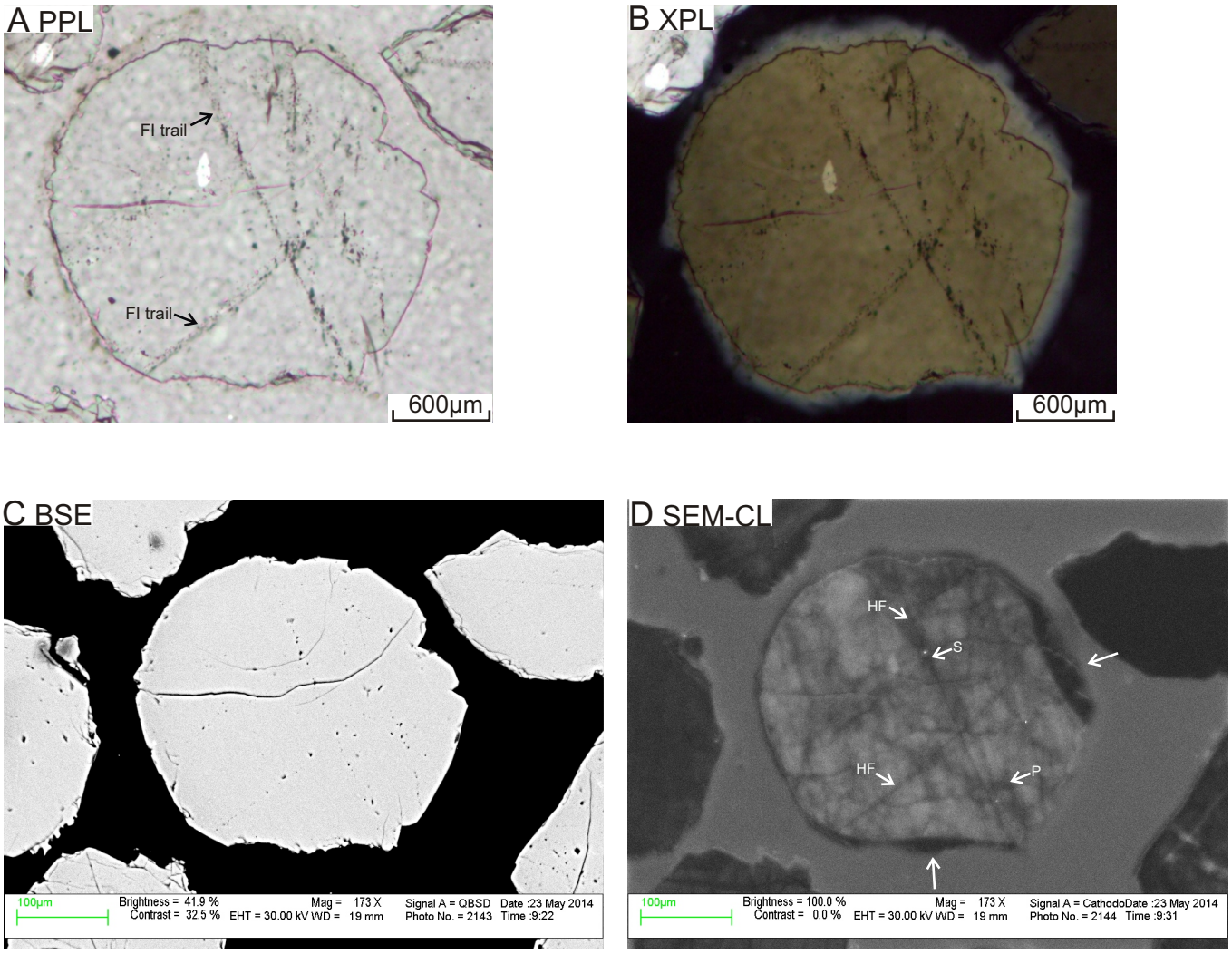

Figure 3A-23: Microphotos under ppl (A) and xpl (B), SEM-BSE image C, and SEM-CL image (D) of quartz grain 23 in sample 2995. The grain is subhedral and well-rounded monocrystalline with weak undulose extinction. Fluid inclusions are common; they are usually associated with secondary porosity and form trails (FI trail) along healed fractures (Fig. A). The grain is microfractured with a set of irregular fractures (Fig. C and D). Healed fractures (HF) and spiders (S) are common (Fig. D). The dark areas indicated by arrows in Fig. D are overgrowth; these areas appear corroded in Fig. C, suggesting secondary porosity.

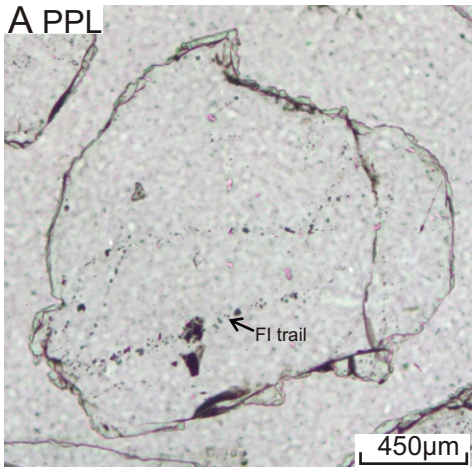

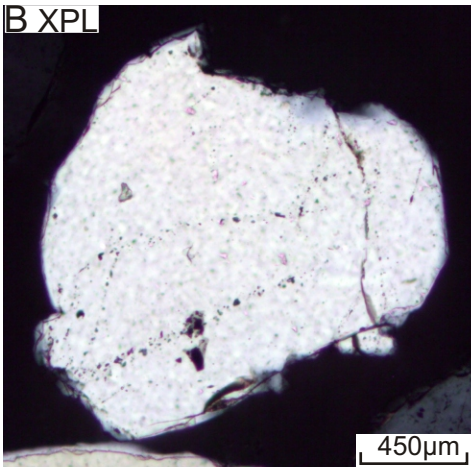

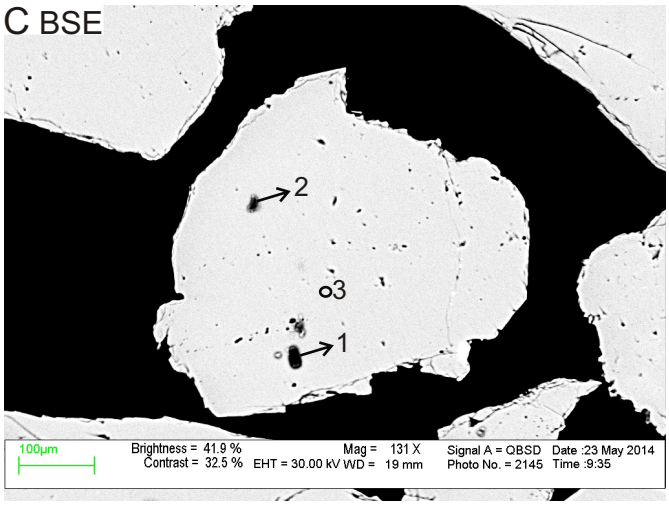

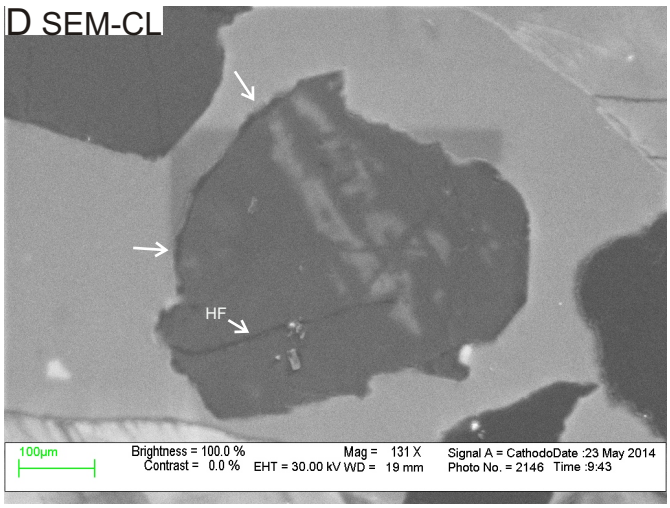

E EDS analyses

Pos#	Min. ID	SiO2	CaO	SO3	Cr2O3	ZnO	Total	Actual total
1	Hole	92.88		1.05	5.72	0.34	100	71
2	Qz	98.19	0.31	1.5			100	115
3	Qz	99.99					100	148

Figure 3A-24: Microphotos under ppl (A) and xpl (B), SEM-BSE image (C), SEM-CL image (D), and EDS analyses table (E) of quartz grain 24 in sample 2995. The grain is subhedral and sub-rounded polycrystalline (only a few sub-grains) with weak undulose extinction and deformation lamellae (Fig. B). Fluid inclusions are common; they are usually associated with secondary porosity and form trails (FI trail) along healed fractures (Fig. A). The grain is microfractured with a set of irregular fractures (Fig. C and D). A few healed fractures (HF) can be seen in Fig. D. The dark areas indicated by arrows in Fig. D are overgrowth; these areas appear corroded in Fig. C, suggesting secondary porosity. The grain shows bright-CL patches in SEM-CL image. Probably these patches are due to deformation, since they have the same orientation of the deformation lamellae in Fig. B.

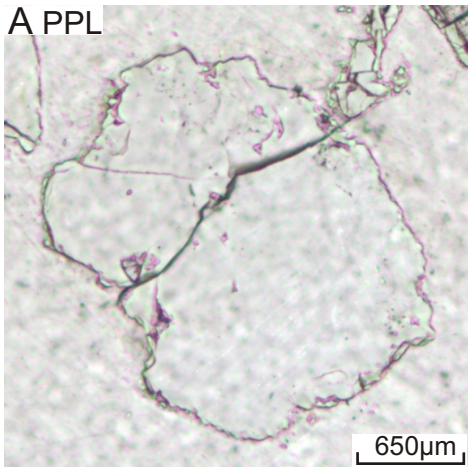

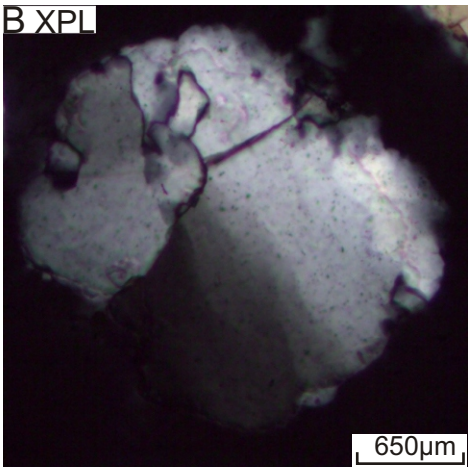

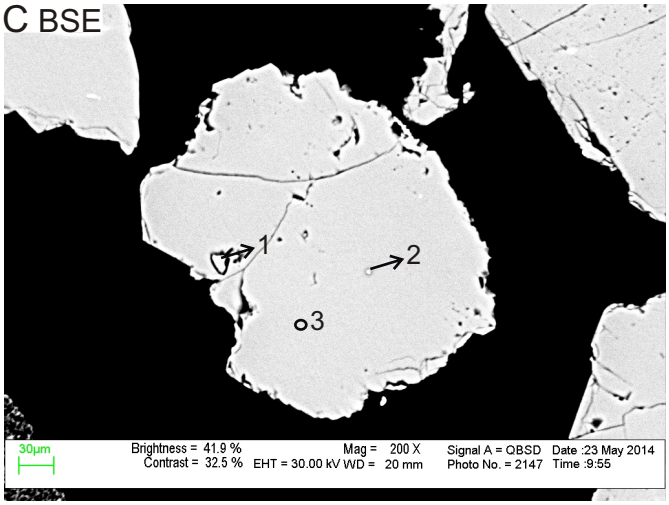

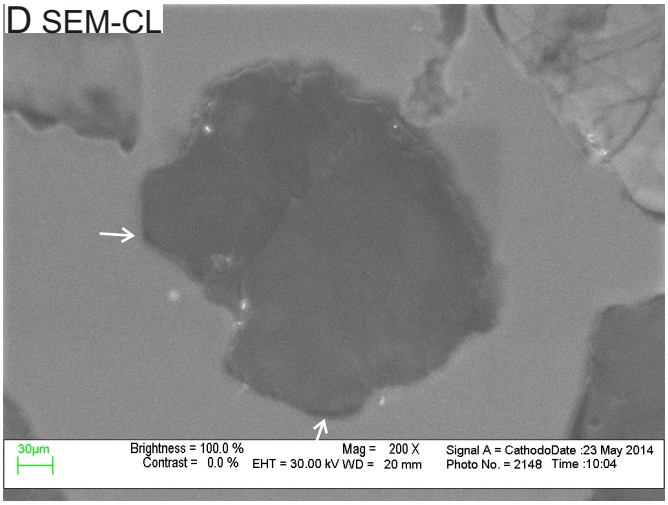

E EDS analyses

Pos#	Min. ID	SiO2	Total	Actual total
1	Qz	99.99	100	131
2	Qz	99.99	100	138
3	Qz	99.99	100	135

Figure 3A-25: Microphotos under ppl (A) and xpl (B), SEM-BSE image (C), SEM-CL image (D), and EDS analyses table (E) of quartz grain 25 in sample 2995. The grain is anhedral and sub-rounded polycrystalline (only a few sub-grains with sutured sub-grain boundaries) with mosaic texture and weak undulose extinction. Fluid inclusions are rare. The grain is weakly microfractured; healed fractures are rare. The dark areas indicated by arrows in Fig. D are overgrowth.

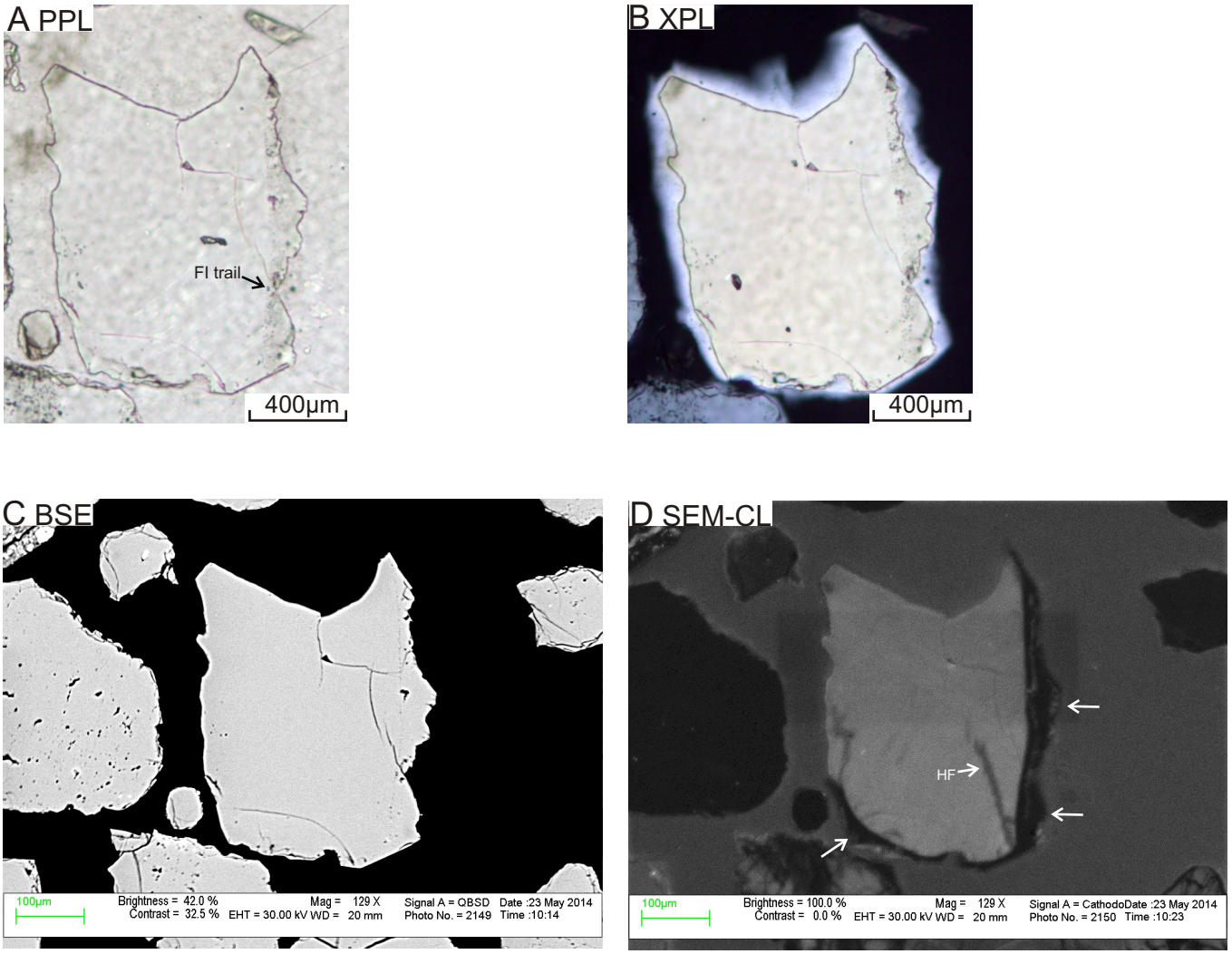

Figure 3A-26: Microphotos under ppl (A) and xpl (B), SEM-BSE image C, and SEM-CL image (D) of quartz grain 26 in sample 2995. The grain is anhedral and angular monocrystalline with strong undulose extinction. Fluid inclusions are present; they form trails at the boundary between the detritral quartz and the overgrowth (Fig. A). The grain is weakly microfractured with a set of irregular fractures (Fig. C and D). Only a few healed fractures (HF) can be seen in Fig. D. The dark areas indicated by arrows in Fig. D are overgrowth; these areas appear corroded in Fig. C, suggesting secondary porosity.

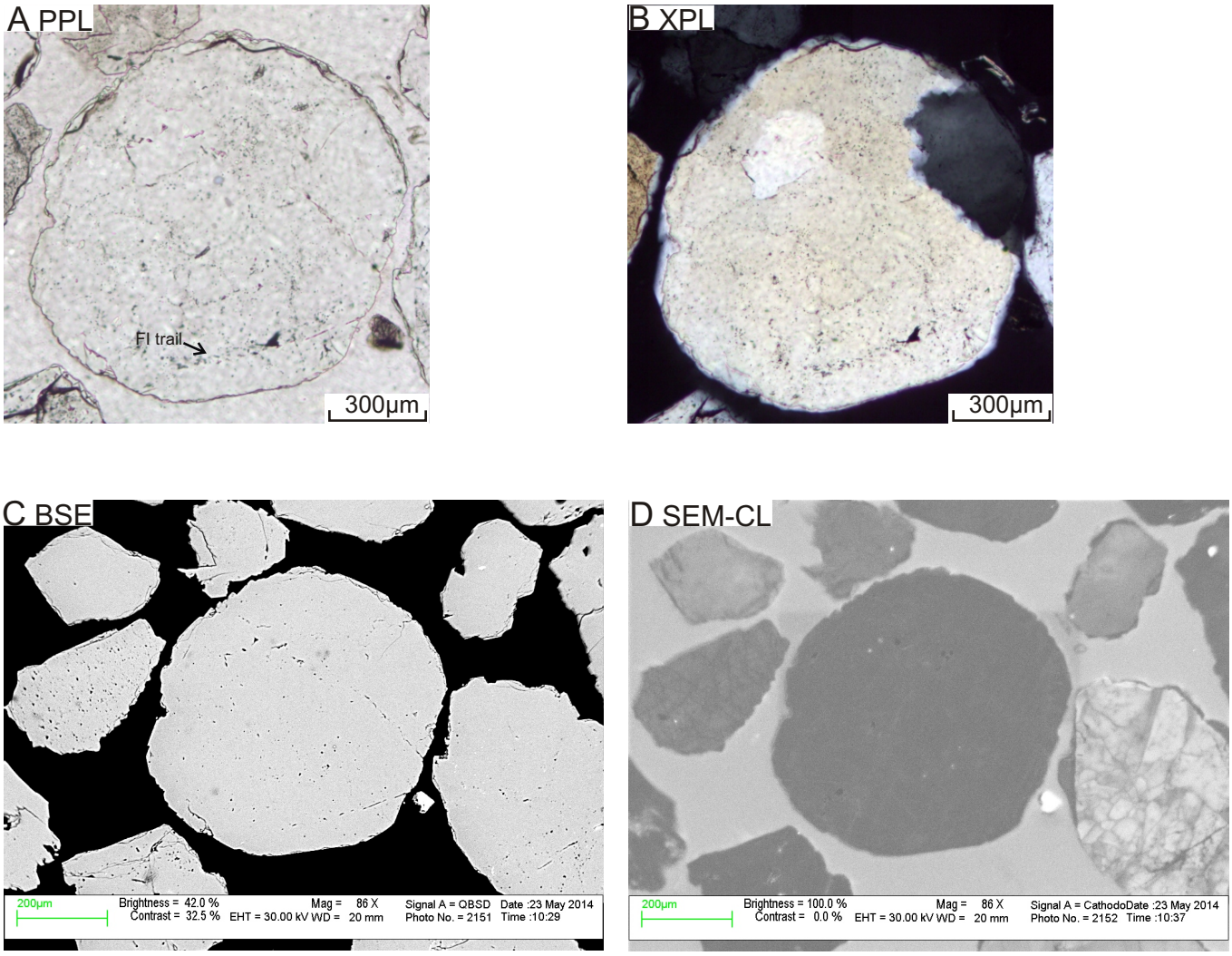

Figure 3A-27: Microphotos under ppl (A) and xpl (B), SEM-BSE image C, and SEM-CL image (D) of quartz grain 27 in sample 2995. The grain is subhedral and well-rounded polycrystalline (only a few sub-grains) with mosaic texture and weak undulose extinction. Fluid inclusion trails are present (Fig. A). The grain is weakly microfractured with irregular fractures.

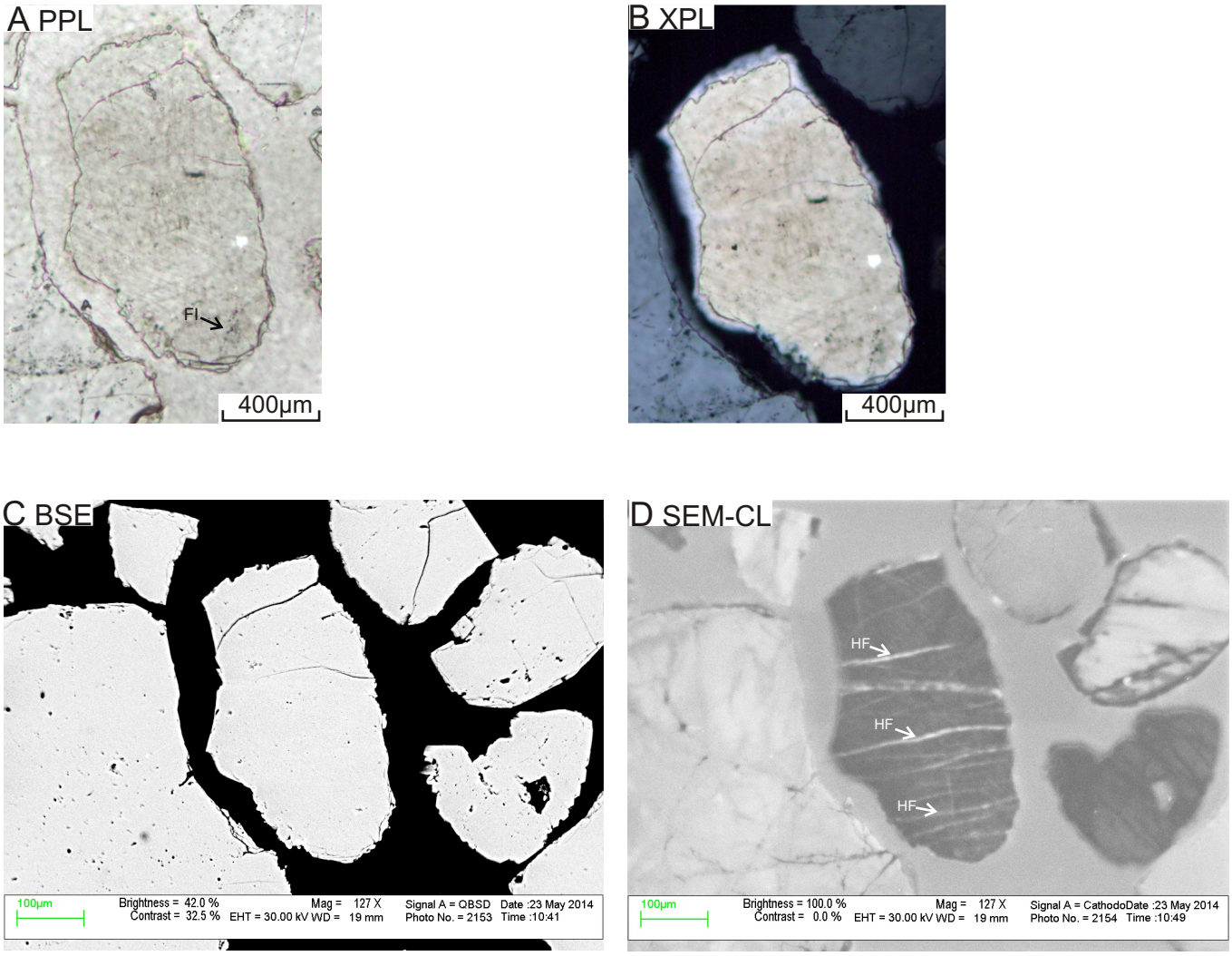

Figure 3A-28: Microphotos under ppl (A) and xpl (B), SEM-BSE image C, and SEM-CL image (D) of quartz grain 28 in sample 2995. The grain is anhedral and sub-rounded polycrystalline (only 2 sub-grains) with mosaic texture, weak undulose extinction and deformation lamellae (Fig. B). Fluid inclusions (FI) are present (Fig. A). The grain is microfractured with a set of parallel fractures (Fig. D). Healed fractures (HF) are common (Fig. D). The grain shows subtle bright-CL mottling texture in SEM-CL image.

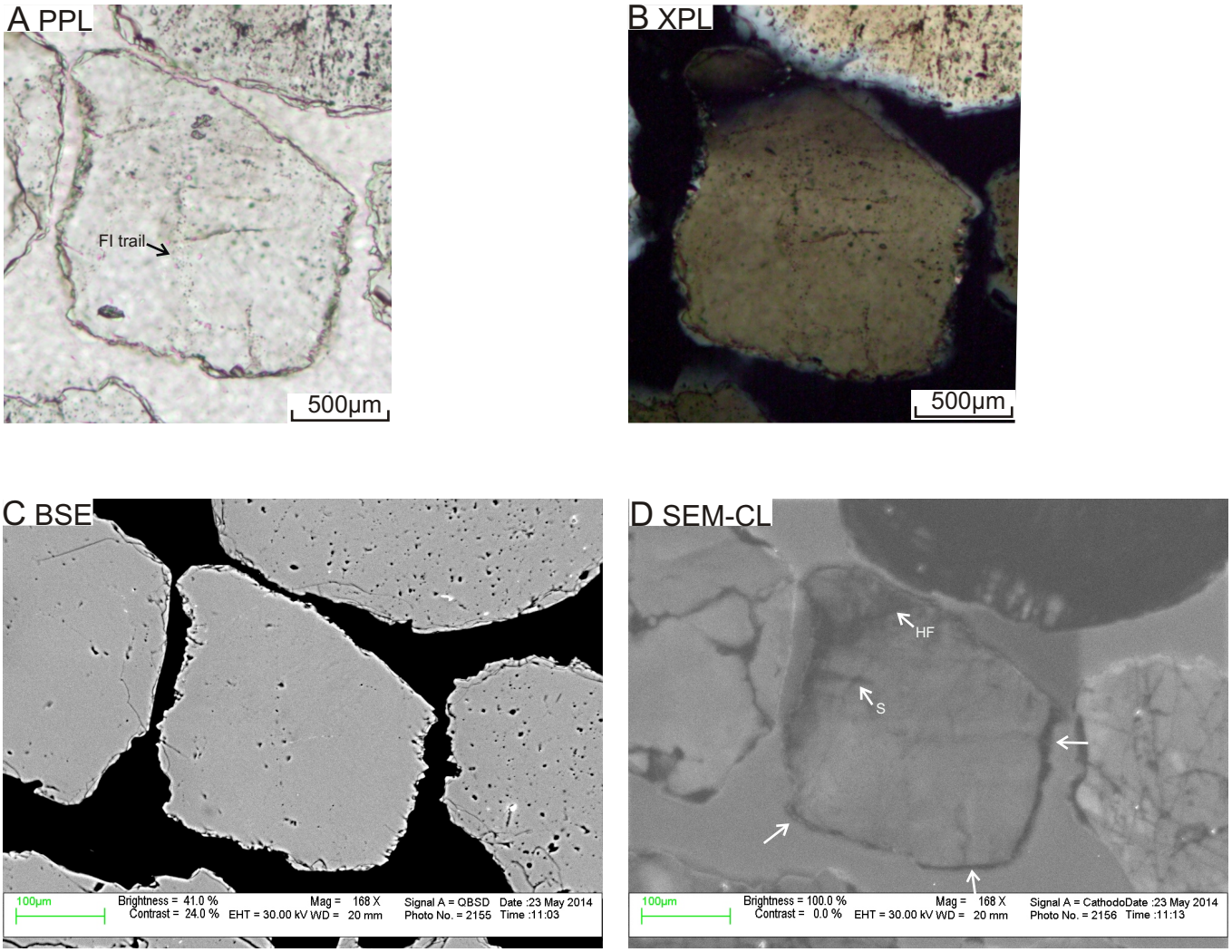

Figure 3A-29: Microphotos under ppl (A) and xpl (B), SEM-BSE image C, and SEM-CL image (D) of quartz grain 29 in sample 2995. The grain is anhedral and sub-rounded monocrystalline with deformation banding and strong undulose extinction. Fluid inclusion trails are common (Fig. A). The grain is weakly microfractured with a set of irregular fractures (Fig. C and D). Only a few healed fractures (HF) and spiders (S) can be seen in Fig. D. The dark areas indicated by arrows in Fig. D are overgrowth; these areas appear corroded in Fig. C, suggesting secondary porosity.

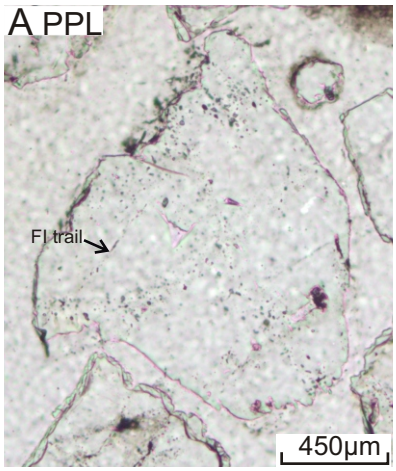

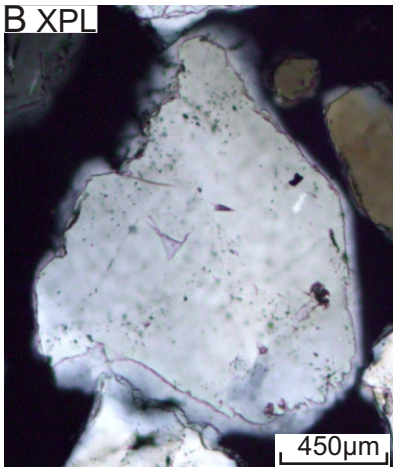

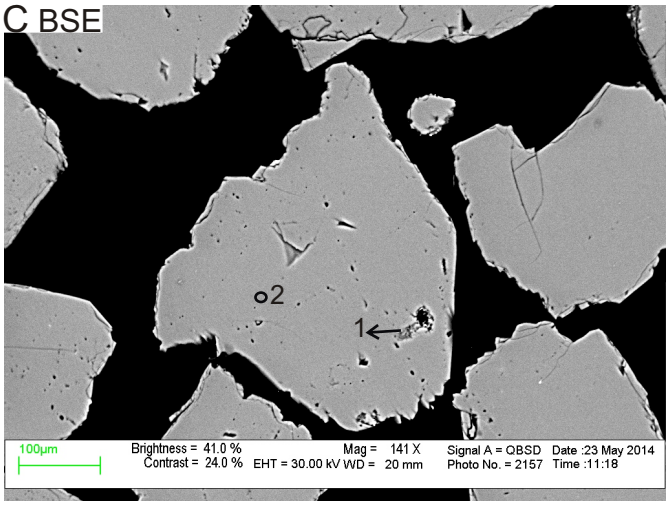

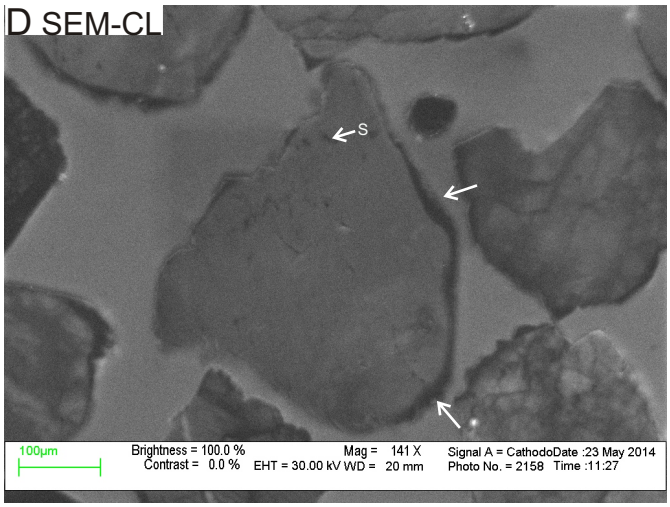

E EDS analyses

Pos#	Min. ID	SiO2	TiO2	Al2O3	FeO	CaO	Total	Actual total
1	Rt	79.15	18.85	1.28	0.36	0.36	100	92
2	Qz	99.99					100	143

Figure 3A-30: Microphotos under ppl (A) and xpl (B), SEM-BSE image (C), SEM-CL image (D), and EDS analyses table (E) of quartz grain 30 in sample 2995. The grain is anhedral and sub-angular monocrystalline with strong undulose extinction. Fluid inclusion trails are present (Fig. A). The grain contains rutile inclusions and is weakly microfractured with irregular fractures (Fig. C). Healed fractures are rare (Fig. D). The dark areas indicated by arrows in Fig. D are overgrowth; these areas appear corroded in Fig. C, suggesting secondary porosity.

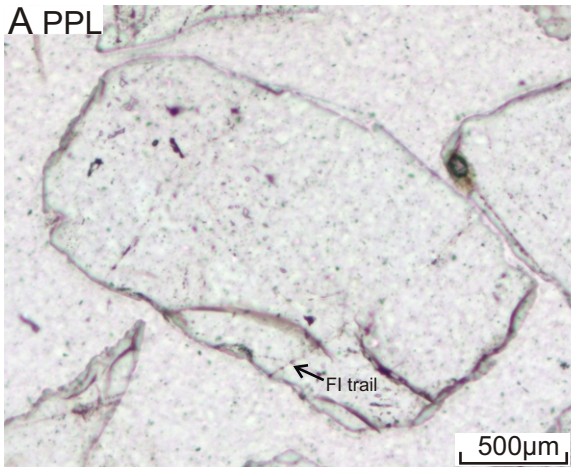

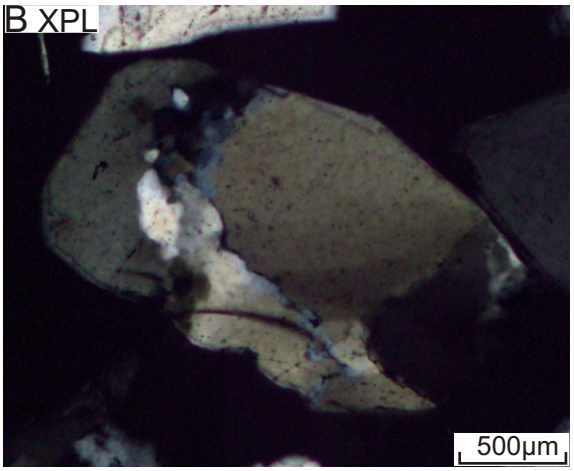

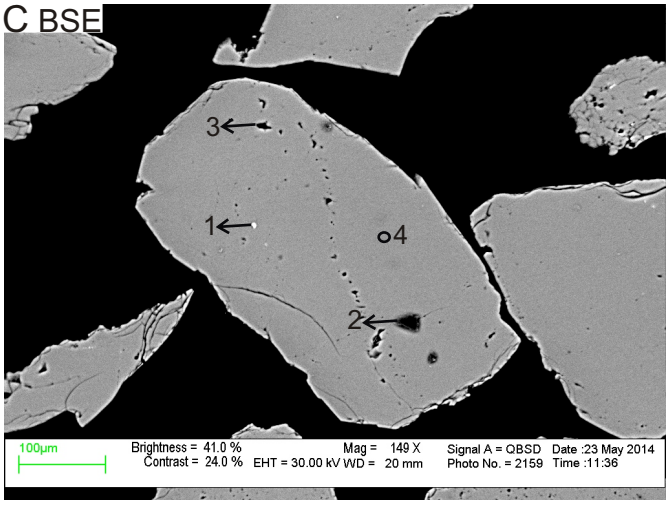

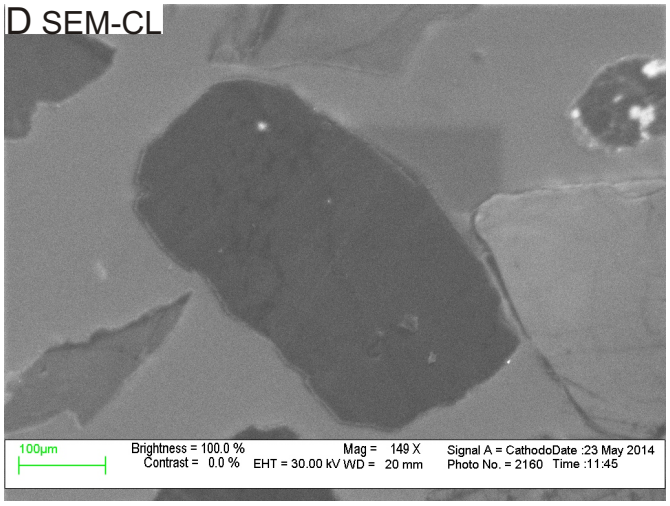

E EDS analyses

Pos#	Min. ID	SiO2	Al2O3	FeO	MgO	CaO	Na2O	K2O	SO3	F	Cl	Total	Actual total
1	Py	43.49		12.5					44			100	185
2	Qz	99.24							0.75			100	112
3	Hole	92.37	0.96	0.35	0.55	0.28	0.31	0.23	0.75	3.85	0.32	100	108
4	Qz	99.99										100	134

Figure 3A-31: Microphotos under ppl (A) and xpl (B), SEM-BSE image (C), SEM-CL image (D), and EDS analyses table (E) of quartz grain 31 in sample 2995. The grain is subhedral and sub-rounded polycrystalline (more than 8 sub-grains) with mosaic texture and weak undulose extinction. Fluid inclusion trails are present (Fig. A). The grain contains pyrite inclusions and is weakly microfractured with a set of irregular curved fractures (Fig. C). Healed fractures are rare.

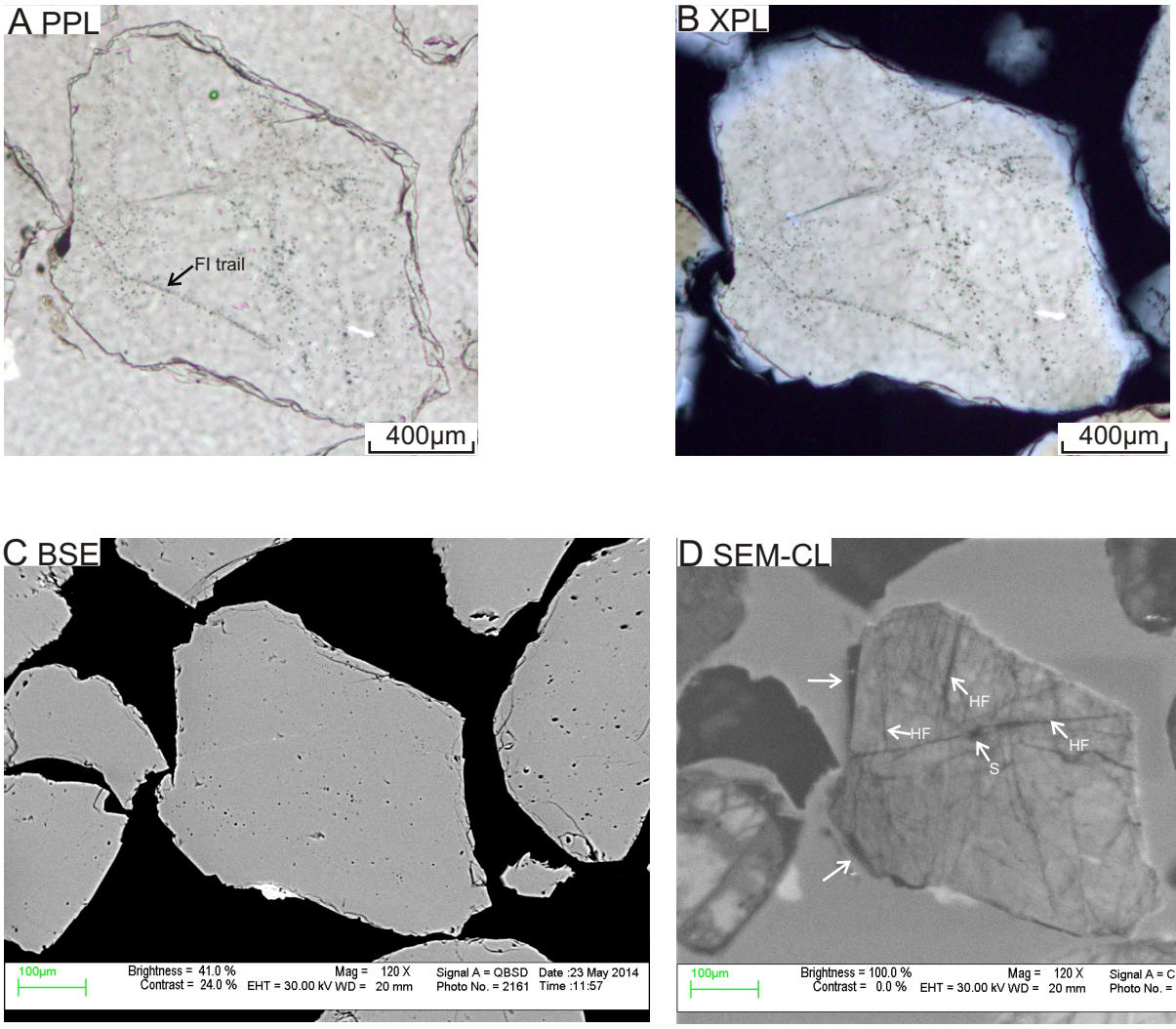

Figure 3A-32: Microphotos under ppl (A) and xpl (B), SEM-BSE image C, and SEM-CL image (D) of quartz grain 32 in sample 2995. The grain is anhedral and sub-rounded monocrystalline with mosaic texture and weak undulose extinction. Fluid inclusions are common; they are usually associated with secondary porosity and form trails along healed fractures (Fig. A). The grain is microfractured with a set of sub-parallel fractures and a set of irregular fractures (Fig. D). Healed fractures (HF) and spiders (S) are common (Fig. D). The dark areas indicated by arrows in Fig. D are overgrowth.

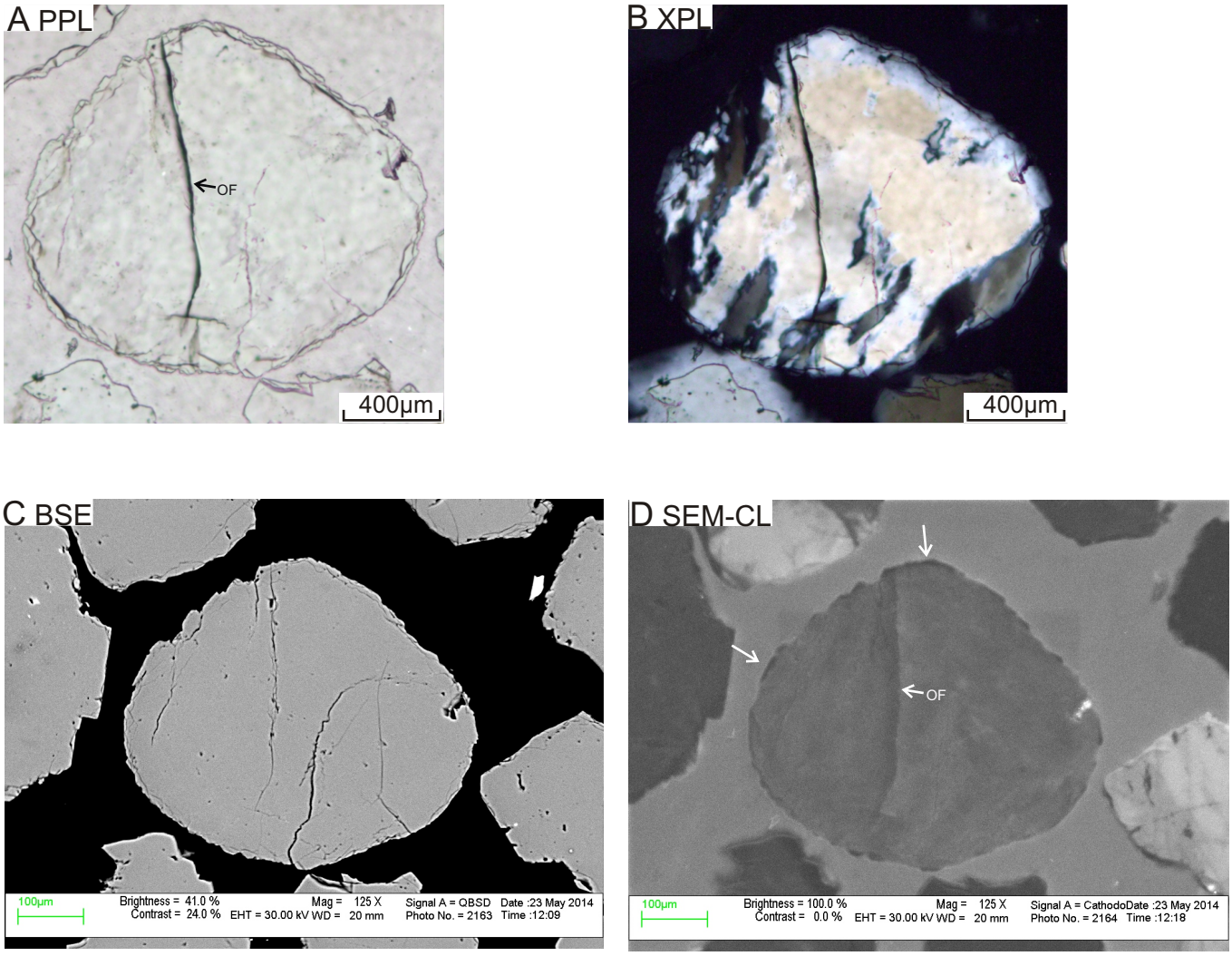

Figure 3A-33: Microphotos under ppl (A) and xpl (B), SEM-BSE image C, and SEM-CL image (D) of quartz grain 33 in sample 2995. The grain is anhedral and well-rounded polycrystalline (more than 10 sub-grains) with mosaic texture and strong undulose extinction. Fluid inclusions are rare. The grain is microfractured with a set of irregular fractures (Fig. A and D). The fractures that appear in CL-SEM image are open fractures (OF) and healed fractures are not common. The dark areas indicated by arrows in Fig. D are overgrowth; these areas appear corroded in Fig. C, suggesting secondary porosity. (Rhyolite)

A PPL

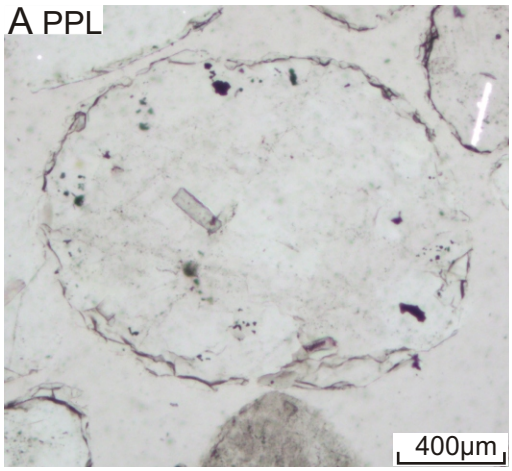

B XPL

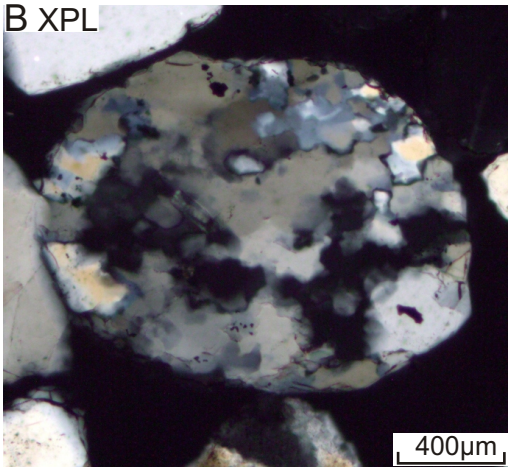

C BSE

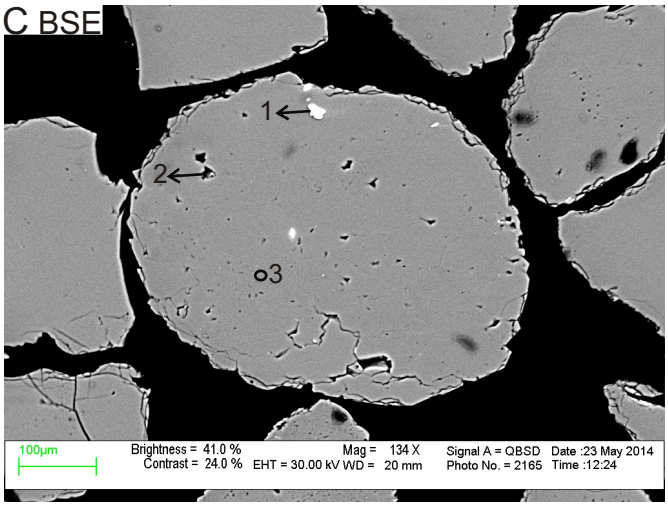

D SEM-CL

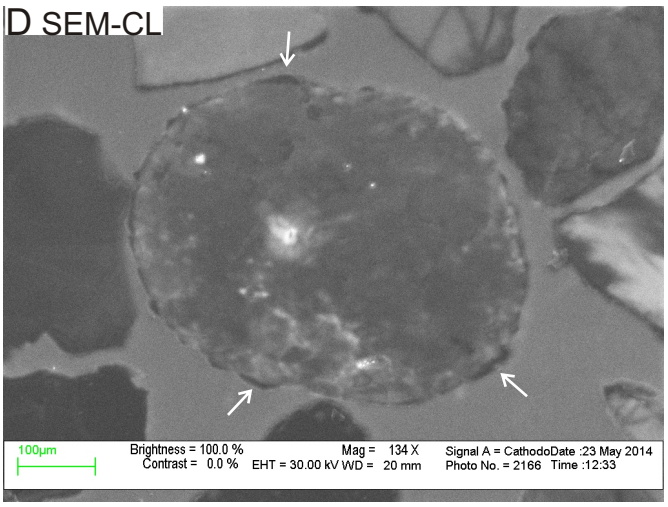

E EDS analyses

Pos#	Min. ID	SiO2	FeO	SO3	Total	Actual total
1	Py	25.69	19.1	55.21	100	194
2	Qz	99.99			100	146
3	Qz	99.99			100	130

Figure 3A-34: Microphotos under ppl (A) and xpl (B), SEM-BSE image (C), SEM-CL image (D), and EDS analyses table (E) of quartz grain 34 in sample 2995. The grain is anhedral and well-rounded polycrystalline (more than 12 sub-grains) with mosaic texture and weak undulose extinction. Fluid inclusions are rare. The grain is microfractured with a set of irregular fractures (Fig. A and C). Healed fractures are rare. The dark areas indicated by arrows in Fig. D are overgrowth.

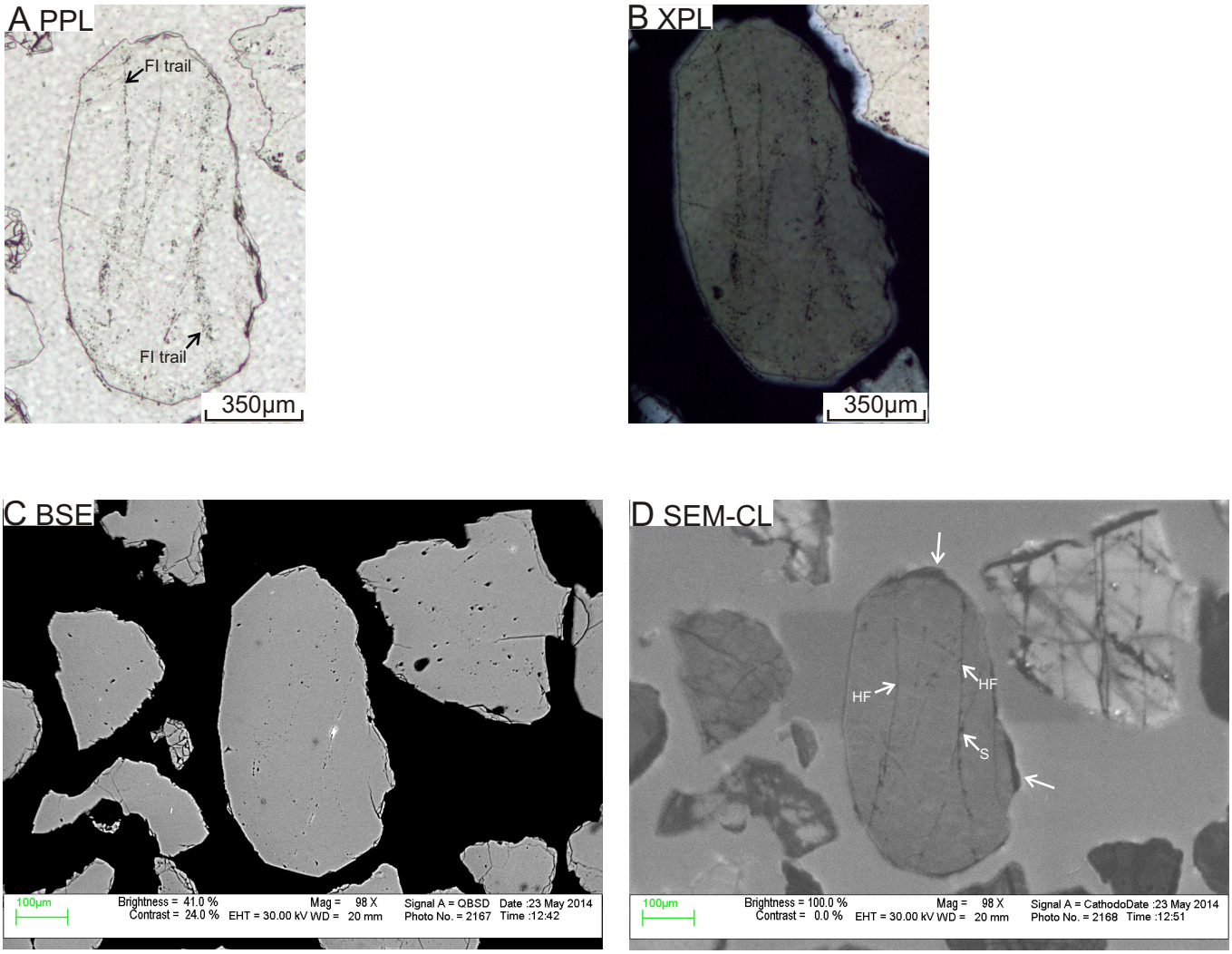

Figure 3A-35: Microphotos under ppl (A) and xpl (B), SEM-BSE image C, and SEM-CL image (D) of quartz grain 35 in sample 2995. The grain is subhedral and rounded monocrystalline with weak undulose extinction. Fluid inclusions are common; they are usually associated with secondary porosity and form trails (FI trail) along healed fractures (Fig. A). The grain is microfractured with a set of sub-parallel fractures (Fig. D). Some healed fractures (HF) and spiders (S) can be seen in Fig. D. The dark areas indicated by arrows in Fig. D are overgrowth.

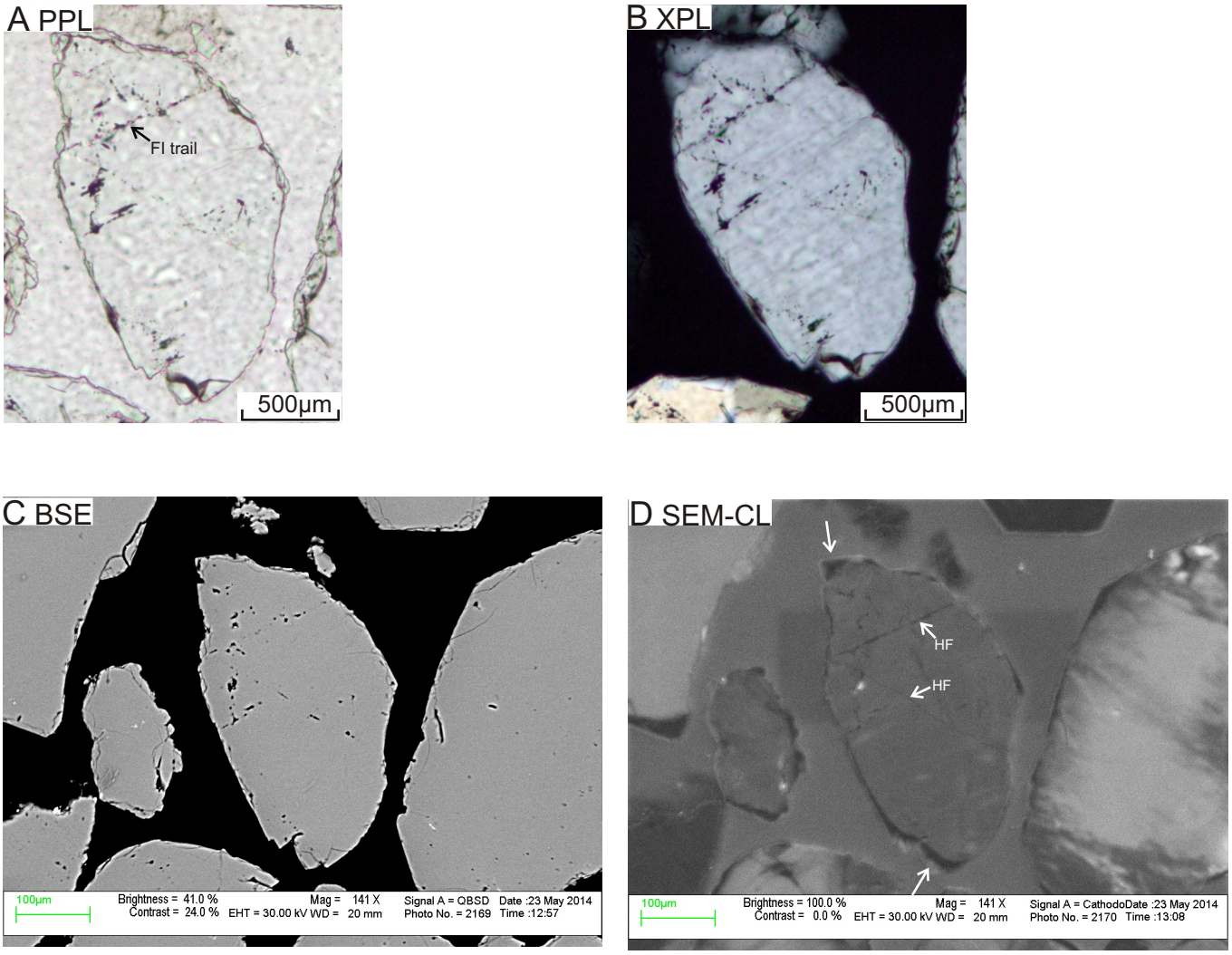

Figure 3A-36: Microphotos under ppl (A) and xpl (B), SEM-BSE image C, and SEM-CL image (D) of quartz grain 36 in sample 2995. The grain is anhedral and sub-rounded monocrystalline with weak undulose extinction and deformation lamellae Fig. A and B). Fluid inclusions are common; they are usually associated with secondary porosity and form trails (FI trail) along healed fractures (Fig. A). The grain is microfractured with irregular fractures (Fig. C and D). A few healed fractures (HF) can be seen in Fig. D. The dark areas indicated by arrows in Fig. D are overgrowth. The grain shows subtle bright-CL mottling texture in SEM-CL image. Probably these patches are due to deformation, since they have the same orientation of the deformation lamellae in Fig. B.

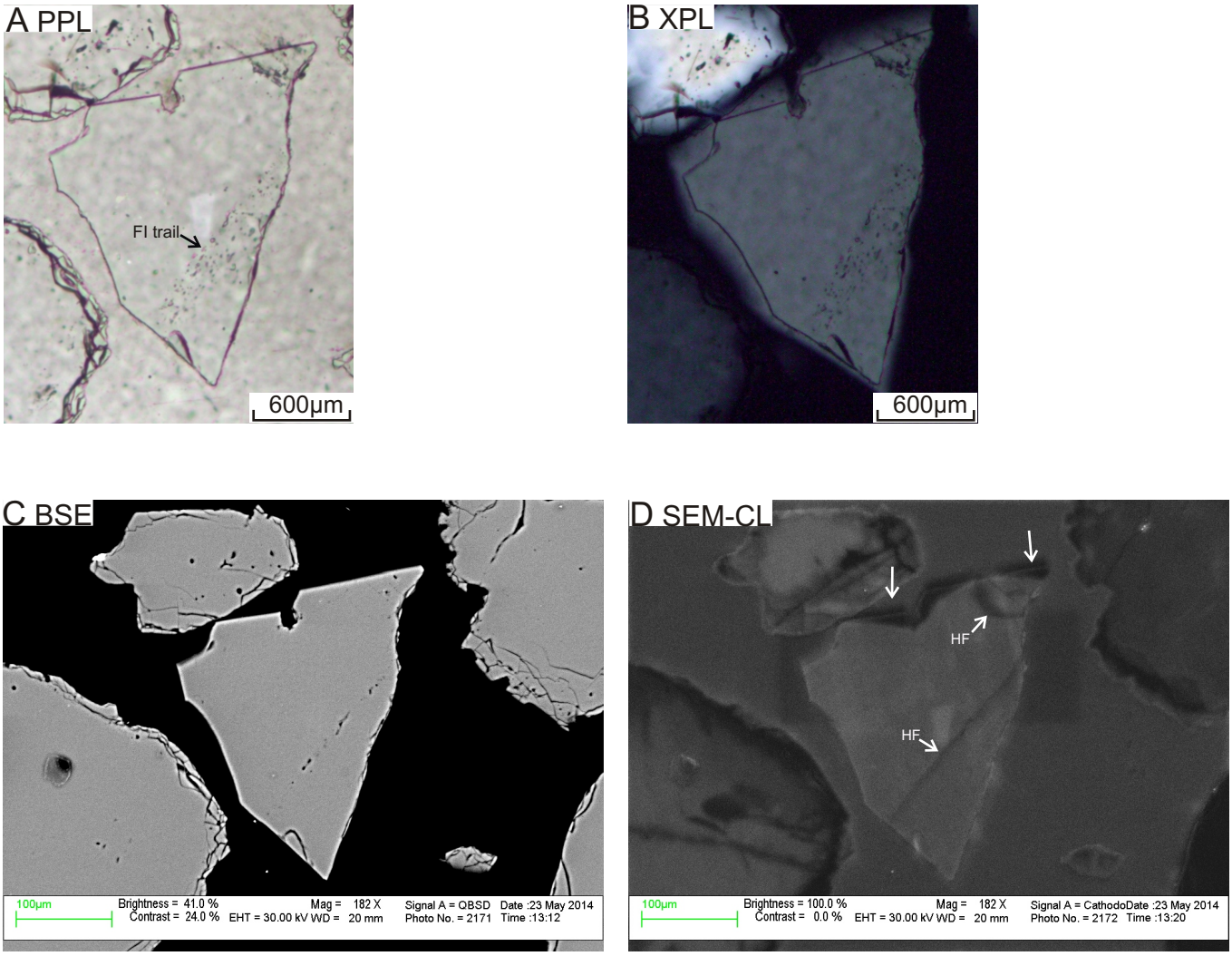

Figure 3A-37: Microphotos under ppl (A) and xpl (B), SEM-BSE image (C), SEM-CL image (D), and EDS analyses table (E) of quartz grain 37 in sample 2995. The grain is anhedral and angular monocrystalline with non-undulose extinction. Fluid inclusions are common; they are associated with secondary porosity and form trails (FI trail) along a healed fracture (Fig. A). The grain is weakly microfractured (Fig. C and D). Some healed fractures (HF) can be seen in Fig. D. The dark areas indicated by arrows in Fig. D are overgrowth.

A PPL

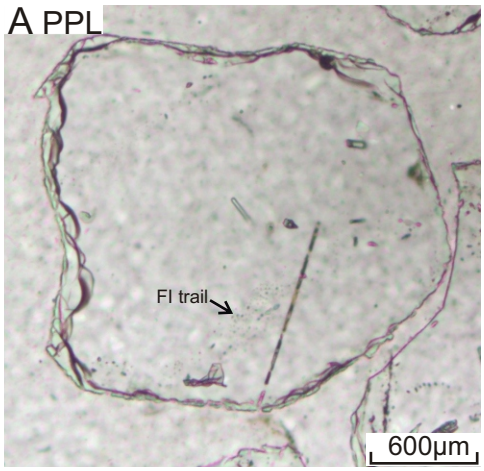

B XPL

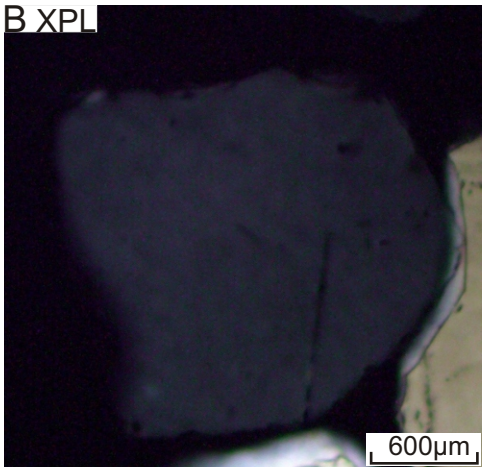

C BSE

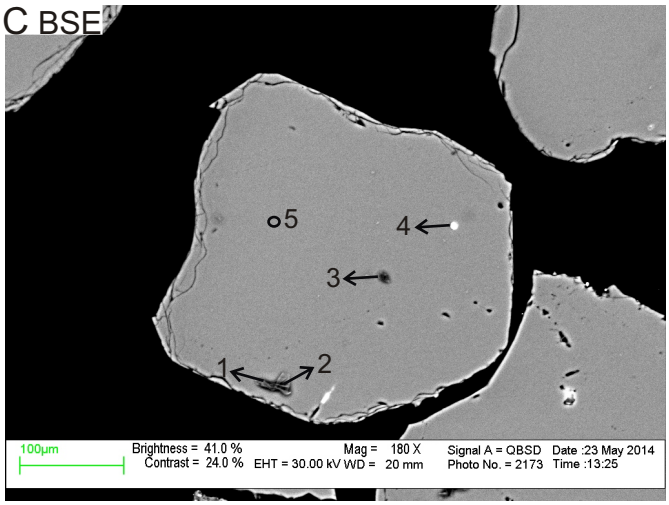

D SEM-CL

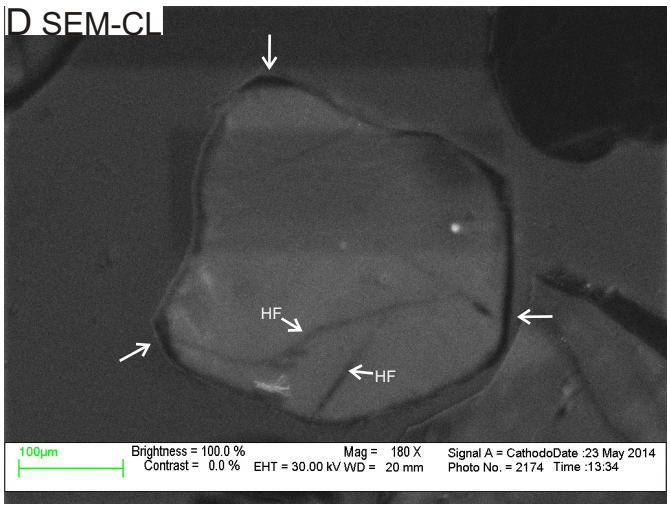

E EDS analyses

Pos#	Min. ID	SiO2	CaO	Na2O	P2O5	F	Total	Actual total
1	Qz	99.99					100	137
2	Qz	99.99					100	137
3	Qz	99.58		0.4			100	117
4	Ap	30.85	30		33.71	5.45	100	153
5	Qz	99.99					100	144

Figure 3A-38: Microphotos under ppl (A) and xpl (B), SEM-BSE image (C), SEM-CL image (D), and EDS analyses table (E) of quartz grain 38 in sample 2995. The grain is subhedral and sub-rounded monocrystalline with non-undulose extinction. Fluid inclusions are present; they form trails along healed fracture (Fig. A). The grain contains apatite inclusion and is weakly microfractured with a set of irregular fractures (Fig. C and D). A few healed fractures (HF) can be seen in Fig. D. The dark areas indicated by arrows in Fig. D are overgrowth.

A PPL

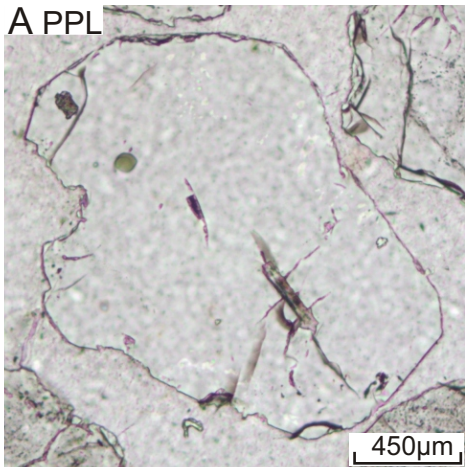

B XPL

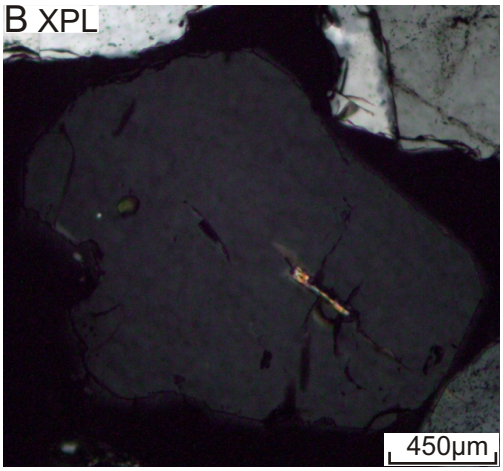

C BSE

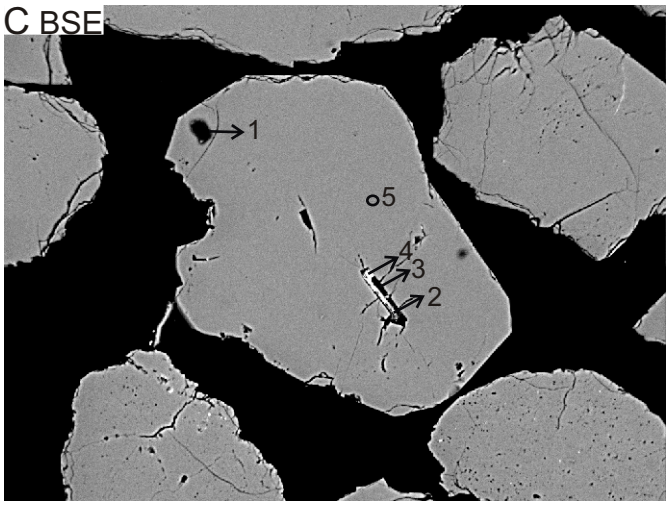

D SEM-CL

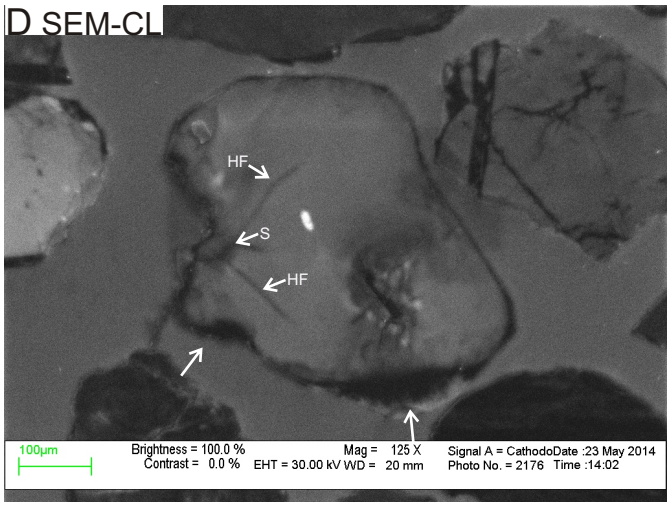

E EDS analyses

Pos#	Min. ID	SiO2	TiO2	Al2O3	FeO	MgO	CaO	Na2O	K2O	SO3	F	Cl	BaO	Total	Actual total
1	Qz	97.31						0.35	0.26	1.5		0.56		100	90
2	Ilt	60.07	3.24	19.2	1.42	1.09	0.38		2.39		2.21			90	78
3	Qz	98.42									1.58			100	130
4	Ilt+Brt	46.57	6.26	12.55	3.63		1.32		4.28	4.05	6.75		14.63	100	28
5	Qz	99.99												100	127

Figure 3A-39: Microphotos under ppl (A) and xpl (B), SEM-BSE image (C), SEM-CL image (D), and EDS analyses table (E) of quartz grain 39 in sample 2995. The grain is subhedral and sub-rounded monocrystalline with embayed margins and non-undulose extinction. Fluid inclusions are rare. The grain contains illite inclusion and illite + barite inclusion, and is microfractured with a set of irregular fractures (Fig. C and D). Some healed fractures (HF) and spiders (S) can be seen in Fig. D. The dark areas indicated by arrows in Fig. D are overgrowth.

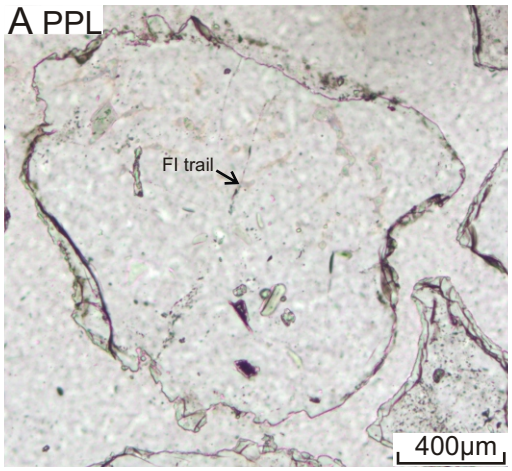

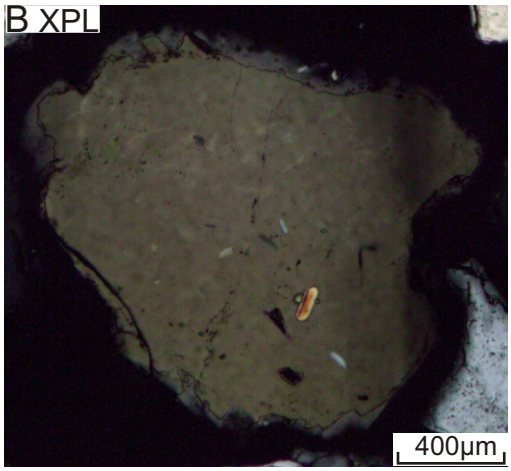

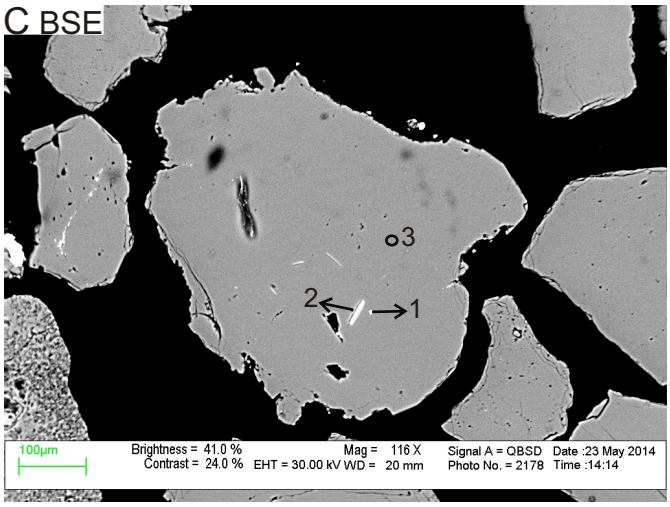

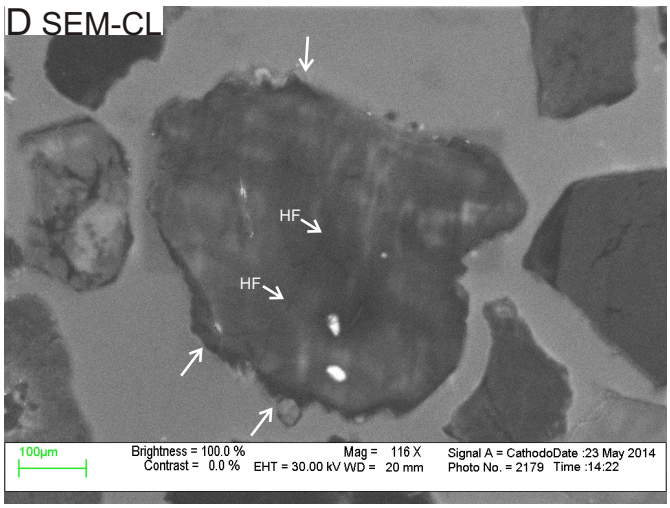

E EDS analyses

Pos#	Min. ID	SiO2	TiO2	Al2O3	FeO	MnO	MgO	CaO	Na2O	K2O	F	Sc2O3	Total	Actual total
1	Tur	63.32	0.2	6.59	11.77	0.34	7.79	7.71	0.94	0.7		0.63	100	131
2	Bt	48.38	0.62	11.48	13.08	0.26	12.45			7.45	2.28		96	131
3	Qz	99.99											100	128

Figure 3A-40: Microphotos under ppl (A) and xpl (B), SEM-BSE image (C), SEM-CL image (D), and EDS analyses table (E) of quartz grain 40 in sample 2995. The grain is anhedral and sub-angular monocrystalline with irregular and embayed margins, and with strong undulose extinction. Fluid inclusion trails are present. The grain contains biotite and tourmaline inclusions, and is weakly microfractured irregular fractures (Fig. C and D). Only a few healed fractures (HF) can be seen in Fig. D. The dark areas indicated by arrows in Fig. D are overgrowth. The grain shows subtle bright-Cl mottling texture in SEM-CL image.

Appendix 3B: Hot cathodoluminescence (HCL) images and blue colour shift analyses of detrital quartz grains in sample 2995.

Notes:

1. All the grains with HCL images correspond to the same grain in SEM-CL images. In all the following organized HCL figures,

   Fig. A shows HCL image taken after 3 seconds;

   Fig. B shows HCL image taken after 12 seconds;

   Fig. C is the histogram of blue colour within the analysed quartz grain in Fig. A and B, where X axis is the intensity of blue colour indicated by the colour bar with values from 0-255 (0=no blue or "black", 255=blue), and Y axis indicates the pixel amount at different blue values;

   Fig. D is the statistical table of blue values within the analysed grain area, where SD corresponds to standard deviation.

2. To classify the blue colour, the following abbreviations are used:

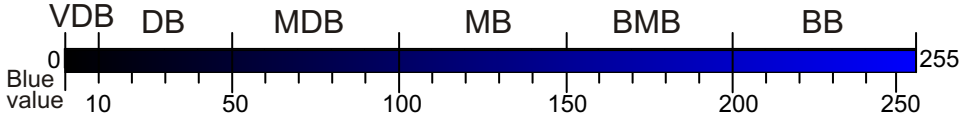

VDB: Very Dark Blue (0-10) **DB**: Dark Blue (11-50)

MDB: Medium Dark Blue (51-100) **MB**: Medium Blue (101-150)

BMB: Bright-Medium Blue (151-200) **BB**: Bright Blue (201-255)

3. To quantify the blue colour shift, the following criteria are used:

   Mean blue value change **< 5**: **No** colour shift

   5 ≤Mean blue value change **< 15**: **Slight** colour shift

   15 ≤Mean blue value change **< 30**: **Moderate** colour shift

   Mean blue value change ≥**30**: **Strong** colour shift

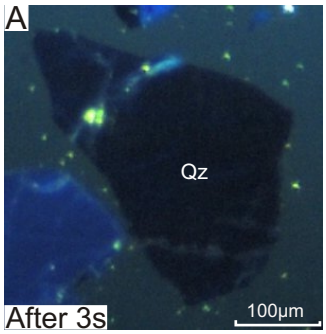

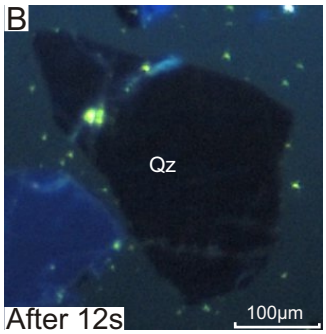

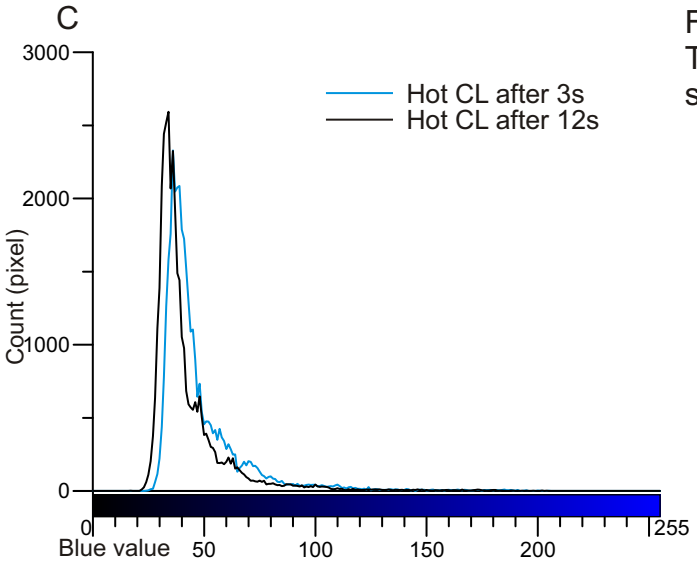

Figure 3B-1: Grain 1. The grain shows slight colour shift.

D

Blue value	Min	Max	Mode	Mean	SD
After 3s	24	205	36	48	19.6
After 12s	17	204	34	42	17.8

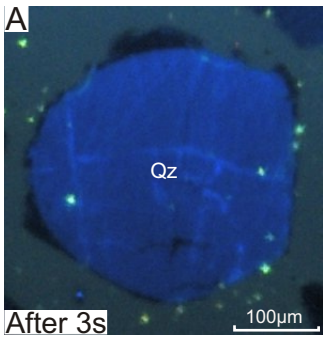

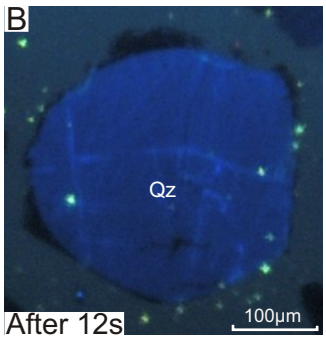

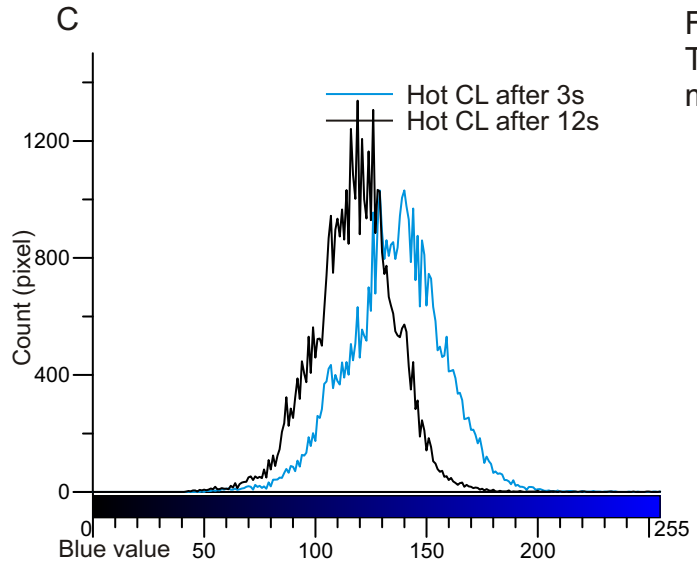

Figure 3B-2: Grain 2. The grain shows moderate colour shift.

D

Blue value	Min	Max	Mode	Mean	SD
After 3s	49	255	129	135	21.4
After 12s	42	255	119	118	18.1

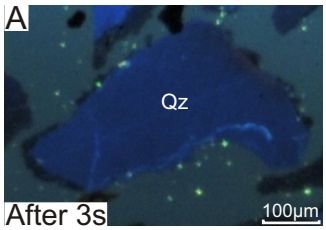

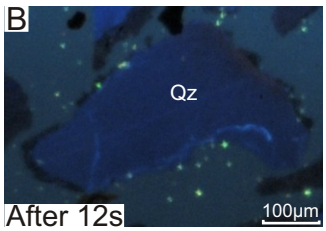

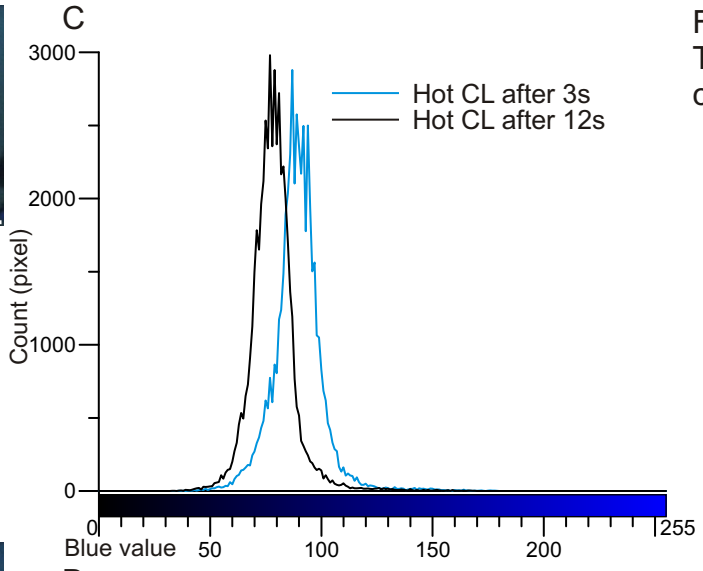

Figure 3B-3: Grain 3. The grain shows slight colour shift.

D

Blue value	Min	Max	Mode	Mean	SD
After 3s	36	179	87	89	11.3
After 12s	33	169	77	78	10.1

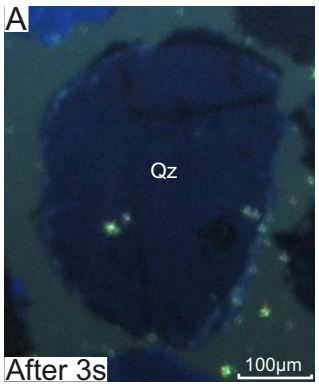



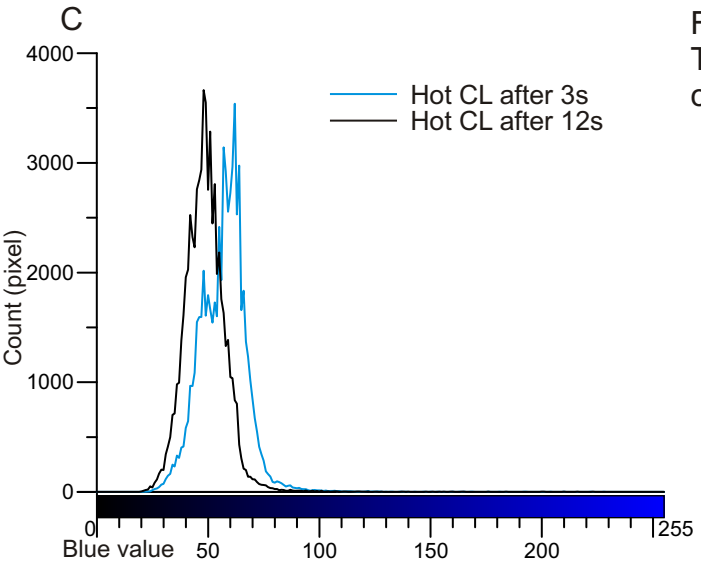

Figure 3B-4: Grain 4. The grain shows slight colour shift.

D

Blue value	Min	Max	Mode	Mean	SD
After 3s	21	228	62	57	10.4
After 12s	20	223	48	49	9.2

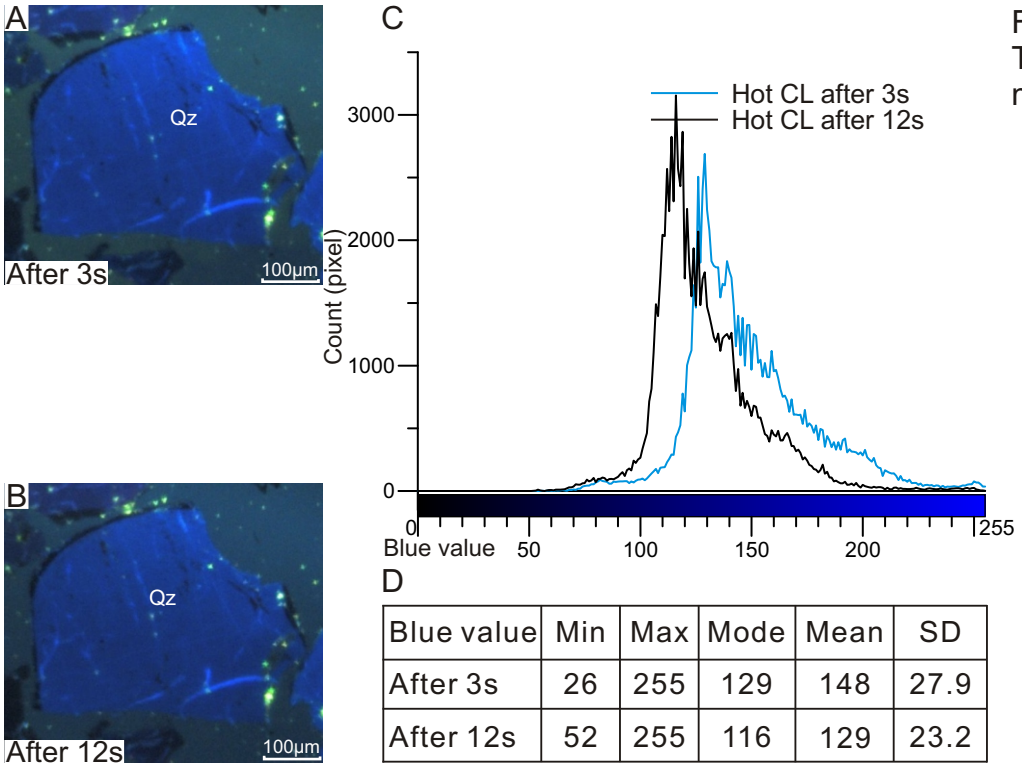

Figure 3B-5: Grain 5. The grain shows moderate colour shift.

D

Blue value	Min	Max	Mode	Mean	SD
After 3s	26	255	129	148	27.9
After 12s	52	255	116	129	23.2

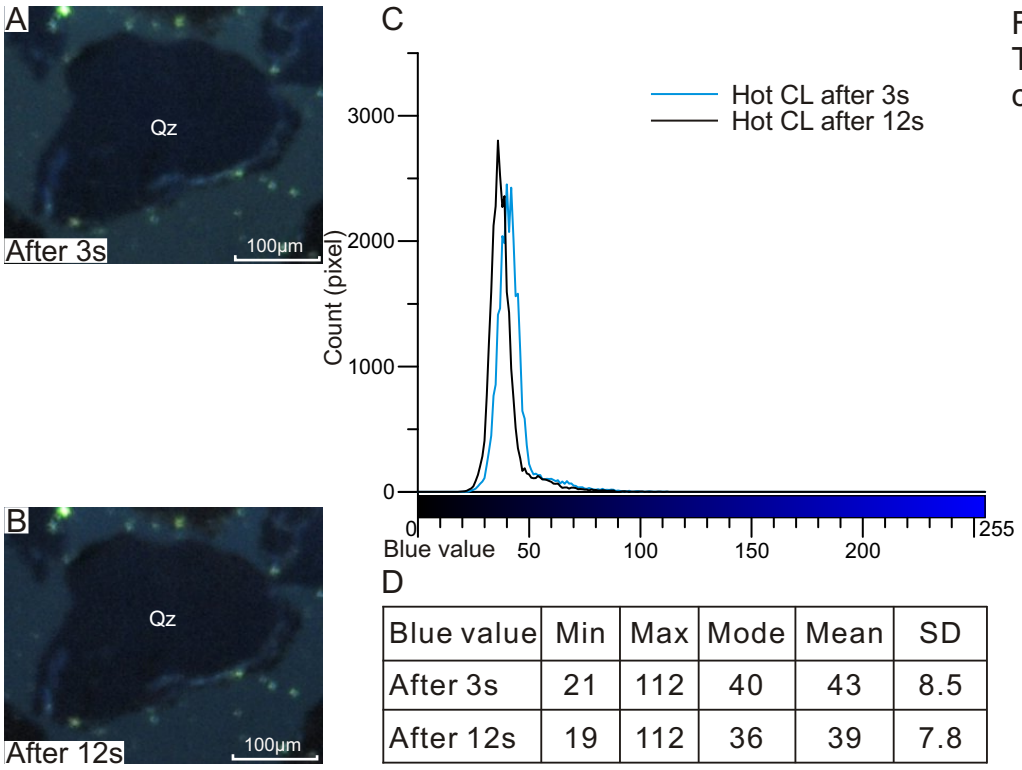

Figure 3B-6: Grain 6. The grain shows no colour shift.

D

Blue value	Min	Max	Mode	Mean	SD
After 3s	21	112	40	43	8.5
After 12s	19	112	36	39	7.8

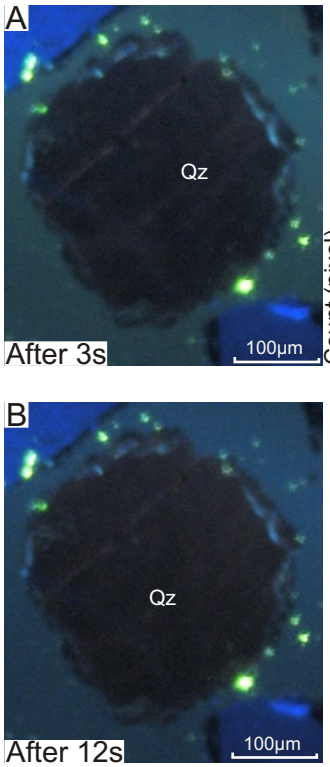

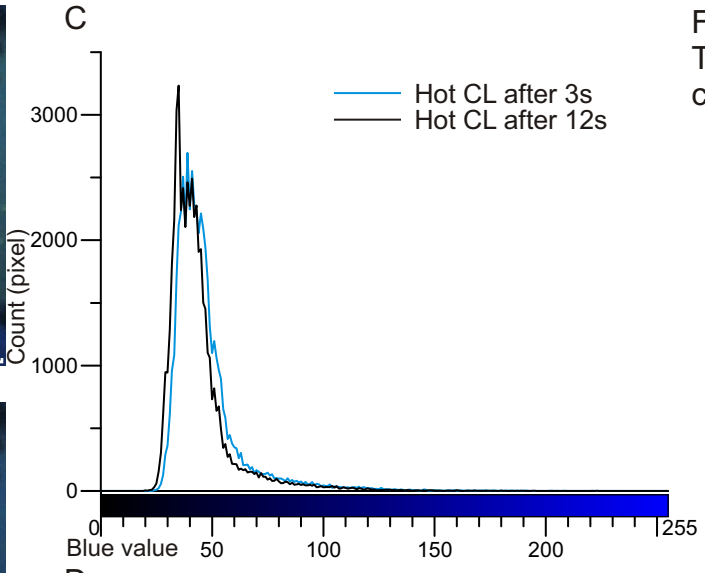

Figure 3B-7: Grain 7. The grain shows no colour shift.

D

Blue value	Min	Max	Mode	Mean	SD
After 3s	24	221	39	47	16.2
After 12s	20	223	35	44	14.8

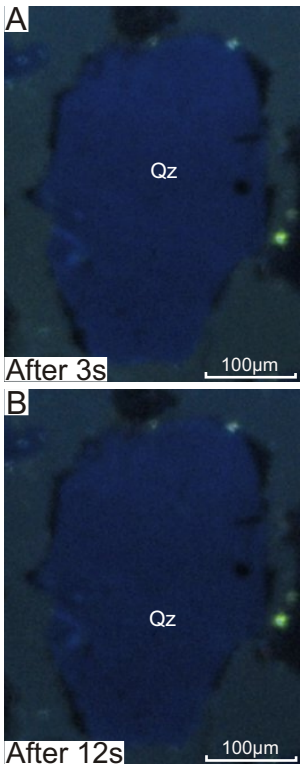

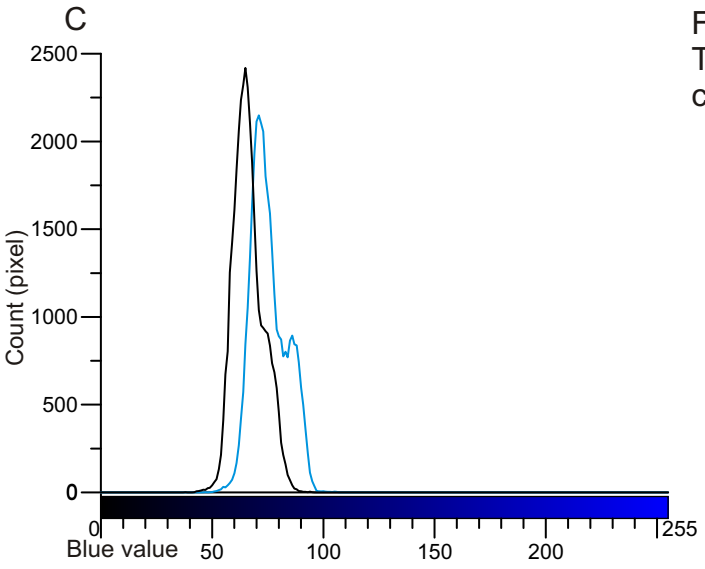

Figure 3B-8: Grain 8. The grain shows slight colour shift.

D

Blue value	Min	Max	Mode	Mean	SD
After 3s	47	106	71	75	7.9
After 12s	38	95	65	66	6.8

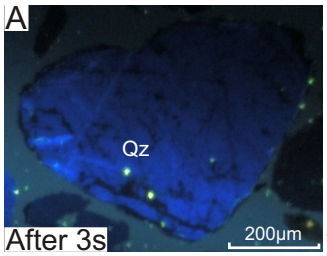

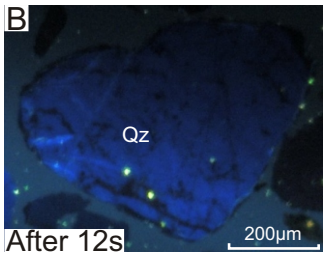

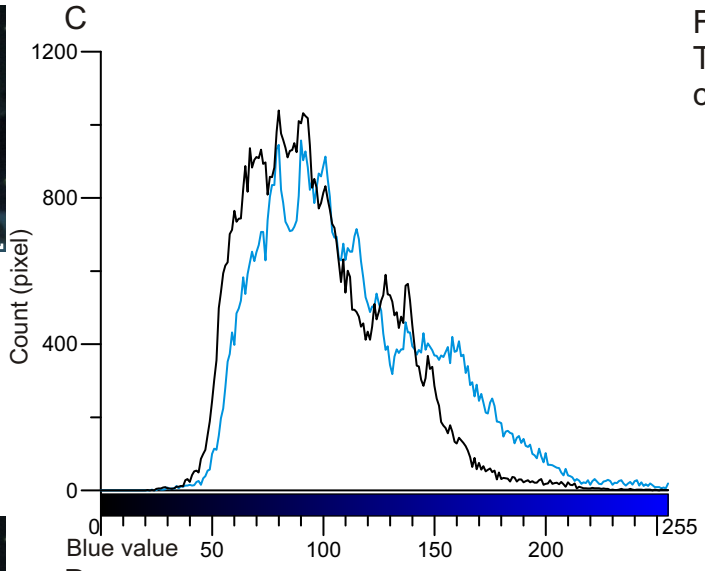

Figure 3B-9: Grain 9. The grain shows slight colour shift.

D

Blue value	Min	Max	Mode	Mean	SD
After 3s	23	255	90	112	38.5
After 12s	21	255	80	98	31.6

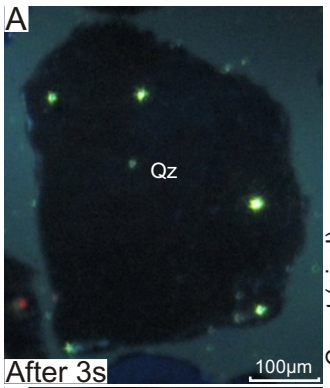

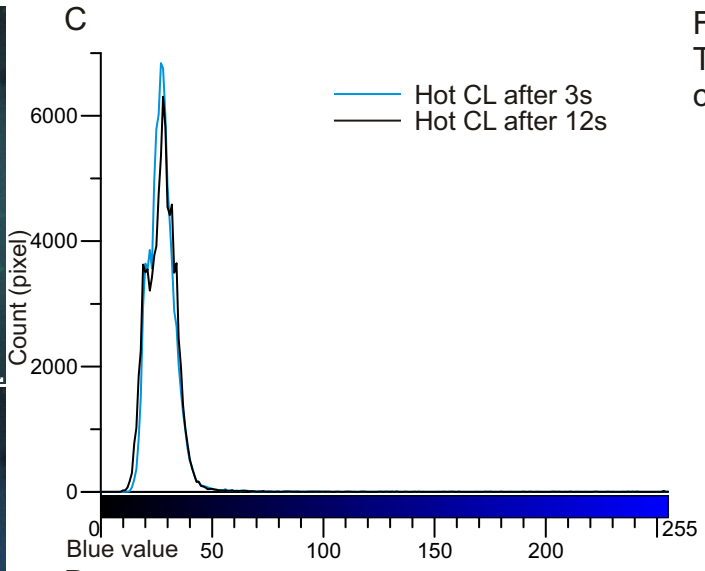

Figure 3B-10: Grain 10. The grain shows no colour shift.

D

Blue value	Min	Max	Mode	Mean	SD
After 3s	11	255	27	28	9.2
After 12s	9	255	28	28	9.7

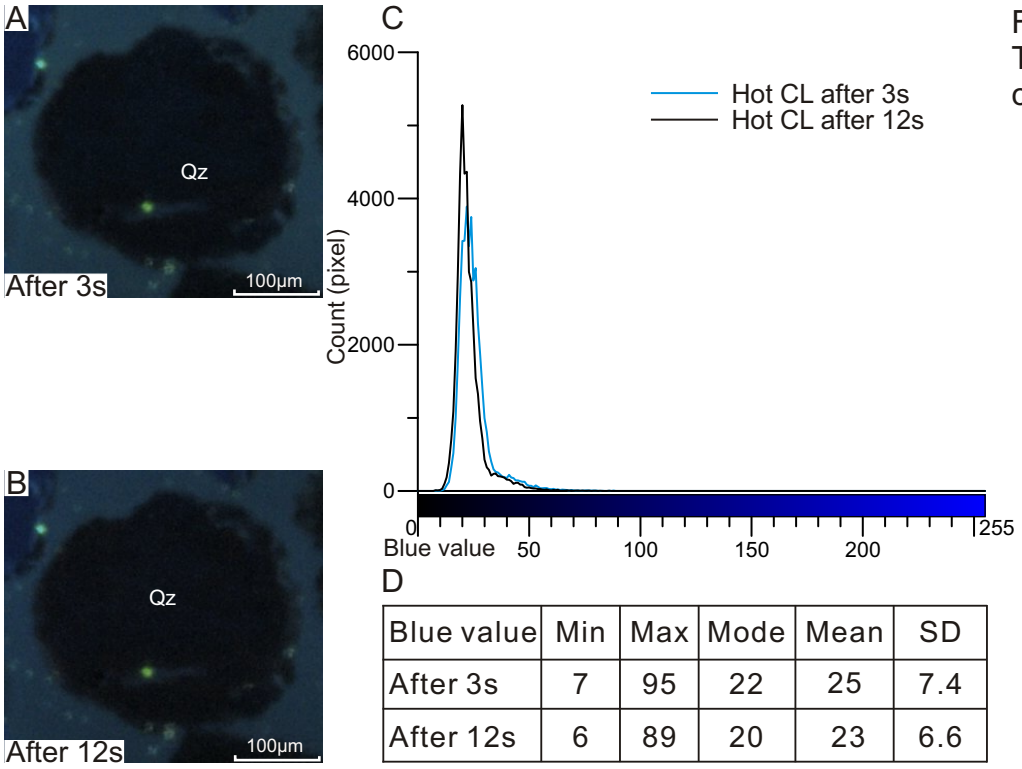

Figure 3B-11: Grain 11. The grain shows no colour shift.

D

Blue value	Min	Max	Mode	Mean	SD
After 3s	7	95	22	25	7.4
After 12s	6	89	20	23	6.6

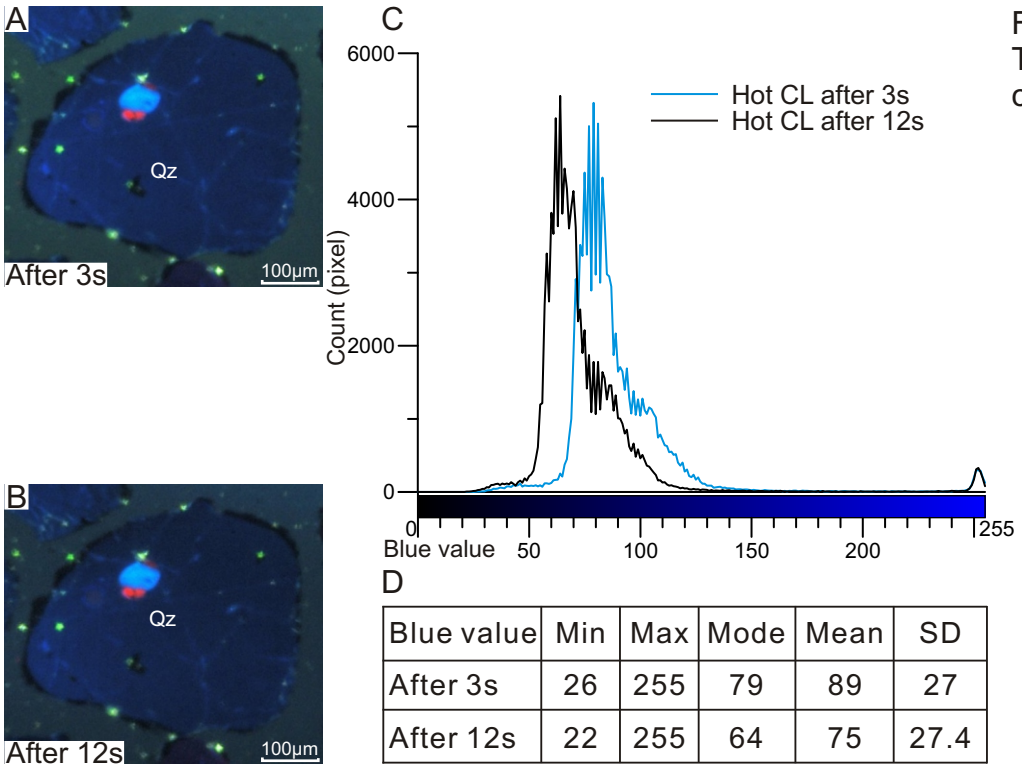

Figure 3B-12: Grain 12. The grain shows slight colour shift.

D

Blue value	Min	Max	Mode	Mean	SD
After 3s	26	255	79	89	27
After 12s	22	255	64	75	27.4

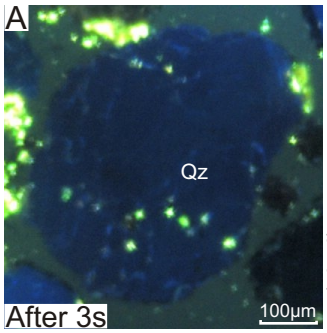

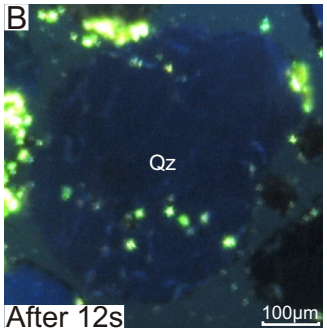

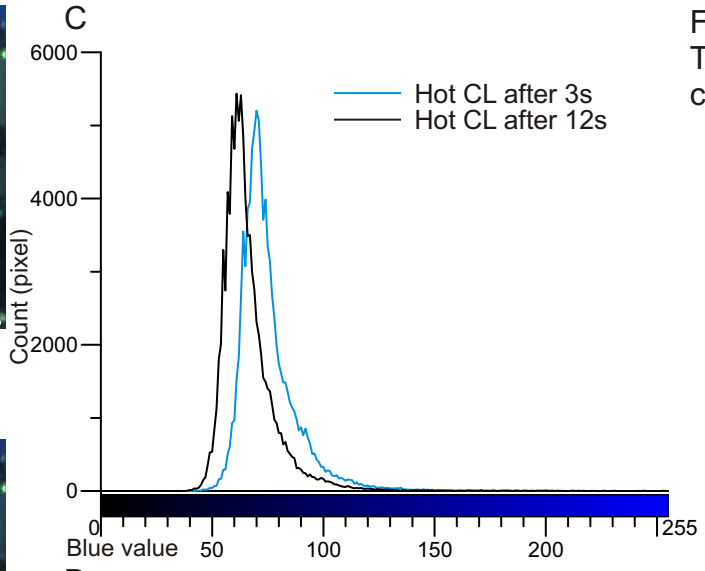

Figure 3B-13: Grain 13. The grain shows slight colour shift.

D

Blue value	Min	Max	Mode	Mean	SD
After 3s	41	255	70	75	13.8
After 12s	38	253	61	66	12.8

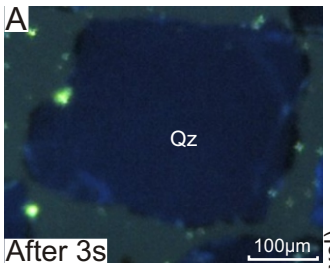

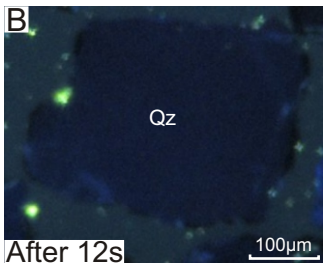

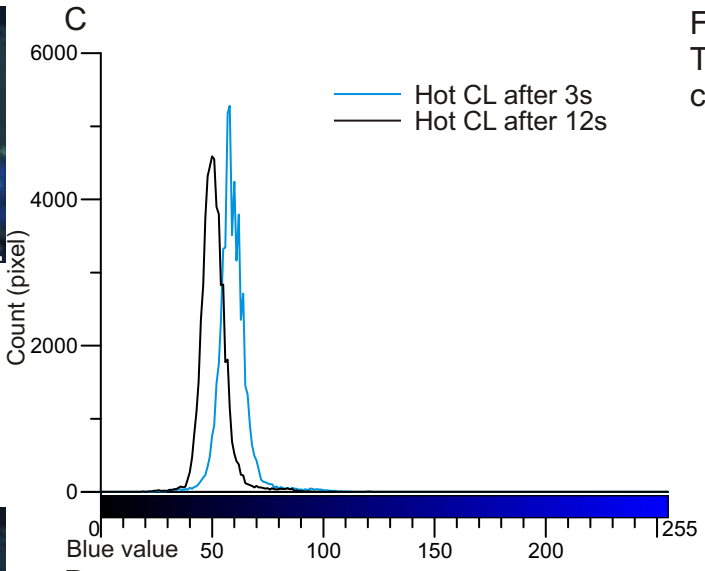

Figure 3B-14: Grain 14. The grain shows slight colour shift.

D

Blue value	Min	Max	Mode	Mean	SD
After 3s	22	143	58	59	7.1
After 12s	19	143	50	51	6.4

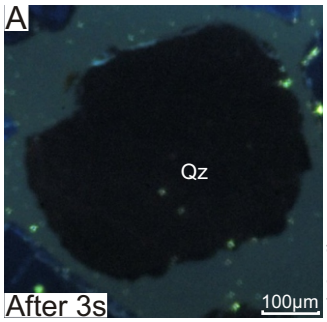

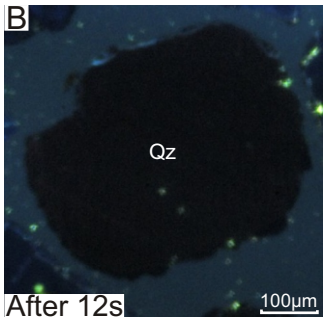

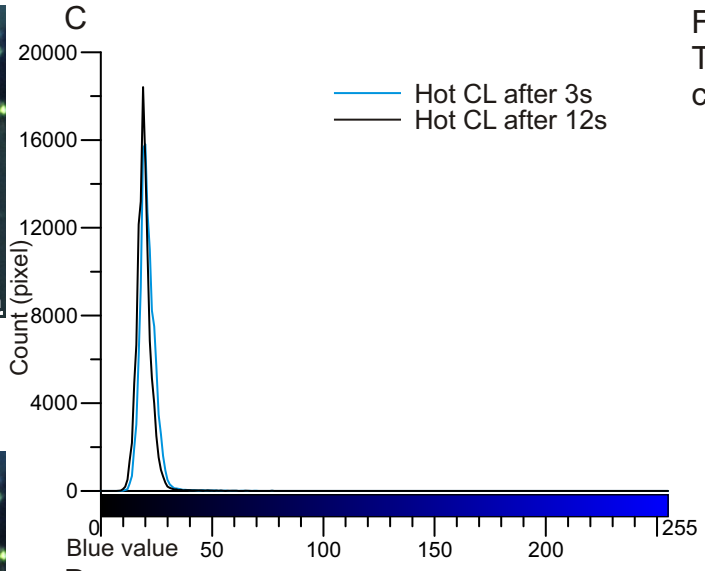

Figure 3B-15: Grain 15. The grain shows no colour shift.

D

Blue value	Min	Max	Mode	Mean	SD
After 3s	8	120	20	21	4.1
After 12s	6	114	19	20	3.9

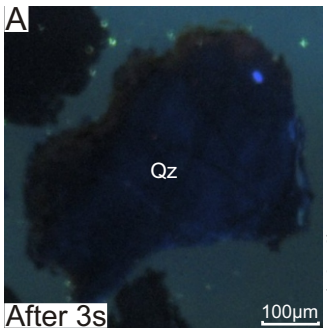

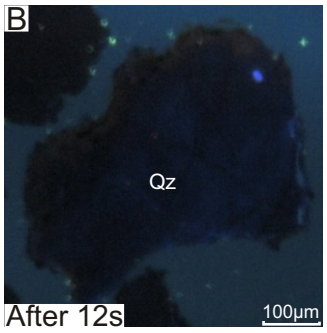

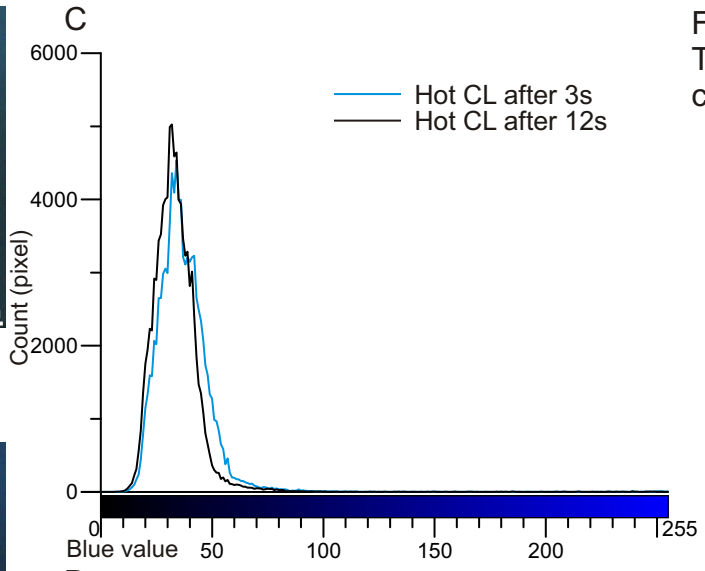

Figure 3B-16: Grain 16. The grain shows no colour shift.

D

Blue value	Min	Max	Mode	Mean	SD
After 3s	6	255	34	37	12.9
After 12s	6	255	32	33	11.4

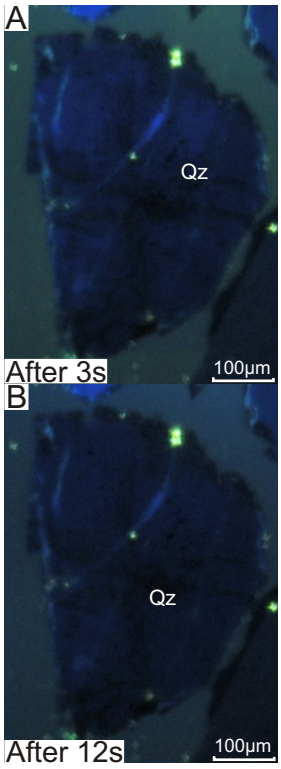

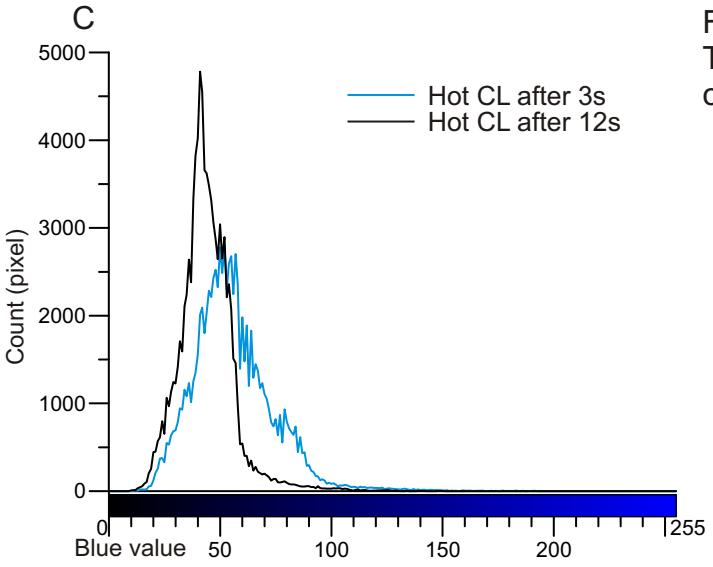

Figure 3B-17: Grain 17. The grain shows slight colour shift.

D

Blue value	Min	Max	Mode	Mean	SD
After 3s	10	213	52	56	18.4
After 12s	8	205	41	44	12.4

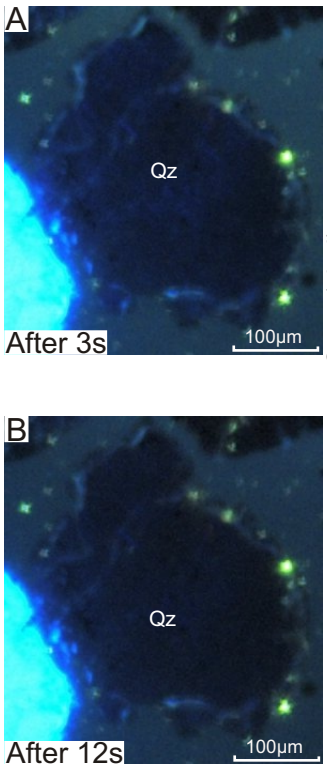

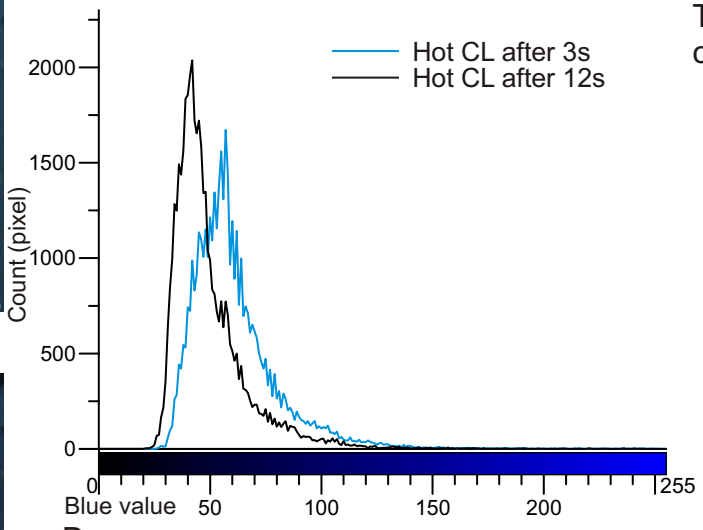

Figure 3B-18: Grain 18. The grain shows slight colour shift.

D

Blue value	Min	Max	Mode	Mean	SD
After 3s	26	251	57	61	19.8
After 12s	21	244	42	50	17.6

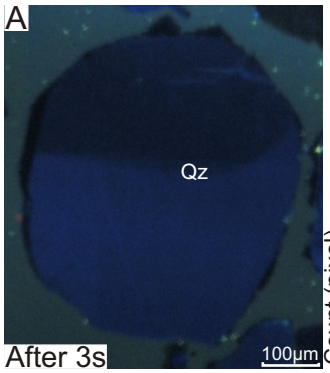

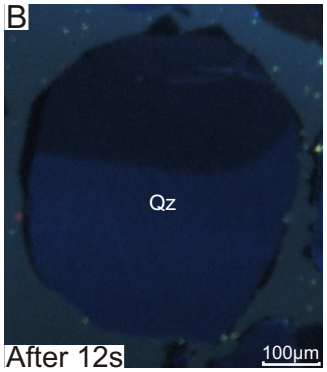

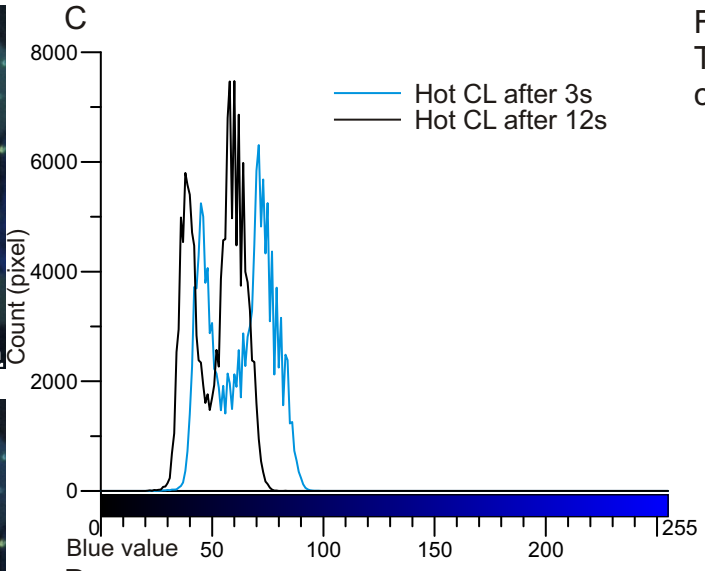

Figure 3B-19: Grain 19. The grain shows slight colour shift.

D

Blue value	Min	Max	Mode	Mean	SD
After 3s	23	98	71	63	13.8
After 12s	20	83	60	52	11.1

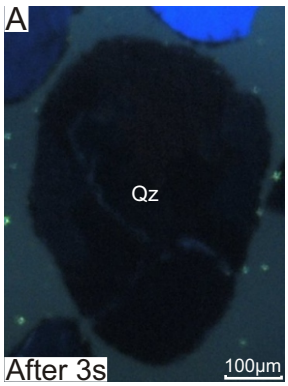

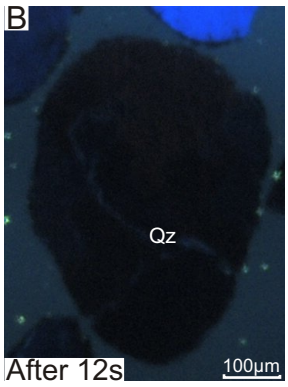

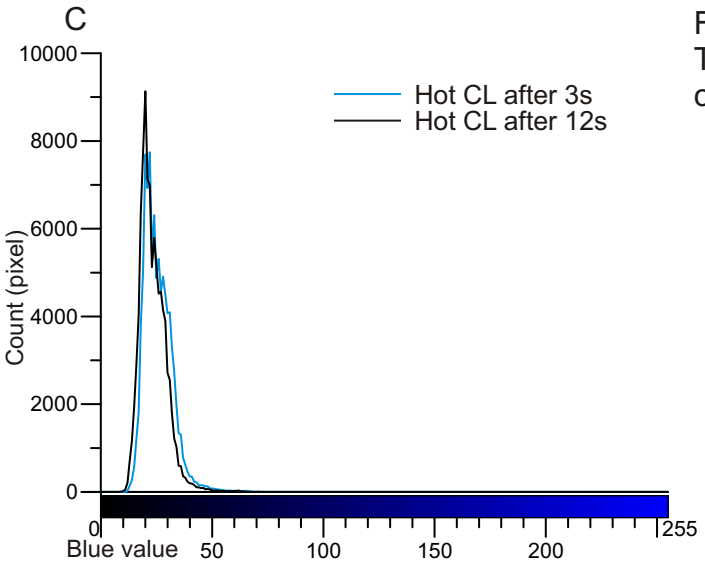

Figure 3B-20: Grain 20. The grain shows no colour shift.

D

Blue value	Min	Max	Mode	Mean	SD
After 3s	12	73	22	26	6.4
After 12s	8	70	20	23	5.9



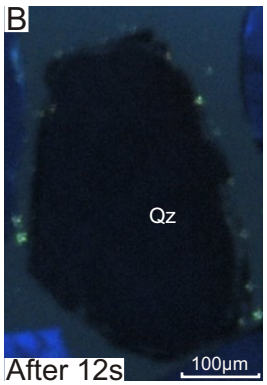

C

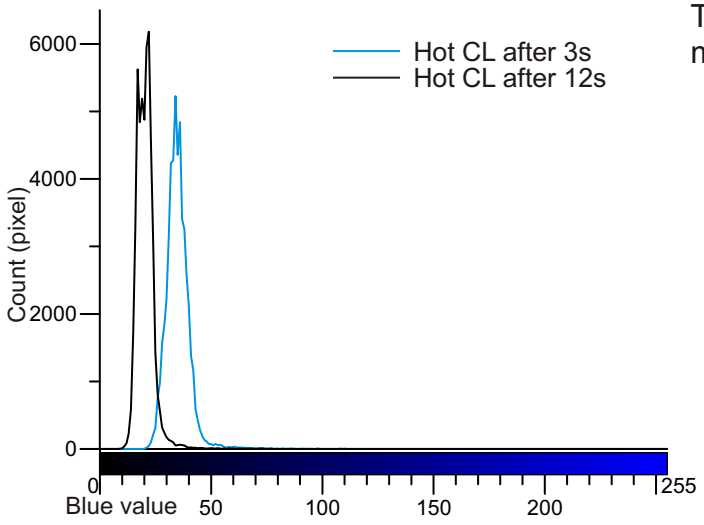

D

Blue value	Min	Max	Mode	Mean	SD
After 3s	20	156	34	35	5.7
After 12s	9	151	22	20	4.7

Figure 3B-21: Grain 21. The grain shows moderate colour shift.

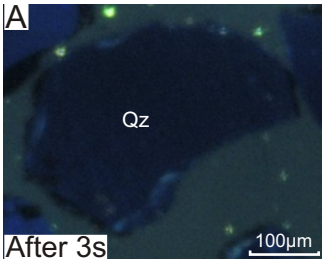

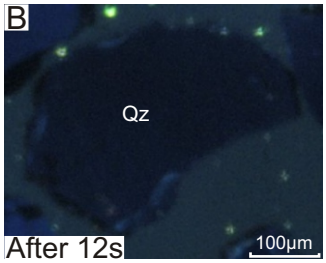

C

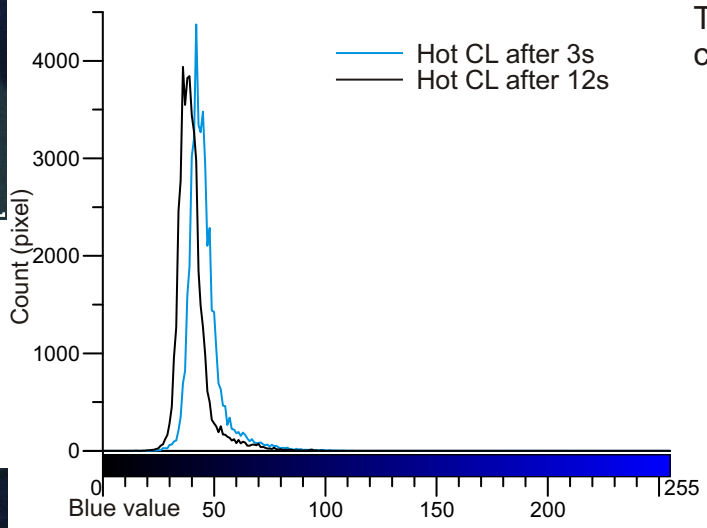

D

Blue value	Min	Max	Mode	Mean	SD
After 3s	22	112	42	46	7.8
After 12s	15	102	36	40	7.1

Figure 3B-22: Grain 22. The grain shows slight colour shift.

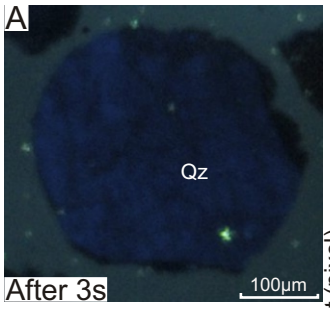

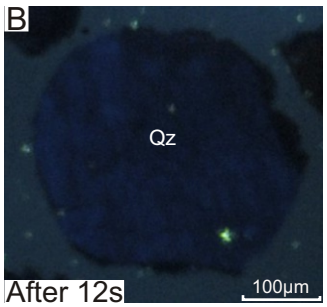

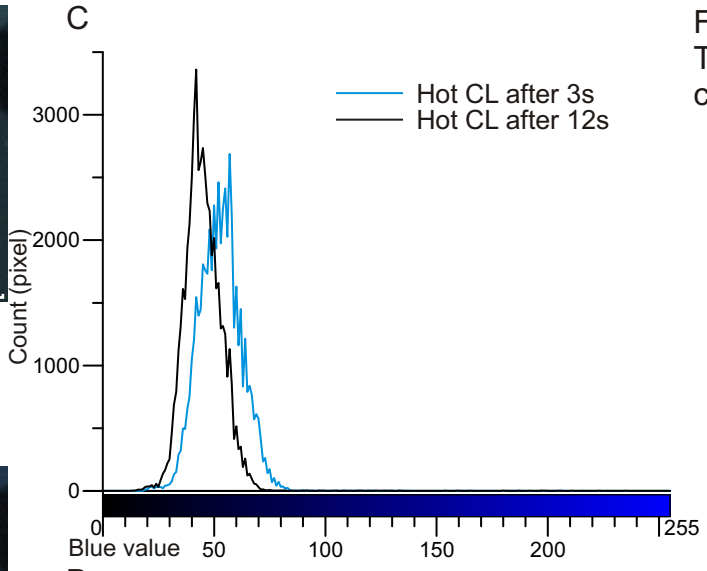

Figure 3B-23: Grain 23. The grain shows slight colour shift.

D

Blue value	Min	Max	Mode	Mean	SD
After 3s	16	239	57	53	9.8
After 12s	13	235	42	45	8.6

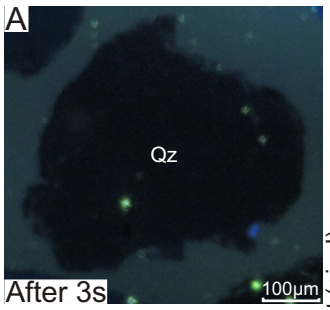

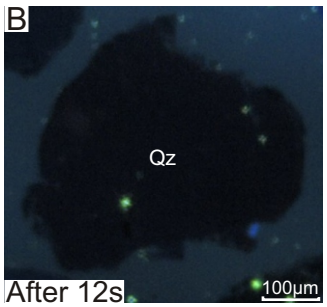

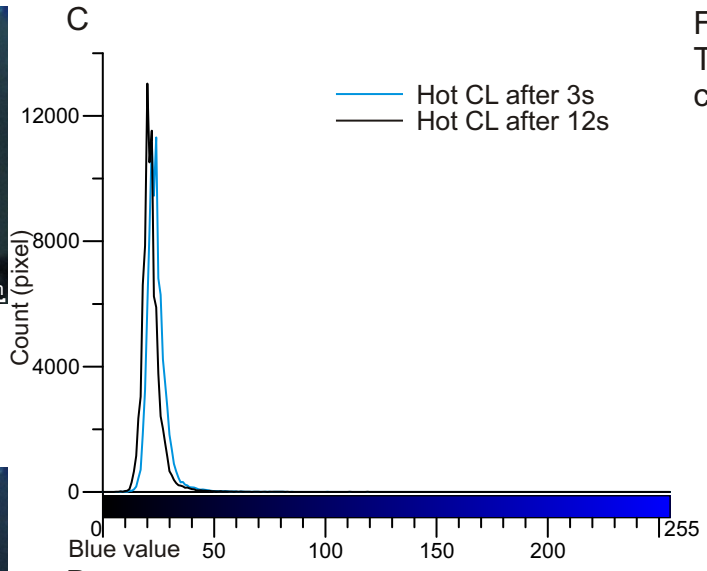

Figure 3B-24: Grain 24. The grain shows no colour shift.

D

Blue value	Min	Max	Mode	Mean	SD
After 3s	5	222	24	24	5.9
After 12s	4	223	20	22	5.9

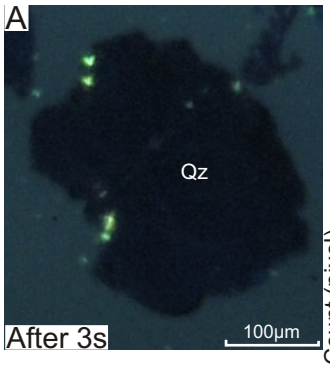

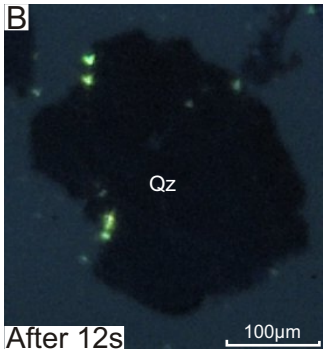

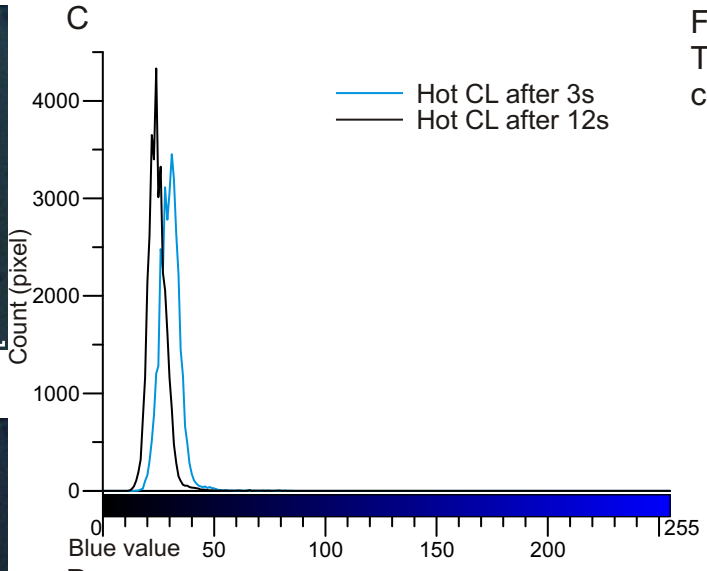

Figure 3B-25: Grain 25. The grain shows slight colour shift.

D

Blue value	Min	Max	Mode	Mean	SD
After 3s	16	85	31	30	4.6
After 12s	12	82	24	25	4.3



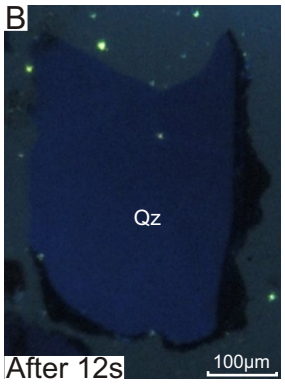

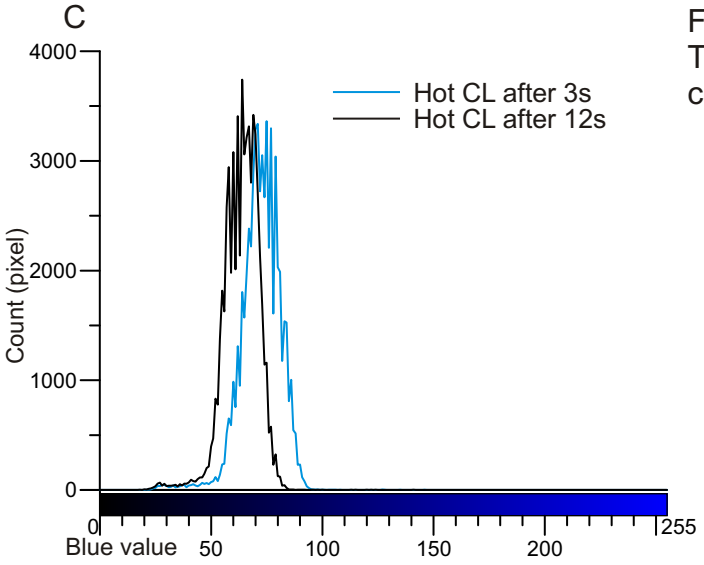

Figure 3B-26: Grain 26. The grain shows slight colour shift.

D

Blue value	Min	Max	Mode	Mean	SD
After 3s	21	146	75	72	8.9
After 12s	18	141	64	64	7.8

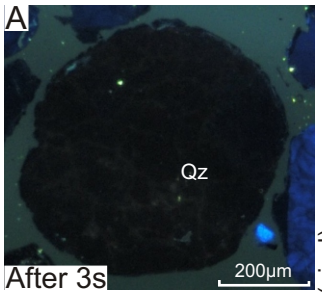

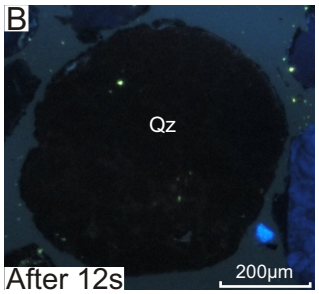

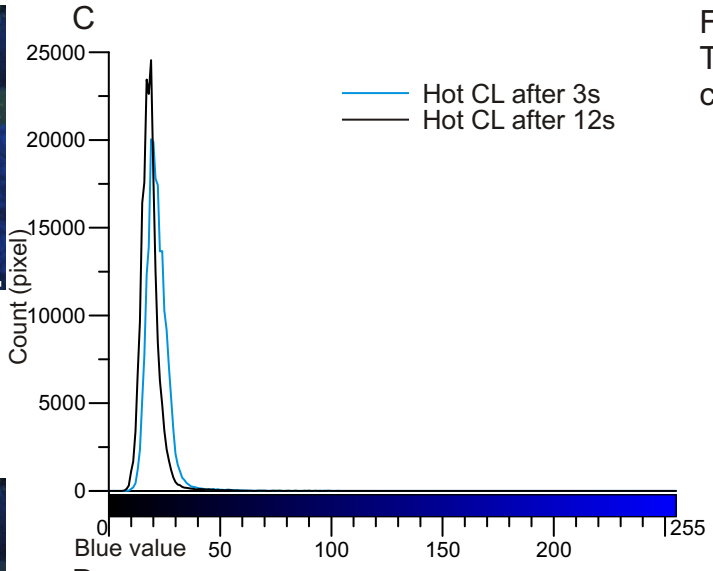

Figure 3B-27: Grain 27. The grain shows no colour shift.

D

Blue value	Min	Max	Mode	Mean	SD
After 3s	7	246	19	22	5.9
After 12s	5	244	19	19	5.5

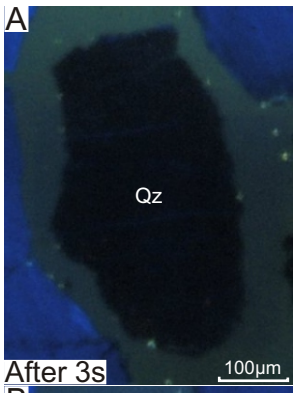



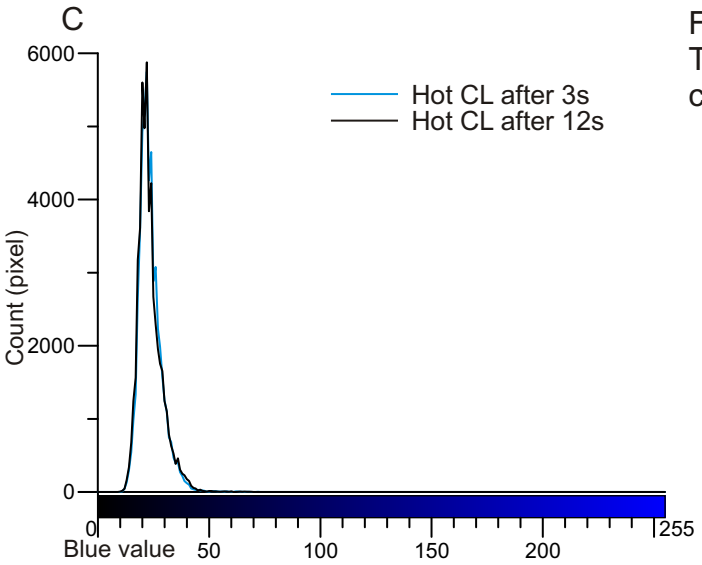

Figure 3B-28: Grain 28. The grain shows no colour shift.

D

Blue value	Min	Max	Mode	Mean	SD
After 3s	10	75	22	24	5.2
After 12s	10	73	22	23	5.5

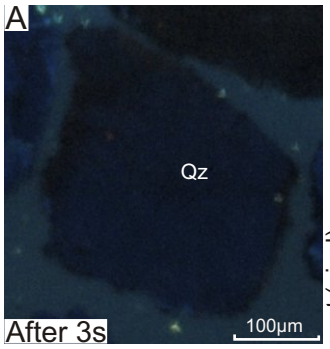

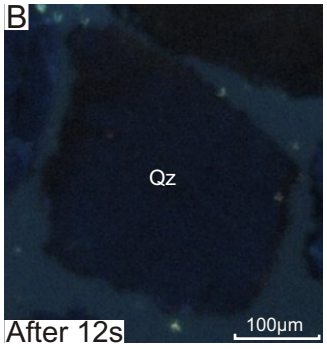

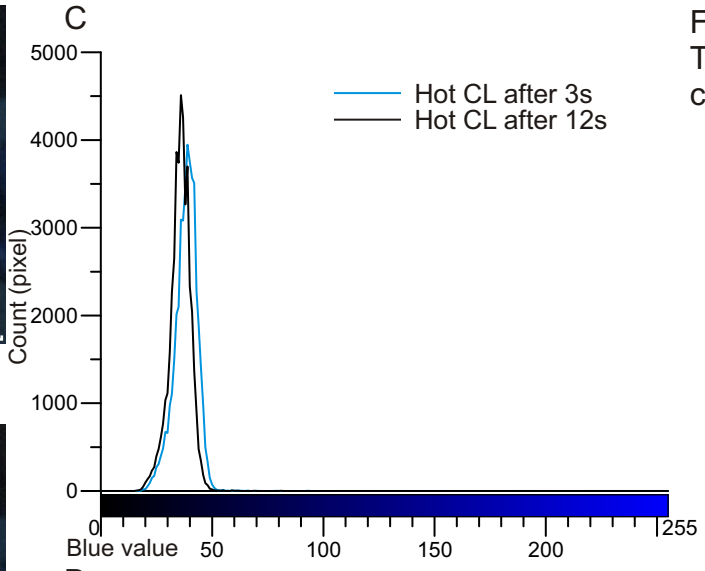

Figure 3B-29: Grain 29. The grain shows no colour shift.

D

Blue value	Min	Max	Mode	Mean	SD
After 3s	16	93	39	38	5.1
After 12s	13	90	36	36	4.7





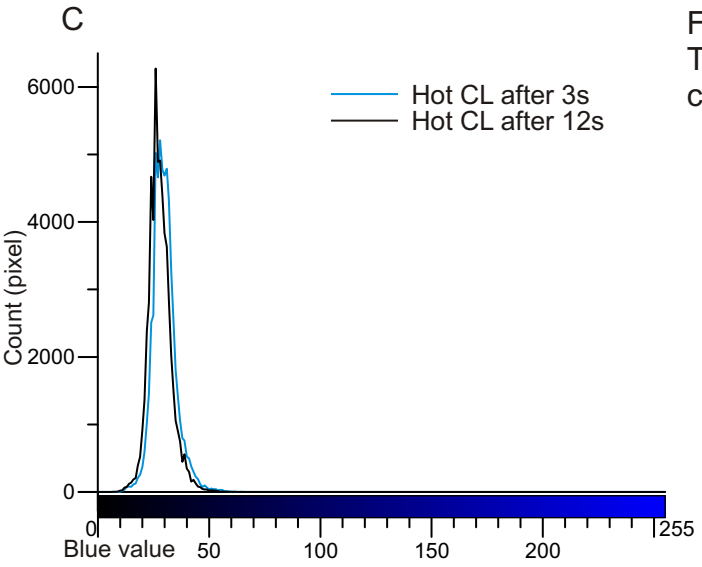

Figure 3B-30: Grain 30. The grain shows no colour shift.

D

Blue value	Min	Max	Mode	Mean	SD
After 3s	7	65	28	30	5.3
After 12s	7	64	26	28	5.1

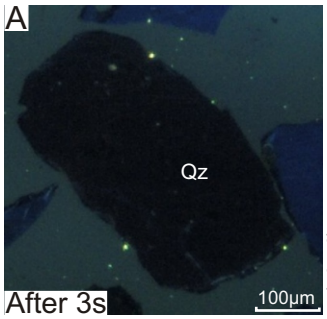

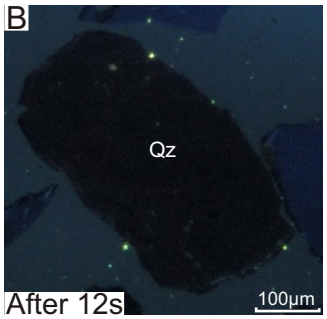

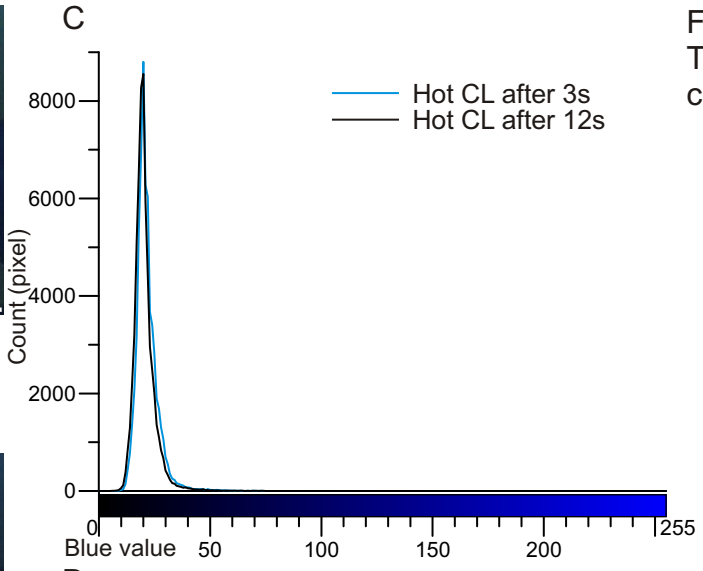

Figure 3B-31: Grain 31. The grain shows no colour shift.

D

Blue value	Min	Max	Mode	Mean	SD
After 3s	8	89	20	22	5
After 12s	6	89	20	20	4.7

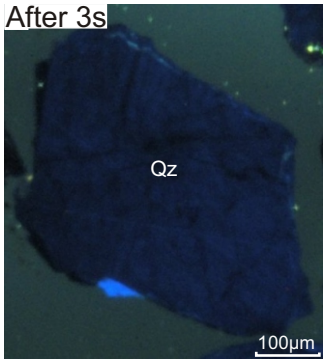

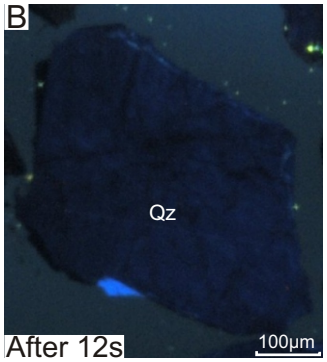

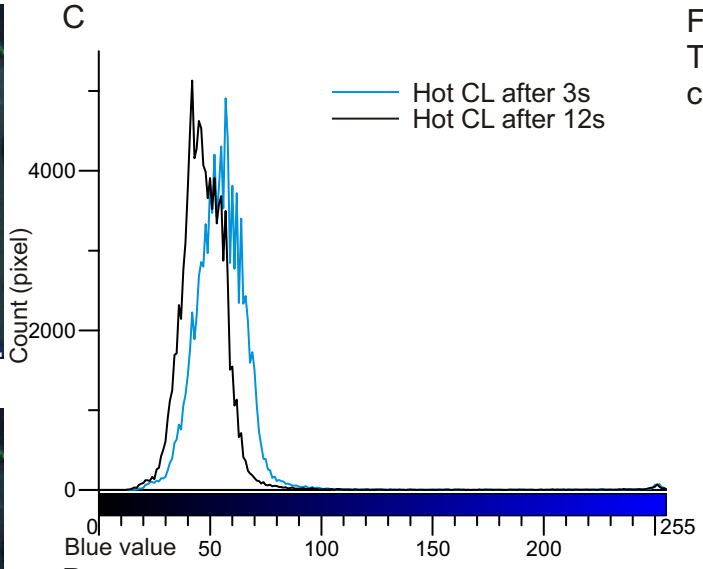

Figure 3B-32: Grain 32. The grain shows slight colour shift.

D

Blue value	Min	Max	Mode	Mean	SD
After 3s	16	255	57	56	17.6
After 12s	12	255	42	48	16.9

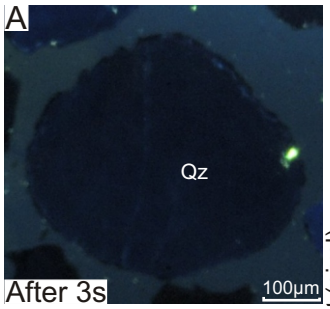

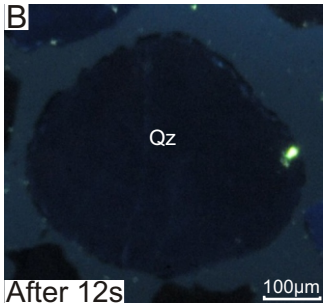

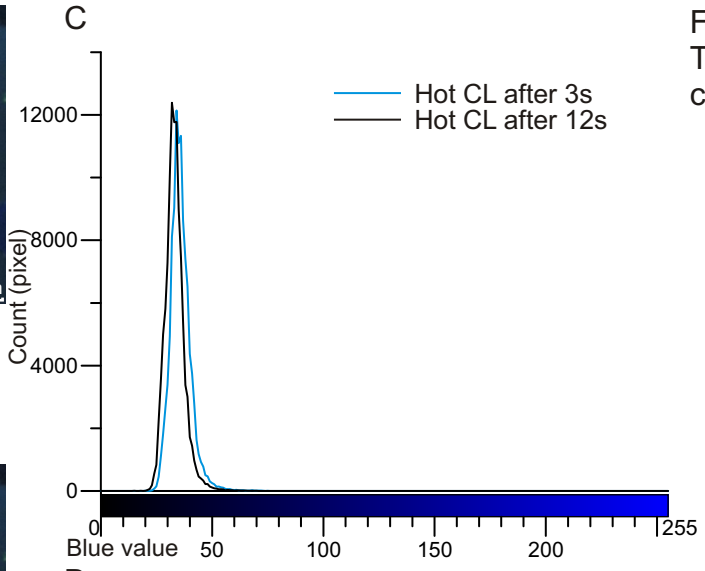

Figure 3B-33: Grain 33. The grain shows no colour shift.

D

Blue value	Min	Max	Mode	Mean	SD
After 3s	17	125	34	36	4.8
After 12s	10	115	32	33	4.5

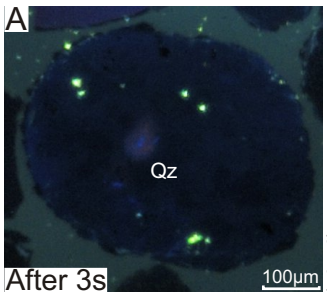

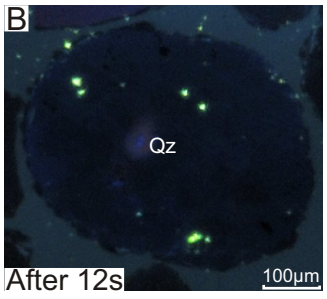

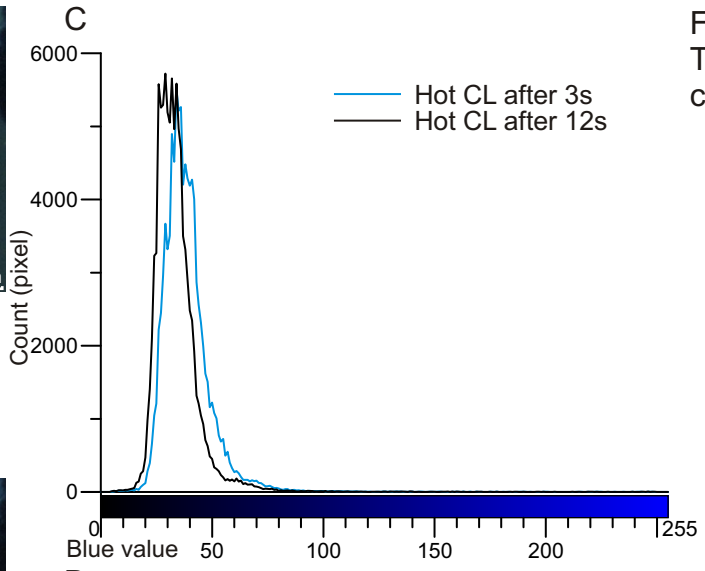

Figure 3B-34: Grain 34. The grain shows slight colour shift.

D

Blue value	Min	Max	Mode	Mean	SD
After 3s	4	253	34	39	12.1
After 12s	4	252	29	34	11.3

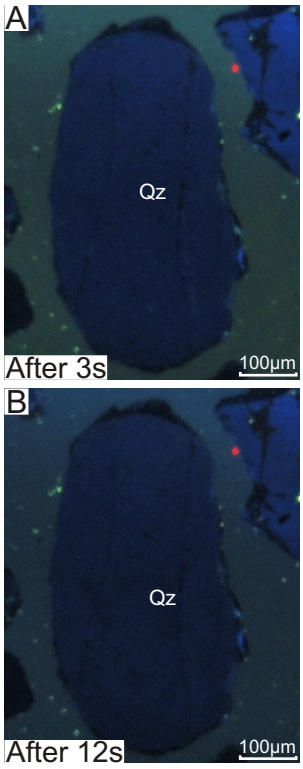

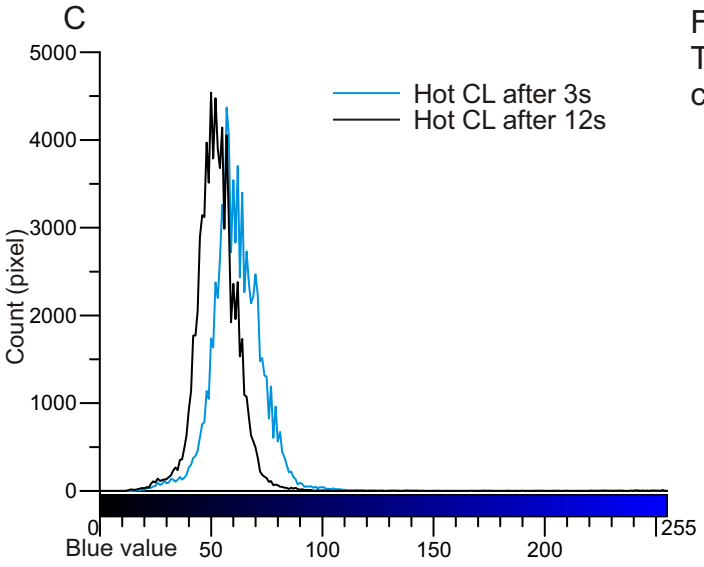

Figure 3B-35: Grain 35. The grain shows slight colour shift.

D

Blue value	Min	Max	Mode	Mean	SD
After 3s	27	154	57	61	9.9
After 12s	19	133	50	52	8.2

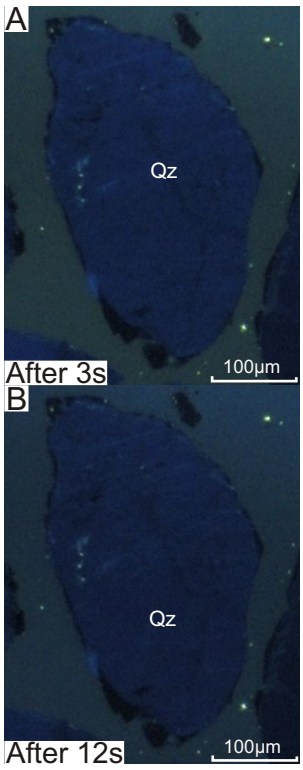

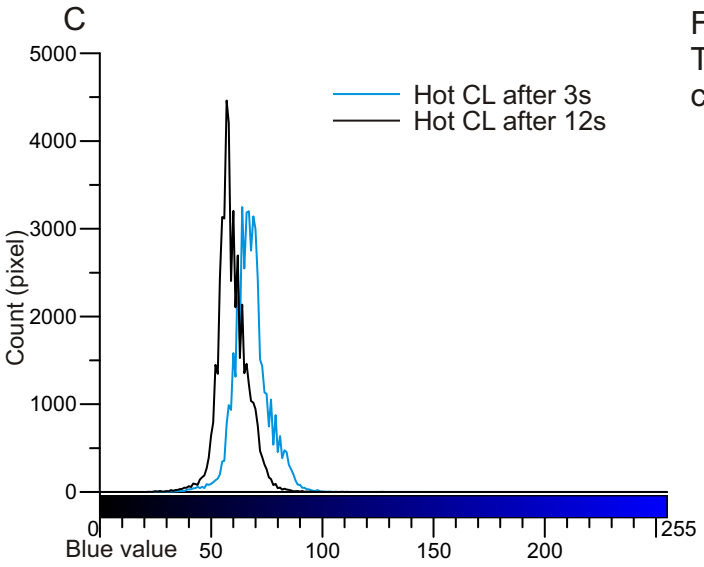

Figure 3B-36: Grain 36. The grain shows slight colour shift.

D

Blue value	Min	Max	Mode	Mean	SD
After 3s	24	131	64	68	7.8
After 12s	21	132	57	60	6.8

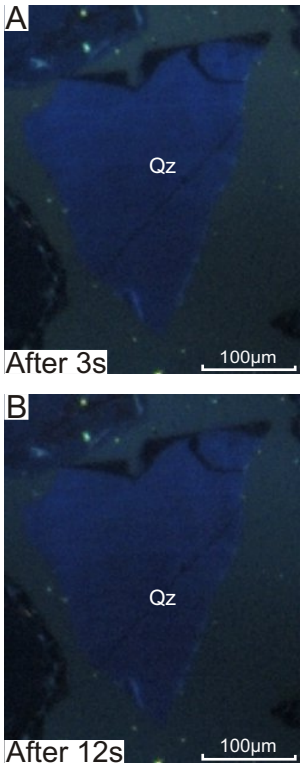

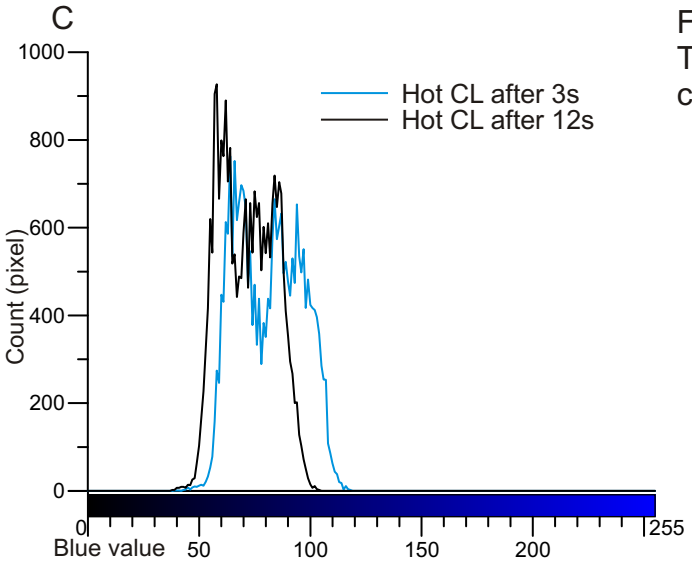

Figure 3B-37: Grain 37. The grain shows slight colour shift.

D

Blue value	Min	Max	Mode	Mean	SD
After 3s	39	118	64	81	14.5
After 12s	38	104	58	72	12.1

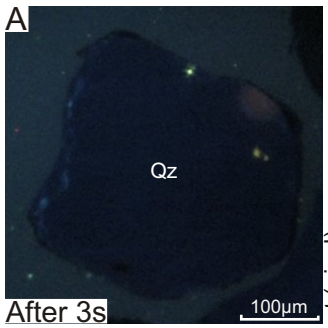

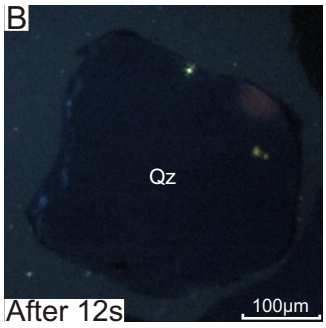

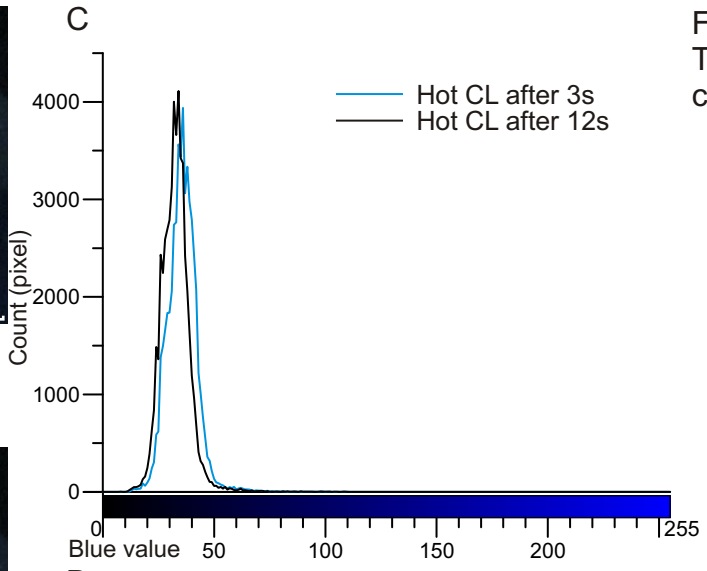

Figure 3B-38: Grain 38. The grain shows no colour shift.

D

Blue value	Min	Max	Mode	Mean	SD
After 3s	11	110	36	36	6.8
After 12s	8	109	34	33	6.4

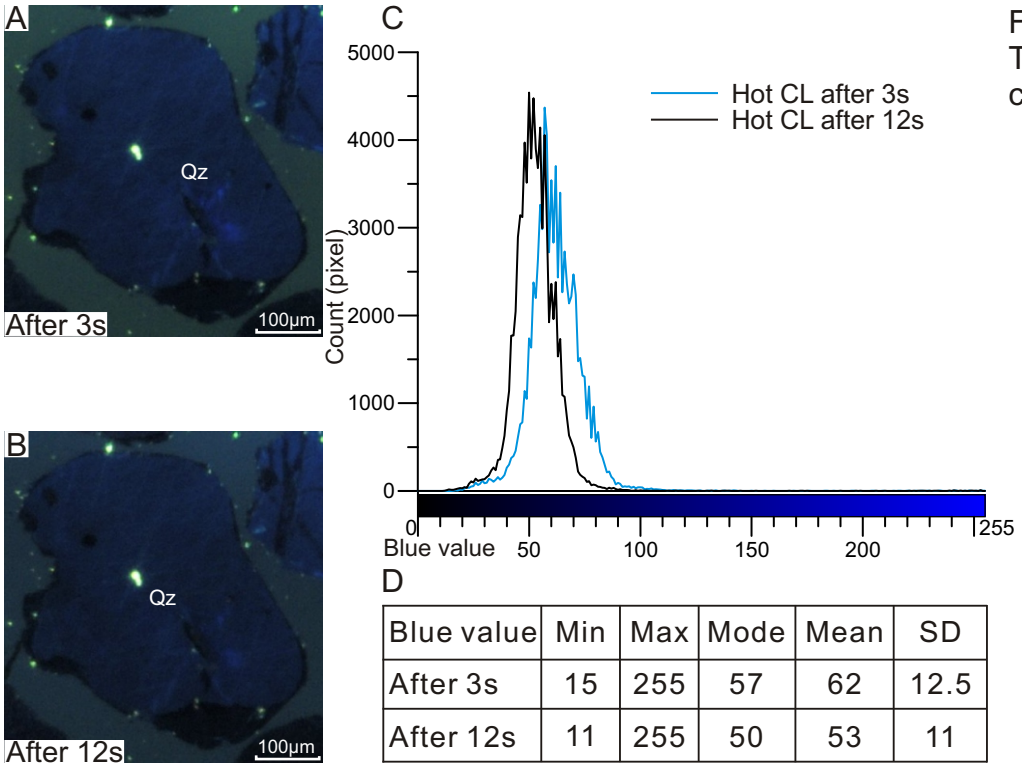

Figure 3B-39: Grain 39. The grain shows slight colour shift.

D

Blue value	Min	Max	Mode	Mean	SD
After 3s	15	255	57	62	12.5
After 12s	11	255	50	53	11

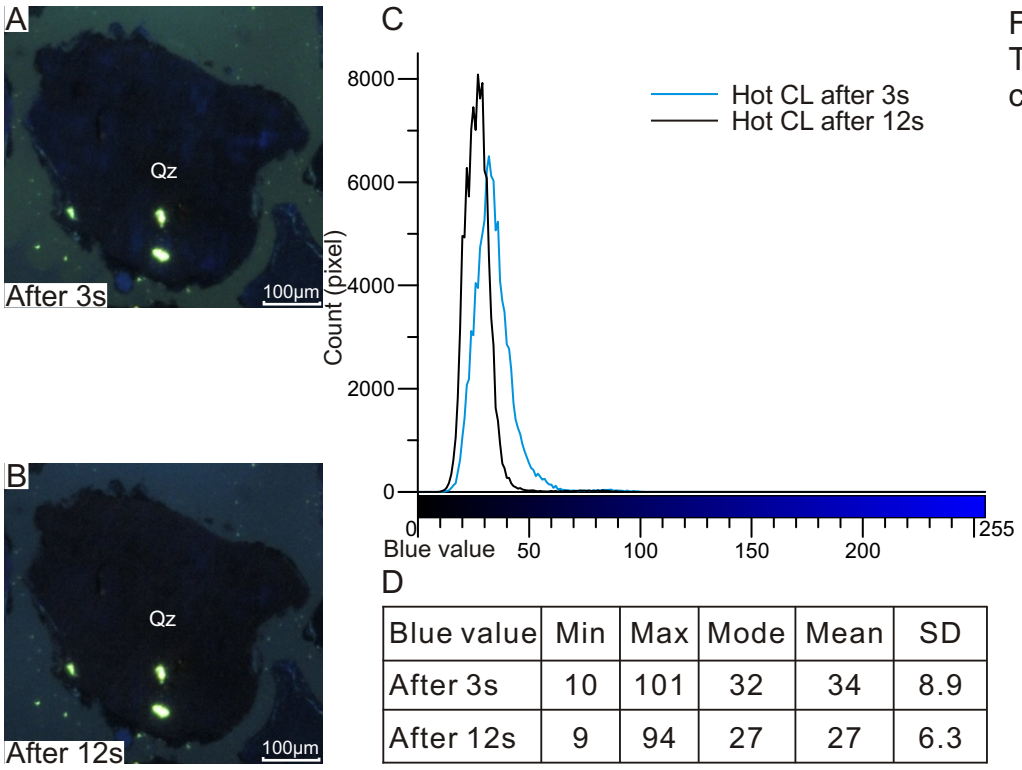

Figure 3B-40: Grain 40. The grain shows slight colour shift.

D

Blue value	Min	Max	Mode	Mean	SD
After 3s	10	101	32	34	8.9
After 12s	9	94	27	27	6.3

Appendix 4A: Microphotos, SEM-BSE images, SEM-CL images, and EDS analyses of detrital quartz grains in sample 3000.

Notes:

1. **Homogenous CL:** Nearly uniform CL intensity across the grain (Fig. 2A).

2. Fractures in quartz have been divided into two types: **healed fractures** (**HF**) and **open fractures** (**OF**).

   Healed fractures are fractures filled with secondary silica that appear as thin (commonly < 10 μm) black lines in SEM-CL images (Fig. 2B). They are usually not shown in back-scattered images (Boggs and Krinsley, 2006).

   Open fractures appear in cathodoluminescense images as CL-dark or CL-bright lines, and they are also visible in back-scattered images and microphotos. A few open fractures are **conchoidal fractures** (**CF**) (Boggs and Krinsley, 2006).

3. **Tectonic deformation lamellae**: Tectonic deformation lamellae (Fig. 2C) appear in SEM-CL image as numerous sets of thin, parallel, closely spaced, dark gray lines (Bernet and Basset, 2005). According to Hamers and Drury (2011), tectonic deformation lamellae can either appear as dark gray lines or bright lines in SEM-CL images, and can show slightly wavy features with varying thickness. They usually also appear in XPL image under petrographic microscope.

4. **Spiders (S):** They are made up of dark-Cl patches and streaks. Dark-CL patches mainly range from 10-100 μm. Streaks are random and irregular in the appearance of black broad (>10 μm) elongated form. The spiders are commonly associated with healed fractures, giving them the appearance in SEM-CL images of spiders sitting on a web (Fig. 2D). They cannot be seen in BSE images, since they are composed by secondary silica (Boggs and Krinsley, 2006).

5. **Bright mottling**: Some grains show irregular CL intensity across grains, creating a mottled pattern due the presence of patches (Boggs and Krinsley, 2006). Three types of bright mottling were seen.

   - **Random bright patches** (Fig. 2E1)
   - **Bright streaky patches fabric** (Fig. 2E2)
   - **Subtle mottling** (Fig. 2E3)

6. **Overgrowth:** Overgrowth appears in SEM-CL images as dark areas in the border of the quartz grains (Fig. 2F).

7. **Fluid inclusion trail** (**FI trail**): Trails formed by **fluid inclusions** (**FI**). They are usually associated with secondary porosity and commonly located along fractures and at boundaries between detritral quartz grain and the overgrowth. They are well observed in microphotos under ppl. The fluid inclusion trails can be separated in two kinds: **detrital fluid inclusion trails (**fluid inclusions that are original from the detrital quartz, they do not cut the quartz overgrowth) and **diagenetic fluid inclusion trails** (fluid inclusions originated from the diagenesis, and they thus cut the quartz overgrowth).

8. **Melt inclusion** (**MI**): Large fluid inclusions (>10 μm) in which crystallized minerals are visible.

9. **Secondary porosity** (**SP**): Porosities usually caused by dissolution and/or fractures. They are easily observed in microphotos under PPL and BSE images.

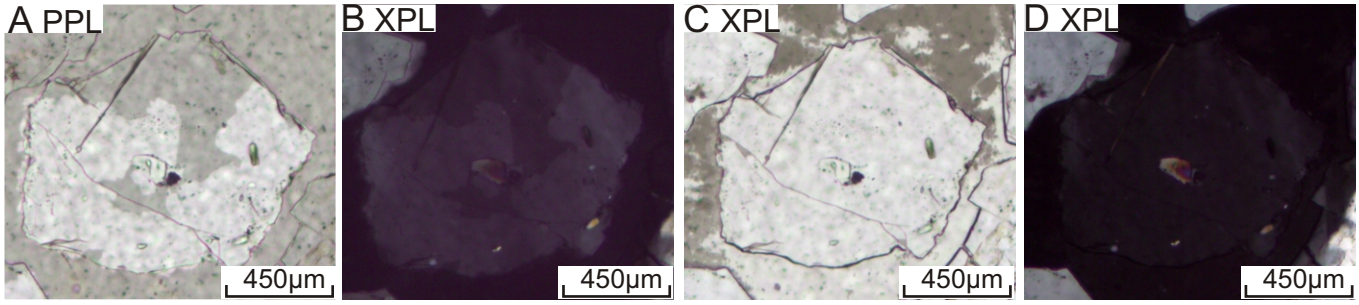

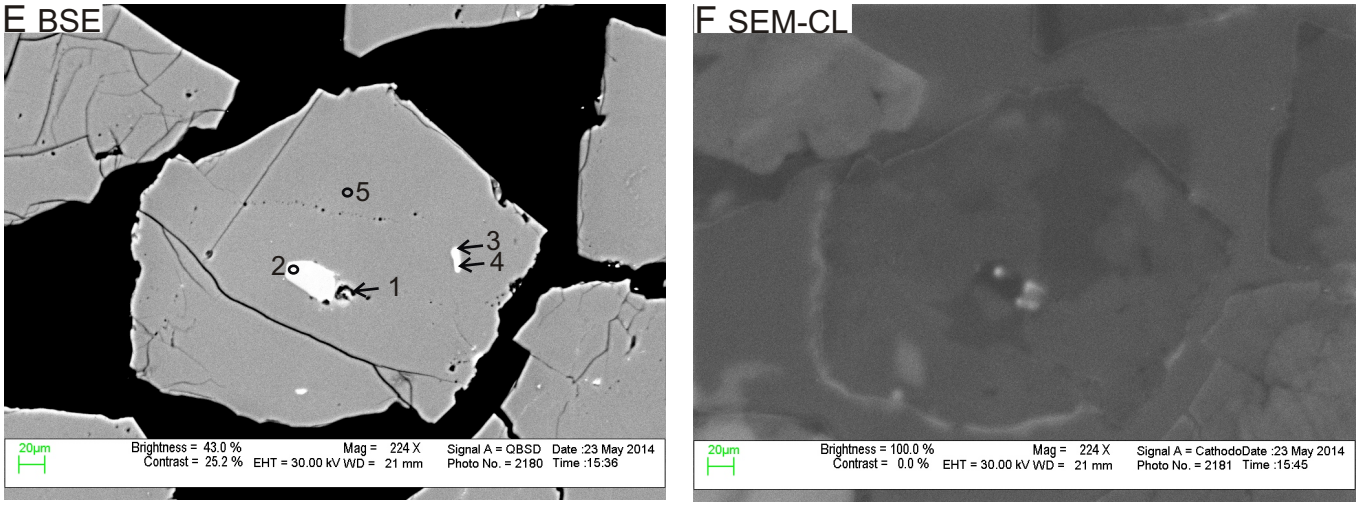

E EDS analyses

Pos#	Min. ID	SiO2	TiO2	Al2O3	FeO	MgO	CaO	Na2O	K2O	P2O5	F	Total	Actual total
1	Ms	47.54	0.40	34.07	1.27	0.55		0.52	10.64			95	94
2	Ap	12.13		10.85	0.31		35.27		2.81	33.66	4.95	100	105
3	Fluid inclusion	86.66	0.35	3.12	5.88	1.72			2.28			100	87
4	Fluid inclusion	77.22	0.63	5.8	9.3	3.37			3.7			100	89
5	Qz	99.99										100	111

Figure 4A-1: Microphotos under ppl (A and C) and xpl (B and D), BSE image (E) and SEM-CL image (F) of quartz grain 1 in sample 3000. Fig. C and D were taken after cleaning the thin section to preclude the possibility of uneven carbon coating. The occurrence of zoning in Fig. A and B, not in Fig. C and D, results from the severely uneven carbon coating on the original thin section. The grain is subhedral and sub-angular monocrystalline with moderate undulose extinction. Fluid inclusions are present. The grain contains muscovite and apatite inclusions, and is microfractured with a set of irregular fractures (Fig. E and F). Healed fractures are rare . The dark area indicated by arrow in Fig. D is overgrowth. The zoning that appears in Fig. F is due the uneven carbon coating on the original thin section.

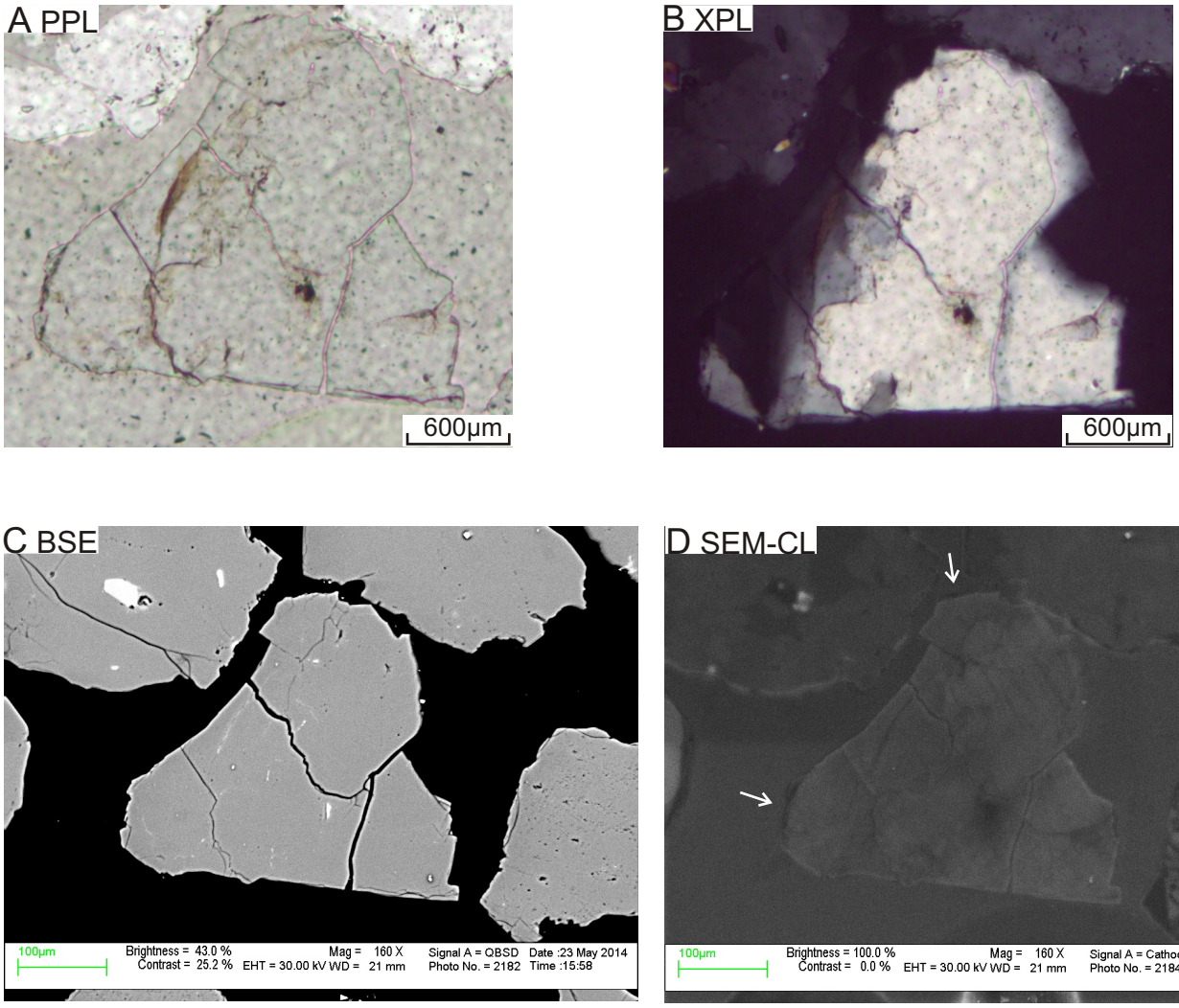

Figure 4A-2: Microphotos under ppl (A) and xpl (B), SEM-BSE image C, and SEM-CL image (D) of quartz grain 2 in sample 3000. The grain is anhedral and sub-angular polycrystalline (only a few sub-grains with sutured sub-grain boundaries) with strong undulose extinction. Fluid inclusions are not common. The grain is weakly microfractured with irregular fractures (Fig. C and D). Healed fractures are rare; the dark-Cl lines in SEM-CL image are the sub-grain boundaries or open fractures. The dark areas indicated by arrows in Fig. D are overgrowth.

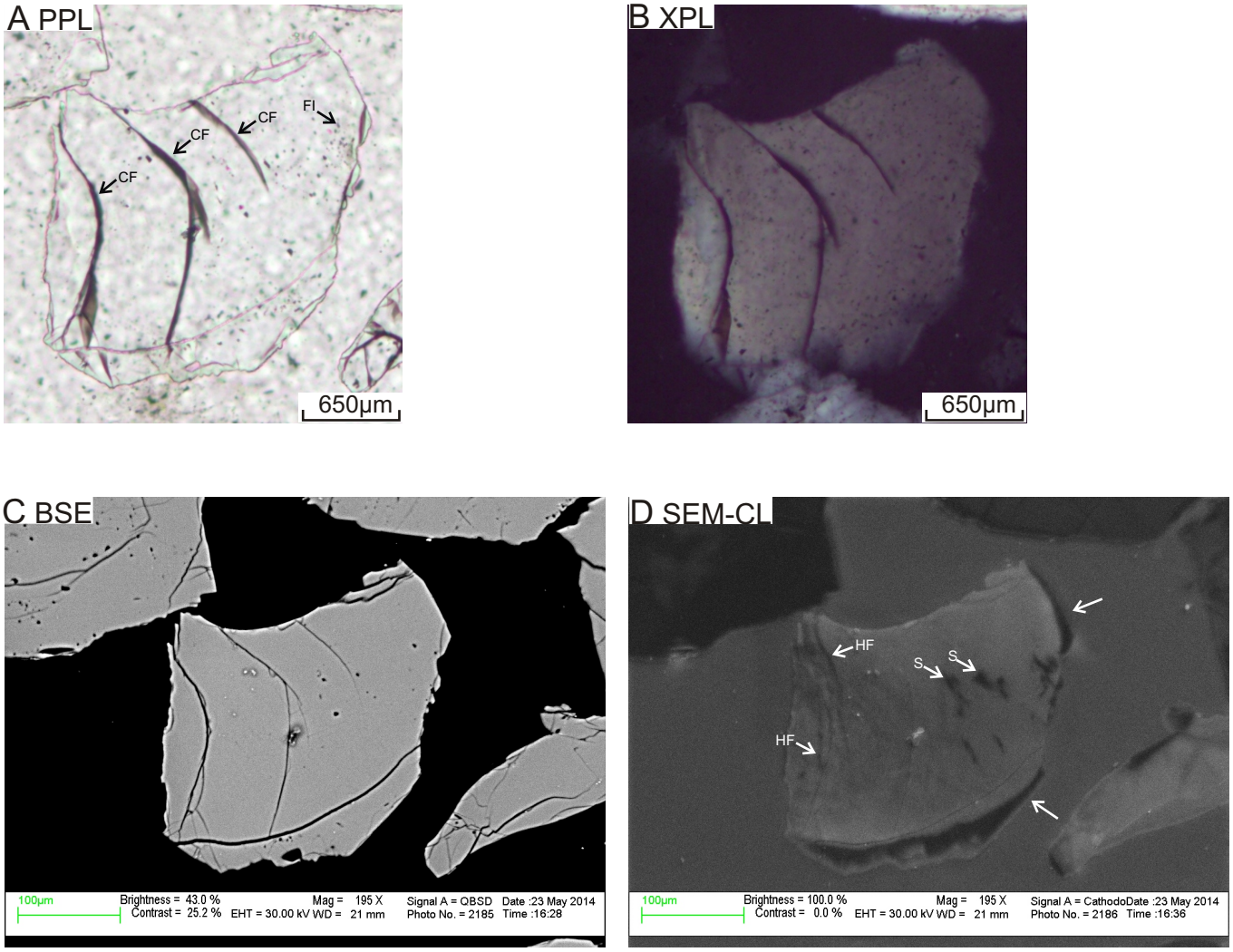

Figure 4A-3: Microphotos under ppl (A) and xpl (B), SEM-BSE image C, and SEM-CL image (D) of quartz grain 3 in sample 3000. The grain is anhedral and sub-angular monocrystalline with strong undulose extinction. Fluid inclusions are present (Fig. A). The grain is microfractured with a set of irregular fractures and a set of conchoidal fractures (CF) (Fig. A and D). A few healed fractures (HF) and spiders (S), which are secondary porosity filled by diagenetic quartz, can be seen in Fig. D. The dark areas indicated by arrows in Fig. D are overgrowth; these areas appear corroded in Fig. C, suggesting secondary porosity.

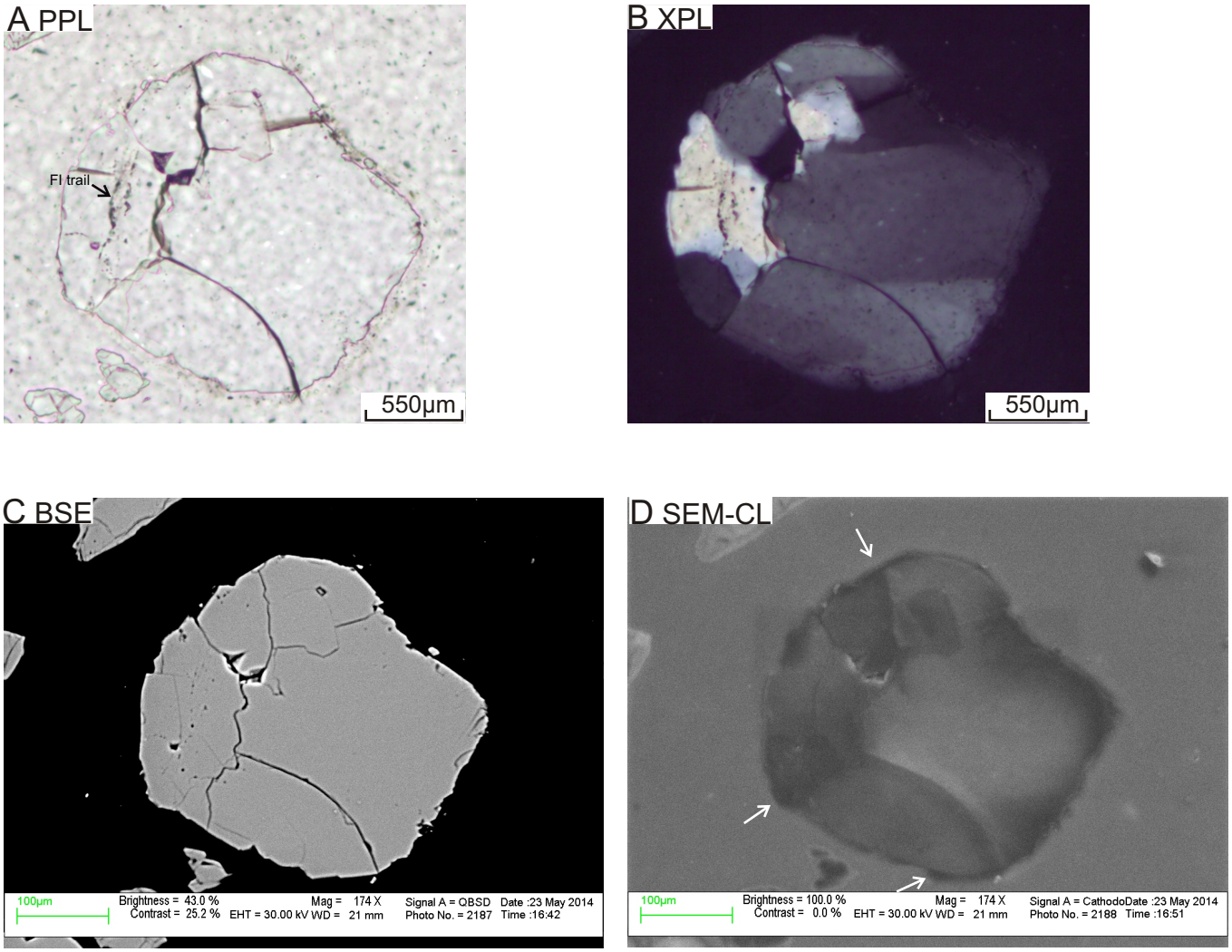

Figure 4A-4: Microphotos under ppl (A) and xpl (B), SEM-BSE image C, and SEM-CL image (D) of quartz grain 4 in sample 3000. The grain is anhedral and sub-angular polycrystalline (only a few sub-grains with sutured sub-grain boundaries) with mosaic texture and weak undulose extinction. Fluid inclusion trails are present (Fig. A). The grain is weakly microfractured with a set of irregular fractures (Fig. C and D). Healed fractures are rare; the dark-CL lines and the bright-CL lines in SEM-CL image are the sub-grain boundaries. The dark areas indicated by arrows in Fig. D are overgrowth.

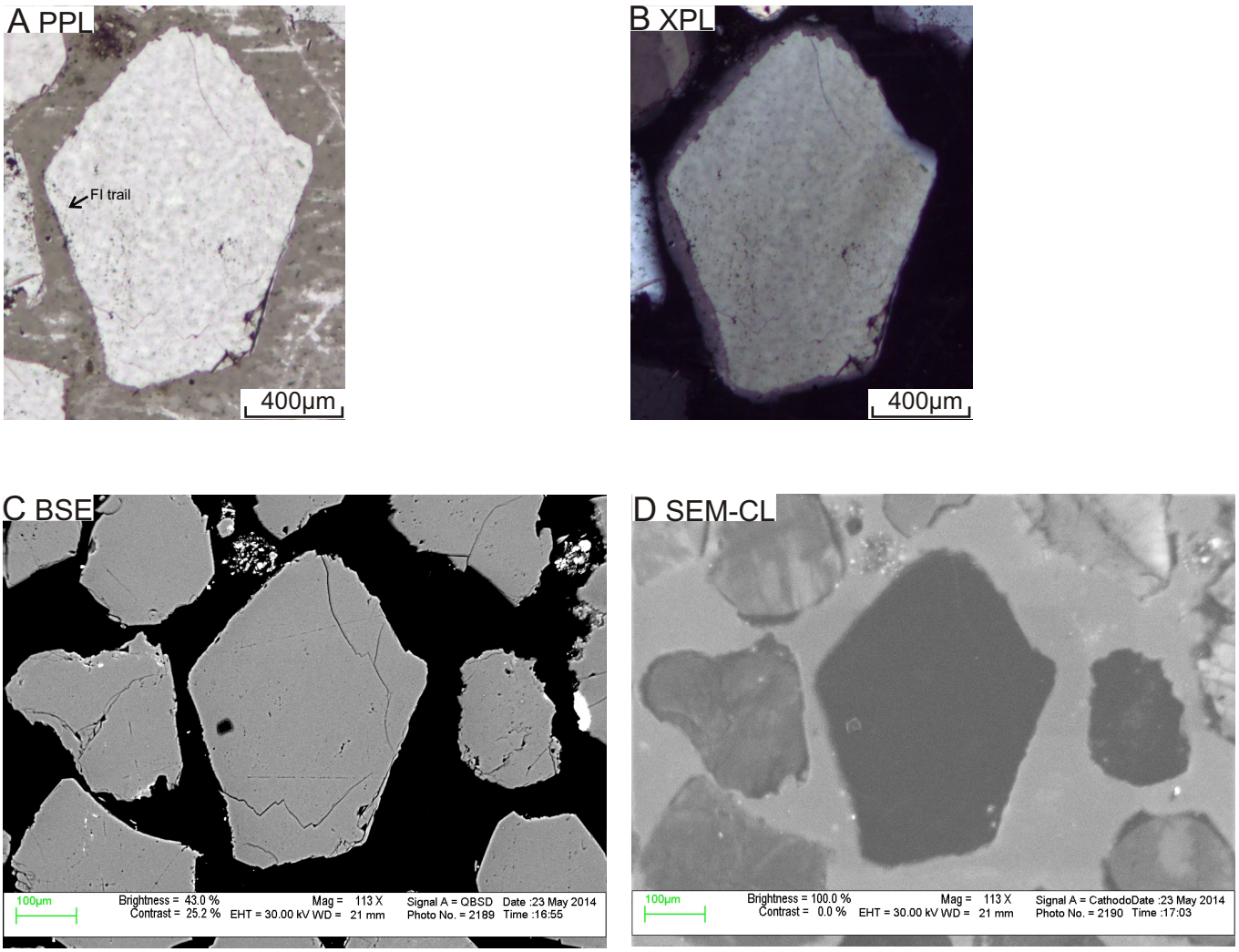

Figure 4A-5: Microphotos under ppl (A) and xpl (B), SEM-BSE image C, and SEM-CL image (D) of quartz grain 5 in sample 3000. The grain is anhedral and sub-angular monocrystalline with mosaic texture and weak undulose extinction. Fluid inclusion trails are present (Fig. A). The grain is weakly microfractured with a set of irregular fractures (Fig. C). Healed fractures are rare. The grains shows homogenous dark-CL in SEM-CL image.

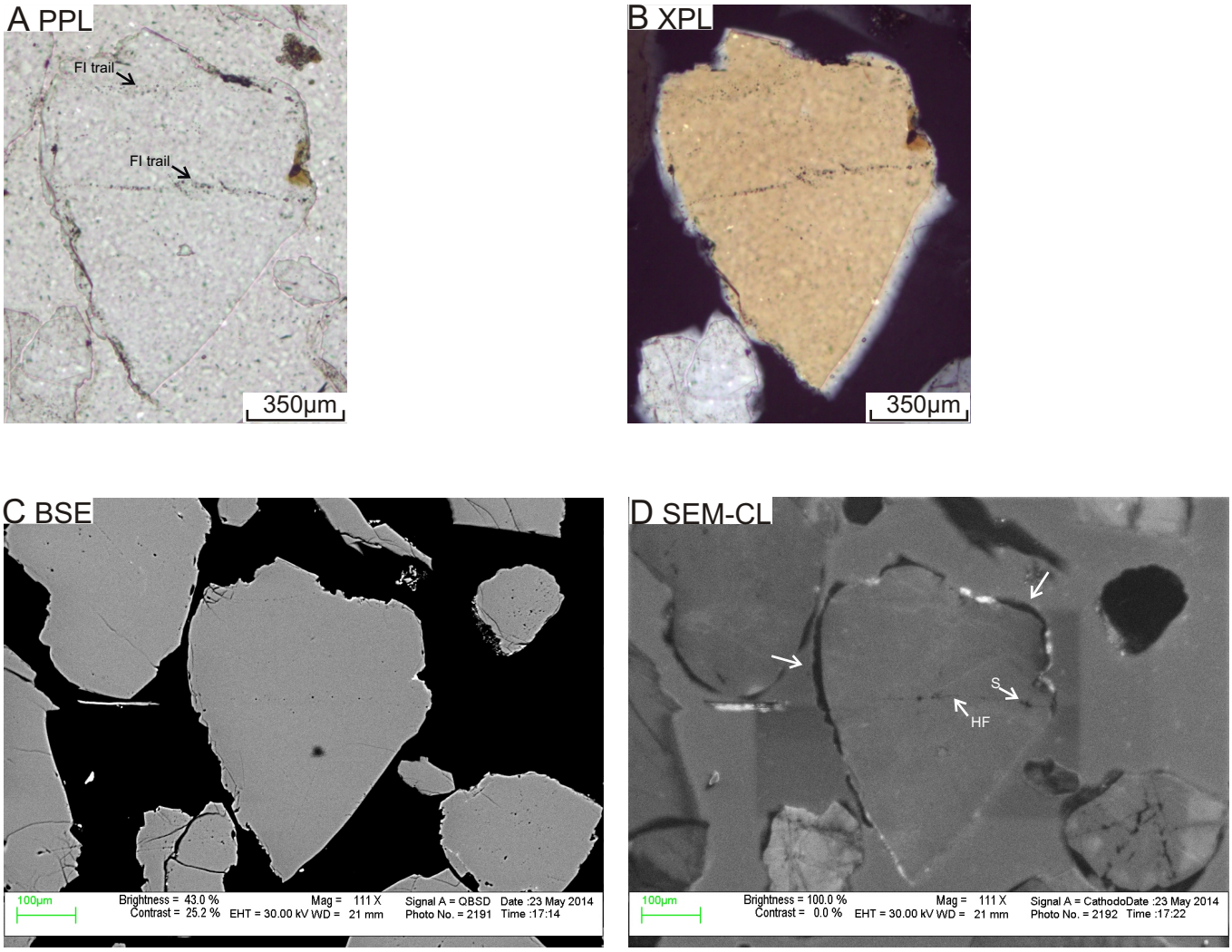

Figure 4A-6: Microphotos under ppl (A) and xpl (B), SEM-BSE image C, and SEM-CL image (D) of quartz grain 6 in sample 3000. The grain is anhedral and sub-angular monocrystalline with weak undulose extinction. Fluid inclusions are present and form trails along healed fractures (Fig. A). The grain is weakly microfractured with irregular fractures (Fig. C and D). A few healed fractures (HF) and spiders (S), which are secondary porosity filled by diagenetic quartz, can be seen in Fig. D. The dark areas indicated by arrows in Fig. D are overgrowth; these areas appear corroded in Fig. C, suggesting secondary porosity.

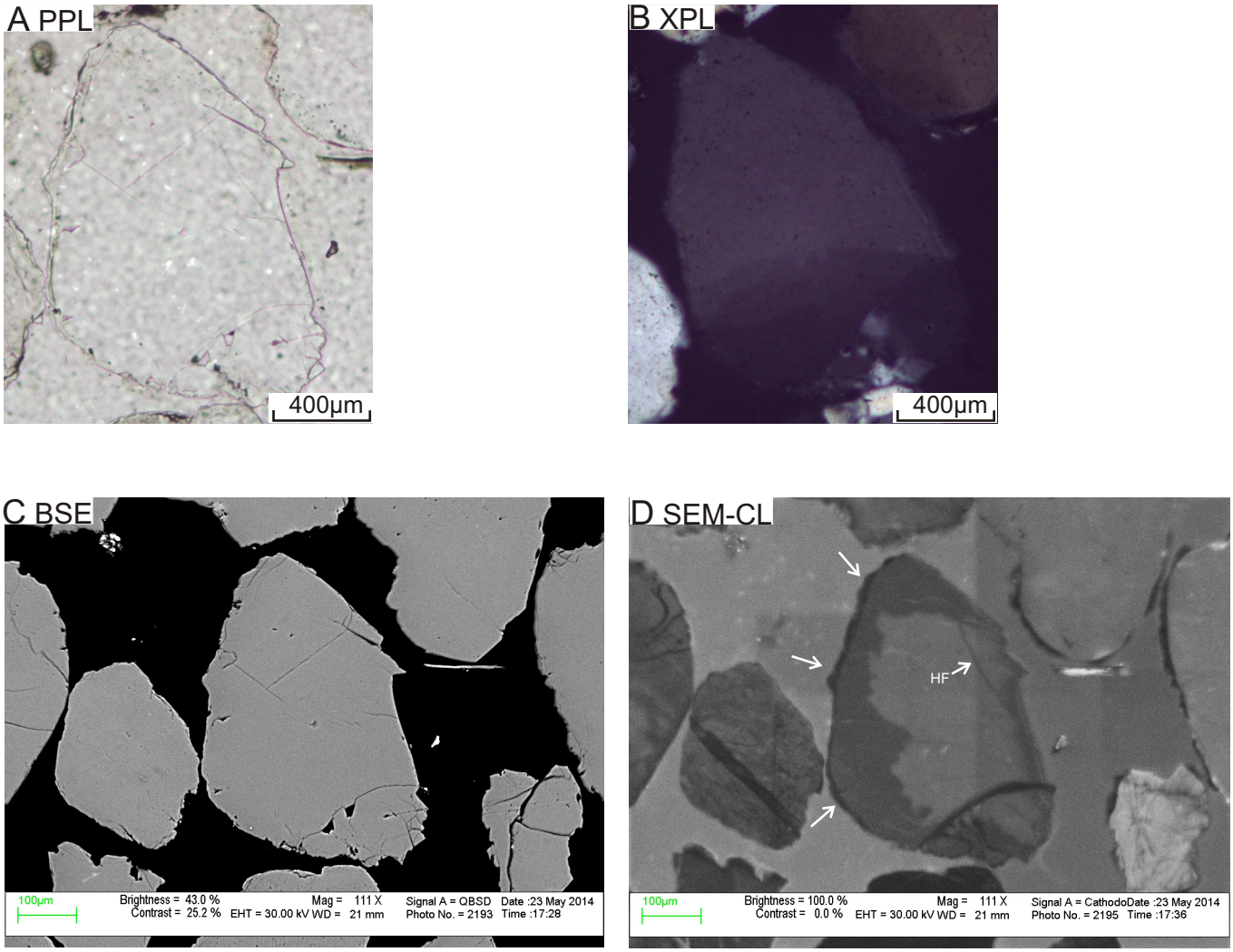

Figure 4A-7: Microphotos under ppl (A) and xpl (B), SEM-BSE image C, and SEM-CL image (D) of quartz grain 7 in sample 3000. The grain is anhedral and sub-rounded polycrystalline (only a few sub-grains) with strong undulose extinction. Fluid inclusions are rare. The grain is microfractured with a set of irregular fractures (Fig. C and D). Only a few healed fractures (HF) can be seen in Fig. D. The dark areas indicated by arrows in Fig. D are overgrowth; these areas appear corroded in Fig. C, suggesting secondary porosity. The grain shows variation in luminescence intensity within two distinct parts in SEM-CL image.

A PPL

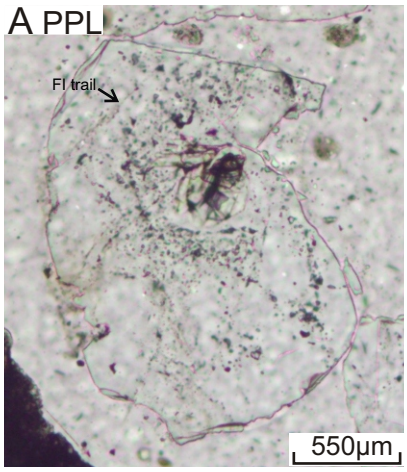

B XPL

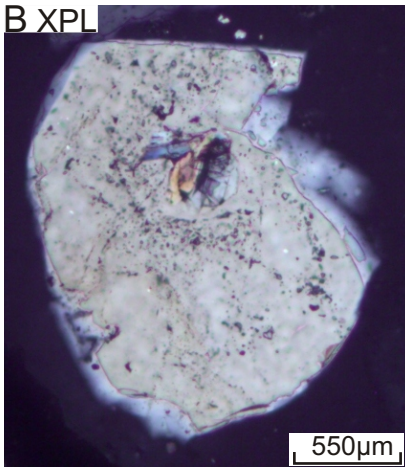

C BSE

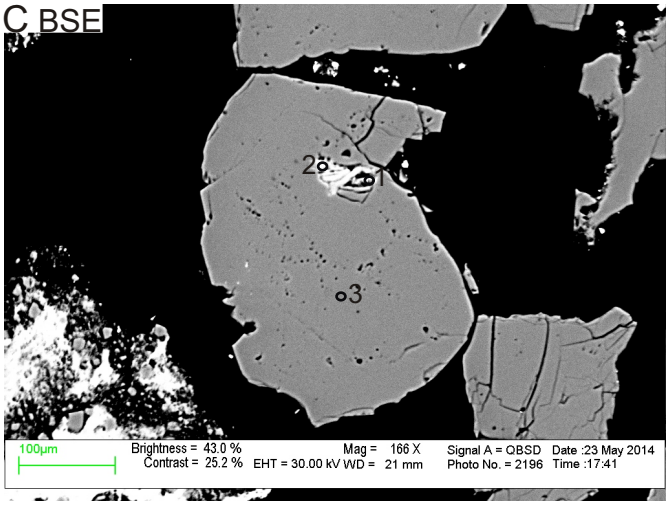

D SEM-CL

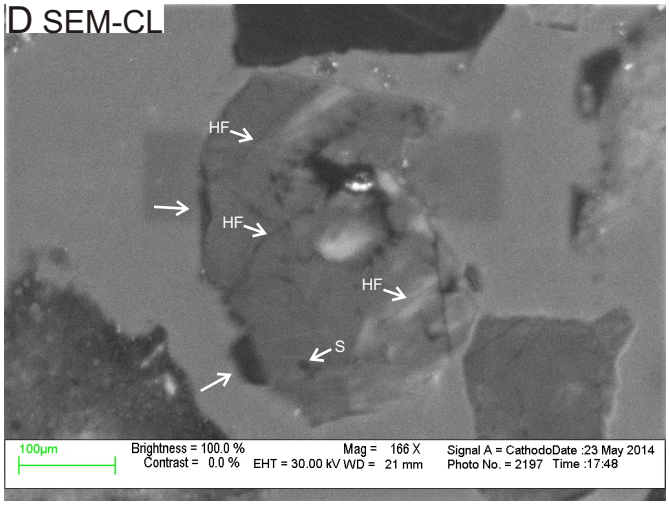

E EDS analyses

Pos#	Min. ID	SiO2	TiO2	Al2O3	FeO	MgO	Na2O	K2O	Total	Actual total
1	Ms	48.35	0.17	33.34	2.57	0.34	0.34	9.89	95	84
2	Ms	53.78	0.22	32.59	2.97	0.36	0.4	9.67	100	94
3	Qz	99.99							100	97

Figure 4A-8: Microphotos under ppl (A) and xpl (B), SEM-BSE image (C), SEM-CL image (D), and EDS analyses table (E) of quartz grain 8 in sample 3000. The grain is anhedral and sub-rounded monocrystalline with embayed margins and weak undulose extinction. Fluid inclusions are common, and they form trails along healed fractures. The grain contains muscovite inclusions and is microfractured with a set of parallel fractures and a set of irregular fractures (Fig. C and D). Some healed fractures (HF) and spiders (S) can be seen in Fig. D. The dark areas indicated by arrows in Fig. D are overgrowth. The grain shows bright streaky patches fabric in SEM-CL image.

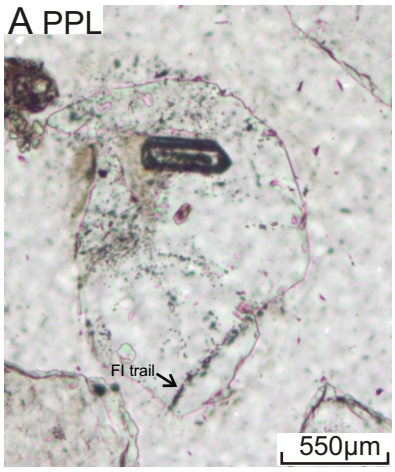

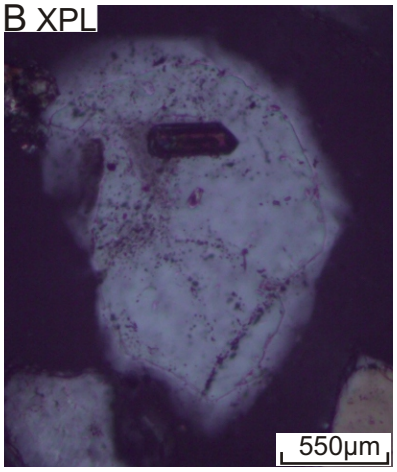

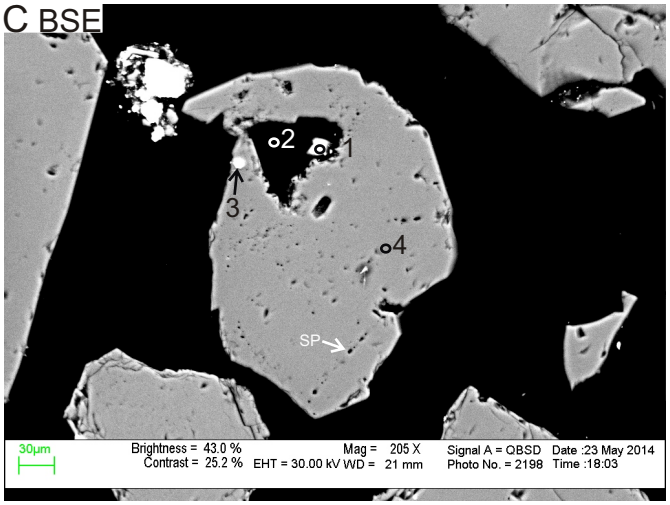

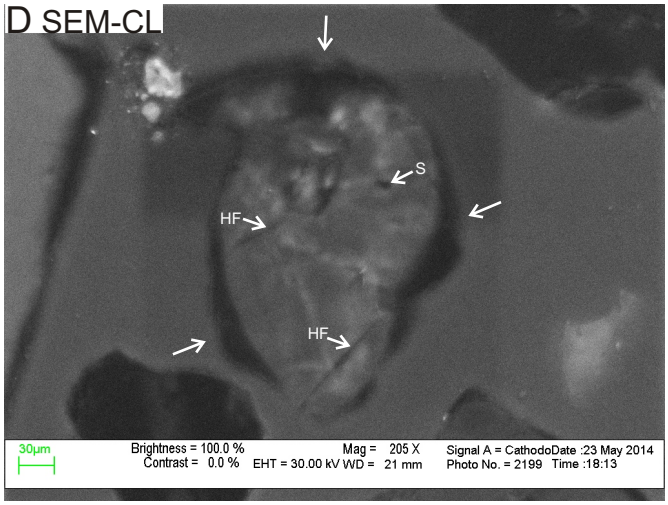

E EDS analyses

Pos#	Min. ID	SiO2	TiO2	Al2O3	FeO	SO3	F	Cl	ZrO2	HfO2	Total	Actual total
1	Zrn	31.19		1.81	0.28		4.15		61.29	1.27	100	79
2	Hole	45.07	6.61	3.06			22.83	2.51	19.92		100	6
3	Py+Qz	21.22			19.4	59.38					100	157
4	Qz	99.99									100	105

Figure 4A-9: Microphotos under ppl (A) and xpl (B), SEM-BSE image (C), SEM-CL image (D), and EDS analyses table (E) of quartz grain 9 in sample 3000. The grain is anhedral and sub-rounded monocrystalline with non-undulose extinction. Fluid inclusions are common; they are usually associated with secondary porosity (SP) and form trails along healed fractures (Fig. A and C). The grain contains zircon and pyrite inclusions, and is microfractured with a set of parallel fractures and a set of irregular fractures (Fig. C and D). Some healed fractures (HF) and spiders (S) can be seen in Fig. D. The dark areas indicated by arrows in Fig. D are overgrowth. The grain shows subtle mottling pattern in SEM-CL image.

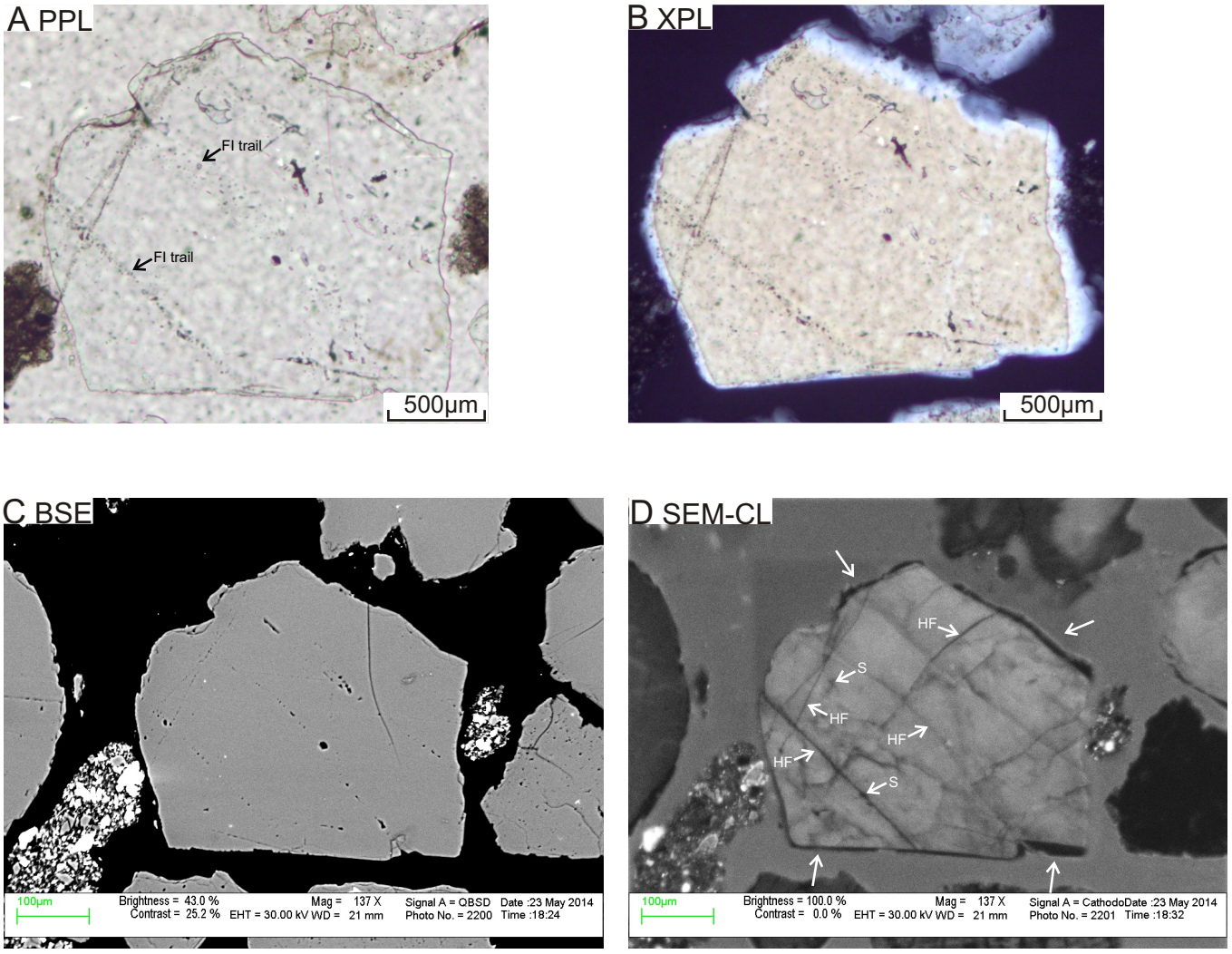

Figure 4A-10: Microphotos under ppl (A) and xpl (B), SEM-BSE image C, and SEM-CL image (D) of quartz grain 10 in sample 3000. The grain is anhedral and sub-angular monocrystalline with mosaic texture and non-undulose extinction. Fluid inclusions are common; they are usually associated with secondary porosity (SP) and form trails along healed fractures (Fig. A and C). The grain is strongly microfractured with two sets of parallel fractures crosscutting each other perpendicularly, and a set of irregular curved fractures (Fig. C and D). Healed fractures (HF) and spiders (S) are common (Fig. D). The dark areas indicated by arrows in Fig. D are overgrowth.

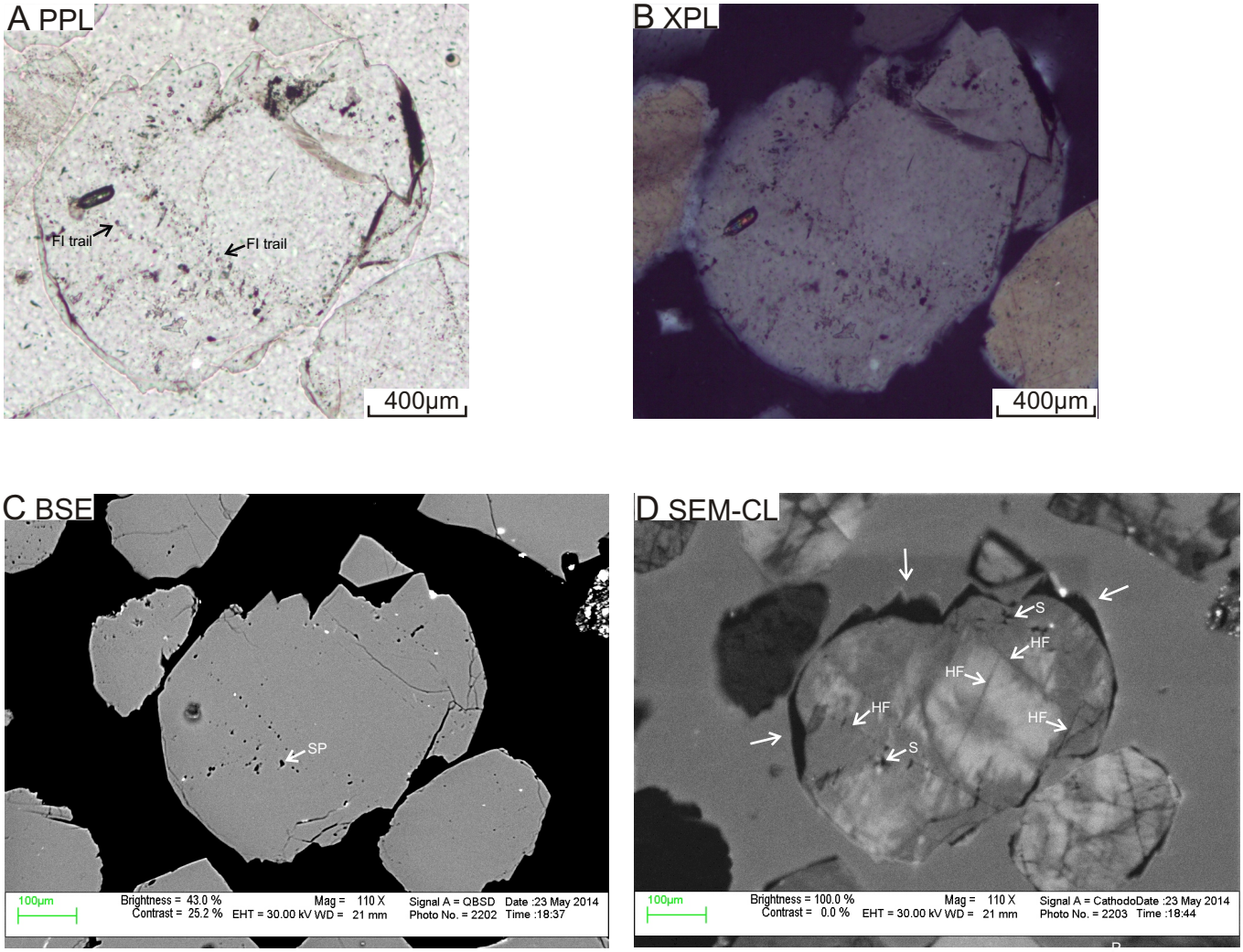

Figure 4A-11: Microphotos under ppl (A) and xpl (B), SEM-BSE image C, and SEM-CL image (D) of quartz grain 11 in sample 3000. The grain is anhedral and sub-rounded monocrystalline with strong undulose extinction. Fluid inclusions are common; they are usually associated with secondary porosity (SP) and form trails along healed fractures (Fig. A and C). The grain is microfractured with two sets of parallel fractures crosscutting each other perpendicularly, and a set of irregular curved fractures (Fig. C and D). Healed fractures (HF) and dark-CL patches (P) are common (Fig. D). The dark areas indicated by arrows in Fig. D are overgrowth. The grain shows streaky bright CL patches fabric in SEM-CL image.

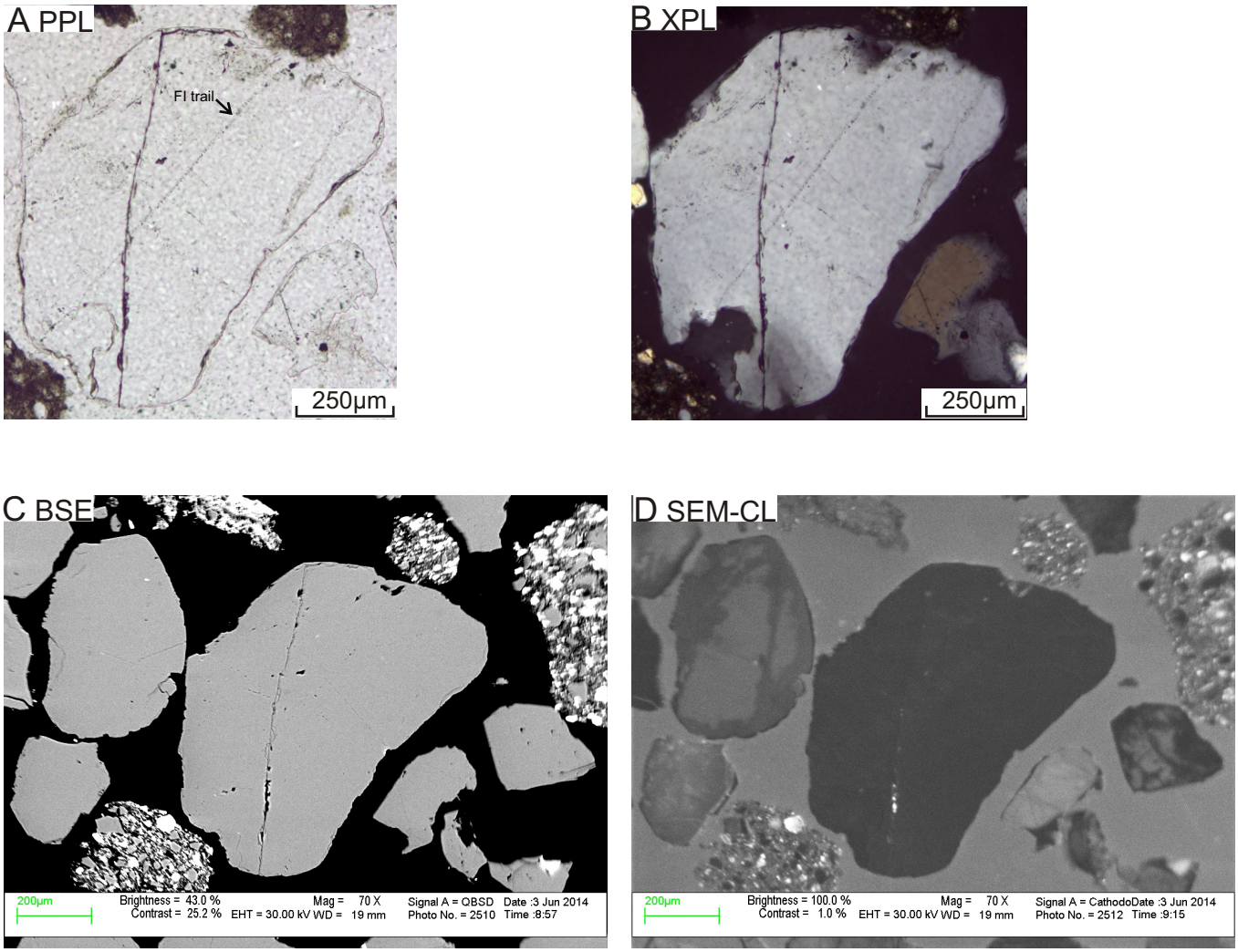

Figure 4A-12: Microphotos under ppl (A) and xpl (B), SEM-BSE image C, and SEM-CL image (D) of quartz grain 12 in sample 3000. The grain is anhedral and rounded polycrystalline (only a few sub-grains with sutured sub-grain boundaries) with mosaic texture and weak undulose extinction. Fluid inclusion trails are present and form trails along healed fractures (Fig. A). The grain is microfractured with irregular fractures (Fig. C). The grain shows homogenous dark-CL colour (Fig. D); therefore, the likely healed fractures cannot be seen in Fig.D.



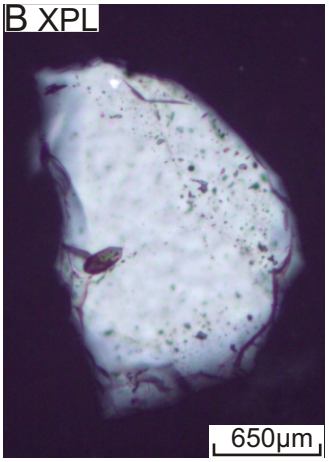

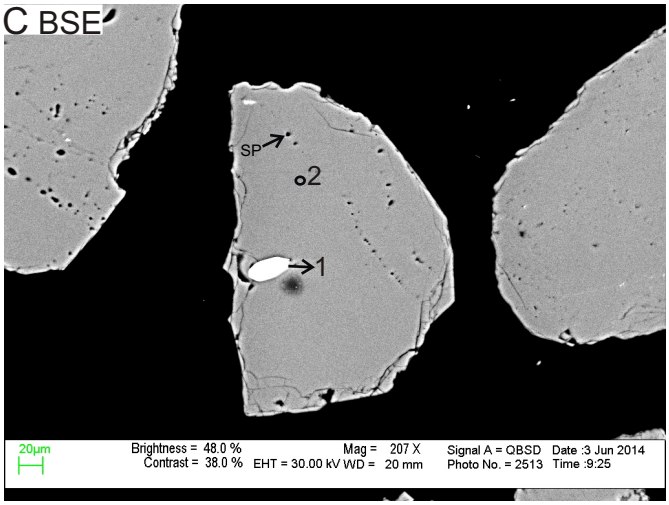

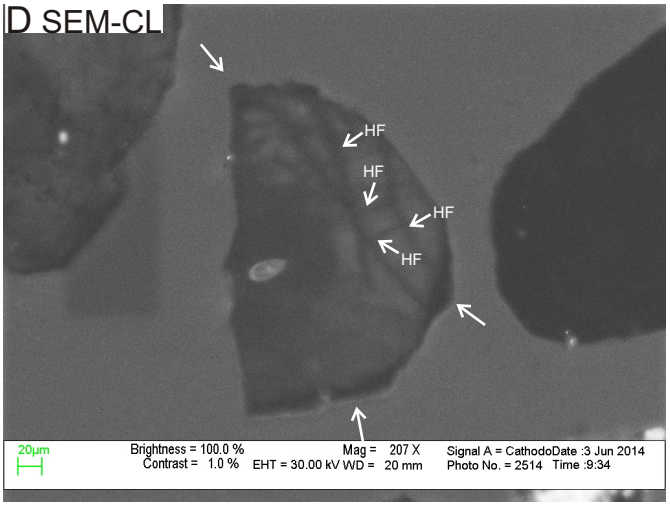

E EDS analyses

Pos#	Min. ID	SiO2	ZrO2	HfO2	Total	Actual total
1	Zrn	32.05	66.15	1.8	100	105
2	Qz	99.99			100	102

Figure 4A-13: Microphotos under ppl (A) and xpl (B), SEM-BSE image (C), SEM-CL image (D), and EDS analyses table (E) of quartz grain 13 in sample 3000. The grain is anhedral and sub-rounded monocrystalline with weak undulose extinction. Fluid inclusions are common; they are usually associated with secondary porosity (SP) and form trails along healed fractures (Fig. A and C). The grain contains a zircon inclusion and is microfractured with two sets of parallel fractures crosscutting each other perpendicularly, and a set of irregular curved fractures (Fig. C and D). Healed fractures (HF) are common (Fig. D). The dark areas indicated by arrows in Fig. D are overgrowth.

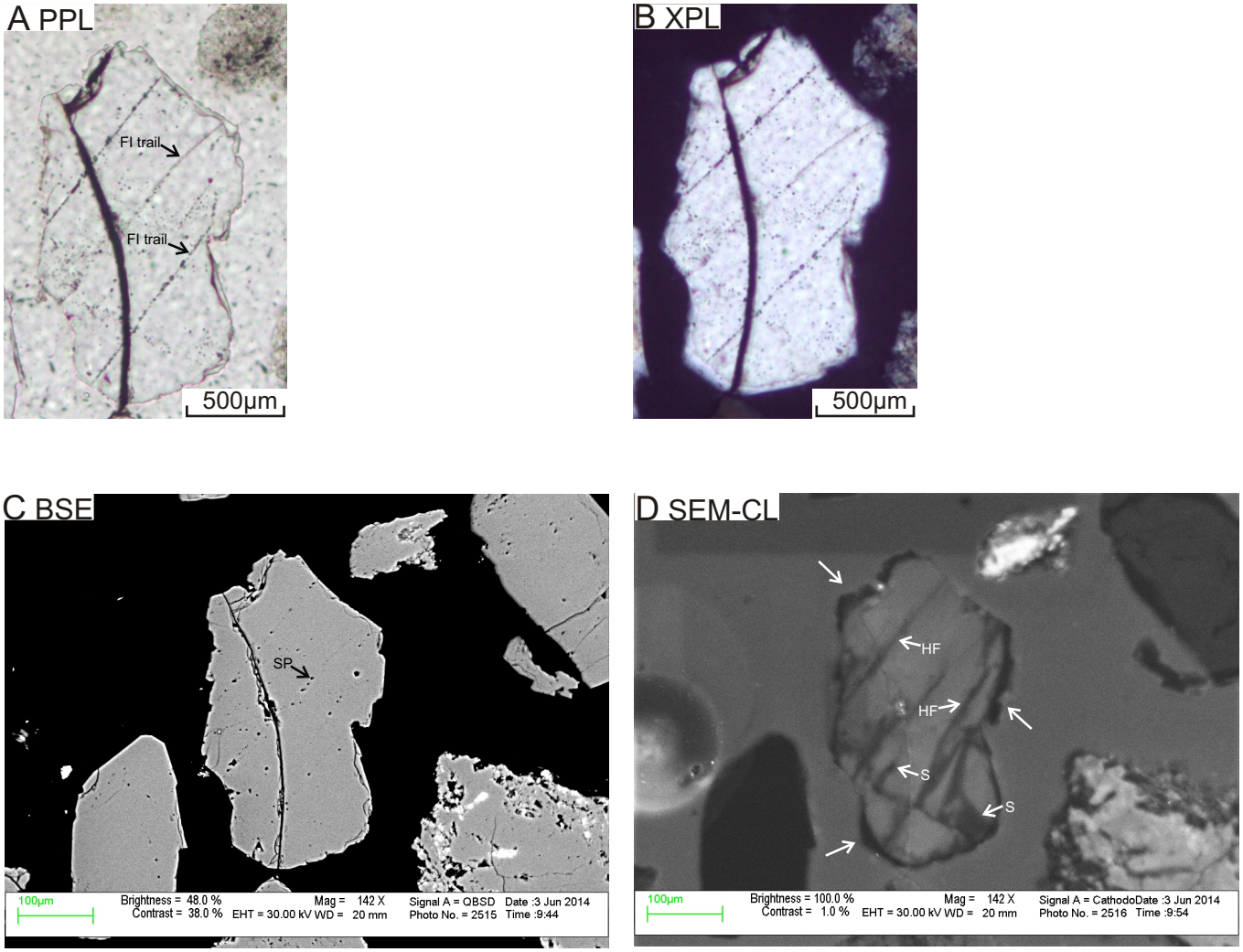

Figure 4A-14: Microphotos under ppl (A) and xpl (B), SEM-BSE image C, and SEM-CL image (D) of quartz grain 14 in sample 3000. The grain is anhedral and sub-angular monocrystalline with strong undulose extinction. Fluid inclusions are common; they are usually associated with secondary porosity (SP) and form trails (FI trail) along healed fractures (Fig. A and C). The grain is microfractured with a set of parallel fractures and a set of irregular curved fractures (Fig. C and D). Healed fractures (HF) and dark-CL patches (P) are common (Fig. D). The dark areas indicated by arrows in Fig. D are overgrowth.

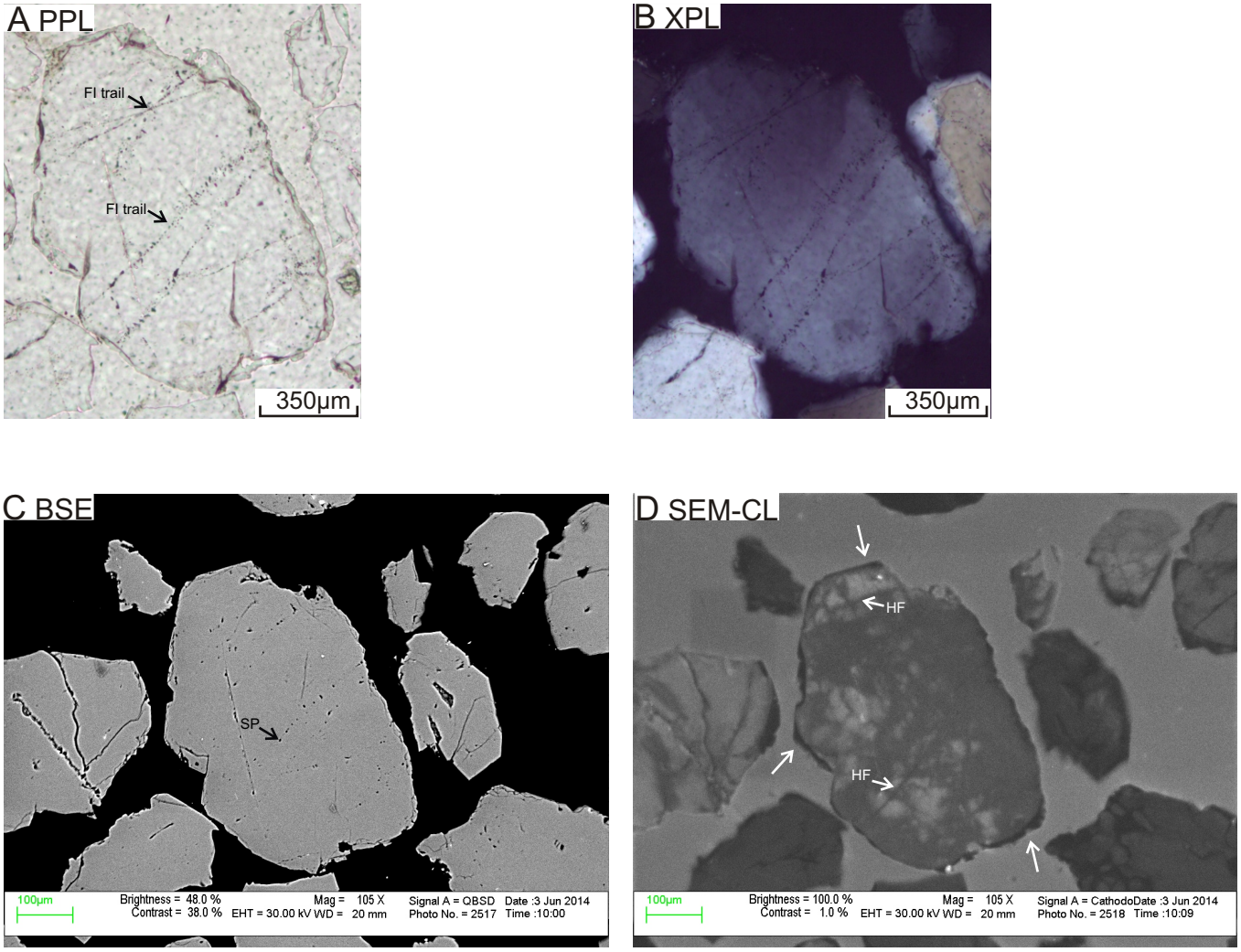

Figure 4A-15: Microphotos under ppl (A) and xpl (B), SEM-BSE image C, and SEM-CL image (D) of quartz grain 15 in sample 3000. The grain is anhedral and sub-rounded monocrystalline with strong undulose extinction. Fluid inclusions are common; they are usually associated with secondary porosity (SP) and form trails (FI trail) along healed fractures (Fig. A and C). The grain is microfractured with a set of irregular fractures (Fig. C and D). Some healed fractures (HF) can be seen in Fig. D. The dark areas indicated by arrows in Fig. D are overgrowth. The grain shows random bright-CL patches in SEM-CL image.

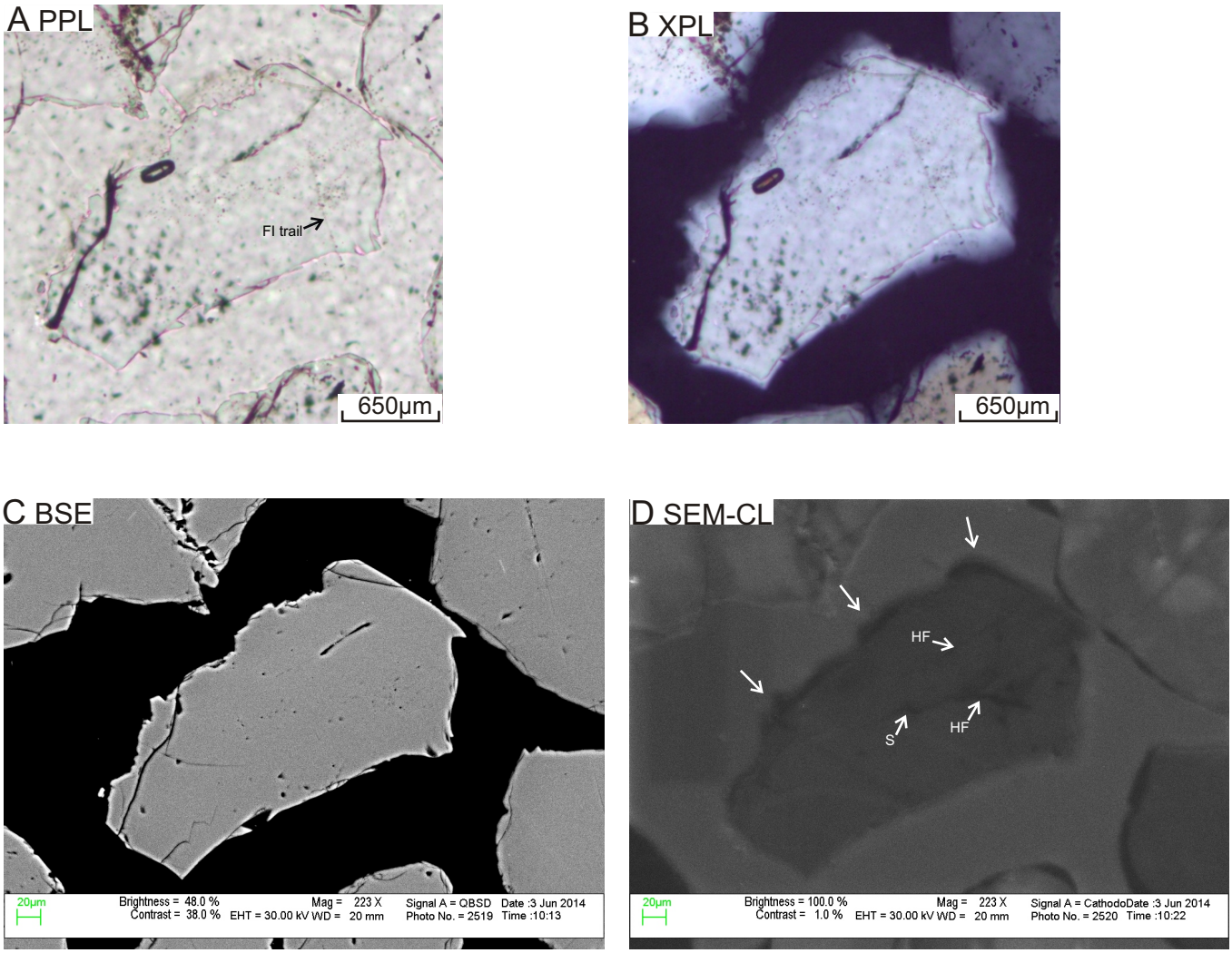

Figure 4A-16: Microphotos under ppl (A) and xpl (B), SEM-BSE image C, and SEM-CL image (D) of quartz grain 16 in sample 3000. The grain is anhedral and angular monocrystalline with weak undulose extinction. Fluid inclusions are common; they form trails (FI trail) along healed fractures (Fig. A). The grain is microfractured with a set of irregular fractures (Fig. C and D). Some healed fractures (HF) and dark-CL patches (P) can be seen in Fig. D. The dark areas indicated by arrows in Fig. D are overgrowth.

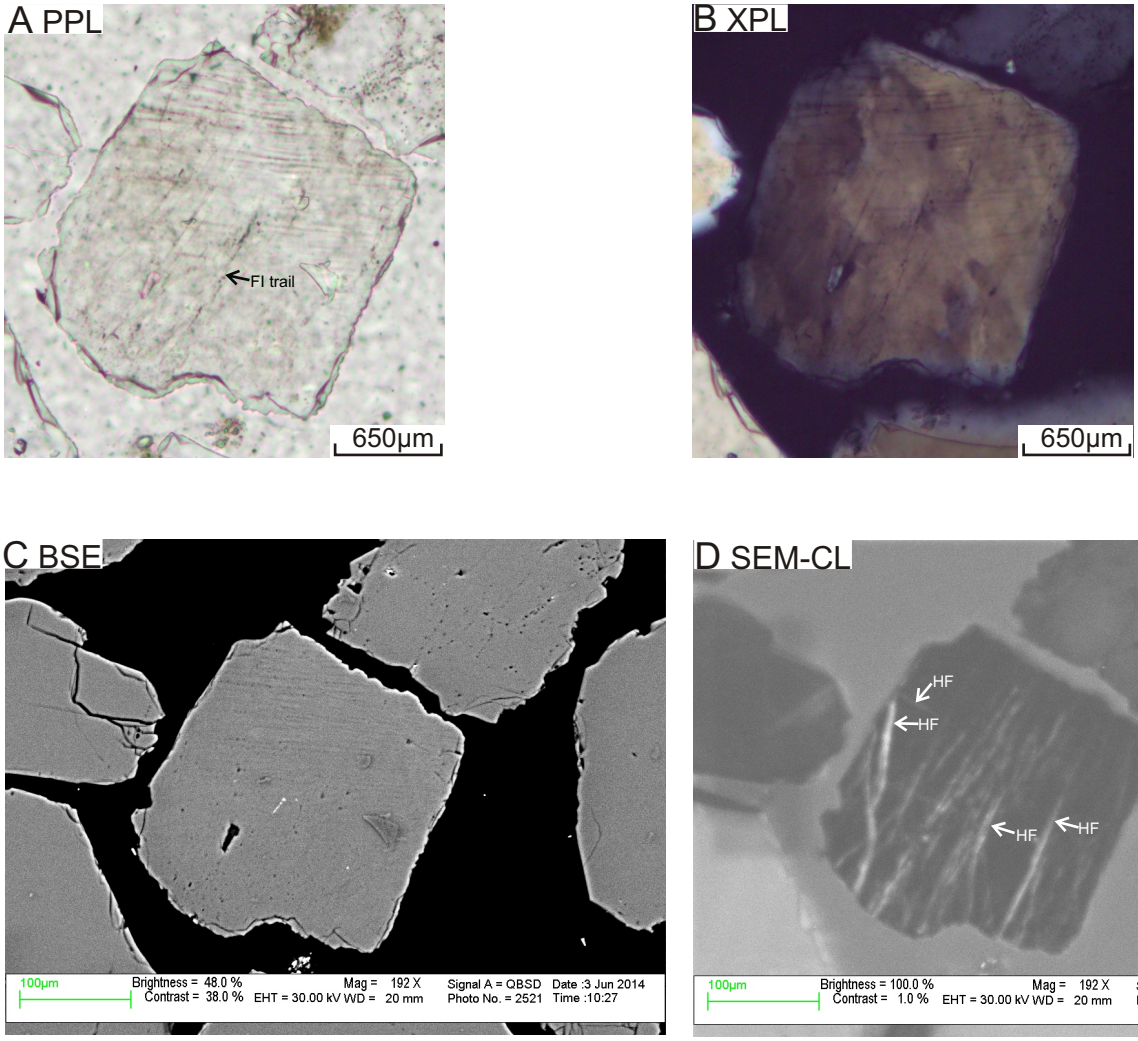

Figure 4A-17: Microphotos under ppl (A) and xpl (B), SEM-BSE image C, and SEM-CL image (D) of quartz grain 17 in sample 3000. The grain is anhedral and sub-rounded monocrystalline with deformation lamellae and strong undulose extinction. Fluid inclusions are common; they form trails (FI trail) along healed fractures (Fig. A). The grain is microfractured with two sets of parallel fractures crosscutting each other perpendicularly (Fig. D). Healed fractures (HF) are common (Fig. D).

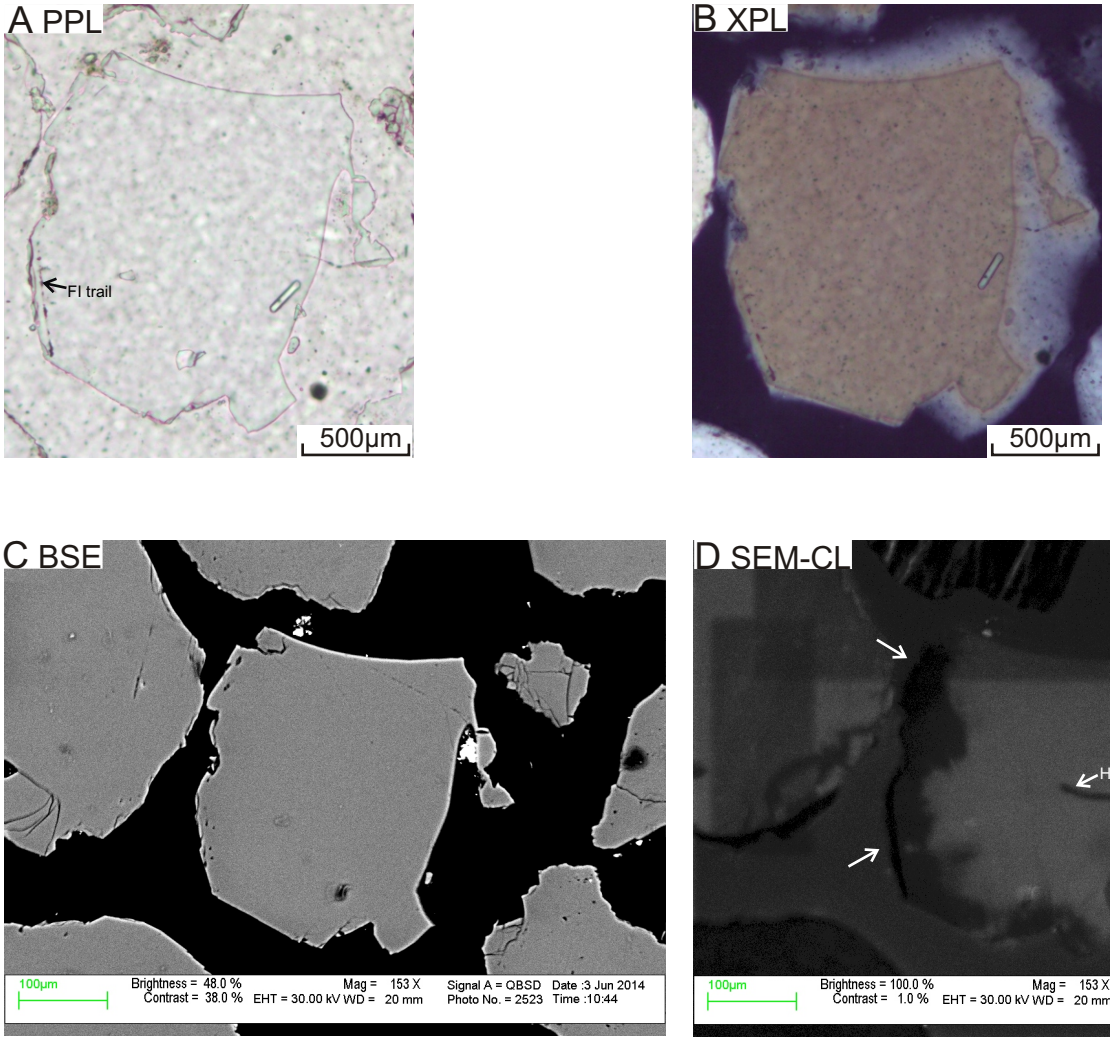

Figure 4A-18: Microphotos under ppl (A) and xpl (B), SEM-BSE image C, and SEM-CL image (D) of quartz grain 18 in sample 3000. The grain is anhedral and sub-angular monocrystalline with weak undulose extinction. Fluid inclusions are present; they form a trail at the contact between the detrital quartz and the overgrowth (Fig. A). The grain is weakly microfractured. Only one healed fracture can be seen in Fig. D. The dark areas indicated by arrows in Fig. D are overgrowth. The grain shows variation in luminescence intensity within two distinct parts in SEM-CL image.

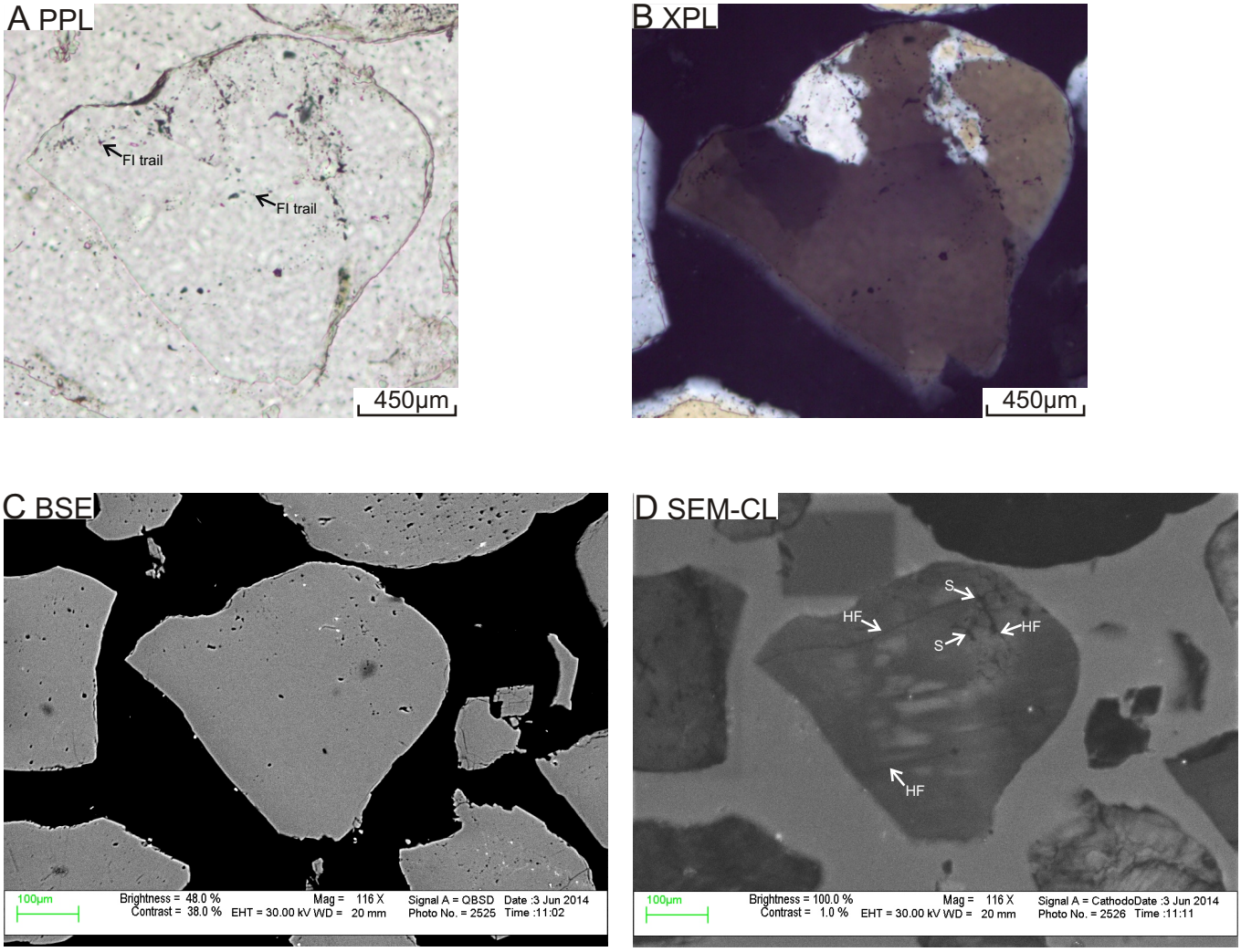

Figure 4A-19: Microphotos under ppl (A) and xpl (B), SEM-BSE image C, and SEM-CL image (D) of quartz grain 19 in sample 3000. The grain is anhedral and sub-rounded polycrystalline (only a few sub-grains) with mosaic texture and weak undulose extinction. Fluid inclusions are common; they form trails (FI trail) along healed fractures (Fig. A). The grain is microfractured with a set of parallel fractures and a set of irregular fractures (Fig. C and D). Some healed fractures (HF) and spiders (S) can be seen in Fig. D. The grain shows bright-CL streaky patches fabric in SEM-CL image.

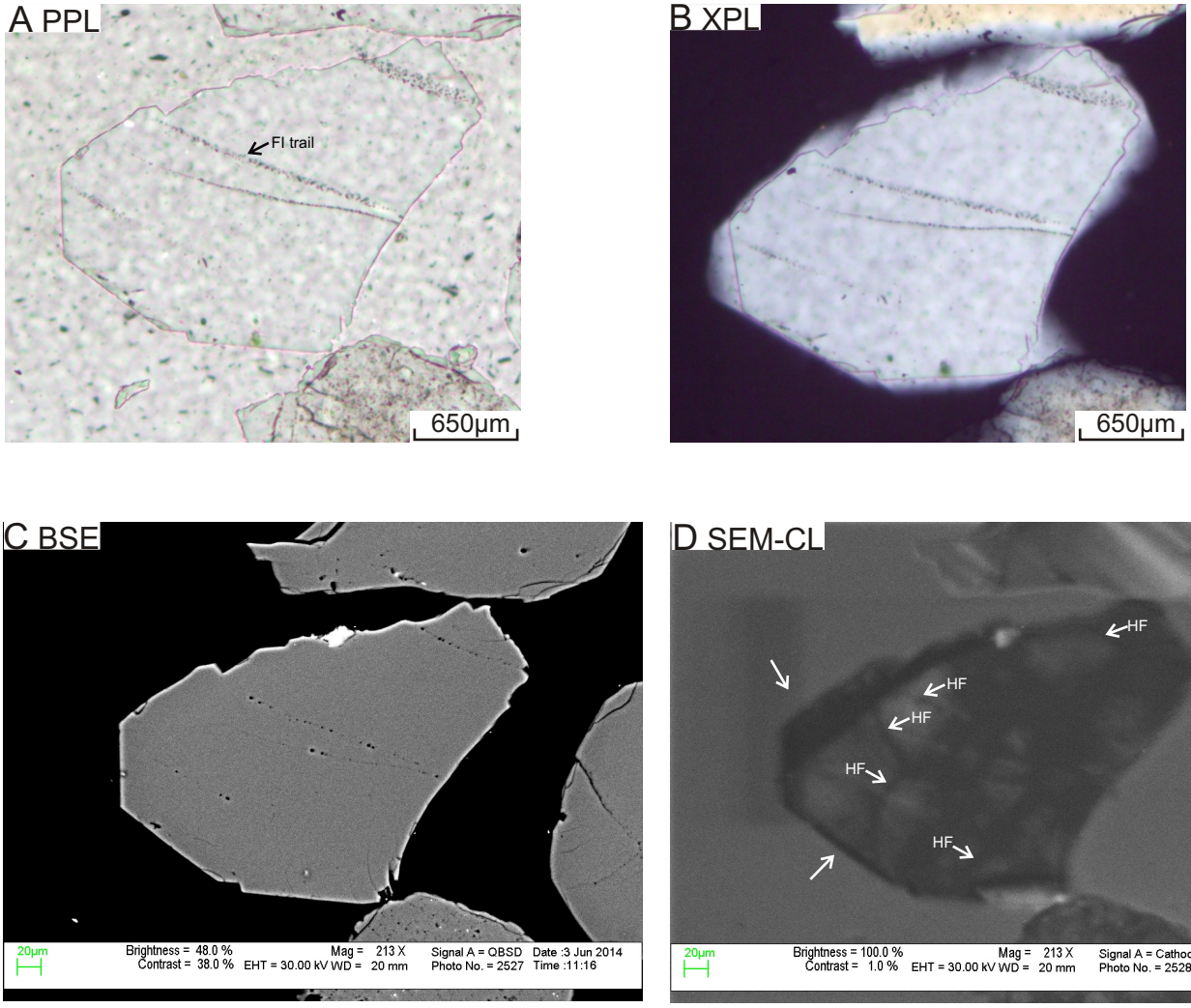

Figure 4A-20: Microphotos under ppl (A) and xpl (B), SEM-BSE image C, and SEM-CL image (D) of quartz grain 20 in sample 3000. The grain is anhedral and angular monocrystalline with weak undulose extinction. Fluid inclusions are common; they are usually associated with secondary porosity (SP) and form trails (FI trail) along healed fractures (Fig. A and C). The grain is microfractured with two distinct sets of parallel fractures crosscutting each other (Fig. D). Healed fractures (HF) are common (Fig. D). The dark areas indicated by arrows in Fig. D are overgrowth. The grain shows bright-CL streaky patches fabric in SEM-CL image.

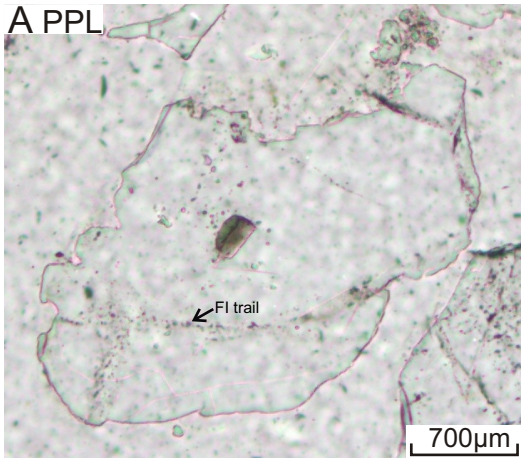

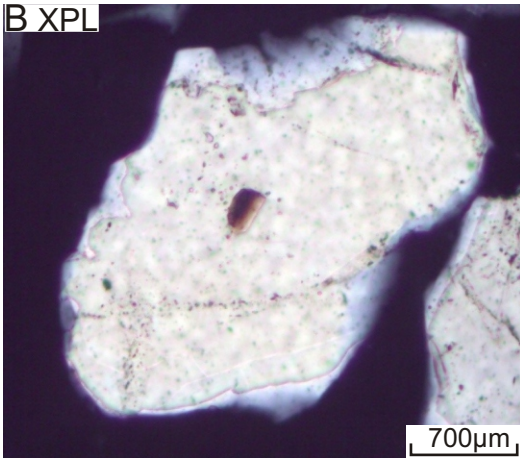

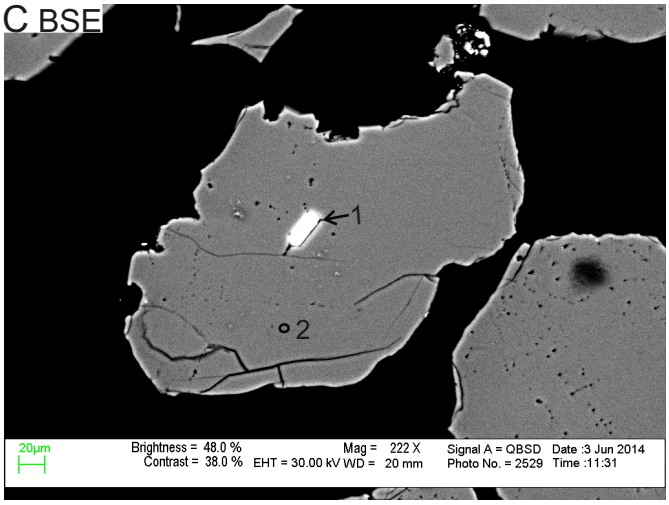

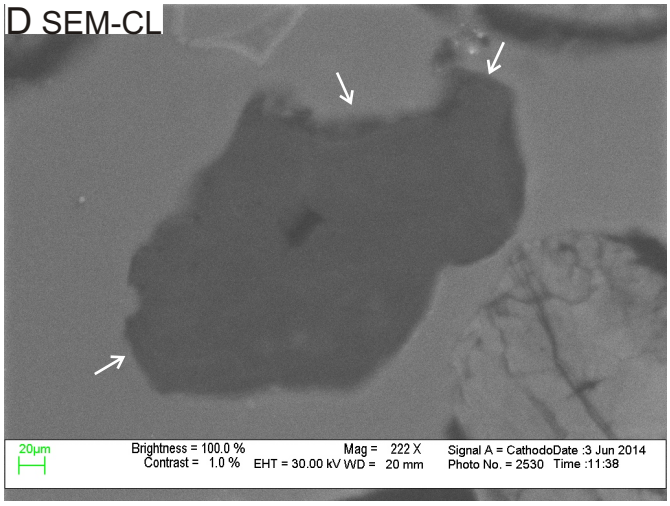

E EDS analyses

Pos#	Min. ID	SiO2	TiO2	Al2O3	FeO	MnO	MgO	K2O	Cl	Total	Actual total
1	Bt	41.52	2.69	16.89	18.89	0.39	9.38	6.05	0.2	96	83
2	Qz	99.99								100	100

Figure 4A-21: Microphotos under ppl (A) and xpl (B), SEM-BSE image (C), SEM-CL image (D), and EDS analyses table (E) of quartz grain 21 in sample 3000. The grain is anhedral and sub-angular monocrystalline with non-undulose extinction. Fluid inclusion trails are common (Fig. A). The grain contains a biotite inclusion and is microfractured with irregular fractures (Fig. C). Healed fractures are rare. The dark areas indicated by arrows in Fig. D are overgrowth.

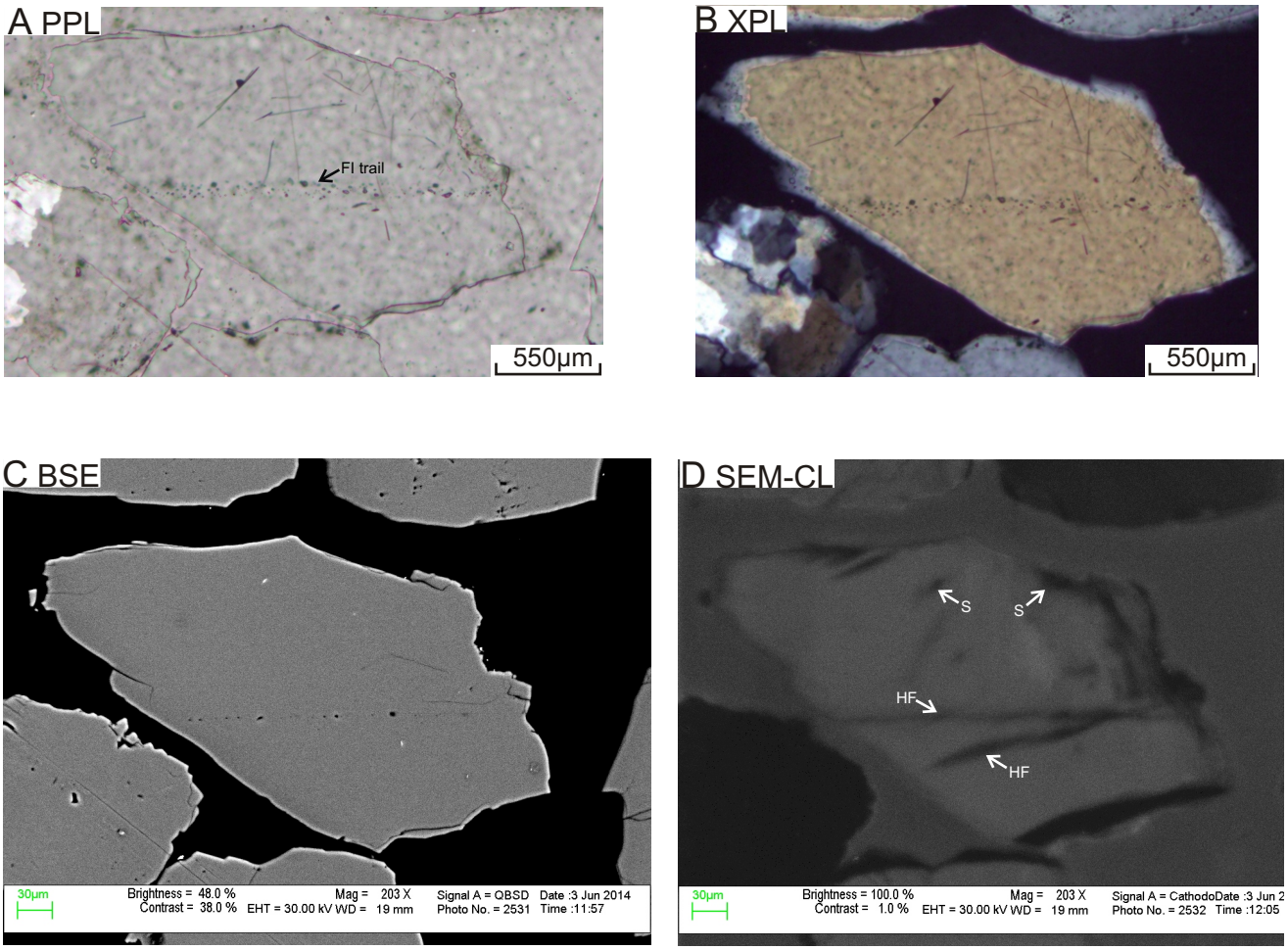

Figure 4A-22: Microphotos under ppl (A) and xpl (B), SEM-BSE image C, and SEM-CL image (D) of quartz grain 22 in sample 3000. The grain is anhedral and angular monocrystalline with non-undulose extinction. Fluid inclusions are common; they form trails along healed fractures (Fig. A). The grain is microfractured with a set of irregular fractures (Fig. D). Some healed fractures (HF) and spiders (S) can be seen in Fig. D.

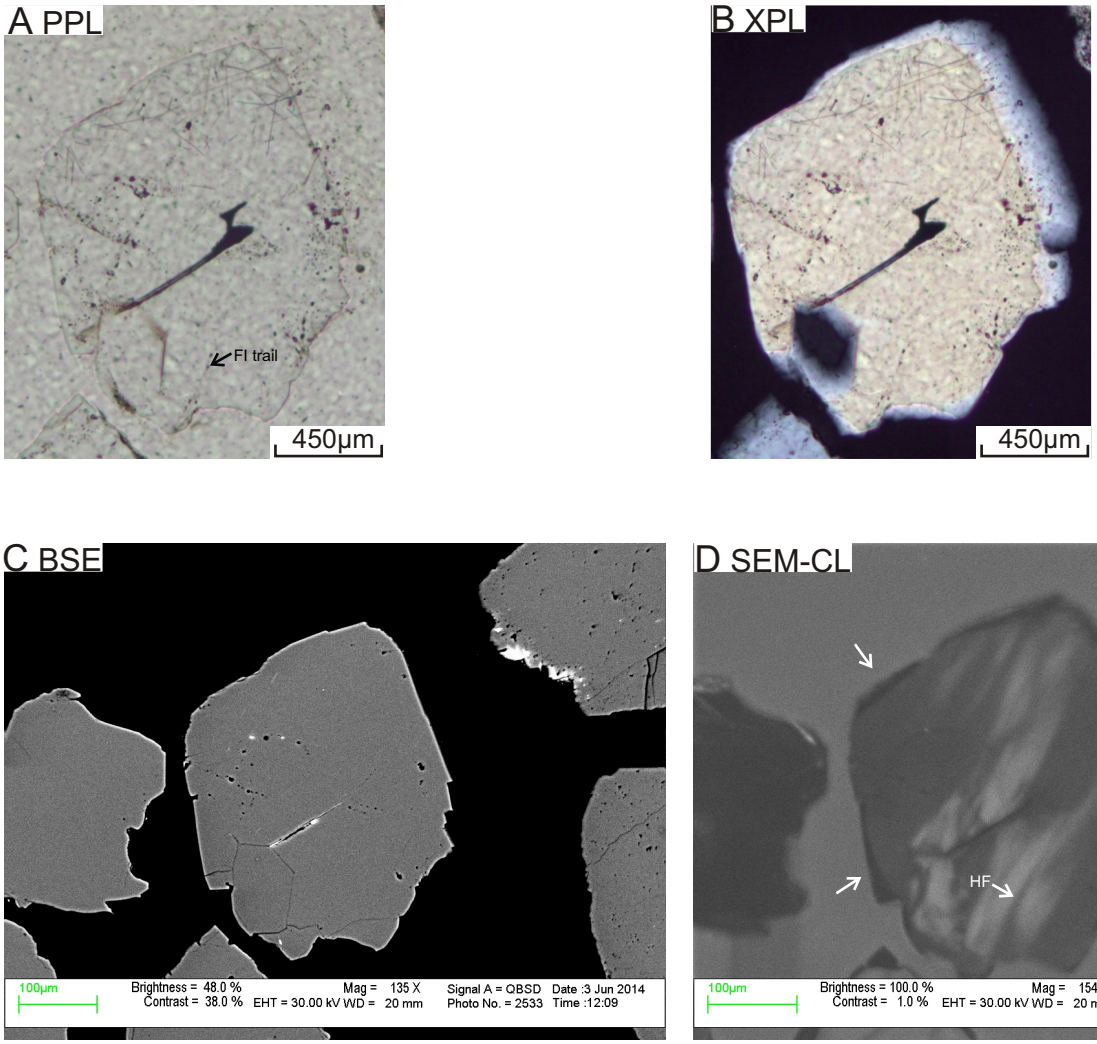

Figure 4A-23: Microphotos under ppl (A) and xpl (B), SEM-BSE image C, and SEM-CL image (D) of quartz grain 23 in sample 3000. The grain is anhedral and sub-rounded monocrystalline with weak undulose extinction. Fluid inclusions are common (Fig. A).The grain is microfractured with a set of irregular fractures (Fig. C and D). A few healed fractures (HF) can be seen in Fig. D. The dark areas indicated by arrows in Fig. D are overgrowth. The grain shows streaky texture in SEM-CL image.

A PPL

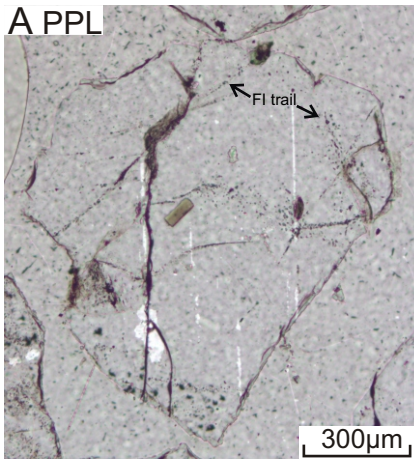

B XPL

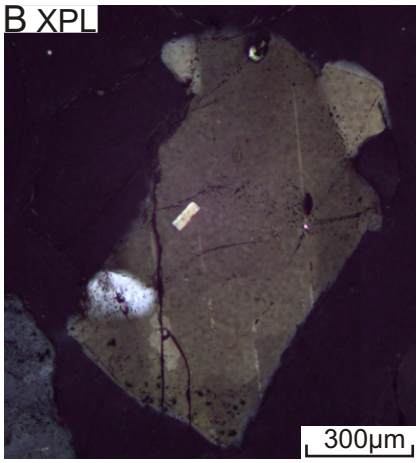

C BSE

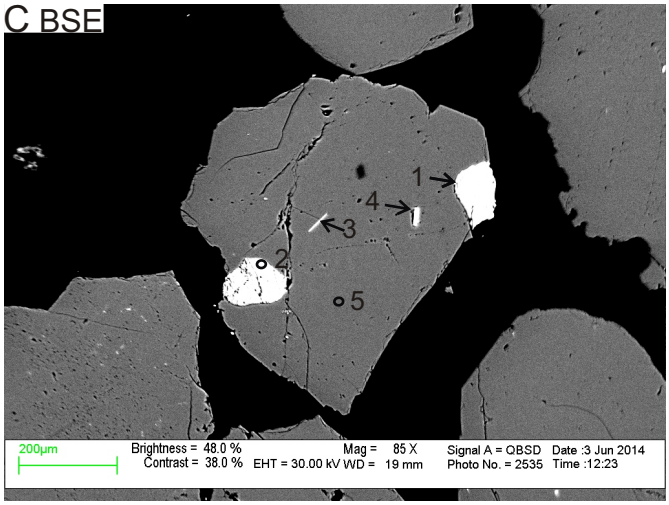

D SEM-CL

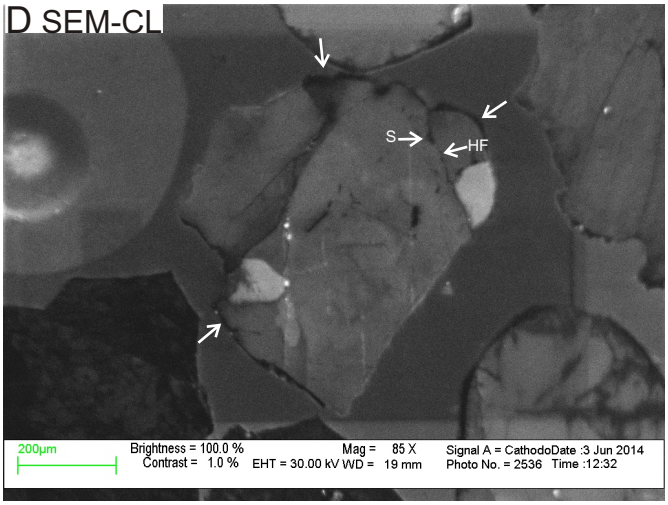

E EDS analyses

Pos#	Min. ID	SiO2	TiO2	Al2O3	FeO	MnO	MgO	Na2O	K2O	BaO	Total	Actual total
1	Kfs	65.31		17.8				1.12	14.55	1.22	100	98
2	Kfs	65.07		17.93				0.98	14.72	1.3	100	91
3	Bt	41.72	4.27	13.86	21.40	0.39	5.71		8.64		96	99
5	Qz	99.99									100	107

Figure 4A-24: Microphotos under ppl (A) and xpl (B), SEM-BSE image (C), SEM-CL image (D), and EDS analyses table (E) of quartz grain 24 in sample 3000. The grain is anhedral and sub-angular polycrystalline (only a few sub-grains with sutured sub-grain boundaries) with mosaic texture and weak undulose extinction. Fluid inclusions are common; they form trails along healed fractures (Fig. A). The grain contains K-feldspar and biotite inclusions and is microfractured with a set of irregular fractures (Fig. C and D). Some healed fractures (HF) and spiders (S) can be seen in Fig. D. The dark areas indicated by arrows in Fig. D are overgrowth.

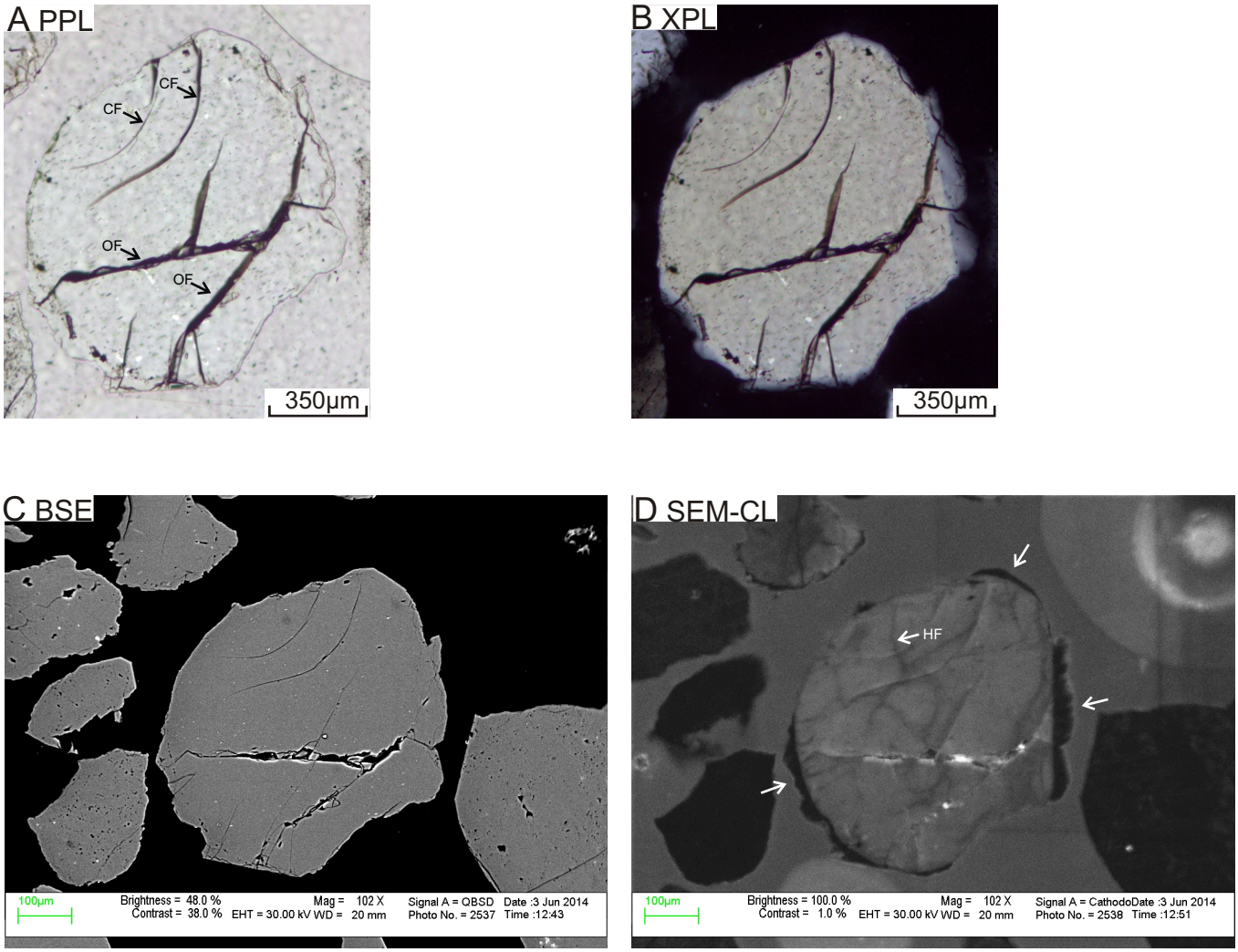

Figure 4A-25: Microphotos under ppl (A) and xpl (B), SEM-BSE image C, and SEM-CL image (D) of quartz grain 25 in sample 3000. The grain is anhedral and rounded monocrystalline with non-undulose extinction. Fluid inclusions are present; they form a trail at the contact between the detrital quartz and the overgrowth (Fig. A). The grain is microfractured with a set of conchoidal fractures (CF) and a set of irregular fractures (Fig. A and D). A few thick open fractures are present (Fig. A). Some healed fractures can be seen in Fig. D. The dark areas indicated by arrows in Fig. D are overgrowth.

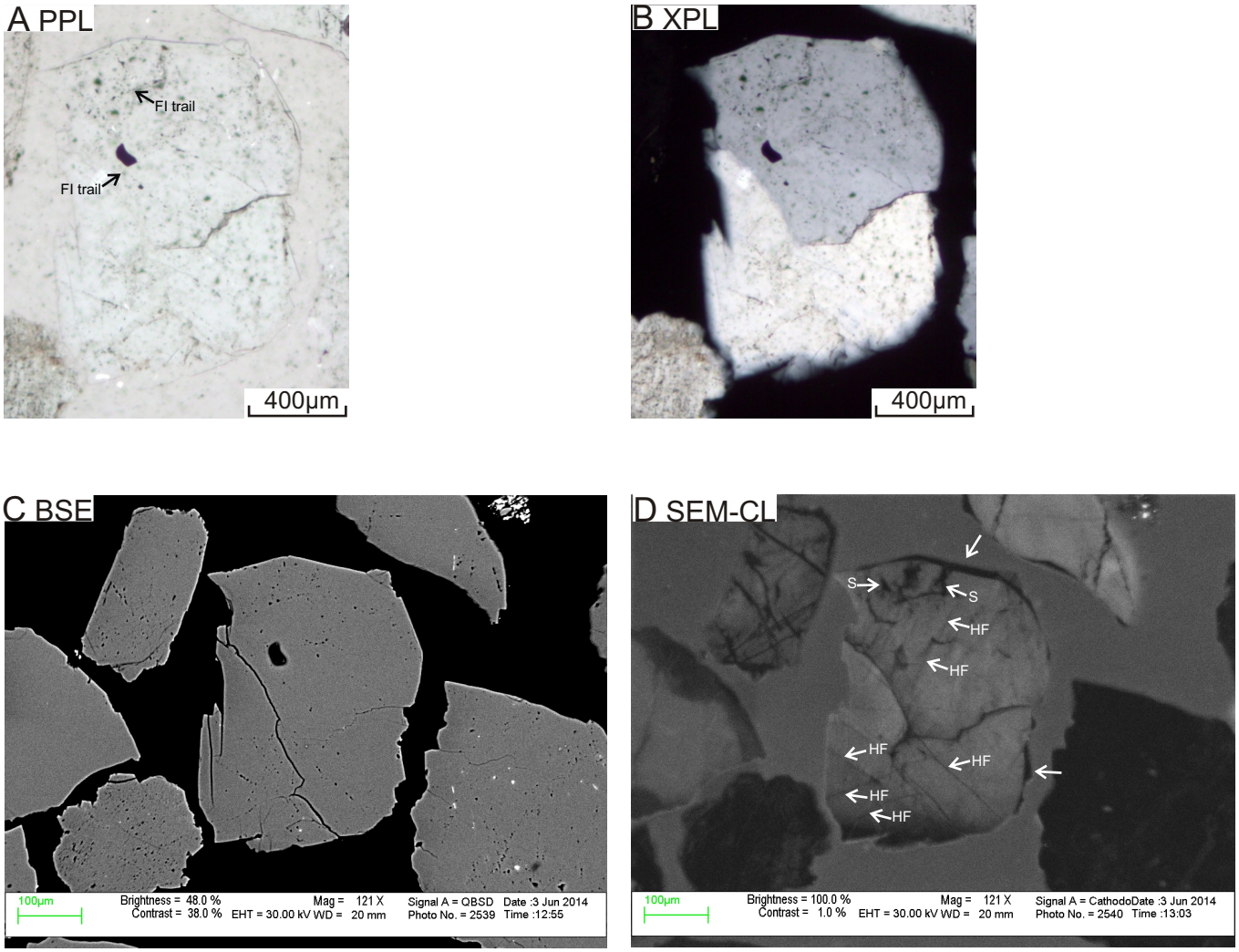

Figure 4A-26: Microphotos under ppl (A) and xpl (B), SEM-BSE image C, and SEM-CL image (D) of quartz grain 26 in sample 3000. The grain is anhedral and sub-angular polycrystalline (only 2 sub-grains) with mosaic texture and weak undulose extinction. Fluid inclusions are common; they form trails along healed fractures (Fig. A). The grain is microfractured with three distinct sets of parallel fractures crosscutting each other and a set of irregular curved fractures (Fig. C and D). Healed fractures (HF) and spiders (S) are common (Fig. D). The dark areas indicated by arrows in Fig. D are overgrowth

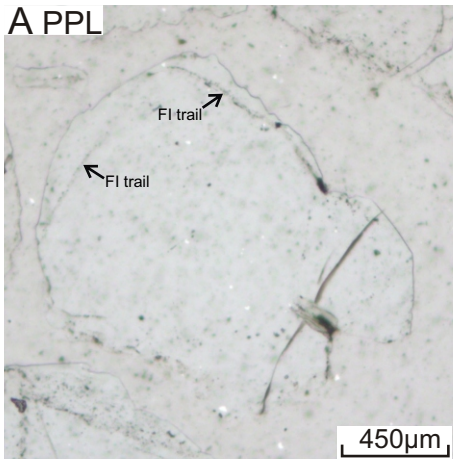

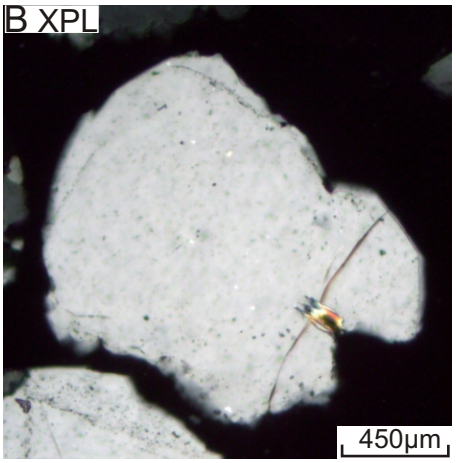

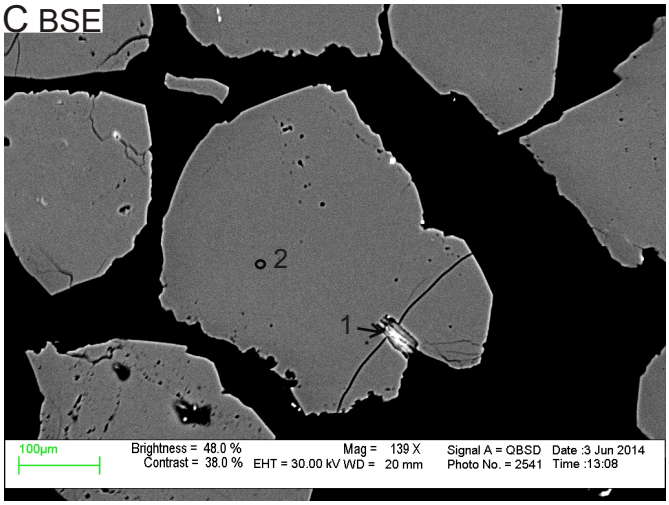

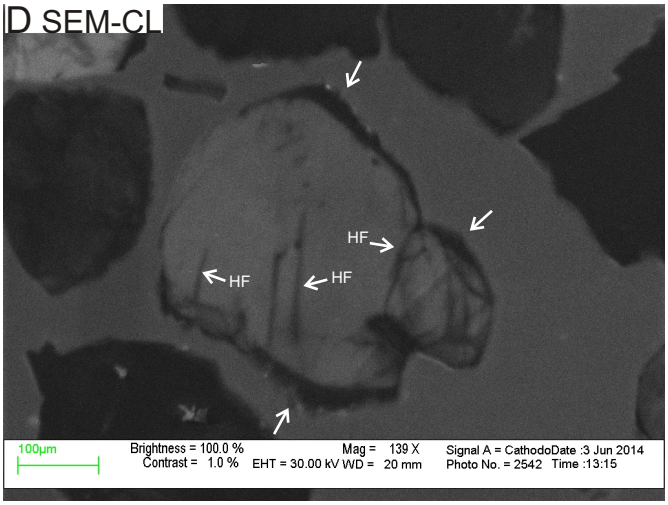

E EDS analyses

Pos#	Min. ID	SiO2	Al2O3	FeO	MgO	CaO	K2O	P2O5	Cr2O3	Ce2O3	Total	Actual total
1	Ilt	50.39	19.46	7.79	2.43	0.64	6.43	1.63	0.21	1.03	90	70
2	Qz	99.99									100	97

Figure 4A-27: Microphotos under ppl (A) and xpl (B), SEM-BSE image (C), SEM-CL image (D), and EDS analyses table (E) of quartz grain 27 in sample 3000. The grain is anhedral and sub-rounded monocrystalline with non-undulose extinction. Fluid inclusions are present; they form trails along healed fractures and at the contact between the detrital quartz and the overgrowth (Fig. A). The grain contains illite inclusions and is microfractured with a set of parallel fractures (Fig. D). Healed fractures are common (Fig. D). The dark areas indicated by arrows in Fig. D are overgrowth; these areas appear corroded in Fig. C, suggesting secondary porosity.

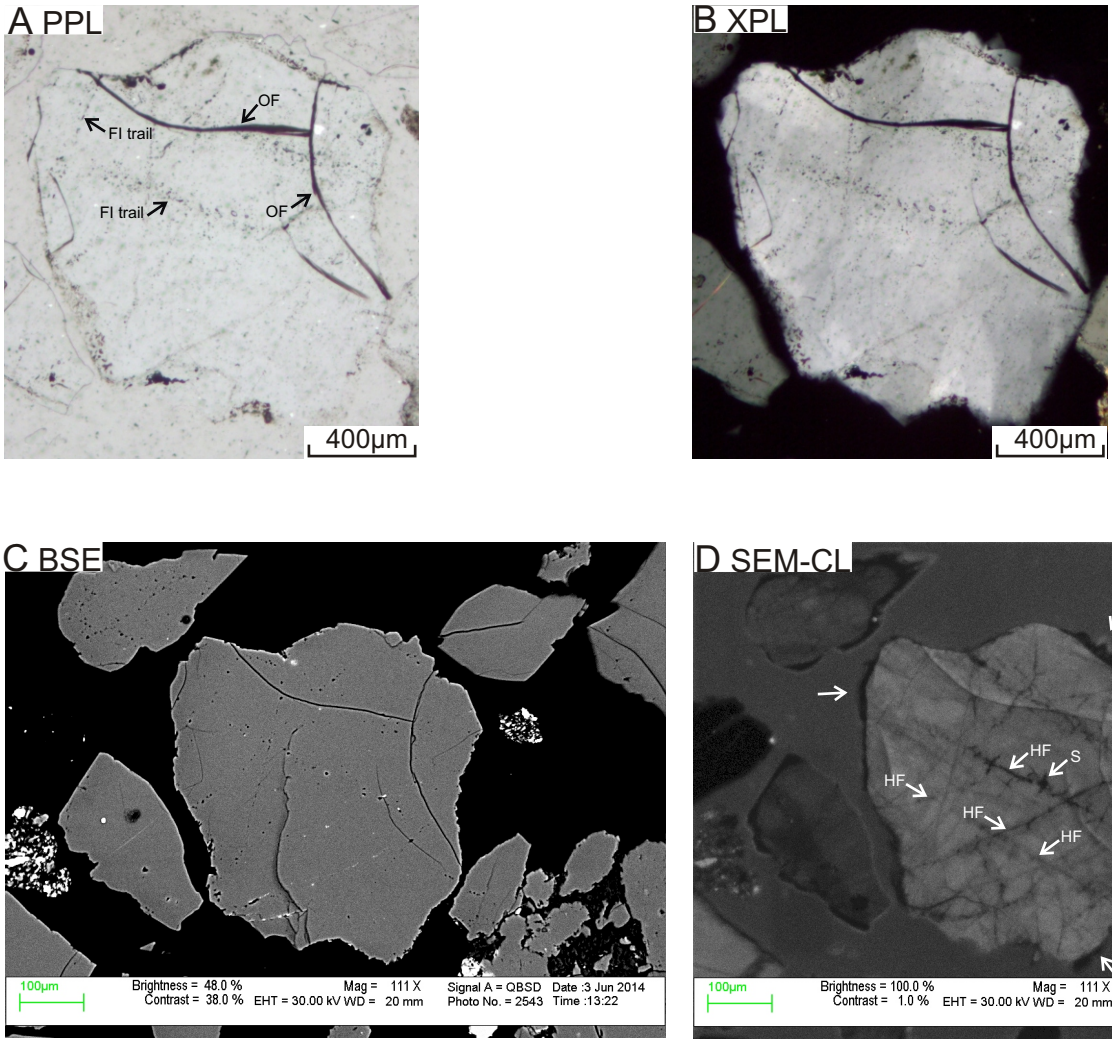

Figure 4A-28: Microphotos under ppl (A) and xpl (B), SEM-BSE image C, and SEM-CL image (D) of quartz grain 28 in sample 3000. The grain is anhedral and sub-rounded monocrystalline with mosaic texture and strong undulose extinction. Fluid inclusions are present; they are usually associated wit secondary porosity and form trails (FI trail) along healed fractures (Fig. A). The grain is strongly microfractured with two sets of parallel fractures crosscutting each other and a set of irregular curved open fractures (OF) (Fig. A and D). Healed fractures and spiders (S) are common (Fig. D). The dark areas indicated by arrows in Fig. D are overgrowth; these areas appear corroded in Fig. C, suggesting secondary porosity.

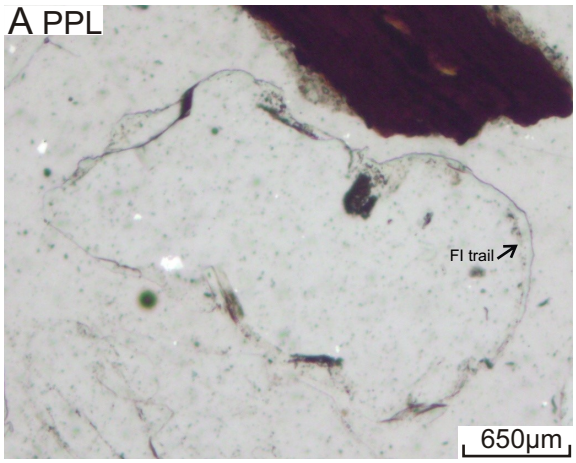

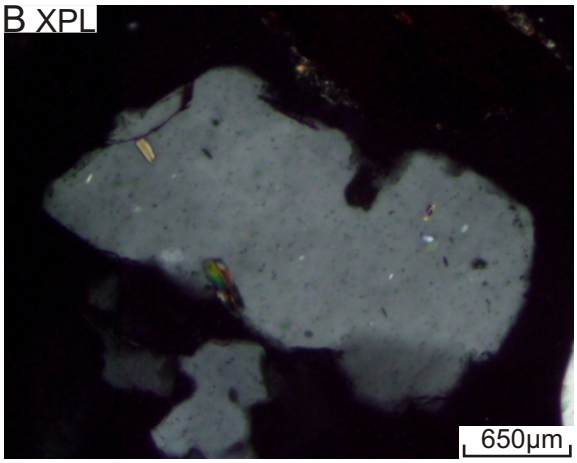

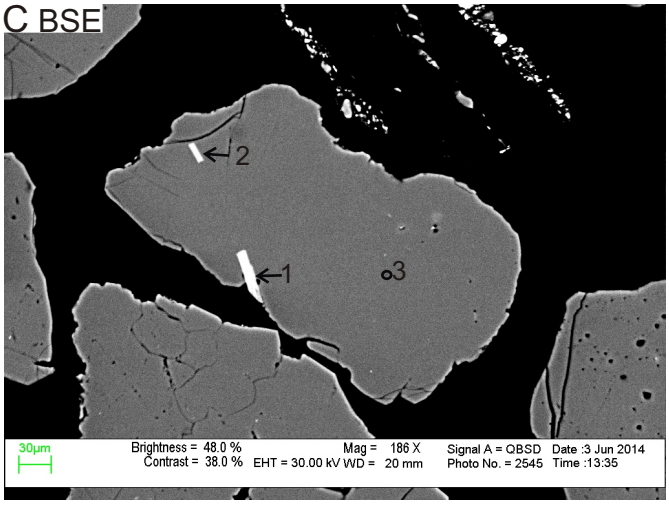

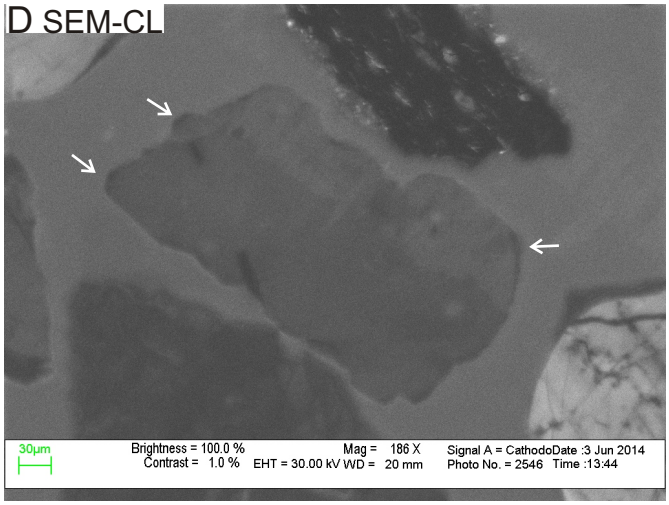

E EDS analyses

Pos#	Min. ID	SiO2	TiO2	Al2O3	FeO	MgO	K2O	Total	Actual total
1	Ms	48.83	1.28	27.75	4.53	1.86	10.74	95	90
2	Ms	56.15	1.07	22.80	4.05	1.75	9.18	95	95
3	Qz	99.99						100	103

Figure 4A-29: Microphotos under ppl (A) and xpl (B), SEM-BSE image (C), SEM-CL image (D), and EDS analyses table (E) of quartz grain 29 in sample 3000. The grain is anhedral and sub-rounded monocrystalline with strong undulose extinction. Fluid inclusions are present; they form trails at the contact between the detrital quartz and the overgrowth (Fig. A). The grain contains muscovite inclusions and is weakly microfractured with curved fractures (Fig. C). Healed fractures are rare. The dark areas indicated by arrows in Fig. D are overgrowth.

A PPL

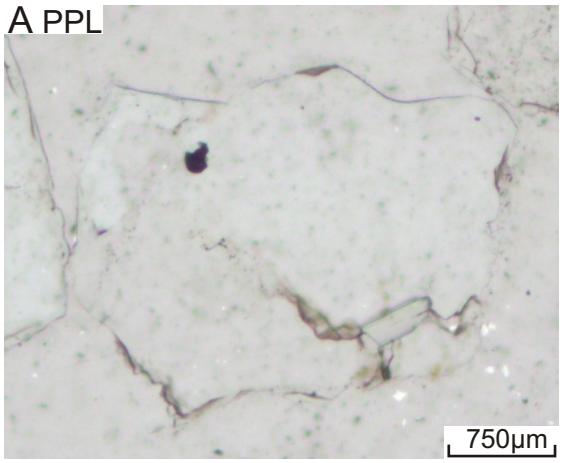

B XPL

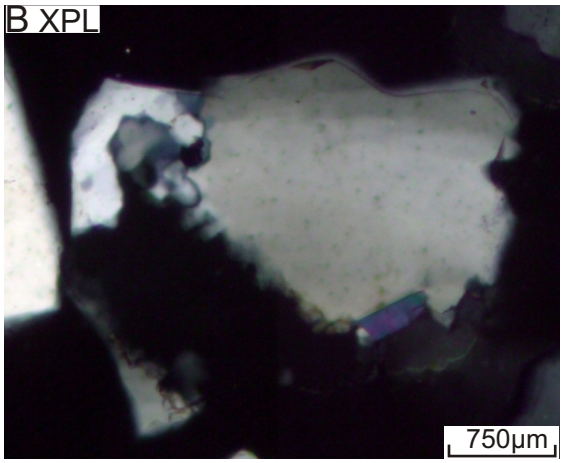

C BSE

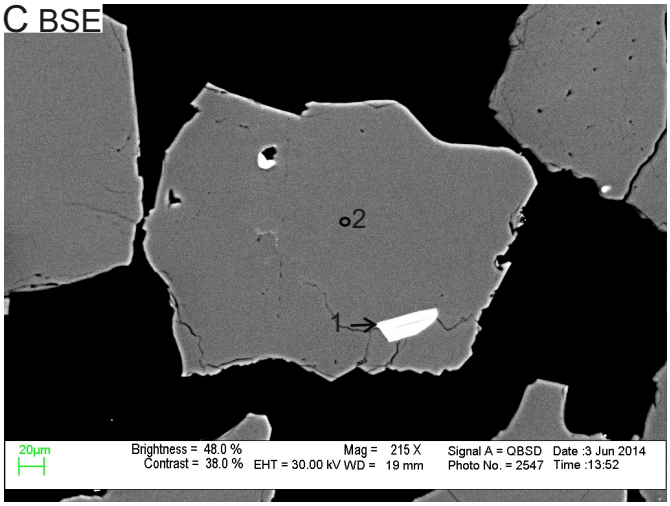

D SEM-CL

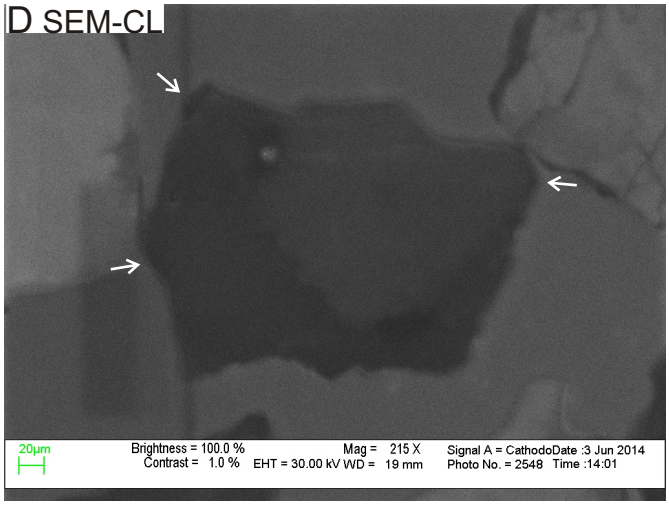

E EDS analyses

Pos#	Min. ID	SiO2	TiO2	Al2O3	FeO	MgO	K2O	Total	Actual total
1	Ms	50.81	0.60	25.94	4.22	2.49	10.95	95	88
2	Qz	99.99						100	97

Figure 4A-30: Microphotos under ppl (A) and xpl (B), SEM-BSE image (C), SEM-CL image (D), and EDS analyses table (E) of quartz grain 30 in sample 3000. The grain is anhedral and sub-angular polycrystalline (more than 6 sub-grains, a few with sutured sub-grain boundaries) with mosaic texture and weak undulose extinction. Fluid inclusions are rare. The grain contains muscovite inclusions; fractures are rare. The dark areas indicated by arrows in Fig. D are overgrowth.

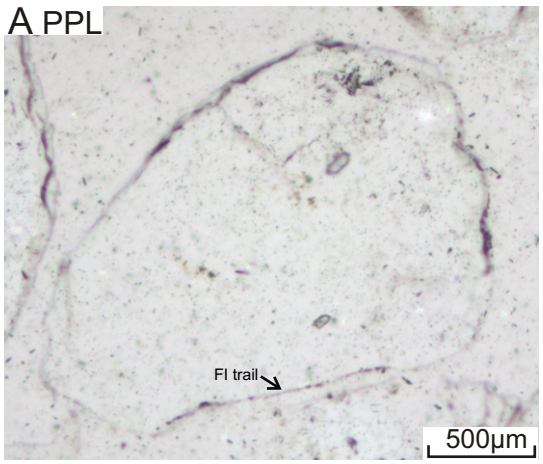

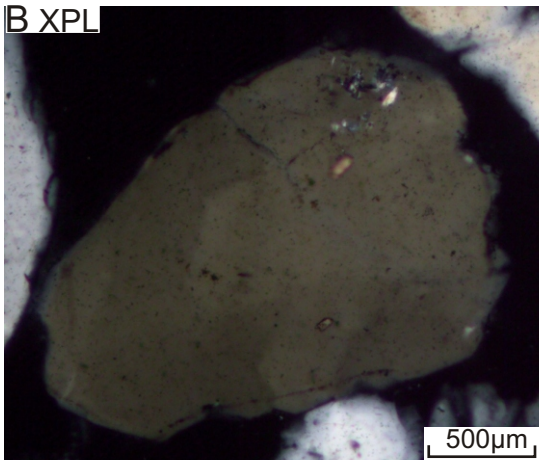

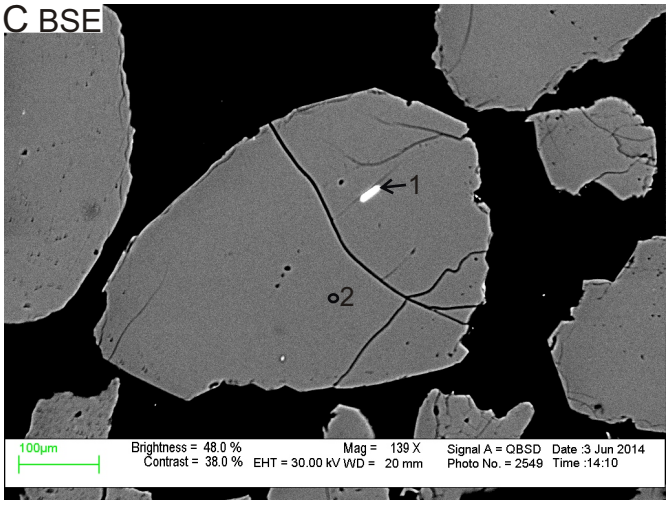

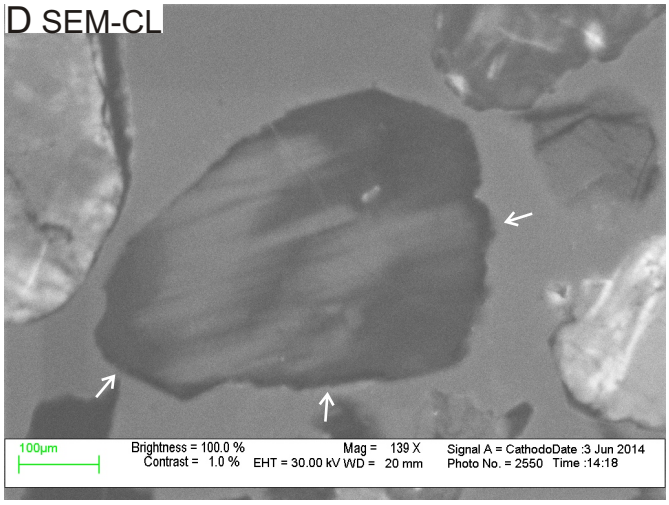

E EDS analyses

Pos#	Min. ID	SiO2	ZrO2	HfO2	Total	Actual total
1	Zrn	46.91	51.95	1.13	100	106
2	Qz	99.99			100	97

Figure 4A-31: Microphotos under ppl (A) and xpl (B), SEM-BSE image (C), SEM-CL image (D), and EDS analyses table (E) of quartz grain 31 in sample 3000. The grain is anhedral and rounded monocrystalline with mosaic texture and weak undulose extinction. Fluid inclusions are present and form trails at the contact between the detrital quartz and the overgrowth (Fig. A). The grain contains zircon inclusions and is microfractured with irregular curved fractures (Fig. C). Healed fractures (HF) are rare. The dark areas indicated by arrows in Fig. D are overgrowth. The grain shows bright CL streaky patches fabric in SEM-CL image.

A PPL

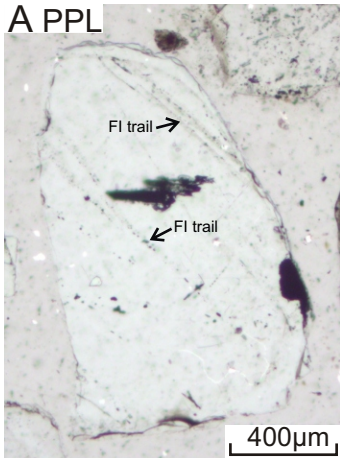

B XPL

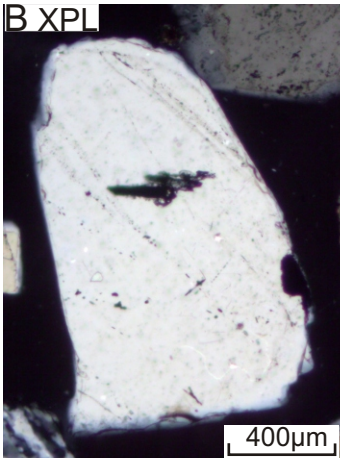

C BSE

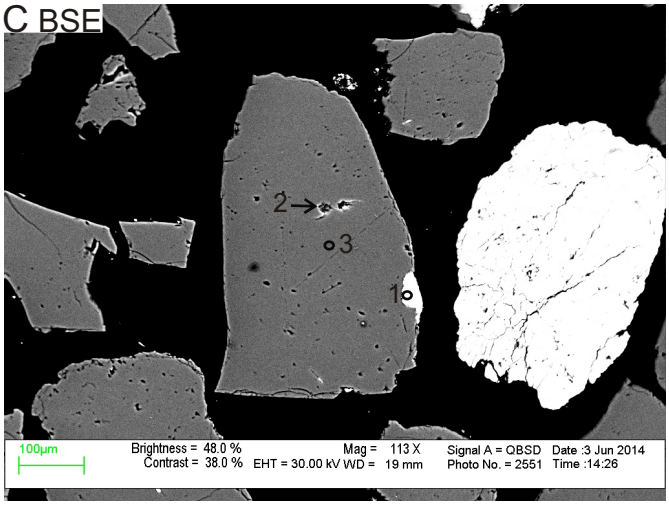

D SEM-CL

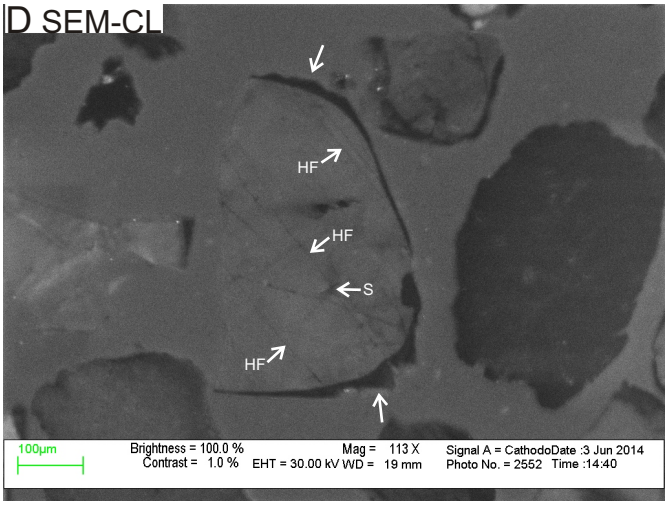

E EDS analyses

Pos#	Min. ID	SiO2	Al2O3	FeO	MgO	CaO	K2O	SO3	F	Cl	Total	Actual total
1	Py	0.17		27.72				72.12			100	175
2	Ilt	45.46	21.76	3.84	2.64	1.76	4.18	7.88	2.30	0.17	90	74
3	Qz	99.99									100	108

Figure 4A-32: Microphotos under ppl (A) and xpl (B), SEM-BSE image (C), SEM-CL image (D), and EDS analyses table (E) of quartz grain 32 in sample 3000. The grain is anhedral and sub-rounded monocrystalline with mosaic texture and weak undulose extinction. Fluid inclusions are common; they are usually associated with secondary porosity and form trails along healed fractures (Fig. A). The grain contains pyrite and illite inclusions and is microfractured with a set of sub-parallel fractures (Fig. D). Some healed fractures (HF) and spiders (S) can be seen in Fig. D. The dark areas indicated by arrows in Fig. D are overgrowth.

A PPL

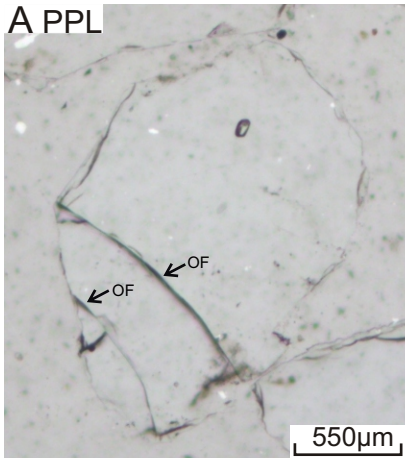

B XPL

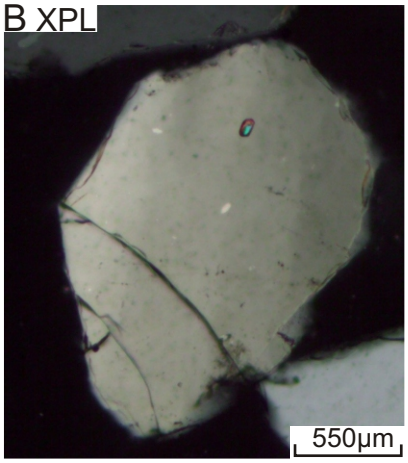

C BSE

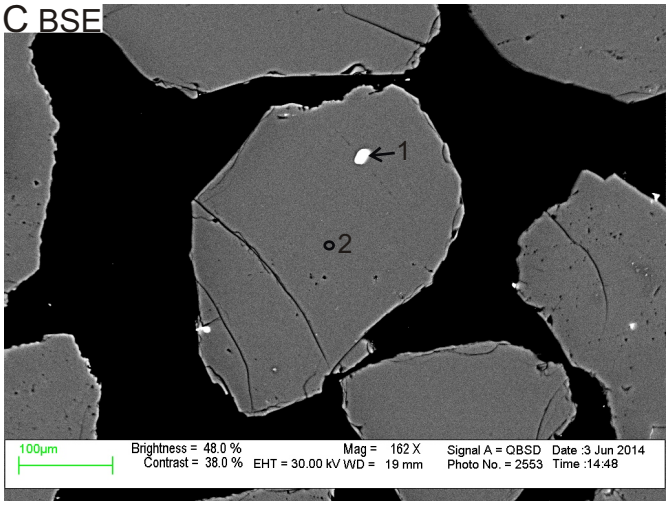

D SEM-CL

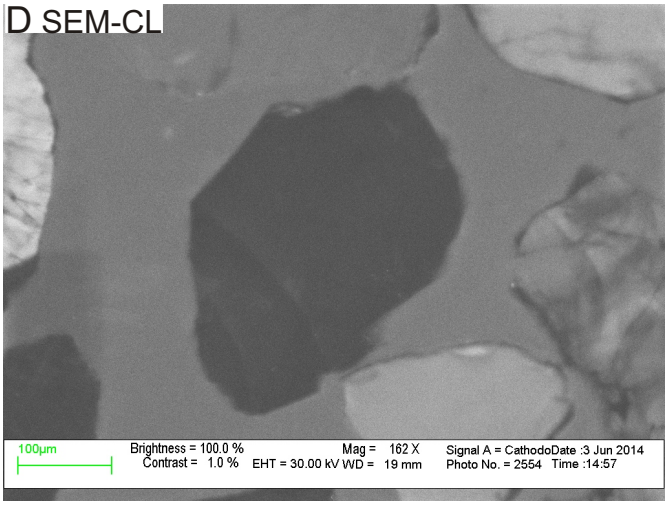

E EDS analyses

Pos#	Min. ID	SiO2	TiO2	Al2O3	FeO	CaO	F	Total	Actual total
1	Ttn	34.1	29.66	4.7	1.89	25.72	3.93	100	92
2	Qz	99.99						100	107

Figure 4A-33: Microphotos under ppl (A) and xpl (B), SEM-BSE image (C), SEM-CL image (D), and EDS analyses table (E) of quartz grain 33 in sample 3000. The grain is anhedral and sub-rounded monocrystalline with mosaic texture and weak undulose extinction. Fluid inclusions are rare. The grain contains titanite inclusions and is microfractured with a set of irregular curved open fractures (OF) (Fig. C). Healed fractures (HF) are rare. The grain shows homogenous dark-CL in SEM-CL image.

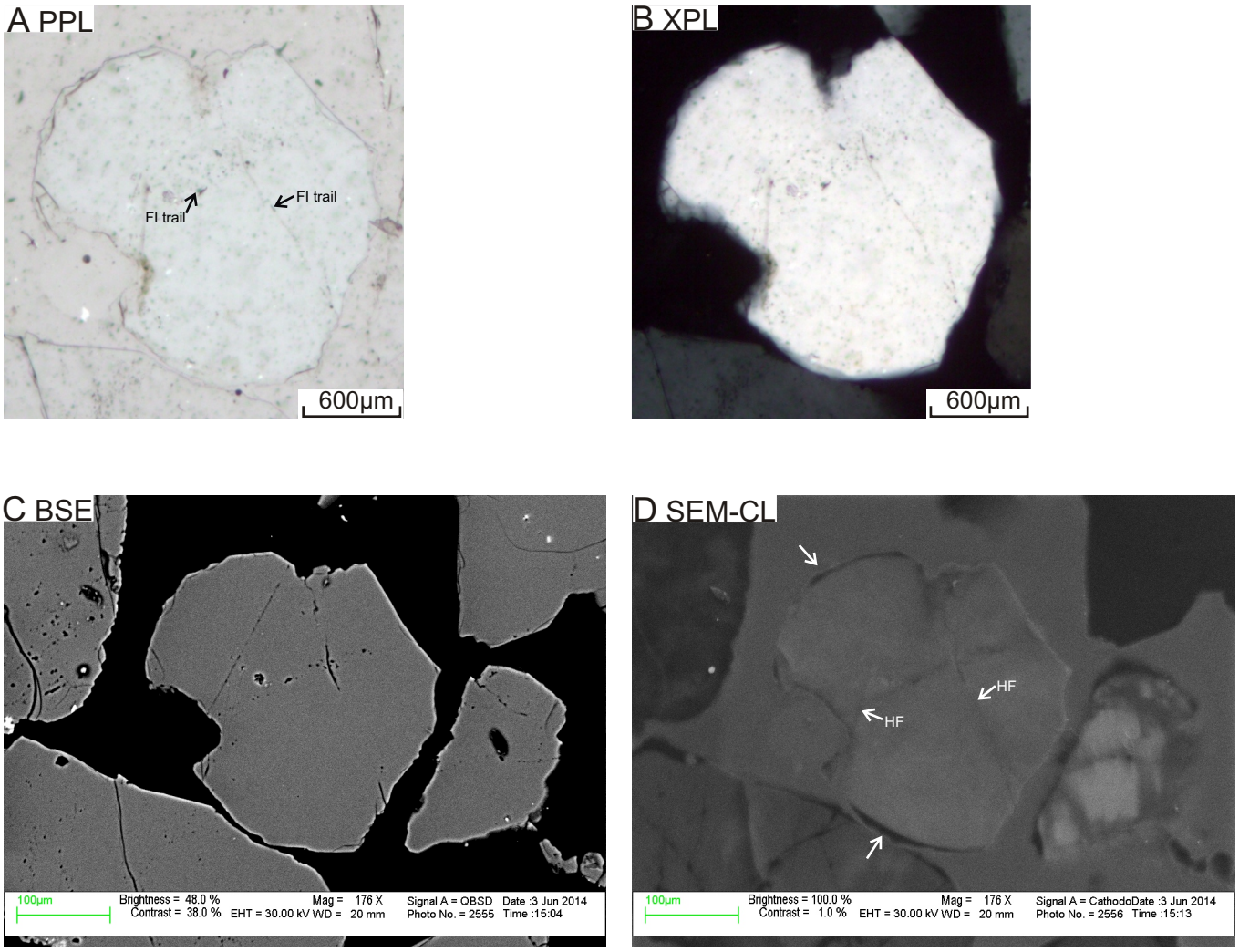

Figure 4A-34: Microphotos under ppl (A) and xpl (B), SEM-BSE image C, and SEM-CL image (D) of quartz grain 34 in sample 3000. The grain is anhedral and sub-rounded monocrystalline with embayed margins and strong undulose extinction. Fluid inclusions are present; they are usually associated with secondary porosity and form trails along healed fractures (Fig. A). The grain is weakly microfractured with a set of irregular fractures (Fig. D). A few healed fractures (HF) can be seen in Fig. D. The dark areas indicated by arrows in Fig. D are overgrowth.

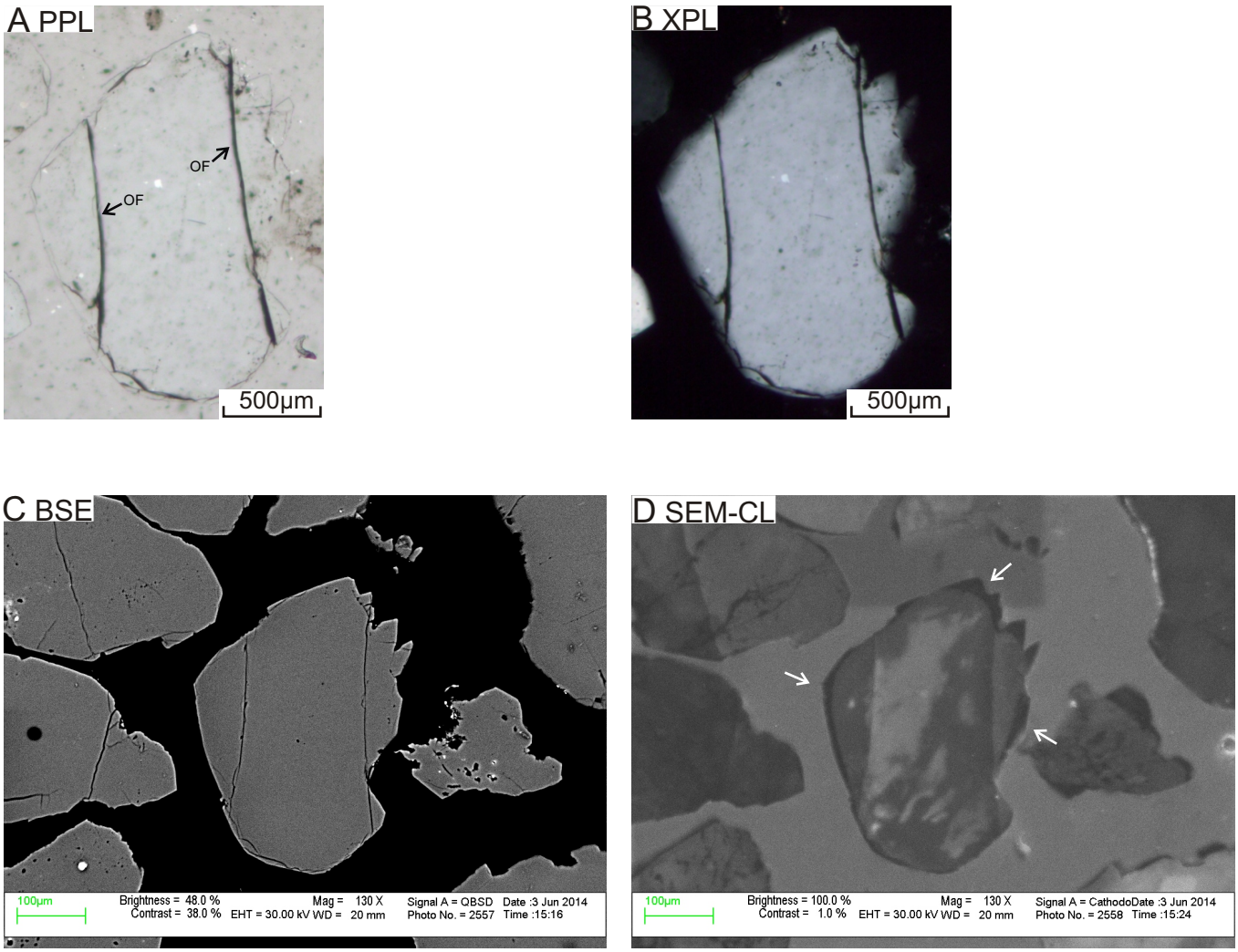

Figure 4A-35: Microphotos under ppl (A) and xpl (B), SEM-BSE image C, and SEM-CL image (D) of quartz grain 35 in sample 3000. The grain is anhedral and sub-rounded monocrystalline with embayed margins and weak undulose extinction. Fluid inclusions are present. The grain is microfractured with a set of irregular open fractures (OF) (Fig. C). Healed fractures (HF) are rare. The dark areas indicated by arrows in Fig. D are overgrowth. The grain shows random bright-CL patches in SEM-CL image.

A PPL

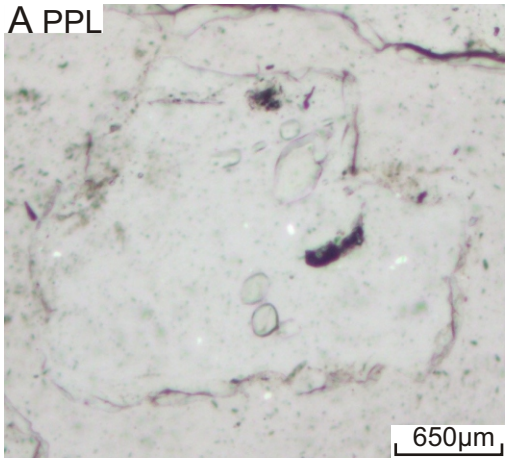

B XPL

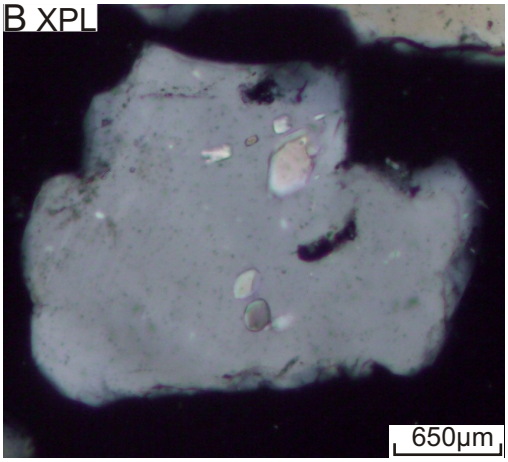

C BSE

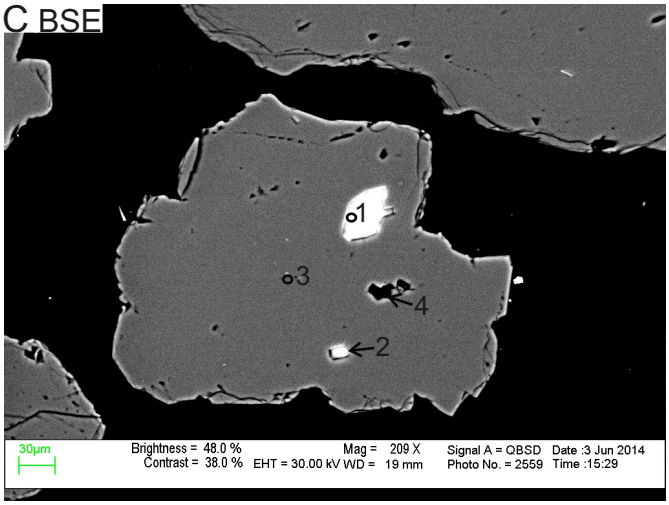

D SEM-CL

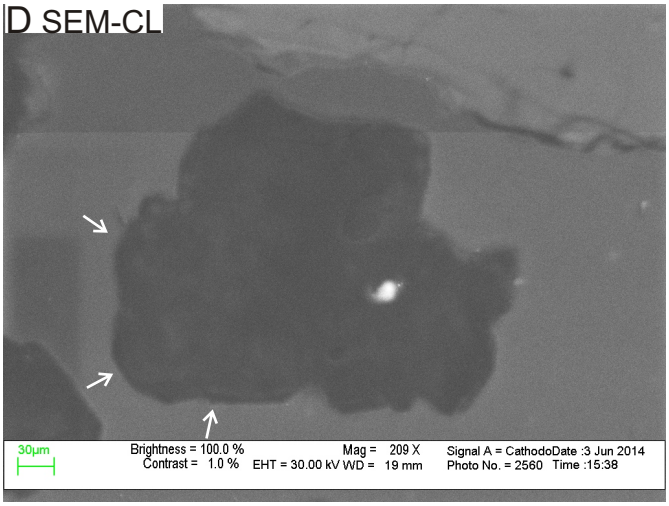

E EDS analyses

Pos#	Min. ID	SiO2	Al2O3	FeO	MnO	MgO	CaO	Na2O	K2O	SO3	F	Cl	Total	Actual total
1	Cal			2.93	2.22	5.26	89.58						100	44
2	Cal+Qz	29.2		1.65	1.24	3.57	64.35						100	54
3	Qz	99.99											100	96
4	Hole	85.8	1.87	0.99		2.32	1.43	0.49	0.37	1.1	5.06	0.59	100	47

Figure 4A-36: Microphotos under ppl (A) and xpl (B), SEM-BSE image (C), SEM-CL image (D), and EDS analyses table (E) of quartz grain 36 in sample 3000. The grain is anhedral and angular monocrystalline with mosaic texture and weak undulose extinction. Fluid inclusions are rare. The grain is weakly microfractured with irregular curved open fractures (Fig. C). Healed fractures are rare. The dark areas indicated by arrows in Fig. D are overgrowth. The grain shows homogenous dark-CL in SEM-CL image.

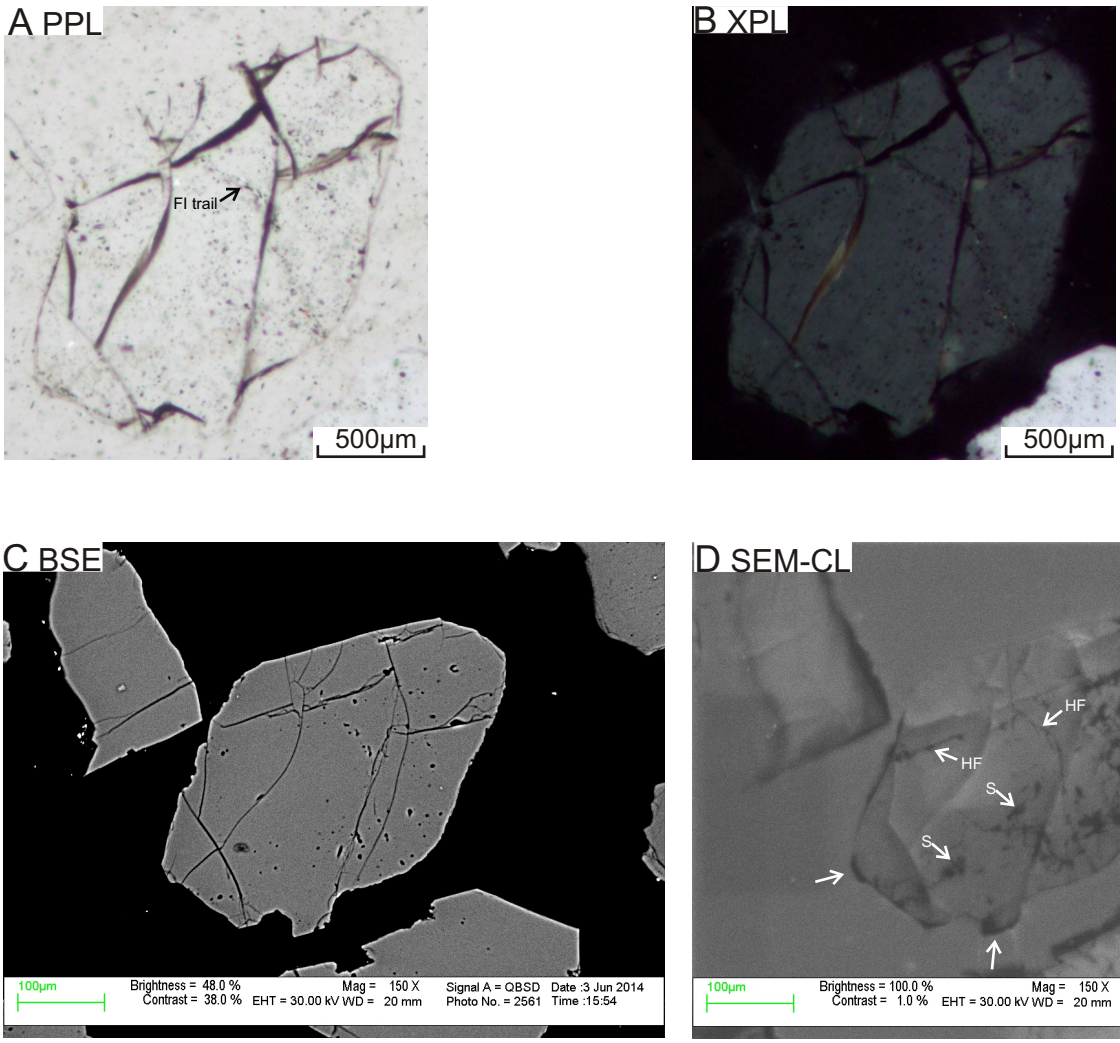

Figure 4A-37: Microphotos under ppl (A) and xpl (B), SEM-BSE image C, and SEM-CL image (D) of quartz grain 37 in sample 3000. The grain is anhedral and sub-rounded monocrystalline with non-undulose extinction. Fluid inclusions are common; they are usually associated with secondary porosity and form trails along healed fractures (Fig. A). The grain is microfractured with a set of irregular fractures (Fig. C and D). Some healed fractures (HF) and spiders (S) can be seen in Fig. D. The dark areas indicated by arrows in Fig. D are overgrowth.

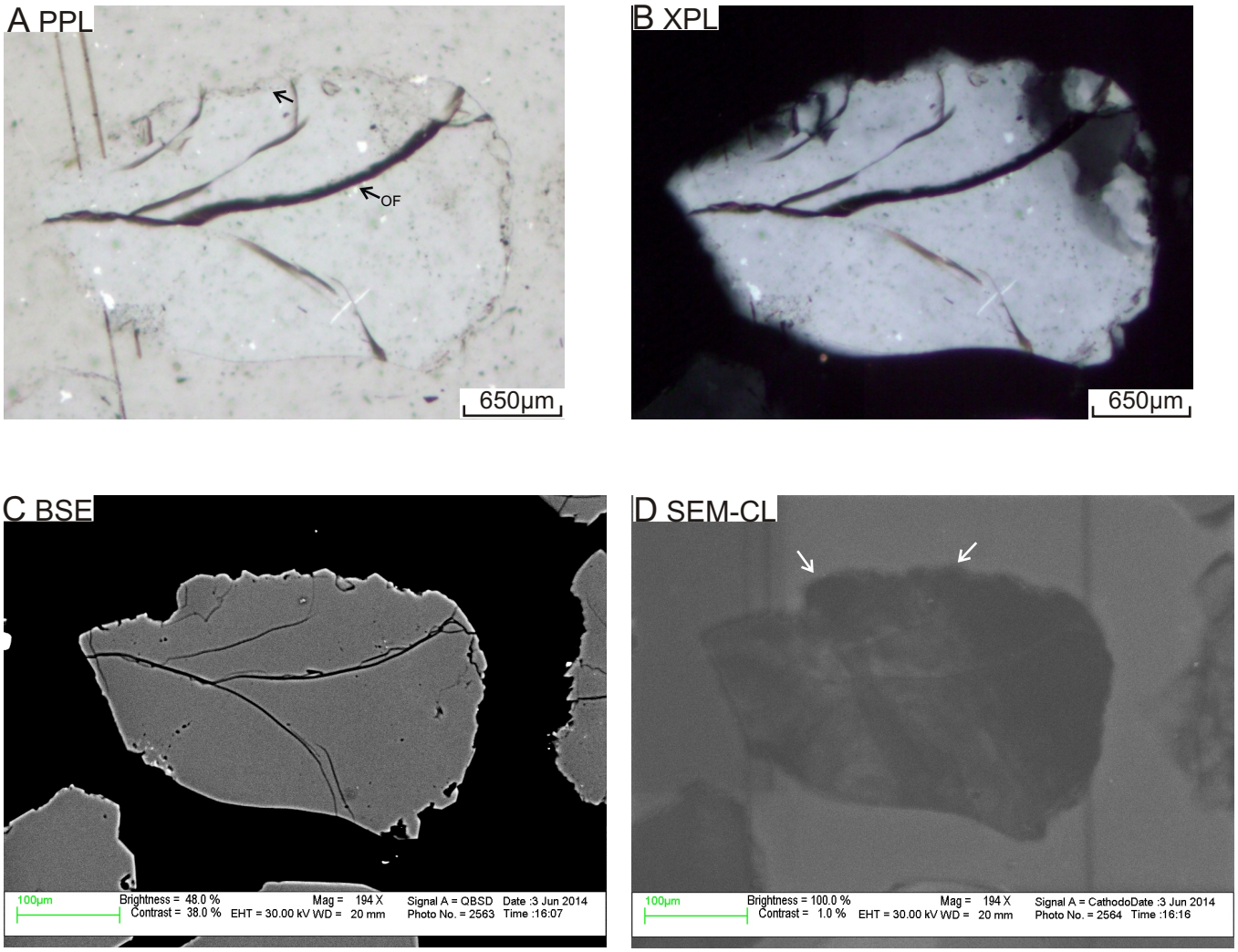

Figure 4A-38: Microphotos under ppl (A) and xpl (B), SEM-BSE image C, and SEM-CL image (D) of quartz grain 38 in sample 3000. The grain is anhedral and sub-rounded polycrystalline (only a few sub-grains) with mosaic texture and strong undulose extinction. Fluid inclusions form trails at the contact between the detrital quartz and the overgrowth (Fig. A). The grain is microfractured with irregular curved open fractures (OF) (Fig. C). Healed fractures are rare. The dark areas indicated by arrows in Fig. D are overgrowth; these areas appear corroded in Fig. C, suggesting secondary porosity.

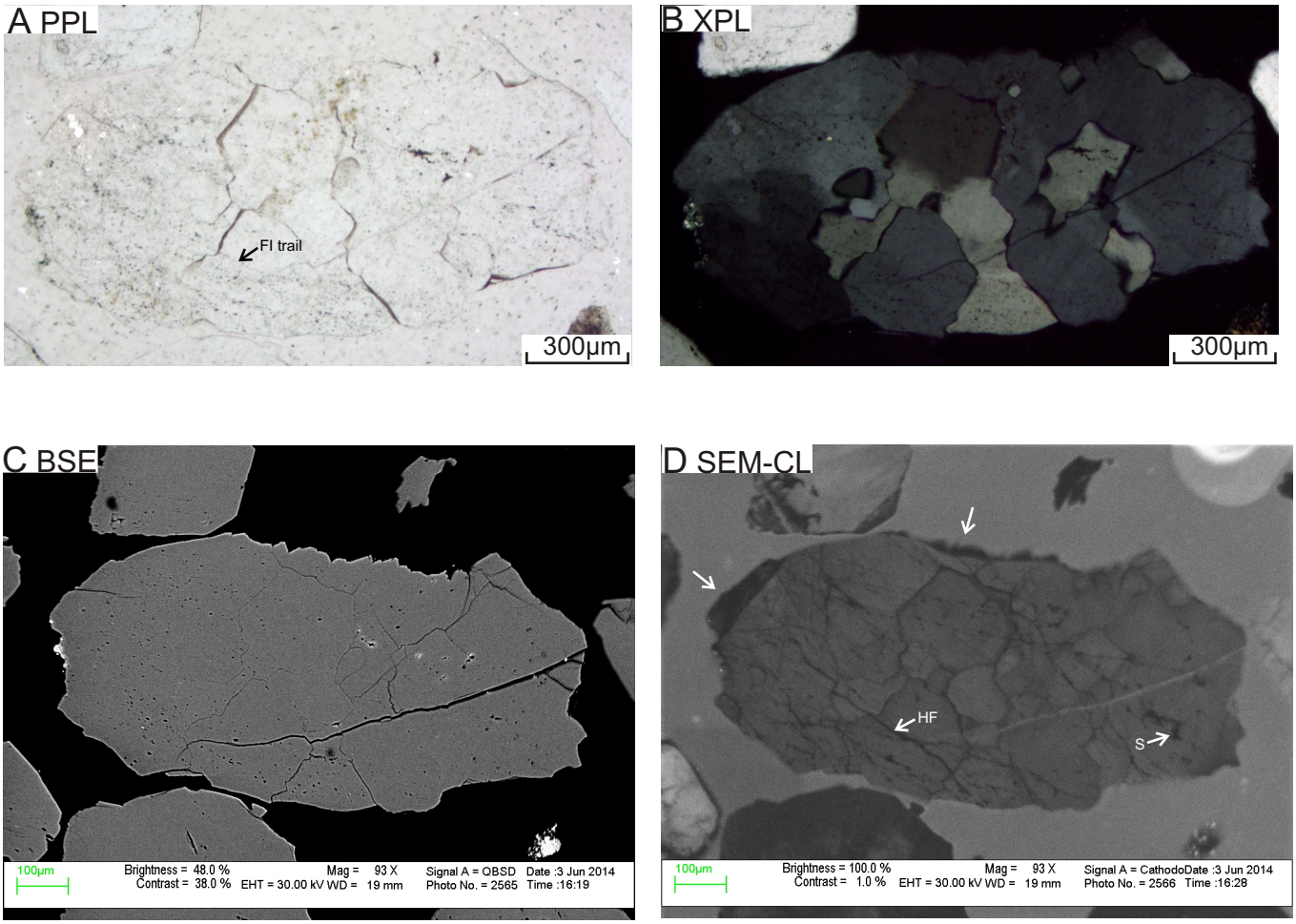

Figure 4A-39: Microphotos under ppl (A) and xpl (B), SEM-BSE image C, and SEM-CL image (D) of quartz grain 39 in sample 3000. The grain is anhedral and sub-rounded polycrystalline (more than 8 sub-grains with sutured sub-grain boundaries) with strong undulose extinction. Fluid inclusions are common; they are usually associated with secondary porosity and form trails along healed fractures (Fig. A). The grain is microfractured with a set of irregular fractures (Fig. C and D). Healed fractures (HF) and spiders (S) are common (Fig. D). The dark areas indicated by arrows in Fig. D are overgrowth.

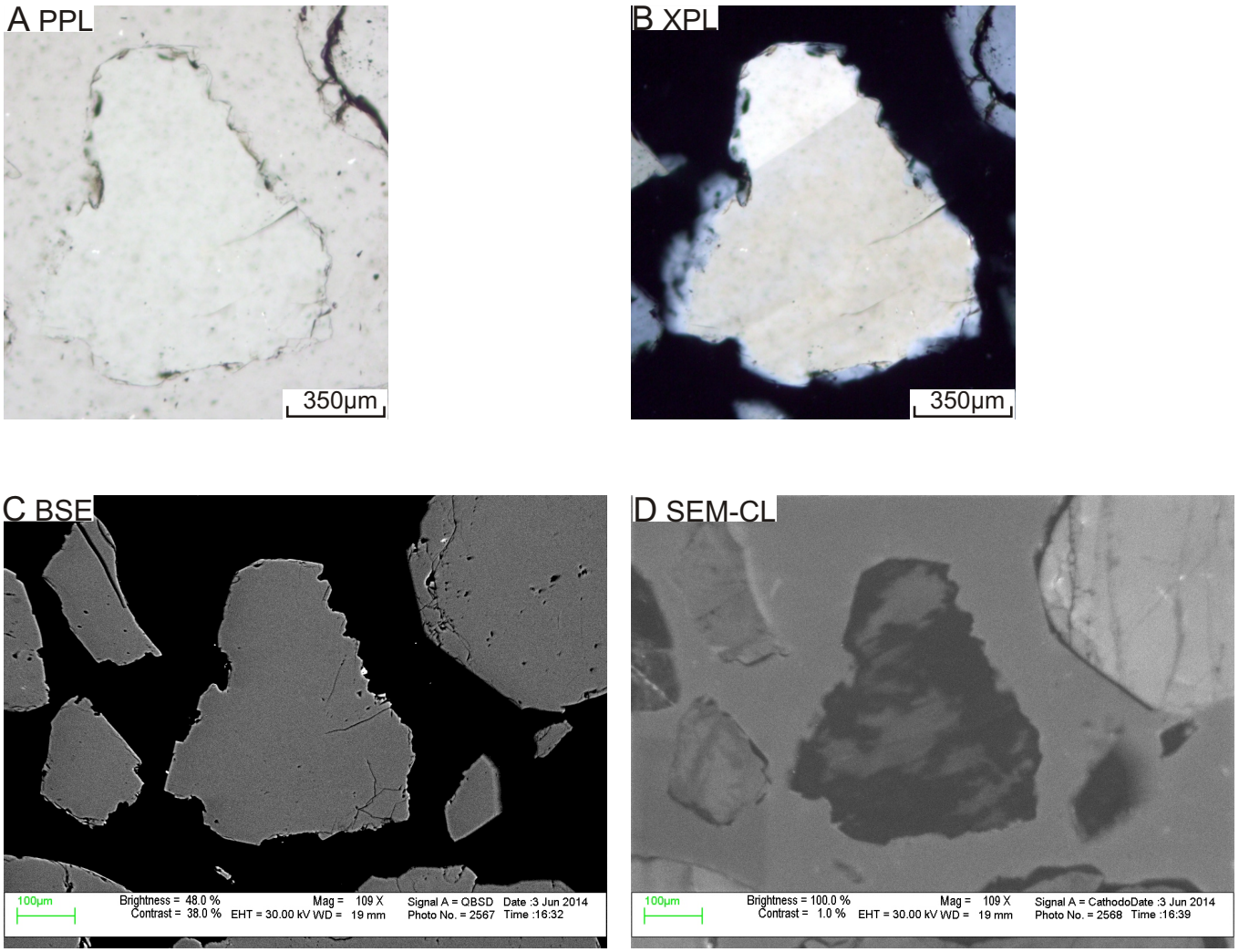

Figure 4A-40: Microphotos under ppl (A) and xpl (B), SEM-BSE image C, and SEM-CL image (D) of quartz grain 40 in sample 3000. The grain is anhedral and sub-rounded monocrystalline with irregular margins and strong undulose extinction. Fluid inclusions are rare. The grain is weakly microfractured with irregular curved open fractures (Fig. C). Healed fractures are rare. The grain shows kink band in Fig.B; the bright streaky patches fabric in SEM-CL image has the same orientation (SW-NE) of the kink band, indicating deformation in the detrital quartz.

Appendix 4B: Hot cathodoluminescence (HCL) images and blue colour shift analyses of detrital quartz grains in sample 3000.

Notes:

1. All the grains with HCL images correspond to the same grain in SEM-CL images. In all the following organized HCL figures,

   Fig. A shows HCL image taken after 3 seconds;

   Fig. B shows HCL image taken after 12 seconds;

   Fig. C is the histogram of blue colour within the analysed quartz grain in Fig. A and B, where X axis is the intensity of blue colour indicated by the colour bar with values from 0-255 (0=no blue or "black", 255=blue), and Y axis indicates the pixel amount at different blue values;

   Fig. D is the statistical table of blue values within the analysed grain area, where SD corresponds to standard deviation.

2. To classify the blue colour, the following abbreviations are used:

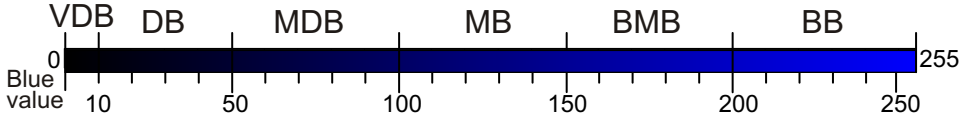

VDB: Very Dark Blue (0-10) **DB**: Dark Blue (11-50)

MDB: Medium Dark Blue (51-100) **MB**: Medium Blue (101-150)

BMB: Bright-Medium Blue (151-200) **BB**: Bright Blue (201-255)

3. To quantify the blue colour shift, the following criteria are used:

   Mean blue value change **< 5**: **No** colour shift

   5 ≤Mean blue value change **< 15**: **Slight** colour shift

   15 ≤Mean blue value change **< 30**: **Moderate** colour shift

   Mean blue value change ≥**30**: **Strong** colour shift

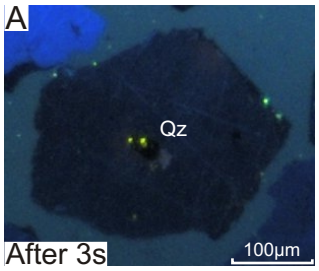

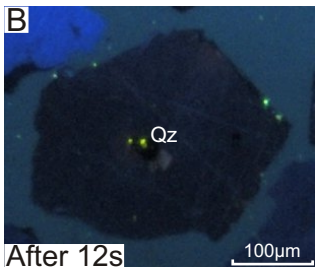

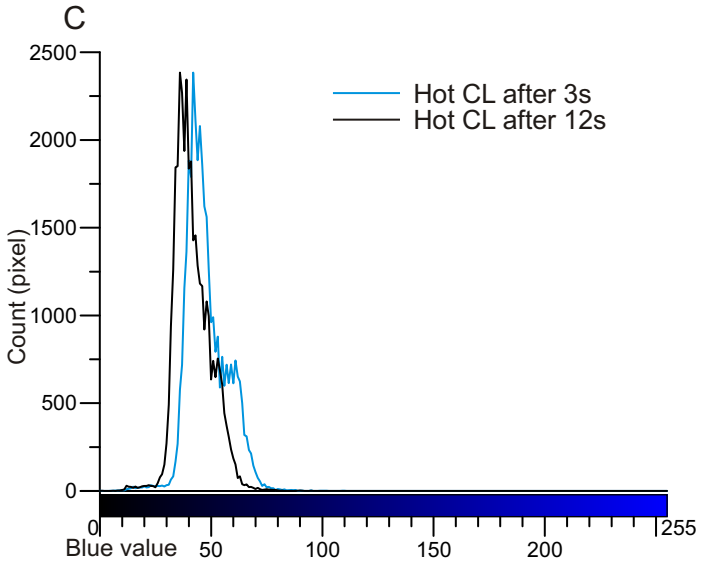

Figure 4B-1: Grain 1. The grain shows slight colour shift.

D

Blue value	Min	Max	Mode	Mean	SD
After 3s	0	110	42	48	9.1
After 12s	1	95	36	42	8

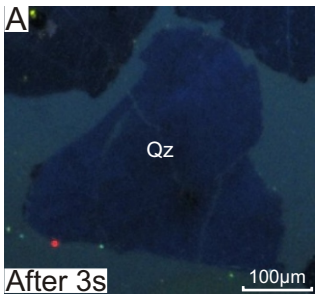

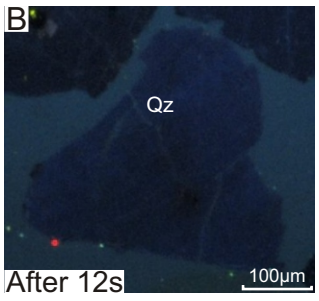

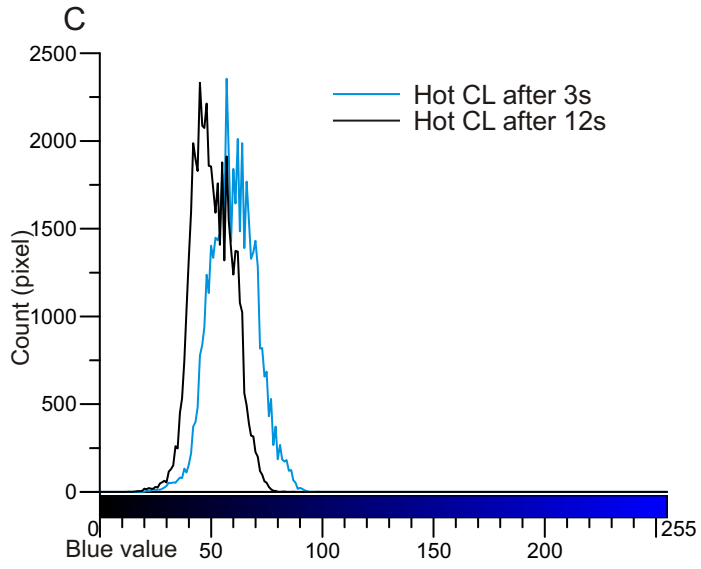

Figure 4B-2: Grain 2. The grain shows slight colour shift.

D

Blue value	Min	Max	Mode	Mean	SD
After 3s	17	98	57	60	10.1
After 12s	13	87	45	51	8.9

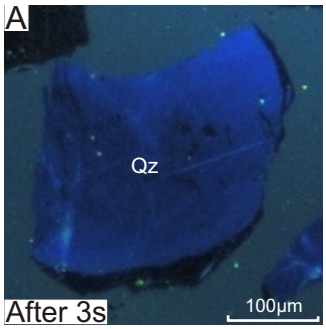

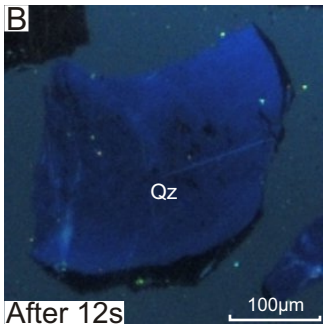

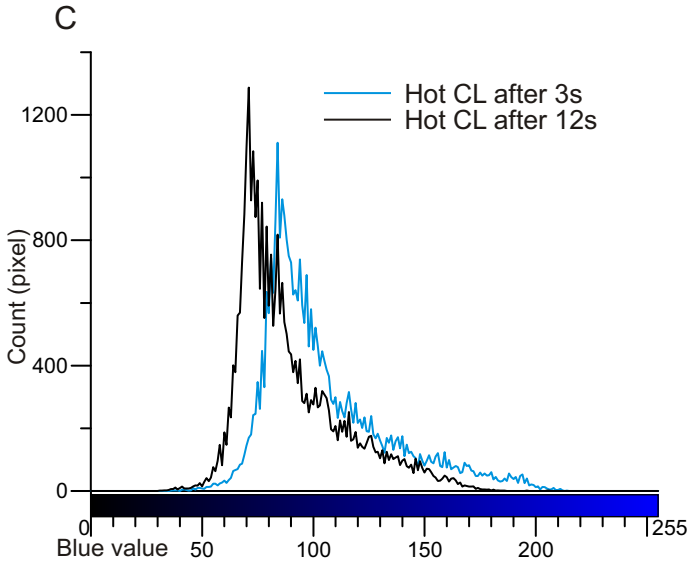

D

Blue value	Min	Max	Mode	Mean	SD
After 3s	36	214	84	105	28.5
After 12s	31	206	71	90	23.9

Figure 4B-3: Grain 3. The grain moderate colour shift.

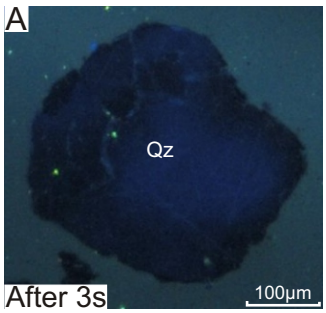

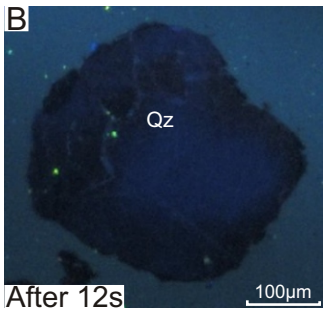

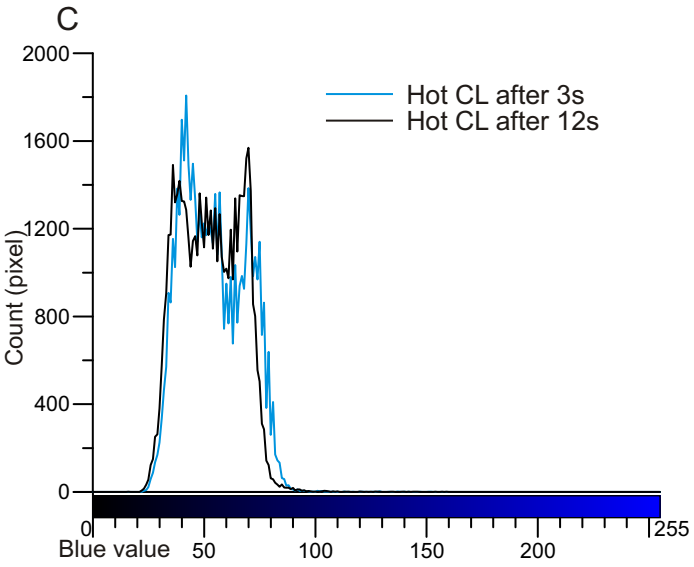

D

Blue value	Min	Max	Mode	Mean	SD
After 3s	22	152	42	54	14.1
After 12s	16	159	70	53	13.6

Figure 4B-4: Grain 4. The grain shows no colour shift.

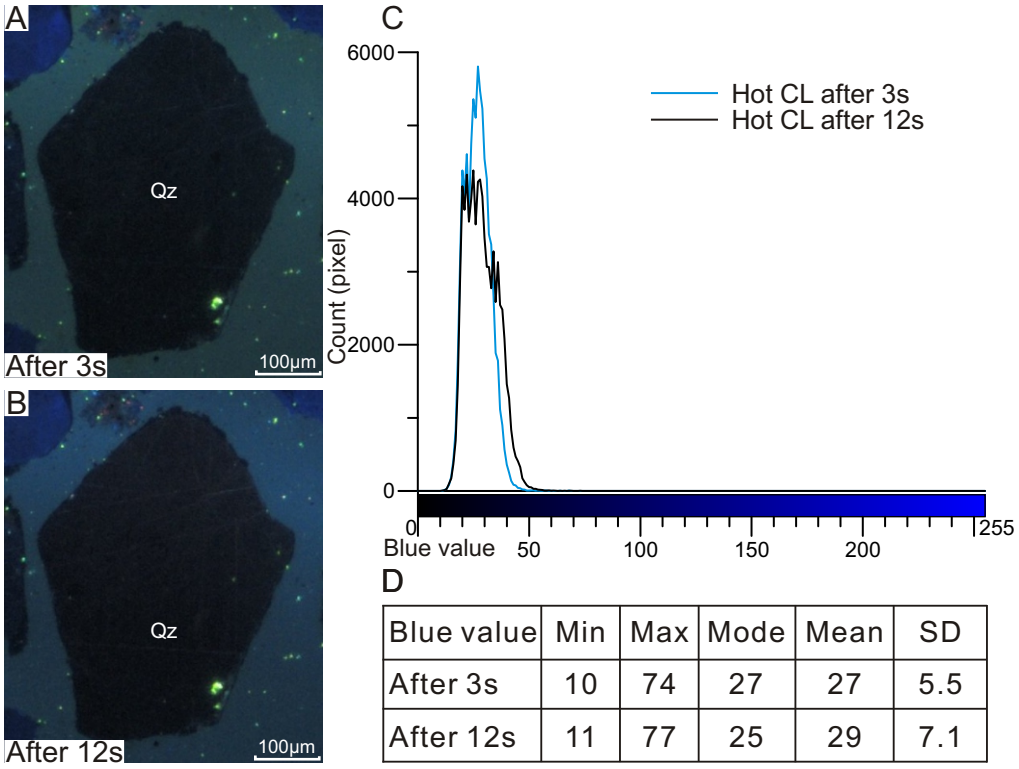

Figure 4B-5: Grain 5. The grain shows no colour shift.

D

Blue value	Min	Max	Mode	Mean	SD
After 3s	10	74	27	27	5.5
After 12s	11	77	25	29	7.1

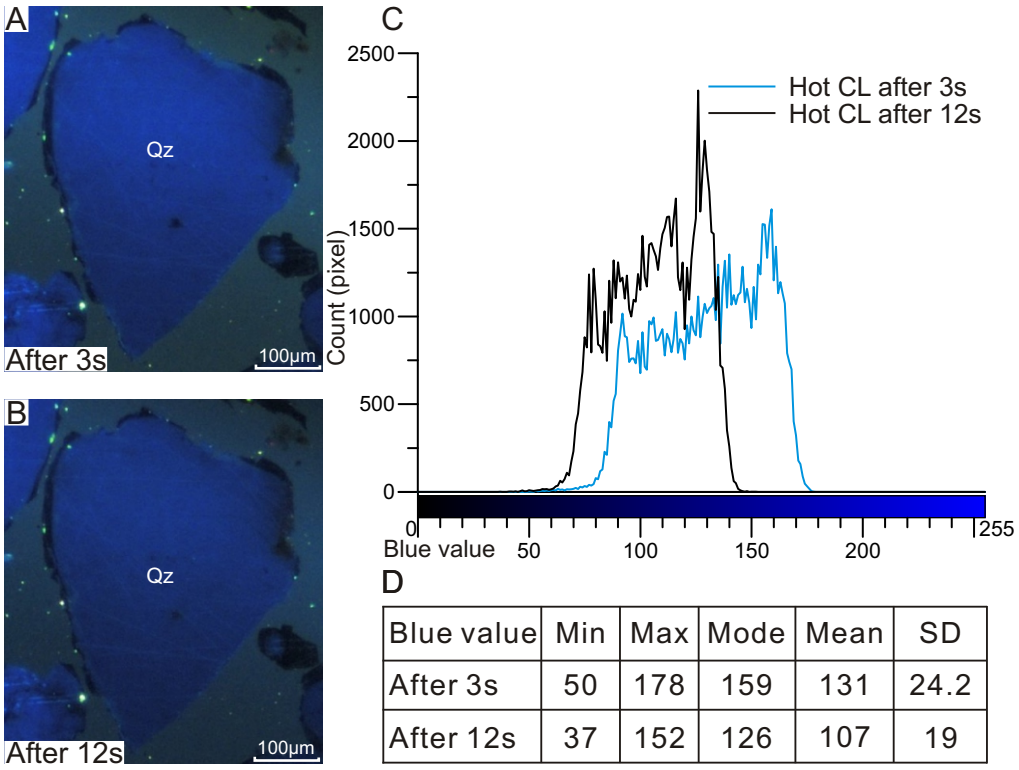

Figure 4B-6: Grain 6. The grain shows moderate colour shift.

D

Blue value	Min	Max	Mode	Mean	SD
After 3s	50	178	159	131	24.2
After 12s	37	152	126	107	19

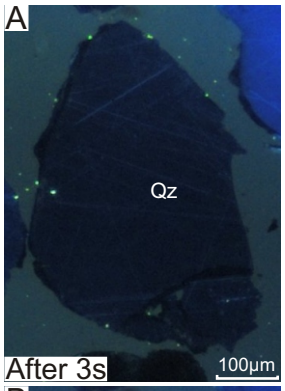

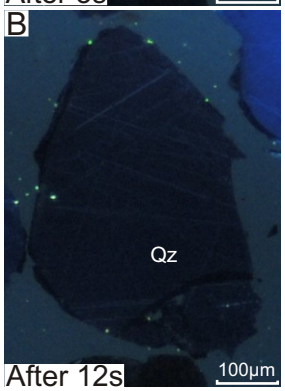

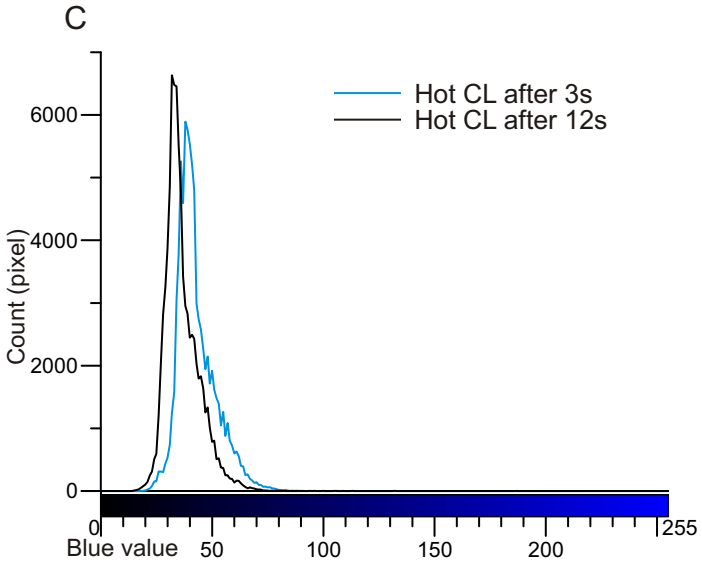

Figure 4B-7: Grain 7. The grain shows slight colour shift.

D

Blue value	Min	Max	Mode	Mean	SD
After 3s	18	223	38	43	8.9
After 12s	13	222	32	37	7.9

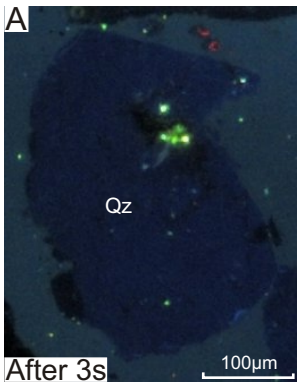

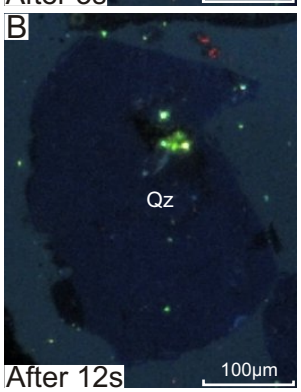

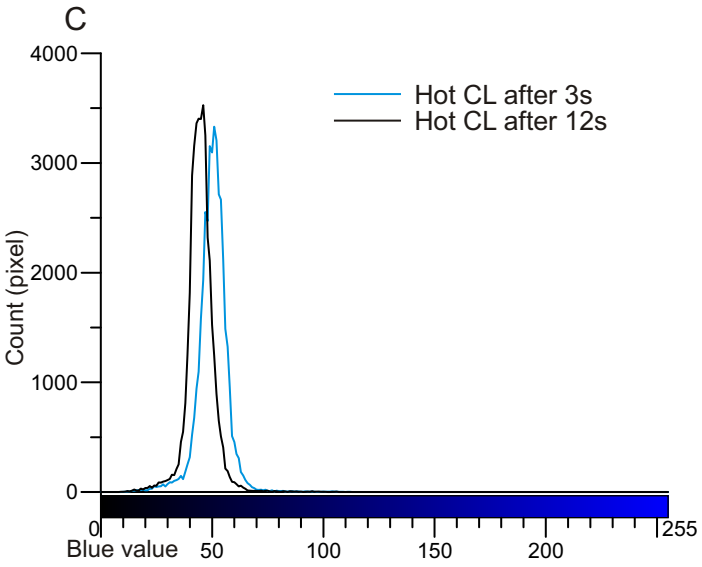

Figure 4B-8: Grain 8. The grain shows slight colour shift.

D

Blue value	Min	Max	Mode	Mean	SD
After 3s	10	112	51	50	6.9
After 12s	9	106	46	45	6.2

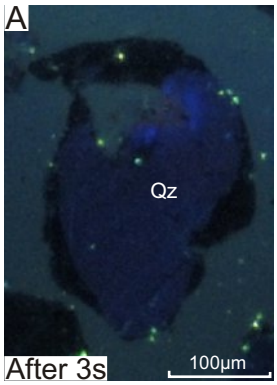

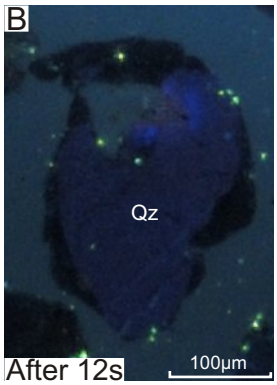

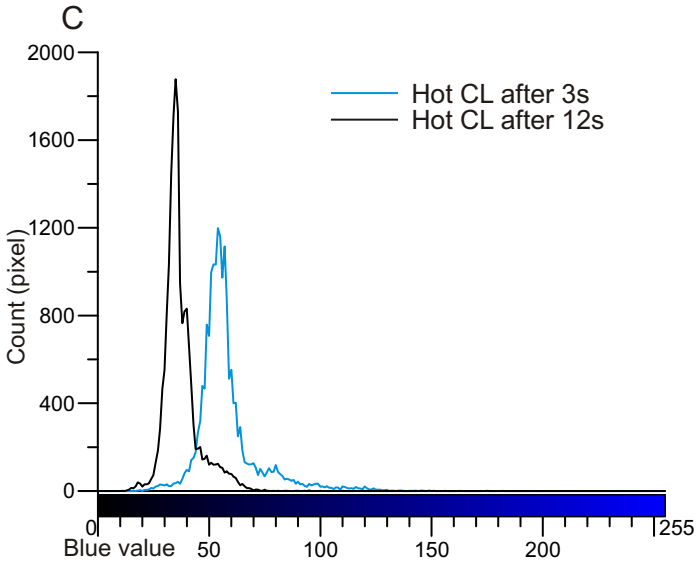

D

Blue value	Min	Max	Mode	Mean	SD
After 3s	18	182	54	58	13.8
After 12s	11	175	35	37	8.1

Figure 4B-9: Grain 9. The grain shows moderate colour shift.

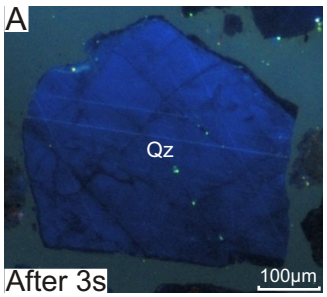

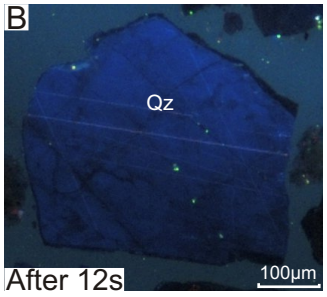

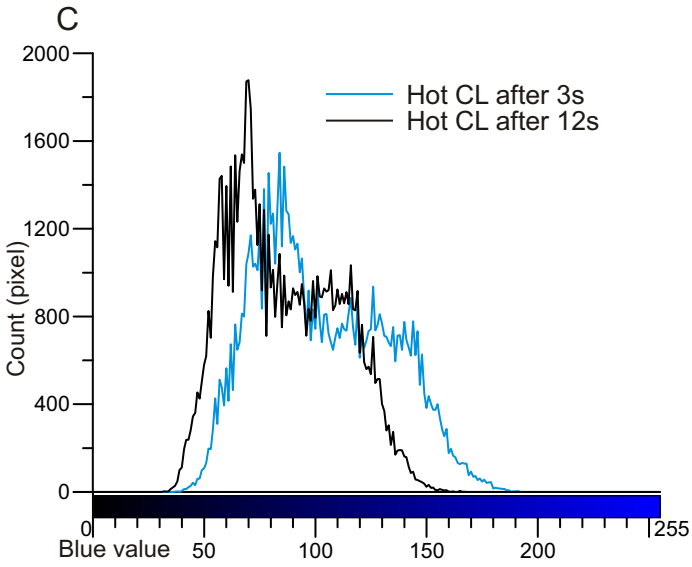

D

Blue value	Min	Max	Mode	Mean	SD
After 3s	37	192	84	103	29.3
After 12s	32	167	70	86	24.9

Figure 4B-10: Grain 10. The grain shows moderate colour shift.

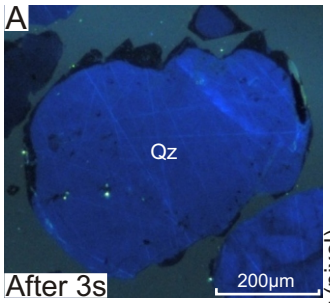

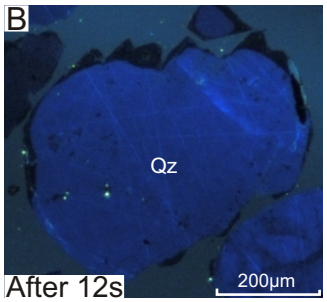

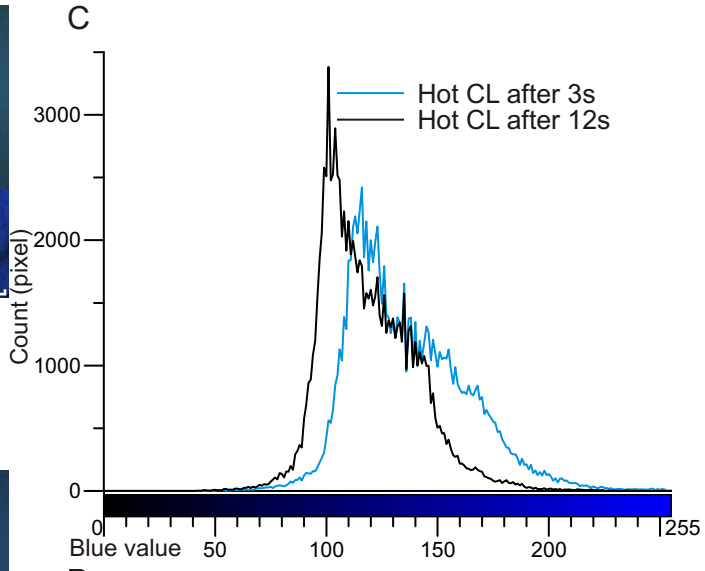

D

Blue value	Min	Max	Mode	Mean	SD
After 3s	50	255	116	136	26.1
After 12s	42	243	101	119	21

Figure 4B-11: Grain 11. The grain shows moderate colour shift.

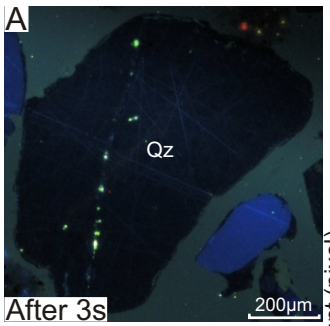

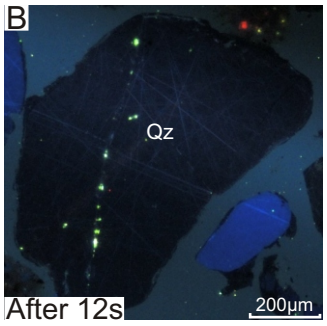

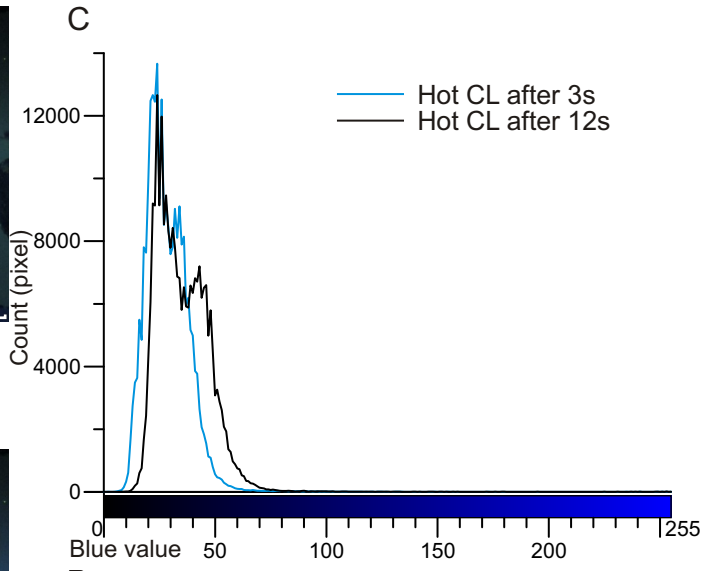

D

Blue value	Min	Max	Mode	Mean	SD
After 3s	2	255	24	28	10.6
After 12s	3	255	24	35	12.7

Figure 4B-12: Grain 12. Probably the first image was taken too early. Therefore, this grain is not useful to analyse the colour shift.

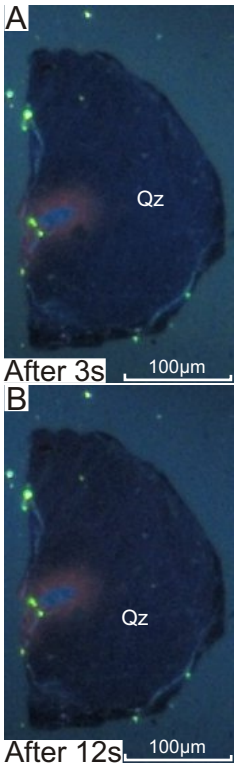

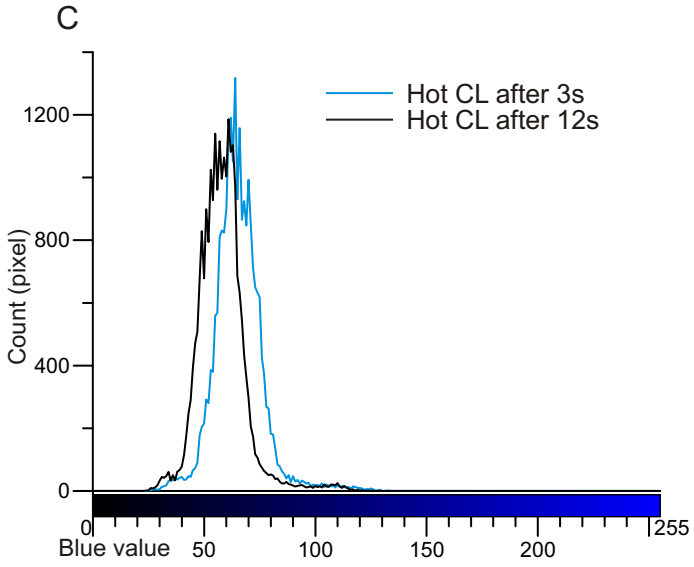

Figure 4B-13: Grain 13. The grain shows slight colour shift.

D

Blue value	Min	Max	Mode	Mean	SD
After 3s	25	133	64	65	10.9
After 12s	24	126	61	58	10.6

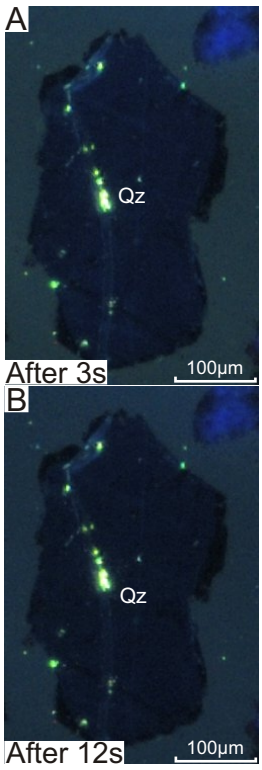

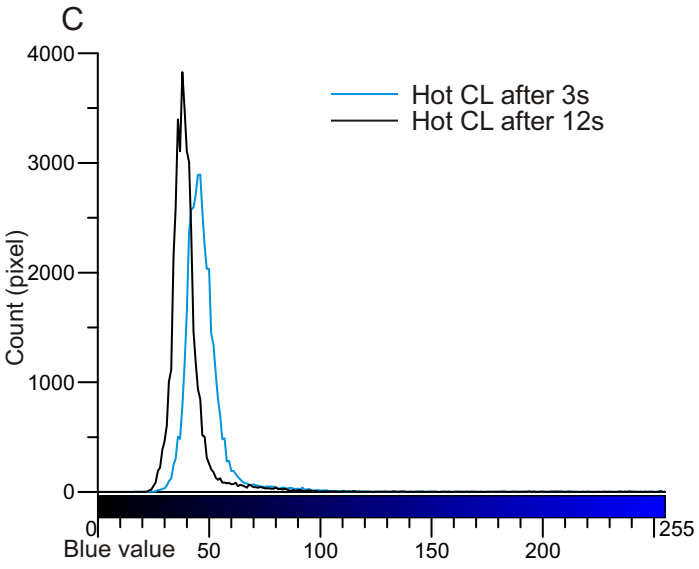

Figure 4B-14: Grain 14. The grain shows slight colour shift.

D

Blue value	Min	Max	Mode	Mean	SD
After 3s	23	253	46	48	13.3
After 12s	17	255	38	41	13

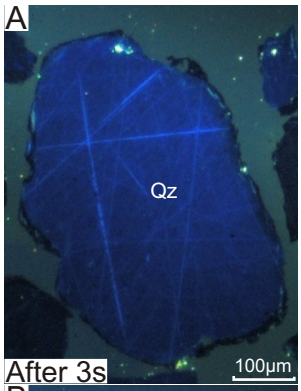

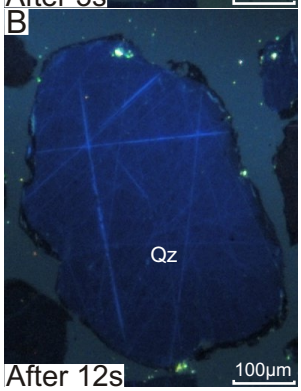

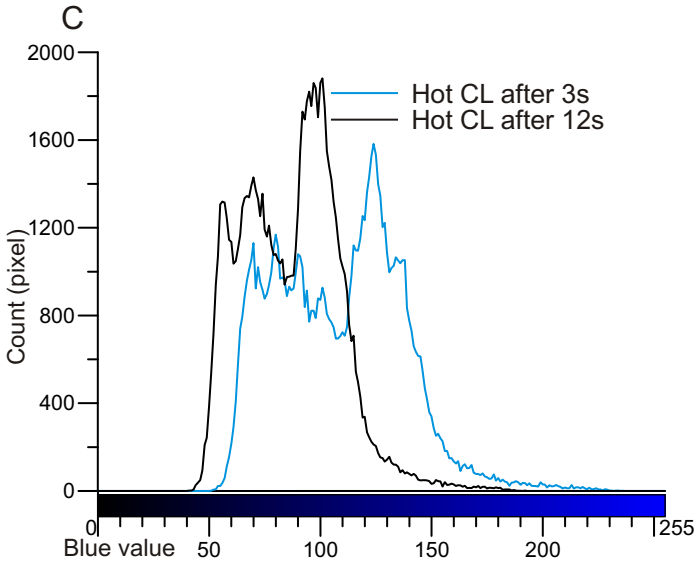

D

Blue value	Min	Max	Mode	Mean	SD
After 3s	51	236	124	109	28.5
After 12s	41	192	101	87	21.7

Figure 4B-15: Grain 15. The grain shows moderate colour shift.

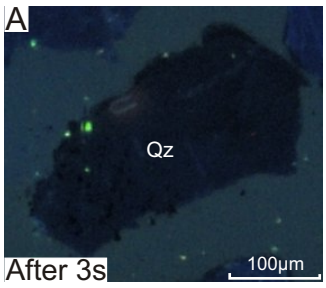

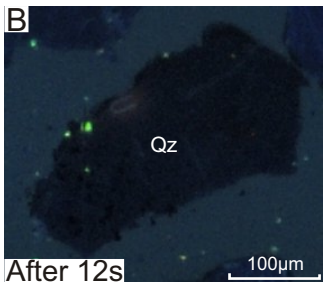

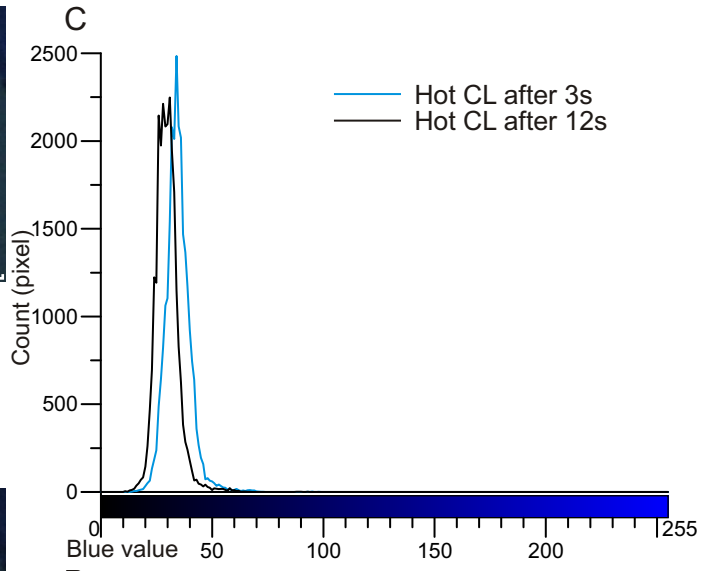

D

Blue value	Min	Max	Mode	Mean	SD
After 3s	14	98	34	35	5.7
After 12s	11	93	31	30	5.2

Figure 4B-16: Grain 16. The grain shows slight colour shift.

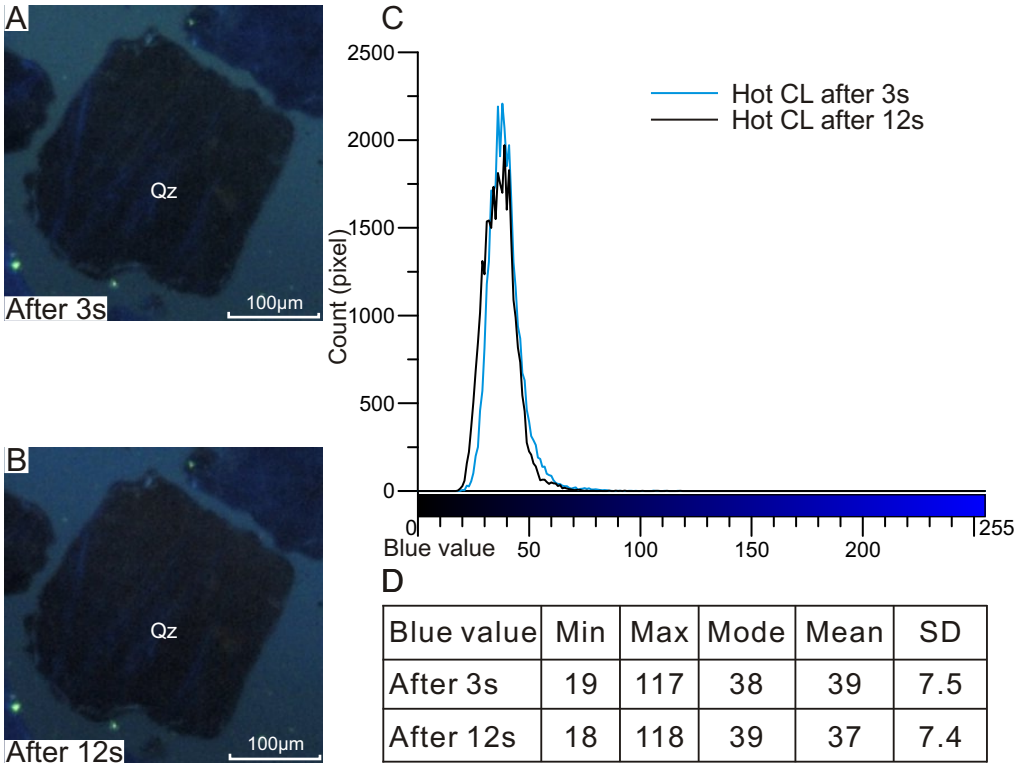

Blue value	Min	Max	Mode	Mean	SD
After 3s	19	117	38	39	7.5
After 12s	18	118	39	37	7.4

Figure 4B-17: Grain 17. The grain shows no colour shift.

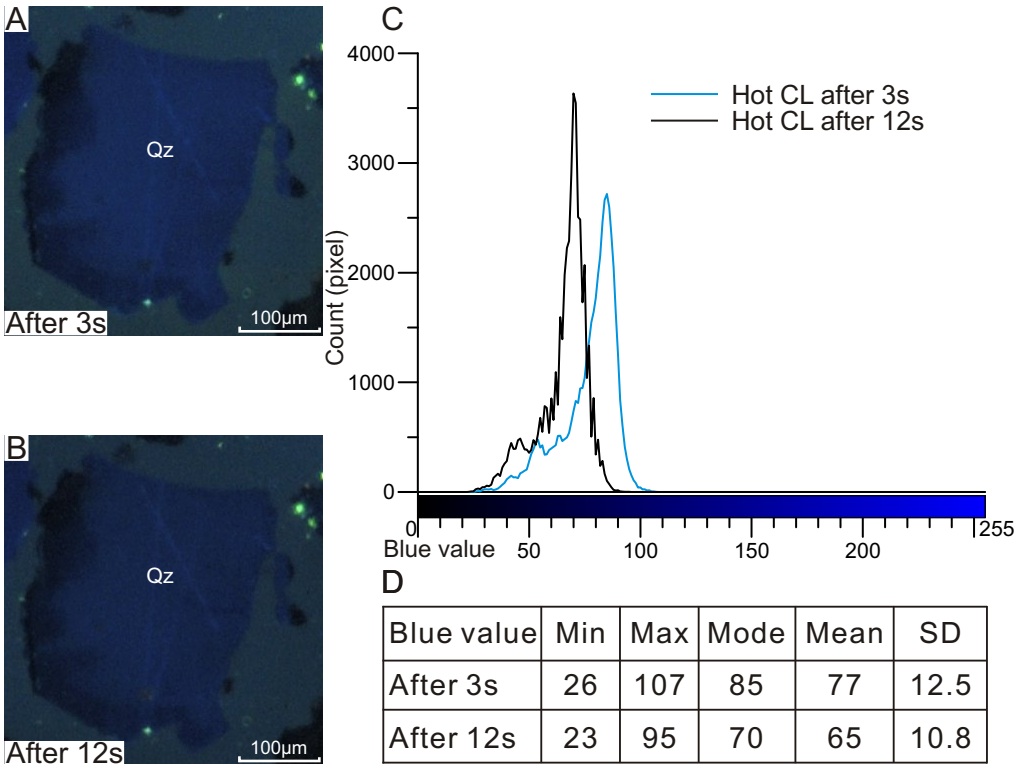

Blue value	Min	Max	Mode	Mean	SD
After 3s	26	107	85	77	12.5
After 12s	23	95	70	65	10.8

Figure 4B-18: Grain 18. The grain shows slight colour shift.

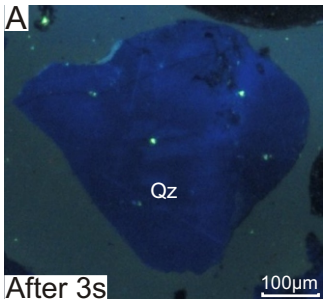

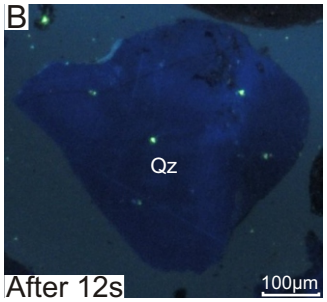

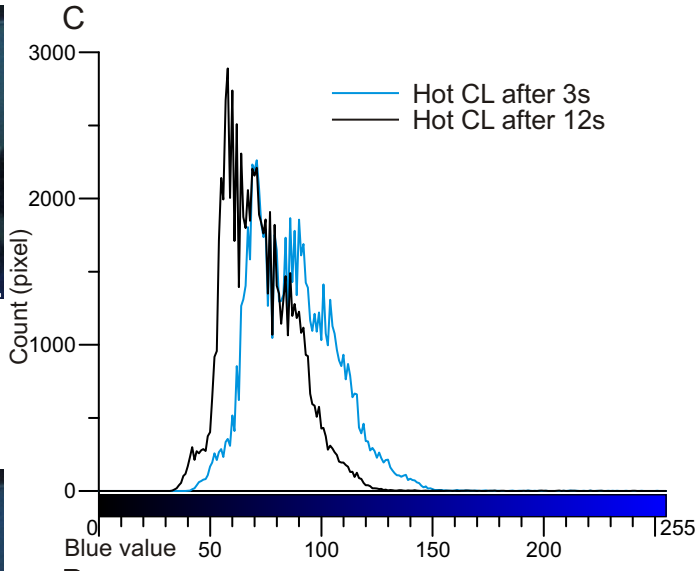

D

Blue value	Min	Max	Mode	Mean	SD
After 3s	40	251	71	87	19
After 12s	33	241	58	72	15.9

Figure 4B-19: Grain 19. The grain shows moderate colour shift.

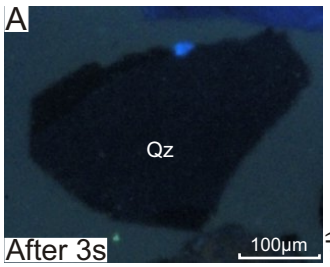

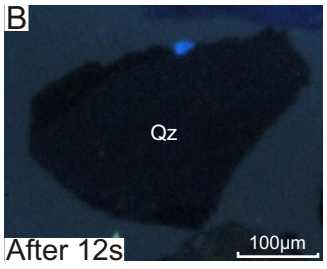

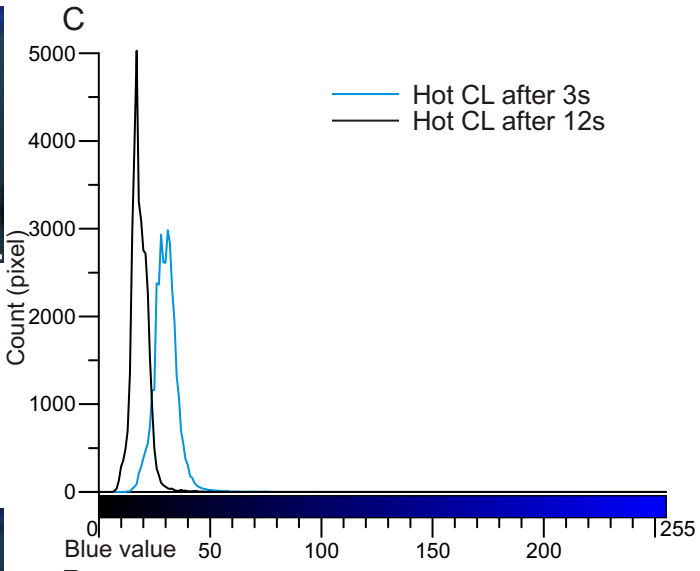

D

Blue value	Min	Max	Mode	Mean	SD
After 3s	13	110	31	30	5.5
After 12s	10	103	26	26	5.1

Figure 4B-20: Grain 20. The grain shows no colour shift.

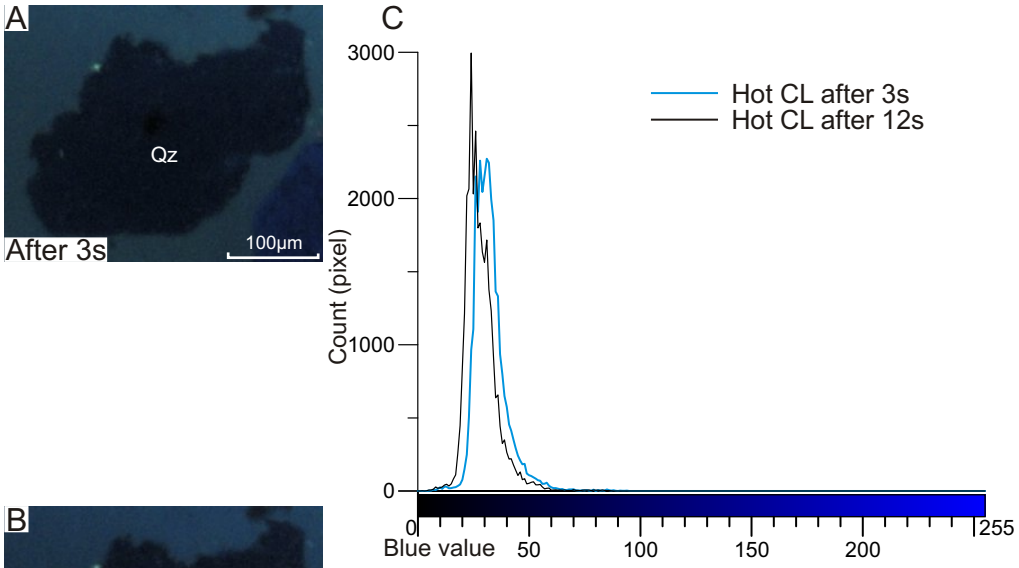

Figure 4B-21: Grain 21. The grain shows no colour shift.

D

Blue value	Min	Max	Mode	Mean	SD
After 3s	5	94	31	32	7.4
After 12s	2	87	24	28	7.2

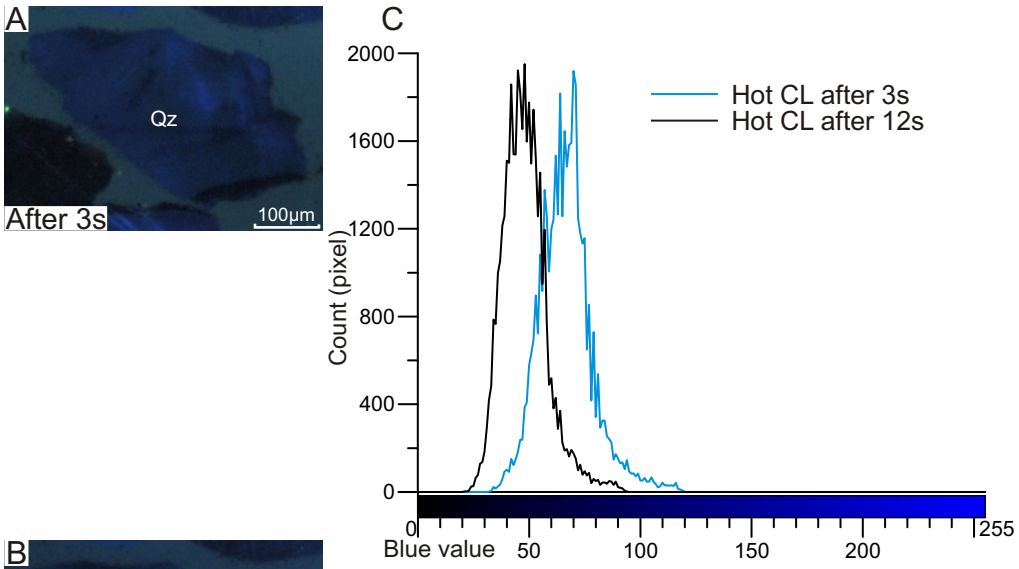

Figure 4B-22: Grain 22. The grain shows moderate colour shift.

D

Blue value	Min	Max	Mode	Mean	SD
After 3s	32	119	70	67	12
After 12s	21	94	48	48	10.1

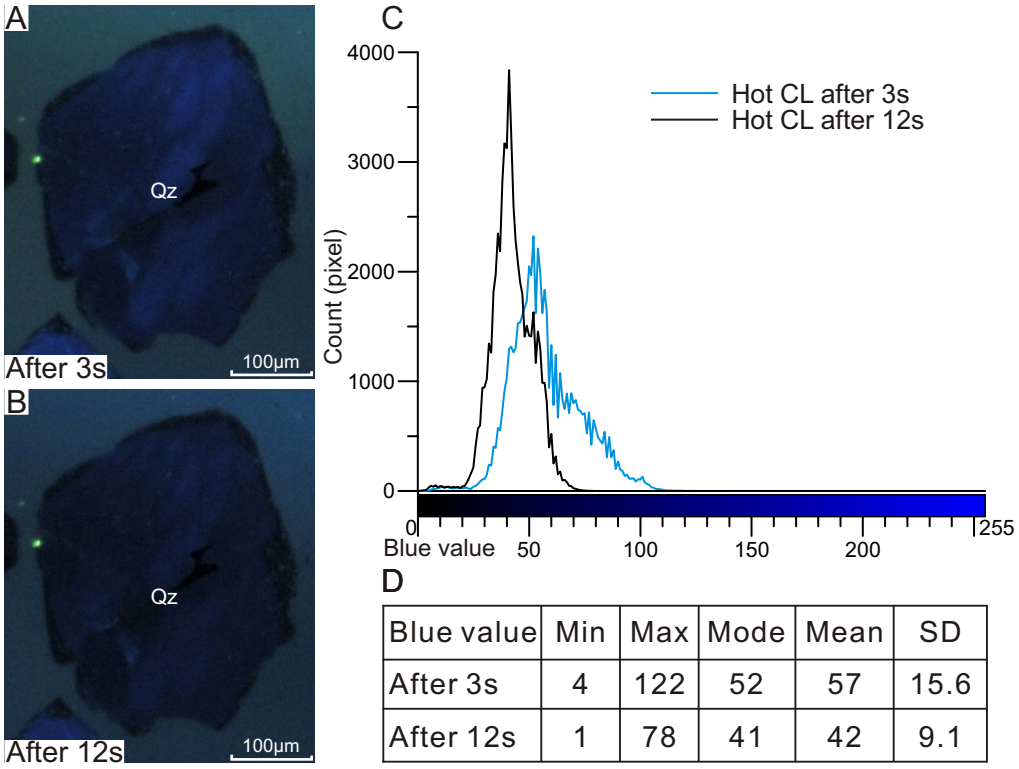

D

Blue value	Min	Max	Mode	Mean	SD
After 3s	4	122	52	57	15.6
After 12s	1	78	41	42	9.1

Figure 4B-23: Grain 23. The grain shows moderate colour shift.

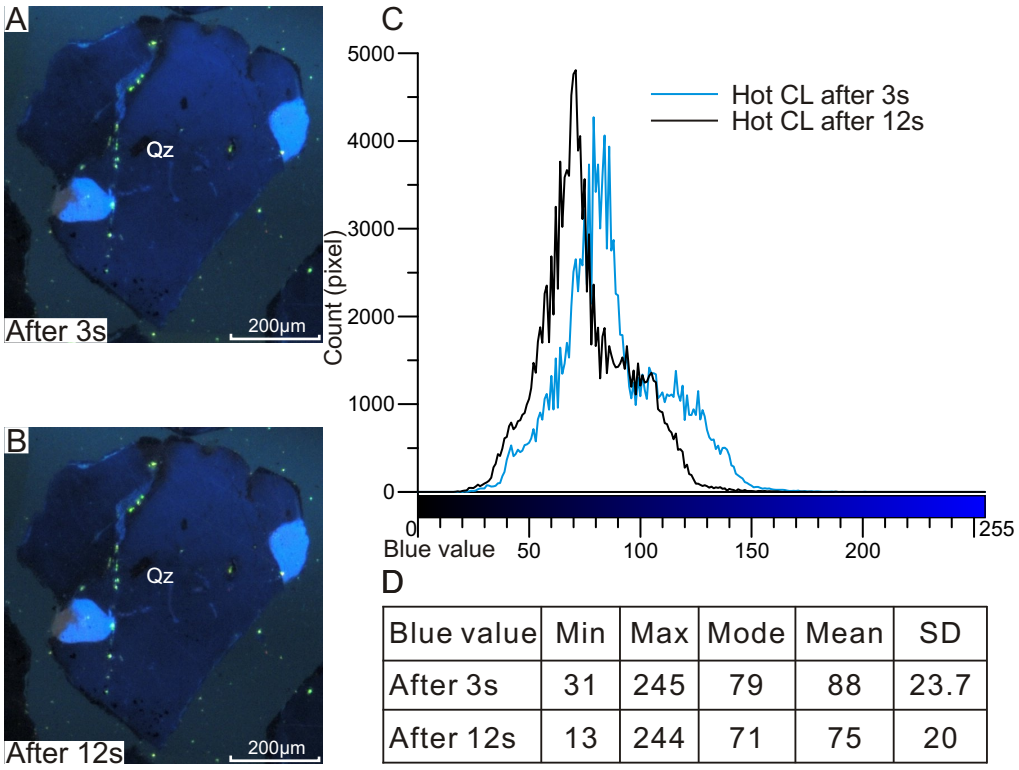

D

Blue value	Min	Max	Mode	Mean	SD
After 3s	31	245	79	88	23.7
After 12s	13	244	71	75	20

Figure 4B-24: Grain 24. The grain shows slight colour shift.

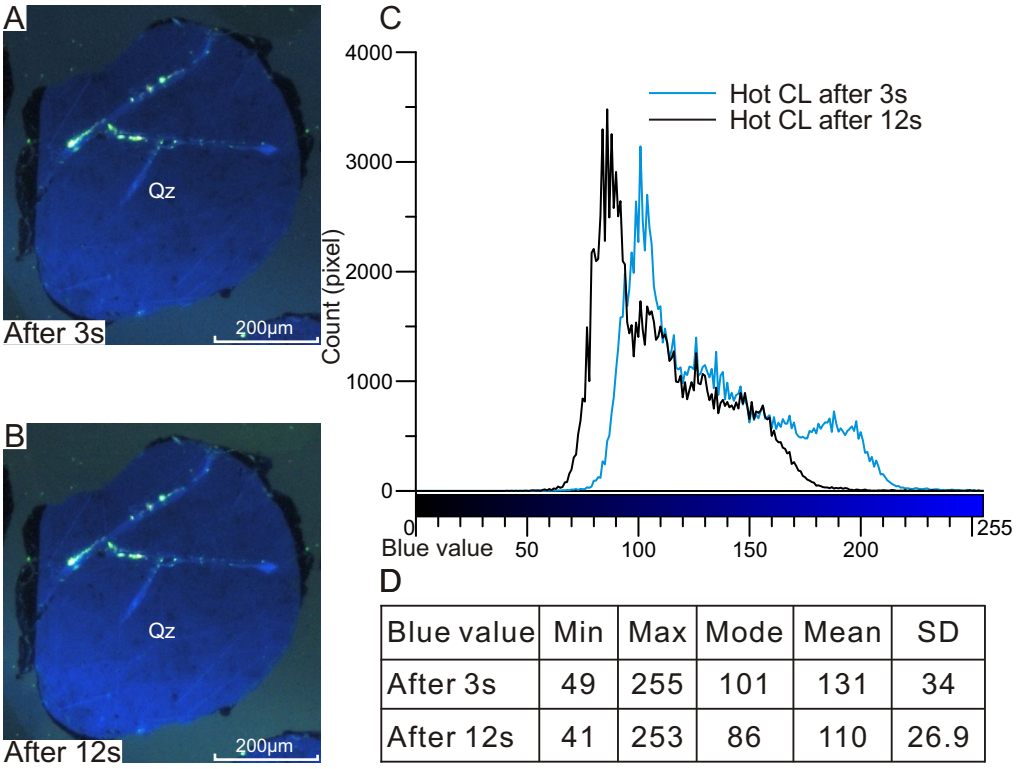

D

Blue value	Min	Max	Mode	Mean	SD
After 3s	49	255	101	131	34
After 12s	41	253	86	110	26.9

Figure 4B-25: Grain 25. The grain shows moderate colour shift.

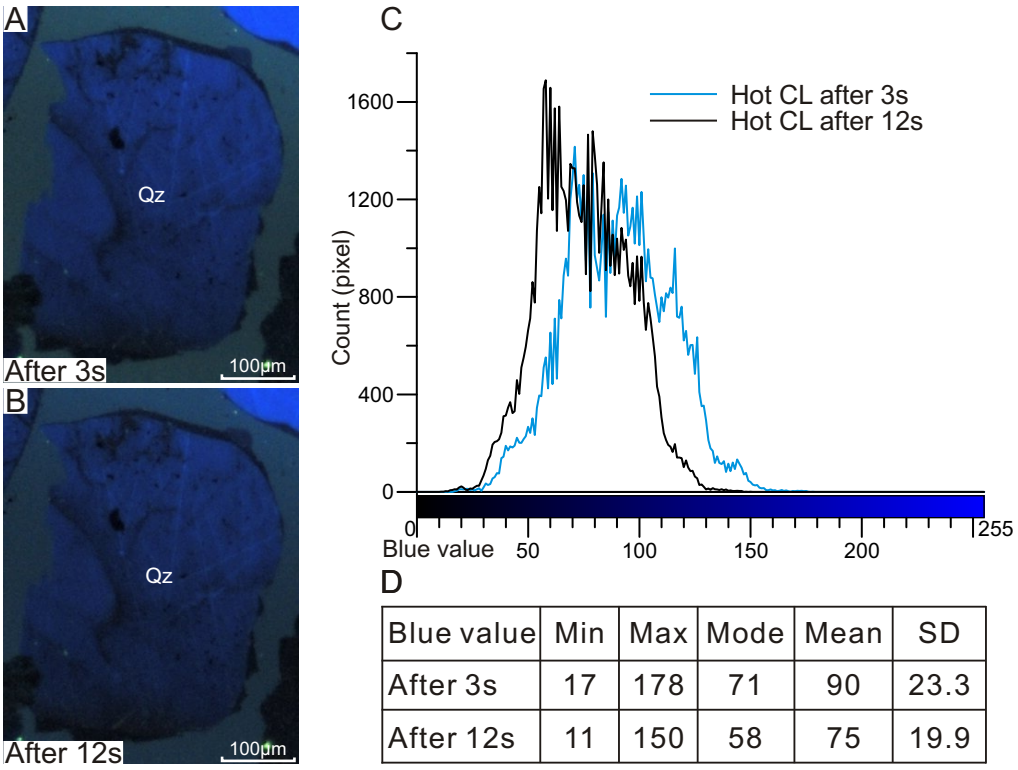

D

Blue value	Min	Max	Mode	Mean	SD
After 3s	17	178	71	90	23.3
After 12s	11	150	58	75	19.9

Figure 4B-26: Grain 26. The grain shows moderate colour shift.

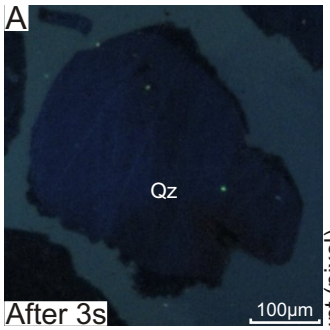

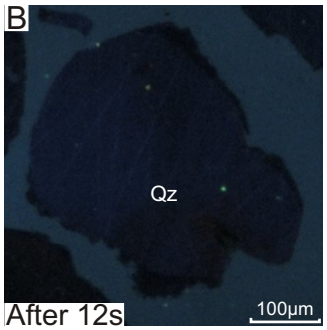

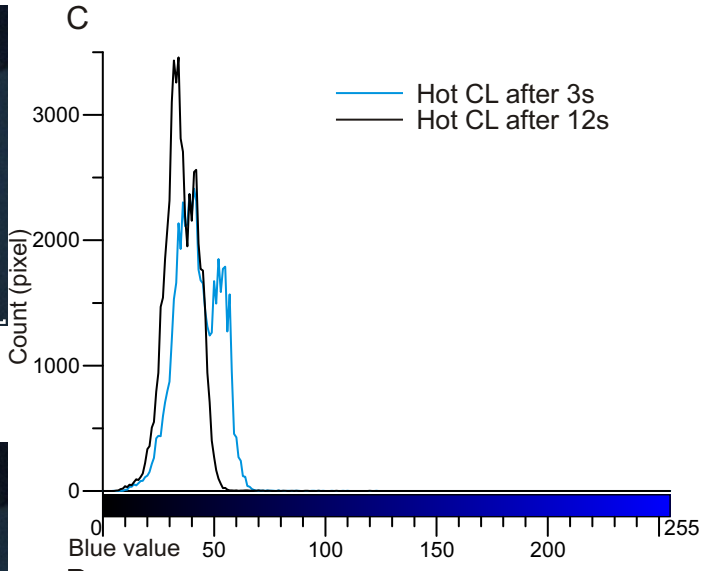

Figure 4B-27: Grain 27. The grain shows slight colour shift.

D

Blue value	Min	Max	Mode	Mean	SD
After 3s	5	123	41	42	9.7
After 12s	6	120	34	35	7.2

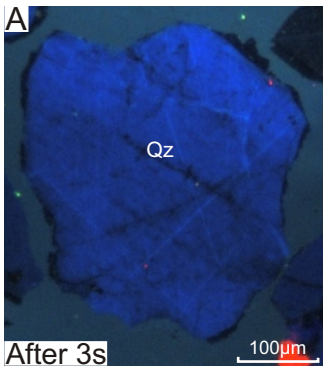

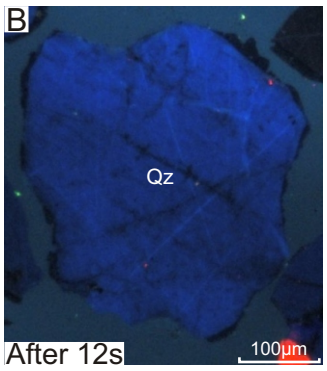

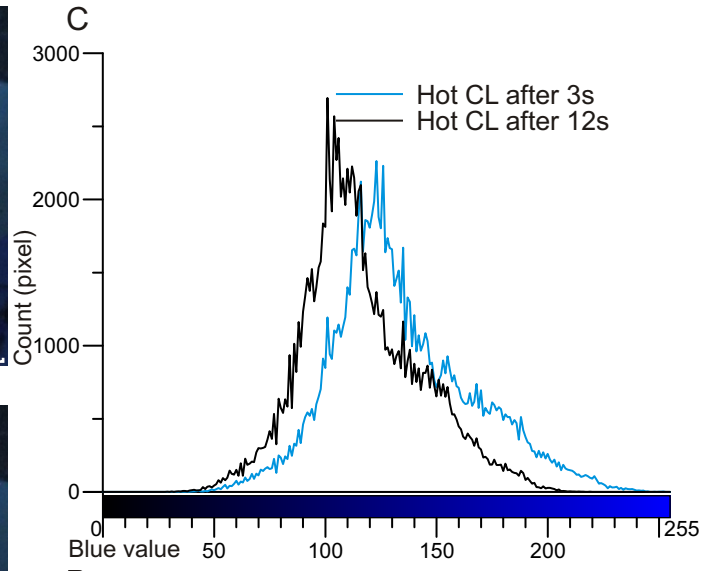

Figure 4B-28: Grain 28. The grain shows moderate colour shift.

D

Blue value	Min	Max	Mode	Mean	SD
After 3s	35	252	123	134	31.6
After 12s	29	219	101	116	26.6

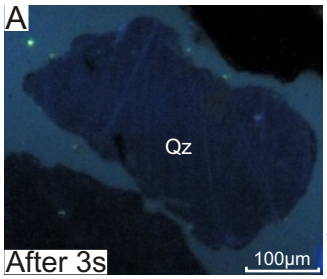

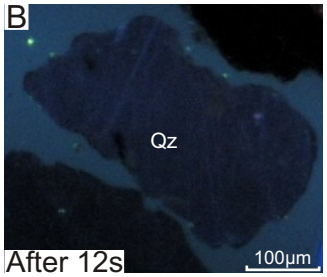

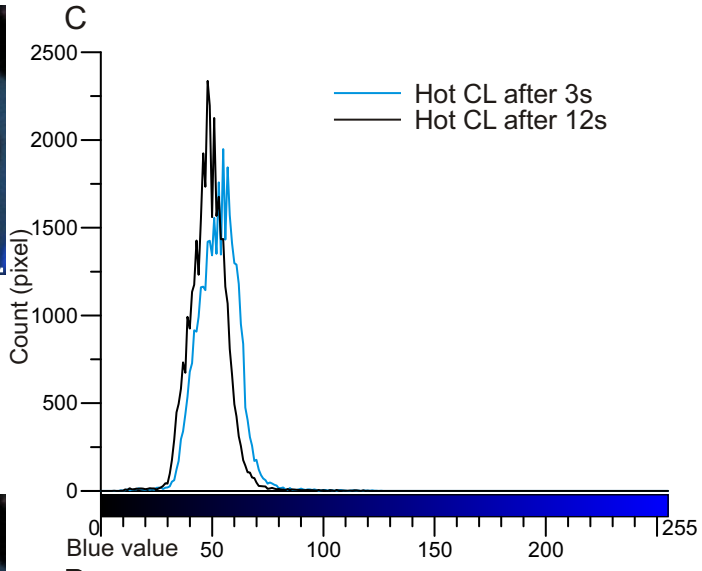

Figure 4B-29: Grain 29. The grain shows slight colour shift.

D

Blue value	Min	Max	Mode	Mean	SD
After 3s	9	126	55	53	9.2
After 12s	6	120	48	48	8.4

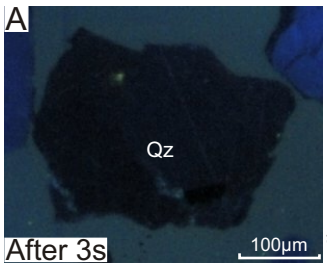

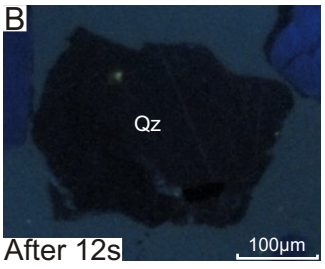

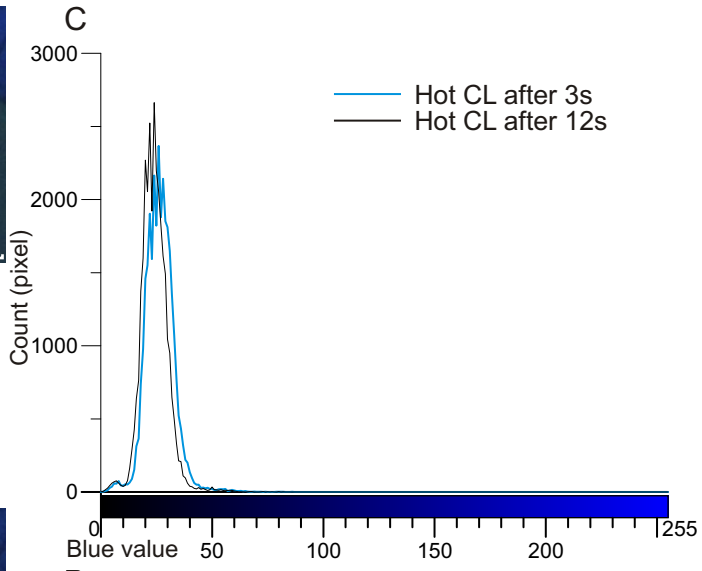

Figure 4B-30: Grain 30. The grain shows no colour shift.

D

Blue value	Min	Max	Mode	Mean	SD
After 3s	1	86	26	26	6.5
After 12s	0	82	24	24	6.1

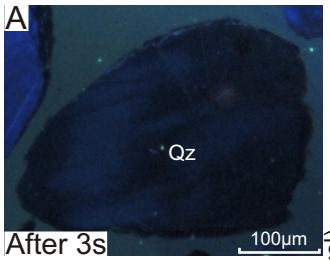

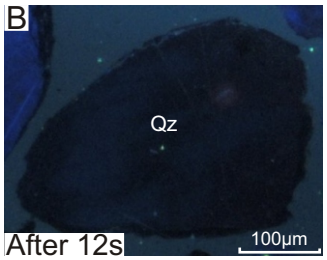

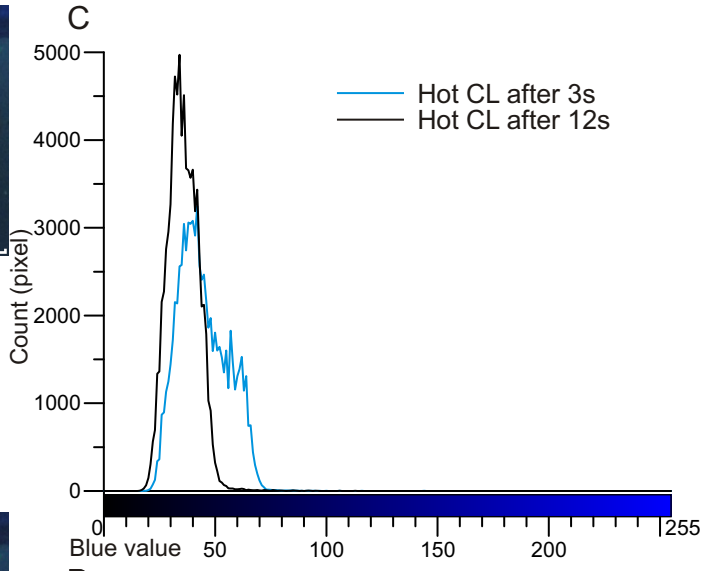

Figure 4B-31: Grain 31. The grain shows slight colour shift.

D

Blue value	Min	Max	Mode	Mean	SD
After 3s	17	149	42	44	10.9
After 12s	16	146	34	36	6.9

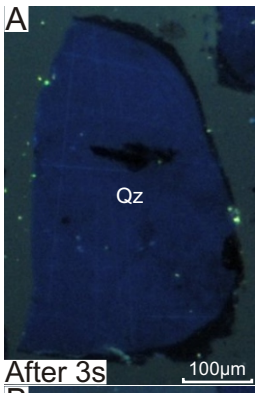

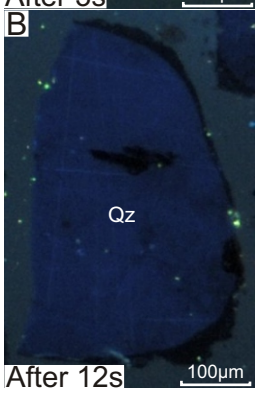

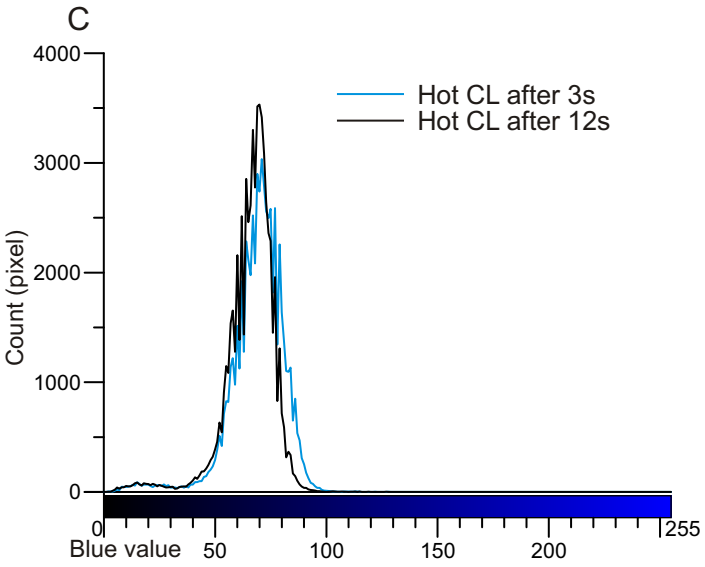

Figure 4B-32: Grain 32. Probably the first image was taken too early. Therefore, this grain is not useful to analyse the colour shift.

D

Blue value	Min	Max	Mode	Mean	SD
After 3s	2	128	71	69	12.4
After 12s	2	127	70	66	11.4

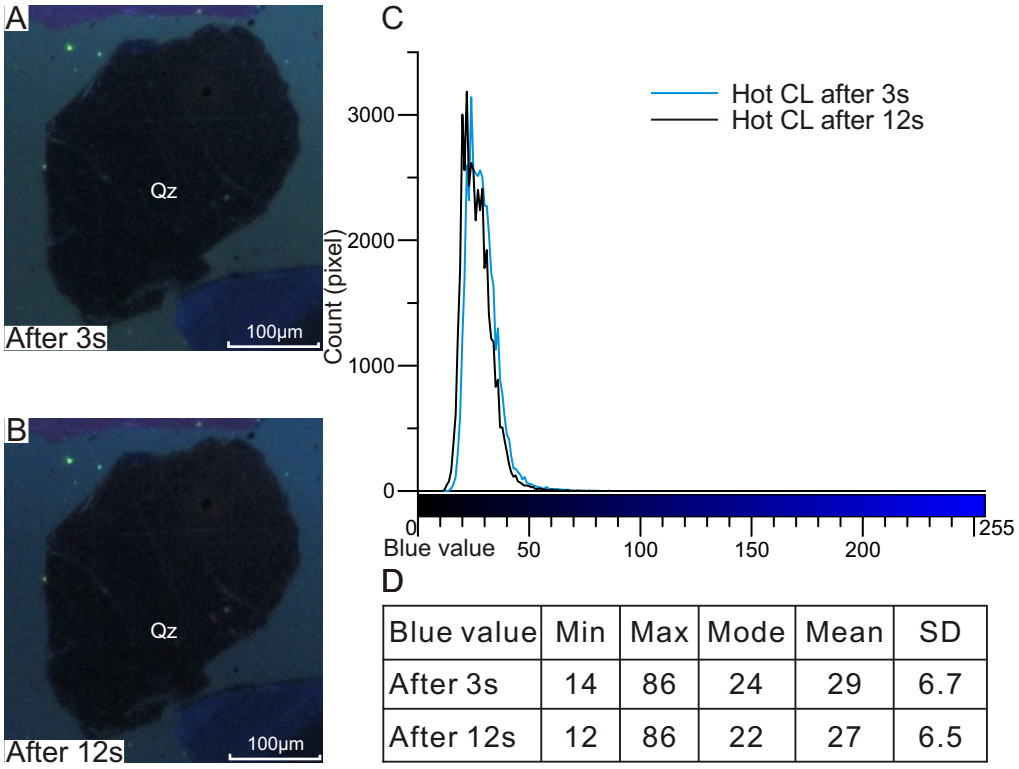

Figure 4B-33: Grain 33. The grain shows no colour shift.

D

Blue value	Min	Max	Mode	Mean	SD
After 3s	14	86	24	29	6.7
After 12s	12	86	22	27	6.5

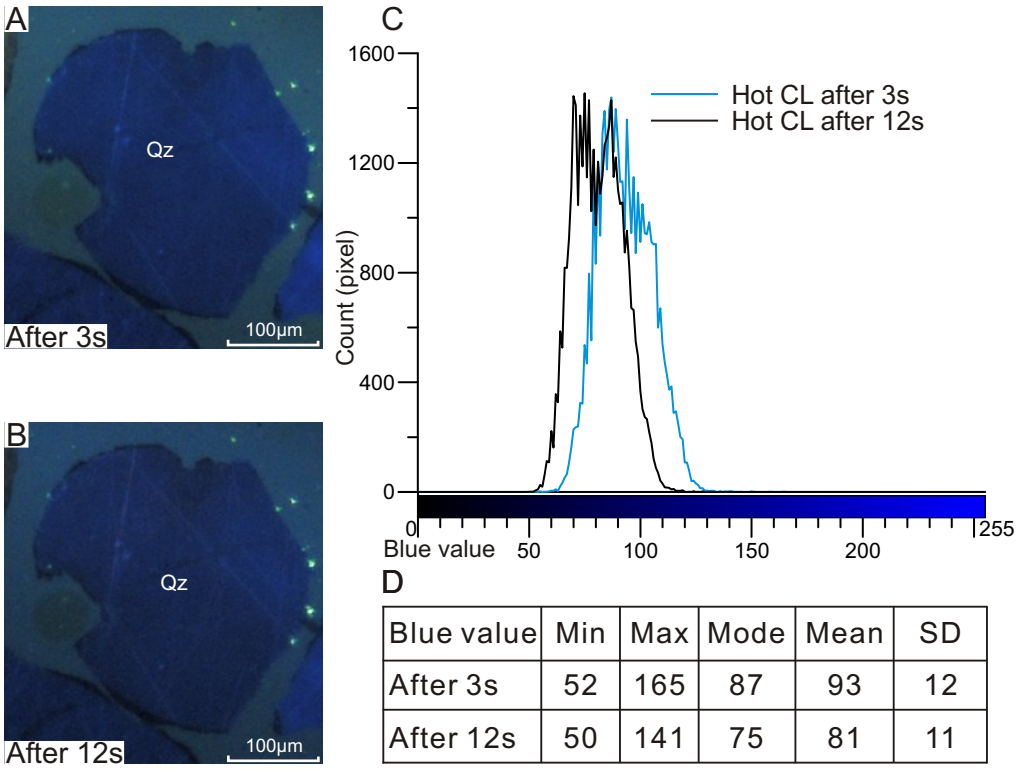

Figure 4B-34: Grain 34. The grain shows slight colour shift.

D

Blue value	Min	Max	Mode	Mean	SD
After 3s	52	165	87	93	12
After 12s	50	141	75	81	11



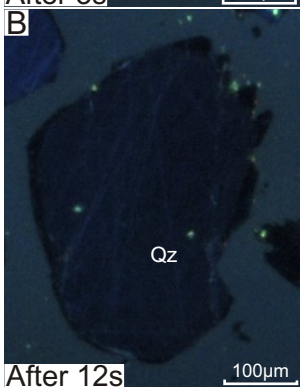

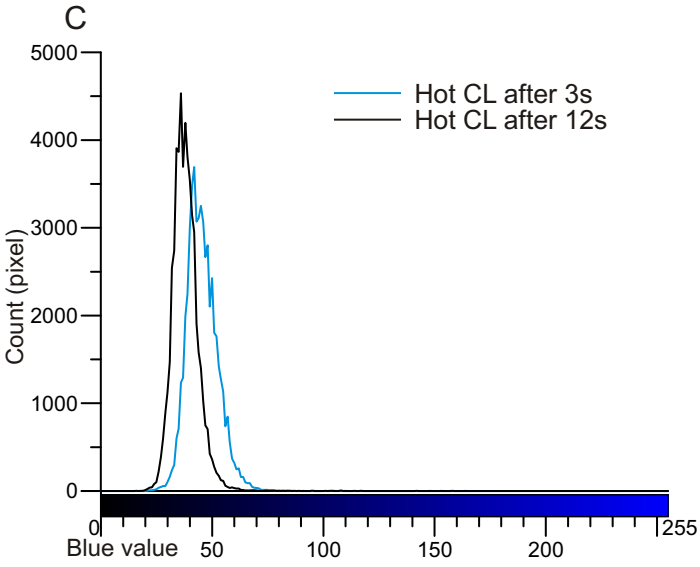

D

Blue value	Min	Max	Mode	Mean	SD
After 3s	19	173	42	46	7.2
After 12s	14	169	36	38	6.1

Figure 4B-35: Grain 35. The grain shows slight colour shift.

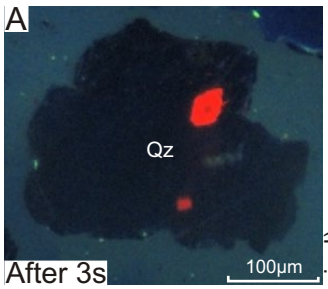

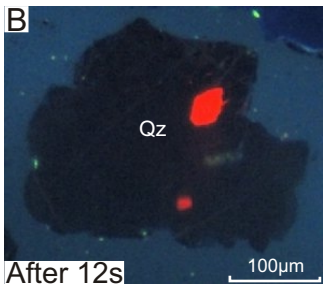

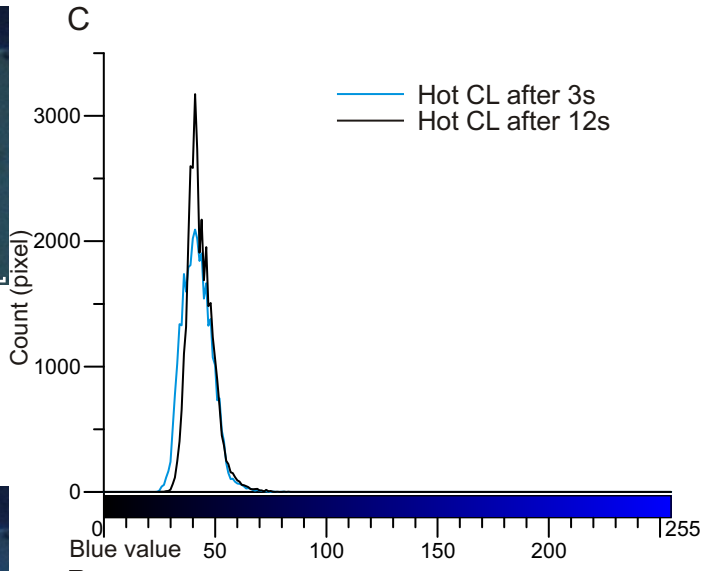

D

Blue value	Min	Max	Mode	Mean	SD
After 3s	24	81	41	42	6.6
After 12s	25	83	41	43	5.8

Figure 4B-36: Grain 36. Probably the first image was taken too early. Therefore, this grain is not useful to analyse the colour shift.

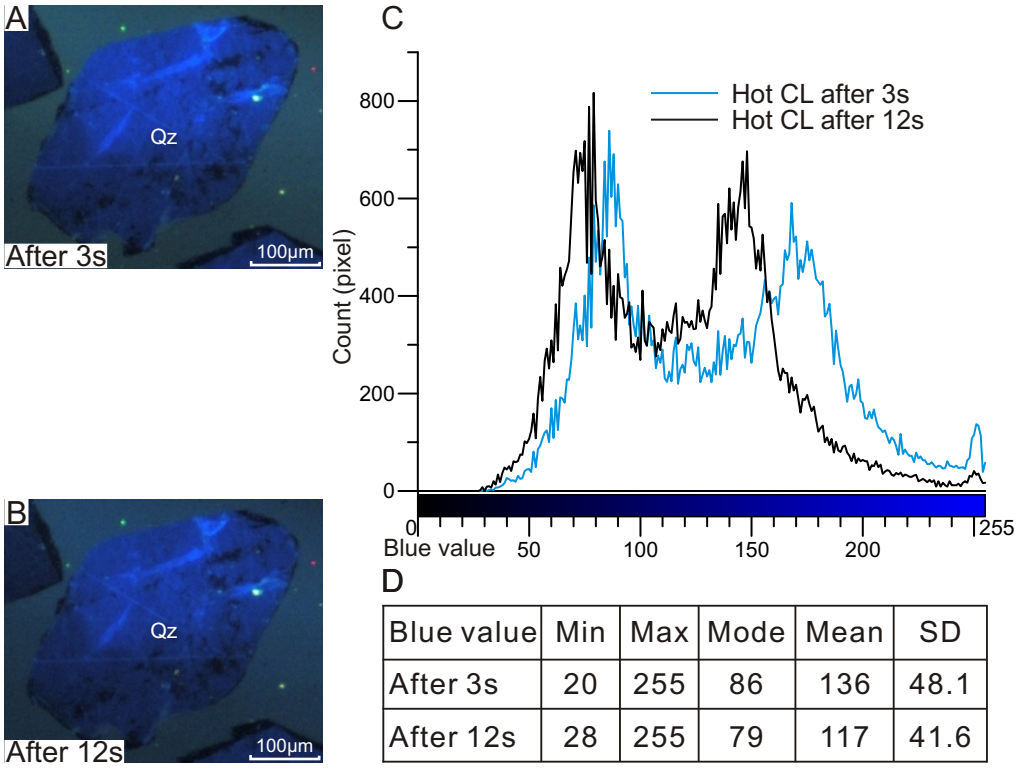

Figure 4B-37: Grain 37. The grain shows moderate colour shift.

D

Blue value	Min	Max	Mode	Mean	SD
After 3s	20	255	86	136	48.1
After 12s	28	255	79	117	41.6

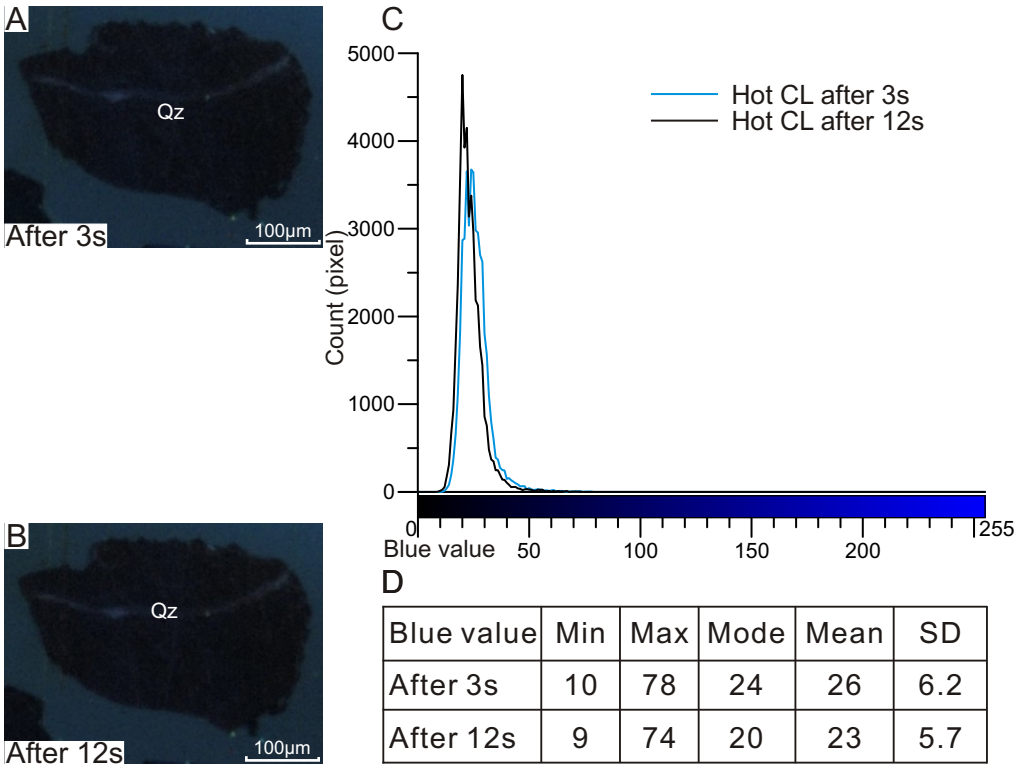

Figure 4B-38: Grain 38. The grain shows no colour shift.

D

Blue value	Min	Max	Mode	Mean	SD
After 3s	10	78	24	26	6.2
After 12s	9	74	20	23	5.7

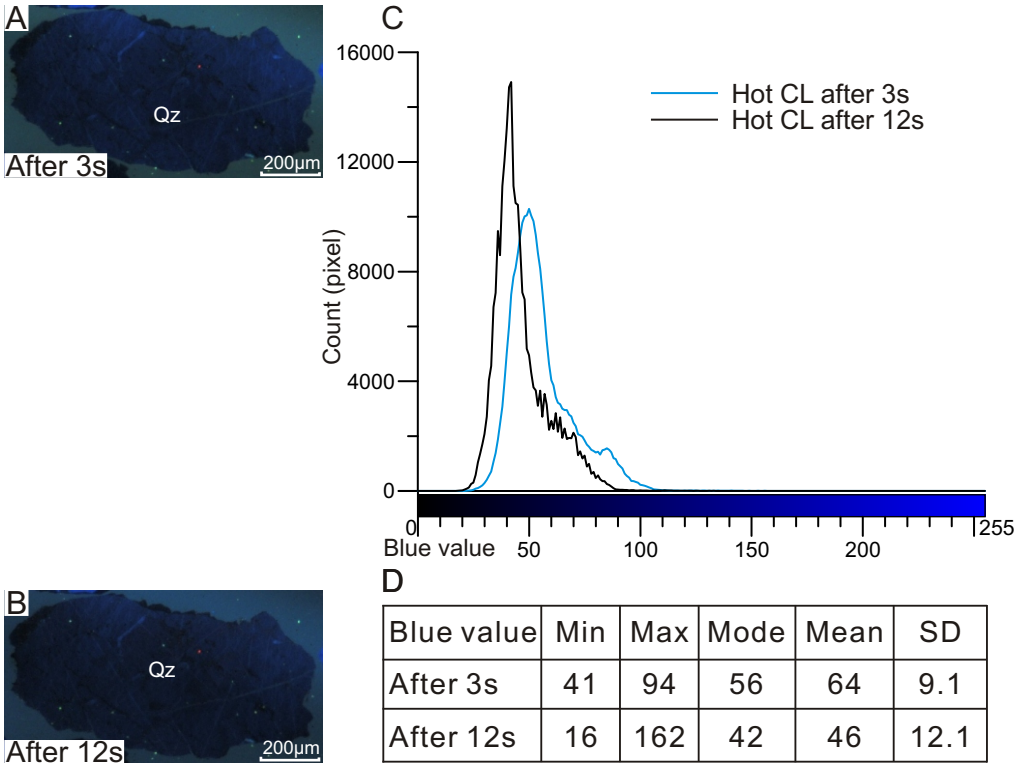

Figure 4B-39: Grain 39. The grain shows moderate colour shift.

D

Blue value	Min	Max	Mode	Mean	SD
After 3s	41	94	56	64	9.1
After 12s	16	162	42	46	12.1

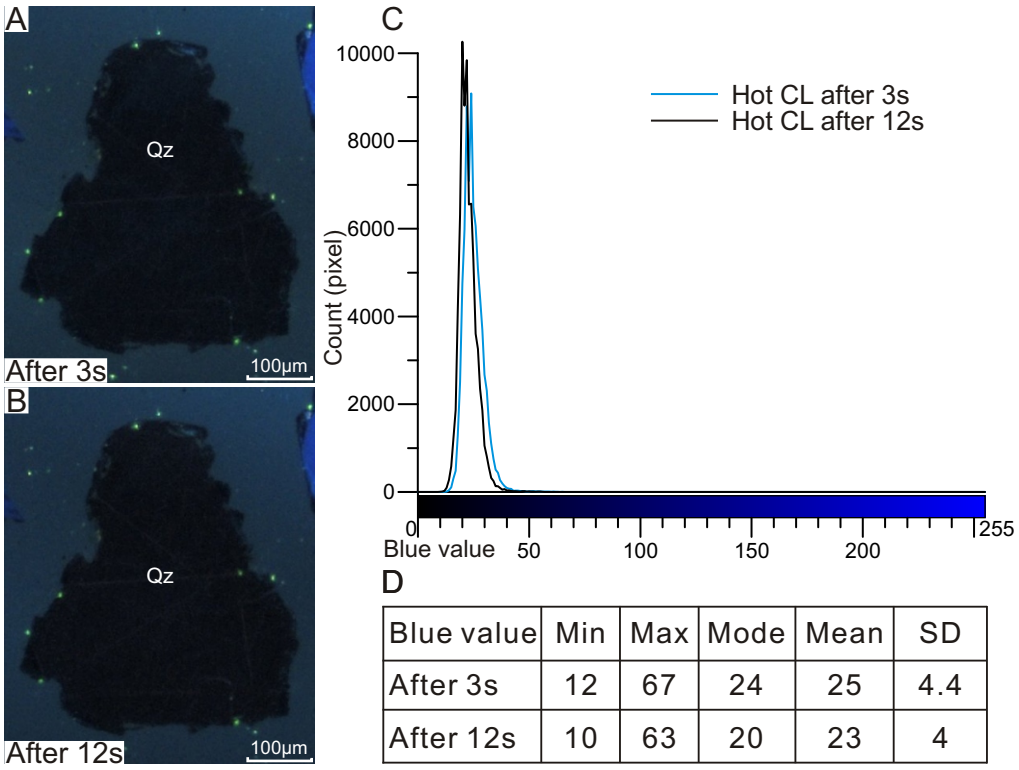

Figure 4B-40: Grain 40. The grain shows no colour shift.

D

Blue value	Min	Max	Mode	Mean	SD
After 3s	12	67	24	25	4.4
After 12s	10	63	20	23	4

Appendix 5A: Microphotos, SEM-BSE images, SEM-CL images, and EDS analyses of detrital quartz grains in sample 3150.

Notes:

1. **Homogenous CL:** Nearly uniform CL intensity across the grain (Fig. 2A).

2. Fractures in quartz have been divided into two types: **healed fractures** (**HF**) and **open fractures** (**OF**).

   Healed fractures are fractures filled with secondary silica that appear as thin (commonly < 10 μm) black lines in SEM-CL images (Fig. 2B). They are usually not shown in back-scattered images (Boggs and Krinsley, 2006).

   Open fractures appear in cathodoluminescense images as CL-dark or CL-bright lines, and they are also visible in back-scattered images and microphotos. A few open fractures are **conchoidal fractures** (**CF**) (Boggs and Krinsley, 2006).

3. **Tectonic deformation lamellae**: Tectonic deformation lamellae (Fig. 2C) appear in SEM-CL image as numerous sets of thin, parallel, closely spaced, dark gray lines (Bernet and Basset, 2005). According to Hamers and Drury (2011), tectonic deformation lamellae can either appear as dark gray lines or bright lines in SEM-CL images, and can show slightly wavy features with varying thickness. They usually also appear in XPL image under petrographic microscope.

4. **Spiders (S):** They are made up of dark-Cl patches and streaks. Dark-CL patches mainly range from 10-100 μm. Streaks are random and irregular in the appearance of black broad (>10 μm) elongated form. The spiders are commonly associated with healed fractures, giving them the appearance in SEM-CL images of spiders sitting on a web (Fig. 2D). They cannot be seen in BSE images, since they are composed by secondary silica (Boggs and Krinsley, 2006).

5. **Bright mottling**: Some grains show irregular CL intensity across grains, creating a mottled pattern due the presence of patches (Boggs and Krinsley, 2006). Three types of bright mottling were seen.

   - **Random bright patches** (Fig. 2E1)
   - **Bright streaky patches fabric** (Fig. 2E2)
   - **Subtle mottling** (Fig. 2E3)

6. **Overgrowth:** Overgrowth appears in SEM-CL images as dark areas in the border of the quartz grains (Fig. 2F).

7. **Fluid inclusion trail** (**FI trail**): Trails formed by **fluid inclusions** (**FI**). They are usually associated with secondary porosity and commonly located along fractures and at boundaries between detritral quartz grain and the overgrowth. They are well observed in microphotos under ppl. The fluid inclusion trails can be separated in two kinds: **detrital fluid inclusion trails (**fluid inclusions that are original from the detrital quartz, they do not cut the quartz overgrowth) and **diagenetic fluid inclusion trails** (fluid inclusions originated from the diagenesis, and they thus cut the quartz overgrowth).

8. **Melt inclusion** (**MI**): Large fluid inclusions (>10 μm) in which crystallized minerals are visible.

9. **Secondary porosity** (**SP**): Porosities usually caused by dissolution and/or fractures. They are easily observed in microphotos under PPL and BSE images.

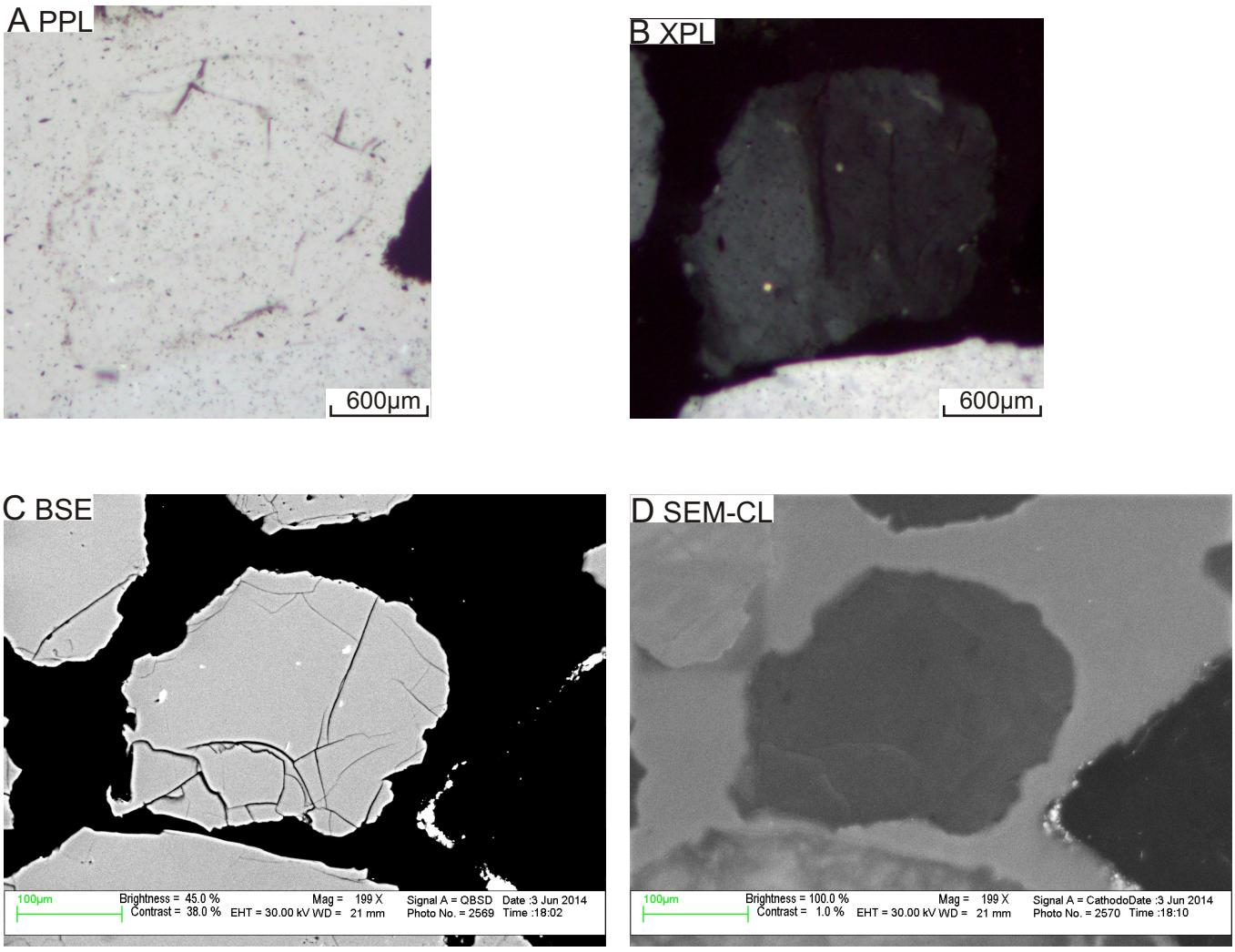

Figure 5A-1: Microphotos under ppl (A) and xpl (B), SEM-BSE image C, and SEM-CL image (D) of quartz grain 1 in sample 3150. The grain is anhedral and sub-rounded monocrystalline with strong undulose extinction. Fluid inclusions are rare. The grain is microfractured with a set of irregular fractures (Fig. C). Healed fractures are rare; the grain shows homogeneous CL in SEM-CL image.

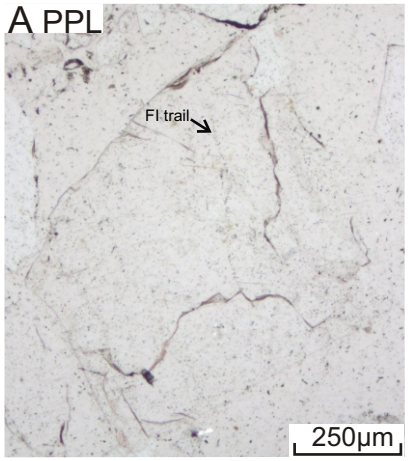

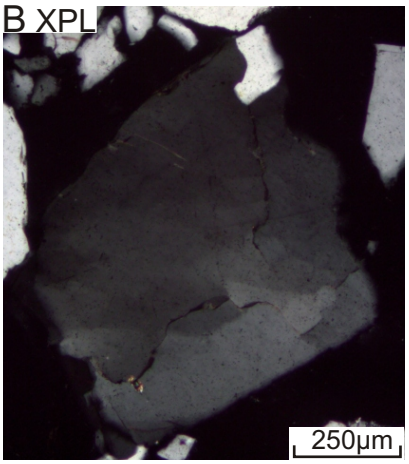

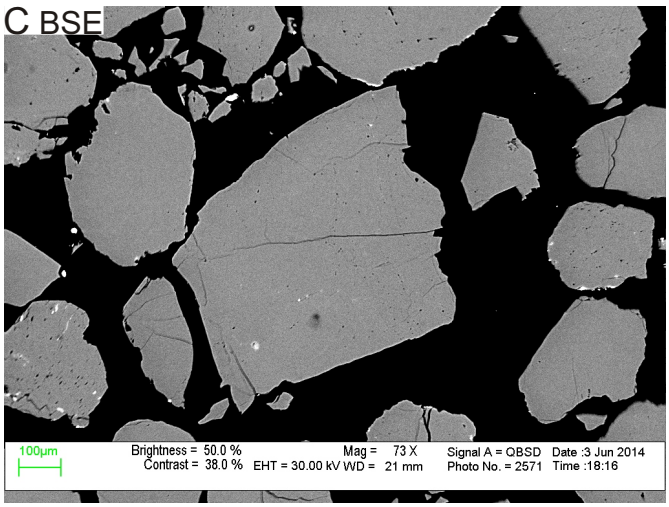

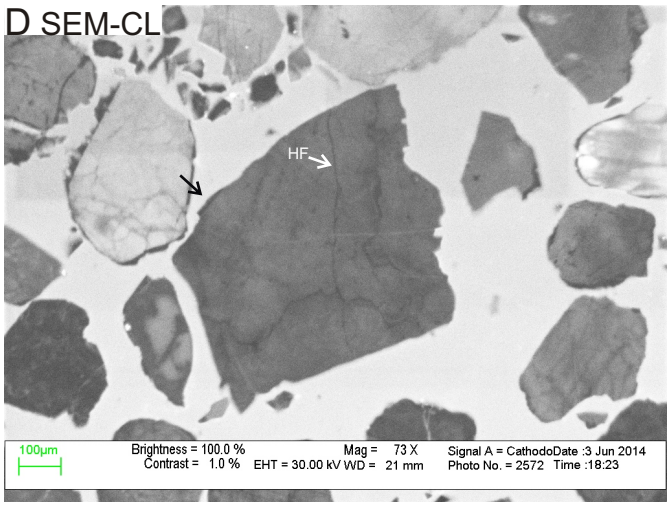

Figure 5A-2: Microphotos under ppl (A) and xpl (B), SEM-BSE image C, and SEM-CL image (D) of quartz grain 2 in sample 3150. The grain is anhedral and sub-angular polycrystalline (more than 4 sub-grains with sutured sub-grain boundaries) with strong undulose extinction. Fluid inclusions are present, and they form trails (FI trail) along healed fractures (Fig. A). The grain is microfractured with a set of irregular fractures (Fig. C and D). Some healed fractures (HF) can be seen in Fig. D. The dark area indicated by arrow in Fig. D is overgrowth.

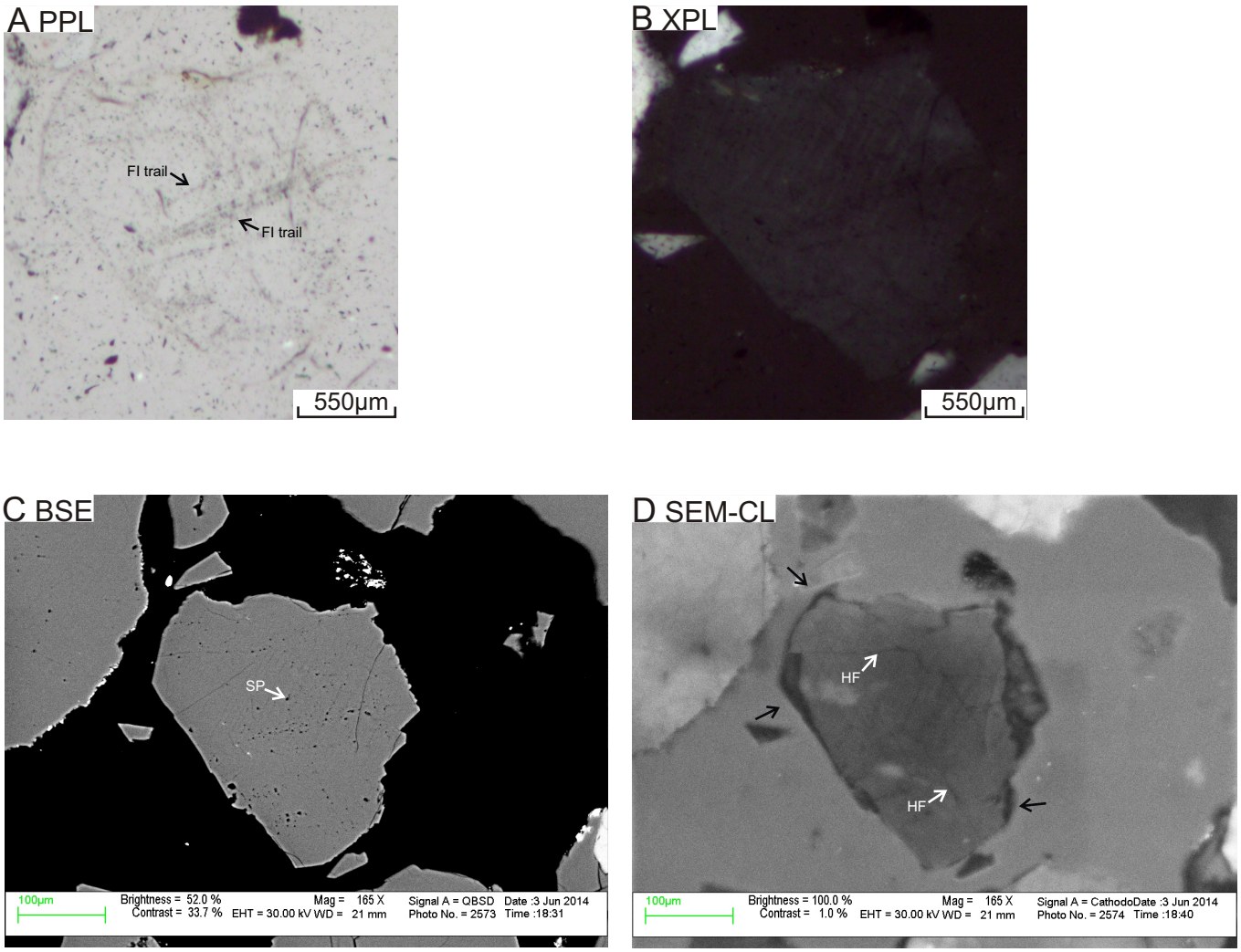

Figure 5A-3: Microphotos under ppl (A) and xpl (B), SEM-BSE image C, and SEM-CL image (D) of quartz grain 3 in sample 3150. The grain is anhedral and sub-angular monocrystalline with deformation lamellae and strong undulose extinction. Fluid inclusions are common; they are usually associated with secondary porosity (SP) and form trails along healed fractures (Fig. A and C). The grain is microfractured with a set of irregular fractures (Fig. C and D). Some healed fractures (HF) can be seen in Fig. D. The dark areas indicated by arrows in Fig. D are overgrowth.

A PPL

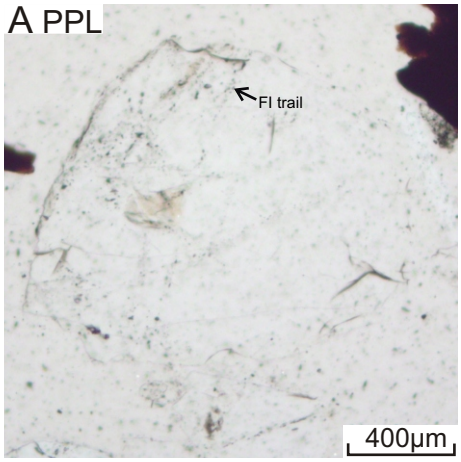

B XPL

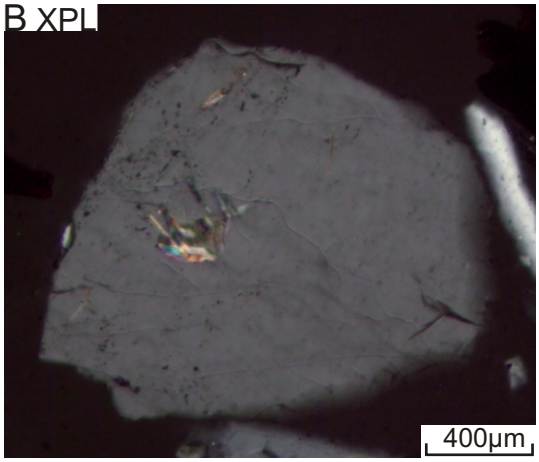

C BSE

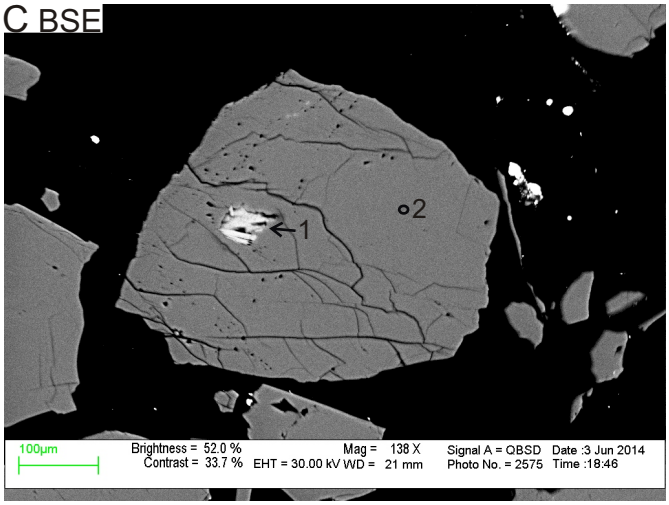

D SEM-CL

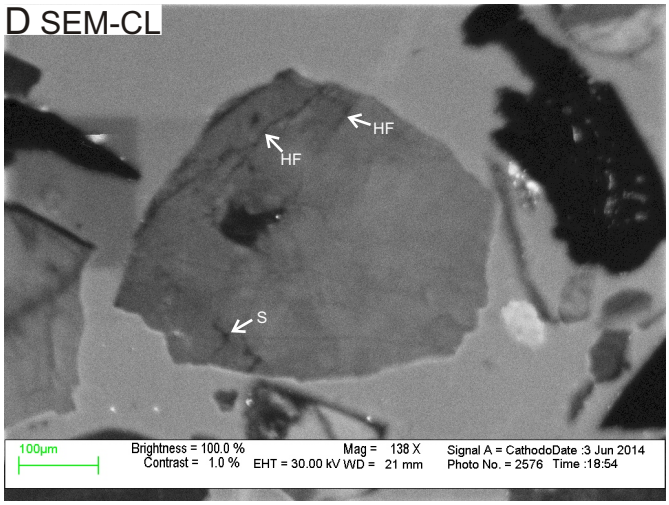

E EDS analyses

Pos#	Min. ID	SiO2	Al2O3	FeO	Na2O	K2O	Total	Actual total
1	Ms	47.57	34.97	1.48	0.54	10.44	95	53
2	Qz	99.99					100	69

Figure 5A-4: Microphotos under ppl (A) and xpl (B), SEM-BSE image (C), SEM-CL image (D), and EDS analyses table (E) of quartz grain 4 in sample 3150. The grain is subhedral and sub-rounded monocrystalline with non-undulose extinction. Fluid inclusions are common; they are usually associated with secondary porosity (SP) and form trails along healed fractures (Fig. A and C). The grain contains muscovite inclusion and is microfractured with a set of irregular fractures (Fig. C and D). Some healed fractures (HF) and spiders (S) can be seen in Fig. D.

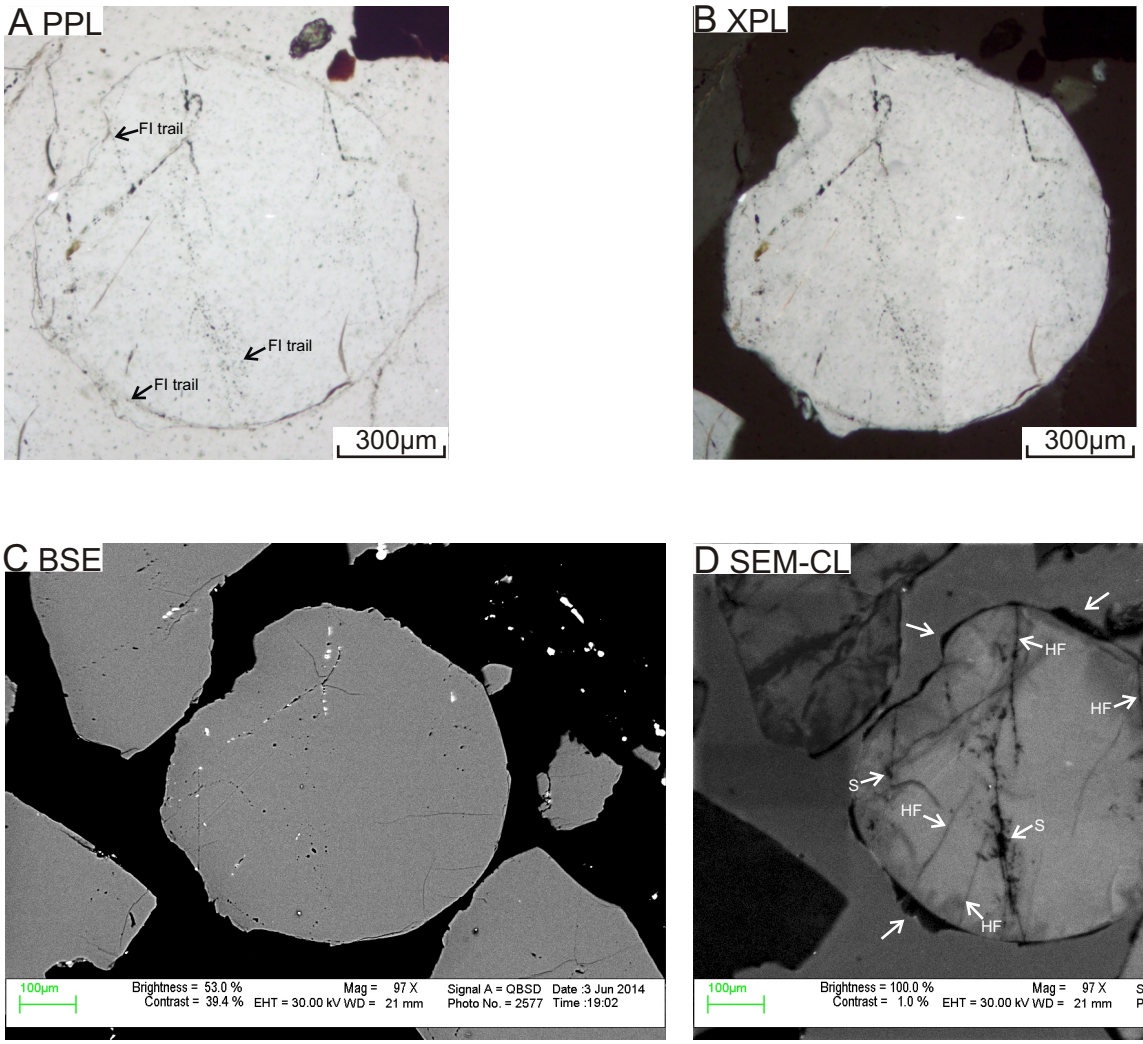

Figure 5A-5: Microphotos under ppl (A) and xpl (B), SEM-BSE image C, and SEM-CL image (D) of quartz grain 5 in sample 3150. The grain is anhedral and well-rounded monocrystalline with weak undulose extinction. Fluid inclusions are common; they are usually associated with secondary porosity and form trails along healed fractures and at the boundary between the detrital quartz and the overgrowth (Fig. A). The grain is microfractured with two distinct sets of sub-parallel fractures (Fig. C and D). Healed fractures (HF) and spiders (S) are common (Fig. D). The dark areas indicated by arrows in Fig. D are overgrowth; these areas appear corroded in Fig. C, suggesting secondary porosity.

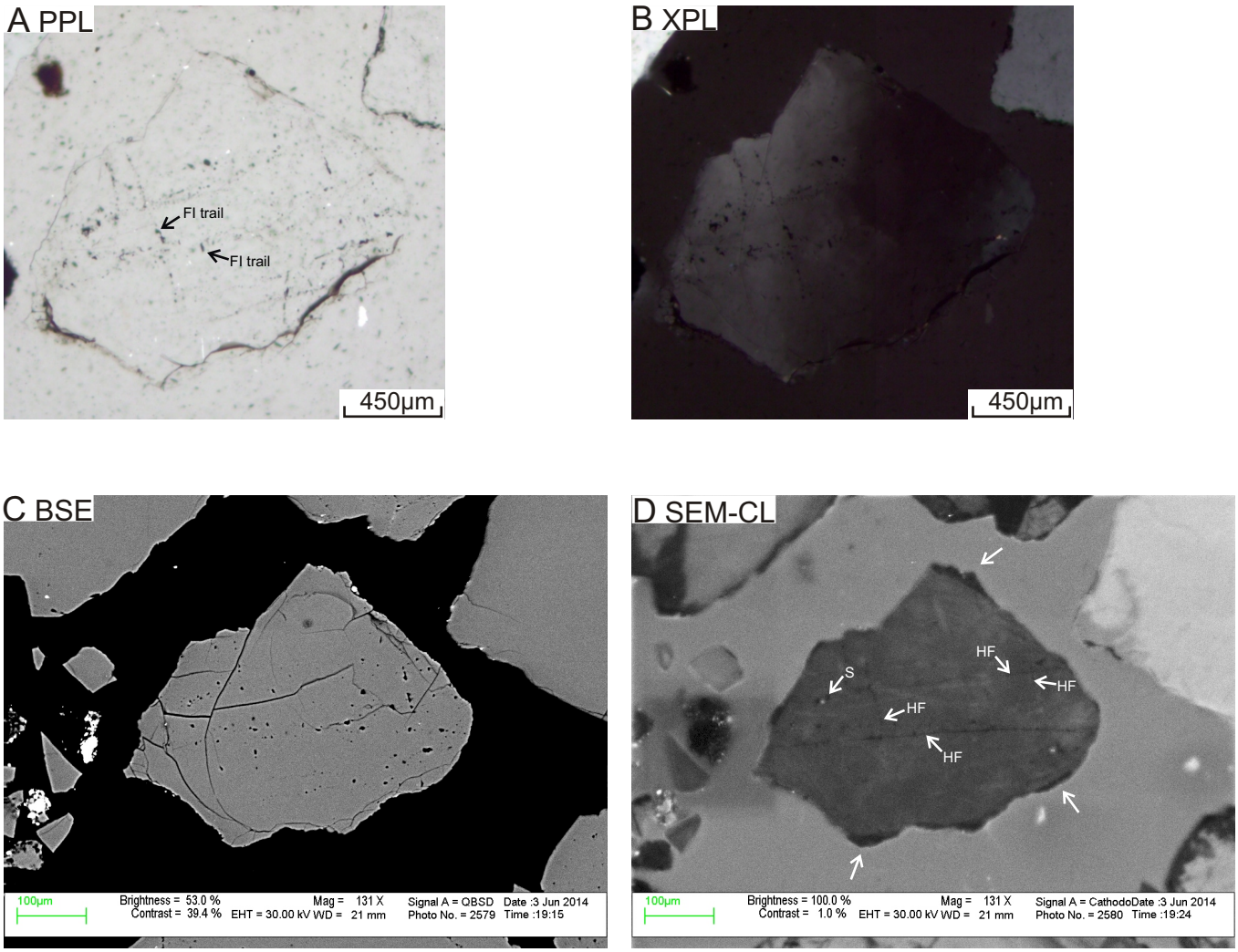

Figure 5A-6: Microphotos under ppl (A) and xpl (B), SEM-BSE image C, and SEM-CL image (D) of quartz grain 6 in sample 3150. The grain is anhedral and sub-angular monocrystalline with strong undulose extinction. Fluid inclusions are common; they are usually associated with secondary porosity and form trails along healed fractures (Fig. A). The grain is microfractured with two sets of parallel healed fractures crosscutting each other and a set of irregular curved open fractures (Fig. C and D). Some healed fractures (HF) and spiders (S) can be seen in Fig, D. The dark areas indicated by arrows in Fig. D are overgrowth.

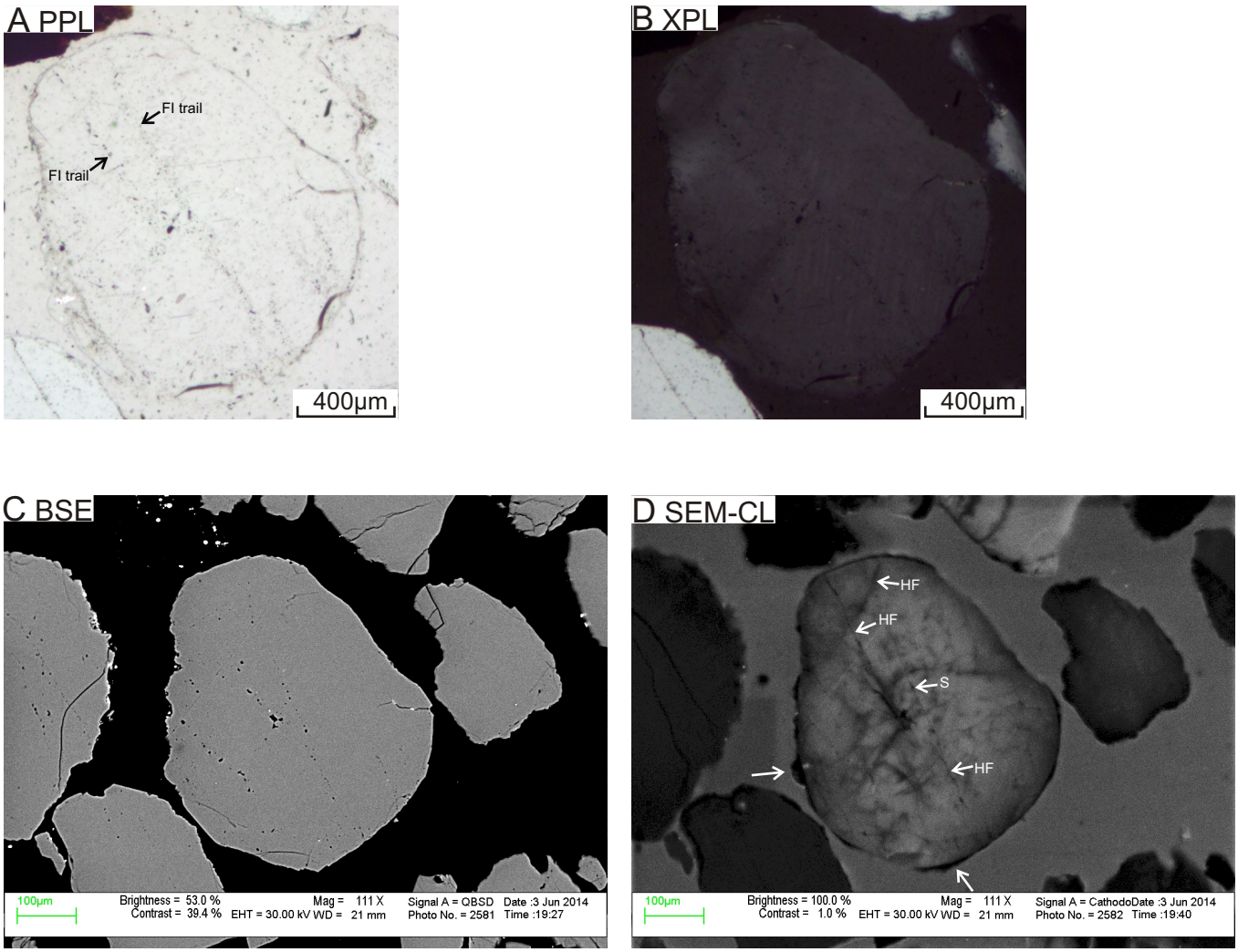

Figure 5A-7: Microphotos under ppl (A) and xpl (B), SEM-BSE image C, and SEM-CL image (D) of quartz grain 7 in sample 3150. The grain is anhedral and rounded monocrystalline with deformation lamellae and strong undulose extinction. Fluid inclusions are common; they are usually associated with secondary porosity and form trails along healed fractures (Fig. A). The grain is microfractured with a set of parallel fractures and a set of irregular fractures (Fig. C and D). Healed fractures (HF) and spiders (S) are common (Fig. D). The dark areas indicated by arrows in Fig. D are overgrowth.

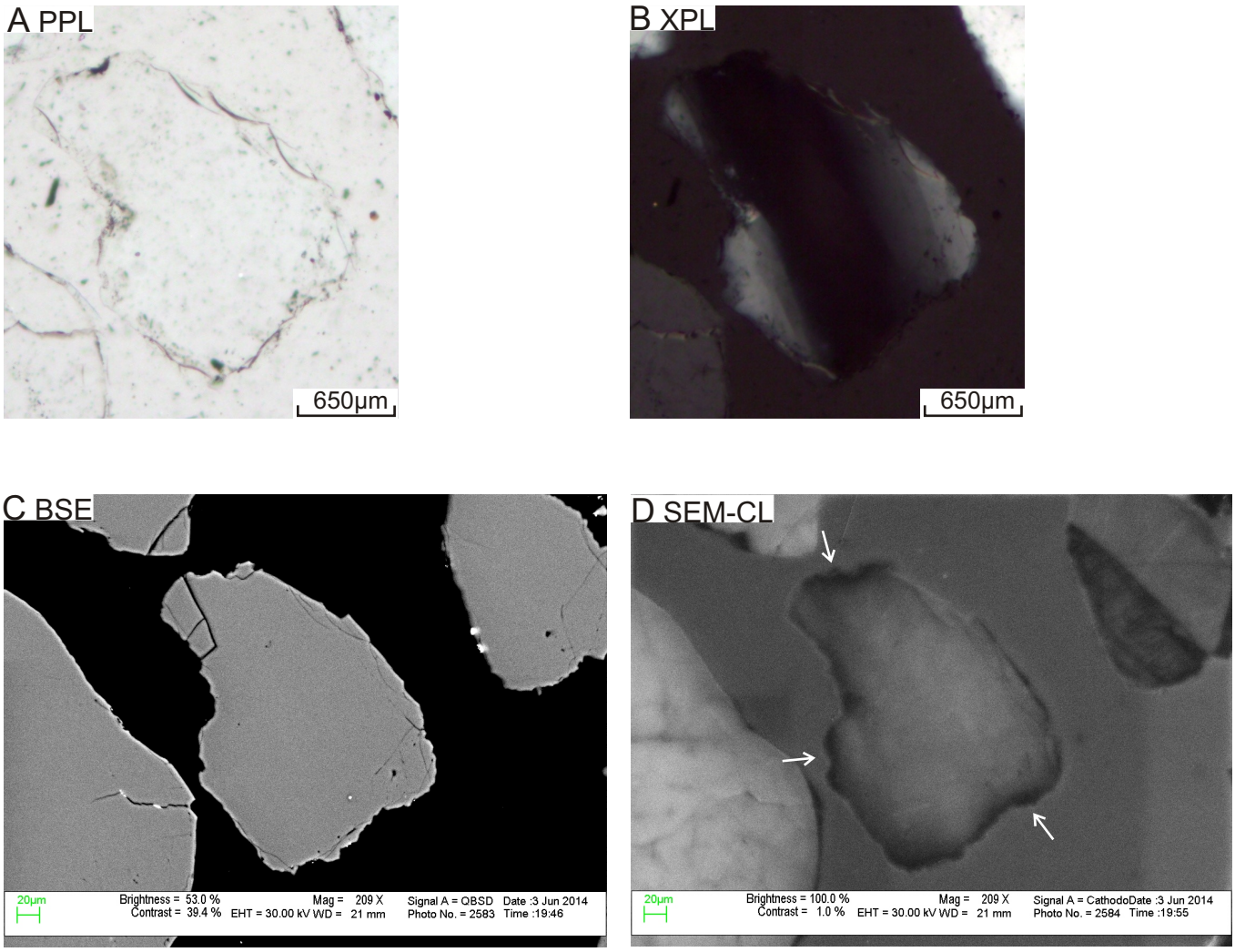

Figure 5A-8: Microphotos under ppl (A) and xpl (B), SEM-BSE image C, and SEM-CL image (D) of quartz grain 8 in sample 3150. The grain is anhedral and sub-rounded monocrystalline with deformation banding and strong undulose extinction. Fluid inclusions are rare. The grain is weakly microfractured with a set of irregular fractures (Fig. C). Healed fractures (HF) and dark-CL patches (P) are rare. The dark areas indicated by arrows in Fig. D are overgrowth; these areas appear corroded in Fig. C, suggesting secondary porosity. The grain shows homogeneous CL in SEM-CL image.

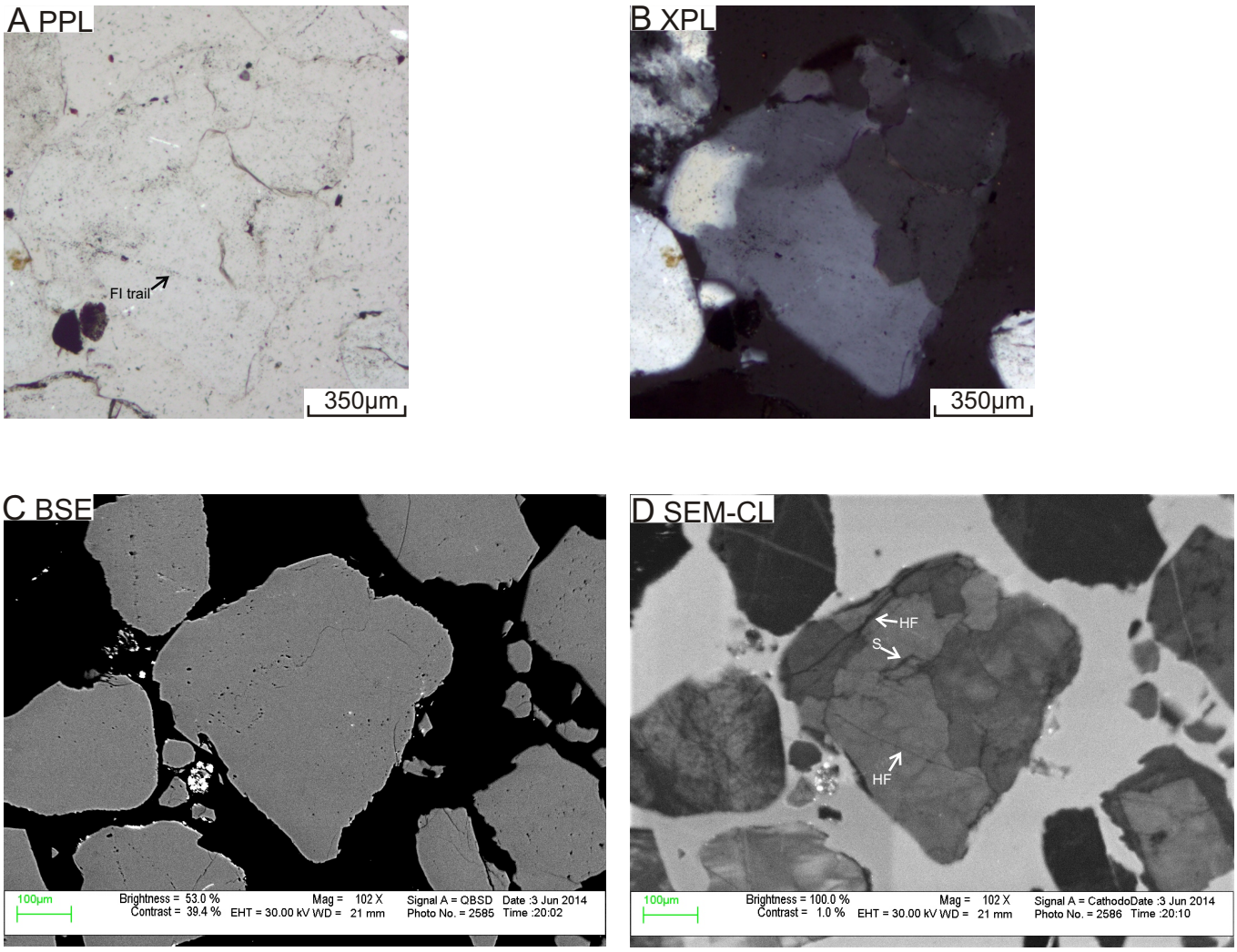

Figure 5A-9: Microphotos under ppl (A) and xpl (B), SEM-BSE image C, and SEM-CL image (D) of quartz grain 9 in sample 3150. The grain is anhedral and sub-rounded polycrystalline (more than 7 sub-grains, a few with sutured sub-grain boundaries) with strong undulose extinction. Fluid inclusions are common; they are usually associated with secondary porosity and form trails along healed fractures (Fig. A). The grain is microfractured with a set of irregular fractures (Fig. C and D). Some healed fractures (HF) and spiders (S) can be seen in Fig. D.

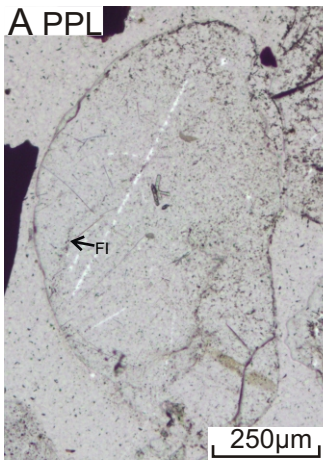

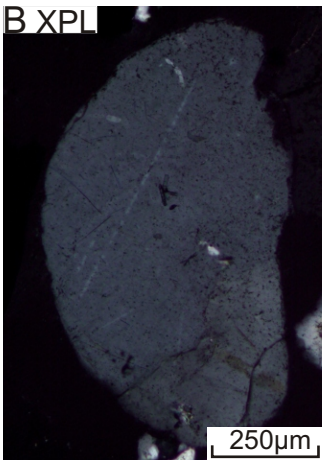

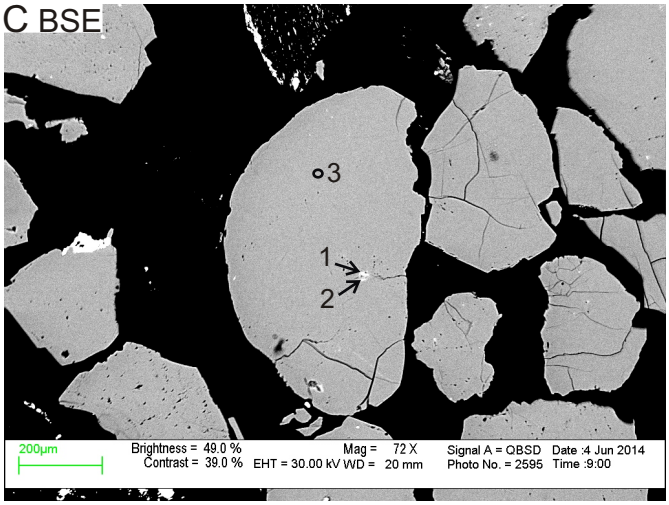

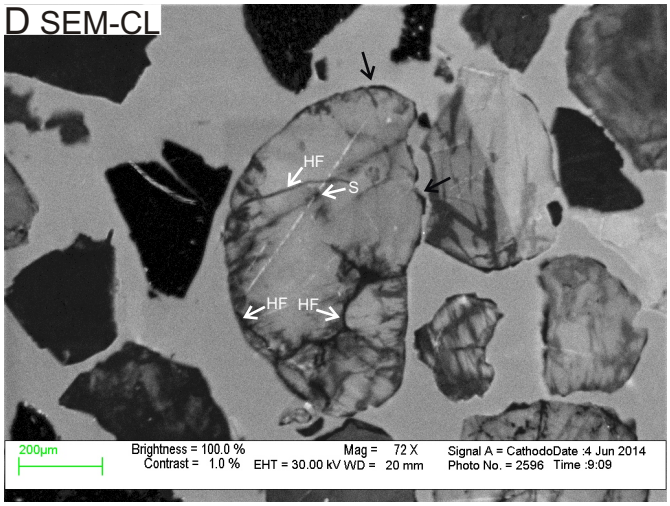

E EDS analyses

Pos#	Min. ID	SiO2	TiO2	Al2O3	FeO	MgO	Na2O	K2O	P2O5	Total	Actual total
1	Ms	51.43	0.21	32.36	0.98	0.48	0.44	9.10		95	103
2	Ms+Qz	78.53		15.72	0.57			4.64	0.53	100	104
3	Qz	99.99								100	114

Figure 5A-10: Microphotos under ppl (A) and xpl (B), SEM-BSE image (C), SEM-CL image (D), and EDS analyses table (E) of quartz grain 10 in sample 3150. The grain is anhedral and rounded polycrystalline (only 2 sub-grains) with weak undulose extinction. Fluid inclusions are common; (Fig. A). The grain contains muscovite inclusions and is microfractured with a set of irregular fractures (Fig. C and D). Healed fractures (HF) and spiders (S) are common (Fig. D). The dark areas indicated by arrows in Fig. D are overgrowth.

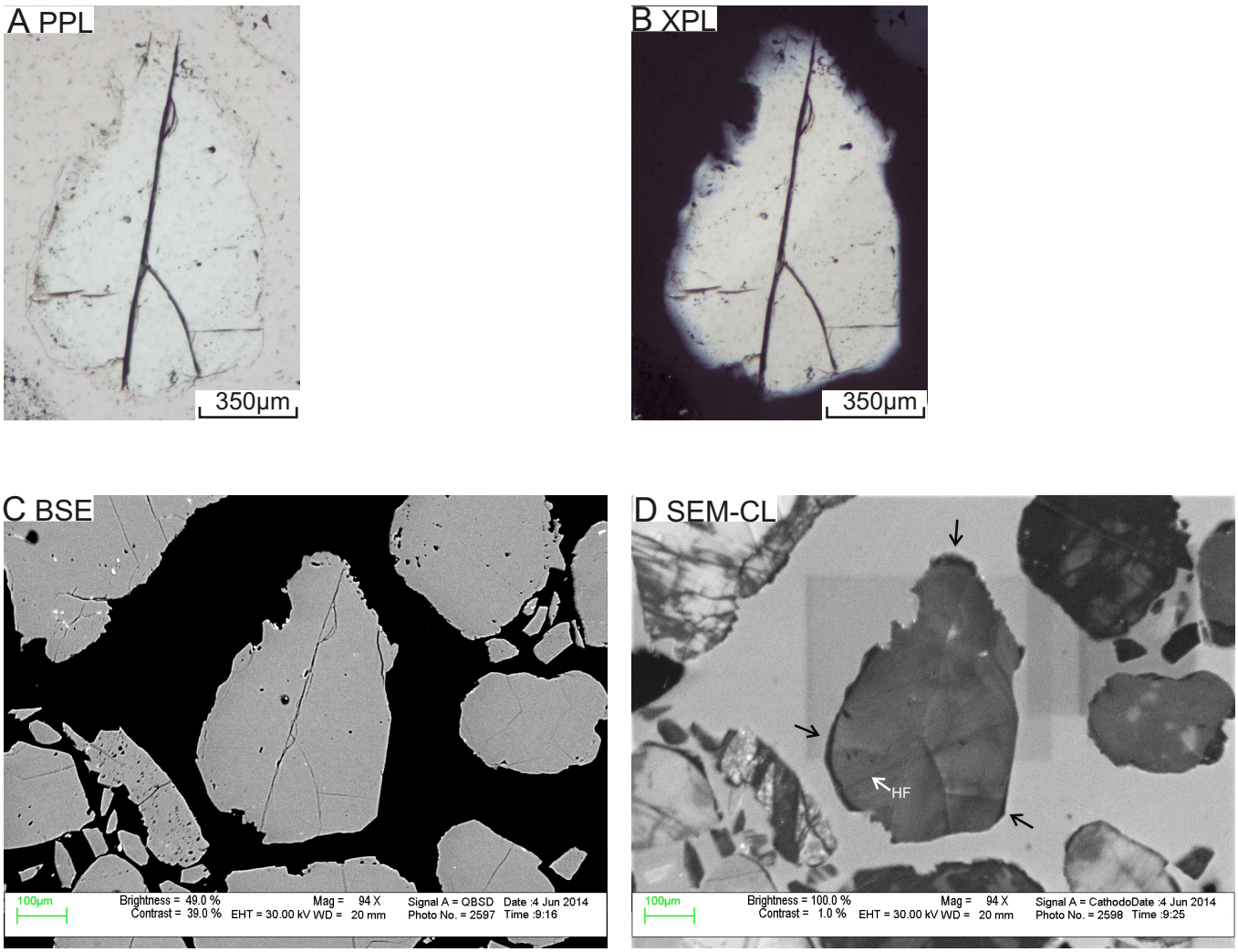

Figure 5A-11: Microphotos under ppl (A) and xpl (B), SEM-BSE image C, and SEM-CL image (D) of quartz grain 11 in sample 3150. The grain is anhedral and sub-angular monocrystalline with embayed margins and strong undulose extinction. Fluid inclusion trails are common and located at the boundary between the detrital quartz and the overgrowth. The grain is microfractured with a set of irregular fractures (Fig. C, and D). Only a few healed fractures (HF) can be seen in Fig. D. The dark areas indicated by arrows in Fig. D are overgrowth.

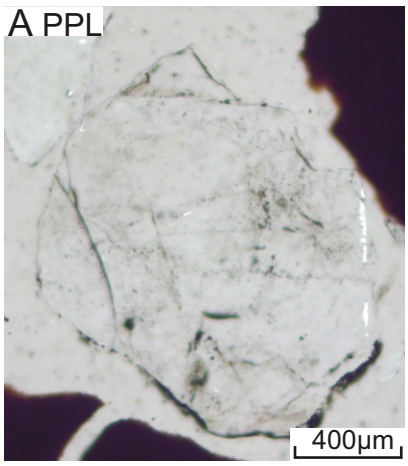

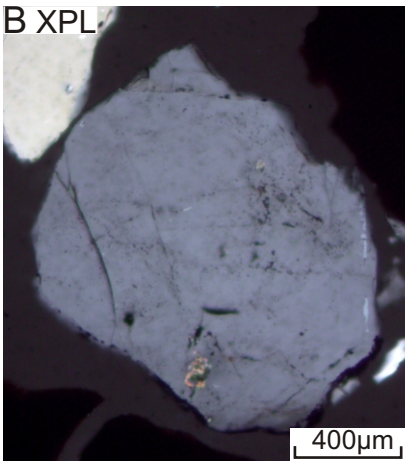

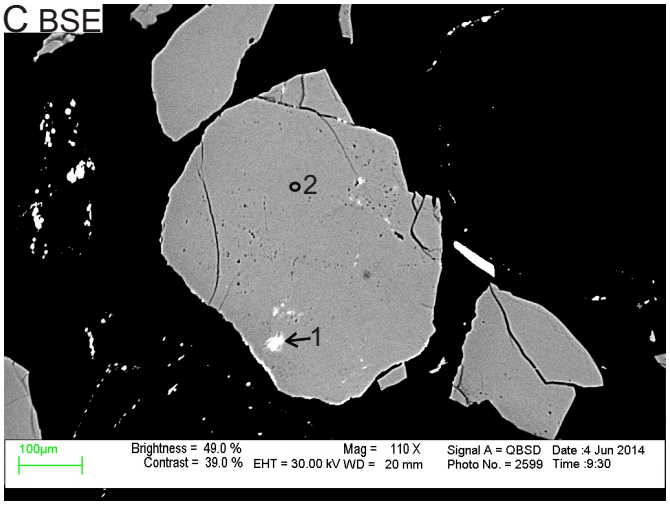

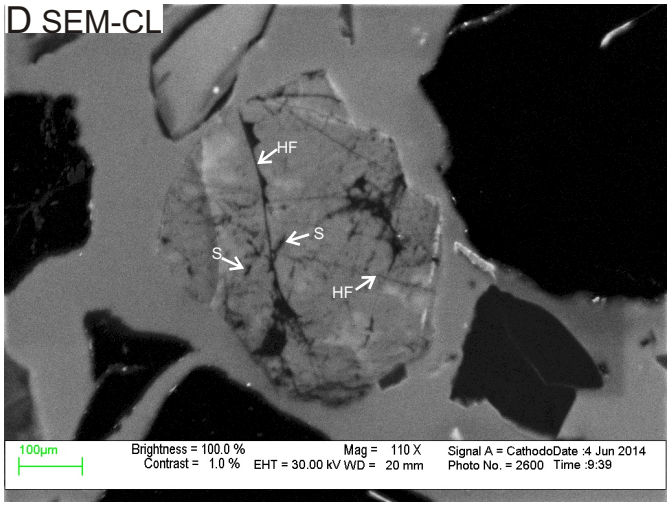

E EDS analyses

Pos#	Min. ID	SiO2	TiO2	Al2O3	FeO	MnO	MgO	Na2O	K2O	P2O5	SO3	Ce2O3	Total	Actual total
1	Ilt	46.95	0.24	24.80	4.78	0.40	0.75	0.44	8.63	0.58	2.07	0.37	90	105
2	Qz	99.99											100	120

Figure 5A-12: Microphotos under ppl (A) and xpl (B), SEM-BSE image (C), SEM-CL image (D), and EDS analyses table (E) of quartz grain 12 in sample 3150. The grain is anhedral and sub-rounded monocrystalline with weak undulose extinction. Fluid inclusions are common; they are usually associated with secondary porosity and form trails along healed fractures (Fig. A). The grain contains illite inclusions and is microfractured with a set of parallel fractures and a set of irregular fractures (Fig. C and D). Healed fractures (HF) and dark-CL spiders (S) are common (Fig. D). The grain shows subtle mottling in SEM-CL image.

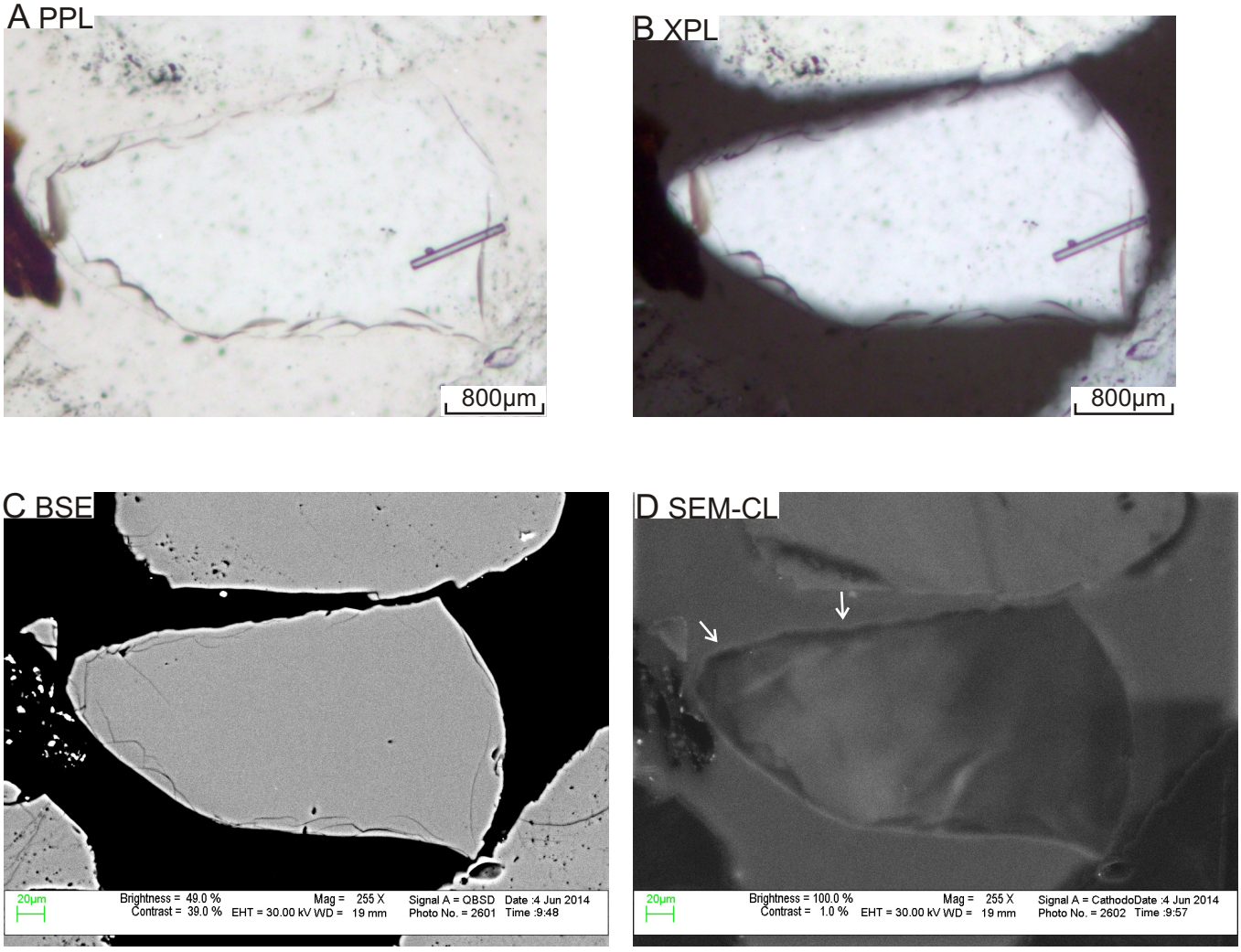

Figure 5A-13: Microphotos under ppl (A) and xpl (B), SEM-BSE image C, and SEM-CL image (D) of quartz grain 13 in sample 3150. The grain is anhedral and sub-rounded monocrystalline with weak undulose extinction. Fluid inclusions are rare. The grain is weakly microfractured with irregular curved fractures (Fig. C). Healed fractures (HF) and dark-CL patches (P) are rare. The dark areas indicated by arrows in Fig. D are overgrowth.

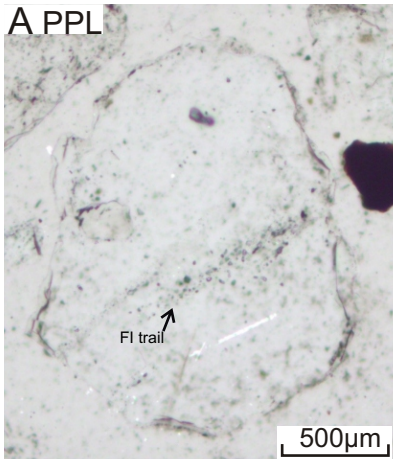

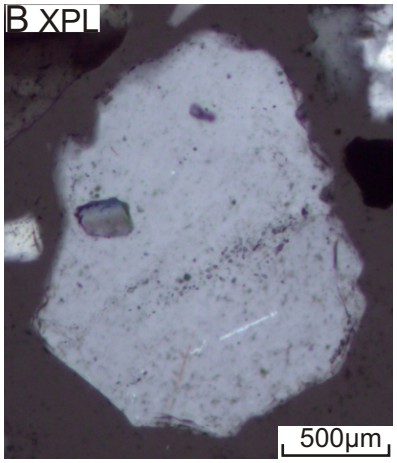

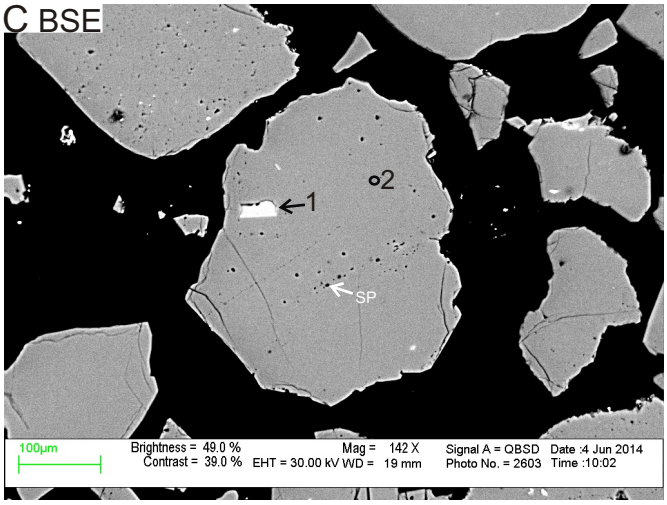

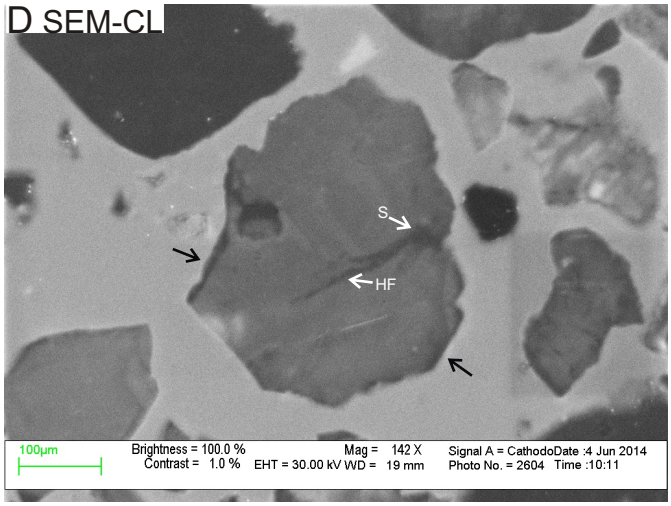

E EDS analyses

Pos#	Min. ID	SiO2	Al2O3	FeO	Na2O	K2O	F	Total	Actual total
1	Ms	45.80	33.59	2.08	0.89	9.60	3.03	95	112
2	Qz	99.99						100	123

Figure 5A-14: Microphotos under ppl (A) and xpl (B), SEM-BSE image (C), SEM-CL image (D), and EDS analyses table (E) of quartz grain 14 in sample 3150. The grain is anhedral and sub-rounded monocrystalline with embayed margins and non-undulose extinction. Fluid inclusions are common; they are usually associated with secondary porosity (SP) and form trails along healed fractures (Fig. A and C). The grain contains a muscovite inclusion and is microfractured with a set of irregular fractures (Fig. C and D). A few healed fractures (HF) and dark-CL spiders (S) can be seen in Fig. D. The dark areas indicated by arrows in Fig. D are overgrowth.

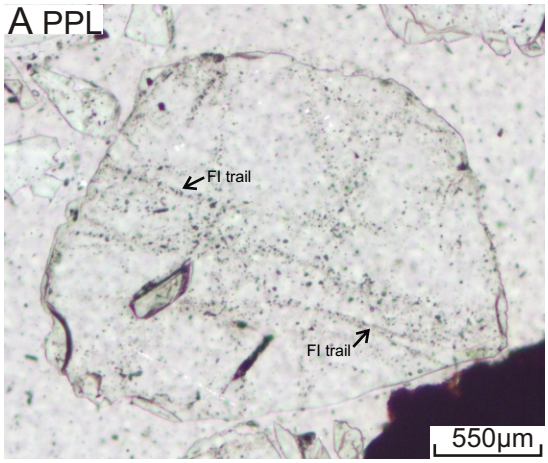

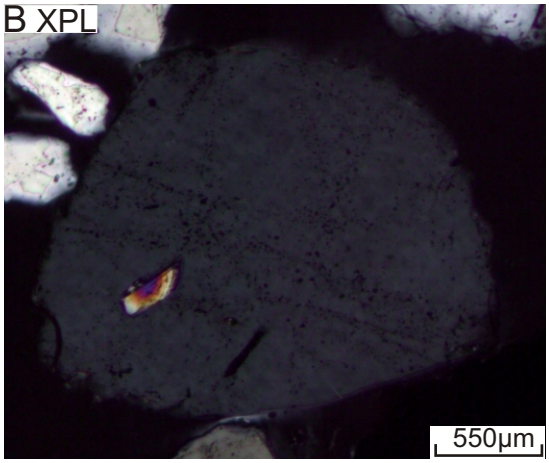

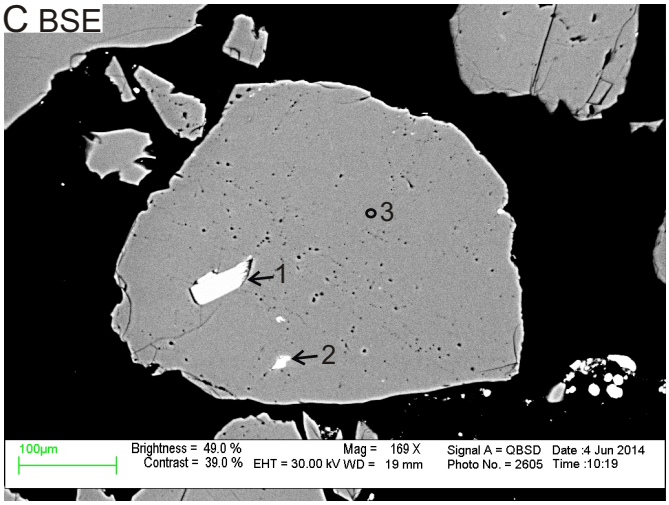

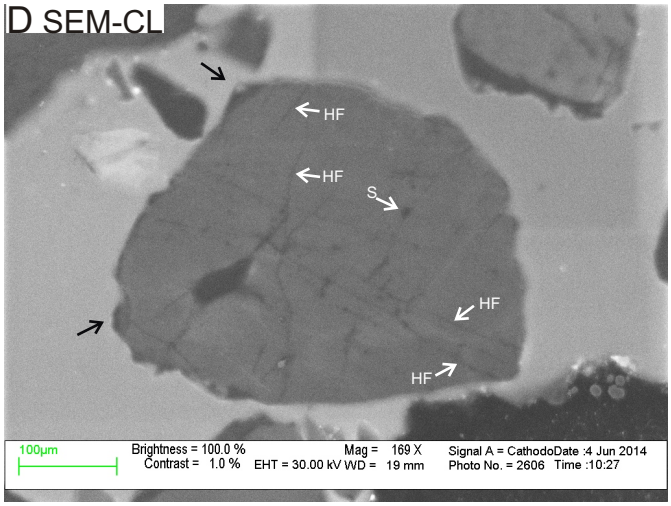

E EDS analyses

Pos#	Min. ID	SiO2	TiO2	Al2O3	FeO	MgO	Na2O	K2O	P2O5	SO3	La2O3	Ce2O3	Nd2O3	Total	Actual total
1	Ms	48.71	0.64	32.59	1.33	1.01	0.92	9.80						95	106
2	Mnz	23.34		9.69	2.51	0.98		1.25	19.61	9.56	6.36	20.58	6.1	100	132
3	Qz	99.99												100	116

Figure 5A-15: Microphotos under ppl (A) and xpl (B), SEM-BSE image (C), SEM-CL image (D), and EDS analyses table (E) of quartz grain 15 in sample 3150. The grain is anhedral and sub-rounded monocrystalline with non-undulose extinction. Fluid inclusions are common; they are usually associated with secondary porosity and form trails along healed fractures (Fig. A). The grain contains muscovite and monazite inclusions and is microfractured with two sets of parallel fractures crosscutting each other perpendicularly (Fig. C and D). Some healed fractures (HF) and spiders (S) can be seen in Fig, D. The dark areas indicated by arrows in Fig. D are overgrowth.

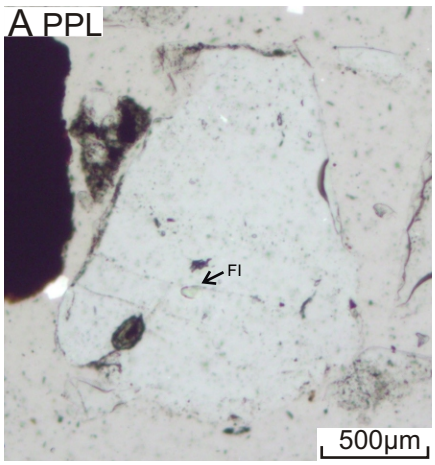

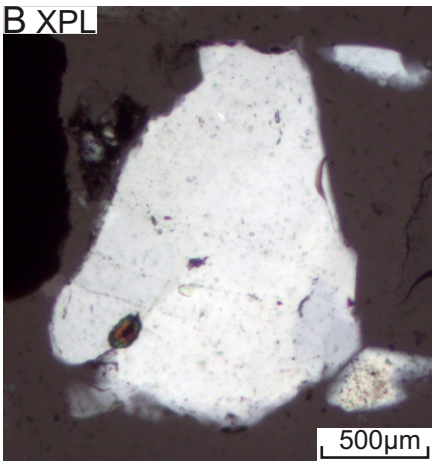

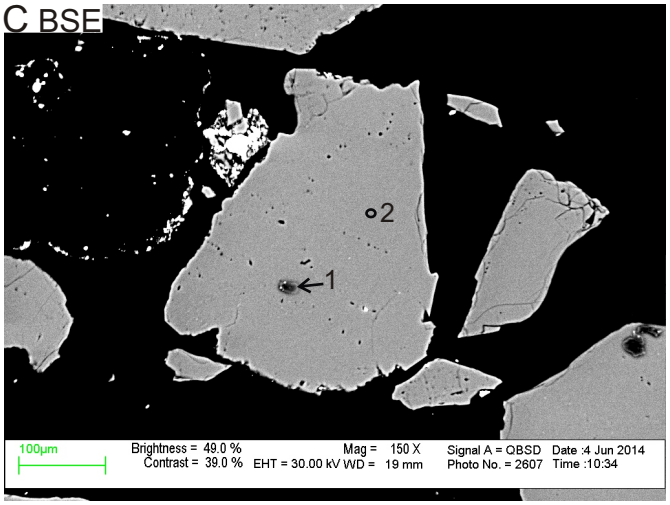

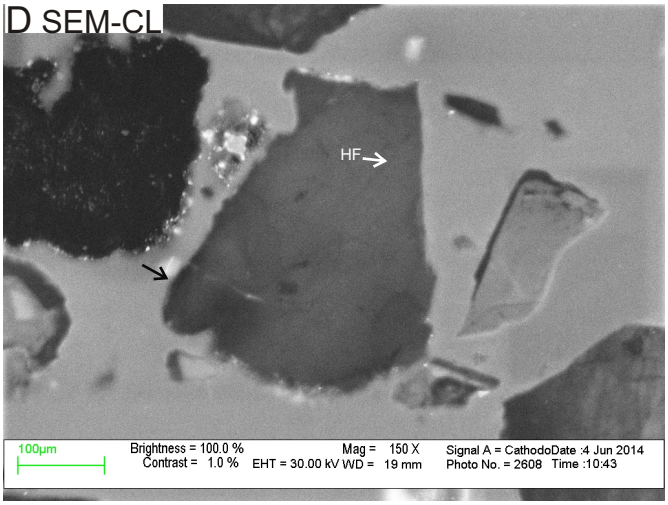

E EDS analyses

Position	Mineral	SiO2	CaO	Na2O	K2O	SO3	F	Cl	CuO	ZnO	Total	Actual total
1	Fluid inclusion	70.19	0.22	3.45	0.31	0.75	1.8	0.73	0.39	0.7	79	104
2	Qz	99.99									100	118

Figure 5A-16: Microphotos under ppl (A) and xpl (B), SEM-BSE image (C), SEM-CL image (D), and EDS analyses table (E) of quartz grain 16 in sample 3150. The grain is anhedral and sub-angular monocrystalline with mosaic texture and weak undulose extinction. Fluid inclusions are present. They are located along fractures and at the boundary between the detrital quartz and the overgrowth (Fig. A). The grain is weakly microfractured with irregular curved fractures (Fig. C). Only a few healed fractures (HF) can be seen in Fig. D. The dark area indicated by arrow in Fig. D is overgrowth.

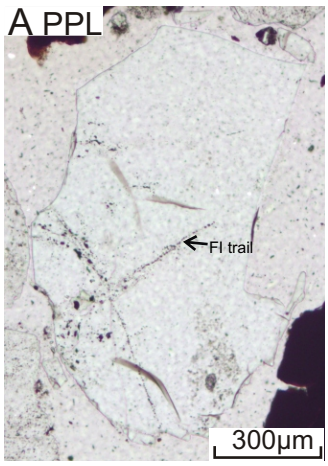

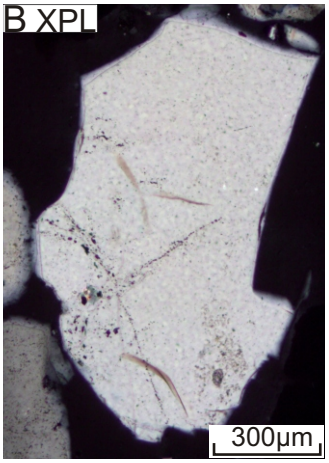

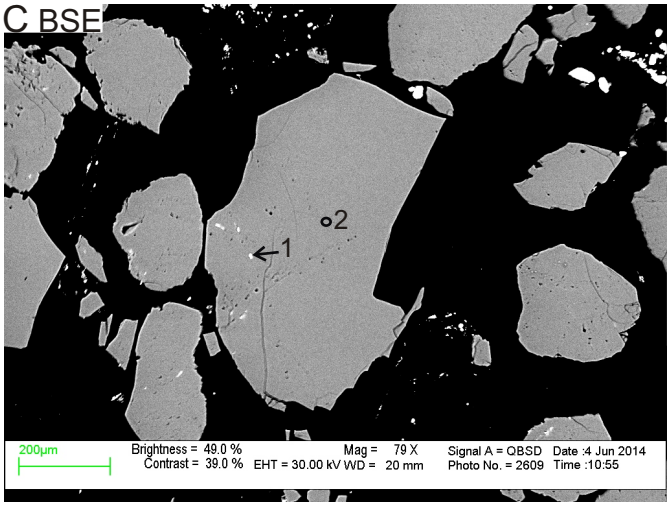

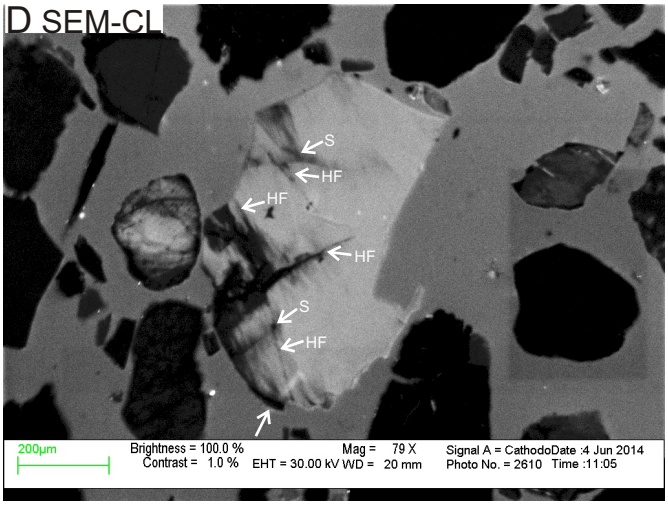

E EDS analyses

Pos#	Min. ID	SiO2	FeO	SO3	Total	Actual total
1	Py+Qz	17.73	22.24	60	100	209
2	Qz	99.99			100	119

Figure 5A-17: Microphotos under ppl (A) and xpl (B), SEM-BSE image (C), SEM-CL image (D), and EDS analyses table (E) of quartz grain 17 in sample 3150. The grain is anhedral and sub-angular monocrystalline with non-undulose extinction. Fluid inclusions are common; they are usually associated with secondary porosity and form trails along healed fractures (Fig. A). The grain contains pyrite inclusions and is microfractured with a set of parallel fractures and a set of irregular fractures (Fig. C and D). Healed fractures (HF) and spiders (S) are common (Fig. D). The dark area indicated by arrow in Fig. D is overgrowth.

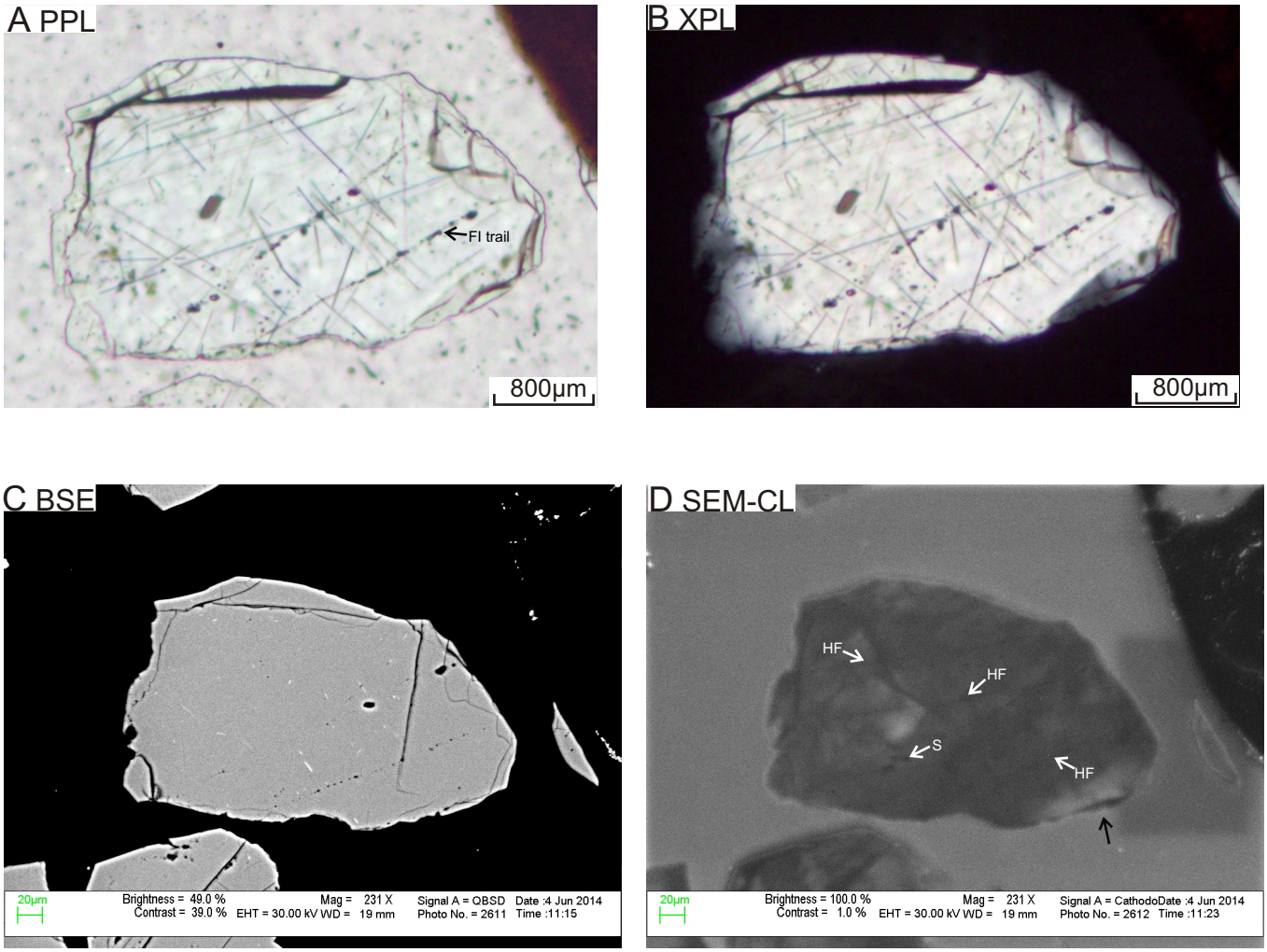

Figure 5A-18: Microphotos under ppl (A) and xpl (B), SEM-BSE image C, and SEM-CL image (D) of quartz grain 18 in sample 3150. The grain is anhedral and sub-rounded monocrystalline with strong undulose extinction. Fluid inclusions are common; they are usually associated with secondary porosity and form trails along healed fractures (Fig. A). The grain is microfractured with a set of parallel healed fractures and a set of irregular open fractures (Fig. C and D). Healed fractures (HF) are common and some spiders (S) can be seen (Fig. D). The dark area indicated by arrow in Fig. D is overgrowth. The grain shows subtle mottling in SEM-CL image.

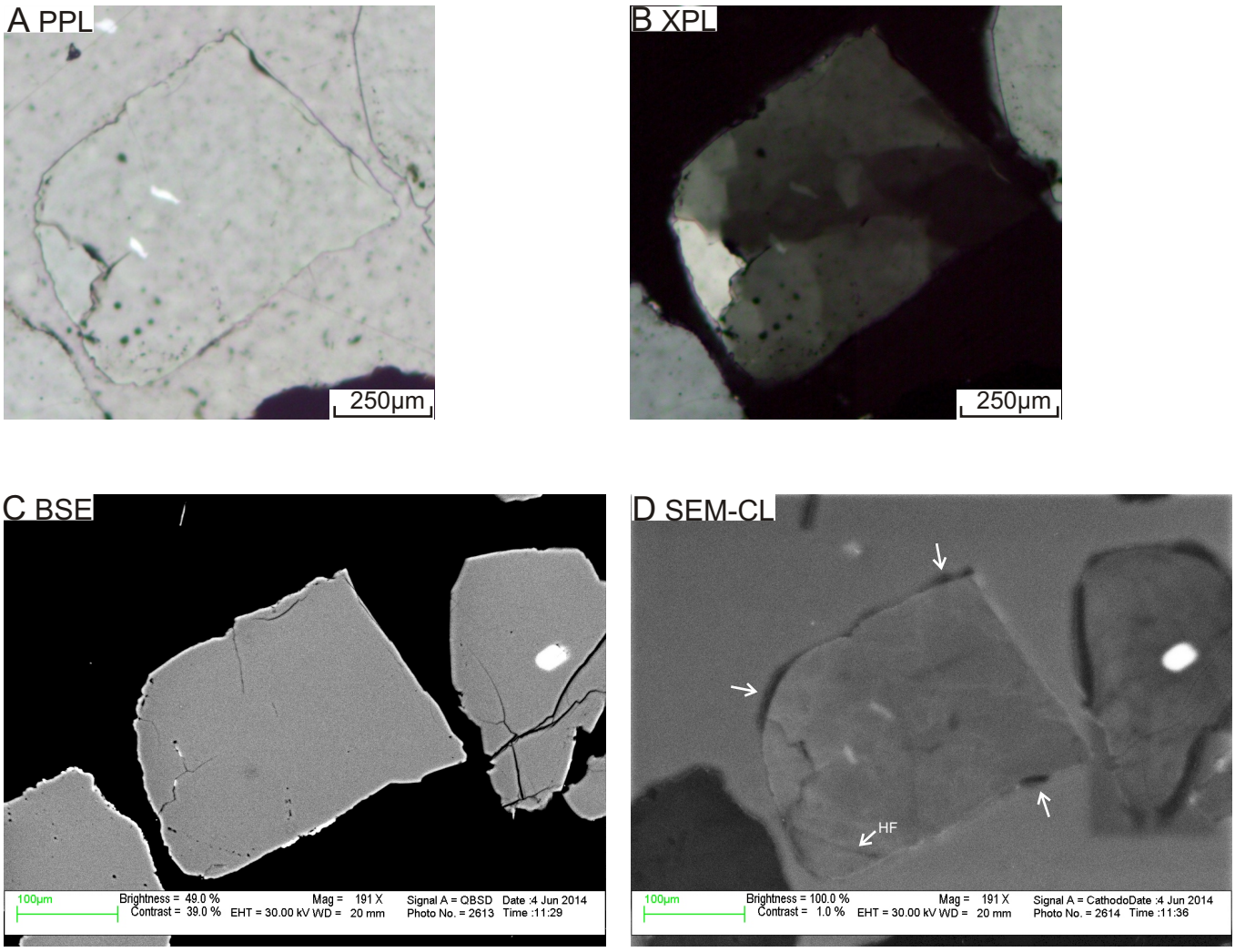

Figure 5A-19: Microphotos under ppl (A) and xpl (B), SEM-BSE image C, and SEM-CL image (D) of quartz grain 19 in sample 3150. The grain is anhedral and sub-rounded polycrystalline (only 2 sub-grains) with mosaic texture and weak undulose extinction. Fluid inclusions are rare. The grain is weakly microfractured with irregular curved fractures (Fig. C). Healed fractures and dark-CL patches are rare. The dark areas indicated by arrows in Fig. D are overgrowth.

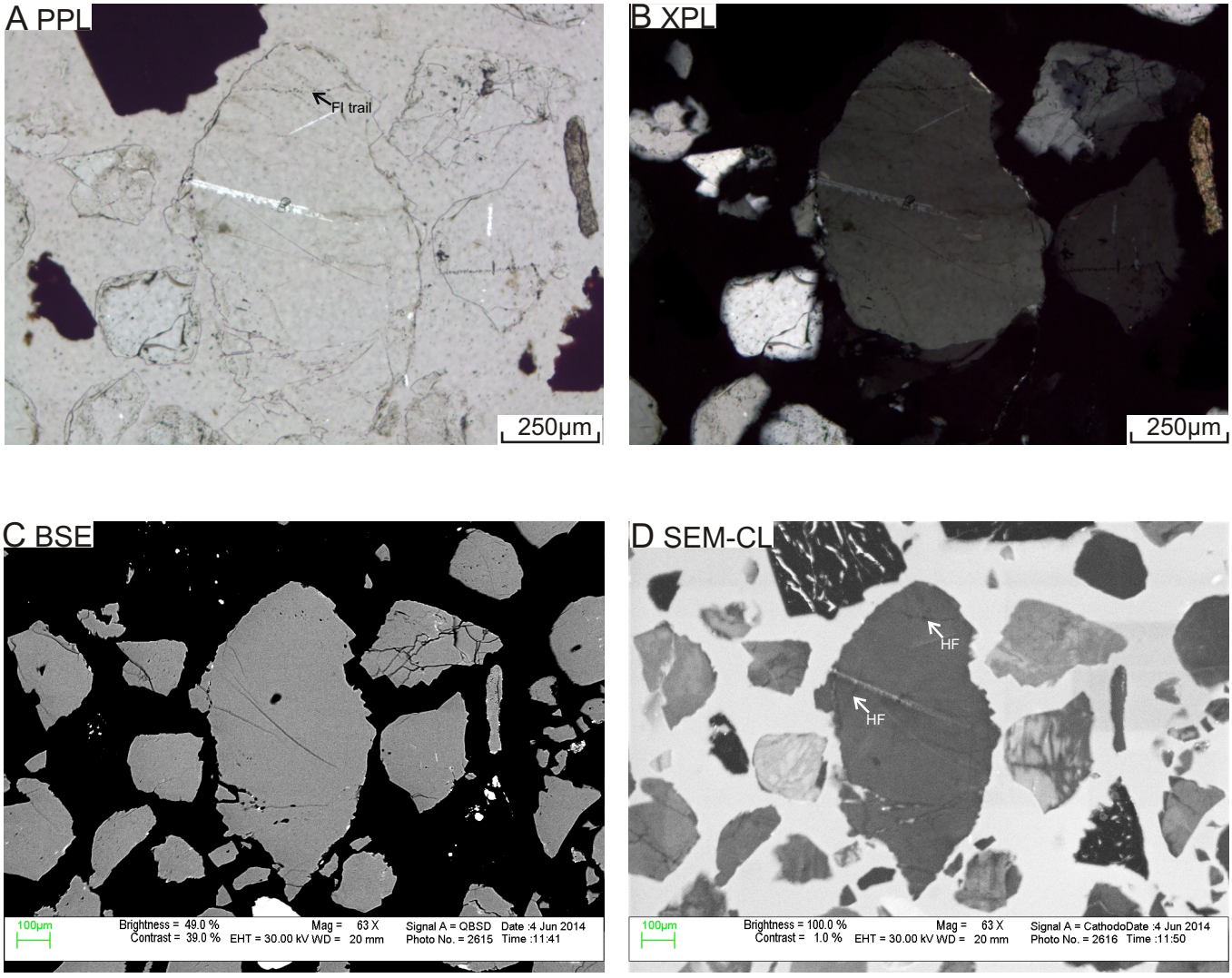

Figure 5A-20: Microphotos under ppl (A) and xpl (B), SEM-BSE image C, and SEM-CL image (D) of quartz grain 20 in sample 3150. The grain is anhedral and sub-angular polycrystalline (only a few sub-grains) with irregular margins and strong undulose extinction. Fluid inclusions are common; they form trails along healed fractures (Fig. A). The grain is microfractured with a set of irregular fractures (Fig. C and D). Some healed fractures (HF) can be seen in Fig. D.

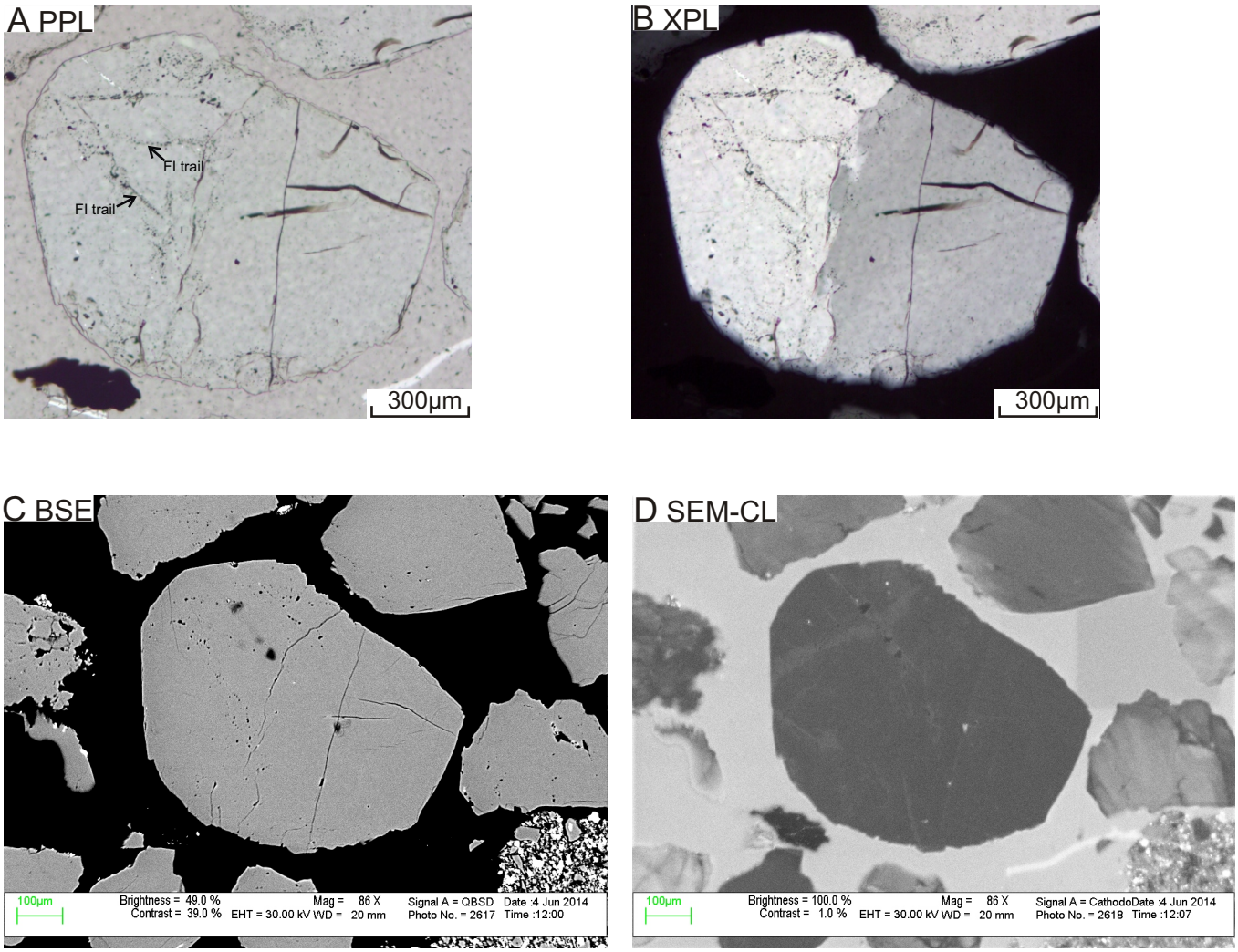

Figure 5A-21: Microphotos under ppl (A) and xpl (B), SEM-BSE image C, and SEM-CL image (D) of quartz grain 21 in sample 3150. The grain is subhedral and rounded polycrystalline (only 2 sub-grains) with mosaic texture and weak undulose extinction. Fluid inclusions are common (Fig. A). The grain is microfractured with a set of irregular fractures (Fig. C and D). Healed fractures are probably camouflaged by the dark-Cl colour of the grain in SEM-CL image.

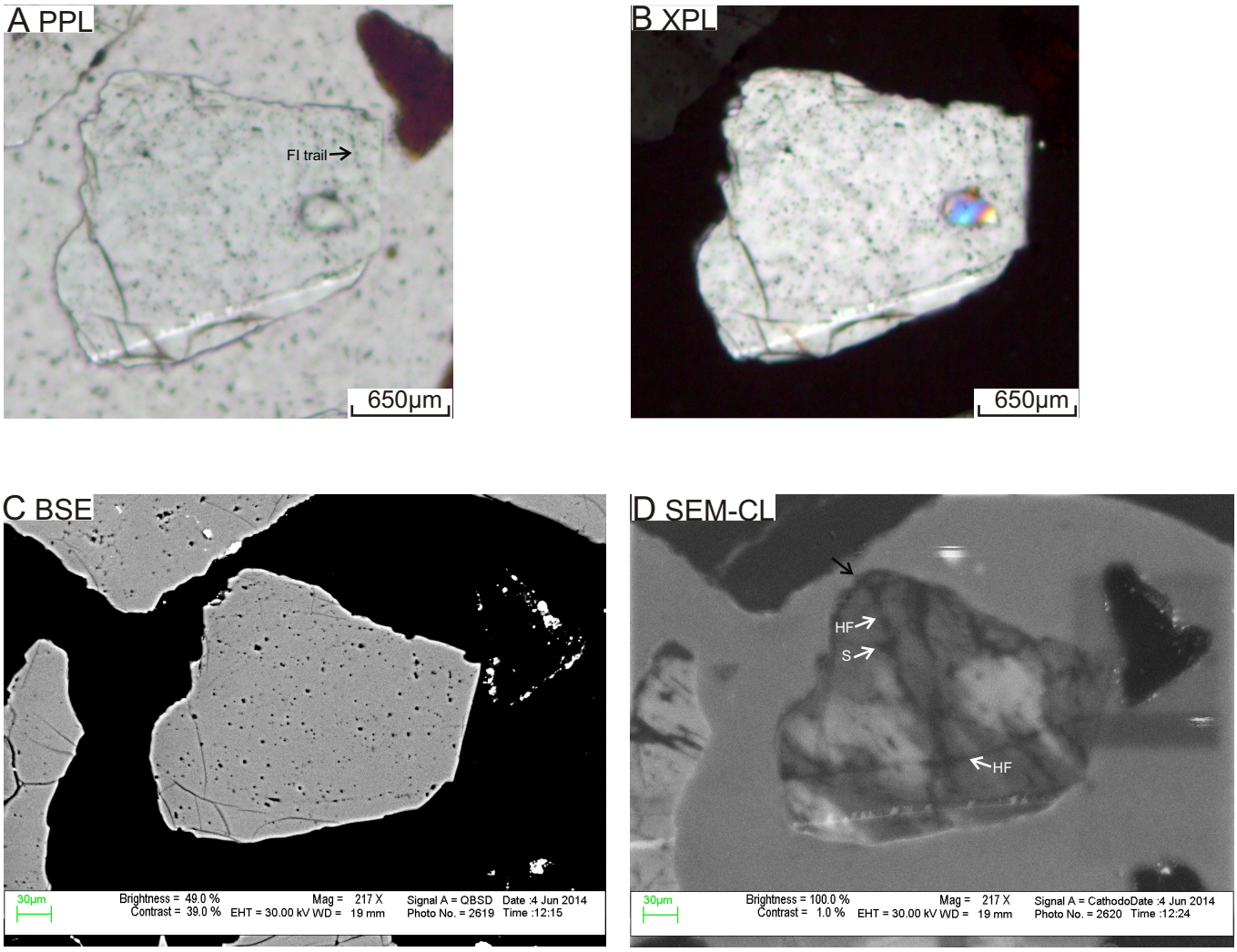

Figure 5A-22: Microphotos under ppl (A) and xpl (B), SEM-BSE image C, and SEM-CL image (D) of quartz grain 22 in sample 3150. The grain is anbhedral and sub-rounded monocrystalline with non-undulose extinction. Fluid inclusions are common; they are usually associated with secondary porosity and form trails along healed fractures (Fig. A). The grain is microfractured with a set of irregular fractures (Fig. C and D). Healed fractures and spiders (S) are common. The dark area indicated by arrow in Fig. D is overgrowth. The grain shows bright streaky patches in Fig. D.

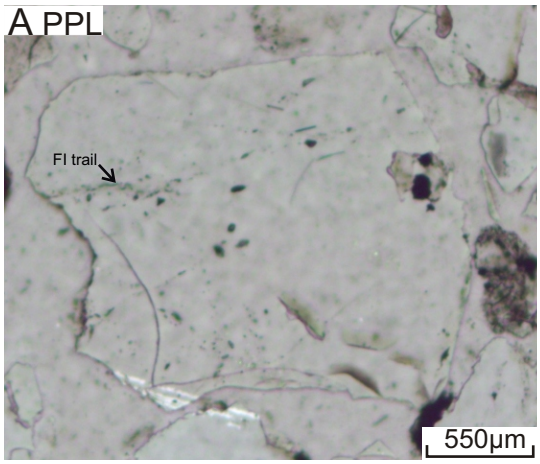

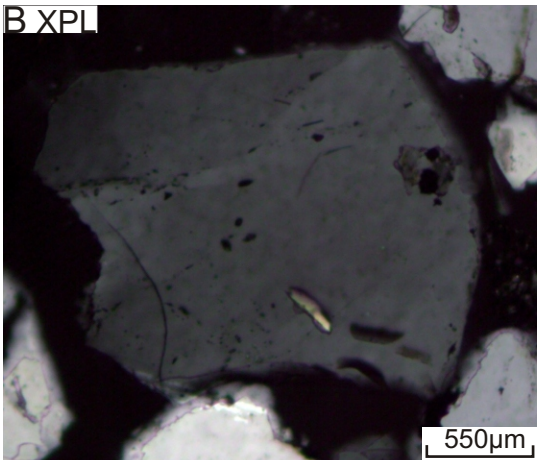

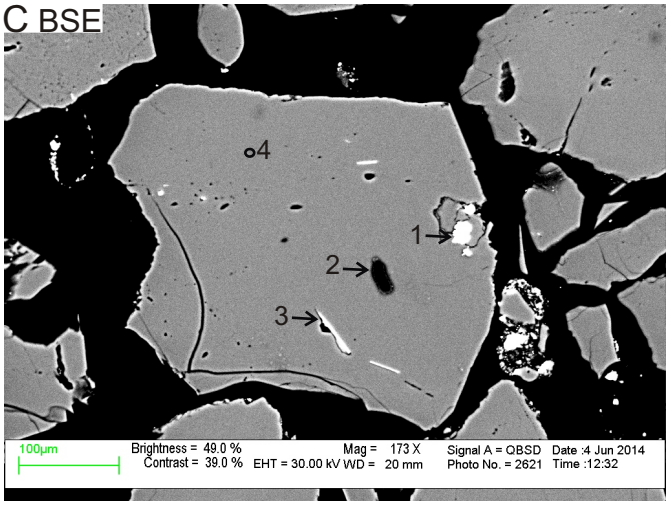

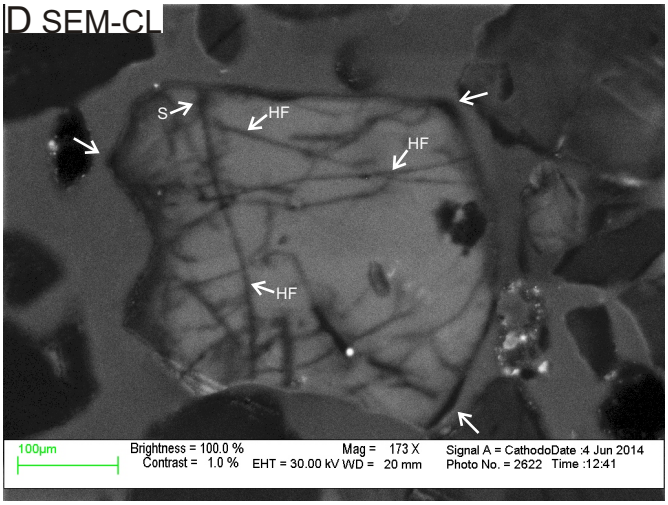

E EDS analyses

Pos#	Min. ID	SiO2	TiO2	Al2O3	FeO	MnO	MgO	CaO	Na2O	K2O	SO3	Cl	Total	Actual total
1	Py	0.3			26.78	1.01					71.92		100	198
2	Hole	73.1						0.17	1.32	0.25	1.02	0.8	77	93
3	Fluid inclusion	71.09	0.93	9.11	8.68		5.62			4.58			100	118
4	Qz	99.99											100	110

Figure 5A-23: Microphotos under ppl (A) and xpl (B), SEM-BSE image (C), SEM-CL image (D), and EDS analyses table (E) of quartz grain 23 in sample 3150. The grain is anhedral and sub-angular monocrystalline with weak undulose extinction. Fluid inclusions are common; they form trails along healed fractures (Fig. A). The grain contains pyrite inclusions and is microfractured with a set of irregular fractures (Fig. C and D). Healed fractures and spiders (S) are common. The dark areas indicated by arrows in Fig. D are overgrowth.

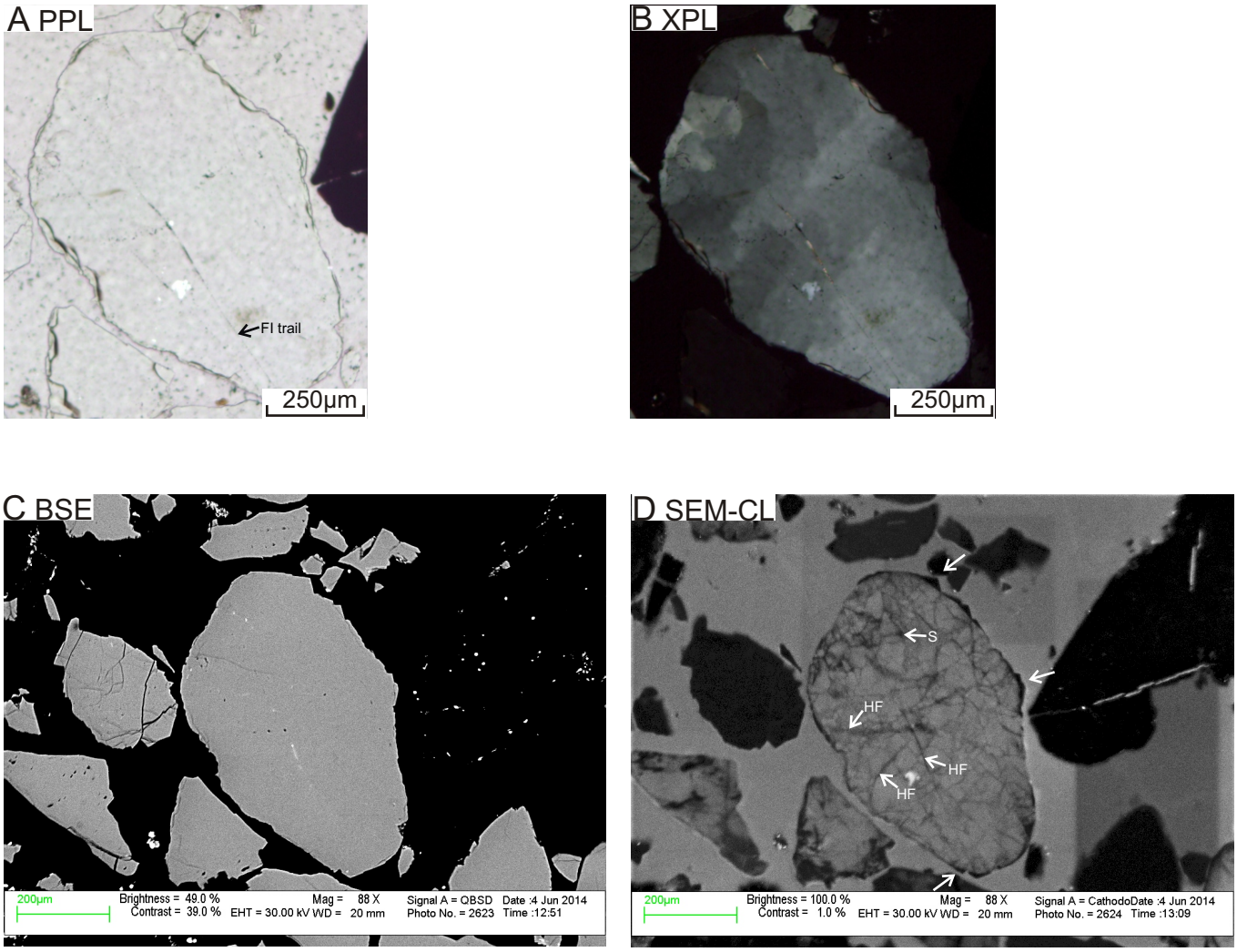

Figure 5A-24: Microphotos under ppl (A) and xpl (B), SEM-BSE image C, and SEM-CL image (D) of quartz grain 24 in sample 3150. The grain is anhedral and sub-rounded polycrystalline (only a few sub-grains) with mosaic texture and non-undulose extinction. Fluid inclusions are present; they form trails along healed fractures (Fig. A). The grain is strongly microfractured with a set of irregular fractures (Fig. C and D). Healed fractures and spiders (S) are common. The dark areas indicated by arrows in Fig. D are overgrowth.

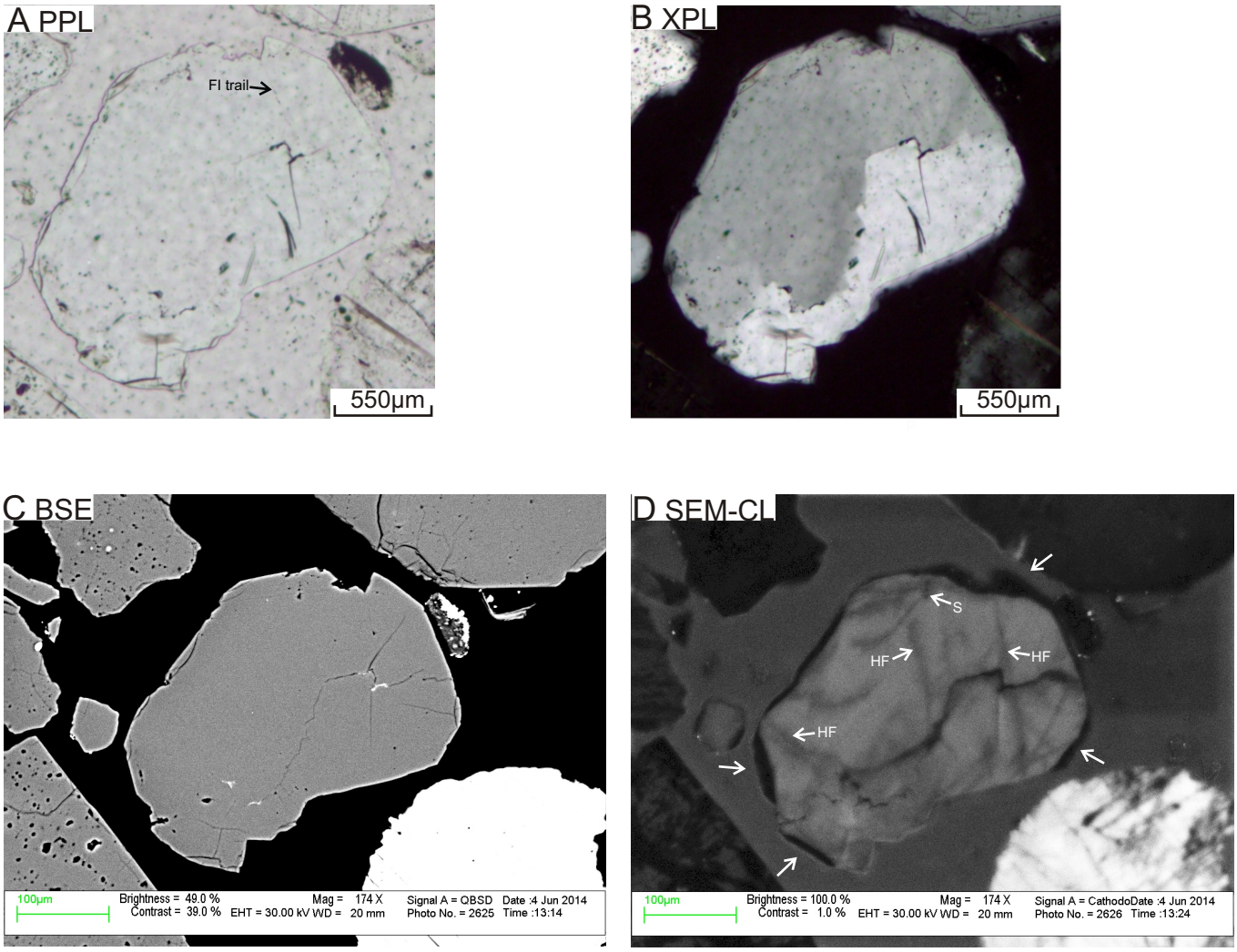

Figure 5A-25: Microphotos under ppl (A) and xpl (B), SEM-BSE image C, and SEM-CL image (D) of quartz grain 25 in sample 3150. The grain is anhedral and sub-rounded polycrystalline (only 2 sub-grains) with weak undulose extinction. Fluid inclusions are present; they form trails along healed fractures (Fig. A). The grain is microfractured with a set of irregular fractures (Fig. C and D). Healed fractures and spiders (S) are common. The dark areas indicated by arrows in Fig. D are overgrowth.

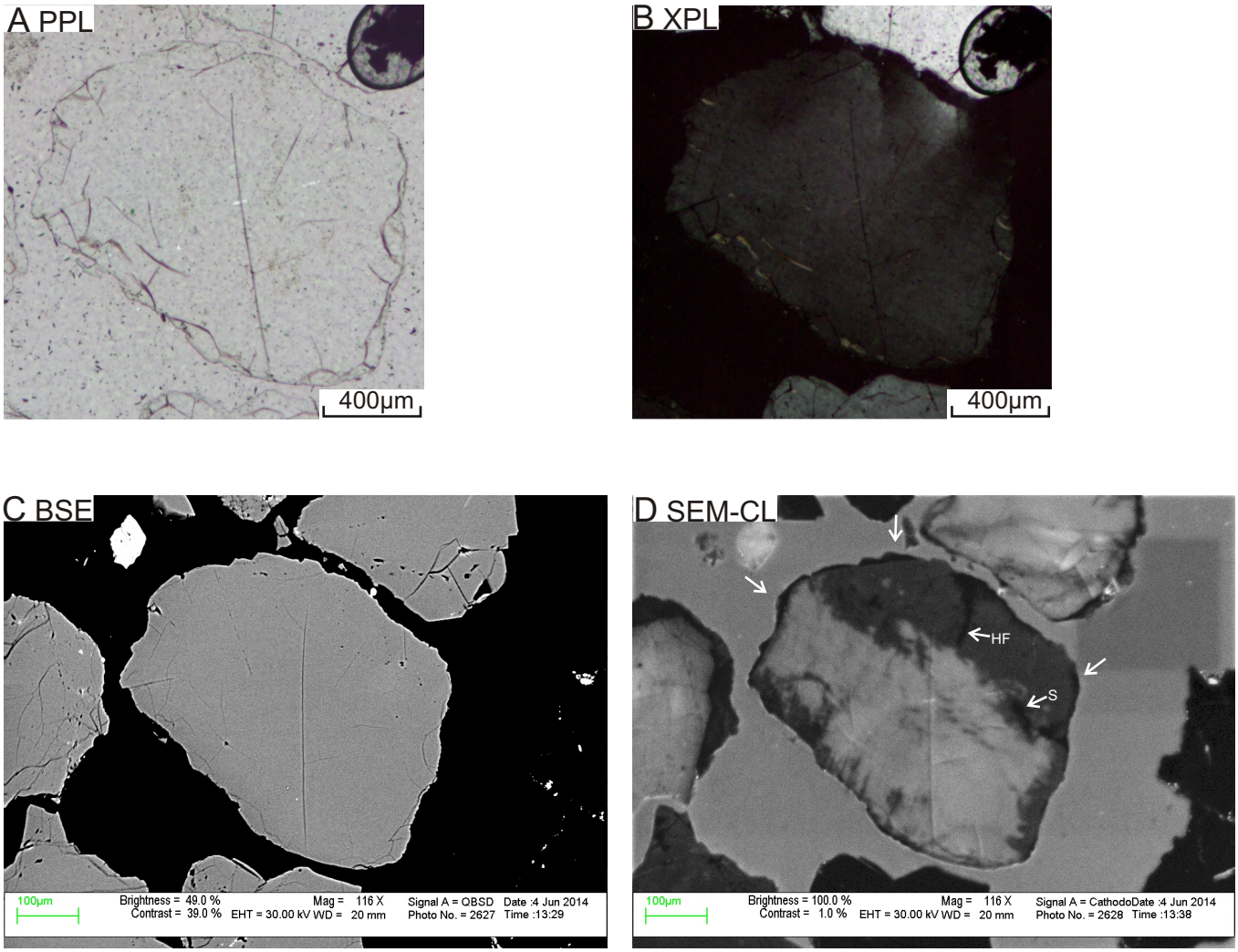

Figure 5A-26: Microphotos under ppl (A) and xpl (B), SEM-BSE image C, and SEM-CL image (D) of quartz grain 26 in sample 3150. The grain is anhedral and sub-rounded monocrystalline with irregular margins and strong undulose extinction. Fluid inclusions are rare. The grain is microfractured with a set of irregular fractures (Fig. C and D). Some healed fractures and spiders (S) can be seen in Fig. D. The dark areas indicated by arrows in Fig. D are overgrowth. The grain shows two distinct colours, bright-CL and dark-CL, in SEM-CL image.

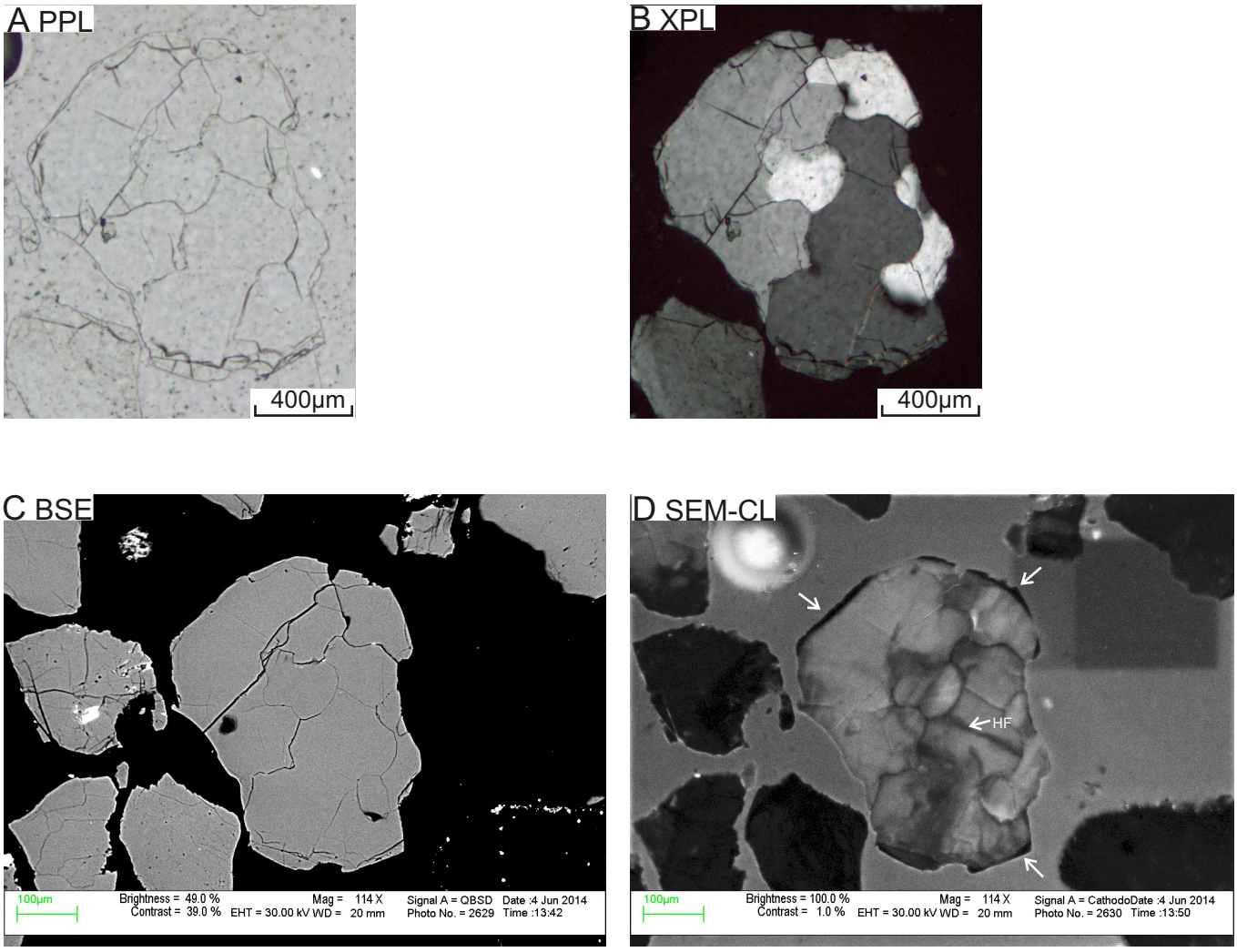

Figure 5A-27: Microphotos under ppl (A) and xpl (B), SEM-BSE image C, and SEM-CL image (D) of quartz grain 27 in sample 3150. The grain is anhedral and sub-rounded polycrystalline (more than 5 sub-grains with sutured sub-grain boundaries) with strong undulose extinction. Fluid inclusions are rare. The grain is microfractured with a set of irregular fractures (Fig. C and D). A few healed fractures can be seen in Fig. D. The dark areas indicated by arrows in Fig. D are overgrowth.

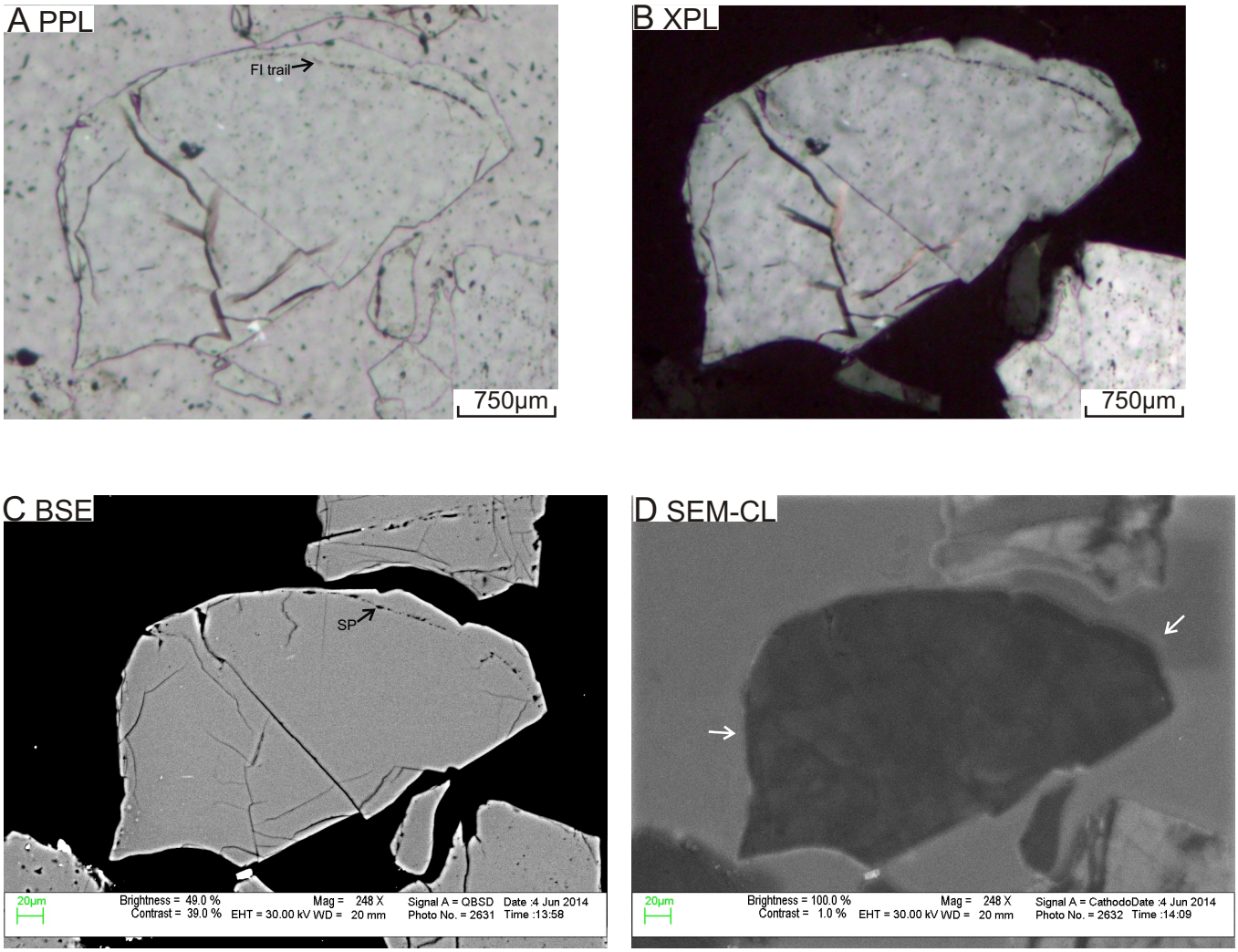

Figure 5A-28: Microphotos under ppl (A) and xpl (B), SEM-BSE image C, and SEM-CL image (D) of quartz grain 28 in sample 3150. The grain is anhedral and sub-angular monocrystalline with strong undulose extinction. Fluid inclusions are present; they are associated with secondary porosity and form trails at the boundary between the detrital quartz and the overgrowth (Fig. A and C). The grain is microfractured with a set of irregular fractures (Fig. C and D). Healed fractures are rare. The dark areas indicated by arrows in Fig. D are overgrowth.

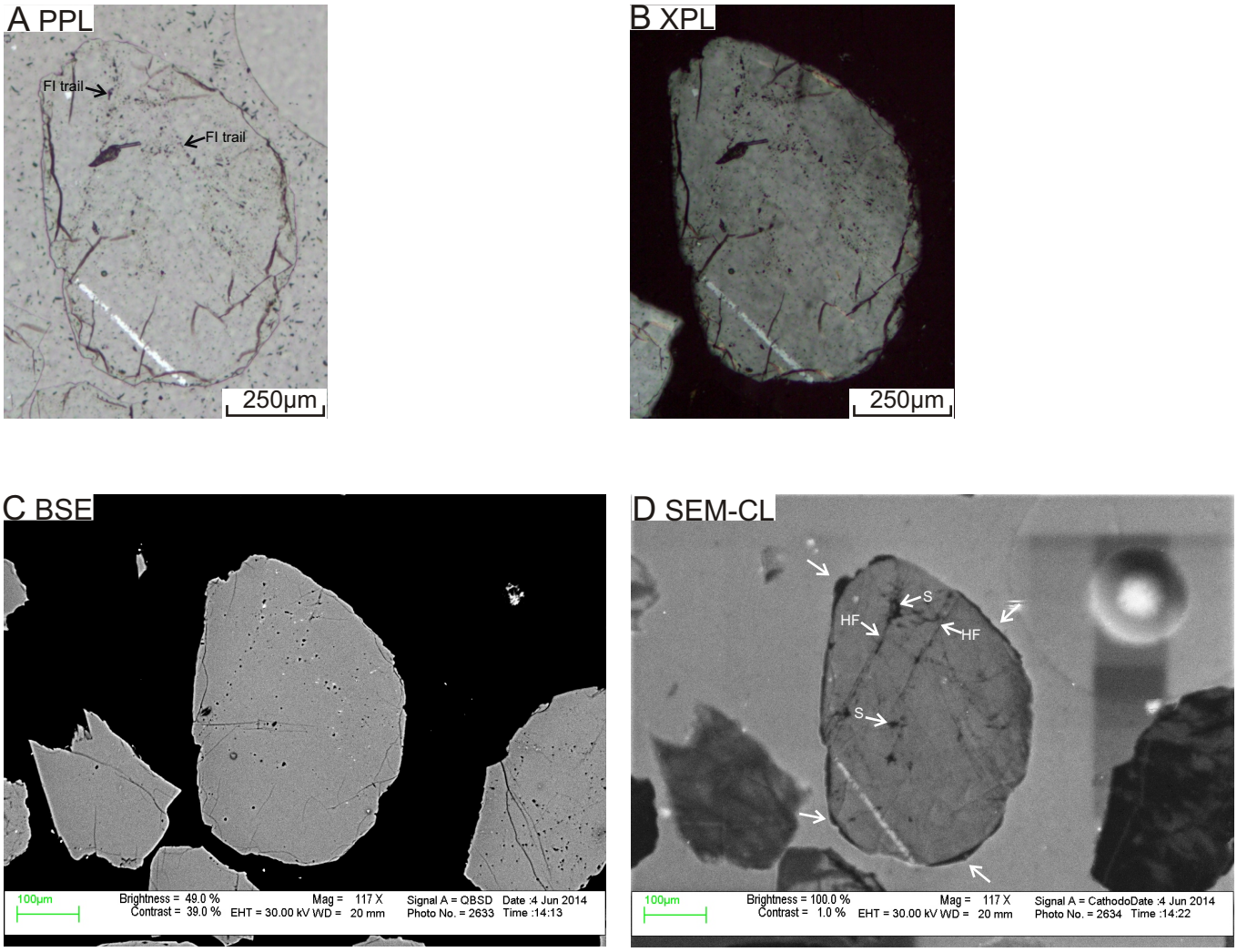

Figure 5A-29: Microphotos under ppl (A) and xpl (B), SEM-BSE image C, and SEM-CL image (D) of quartz grain 29 in sample 3150. The grain is anhedral and rounded monocrystalline with weak undulose extinction. Fluid inclusions are common; they are usually associated with secondary porosity and form trails along healed fractures (Fig. A). The grain is microfractured with a set of parallel fractures and a set of irregular fractures (Fig. C and D). Healed fractures and spiders (S) are common. The dark areas indicated by arrows in Fig. D are overgrowth.

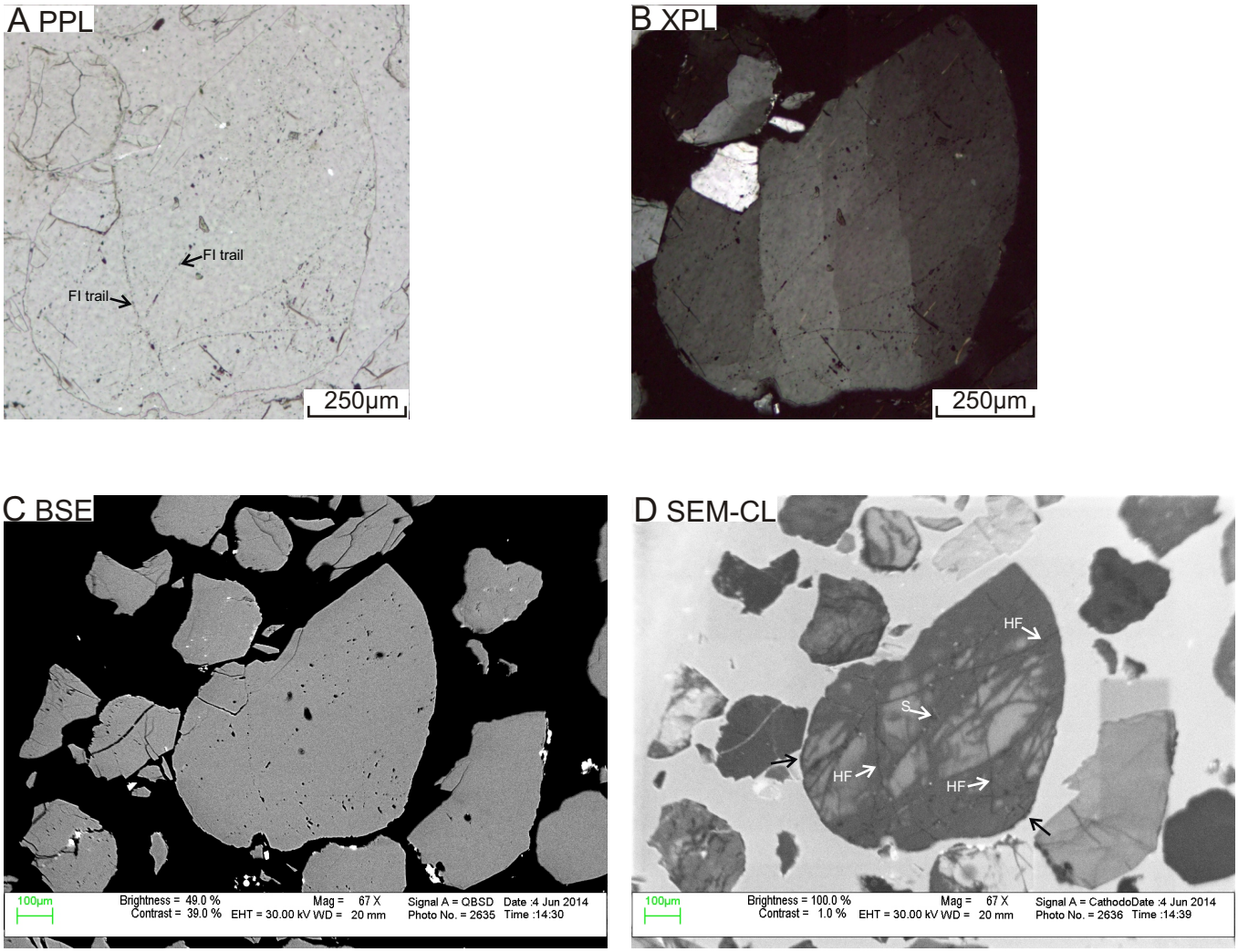

Figure 5A-30: Microphotos under ppl (A) and xpl (B), SEM-BSE image C, and SEM-CL image (D) of quartz grain 30 in sample 3150. The grain is anhedral and sub-rounded polycrystalline (only 2 sub-grains with sutured sub-grain boundaries) with mosaic texture and strong undulose extinction. Fluid inclusions are common; they are usually associated with secondary porosity and form trails along healed fractures (Fig. A). The grain is microfractured with a set of irregular fractures (Fig. C and D). Healed fractures and spiders (S) are common. The dark areas indicated by arrows in Fig. D are overgrowth. The grain shows bright streaky patches in Fig. D.

A PPL

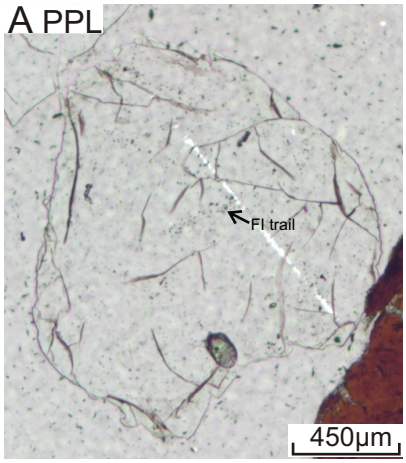

B XPL

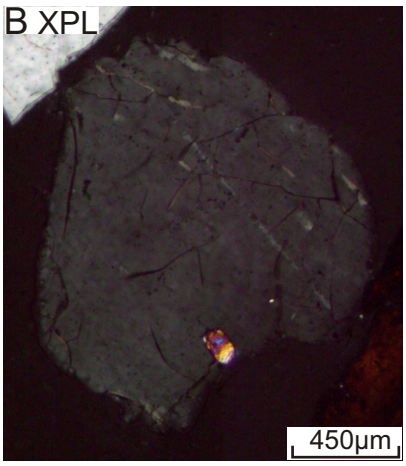

C BSE

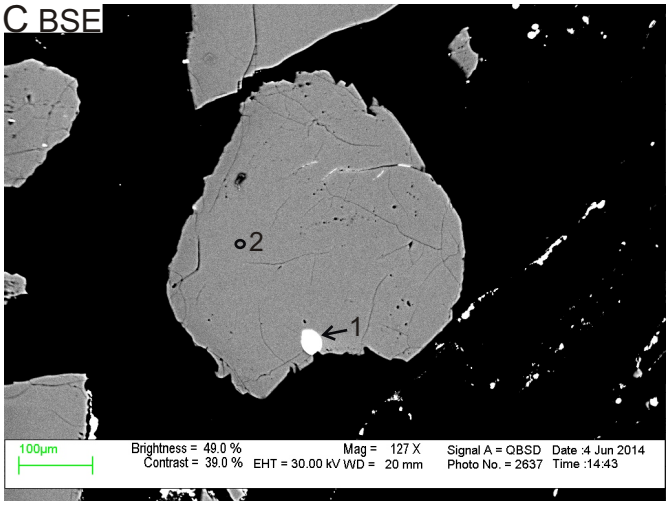

D SEM-CL

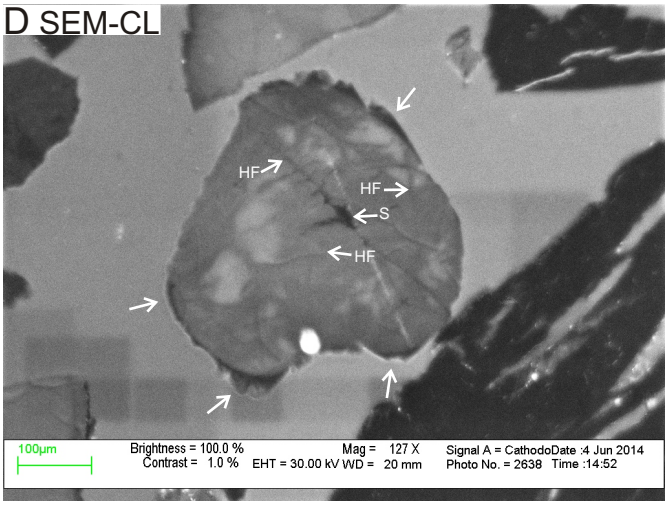

E EDS analyses

Pos#	Min. ID	SiO2	ZrO2	HfO2	Total	Actual total
1	Zrn	28.96	59.58	1.17	90	112
2	Qz	99.99			100	111

Figure 5A-31: Microphotos under ppl (A) and xpl (B), SEM-BSE image (C), SEM-CL image (D), and EDS analyses table (E) of quartz grain 31 in sample 3150. The grain is anhedral and sub-rounded monocrystalline with non-undulose extinction. Fluid inclusions are common; they are usually associated with secondary porosity and form trails along healed fractures (Fig. A). The grain contains a zircon inclusion and is microfractured with a set of irregular fractures (Fig. C and D). Healed fractures (HF) and spiders (S) are common (Fig. D). The dark areas indicated by arrows in Fig. D are overgrowth. The grain shows random bright-CL patches in SEM-CL image.

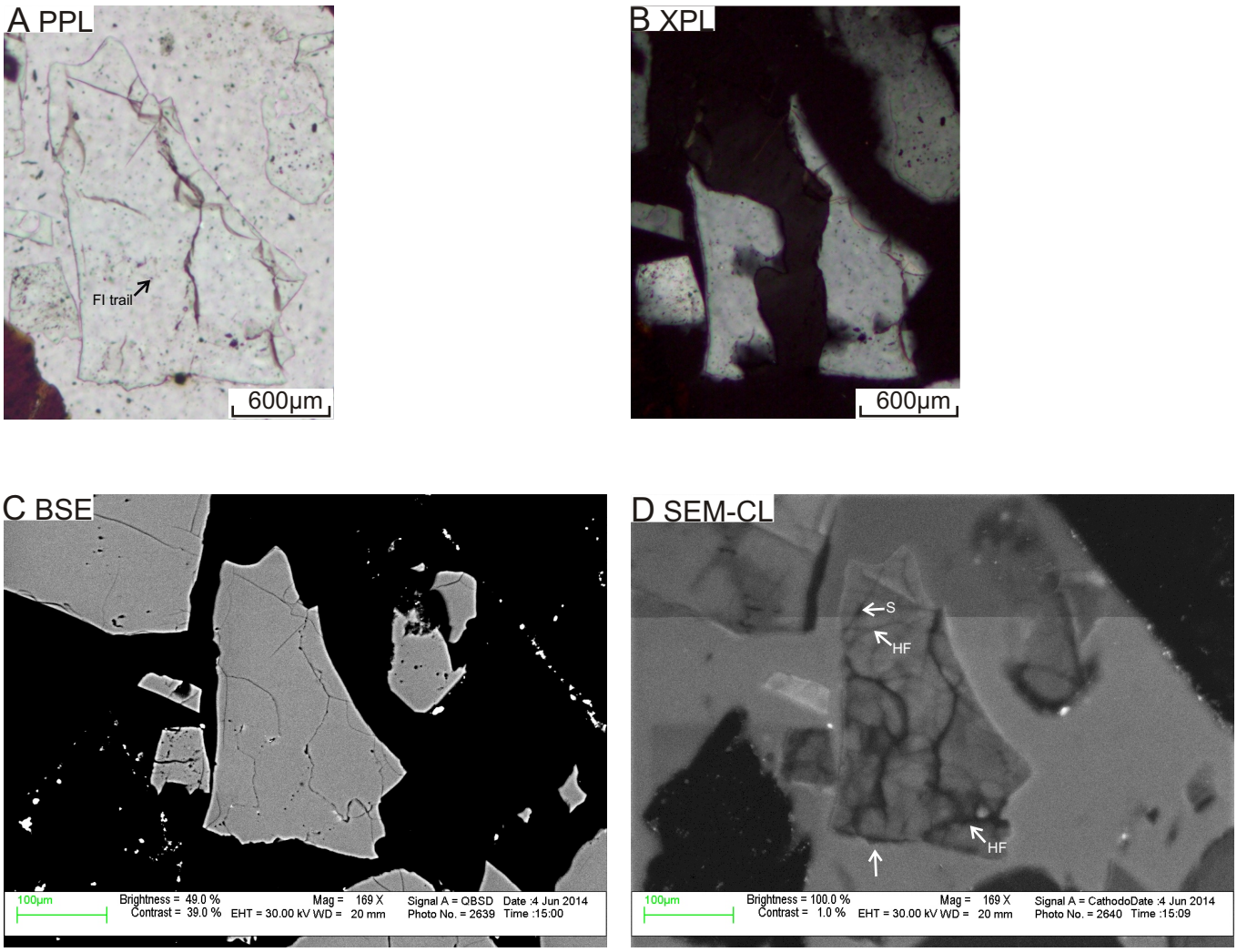

Figure 5A-32: Microphotos under ppl (A) and xpl (B), SEM-BSE image C, and SEM-CL image (D) of quartz grain 32 in sample 3150. The grain is anhedral and angular polycrystalline (only a few sub-grains with sutured sub-grain boundaries) with weak undulose extinction. Fluid inclusion trails are present (Fig. A). The grain is microfractured with a set of irregular fractures (Fig. C and D). Healed fractures (HF) are common (Fig. D). The dark area indicated by arrow in Fig. D is overgrowth.

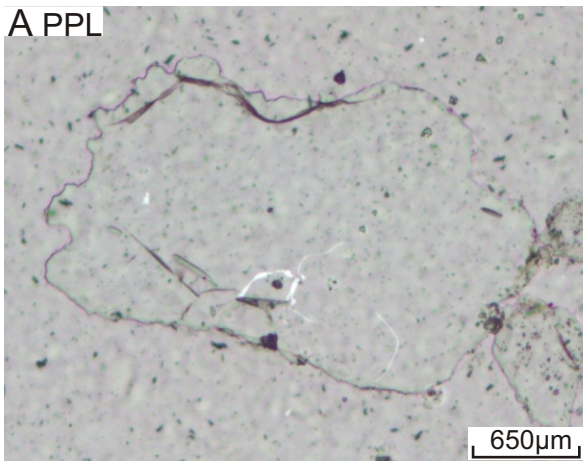

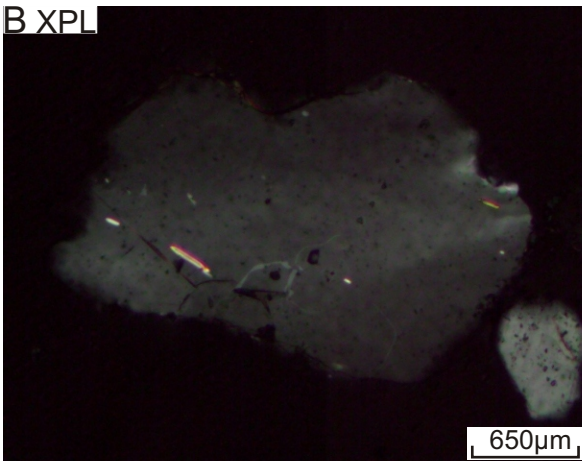

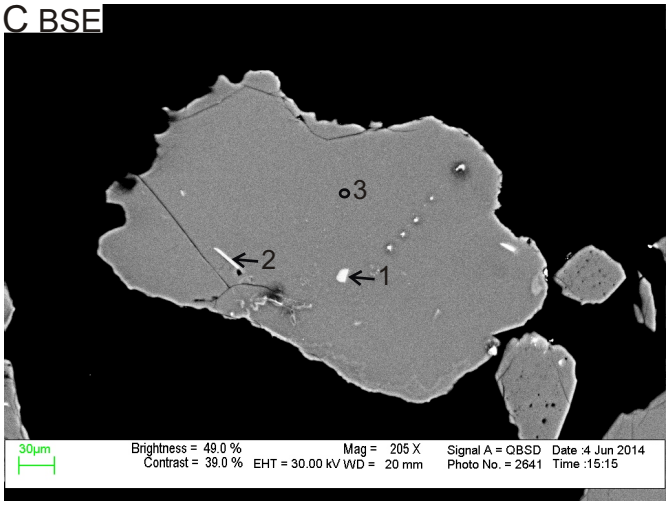

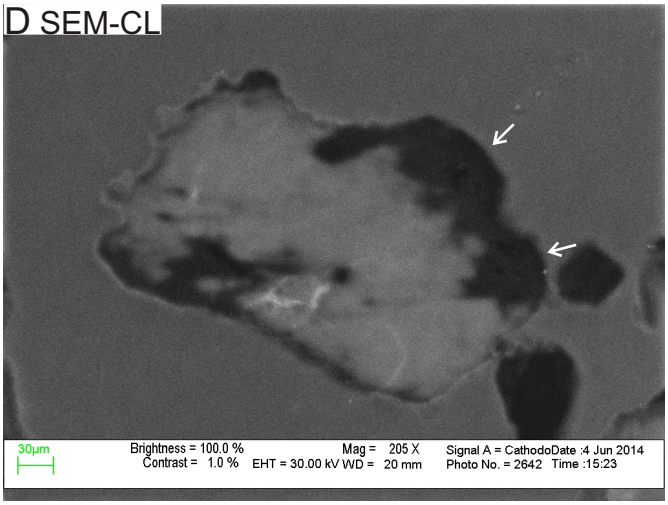

E EDS analyses

Pos#	Min. ID	SiO2	TiO2	Al2O3	FeO	MgO	Na2O	K2O	F	Total	Actual total
1	Kfs	59.11	0.48	28.42	0.64	0.6	0.8	8.08	1.88	100	106
2	Kfs	66.08	0.2	23.34	0.57	0.46	0.67	6.83	1.83	100	110
3	Quartz	99.99								100	106

Figure 5A-33: Microphotos under ppl (A) and xpl (B), SEM-BSE image (C), SEM-CL image (D), and EDS analyses table (E) of quartz grain 33 in sample 3150. The grain is anhedral and sub-rounded monocrystalline with strong undulose extinction. Fluid inclusions are rare. The grain contains K-feldspar inclusions and weakly microfractured with irregular fractures (Fig. C and D). Healed fractures are rare. The dark area indicated by arrow in Fig. D is overgrowth. The grain shows two distinct colours, bright-CL and dark-CL, in SEM-CL image.

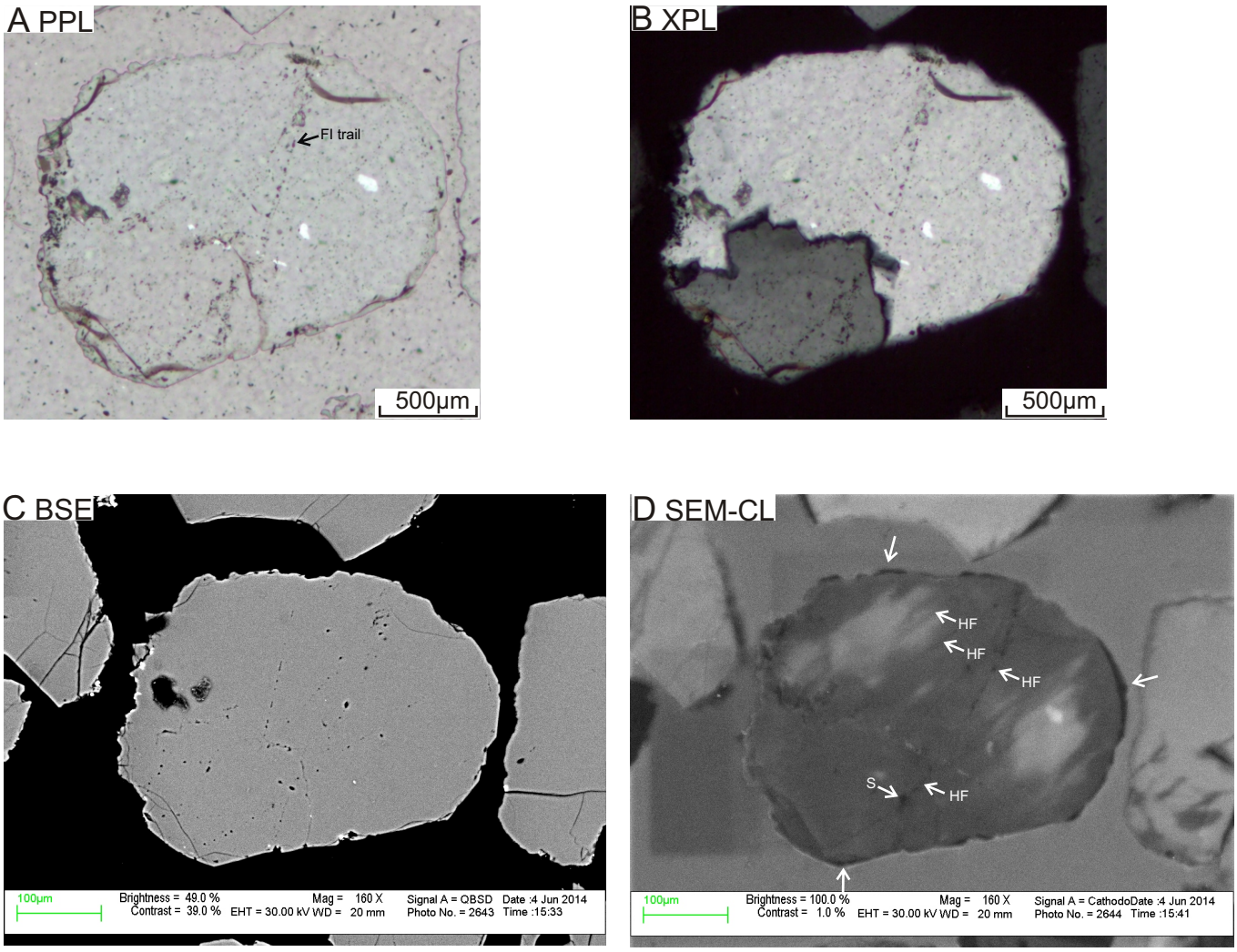

Figure 5A-34: Microphotos under ppl (A) and xpl (B), SEM-BSE image C, and SEM-CL image (D) of quartz grain 34 in sample 3150. The grain is anhedral and rounded polycrystalline (only 2 sub-grains with sutured sub-grain boundaries) with mosaic texture and weak undulose extinction. Fluid inclusions are common; they are usually associated with secondary porosity and form trails along healed fractures (Fig. A). The grain is microfractured with a set of sub-parallel fractures and a set of irregular fractures (Fig. C and D). Some healed fractures (HF) and spiders (S) can be seen in Fig. D. The dark areas indicated by arrows in Fig. D are overgrowth. The grain shows bright-CL streaky patches fabric with the same orientation of the set of sub-parallel fractures(Fig. D).

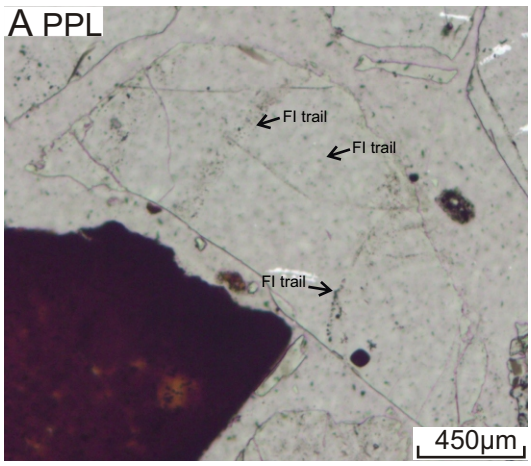

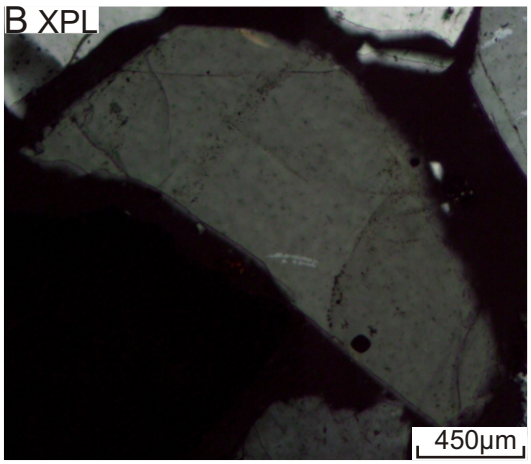

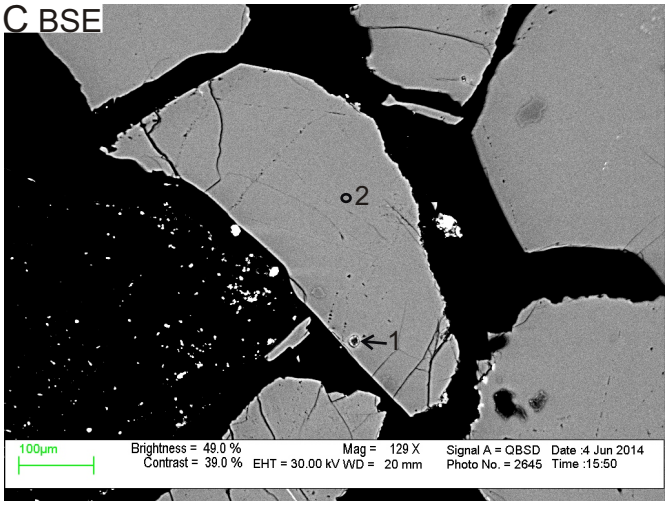

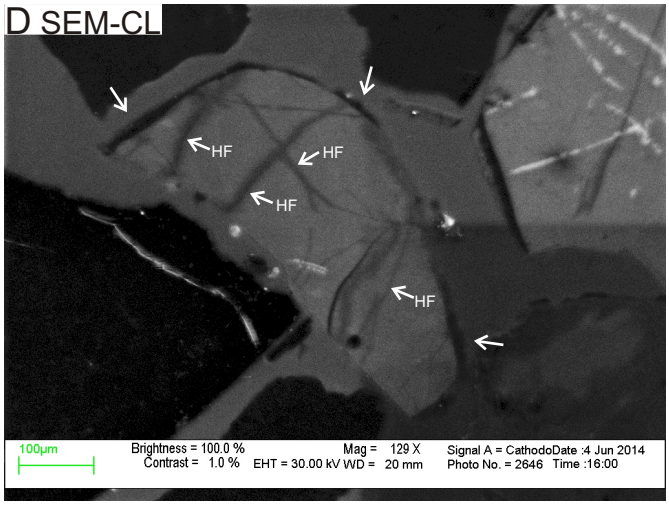

E EDS analyses

Pos#	Min. ID	SiO2	TiO2	Al2O3	FeO	K2O	Total	Actual total
1	Kfs	59.21	0.25	26.06	4.23	10.24	100	82
2	Qz	99.99					100	110

Figure 5A-35: Microphotos under ppl (A) and xpl (B), SEM-BSE image (C), SEM-CL image (D), and EDS analyses table (E) of quartz grain 35 in sample 3150. The grain is anhedral and angular monocrystalline with non-undulose extinction. Fluid inclusions are common; they are usually associated with secondary porosity and form trails along healed fractures (Fig. A). The grain contains a K-feldspar inclusion and is microfractured with a set of parallel fractures and a set of irregular fractures (Fig. C and D). Healed fractures (HF) are common (Fig. D). The dark areas indicated by arrows in Fig. D are overgrowth.

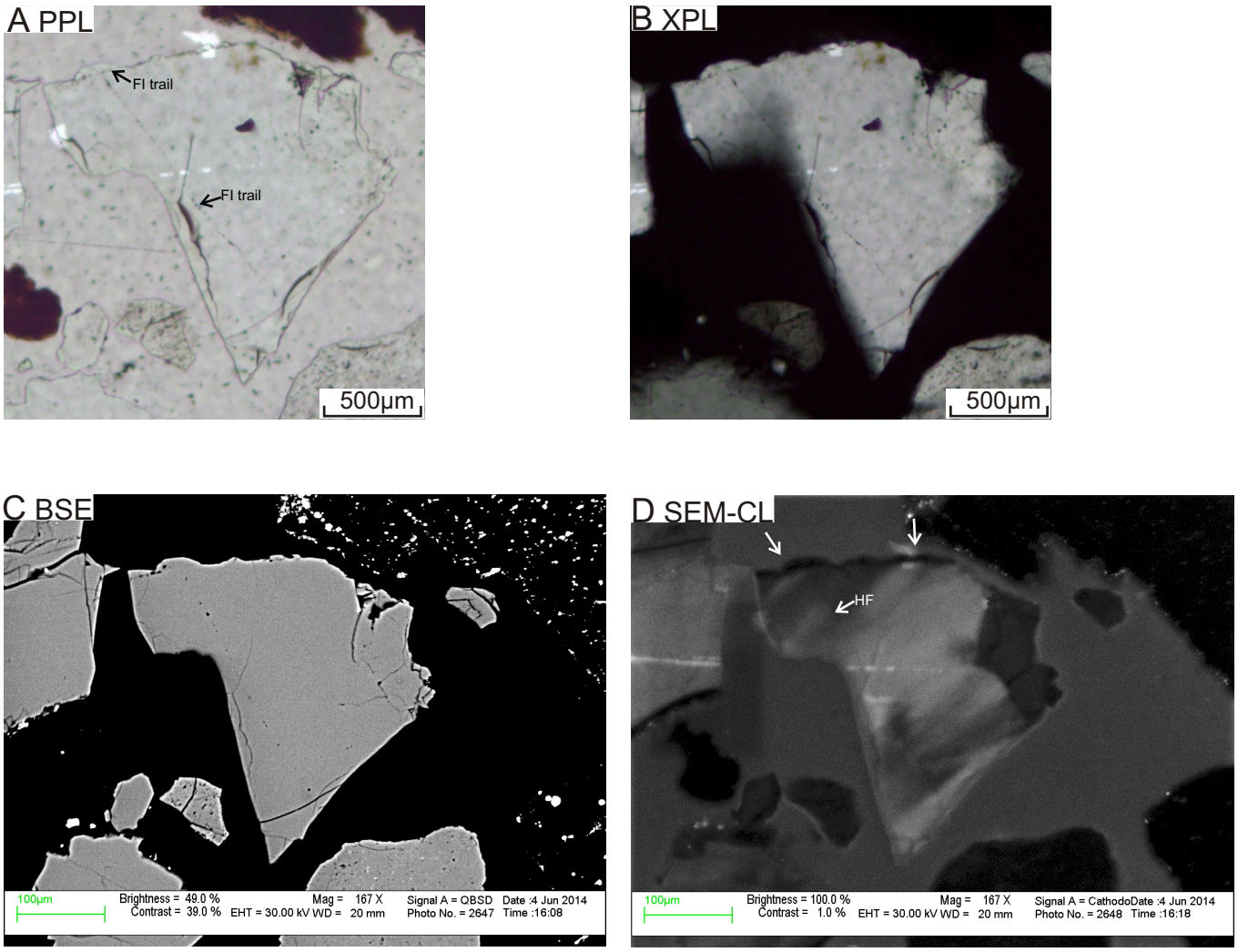

Figure 5A-36: Microphotos under ppl (A) and xpl (B), SEM-BSE image C, and SEM-CL image (D) of quartz grain 36 in sample 3150. The grain is anhedral and angular monocrystalline with strong undulose extinction. Fluid inclusions are present; they form trails along healed fractures and at the boundary between the detritral quartz and the overgrowth (Fig. A). The grain is microfractured with a set of irregular fractures (Fig. C and D). A few healed fractures (HF) can be seen in Fig. D. The dark areas indicated by arrows in Fig. D are overgrowth. The grain shows bright-CL streaky patches fabric and two distinct colours, bright-CL and dark-CL, in SEM-CL image.

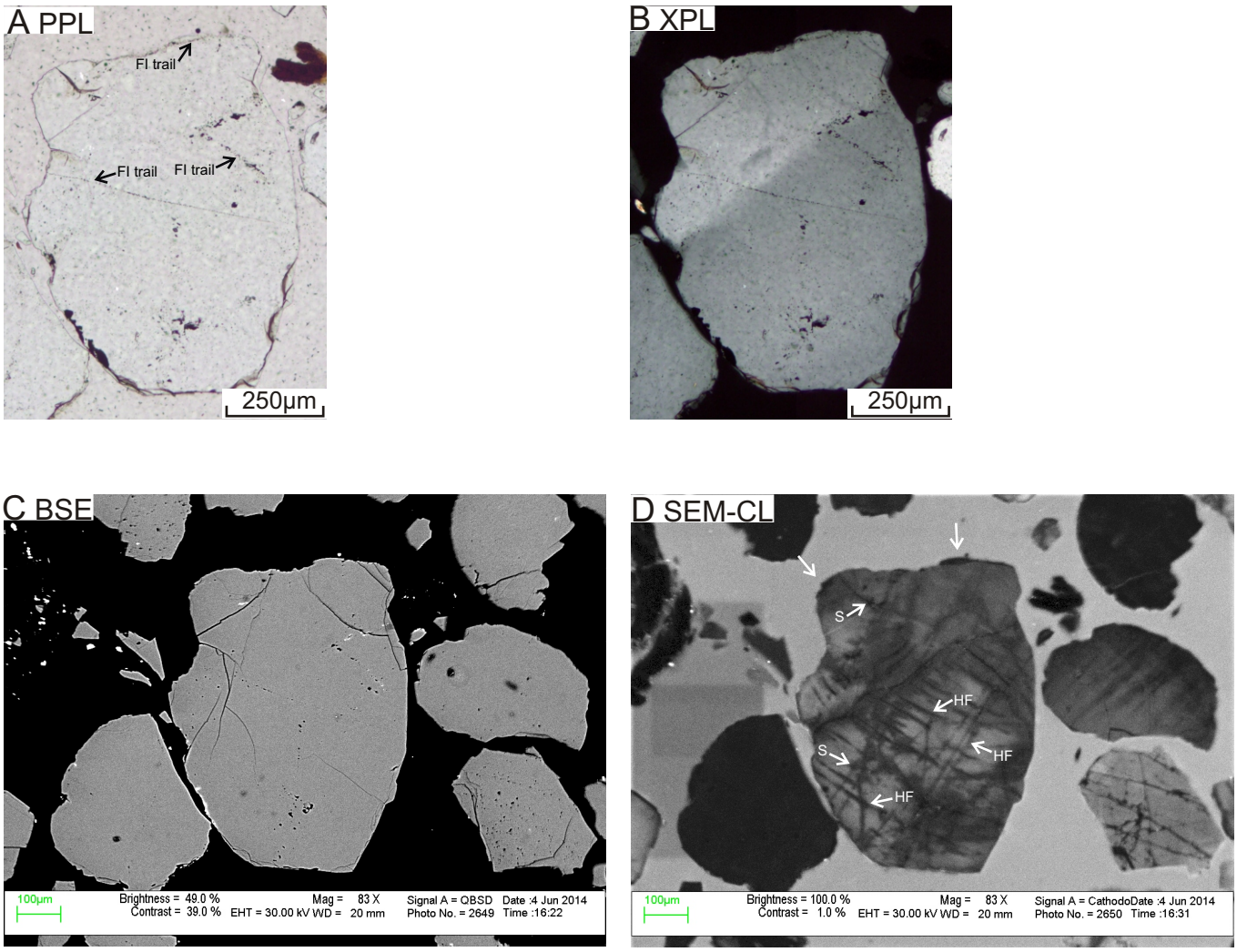

Figure 5A-37: Microphotos under ppl (A) and xpl (B), SEM-BSE image C, and SEM-CL image (D) of quartz grain 37 in sample 3150. The grain is anhedral and sub-rounded monocrystalline with strong undulose extinction. Fluid inclusions are common; they are usually associated with secondary porosity and form trails along healed fractures and at the boundary between the detritral quartz and the overgrowth (Fig. A). The grain is microfractured with two sets of parallel healed fractures crosscutting each other perpendicularly and a set of irregular, curved open fractures (Fig. C and D). Healed fractures (HF) and spiders (S) are common (Fig. D). The parallel healed fractures are probably caused by brittle deformation. The dark areas indicated by arrows in Fig. D are overgrowth. The grain shows bright-CL streaky patches fabric in SEM-CL image.

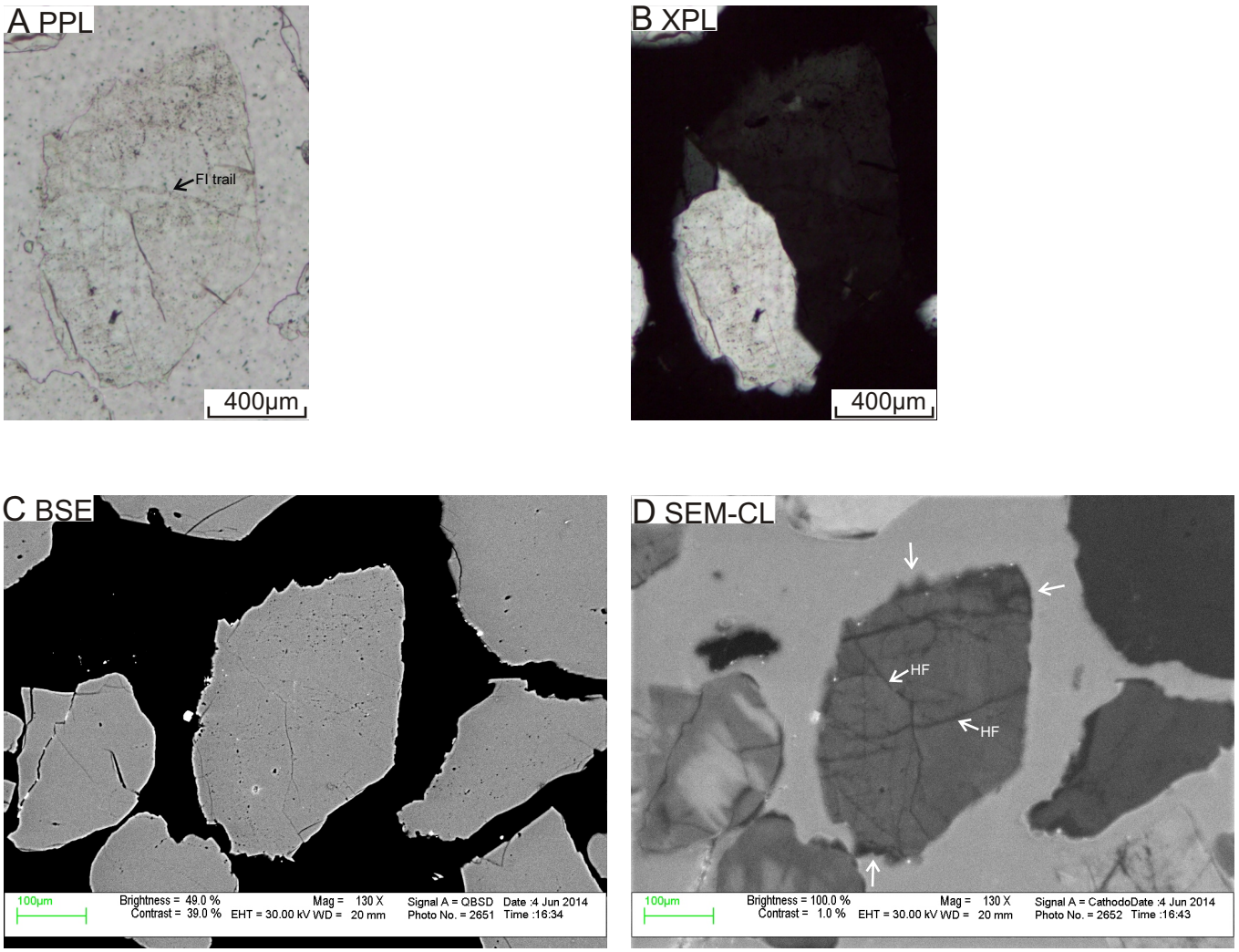

Figure 5A-38: Microphotos under ppl (A) and xpl (B), SEM-BSE image C, and SEM-CL image (D) of quartz grain 38 in sample 3150. The grain is anhedral and sub-angular polycrystalline (only a few sub-grains) with irregular margins and strong undulose extinction. Fluid inclusions are common; they are usually associated with secondary porosity and form trails along healed fractures (Fig. A). The grain is microfractured with a set of irregular fractures (Fig. C and D). Healed fractures (HF) are common (Fig. D). The dark areas indicated by arrows in Fig. D are overgrowth.

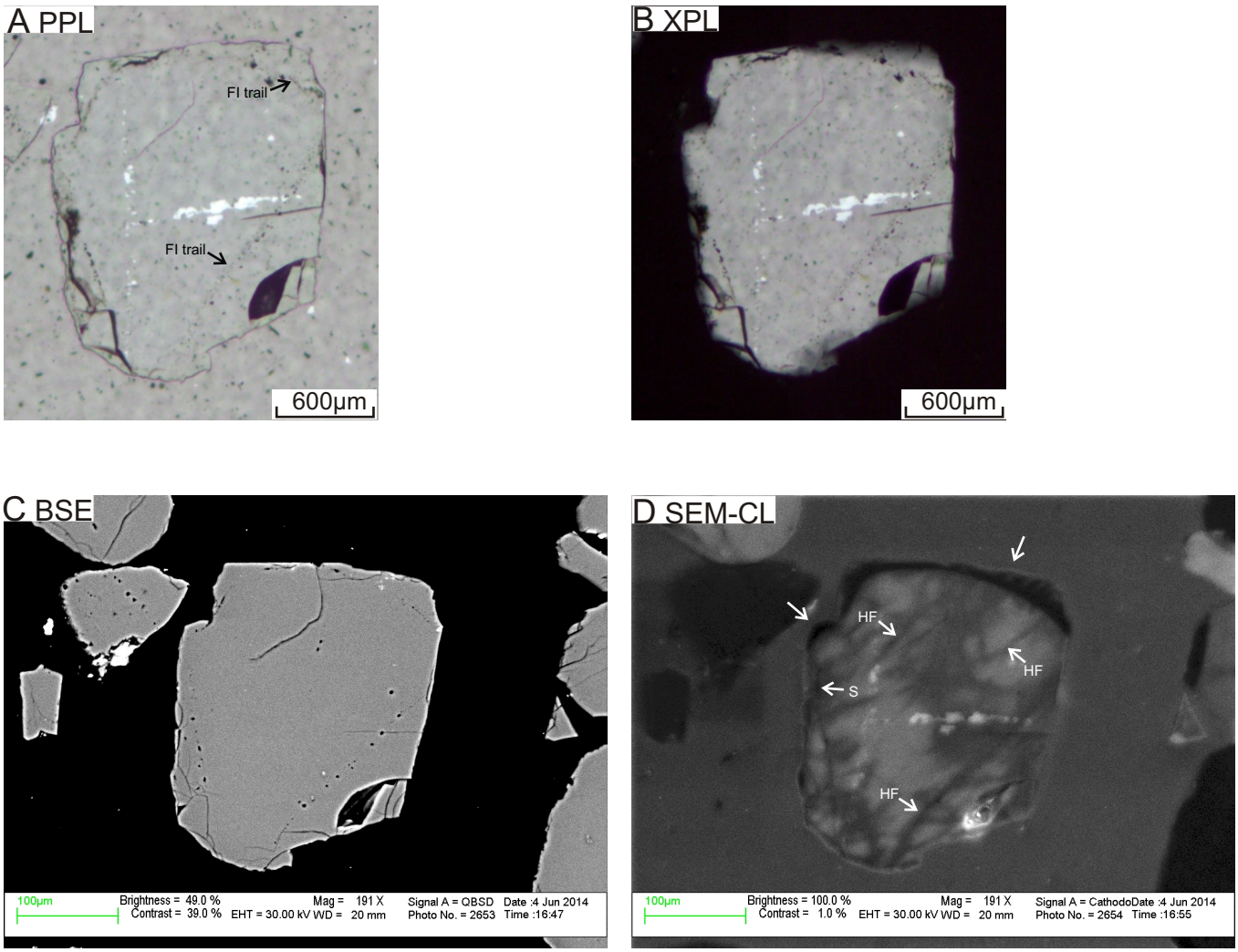

Figure 5A-39: Microphotos under ppl (A) and xpl (B), SEM-BSE image C, and SEM-CL image (D) of quartz grain 39 in sample 3150. The grain is anhedral and sub-rounded monocrystalline with strong undulose extinction. Fluid inclusions are common; they are usually associated with secondary porosity and form trails along healed fractures and at the boundary between the detritral quartz and the overgrowth (Fig. A). The grain is microfractured with a set of parallel fractures and a set of irregular fractures (Fig. C and D). Healed fractures (HF) and spiders (S) are common (Fig. D). The dark areas indicated by arrows in Fig. D are overgrowth. The grain shows bright-CL streaky patches fabric in SEM-CL image.

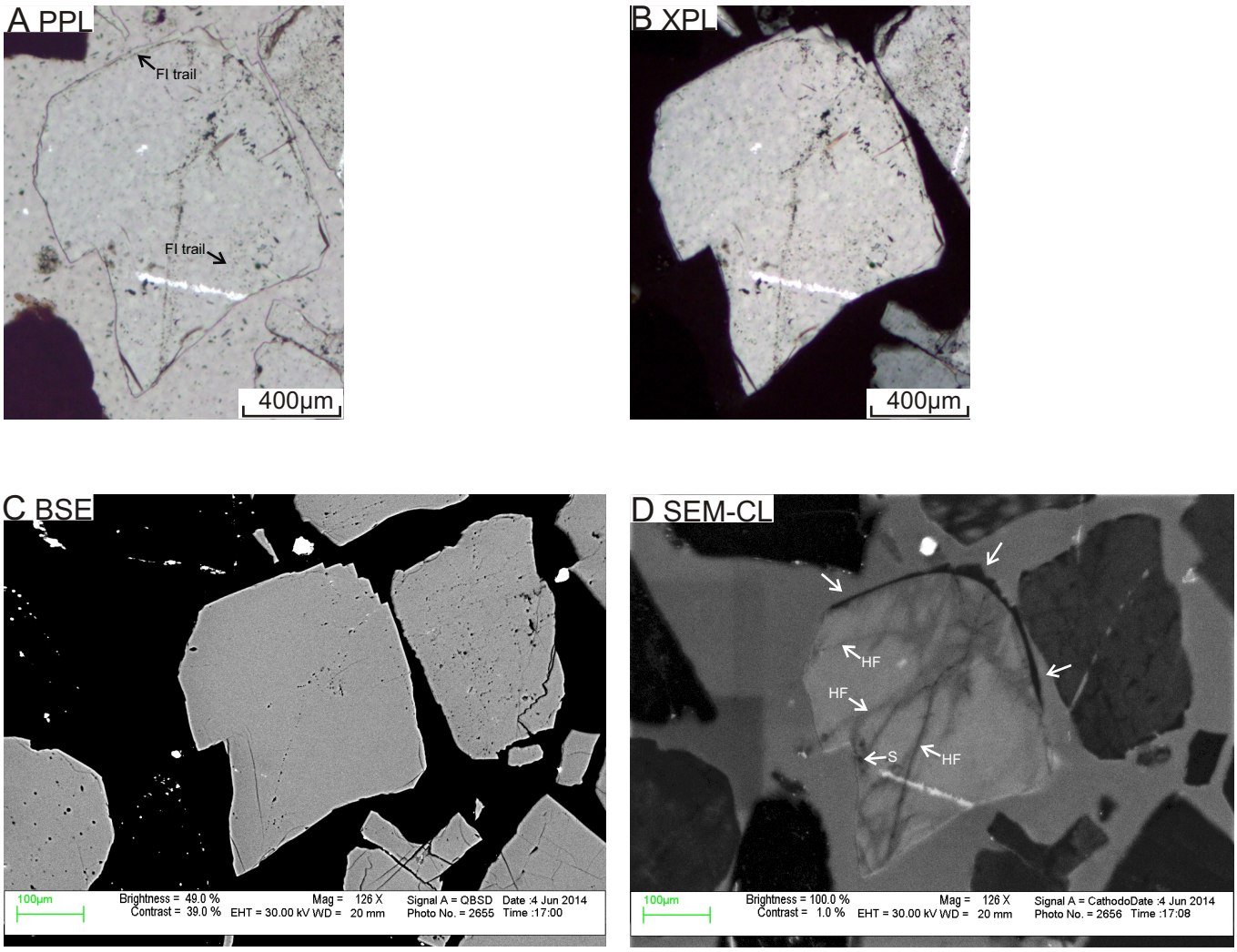

Figure 5A-40: Microphotos under ppl (A) and xpl (B), SEM-BSE image C, and SEM-CL image (D) of quartz grain 40 in sample 3150. The grain is anhedral and angular monocrystalline with non-undulose extinction. Fluid inclusions are common; they are usually associated with secondary porosity and form trails along healed fractures and at the boundary between the detritral quartz and the overgrowth (Fig. A). The grain is microfractured with a set of irregular fractures (Fig. C and D). Healed fractures (HF) and spiders (S) are common (Fig. D). The dark areas indicated by arrows in Fig. D are overgrowth. The grain shows bright-CL streaky patches fabric in SEM-CL image.

Appendix 5B: Hot cathodoluminescence (HCL) images and blue colour shift analyses of detrital quartz grains in sample 3150.

Notes:

1. All the grains with HCL images correspond to the same grain in SEM-CL images. In all the following organized HCL figures,

   Fig. A shows HCL image taken after 3 seconds;

   Fig. B shows HCL image taken after 12 seconds;

   Fig. C is the histogram of blue colour within the analysed quartz grain in Fig. A and B, where X axis is the intensity of blue colour indicated by the colour bar with values from 0-255 (0=no blue or "black", 255=blue), and Y axis indicates the pixel amount at different blue values;

   Fig. D is the statistical table of blue values within the analysed grain area, where SD corresponds to standard deviation.

2. To classify the blue colour, the following abbreviations are used:

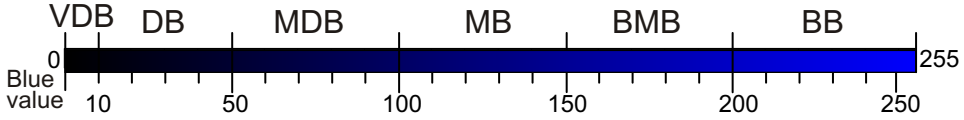

VDB: Very Dark Blue (0-10) **DB**: Dark Blue (11-50)

MDB: Medium Dark Blue (51-100) **MB**: Medium Blue (101-150)

BMB: Bright-Medium Blue (151-200) **BB**: Bright Blue (201-255)

3. To quantify the blue colour shift, the following criteria are used:

   Mean blue value change **< 5**: **No** colour shift

   5 ≤Mean blue value change **< 15**: **Slight** colour shift

   15 ≤Mean blue value change **< 30**: **Moderate** colour shift

   Mean blue value change ≥**30**: **Strong** colour shift

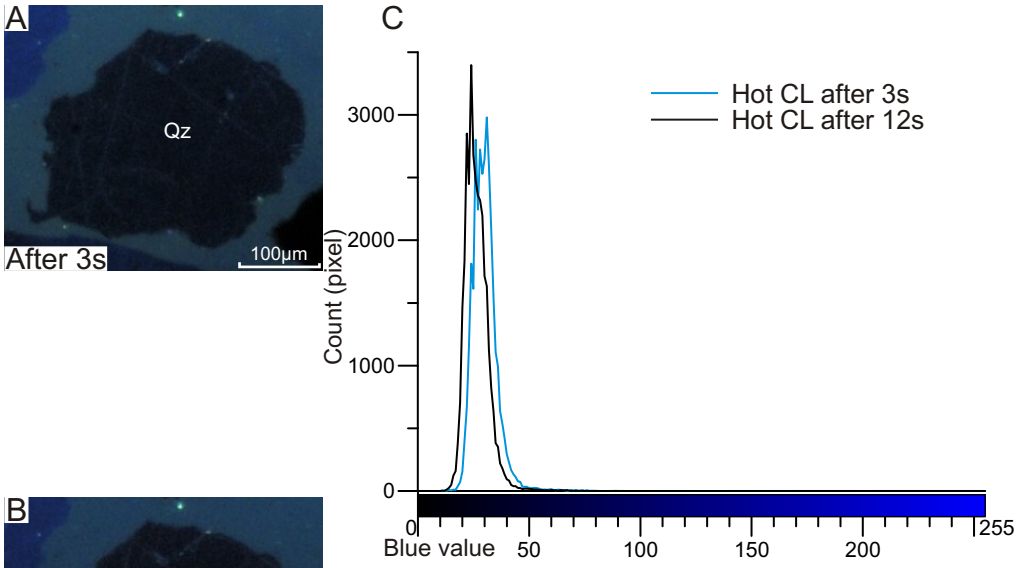

Figure 5B-1: Grain 1. The grain shows no colour shift.

D

Blue value	Min	Max	Mode	Mean	SD
After 3s	11	89	31	30	5.5
After 12s	11	76	24	26	5.3

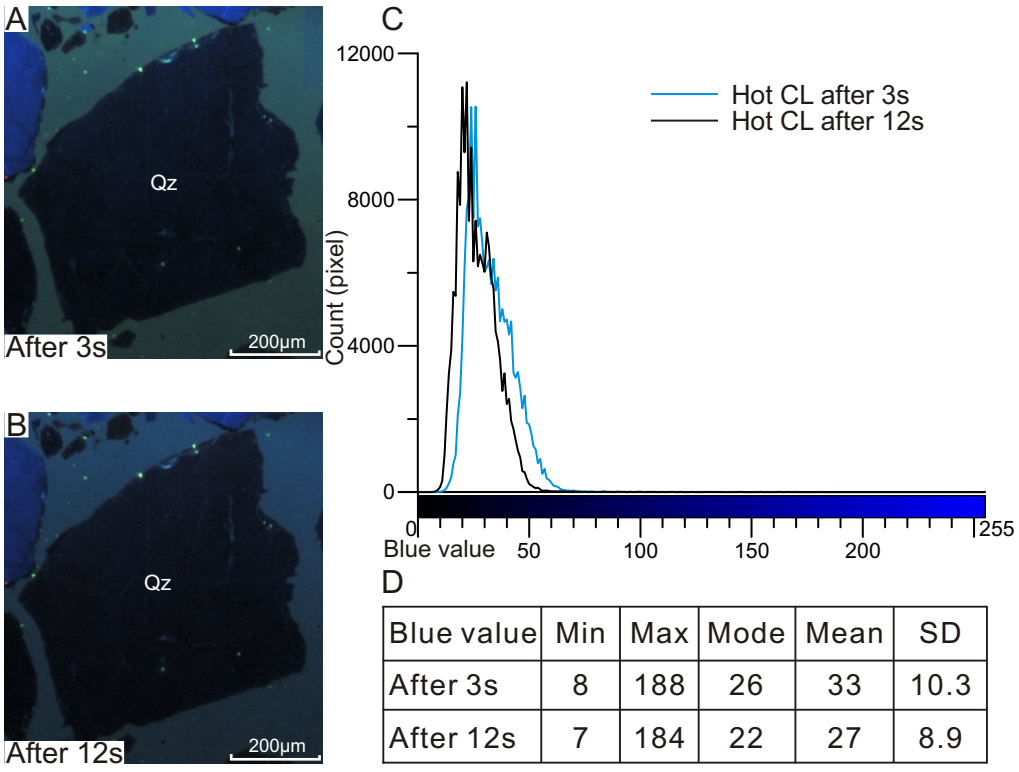

Figure 5B-2: Grain 2. The grain shows slight colour shift.

D

Blue value	Min	Max	Mode	Mean	SD
After 3s	8	188	26	33	10.3
After 12s	7	184	22	27	8.9

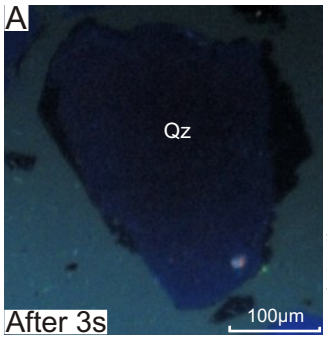

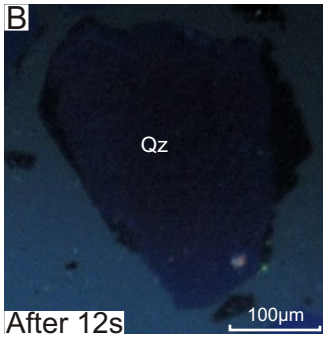

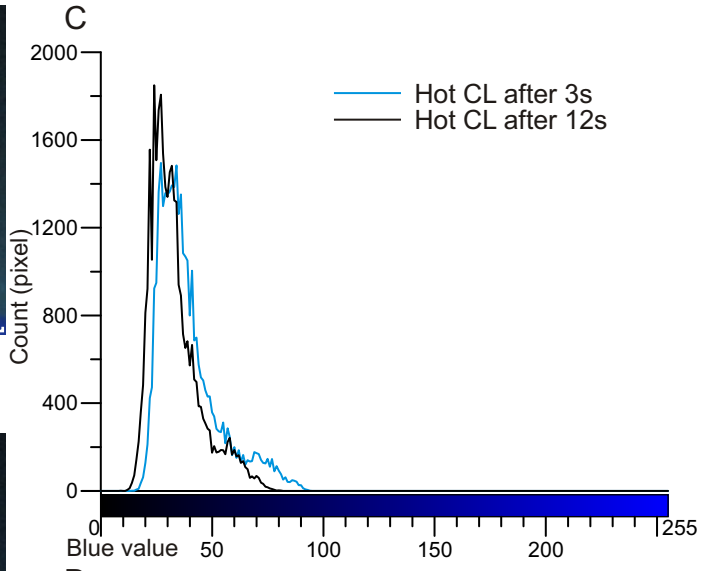

Figure 5B-3: Grain 3. The grain shows slight colour shift.

D

Blue value	Min	Max	Mode	Mean	SD
After 3s	14	94	27	39	14
After 12s	9	81	24	33	11.3

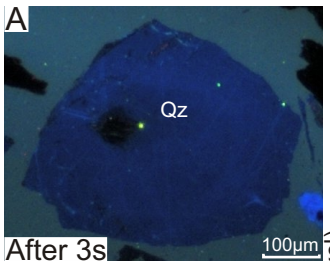

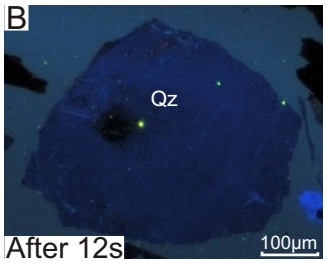

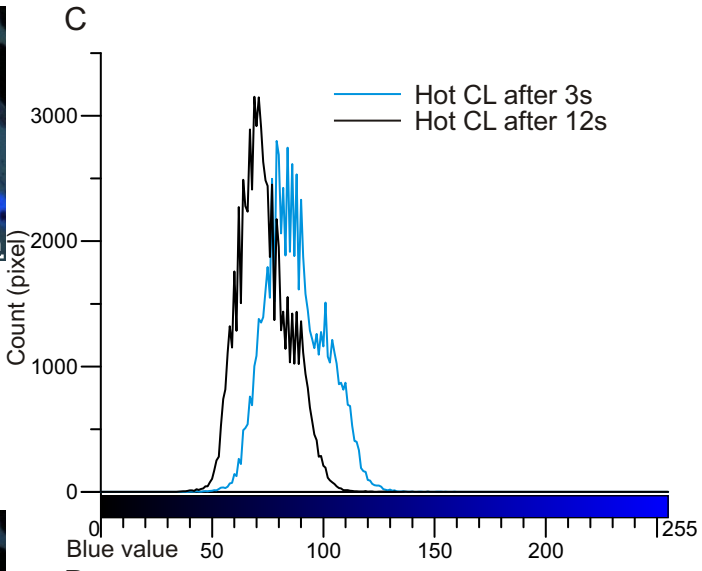

Figure 5B-4: Grain 4. The grain shows slight colour shift.

D

Blue value	Min	Max	Mode	Mean	SD
After 3s	40	159	70	88	13.3
After 12s	35	147	69	74	11.2

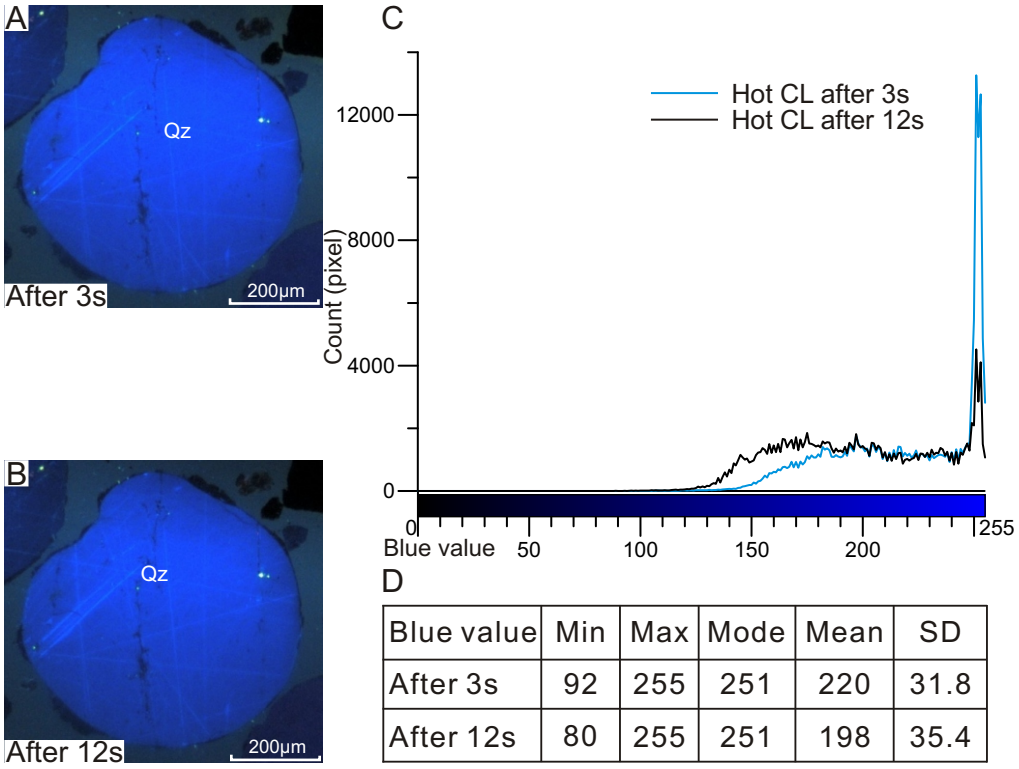

D

Blue value	Min	Max	Mode	Mean	SD
After 3s	92	255	251	220	31.8
After 12s	80	255	251	198	35.4

Figure 5B-5: Grain 5. The grain shows moderate colour shift.

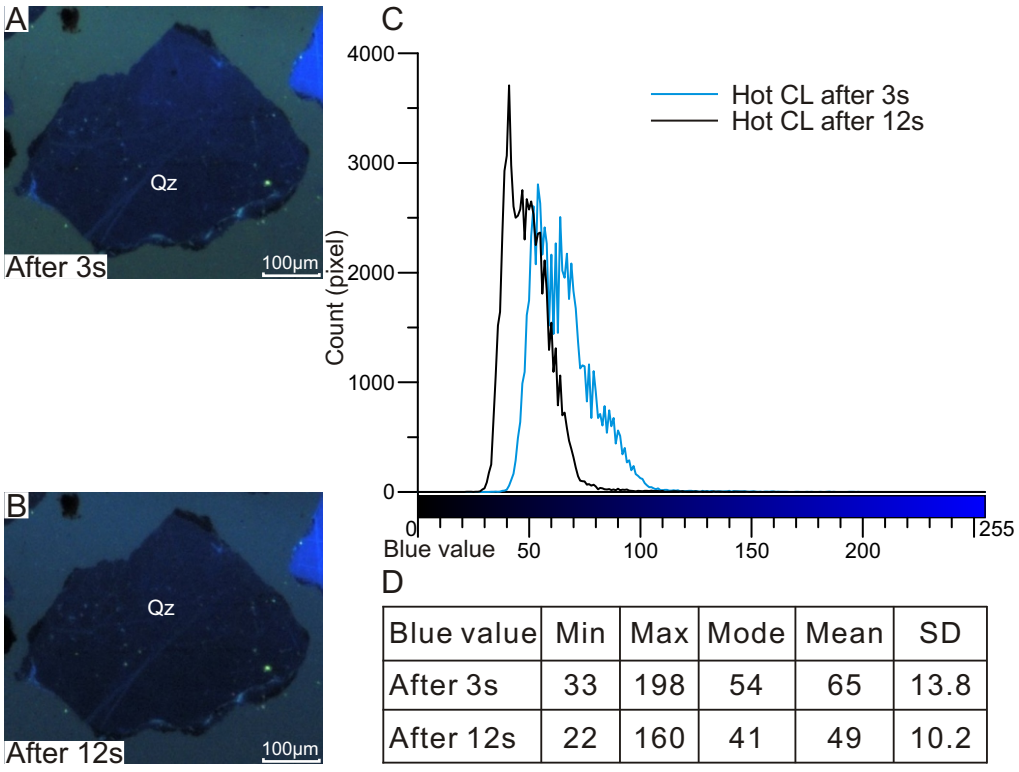

D

Blue value	Min	Max	Mode	Mean	SD
After 3s	33	198	54	65	13.8
After 12s	22	160	41	49	10.2

Figure 5B-6: Grain 6. The grain shows moderate colour shift.

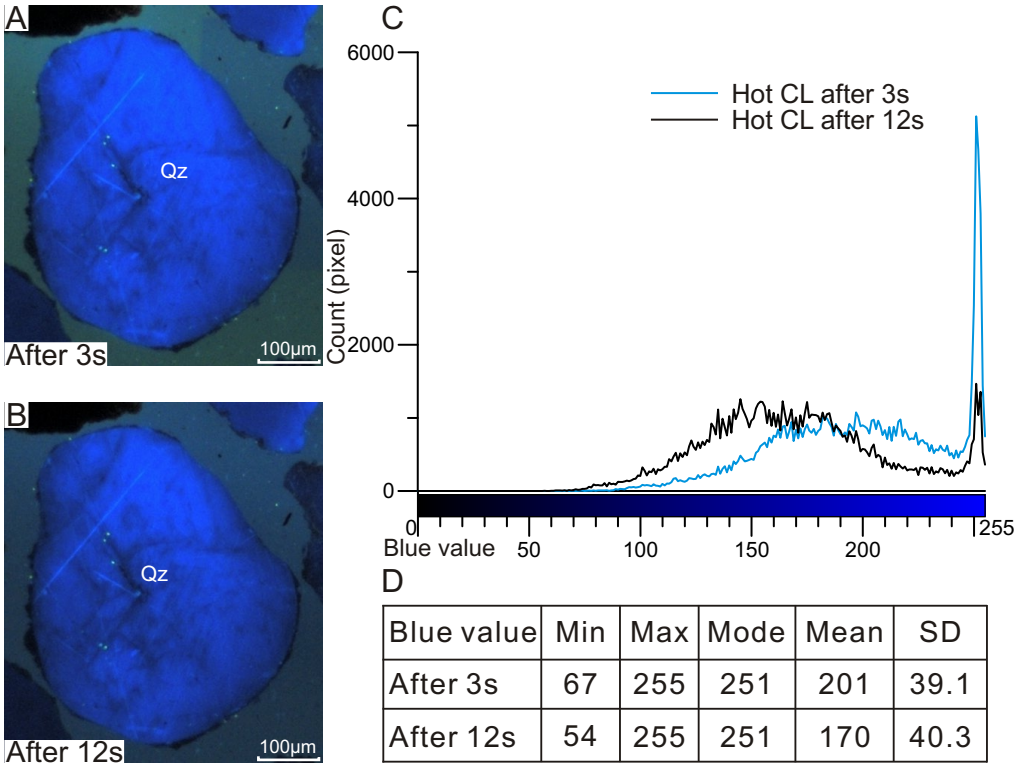

D

Blue value	Min	Max	Mode	Mean	SD
After 3s	67	255	251	201	39.1
After 12s	54	255	251	170	40.3

Figure 5B-7: Grain 7. The grain shows strong colour shift.

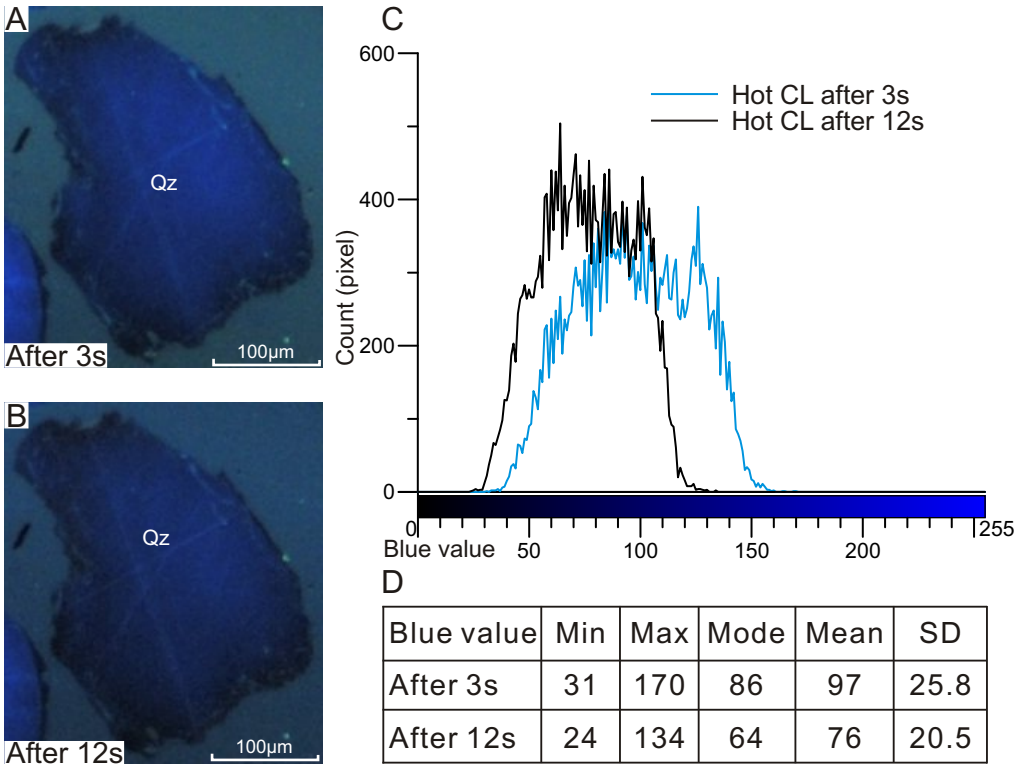

D

Blue value	Min	Max	Mode	Mean	SD
After 3s	31	170	86	97	25.8
After 12s	24	134	64	76	20.5

Figure 5B-8: Grain 8. The grain shows moderate colour shift.

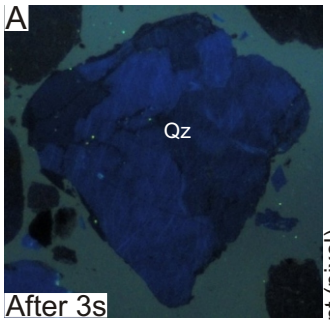

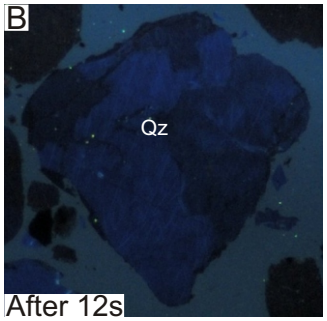

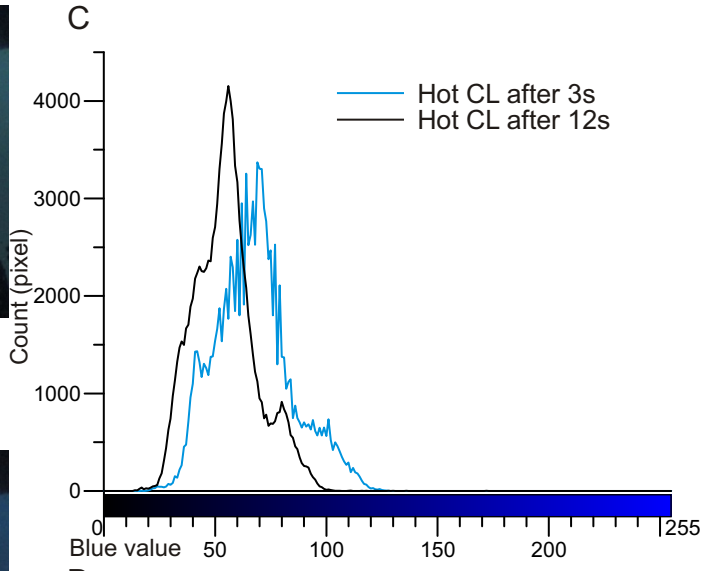

D

Blue value	Min	Max	Mode	Mean	SD
After 3s	17	128	69	67	17.3
After 12s	14	172	56	55	14.1

Figure 5B-9: Grain 9. The grain shows slight colour shift.

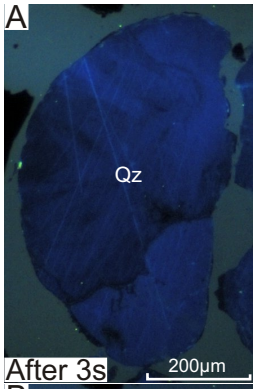

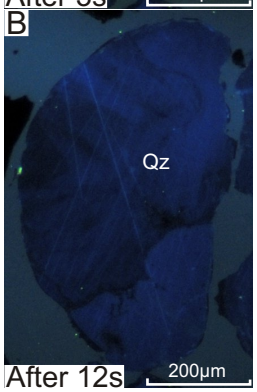

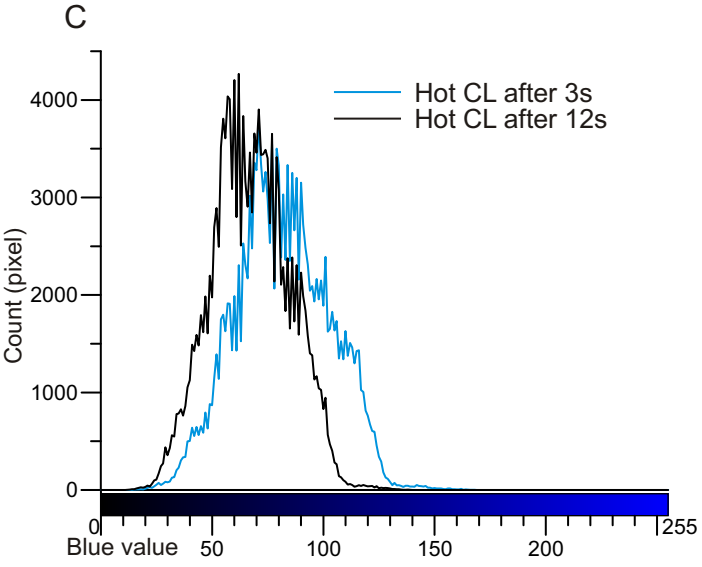

D

Blue value	Min	Max	Mode	Mean	SD
After 3s	15	168	71	82	20.9
After 12s	12	139	62	67	17.4

Figure 5B-10: Grain 10. The grain shows slight colour shift.

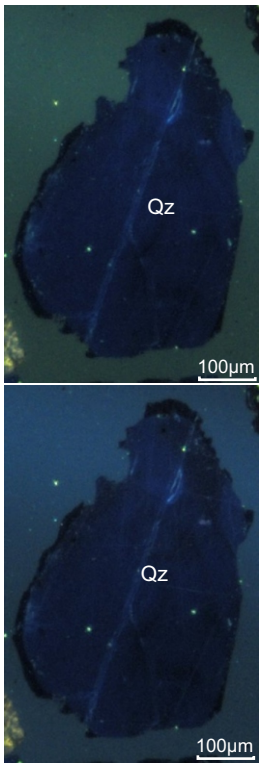

C

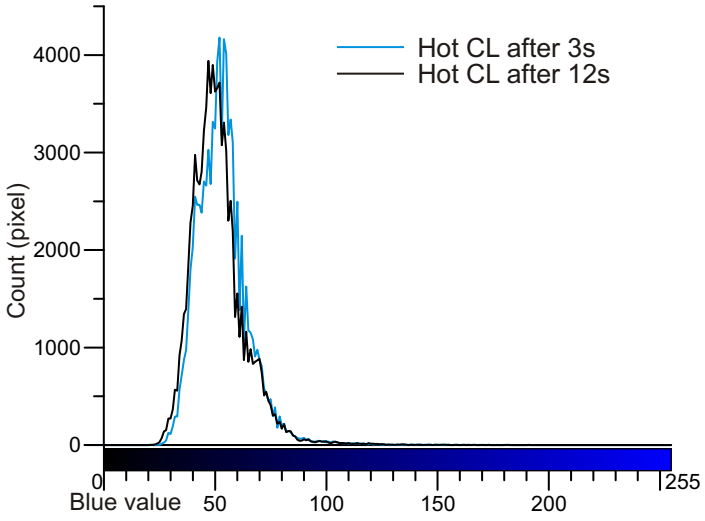

D

Blue value	Min	Max	Mode	Mean	SD
After 3s	21	180	52	53	11.7
After 12s	21	191	47	51	12.2

Figure 5B-11: Grain 11. The grain shows no colour shift.

A

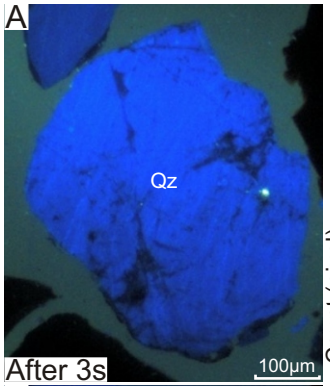

B

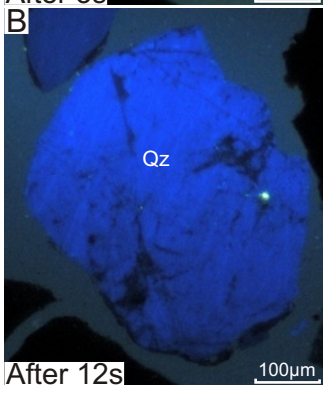

C

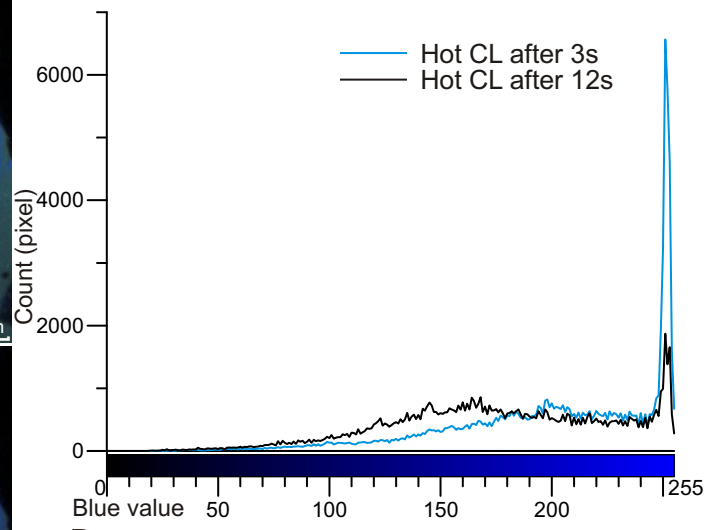

D

Blue value	Min	Max	Mode	Mean	SD
After 3s	24	255	251	204	46.8
After 12s	19	255	251	177	49.5

Figure 5B-12: Grain 12. The grain shows moderate colour shift.

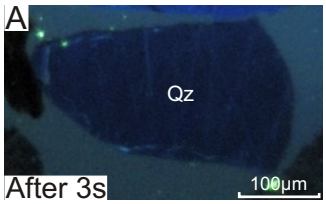

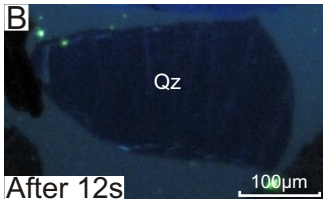

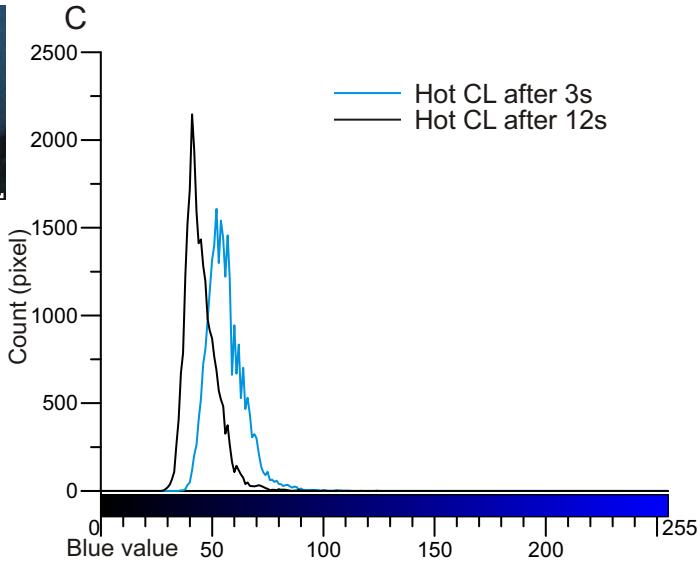

D

Blue value	Min	Max	Mode	Mean	SD
After 3s	36	124	52	56	8.3
After 12s	28	108	41	45	7.1

Figure 5B-13: Grain 13. The grain shows slight colour shift.

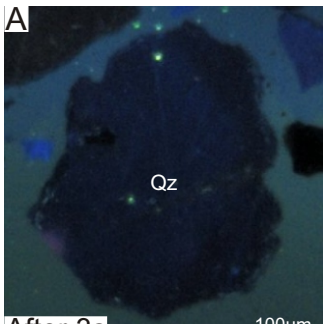

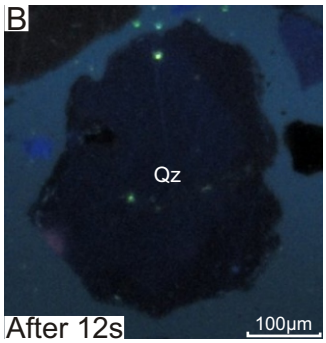

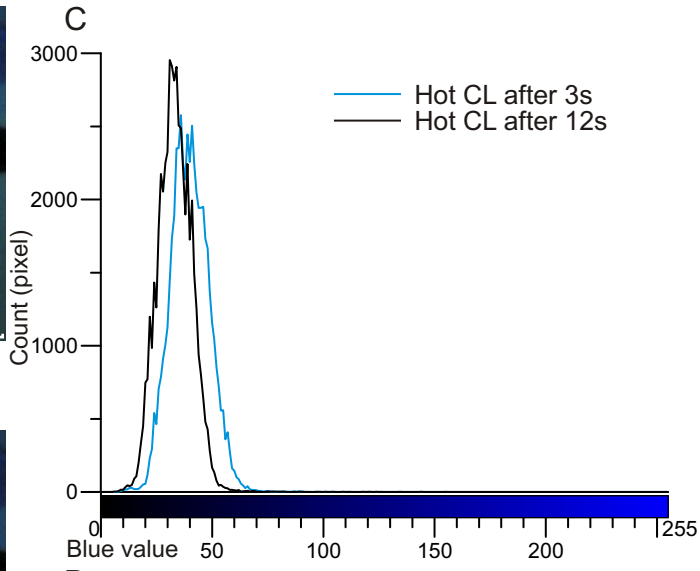

D

Blue value	Min	Max	Mode	Mean	SD
After 3s	8	155	36	40	8.5
After 12s	6	144	31	33	7.6

Figure 5B-14: Grain 14. The grain shows slight colour shift.

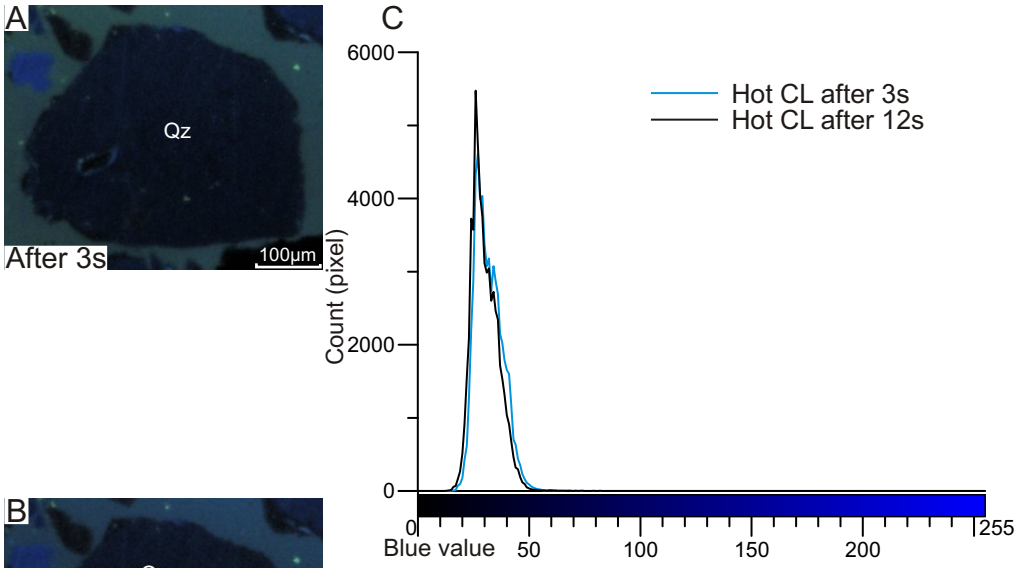

Figure 5B-15: Grain 15. The grain shows no colour shift.

D

Blue value	Min	Max	Mode	Mean	SD
After 3s	14	81	27	32	6.1
After 12s	11	86	26	30	5.9

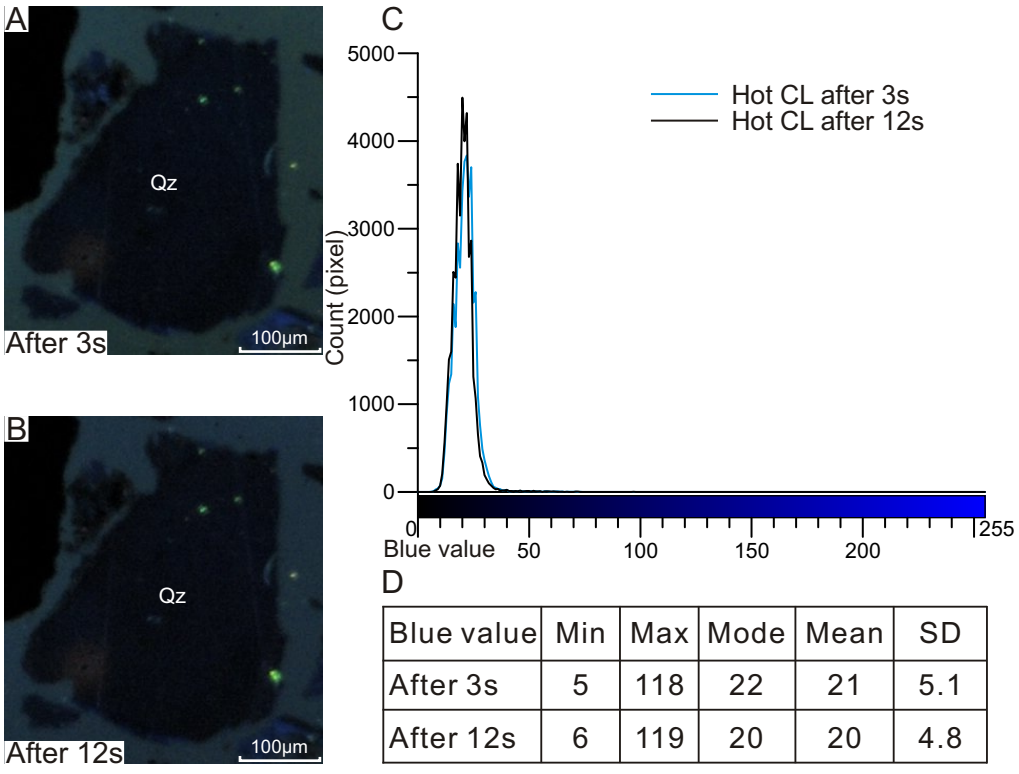

Figure 5B-16: Grain 16. The grain shows no colour shift.

D

Blue value	Min	Max	Mode	Mean	SD
After 3s	5	118	22	21	5.1
After 12s	6	119	20	20	4.8

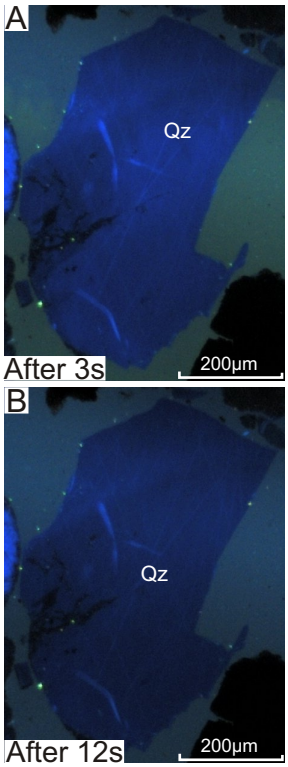

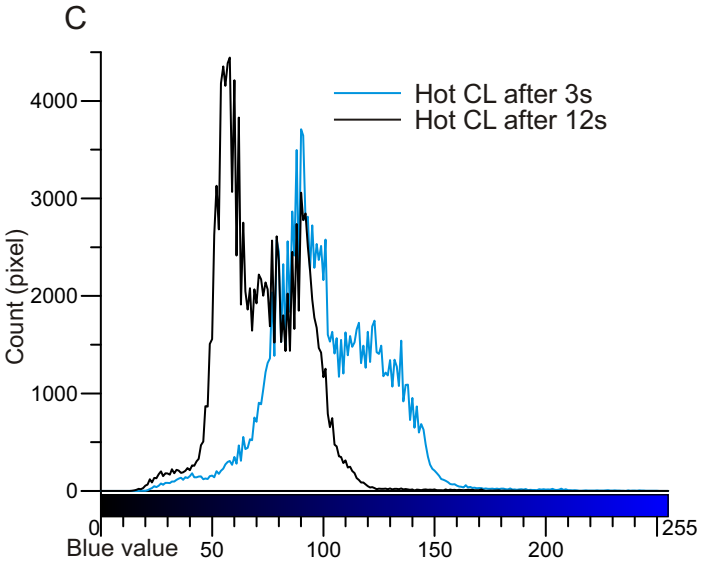

D

Blue value	Min	Max	Mode	Mean	SD
After 3s	18	250	90	101	24.8
After 12s	14	193	58	72	18.8

Figure 5B-17: Grain 17. The grain shows moderate colour shift.

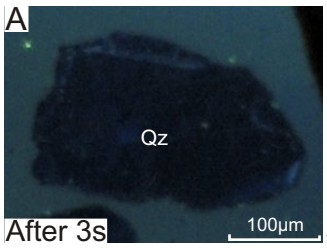

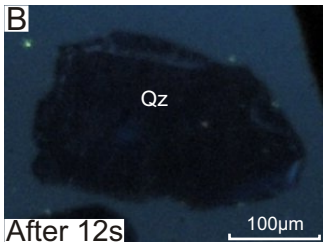

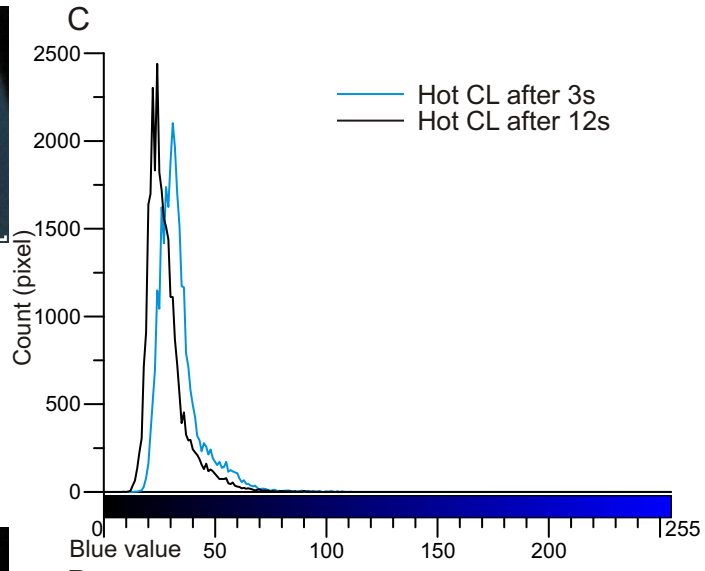

D

Blue value	Min	Max	Mode	Mean	SD
After 3s	14	111	31	34	9.7
After 12s	9	97	24	28	8.8

Figure 5B-18: Grain 18. The grain shows slight colour shift.

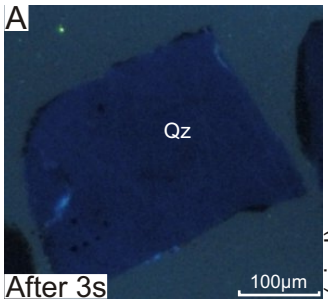

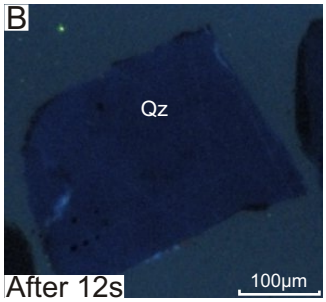

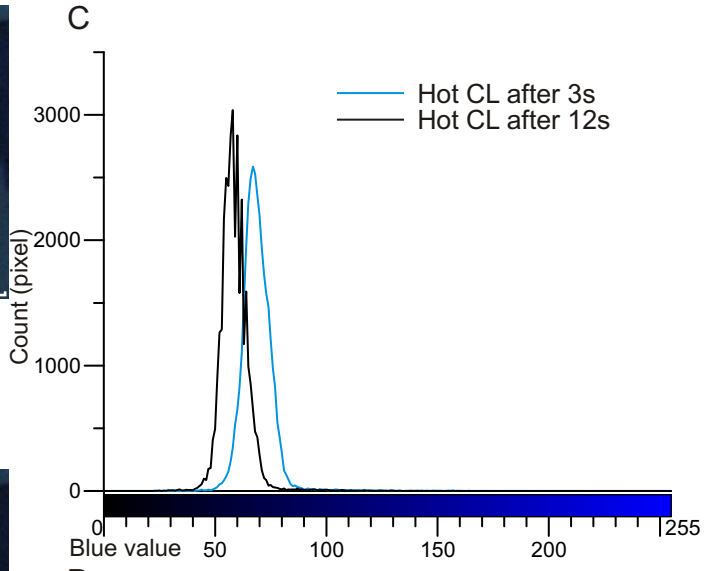

Figure 5B-19: Grain 19. The grain shows slight colour shift.

D

Blue value	Min	Max	Mode	Mean	SD
After 3s	37	164	67	69	7.2
After 12s	23	133	58	59	6.5





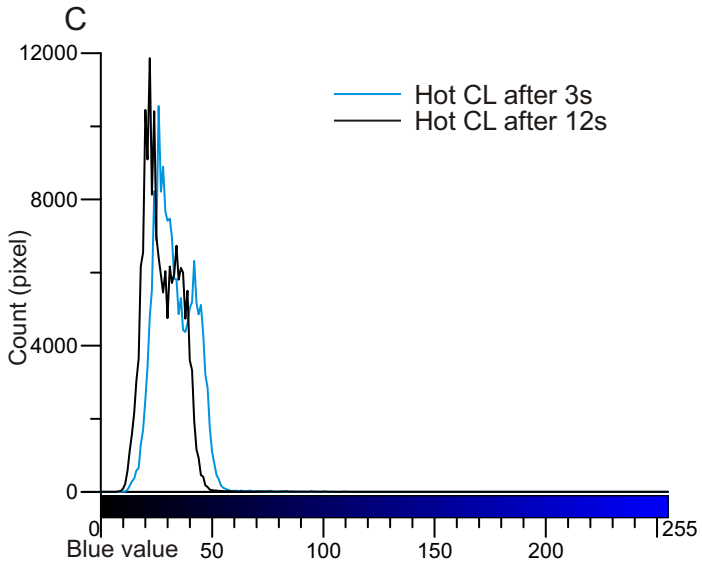

Figure 5B-20: Grain 20. The grain shows slight colour shift.

D

Blue value	Min	Max	Mode	Mean	SD
After 3s	10	116	26	33	8.6
After 12s	8	128	22	28	8.1

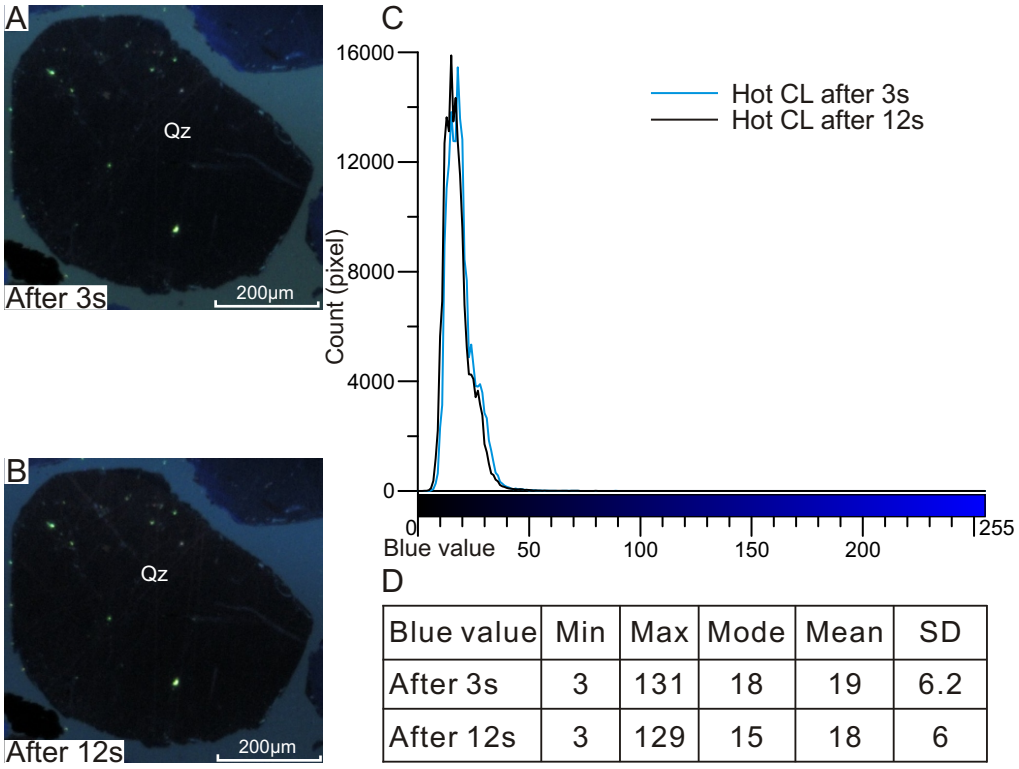

Figure 5B-21: Grain 21. The grain shows no colour shift.

D

Blue value	Min	Max	Mode	Mean	SD
After 3s	3	131	18	19	6.2
After 12s	3	129	15	18	6

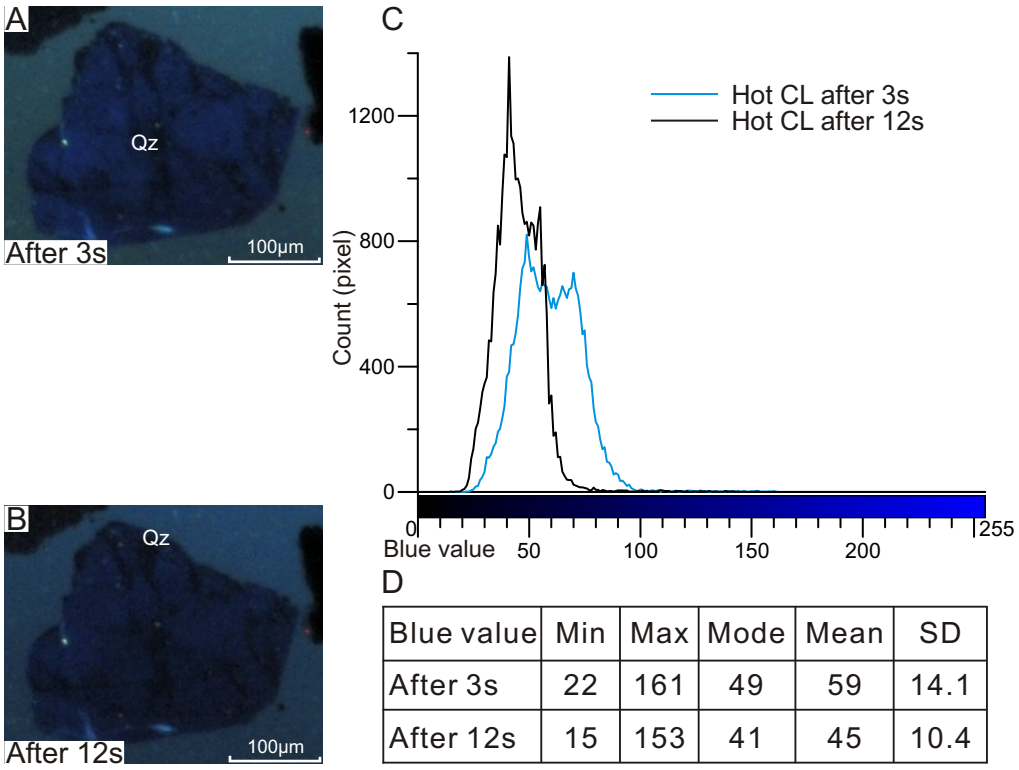

Figure 5B-22: Grain 22. The grain shows slight colour shift.

D

Blue value	Min	Max	Mode	Mean	SD
After 3s	22	161	49	59	14.1
After 12s	15	153	41	45	10.4

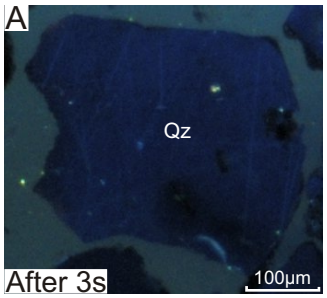

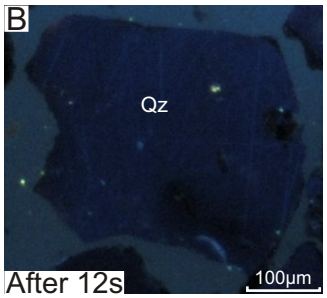

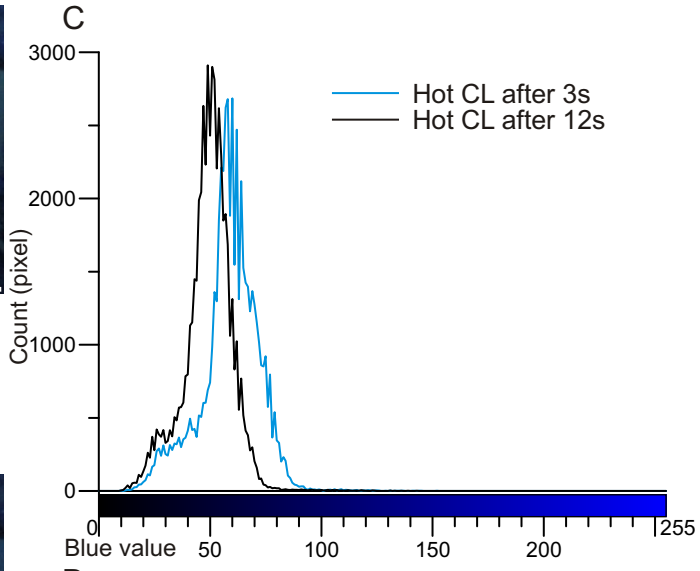

D

Blue value	Min	Max	Mode	Mean	SD
After 3s	10	152	60	59	13.1
After 12s	10	143	90	49	10.9

Figure 5B-23: Grain 23. The grain shows slight colour shift.

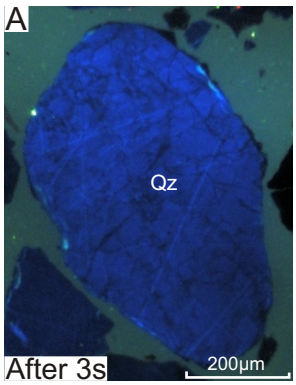

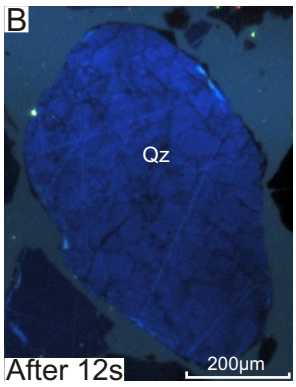

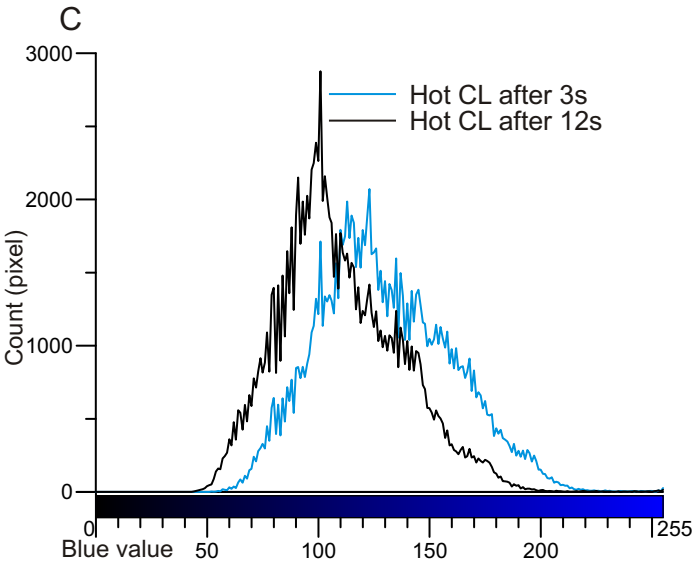

D

Blue value	Min	Max	Mode	Mean	SD
After 3s	52	255	123	130	29.9
After 12s	44	255	101	110	27.3

Figure 5B-24: Grain 24. The grain shows moderate colour shift.

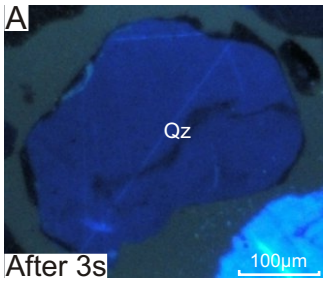

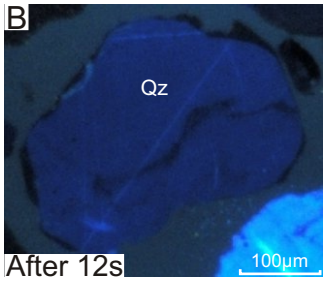

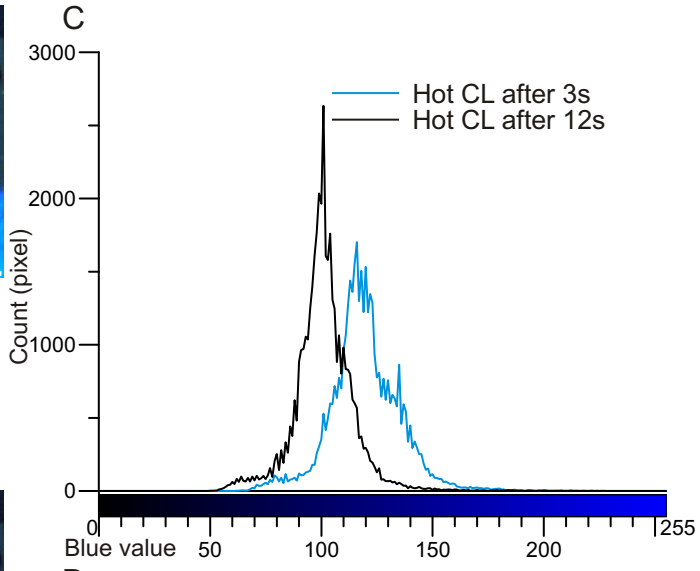

Figure 5B-25: Grain 25. The grain shows moderate colour shift.

D

Blue value	Min	Max	Mode	Mean	SD
After 3s	62	227	116	120	16
After 12s	50	200	101	101	13.2

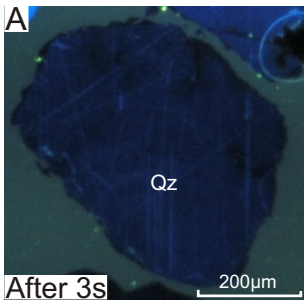

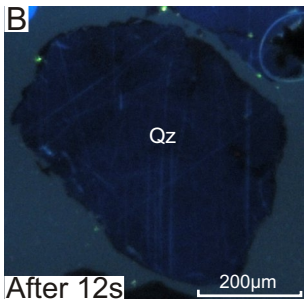

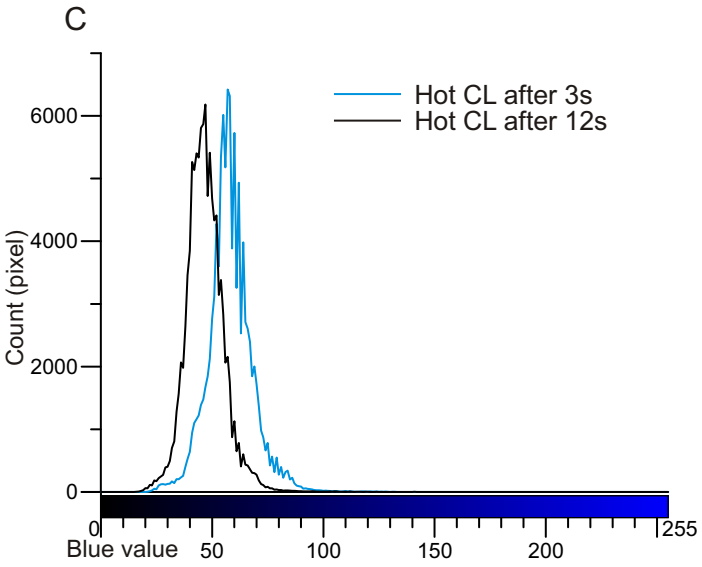

Figure 5B-26: Grain 26. The grain shows slight colour shift.

D

Blue value	Min	Max	Mode	Mean	SD
After 3s	18	133	57	58	10.1
After 12s	13	147	47	47	8.6

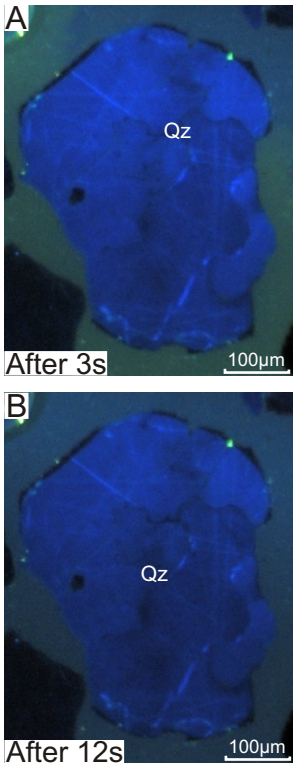

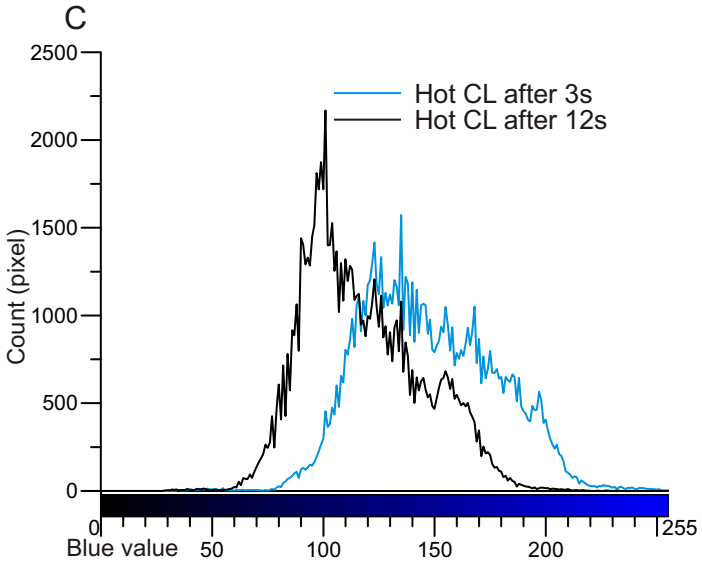

D

Blue value	Min	Max	Mode	Mean	SD
After 3s	32	255	135	147	29.8
After 12s	29	238	101	118	26.6

Figure 5B-27: Grain 27. The grain shows moderate colour shift.

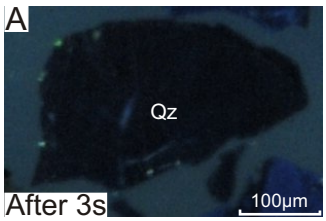

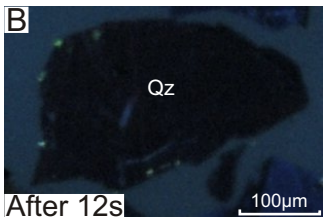

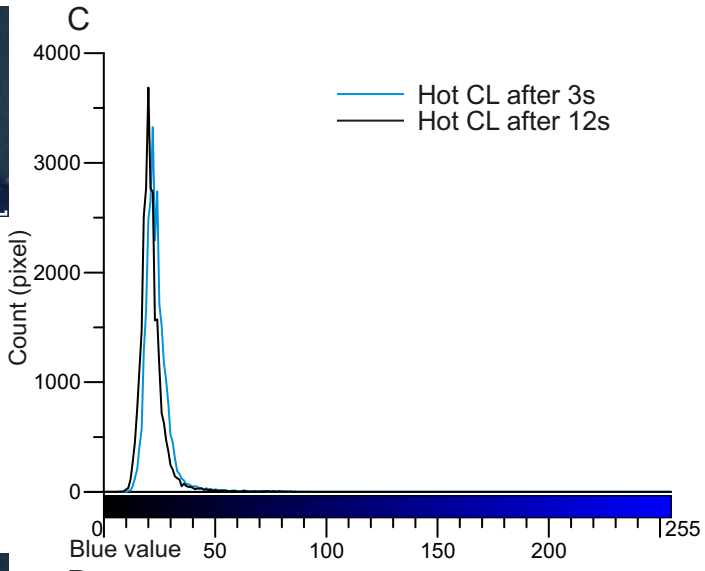

D

Blue value	Min	Max	Mode	Mean	SD
After 3s	11	92	22	24	6.2
After 12s	7	84	20	22	5.9

Figure 5B-28: Grain 28. The grain shows no colour shift.

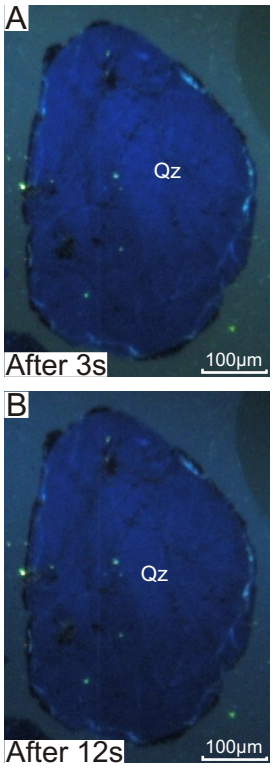

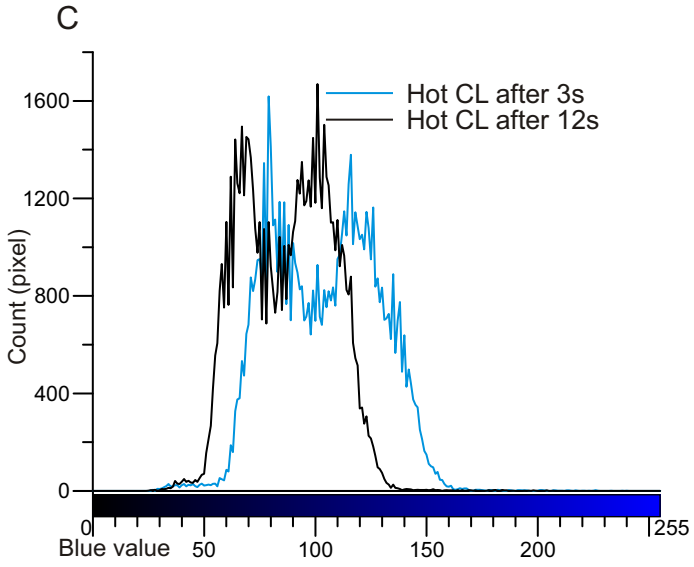

D

Blue value	Min	Max	Mode	Mean	SD
After 3s	26	240	79	104	23.9
After 12s	25	207	101	87	19.9

Figure 5B-29: Grain 29. The grain shows moderate colour shift.

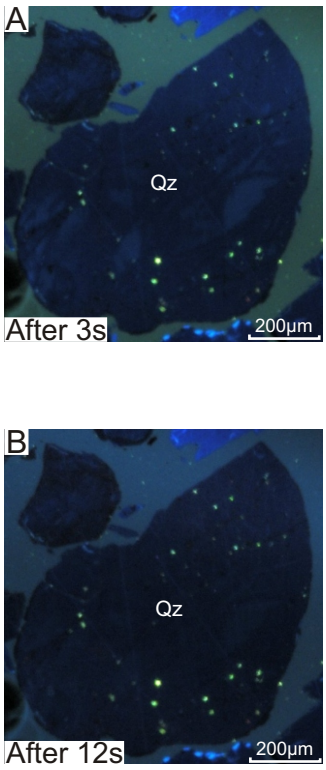

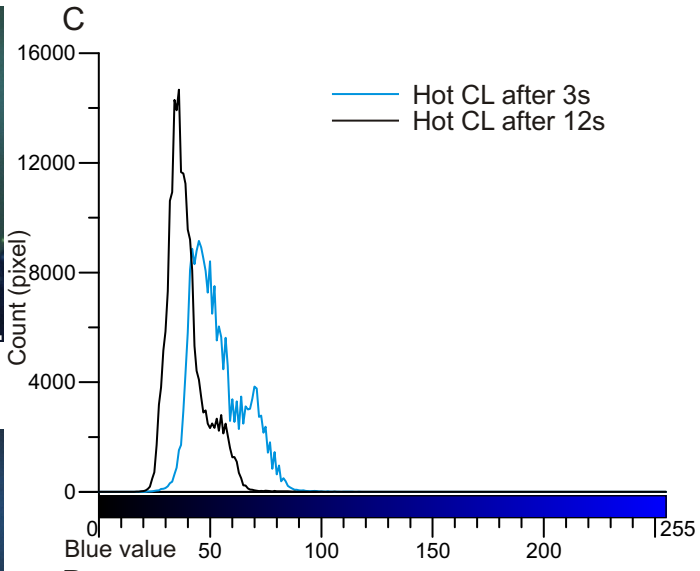

D

Blue value	Min	Max	Mode	Mean	SD
After 3s	18	231	45	53	11.8
After 12s	15	229	36	39	8.8

Figure 5B-30: Grain 30. The grain shows slight colour shift.

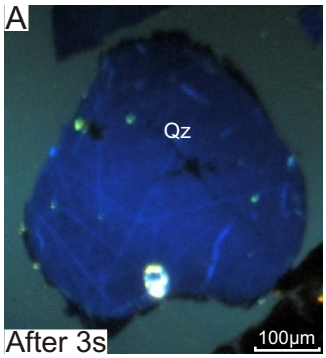

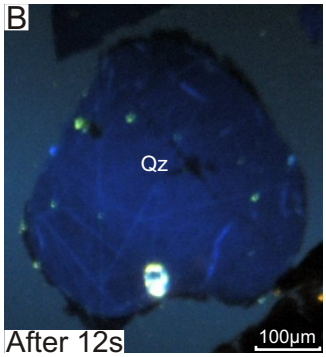

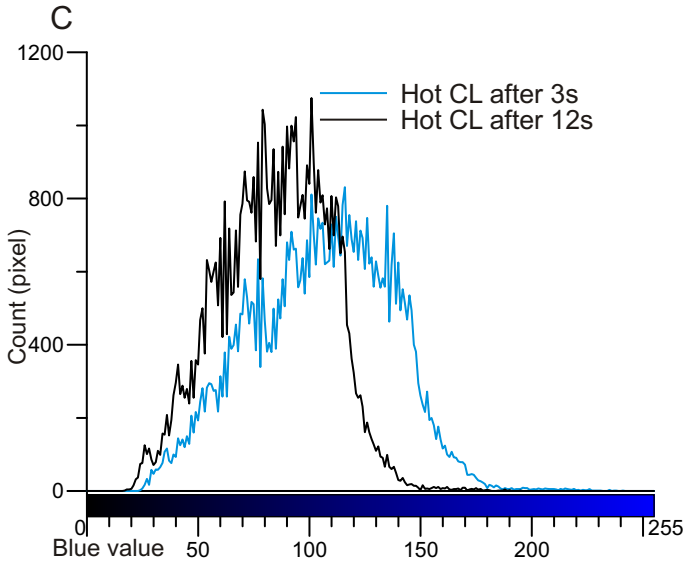

D

Blue value	Min	Max	Mode	Mean	SD
After 3s	24	241	116	105	31.3
After 12s	17	195	101	84	24.5

Figure 5B-31: Grain 31. The grain shows moderate colour shift.

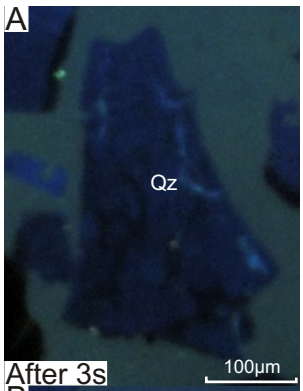

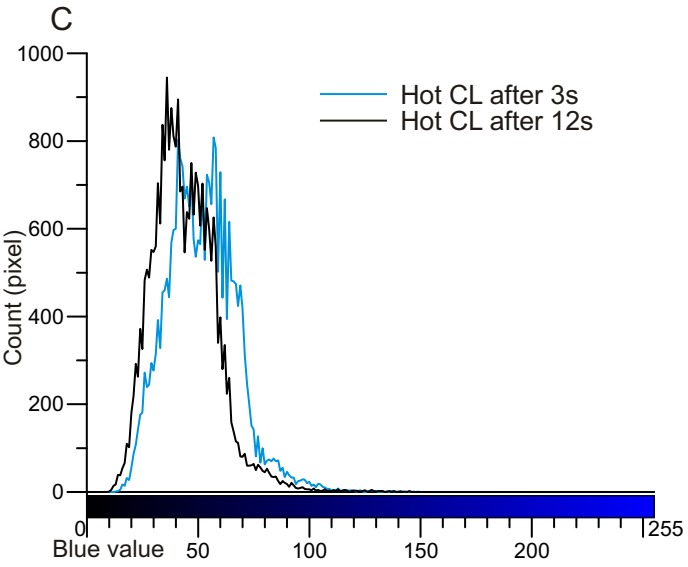

D

Blue value	Min	Max	Mode	Mean	SD
After 3s	13	149	57	52	15.6
After 12s	10	145	36	44	14.4

Figure 5B-32: Grain 32. The grain shows slight colour shift.

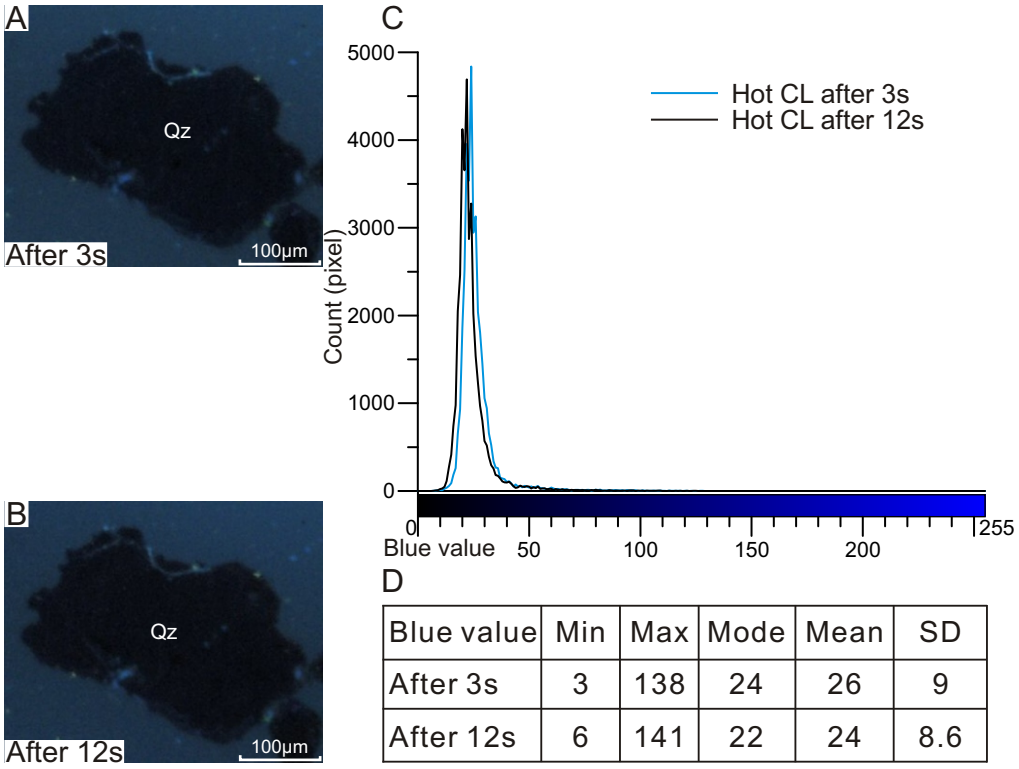

D

Blue value	Min	Max	Mode	Mean	SD
After 3s	3	138	24	26	9
After 12s	6	141	22	24	8.6

Figure 5B-33: Grain 33. The grain shows no colour shift.

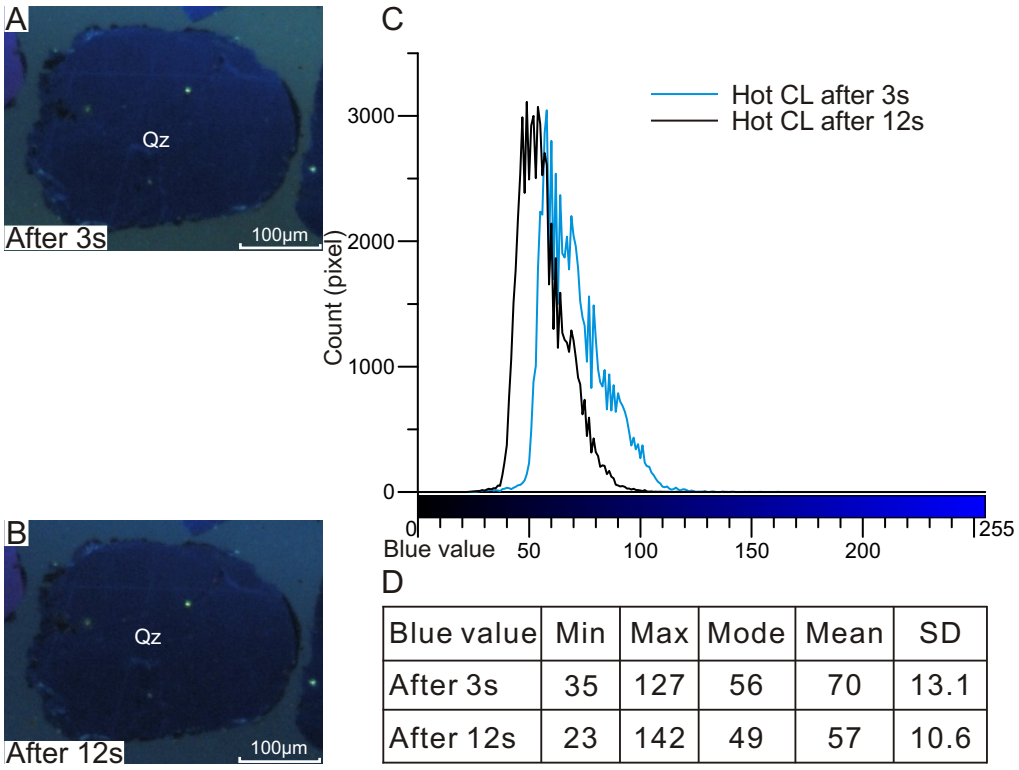

D

Blue value	Min	Max	Mode	Mean	SD
After 3s	35	127	56	70	13.1
After 12s	23	142	49	57	10.6

Figure 5B-34: Grain 34. The grain shows slight colour shift.

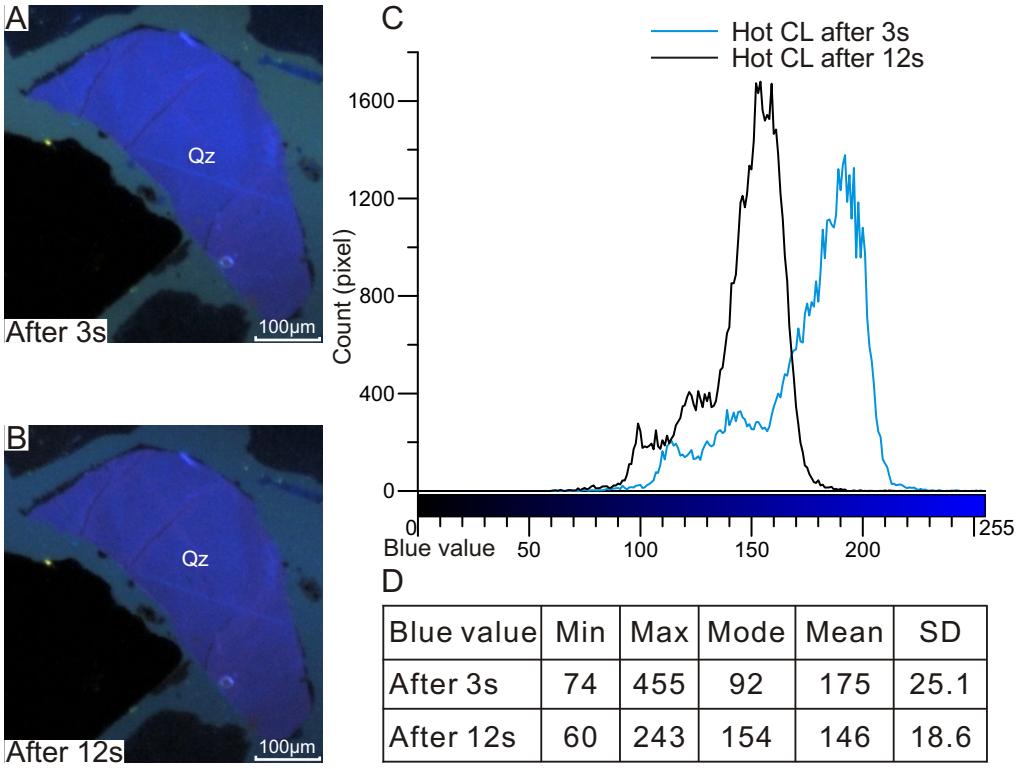

D

Blue value	Min	Max	Mode	Mean	SD
After 3s	74	455	92	175	25.1
After 12s	60	243	154	146	18.6

Figure 5B-35: Grain 35. The grain shows moderate colour shift.

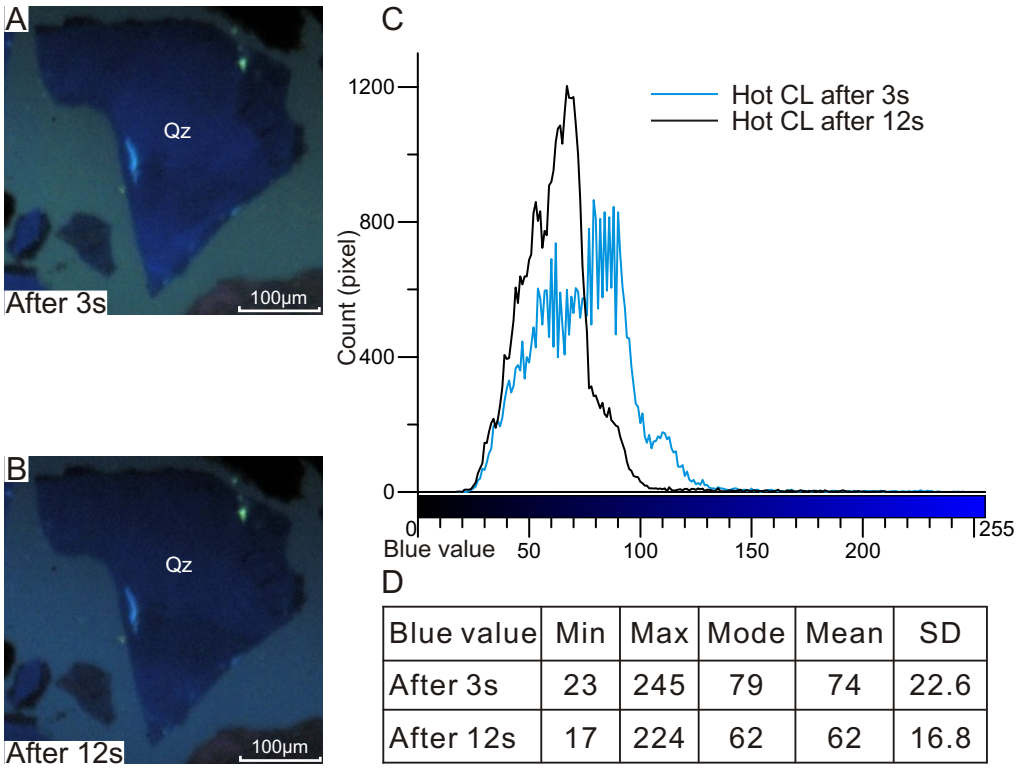

D

Blue value	Min	Max	Mode	Mean	SD
After 3s	23	245	79	74	22.6
After 12s	17	224	62	62	16.8

Figure 5B-36: Grain 36. The grain shows slight colour shift.

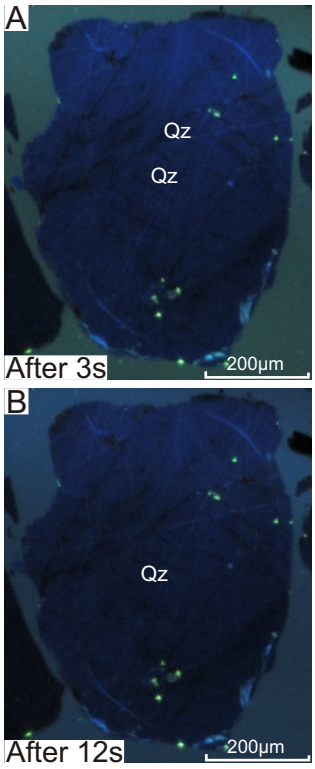

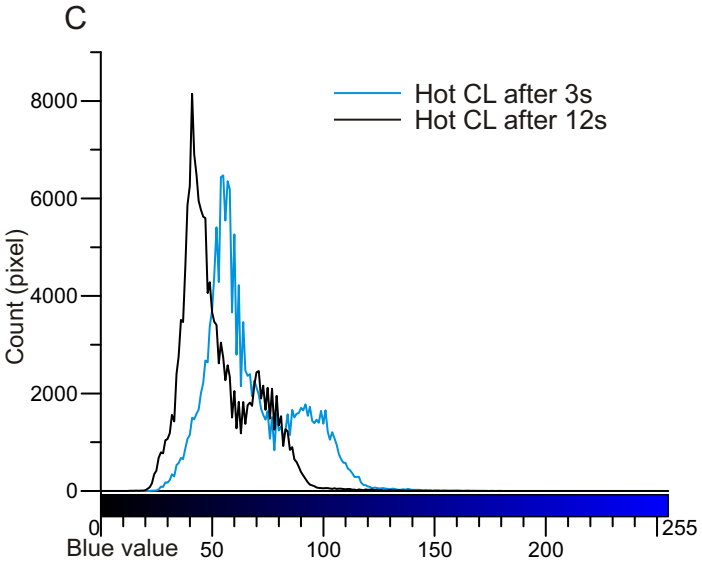

D

Blue value	Min	Max	Mode	Mean	SD
After 3s	21	194	55	67	20.2
After 12s	12	179	41	53	16.2

Figure 5B-37: Grain 37. The grain shows slight colour shift.

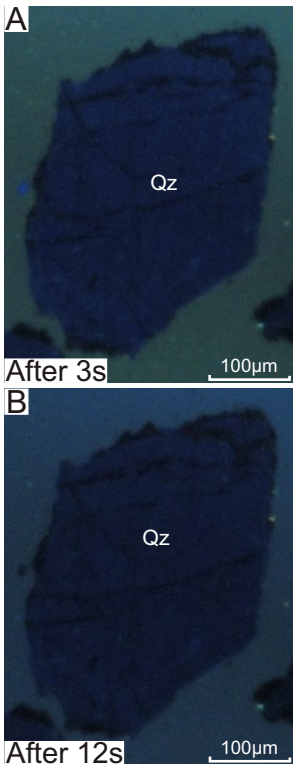

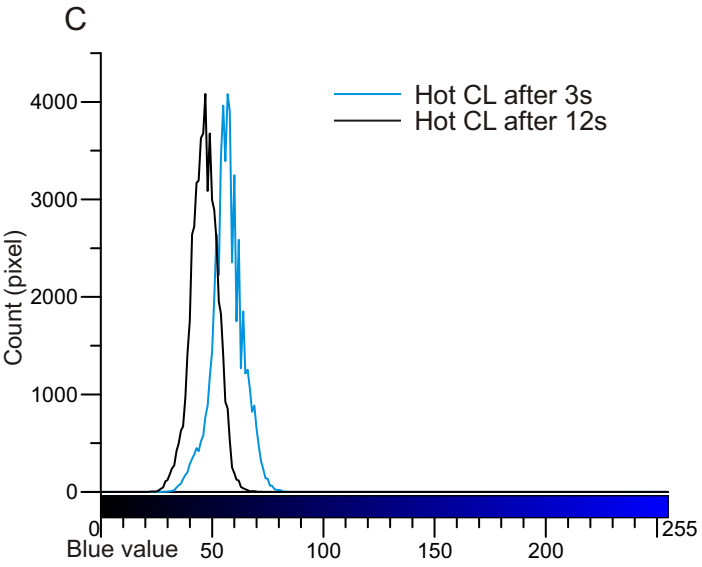

D

Blue value	Min	Max	Mode	Mean	SD
After 3s	28	83	57	57	7
After 12s	22	72	47	47	5.9

Figure 5B-38: Grain 38. The grain shows slight colour shift.

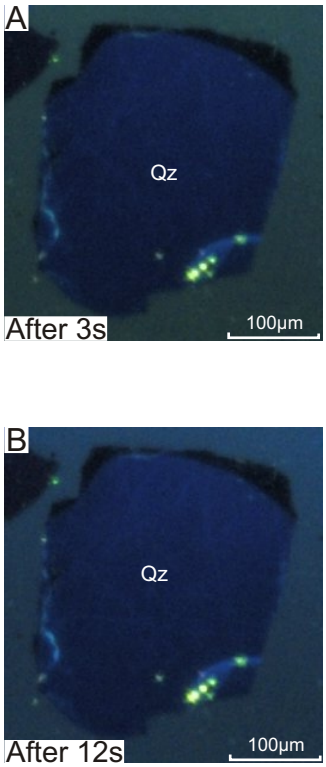

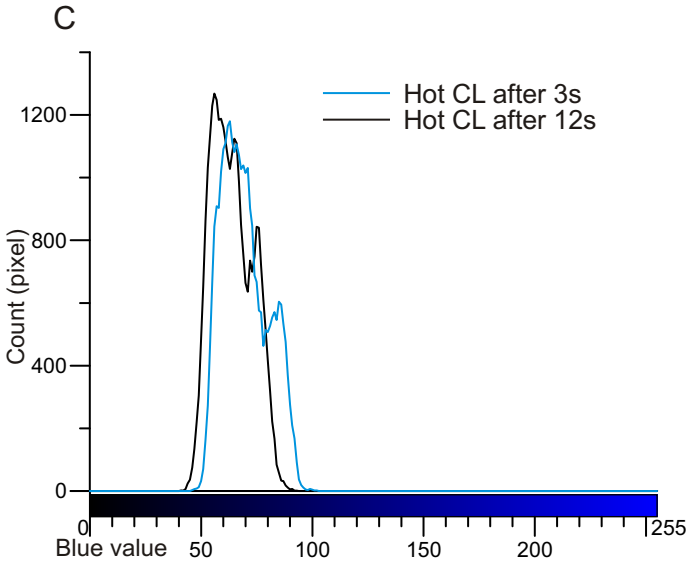

D

Blue value	Min	Max	Mode	Mean	SD
After 3s	41	93	56	64	9.1
After 12s	42	106	63	69	10.2

Figure 5B-39: Grain 39. Probably the first image was taken too early. Therefore, this grain is not useful to analyse the colour shift.

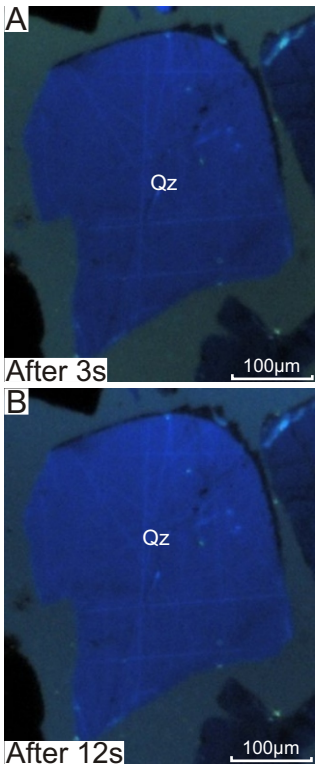

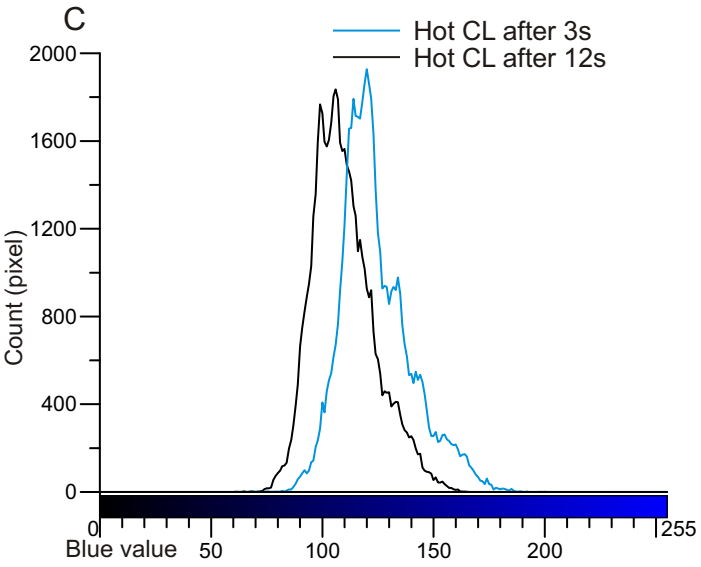

D

Blue value	Min	Max	Mode	Mean	SD
After 3s	61	165	106	110	14.6
After 12s	35	128	65	110	13.9

Figure 5B-40: Grain 40. The grain shows no colour shift.

Appendix 6A: Microphotos, SEM-BSE images, SEM-CL images, and EDS analyses of detrital quartz grains in sample 3425.

Notes:

1. **Homogenous CL:** Nearly uniform CL intensity across the grain (Fig. 2A).

2. Fractures in quartz have been divided into two types: **healed fractures** (**HF**) and **open fractures** (**OF**).

   Healed fractures are fractures filled with secondary silica that appear as thin (commonly < 10 μm) black lines in SEM-CL images (Fig. 2B). They are usually not shown in back-scattered images (Boggs and Krinsley, 2006).

   Open fractures appear in cathodoluminescense images as CL-dark or CL-bright lines, and they are also visible in back-scattered images and microphotos. A few open fractures are **conchoidal fractures** (**CF**) (Boggs and Krinsley, 2006).

3. **Tectonic deformation lamellae**: Tectonic deformation lamellae (Fig. 2C) appear in SEM-CL image as numerous sets of thin, parallel, closely spaced, dark gray lines (Bernet and Basset, 2005). According to Hamers and Drury (2011), tectonic deformation lamellae can either appear as dark gray lines or bright lines in SEM-CL images, and can show slightly wavy features with varying thickness. They usually also appear in XPL image under petrographic microscope.

4. **Spiders (S):** They are made up of dark-Cl patches and streaks. Dark-CL patches mainly range from 10-100 μm. Streaks are random and irregular in the appearance of black broad (>10 μm) elongated form. The spiders are commonly associated with healed fractures, giving them the appearance in SEM-CL images of spiders sitting on a web (Fig. 2D). They cannot be seen in BSE images, since they are composed by secondary silica (Boggs and Krinsley, 2006).

5. **Bright mottling**: Some grains show irregular CL intensity across grains, creating a mottled pattern due the presence of patches (Boggs and Krinsley, 2006). Three types of bright mottling were seen.

   - **Random bright patches** (Fig. 2E1)
   - **Bright streaky patches fabric** (Fig. 2E2)
   - **Subtle mottling** (Fig. 2E3)

6. **Overgrowth:** Overgrowth appears in SEM-CL images as dark areas in the border of the quartz grains (Fig. 2F).

7. **Fluid inclusion trail** (**FI trail**): Trails formed by **fluid inclusions** (**FI**). They are usually associated with secondary porosity and commonly located along fractures and at boundaries between detritral quartz grain and the overgrowth. They are well observed in microphotos under ppl. The fluid inclusion trails can be separated in two kinds: **detrital fluid inclusion trails (**fluid inclusions that are original from the detrital quartz, they do not cut the quartz overgrowth) and **diagenetic fluid inclusion trails** (fluid inclusions originated from the diagenesis, and they thus cut the quartz overgrowth).

8. **Melt inclusion** (**MI**): Large fluid inclusions (>10 μm) in which crystallized minerals are visible.

9. **Secondary porosity** (**SP**): Porosities usually caused by dissolution and/or fractures. They are easily observed in microphotos under PPL and BSE images.

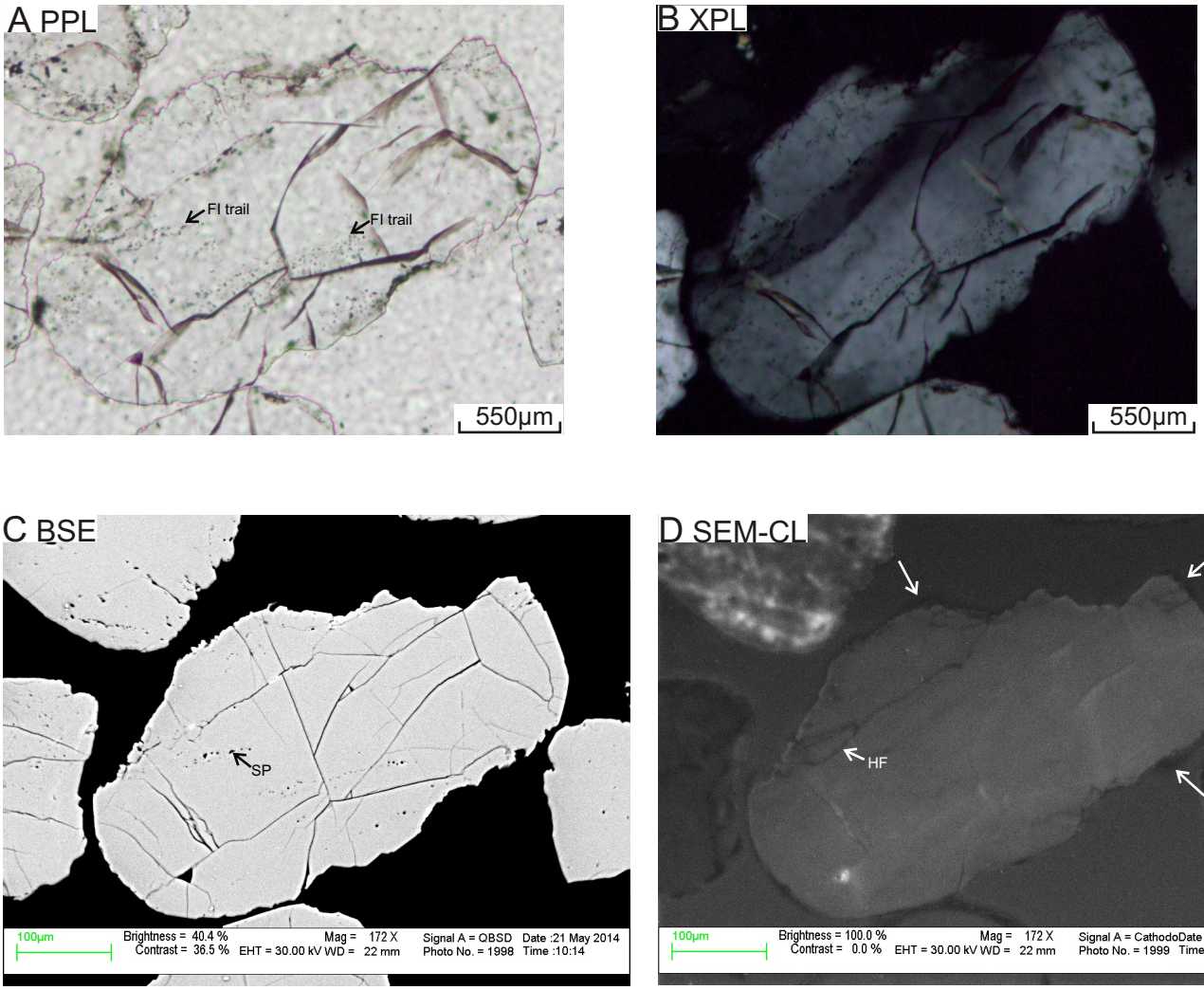

Figure 6A-1: Microphotos under ppl (A) and xpl (B), SEM-BSE image (C) and SEM-CL image (D) of quartz grain 1 in sample 3425. The grain is anhedral and subrounded monocrystalline with strong undulose extinction. Fluid inclusions are common; they are usually associated with secondary porosity (SP) and form trails (FI trail) along healed fractures (Fig. A and C). The grain is microfractured with a set of irregular fractures (Fig. C and D). A few healed fractures (HF) can be seen in Fig, D. The dark areas indicated by arrows in Fig. D are overgrowth; these areas appear corroded in Fig. C, suggesting secondary porosity.

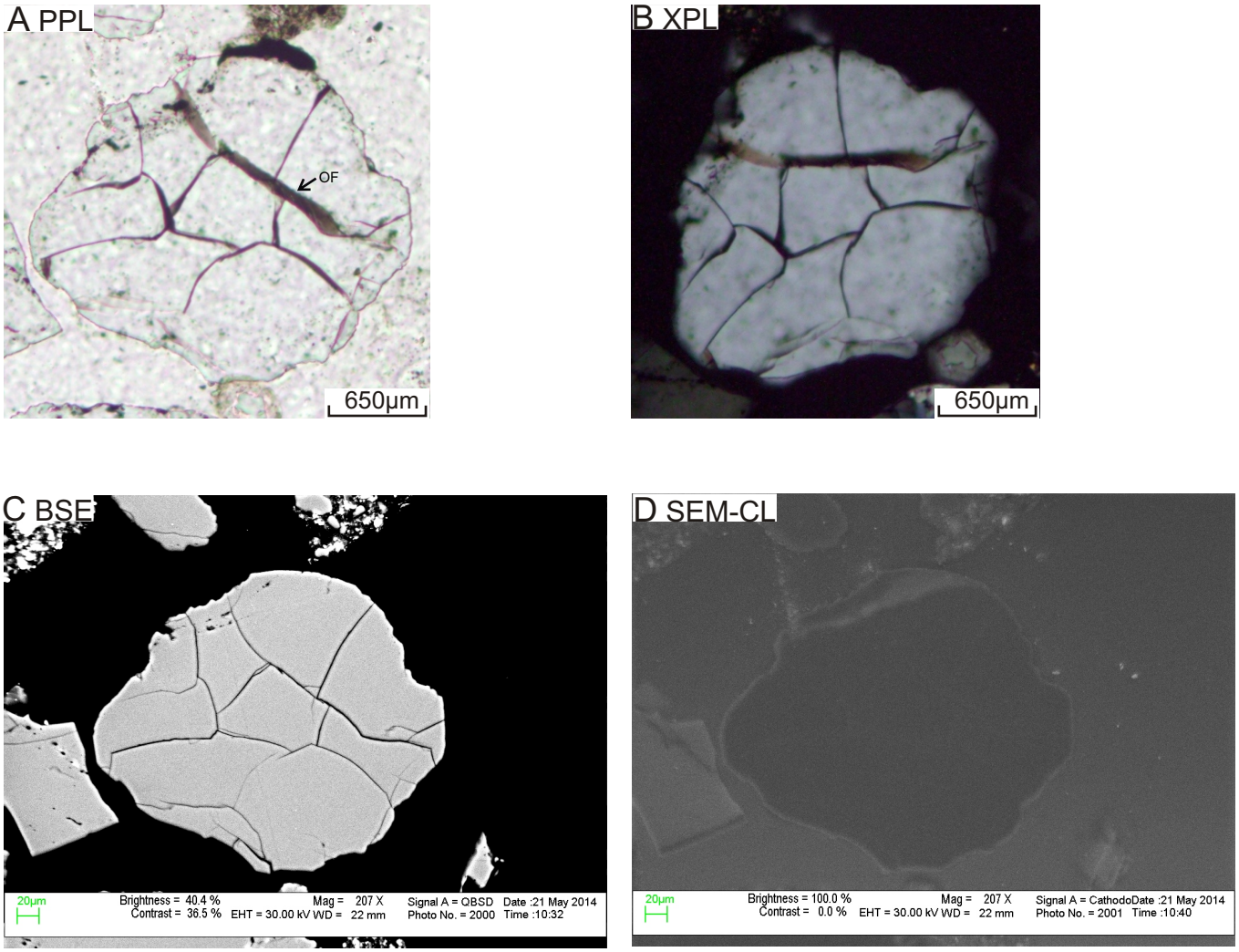

Figure 6A-2: Microphotos under ppl (A) and xpl (B), SEM-BSE image (C) and SEM-CL image (D) of quartz grain 2 in sample 3425. The grain is anhedral and sub-rounded monocrystalline with strong undulose extinction. Fluid inclusion trails are present (Fig. A). The grain is microfractured with a set of irregular open fractures (OF) (Fig. A and C). Healed fractures are rare.

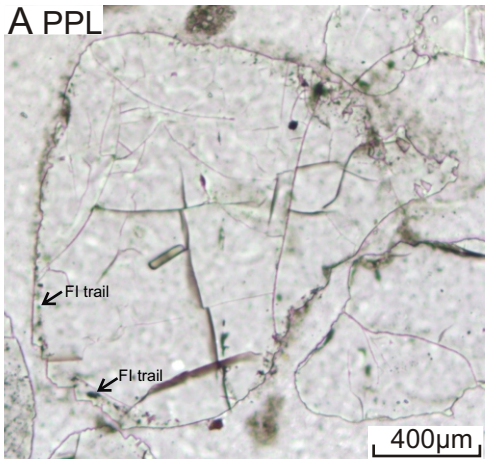

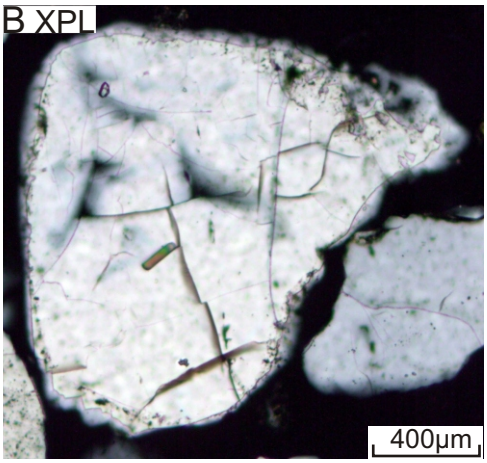

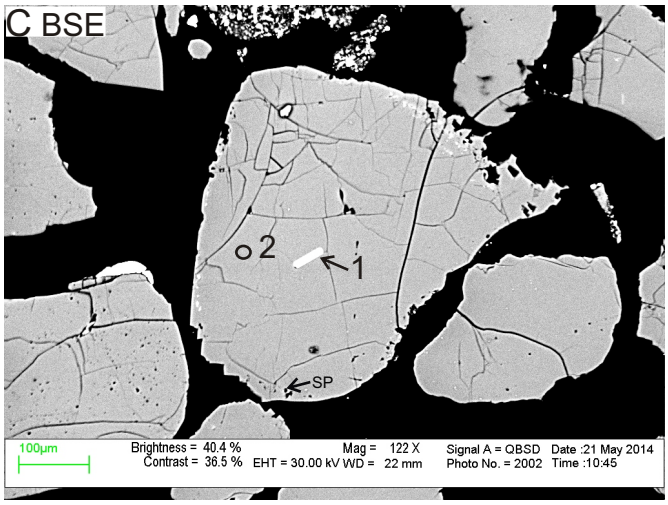

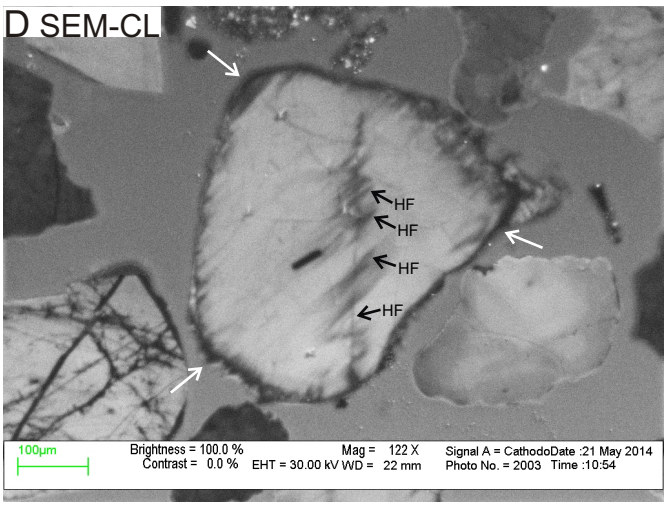

E EDS analyses

Pos#	Min. ID	SiO2	TiO2	Al2O3	FeO	MgO	K2O	ZnO	Total	Actual Total
1	Bt	39.51	0.88	21.08	15	10.1	8.66	0.43	96	73
2	Qz	99.71						0.3	100	79

Figure 6A-3: Microphotos under ppl (A) and xpl (B), SEM-BSE image (C), SEM-CL image (D), and EDS analyses table (E) of quartz grain 3 in sample 3425. The grain is anhedral and sub-rounded monocrystalline with strong undulose extinction. Fluid inclusions are common; they are usually associated with secondary porosity (SP) and form trails (FI trail) at the boundary between the detrital quartz and the overgrowth (Fig. A). The grain contains a biotite inclusion and is microfractured with a set of parallel fractures and a set of irregular fractures (Fig. C and D). Healed fractures (HF) are common (Fig. D). The dark areas indicated by arrows in Fig. D are overgrowth; these areas appear corroded in Fig. C, indicating secondary porosity. The grain shows bright-CL streaky patches fabric in SEM-CL Image. The streaky patches have the same orientation as the set of parallel healed fractures, indicating brittle deformation.

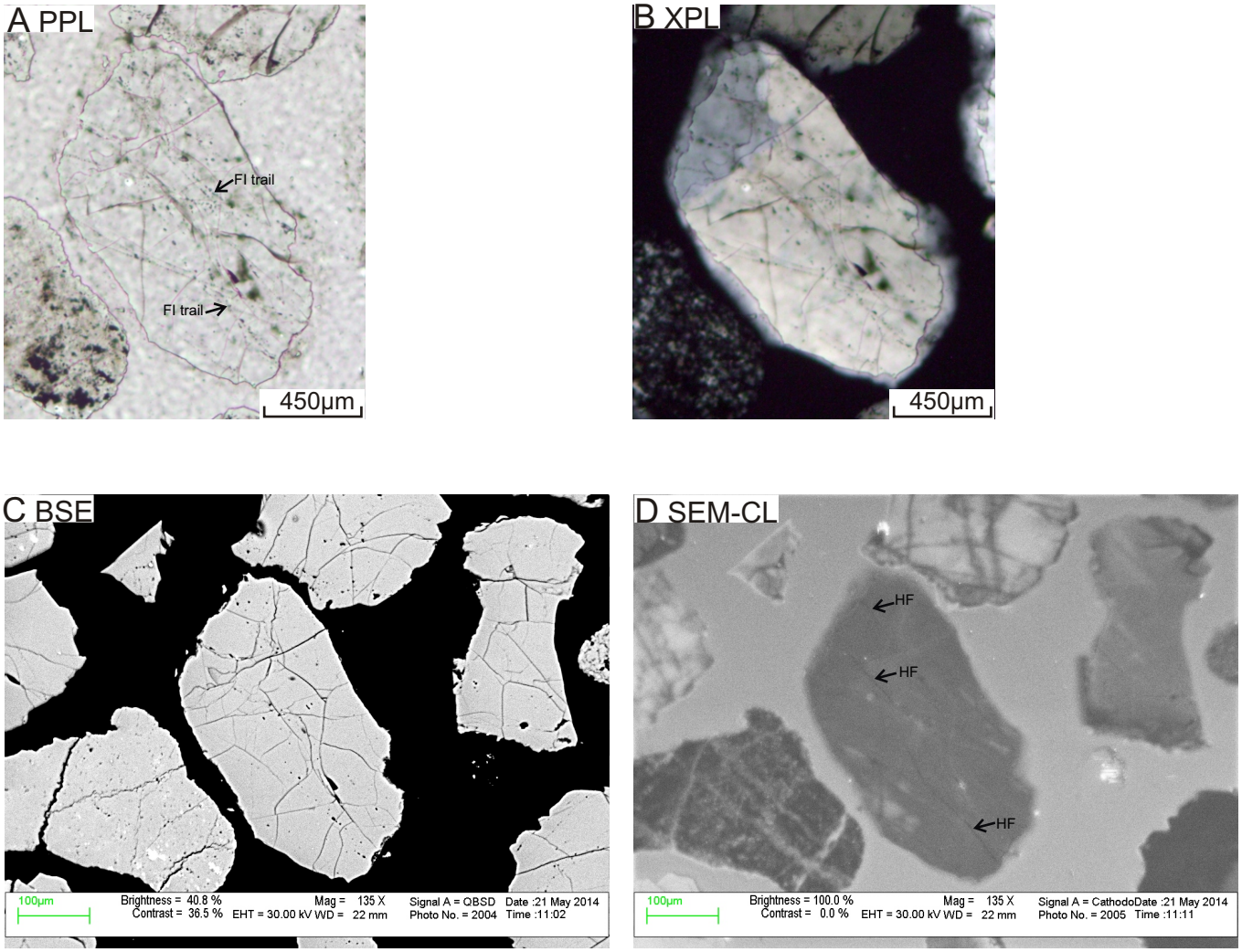

Figure 6A-4: Microphotos under ppl (A) and xpl (B), SEM-BSE image (C) and SEM-CL image (D) of quartz grain 4 in sample 3425. The grain is anhedral and sub-rounded polycrystalline (only two sub- grains) with strong undulose extinction. Fluid inclusions are common; they are usually associated with secondary porosity and form trails (FI trail) along healed fractures (Fig. A). The grain is microfractured with a set of sub-parallel healed fractures and a set of irregular open fractures (Fig. C and D). The grain shows bright-CL streaky patches fabric in SEM-CL Image. The streaky patches have the same orientation of the set of parallel healed fractures, indicating brittle deformation.

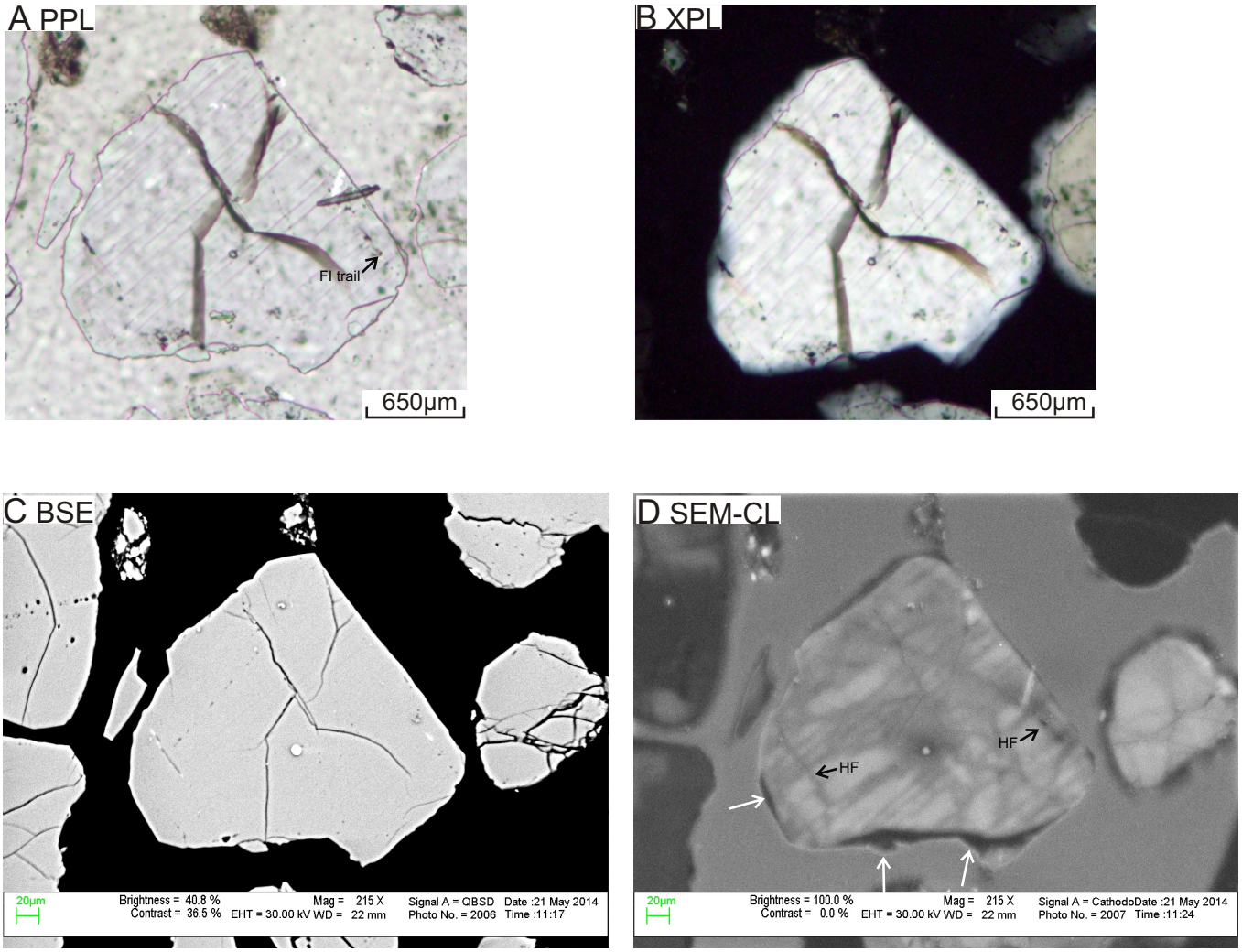

Figure 6A-5: Microphotos under ppl (A) and xpl (B), SEM-BSE image (C) and SEM-CL image (D) of quartz grain 5 in sample 3425. The grain is anhedral and sub-angular monocrystalline with deformation lamellae and weak undulose extinction. Fluid inclusions are present; they form trails (FI trail) along healed fractures (Fig. A). The grain is microfractured with a set of irregular fractures (Fig. C and D). Some healed fractures (HF) can be seen in Fig. D. The dark areas indicated by arrows in Fig. D are overgrowth. The grain shows streaky texture in SEM-CL image due to the deformation lamellae.

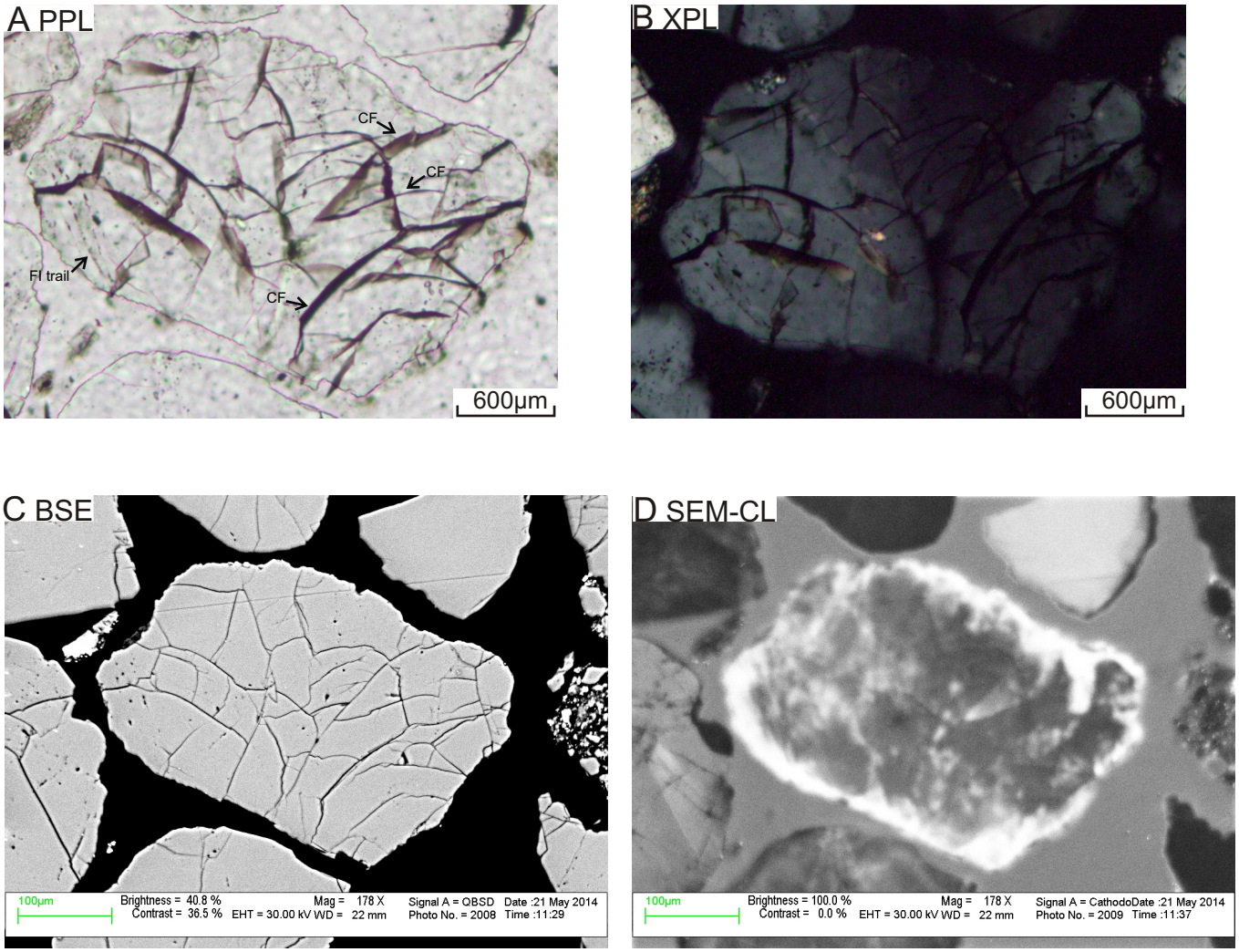

Figure 6A-6: Microphotos under ppl (A) and xpl (B), SEM-BSE image (C) and SEM-CL image (D) of quartz grain 6 in sample 3425. The grain is anhedral and sub-rounded monocrystalline with strong undulose extinction. Fluid inclusion trails are present (Fig. A). The grain is strongly microfractured with a set of irregular fractures and a set of conchoidal fractures (CF) (Fig. C). Healed fractures are rare. The grain shows subtle mottling CL- texture in SEM-CL image.

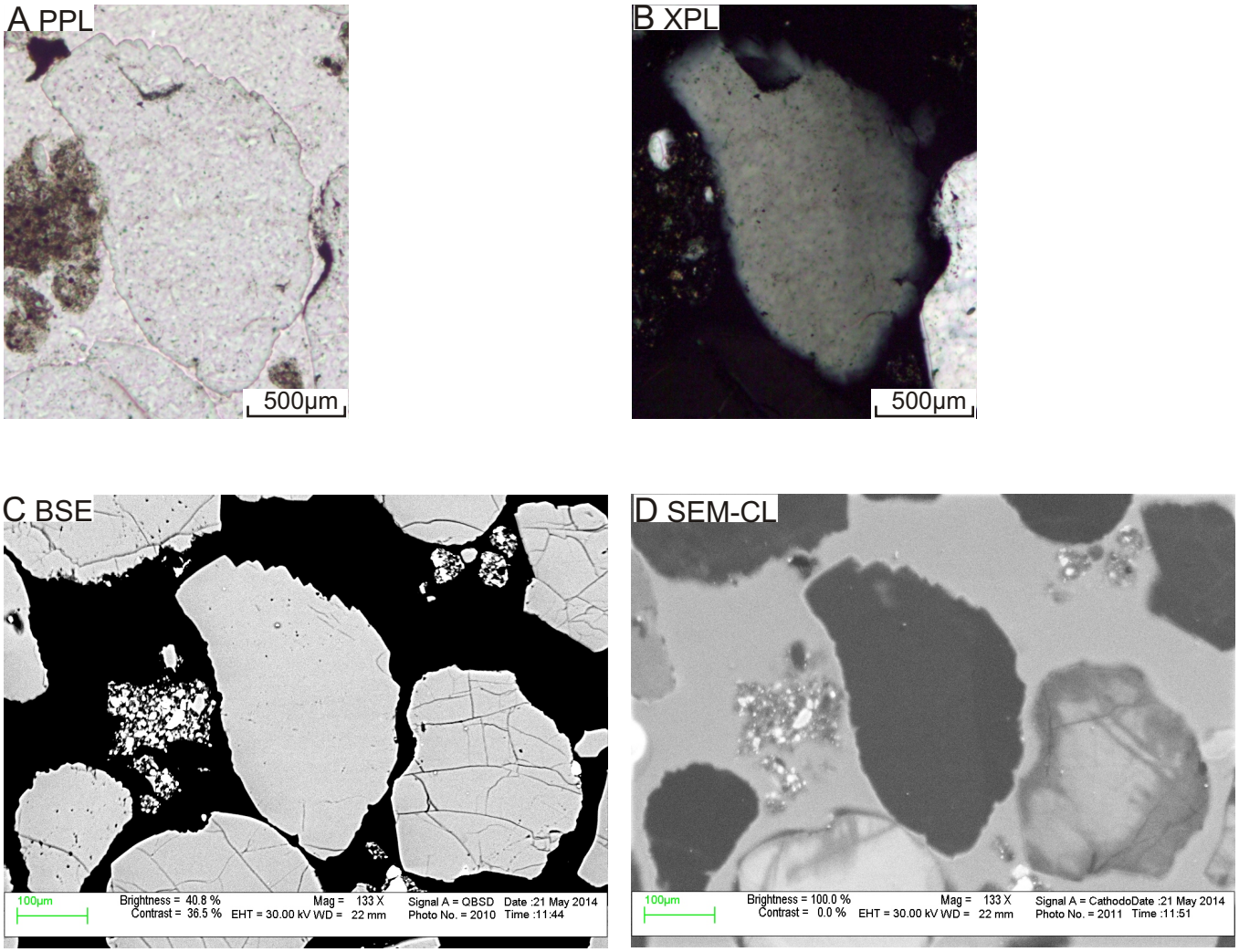

Figure 6A-7: Microphotos under ppl (A) and xpl (B), SEM-BSE image (C) and SEM-CL image (D) of quartz grain 7 in sample 3425. The grain is anhedral and sub-rounded polycrystalline (only two sub-grains) with mosaic texture and weak undulose extinction. Fluid inclusion are rare (Fig. A). The grain is weakly microfractured with irregular fractures (Fig. C). Healed fractures are rare. The grain shows homogeneous dark-CL in SEM-CL image.

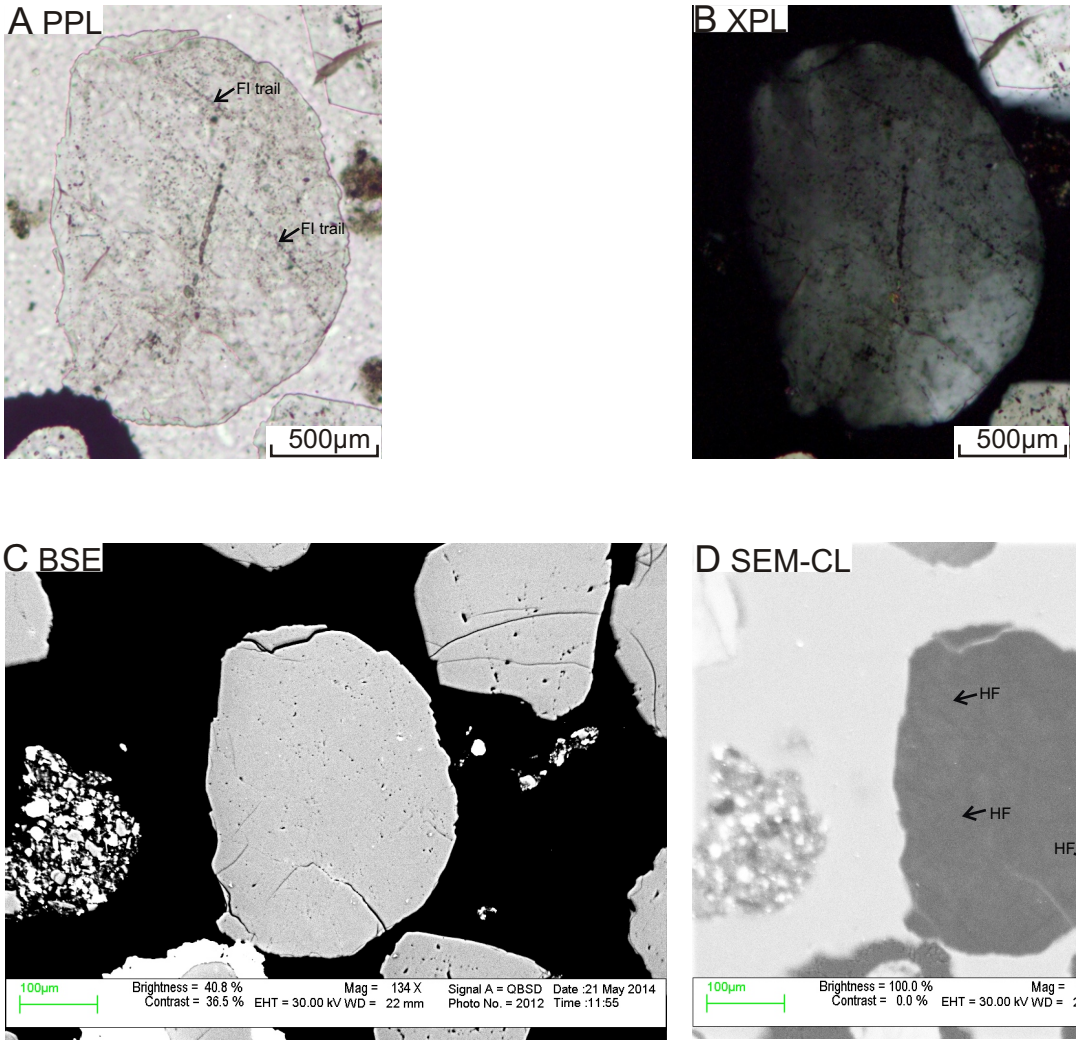

Figure 6A-8: Microphotos under ppl (A) and xpl (B), SEM-BSE image (C) and SEM-CL image (D) of quartz grain 8 in sample 3425. The grain is anhedral and rounded monocrystalline with mosaic texture and weak undulose extinction. Fluid inclusions are common; they are usually associated with secondary porosity and form trails (FI trail) along healed fractures (Fig. A). The grain is microfractured with a set of irregular fractures (Fig. C and D). The healed fractures are camouflaged by the homogeneous dark-CL image.

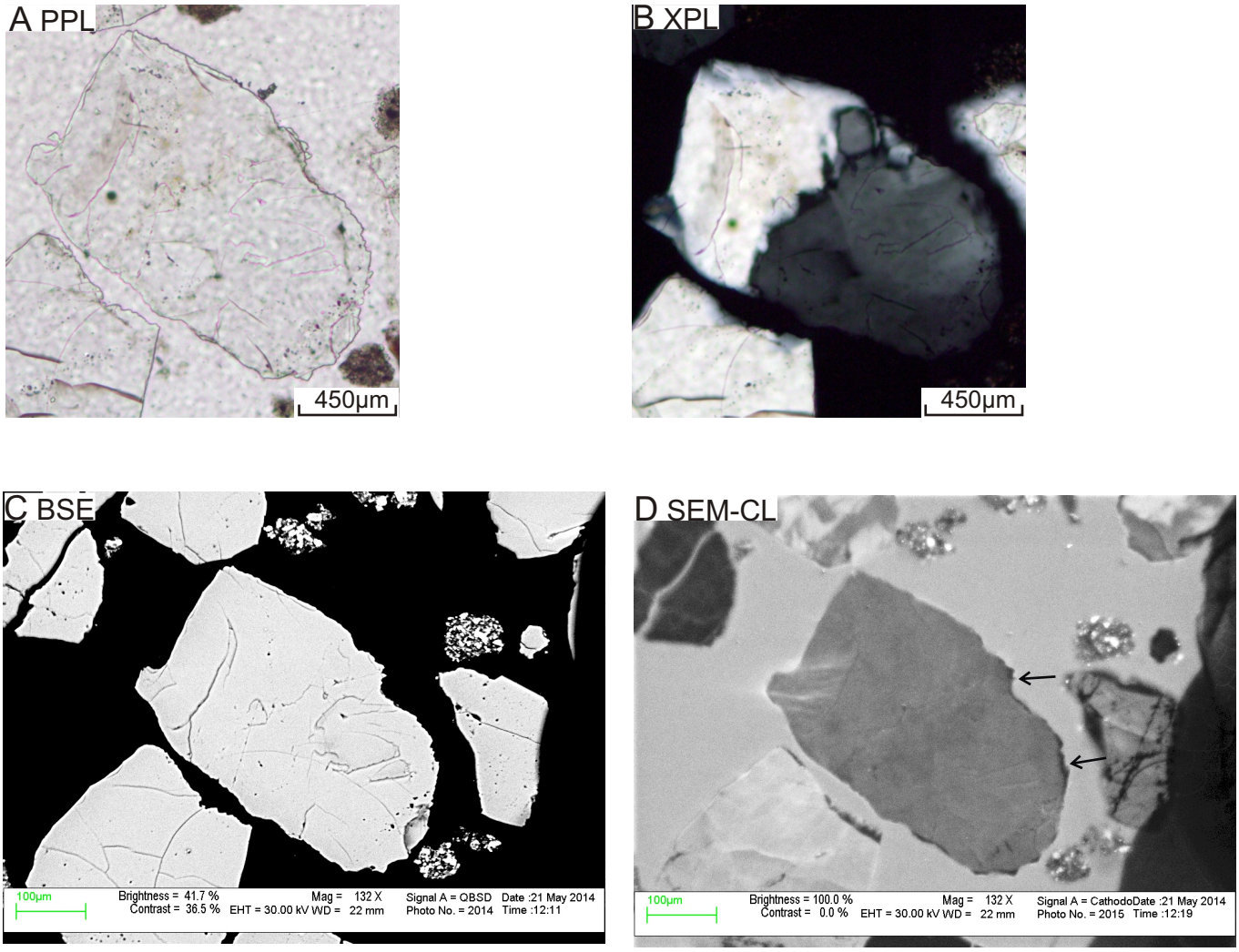

Figure 6A-9: Microphotos under ppl (A) and xpl (B), SEM-BSE image (C) and SEM-CL image (D) of quartz grain 9 in sample 3425. The grain is anhedral and sub-rounded polycrystalline (more than 4 sub-grains with sutured sub-grain boundaries) with mosaic texture and weak undulose extinction. Fluid inclusions trails are rare. The grain is microfractured with a set of irregular fractures (Fig. C and D). Healed fractures are rare. The dark areas indicated by arrows in Fig. D are overgrowth.

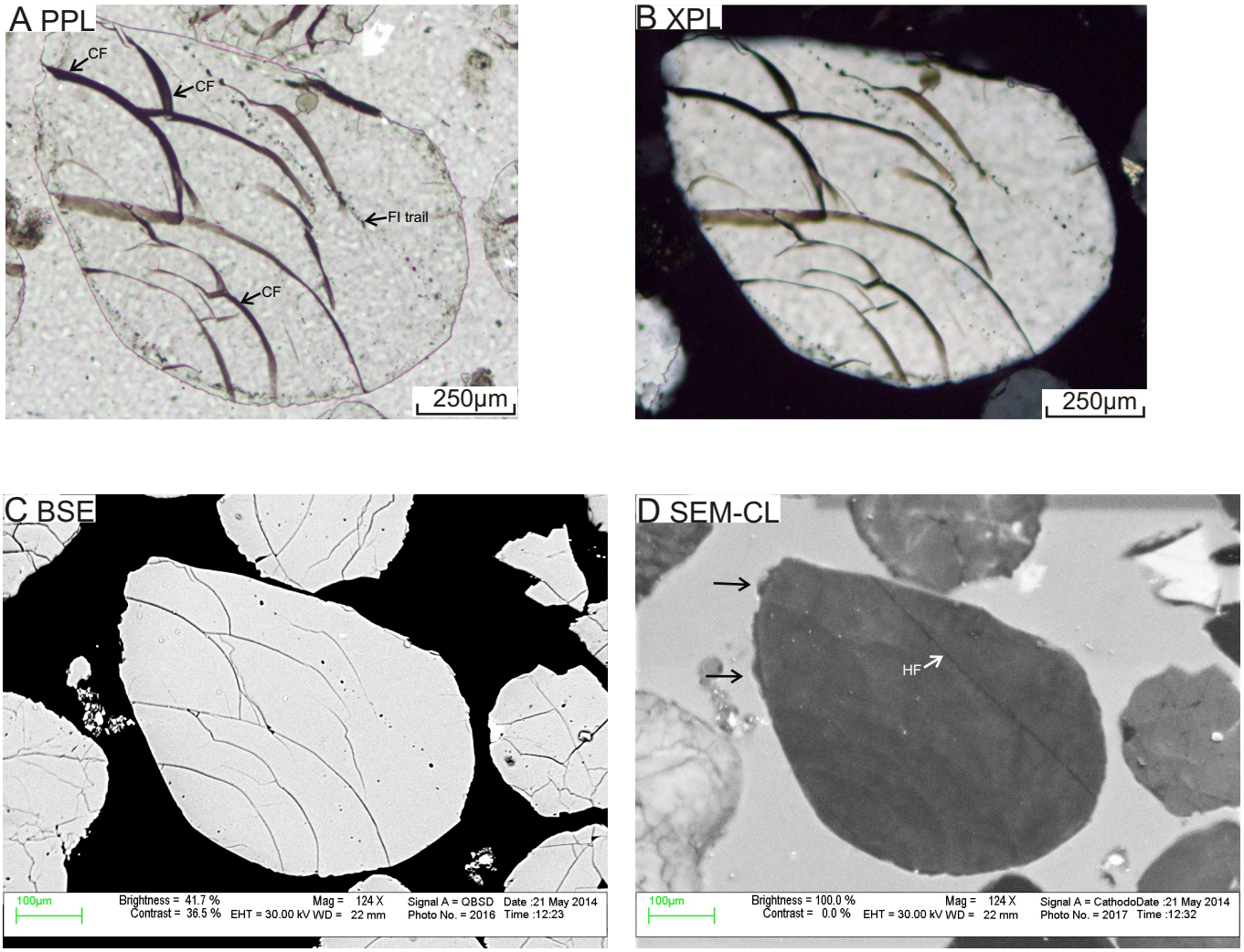

Figure 6A-10: Microphotos under ppl (A) and xpl (B), SEM-BSE image (C) and SEM-CL image (D) of quartz grain 10 in sample 3425.The grain is anhedral and rounded monocrystalline with weak undulose extinction. Fluid inclusion trails are present (Fig. A). The grain is microfractured with a set of conchoidal open fractures (CF) and only one healed fracture (Fig. A and D). The grain shows homogeneous SEM-CL image.

A PPL

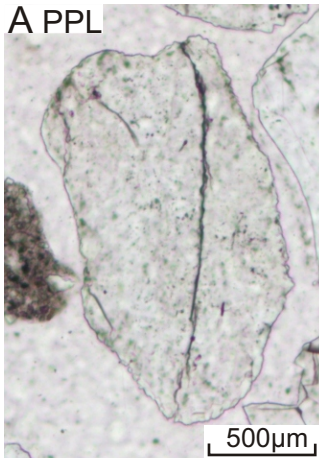

B XPL



C BSE

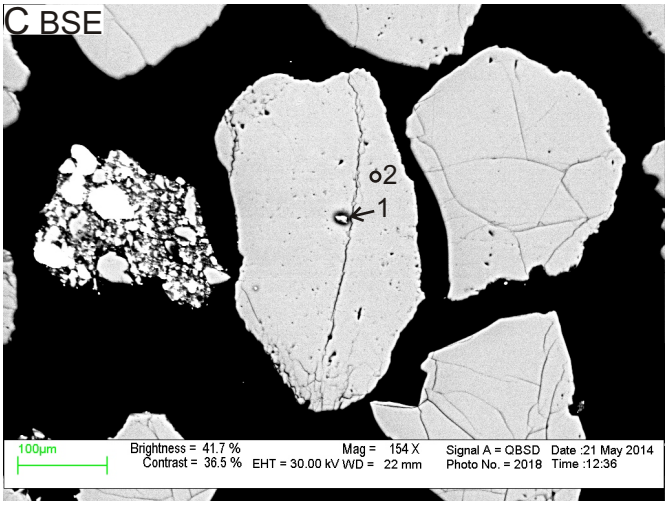

D SEM-CL

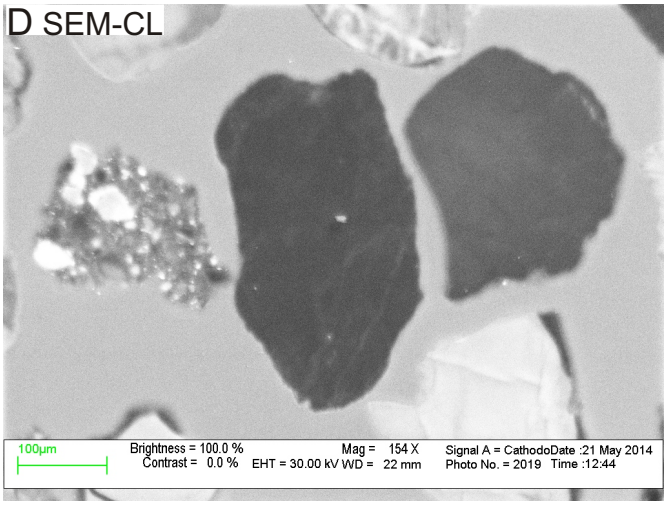

E EDS analyses

Pos#	Min. ID	SiO2	Al2O3	K2O	Total	Actual Total
1	Hole	79.06	11.34	9.6	100	5
2	Qz	99.99			100	73

Figure 6A-11: Microphotos under ppl (A) and xpl (B), SEM-BSE image (C), SEM-CL image (D), and EDS analyses table (E) of quartz grain 13 in sample 3425. The grain is anhedral and sub-rounded polycrystalline (more than 12 sub-grains) with mosaic texture and weak undulose extinction (Fig. A and B). Fluid inclusion trails are common (Fig. A). The grain is microfractured with a set of irregular fractures (Fig. C). Healed fractures are rare.

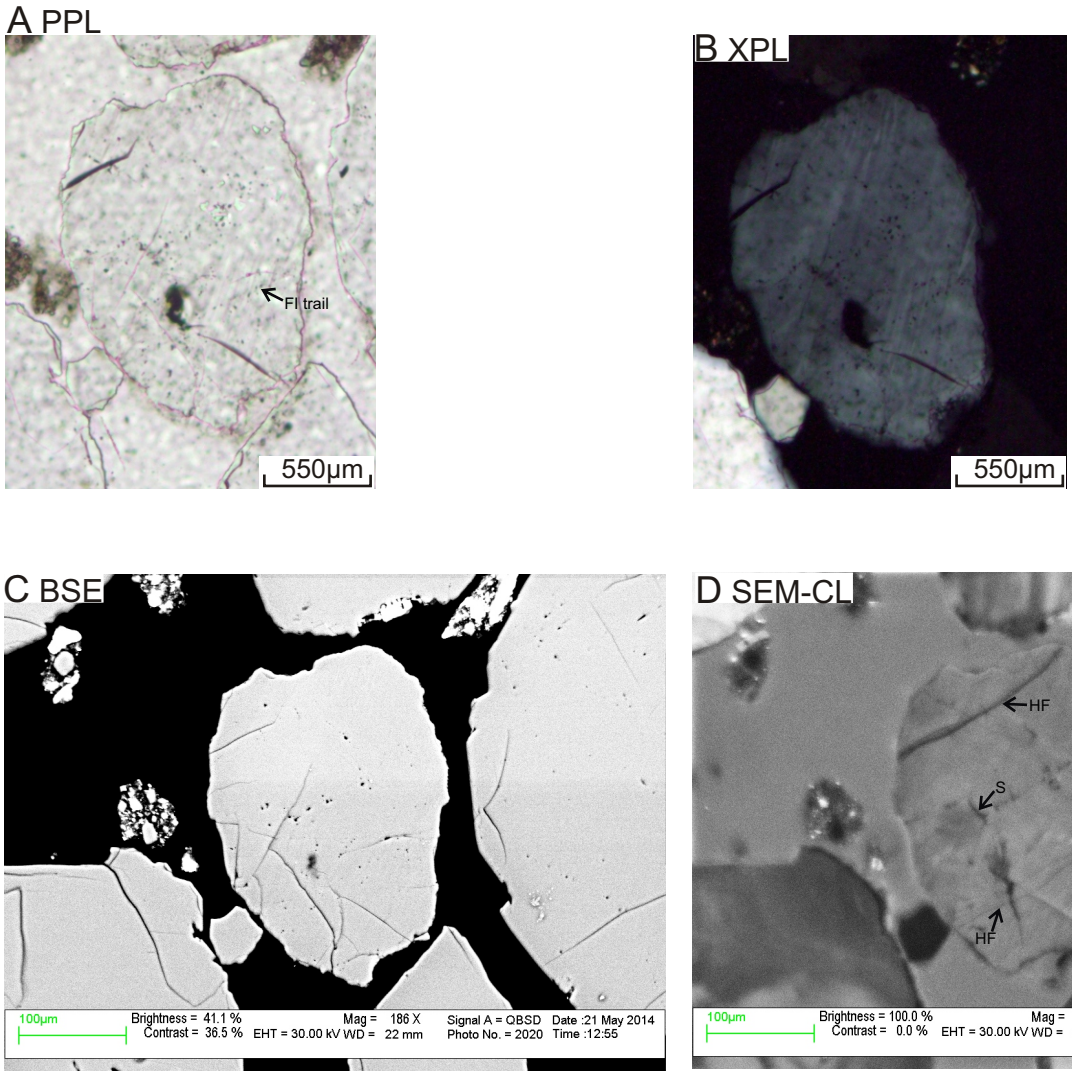

Figure 6A-12: Microphotos under ppl (A) and xpl (B), SEM-BSE image (C) and SEM-CL image (D) of quartz grain 12 in sample 3425. The grain is anhedral and sub-rounded monocrystalline with deformation lamellae and strong undulose extinction (Fig. A and B). Fluid inclusions are present; they are usually associated with secondary porosity and form trails (FI trail) along healed fractures (Fig. A). The grain is microfractured with a set of parallel fractures and a set of irregular fractures (Fig. C and D). Some healed fractures (HF) and spiders (S) can be seen in Fig. D.

A PPL

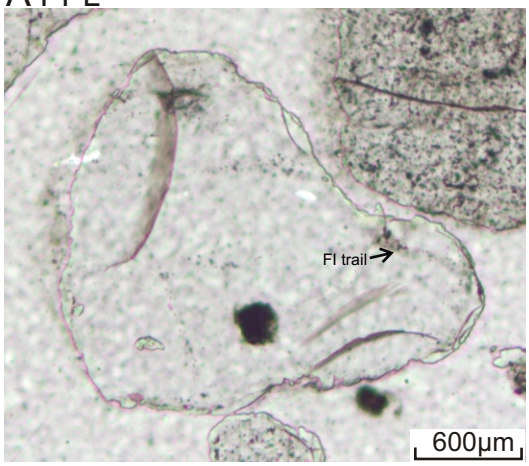

B XPL

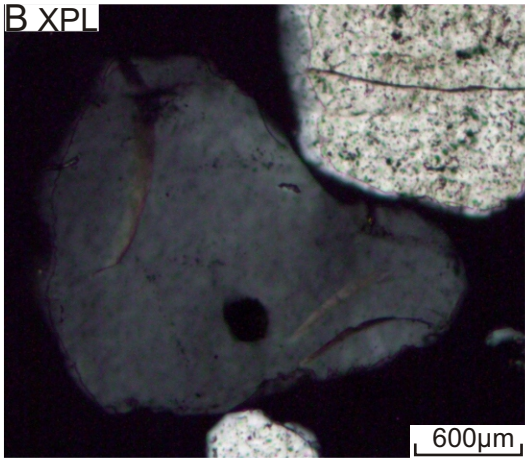

C BSE

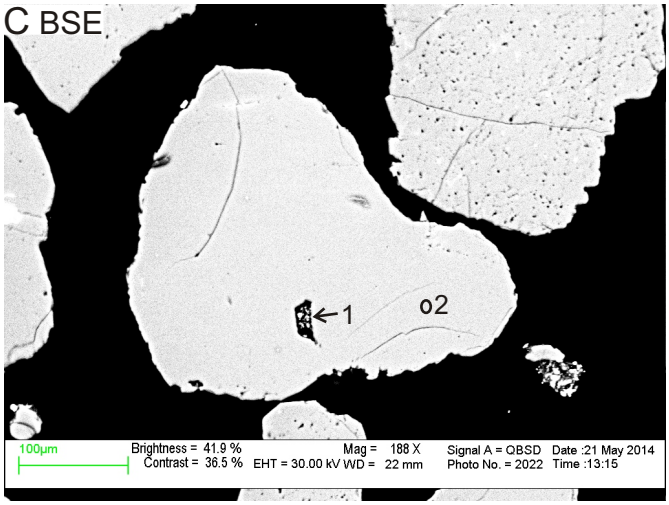

D SEM-CL

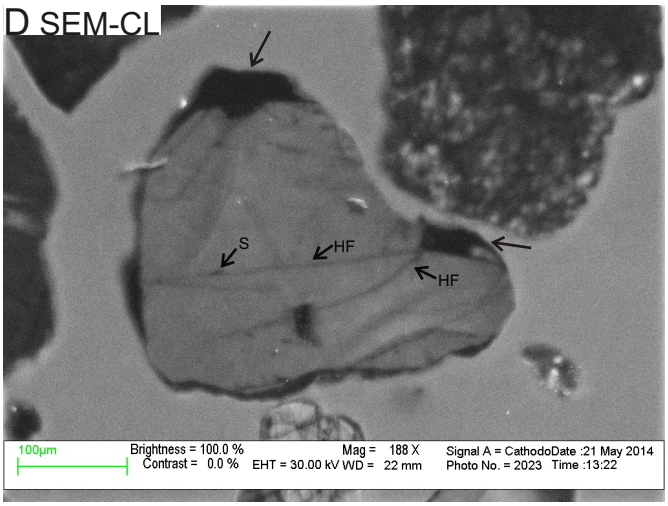

E EDS analyses

Pos#	Min. ID	SiO2	Al2O3	FeO	MgO	CaO	Cl	Total	Actual Total
1	Chl	58.85	0.76	23.42	1.33	0.38	0.26	85	46
2	Qz	99.99						100	76

Figure 6A-13: Microphotos under ppl (A) and xpl (B), SEM-BSE image (C), SEM-CL image (D), and EDS analyses table (E) of quartz grain 13 in sample 3425. The grain is anhedral and sub-rounded monocrystalline with strong undulose extinction. Fluid inclusions are common; they form trails along healed fractures and at the boundary between the detrital quartz and the overgrowth (Fig. A). The grain contains chlorite inclusion and is microfractured with a set of irregular fractures (Fig. C and D). Some healed fractures (HF) and spiders (S) can be seen in Fig. D. The dark areas indicated by arrows in Fig. D are overgrowth.

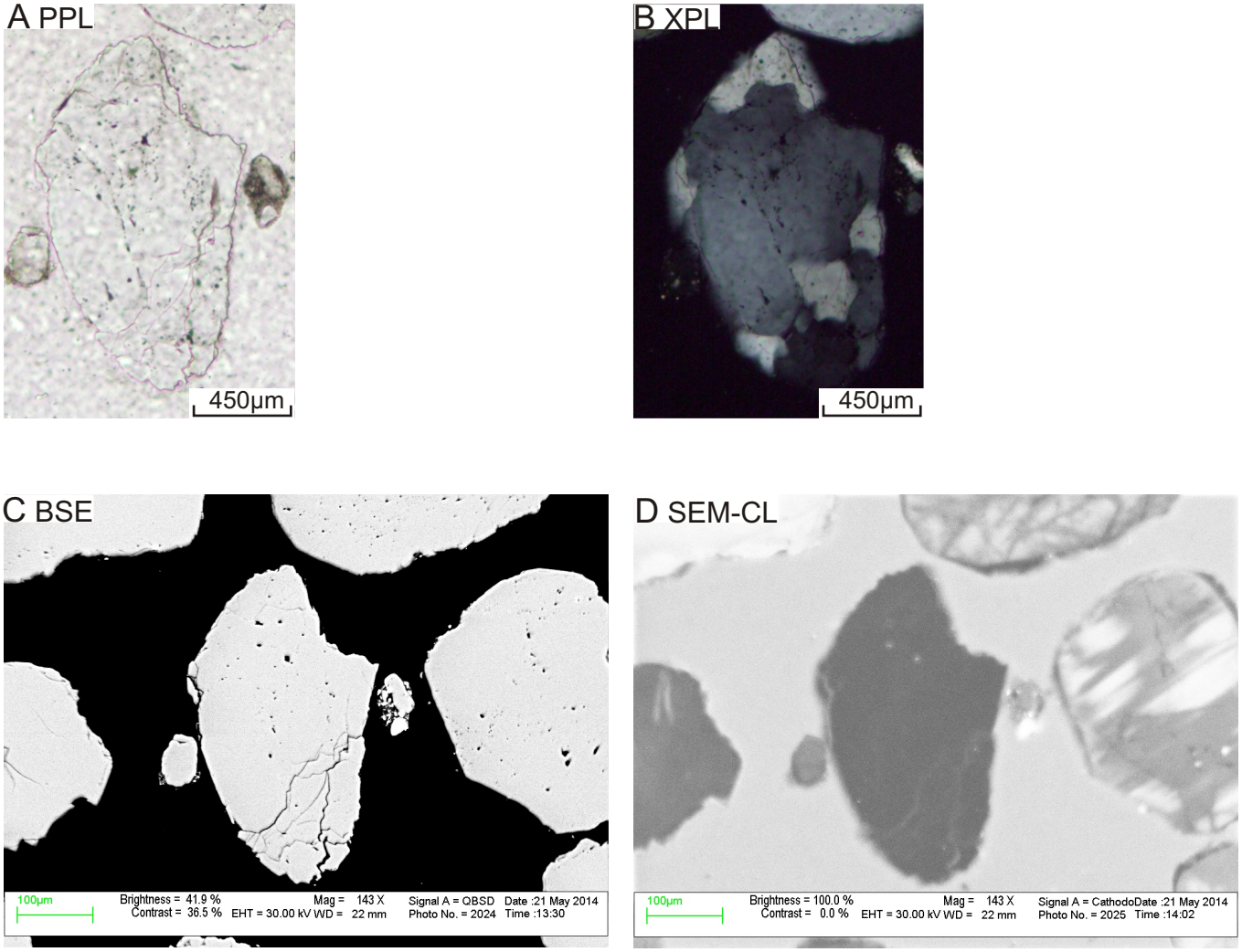

Figure 6A-14: Microphotos under ppl (A) and xpl (B), SEM-BSE image (C) and SEM-CL image (D) of quartz grain 14 in sample 3425. The grain is anhedral and sub-rounded polycrystalline (more than 6 sub-grains) with strong undulose extinction. The grain contains fluid inclusion trails and is microfractured with a set of irregular fractures (Fig. C). Healed cracks are rare.

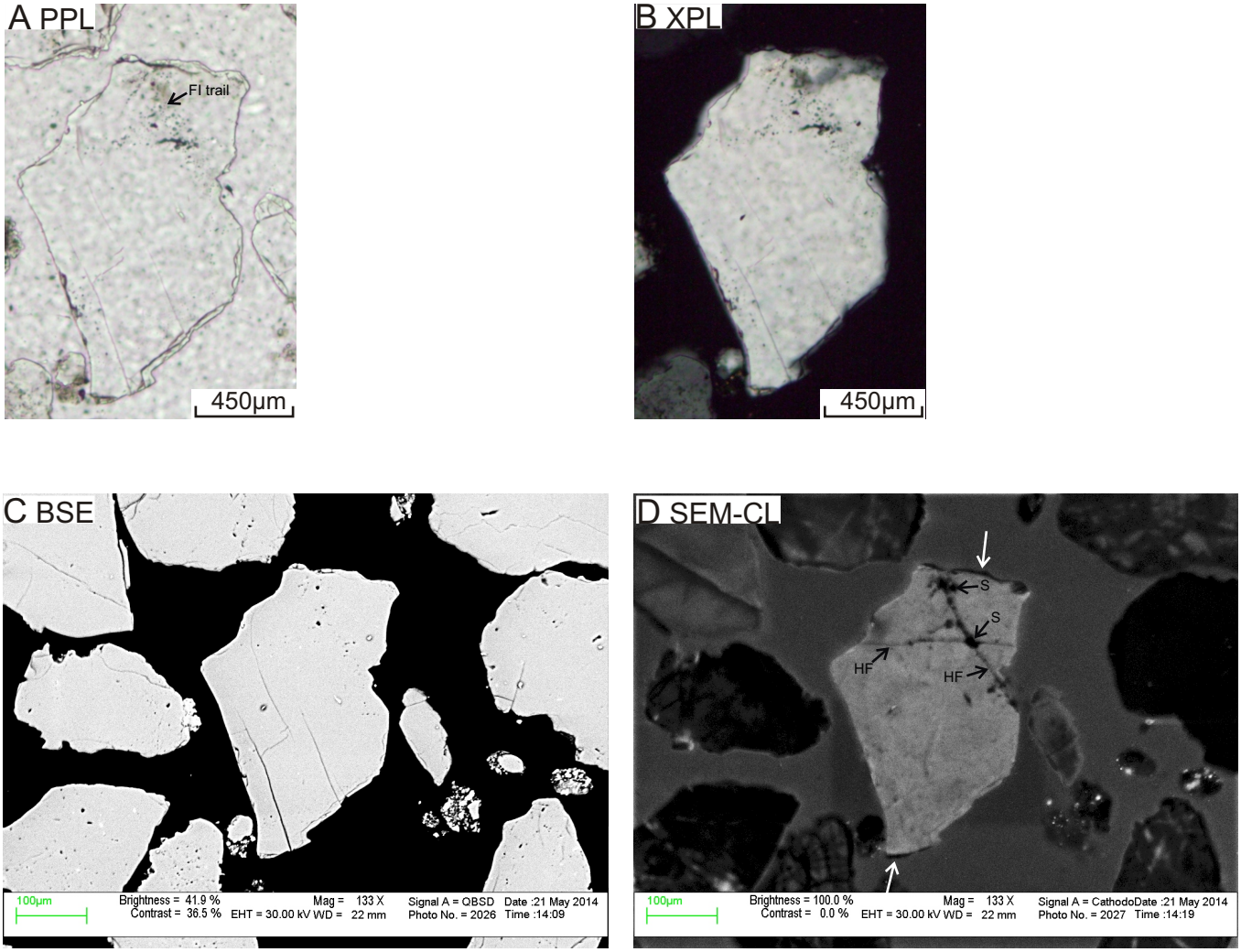

Figure 6A-15: Microphotos under ppl (A) and xpl (B), SEM-BSE image (C) and SEM-CL image (D) of quartz grain 15 in sample 3425. The grain is anhedral and sub-angular monocrystalline with embayed margins and non undulose extinction. Fluid inclusions are common; they form trails along healed fractures (Fig. A). The grain is microfractured with a set of irregular fractures (Fig. C and D). Some healed fractures (HF) and spiders (S) can be seen in Fig. D. The dark areas indicated by arrows in Fig. D are overgrowth.

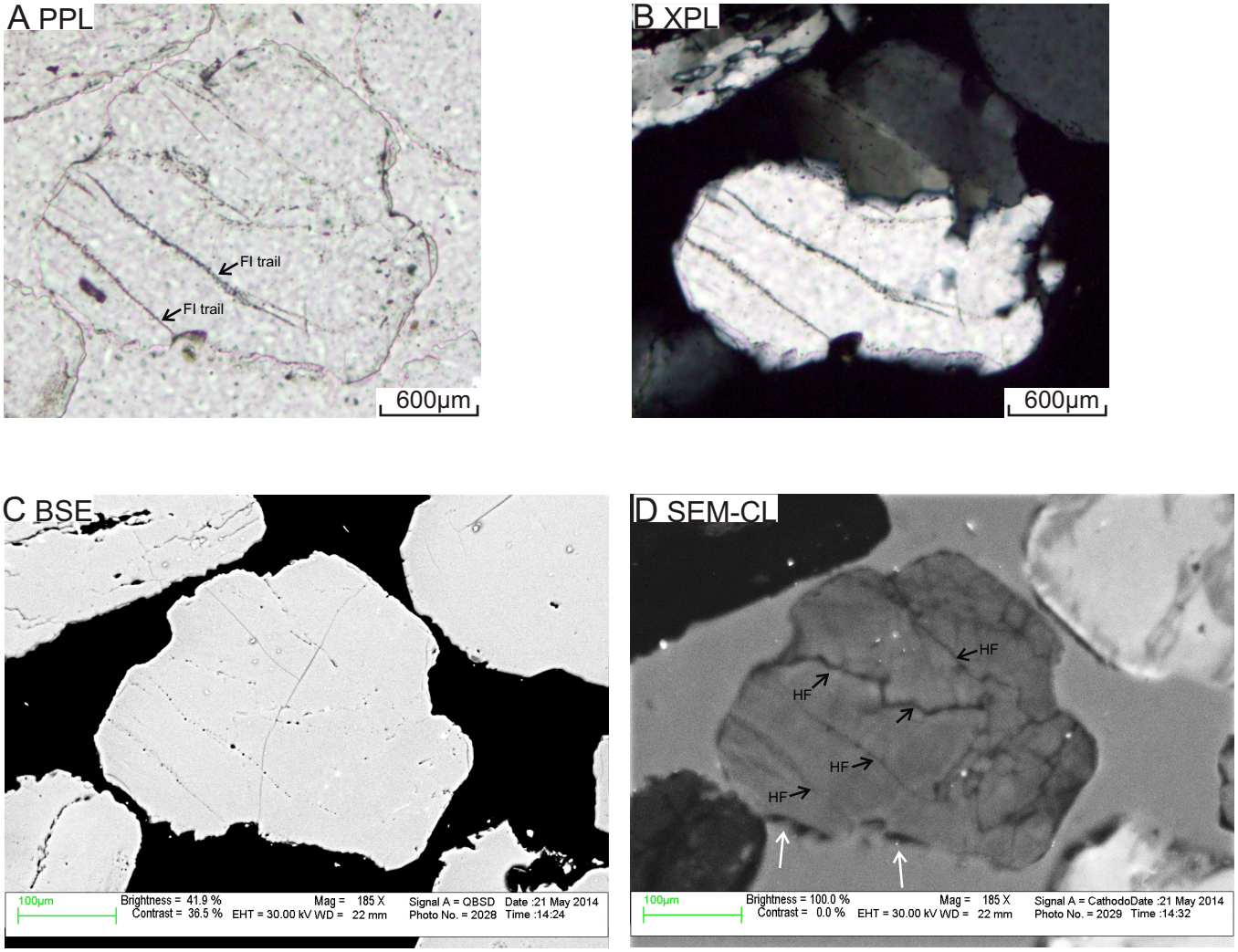

Figure 6A-16: Microphotos under ppl (A) and xpl (B), SEM-BSE image (C) and SEM-CL image (D) of quartz grain 16 in sample 3425. The grain is anhedral and sub-rounded polycrystalline (more than 5 sub-grains with sutured sub-grain boundaries) with strong undulose extinction. Fluid inclusions are common; they are usually associated with secondary porosity and form trails along healed fractures (Fig. A). The grain is microfractured with a set of parallel fractures and a set of irregular fractures (Fig. C and D). Healed fractures (HF) are common (Fig. D). The dark areas indicated by arrows in Fig. D are overgrowth; these areas appear corroded in Fig. C, suggesting secondary porosity.

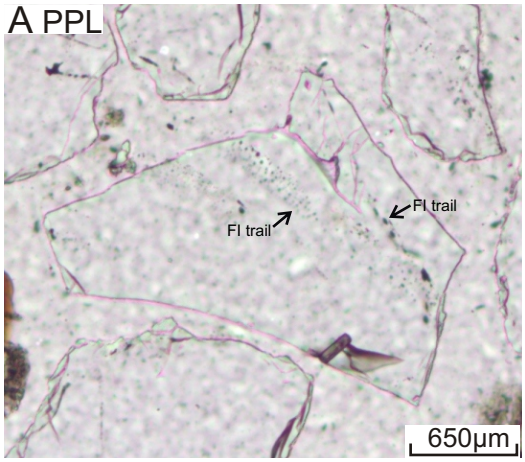

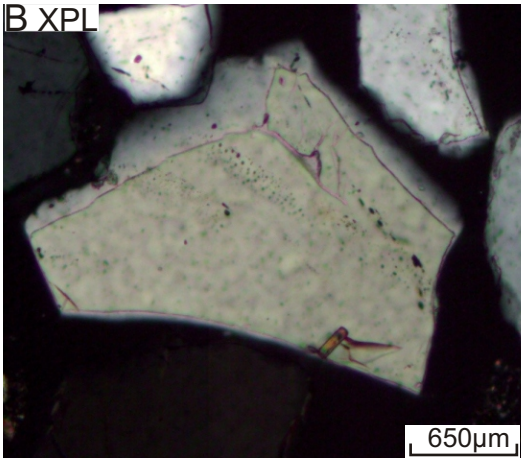

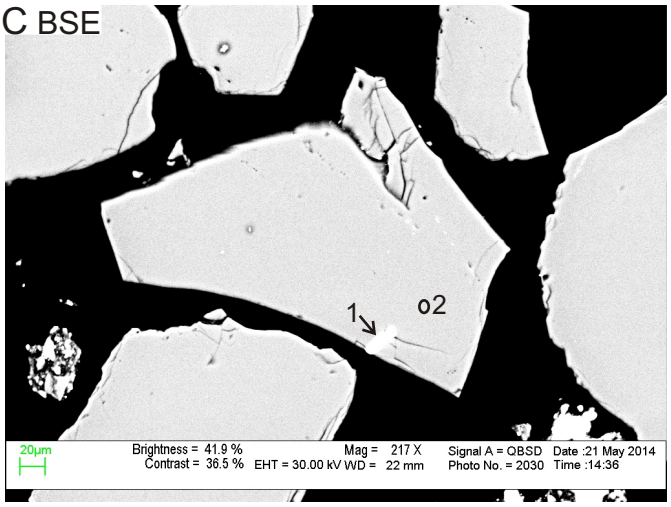

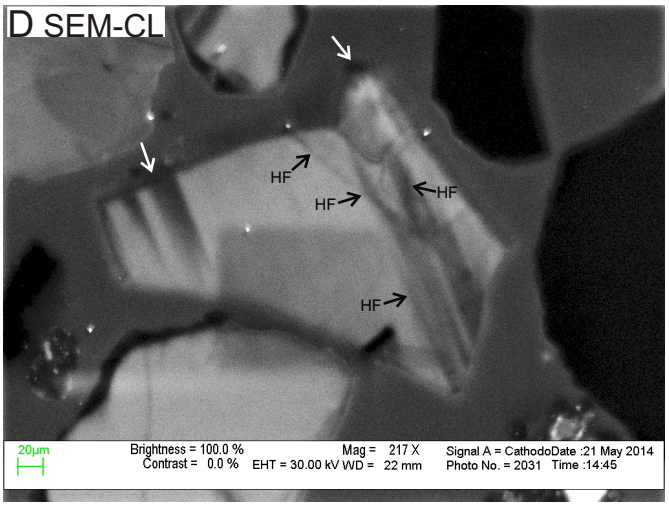

E EDS analyses

Pos#	Min. ID	SiO2	TiO2	Al2O3	FeO	MnO	MgO	K2O	Total	Actual Total
1	Bt	40.98	3.3	18.5	16.9	0.52	6.82	8.98	96	66
2	Qz	99.99							100	75

Figure 6A-17: Microphotos under ppl (A) and xpl (B), SEM-BSE image (C), SEM-CL image (D), and EDS analyses table (E) of quartz grain 17 in sample 3425. The grain is anhedral and angular monocrystalline with weak undulose extinction. Fluid inclusions are common; they form trails along healed fractures (Fig. A). The grain contains a biotite inclusion and is microfractured with a set of parallel healed fractures and a set of irregular open fractures (Fig. C and D). Healed fractures (HF) are common (Fig. D). The grains shows streaky texture in CL-image due the presence of the set of parallel healed fractures.

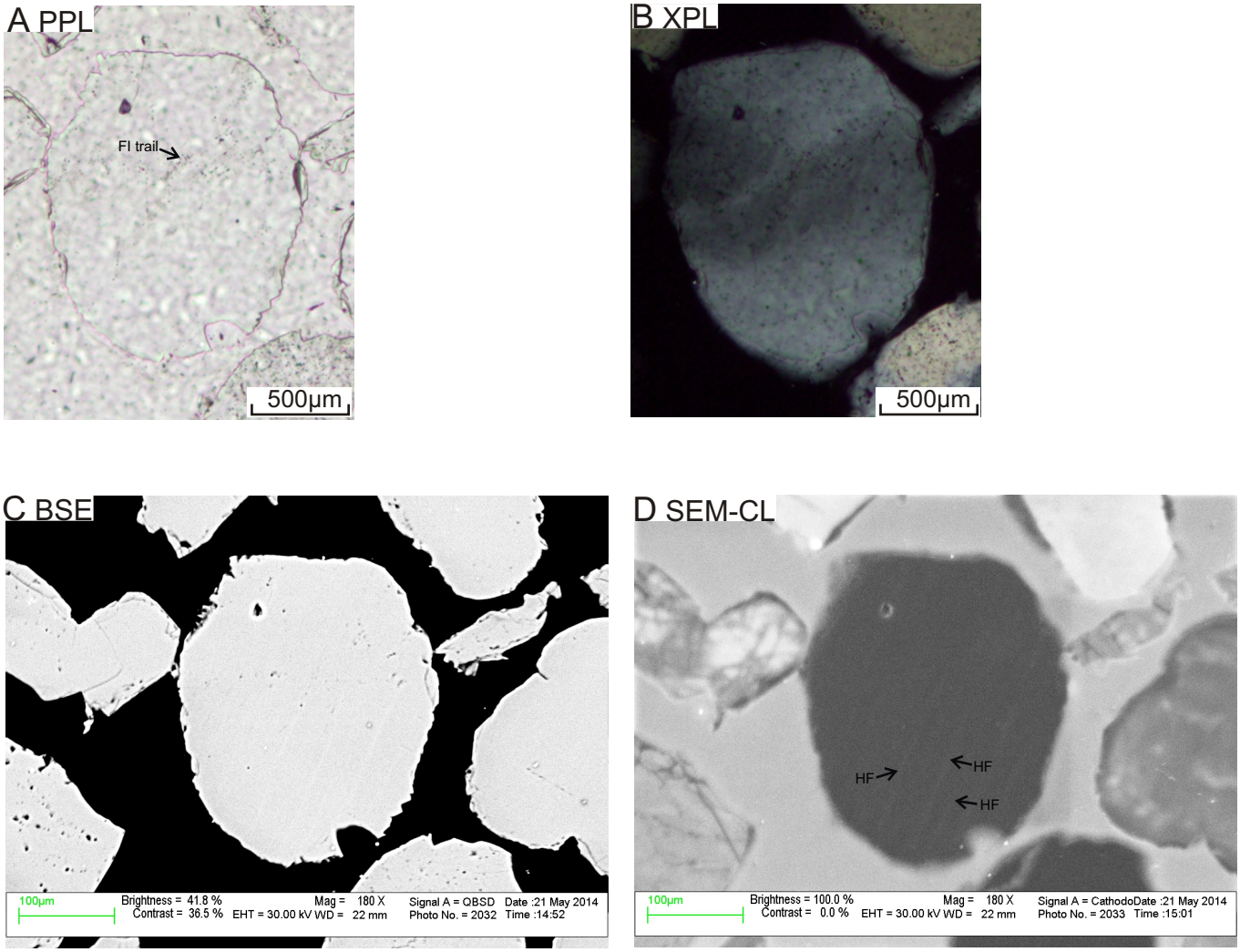

Figure 6A-18: Microphotos under ppl (A) and xpl (B), SEM-BSE image (C) and SEM-CL image (D) of quartz grain 18 in sample 3425. The grain is anhedral and rounded monocrystalline with strong undulose extinction. Fluid inclusion trails are present (Fig. A). Fractures are rare.

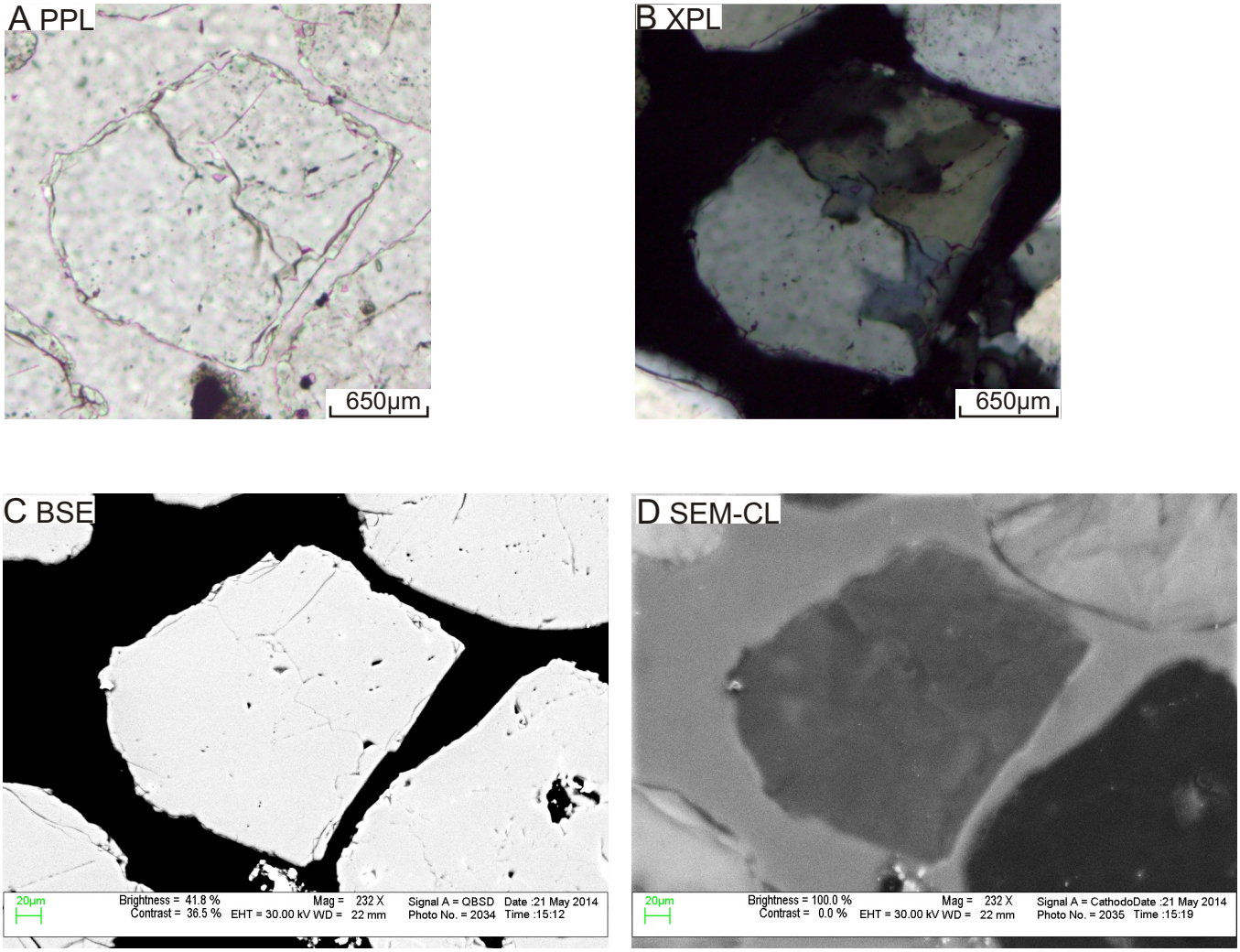

Figure 6A-19: Microphotos under ppl (A) and xpl (B), SEM-BSE image (C) and SEM-CL image (D) of quartz grain 19 in sample 3425. The grain is anhedral and sub-rounded polycrystalline (more than 7 sub-grains with sutured sub-grain boundaries) with mosaic texture and weak undulose extinction. Fluid inclusions are rare (Fig. A). The grain is weakly microfractured with a set of irregular fractures (Fig. C and D). Healed fractures are rare (Fig. D). The grain shows subtle mottling in SEM-CL image.

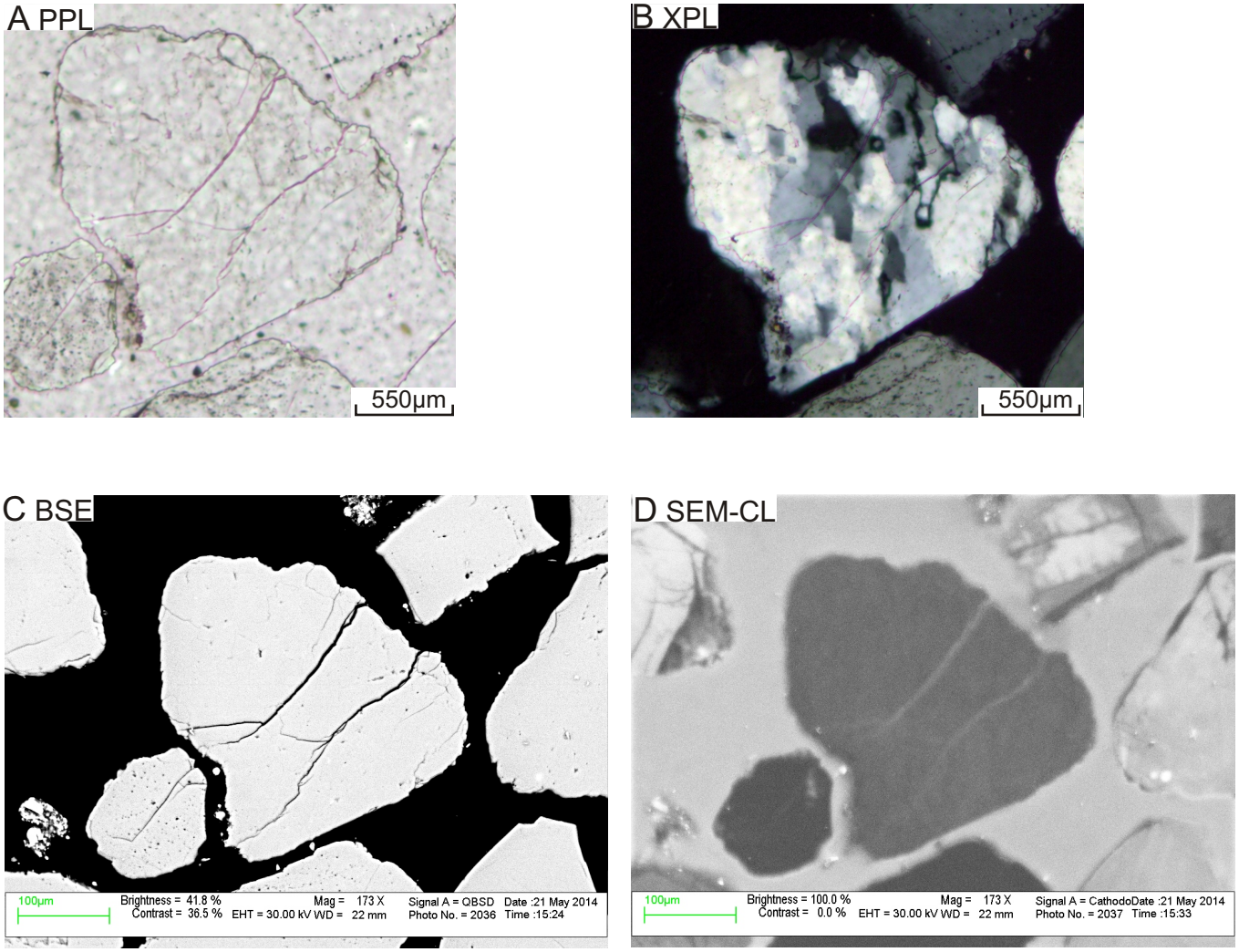

Figure 6A-20: Microphotos under ppl (A) and xpl (B), SEM-BSE image (C) and SEM-CL image (D) of quartz grain 20 in sample 3425. The grain is anhedral and sub-rounded polycrystalline (more than 10 sub-grains sutured sub-grain boundaries) with mosaic texture and weak undulose extinction. Fluid inclusions are rare. The grain is microfractured with a set of irregular fractures (Fig. A and C). Healed fractures are rare.

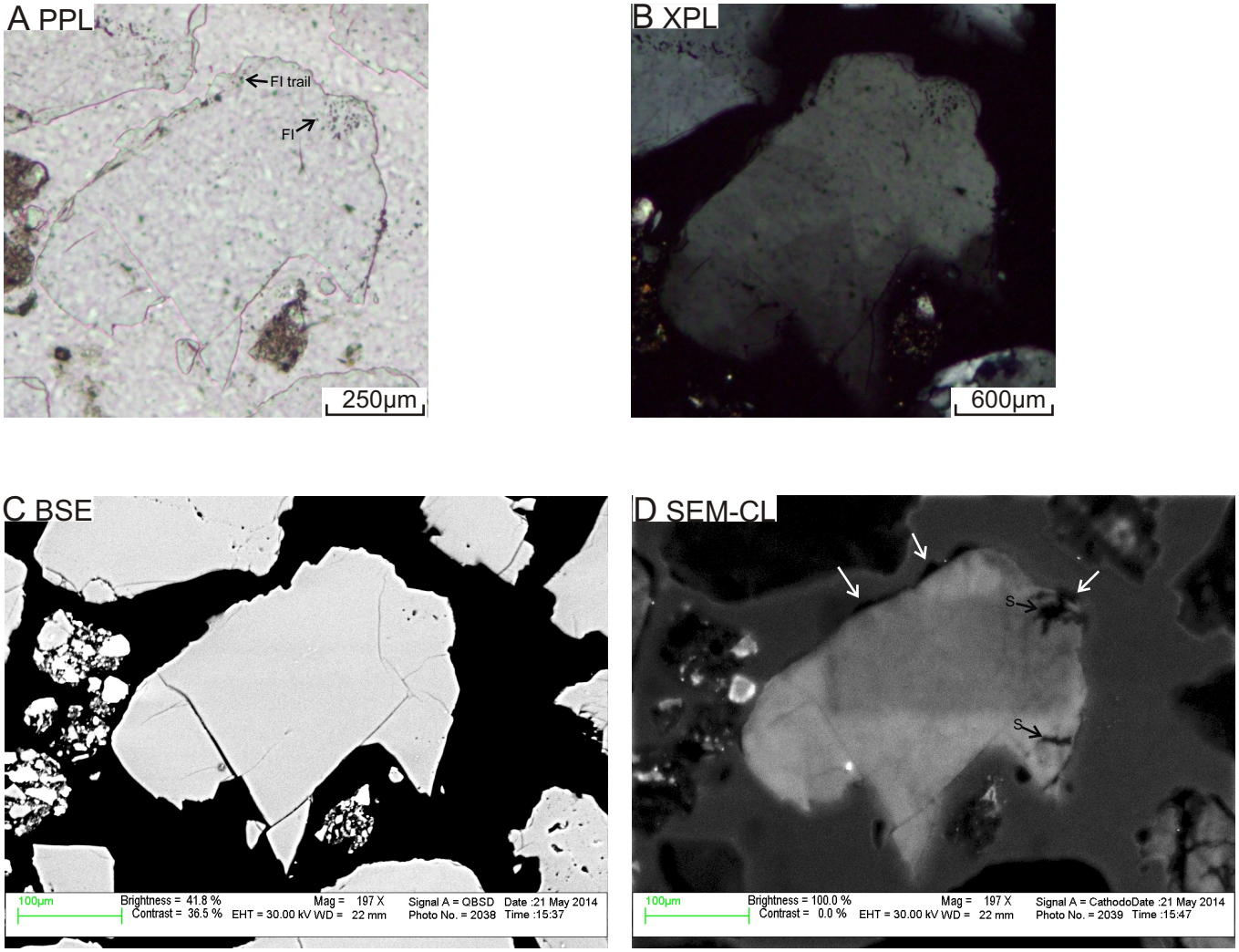

Figure 6A-21: Microphotos under ppl (A) and xpl (B), SEM-BSE image (C) and SEM-CL image (D) of quartz grain 21 in sample 3425. The grain is anhedral and angular monocrystalline with strong undulose extinction. Fluid inclusions are present; they form trails (FI trail) at the boundary between the detrital quartz and the overgrowth (Fig. A). The grain is weakly microfractured with a set of irregular fractures (Fig. C and D). Healed fractures are rare. However, some spiders (S) can be seen in Fig. D. The dark areas indicated by arrows in Fig. D are overgrowth.

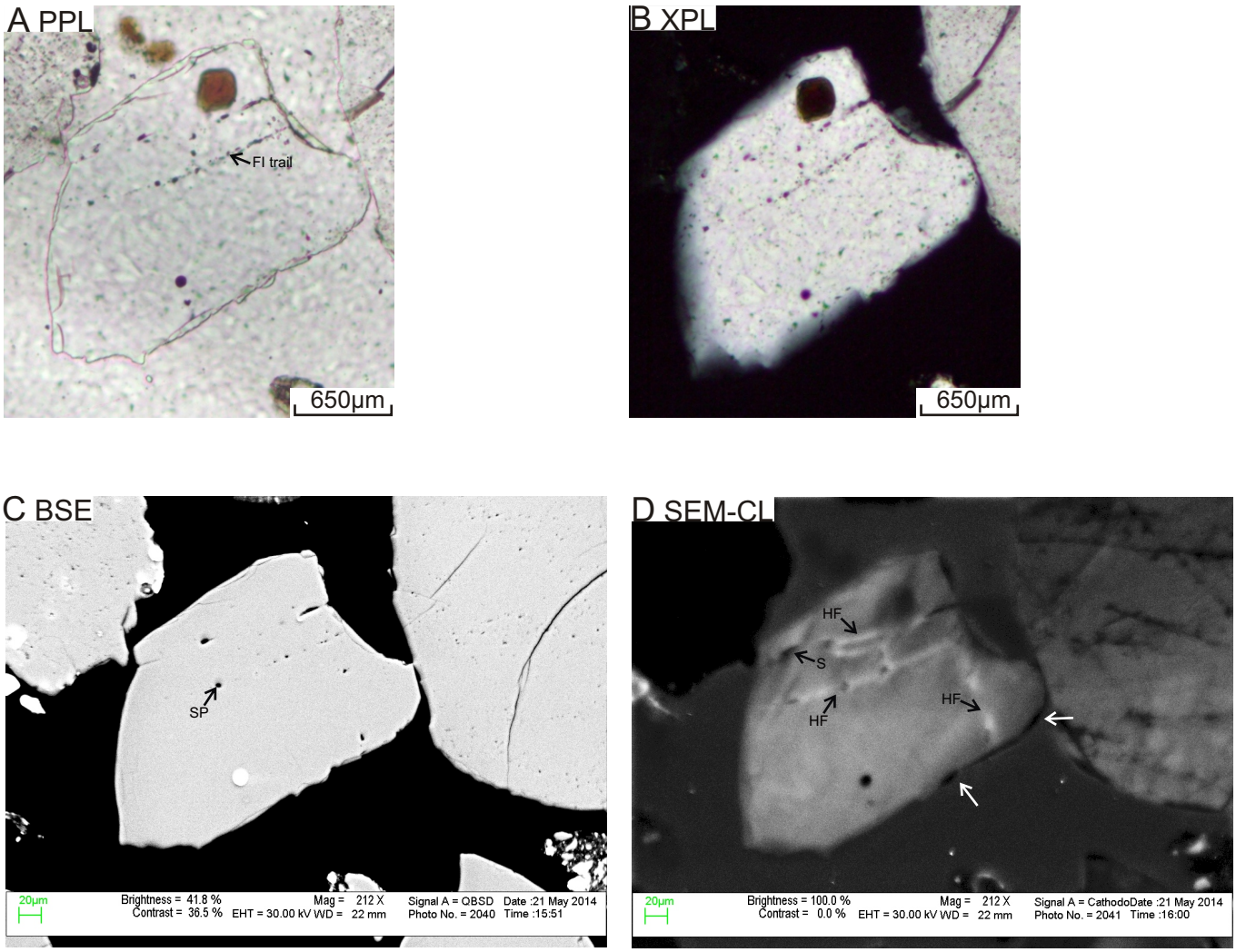

Figure 6A-22: Microphotos under ppl (A) and xpl (B), SEM-BSE image (C) and SEM-CL image (D) of quartz grain 22 in sample 3425. The grain is anhedral and sub-rounded monocrystalline with non-undulose extinction. Fluid inclusions are common; they are usually associated with secondary porosity (SP) and form trails (FI trail) along healed fractures (Fig. A and C). The grain is microfractured with a set of irregular fractures (Fig. C and D). Some healed fractures (HF) and spiders (S) can be seen in Fig. D. The dark areas indicated by arrows in Fig. D are overgrowth.

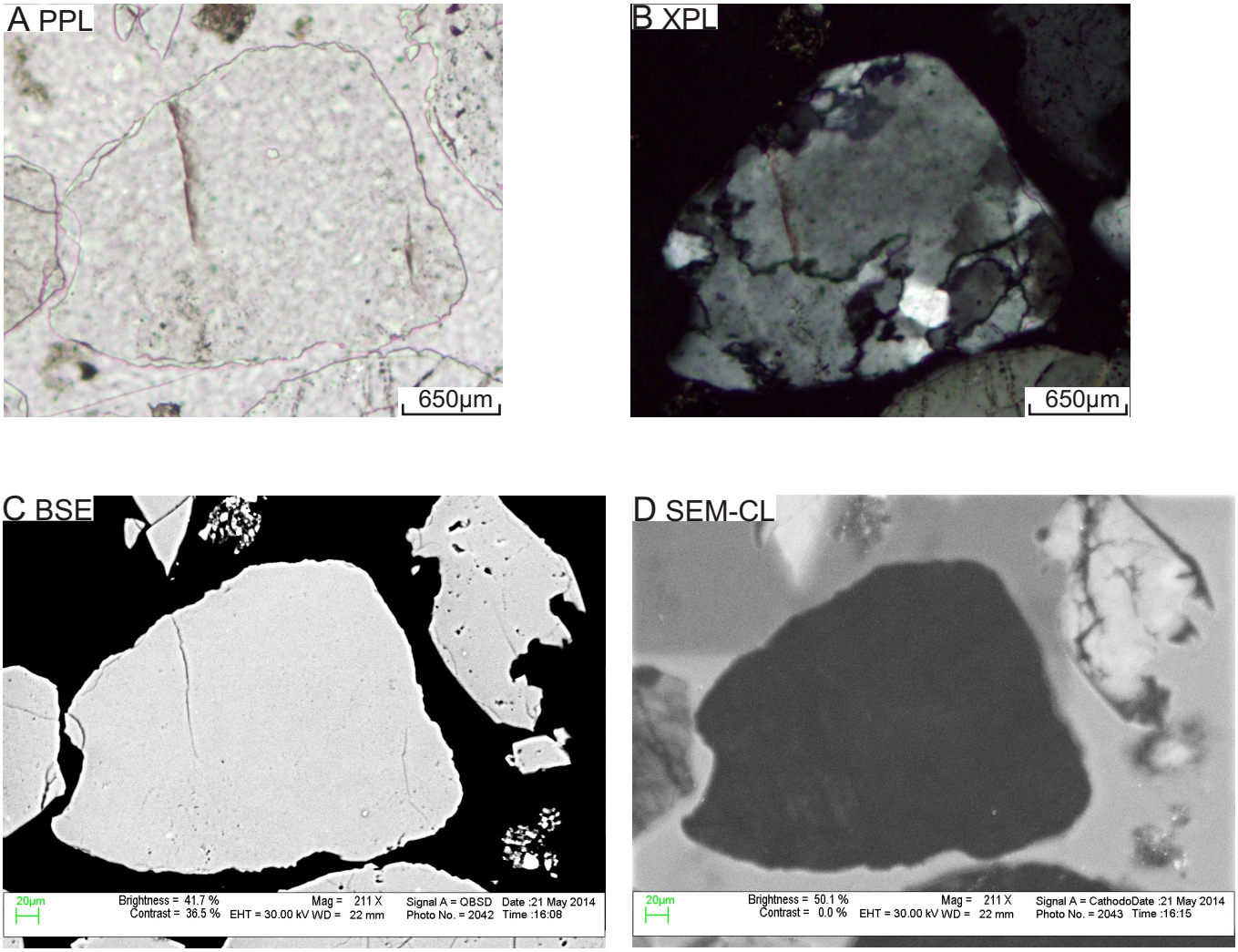

Figure 6A-23: Microphotos under ppl (A) and xpl (B), SEM-BSE image (C) and SEM-CL image (D) of quartz grain 23 in sample 3425. The grain is anhedral and sub-rounded polycrystalline (more than 10 sub-grains with sutured sub-grain boundaries) with mosaic texture and weak undulose extinction. The grain contains fluid inclusion trails and is weakly microfractured with a set of irregular fractures (Fig. A and C).

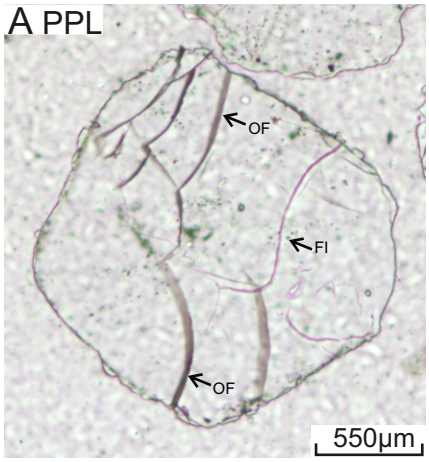

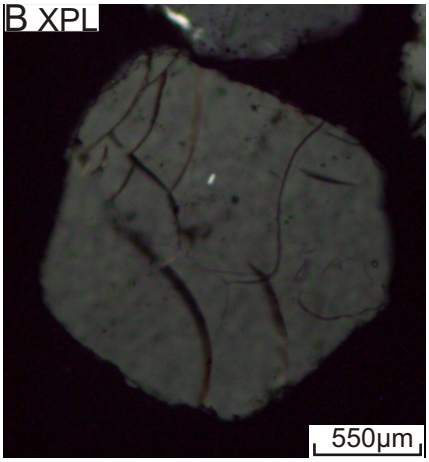

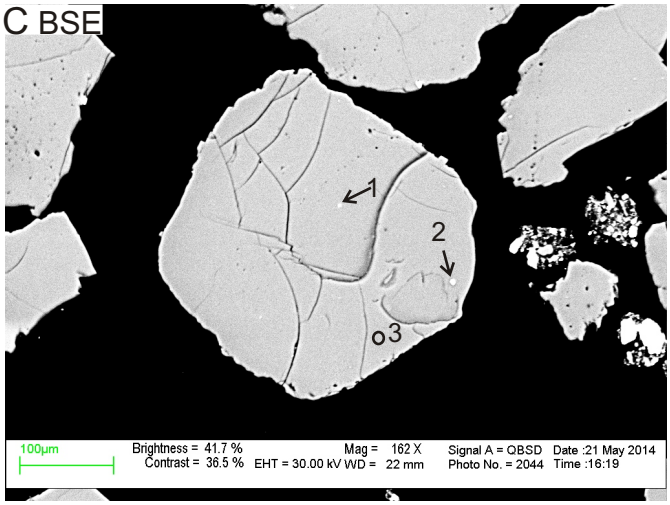

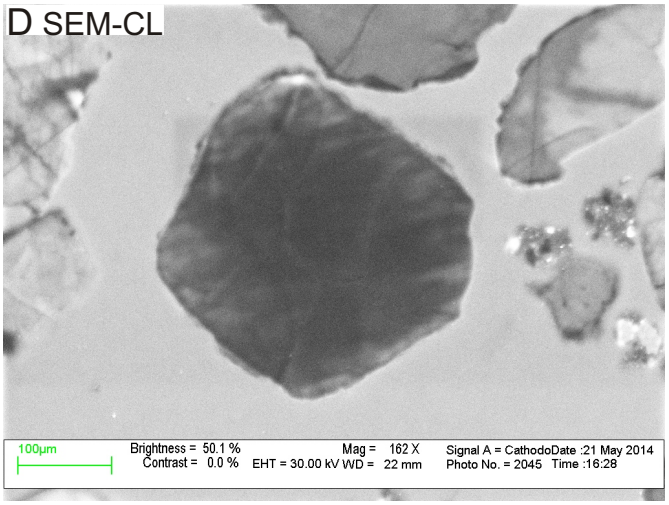

E EDS analyses

Pos#	Min. ID	SiO2	TiO2	Al2O3	CaO	F	Total	Actual Total
1	Qz+Ttn	83.45	8.26	0.89	7.39		100	74
2	Qz+Ttn	69.95	13.73	1.97	11.7	2.66	100	72
3	Qz	99.99					100	73

Figure 6A-24: Microphotos under ppl (A) and xpl (B), SEM-BSE image (C), SEM-CL image (D), and EDS analyses table (E) of quartz grain 24 in sample 3425. The grain is anhedral and rounded monocrystalline with weak undulose extinction. Fluid inclusions are present (Fig. A). The grain contains titanite inclusions and is microfractured with a set of irregular curved open fractures (Fig. A and C). Healed fractures are rare. The grain shows bright-CL streaky patches fabric in SEM-CL image.

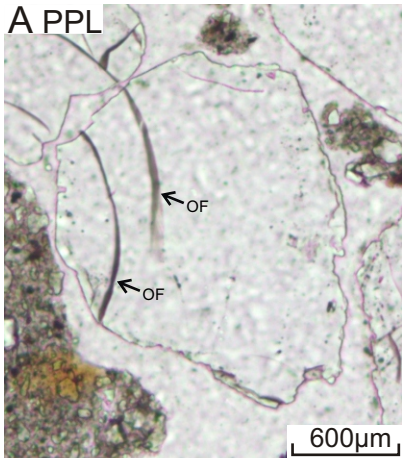

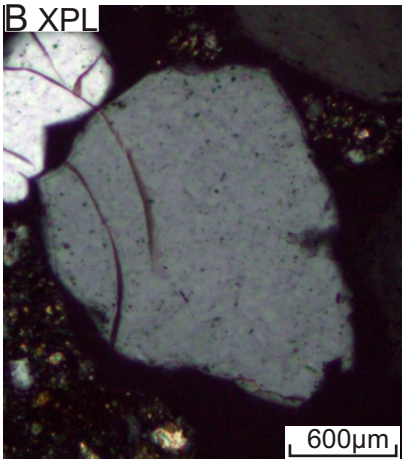

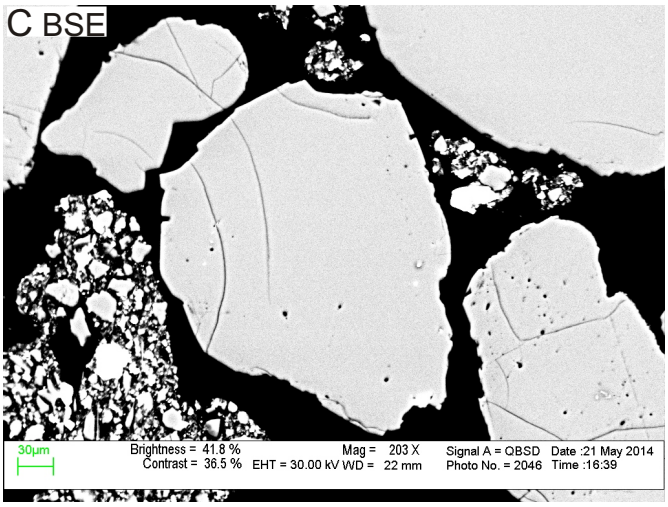

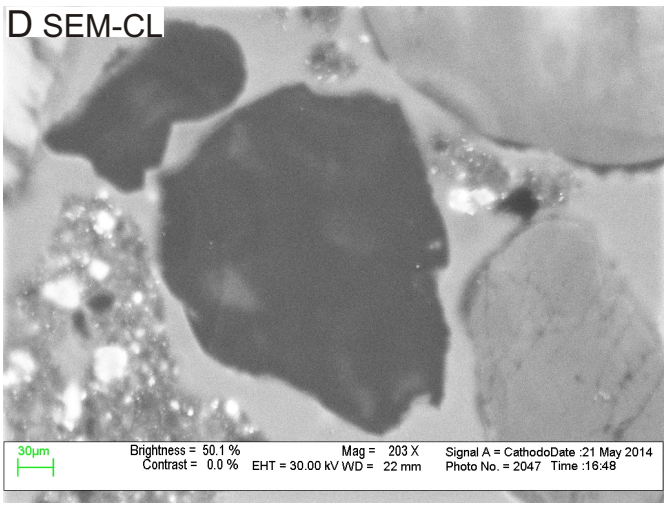

Figure 6A-25: Microphotos under ppl (A) and xpl (B), SEM-BSE image (C) and SEM-CL image (D) of quartz grain 25 in sample 3425. The grain is anhedral and sub-rounded monocrystalline with weak undulose extinction. Fluid inclusions are rare (Fig. A). The grain is microfractured with a set of irregular curved open fractures (Fig. A and C). Healed fractures are rare. The grain shows subtle mottling in SEM-CL image.

A PPL

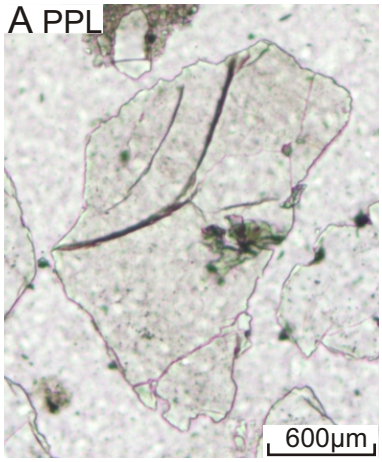

B XPL

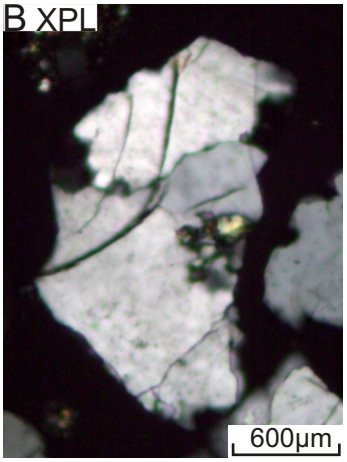

C BSE

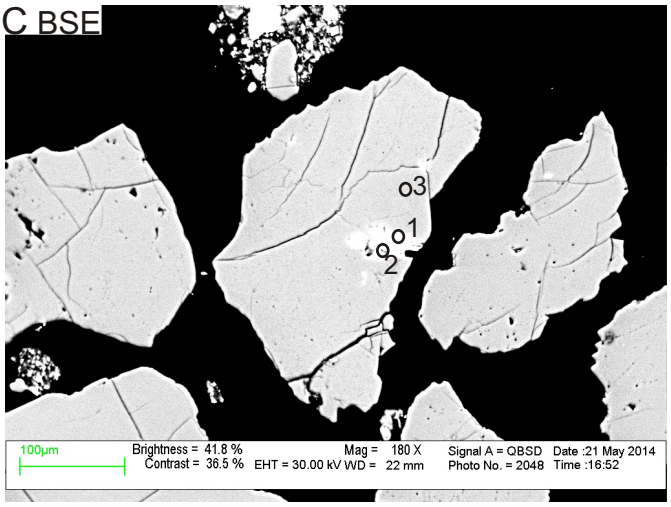

D SEM-CL

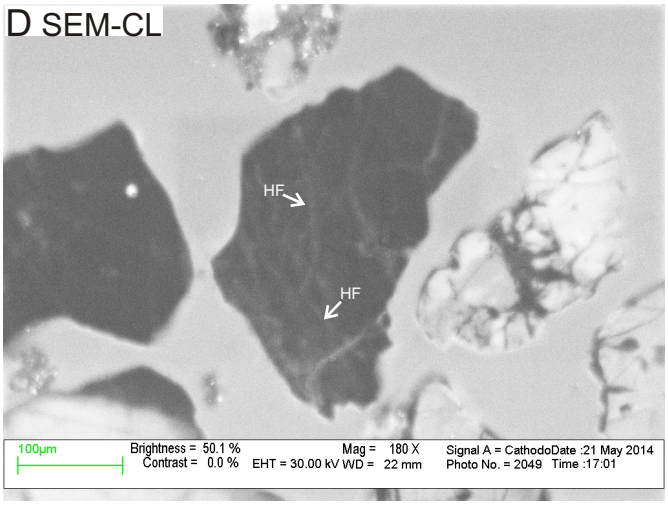

E EDS analyses

Pos#	Min. ID	SiO2	Al2O3	FeO	MnO	MgO	CaO	Na2O	Cr2O3	Total	Actual Total
1	Chl	30.6	21.07	28.21	0	4.6	0.29	0	0.22	85	54
2	Chl	34.84	18.49	26.94	0.23	3.83	0.21	0.451	0	85	54
3	Qz	99.99								100	71

Figure 6A-26: Microphotos under ppl (A) and xpl (B), SEM-BSE image (C), SEM-CL image (D), and EDS analyses table (E) of quartz grain 26 in sample 3425. The grain is anhedral and sub-angular polycrystalline (more than 6 sub-grains with sutured sub-grain boundaries) with mosaic texture and weak undulose extinction. Fluid inclusions are rare (Fig. A). The grain contains chlorite inclusions and is microfractured with a set of irregular curved fractures (Fig. C and D). Some healed fractures can be seen in Fig, D.

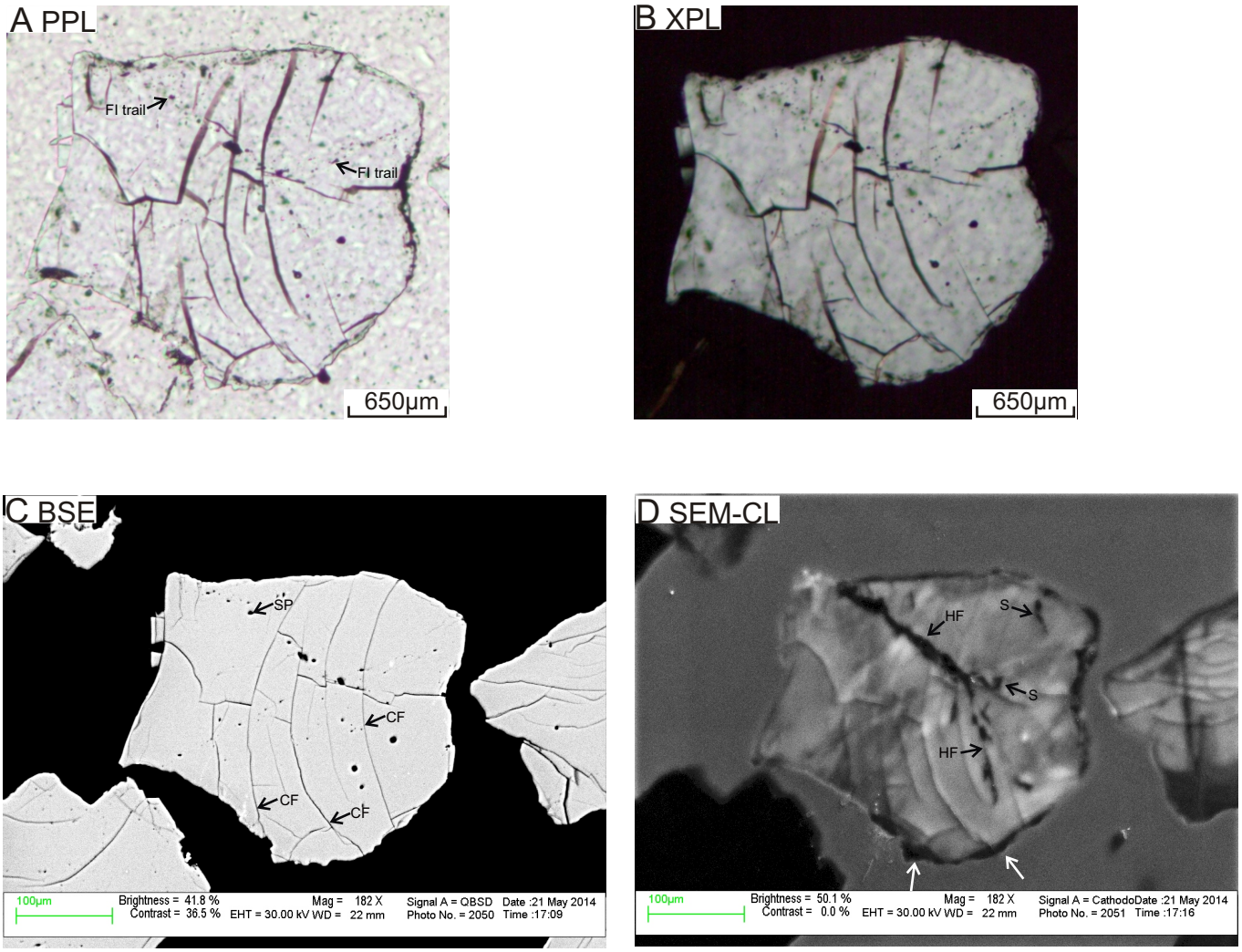

Figure 6A-27: Microphotos under ppl (A) and xpl (B), SEM-BSE image (C) and SEM-CL image (D) of quartz grain 27 in sample 3425. The grain is anhedral and sub-angular monocrystalline with non-undulose extinction. Fluid inclusions are common; they are usually associated with secondary porosity (SP) and form trails (FI trail) along healed fractures (Fig. A and C). The grain is microfractured with a set of conchoidal open fractures (CF) and a set of irregular fractures (Fig. C and D). Some healed fractures (HF) and spiders (S) can be seen in Fig, D. The dark areas indicated by arrows in Fig. D are overgrowth. The grain show random bright-CL patches in SEM-CL image.

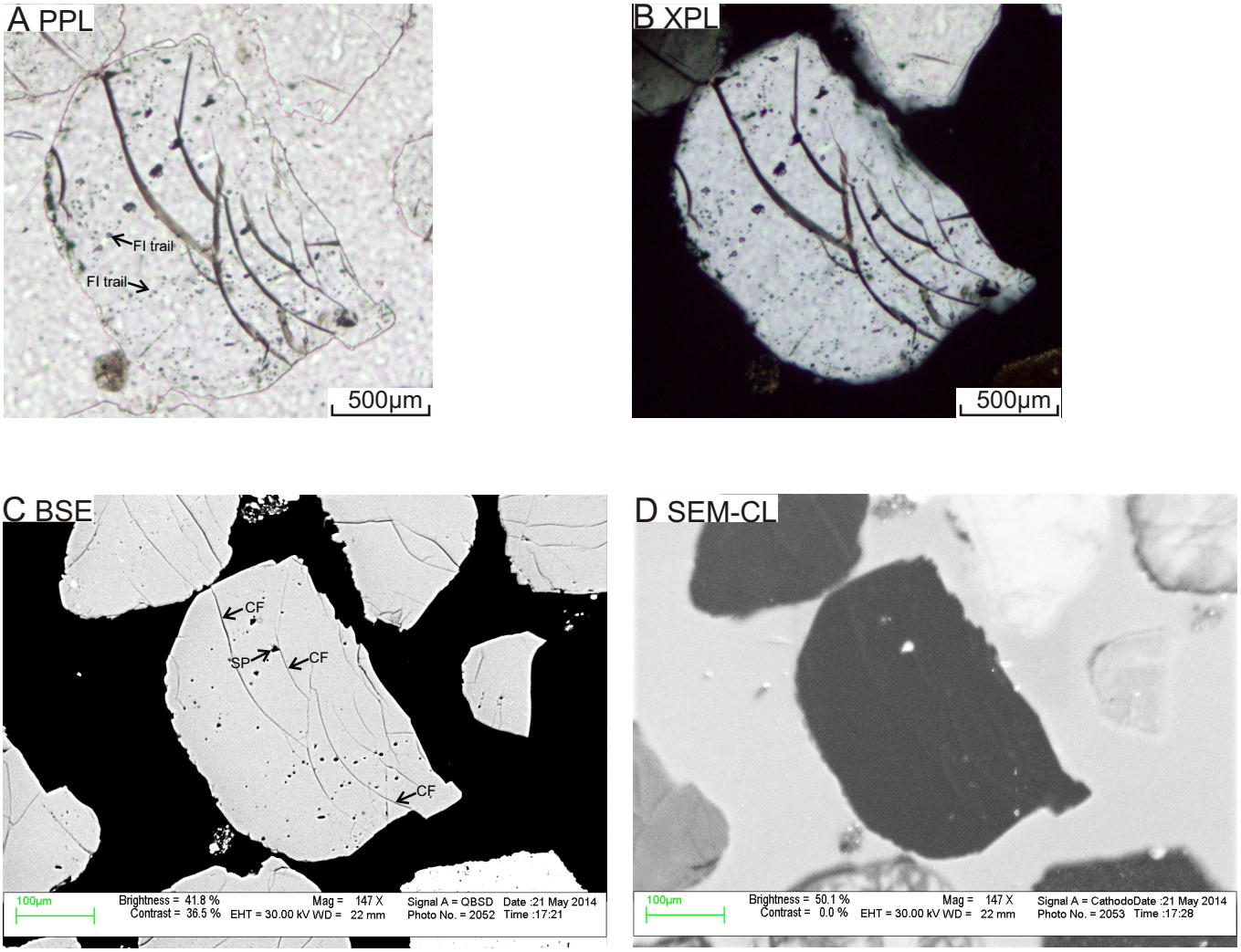

Figure 6A-28: Microphotos under ppl (A) and xpl (B), SEM-BSE image (C) and SEM-CL image (D) of quartz grain 28 in sample 3425. The grain is anhedral and sub-rounded monocrystalline with weak undulose extinction. Fluid inclusions are common; they are usually associated with secondary porosity (SP) and form trails (FI trail) along healed fractures (Fig. A and C). The grain is microfractured with a set of conchoidal open fractures (Fig. C). Healed fractures are probably camouflaged by the homogeneous dark-CL image (Fig. D).

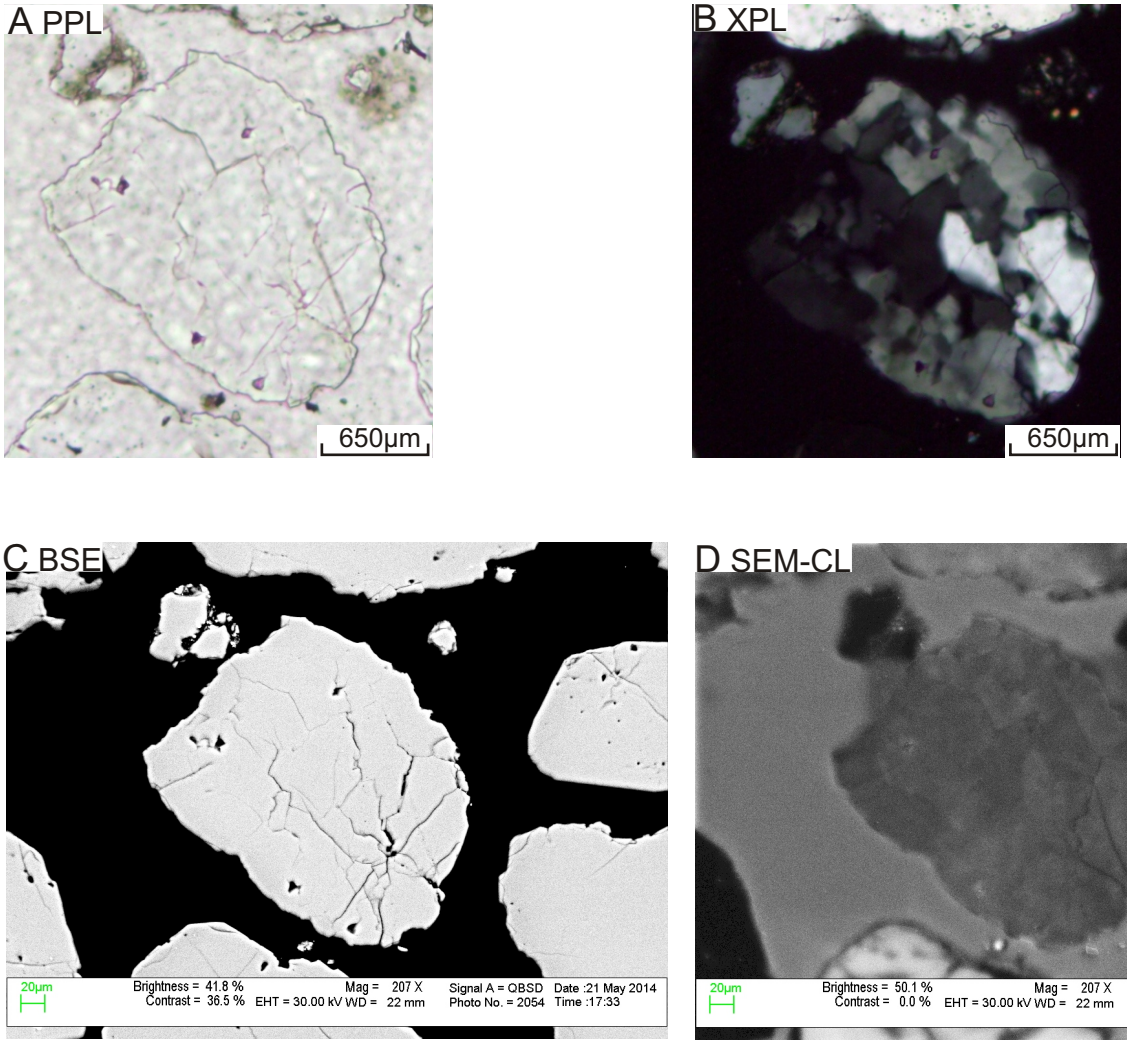

Figure 6A-29: Microphotos under ppl (A) and xpl (B), SEM-BSE image (C) and SEM-CL image (D) of quartz grain 29 in sample 3425. The grain is anhedral and sub-rounded polycrystalline (more than 10 sub-grains with sutured sub-grain boundaries) with mosaic texture and weak undulose extinction. The grain is weakly microfractured with a set of irregular fractures (Fig. A and C). Healed fractures are rare. The grain shows subtle mottling in SEM-CL image.

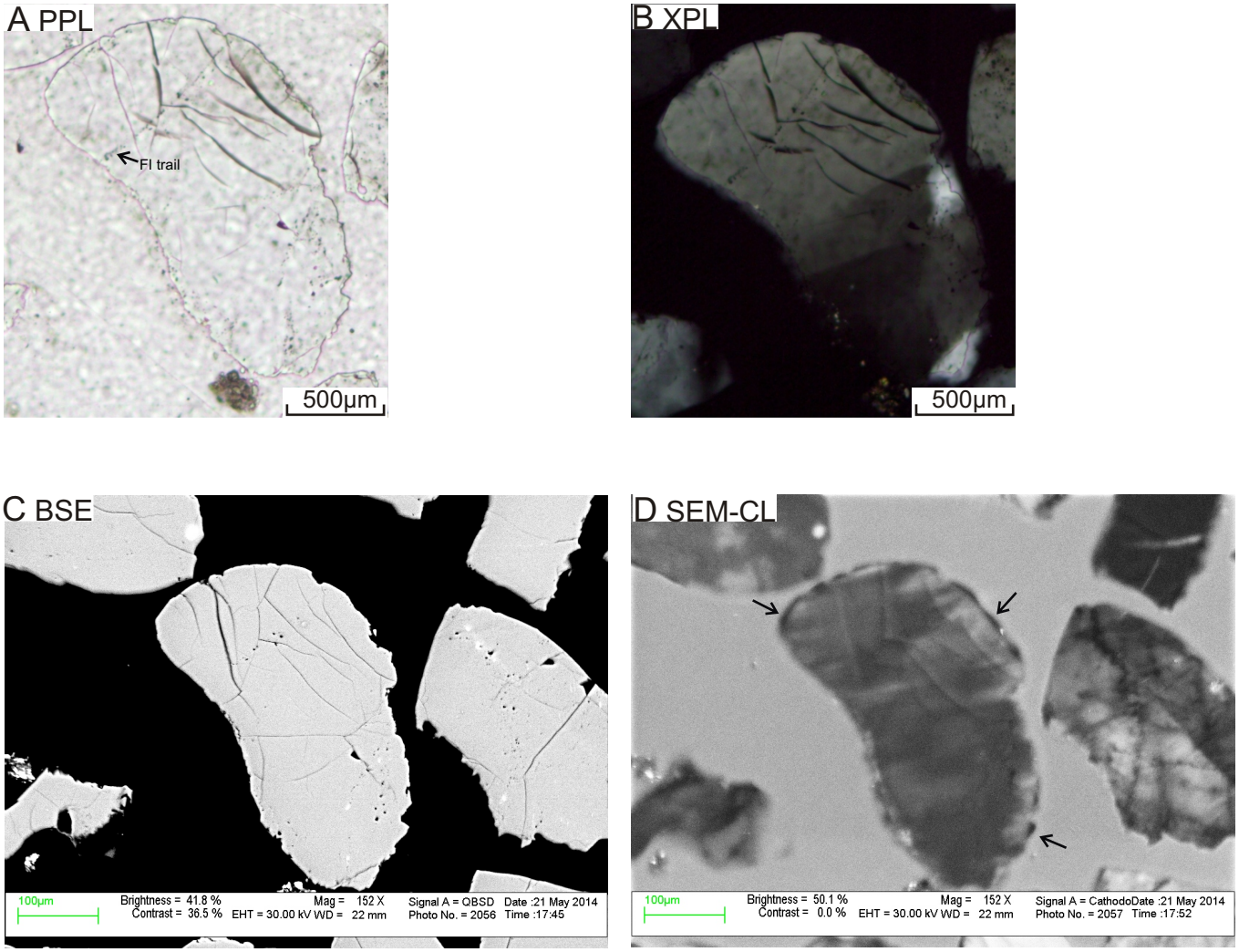

Figure 6A-30: Microphotos under ppl (A) and xpl (B), SEM-BSE image (C) and SEM-CL image (D) of quartz grain 30 in sample 3425. The grain is anhedral and sub-rounded monocrystalline with strong undulose extinction. Fluid inclusion trails are present (Fig. A). The grain is microfractured with a set of irregular curved fractures (Fig. C and D). Healed fractures are rare. The grain shows bright-CL streaky patches fabric in SEM-CL image.

A PPL

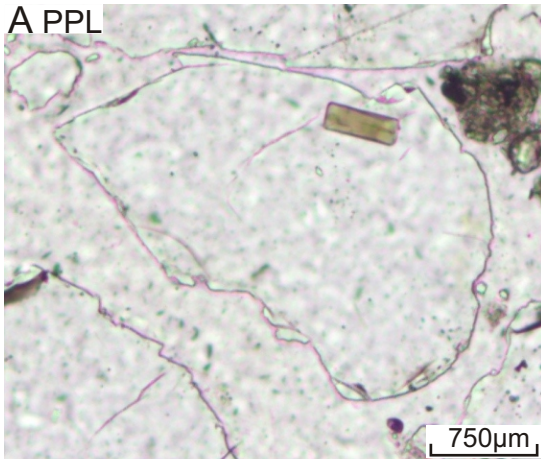

B XPL

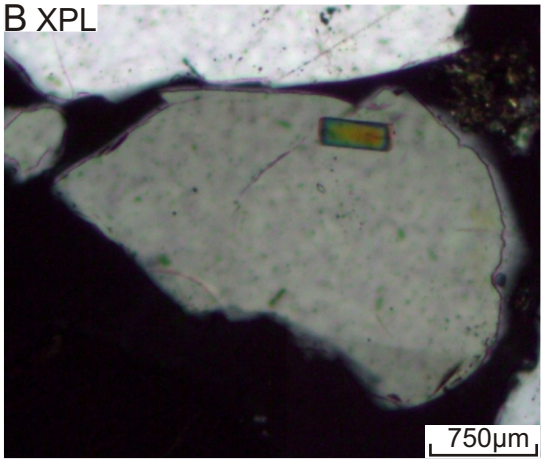

C BSE

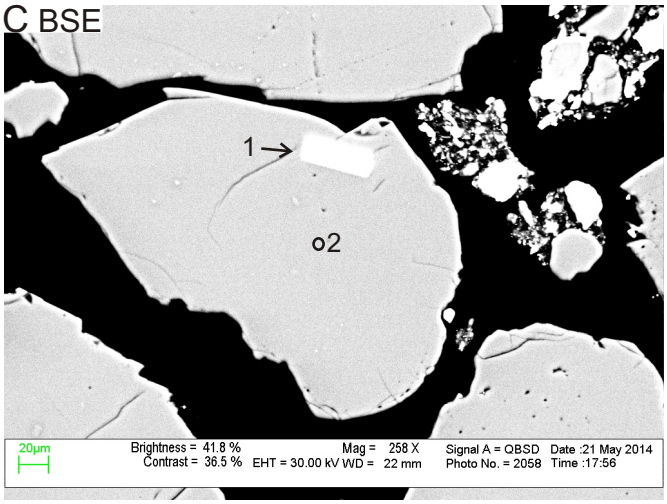

D SEM-CL

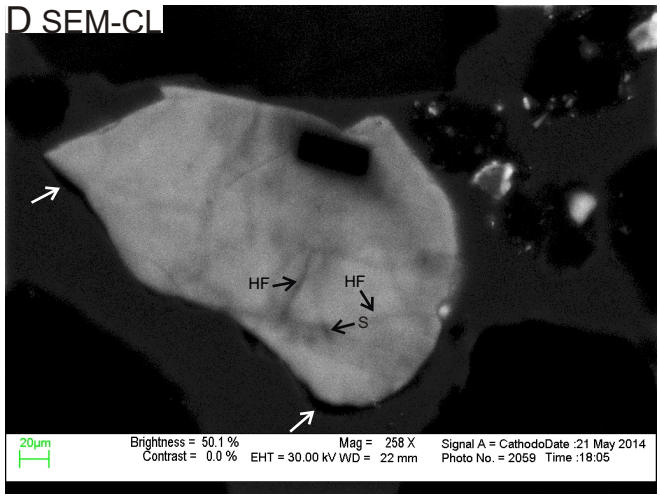

E EDS analyses

Pos#	Min. ID	SiO2	TiO2	Al2O3	FeO	MgO	K2O	Total	Actual Total
1	Bt	40.89	2.9	16.09	8.44	17.89	9.79	96	67
2	Qz	99.99						100	77

Figure 6A-31: Microphotos under ppl (A) and xpl (B), SEM-BSE image (C), SEM-CL image (D), and EDS analyses table (E) of quartz grain 31 in sample 3425. The grain is anhedral and sub-angular monocrystalline with weak undulose extinction. Fluid inclusions are rare (Fig. A). The grain contains a biotite inclusion and is weakly microfractured with irregular fractures (Fig. A and C). Some healed fractures (HF) and spiders (S) can be seen in Fig. D. The dark areas indicated by arrows in Fig. D are overgrowth.

A PPL

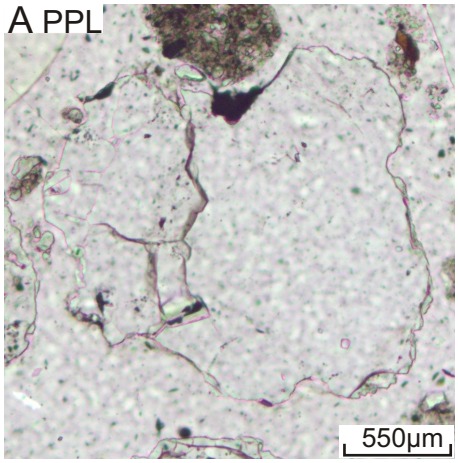

B XPL

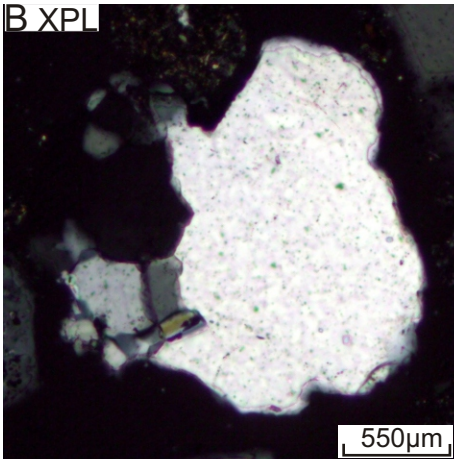

C BSE

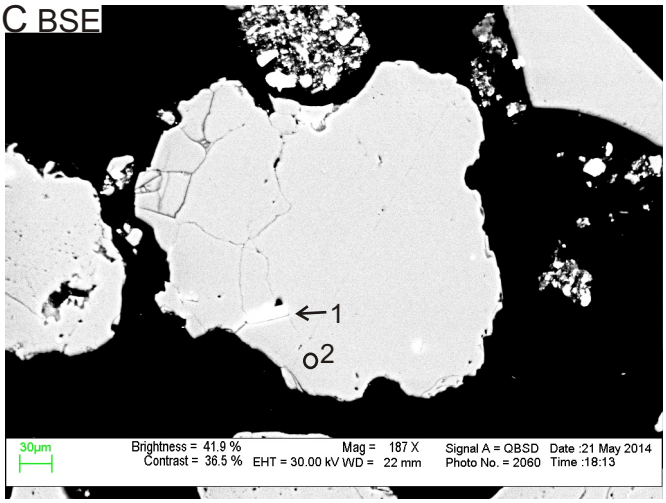

D SEM-CL

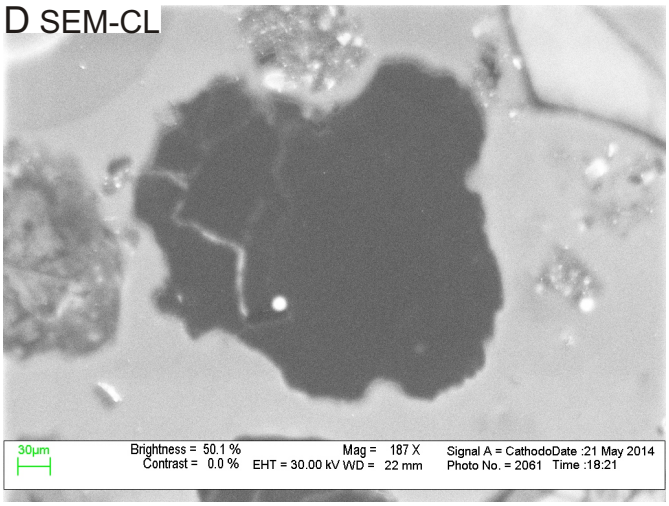

E EDS analyses

Pos#	Min. ID	SiO2	TiO2	Al2O3	FeO	MgO	K2O	SO3	Total	Actual Total
1	Chloritized Ms	51.99	0.27	27.29	3.78	1.8	10.01	0.86	96	68
2	Qz	99.99							100	75

Figure 6A-32: Microphotos under ppl (A) and xpl (B), SEM-BSE image (C), SEM-CL image (D), and EDS analyses table (E) of quartz grain 32 in sample 3425. The grain is anhedral and sub-angular polycrystalline (more than 7 sub-grains with sutured sub-grain boundaries) with irregular and embayed margins, mosaic texture and weak undulose extinction. Fluid inclusions are rare (Fig. A). The grain contains a chloritized muscovite inclusion and is weakly microfractured with irregular fractures (Fig. A and C). Healed fractures are rare. The grain show homogeneous dark-CL (Fig. D).

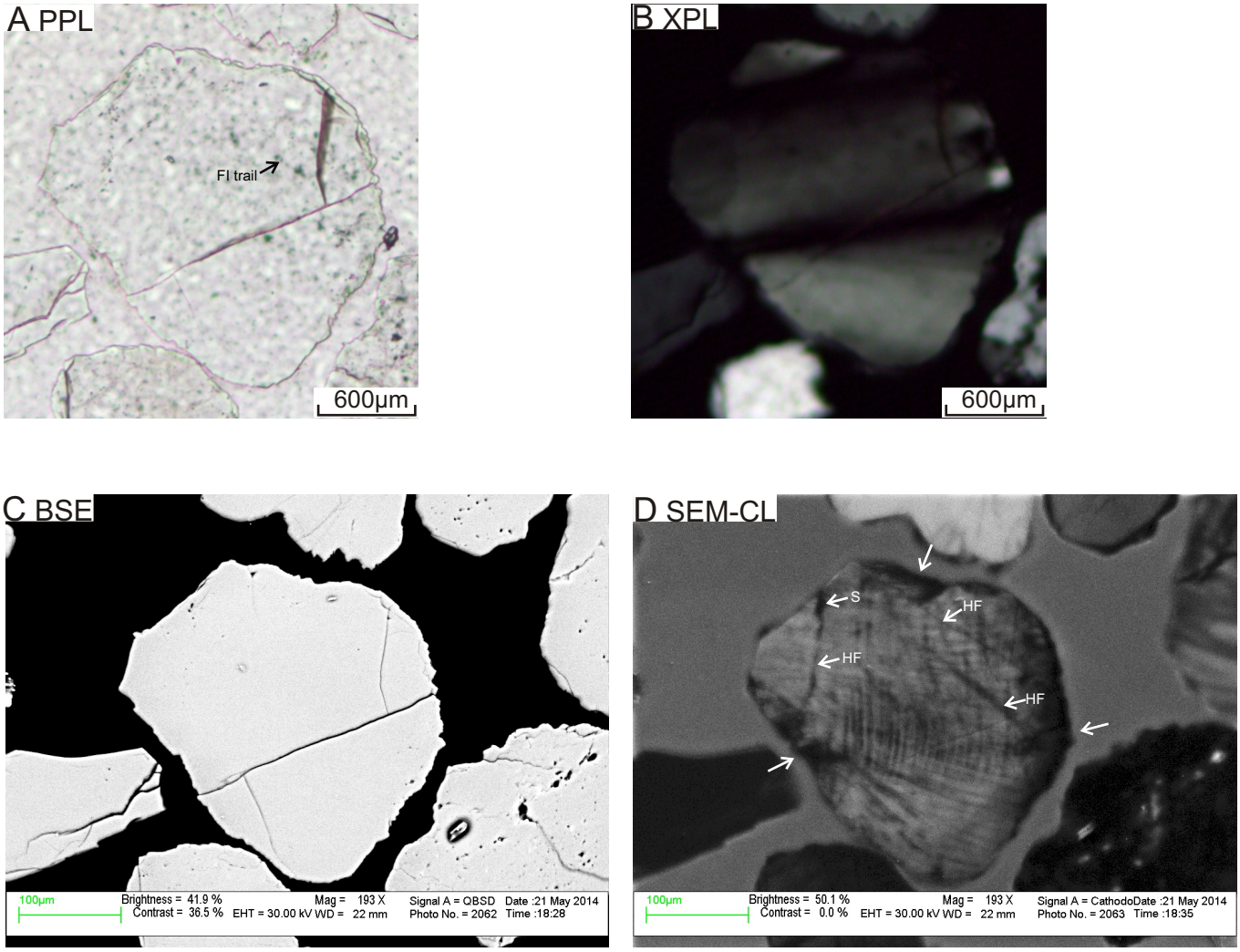

Figure 6A-33: Microphotos under ppl (A) and xpl (B), SEM-BSE image (C) and SEM-CL image (D) of quartz grain 33 in sample 3425. The grain is anhedral and sub-angular polycrystalline (only 2 sub-grains) with strong undulose extinction and deformation lamellae. Fluid inclusions are present and form trails along healed fractures (Fig. A). The grain is microfractured with a set of irregular fractures (Fig. C and D). Some healed fractures (HF) and spiders (S) are present (Fig. D). The dark areas indicated by arrows in Fig. D are overgrowth. The SEM-CL image shows the presence of two sets of sub-parallel CL-dark lines, indicating deformation lamellae. The different orientation of these sets suggests two different deformational events.

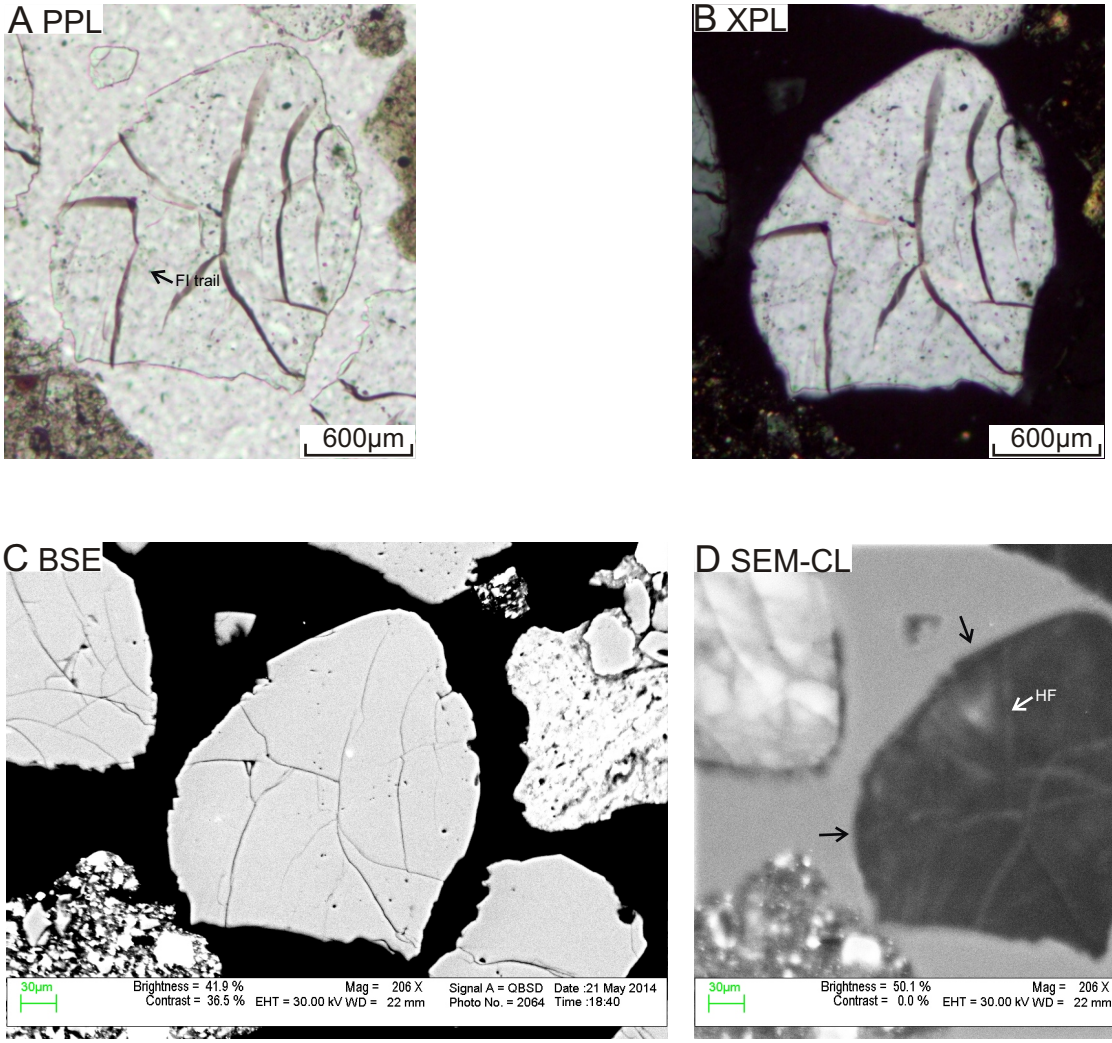

Figure 6A-34: Microphotos under ppl (A) and xpl (B), SEM-BSE image (C) and SEM-CL image (D) of quartz grain 34 in sample 3425. The grain is anhedral and sub-rounded monocrystalline with mosaic texture and weak undulose extinction. Fluid inclusions are present and form trails along healed fractures (Fig. A). The grain is microfractured with a set of irregular fractures (Fig. C and D). A few healed fractures (HF)are present (Fig. D). The dark areas indicated by arrows in Fig. D are overgrowth. The grain shows subtle mottling in SEM-CL image.

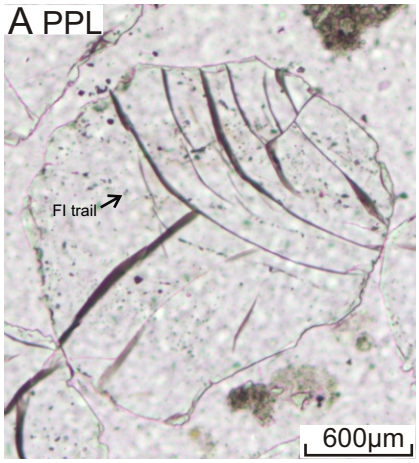

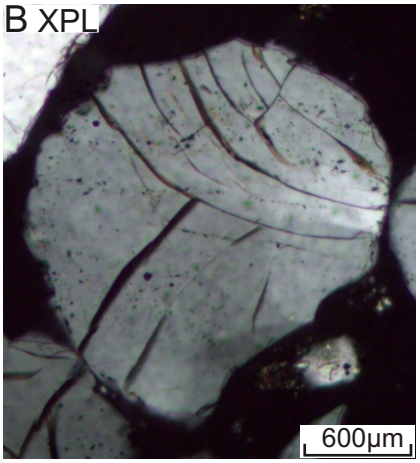

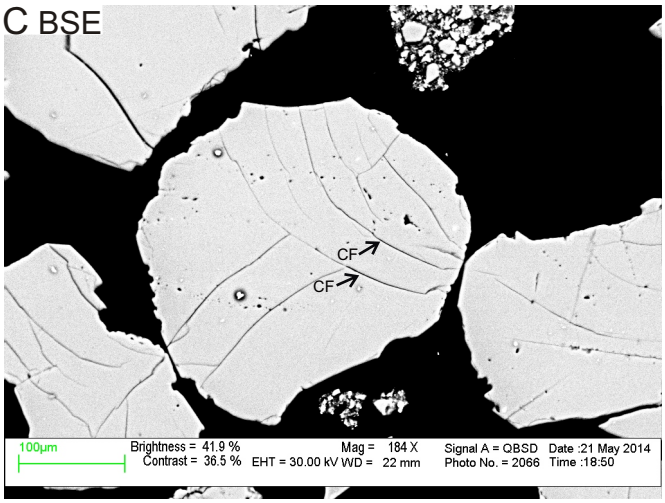

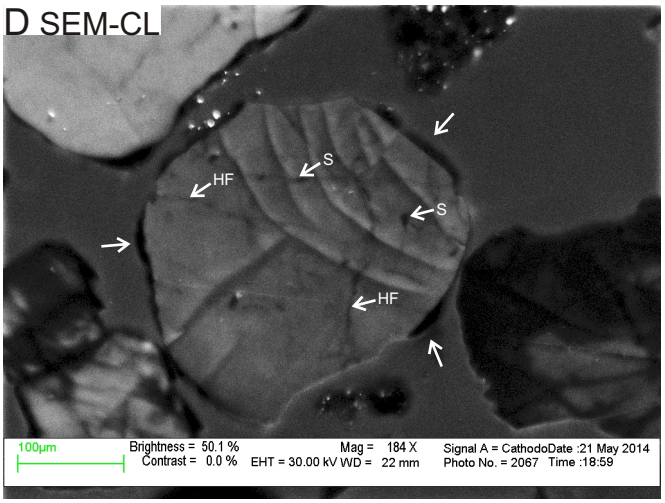

Figure 6A-35: Microphotos under ppl (A) and xpl (B), SEM-BSE image (C) and SEM-CL image (D) of quartz grain 35 in sample 3425. The grain is anhedral and sub-rounded monocrystalline with mosaic texture and weak undulose extinction. Fluid inclusions are common; they are usually associated with secondary porosity and form trails (FI trail) along healed fractures (Fig. A). The grain is microfractured with a set of conchoidal open fractures (Fig. C) and a set of irregular fractures. Some healed fractures (HF) and spiders (S) are present (Fig. D). The dark areas indicated by arrows in Fig. D are overgrowth.

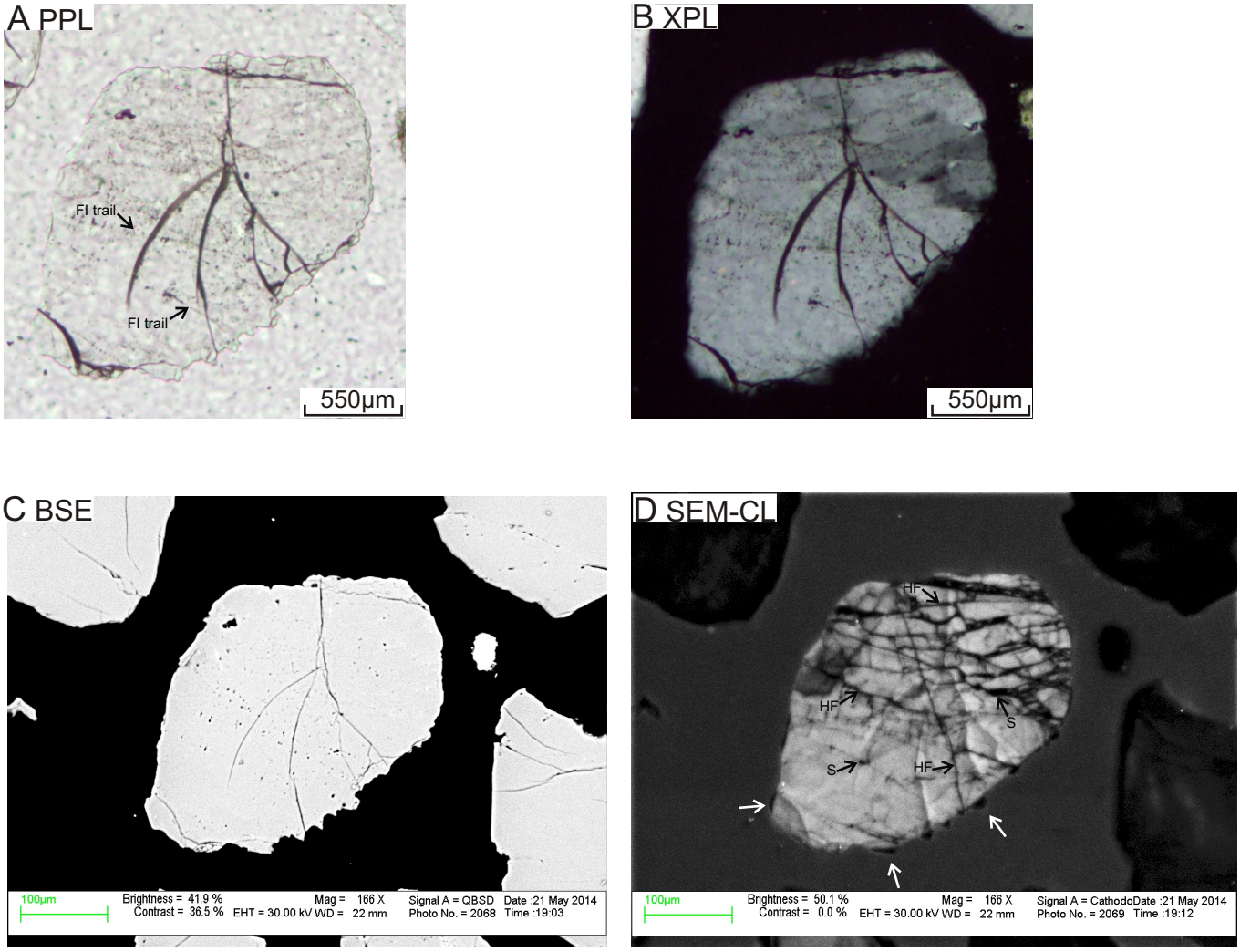

Figure 6A-36: Microphotos under ppl (A) and xpl (B), SEM-BSE image (C) and SEM-CL image (D) of quartz grain 36 in sample 3425. The grain is anhedral and sub-rounded polycrystalline (only 3 sub-grains) with mosaic texture and weak undulose extinction. Fluid inclusions are common; they are usually associated with secondary porosity and form trails (FI trail) along healed fractures (Fig. A). The grain is strongly microfractured with a set of sub-parallel fractures and a set of irregular fractures (Fig. C and D). Healed fractures (HF) and spiders (S) are common (Fig. D). The dark areas indicated by arrows in Fig. D are overgrowth.

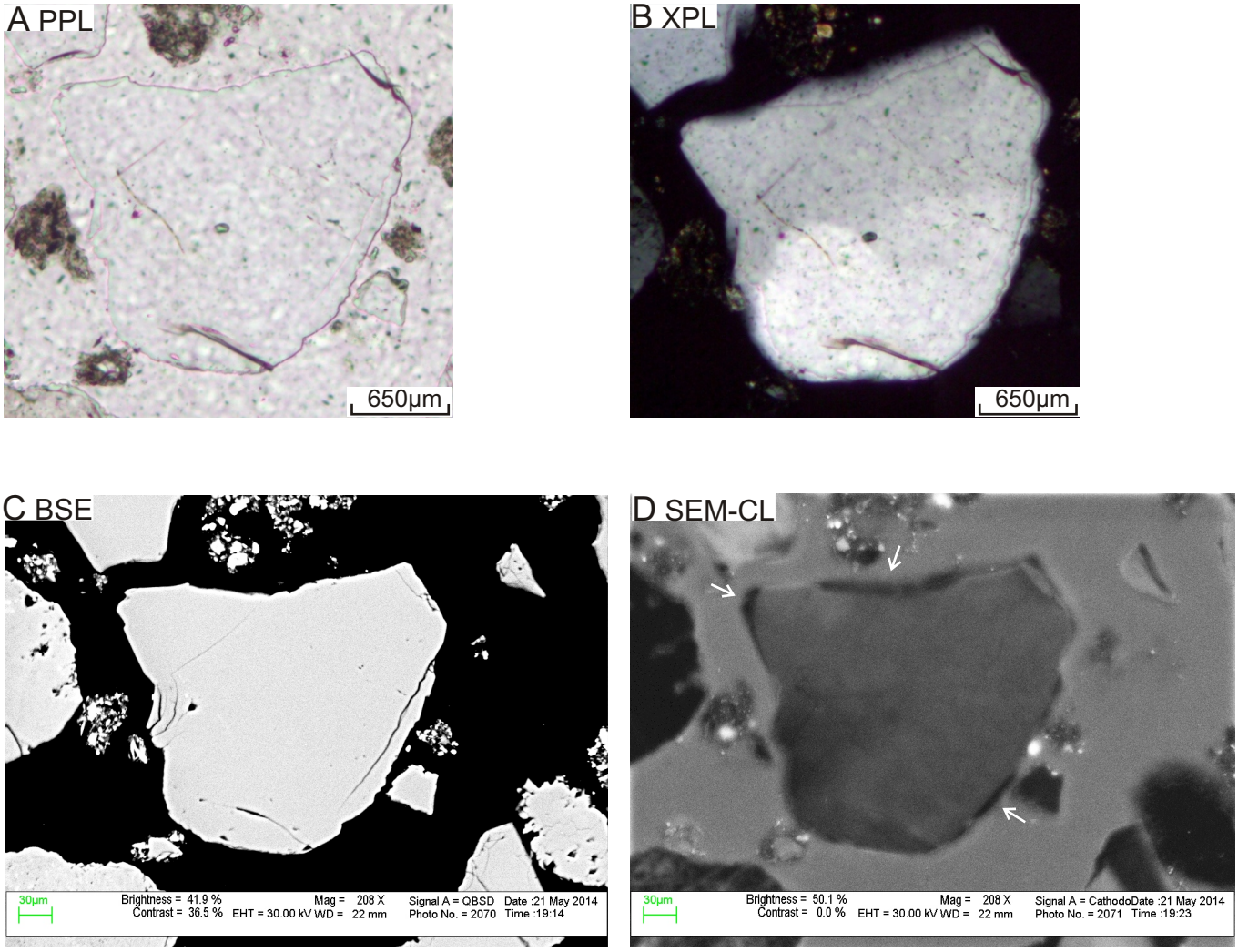

Figure 6A-37: Microphotos under ppl (A) and xpl (B), SEM-BSE image (C) and SEM-CL image (D) of quartz grain 37 in sample 3425. The grain is anhedral and sub-rounded monocrystalline with mosaic texture and strong undulose extinction. Fluid inclusions are rare. The grain is weakly microfractured with irregular fractures (Fig. A and C). Healed fractures are rare (Fig. D). The dark areas indicated by arrows in Fig. D are overgrowth. The grain shows homogenous SEM-CL image.

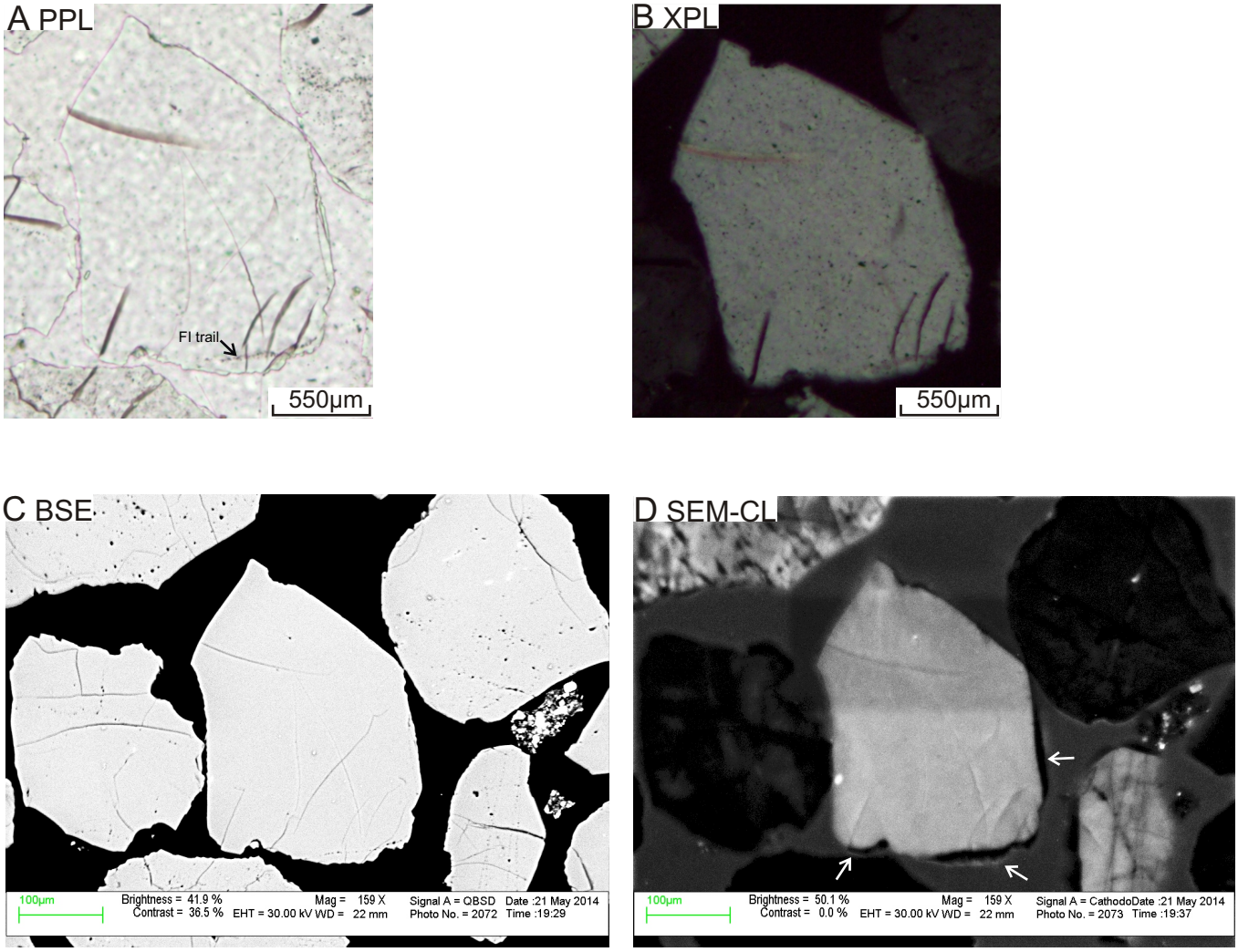

Figure 6A-38: Microphotos under ppl (A) and xpl (B), SEM-BSE image (C) and SEM-CL image (D) of quartz grain 38 in sample 3425. The grain is anhedral and sub-angular monocrystaline with non-undulose extinction. Fluid inclusion trail is present, they are located in the boundary between the detrital quartz and the overgrowth. The grain is weakly microfractured with a set of irregular curved fractures (Fig. A and C). Healed fractures are rare (Fig. D). The dark areas indicated by arrows in Fig. D are overgrowth. The grain shows homogenous SEM-CL image.

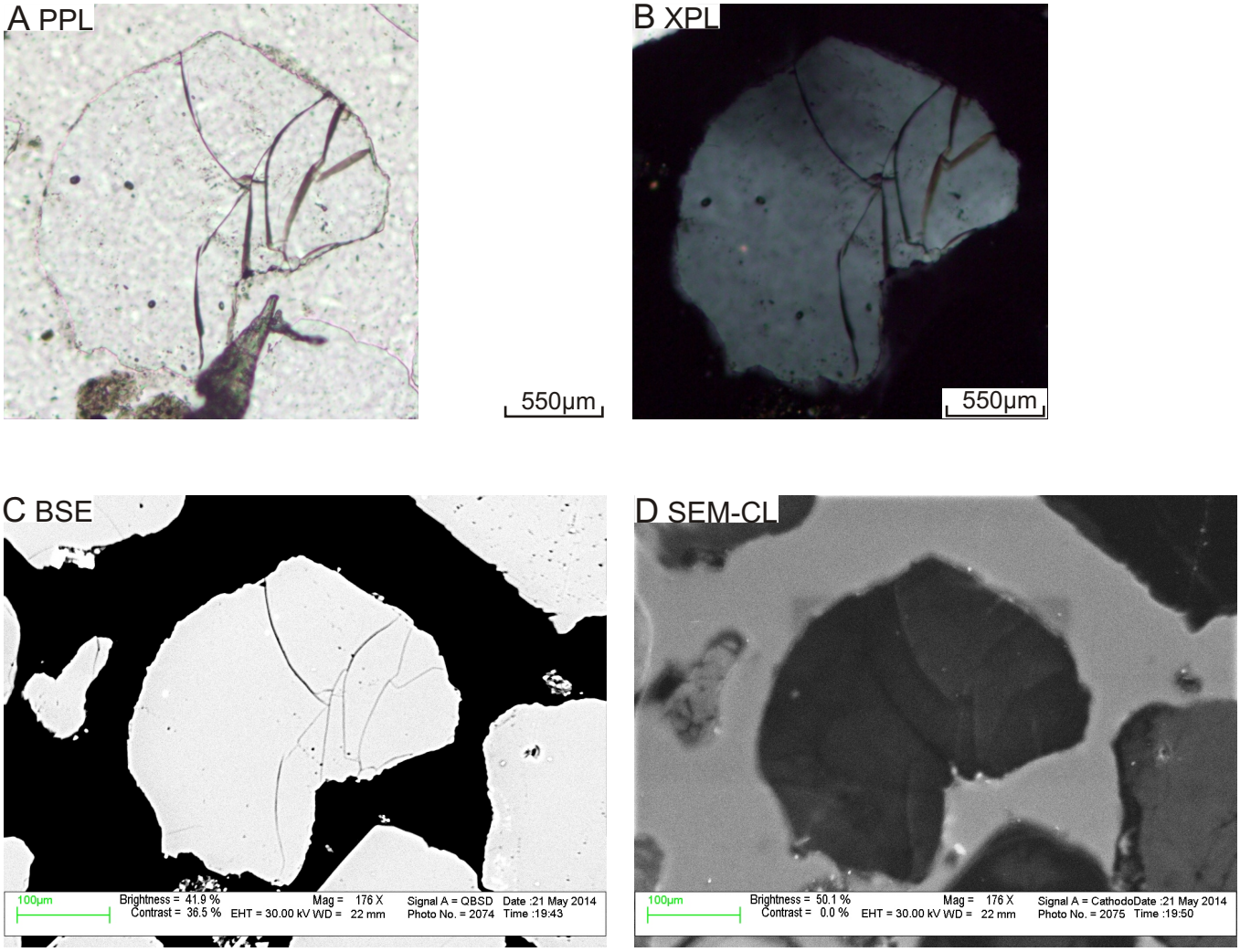

Figure 6A-39: Microphotos under ppl (A) and xpl (B), SEM-BSE image (C) and SEM-CL image (D) of quartz grain 39 in sample 3425. The grain is anhedral and sub-rounded monocrystalline with strong undulose extinction. Fluid inclusion trails are present (Fig. A). The grain is microfractured with a set of irregular fractures (Fig. C and D). Healed fractures are rare. The grain shows homogeneous SEM-CL image.

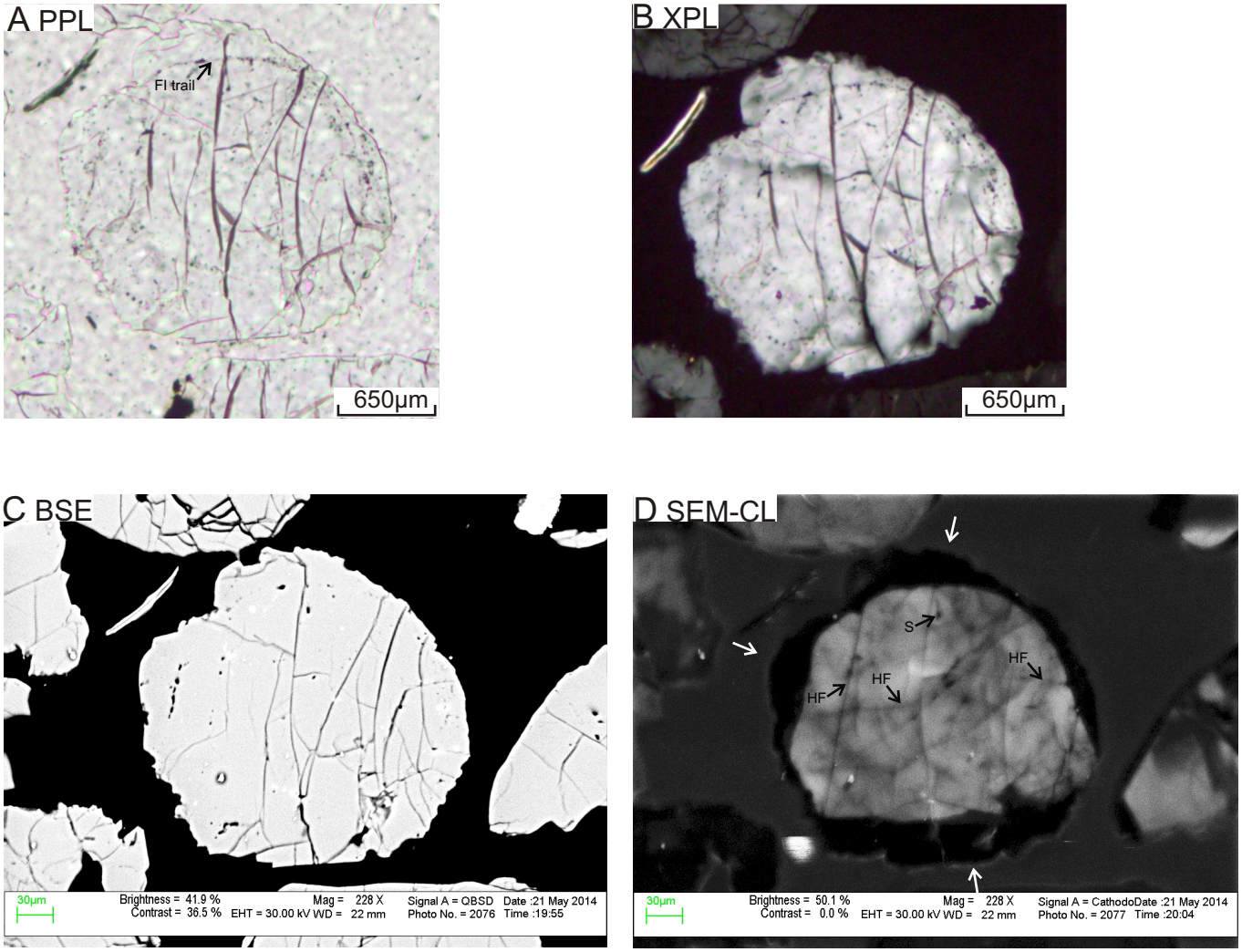

Figure 6A-40: Microphotos under ppl (A) and xpl (B), SEM-BSE image (C) and SEM-CL image (D) of quartz grain 40 in sample 3425. The grain is anhedral and sub-rounded monocrystalline with strong undulose extinction. Fluid inclusions are common; they are usually associated with secondary porosity and form trails (FI trail) along healed fractures and at the boundary between the detrital quartz and the overgrowth (Fig. A). The grain is strongly microfractured with a set of parallel fractures disposed vertically and a set of irregular fractures (Fig. C and D). Healed fractures (HF) and spiders (S) are common (Fig. D). The dark areas indicated by arrows in Fig. D are overgrowth; these areas appear corroded in Fig. C, suggesting secondary porosity.

Appendix 6B: Hot cathodoluminescence (HCL) images and blue colour shift analyses of detrital quartz grains in sample 3425.

Notes:

1. All the grains with HCL images correspond to the same grain in SEM-CL images. In all the following organized HCL figures,

   Fig. A shows HCL image taken after 3 seconds;

   Fig. B shows HCL image taken after 12 seconds;

   Fig. C is the histogram of blue colour within the analysed quartz grain in Fig. A and B, where X axis is the intensity of blue colour indicated by the colour bar with values from 0-255 (0=no blue or "black", 255=blue), and Y axis indicates the pixel amount at different blue values;

   Fig. D is the statistical table of blue values within the analysed grain area, where SD corresponds to standard deviation.

2. To classify the blue colour, the following abbreviations are used:

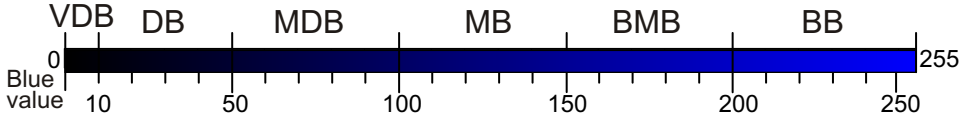

VDB: Very Dark Blue (0-10) **DB**: Dark Blue (11-50)

MDB: Medium Dark Blue (51-100) **MB**: Medium Blue (101-150)

BMB: Bright-Medium Blue (151-200) **BB**: Bright Blue (201-255)

3. To quantify the blue colour shift, the following criteria are used:

   Mean blue value change **< 5**: **No** colour shift

   5 ≤Mean blue value change **< 15**: **Slight** colour shift

   15 ≤Mean blue value change **< 30**: **Moderate** colour shift

   Mean blue value change ≥**30**: **Strong** colour shift

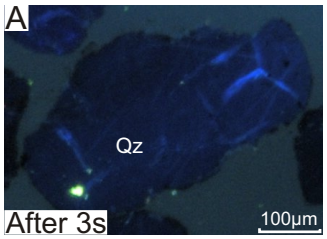

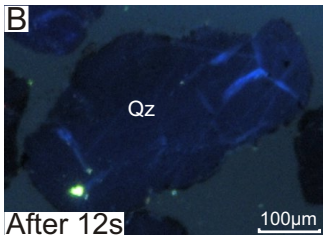

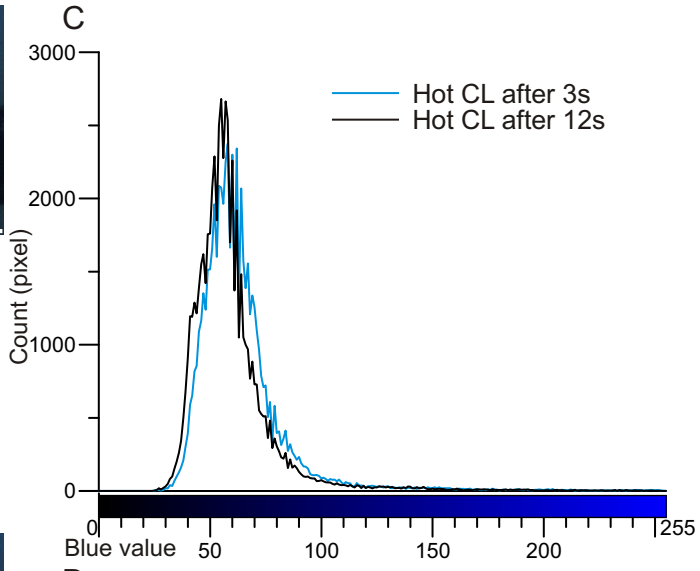

Figure 6B-1: Grain 1. The grain shows no colour shift.

D

Blue value	Min	Max	Mode	Mean	SD
After 3s	25	254	28	64	21.4
After 12s	25	252	55	60	20

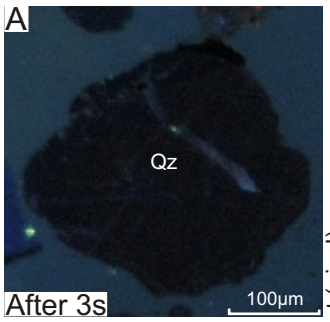

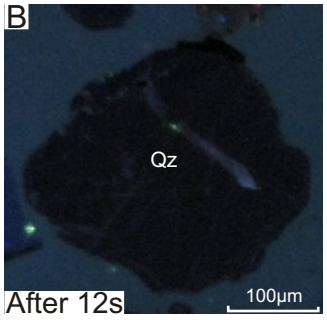

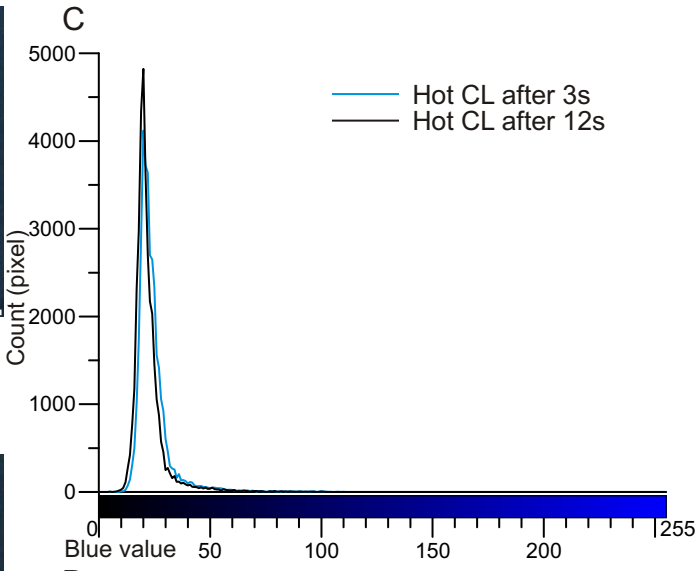

Figure 6B-2: Grain 2. The grain shows no colour shift.

D

Blue value	Min	Max	Mode	Mean	SD
After 3s	10	131	20	24	8.2
After 12s	5	123	20	22	7.6

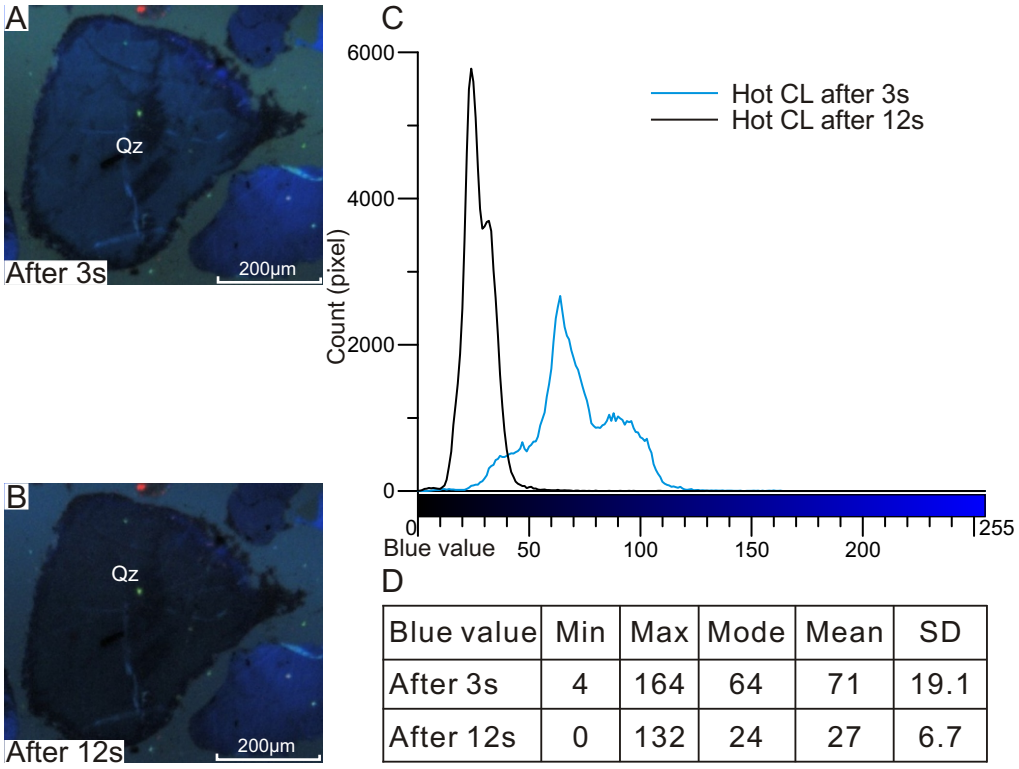

Figure 6B-3: Grain 3. The grain shows strong colour shift.

D

Blue value	Min	Max	Mode	Mean	SD
After 3s	4	164	64	71	19.1
After 12s	0	132	24	27	6.7

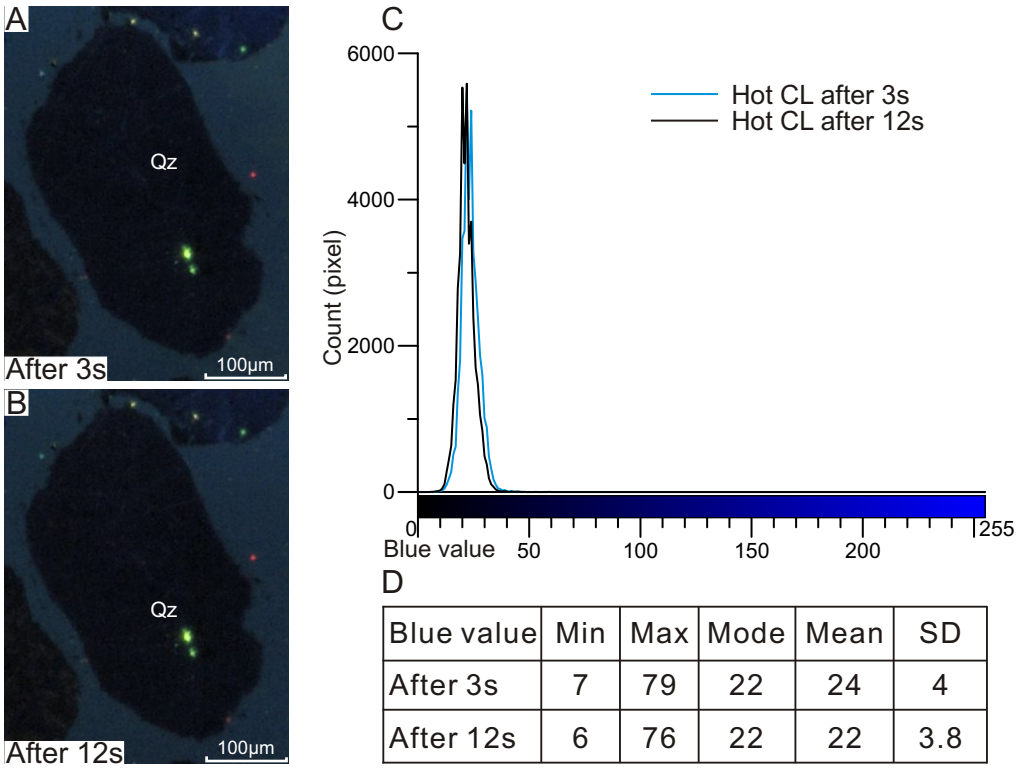

Figure 6B-4: Grain 4. The grain shows no colour shift.

D

Blue value	Min	Max	Mode	Mean	SD
After 3s	7	79	22	24	4
After 12s	6	76	22	22	3.8

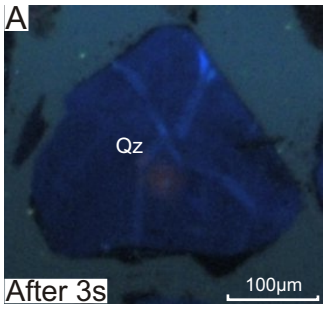

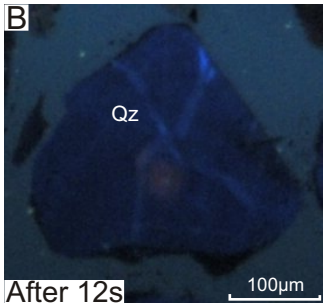

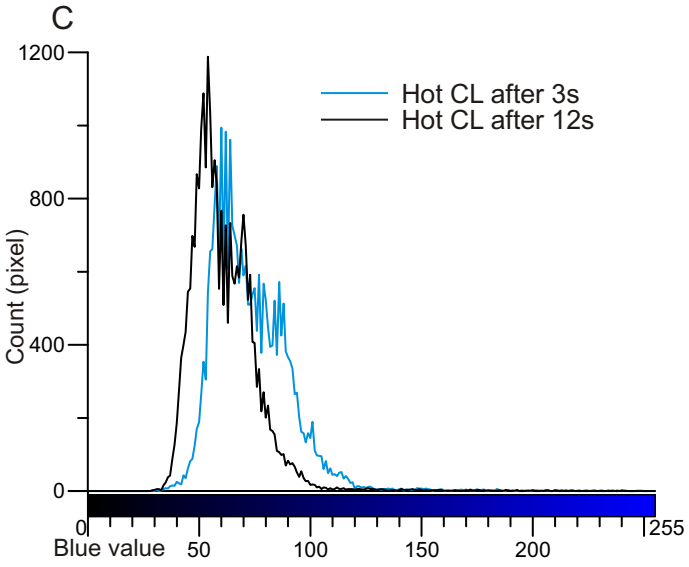

D

Blue value	Min	Max	Mode	Mean	SD
After 3s	29	249	60	73	18.2
After 12s	29	218	54	61	14.9

Figure 6B-5: Grain 5. The grain shows slight colour shift.

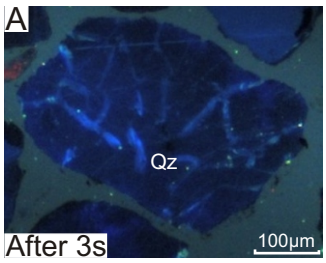

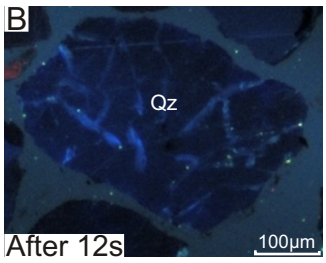

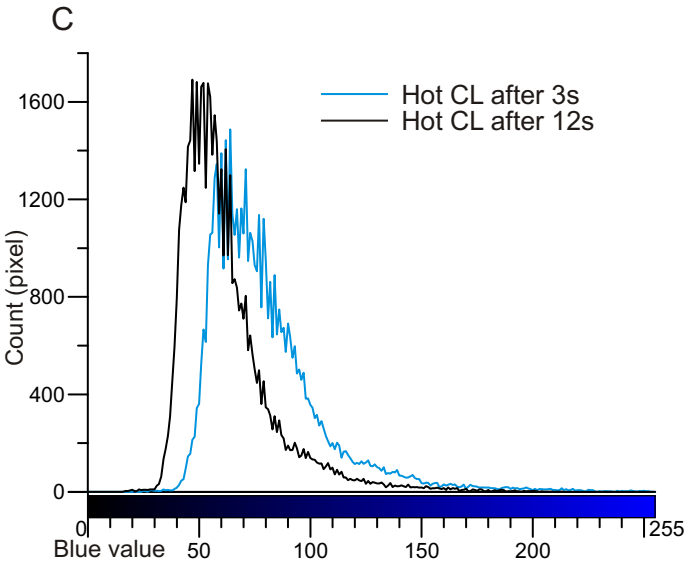

D

Blue value	Min	Max	Mode	Mean	SD
After 3s	21	252	64	80	26.5
After 12s	16	213	47	62	21.2

Figure 6B-6: Grain 6. The grain shows moderate colour shift.

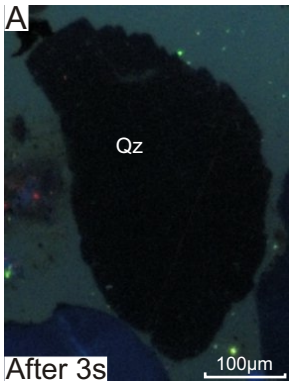

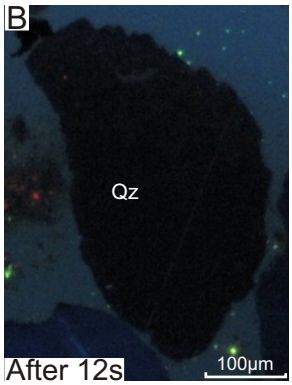

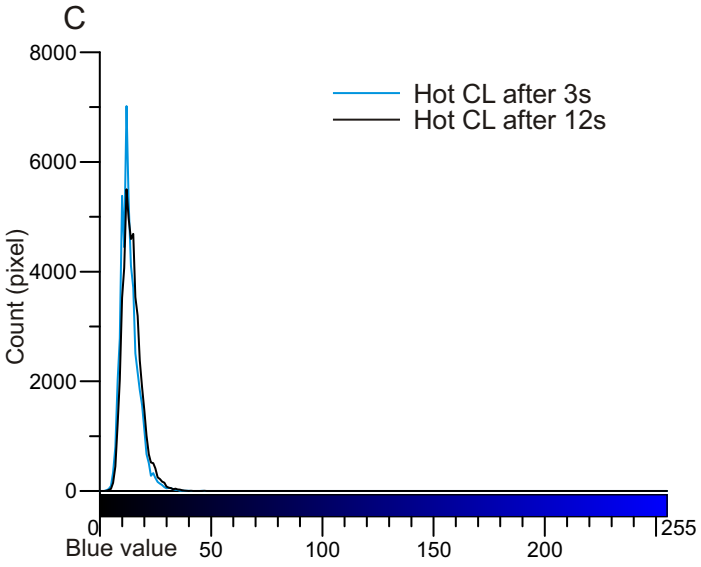

Figure 6B-7: Grain 7. The grain shows no colour shift.

D

Blue value	Min	Max	Mode	Mean	SD
After 3s	3	54	12	13	4.2
After 12s	2	57	12	15	4.4



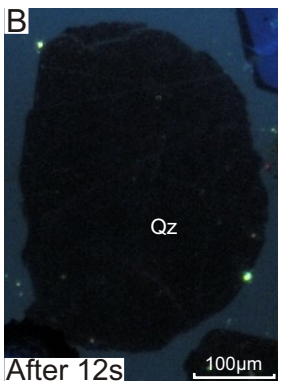

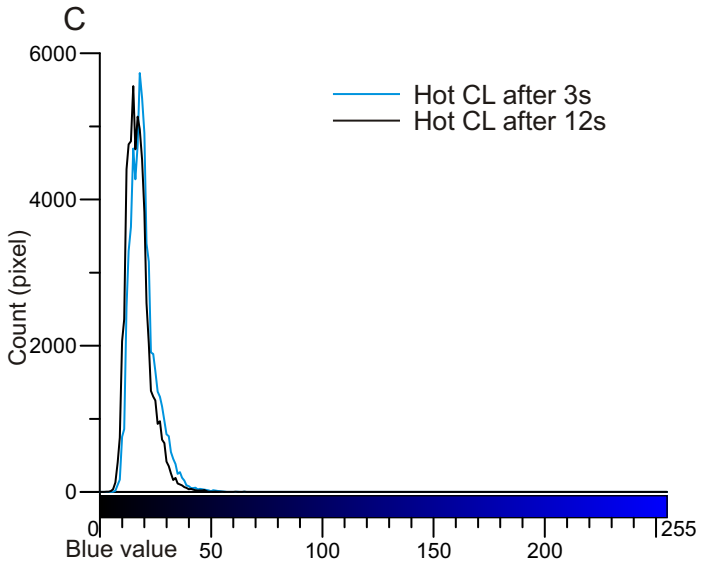

Figure 6B-8: Grain 8. The grain shows no colour shift.

D

Blue value	Min	Max	Mode	Mean	SD
After 3s	3	71	18	20	6
After 12s	3	69	15	17	5.5

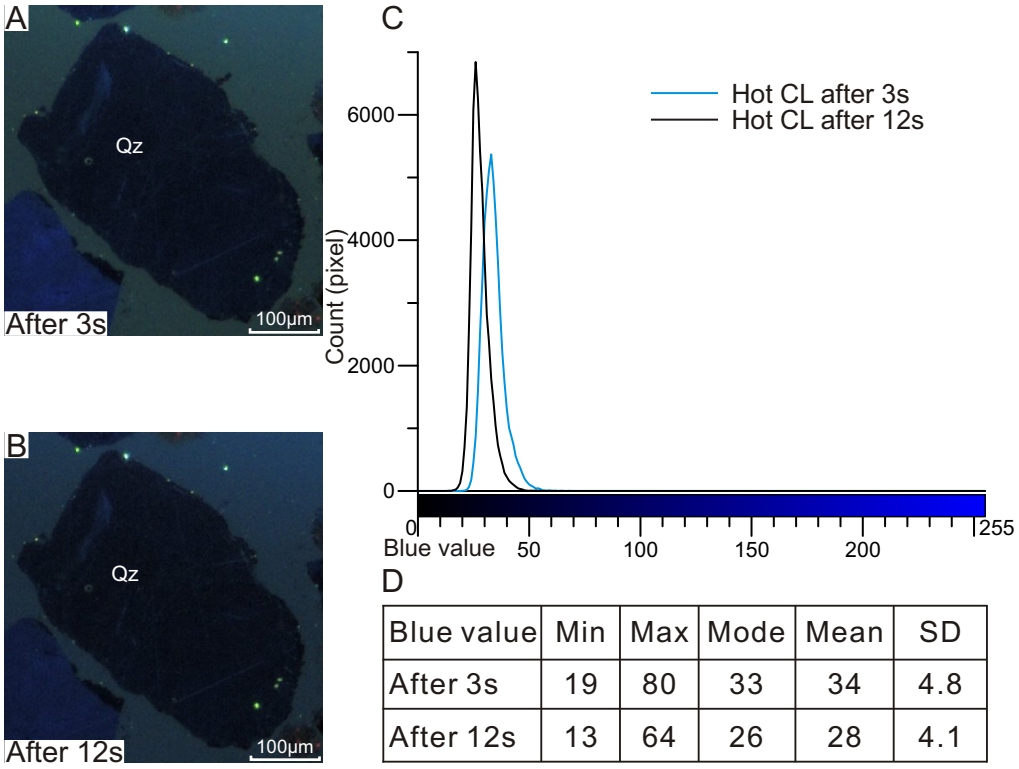

Blue value	Min	Max	Mode	Mean	SD
After 3s	19	80	33	34	4.8
After 12s	13	64	26	28	4.1

Figure 6B-9: Grain 9. The grain shows slight colour shift.

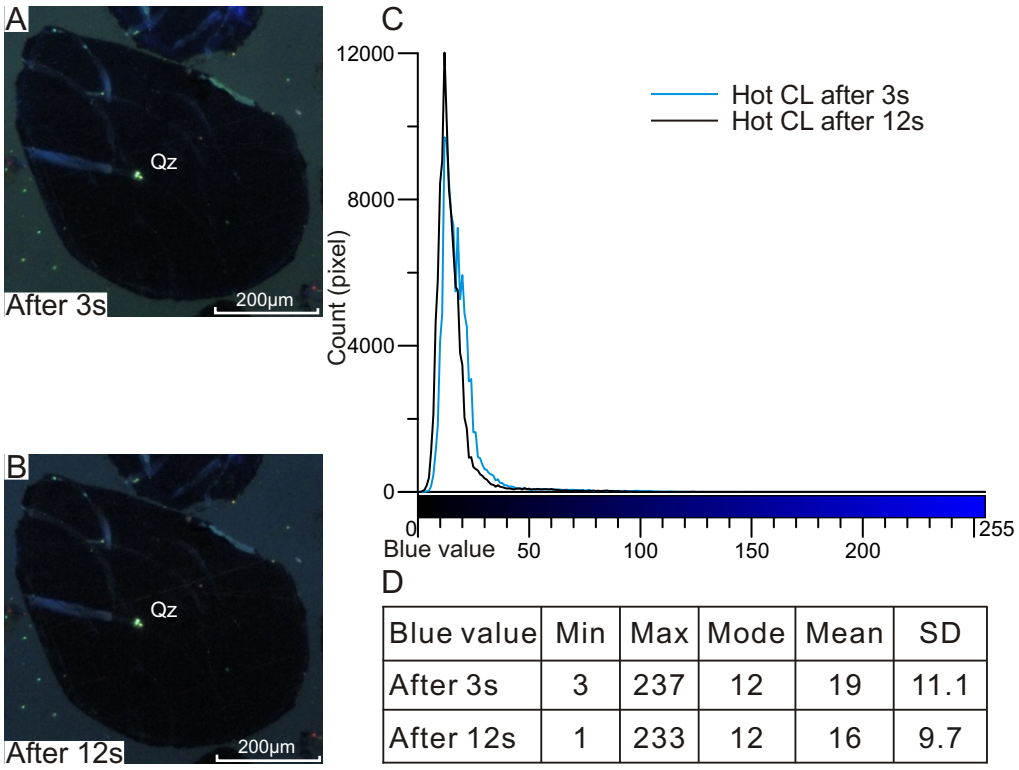

Blue value	Min	Max	Mode	Mean	SD
After 3s	3	237	12	19	11.1
After 12s	1	233	12	16	9.7

Figure 6B-10: Grain 10. The grain shows no colour shift.

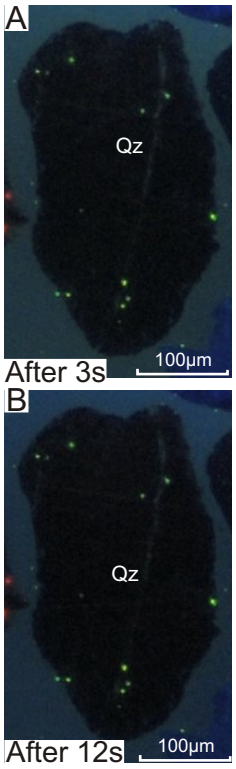

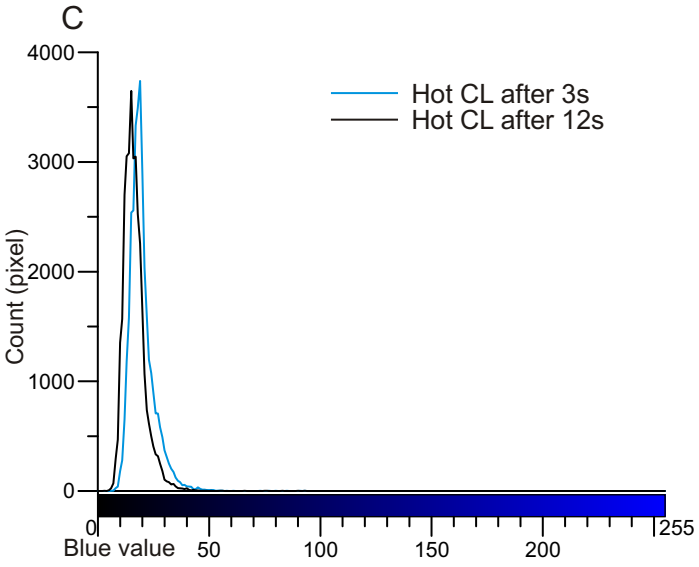

Figure 6B-11: Grain 11. The grain shows no colour shift.

D

Blue value	Min	Max	Mode	Mean	SD
After 3s	6	93	19	20	5.5
After 12s	3	93	15	16	4.9

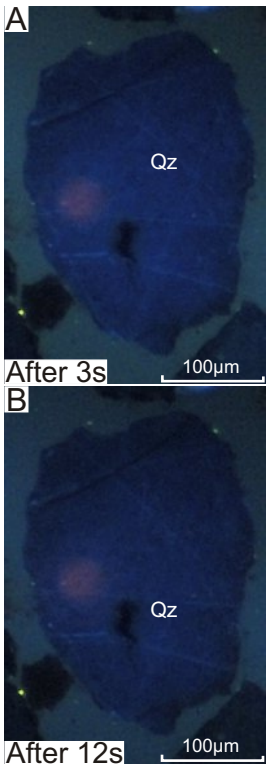

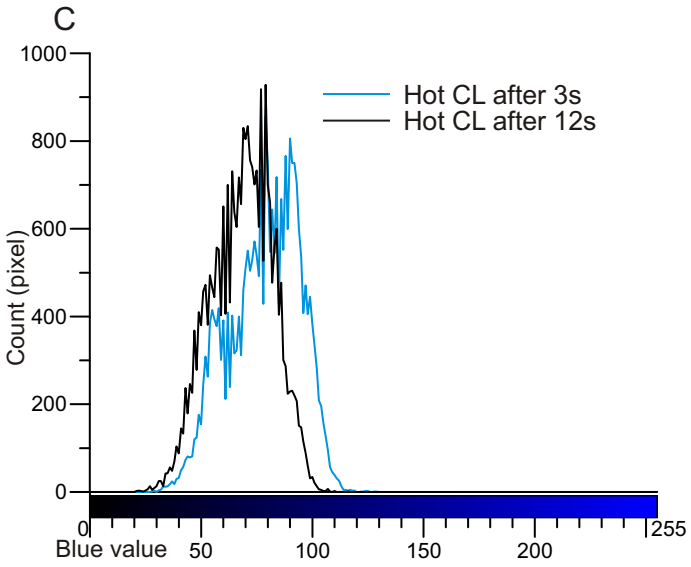

Figure 6B-12: Grain 12. The grain shows slight colour shift.

D

Blue value	Min	Max	Mode	Mean	SD
After 3s	28	129	79	78	15.7
After 12s	21	116	79	68	13.8

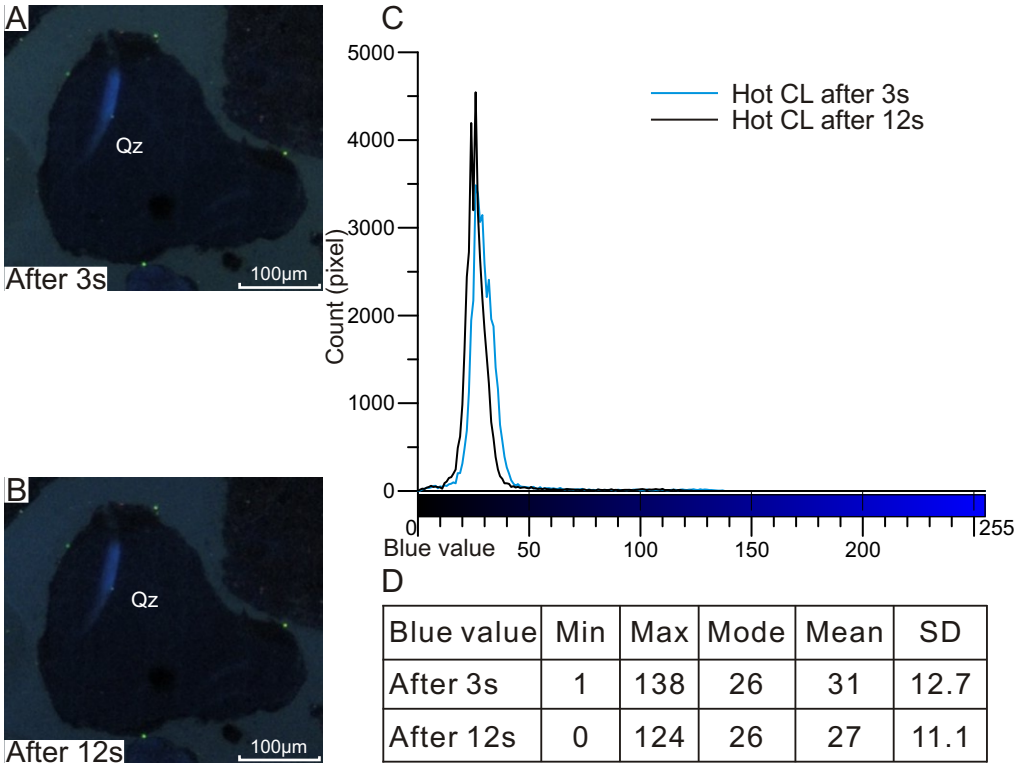

Figure 6B-13: Grain 13. The grain shows no colour shift.

D

Blue value	Min	Max	Mode	Mean	SD
After 3s	1	138	26	31	12.7
After 12s	0	124	26	27	11.1

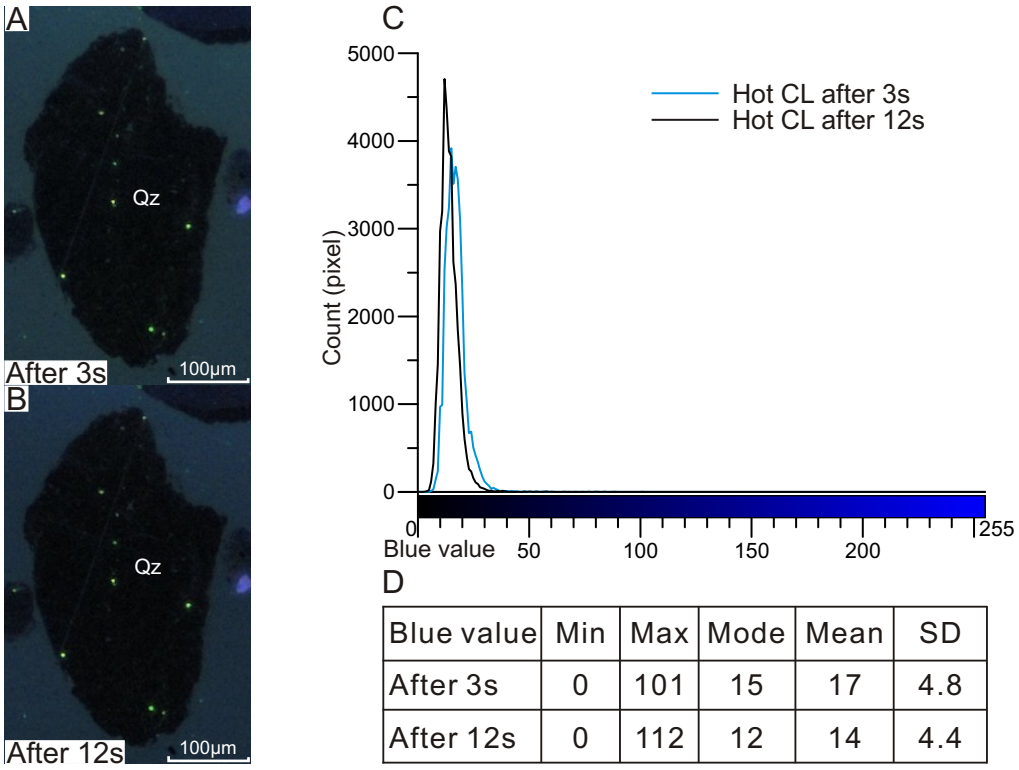

Figure 6B-14: Grain 14. The grain shows no colour shift.

D

Blue value	Min	Max	Mode	Mean	SD
After 3s	0	101	15	17	4.8
After 12s	0	112	12	14	4.4

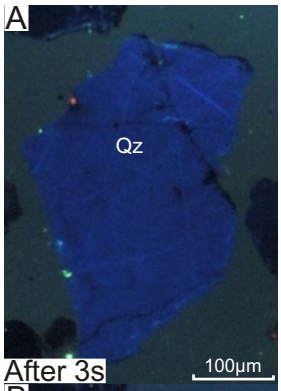

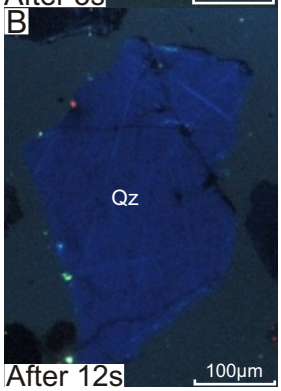

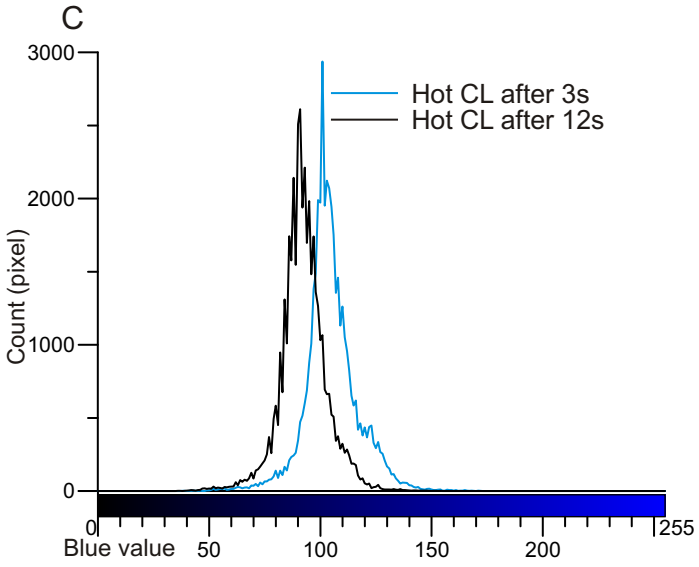

Figure 6B-15: Grain 15. The grain shows slight colour shift.

D

Blue value	Min	Max	Mode	Mean	SD
After 3s	38	172	101	105	11.9
After 12s	36	154	91	92	10.5

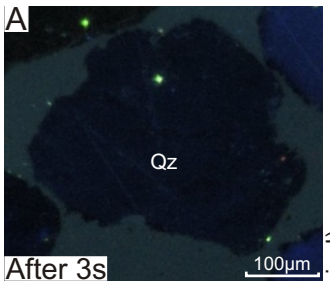

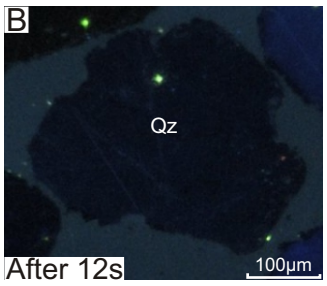

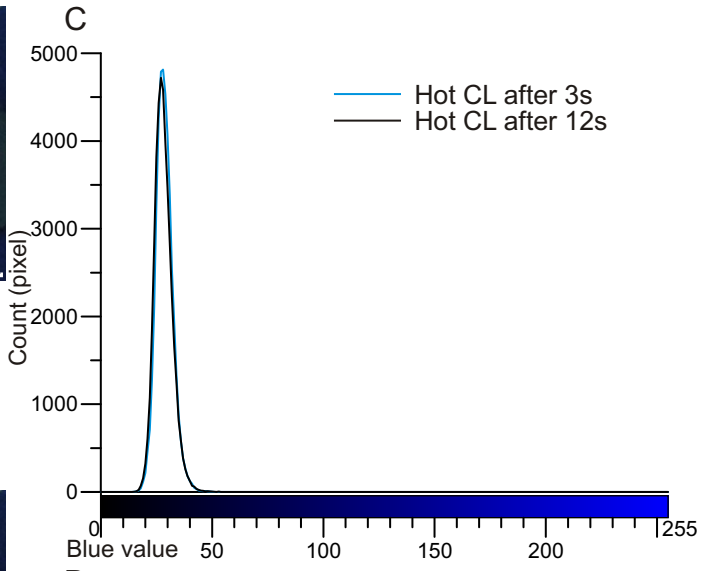

Figure 6B-16: Grain 16. The grain shows no colour shift.

D

Blue value	Min	Max	Mode	Mean	SD
After 3s	15	61	28	29	3.8
After 12s	13	65	27	28	4

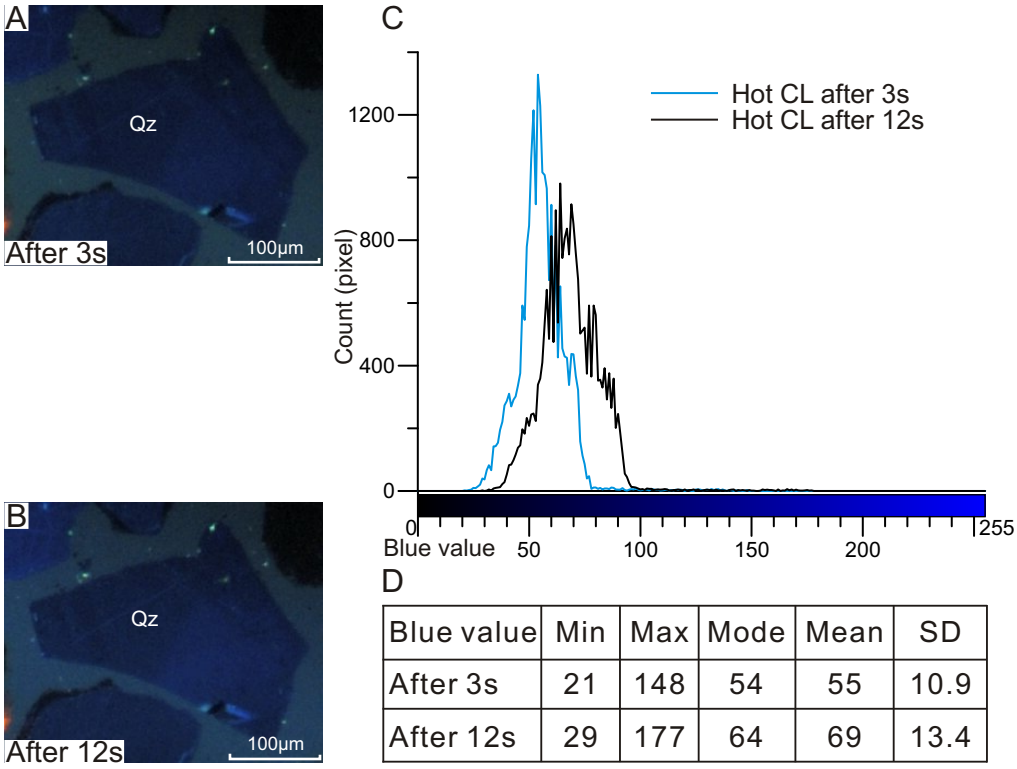

Figure 6B-17: Grain 17. Probably the first image was taken too early. Therefore, this grain is not useful to analyse the colour shift..

D

Blue value	Min	Max	Mode	Mean	SD
After 3s	21	148	54	55	10.9
After 12s	29	177	64	69	13.4

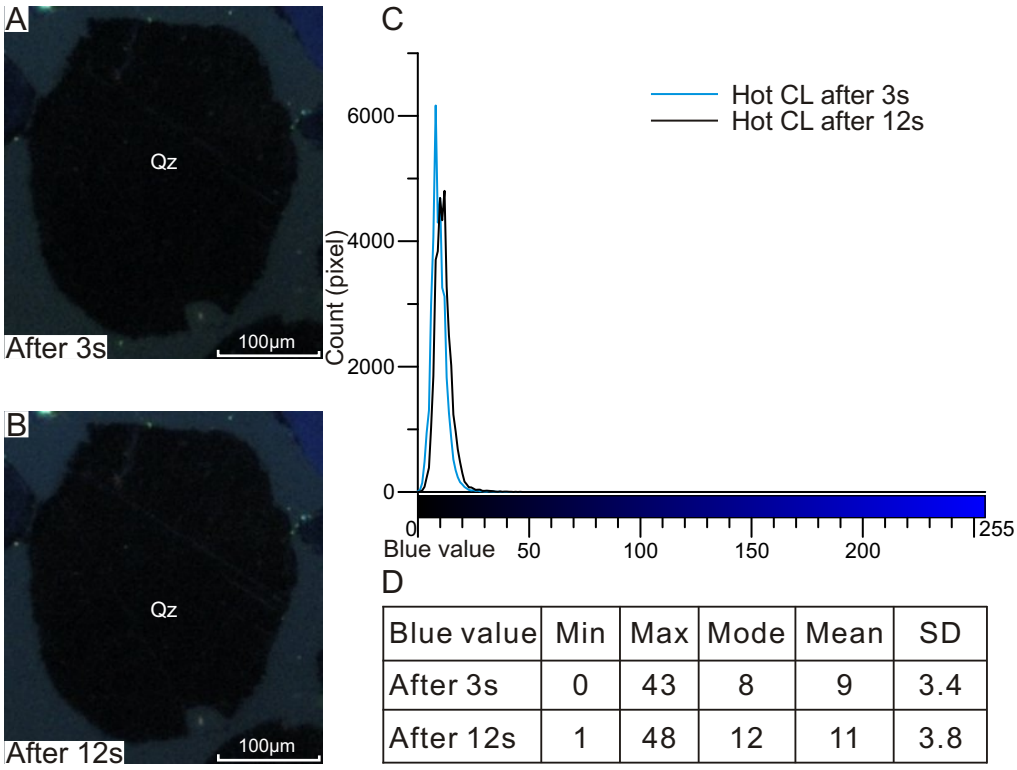

Figure 6B-18: Grain 18. Probably the first image was taken too early. Therefore, this grain is not useful to analyse the colour shift.

D

Blue value	Min	Max	Mode	Mean	SD
After 3s	0	43	8	9	3.4
After 12s	1	48	12	11	3.8

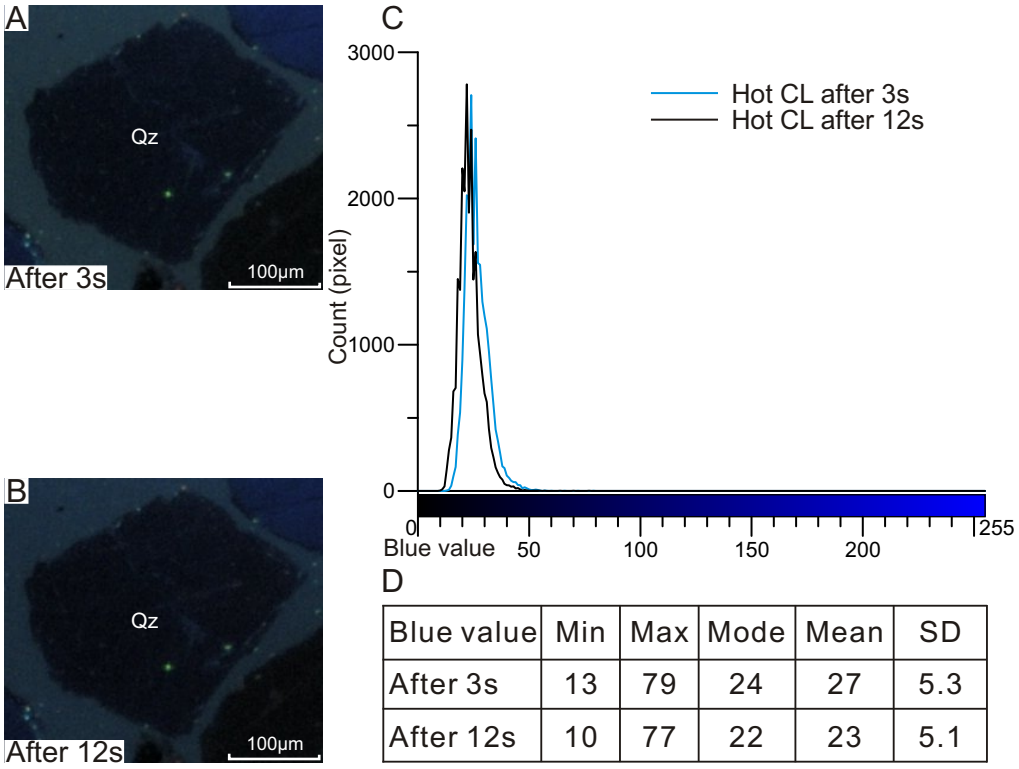

Figure 6B-19: Grain 19. The grain shows no colour shift.

D

Blue value	Min	Max	Mode	Mean	SD
After 3s	13	79	24	27	5.3
After 12s	10	77	22	23	5.1

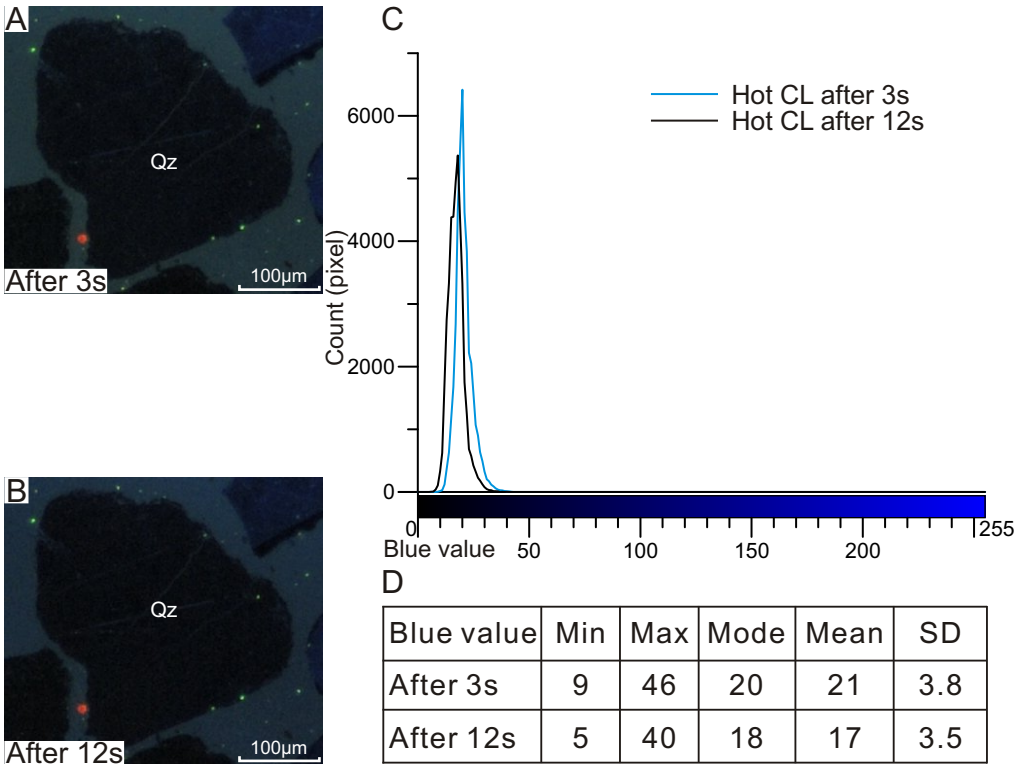

Figure 6B-20: Grain 20. The grain shows no colour shift.

D

Blue value	Min	Max	Mode	Mean	SD
After 3s	9	46	20	21	3.8
After 12s	5	40	18	17	3.5

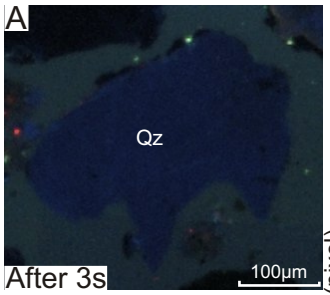

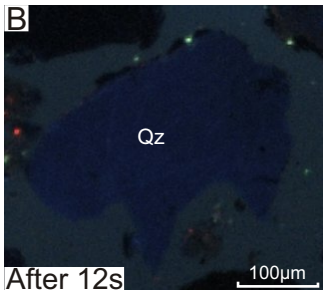

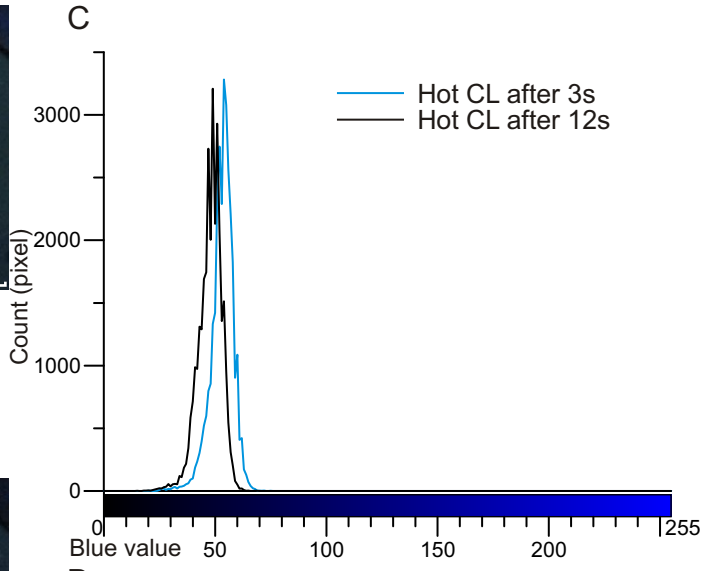

Figure 6B-21: Grain 21. The grain shows slight colour shift.

D

Blue value	Min	Max	Mode	Mean	SD
After 3s	20	75	54	53	5.1
After 12s	15	69	49	48	5.3

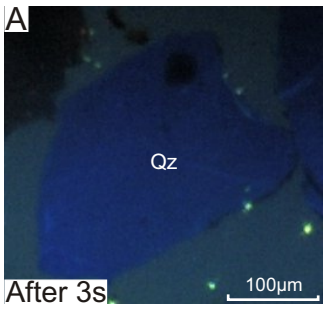

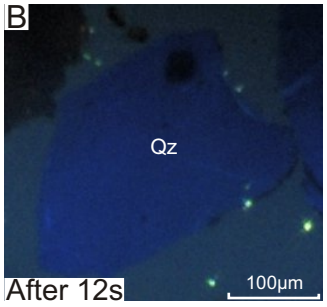

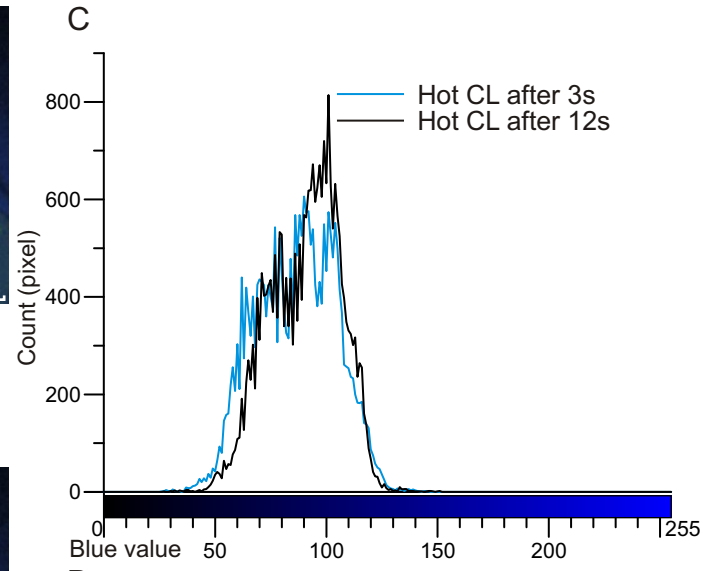

Figure 6B-22: Grain 22. The grain shows no colour shift.

D

Blue value	Min	Max	Mode	Mean	SD
After 3s	26	146	90	86	17.8
After 12s	27	151	101	90	15.7

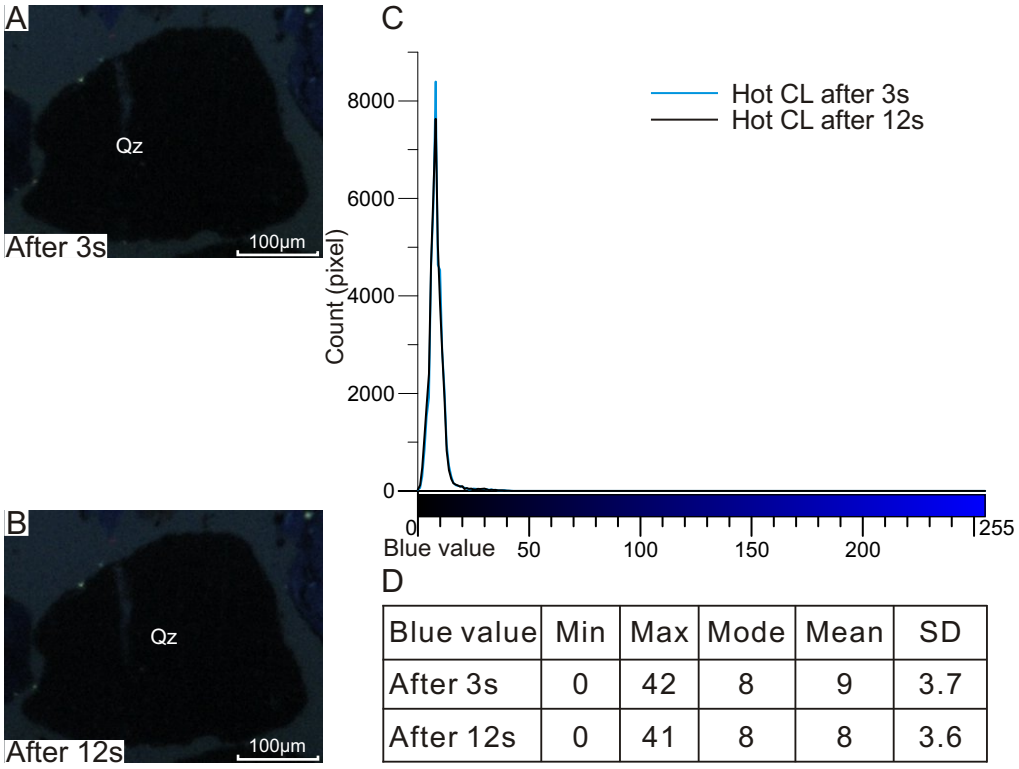

Figure 6B-23: Grain 23. The grain shows no colour shift.

D

Blue value	Min	Max	Mode	Mean	SD
After 3s	0	42	8	9	3.7
After 12s	0	41	8	8	3.6

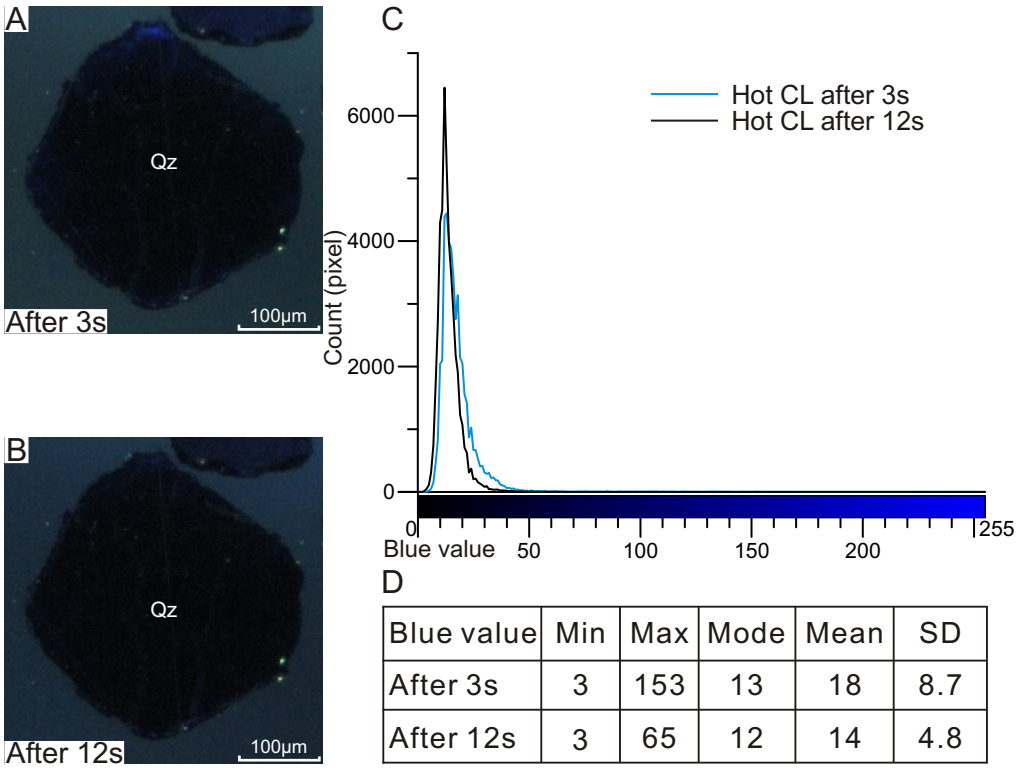

Figure 6B-24: Grain 24. The grain shows no colour shift.

D

Blue value	Min	Max	Mode	Mean	SD
After 3s	3	153	13	18	8.7
After 12s	3	65	12	14	4.8

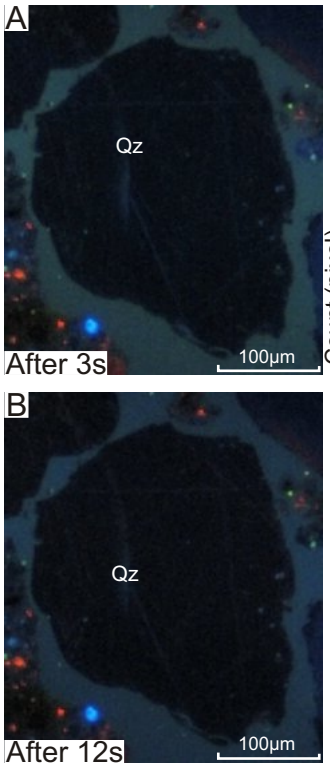

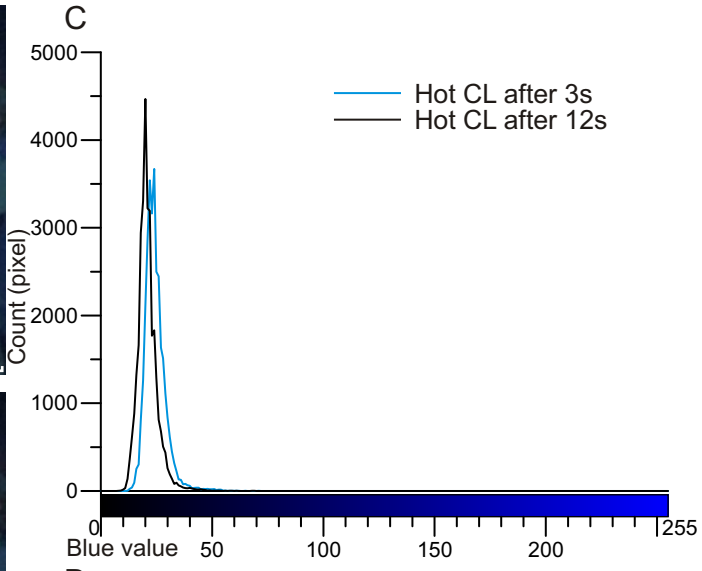

D

Blue value	Min	Max	Mode	Mean	SD
After 3s	12	79	24	24	4.8
After 12s	8	75	20	21	4.5

Figure 6B-25: Grain 25. The grain shows no colour shift.

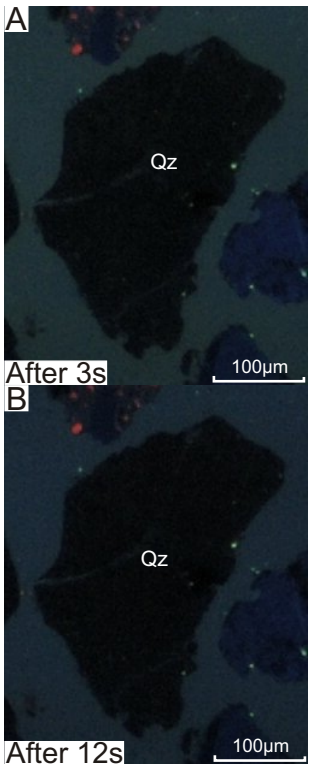

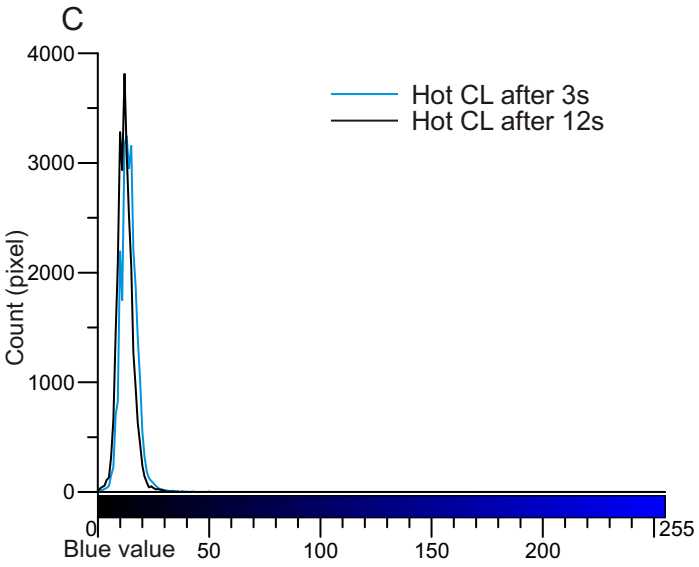

D

Blue value	Min	Max	Mode	Mean	SD
After 3s	0	50	13	14	3.7
After 12s	0	50	12	12	3.5

Figure 6B-26: Grain 26. The grain shows no colour shift.

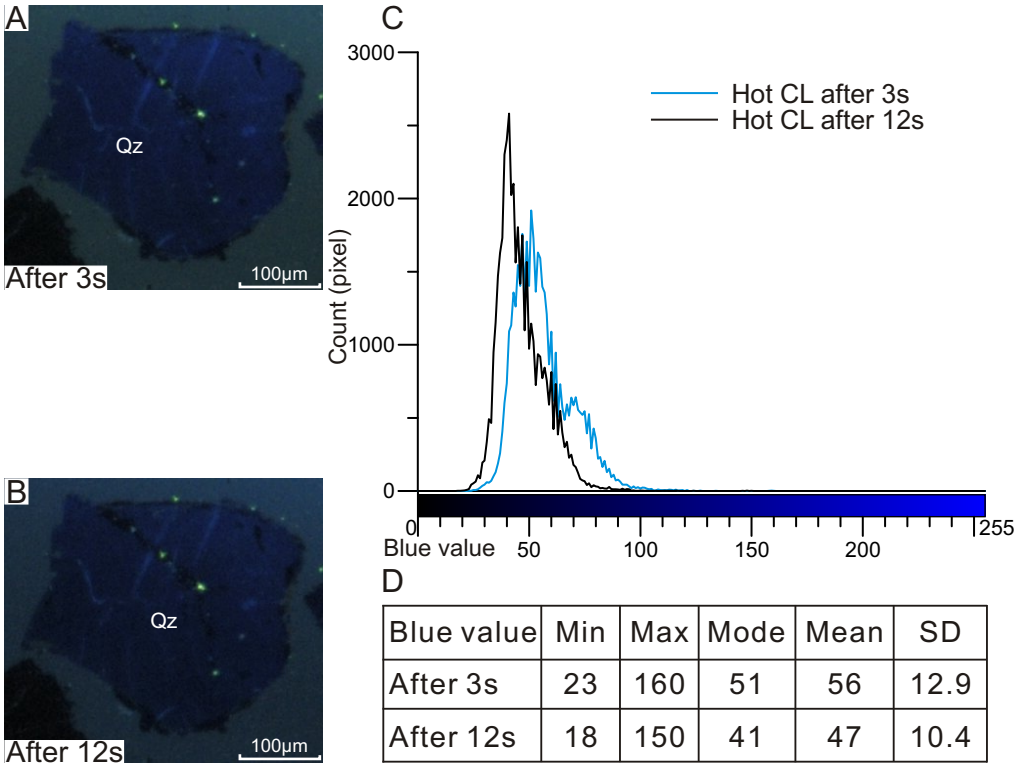

Figure 6B-27: Grain 27. The grain shows slight colour shift.

D

Blue value	Min	Max	Mode	Mean	SD
After 3s	23	160	51	56	12.9
After 12s	18	150	41	47	10.4

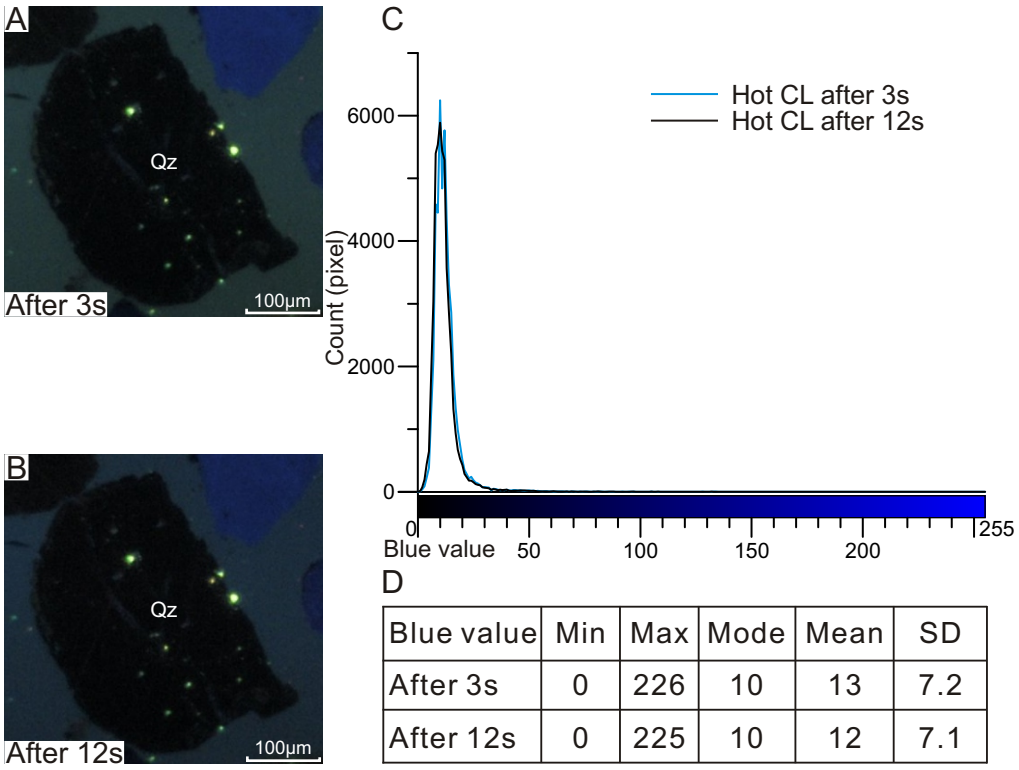

Figure 6B-28: Grain 28. The grain shows no colour shift.

D

Blue value	Min	Max	Mode	Mean	SD
After 3s	0	226	10	13	7.2
After 12s	0	225	10	12	7.1

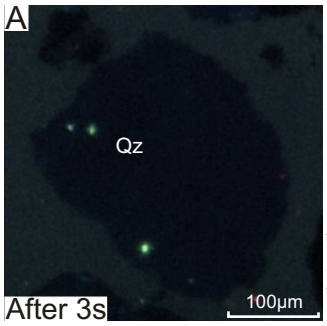

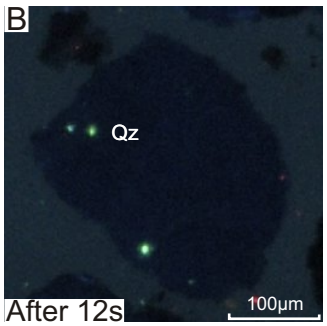

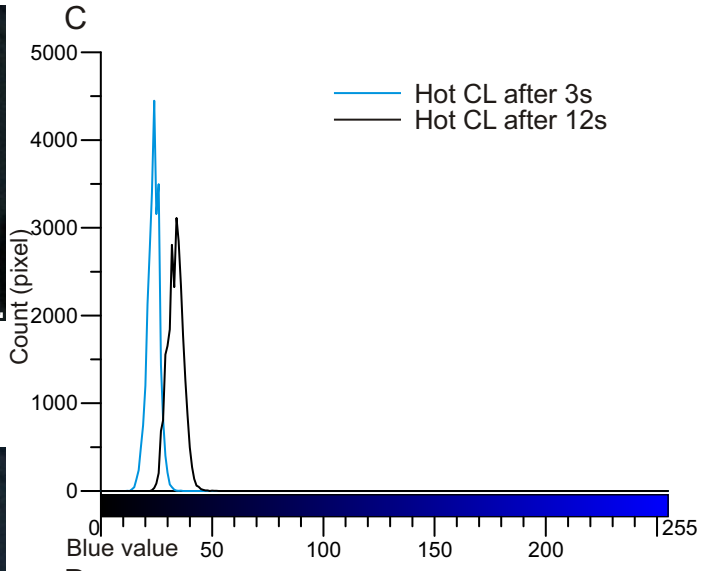

D

Blue value	Min	Max	Mode	Mean	SD
After 3s	10	38	24	24	2.7
After 12s	20	52	34	34	3.5

Figure 6B-29: Grain 29. Probably the first image was taken too early. Therefore, this grain is not useful to analyse the colour shift.

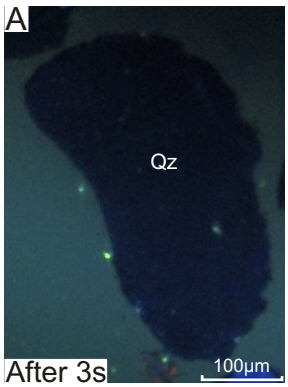

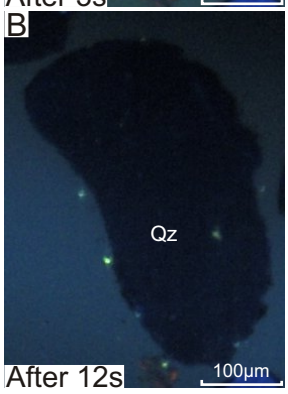

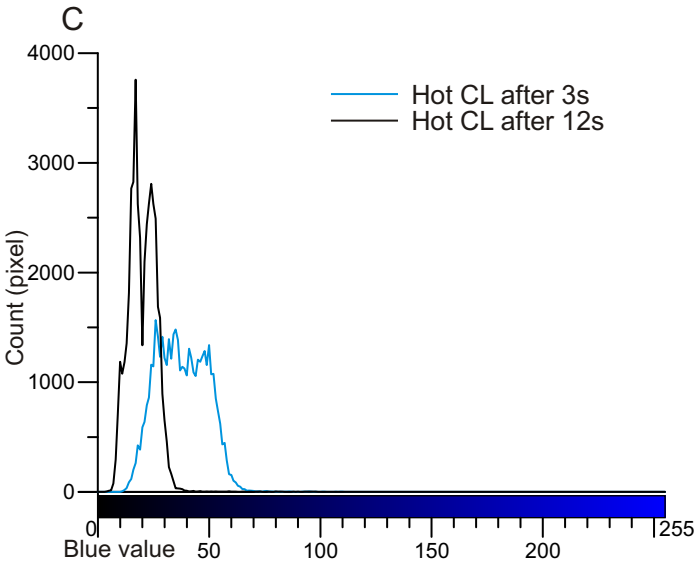

D

Blue value	Min	Max	Mode	Mean	SD
After 3s	11	110	26	38	11.1
After 12s	4	98	17	20	6

Figure 6B-30: Grain 30. The grain shows moderate colour shift.

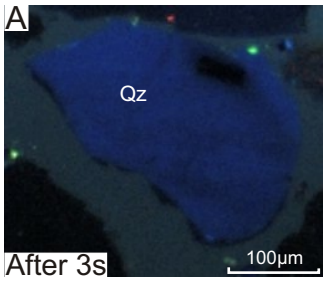

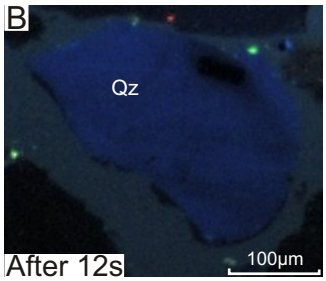

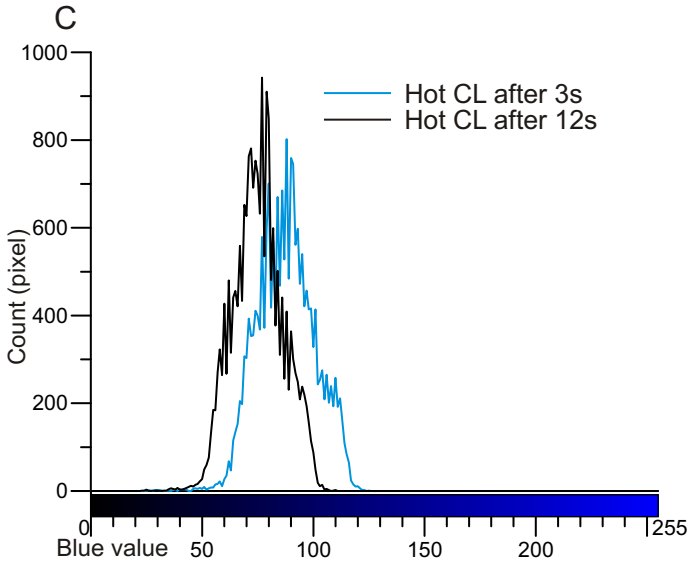

Figure 6B-31: Grain 31. The grain shows slight colour shift.

D

Blue value	Min	Max	Mode	Mean	SD
After 3s	25	125	88	88	12.8
After 12s	23	110	77	75	11.2

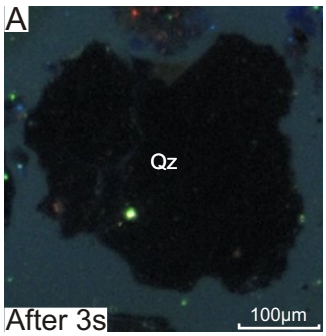

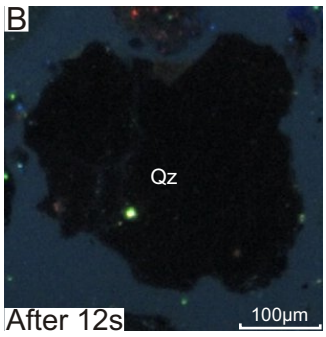

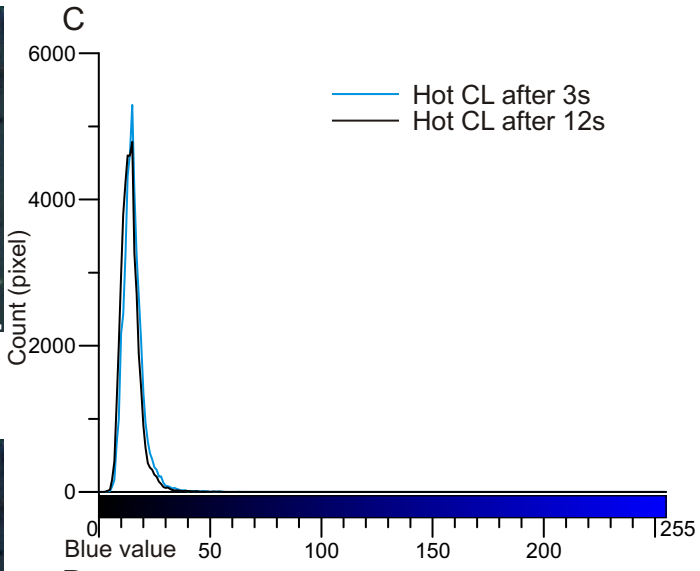

Figure 6B-32: Grain 32. The grain shows no colour shift.

D

Blue value	Min	Max	Mode	Mean	SD
After 3s	3	69	15	15	4.7
After 12s	3	69	15	14	4.4

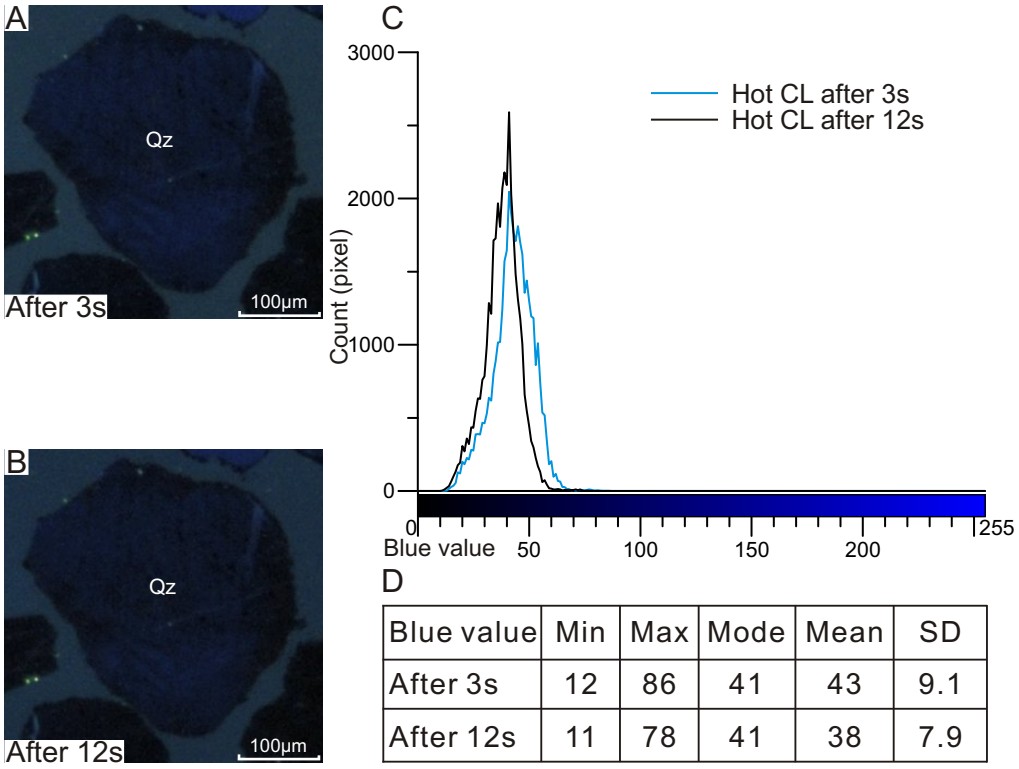

Figure 6B-33: Grain 33. The grain shows slight colour shift.

D

Blue value	Min	Max	Mode	Mean	SD
After 3s	12	86	41	43	9.1
After 12s	11	78	41	38	7.9

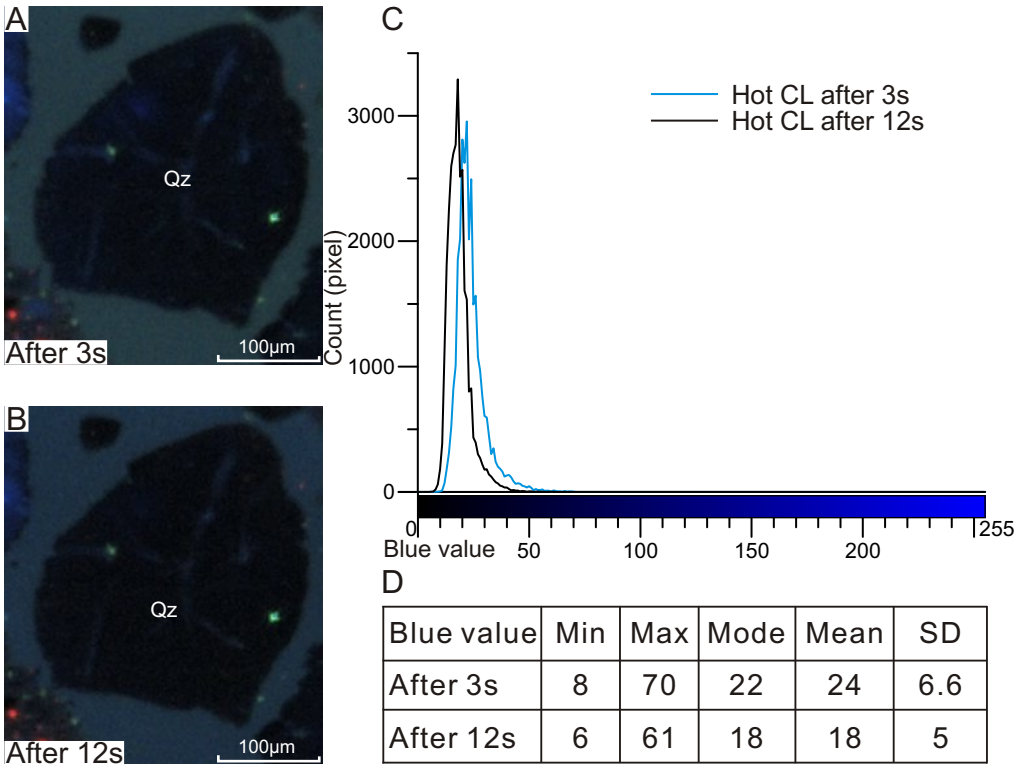

Figure 6B-34: Grain 34. The grain shows slight colour shift.

D

Blue value	Min	Max	Mode	Mean	SD
After 3s	8	70	22	24	6.6
After 12s	6	61	18	18	5

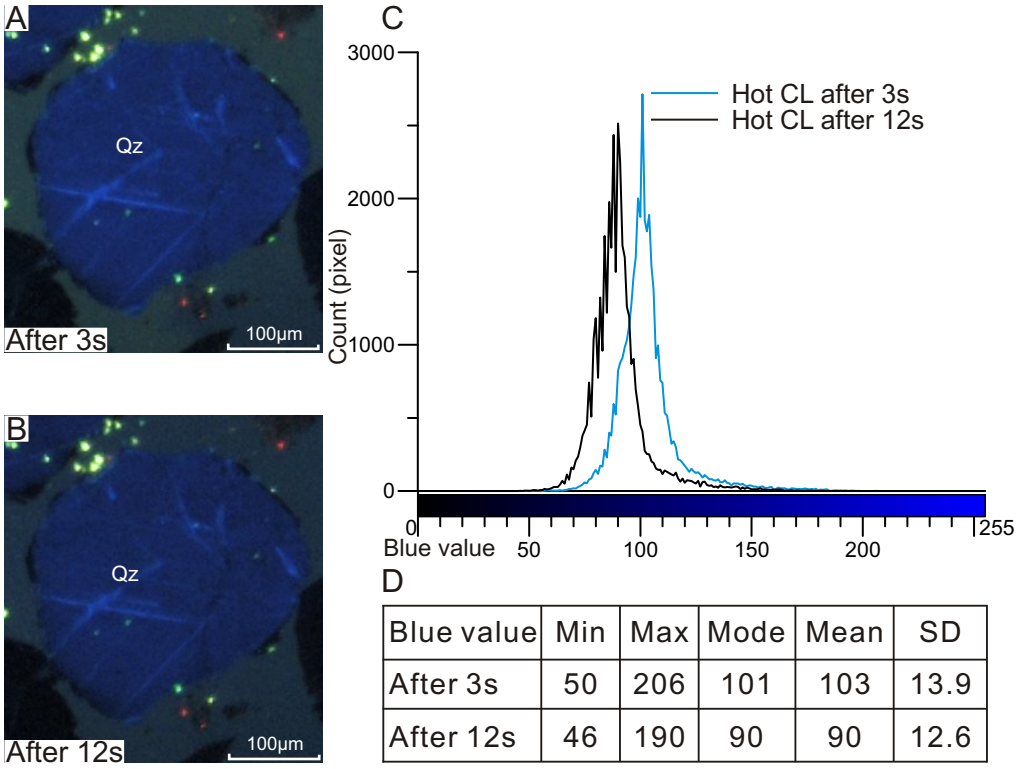

D

Blue value	Min	Max	Mode	Mean	SD
After 3s	50	206	101	103	13.9
After 12s	46	190	90	90	12.6

Figure 6B-35: Grain 35. The grain shows slight colour shift.

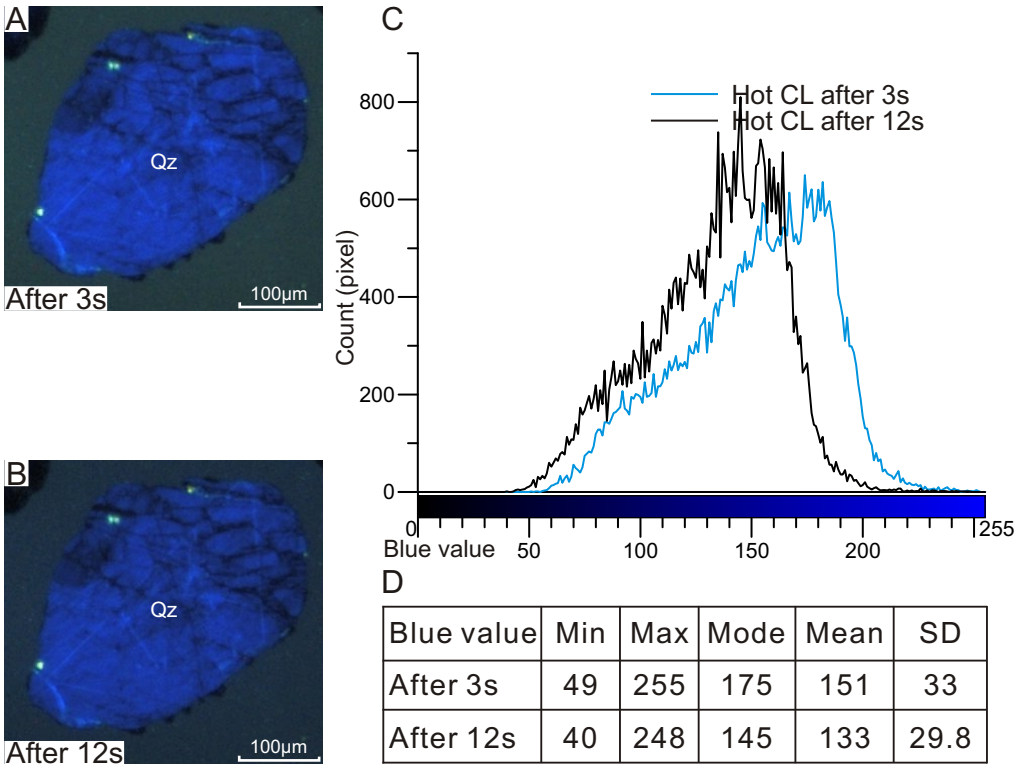

D

Blue value	Min	Max	Mode	Mean	SD
After 3s	49	255	175	151	33
After 12s	40	248	145	133	29.8

Figure 6B-36: Grain 36. The grain shows moderate colour shift.

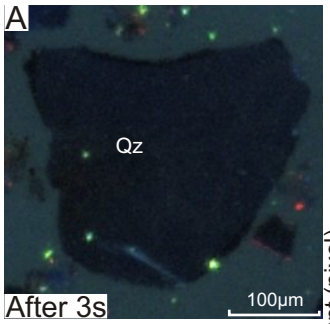

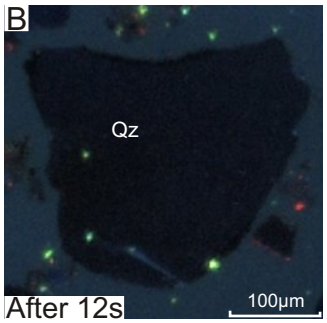

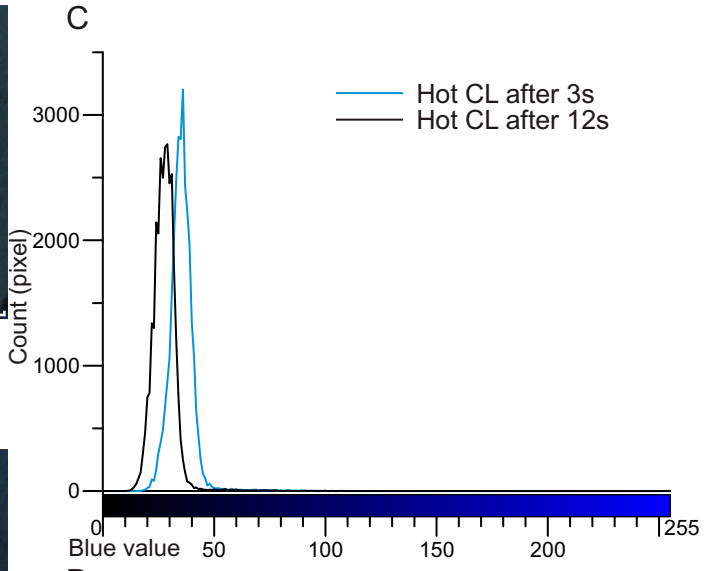

D

Blue value	Min	Max	Mode	Mean	SD
After 3s	14	114	36	35	5.7
After 12s	11	107	29	28	5.4

Figure 6B-37: Grain 37. The grain shows slight colour shift.

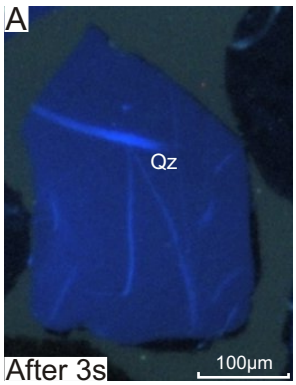

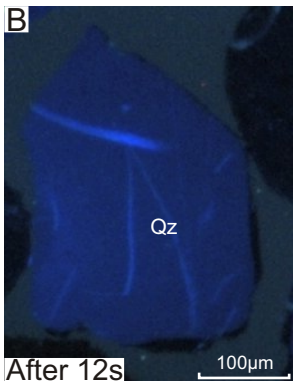

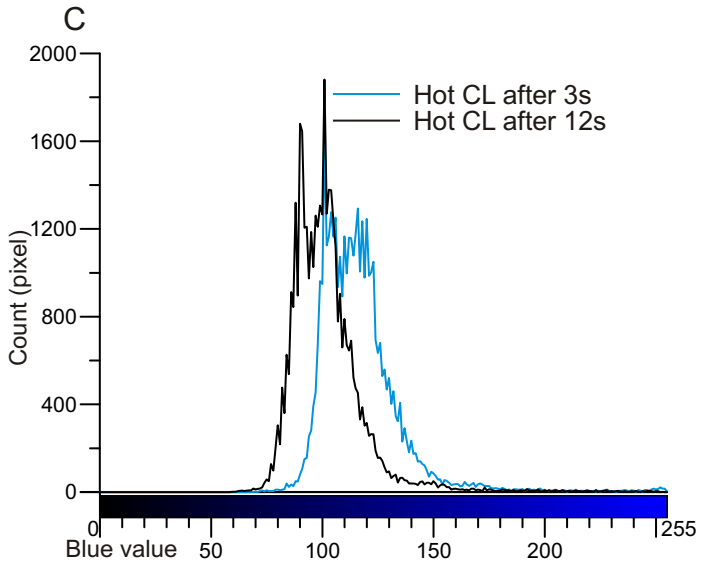

D

Blue value	Min	Max	Mode	Mean	SD
After 3s	68	255	101	117	19.4
After 12s	59	253	101	102	17.6

Figure 6B-38: Grain 38. The grain shows moderate colour shift.

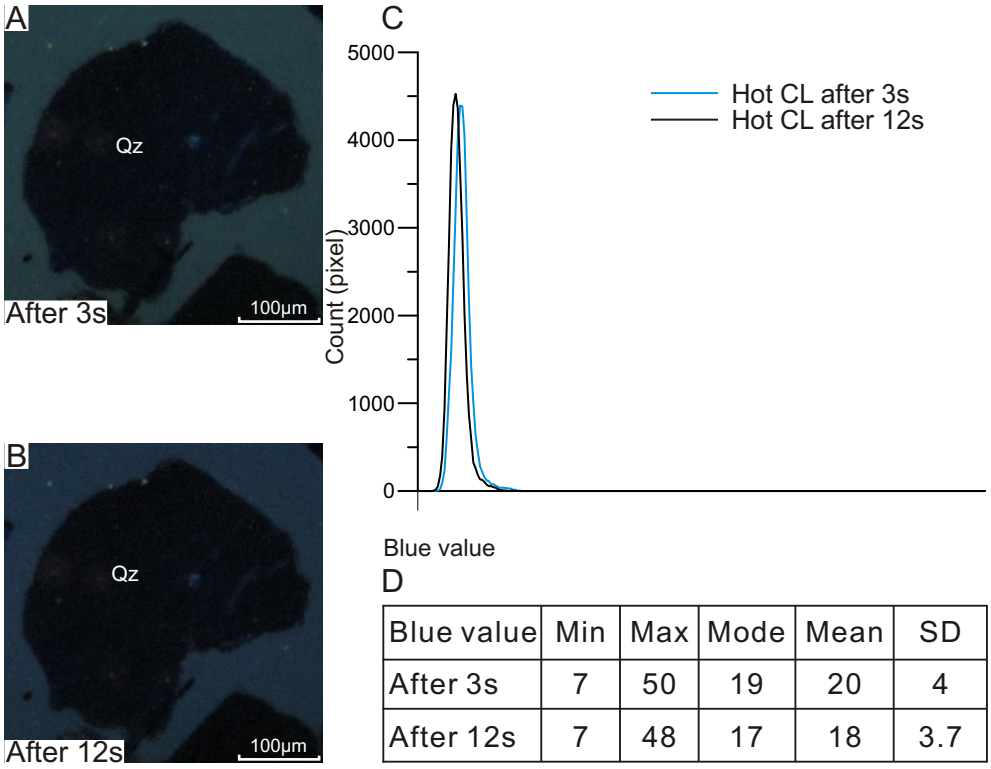

Figure 6B-39: Grain 39. The grain shows no colour shift.

D

Blue value	Min	Max	Mode	Mean	SD
After 3s	7	50	19	20	4
After 12s	7	48	17	18	3.7

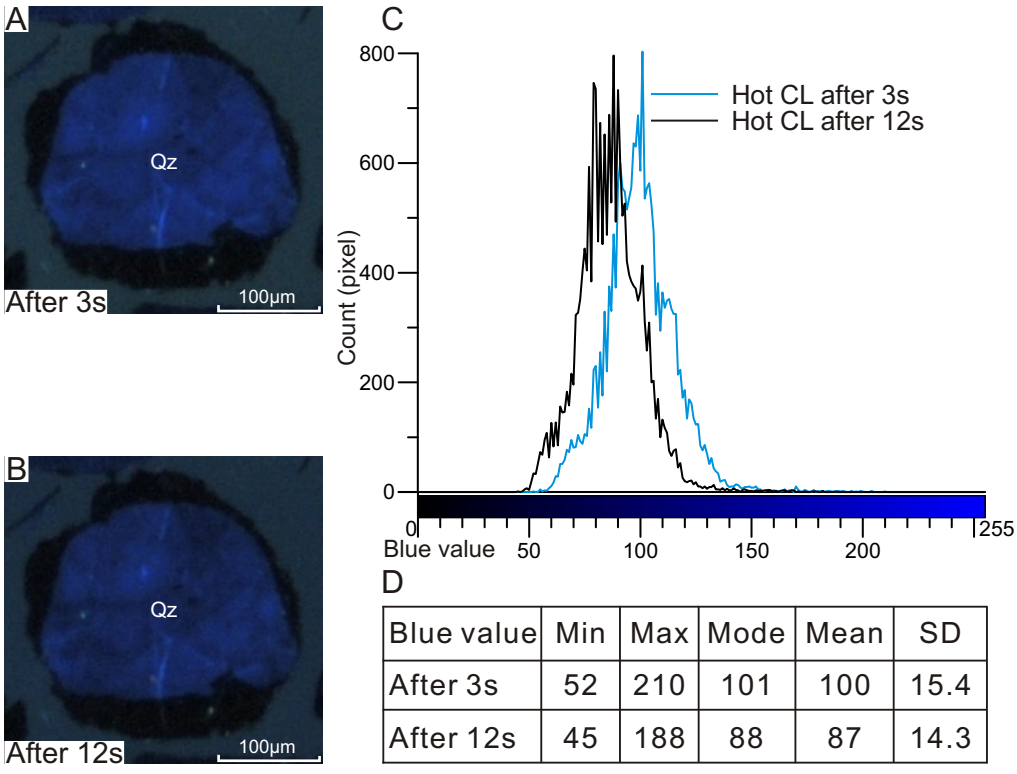

Figure 6B-40: Grain 40. The grain shows slight colour shift.

D

Blue value	Min	Max	Mode	Mean	SD
After 3s	52	210	101	100	15.4
After 12s	45	188	88	87	14.3

Appendix 7A: Microphotos, SEM-BSE images, SEM-CL images, and EDS analyses of detrital quartz grains in sample 3900.

Notes:

1. **Homogenous CL:** Nearly uniform CL intensity across the grain (Fig. 2A).

2. Fractures in quartz have been divided into two types: **healed fractures** (**HF**) and **open fractures** (**OF**).

   Healed fractures are fractures filled with secondary silica that appear as thin (commonly < 10 μm) black lines in SEM-CL images (Fig. 2B). They are usually not shown in back-scattered images (Boggs and Krinsley, 2006).

   Open fractures appear in cathodoluminescense images as CL-dark or CL-bright lines, and they are also visible in back-scattered images and microphotos. A few open fractures are **conchoidal fractures** (**CF**) (Boggs and Krinsley, 2006).

3. **Tectonic deformation lamellae**: Tectonic deformation lamellae (Fig. 2C) appear in SEM-CL image as numerous sets of thin, parallel, closely spaced, dark gray lines (Bernet and Basset, 2005). According to Hamers and Drury (2011), tectonic deformation lamellae can either appear as dark gray lines or bright lines in SEM-CL images, and can show slightly wavy features with varying thickness. They usually also appear in XPL image under petrographic microscope.

4. **Spiders (S):** They are made up of dark-Cl patches and streaks. Dark-CL patches mainly range from 10-100 μm. Streaks are random and irregular in the appearance of black broad (>10 μm) elongated form. The spiders are commonly associated with healed fractures, giving them the appearance in SEM-CL images of spiders sitting on a web (Fig. 2D). They cannot be seen in BSE images, since they are composed by secondary silica (Boggs and Krinsley, 2006).

5. **Bright mottling**: Some grains show irregular CL intensity across grains, creating a mottled pattern due the presence of patches (Boggs and Krinsley, 2006). Three types of bright mottling were seen.

   - **Random bright patches** (Fig. 2E1)
   - **Bright streaky patches fabric** (Fig. 2E2)
   - **Subtle mottling** (Fig. 2E3)

6. **Overgrowth:** Overgrowth appears in SEM-CL images as dark areas in the border of the quartz grains (Fig. 2F).

7. **Fluid inclusion trail** (**FI trail**): Trails formed by **fluid inclusions** (**FI**). They are usually associated with secondary porosity and commonly located along fractures and at boundaries between detritral quartz grain and the overgrowth. They are well observed in microphotos under ppl. The fluid inclusion trails can be separated in two kinds: **detrital fluid inclusion trails (**fluid inclusions that are original from the detrital quartz, they do not cut the quartz overgrowth) and **diagenetic fluid inclusion trails** (fluid inclusions originated from the diagenesis, and they thus cut the quartz overgrowth).

8. **Melt inclusion** (**MI**): Large fluid inclusions (>10 μm) in which crystallized minerals are visible.

9. **Secondary porosity** (**SP**): Porosities usually caused by dissolution and/or fractures. They are easily observed in microphotos under PPL and BSE images.

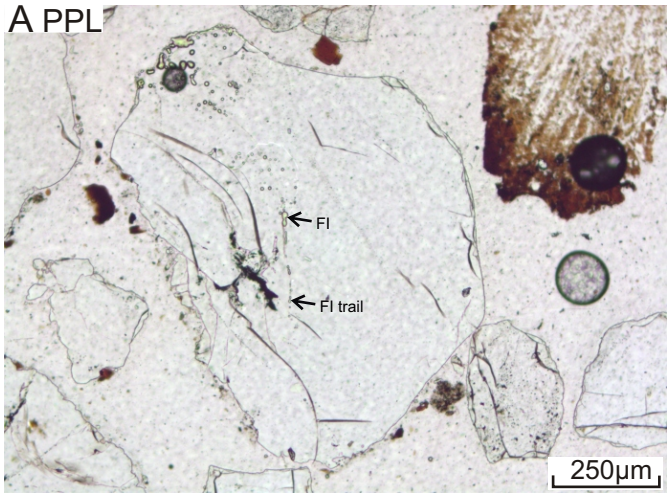

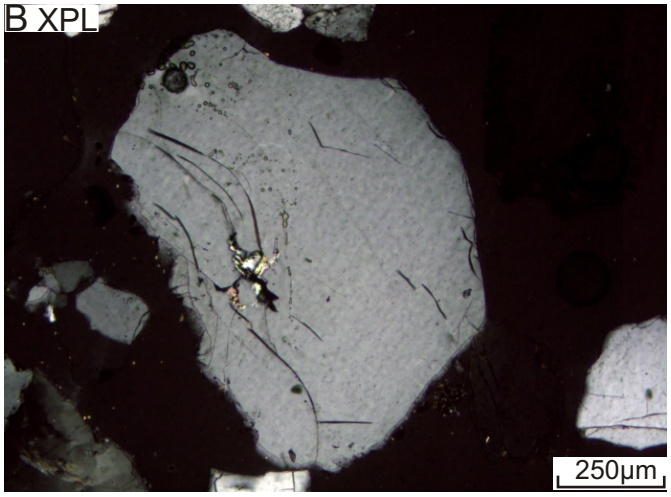

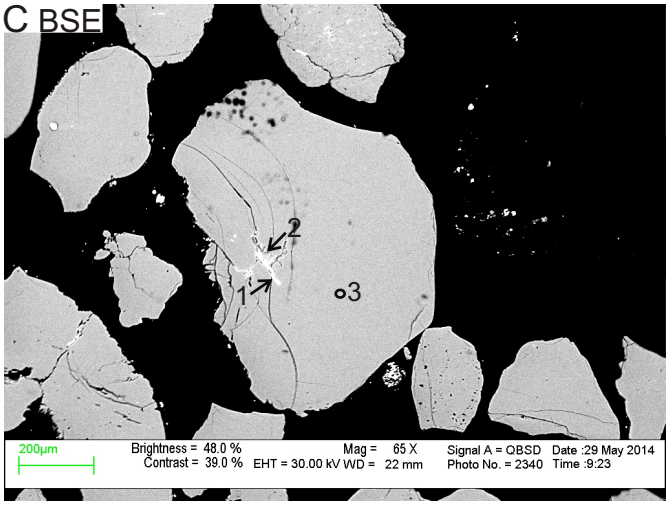

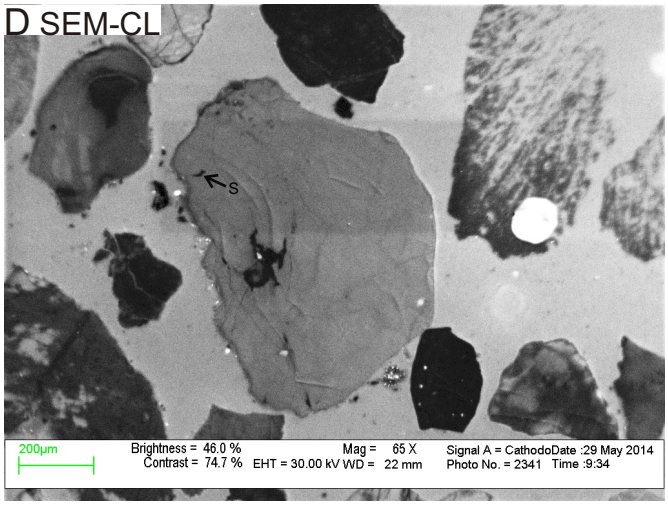

E EDS analyses

Pos#	Min. ID	SiO2	Al2O3	FeO	MgO	CaO	Na2O	K2O	P2O5	SO3	Total	Actual total
1	Ilt+Ap+Py	37.63	23.15	5.17	0.73	8.68	3.53	3.84	3.69	13.58	100	51
2	Qz	99.99									100	62
3	Ilt	48.37	31.34	1.20	1.11		4.33	3.66			90	54

Figure 7A-1: Microphotos under ppl (A) and xpl (B), SEM-BSE image (C), SEM-CL image (D), and EDS analyses table (E) of quartz grain 1 in sample 3900. The grain is anhedral and sub-rounded monocrystalline with non-undulose extinction. Fluid inclusions (FI) are present, some of the form trails (Fig. A). The grain contains illite, pyrite, and apatite inclusions and is microfractured with a set of irregular curved fractures (Fig. C and D). Healed fractures (HF) are rare, and a few spiders (S) can be seen in Fig. D.

A PPL

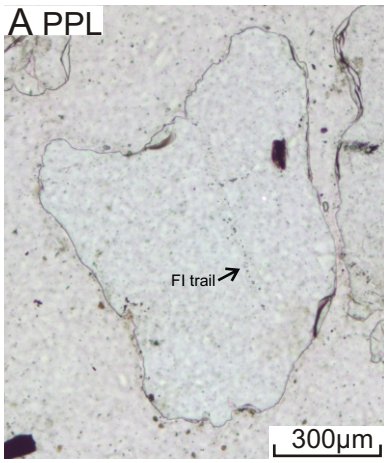

B XPL

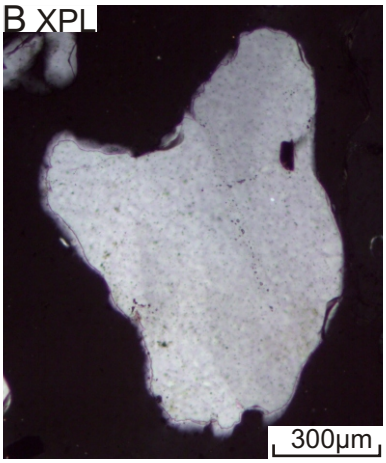

C BSE

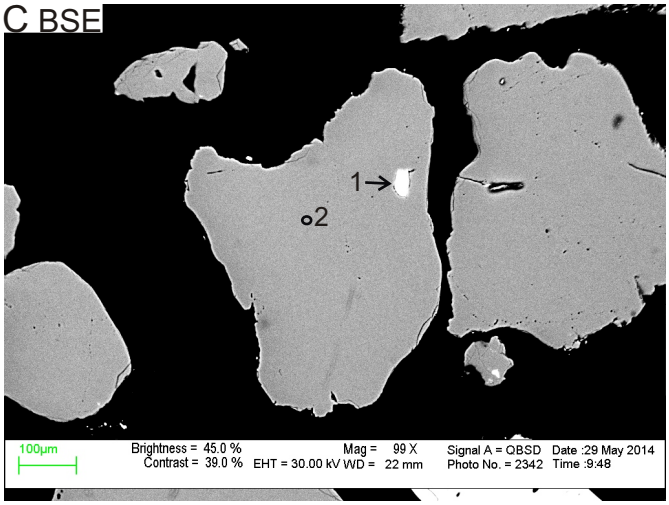

D SEM-CL

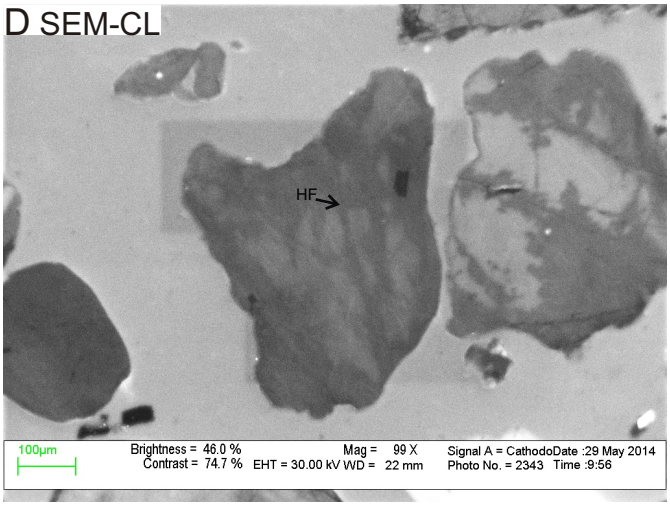

E EDS analyses

Pos#	Min. ID	SiO2	TiO2	Al2O3	FeO	MgO	K2O	SO3	Total	Actual total
1	Py+Ilt	18.5	2.87	11.28	22.36	4.84	2.38	37.78	100	67
2	Quartz	99.99							100	57

Figure 7A-2: Microphotos under ppl (A) and xpl (B), SEM-BSE image (C), SEM-CL image (D), and EDS analyses table (E) of quartz grain 2 in sample 3900. The grain is anhedral and sub-rounded monocrystalline with strong undulose extinction. Fluid inclusions are present; they form trails (FI trail) along healed fractures (Fig. A). The grain contains pyrite + illite inclusions and is weakly microfractured with a set of irregular fractures (Fig. D). A few healed fractures can be seen in Fig. D. The grain shows random bright-CL patches in SEM-CI image.

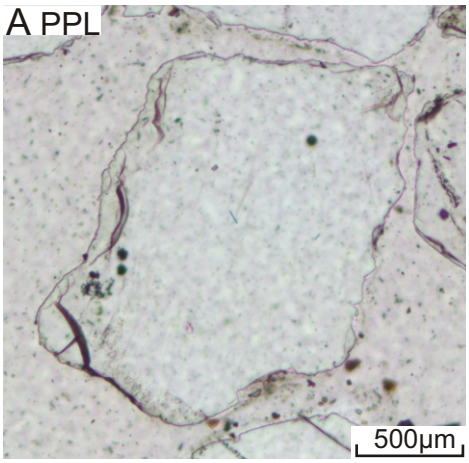

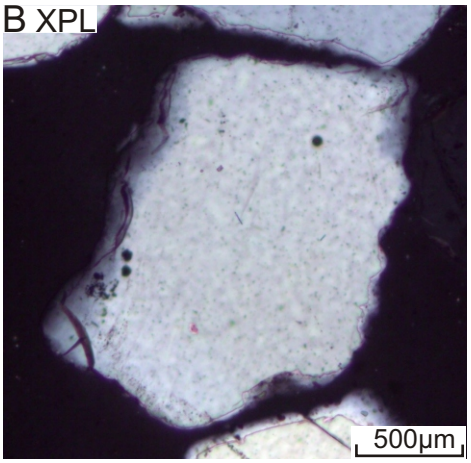

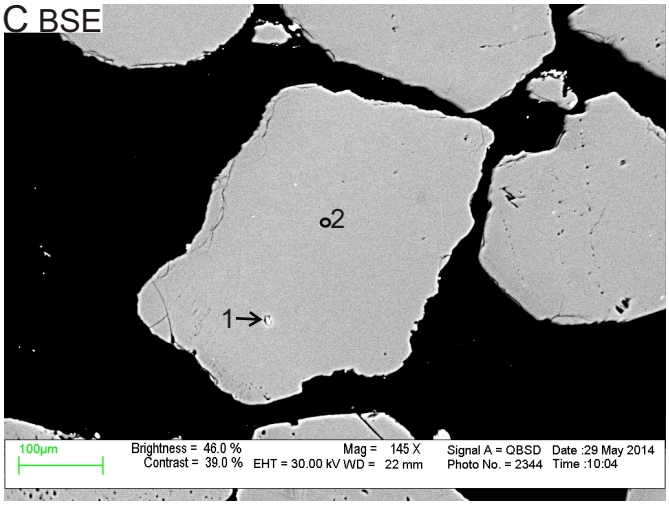

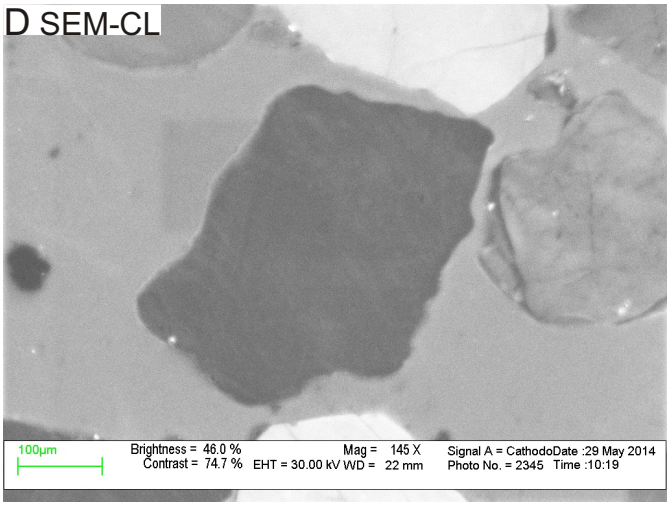

E EDS analyses

Pos#	Min. ID	SiO2	CaO	F	Total	Actual total
1	Qz+Cal	70.76	26.64	2.6	100	43
2	Quartz	99.99			100	59

Figure 7A-3: Microphotos under ppl (A) and xpl (B), SEM-BSE image (C), SEM-CL image (D), and EDS analyses table (E) of quartz grain 4 in sample 3900. The grain is anhedral and sub-rounded monocrystalline with strong undulose extinction. Fluid inclusions are rare. The grain contains a calcite inclusion and is weakly microfractured with irregular open fractures (Fig. C). Healed fractures (HF) are rare. The grain shows homogeneous dark-CL in SEM-CL image.

A PPL

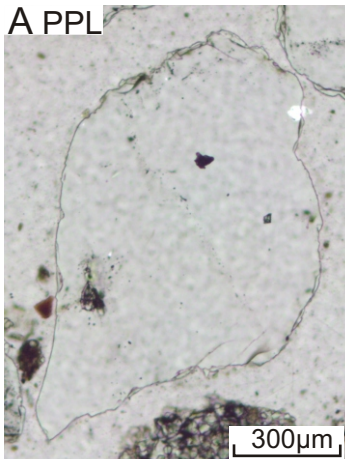

B XPL

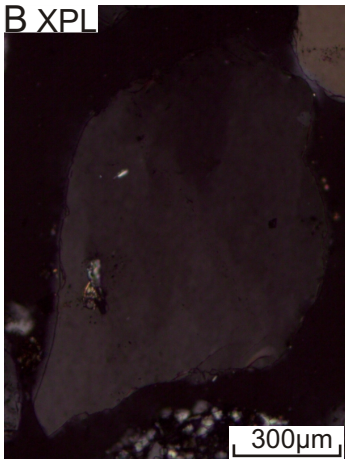

C BSE

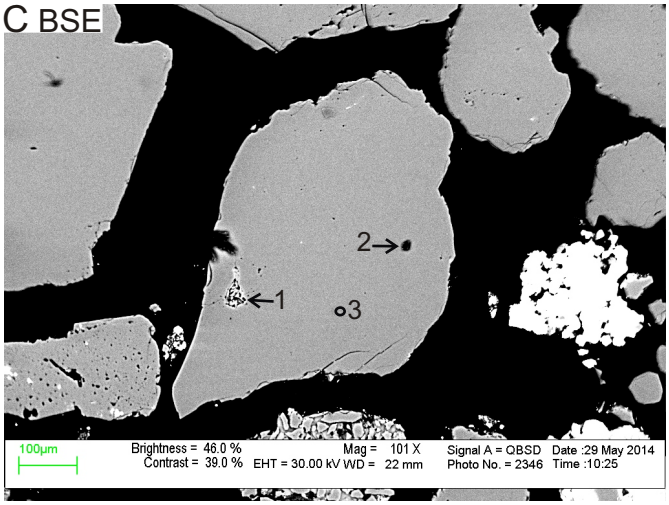

D SEM-CL

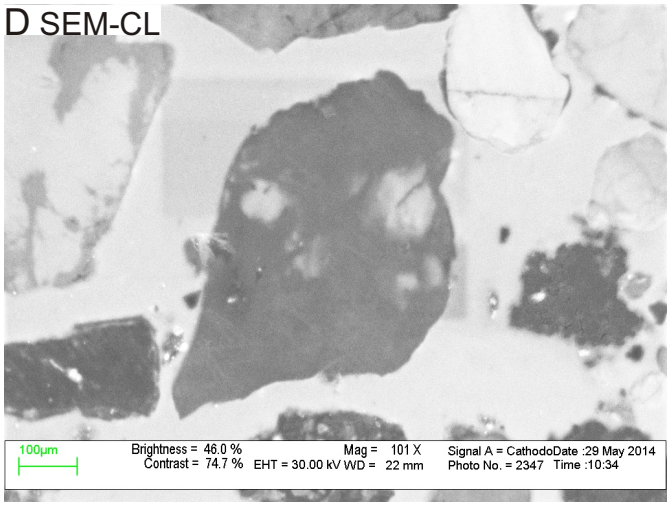

E EDS analyses

Pos#	Min. ID	SiO2	TiO2	Al2O3	FeO	MgO	Na2O	K2O	SO3	F	Cl	Total	Actual total
1	Ms	49.34	0.29	31.92	1.74	0.96		9.01		1.75		95	45
2	Qz+Fluid inclusion	70.14					1.11	0.3	23.15	2.28	3.01	100	55
3	Qz	99.99										100	58

Figure 7A-4: Microphotos under ppl (A) and xpl (B), SEM-BSE image (C), SEM-CL image (D), and EDS analyses table (E) of quartz grain 4 in sample 3900. The grain is anhedral and sub-rounded monocrystalline with strong undulose extinction. Fluid inclusions are present. The grain contains muscovite inclusions and is weakly microfractured with irregular open fractures (Fig. C). Healed fractures (HF) are rare. The grain shows random bright-CL patches in SEM-CL image.

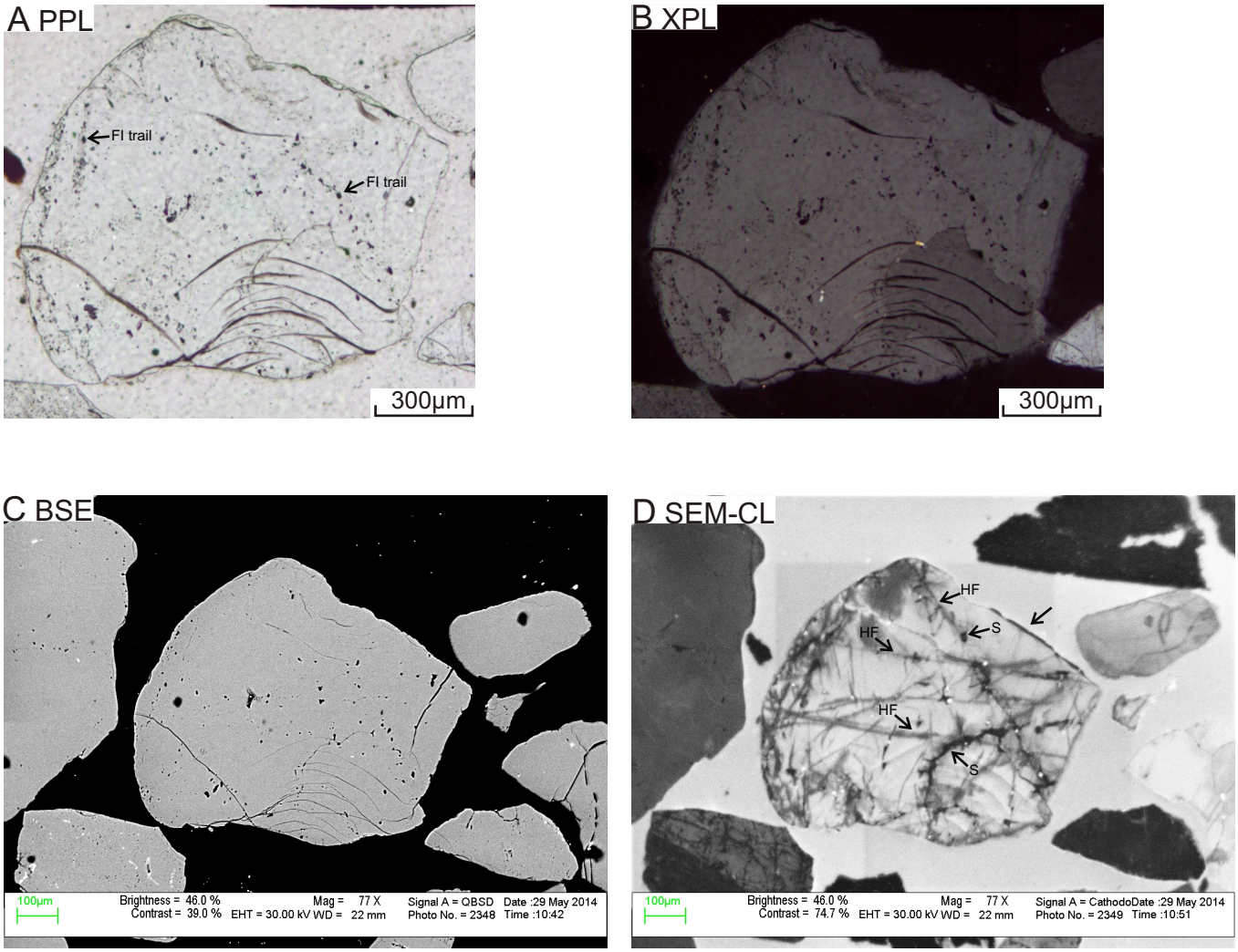

Figure 7A-5: Microphotos under ppl (A) and xpl (B), SEM-BSE image C, and SEM-CL image (D) of quartz grain 5 in sample 3900. The grain is anhedral and sub-rounded monocrystalline with non-undulose extinction. Fluid inclusions are common; they are usually associated with secondary porosity and form trails (FI trail) along healed fractures (Fig. A). The grain is strongly microfractured with a set of conchoidal open fractures (CF), a set of parallel healed fractures and a set of irregular fractures (Fig. C and D). Healed fractures (HF) and spiders (S) are common (Fig. D). The dark area indicated by arrow in Fig. D is overgrowth.

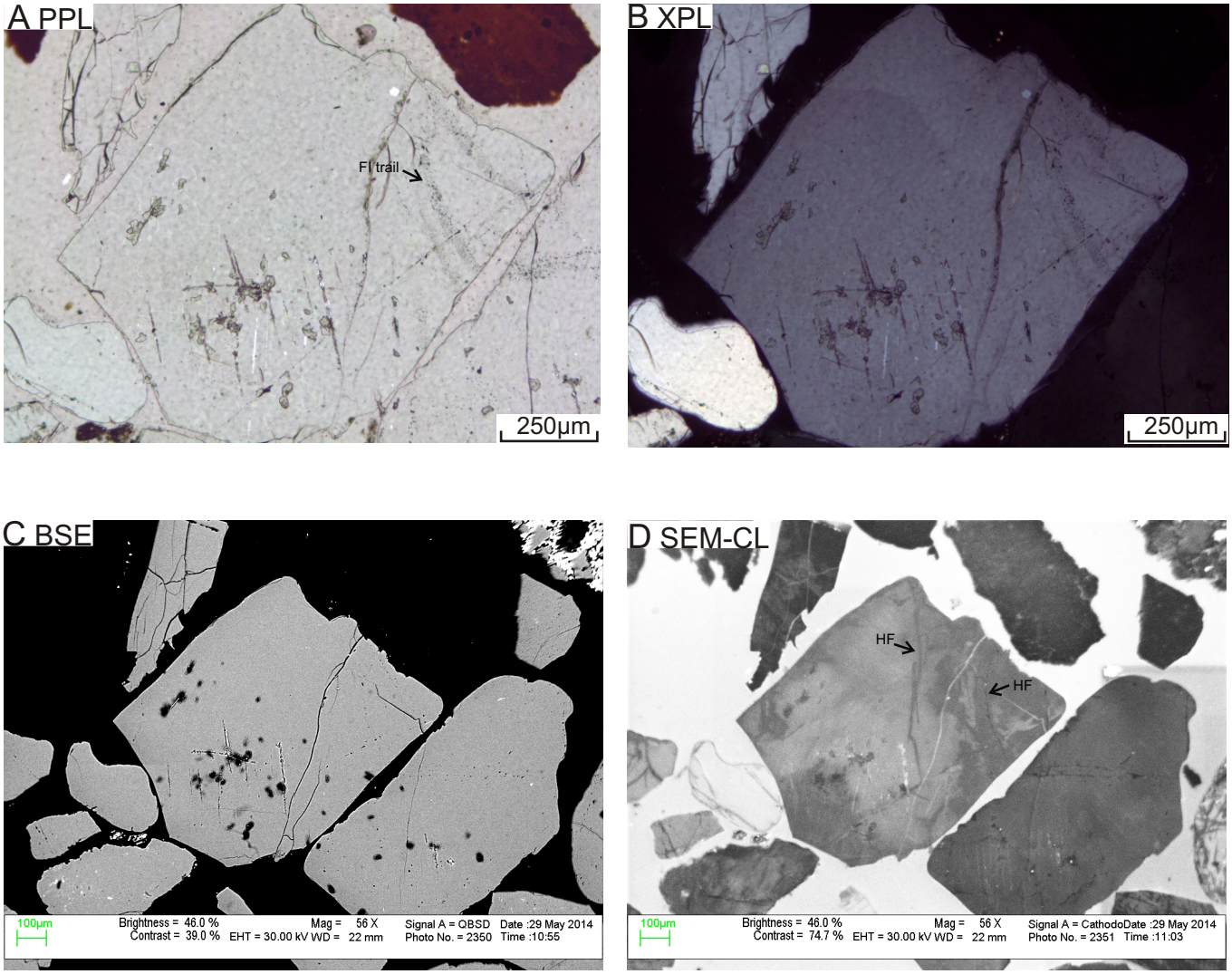

Figure 7A-6: Microphotos under ppl (A) and xpl (B), SEM-BSE image C, and SEM-CL image (D) of quartz grain 6 in sample 3900. The grain is anhedral and sub-rounded monocrystalline with non-undulose extinction. Fluid inclusions are common; they form trails (FI trail) along healed fractures (Fig. A). The grain is microfractured with a set of irregular fractures (Fig. C and D). Healed fractures (HF) and present (Fig. D). The grain shows random bright-CL patches in SEM-CL image.

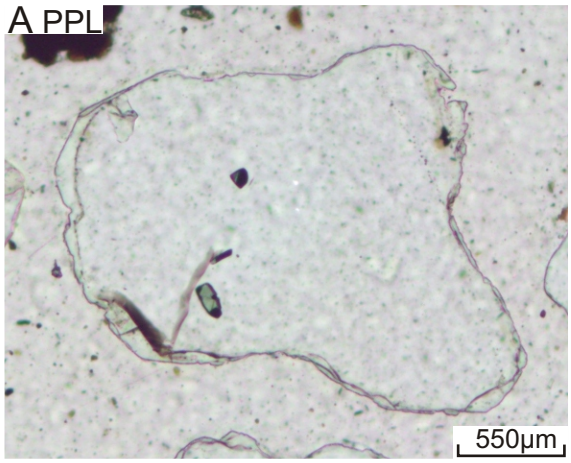

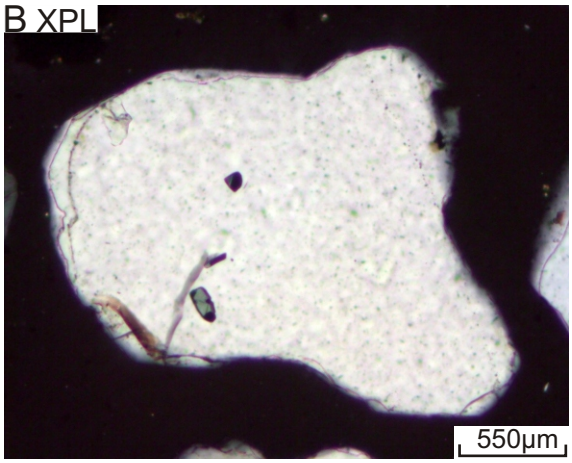

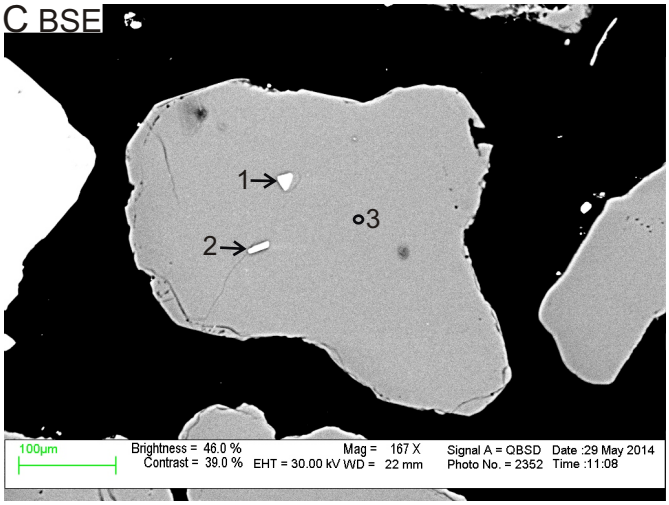

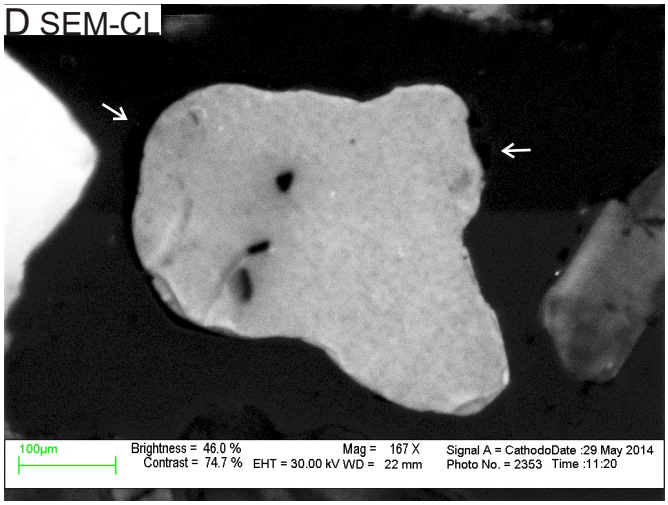

E EDS analyses

Pos#	Min. ID	SiO2	Al2O3	FeO	MgO	Total	Actual total
1	Hc	0.68	62	29.09	8.24	100	52
2	Hc+Fe oxide+Qz	10.59	32.1	52.22	5.11	100	62
3	Qz	99.99				100	59

Figure 7A-7: Microphotos under ppl (A) and xpl (B), SEM-BSE image (C), SEM-CL image (D), and EDS analyses table (E) of quartz grain 7 in sample 3900. The grain is anhedral and rounded monocrystalline with weak undulose extinction. Fluid inclusions are present, they form trails at boundaries between detritral quartz grain and the overgrowth.The grain contains hercynite and iron oxide inclusions and is weakly microfractured with irregular open fractures. Healed fractures are rare. The grain shows homogeneous-CL in SEM -CL image.

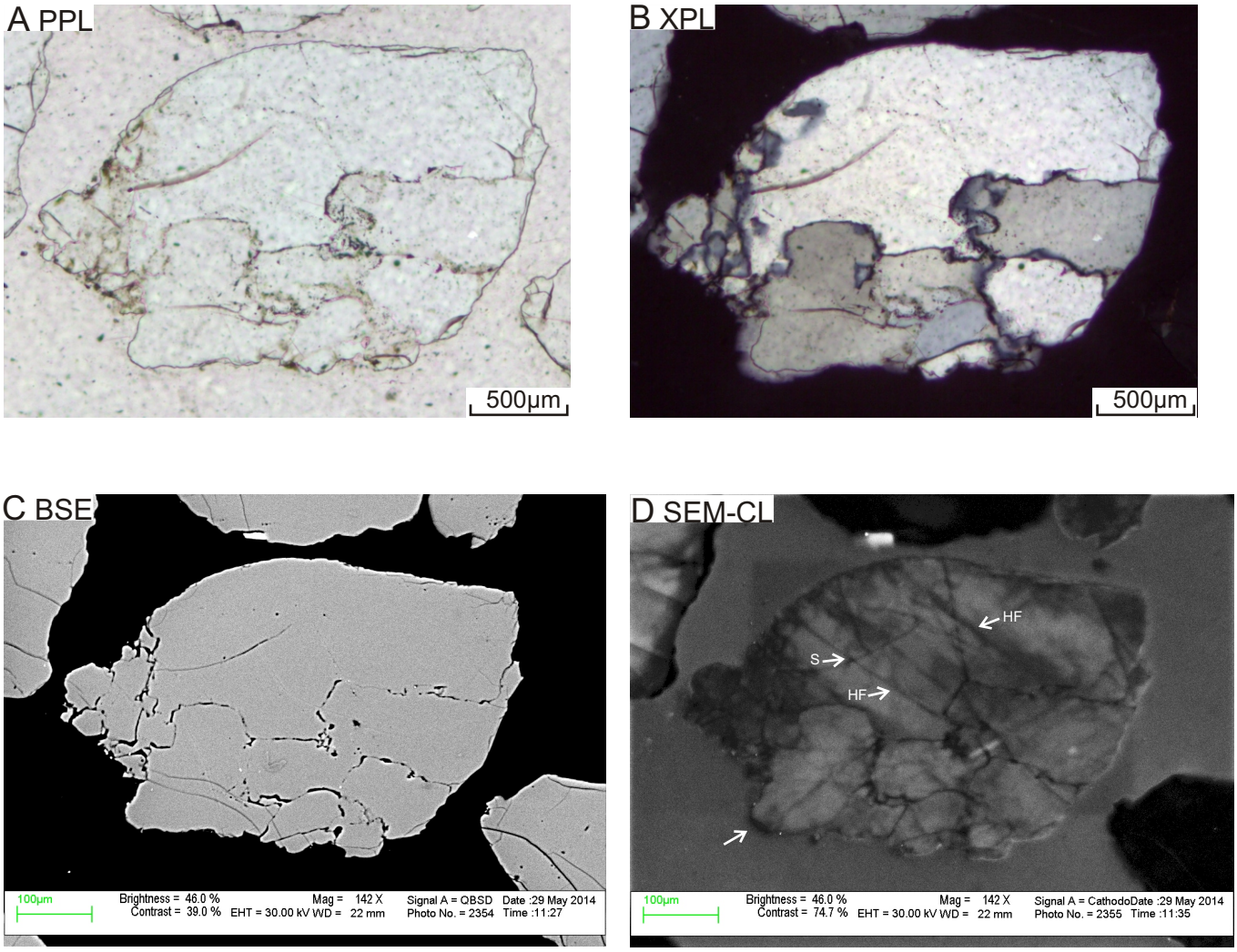

Figure 7A-8: Microphotos under ppl (A) and xpl (B), SEM-BSE image C, and SEM-CL image (D) of quartz grain 8 in sample 3900. This grain is anhedral and sub-rounded polyctystalline (more than 9 subgrains with sutured sub-grain boundaries) with mosaic texture and weak undulose extinction. Fluid inclusions are present. The grain is microfractured with a set of sub-parallel fractures and a set of irregular fractures. Healed Fractures (HF) and spiders (S) are common (Fig. D). The grain shows random bright-CL patches in SEM-CL image.

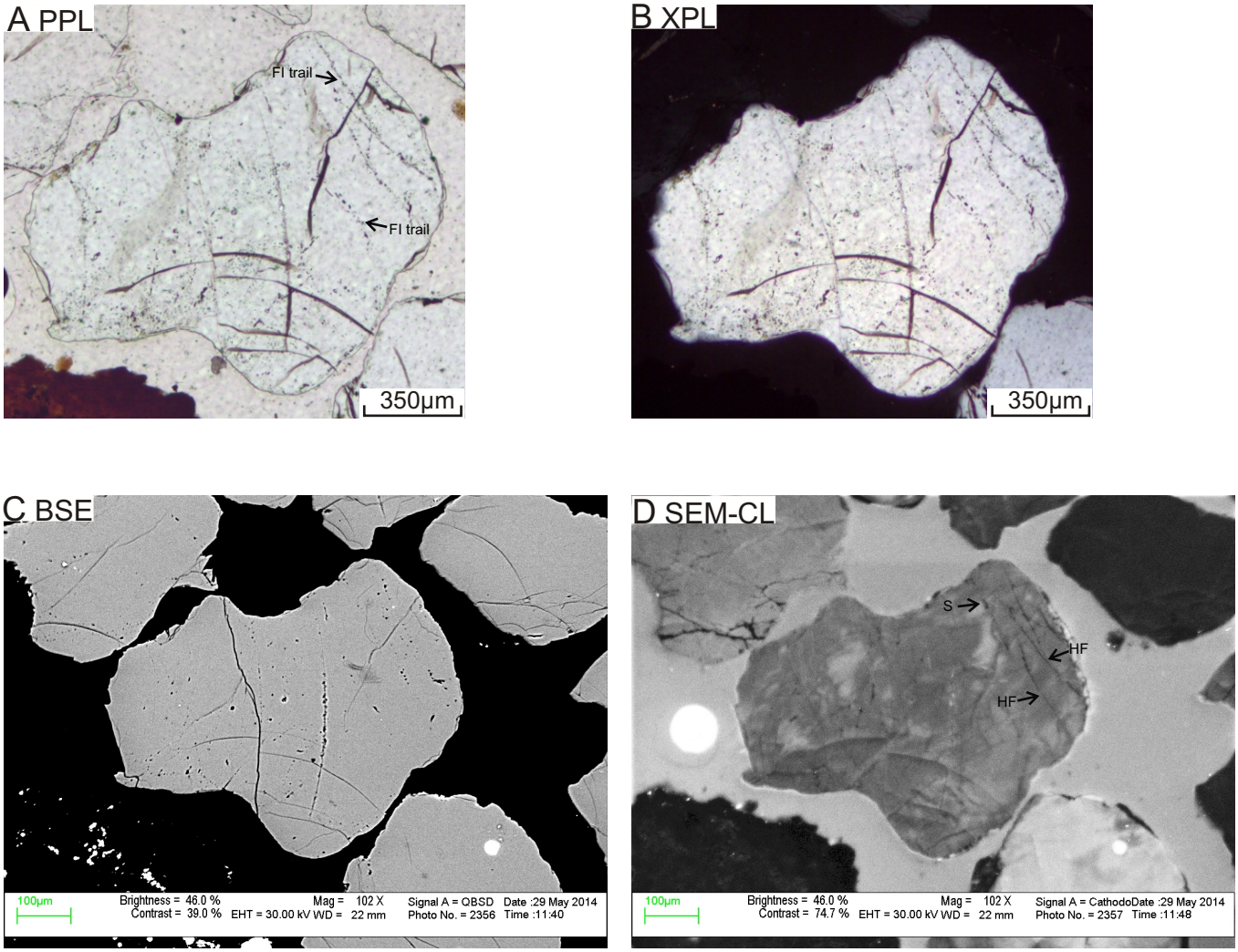

Figure 7A-9: Microphotos under ppl (A) and xpl (B), SEM-BSE image C, and SEM-CL image (D) of quartz grain 9 in sample 3900. The grain is anhedral and sub-rounded monocrystalline with strong undulose extinction. Fluid inclusions are common; they are usually associated with secondary porosity and form trails (FI trail) along healed fractures (Fig. A). The grain is microfractured with a set of irregular fractures (Fig. C and D). Healed fractures (HF) are common. Some spiders (S) are present (Fig. D). The grain shows bright streaky patches fabric in SEM-CL image.

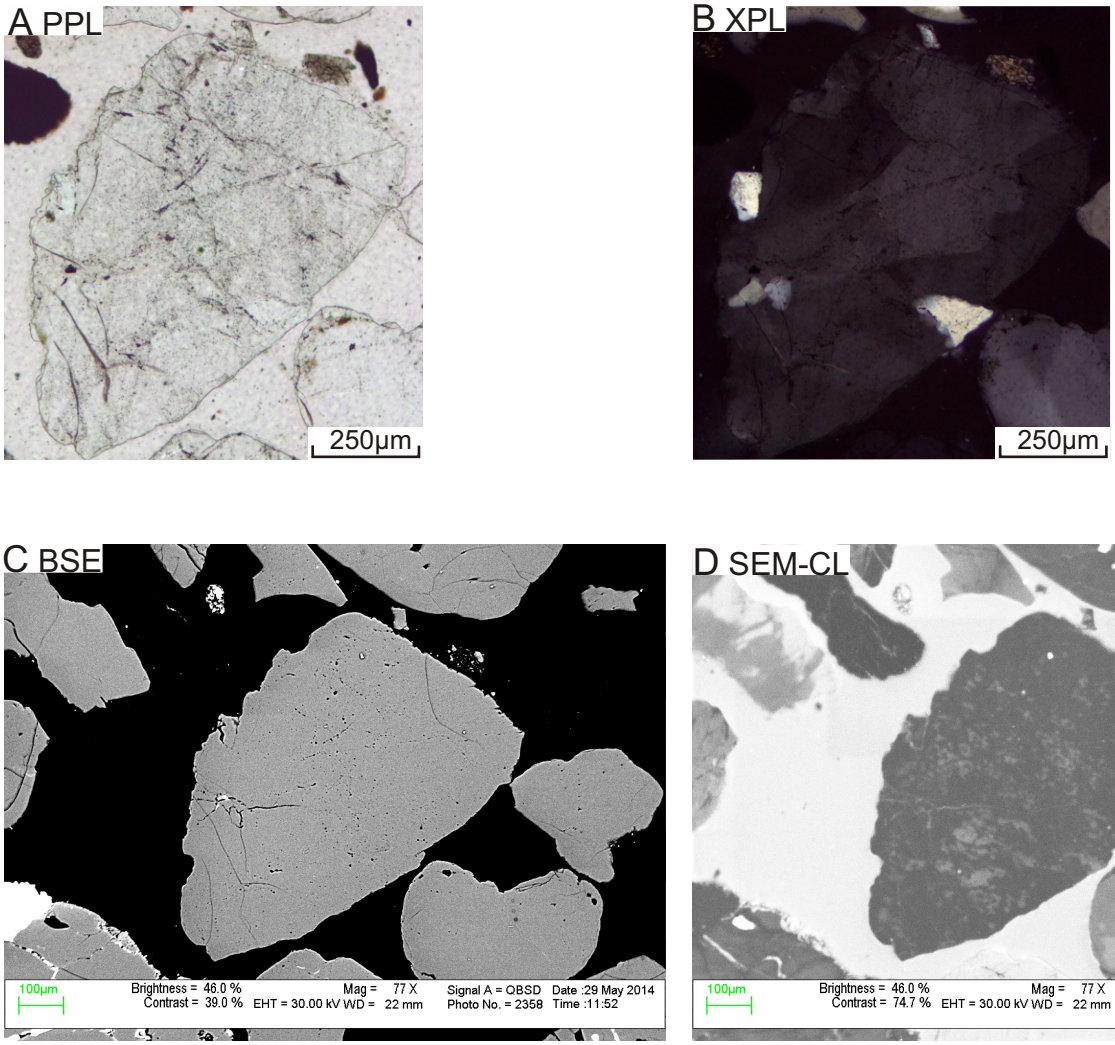

Figure 7A-10: Microphotos under ppl (A) and xpl (B), SEM-BSE image C, and SEM-CL image (D) of quartz grain 10 in sample 3900. The grain is anhedral and sub-rounded polycrystalline (more than 9 sub-grains) with mosaic texture and weak undulose extinction. Fluid inclusions are common and form trails. The grain is microfractured with a set of irregular fractures (Fig. C and D). The grain shows subtle mottling in SEM-CL image.

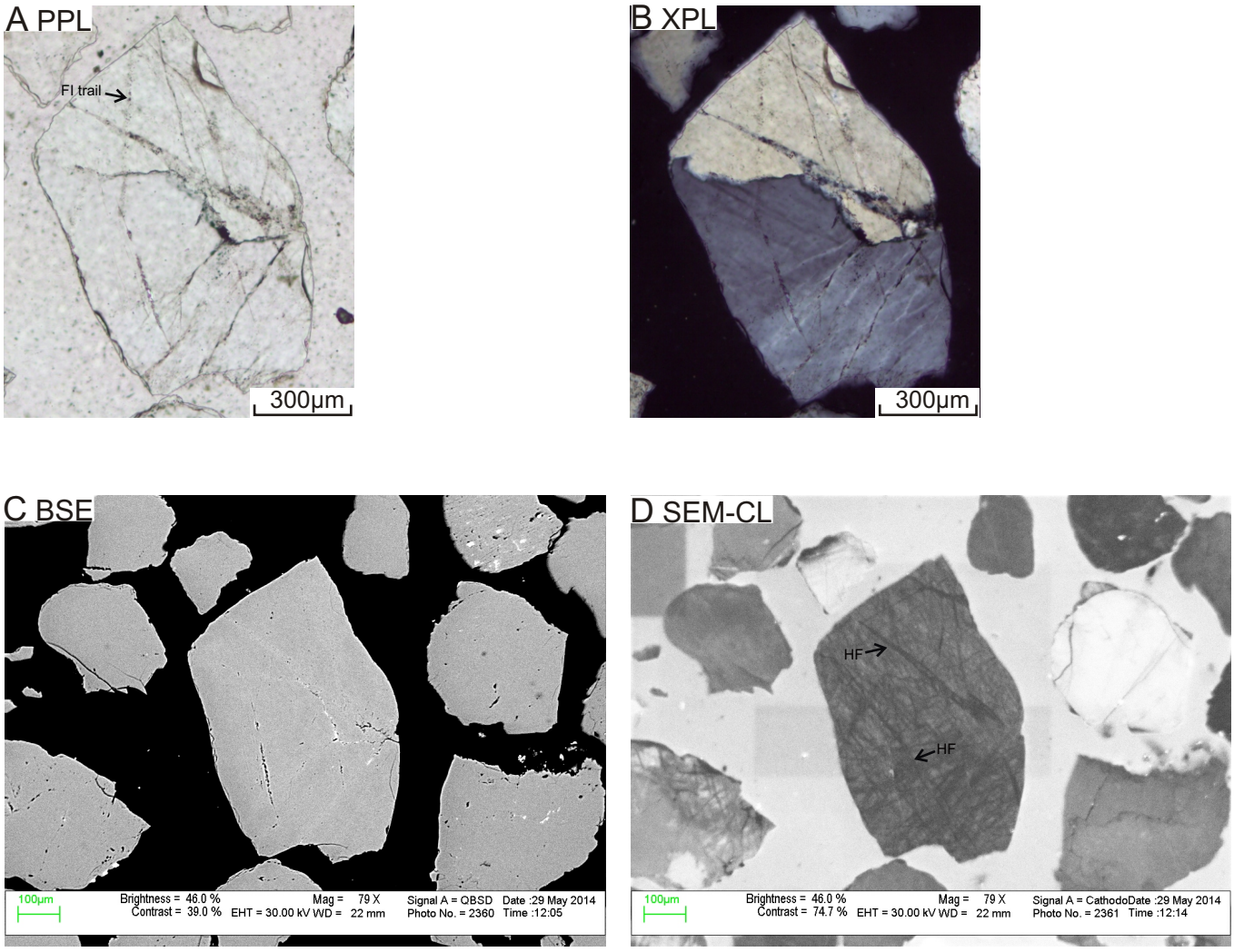

Figure 7A-11: Microphotos under ppl (A) and xpl (B), SEM-BSE image C, and SEM-CL image (D) of quartz grain 11 in sample 3900. The grain is anhedral and sub-angular polycrystalline (only 2 sub-grains with sutured sub-grain boundaries) with deformation lamellae and strong undulose extinction. Detrital fluid inclusions are common; they form trails (FI trail) along healed fractures (Fig. A). The grain is strongly microfractured with a set of parallel fractures and a set of irregular fractures (Fig. C and D). Healed fractures (HF) are common (Fig. D).

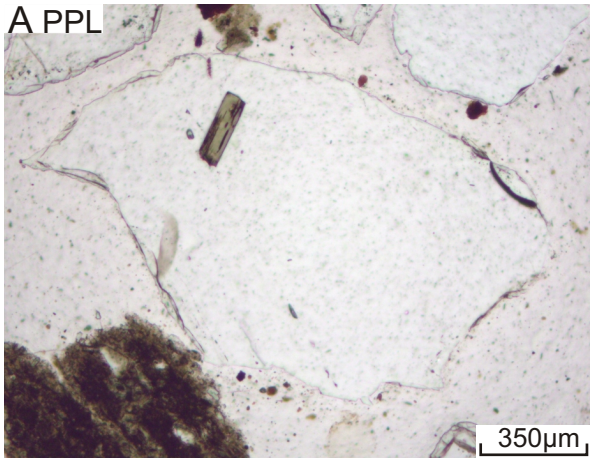

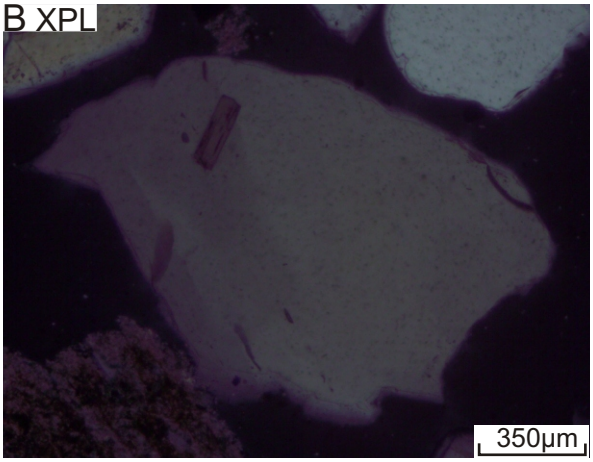

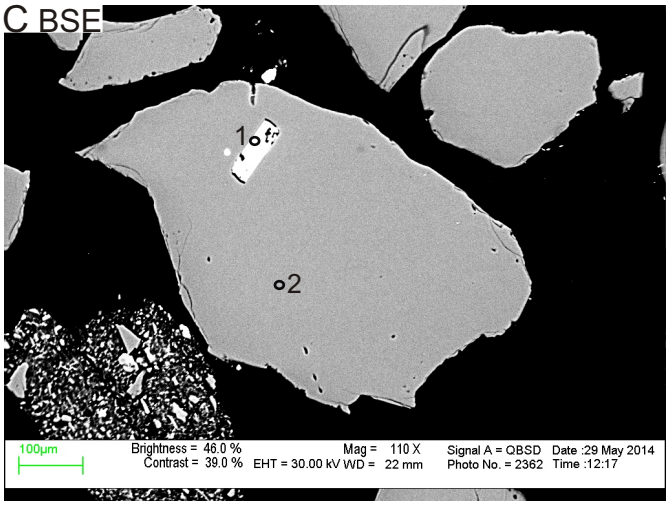

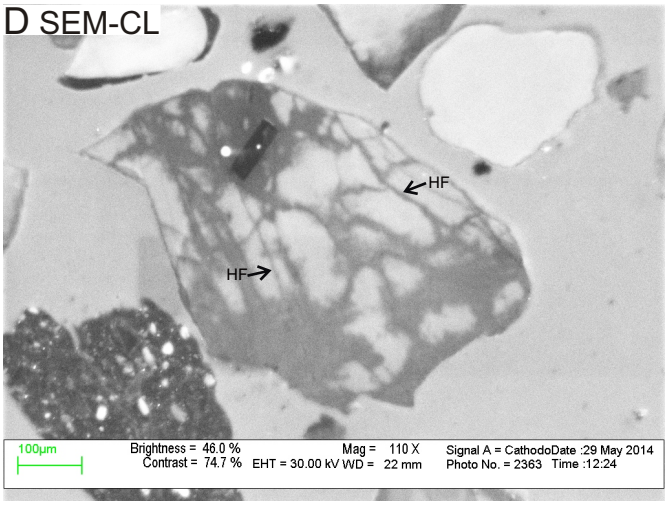

E EDS analyses

Pos#	Min. ID	SiO2	TiO2	Al2O3	FeO	MnO	MgO	K2O	Total	Actual total
1	Bt	39.64	3.12	15.52	16.43	0.26	11.43	9.59	96	49
2	Qz	99.99							100	61

Figure 7A-12: Microphotos under ppl (A) and xpl (B), SEM-BSE image (C), SEM-CL image (D), and EDS analyses table (E) of quartz grain 12 in sample 3900. The grain is anhedral and sub-angular monocrystalline with strong undulose extinction. Fluid inclusions are rare. The grain is microfractured with a set of irregular fractures (Fig. D) and contains a biotite inclusion. Healed fractures (HF) are common (Fig. D). The grain shows random bright-CL patches in SEM-CL image.

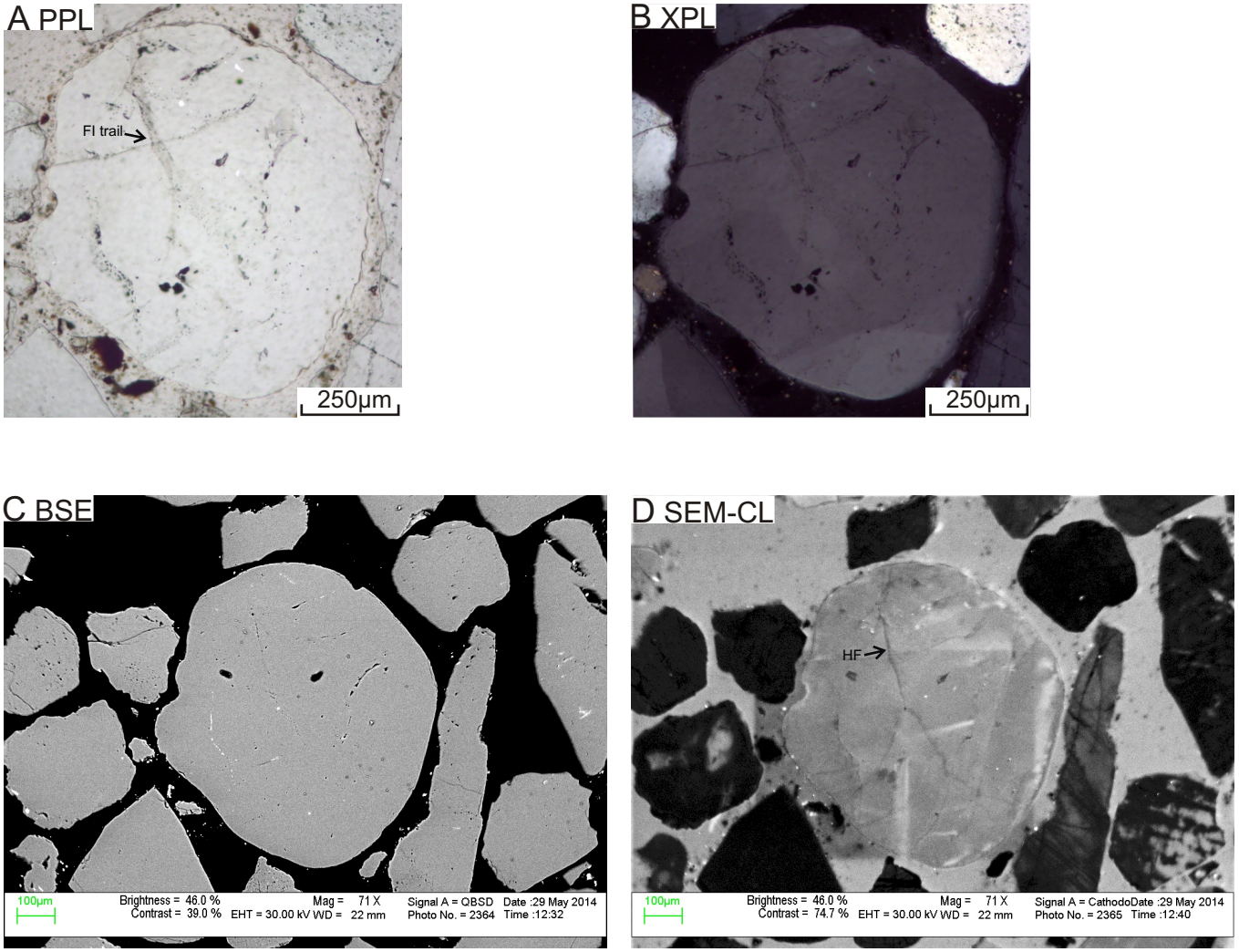

Figure 7A-13: Microphotos under ppl (A) and xpl (B), SEM-BSE image C, and SEM-CL image (D) of quartz grain 13 in sample 3900. The grain is anhedral and well-rounded monocrystalline with weak undulose extinction. Detrital fluid inclusion trails (FI trail) are present. The grain is weakly microfractured with a set of irregular fractures (Fig. D). Healed fractures (HF) are present (Fig. D). The grain shows some bright streaky patches in SEM-CL image.

A PPL

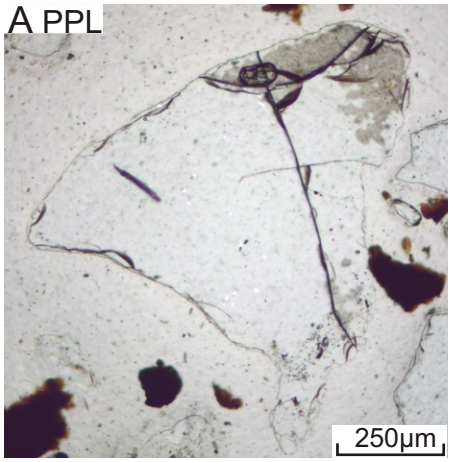

B XPL

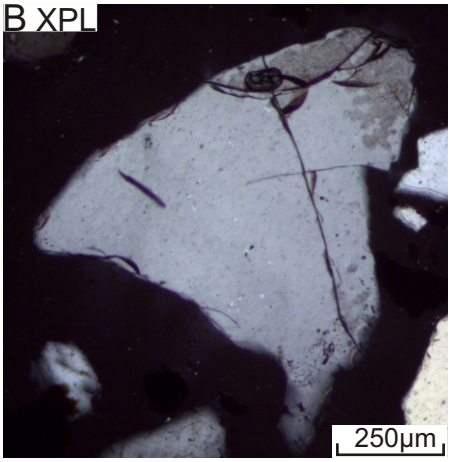

C BSE

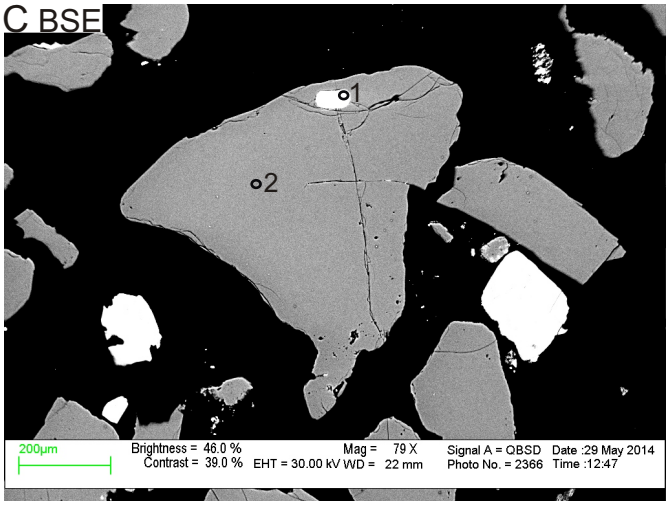

D SEM-CL

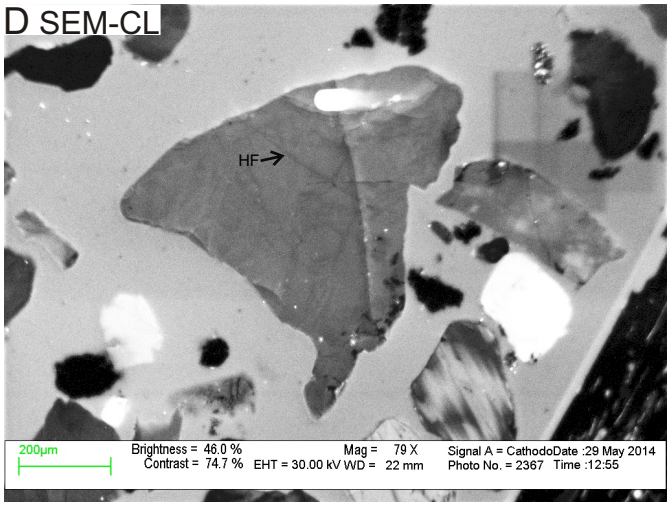

E EDS analyses

Pos#	Min. ID	SiO2	CaO	P2O5	F	Total	Actual total
1	Ap		47.52	45.1	7.4	100	49
2	Qz	99.99				100	48

Figure 7A-14: Microphotos under ppl (A) and xpl (B), SEM-BSE image (C), SEM-CL image (D), and EDS analyses table (E) of quartz grain 14 in sample 3900. The grain is anhedral and sub-angular monocrystalline with non-undulose extinction. Fluid inclusions are rare. The grain contains a apatite inclusion and is microfractured with a set of irregular fractures. A few healed fractures (HF) are present.

A PPL

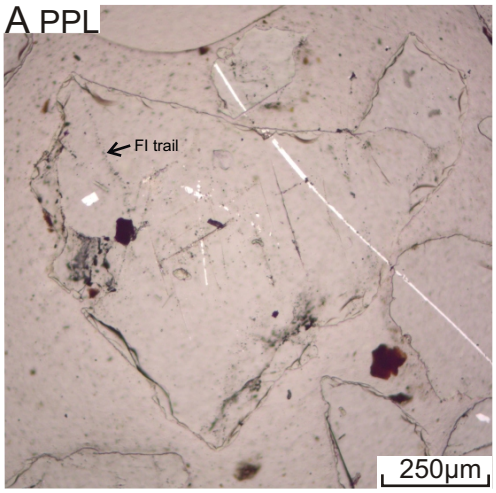

B XPL

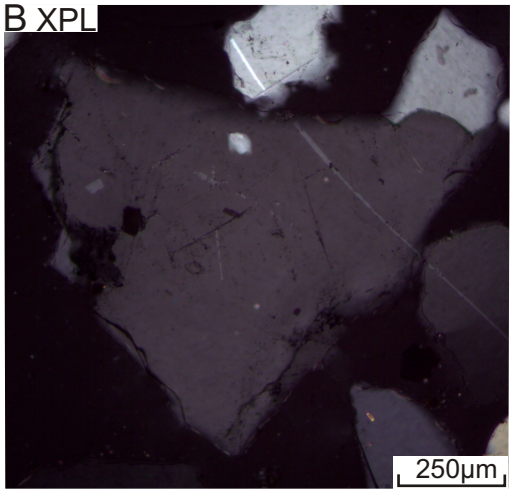

C BSE

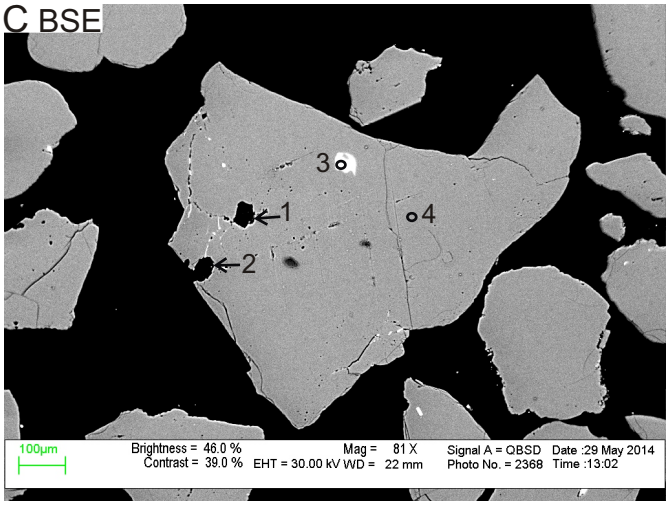

D SEM-CL

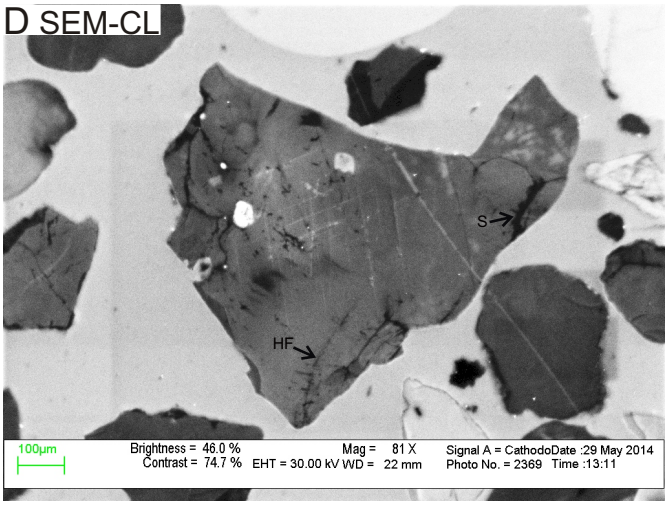

E EDS analyses

Pos#	Min. ID	SiO2	TiO2	Al2O3	FeO	MgO	CaO	Na2O	K2O	SO3	F	Cl	Total	Actual total
1	Kln+Py+Hole	59.53		28.82	0.96	1.99	0.73	1.27	0.52	1.95	3.99	0.26	100	26
2	Hole	27.62	2.62	16.8	2.16		9.21			22.57	17.22	1.81	100	6
3	Kfs	66.51		18.08				1.38	14.03				100	50
4	Qz	99.99											100	58

Figure 7A-15: Microphotos under ppl (A) and xpl (B), SEM-BSE image (C), SEM-CL image (D), and EDS analyses table (E) of quartz grain 15 in sample 3900. The grain is anhedral and angular polycrystalline (only 3 sub-grains with sutured sub-grain boundaries) with non-undulose extinction. Detrital fluid inclusion trails (FI trail) are present (Fig. A). The grain contains kaolinite, pyrite, and K-feldspar inclusions, and is microfractured with a set of irregular fractures. Spiders (S) and healed fractures (HF) are common (Fig. D).

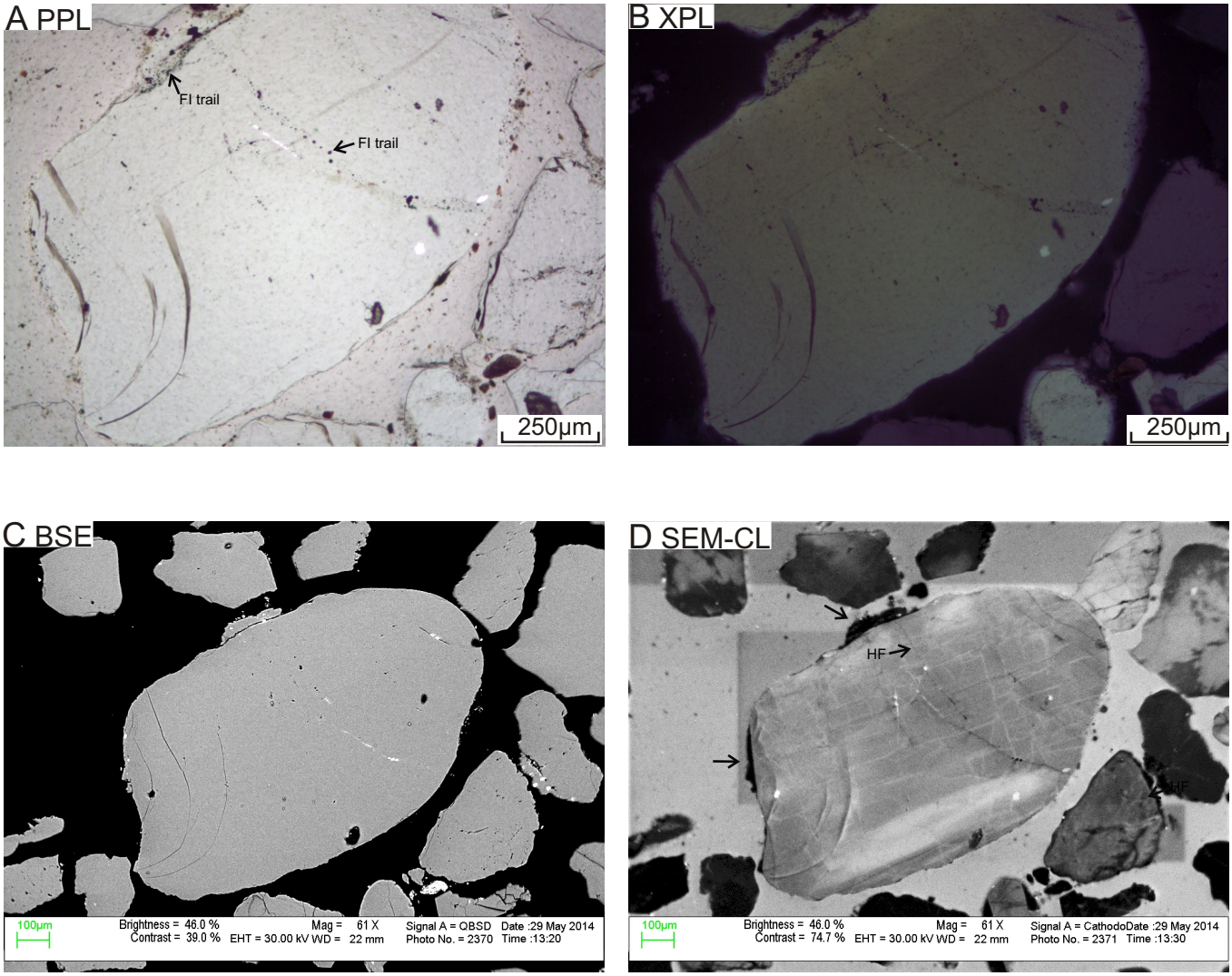

Figure 7A-16: Microphotos under ppl (A) and xpl (B), SEM-BSE image C, and SEM-CL image (D) of quartz grain 16 in sample 3900. The grain is anhedral and well-rounded monocrystalline with mosaic texture and weak undulose extinction. Detrital fluid inclusion trails and diagenetic fluid inclusion trails are present, the latter located at the boundary between the overgrowth and the detrital quartz . The grain is microfractured with a set of irregular fractures (Fig. D). Some healed fractures (HF) and spiders (S) are present (Fig. D). The dark areas indicated by arrows in Fig. D are overgrowth. The grain shows bright-CL streaky patches fabric in SEM-CL image.

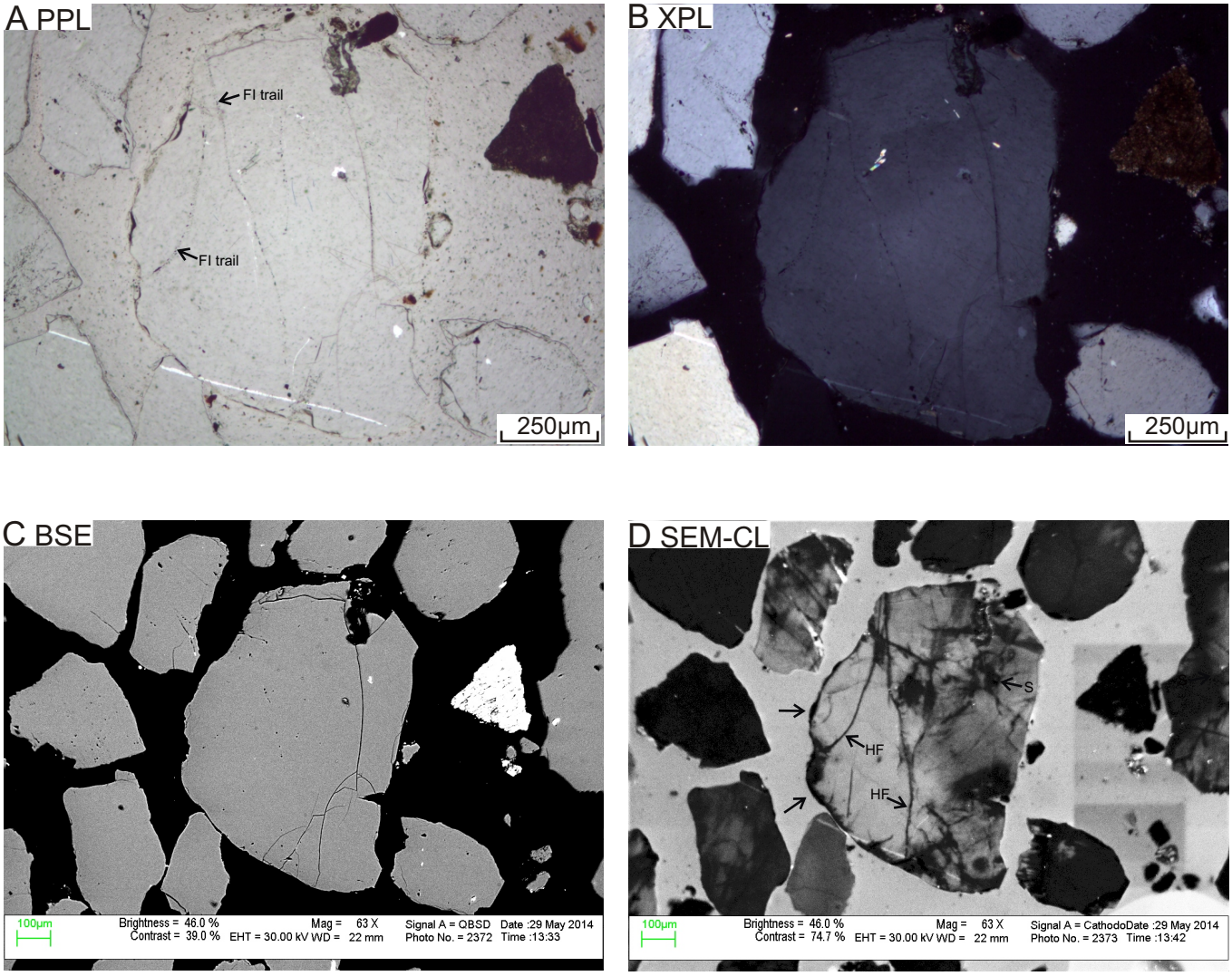

Figure 7A-17: Microphotos under ppl (A) and xpl (B), SEM-BSE image C, and SEM-CL image (D) of quartz grain 17 in sample 3900. The grain is anhedral and sub-rounded monocrystalline with non-undulose extinction. Detrital fluid inclusions are common; they form trails (FI trail) along healed fractures (Fig. A). The grain is strongly microfractured with a set of irregular fractures (Fig. C and D). Healed fractures (HF) and spiders (S) are common (Fig. D). The dark areas indicated by arrows in Fig. D are overgrowth.

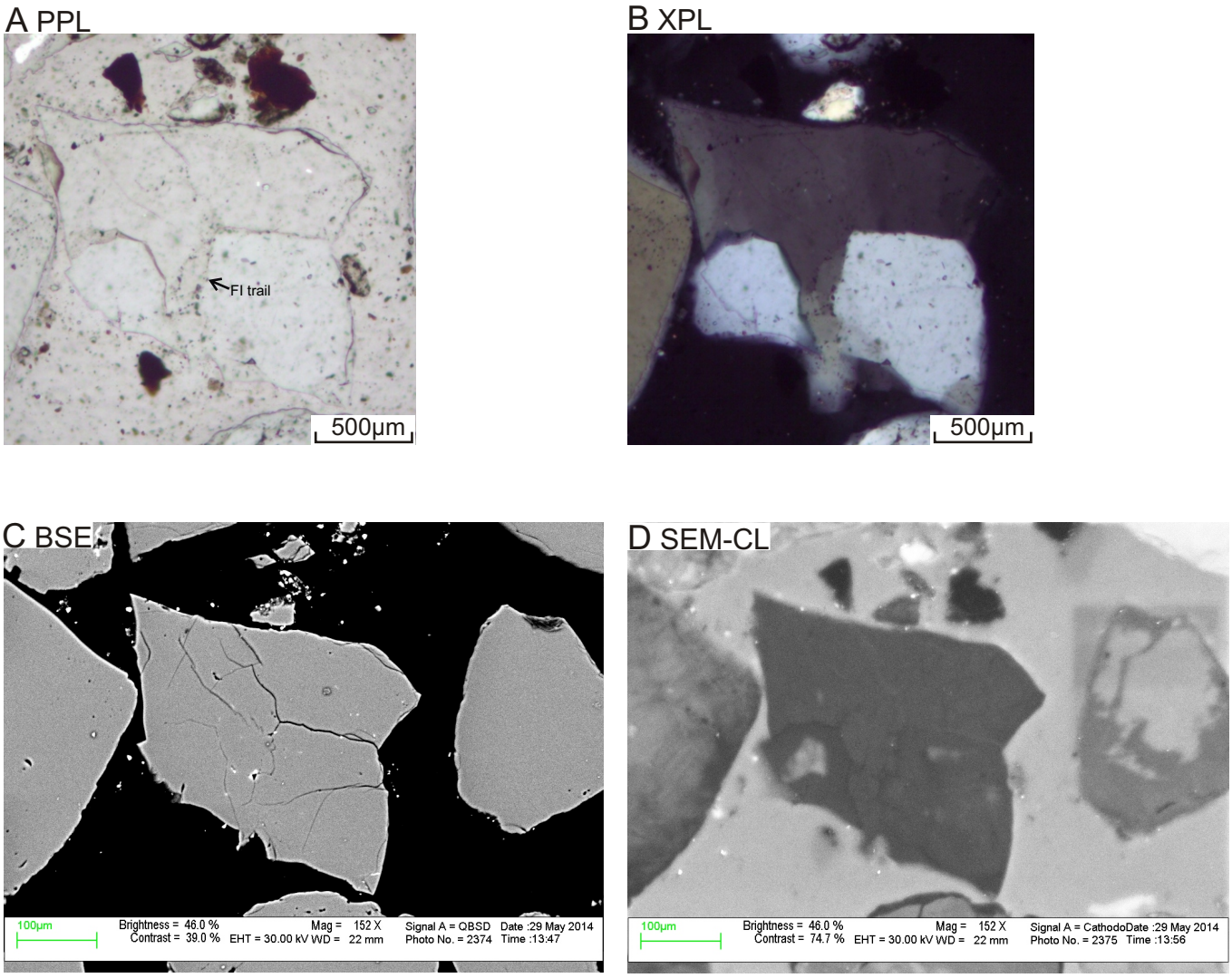

Figure 7A-18: Microphotos under ppl (A) and xpl (B), SEM-BSE image C, and SEM-CL image (D) of quartz grain 18 in sample 3900. The grain is anhedral and angular polycrystalline (6 sub-grains) with mosaic texture and weak undulose extinction. Detrital fluid inclusion trails are present (Fig. A). The grain is microfractured with a set of irregular open fractures (Fig. C). Healed fractures are rare (Fig. D).The grain shows subtle molting in SEM-CL image.

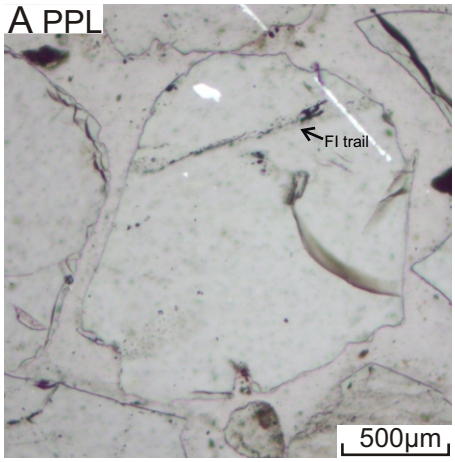

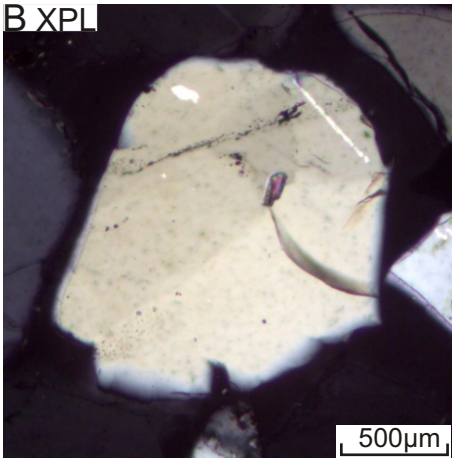

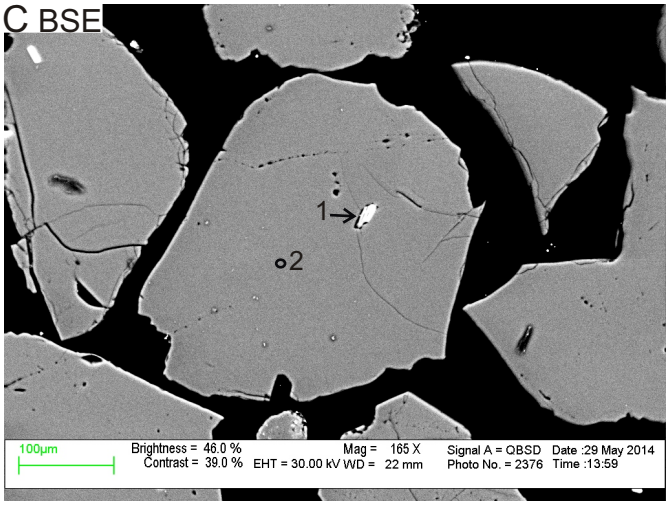

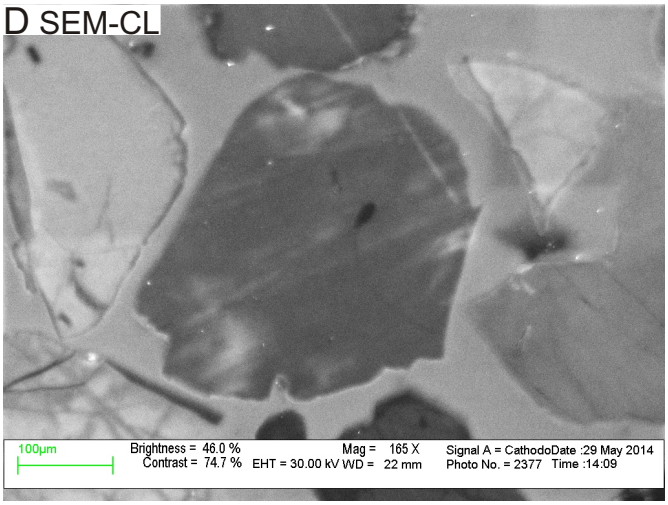

E EDS analyses

Pos#	Min. ID	SiO2	TiO2	Al2O3	FeO	MgO	Na2O	K2O	SO3	Total	Actual total
1	Ms	48.89	0.81	30.12	2.56	1.18	0.44	9.86	1.14	95	46
2	Qz	99.99								100	53

Figure 7A-19: Microphotos under ppl (A) and xpl (B), SEM-BSE image (C), SEM-CL image (D), and EDS analyses table (E) of quartz grain 19 in sample 3900. The grain is anhedral and sub-rounded monocrystalline with mosaic texture and weak undulose extinction. Detrital fluid inclusion trails are present (Fig. A). The grain contains a muscovite inclusion and is microfractured with a set of irregular open fractures (Fig. C). Healed fractures are rare (Fig. D). The grain shows bright-CL streaky patches fabric in SEM-CL image.

A PPL

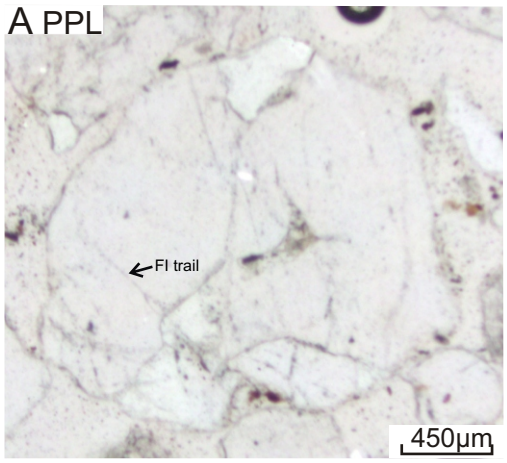

B XPL

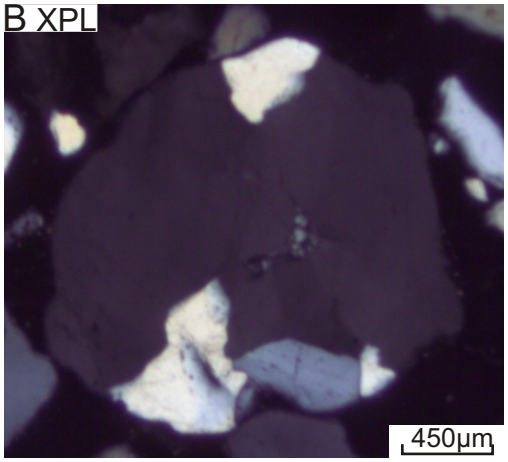

C BSE

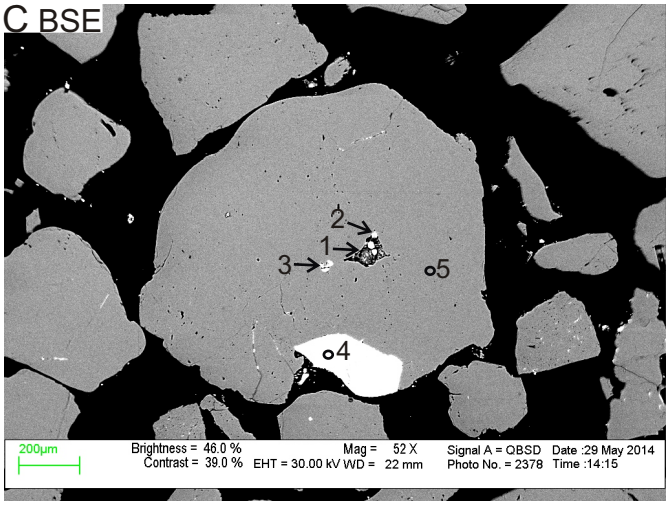

D SEM-CL

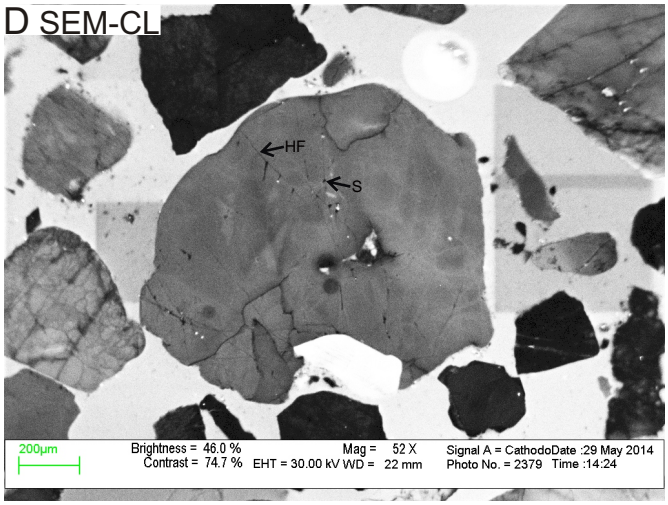

E EDS analyses

Pos#	Min. ID	SiO2	TiO2	Al2O3	FeO	MnO	MgO	CaO	Na2O	K2O	P2O5	SO3	F	Total	Actual total
1	Ilt	45.03		33.16	1.55		0.39	0.57		2.05	2.83	1.50	2.93	90	40
2	Kfs	66.14		18.16					0.42	15.27				100	50
3	Bt+Py	45.56	2.25	15.63	19	0.22	5.39			5.18		6.79		100	47
4	Kfs	66.55		18.05						15.41				100	46
5	Qz	99.99												100	44

Figure 7A-20: Microphotos under ppl (A) and xpl (B), SEM-BSE image (C), SEM-CL image (D), and EDS analyses table (E) of quartz grain 20 in sample 3900. The grain is subhedral and sub-rounded polycrystalline (5 sub-grains) with mosaic texture and weakundulose extinction. Detrital fluid inclusions are present; they form trails (FI trail) along healed fractures (Fig. A). The grain contains fluid inclusion trails, ilite, k-feldspar, biotite , and pyrite inclusions and is microfractured with a set of irregular fractures (Fig. C and D). Healed fractures (HF) and spiders (S) are present (Fig. D).

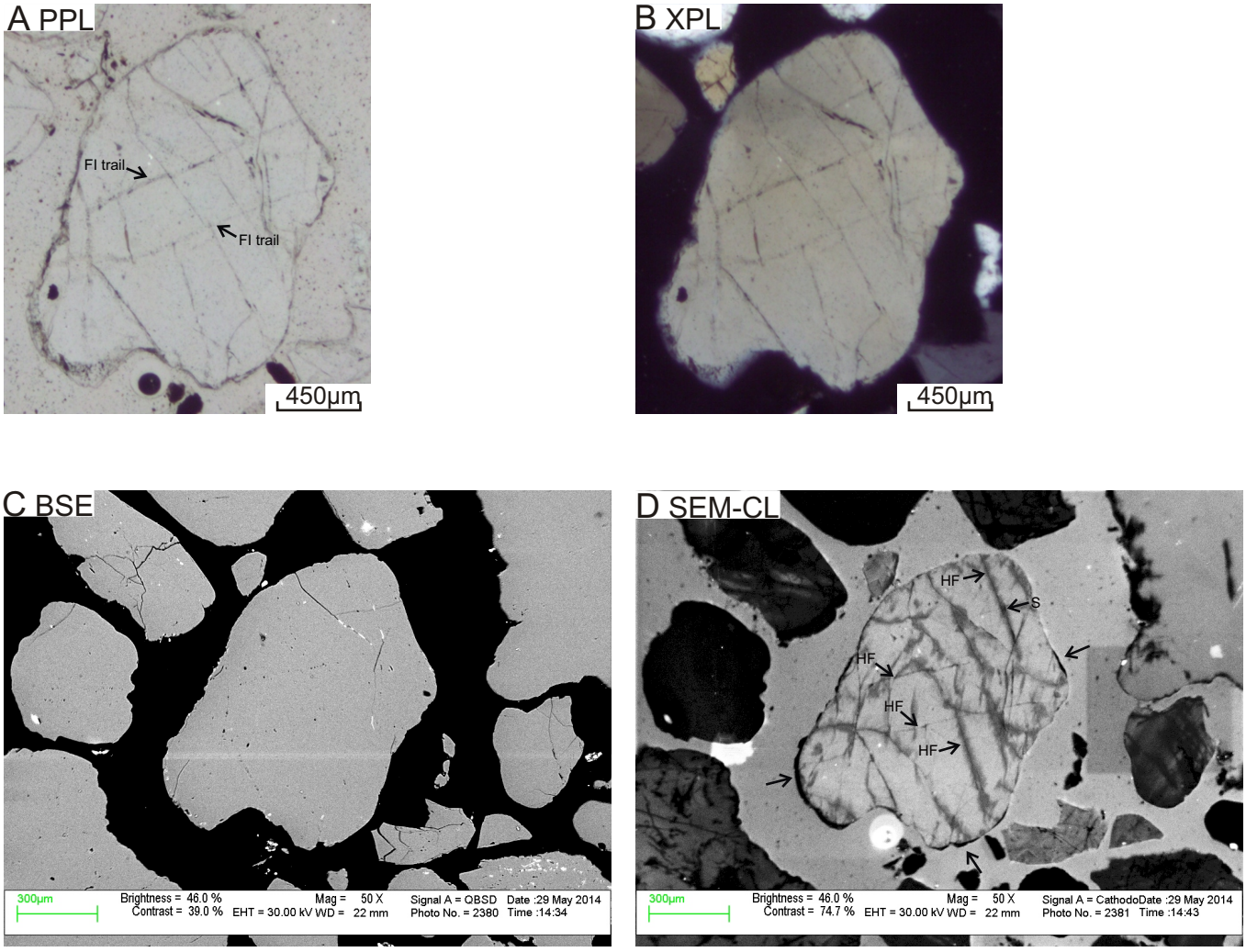

Figure 7A-21: Microphotos under ppl (A) and xpl (B), SEM-BSE image C, and SEM-CL image (D) of quartz grain 21 in sample 3900. The grain is anhedral and rounded monocrystalline with embayed margins, mosaic texture and non-undulose extinction. Detrital fluid inclusions are common; they form trails (FI trail) along healed fractures (Fig. A). The grain is strongly microfractured with two sets of parallel healed fractures crosscutting each other perpendicularly and a set of irregular open fractures (Fig. C and D). Healed fractures (HF) and spiders (S) are common (Fig. D). The dark areas indicated by arrows in Fig. D are overgrowth.

A PPL

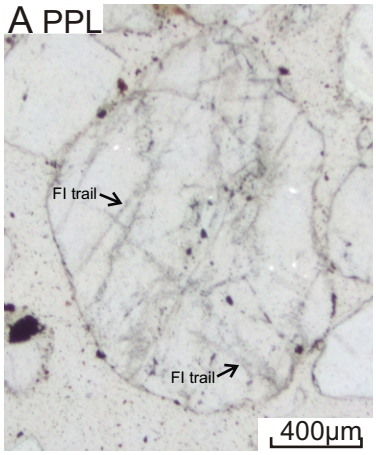

B XPL

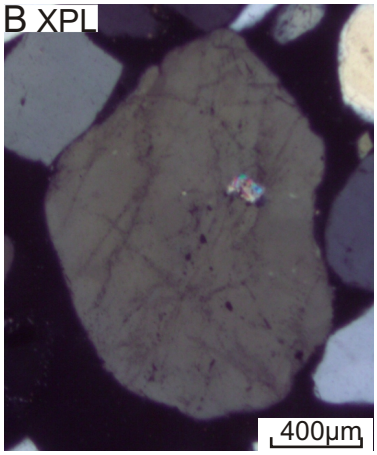

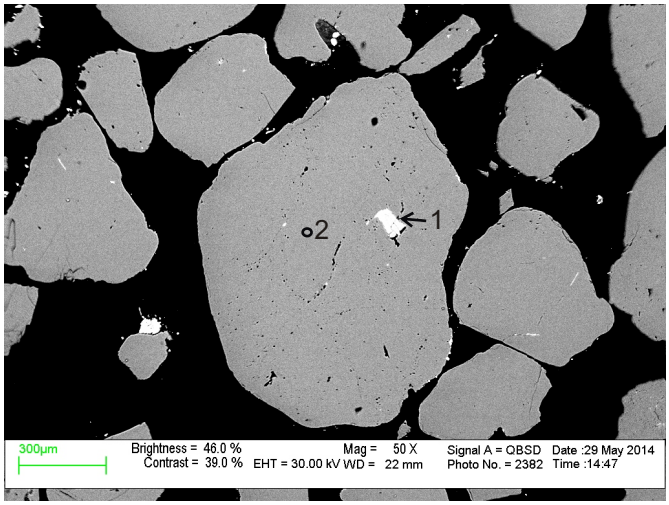

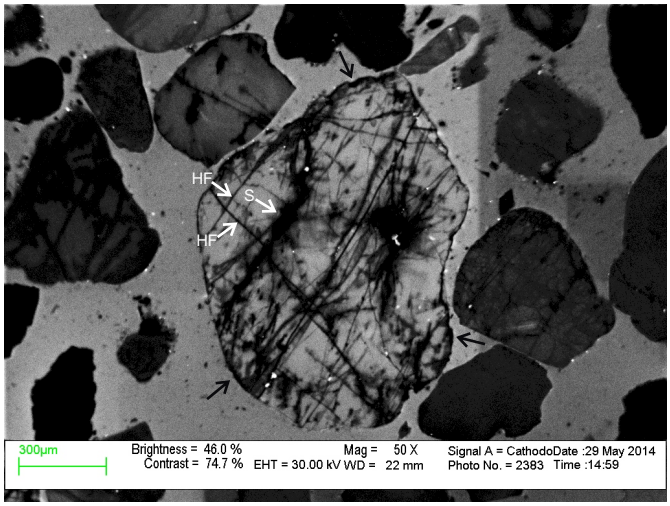

E EDS analyses

Pos#	Min. ID	SiO2	TiO2	Al2O3	FeO	MgO	Na2O	K2O	Total	Actual total
1	Ms	47.54	0.54	32.33	3.33	0.48	0.59	10.19	95	49
2	Qz	99.99							100	48

Figure 7A-22: Microphotos under ppl (A) and xpl (B), SEM-BSE image (C), SEM-CL image (D), and EDS analyses table (E) of quartz grain 22 in sample 3900. The grain is anhedral and rounded monocrystalline with weak undulose extinction. Detrital fluid inclusions are common; they form trails (FI trail) along healed fractures (Fig. A). The grain contains a muscovite inclusion and is strongly microfractured with two sets of parallel healed fractures crosscutting each other perpendicularly (Fig. D). Healed fractures (HF) and spiders (S) are common (Fig. D). The dark areas indicated by arrows in Fig. D are overgrowth.

A PPL

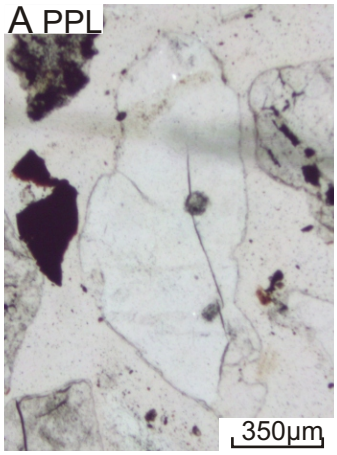

B XPL

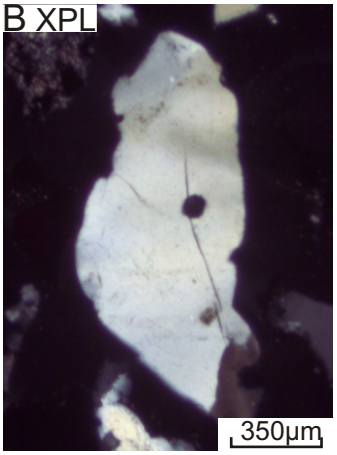

C BSE

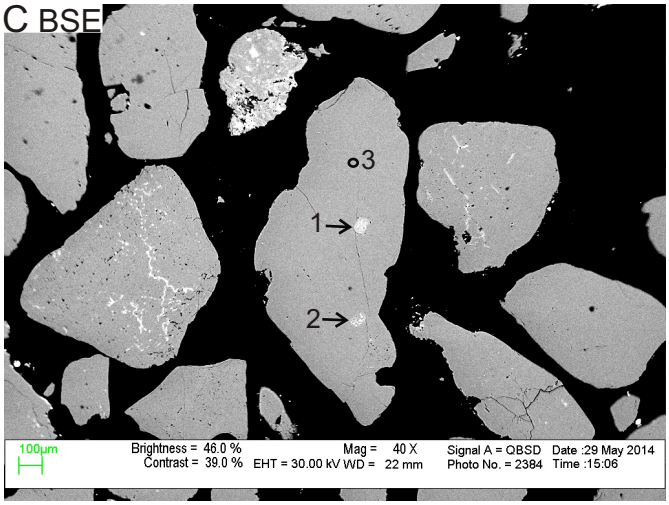

D SEM-CL

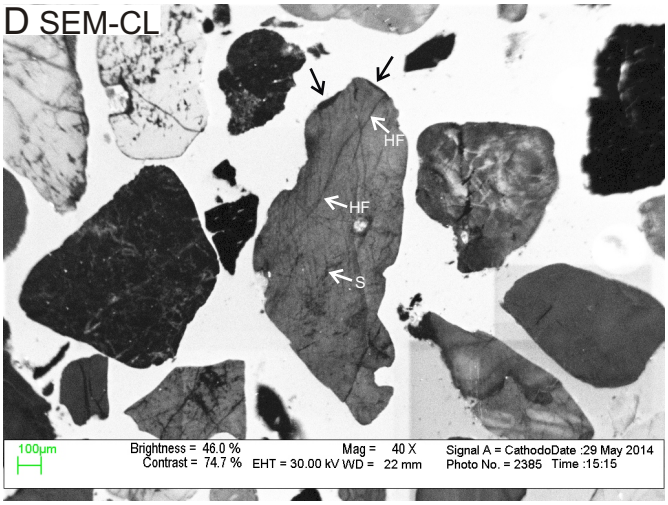

E EDS analyses

Pos#	Min. ID	SiO2	Al2O3	FeO	CaO	Na2O	Total	Actual total
1	Pl	63.62	21.33		4.27	10.77	100	53
2	Pl	66.17	20.31	0.23	2.49	10.8	100	51
3	Quartz	99.99					100	49

Figure 7A-23: Microphotos under ppl (A) and xpl (B), SEM-BSE image (C), SEM-CL image (D), and EDS analyses table (E) of quartz grain 23 in sample 3900. The grain is anhedral and sub-angular monocrystalline with mosaic texture and weak undulose extinction. Fluid inclusions are rare. The grain contains plagioclase inclusions and is microfractured with a set of parallel fractures and a set of irregular fractures (Fig. C and D). Healed fractures (HF) and spiders are common (Fig. D). The dark areas indicated by arrows in Fig. D are overgrowth.

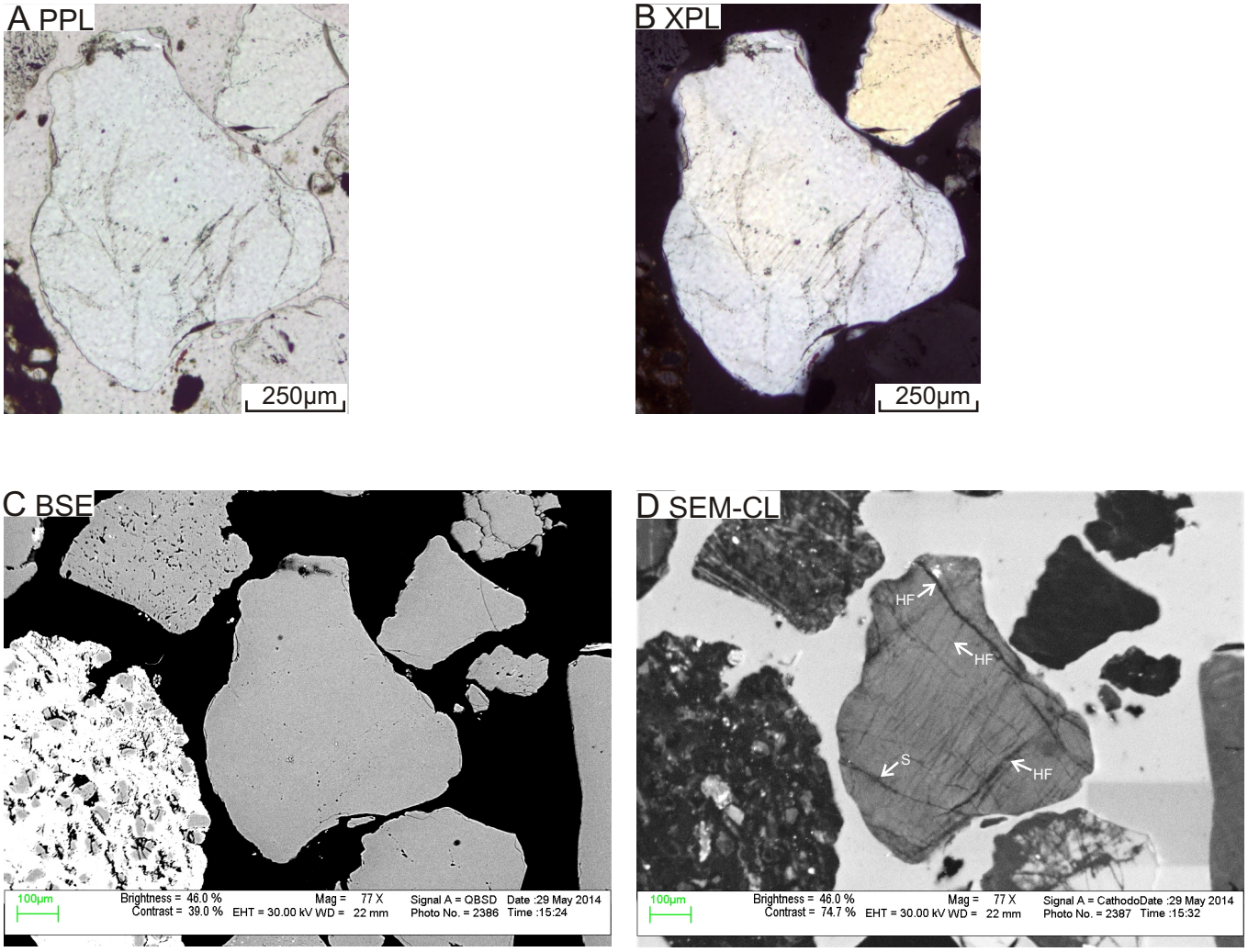

Figure 7A-24: Microphotos under ppl (A) and xpl (B), SEM-BSE image C, and SEM-CL image (D) of quartz grain 24 in sample 3900. The grain is anhedral and sub-rounded monocrystalline with mosaic texture and weak undulose extinction. Detrital fluid inclusions are common; they form trails (FI trail) along healed fractures (Fig. A). The grain is strongly microfractured with two sets of parallel healed fractures crosscutting each other perpendicularly (Fig. D). Healed fractures (HF) and spiders (S) are common (Fig. D).

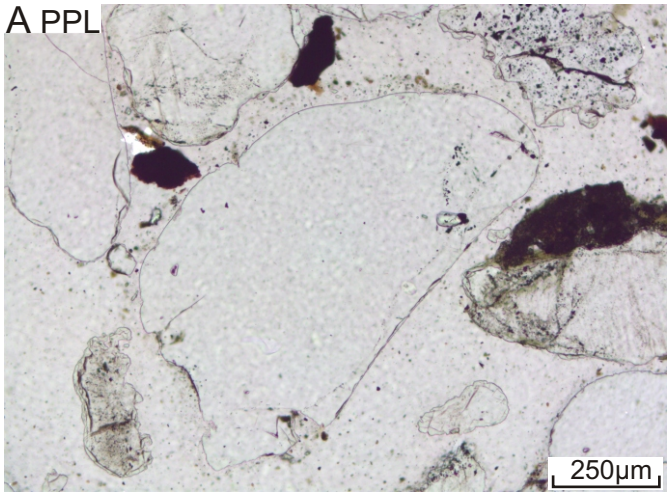

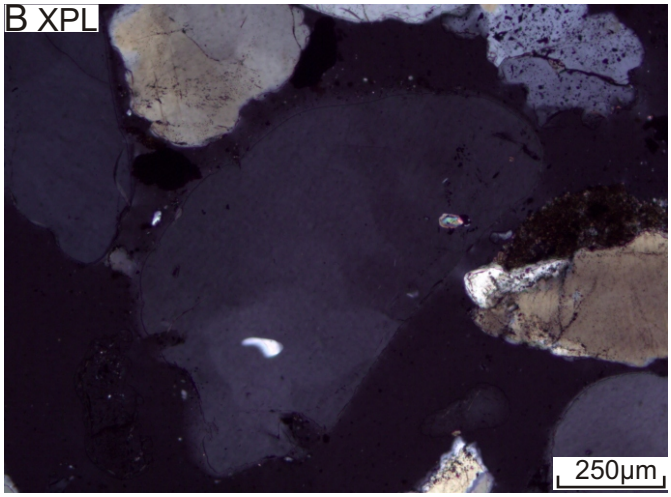

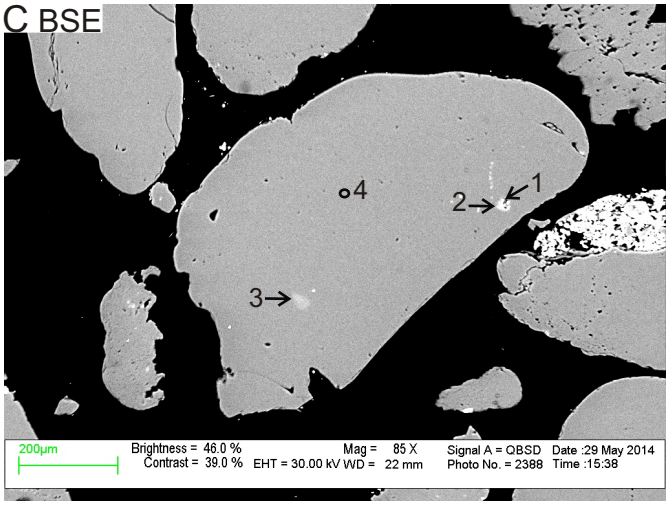

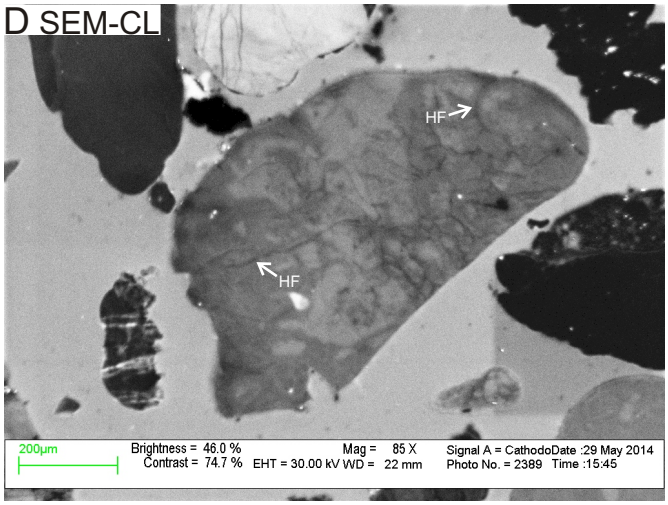

E EDS analyses

Pos#	Min. ID	SiO2	TiO2	Al2O3	FeO	MgO	CaO	Na2O	K2O	SO3	Total	Actual total
1	Ms+Py	37.29	1.95	26.45	8.72	0.93		0.43	5.94	18.3	100	52
2	Ms	49.33	0.69	30.29	2.76	1.22	0.00	0.59	10.12	0.00	95	51
3	Ab	67.09		20.26			1.11	11.57			100	50
4	Qz	99.99									100	56

Figure 7A-25: Microphotos under ppl (A) and xpl (B), SEM-BSE image (C), SEM-CL image (D), and EDS analyses table (E) of quartz grain 25 in sample 3900. The grain is anhedral and sub-rounded monocrystalline with mosaic texture and non-undulose extinction. Fluid inclusions are rare. The grain contain muscovite, pyrite and albite inclusions and is microfractured with a set of irregular fractures (Fig. D). Healed fractures (HF) are common (Fig. D). The grain shows random bright-CL patches in SEM-CL.

A PPL

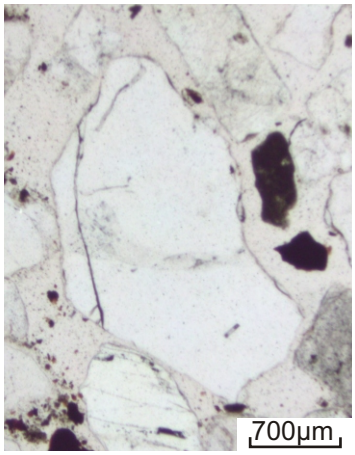

B XPL

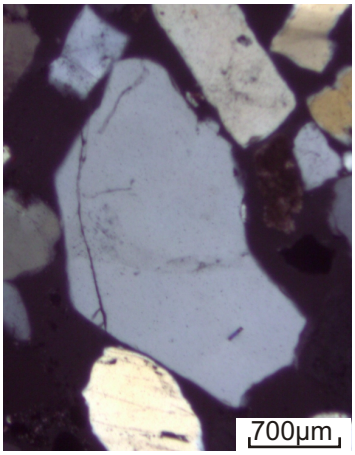

C BSE

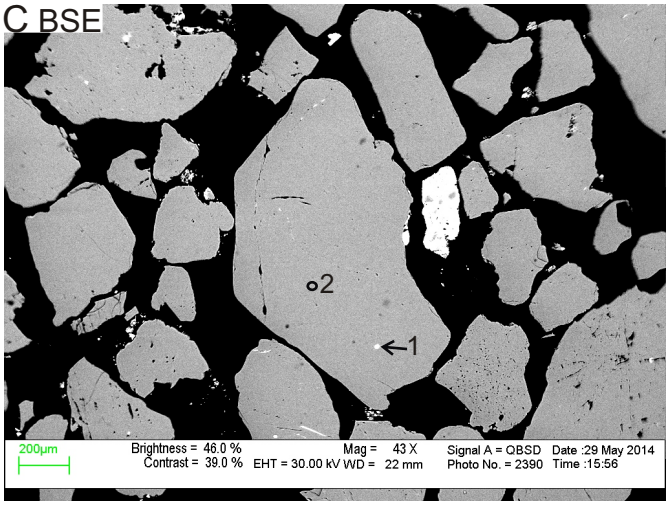

D SEM-CL

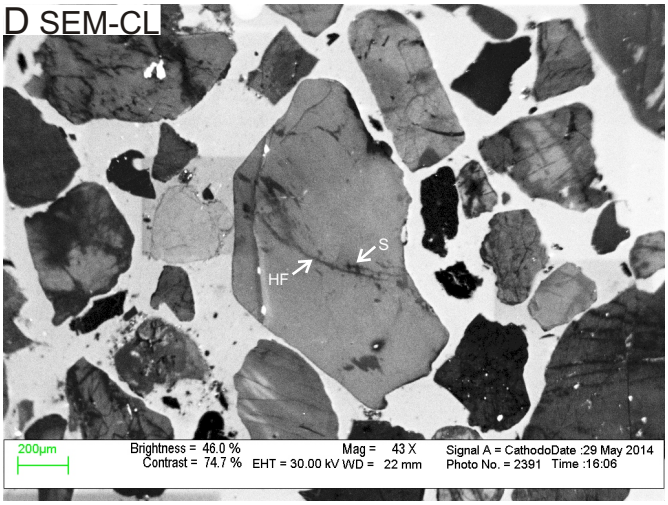

E EDS analyses

Pos#	Min. ID	SiO2	ZrO2	HfO2	Total	Actual total
1	Zrn	31.62	67.19	1.2	100	54
2	Qz	99.99			100	59

Figure 7A-26: Microphotos under ppl (A) and xpl (B), SEM-BSE image (C), SEM-CL image (D), and EDS analyses table (E) of quartz grain 26 in sample 3900. The grain is anhedral and sub-angular monocrystalline with moderate undulose extinction. Fluid inclusions are rare. The grain contain zircon inclusions and is microfractured with a set of irregular fractures (Fig. D). Healed fractures (HF) and spiders (S) are present (Fig. D).

A PPL

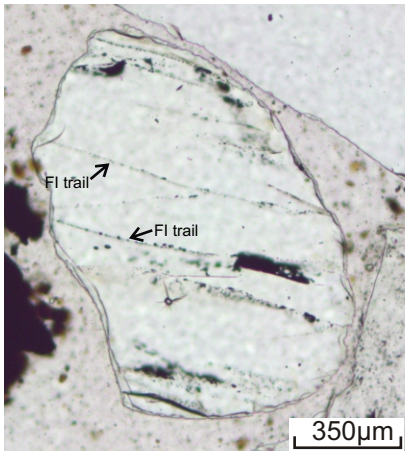

B XPL

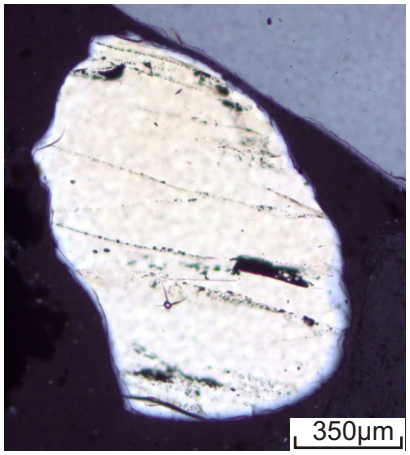

C BSE

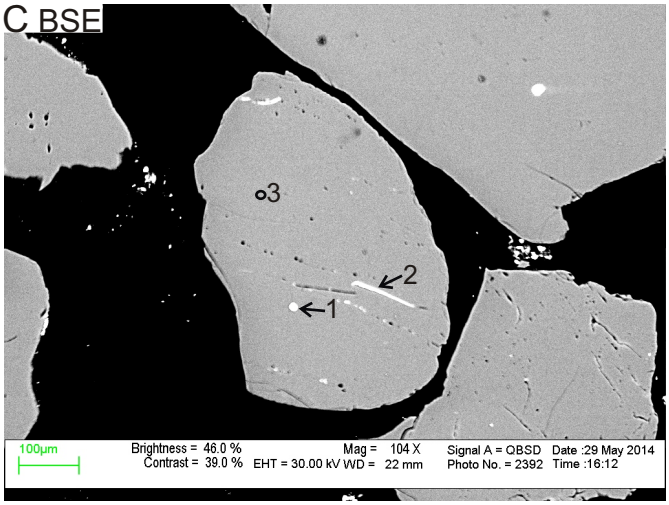

D SEM-CL

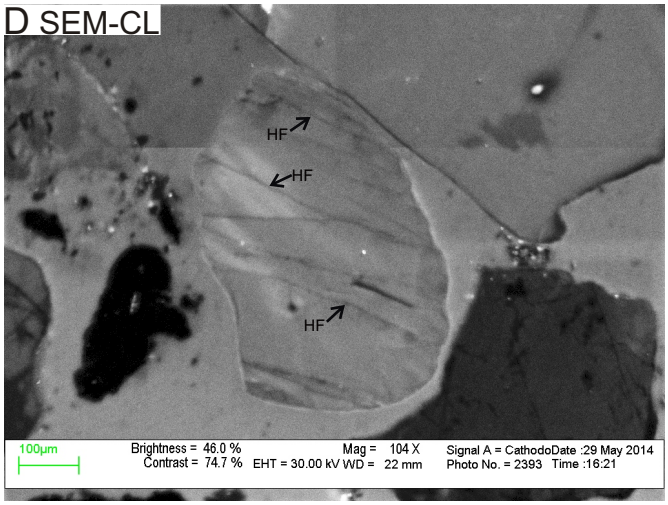

E EDS analyses

Pos#	Min. ID	SiO2	FeO	SO3	ZrO2	HfO2	Total	Actual total
1	Zrn	32.86			64.38	2.77	100	53
2	Py+Qz	41.95	14.07	43.97			100	82
3	Qz	99.99					100	55

Figure 7A-27: Microphotos under ppl (A) and xpl (B), SEM-BSE image (C), SEM-CL image (D), and EDS analyses table (E) of quartz grain 27 in sample 3900. The grain is anhedral and sub-rounded monocrystalline with weak undulose extinction. Detrital fluid inclusions are common; they are usually associated with secondary porosity and form trails (FI trail) along healed fractures (Fig. A). The grain contains zircon and pyrite inclusions and is microfractured with a set of sub-parallel healed fractures (Fig. D). Healed fractures (HF) are common (Fig. D). The grain shows bright streaky patches fabric in SEM -CL image.

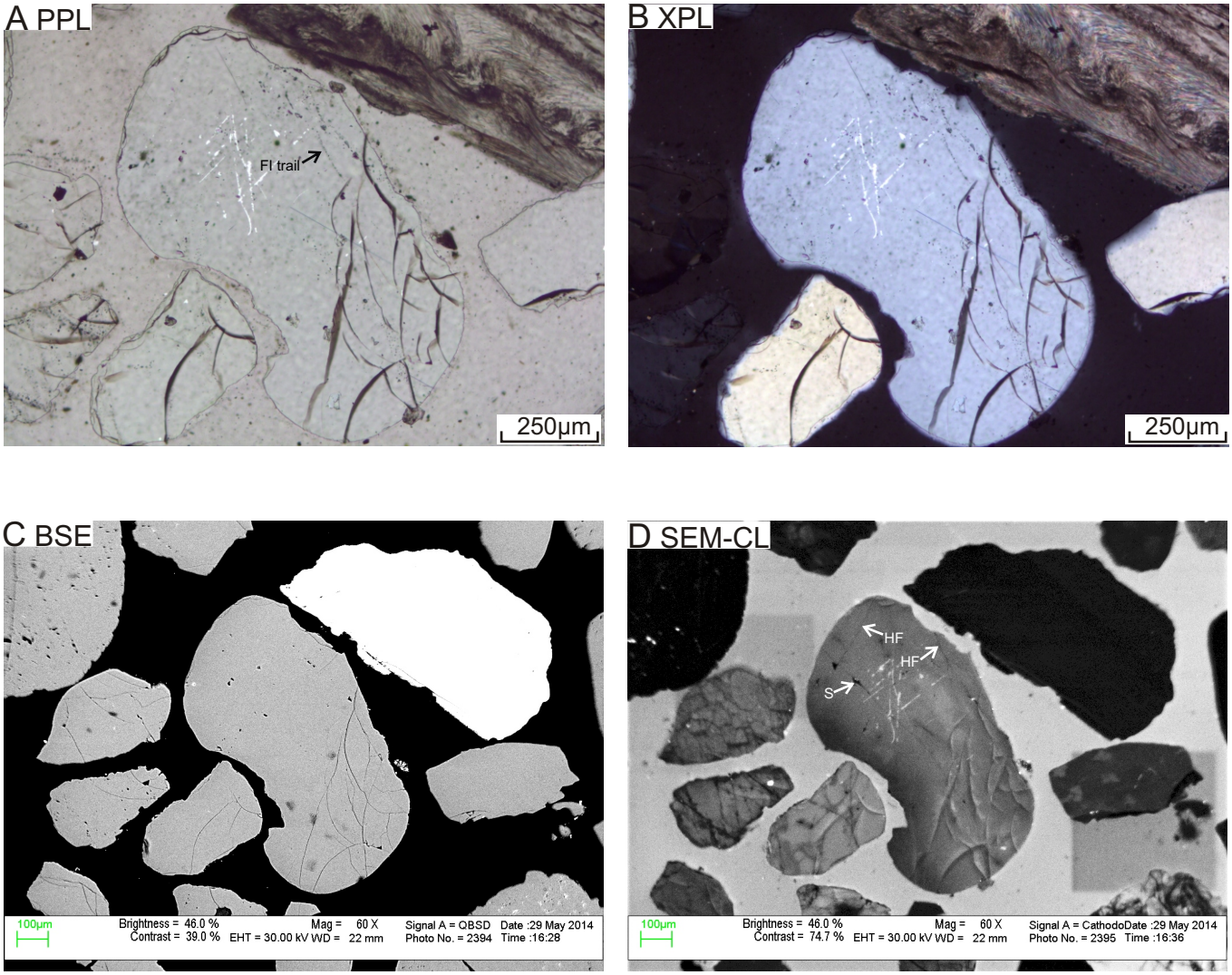

Figure 7A-28: Microphotos under ppl (A) and xpl (B), SEM-BSE image C, and SEM-CL image (D) of quartz grain 28 in sample 3900. The grain is anhedral and rounded monocrystalline with embayed margins and weak undulose extinction. Detrital fluid inclusion trails (FI trail) are present. (Fig. A). The grain is microfractured with a set of irregular fractures (Fig. C and D). Some healed fractures (HF) and spiders (S) are present (Fig. D).

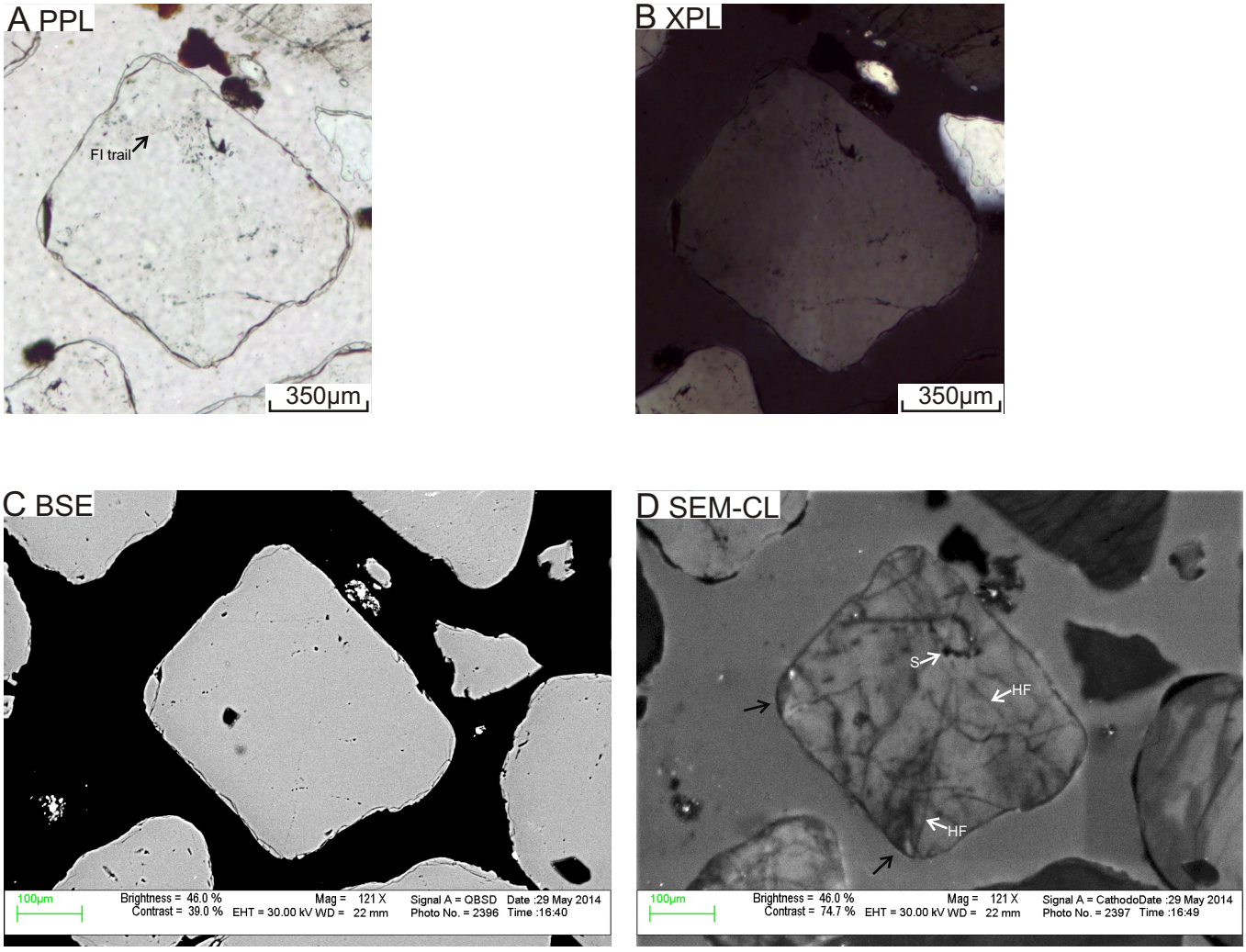

Figure 7A-29: Microphotos under ppl (A) and xpl (B), SEM-BSE image C, and SEM-CL image (D) of quartz grain 29 in sample 3900. The grain is anhedral and sub-rounded monocrystalline with strong undulose extinction. Detrital fluid inclusion trails are present (Fig. A). The grain is microfractured with a set of irregular healed fractures (Fig. D). Healed fractures (HF) and spiders (S) are common (Fig. D). The dark areas indicated by arrows in Fig. D are overgrowth. The grain shows subtle mottling in SEM-CL image.

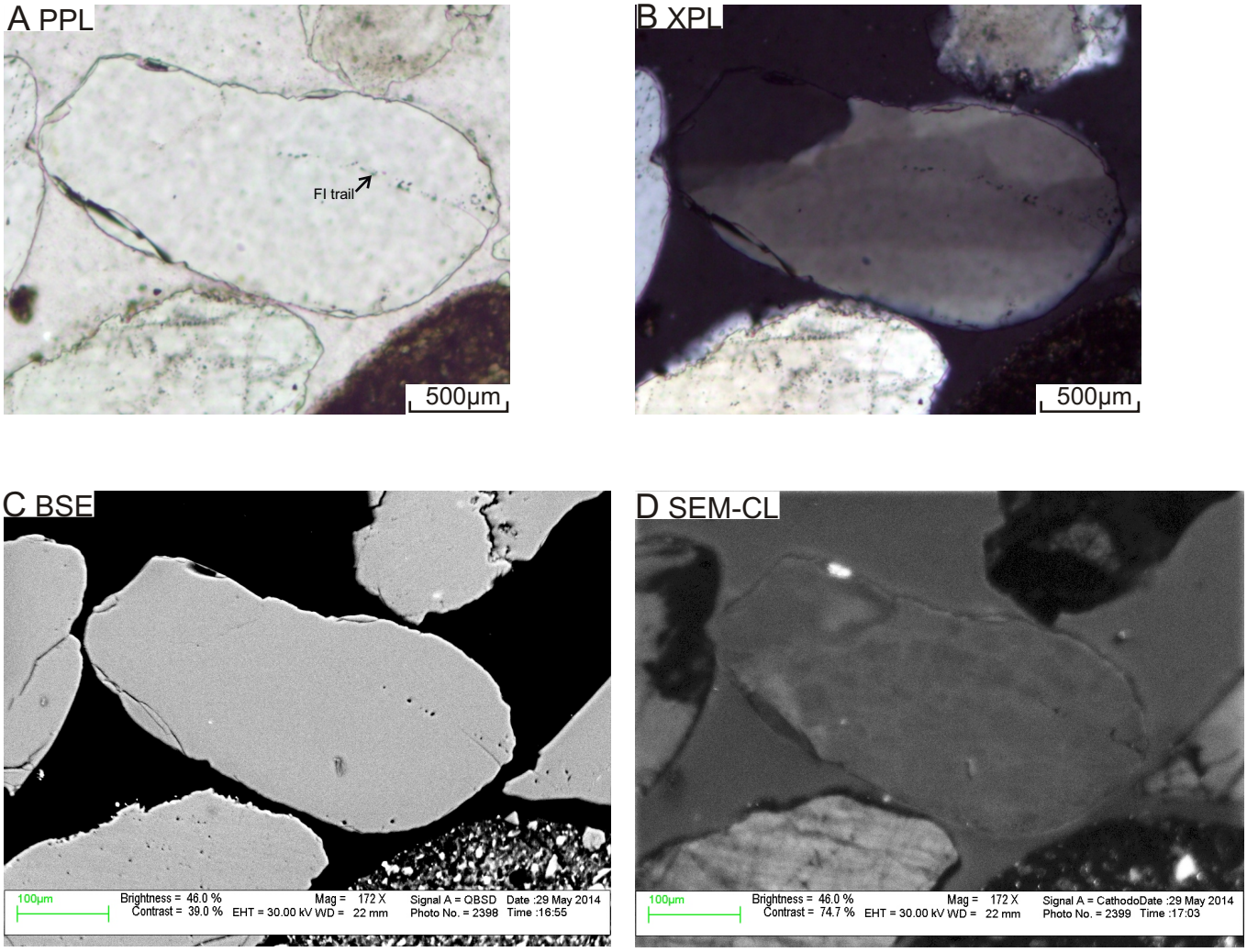

Figure 7A-30: Microphotos under ppl (A) and xpl (B), SEM-BSE image C, and SEM-CL image (D) of quartz grain 30 in sample 3900. The grain is anhedral and rounded monocrystalline with mosaic texture and weak undulose extinction. Fluid inclusions are present (Fig. A). The grain is weakly microfractured (Fig. D). Healed fractures are rare. The grain shows subtle bright mottling in SEM-CL image.

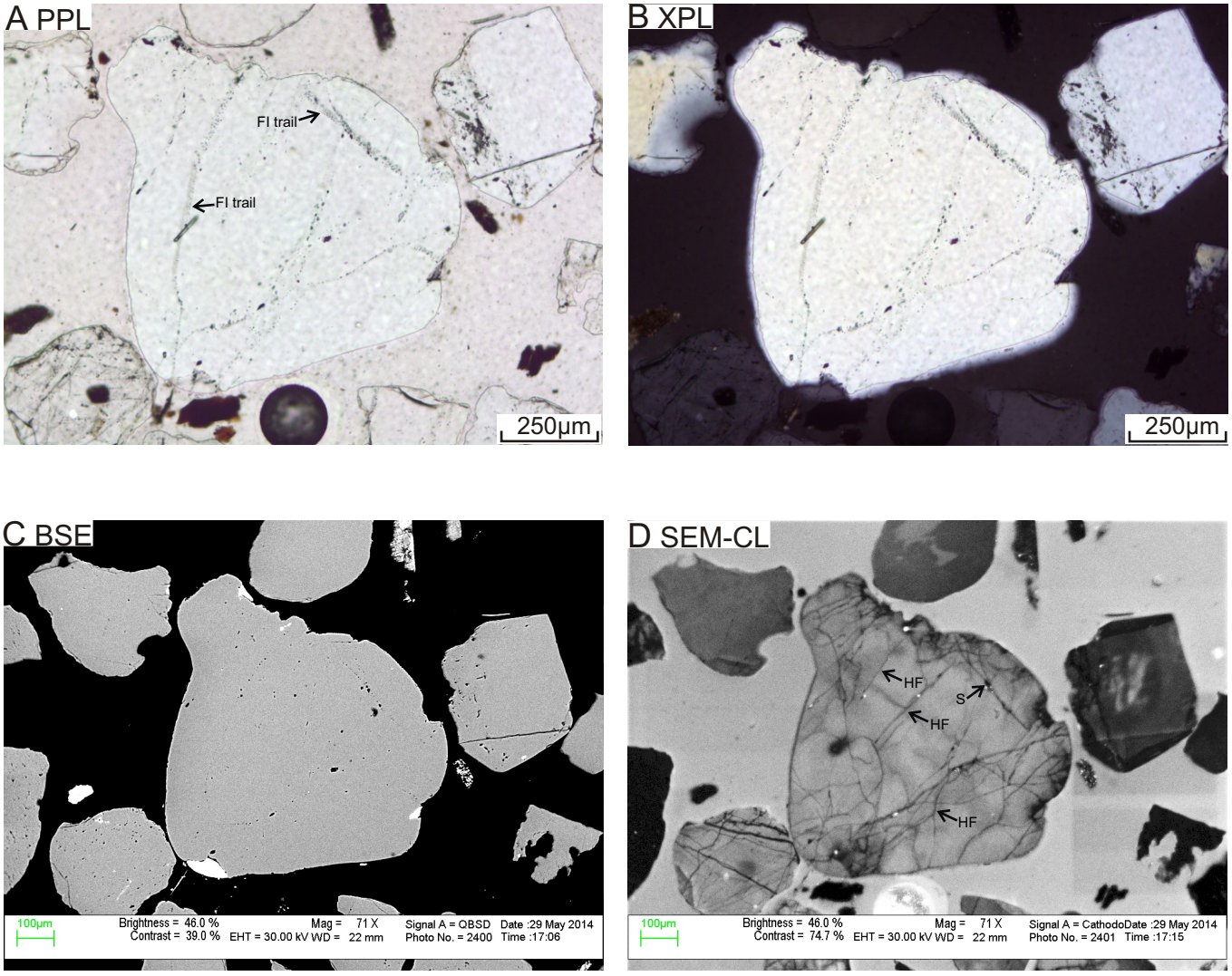

Figure 7A-31: Microphotos under ppl (A) and xpl (B), SEM-BSE image C, and SEM-CL image (D) of quartz grain 31 in sample 3900. The grain is anhedral and sub-rounded monocrystalline with non-undulose extinction. Detrital fluid inclusions are common, they form trails (FI trail) along healed fractures (Fig. A). The grain is strongly microfractured with a set of irregular fractures. Healed fractures (HF) and spiders (S) are common.

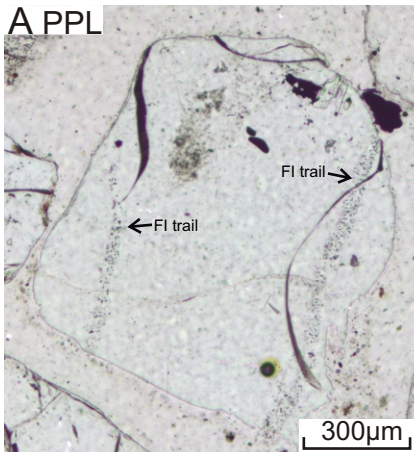

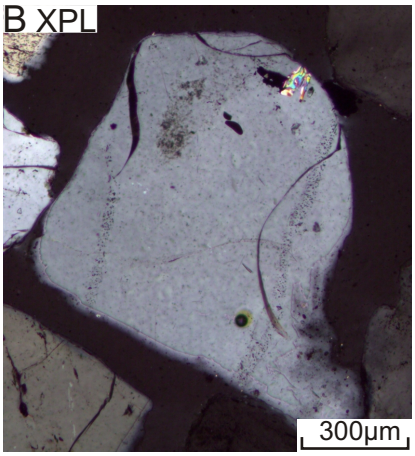

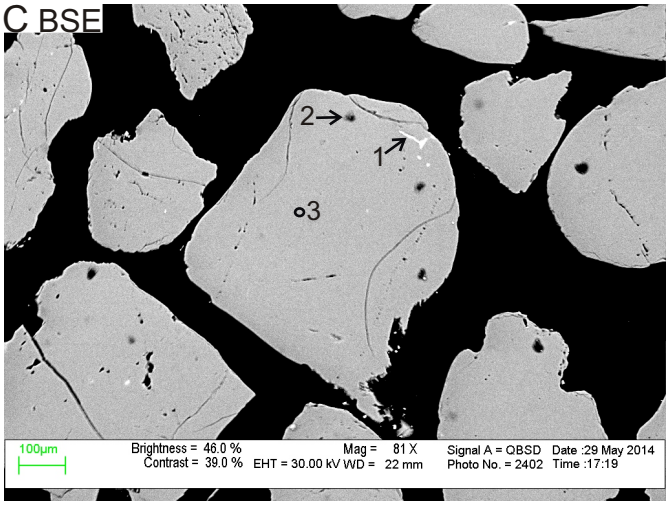

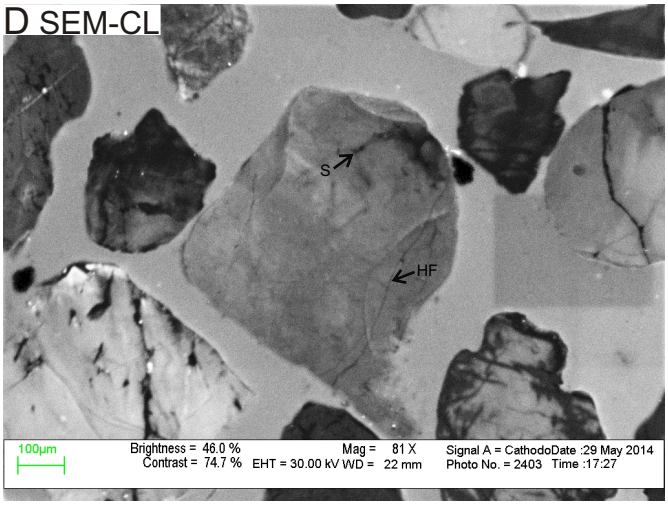

E EDS analyses

Pos#	Min. ID	SiO2	FeO	CaO	Na2O	K2O	SO3	F	Cl	Total	Actual total
1	Qz+Fluid Inclusion	61.37	9.35		1.01		28.27			100	70
2	Qz+Fluid inclusion	87.13		0.42	5.22	0.39	2.82	3.28	0.74	100	52
3	Qz	99.99								100	61

Figure 7A-32: Microphotos under ppl (A) and xpl (B), SEM-BSE image (C), SEM-CL image (D), and EDS analyses table (E) of quartz grain 32 in sample 3900. The grain is anhedral and sub-rounded monocrystalline with non-undulose extinction. Detrital fluid inclusions are common. They form trails (FI trail) along healed fractures (Fig. A). The grain is microfractured with a set of irregular fractures. Healed fractures (HF) and spiders are present.

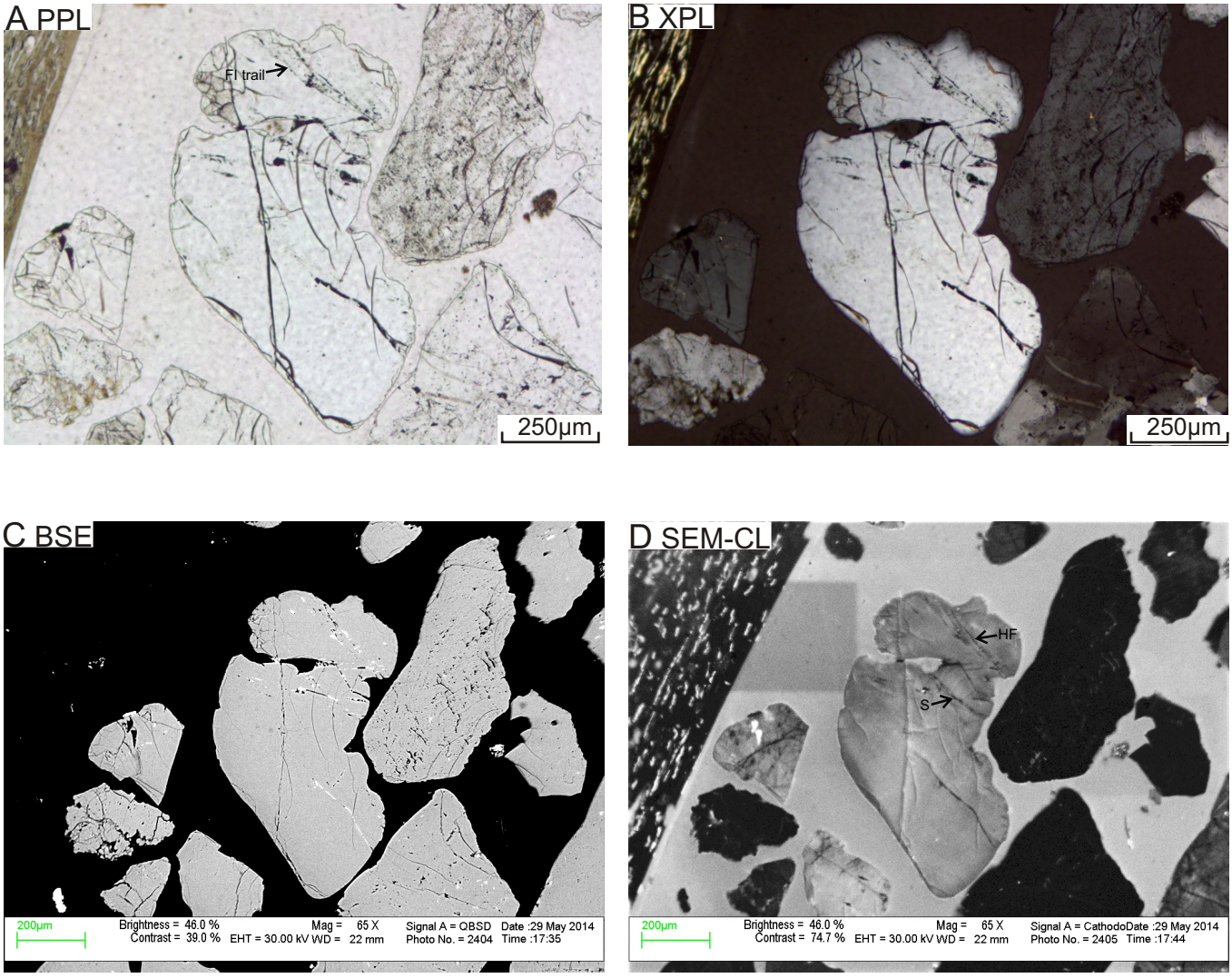

Figure 7A-33: Microphotos under ppl (A) and xpl (B), SEM-BSE image C, and SEM-CL image (D) of quartz grain 33 in sample 3900. The grain is anhedral and sub-rounded monocrystalline with embayed margins and non-undulose extinction. Detrital fluid inclusion trails are present (Fig. A). The grain is microfractured with a set of irregular fractures. Healed fractures (HF) and spiders are present.

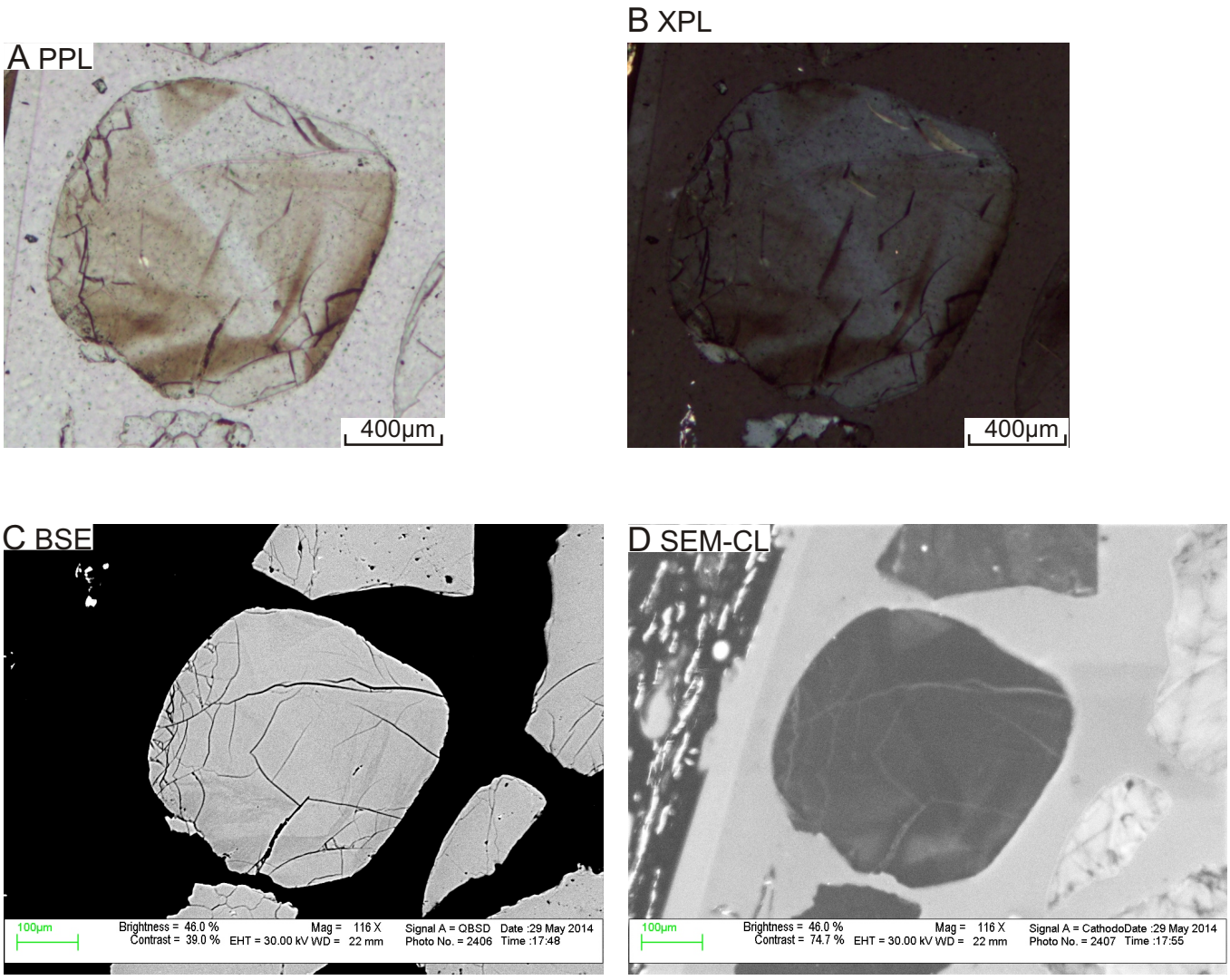

Figure 7A-34: Microphotos under ppl (A) and xpl (B), SEM-BSE image C, and SEM-CL image (D) of quartz grain 34 in sample 3900. The grain is anhedral and well-rounded monocrystalline with weak undulose extinction. Fluid inclusions are rare. The grain is microfractured with a set of irregular open fractures. Healed fractures are rare. The grain shows subtle bright mottling in SEM-CL image.

A PPL

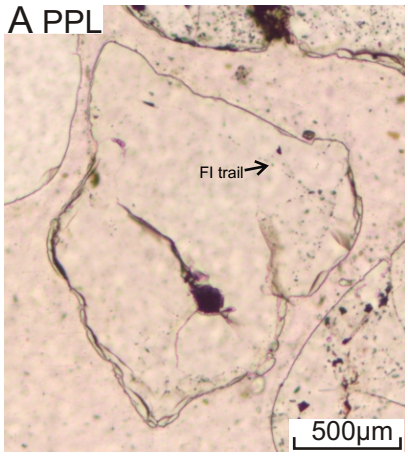

B XPL

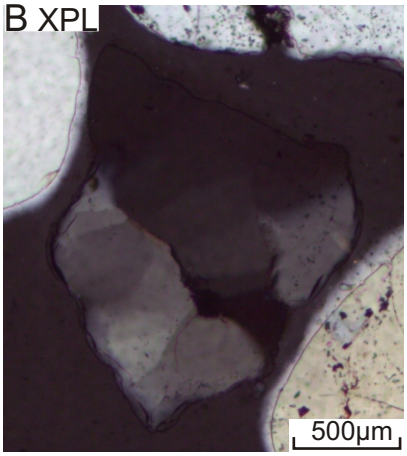

C BSE

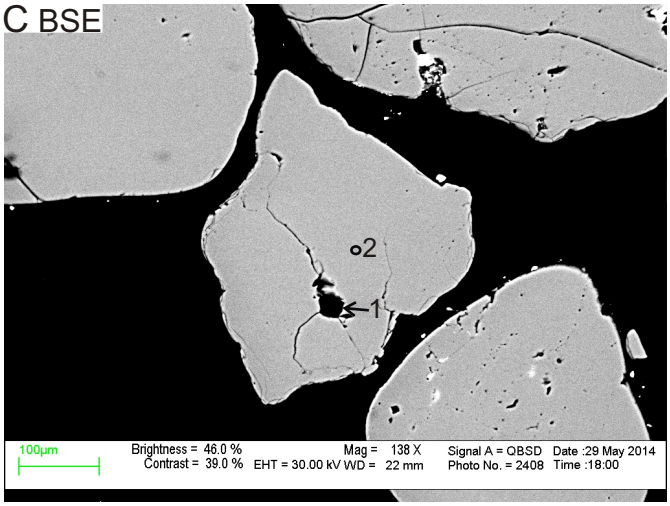

D SEM-CL

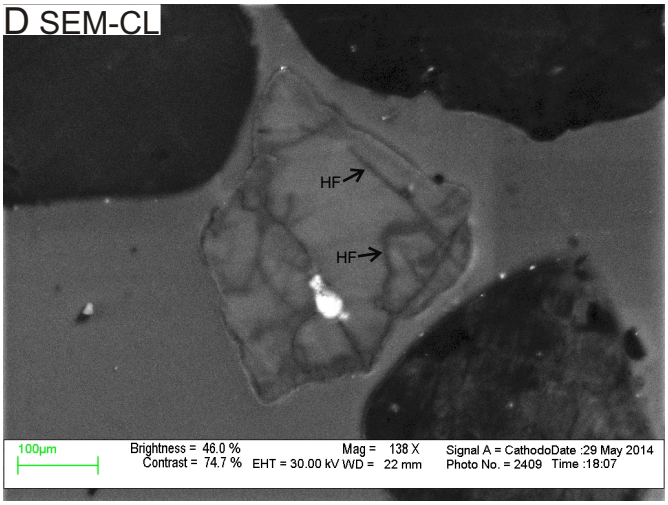

E EDS analyses

Pos#	Min. ID	SiO2	Al2O3	FeO	MgO	CaO	F	Cl	Total	Actual total
1	Hole	80.22	2.29	1.42	4.41	2.59	7.19	1.89	100	8
2	Qz	99.99							100	61

Figure 7A-35: Microphotos under ppl (A) and xpl (B), SEM-BSE image (C), SEM-CL image (D), and EDS analyses table (E) of quartz grain 35 in sample 3900. The grain is anhedral and sub-angular Polycrystalline (4 sub-grains) with mosaic texture and weak undulose extinction. Fluid inclusions are present. They form trails (FI trail) along healed fractures (Fig. A). The grain is microfractured with a set of irregular fractures. Healed fractures (HF) are common.

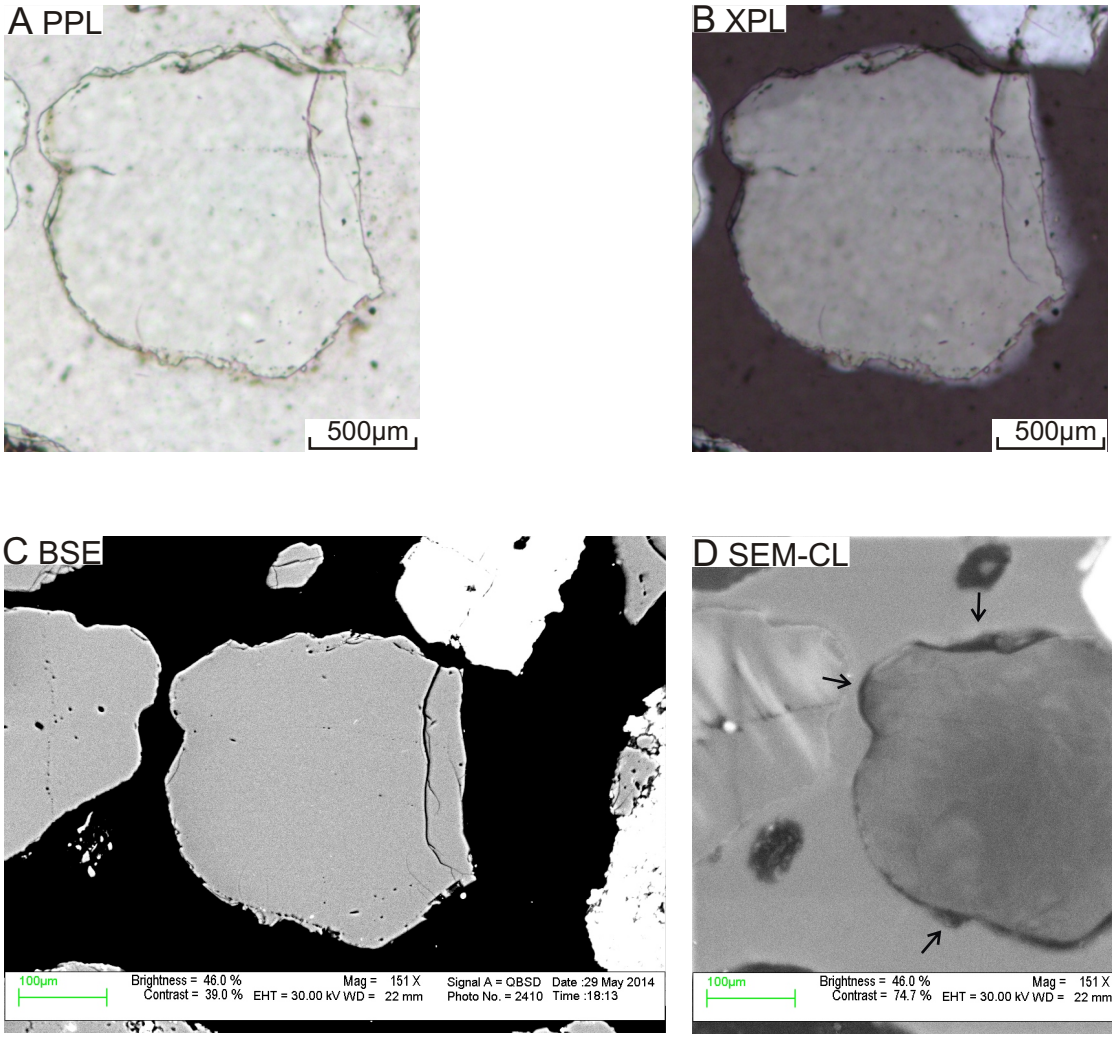

Figure 7A-36: Microphotos under ppl (A) and xpl (B), SEM-BSE image C, and SEM-CL image (D) of quartz grain 36 in sample 3900. The grain is anhedral and sub-rounded monocrystalline with weak undulose extinction. Fluid inclusions are present. They are diagenetic since they form trails at the boundary between the detrital quartz and the overgrowth. The grain is weakly microfractured. Healed fractures are rare.



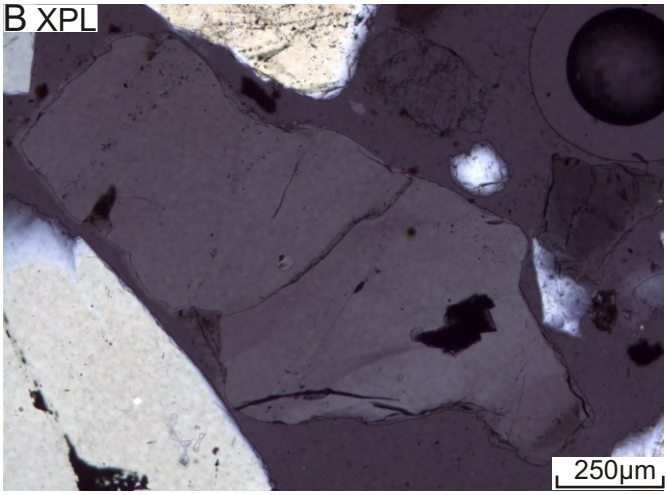

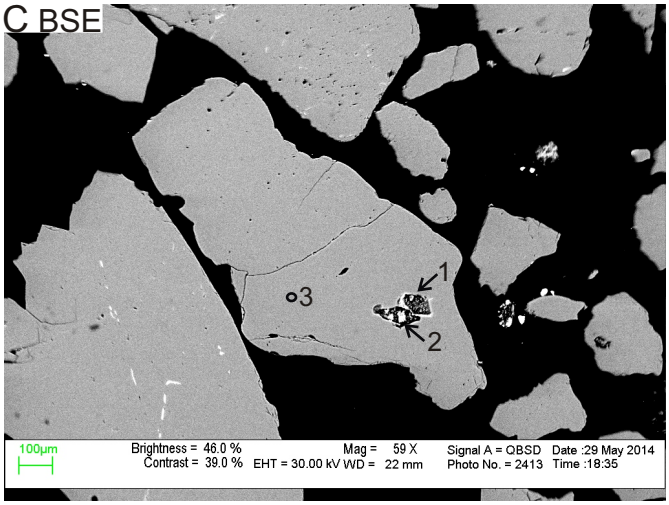

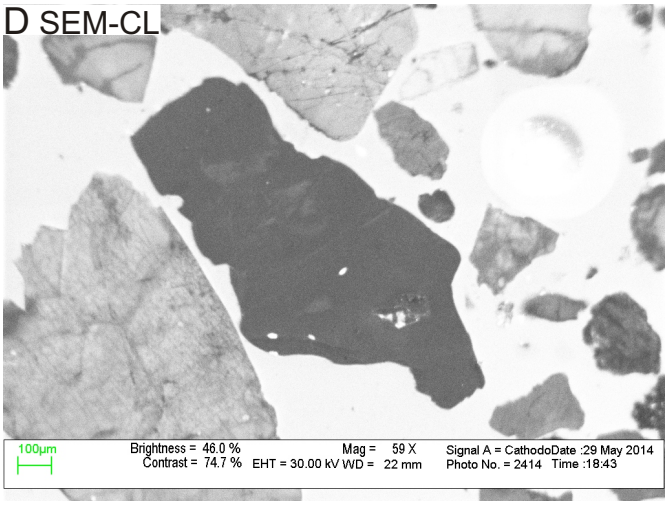

E EDS analyses

Pos#	Min. ID	SiO2	TiO2	Al2O3	FeO	CaO	Na2O	K2O	SO3	Total	Actual total
1	Py+Kln	45.67	3.45	33.07	5.56	0.18		0.28	11.79	100	42
2	Kfs	63.51	0.67	20.03	0.68		0.42	12.77	1.9	100	53
3	Qz	99.99								100	60

Figure 7A-37: Microphotos under ppl (A) and xpl (B), SEM-BSE image (C), SEM-CL image (D), and EDS analyses table (E) of quartz grain 37 in sample 3900. The grain is anhedral and sub-angular monocrystalline with embayed margins and weak undulose extinction. Detrital fluid inclusions are present (Fig. A). The grain contains pyrite + kaolinite inclusions, k-feldspar inclusions and is microfractured with a set of irregular fractures. Healed fractures probably are camouflaged by the dark-CL colour (Fig. D). The grain shows subtle mottling in SEM-CL image.

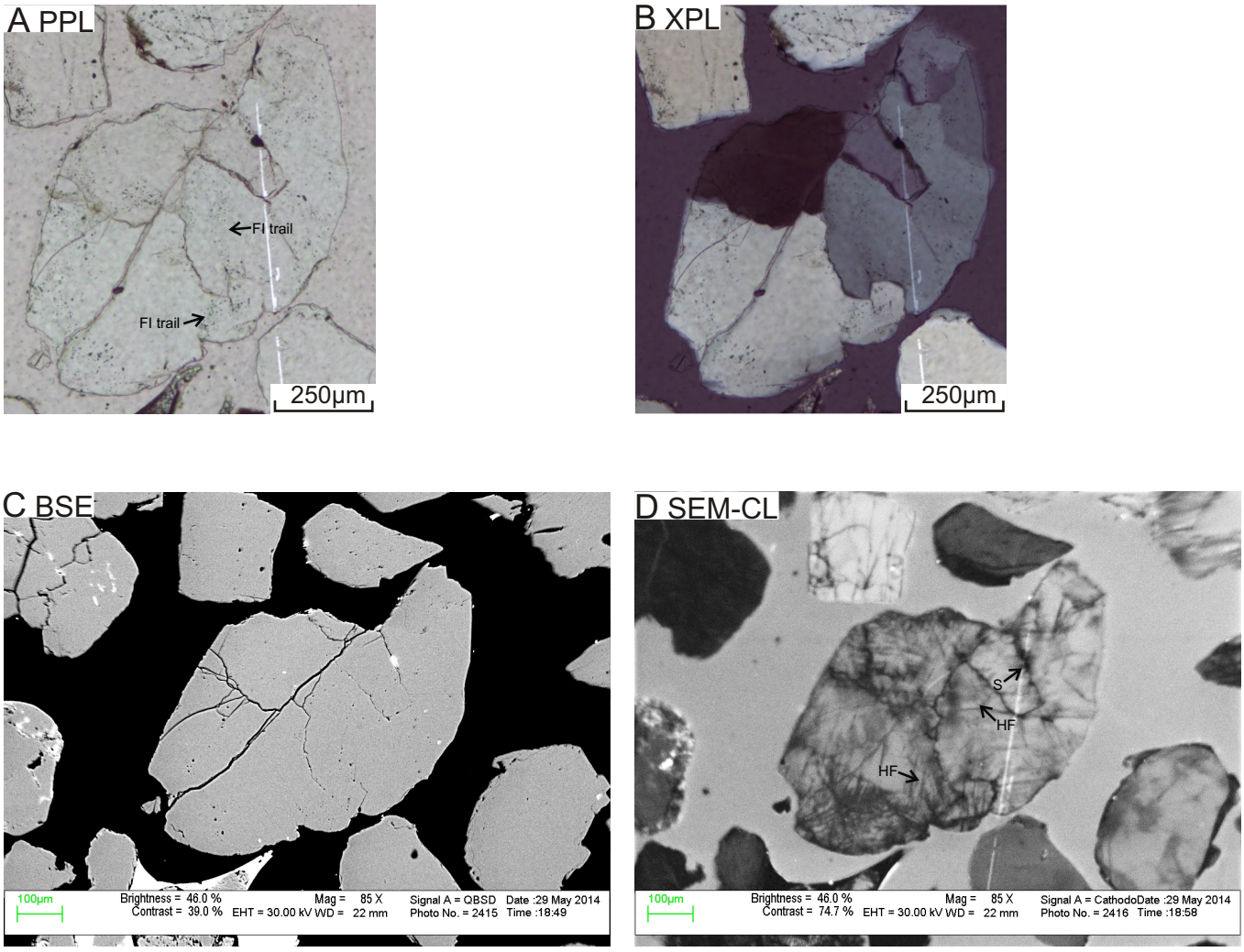

Figure 7A-38: Microphotos under ppl (A) and xpl (B), SEM-BSE image C, and SEM-CL image (D) of quartz grain 38 in sample 3900. The grain is anhedral and sub-rounded polycrystalline (5 sub-grains with sutured sub-grain boundaries) with deformation lamellae and strong undulose extinction. Detrital fluid inclusions are common. They form trails (FI trail) along healed fractures (Fig. A). The grain is strongly microfractured with two sets of parallel fractures crosscutting each other and a set of irregular fractures. Healed fractures (HF) and spiders (S) are common.

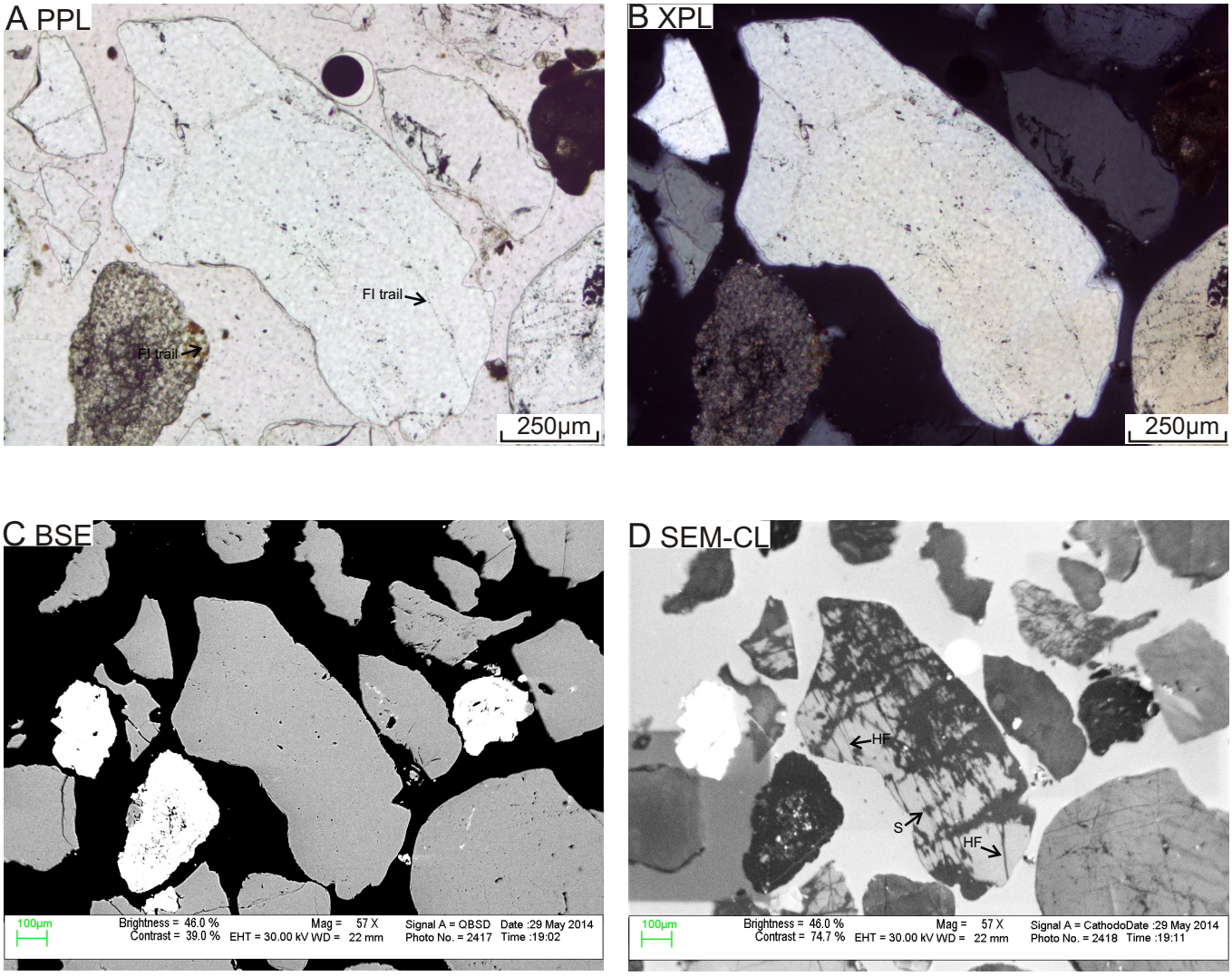

Figure 7A-39: Microphotos under ppl (A) and xpl (B), SEM-BSE image C, and SEM-CL image (D) of quartz grain 39 in sample 3900. The grain is anhedral and sub-angular monocrystalline with mosaic texture and weak undulose extinction. Detrital fluid inclusions are common, they form trails (FI trail) along healed fractures (Fig. A). The grain is strongly microfractured with a set of parallel fractures and a set of irregular fractures. Healed fractures (HF) and spiders are common.

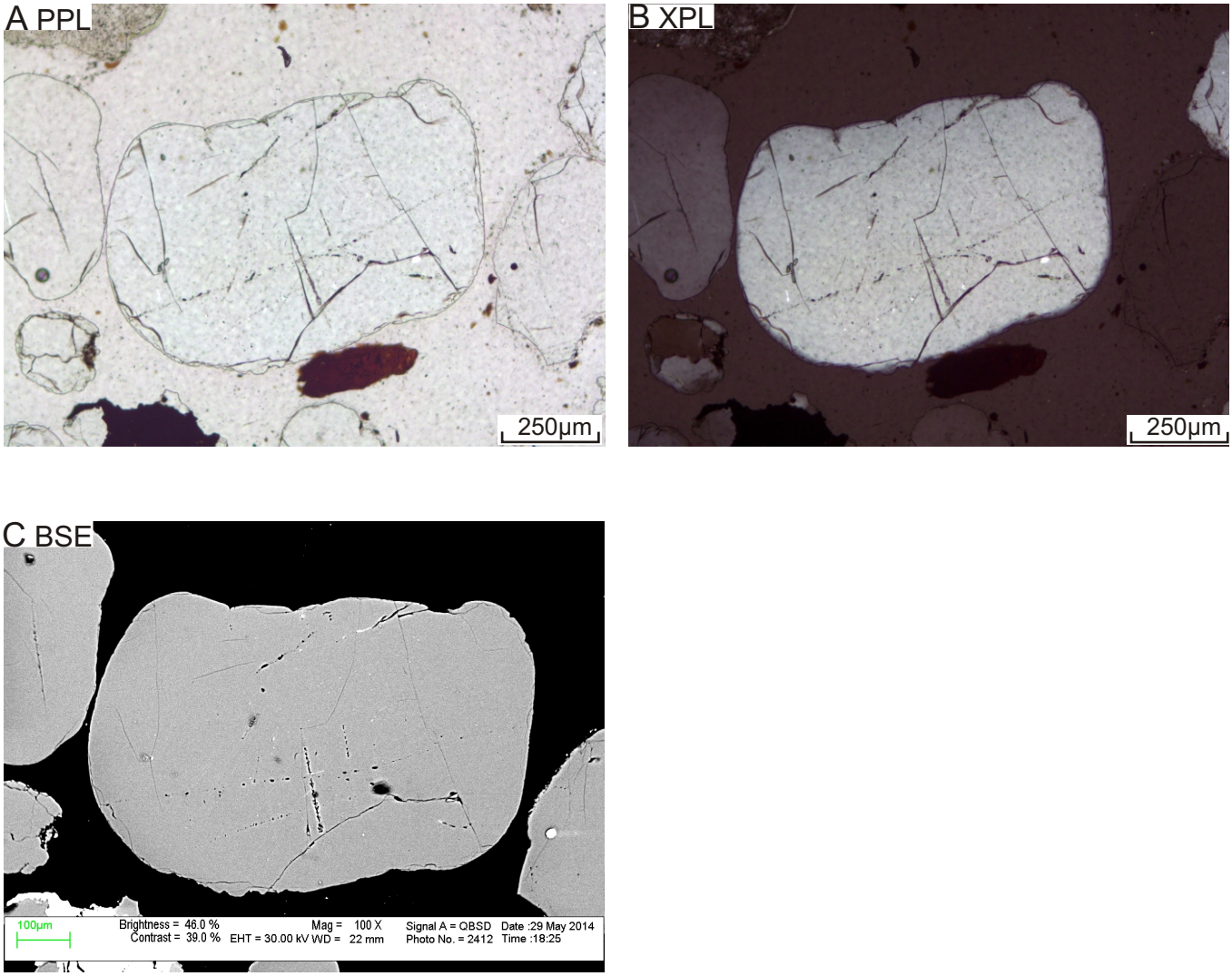

Figure 7A-40: Microphotos under ppl (A) and xpl (B), and SEM-BSE image C of quartz grain 40 in sample 3900. The grain is anhedral and rounded monocrystalline with mosaic texture and weak undulose extinction. Fluid inclusion trails are common (Fig. A).

Appendix 7B: Hot cathodoluminescence (HCL) images and blue colour shift analyses of detrital quartz grains in sample 3900.

Notes:

1. All the grains with HCL images correspond to the same grain in SEM-CL images. In all the following organized HCL figures,

   Fig. A shows HCL image taken after 3 seconds;

   Fig. B shows HCL image taken after 12 seconds;

   Fig. C is the histogram of blue colour within the analysed quartz grain in Fig. A and B, where X axis is the intensity of blue colour indicated by the colour bar with values from 0-255 (0=no blue or "black", 255=blue), and Y axis indicates the pixel amount at different blue values;

   Fig. D is the statistical table of blue values within the analysed grain area, where SD corresponds to standard deviation.

2. To classify the blue colour, the following abbreviations are used:

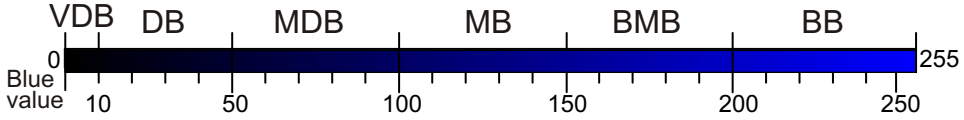

VDB: Very Dark Blue (0-10) **DB**: Dark Blue (11-50)

MDB: Medium Dark Blue (51-100) **MB**: Medium Blue (101-150)

BMB: Bright-Medium Blue (151-200) **BB**: Bright Blue (201-255)

3. To quantify the blue colour shift, the following criteria are used:

   Mean blue value change **< 5**: **No** colour shift

   5 ≤Mean blue value change **< 15**: **Slight** colour shift

   15 ≤Mean blue value change **< 30**: **Moderate** colour shift

   Mean blue value change ≥**30**: **Strong** colour shift

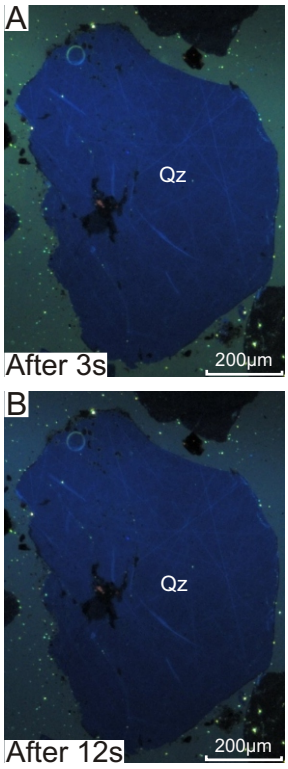

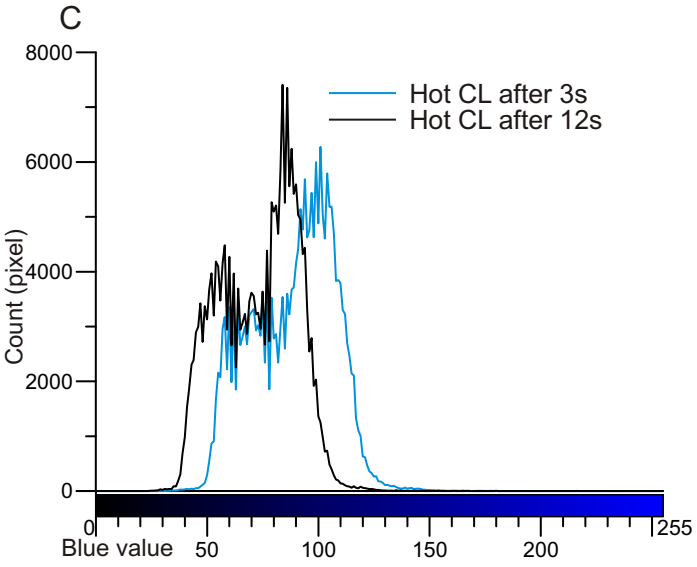

D

Blue value	Min	Max	Mode	Mean	SD
After 3s	24	216	101	89	18.5
After 12s	24	207	84	73	17.3

Figure 7B-1: Grain 1. The grain shows moderate colour shift.

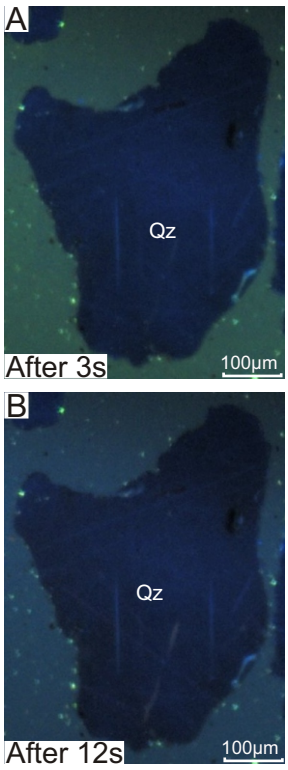

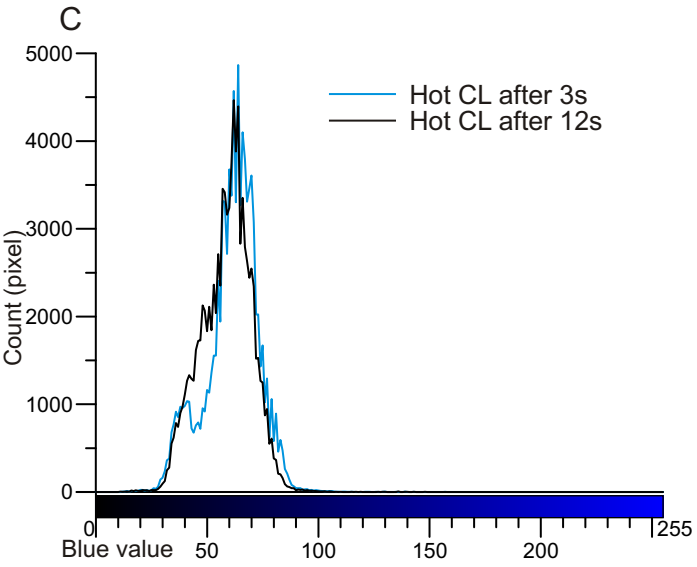

D

Blue value	Min	Max	Mode	Mean	SD
After 3s	11	80	64	61	12.1
After 12s	90	166	62	59	11.4

Figure 7B-2: Grain 2. The grain shows no colour shift.

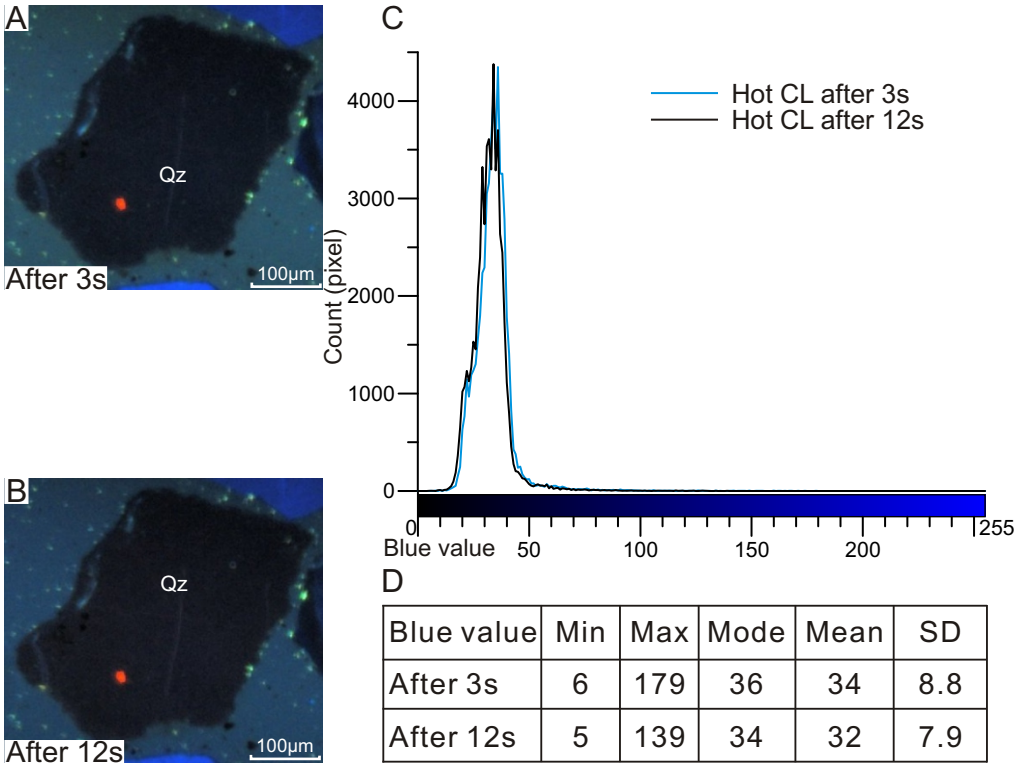

Figure 7B-3: Grain 3. The grain shows no colour shift.

D

Blue value	Min	Max	Mode	Mean	SD
After 3s	6	179	36	34	8.8
After 12s	5	139	34	32	7.9

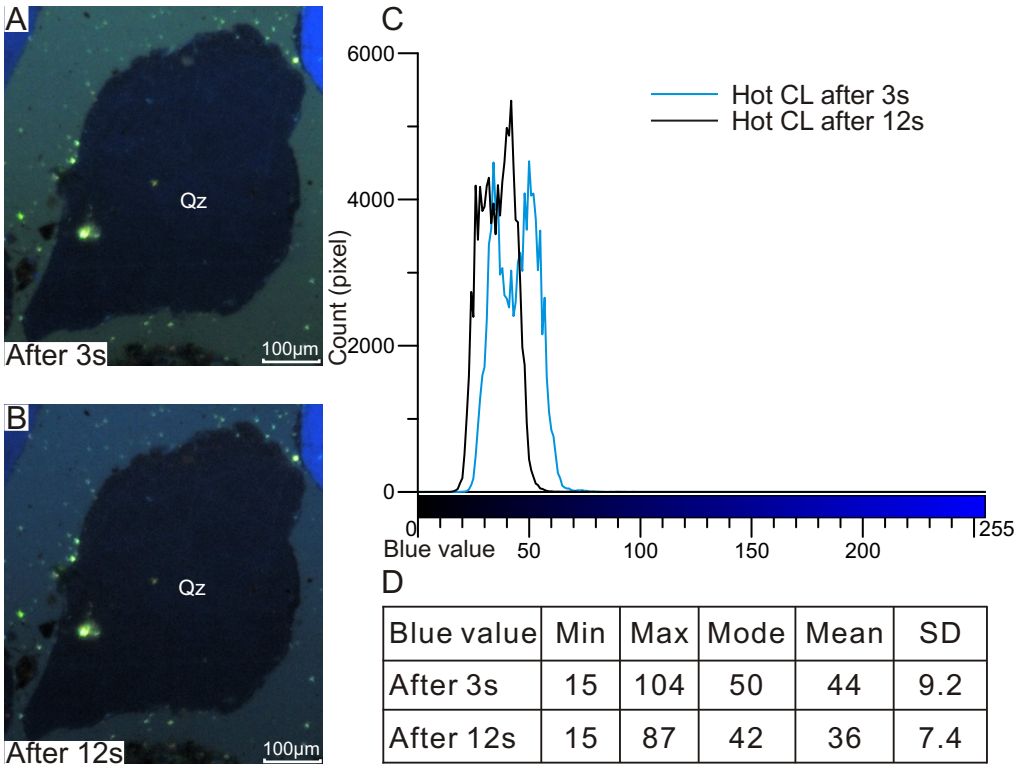

Figure 7B-4: Grain 4. The grain shows slight colour shift.

D

Blue value	Min	Max	Mode	Mean	SD
After 3s	15	104	50	44	9.2
After 12s	15	87	42	36	7.4

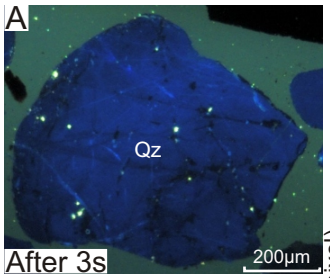

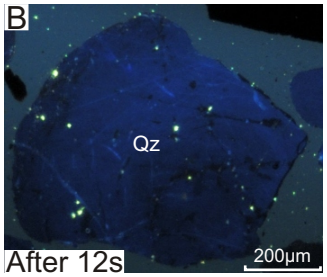

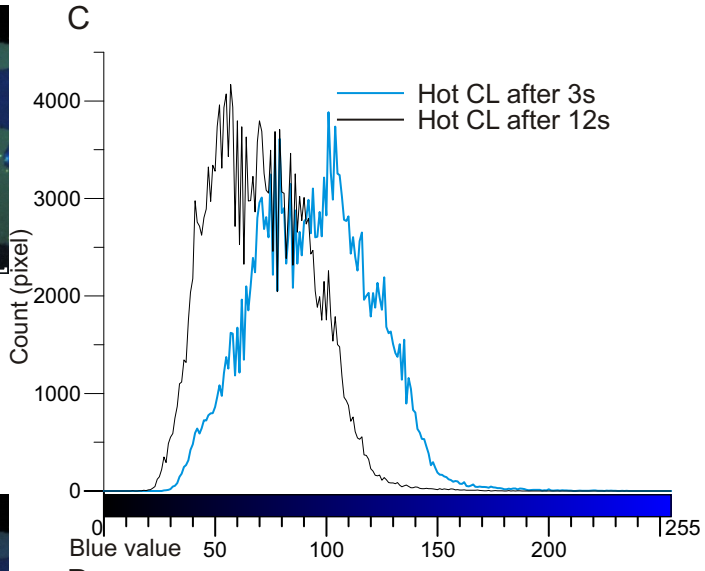

D

Blue value	Min	Max	Mode	Mean	SD
After 3s	27	235	101	94	26.1
After 12s	13	187	57	70	22

Figure 7B-5: Grain 5. The grain shows moderate colour shift.

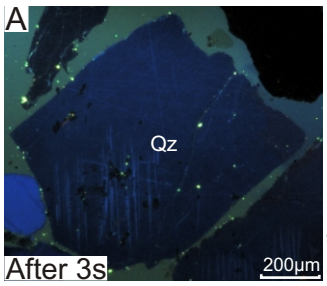

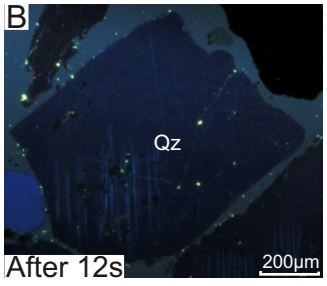

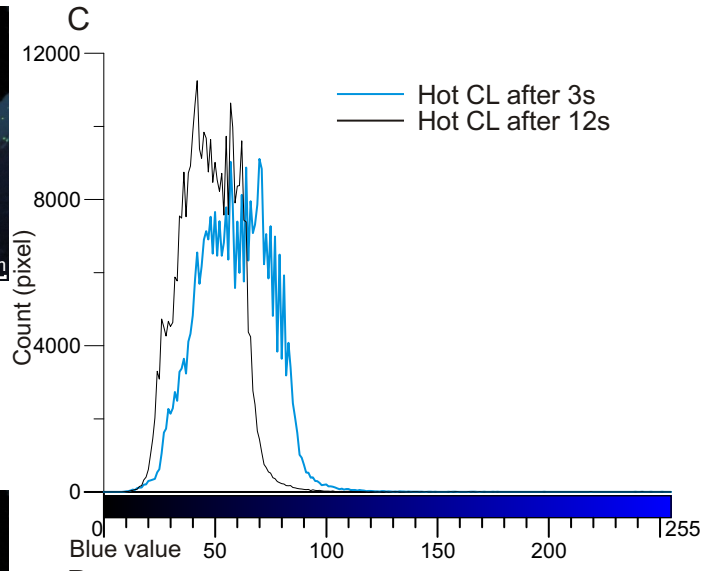

D

Blue value	Min	Max	Mode	Mean	SD
After 3s	8	255	70	60	16.2
After 12s	9	255	42	47	12.9

Figure B7-6: Grain 6. The grain shows slight colour shift.

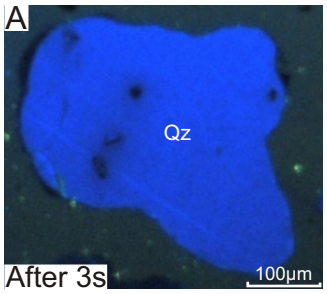

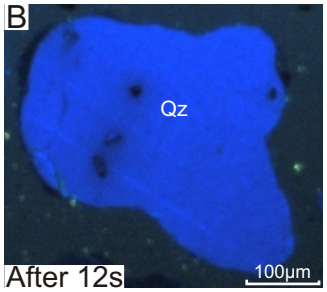

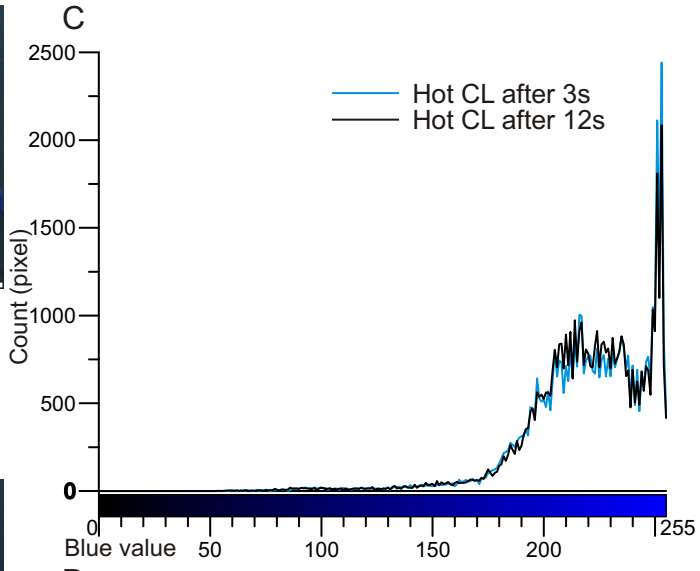

Figure 7B-7: Grain 7. The grain shows no colour shift.

D

Blue value	Min	Max	Mode	Mean	SD
After 3s	55	255	253	220	27.4
After 12s	53	255	253	220	27

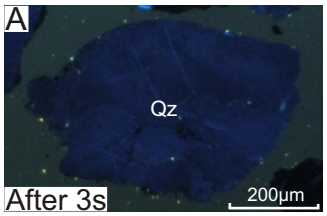

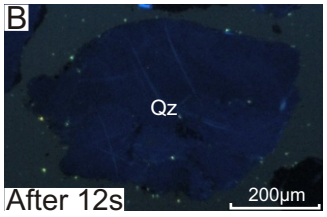

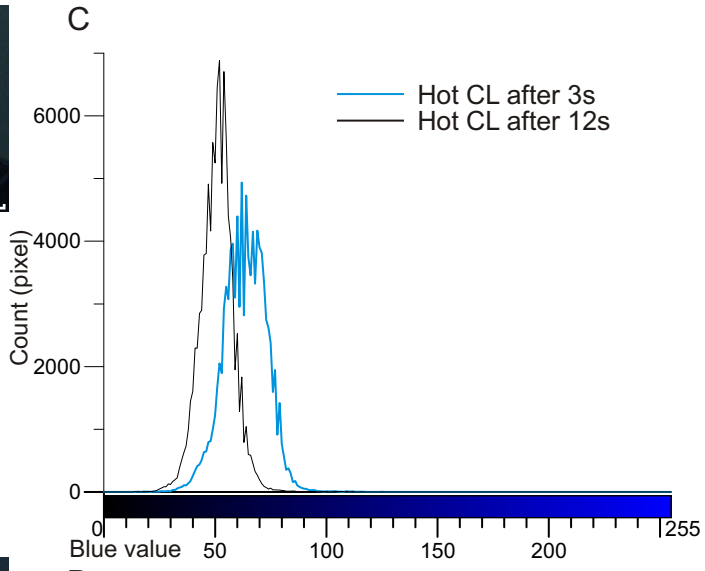

Figure 7B-8: Grain 8. The grain shows slight colour shift.

D

Blue value	Min	Max	Mode	Mean	SD
After 3s	15	133	62	63	9.5
After 12s	13	121	52	51	7.5

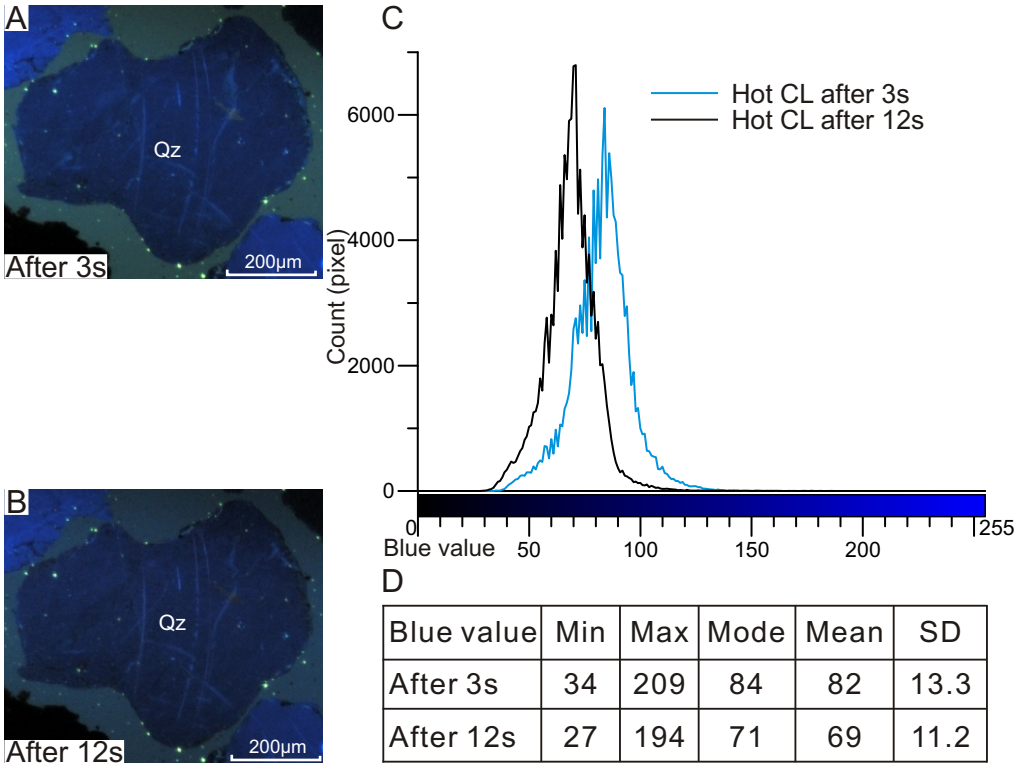

D

Blue value	Min	Max	Mode	Mean	SD
After 3s	34	209	84	82	13.3
After 12s	27	194	71	69	11.2

Figure 7B-9: Grain 9. The grain shows slight colour shift.

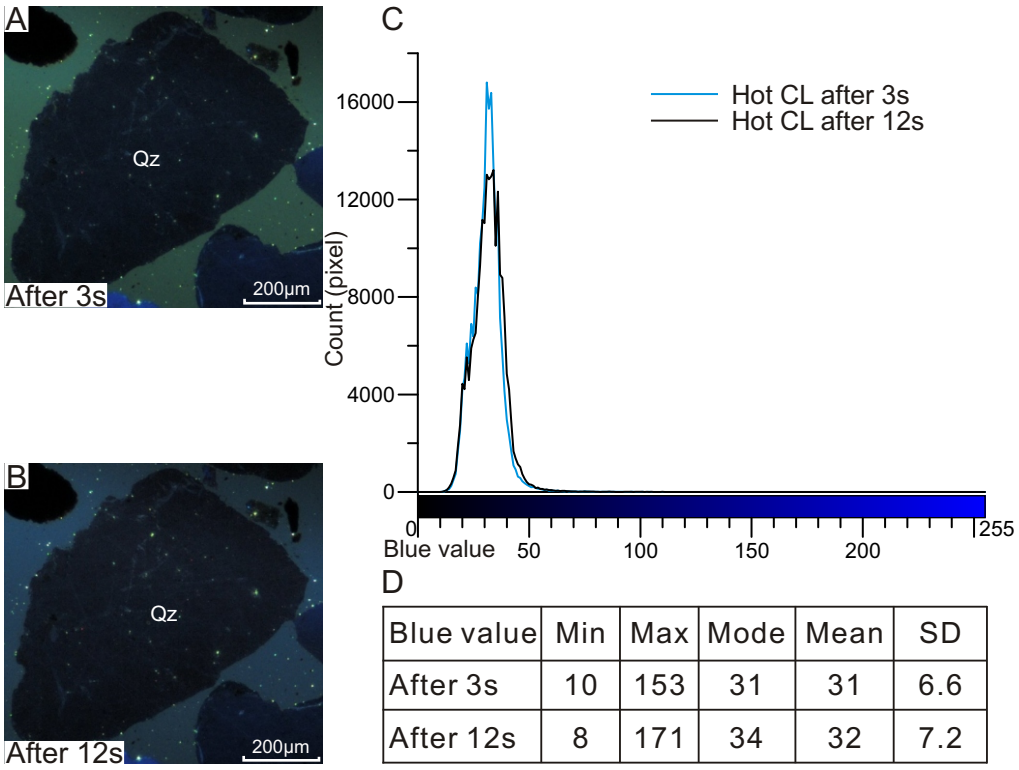

D

Blue value	Min	Max	Mode	Mean	SD
After 3s	10	153	31	31	6.6
After 12s	8	171	34	32	7.2

Figure 7B-10: Grain 10. The grain shows no colour shift.

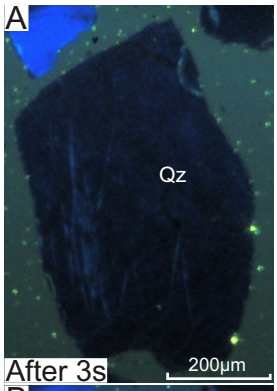

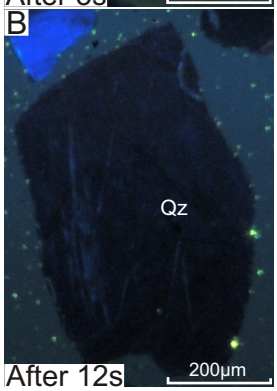

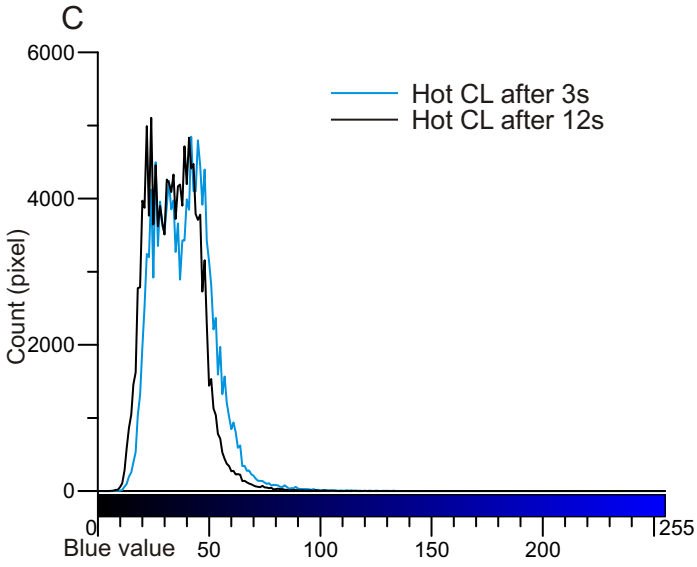

Figure 7B-11: Grain 11. The grain shows slight colour shift.

D

Blue value	Min	Max	Mode	Mean	SD
After 3s	6	133	42	39	12.7
After 12s	6	123	24	34	11.4

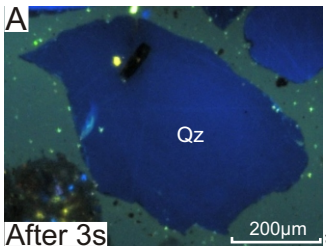

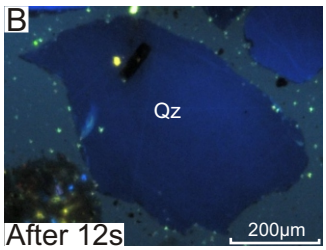

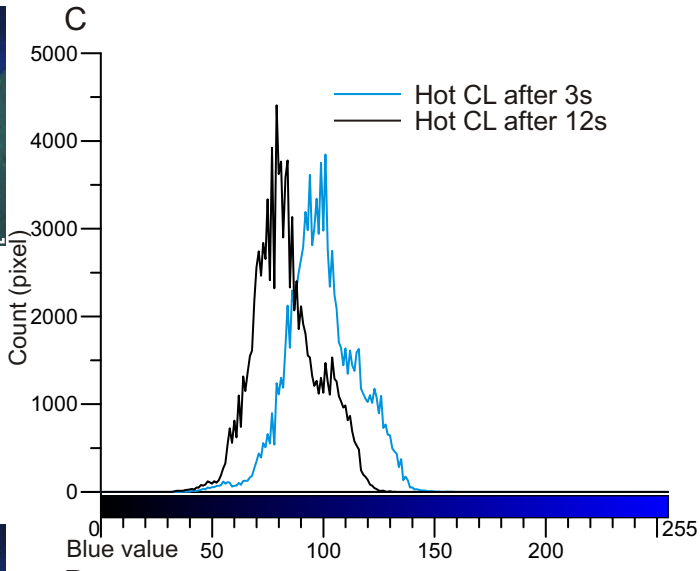

Figure 7B-12: Grain 12. The grain shows moderate colour shift.

D

Blue value	Min	Max	Mode	Mean	SD
After 3s	35	158	101	99	15.4
After 12s	32	135	79	84	14.5

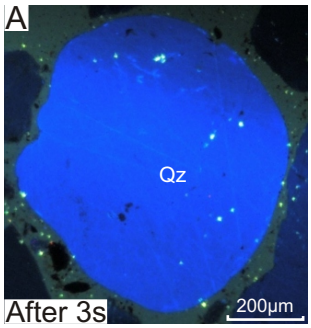

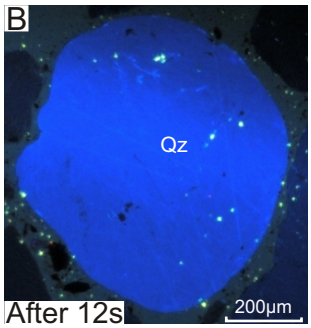

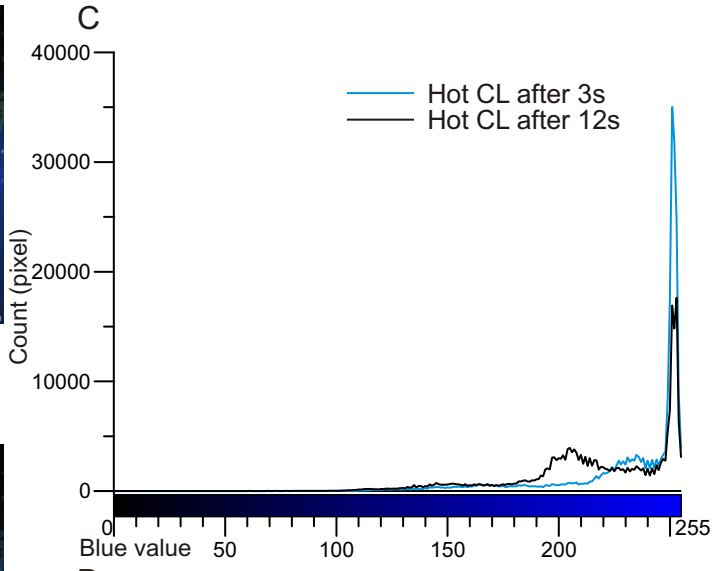

D

Blue value	Min	Max	Mode	Mean	SD
After 3s	45	255	251	234	29.3
After 12s	36	255	253	218	34

Figure 7B-13: Grain 13. The grain shows moderate colour shift.

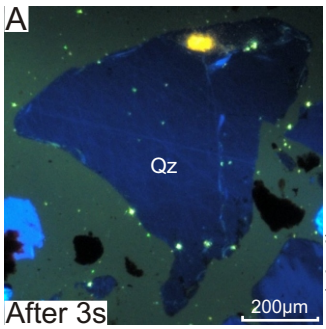

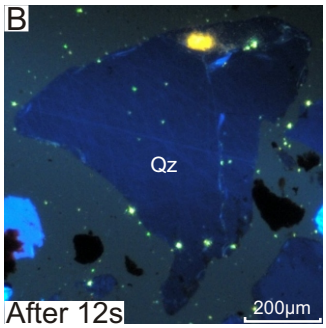

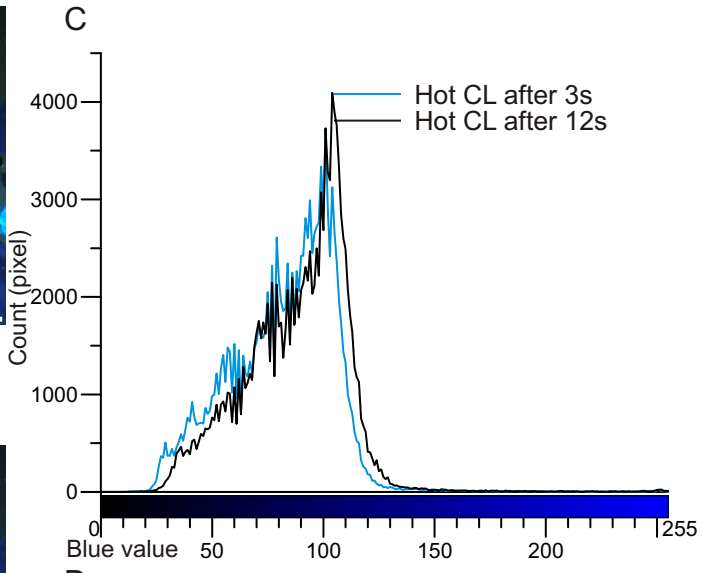

D

Blue value	Min	Max	Mode	Mean	SD
After 3s	10	255	101	82	23.6
After 12s	14	255	104	88	23.4

Figure 7B-14: Grain 14. Probably the first image was taken too early. Therefore, this grain is not useful to analyse the colour shift.

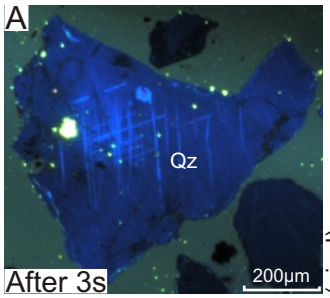

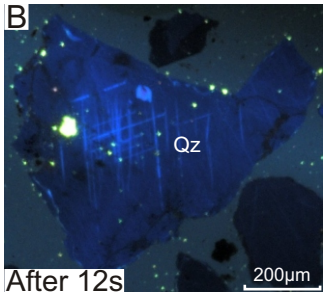

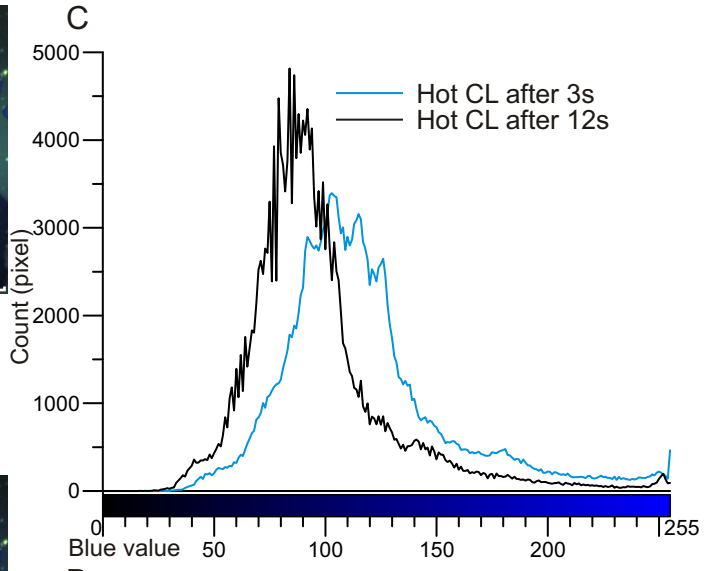

D

Blue value	Min	Max	Mode	Mean	SD
After 3s	27	255	103	118	37.3
After 12s	16	255	84	97	33

Figure 7B-15: Grain 15. The grain shows moderate colour shift.

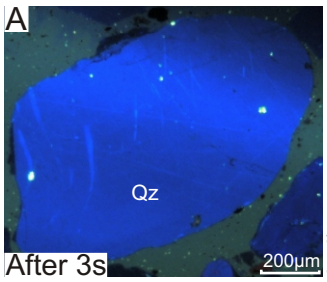

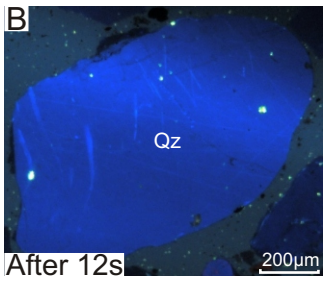

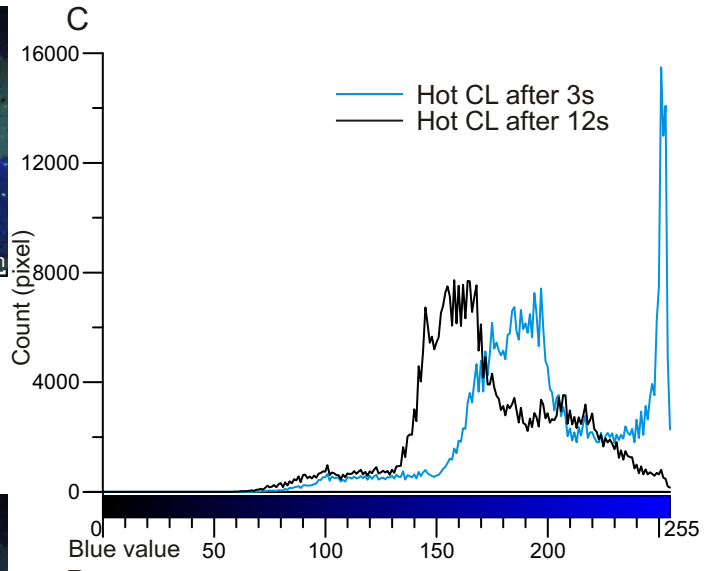

D

Blue value	Min	Max	Mode	Mean	SD
After 3s	66	255	251	199	37
After 12s	57	255	158	172	34

Figure 7B-16: Grain 16. The grain shows moderate colour shift.

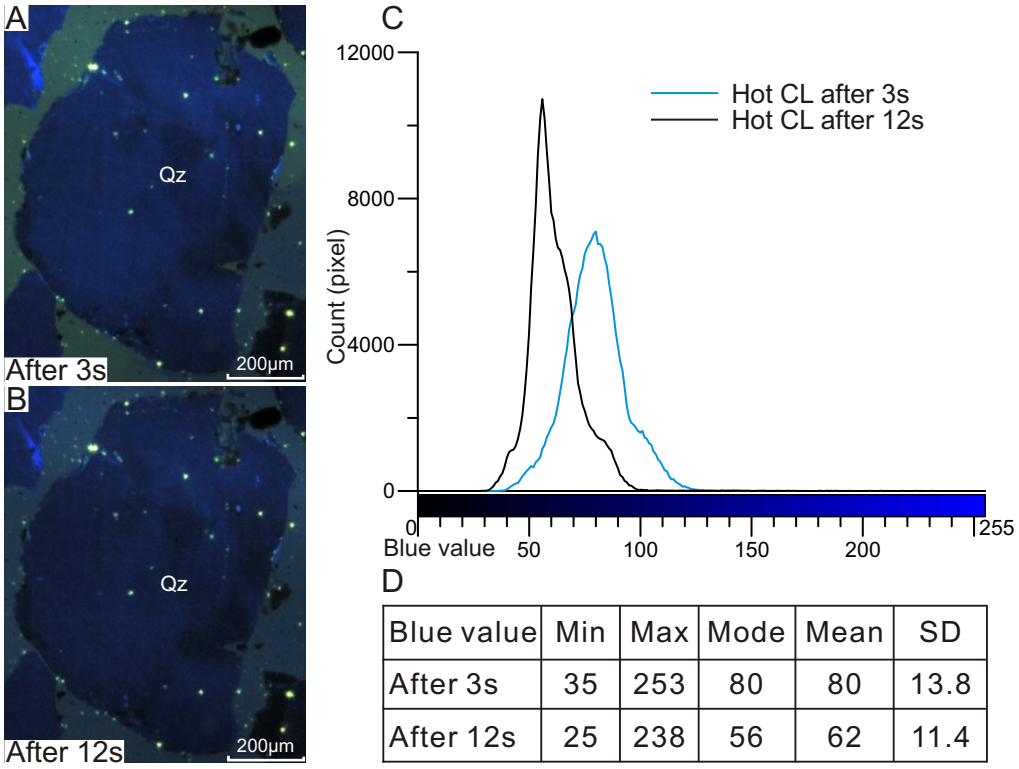

D

Blue value	Min	Max	Mode	Mean	SD
After 3s	35	253	80	80	13.8
After 12s	25	238	56	62	11.4

Figure 7B-17: Grain 17. The grain shows moderate colour shift.

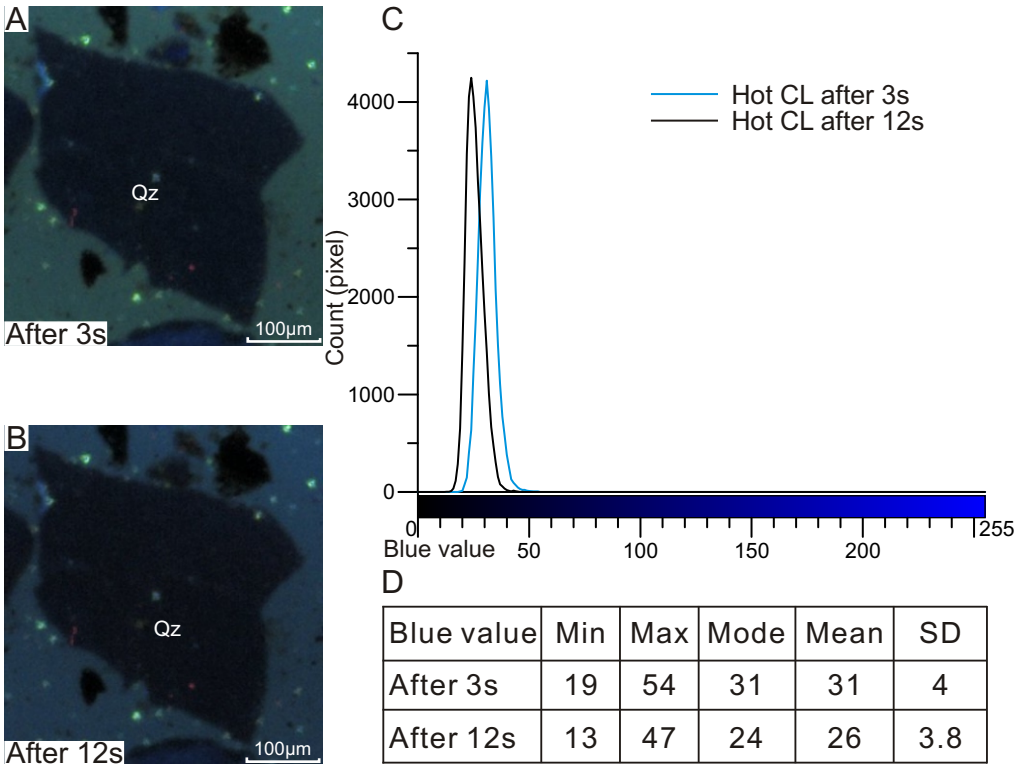

D

Blue value	Min	Max	Mode	Mean	SD
After 3s	19	54	31	31	4
After 12s	13	47	24	26	3.8

Figure 7B-18: Grain18 . The grain shows slight colour shift.

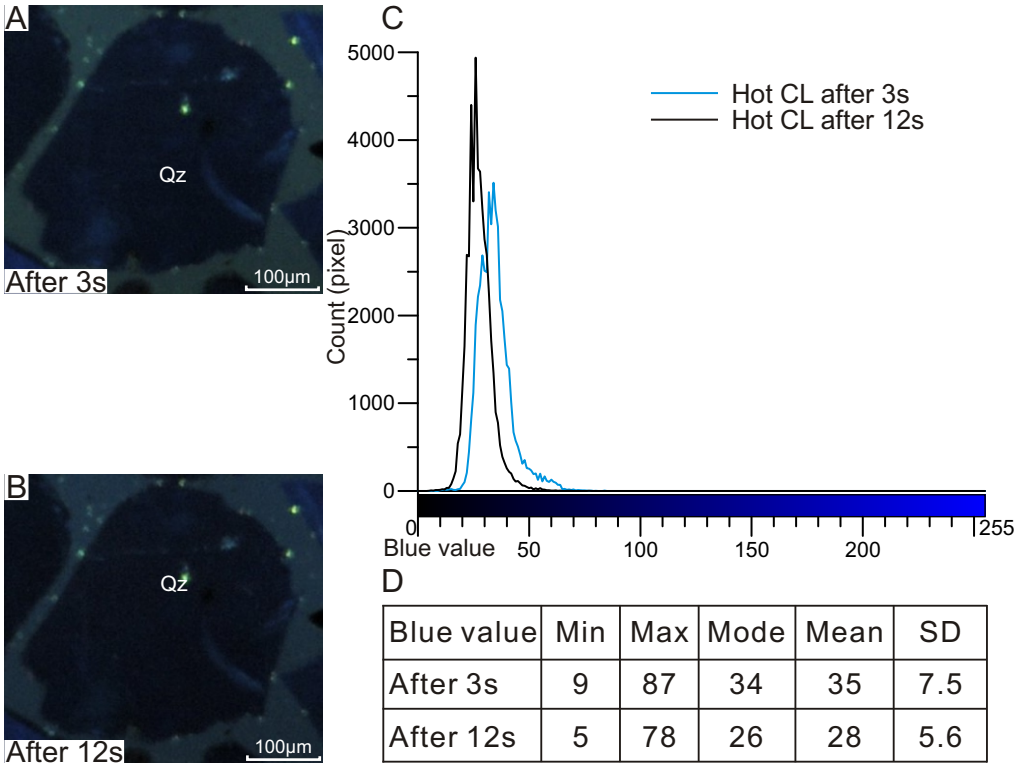

Figure 7B-19: Grain 19. The grain shows slight colour shift.

D

Blue value	Min	Max	Mode	Mean	SD
After 3s	9	87	34	35	7.5
After 12s	5	78	26	28	5.6

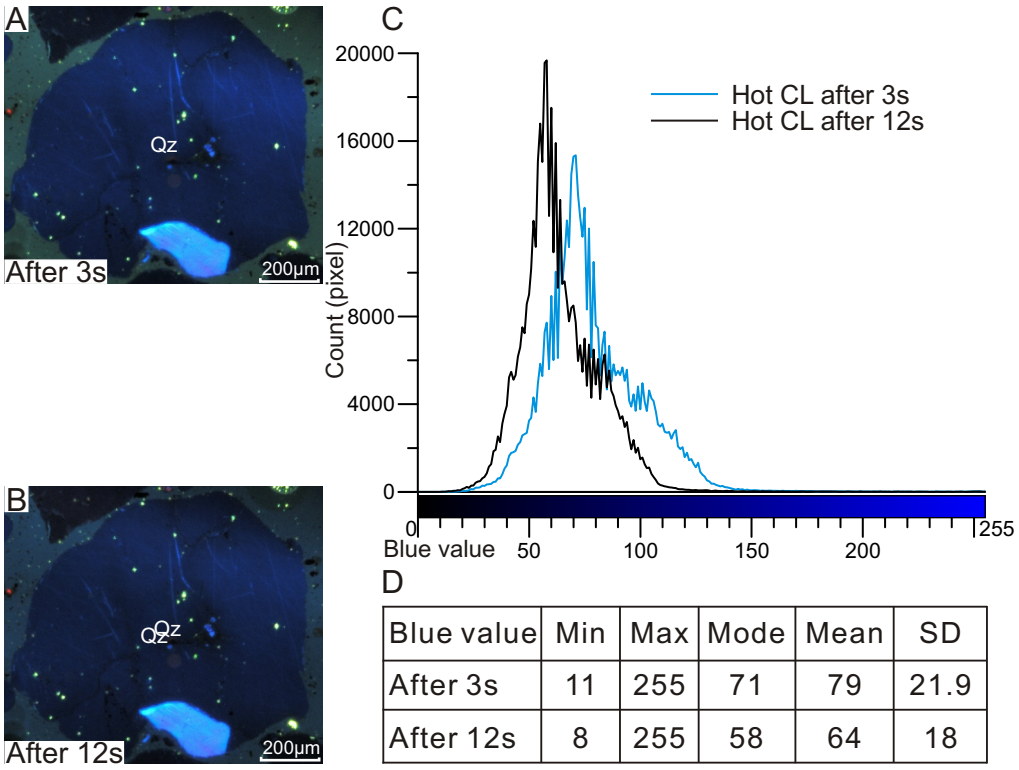

Figure 7B-20: Grain 20. The grain shows moderate colour shift.

D

Blue value	Min	Max	Mode	Mean	SD
After 3s	11	255	71	79	21.9
After 12s	8	255	58	64	18

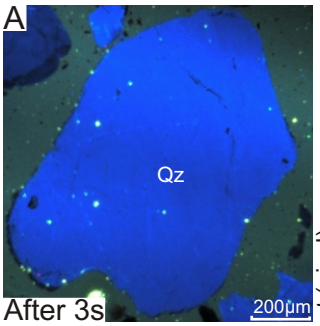

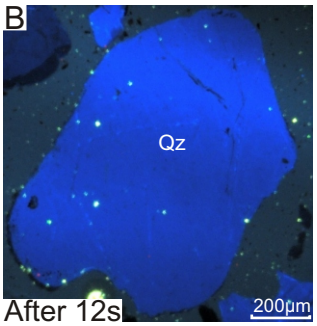

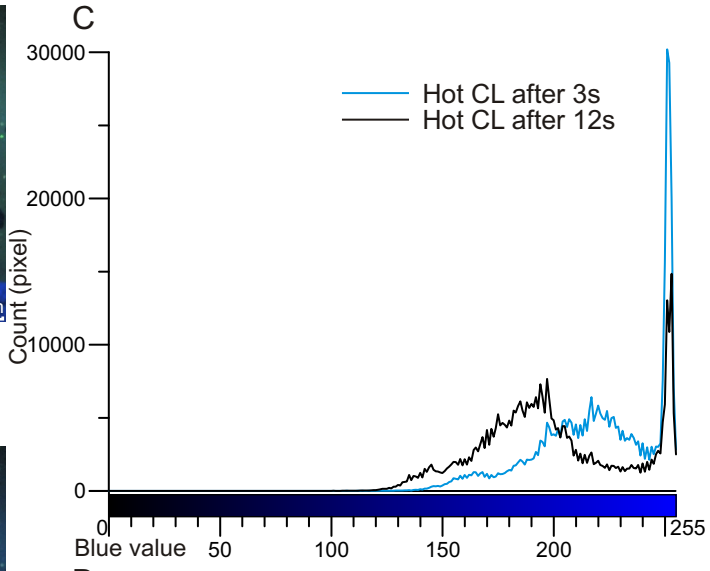

Figure 7B-21: Grain 21. The grain shows moderate colour shift.

D

Blue value	Min	Max	Mode	Mean	SD
After 3s	92	255	251	222	27.3
After 12s	81	255	253	200	32.6

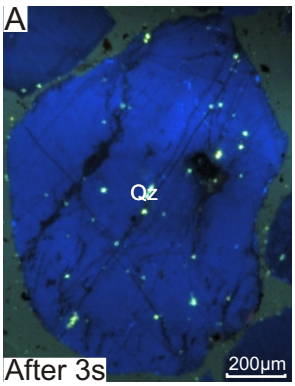

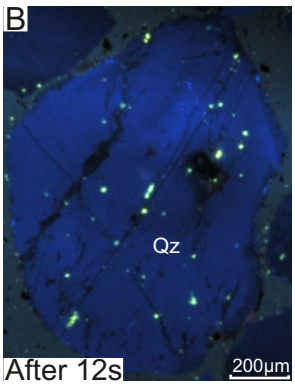

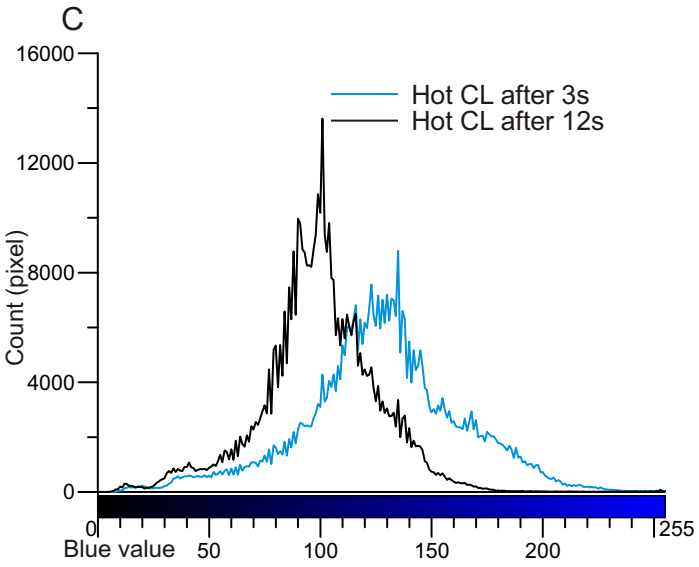

Figure 7B-22: Grain 22. The grain shows moderate colour shift.

D

Blue value	Min	Max	Mode	Mean	SD
After 3s	7	255	135	127	35.7
After 12s	5	255	101	99	26.4

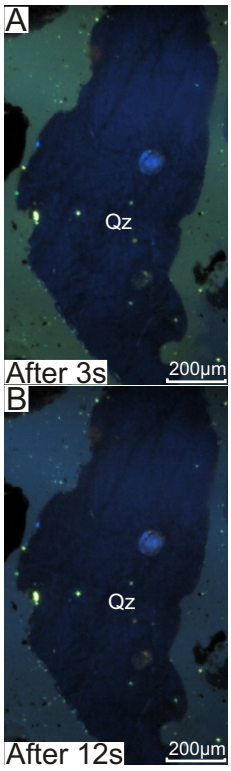

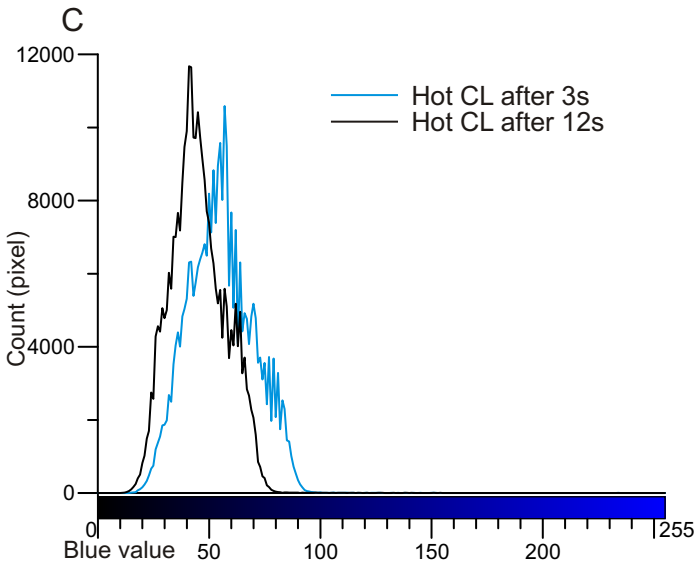

D

Blue value	Min	Max	Mode	Mean	SD
After 3s	12	249	57	55	14.6
After 12s	11	248	41	45	12.3

Figure 7B-23: Grain 23. The grain shows slight colour shift.

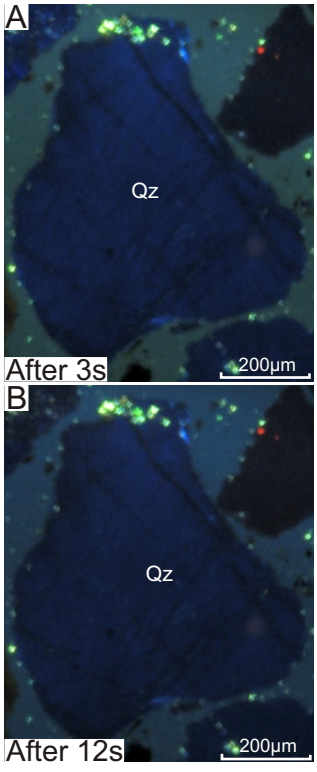

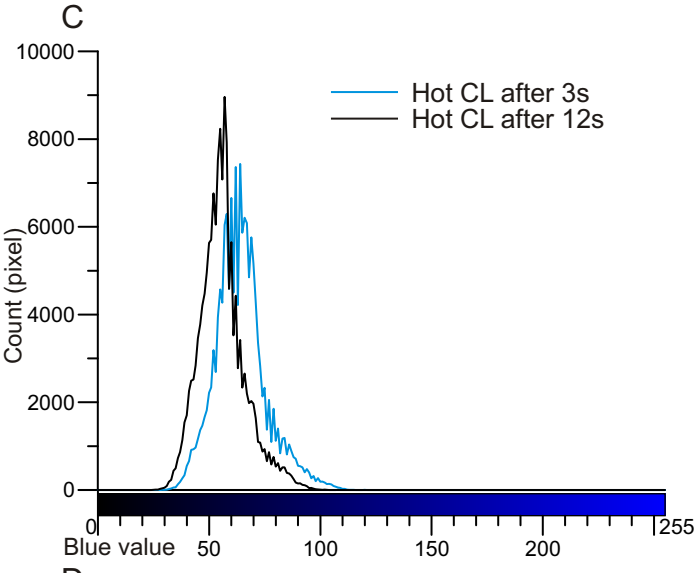

D

Blue value	Min	Max	Mode	Mean	SD
After 3s	28	139	64	64	11.7
After 12s	23	117	57	56	10.4

Figure 7B-24: Grain 24. The grain shows slight colour shift.

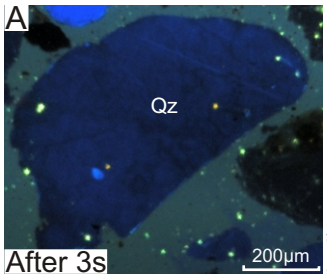

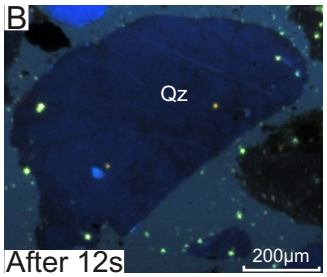

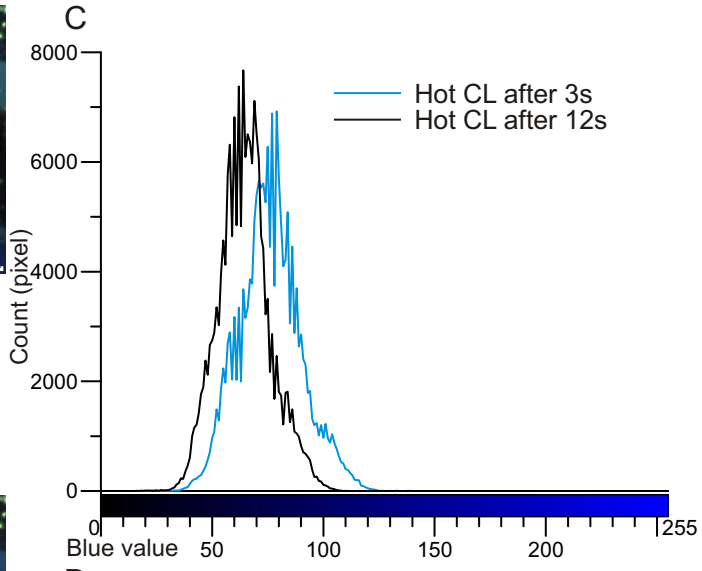

D

Blue value	Min	Max	Mode	Mean	SD
After 3s	13	153	79	76	13.9
After 12s	12	141	64	65	11.8

Figure 7B-25: Grain 25. The grain shows slight colour shift.

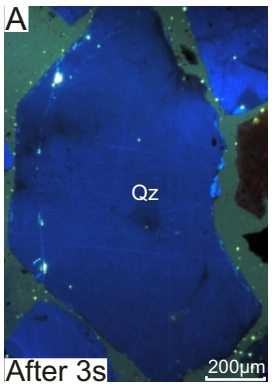

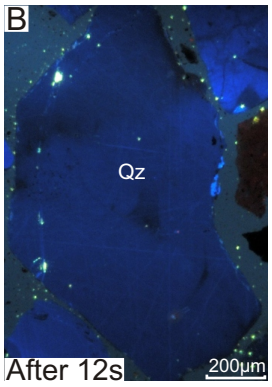

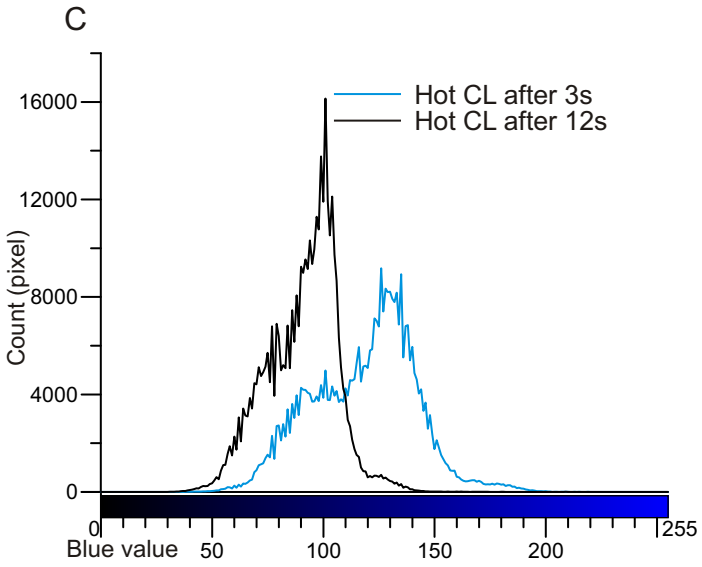

D

Blue value	Min	Max	Mode	Mean	SD
After 3s	34	255	126	119	23.4
After 12s	25	243	101	91	15.9

Figure 7B-26: Grain 26. The grain shows moderate colour shift.

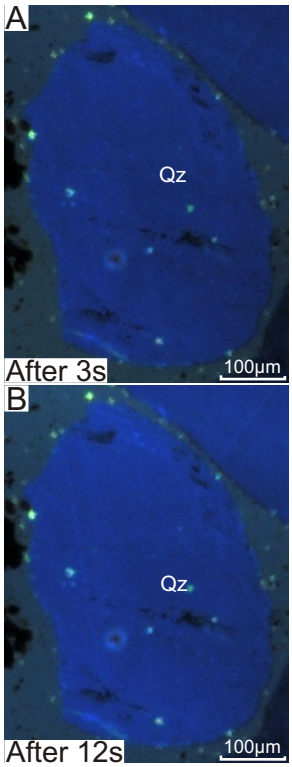

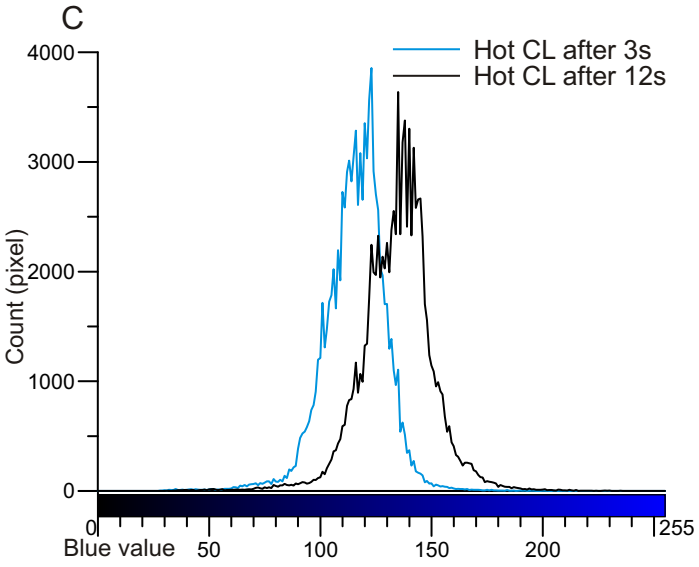

D

Blue value	Min	Max	Mode	Mean	SD
After 3s	28	208	123	116	14
After 12s	31	235	135	134	16.4

Figure 7B-27: Grain 27. Probably the first image was taken too early. Therefore, this grain is not useful to analyse the colour shift.

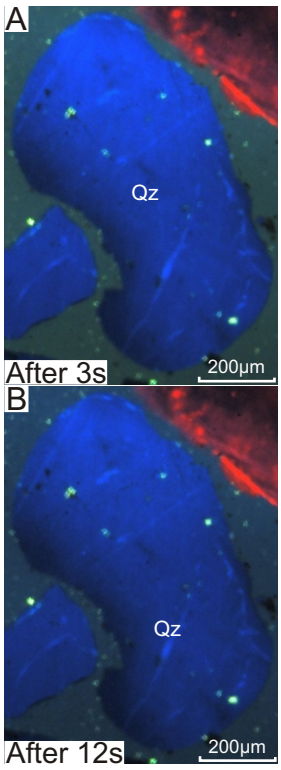

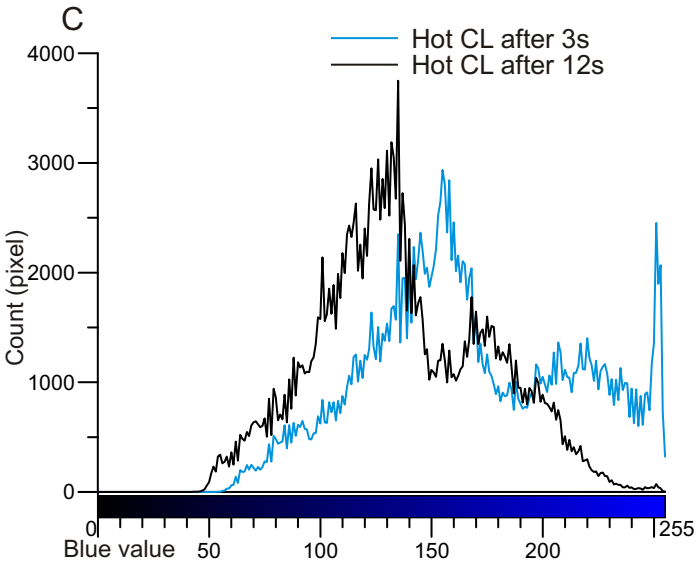

D

Blue value	Min	Max	Mode	Mean	SD
After 3s	54	255	155	167	46.2
After 12s	43	255	135	137	38.3

Figure 7B-28: Grain 28. The grain shows strong colour shift.

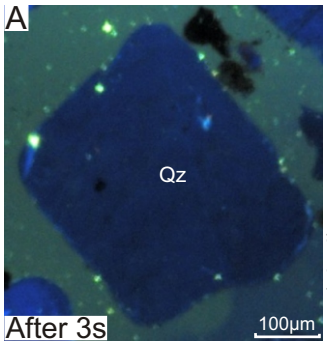

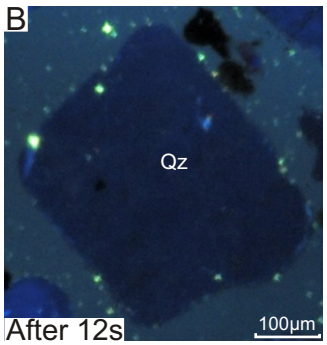

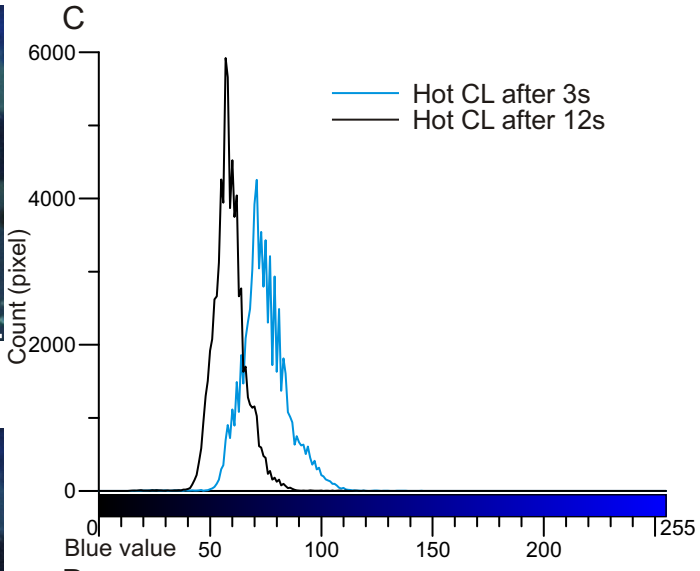

D

Blue value	Min	Max	Mode	Mean	SD
After 3s	16	148	71	75	10.2
After 12s	13	130	57	59	7.3

Figure 7B-29: Grain 29. The grain shows moderate colour shift.

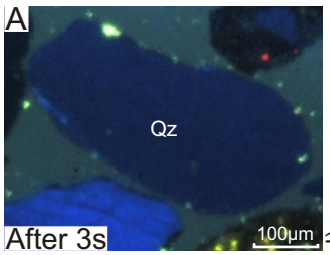

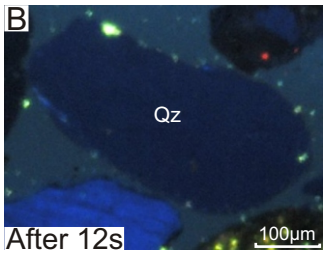

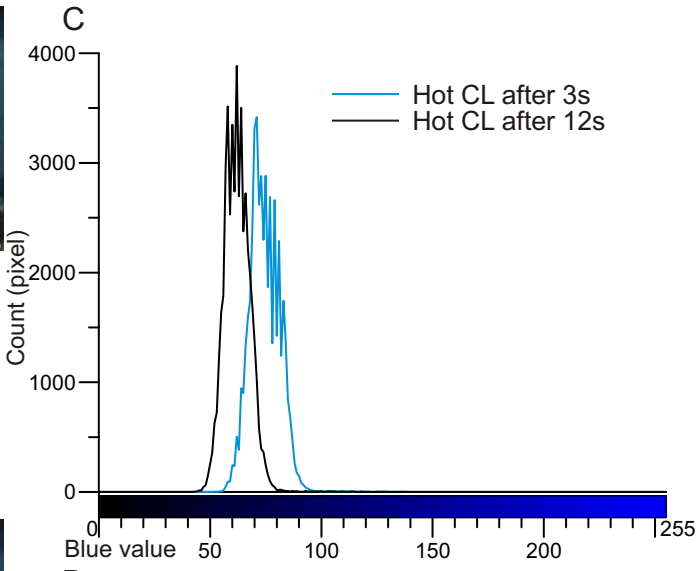

D

Blue value	Min	Max	Mode	Mean	SD
After 3s	52	141	71	74	6.8
After 12s	43	121	62	62	5.8

Figure 7B-30: Grain 30. The grain shows slight colour shift.

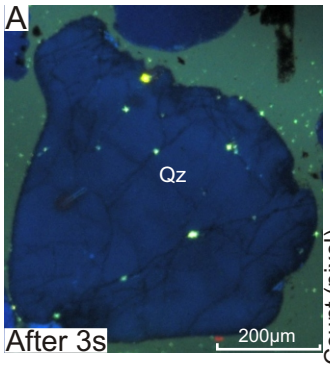

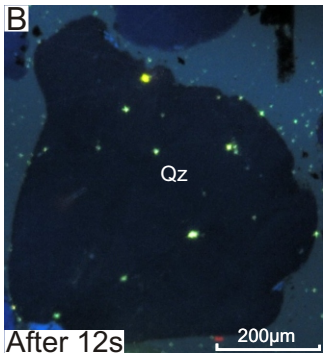

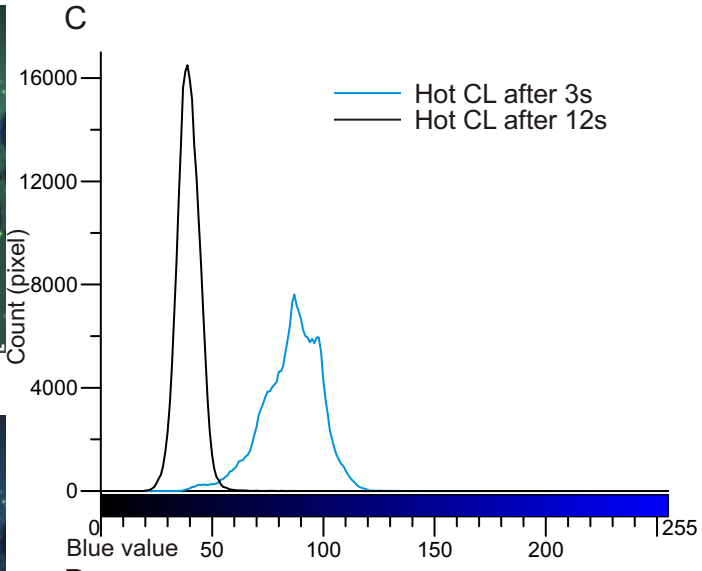

D

Blue value	Min	Max	Mode	Mean	SD
After 3s	33	168	87	86	12.9
After 12s	19	109	39	39	5.1

Figure 7B-31: Grain 31. The grain shows strong colour shift.

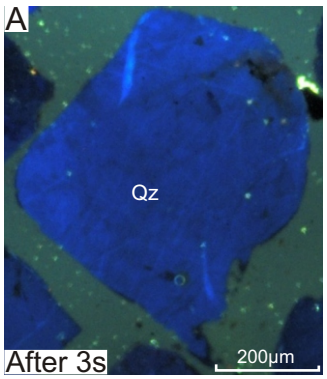

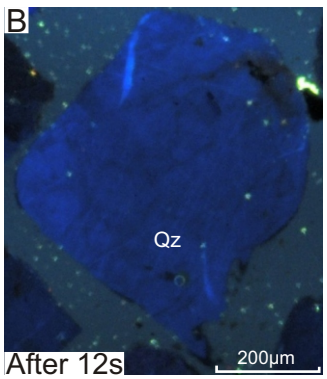

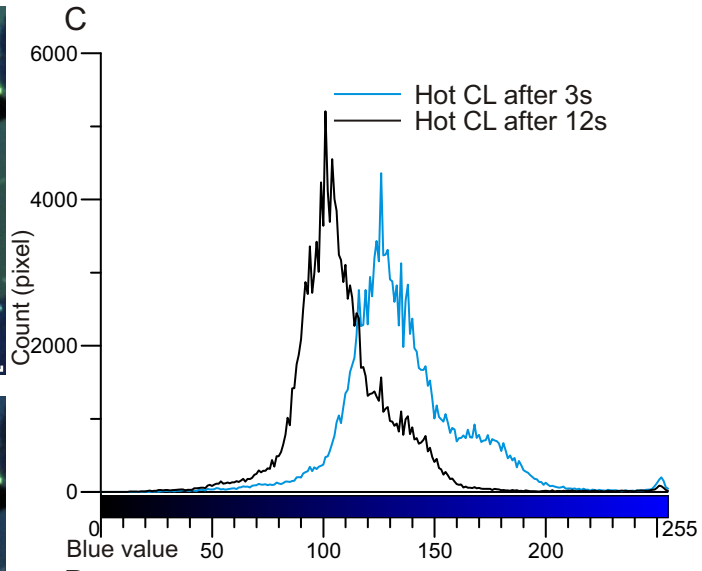

D

Blue value	Min	Max	Mode	Mean	SD
After 3s	20	255	126	136	27.1
After 12s	12	255	101	109	22.9

Figure 7B-32: Grain 32. The grain shows moderate colour shift.

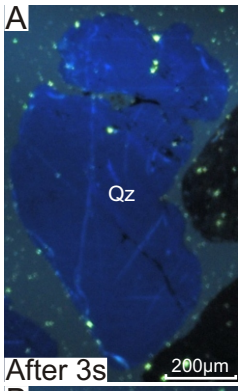

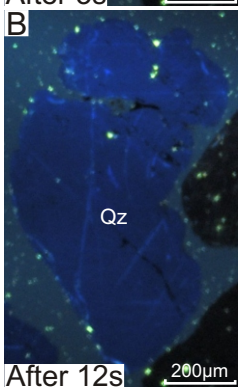

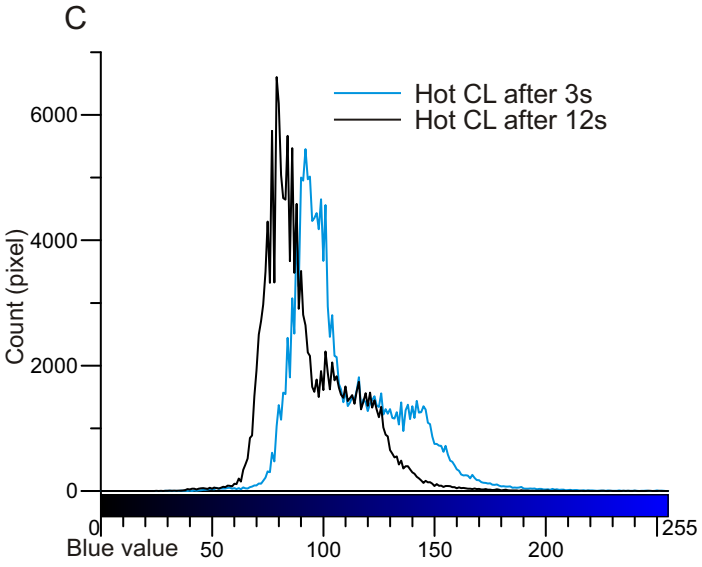

D

Blue value	Min	Max	Mode	Mean	SD
After 3s	28	255	92	110	24
After 12s	23	252	79	93	19.9

Figure 7B-33: Grain 33. The grain shows moderate colour shift.

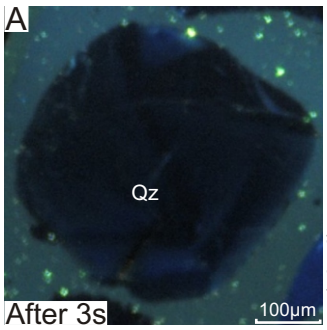

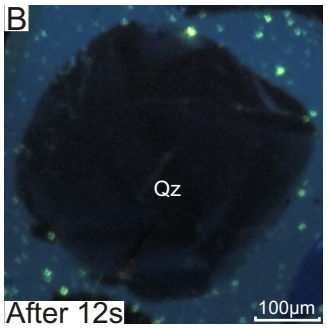

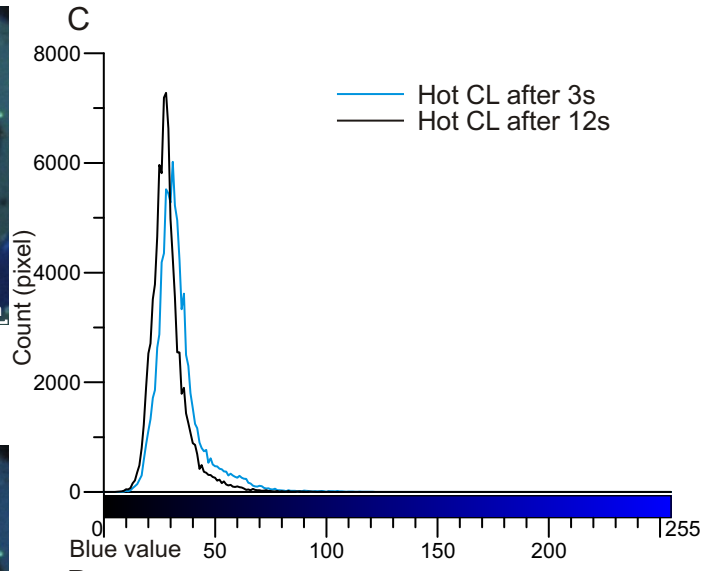

D

Blue value	Min	Max	Mode	Mean	SD
After 3s	8	121	31	34	10.8
After 12s	4	110	28	29	8.2

Figure 7B-34: Grain 34. The grain shows slight colour shift.

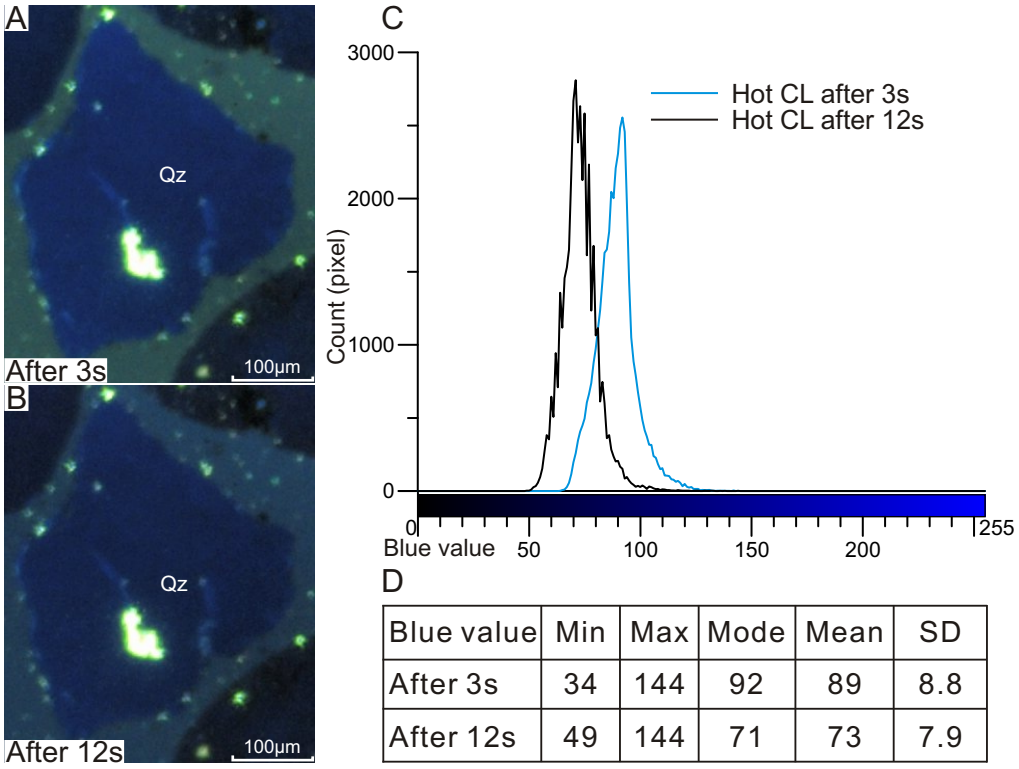

D

Blue value	Min	Max	Mode	Mean	SD
After 3s	34	144	92	89	8.8
After 12s	49	144	71	73	7.9

Figure 7B-35: Grain 35. The grain shows moderate colour shift.

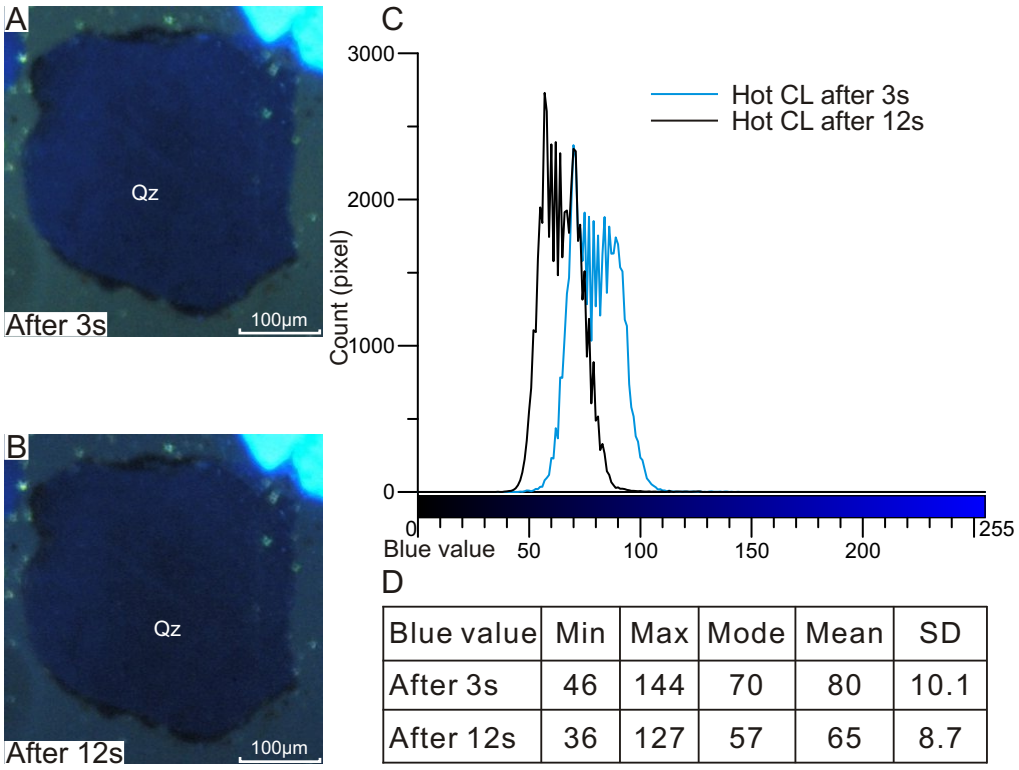

D

Blue value	Min	Max	Mode	Mean	SD
After 3s	46	144	70	80	10.1
After 12s	36	127	57	65	8.7

Figure 7B-36: Grain 36. The grain shows moderate colour shift.

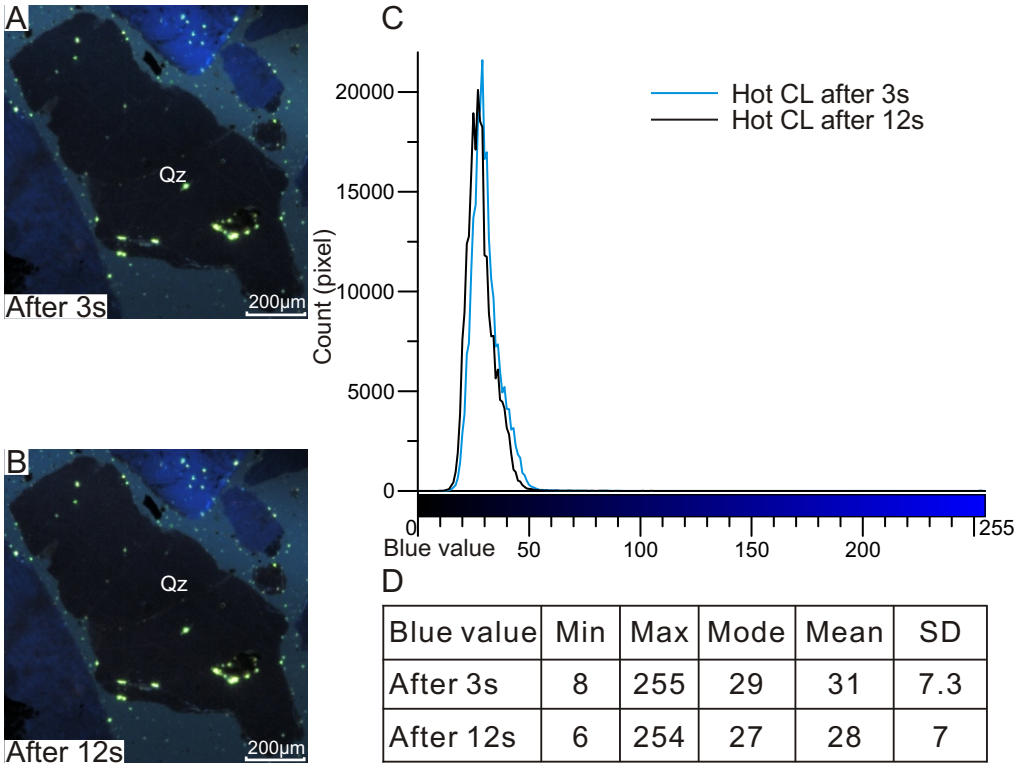

Figure 3B-37: Grain 37. The grain shows no colour shift.

D

Blue value	Min	Max	Mode	Mean	SD
After 3s	8	255	29	31	7.3
After 12s	6	254	27	28	7

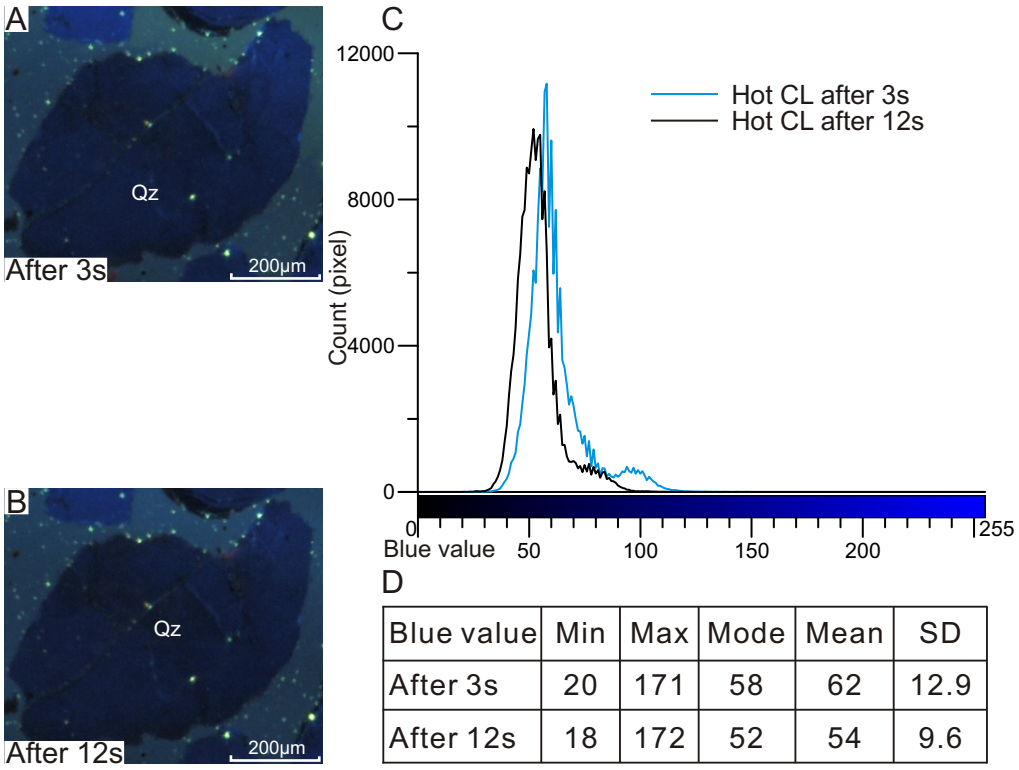

Figure 7B-38: Grain 38. The grain shows slight colour shift.

D

Blue value	Min	Max	Mode	Mean	SD
After 3s	20	171	58	62	12.9
After 12s	18	172	52	54	9.6

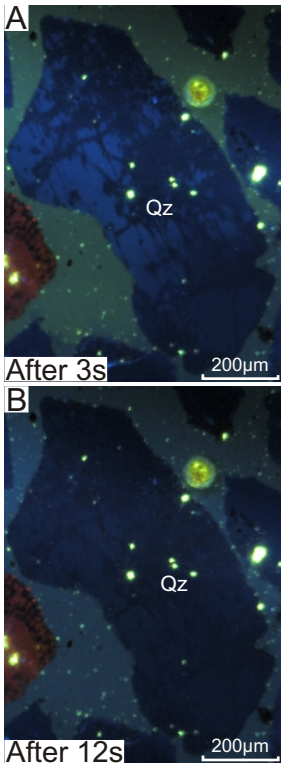

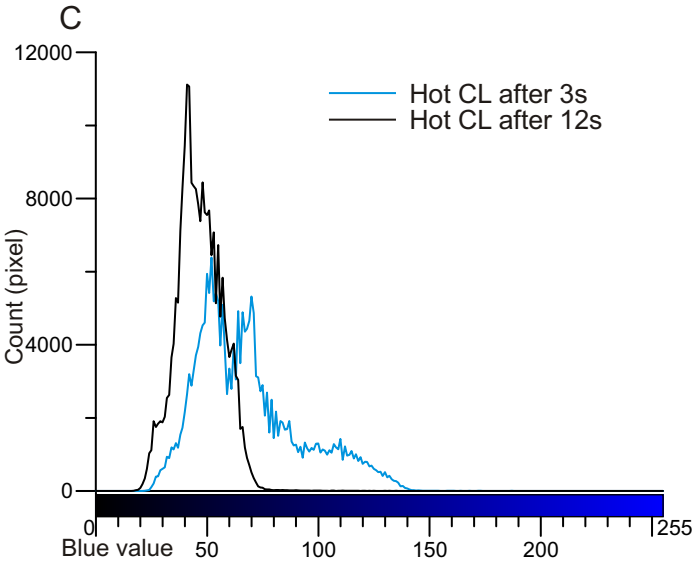

D

Blue value	Min	Max	Mode	Mean	SD
After 3s	20	255	52	69	23.9
After 12s	16	255	41	47	10.3

Figure 7B-39: Grain 39. The grain shows moderate colour shift.

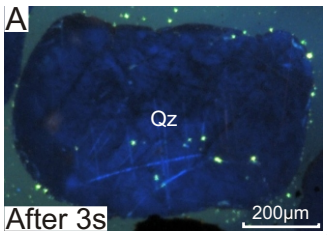

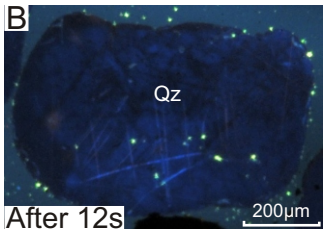

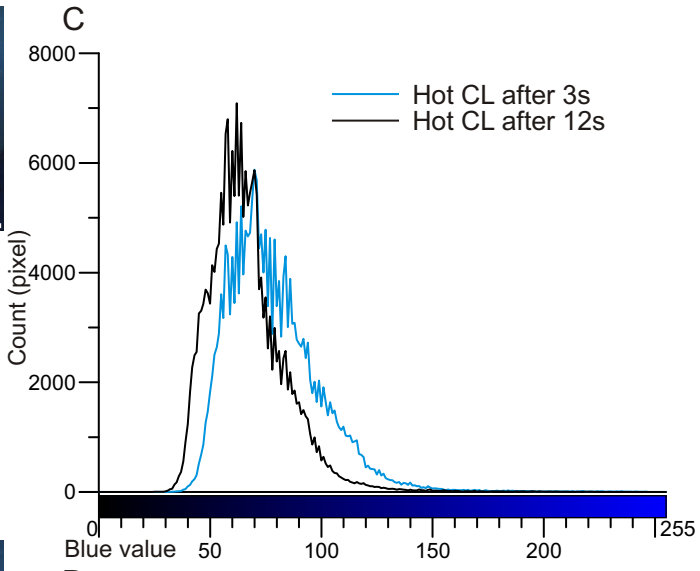

D

Blue value	Min	Max	Mode	Mean	SD
After 3s	31	251	70	79	21.4
After 12s	24	232	62	67	17.6

Figure 7B-40: Grain 40. The grain shows slight colour shift.